

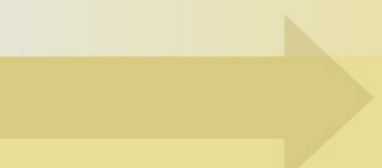
Jesús A. De Loera
Jörg Rambau
Francisco Santos

ALGORITHMS AND COMPUTATION
IN MATHEMATICS

25

Triangulations

Structures for Algorithms
and Applications



[ACM]



Algorithms and Computation in Mathematics • Volume 25

Editors

Manuel Bronstein Arjeh M. Cohen

Henri Cohen David Eisenbud

Bernd Sturmfels

For further volumes:
<http://www.springer.com/series/3339>

Jesús A. De Loera
Jörg Rambau
Francisco Santos

Triangulations

Structures for Algorithms
and Applications

With 550 Figures and 14 Tables

Jesús A. De Loera
University of California, Davis
Department of Mathematics
Shields Ave. 1
95616-8633 Davis California
USA
deloera@math.ucdavis.edu

Francisco Santos
Universidad de Cantabria
Depto. Matemáticas Estadística y
Computación
Avenida de los Castros s/n
39005 Santander
Spain
francisco.santos@unican.es

Jörg Rambau
Universität Bayreuth
Lehrstuhl für Wirtschaftsmathematik
95440 Bayreuth
Germany
joerg.rambau@uni-bayreuth.de

ISSN 1431-1550
ISBN 978-3-642-12970-4 e-ISBN 978-3-642-12971-1
DOI 10.1007/978-3-642-12971-1
Springer Heidelberg Dordrecht London New York

Library of Congress Control Number: 2010933308

© Springer-Verlag Berlin Heidelberg 2010

This work is subject to copyright. All rights are reserved, whether the whole or part of the material is concerned, specifically the rights of translation, reprinting, reuse of illustrations, recitation, broadcasting, reproduction on microfilm or in any other way, and storage in data banks. Duplication of this publication or parts thereof is permitted only under the provisions of the German Copyright Law of September 9, 1965, in its current version, and permission for use must always be obtained from Springer. Violations are liable to prosecution under the German Copyright Law.

The use of general descriptive names, registered names, trademarks, etc. in this publication does not imply, even in the absence of a specific statement, that such names are exempt from the relevant protective laws and regulations and therefore free for general use.

Cover design: deblik, Berlin

Printed on acid-free paper

Springer is part of Springer Science+Business Media (www.springer.com)

Preface

Triangulations appear in many different parts of mathematics and computer science since they are the natural way to decompose a region of space into smaller, easy-to-handle pieces. From volume computations and meshing to algebra and topology, there are many natural situations in which one has a fixed set of points that can be used as vertices for the triangulation. Typically one wants to find an optimal triangulation of those points or to explore the set of their all triangulations. The given points may represent the “sites” for a Delaunay triangulation computation, the test points for a surface reconstruction, or a set of monomials, represented as lattice points in \mathbb{Z}^d , in an algebraic-geometric meaning.

A central theme of this book is to use the rich geometric structure of the space of triangulations of a given set of points to solve computational problems (e.g., counting the number of triangulations or finding optimal triangulations with respect to various criteria), and for setting up connections to novel applications in algebra, computer science, combinatorics, and optimization. Thus at the heart of the book is a comprehensive treatment of the theory of regular subdivisions, secondary polytopes, flips, chambers, and their interactions. Again, we firmly believe that understanding the fundaments of geometry and combinatorics pays up for algorithms and applications.

The book is designed to serve as a textbook or for self-guided study. It was written with graduate students or advanced undergraduates as the target audience (in fact, several groups of students were kind enough to let us test the book with them). Beyond good knowledge of linear algebra, all that is required to use this book is maturity to read and understand proofs. With many examples and exercises, and with over five hundred illustrations, we aim to gently introduce beginners to the properties of the spaces of triangulations of “highly-structured” (e.g., cubes, cyclic polytopes, lattice polytopes, etc.) and “pathological” situations (e.g., disconnected spaces of triangulations, NP-hardness constructions, etc.). We do this in arbitrary dimension, while using only elementary geometric principles. We are excited to present many open questions. Some are new, but many have been open for some time. Also, the book contains many new results appearing here for the first time, besides corrections and simpler proofs of well-known theorems.

Chapter 1 describes several instances where triangulations of a point set naturally arise in combinatorics, optimization, and algebra, as motivation for the rest. A reader may select which parts he or she is most interested in and skip the rest. None of the material is a prerequisite for later chapters, but we hope to communicate some of the exciting and diverse applications possible and to show that triangulations are worth studying by outsiders.

Chapters 2 and 4 lay out the formal language, notation, and basic constructions. Concerning the language, we have decided to distinguish between the points (or vectors) of a configuration and the labels used to denote them. This may look awkward to the beginner at first sight but it has many advantages in the long run.

Chapter 3, is an “interlude” devoted specifically to what happens in two dimensions and a quick glance at dimension three. This chapter is almost independent from the rest and we hope it will help the reader to build intuition and to motivate, in a visual way, the challenges to come in arbitrary dimension (e.g., the notion of flip, enumeration, optimization, etc.). Because Chapter 3 lies in between two more technical chapters we included more examples and applications that helped balance the presentation. It is a fun detour through a very active area of computational geometry.

Chapter 5 contains what is probably the central theorem of the book: Gelfand, Kapranov, and Zelevinsky’s ground-breaking construction of a polytope with face lattice equal to the poset of *regular subdivisions* for any given configuration. This theorem is the central tool for flipping algorithms such as the incremental randomized construction of Delaunay triangulations, customary in Computational Geometry.

The next two chapters are devoted to the study of important examples of configurations (Chapter 6) and triangulations (Chapter 7). In the first one, nice combinatorial structures allow for a deeper study of the properties of

these examples, while in the latter the focus is on ingenious constructions of pathological triangulations (disconnected flip-graphs, and triangulations with very few or no flips).

Chapter 8 focuses on computation and algorithms. We start with a discussion of data structures and discuss methods for enumeration and optimization in triangulations of arbitrary dimension. Here we prove that the structural understanding helps with the design algorithms, software, and the analysis of computational complexity.

Finally, Chapter 9 explores generalizations or different ways of looking at some of the structures in the rest of the book. Some of these “further topics” are so rich they could be themselves central topics of books. Interesting directions discussed include fiber polytopes, Cayley’s construction, Gröbner bases, connections to lattice points and Ehrhart functions, and the combinatorics of simplicial spheres.

If you are a teacher planning to give a one semester course based on this book, the core of it should be Chapters 2, 4 and 5, ending with Section 5.3. These chapters develop the structure on which most of the rest is based. Some parts can be omitted if you need to go to the essentials. These include Sections 2.6 and 4.5. The former relates triangulations with classical topics in polytope theory and the latter is meant as a comprehensive reference list of different ways in which triangulations can be characterized.

Despite our very best intentions there surely remain some errors or typos in the text. We take full responsibility for that and plan to post a list of errors and typos at our web sites. Please do let us know via email (our web addresses are listed below) if you find any. (And feel free to write to us with your triangulation stories too!)

This book took too long to write and required the help of many friends and colleagues who taught us and inspired us with their mathematics and wisdom. We are truly grateful to the following people for their ideas, corrections, comments, questions, suggestions, or simply because they patiently kept asking about our seemingly never-ending book project:

Manuel Abellanas, Oswin Aichholzer, Nina Amenta, Christos Athanasiadis, David Avis, Miguel Azaola, Eric Babson, Imre Bárány, David Barnette, Alexander Barvinok, Margaret Bayer, Matthias Beck, Alexander Below, Andrew Berget, Marshall Bern, Louis J. Billera, Anders Björner, Jürgen Bokowski, Prosejit Bose, Lewis Bowen, Javier Bracho, David Bremner, Winfried Bruns, Igor Chaylygin, Robert Connelly, Mike Develin, Herbert Edelsbrunner, Richard Ehrenborg, David Eppstein, Komei Fukuda, Isidoro Gitler, David Gove, Peter Gritzmann, Joseph Gubeladze, Christian Haase, David Haws, Raymond Hemmecke, Martin Henk, Sven Herrmann, Takayuki Hibi, Serkan Hoşten, Katherine Jones, Michael Joswig, Gil Kalai, Jean-Michel Kantor, Victor Klee, Steve Klee, Edward D. Kim, Matthias Köppe, Francisco Larrión, James Lawrence, Carl W. Lee, Fu Liu, Monika Ludwig, Frank Lutz, Diane Maclagan, Peter Malkin, Jirka Matoušek, Tyrrell McAllister, Luis Montejano, Walter Morris, Oleg Musin, Victor Neumann-Lara, Eran Nevo, Isabella Novik, Mohamed Omar, Shmuel Onn, David Orden, Joseph O’Rourke, Edwin O’Shea, Lior Pachter, Igor Pak, Julian Pfeifle, Vincent Pilaud, Richard Pollack, Alexander Postnikov, Pedro Ramos, Tomás Recio, Victor Reiner, Jürgen Richter-Gebert, Leni Rostock, Günter Rote, Raman Sanyal, Achill Schürmann, József Solymosi, Richard P. Stanley, Mike Stillman, Ileana Streinu, Bernd Sturmfels, Francis Su, Thorsten Theobald, Rekha Thomas, Jorge Urrutia, Frank Vallentin, Michèle Vergne, Rafael Villarreal, Robert Weismantel, Roger J-B Wets, Emo Welzl, Jörg Wills, Andrei Zelevinsky, Günter M. Ziegler, and Chuanming Zong. Last, but not least, we thank the anonymous referees who gave us excellent comments and suggestions for the book.

Several institutions supported us during the writing journey and hosted the other visiting co-authors several times. Of course, our home institutions, University of California, Davis, Universität Bayreuth, and Universidad de Cantabria, were key hosts of our book activities, but earlier versions of the book were also discussed, taught, or written during our various stays at the Geometry Center of the University of Minnesota, ZIB-Berlin, ETH-Zürich, MSRI-Berkeley, and Universität Magdeburg. The Universidad de Cantabria and the Mathematical Sciences Research Institute at UC Berkeley gave us the unique opportunity to deliver Summer courses in 2001 and 2003 on the topic of the book, which very much shaped its current contents and format. The Mathematisches Forschungsinstitut Oberwolfach allowed us to meet in their “Research in Pairs” program for two weeks in the Summer of 2005. This book benefited from the financial support received through grants from the National Science Foundation (DMS-0914107, DMS-0608785, DMS-0309694, and DMS-0073815), the Alexander von Humboldt Foundation,

and the Spanish Ministry of Science and Innovation. We are grateful for the support we received.

Above all we are truly grateful to our wives Ingrid, Nicole, and Mónica, and our three pairs of children Antonio and Andrés, Magdalena and Anna, Jon Ander and Íñigo, for their love, encouragement and support. Whenever we were meeting for the book, either in Davis, Bayreuth, or Santander, we enjoyed the warm hospitality of the respective host family, their friendship, and their appreciation for our work on the book. Most of all we thank them for being with us in the first place. In a way this book belongs to them!

Jesús A. De Loera, Jörg Rambau, and Francisco Santos

April 2010

Contents

Preface	v
1 Triangulations in Mathematics	1
1.1 Combinatorics and triangulations	2
1.2 Optimization and triangulations	13
1.3 Algebra and triangulations	21
1.4 The rest of this book	34
<i>Exercises</i>	38
2 Configurations, Triangulations, Subdivisions, and Flips	43
2.1 The official languages in the land of triangulations	43
2.1.1 Polyhedra and cones	43
2.1.2 Point configurations	47
2.1.3 Geometry of point configurations	50
2.2 A closer look at the definition of triangulation	53
2.2.1 There is always a triangulation	54
2.2.2 A famous example: the Delaunay triangulation	56
2.2.3 Regular subdivisions and their structure	59
2.3 A bullet-proof definition of polyhedral subdivisions	62
2.3.1 Polyhedral subdivisions	62
2.3.2 Regular subdivisions, again	67
2.4 Flips and the graph of triangulations	72
2.4.1 Corank-one configurations and circuits	72
2.4.2 Almost-triangulations and flips	74
2.5 Vector configurations and their triangulations	76
2.5.1 Vector configurations	77
2.5.2 Polyhedral subdivisions of vector configurations	79
2.5.3 Regular subdivisions of vector configurations	81
2.6 Triangulations as simplicial complexes	83
2.6.1 Simplicial complexes	83
2.6.2 The f -vector of a simplicial complex	84
2.6.3 Linear constraints on the f -vector	87
<i>Exercises</i>	90
3 Life in Two Dimensions	93
3.1 Some basic properties	93
3.2 A few examples of triangulations in the plane	95
3.2.1 Placing and pulling triangulations	96
3.2.2 Delaunay triangulations	97
3.2.3 Greedy and minimum weight triangulations	102
3.3 The set of all triangulations of a point set	107
3.3.1 The exact number of triangulations	107

3.3.2	The maximum possible number of triangulations	112
3.3.3	The minimum possible number of triangulations	115
3.3.4	The poset of subdivisions	116
3.4	Flips in triangulations	119
3.4.1	All triangulations of a point set in the plane are connected by flips	120
3.4.2	Effective enumeration of triangulations	123
3.4.3	Further properties of the graph of flips	128
3.5	Pseudo-triangulations	131
3.6	Life in three dimensions	133
3.6.1	The number of tetrahedra	134
3.6.2	Monotone flipping does not (always) work	137
3.6.3	The number of flips	141
3.7	Notes and References	145
	<i>Exercises</i>	146
4	A Tool Box	149
4.1	Combinatorics of configurations	149
4.1.1	Dependences, circuits, and the intersection property	150
4.1.2	Evaluations, cocircuits, and the union property	155
4.1.3	Gale transforms and the duality between circuits and cocircuits	160
4.2	Manipulating vector configurations	165
4.2.1	Pyramids and joins	165
4.2.2	Prisms and products	167
4.2.3	Deletion	169
4.2.4	Contraction	171
4.2.5	One-point suspension	175
4.3	Generating polyhedral subdivisions	178
4.3.1	The placing (or pushing) triangulation	178
4.3.2	The pulling triangulation	181
4.3.3	Lexicographic triangulations	182
4.3.4	Pushing and pulling refinements	183
4.4	Two equivalent characterizations of flips	185
4.4.1	Flips via circuits	186
4.4.2	Flips via walls	188
4.5	More characterizations of triangulations and subdivisions	190
4.5.1	Geometric characterizations	191
4.5.2	Combinatorial characterizations	203
	<i>Exercises</i>	207
5	Regular Triangulations and Secondary Polytopes	209
5.1	The secondary polytope	210
5.1.1	Motivating examples	210
5.1.2	Statement of the main theorem	214
5.1.3	Dimension and affine span of the secondary polytope	217
5.2	The normal fan of the secondary polytope	221
5.2.1	Secondary cones	221
5.2.2	The secondary fan	225
5.2.3	Proof of the main theorem	229

5.3	Structure of the secondary polytope	233
5.3.1	Edges of the secondary polytope	233
5.3.2	Monotone paths on the secondary polytope	236
5.3.3	Facets of the secondary polytope	241
5.4	Chambers	243
5.4.1	The chamber fan	243
5.4.2	Flips in the chamber fan	248
5.5	Configurations with fixed corank	257
5.5.1	Configurations with $d + 3$ points	257
5.5.2	Configurations with $d + 4$ points	261
5.5.3	Lawrence polytopes and the complexity of secondary polytopes	264
	Exercises	270
6	Some Interesting Configurations	275
6.1	Cyclic polytopes	275
6.1.1	Warm-up example: two dimensions	276
6.1.2	Combinatorial properties of cyclic polytopes	277
6.1.3	Triangulations as sections of the canonical projection	283
6.1.4	Higher Stasheff-Tamari posets	285
6.1.5	The structure theorem for the first Stasheff-Tamari poset	287
6.1.6	Cyclic polytopes have many triangulations	290
6.2	Products of two simplices	294
6.2.1	The prism over a simplex	294
6.2.2	The product of simplices	299
6.2.3	Staircase triangulations	301
6.2.4	Non-regular triangulations of products of simplices	304
6.3	Cubes and their subpolytopes	311
6.3.1	Small 0/1 non-regular triangulations	311
6.3.2	Two simple ways to triangulate any cube	314
6.3.3	Triangulating high-dimensional cubes. State of the art	316
6.3.4	Cubes of three dimensions	319
6.3.5	Cubes of four dimensions	322
6.3.6	Slices of cubes: triangulations of hypersimplices	325
6.3.7	Birkhoff's polytope	330
	Exercises	334
7	Some Interesting Triangulations	337
7.1	The mother of all examples, and some relatives	338
7.1.1	A theme with many variations	338
7.1.2	Twelve proofs of non-regularity	342
7.2	Highly flip-deficient triangulations	345
7.2.1	Dimension 3: A zig-zag grid	345
7.2.2	Locally acyclic orientations and triangulations of products	349
7.2.3	Locally acyclic orientations without reversible edges	352
7.2.4	Dimension 4: Layers of prisms	356
7.3	Dimension 5: A disconnected graph of triangulations with unimodular triangulations	358
7.3.1	Locally acyclic orientations of boundary subcomplexes	358
7.3.2	Unimodular triangulations in different components of the graph of triangulations	360

7.3.3	Exponential number of components in the graph of flips	361
7.4	Dimension 6: A disconnected graph of triangulations in general position	362
7.4.1	The building block: Gale octagons	363
7.4.2	Seventeen points in special position	365
7.4.3	A disconnected space of triangulations in general position	369
	<i>Exercises</i>	374
8	Algorithmic Issues	377
8.1	Tools for computation	377
8.1.1	Chirotopes	377
8.1.2	Computing the chirotope	378
8.1.3	Computing circuit and cocircuit signatures from the chirotope	383
8.2	Verification and realizability	385
8.2.1	Constructing regular triangulations in practice	386
8.2.2	Checking regularity of a triangulation	387
8.3	Listing and enumerating triangulations	388
8.3.1	Exploring a flip-graph component	389
8.3.2	Enumeration of all triangulations	390
8.3.3	Enumeration with symmetry	392
8.3.4	Implementation issues	393
8.4	Bounding the number of triangulations	396
8.5	Optimization	398
8.5.1	A linear optimization approach: the universal polytope	400
8.5.2	Relaxations of the universal polytope and its edges	406
8.5.3	Equidecomposable and weakly neighborly polytopes	410
8.6	Computational complexity of triangulation problems	413
8.6.1	A very quick review of complexity classes	413
8.6.2	The hardness of the planar constrained triangulation problem	415
8.6.3	Hardness of minimum length triangulations in the plane	422
8.6.4	Hardness of minimal size triangulations of convex polytopes	425
	<i>Exercises</i>	429
9	Further Topics	433
9.1	Fiber polytopes	433
9.1.1	Monotone paths	433
9.1.2	Zonotopal tilings	436
9.1.3	Polyhedral subdivisions	438
9.1.4	Compatible subdivisions and the fiber polytope	438
9.2	Mixed subdivisions and the Cayley trick	445
9.2.1	An example	445
9.2.2	Mixed subdivisions and the Minkowski projection	447
9.2.3	Subdivisions in the Cayley embedding and the Cayley projection	452
9.2.4	The Cayley trick	454
9.2.5	Product of a triangle and k -simplex	459
9.3	Lattice polytopes and unimodular triangulations	463
9.3.1	Triangulations of lattice polygons	465
9.3.2	Existence of unimodular triangulations	469
9.3.3	Ehrhart polynomials and unimodular triangulations	475

9.4	Triangulations and Gröbner bases	478
9.4.1	Gröbner bases and toric ideals	479
9.4.2	Sturmfels' correspondence	481
9.5	Polytopal complexes and regular triangulations	488
9.5.1	Central and normal fans as regular triangulations	489
9.5.2	Shellings, flips, and face vectors	493
9.5.3	Polytopality via regular triangulations	502
	<i>Exercises</i>	509
	Bibliography	513
	Index	531

1

Triangulations in Mathematics

When solving a difficult problem it is a natural idea to decompose complicated objects into smaller, easy-to-handle pieces. In this book we study such decompositions: *triangulations of point configurations*. We will look at triangulations from many different points of view. We will explore their combinatorial and geometric properties, as well as some algorithmic issues arising along the way.

This first chapter is designed to informally introduce the fundamental notions to come in later chapters. We provide motivating examples to convince the reader that triangulations are useful and that they appear in many areas of mathematics. The reader can skip most of this chapter safely, or read the sections in an order different than the one presented. The examples also provide an entry door for non-discrete-geometers (e.g., algebraic geometers, computer scientists, linear programming enthusiasts, etc.) that wish to learn about triangulations for their research, connecting our book to their topic. Without further delay we begin.

A *point configuration*¹ is a finite collection of points $\mathbf{A} = \{\mathbf{a}_1, \dots, \mathbf{a}_n\}$ in Euclidean space \mathbb{R}^d .

The *convex hull* of \mathbf{A} is by definition the intersection of all convex sets containing the points in \mathbf{A} . We denote it by $\text{conv}(\mathbf{A})$.

A k -simplex is the convex hull of $k+1$ affinely independent points in \mathbb{R}^d (clearly $d \geq k$). Simplices are the simplest of polyhedra: points, segments, triangles, tetrahedra, etc. A j -face of a k -simplex is the convex hull of $j+1$ of its vertices and thus in particular is a j -simplex itself. We say that the empty set is a (-1) -dimensional face common to all simplices, so that every k -simplex has exactly $\binom{k+1}{j+1}$ j -faces for $j = -1, 0, 1, \dots, k$. A simplex of \mathbf{A} is a simplex whose vertices are taken from \mathbf{A} .

Here is the main actor in this play:

Definition 1.0.1. A *triangulation* of a point configuration $\mathbf{A} \in \mathbb{R}^d$ is a collection \mathcal{T} of d -simplices all of whose vertices are points in \mathbf{A} that satisfies the following two properties:

1. The union of all these simplices equals $\text{conv}(\mathbf{A})$. (*Union Property*)
2. Any pair of these simplices intersects in a common face (possibly empty). (*Intersection Property*)

¹The word *configuration* is used to distinguish this from a *set* of points: in a subset of \mathbb{R}^d there can be no multiple points, whereas in a configuration we, in principle, are allowed to have $\mathbf{a}_i = \mathbf{a}_j$ for some $i \neq j$ and still consider \mathbf{a}_i and \mathbf{a}_j two different elements of \mathbf{A} . See Chapter 2 for explanations and justifications of this.

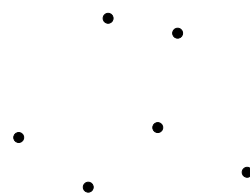


Figure 1.1: A point configuration.

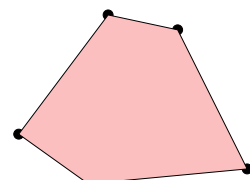


Figure 1.2: Its convex hull.

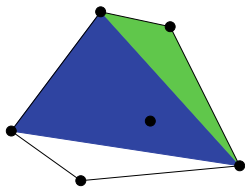


Figure 1.3: The union of simplices is not the whole convex hull (union property fails).

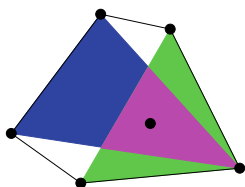


Figure 1.4: The intersection of simplices is not proper (intersection property fails).

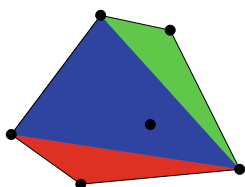


Figure 1.5: This example satisfies both the union and intersection properties, thus it is a triangulation.

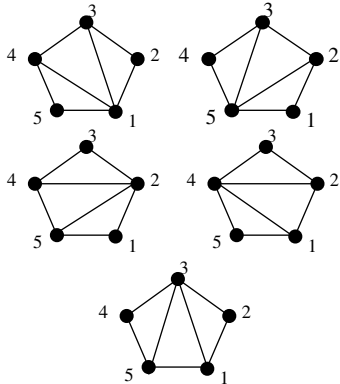


Figure 1.6: The five triangulations of a pentagon.
In this case all triangulations are full.

As a particular case, by a triangulation of a convex polytope \mathbf{P} we mean a triangulation of the point configuration given by the vertices of \mathbf{P} .

In Figures 1.3 and 1.4 we show examples of the possible pathologies that may prevent a triangulation.

Let us emphasize two features that distinguish our definition from other definitions of the word triangulation that the reader may have seen before:

1. With very few exceptions, we will fix in advance the set \mathbf{A} of points that can be used as vertices, and it is a finite set. In particular, the number of triangulations of a point configuration is always finite. This does not happen in classic combinatorial topology or in some applications, where one is free to use arbitrary additional points.
2. We do not insist that all points of \mathbf{A} are used as vertices in a triangulation. For example, if our point configuration consists of points in \mathbb{R} , then there is one triangulation with only one simplex (the whole segment $\text{conv}(\mathbf{A})$) and two vertices (the two convex hull extremes of the line segment $\text{conv}(\mathbf{A})$), regardless of how many points we may have in \mathbf{A} . This differs from the standard use of triangulations in Computational Geometry, where one usually requires all the points to be used. Thus we make the following definition:

Definition 1.0.2. Let $\mathbf{A} \subset \mathbb{R}^d$ be a point configuration. We call a triangulation of \mathbf{A} *full* if all the points of \mathbf{A} are vertices of it.

The first of these two features gives our setting a strong combinatorial flavor. Actually, to describe a particular triangulation we will normally number the points of \mathbf{A} from 1 to n and give the list of vertex sets of the d -simplices in the triangulation. For example, the five triangulations of a pentagon would be written as:

$$\begin{aligned} & \{ \{1,2,3\}, \{1,3,4\}, \{1,4,5\} \}, & \{ \{1,2,5\}, \{2,3,5\}, \{3,4,5\} \}, \\ & \{ \{1,2,5\}, \{2,4,5\}, \{2,3,4\} \}, & \{ \{1,4,5\}, \{1,2,4\}, \{2,3,4\} \}, \\ & \text{and} & \{ \{1,2,3\}, \{1,3,5\}, \{3,4,5\} \}. \end{aligned}$$

We will even abbreviate $\{1,2,3\}$ as 123 and so on, whenever this creates no confusion.

Why should anyone care about studying triangulations of point configurations? It is our intention to illustrate, with some examples, how several of the fundamental defining properties of triangulations draw themselves into topics that, at first sight, seem far apart from the geometry of triangulations.

1.1 Combinatorics and triangulations

It is well-known that polyhedra can be quite useful when dealing with combinatorial problems. In this section we show two examples of combinatorial identities that have interpretations in terms of triangulations. Let us start with what is possibly the simplest example of the structures studied

in this book: the set of triangulations of a convex polygon. Let \mathbf{C}_n be a convex polygon with n vertices, numbered from 1 to n in clockwise order. The first observation is that the number of triangulations does not depend on the coordinates of the vertices. Indeed, a triangulation will be given by any $n - 3$ diagonals not crossing one another, and two diagonals cross if and only if they involve four vertices in an alternating way. That is to say, if $1 \leq i < j < k < l \leq n$, then the only two diagonals involving these four points and crossing each other are ik and jl .

In particular, the number of triangulations of a convex n -gon is a number depending only on n and that we will denote by t_n . The first instances are easy to compute: $t_3 = 1$, $t_4 = 2$, $t_5 = 5$ (see Figure 1.6), and $t_6 = 14$ (see Figure 1.15).

Proposition 1.1.1. *Setting $t_2 = 1$ by convention, the sequence of numbers t_2, t_3, t_4, \dots satisfies the following recurrence relation:*

$$t_n = t_2 t_{n-1} + t_3 t_{n-2} + \cdots + t_{n-1} t_2.$$

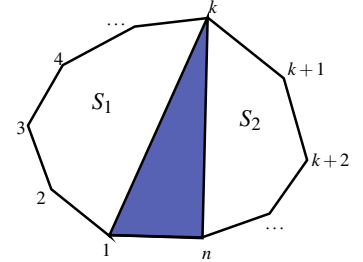


Figure 1.7: Setting up a recursion for $R(n)$.

Proof. In every triangulation of \mathbf{C}_n the edge $\{1, n\}$ is a side of exactly one of the triangles, say $\{1, k, n\}$. The total number of triangulations, then, is the sum of the triangulations using the triangle $\{1, k, n\}$ for k ranging from 2 to $n - 1$.

For a fixed k , the complement of the triangle $\{1, k, n\}$ consists of two polygons S_1 and S_2 with k and $n - k + 1$ vertices, respectively. Since the polygons S_1 and S_2 can be triangulated independently, the number of triangulations of \mathbf{C}_n using the triangle $\{1, k, n\}$ equals $t_k t_{n-k+1}$. (Of course, we admit S_1 or S_2 being a single edge, or a “2-gon”, if $k = 2$ or $k = n - 1$. We take $t_2 = 1$ because this makes $t_2 t_{n-1}$ be equal to t_{n-1} .)

The recurrence formula is obtained by adding this for $k = 2, \dots, n - 1$. \square

The recurrence formula in the statement allows us to easily compute further terms in the sequence, for example $t_7 = 1 \cdot 14 + 1 \cdot 5 + 2 \cdot 2 + 5 \cdot 1 + 14 \cdot 1 = 42$ and $t_8 = 1 \cdot 42 + 1 \cdot 14 + 2 \cdot 5 + 5 \cdot 2 + 14 \cdot 1 + 42 \cdot 1 = 132$. A closed formula for t_i can be deduced from the recurrence with the method of *generating functions* (see Exercise 1.5), but here we use a more direct approach to find it.

Theorem 1.1.2. *The number t_n of triangulations of a convex n -gon equals*

$$\frac{1}{n-1} \binom{2n-4}{n-2}.$$

Proof. As before, we assume the vertices of the n -gon to be labeled from 1 to n in clockwise order. Denote by $\Delta(\mathbf{C}_n)$ the set of all triangulations of an n -gon, and their number by t_n . We are going to set up a simple surjective map f from $\Delta(\mathbf{C}_{n+1})$ onto $\Delta(\mathbf{C}_n)$. A triangulation in $\Delta(\mathbf{C}_{n+1})$ is mapped to the triangulation in $\Delta(\mathbf{C}_n)$ obtained by contracting the boundary edge $\{1, n+1\}$ (see Figure 1.8).

Our crucial observation is that the number of triangulations in $\Delta(\mathbf{C}_{n+1})$ mapped to a certain triangulation \mathcal{T} in $\Delta(\mathbf{C}_n)$ equals the number of edges

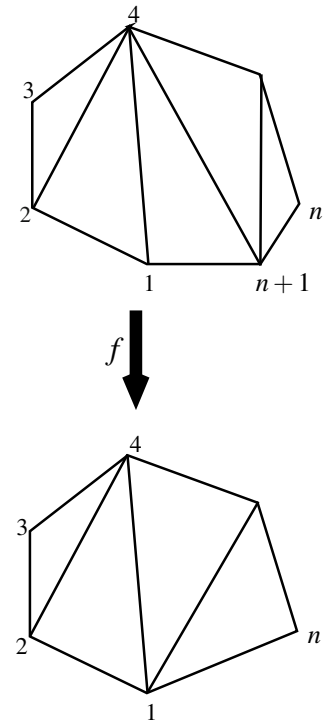


Figure 1.8: The contracting map.

incident to vertex 1 in \mathcal{T} (the *degree* of vertex 1 in \mathcal{T}). This is true because, to reverse the map f , we must choose one edge incident to 1 and “double” it to obtain a triangle incident to the edge $\{1, n+1\}$ (For example, in Figure 1.8 one has to double the edge $\{1, 4\}$). This implies that

$$t_{n+1} = \sum_{\mathcal{T} \in \Delta(\mathbf{C}_n)} \deg_{\mathcal{T}}(1).$$

By cyclic symmetry of the n -gon, this same formula must hold for any other vertex of it. Hence:

$$nt_{n+1} = \sum_{i=1}^n \sum_{\mathcal{T} \in \Delta(\mathbf{C}_n)} \deg_{\mathcal{T}}(i) = \sum_{\mathcal{T} \in \Delta(\mathbf{C}_n)} \sum_{i=1}^n \deg_{\mathcal{T}}(i).$$

But it turns out that the sum $\sum_{i=1}^n \deg_{\mathcal{T}}(i)$ is independent of \mathcal{T} ; it equals twice the number of edges of \mathcal{T} , that is, $2(2n - 3)$. Hence:

$$t_{n+1} = \frac{2(2n - 3)}{n} t_n, \quad \text{or} \quad t_n = \frac{2(2n - 5)}{n - 1} t_{n-1}.$$

From this we conclude that:

$$t_n = \frac{2^{n-2}(2n-5)(2n-7)\cdots 3 \cdot 1}{(n-1)(n-2)\cdots 3 \cdot 2} \quad (1.1)$$

$$= \frac{(2n-4)!}{(n-1)!(n-2)!} = \frac{1}{n-1} \binom{2n-4}{n-2}. \quad (1.2)$$

□

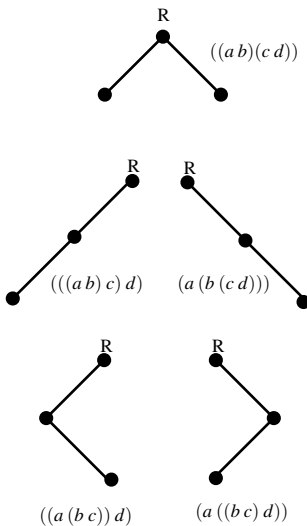


Figure 1.9: The five binary trees in 3 nodes, with their associated parenthesizations.

The sequence of numbers we have just found is known as the *Catalan numbers* (see Definition 1.1.4 below) and is one of the most important number sequences in combinatorics, perhaps comparable to the well-known Fibonacci sequence. We remark that asymptotically these numbers grow (up to a constant factor) like $4^n n^{-3/2}$. This may be seen by using Stirling’s approximation of the factorial. As an example of the ubiquity of the Catalan numbers, the following statement lists four other combinatorial structures whose cardinality is given by the Catalan sequence, and Exercise 6.19 in [307, p. 219] contains 61 additional such examples.

Theorem 1.1.3. *There are as many triangulations of a convex polygon with $n + 2$ vertices as:*

- (i) *Binary trees with n nodes (and hence $n - 1$ edges).*
- (ii) *Parenthesizations of the product of $n + 1$ factors, that is to say, ways of placing n pairs of parentheses in order to perform the product.*
- (iii) *Sequences of length $2n$ consisting of n plus signs and n minus signs, with the property that in every initial segment of the sequence there are at least as many pluses as minuses.*

- (iv) Monotone paths in the integer grid, going from $(0,0)$ to (n,n) by steps of length 1 in the positive directions of the axes, and never going above the diagonal.

One interesting feature of the equivalence to sign sequences is that it immediately shows that the number of triangulations of an n -gon is bounded above by 2^{2n-4} . Of course, that is also clear from Theorem 1.1.2, but its proof needed some work. Moreover, the equivalence explicitly tells us how to write a given triangulation as a binary number of length $2n - 4$.

Before proving Theorem 1.1.3, let us recall the definition of binary trees. A *tree* is a connected simple graph with no cycles [63]. We are interested in rooted trees, i.e., trees with a special distinguished node, called the *root*. In rooted trees, one can direct the edges naturally along the unique paths from each node to the root node. This establishes a hierarchy among the nodes: node v_1 becomes a *child of node v_2* if they are adjacent and the edge joining them is directed from v_2 to v_1 (v_2 is the *parent of v_1*). Rooted trees are normally drawn with the root on top and with parents above their children.

A *binary tree* is a rooted tree in which each edge is marked as a *right* or *left* edge of its parent and each node has at most one right child and at most one left child (in particular, each node has either 0, 1 or 2 children). In Figure 1.9 we show the five different binary trees on three nodes. As it is customary, a left child is drawn toward the left-down direction and a right child is drawn toward the right-down direction. Binary trees are very useful combinatorial structures due to applications in data structures and the design of algorithms (see for example [194]).

Proof of Theorem 1.1.3.

1. From triangulations to binary trees: Let us see how to build up a binary tree from a given triangulation of the $(n + 2)$ -gon. As usual, we assume the vertices of the polygon are labeled from 1 to $n + 2$. We call the edge $\{1, n + 2\}$ the *reference edge* of the polygon. We draw a node of the binary tree inside each of the n triangles of the triangulation, and join nodes of adjacent triangles by an edge. We declare the root of the tree to be the node of the unique triangle that contains the reference edge. The three sides of each triangle can be clearly identified as a “parent edge” (the one towards the root), a “right edge” (the next one in the clockwise direction) and a “left edge” (the third one). In particular, every node in the tree has a parent (unless it is the root node) and its children are labeled as right or left depending on whether the corresponding edge in the triangle is the right or the left one. See Figure 1.10.

To show that this construction is indeed a bijection, it suffices to show that it can be reversed: Starting with a binary tree, draw a triangle for the root and call its edges “parent”, “right” and “left” appropriately. Then glue triangles to its right and left edge for the right and left children of the root, if they exist. Recursively continue with grand children and all the other descendants (great-grand-children, etc.) and, after you have finished, number the vertices of the $(n + 2)$ -gon starting and ending with the end-points of the parent edge of the root triangle.

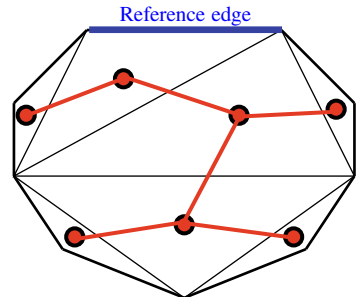
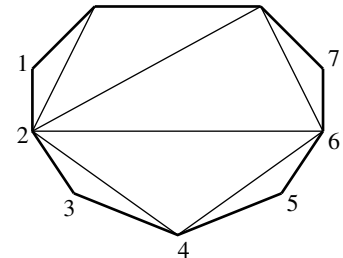
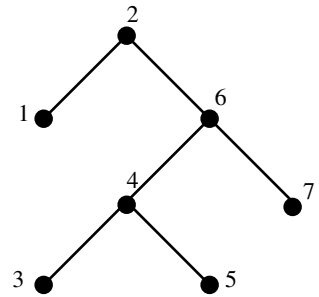


Figure 1.10: A binary tree dual of a triangulation.



+ - + + - + + - + + -
1 1 2 3 3 4 5 5 4 6 7 7 6 2

Figure 1.11: A binary tree with its symmetric order traversal, its associated triangulation, and its associated sequence of signs.

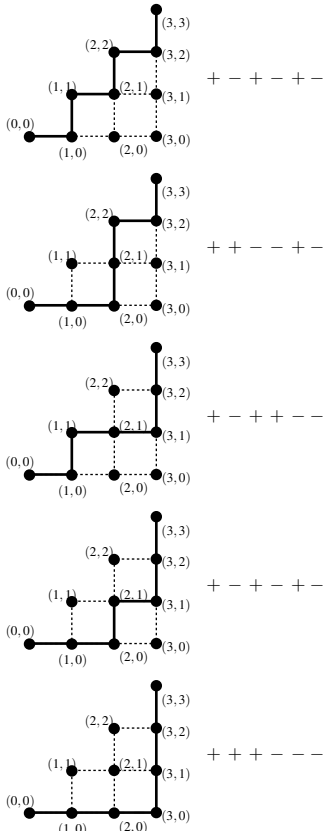


Figure 1.12: The five monotone paths/sign sequences of length six.

There is actually a nice correspondence between the n nodes in the binary tree and the n vertices of the $(n+2)$ -gon out of the reference edge, exhibited in Figure 1.11. It is given by the *symmetric order traversal* of the nodes of a binary tree: Start with the root node. If a node has at least one child, then process recursively first its left subtree, then insert the node itself into your order, then process recursively its right subtree, and finally return to its parent. We give numbers 1 to n to the n nodes as we visit them during the traversal. If a node has no children, then simply visit it by assigning to it the next available number from 1 to n , and return to its parent. We will use the symmetric order traversal a bit later.

2. From binary trees to parenthesizations: The bijection between binary trees with n nodes and parenthesizations of products of $n+1$ factors was displayed in Figure 1.9. We place a pair of parentheses for each node of the binary tree, starting with the root parentheses which enclose the whole product and inserting inner parentheses for children with the following rule: if the right/left child of a given parent node has k descendants, the corresponding parentheses will enclose the $k+1$ leftmost/rightmost factors within the ones enclosed by the parent parentheses. Alternatively, one can start drawing parentheses for the leaves of the tree (leaving place holders for the two variables they contain, which we cannot still identify) and add greater and greater parentheses for their parents, inserting right or left factors (place-holders) depending on the type of edge leading to the parent. We leave it to the reader to convince him or herself that this is indeed a bijection.

3. From binary trees to sign sequences: Clearly, there is going to be a plus and a minus sign corresponding to each node in the tree, and the plus sign will appear before the minus to guarantee that every initial segment has at least as many pluses as minuses. The way to construct the sequence is: Go along the tree in the symmetric order traversal presented above. When visiting a node, first process its left subtree, then place the plus sign for this node, then visit the right subtree, then place the minus sign. Figure 1.11 shows an example where, to make things clear, each plus or minus is labeled by its corresponding vertex of the tree.

In the exercises you will see how to construct the sequences of signs directly from the triangulation.

4. From sign sequences to monotone paths: Figure 1.12 shows the monotone paths under consideration and, at the same time, their bijection to sign sequences. Essentially, plus signs correspond to steps to the right and minus signs to steps upwards. The condition that the monotone paths do not cross the diagonal is exactly equivalent to saying that every initial segment has at least as many plus signs as minus signs.

□

Definition 1.1.4. The n -th Catalan number, where $n = 0, 1, 2, \dots$, is the number C_n defined by the following recurrence formula:

$$C_0 = 1, \quad C_n = \sum_{k=0}^{n-1} C_k C_{n-k-1}, \quad \forall n > 0. \quad (1.3)$$

Equivalently, it is the number of triangulations of the convex $(n+2)$ -gon,

which equals

$$C_n = \frac{1}{n+1} \binom{2n}{n}. \quad (1.4)$$

Theorem 1.1.3 can be read as saying that the five combinatorial structures described there are just different formulations of one and the same structure, that we can call the “Catalan structure”. Having the different formulations, besides its mathematical appeal, has practical consequences: properties which are obvious in one formulation may be invisible in others, and the many appearances of the structure provide additional insight and more tools to attack Catalan-type problems with.

As an example, our proof of Theorem 1.1.2 is heavily based on the cyclic symmetry of the convex n -gon, while none of the four other structures of Theorem 1.1.3 have a cyclic symmetry at all.

Once we know the cardinality of the set $\Delta(\mathbf{C}_n)$ of triangulations of the convex n -gon, let us see that it is “more than a set”, that there are natural relations between pairs of triangulations. Every internal edge in a triangulation is a diagonal of a convex quadrilateral formed by two adjacent triangles. One can change this diagonal to the opposite one and get a triangulation which is as similar as possible to the initial one. This operation is called a *diagonal flip* or simply a *flip* for short. Figure 1.13 shows a flip between two triangulations of a hexagon.

We can thus consider the set of triangulations of the n -gon as the vertices of a graph whose edges are diagonal flips. This graph is called the *graph of flips* of the triangulations of the n -gon. Some straightforward properties of the graph are:

1. It is regular of degree $n - 3$ (that is to say, every triangulation has exactly $n - 3$ flips). This is so because there is one flip associated to each internal diagonal.
2. It is connected. To prove this, let us pick any particular vertex, say the i -th one, and consider the unique triangulation in which all the triangles are incident to i . We call this the i -th *standard triangulation* of the n -gon. An example is in the right part of Figure 1.13. In any triangulation other than this one there is always at least one flip which increases the degree of vertex i : just flip the diagonal jk for any triangle ijk with j and k not consecutive vertices of the n -gon. This shows that every triangulation can be transformed into the standard one by a sequence of at most $n - 3$ flips.

Other not-so-easy properties of the graph of flips of the n -gon are that it is Hamiltonian [220] and that it is the graph of a convex and simple polytope of dimension $n - 3$ called the *associahedron* [205] (see also [339, Chapter 0]). The associahedron is a particular case of the *secondary polytope* or “polytope of triangulations and flips”, which exists for any finite point configuration in any dimension. Flips and secondary polytopes are introduced in Chapters 2 and 5, and are among the central topics in this book. See Figure 1.15 for a

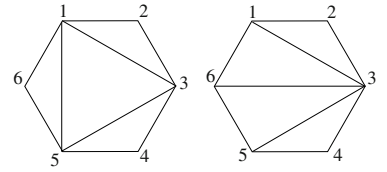


Figure 1.13: A diagonal flip in the quadrilateral 1356.

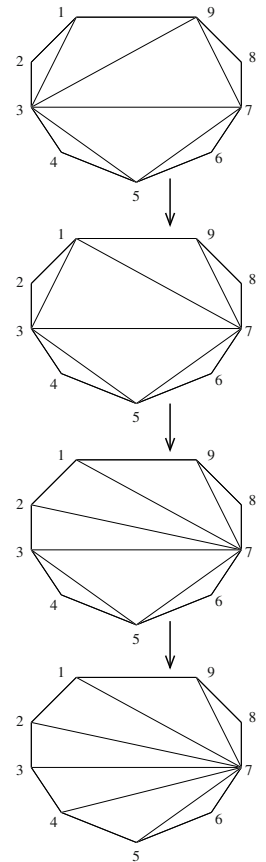


Figure 1.14: Flipping towards the 7th standard triangulation.

picture of the graph of flips on triangulations of a hexagon (well, we have forgotten to draw one edge; can you find it?). You should try to verify in the picture all the properties of the graph mentioned so far.

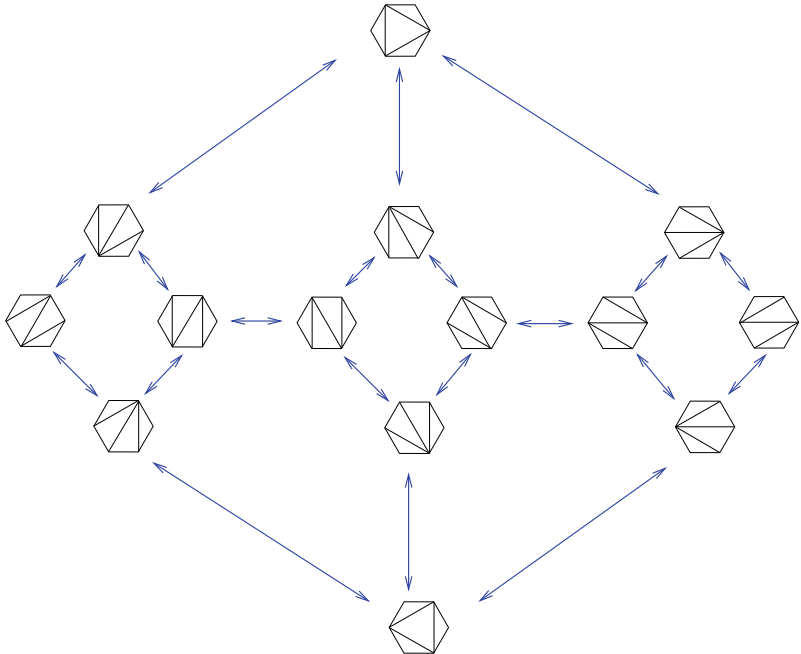


Figure 1.15: The graph of flips for a hexagon, with one edge missing.

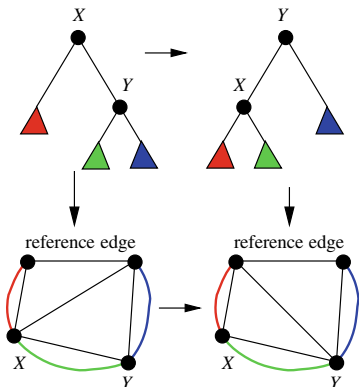


Figure 1.16: The diagonal flip corresponding to a rotation.

You may be wondering whether the graph of flips is meaningful in the other formulations of the Catalan structure that we have mentioned. The answer is yes and no. For example, the monotone path formulation possesses its own natural notion of flip (move the path along a single square of the grid), but these flips are certainly not equivalent to the flips in triangulations: In Figure 1.12 you can see paths with one, two, and three flips.

In the context of binary trees, however, diagonal flips can be described easily: They arise as the so-called “rotation of an edge”. If an edge connects a node X to its right child Y , let P, A, B , and C denote the parent subtree of X , left subtree of X , left subtree of Y , and right subtree of Y , respectively. The rotation changes this to the binary tree in which X is a left child of Y and P, A, B , and C are, respectively, the parent subtree of Y , left subtree of X , right subtree of X , and right subtree of Y . A rotation and its correspondence to a flip in triangulations are depicted in Figure 1.16. In the context of parenthesizations a flip is given by a single application of the associative law $A(BC) \mapsto (AB)C$.

But how many flips does it take to move from one triangulation to another? Remember that the distance between two nodes in a connected graph is the minimal number of edges needed to go from one node to the other, and that the diameter of the graph is the maximum distance between nodes.

It is interesting to say something about the diameter of the graph of flips:

Proposition 1.1.5. *Let $D(\mathbf{C}_n)$ be the diameter of the graph of flips between triangulations of the convex n -gon. Then:*

- (i) $D(\mathbf{C}_n) \leq 2n - 10 + 12/n$ for every n (in particular, it is bounded by $2n - 10$ for every $n \geq 12$).
- (ii) $D(\mathbf{C}_n) + 1 \leq D(\mathbf{C}_{n+1}) \leq D(\mathbf{C}_n) + 3$ for every n .

Proof. Part (i) can be proved by slightly refining the argument that proved connectedness. Let \mathcal{T} and \mathcal{T}' be two triangulations, and let d_j and d'_j denote the degrees of the vertex j in \mathcal{T} and \mathcal{T}' respectively, for each $j = 1, \dots, n$. What we have shown is that for every $i = 1, \dots, n$ there is a path from \mathcal{T} to \mathcal{T}' consisting of $2n - 2 - d_i - d'_i$ flips: just start flipping from \mathcal{T} and \mathcal{T}' in a way that always increases the degree of the i -th vertex. Now we wonder what is the minimum length of these n paths we constructed. This is a difficult question so we look instead at the *average* length, which is:

$$\frac{1}{n} \sum_{i=1}^n (2n - 2 - d_i - d'_i) = 2n - 2 - \frac{1}{n} \left(\sum_{i=1}^n d_i + \sum_{i=1}^n d'_i \right) \quad (1.5)$$

$$= 2n - 2 - \frac{8n - 12}{n} \quad (1.6)$$

$$= 2n - 10 + \frac{12}{n}. \quad (1.7)$$

In Equation (1.6) we have used that $\sum d_i$ equals twice the number $2n - 3$ of edges, a property already used in the proof of Theorem 1.1.2.

Part (ii) is left as an exercise. For the left inequality, use the contraction map of Theorem 1.1.2. For the other one, use the arguments of Part (i), but flip through an “anti-standard” triangulation, that is to say, a triangulation with no internal edge at the given vertex i . \square

Part (ii) says that the bound in Part (i) is not too bad, but the following statement says more; it gives the exact diameter for almost all values of n :

Theorem 1.1.6 (Sleator, Tarjan, Thurston). *The diameter of the graph of flips of an n -gon is $2n - 10$ for all sufficiently large values of n .*

No purely combinatorial proof of the lower bound implicit in this theorem is known. The proof contained in [300] is far from elementary and we will avoid all the details, but we will sketch the main idea. We wish to give a lower estimate on how many flips are necessary to move from one triangulation \mathcal{T} to another \mathcal{T}' . For this, we associate to every sequence of flips going from \mathcal{T} to \mathcal{T}' an abstract simplicial complex in the following fashion:

Start with one of the triangulations, \mathcal{T} , and consider it as an abstract 2-dimensional simplicial complex. Then attach to this complex one tetrahedron for each flip in the sequence, in the same order. More precisely, if a flip exchanges the diagonals pq and rs , add the tetrahedron $pqrs$ to the

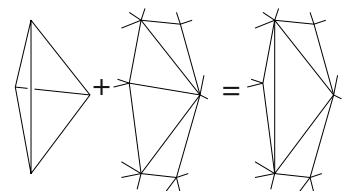


Figure 1.17: A diagonal flip viewed as glueing a tetrahedron to a surface.

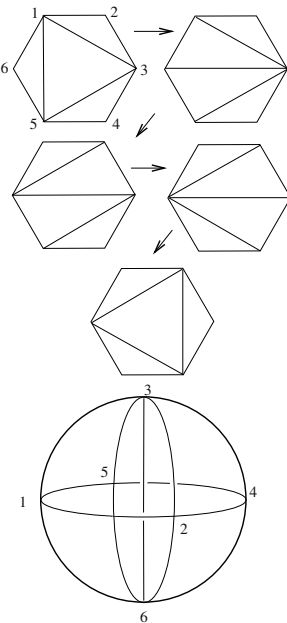


Figure 1.18: Four flips in a hexagon and the corresponding triangulated 3-ball.

already constructed simplicial complex. This tetrahedron has two triangles in common to the complex we had before the flip, and it creates two new boundary triangles (see Figure 1.17). This interpretation of flips is also very popular in the context of Delaunay triangulations [129], as we will see in Theorem 3.4.2 of Chapter 3.

After we do this for all the flips in the sequence we get a simplicial complex that is topologically a 3-dimensional ball \mathcal{B} and whose boundary, a 2-dimensional sphere, is made by glueing \mathcal{T} and \mathcal{T}' along their boundaries. (This is unless \mathcal{T} and \mathcal{T}' have interior edges in common; one step in the proof is to show that there is no loss of generality in assuming this.) Figure 1.18 shows an example where four flips in a hexagon give a triangulated ball with the four tetrahedra $\{1, 3, 5, 6\}$, $\{1, 2, 3, 6\}$, $\{3, 4, 5, 6\}$, $\{2, 3, 4, 6\}$. With this we get the following interesting result:

Lemma 1.1.7. *If the triangulated 2-sphere obtained by glueing \mathcal{T} to \mathcal{T}' along their boundaries cannot be extended to a triangulation of the 3-ball with less than k tetrahedra, then every sequence of flips going from \mathcal{T} to \mathcal{T}' has length at least k .*

In other words, the problem of finding paths in the flip-graph of a polygon is related to the problem of finding combinatorial simplicial 3-polytopes that do not admit small triangulations. This gives an easy way to remember where the number $2n - 10$ comes from: It follows easily from Euler's formula that a triangulated 2-sphere with n vertices has exactly $2n - 4$ triangles and, if $n \geq 13$, a vertex of degree at least six. Using this we can easily triangulate the 3-ball into at most $2n - 10$ tetrahedra: just cone the highest degree vertex to all the triangles not incident to it.

But to obtain *lower bounds* for the flip distance we need to find 3-polytopes without small triangulations and, what is more difficult, prove that they do not have small triangulations. How can one do that? The key idea in [300] is to use hyperbolic polytopes. A useful fact about hyperbolic 3-space is that the volume of all hyperbolic tetrahedra is bounded by a certain constant σ , so that a hyperbolic 3-polytope of volume V clearly needs at least V/σ many tetrahedra to be triangulated. What the paper [300] proves is that for sufficiently big n , there are n -vertex hyperbolic 3-polyhedra with volume $(2n - 10)\sigma$. We must remark, however, that this paper does not say how big n needs to be for the lower bound to be exact. The conjecture is that $n = 13$ is enough, and a related conjecture is the following:

Conjecture 1.1.8. *For every $n \geq 13$ there is a simplicial 3-polytope with n vertices whose interior cannot (even combinatorially) be triangulated with less than $2n - 10$ tetrahedra.*

Let us also mention that the same idea of using hyperbolic volumes, now in arbitrary dimension, was used by W. Smith to give the best lower bound known for the size of the smallest triangulations of combinatorial n -dimensional cubes [301].

Triangulating and computing volumes are intimately related activities. Since the volume formula of a simplex in Euclidean space is just a determinant, an easy way to compute the Euclidean volume of a polytope is to

add the volumes of simplices of any triangulation of it. Of course, for this to be a general algorithm we need the fact that every convex polytope can be triangulated (if you do not see why, read Proposition 2.2.4 in the next chapter.)

Volume computations are useful throughout mathematics. For example, the calculation of volumes of hyperbolic convex polytopes has become of interest in topology. The reason is that every hyperbolic manifold can be obtained by identifying the faces of a convex polytope in hyperbolic space, and its volume is a topological invariant. The volume has been used in the classification of hyperbolic manifolds (see [269] for references). (It should be said, however, that the calculation of the volume of a simplex in hyperbolic space is much more complicated than in Euclidean space.)

The computation of volumes of polytopes in Euclidean space is also used in algebra [46, 140, 312]. But more important for us are the fascinating connections to combinatorics [306]. Here we show how the computation of volume is equivalent to counting linear extensions of posets, and that the linear extensions are simplices of a triangulation! This was first observed by R. Stanley in [305]:

Definition 1.1.9. We define:

- (i) A partially ordered set (or *poset*) is a finite set P with an ordering $<$ that is reflexive, antisymmetric, and transitive.
- (ii) A *linear extension* of a poset on n vertices is a bijection λ from the set of vertices of P to $\{1, \dots, n\}$ such that $\lambda(a) < \lambda(b)$ whenever $a < b$ in P .
- (iii) An *order ideal* of a poset is a subset of the poset P such that if $a \in I$ and $b < a$, then $b \in I$.

Usually, a poset is represented by a graph, its *Hasse diagram*. We recommend Chapter 3 of [308] for a thorough discussion of posets. Here we simply show in Figure 1.19 the Hasse diagram for the poset of subsets of the set $\{1, 2, 3\}$ ordered by containment, as well as two of its order ideals (black dots) and two linear orderings, only one of them extending the partial ordering. Given a poset P with elements a_1, \dots, a_n , one can define the *order polytope* $\mathbf{O}(P)$ in \mathbb{R}^n (see [305]) by the following linear constraints:

$$\mathbf{O}(P) = \{(x_1, \dots, x_n) \in \mathbb{R}^n : 0 \leq x_i \leq 1, \text{ and } x_i \geq x_j \text{ if } a_i > a_j \text{ in } P\}.$$

Theorem 1.1.10. The following properties hold for the order polytope $\mathbf{O}(P)$ of a poset P :

- (i) The vertices of the order polytope $\mathbf{O}(P)$ are vectors with 0–1 entries. They are in bijection with the order ideals of the poset P .
- (ii) The number of distinct linear extensions of the poset P equals the number of simplices in a maximal size triangulation of the order polytope $\mathbf{O}(P)$.

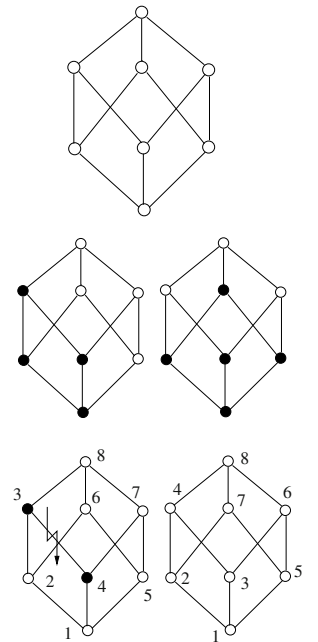


Figure 1.19: A poset P with two order ideals and two bijections $P \rightarrow \{1, \dots, 8\}$. Only one of them is a linear extension.

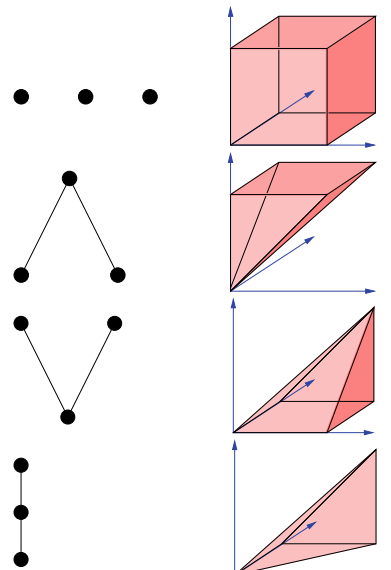


Figure 1.20: Some posets with three elements and their order polytopes.

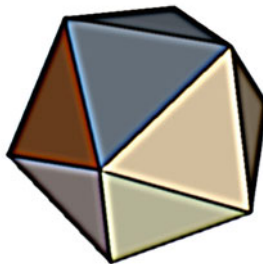


Figure 1.21: The volume of this icosahedron ...

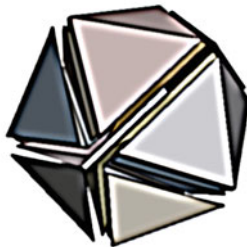


Figure 1.22: ... can be computed by triangulating it ...



Figure 1.23: ... and adding up the volumes of the simplices.

Remark 1.1.11. For a poset with n elements, $\mathbf{O}(P)$ is always contained in the n -cube. If P has no relations at all, then $\mathbf{O}(P)$ is the whole n -cube. In particular, the previous theorem yields a triangulation of the n -cube. See Figure 1.20 for some order polytopes of posets with three elements. One more is asked for in Exercise 1.12.

Proof. We prove first that the coordinates of the vertices of $\mathbf{O}(P)$ are 0 or 1: Let $\mathbf{x} = (x_1, \dots, x_n) \in \mathbf{O}(P)$ have some entry not zero or one. Let $\alpha \in \{x_j : 0 < x_j < 1\}$. Then, increasing by a sufficiently small ε all coordinates of \mathbf{x} equal to α we get a new point $\mathbf{x}^+ \in \mathbf{O}(P)$, and by decreasing the same coordinates by the same amount we get another one $\mathbf{x}^- \in \mathbf{O}(P)$, with the property that \mathbf{x} is in the interior of the segment $\mathbf{x}^- \mathbf{x}^+$. Hence, \mathbf{x} is not a vertex.

The correspondence of vertices and order ideals is the following:

$$\mathbf{p} = (p_1, \dots, p_n) \in \text{vert}(\mathbf{O}(P)) \rightarrow S_{\mathbf{p}} = \{a_j : p_j = 0\}.$$

We should verify that $S_{\mathbf{p}}$ is an ideal: Suppose $a_k < a_j$ in the poset and $a_j \in S_{\mathbf{p}}$, then clearly by definition of $\mathbf{O}(P)$ we have $0 \leq p_k \leq p_j = 0$, which says $p_k = 0$ too, thus $a_k \in S_{\mathbf{p}}$, the order ideal associated to vertex \mathbf{p} . Different vertices have different support so they give different order ideals. Now given an order ideal S , we construct a 0/1 vector by following the convention $p_j = 1$ if and only if $a_j \notin S$. The inequalities are satisfied inside $\mathbf{O}(P)$, thus the resulting vector lies inside $\mathbf{O}(P)$ and it must be a vertex.

Any of the $n!$ total orderings $a_{\lambda(1)} < a_{\lambda(2)} < \dots < a_{\lambda(n)}$ defines a simplex $\{\mathbf{x} \in [0, 1]^n : x_{\lambda(1)} < x_{\lambda(2)} < \dots < x_{\lambda(n)}\}$ inside the unit n -cube. Call such simplices *total order simplices*. The cube is partitioned into $n!$ total order simplices. Why? No two intersect in the interior, and the union of all of those equals the cube. It is important to notice that all these simplices have the same volume $1/n!$. Now, given a poset P , all its linear extensions correspond to simplices that form a triangulation of $\mathbf{O}(P)$. This is because $\mathbf{O}(P)$ contains one such simplex if and only if the ordering where it came from is a linear extension, and all of $\mathbf{O}(P)$ is covered: by construction, if you pick any point \mathbf{x} of $\mathbf{O}(P)$ and choose any total ordering of its entries, this defines a total order simplex that contains \mathbf{x} . The number of simplices in the triangulation equals the number of linear extensions for the poset P . Because the simplices of a cube cannot have smaller volume, we have a maximal triangulation of $\mathbf{O}(P)$. \square

Brightwell and Winkler [66] proved that enumerating the linear extensions of a finite poset is a #P-complete problem. Therefore, from the previous theorem we get the following:

Corollary 1.1.12. *It is #P-hard to compute the volume of a d -dimensional polytope P represented by its facets.*

This means that, computationally, the problem is at least as hard as a number of other computational problems that are already known to be “extremely hard” in a well-defined way. The class of #P-hard problems

includes counting problems such as “How many Hamiltonian cycles are there in a finite graph?”, “How many matchings are there in a bipartite graph?”, “How many different 3-colorings are possible of a planar graph?”, and many more (see [134]). More precisely, if it were the case that computing the volume admits a fast solution, all the other members of the same family of problems would have a fast solution too. This indicates that it is more than likely that we will never find a fast algorithm.

The enumeration of vertices in face-presented polytopes is also a hard problem [261], as well as computing the volume of a vertex-presented polytope [109, 186]. We even know that it is hard to compute the volume of *zonotopes* [111] (Zonotopes are centrally symmetric polytopes that arise as projections of cubes or, equivalently, as Minkowski sums of line segments [339, Chapter 7]). We refer the reader to the paper [70] for a survey and evaluation of practical methods to compute the volume of a convex polyhedron.

How about the problem of approximating the volume? It is possible to have fast randomized approximation [110] although for general convex sets the situation is much worse: It was proved by Elekes (see [120]) that the volume of the convex hull of any m points in an n -dimensional ball with volume V is at most $Vm/2^n$. This implies that no polynomial-time algorithm can compute the volume of convex sets (specified by a membership oracle) with less than exponential relative error.

1.2 Optimization and triangulations

Triangulations of polyhedra and point configurations appear in the context of optimization problems and we wish to present two examples here. First, in connection to linear optimization and then in the computation of equilibrium points.

Linear programming (also called linear optimization) is the process of minimizing a linear objective function subject to a finite number of linear equality and inequality constraints. Not only linear programs have many real world applications, but the theory of linear programming has been used in solutions of problems in combinatorics and theoretical computer science (e.g., efficient algorithms for maximum flows on networks, matchings of graphs, etc). An important class of linear programming problems are *parametric linear programs*. These problems have parameters instead of fixed input entries. They often arise from the recognition that data has uncertainty or from the wish to analyze the effects of deviations from the initial values. We wish to outline the beautiful relationship between triangulations and parametric linear optimization problems.

Let us begin with a review a few facts about linear optimization now in terms of point configurations. We hope this will suffice for readers unfamiliar with linear programming, but a complete introduction to the subject is available in the wonderful books [226, 291].

It is commonly assumed that a linear program is given in the form presented in Figure 1.24, where \mathbf{A} is $d \times n$ integral of rank d and \mathbf{b} is an integral d -vector. For us the columns of the matrix A will be the points of a

$$\begin{aligned} & \min \mathbf{c} \cdot \mathbf{x} \\ & \text{subject to} \\ & \mathbf{Ax} = \mathbf{b} \\ & \mathbf{x} \geq 0 \end{aligned}$$

Figure 1.24: A linear program with $\mathbf{A} \in \mathbb{R}^{d \times n}$,

$\mathbf{b} \in \mathbb{R}^n$, and $\mathbf{c} \in \mathbb{R}^d$.

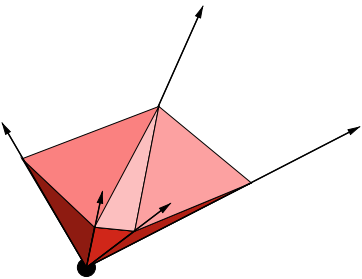


Figure 1.25: A triangulation of a pointed cone, cut off by an affine hyperplane; this section of the cone looks like a triangulation of a point configuration.

configuration. Denote by $\text{cone}(\mathbf{A})$ the *cone* generated by the nonnegative linear combinations of the columns of the matrix \mathbf{A} . For each subset $B \subset [n]$ of columns let \mathbf{A}_B denote the sub-matrix formed by those columns. A *cone subdivision* of $\text{cone}(\mathbf{A})$ is a finite collection \mathcal{S} of subcones $\text{cone}(\mathbf{A}_B)$, such that the intersection of any pair of subcones in \mathcal{S} is a face of both and the union of all the subcones is $\text{cone}(\mathbf{A})$. By a *cone triangulation* we mean a cone subdivision all of whose cones are simplicial cones, that is, all the submatrices are square matrices. Note that this definition is essentially our original definition of triangulation but uses vectors (the columns of \mathbf{A}) instead of points.

Fix a matrix \mathbf{A} as above, and for each cost vector $\mathbf{c} \in \mathbb{R}^n$ and right-hand-side vector $\mathbf{b} \in \text{cone}(\mathbf{A}) \subset \mathbb{R}^d$, consider the linear programming problem (for short LP) $\text{LP}_{\mathbf{A}, \mathbf{c}}(\mathbf{b}) := \min \{ \mathbf{c} \cdot \mathbf{x} : \mathbf{Ax} = \mathbf{b}, \mathbf{x} \geq 0 \}$. Here, $\mathbf{x} \geq 0$ means that all the entries of \mathbf{x} are non-negative.

By definition of a cone(\mathbf{A}), $\text{LP}_{\mathbf{A}, \mathbf{c}}(\mathbf{b})$ has a solution x if and only if the right-hand side \mathbf{b} lies in $\text{cone}(\mathbf{A})$. In the terminology of linear programming we say the LP is *feasible*. When a subcone $\text{cone}(\mathbf{A}_B)$ corresponds to a full-rank matrix (i.e., d linearly independent columns) we say \mathbf{A}_B is a *basis*. The reader must note that for a basis cone(\mathbf{A}_B) is a *simplicial cone*. From a basis with indices $B = \{j_1, j_2, \dots, j_d\}$ and $j_1 < j_2 < \dots < j_d$ we can immediately construct a tentative feasible solution of the LP. Set to zero any variable x_l where $l \notin B$ and for x_{j_k} with $j_k \in B$ set the variable x_{j_k} to the value of the k -th component of $(\mathbf{A}_B)^{-1}\mathbf{b}$. This is just a tentative solution because some of the x_{j_k} 's may be negative, but if all of them are non-negative then the vector x is a *basic feasible solution* of our LP. Note that there are only finitely many basic feasible solutions possible because each of them is determined by d -subset of the columns of \mathbf{A} , the number of basic feasible solutions is at most $\binom{n}{d}$.

It is well-known (see e.g., Theorem 4.2.3 in [226]) that if there is at least one feasible solution and the objective function $\mathbf{c} \cdot \mathbf{x}$ is bounded (a reasonable assumption!), an optimal solution exists and in fact there is a basic feasible solution to the LP which is optimal. Thus, an optimum of $\text{LP}_{\mathbf{A}, \mathbf{c}}(\mathbf{b})$ is achieved at a vector \mathbf{x} where at least $n - d$ coordinates are zero. If \mathbf{b} and \mathbf{c} are sufficiently generic, then *exactly* $n - d$ coordinates are zero. We can then consider \mathbf{b} as selecting the maximal rank square $d \times d$ submatrix of \mathbf{A} , the *basis*, within the set of columns corresponding to non-zero entries. Please note that when we select a basic feasible solution for the right-hand-side vector \mathbf{b} we also select a simplex of our triangulation.

From what we just discussed linear programming is a finite problem! We just need to scan all of the (exponentially many) basic feasible solutions in order to find an optimal point. We will not discuss it here but the famous *simplex algorithm* is nothing more than a clever way to scan them, but not all of them. The algorithm starts from an arbitrary basic feasible solution and ideally finds a sequence of cheaper and cheaper alternatives. If no alternative cheaper basic feasible solution can be found then it is because we are at an optimal solution already. Of course this is very simplistic and we recommend the reader to learn this beautiful algorithm (claimed to be

one of the top ten algorithms of the 20th century [82]). It is also worth learning about the ellipsoid method and the interior-point algorithms used today to solve linear programs see [291]

To conclude our minimalistic review of linear programming we will state a basic fundamental fact from the theory of linear programming which truly sets up the connection between linear programs and triangulations and will be used in our forthcoming proof of the main result (Theorem 1.2.2). See e.g., [291, Section 7.9] for a proof.

Lemma 1.2.1 (Complementary slackness). *Let \mathbf{A} be a matrix, \mathbf{b} and \mathbf{c} the right-hand-side and cost vectors of $\text{LP}_{\mathbf{A}, \mathbf{c}}(\mathbf{b}) = \min \{ \mathbf{c}\mathbf{x} : \mathbf{Ax} = \mathbf{b}, \mathbf{x} \geq 0 \}$. There is an associated dual problem, and the following duality equation holds:*

$$\max \{ \mathbf{y}\mathbf{b} : \mathbf{y}\mathbf{A} \leq \mathbf{c} \} = \min \{ \mathbf{c}\mathbf{x} : \mathbf{Ax} = \mathbf{b}, \mathbf{x} \geq 0 \}. \quad (1.8)$$

If both optima are finite and \mathbf{x}^* and \mathbf{y}^* are feasible solutions, then the following conditions are equivalent:

- (i) \mathbf{x}^* and \mathbf{y}^* are optimum solutions of their problems.
- (ii) If a component of \mathbf{x}^* is positive, the corresponding inequality in $\mathbf{y}\mathbf{A} \leq \mathbf{c}$ is satisfied by \mathbf{y}^* with equality, i.e., $\mathbf{x}^*(\mathbf{c} - \mathbf{y}^*\mathbf{A}) = 0$.

In other words, the minimum value of $\text{LP}_{\mathbf{A}, \mathbf{c}}(\mathbf{b})$ is attained at a vector \mathbf{x}^* if and only if there exists a \mathbf{y} such that $\mathbf{y}\mathbf{A}_j \leq \mathbf{c}_j$ for all $j = 1, \dots, n$ and for all indices either $\mathbf{x}_j^* = 0$ or $\mathbf{y}\mathbf{A}_j = \mathbf{c}_j$.

Using the principle of complementary slackness, one can solve a linear program by considering the primal (original) problem and its dual problem together and seeking a pair of vectors w, u , the first primal feasible solution and the second a dual feasible solution. If they satisfy the complementary slackness then they must be a pair of primal dual optima. Note that in this way no explicit mention of the objective function is made.

Our focus will be now the study of the *parametric family of linear programs*

$$\text{LP}_{\mathbf{A}, \mathbf{c}} = \{ \text{LP}_{\mathbf{A}, \mathbf{c}}(\mathbf{b}) : \mathbf{b} \in \text{cone}(\mathbf{A}) \},$$

for fixed \mathbf{c} and varying \mathbf{b} . The main idea is that $\text{cone}(\mathbf{A})$ will be triangulated by each choice of cost vector \mathbf{c} . Let us see how this works.

For simplicity, we will usually assume that $\ker(\mathbf{A}) \cap \mathbb{R}_+^n = \{0\}$, where $\ker(\mathbf{A}) = \{\mathbf{x} \in \mathbb{R}^n : \mathbf{Ax} = 0\}$ and $\mathbb{R}_+^n = \{\mathbf{x} \in \mathbb{R}^n : \mathbf{x} \geq 0\}$. This assumption on \mathbf{A} makes $\text{LP}_{\mathbf{A}, \mathbf{c}}$ a family of bounded linear programs (so the minimum exists in all cases, no matter what \mathbf{c} and \mathbf{b}).

What happens to the linear program as \mathbf{b} moves within the cone? What are the optimal bases for each \mathbf{b} ? The main intuition is that $\text{cone}(\mathbf{A})$ will be divided into regions consisting of “equivalent” linear programs. And it turns out that the subdivision is a cone subdivision and, if \mathbf{c} is generic, a triangulation. This was first observed by Walkup and Wets [330]. The geometric theory of parametric linear programs has recently been extended to parametric integer programs (see [315]).

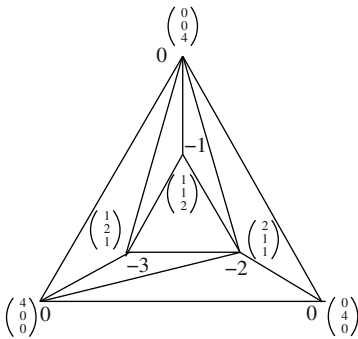


Figure 1.26: The cone triangulation associated with the cost vector \mathbf{c} . This shows a two-dimensional slice of the cone.

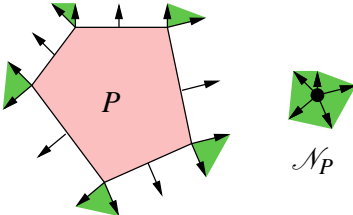


Figure 1.27: The normal fan of a polygon.

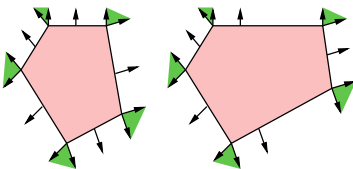


Figure 1.28: Normally equivalent polygons.

Theorem 1.2.2 (Walkup-Wets). *Let $\text{LP}_{\mathbf{A}, \mathbf{c}}(\mathbf{b})$ denote the linear program*

$$\min\{\mathbf{c}\mathbf{x} : \mathbf{Ax} = \mathbf{b}, \mathbf{x} \geq 0\},$$

for each \mathbf{c} and \mathbf{A} . $\text{LP}_{\mathbf{A}, \mathbf{c}}(\mathbf{b})$ is bounded, then for each generic cost vector \mathbf{c} there exists a triangulation $\mathcal{T}(\mathbf{c})$ of $\text{cone}(\mathbf{A})$ such that, for each $\mathbf{b} \in \text{cone}(\mathbf{A})$, the extreme rays of any d -dimensional cone of $\mathcal{T}(\mathbf{c})$ containing \mathbf{b} are an optimal basis for $\text{LP}_{\mathbf{A}, \mathbf{c}}(\mathbf{b})$.

Here is an example. Consider the parametric linear programming problems $\text{LP}_{\mathbf{A}, \mathbf{c}}(\mathbf{b})$ with

$$\mathbf{c} = (0, 0, 0, -2, -3, -1), \quad (\text{cost})$$

$$\mathbf{A} = \begin{bmatrix} 4 & 0 & 0 & 2 & 1 & 1 \\ 0 & 4 & 0 & 1 & 2 & 1 \\ 0 & 0 & 4 & 1 & 1 & 2 \end{bmatrix}, \quad (\text{coefficients})$$

$$\mathbf{b} = (b_1, b_2, b_3). \quad (\text{right-hand side})$$

According to Theorem 1.2.2 we can find a triangulation $\mathcal{T}(\mathbf{c})$ of $\text{cone}(\mathbf{A})$ associated with \mathbf{c} , and the simplicial cones in $\mathcal{T}(\mathbf{c})$ are useful for finding optimal solutions. We can visualize the triangulation of $\text{cone}(\mathbf{A})$ for the above example by taking a 2-dimensional slice of the 3-dimensional cone(\mathbf{A}). The triangulation for the cost vector $\mathbf{c} = (0, 0, 0, -2, -3, -1)$ is shown in Figure 1.26.

Proof of Theorem 1.2.2. To simplify the exposition let us assume that the cost vector \mathbf{c} is generic. More precisely, we assume that there is no set of more than d columns of \mathbf{A} with the property that the subsystem of $\mathbf{yA} = \mathbf{c}$ indexed by those columns is feasible.

Let \mathbf{A}_i denote the i th column of \mathbf{A} . Moreover, let $\{\mathbf{A}_{i_1}, \dots, \mathbf{A}_{i_d}\}$ be a set of columns such that there exist a vector \mathbf{y} with $\mathbf{yA}_{i_k} = \mathbf{c}_{i_k}$ for all $i_k \in \{i_1, \dots, i_d\}$. Then the cones $\text{cone}(\{\mathbf{A}_{i_1}, \dots, \mathbf{A}_{i_d}\})$ are all cone-simplices, and they form a triangulation of $\text{cone}(\mathbf{A})$ that we denote by $\mathcal{T}_{\mathbf{c}}$.

Now, take any d -dimensional simplicial cone $\text{cone}(\{\mathbf{A}_{i_1}, \dots, \mathbf{A}_{i_d}\})$. By the complementary slackness theorem (Lemma 1.2.1), the columns of \mathbf{A} which are extreme rays of the cone are indeed a basis that supports an optimal solution. \square

We emphasize that not all cone triangulations of $\text{cone}(\mathbf{A})$ come from the use of some cost vector. The ones that actually do are called *regular*. Regularity of triangulations is probably the most important concept in this book and will be discussed in full detail in the following chapters.

Let us look at another subdivision of $\text{cone}(\mathbf{A})$ related to the family of linear programs. For each \mathbf{b} , we have a polytope $\mathbf{P}_\mathbf{b} := \{\mathbf{x} : \mathbf{Ax} = \mathbf{b}, \mathbf{x} \geq 0\}$. We say that $\mathbf{P}_\mathbf{b}$ and $\mathbf{P}_\mathbf{b}'$ are *normally equivalent* if their *normal fans* coincide. The normal fan of a polytope $\mathbf{P} \subset \mathbb{R}^d$ is the decomposition of \mathbb{R}^d (now regarded as the space of linear functionals on \mathbf{P}) into functionals that are maximized at the same face of \mathbf{P} . Being normally equivalent means,

in particular, that the polytopes look combinatorially the same (same face lattice) and, more strongly, that corresponding facets are parallel [339].

Now, the notion of normally equivalent polyhedra creates an equivalence relation on the right-hand-side vectors \mathbf{b} . We can say that right-hand-side vectors \mathbf{b}, \mathbf{b}' inside $\text{cone}(\mathbf{A})$ are equivalent if $\mathbf{P}_\mathbf{b}$ and $\mathbf{P}_{\mathbf{b}'}$ are normally equivalent. This provides us now with yet another partition of $\text{cone}(\mathbf{A})$ into polyhedral cones. This partition is *not* a cone subdivision in the sense defined above. Among other things, some new vertices are introduced.

We call the cells in this partition *chambers*. They are the maximal cells in the common polyhedral refinement of *all* triangulations of $\text{cone}(\mathbf{A})$. In other words, a chamber γ is the intersection of a finite collection Γ_γ of simplicial subcones with the following properties: (a) each $B \in \Gamma_\gamma$ is generated by $\text{rank}(\mathbf{A})$ many linearly independent columns of \mathbf{A} , (b) the intersection $\cap_{B \in \Gamma_\gamma} B$ has non-empty interior, and (c) Γ_γ is maximal with respect to property (b).

Figure 1.29 shows the polyhedral complex that we obtain by “overlapping” of all cost-vector-induced triangulations. We show the regular triangulations for our running example in the upper part of Figure 1.30. The lower part of Fig. 1.30 shows all triangulations.

First, we allowed the right-hand-side vector \mathbf{b} to move with \mathbf{c} fixed and discovered a triangulation of $\text{cone}(\mathbf{A})$; then, we let \mathbf{c} change as well to discover that the points \mathbf{b} that produce the same optimal solution for every \mathbf{c} are contained in a chamber of $\text{cone}(\mathbf{A})$ and that chambers are indeed what results from overlapping all triangulations of $\text{cone}(\mathbf{A})$. Now there is a final surprise: the different triangulations of $\text{cone}(\mathbf{A})$ that appear when we let the cost vector \mathbf{c} vary are “connected” to one another in a rather nice way. They form a graph with the structure of a polytope: the secondary polytope that we have already seen a couple of times in this chapter. We show in Figure 1.30 the vertices and edges of the secondary polytope of the point configuration in Figure 1.26.

Take two generic cost vectors \mathbf{c} and \mathbf{c}' . Then $\text{LP}_{\mathbf{A}, \mathbf{c}}(\mathbf{b})$ and $\text{LP}_{\mathbf{A}, \mathbf{c}'}(\mathbf{b})$ have the same set of optimal solutions for every value of \mathbf{b} if and only if \mathbf{c} and \mathbf{c}' define the same cone triangulation. Define an equivalence relation among the cost vectors (vectors in \mathbb{R}^n): We say \mathbf{c} is equivalent to \mathbf{c}' if they define the same triangulation. This equivalence relation decomposes \mathbb{R}^n into finitely many equivalence classes, each of them is a convex polyhedral cone. The collections of all such cones covers \mathbb{R}^n and receives the name of the *secondary fan*. Gelfand, Kapranov, and Zelevinsky demonstrated that this fan is actually the normal fan of the *secondary polytope* of \mathbf{A} via cost variations.

The connection of triangulations of point configurations with linear optimization problems does not end here. One can consider a similar study of parametric integer programming problems. There are several methods to attack such problems [291], but a new algebraic approach, presented in [84] and extended in [320], provides a nice connection of the theory of Gröbner bases of toric ideals to our setting (we will see more on this in Chapter 9).

Let us now turn our attention to fixed points of continuous maps, which is another topic in optimization where triangulations play an important role. In

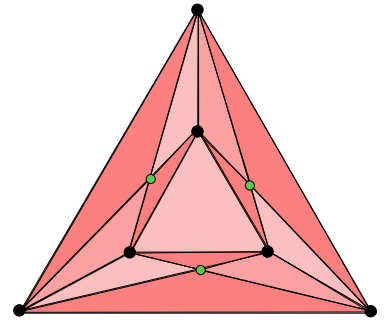


Figure 1.29: The chamber complex of $\text{cone}(\mathbf{A})$ for the example. As before, for the ease of drawing, we show a 2-dimensional slice.

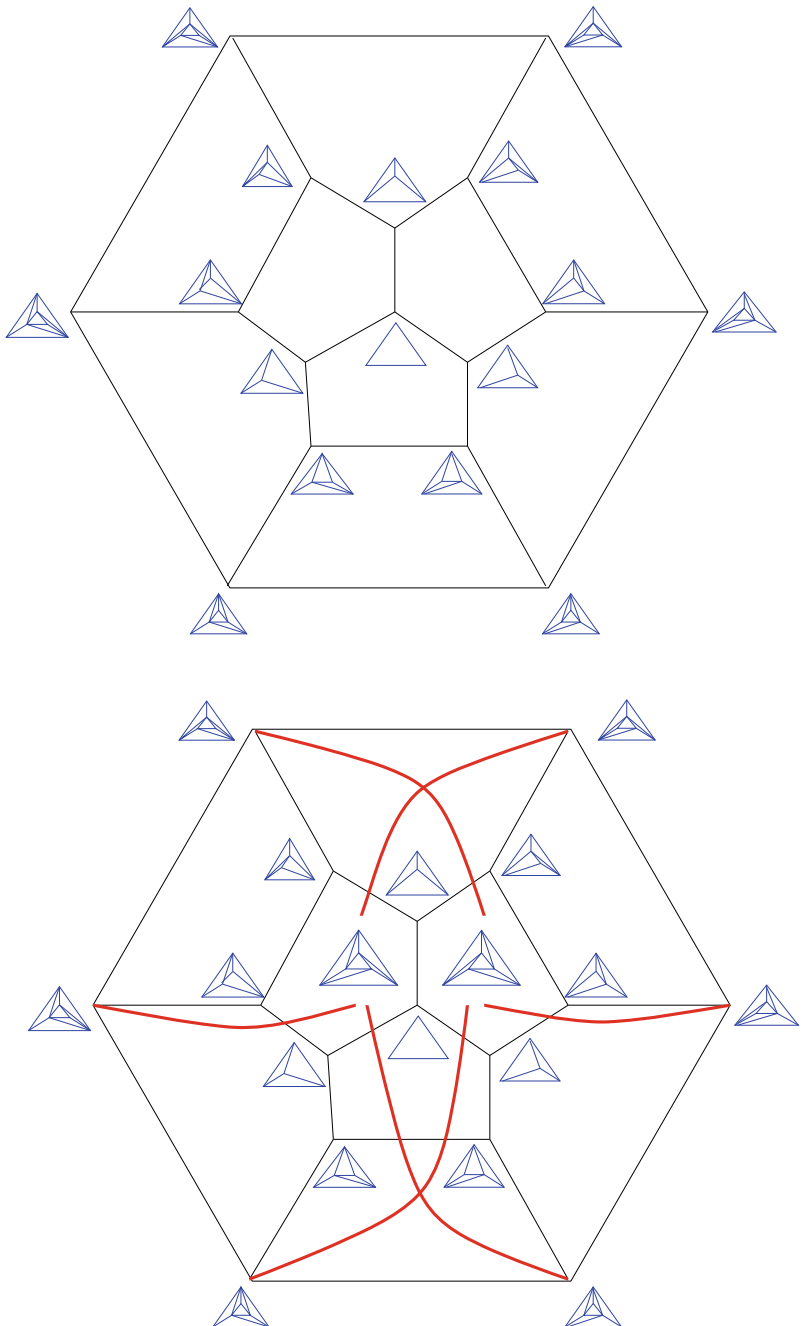


Figure 1.30: The flip graph of all regular triangulations (top) and all triangulations (bottom) of the point configuration in Figure 1.26.

game theory and economics the notion of equilibrium is very important [289]. Mathematically, an equilibrium is a fixed point of a continuous mapping. Finding a fixed point is then an issue of practical importance. A wide variety

of algorithms have been proposed and there is an extensive literature in the mathematical programming community. One of the most famous theorems about fixed points is due to the Dutch mathematician L. E. J. Brouwer:

Theorem 1.2.3 (Brouwer). *If \mathbf{C} is a topological d -dimensional ball and $f : \mathbf{C} \mapsto \mathbf{C}$ is a continuous function, then f has a fixed point, namely, there is a point \mathbf{x}^* in \mathbf{C} with $f(\mathbf{x}^*) = \mathbf{x}^*$.*

Recall that a homeomorphism is a one-to-one and onto continuous function whose inverse is also continuous. A topological d -ball is the image of the standard unit ball $B^d = \{ \mathbf{x} \in \mathbb{R}^d : \sum_i x_i^2 \leq 1 \}$ under a homeomorphism. A simplex is our favorite example of a topological ball. Brouwer's original proof says nothing about how to find the fixed point or a good approximation to a fixed point, not even in the case when \mathbf{C} is a simplex. In the case of a simplex Brouwer's theorem may be demonstrated via a combinatorial result about labeling triangulations due to Sperner (see exercises for an extension). Sperner's lemma provides an algorithmic way for finding fixed points of continuous maps:

Lemma 1.2.4 (Sperner). *Let \mathbf{A} be a point configuration whose convex hull is a d -dimensional simplex \mathbf{D} and \mathcal{T} a triangulation of \mathbf{A} . There are $d+1$ facets $\mathbf{D}_1, \dots, \mathbf{D}_{d+1}$ in the simplex \mathbf{D} . Label all the vertices of \mathcal{T} using the numbers $1, 2, \dots, d+1$ in such a way that no vertex that lies on the facet \mathbf{D}_i receives the label i . Equivalently, one labels the vertices of \mathcal{T} that belong to a face \mathbf{F} only using the label indices assigned to the vertices of that face. Then there is a simplex in \mathcal{T} whose vertices carry all the different $d+1$ labels.*

A rather easy proof can be derived by induction on the dimension of the simplex (see exercises). Curiously, Sperner's lemma has a simple generalization to labelings of triangulations of arbitrary polytopes (see Figure 1.32 for an example and [99, 233] for details concerning the following theorem and a strengthening).

Theorem 1.2.5 (Polytopal Sperner Lemma). *Let \mathbf{P} be a d -dimensional polytope with n vertices $\mathbf{v}_1, \mathbf{v}_2, \dots, \mathbf{v}_n$. Let \mathcal{T} be a triangulation of \mathbf{P} , possibly using additional vertices. Label the vertices of \mathcal{T} by $1, 2, \dots, n$ in such a way that a vertex of \mathcal{T} belonging to a face \mathbf{F} of \mathbf{P} can only be labeled by j if \mathbf{v}_j is a vertex of \mathbf{F} . In particular, each vertex \mathbf{v}_i is labeled i . Using this labeling rule, one can guarantee that there are at least $n-d$ full dimensional simplices of \mathcal{T} labeled with $d+1$ different labels each.*

Now, how can one use Sperner's lemma, or its generalization, to prove Brouwer's fixed-point theorem for simplices? Triangulate the simplex and apply a labeling related to a particular continuous function f : Associate to a vertex \mathbf{a} of the triangulation the label i if the i th-barycentric coordinate of \mathbf{a} is smaller than or equal to the i th-barycentric coordinate of $f(\mathbf{a})$. (Intuitively, you label \mathbf{a} with i if f moves \mathbf{a} more or less towards the i -th vertex.) There will be at least one such index for each vertex, unless the vertex is a fixed point, because the barycentric coordinates add up to one. If there are

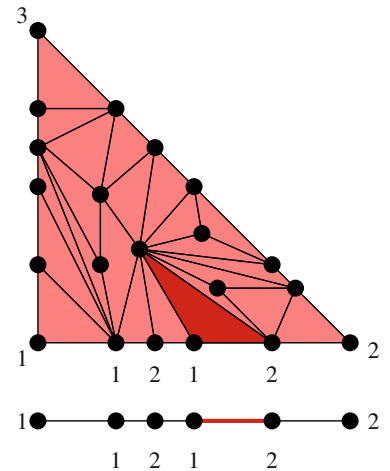


Figure 1.31: In order to find a fully labeled simplex, one can start with a fully labeled simplex of one dimension less in the boundary; then, one dives into the interior until a fully labeled simplex is reached; Exercise 1.15 asks you to make this idea rigorous.

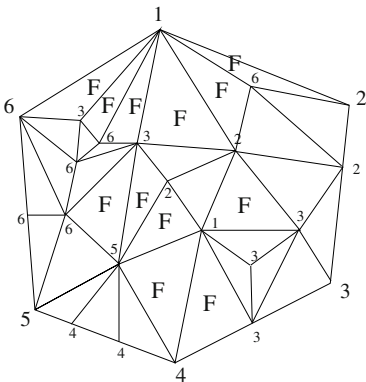


Figure 1.32: A Sperner labeling of a triangulated hexagon, with many extra vertices, and its fully labeled cells.

several such indices, simply make an arbitrary choice among them. Now, by Sperner's lemma, a simplex of \mathcal{T} can be found with its vertices labeled with all the numbers 1 to $d + 1$ and so that the i -th barycentric coordinate of the vertex labeled i is *not* increased by f (the reader should check that our labeling satisfies the hypothesis of Sperner's lemma).

Re-triangulate again and again adding more and more points in such a way that the maximum diameter of the simplices appearing in the triangulation goes to zero. At each step find a fully labeled simplex. The barycenters of all such simplices will produce an infinite sequence of points and, since it is a bounded sequence, it contains a convergent subsequence. Let \mathbf{x}^* be the limit of this subsequence. Since the map f is continuous, the i th-barycentric coordinate of \mathbf{x}^* is smaller or equal than the i th-barycentric coordinate of $f(\mathbf{x}^*)$ for every i (the difference is smaller than any positive epsilon) and therefore \mathbf{x}^* is a fixed point of the map.

There are some practical difficulties on using Sperner's lemma to explicitly find an approximation to the fixed point. First, finite versions of this method do not, in general, find a point arbitrarily close to a fixed point but rather a point that is arbitrarily close to being a fixed point, i.e., whose image is arbitrarily close to itself. Second, and most important, the number of vertices necessary to refine the successive triangulations may be very large and there is no clear procedure to find the special simplices that receive all the labelings. Today there is a large set of triangulation-based techniques to compute fixed points (see [321]). The development of triangulation-based algorithms is still active and has brought new interesting questions [169, 322] and neat applications [316].

All such algorithms use an essential property of triangulations: If \mathcal{T} is a triangulation of a point set in \mathbb{R}^d and τ is a $(d - 1)$ -simplex that is a facet of a simplex of \mathcal{T} , then either (1) τ belongs to the boundary of $\text{conv}(A)$, or (2) τ is a face of precisely two simplices in \mathcal{T} . You can easily verify from Definition 1.0.1 that this is true. This simple property makes triangulations useful because one can iteratively search for a “fully labeled” simplex of the triangulation by moving to an adjacent simplex. Even non-triangulation-based algorithms use a similar pivoting property [288, 289].

Computational experience with various fixed-point algorithms has shown a considerable sensitivity to the triangulation used. Is there a theoretical measure that can predict the relative efficiency? When we want to find the “approximate fixed point” the general principle is to move from a simplex to an adjacent simplex until we reach a fully labeled simplex. Hence, a rough measure of efficiency of a triangulation would be the number of simplices used. This has brought attention to the problem of finding triangulations of point sets that use the fewest simplices.

For example, take the vertices of a standard 3-dimensional cube. As we will see in Example 3.6.5, it has six types of triangulations modulo symmetry, displayed in Figure 1.33. They are all regular triangulations, which in this case means they can be obtained from the projection of the lower convex hull of a polytope (much more details later). Figure 1.33 shows lifting vectors producing the polytopes, which should help to visualize them.

(Hint: A high cost vector implies that the corresponding vertex is “cut” from the rest of the cube by one tetrahedron). The one of type (A) has five tetrahedra (a regular simplex plus one incident to each facet of it), while the rest have six (they can almost all be constructed by splitting the cube into two prisms and then triangulating the prisms separately. Can you spot the only one that does not fit this description?). It is a famous open problem to determine the size of the smallest triangulation of the regular d -cube. So far the answer is only known up to $d = 7$, where it equals 1493 [169]. We will further discuss this topic in Chapter 8.

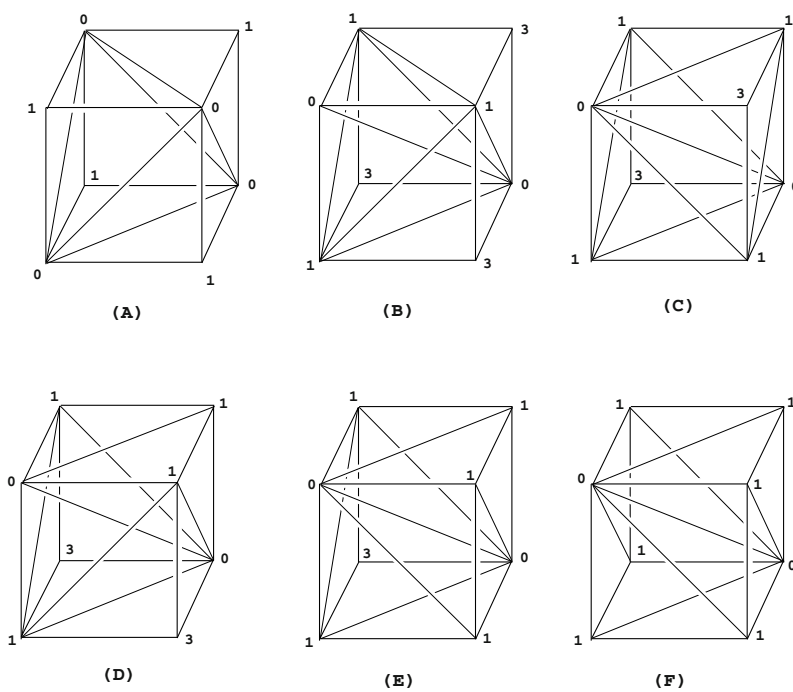


Figure 1.33: The six non-isomorphic triangulations of a regular cube.

1.3 Algebra and triangulations

Consider the system of polynomial equations

$$ax + by + c = 0 \quad \text{and} \quad dx^3y^3 + ex^3 + fy^3 + g = 0.$$

The coefficients a, b, c, d, e, f, g are non-zero complex parameters (this particular system is a counterexample to an important conjecture, see [210]). The question that we would like to ask is how many roots over \mathbb{C}^2 should one expect for the system as the parameters change? We are looking for bounds that will be valid for “almost all” values. We certainly know of these kinds of bounds, for instance, Bézout’s theorem. We now recall two versions of this theorem. The second version is very specific for discussing

real solutions and will be used later, the first version is more useful for us now. The books [87] and [329] have nice expositions about this theorem.

Theorem 1.3.1 (Bézout). *There are the following bounds on the roots of a system of polynomial equations:*

- Affine complex version: *Let $f_1(x, y) = 0$ and $f_2(x, y) = 0$ be a system of two polynomial equations in two unknowns. If it has only finitely many common complex roots $(x, y) \in \mathbb{C}^2$, then the number of those roots is at most $\deg(f_1)\deg(f_2)$.*
- Projective smooth real curve version: *If $\mathbf{C}_{f_1}, \mathbf{C}_{f_2}$ are two non-singular real projective curves, given by the homogeneous polynomials f_1 and f_2 respectively, and the intersection $\mathbf{C}_{f_1} \cap \mathbf{C}_{f_2}$ is a finite set of points, then its cardinality is at most $\deg(f_1)\deg(f_2)$. If, in addition, f_1 and f_2 intersect transversally, then $|\mathbf{C}_{f_1} \cap \mathbf{C}_{f_2}| \equiv \deg(f_1)\deg(f_2)$ (modulo 2).*

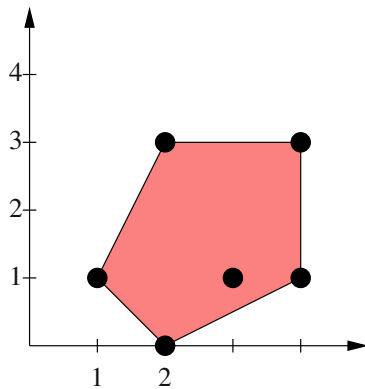


Figure 1.34: The Newton polytope for the polynomial $x^2 + xy + x^3y + x^4y + x^2y^3 + x^4y^3$.

In our particular example the bound is six roots. In most instances, the Bézout bound will not be too tight (though we will later prove that in this example it is sharp) because Bézout's bound counts solutions at infinity as well. Our example is a sparse system, missing many of the terms of degree six that can be formed with two variables. We would like to have a bound that reflects somehow the “shape” of the system and possibly a method that finds the solution without changing its shape as with Gröbner bases techniques. We must then define what we mean by the shape of a system:

Definition 1.3.2. The *support* of a polynomial $f(x_1, \dots, x_n)$ is the set of monomials that appear with non-zero coefficient. Each monomial is regarded as an *exponent vector* in \mathbb{N}^n , i.e., its coordinates are the exponents of the n variables. The *Newton polytope* of f , denoted by $N(f)$, is the convex hull of the exponent vectors of the monomials in the support of f .

In this way the Newton polytope of the polynomials presented at the beginning are a triangle and a rectangle. Note that in some situations the vertices of the Newton polytope may not equal the support of the polynomial. The *Minkowski sum* of two convex polytopes \mathbf{P} and \mathbf{Q} , denoted $\mathbf{P} + \mathbf{Q}$, is the convex polytope $\{\mathbf{p} + \mathbf{q} : \mathbf{p} \in \mathbf{P}, \mathbf{q} \in \mathbf{Q}\}$. The vertices (respectively faces) of $\mathbf{P} + \mathbf{Q}$ are sums of vertices (faces) of \mathbf{P} and \mathbf{Q} . Note that the Minkowski sum of the Newton polytopes of two polynomials f and g equals the Newton polytope $N(fg)$. We can see an example of a Minkowski sum in Figure 1.35.

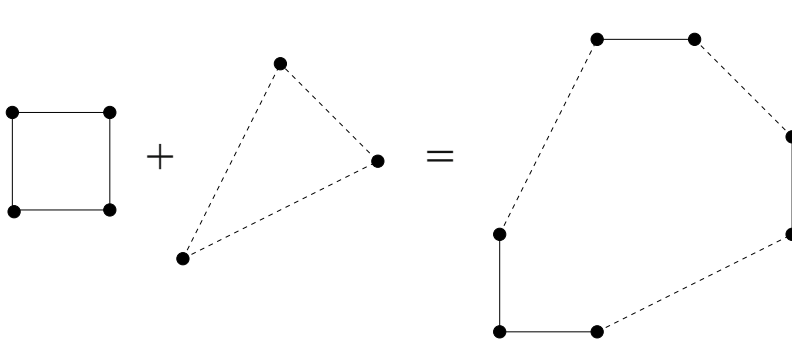


Figure 1.35: Minkowski sum of a triangle and a rectangle.

Definition 1.3.3. Given d polytopes $\mathbf{Q}_1, \mathbf{Q}_2, \dots, \mathbf{Q}_d$ in \mathbb{R}^d , their *mixed volume* $\mu(\mathbf{Q}_1, \mathbf{Q}_2, \dots, \mathbf{Q}_d)$ equals the following alternating sum of ordinary volumes:

$$\sum_{I \subset \{1, 2, \dots, d\}} (-1)^{|I|} \text{vol}(\sum_{j \in I} \mathbf{Q}_j).$$

A perhaps more meaningful way to define the mixed volume is:

Lemma 1.3.4. For given polytopes $\mathbf{Q}_1, \mathbf{Q}_2, \dots, \mathbf{Q}_d$ in \mathbb{R}^d consider the following function on d indeterminates x_1, \dots, x_d :

$$V(x_1, \dots, x_d) = \text{vol}(x_1 \mathbf{Q}_1 + \dots + x_d \mathbf{Q}_d).$$

Then, $V(x_1, \dots, x_d)$ is a homogeneous polynomial of degree d , and the mixed volume $\mu(\mathbf{Q}_1, \mathbf{Q}_2, \dots, \mathbf{Q}_d)$ equals the coefficient of the monomial $x_1 x_2 \cdots x_d$ in it.

This is a concrete way of defining a certain real number, but how does one compute its value? This has to do with the following lifting construction, which is a version of the one we saw in the previous section when speaking of linear programming. Let $\mathbf{A}_1, \mathbf{A}_2, \dots, \mathbf{A}_d$ be a collection of lattice point configurations, $\mathbf{A}_i \subset \mathbb{Z}^d$ (you can think of them as the support exponent vectors for certain polynomials). Denote by \mathbf{Q}_i the convex hull of \mathbf{A}_i . Now let us perform the following construction:

1. Choose random values $\omega_i(\mathbf{a})$ for each of the points $\mathbf{a} \in \mathbf{A}_i$. Do this for each set \mathbf{A}_i . Consider the polytope

$$\overline{\mathbf{Q}}_i = \text{conv}(\{(\mathbf{a}, \omega_i(\mathbf{a})) : \mathbf{a} \in \mathbf{A}_i\}).$$

Note that $\overline{\mathbf{Q}}_i$ is a polytope in \mathbb{R}^{d+1} .

2. Compute the lower convex hull \mathbf{L} of the Minkowski sum $\overline{\mathbf{Q}}_1 + \dots + \overline{\mathbf{Q}}_d$. The facets of \mathbf{L} are of the form $\overline{\mathbf{F}}_1 + \overline{\mathbf{F}}_2 + \dots + \overline{\mathbf{F}}_d$ where $\overline{\mathbf{F}}_i$ is a face of $\overline{\mathbf{Q}}_i$ and $\sum_{i=1}^d \dim(\overline{\mathbf{F}}_i) = d$. We say one such facet is *mixed* if $\dim(\overline{\mathbf{F}}_i) = 1$ for all i .

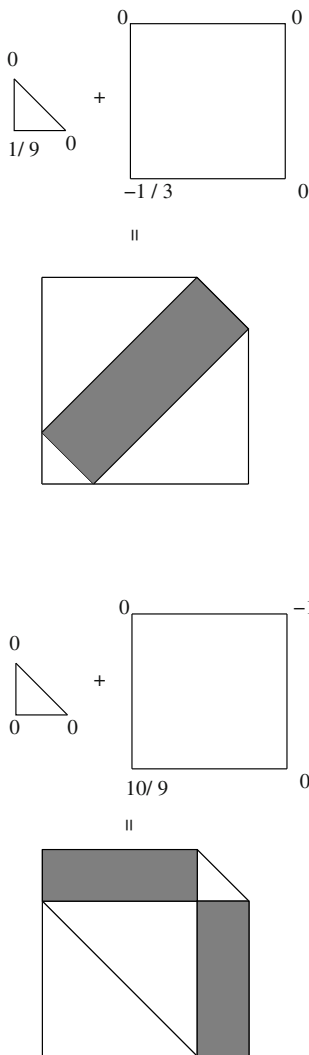


Figure 1.36: Mixed subdivision obtained by specified height vectors; mixed cells are drawn grey again.

Theorem 1.3.5. *The image of the polyhedral complex \mathbf{L} under the projection that forgets the last coordinate of every point is a polyhedral subdivision of the Minkowski sum $\sum_{i=1}^d \mathbf{Q}_i$. The mixed volume $\mu(\mathbf{Q}_1, \dots, \mathbf{Q}_d)$ equals the sum of the volumes of the mixed cells.*

The subdivisions obtained in this way are called *regular mixed subdivisions*. Observe that the mixed subdivision may depend on the choice of the values $\omega_i(\mathbf{a})$, but the mixed volume computed from it does not, as long as the values are “random” (more technically, “sufficiently generic”; see the discussion in [166]). Also, adding interior points to \mathbf{A}_i will affect the subdivisions, but not the mixed volume.

In Figure 1.36 we show an example of two mixed subdivisions of the Minkowski sum of the Newton polytopes of the system of polynomials $ax + by + c = 0$ and $dx^3y^3 + ex^3 + fy^3 + g = 0$. Each is obtained as the Minkowski sum of two polytopes, one is a lifting of a square (in fact, a tetrahedron), and the other a lifted triangle. To compute the mixed volume we must simply identify the mixed cells (in this case, we show them highlighted in the picture).

The mixed volume is equal to six in this particular example. Note that as we change the heights or the lifting values we use for the points, we obtain different subdivisions. We can find the equivalence classes of the height vectors that induced the same mixed subdivisions and we obtain a collection of polyhedral cones partitioning real space. It follows from the theory of fiber polytopes, developed by L. Billera and B. Sturmfels [53], that this is the normal fan of a polytope. We show a diagram of the polytope for our example in Figure 1.37. Readers that carefully read the previous sections will feel a sense of déjà-vu, especially comparing this figure to Figures 1.15 and 1.30. Indeed, the polytope in question is the same as the secondary polytope of a certain three-dimensional point set. This is not a coincidence as we will see in Section 9.2.

Now we are ready to state the main result of this section (see [46] and [166] for proofs of the theorem, as well as the closely related papers [188] and [197]). The word *sparse* in the statement has the precise meaning that we are looking at a family of polynomial systems depending on certain parameters $c_{i,\mathbf{a}}$, but we are fixing the monomials that are used by all these systems.

Theorem 1.3.6 (D.N. Bernstein, 1976). *Given d subsets $\mathbf{A}_1, \dots, \mathbf{A}_d$ of \mathbb{Z}^d and $\mathbf{Q}_i = \text{conv}(\mathbf{A}_i)$, consider the sparse polynomial system of equations*

$$\sum_{\mathbf{a} \in \mathbf{A}_1} c_{1,\mathbf{a}} x_1^{a_1} x_2^{a_2} \dots x_d^{a_d} = 0, \quad (1.9)$$

$$\sum_{\mathbf{a} \in \mathbf{A}_2} c_{2,\mathbf{a}} x_1^{a_1} x_2^{a_2} \dots x_d^{a_d} = 0, \quad (1.10)$$

$$\vdots$$

$$\sum_{\mathbf{a} \in \mathbf{A}_d} c_{d,\mathbf{a}} x_1^{a_1} x_2^{a_2} \dots x_d^{a_d} = 0. \quad (1.11)$$

For almost all choices of coefficients $(c_{i,\mathbf{a}})_{i \in [d], \mathbf{a} \in \mathbf{A}_i}$, the number of roots of this system in $(\mathbb{C}^*)^d$ equals the mixed volume $\mu(\mathbf{Q}_1, \dots, \mathbf{Q}_d)$.

As usual, \mathbb{C}^* denotes $\mathbb{C} \setminus \{0\}$. That is, the roots to which the theorem applies are those with no zero coordinate. In algebraic geometry, $(\mathbb{C}^*)^d$ is usually called the *complex torus* of dimension d .

As an application of Bernstein's theorem, consider the system of equations $ax^3y^2 + bx + cy^2 + d = 0$ and $exy^4 + fx^3 + gy = 0$. The Bézout bound estimates 25 complex roots. The number of roots in the torus $(\mathbb{C}^*)^2$ predicted by Bernstein's Theorem is 18. Using Gröbner bases one can see that 18 is in fact the actual number of roots in \mathbb{C}^2 .

Note that if the polynomials of a certain system are each multiplied by a certain monomial, the number of roots in the torus $(\mathbb{C}^*)^d$ does not change. This is in accordance with the fact that the Newton polytopes of the new system are just translated copies of the old ones, so their mixed volume does not change. The total number of affine solutions may, however, change. There has been work trying to extend Bernstein's Theorem to counting affine solutions [166], [274]. For sparse systems there exist *homotopy methods* for finding all roots. These are algorithms resulting from the combination of numerical and polyhedral techniques. They have been explored, for instance, in [166], [325].

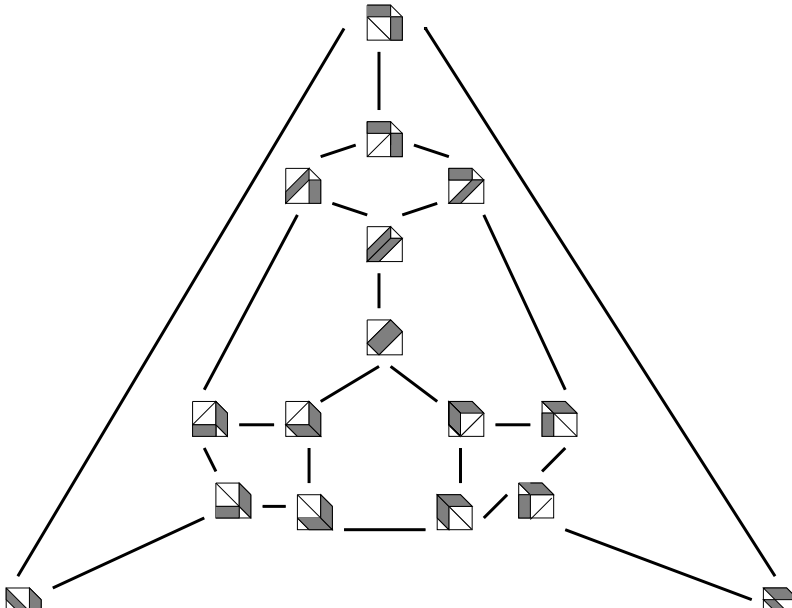


Figure 1.37: All mixed subdivisions of a Minkowski sum. The gray cells are mixed cells. The meaning of the edges in this picture will be discussed in Section 9.2.

How many of the complex roots given by Bernstein's Theorem can be *real*? One would like to generalize the case with one variable, where Descartes' rule of signs [58] indicates that the number of positive real solu-



David Hilbert c. 1900

Figure 1.38: David Hilbert around the time he proposed 23 open problems.

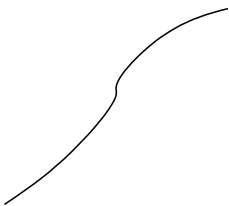


Figure 1.39: A pseudoline. Its complement has one component, homeomorphic to an open circle. The picture only shows the “affine part”; you have to think of the two ends as meeting at infinity.

tions of a polynomial is bounded by the number of monomials. Can something similar be done for multivariate systems? This is still unknown. On a positive note, Khovanskii [189] made a major breakthrough when he provided a bound that did not depend on the degrees of the equations. On the negative side, Kushnirenko had conjectured that, if $f_1 = f_2 = \dots = f_k = 0$ are k polynomial equations in k variables, and m_i is the number of terms of f_i , the number of nondegenerate isolated positive roots of this system is at most

$$(m_1 - 1)(m_2 - 1) \dots (m_k - 1).$$

Bertrand Haas found a counterexample that consists of two polynomials in two variables with three terms having five roots (instead of the conjectured four). The example can be easily generalized to more variables [152].

In preparation for our next algebraic topic, it is relevant to mention the work of Sturmfels, who gave lower bounds on the number of real roots for sparse systems of equations from studying the signs of the coefficients and marking with them the mixed cells of the mixed subdivisions [311]. This is a generalization of O. Viro’s method for complete intersections. In this way one can construct zero dimensional polynomial systems that have an “easy to count” number of real roots. The roots are in fact cells of a mixed subdivision of the type we saw before. It was proposed by Itenberg and Roy [175] that this construction could provide a combinatorial bound for the number of real solutions of a polynomial system with fixed Newton polytopes. Unfortunately, this was disproved by Li and Wang [210]. For a nice introduction to the topic of solving systems of polynomial equations, we highly recommend the book [313].

Now we move to another application in algebraic geometry. The study of the topology of smooth real algebraic curves has a long history (perhaps the earliest result is the well-known theorem of projective geometry, due to Poncelet, which says that any pair of smooth conics are equivalent under projective transformations). Informally, it deals with the following question: What are the possible topological types of smooth real curves with a given degree? Hilbert popularized this question by including a version of it in his famous collection of problems, proposed in 1900. He asked about the classification of curves of degree six and surfaces of degree four. Both cases were solved by 1977, but only the curves of degree seven have been classified since then, and hardly anything is known for real smooth hypersurfaces of arbitrary degree.

For the classification, two types of results are needed. On the one hand, it is necessary to describe “prohibitions” or obstructions that narrow down the possible topological types. On the other hand, the interested researcher must construct hypersurfaces for the topological types allowed by the obstructions. This part of the book considers in detail the construction of hypersurfaces with prescribed topology. We focus on the work of Oleg Viro [326, 327], who developed a very successful combinatorial technique based on the triangulations of point sets associated with the possible monomials of a polynomial function. For simplicity, the discussion will be done for the case of plane curves, but the theory works in arbitrary dimension. See also [334] for an introduction to Hilbert’s Sixteenth problem.

Let us carefully see what the problem actually looks like. Let

$$f(x, y, z) = \sum_{i+j+k=d} a_{i,j,k} x^i y^j z^k$$

be a smooth homogeneous polynomial of degree d . The solution set of f is the collection $\mathbf{C}_f = \{(x, y, z) \in \mathbb{R}^3 : f(x, y, z) = 0\}$. The solution set is a closed subvariety of dimension one inside \mathbb{RP}^2 . Since it is smooth, each component is homeomorphic to a circle. But there are two topologically different (i.e., non-isotopic) ways to embed a circle in \mathbb{RP}^2 : It can be isotopic to a conic, or to a line. The two cases are called, respectively, an *oval* and a *pseudoline*. The main difference is that the complement of a pseudoline has only one connected component (for example, the “line at infinity” is a pseudoline whose complement is the affine plane), while the complement of an oval has two connected components: one homeomorphic to an open disk, which we call the interior of the oval, and one homeomorphic to a Möbius band; see Figures 1.39 and 1.40. The two cases are also distinguishable by the double cover of \mathbb{RP}^2 by the 2-dimensional sphere S^2 . An oval is covered by two ovals in the sphere, and a pseudoline by only one, which wraps around twice.

Ovals can be nested; that is to say, one contained in the interior of the other, or not. A nest of ovals (of depth k) consists of k ovals each nested in the previous one. Also relevant to the question we want to study is that an oval meets any generic line (or pseudoline, for that matter) in an even number of points, while two generic pseudolines always meet in an odd number of points. In particular:

Corollary 1.3.7. *The following holds for all real planar curves:*

- (i) *A smooth plane curve of degree d has a pseudoline if and only if d is odd, and in this case it only has one. In particular, a curve of odd degree is never empty.*
- (ii) *If a curve of degree d has two nests, of depths i and j , then $i + j \leq d/2$. Here i and j are allowed to be zero.*
- (iii) *If the ovals of a curve of degree d are distributed into at most five nests, then there are at most d ovals in the curve.*

Proof. For the first part, take a line \mathbf{l} cutting the whole curve transversally. The cardinality of $\mathbf{l} \cap \mathbf{C}_f$ is congruent to d modulo 2, by Bézout’s Theorem, so the number of pseudolines has the same parity as the degree. But two pseudolines cannot appear, because they would produce at least a singular point, which proves the first part. Similarly for the second part we can find a line that passes through the center of the innermost ovals in the two nests. For the last assertion, we consider the conic that passes through points inside of the innermost ovals in the five (or less) nests. \square

This is a result of the type we have called “prohibitions”. The first part is particularly important. It says that the classification of curves of a certain

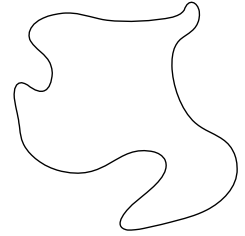


Figure 1.40: An oval. Its interior is a (topological) circle and its exterior is a Möbius band.

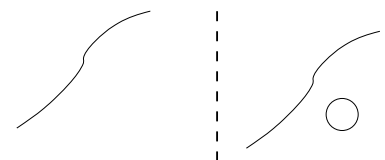


Figure 1.41: Two configurations are possible in degree 3.

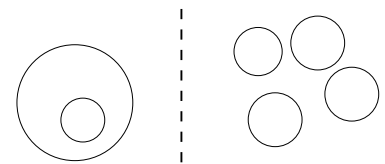


Figure 1.42: Six configurations are possible in degree 4. Only the two maximal ones are shown.

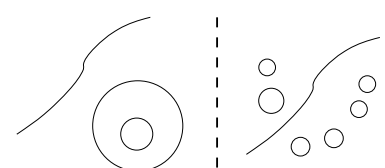


Figure 1.43: Eight configurations are possible in degree 5. Only the two maximal ones are shown.

degree consists just in telling how many different ovals can appear and what the possible nesting structures are. In other words, we want to know which partially ordered sets (posets) can arise in this way from a smooth curve of given degree. The equivalence class of curves that induce the same poset is an isotopy class.

A second example of prohibition is Harnack's Theorem, known well before Hilbert (there are many more beautiful prohibition type results but this is not the point of these notes, so we abstain from showing more):

Theorem 1.3.8 (Harnack). *The number of connected components of a non-singular algebraic curve f of degree d is at most $(d^2 - 3d + 4)/2$, or, equivalently, one plus the genus of the Riemann surface associated with f .*

This theorem already allows us to easily give the full classification of real smooth plane curves up to dimension five. Observe that, by Part (ii) of Corollary 1.3.7, nesting appears only in dimensions four and higher. Moreover, in dimensions four and five only a single nest of two ovals is allowed, and if the nest appears then no more ovals can be present. This gives only the following possibilities, displayed in Figures 1.41, 1.42, and 1.43.

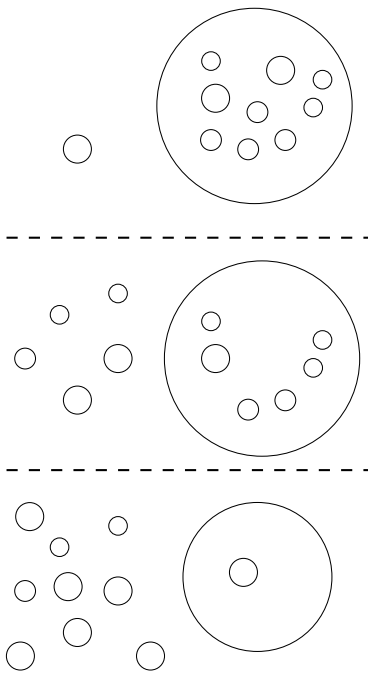


Figure 1.44: The three curves of degree six with eleven ovals.

1. In degree one and two, we can have only one connected component, and it is a pseudoline or oval depending on the degree (well, we knew this already, didn't we?). In degree one we have a line, and in dimension two we have a conic, which in the projective plane is indeed an oval.
2. In degree three, there is a pseudoline together with zero or one ovals.
3. In degree four, there is either a nest of two ovals or a number of unnested ovals ranging from 0 to 4 (only the maximal case is shown in Figure 1.42).
4. In degree five, there is a pseudoline together with either a nest of two ovals or a number of unnested ovals ranging from 0 to 6 (again, only the maximal case is shown).

As it turns out, all the degree five non-prohibited configurations can (easily) be constructed algebraically. But in degree six constructing new curves starts to be much more complicated. By Corollary 1.3.7, you cannot get two nests of depth at least two for a curve of degree six, and if there is a nest of depth three then there is nothing else. Hence, the possibilities are:

- A single nest with three ovals.
- A number of zero to eleven unnested ovals.
- An oval having i ovals inside (unnested to one another) and j ovals outside, with $i + j \leq 10$.

For instance, there are only three configurations of degree six curves with 11 ovals, see Figure 1.44. Two of these three curves were already

constructed in the times of Hilbert. Gudkov's achievement was an elegant construction of the third one.

A big boost to the “constructions” part of the problem was given by O. Viro around 1990. His construction uses triangulations in an essential way. Consider the point configuration

$$\mathbf{A}_d = \{(i, j) : i + j \leq d, i, j \in \mathbb{Z}, i, j \geq 0\}.$$

We denote the convex hull of \mathbf{A}_d by \mathbf{Q}_d . (How many points do you have in \mathbf{A}_d ?) Take a triangulation \mathcal{T} of \mathbf{A}_d . Later we will need \mathcal{T} to be regular, but for now this is not necessary. Consider also a sign function $\sigma : \mathbf{A}_d \rightarrow \{+, -\}$. Denote by $\mathbb{R}P_{++}^2 = \{(x : y : z) : x \geq 0, y \geq 0, z \geq 0\}$ the real projective plane.

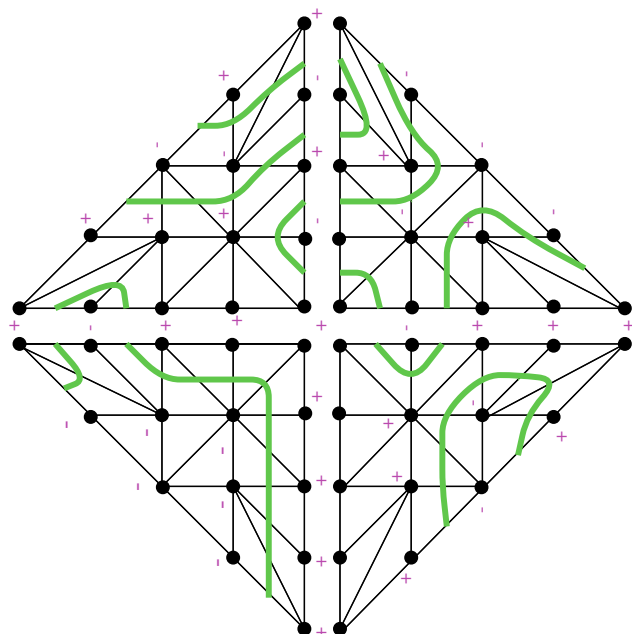


Figure 1.45: The graph $G_{T,\sigma}$ of degree 4.

Take three more copies of the triangulation \mathcal{T} , obtained by reflecting \mathcal{T} over the coordinate axis. Glue these four copies together to build a model of the real projective plane, so that opposite sides are glued in opposite directions. We also extend the sign function σ to the other three copies of \mathcal{T} , but modified according to which orthant we are working on. That is to say, $\sigma(i, j) = \sigma(i, j)(-1)^i$ for $\mathbb{R}P_{+-}^2$, $\sigma(i, j) = \sigma(i, j)(-1)^j$ for $\mathbb{R}P_{-+}^2$, $\sigma(i, j) = \sigma(i, j)(-1)^{i+j}$ for $\mathbb{R}P_{--}^2$. We are going to define a graph $G_{\mathcal{T},\sigma}$ whose vertices are the midpoints of those edges of \mathcal{T} and whose endpoints have distinct signs under σ . Two of these nodes will be connected if and only if they lie in a common triangle of \mathcal{T} . The graph is embedded in the combinatorial model of the projective plane. Figure 1.45 shows an example. We are now ready to state the main theorem of Viro:

Theorem 1.3.9. Assume that the triangulation \mathcal{T} is regular, that is, it is defined by a certain height function $\omega : \mathbf{A}_d \rightarrow \mathbb{Z}$. Let

$$f_t(x, y, z) = \sum c_{i,j} x^i y^j z^{d-i-j} t^{\omega(i,j)},$$

where the $c_{i,j}$'s are arbitrary constants with $\text{sign}(c_{i,j}) = \sigma(i,j)$.

Then, for t large enough, f_t is an affine equation for a smooth plane algebraic curve, and there exists a homeomorphism between $\mathbb{R}P^2$ and its combinatorial model which maps the curve $\{f_t = 0\}$ into the graph $G_{\mathcal{T},\sigma}$.

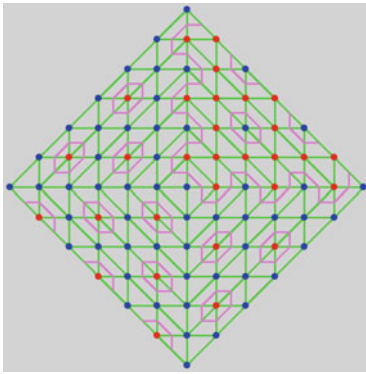


Figure 1.46: A curve of degree 6 constructed by using Viro's method.

Let us recall what it means for a triangulation to be regular. Roughly speaking, a triangulation is regular when it is isomorphic to the lower hull of a convex polytope. More precisely, the triangulation is regular if we can lift each of the vertices \mathbf{a} of \mathcal{T} to a height $\omega(\mathbf{a})$ and obtain a convex polyhedral surface combinatorially equivalent to \mathcal{T} . Therefore a regular triangulation \mathcal{T} is given by a generic height vector $\omega : \mathbf{A}_d \rightarrow \mathbb{Z}$. Our running example is in fact a good piecewise linear picture of a certain smooth curve of degree four. Perhaps the reader should play with this construction.

The construction is powerful enough to obtain all the maximal curves of degree six. Figure 1.46 shows one.

We finish with a very successful application of Viro's construction. Virginia Ragsdale conjectured in her 1906 paper [262] that the following inequalities would be satisfied by all non-singular curves of degree $2k$ (the second equation is in fact a correction by O. Viro to the original statement of Ragsdale). Denote by e and o the number of even and odd ovals respectively, then

$$e \leq 3/2(k^2 - k) + 1, \quad o \leq 3/2(k^2 - k) + 1.$$

She obtained this conjecture from her extensive analysis of Hilbert's and Harnack's results. This condition was first proved to be false by Ilia Itenberg in 1993 (see [173]). Itenberg used Viro's construction to show that there are examples of curves with $(3k^2 - 3k + 2)/2 + h(k)$ even ovals, where $h(k)$ is a quadratic function of k . We present in Figure 1.47 the case for $k = 5$. Itenberg's construction gives $\frac{13}{32}d^2 \pm O(d)$ positive ovals. Bertrand Haas improved the result to $\frac{10}{24}d^2 \pm O(d)$ [150].

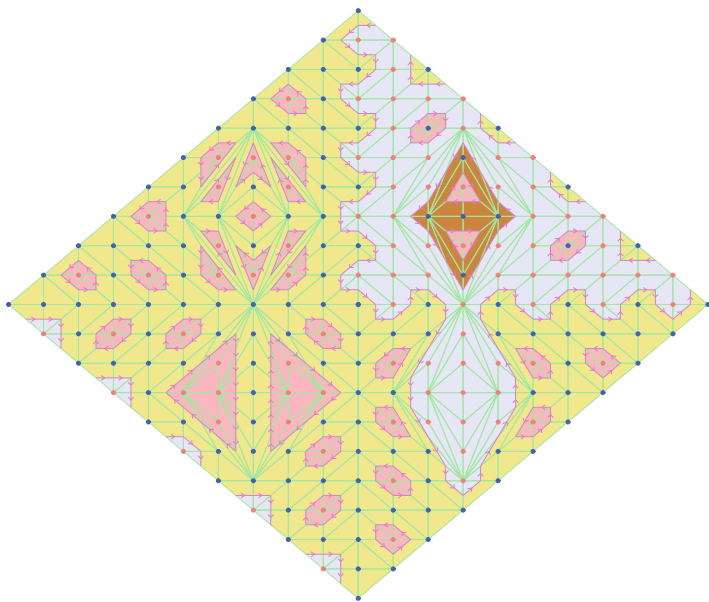


Figure 1.47: Itenberg's counterexample to Ragsdale's conjecture (degree 10).

This shows the power of Viro's construction. The construction of Viro in principle is purely combinatorial and depends on a triangulated point set. The algorithms can be carried out even for non-regular triangulations. It has to be emphasized, though, that only regular triangulations are guaranteed to produce algebraic curves. For non-regular triangulations, the construction provides a curve embedded in the projective plane, but there is no evidence that these curves are always algebraic. However, up to this point no counterexample is known. Several properties of algebraic curves seem to be also valid for curves arising from arbitrary triangulations [102, 151].

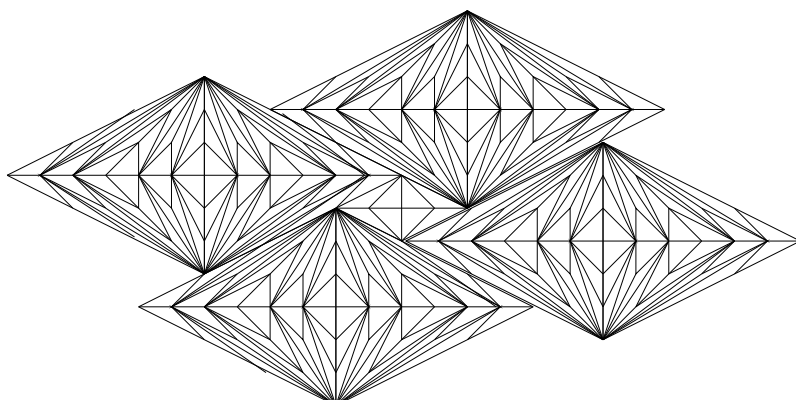


Figure 1.48: A portion of a non-regular triangulation related to Ragsdale's conjecture.

For example, using non-regular triangulations it is possible to construct curves with $\frac{17}{40}d^2 \pm O(d)$ positive ovals, which would be the “best” counterexamples to Ragsdale’s conjecture. Figure 1.48 shows a look at the triangulations needed for this, which is a modification of the construction of Haas mentioned above [150] (Haas’ construction gives fewer ovals, but it is a regular triangulation).

Viro’s construction generalizes naturally to the case of real smooth hypersurfaces of higher dimension [187, 174], for the construction of singular curves with prescribed collection of singularities [297], and for the construction of planar polynomial vector fields with large number of limit cycles [176].

Triangulations often arise in *representation theory* too, in particular in the representation theory of Lie algebras. Remember that complex simple finite-dimensional Lie algebras are classified via their *crystallographic root systems* (see [170] for details), which are nothing but finite sets of vectors in \mathbb{R}^r . It is well-known that there are the following four infinite series plus five “Exceptional” root systems:

- $A_r = \{e_i - e_j, \delta + e_i\}_{i \neq j}$, where $\delta = \sum_{k=1}^r e_k$. This system corresponds to the Lie algebra \mathfrak{sl}_{r+1} .
- $B_r = \{\pm e_i \pm e_j\}_{i < j} \cup \{e_i\}$. This system corresponds to \mathfrak{so}_{2r+1} .
- $C_r = \{\pm e_i \pm e_j\}_{i < j} \cup \{2e_i\}$. This system corresponds to \mathfrak{sp}_{2r} .
- $D_r = \{\pm e_i \pm e_j\}_{i < j}$. This system corresponds to \mathfrak{so}_{2r} .
- The five exceptional root systems G_2, F_4, E_6, E_7, E_8 .

All these appear, for example, in the classification of finite reflection, or Coxeter, groups. Indeed, the root vectors are essentially the normals to the hyperplanes in the arrangement for the Coxeter group.

Given an irreducible crystallographic root system Φ , one can define the following rich family of polyhedra, the *alcoved polytopes*, defined as the intersections of half-spaces bounded by inequalities of the form

$$b_\alpha \leq (\alpha, x) \leq c_\alpha, \quad \alpha \in \Phi,$$

where b_α, c_α are some integer parameters. So alcoved polytopes are unions of cells in *affine Coxeter hyperplane arrangements*.

Of course, by definition, an alcoved polytope for a certain root system Φ is simply a polytope whose set of normal vectors is contained in Φ . As we will see in Section 2.5, this is the same as saying that:

Definition 1.3.10. An alcoved polytope for a root system Φ is a polytope whose normal fan is a regular triangulation of Φ obtained with an integer height function ω .

To emphasize how rich alcoved polytopes really are one can note that hypersimplices, order polytopes, and some special kinds of matroid polytopes appear as examples of them. In [199], the authors investigate alcoved

polytopes for the root system A_n and uncover some beautiful combinatorics for their triangulations. They proved that two seemingly unrelated ways of triangulating a hypersimplex, one given by R. P. Stanley [303] and the other by B. Sturmfels [312], are in fact the same, and a manifestation of a more general construction on alcoved polytopes. Using their triangulations the authors are able to calculate volumes of alcoved polytopes and provide generalizations of the descent and major index statistics on permutations, which appear as volumes of hypersimplices (see Subsection 6.3.6), within this more general context.

Triangulations of root systems already arised in the work of Gelfand, Graev, and Postnikov on hypergeometric functions. There, they considered the problem of computing the normalized volume of the convex hull in \mathbf{R}^n of a finite subset \mathbf{A} of \mathbf{Z}^n . This quantity is of course easy to compute from a triangulation of the convex hull of \mathbf{A} . Of particular interest were the classical root configurations, denoted by $A_n^{(+)}, B_n^{(+)}, C_n^{(+)}$, and $D_n^{(+)}$, that arise as the set of *positive roots* of the classical root systems. For example, they showed that the volume of $A_n^{(+)}$ is precisely the Catalan number C_n that also counts triangulations of an $(n+2)$ -gon by constructing a triangulation of it with that many simplices. The key idea is that there is an explicit bijection between the maximal simplices in the constructed triangulation of $A_n^{(+)}$ and the set of so-called “anti-standard trees” on n elements. Since the number of anti-standard trees is the Catalan number, (and since all simplices in their triangulation are unimodular) it follows that the normalized volume of $\text{conv}(A_n^{(+)})$ equals the Catalan number. We will show this triangulation in Section 9.5.3.

In fact, their construction (if properly polarized) gives a construction of the associahedron as an alcoved polytope! Remember that in Section 1.1 we previewed the associahedron (or *Stasheff polytope*, as it is more known in algebraic circles) as the *secondary polytope* of an $(n+2)$ -gon \mathbf{C}_{n+2} .

Their ideas where continued by W. Fong in her thesis [127], where she found the normalized volume in the other root systems. Fong’s formulas were later revisited by Ohsugi and Hibi in the language of initial ideals and Gröbner bases that we will see in Section 9.4. As stated in the Sturmfels’ correspondence of Theorem 9.4.5, if an initial ideal of a toric ideal $I_{\mathbf{A}}$ is square-free then the generators of the toric ideal give the *minimal non-faces* of a unimodular triangulation of the undrlying configuration \mathbf{A} . Most recently, K. Meszaros has continued the study of root polytopes and used triangulations to prove a conjecture of A. N. Kirillov about the uniqueness of the reduced form of a Coxeter type element in the bracket algebra of type C_n (see [232]).

A different construction of the associahedron as an alcoved polytope for the type A_n was devised by J.-L. Loday in [217]. In a subsequent paper he constructed a triangulation of it related to parking functions: A sequence of (possibly repeated) positive integers (i_1, \dots, i_n) is called a *parking function* if the permuted sequence (j_1, \dots, j_n) with $j_1 \leq \dots \leq j_n$ satisfies $j_k \leq k$ for

every k . Put differently, it is a parking function if

$$\#\{i_k : i_k \leq k\} \geq k, \quad \forall k = 1, \dots, n.$$

One can show that for fixed n , there are exactly $(n+1)^{n-1}$ parking functions of length n . The set of them is denoted PF_n . In [218, Theorem 2.1], a triangulation of the associahedron $\Sigma\text{-poly}(\mathbf{C}_n)$ by oriented n -simplices is constructed, such that the oriented edges are in accordance with the natural *Tamari order* on the triangulations of the n -gon (we will define the Tamari order in Section 6.1). Moreover, via a new recursive formula involving $\text{PF}_p, \text{PF}_{n-p-1}$, and the set of $(p, n-p-1)$ -shuffles, the author shows that the top dimensional simplices of this triangulation of the associahedron $\Sigma\text{-poly}(\mathbf{C}_n)$ are in bijection to the parking functions (Theorem 3.2). So, once more, triangulations have a nice combinatorial meaning.

One cannot mention the incredible associahedron without remembering *cluster algebras* (see [125]). These are commutative rings equipped with a distinguished set of generators (cluster variables) grouped into overlapping subsets (clusters) of the same finite cardinality (the rank of an algebra in question). Cluster algebras are constructed by an iterative process of *mutations* which in some sense generalize flips. In [76] the authors showed the cluster complex (the simplicial complex whose vertices are cluster variables and whose maximal simplices are clusters) can be identified with the dual face complex of a simple convex polytope, the *generalized associahedron*. These polytopes include, as a special case, the Stasheff's *associahedron* and others.

1.4 The rest of this book

Now the reader has a minimal familiarity with the objects to be studied and why triangulations are relevant in mathematics. For a given point set \mathbf{A} there are many questions that one can ask about their triangulations. Here is a sample of general issues that will be of interest for us in the rest of the book:

1. *Count the number* of different triangulations.
2. *Decide* whether there is a triangulation with *property X*.
3. *Find* an “*optimal*” such triangulation.
4. *Study* the algebraic or topological *structure* of the set of all triangulations, or special subsets.

Chapter 2 lays out the language and main objects for the rest of the book. The first point we make is we want to convince the reader of the convenience of clearly distinguishing between the points (or vectors) of a configuration and the labels used to denote it. Following the tradition common in combinatorial topology and geometry (including, by the way, graph theory) a “simplex” or a “cell” is a set of labels, and a triangulation or subdivision is a family of them, with certain properties. This may look awkward at the beginning but it has many advantages in the long run. Among

other things, it allows you to “play” with your configuration (move its points, project it, lift it, etc.) and keep the same labels for the elements, which makes it natural to ask what happens with triangulations (are they the same after the transformation?). It is also very handy in the context of *regular triangulations* where you construct triangulations of a configuration by lifting it to higher dimension and then projecting its lower envelope. All this is introduced and worked out in Sections 2.1 to 2.3. The other three sections in this chapter are devoted to three different topics:

- The notion of *flip* between triangulations, which is central to the book. We took as a definition that a “flip” is simply a subdivision that is refined only by two triangulations, and leave more operational characterizations for Chapter 4.
- *Vector configurations* and triangulations of them. These generalize *point configurations* (which arise as the *homogeneous* case) and are useful in several contexts. Among other things, they are essential for the Gale duality introduced in Chapter 4.
- *Simplicial complexes* in general, with focus on the face vectors of simplicial balls and spheres, of which triangulations of vector configurations are a special instance.

Triangulations in dimension two have deserved special attention in Computational Geometry, both for their applications and for their simplicity. We study them in Chapter 3 focusing on special constructions (Section 3.2), how many can a given point set have (Section 3.3) and how to move from one to another via flips (Section 3.4). We finish the chapter by showing that triangulations in dimension three (and higher) fail to have most of the properties of two-dimensional triangulations:

- Different triangulations of the same configuration may have different numbers of simplices.
- Monotone flipping does not always work, which leaves open (in dimensions three and four) the question of whether graphs of flips are always connected.
- Triangulations exist with fewer flips than expected.

Chapter 4 continues with the work of Chapter 2, providing the reader with a tool box of constructions and results to use when needed. Section 4.1 isolates the properties of a given configuration that are relevant to study its set of triangulations. This is basically the *oriented matroid* of the configuration (sometimes called its *order type*) which can be described in several ways. This opens the door to easily manipulate configurations and get new ones from old ones. In Section 4.2 we show how triangulations behave with respect to the matroid operations of contraction and deletion, as well as to other natural operations such as pyramids and products. Special attention deserves the *one-point suspension* operation introduced in Subsection 4.2.5.

It shows, among other things, that configurations in convex position are not simpler than arbitrary configurations, unless you are working in fixed dimension. Section 4.3 basically repeats the constructions of Section 3.2 in arbitrary dimension. Section 4.4 retakes the topic of flips, showing two characterizations of them. The final section in this chapter is a compilation of many different ways in which triangulations and subdivisions can be characterized, grouped in two basic blocks: “geometric” and “combinatorial”.

This leads to what may be the central chapter of the book, Chapter 5 devoted to the construction and properties of secondary polytopes. After motivating the secondary polytope with several examples we introduce in Section 5.2 the *secondary fan* of a configuration, as follows: if we are given a configuration \mathbf{A} of n points or vectors, we can stratify the vector space of all heights $\omega \in \mathbb{R}^n$ that we can use to construct regular triangulations of \mathbf{A} , according to the actual triangulation they produce. This stratification is a *polyhedral fan* and it turns out to be (if \mathbf{A} is *acyclic*, that is, if it is equivalent to a *point* configuration) the normal fan of a polytope: the secondary polytope of \mathbf{A} , whose face lattice is the poset of *regular subdivisions* of \mathbf{A} .

Then we devote Section 5.3 to a closer look at some features of secondary polytopes. We want to emphasize a result which surprised us and was one of the latest additions to the book: Contrary to general belief, the graph of the secondary polytope is *not equal* to the graph of flips among regular triangulations, since there can be “non-regular flips” connecting regular triangulations. This has been wrongly stated several times in the literature, and we devoted some effort to try to prove the wrong statement before finding (surprisingly simple) counter-examples.

In the construction of the secondary fan, the Gale transform of our configuration played a significant role. This is emphasized by the concept of *chamber complex* introduced in Section 5.4. Although it can be considered simply a different name for the secondary fan, its explicit definition in terms of the Gale transform clarifies its structure a lot and opens the door to a deeper understanding of triangulations of configurations with few elements, which is undertaken in Section 5.5.

Chapter 6 takes a closer look at triangulations of certain specially structured configurations: vertex sets of cyclic polytopes (Section 6.1), products of simplices 6.2, and cubes or, more generally, configurations with 0/1 coordinates 6.3. Cyclic polytopes play a fundamental role in polytope theory, as they give examples of the biggest number of facets (and faces of all dimensions) possible in polytopes with a given dimension and number of vertices. For us, they are interesting because they are a family of polytopes very well behaved with respect to the deletion, contraction, projection, and lifting operations. Understanding this good behavior one can prove, for example, that their graphs of triangulations are connected. Also, they give examples of configurations with (at least asymptotically) the biggest number of triangulations possible. Products of two simplices are also very well behaved: the simplices they contain are in bijection with spanning trees in complete bipartite graphs, which allows to nicely describe and understand

specific triangulations of them. One can, for example, completely characterize which products of two simplices possess non-regular triangulations. Finally, cubes and 0/1 polytopes, although a bit less structured in general, are very important in polyhedral optimization, so it is worth having a look at their triangulations.

Chapter 7 is devoted to “pathological” triangulations. As a warm-up for later constructions, it starts with a very close look at the smallest configuration having non-regular triangulations, which we call “the mother of all examples”. We have already introduced it in Figure 1.30 and it shows up again and again in the book. Section 7.2 then shows triangulations in dimensions three and four having *very few flips*. For example, with a construction based on taking several copies of the vertices of a 24-cell one can build arbitrarily large triangulations in dimension four with a constant number of flips. The next two sections show two constructions of point sets with a disconnected graph of triangulations: the first in dimension five and the second in dimension six. Each of them has an added special feature: the second one is in general position, and the first one has unimodular triangulations in the non-regular components of the graph, a property that makes it very interesting for algebraic geometric applications.

Chapter 8 focuses on computational and algorithmic aspects. The first three sections describe, respectively, how to implement the oriented matroid of a configuration in a computer, the construction and test of regular triangulations, and the enumeration of regular and non-regular triangulations. Section 8.4 is an account of the known bounds for the numbers of triangulations that a point set can have. Section 8.5 introduces a very general framework for optimization in the space of triangulations of a configuration: the *universal polytope*. Following a standard procedure in polyhedral optimization, the universal polytope is simply the convex hull of the characteristic vectors of all triangulations of a configuration. This is a very powerful concept, except it typically (and our case is not an exception) requires you to use integer programming, rather than linear programming, to solve specific optimization problems. This is not a drawback of the method, but rather a reflection of the intrinsic difficulty of some optimization problems in triangulations. We show in Section 8.6 three problems that can be expressed as linear optimization problems over the universal polytope and for which there are NP-hardness proofs.

In the final chapter we address five almost independent topics that continue the theory laid down in the book:

- Section 9.1 shows that secondary polytopes and posets of subdivisions are just a special instance of a more general construction (fiber polytopes and posets of projection-compatible subdivisions) which includes as other significant cases that of zonotopal tilings in a zonotope and monotone paths in an arbitrary polytope.
- Elaborating further on this, Section 9.2 shows a nice relation between mixed subdivisions of a Minkowski sum of polytopes (which we have

already encountered in Section 1.3) and arbitrary subdivisions of certain special polytopes, the so-called Cayley embeddings.

- In Section 9.3 we look at special properties and questions concerning triangulations of integer point configurations, which are of special interest in algebra and combinatorics.
- Section 9.4 shows the relation between the secondary fan of an integer point configuration \mathbf{A} and the Gröbner fan of the toric (or binomial) ideal $I_{\mathbf{A}}$ associated to it. The first parametrizes the regular subdivisions of \mathbf{A} and the second parametrizes the initial ideals of $I_{\mathbf{A}}$.
- To finish the book, in Section 9.5 we want to stress an obvious fact that should, in our opinion, be paid more attention: a simplicial complex is *polytopal* if and only if it is a regular triangulation of some “totally cyclic” configuration. Having this in mind, we show the relation between the g -vector of a polytope and a monotone flip sequence constructing its face lattice from that of a simplex, and also lay out a general method for checking whether a simplicial complex is polytopal. As an application, we show that (the polar complex of) the associahedron is a regular triangulation of the root system of type A , which in particular shows its polytopality.

Exercises

Exercise 1.1. Identify how the five binary trees with 3 nodes (Figure 1.9) biject to the five triangulations of a pentagon (Figure 1.6, but you should turn the figure upside-down and check that rotations correspond to diagonal flips).

Exercise 1.2. Prove that any point set with four elements in the plane, not all in a line, has exactly two triangulations.

Exercise 1.3. Take a regular tetrahedron. Can you triangulate it, with the help of extra interior points, in such a way that only regular tetrahedra appear inside? (*Hint:* find the dihedral angle between adjacent facets of a tetrahedron.)

Exercise 1.4. Prove that the graph of flips of a 6-gon is Hamiltonian (this holds in general for any n -gon; see [220]).

Exercise 1.5. (Catalan numbers via generating functions.) Find formula (1.4) for the Catalan number C_n from the recurrence relation (1.3) of Definition 1.1.4. In other words, prove Theorem 1.1.2 from Proposition 1.1.1.

For this, call $F(x)$ the *generating function* of the sequence C_i ; that is to say the series

$$F(x) = \sum_{i=0}^{\infty} C_i x^i.$$

1. Prove that $F^2(x) = \sum_{i=0}^{\infty} C_{i+1} x^i = \frac{F(x)-1}{x}$.

2. Deduce that

$$F(x) = \frac{1 + \sqrt{1 - 4x}}{2x}.$$

(Hint: solve for F in $xF^2 = F - 1$, and discard the solution which diverges when $x \rightarrow 0^+$; our function must have $\lim_{x \rightarrow 0^+} F(x) = 1$.)

3. Recall Newton's binomial theorem:

$$(1+z)^{1/2} = \sum_{k=0}^{\infty} \binom{1/2}{k} z^k,$$

where the fractional binomial is defined as:

$$\binom{1/2}{k} = \frac{1/2(1/2-1)(1/2-2)\dots(1/2-k+1)}{k!}.$$

Apply it to $z = -4x$ and express the fractional binomial in terms of $\binom{2k}{k}$.

Exercise 1.6. For each of the four “Catalan structures” of Theorem 1.1.3 (other than triangulations), show that the recurrence formula (1.3) holds.

Exercise 1.7. (From triangulations to sign sequences) Show that the way we have constructed sign sequences in Theorem 1.1.3 is equivalent to the following one: Given a triangulation of the $(n+2)$ -gon, the sequence consists of $n+1$ blocks, one for each vertex of the polygon other than the first one. The $(i-1)$ -th block ($i = 2, \dots, n+2$) has length equal to the number of edges j_i , with $j < i$, except we do not count the reference edge $\{1, n+2\}$ in the last block. Each block consists of zero or more minuses ending in a single plus, except the last block where we only put minuses. Figure 1.49 shows the construction and also hints at an alternative description of it, where a sign is assigned to every edge other than the reference edge.

Exercise 1.8. Let $D(\mathbf{C}_n)$ denote the diameter of the graph of flips of the convex n -gon. Show that

$$D(\mathbf{C}_n) + 1 \leq D(\mathbf{C}_{n+1}) \leq D(\mathbf{C}_n) + 3$$

for every $n \geq 3$. (This is Part ii of Proposition 1.1.5. See the hints given there.)

Exercise 1.9. Prove that the diameter of the graph of flips in a convex n -gon is at least $\lfloor \frac{3n}{2} - 5 \rfloor$ for every n . More precisely, prove that for every even n , at least that number of flips is needed to go from a triangulation with no internal edges incident to even vertices to a triangulation with no internal edges incident to odd vertices, such as the ones in the figure.

Exercise 1.10. Adapt your solution of the previous exercise (or vice-versa) to show that the m -antiprism cannot be triangulated with less than $3m - 5$ tetrahedra [100]. Recall that the antiprism is the convex hull of two horizontal copies of an m -gon in \mathbb{R}^3 , at different heights and rotated to one another an angle π/m , as in Figure 1.51.

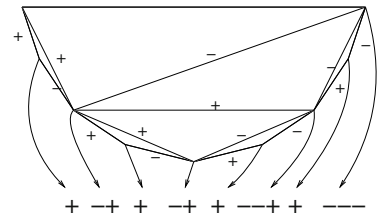


Figure 1.49: The sign sequence associated to a triangulation. Compare with Figure 1.11.

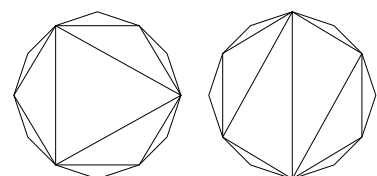


Figure 1.50: At least thirteen flips are needed to transform these triangulations to one another.

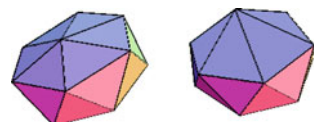


Figure 1.51: This polyhedron needs at least 13 tetrahedra to be triangulated.

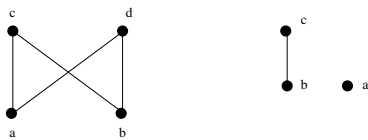


Figure 1.52: Describe the order polytopes associated to these two posets.

Exercise 1.11. Suppose you are given a planar polygon, but the subroutine that computes triangulations of polygons is broken. How can you still calculate the area of the polygon without using a triangulation? (*Hint:* essentially you only know the boundary of the polygon right?)

Exercise 1.12. Describe as completely as you can (dimension, vertices, facets, address, age, etc.) the order polytopes of the two posets in the Figure 1.52.

Exercise 1.13. Provide a proof of Sperner's lemma for arbitrary dimension. (*Hint:* Start with dimension two, then apply induction.)

Exercise 1.14. Prove that Brouwer's theorem is true for all homeomorphic balls if it is true for the simplex.

Exercise 1.15. Prove Sperner's lemma using Brouwer's theorem.

Exercise 1.16. Take a “deformed” combinatorial 3-cube, say the Cartesian product of a trapezoid with a segment, and find all possible triangulations. How many are there?

Exercise 1.17. Consider the family of parametric linear programming problems $\text{LP}_{\mathbf{A}, \mathbf{c}}(\mathbf{b})$, where \mathbf{A} is given by the 3×6 matrix

$$\mathbf{A} = \begin{bmatrix} 2 & 1 & 1 & 0 & 0 & 0 \\ 0 & 1 & 0 & 2 & 1 & 0 \\ 0 & 0 & 1 & 0 & 1 & 2 \end{bmatrix}.$$

1. Describe all the triangulations associated to the columns of \mathbf{A} (hint: there are 14 of them).
2. Prove that all triangulations are regular.
3. Consider the cost vector $\mathbf{c} = (1, 2, 1, 2, 1, 2)$. Find the regular triangulation associated to it. Find an optimal basis for the right-hand-side vector $\mathbf{b} = (1, 1, 1)$. Is it unique?
4. Draw the graph of flips. A flip in this example is either a change of diagonals or inserting or deleting one point in the triangulation. This is the graph of the secondary polytope. Does it look familiar?

Exercise 1.18. Consider the parametric system of equations

$$a_0xy^3 + a_1x^3 + a_2 = 0, \quad (1.12)$$

$$b_0x^2y^2 + b_1x^2 + b_2y^2 + b_3 = 0. \quad (1.13)$$

Determine bounds for the number of complex roots of the system using mixed subdivisions. If you are familiar with some computer algebra system, try to verify your answer using, for example, Gröbner bases.

Exercise 1.19 (See [121]). Consider the problem of finding an eigenvalue λ of an $n \times n$ matrix \mathbf{M} with rows \mathbf{M}_k , $k = 1, \dots, n$, together with a corresponding eigenvector $\mathbf{v} = (v_1, \dots, v_n)$ of norm one, all considered over the complex numbers. These objects can be considered as the solution of a system of polynomial equations:

$$\langle \mathbf{M}_k, \mathbf{v} \rangle = \lambda v_k \quad \forall k = 1, \dots, n \quad (\text{eigenvalue/eigenvector})$$

$$\sum_{k=1}^n (v_k)^2 = 1 \quad (\text{norm})$$

1. What is the maximal number of common solutions of this system according to the Bézout's bound?
2. What is the maximal number of common solutions of this system according to the Bernstein's bound?
3. What is the number of solutions of this system?

Exercise 1.20. Use Viro's method to construct the three isotopy types of maximal curves of degree six shown as in Figure 1.44. How many distinct triangulations did you need?

Exercise 1.21. Check that there are exactly 53 configurations of ovals that you can get from the three in Figure 1.44 by removing some of the ovals. (These 53, together with a single nest of three ovals and the two configurations in Figure 1.53, form the 56 possible configurations of real algebraic curves of degree six.)

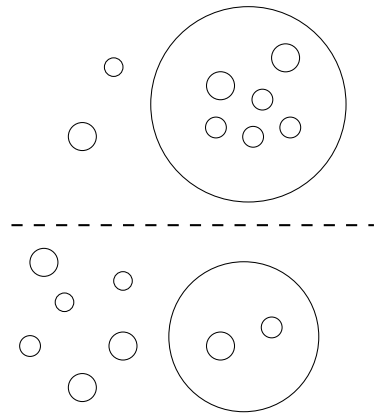


Figure 1.53: Two configurations which are possible in degree six.

Configurations, Triangulations, Subdivisions, and Flips

2

The first goal of this chapter is to introduce the necessary mathematical language to work with triangulations. This language includes the geometry of polyhedra and cones [339] and the combinatorics of point and vector configurations, as described by their oriented matroids [55]. These two books are recommended for more details. The second goal is to provide the reader with formal definitions and notation that are strong but flexible enough to cover all kinds of point configurations, and even the more general case of vector configurations. These definitions should include degeneracies, such as collinearities and repetition of points. We will do this slowly, intending to help the reader to see why a naive definition may lead to problems.

2.1 The official languages in the land of triangulations

When one looks at their purely geometric aspects, triangulations are made of polyhedra and thus they are described by convex geometry concepts like polytopes, cones, hyperplanes, etc. But when one cares about data structures, or if one is interested in combinatorial aspects, then combinatorics comes into play, and one is concerned about such things as labels, sign vectors, simplicial complexes, posets, etc. In this chapter we develop the “bilingual” setting that we use throughout the book.

2.1.1 Polyhedra and cones

A *convex combination* of a finite set of points $\mathbf{x}_1, \dots, \mathbf{x}_k$ in \mathbb{R}^m is any point \mathbf{x} that can be expressed as

$$\sum_{i=1}^k \lambda_i \mathbf{x}_i$$

with the $\lambda_i \in \mathbb{R}$ non-negative and summing to one. If non-negativity is dropped, then \mathbf{x} is an *affine combination*.

The *convex hull* of a set $\mathbf{X} \subset \mathbb{R}^m$, denoted $\text{conv}(\mathbf{X})$, is the intersection of all convex sets containing \mathbf{X} . Equivalently, a point \mathbf{x} is in $\text{conv}(\mathbf{X})$ if it is a convex combination of some finite subset of points in \mathbf{X} . Similarly, the set of all affine combinations of points in $\text{conv}(\mathbf{X})$ is called the *affine hull* or *affine span* of \mathbf{X} . Affine spans are always *affine subspaces*, also called *flats* of \mathbb{R}^m . That is, every affine span is a translated copy of a linear subspace (conversely, linear subspaces are affine subspaces passing through the origin).

The convex hull of finitely many points is called a *convex polytope*, but we will usually just call it a *polytope* since we will very rarely be concerned with non-convex ones (which we do not even define here). A *face* of a

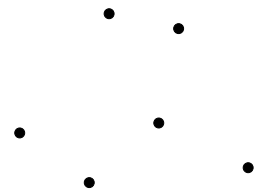


Figure 2.1: Points forming a set \mathbf{X}

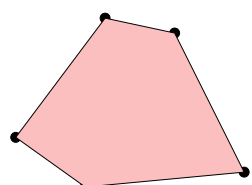


Figure 2.2: ... and the convex hull of \mathbf{X} .

polytope \mathbf{P} is the locus $\{\mathbf{x} \in \mathbf{P} : \psi(\mathbf{x}) \geq \psi(\mathbf{y}), \forall \mathbf{y} \in \mathbf{P}\}$ where a certain linear form $\psi : \mathbb{R}^m \rightarrow \mathbb{R}$ is maximized (or minimized). The whole \mathbf{P} is a face (obtained with $\psi = 0$) and, for convenience, the empty set is also accepted as a face. It is easy to prove that faces of a polytope are themselves polytopes and that faces of a face of \mathbf{P} are faces of \mathbf{P} as well. The *dimension* of a polytope, or of a face, is the dimension of its affine span. Faces of dimension zero, one, and $\dim(\mathbf{P}) - 1$ are called *vertices*, *edges*, and *facets* of \mathbf{P} , respectively.

Remark 2.1.1. Of course, if a polytope $\mathbf{P} \subseteq \mathbb{R}^m$ has dimension d , we can always find a projection $\mathbb{R}^m \rightarrow \mathbb{R}^d$ that “embeds” \mathbf{P} in dimension d keeping all its properties of interest (face lattice, triangulations, etc). But sometimes it is easier to define, or study, a d -dimensional polytope as lying in a proper flat of a higher dimensional space. For example, the standard d -dimensional simplex is better represented in \mathbb{R}^{d+1} as the intersection of the positive orthant with the hyperplane of coordinate sum equal to one. This representation preserves its symmetries. Also, one of the most important polytopes in this book, the *secondary polytope* of a point configuration, comes naturally embedded in a dimension much higher than its intrinsic dimension.

For this and other reasons (see Section 2.1.2, for example) we will make a distinction between the intrinsic dimension of \mathbf{P} , typically denoted d , and the ambient dimension, for which we usually reserve the letter m .

We write $\mathbf{F} \leq \mathbf{P}$ to mean that \mathbf{F} is a face of \mathbf{P} and $\mathbf{F} < \mathbf{P}$ to mean that \mathbf{F} is a proper face. If \mathbf{F} is a non-empty proper face and ψ is a functional defining it, the hyperplane $\{\mathbf{y} \in \mathbb{R}^m : \psi(\mathbf{x}) = \psi(\mathbf{y}), \forall \mathbf{x} \in \mathbf{F}\}$ is called a *supporting hyperplane*. Equivalently, a supporting hyperplane is a hyperplane whose intersection with \mathbf{P} is a non-empty face.

It is a well-known and fundamental theorem (see Chapters one and two of [339]) that a polytope can be described as either the convex hull of its set of vertices, or as the intersection of the half-spaces given by its facets. Here, a *half-space* is a set of the form $\{\mathbf{x} \in \mathbb{R}^m : \psi(\mathbf{x}) \geq c\}$, where ψ is a linear functional and $c \in \mathbb{R}$ is a constant. Any finite intersection of half-spaces is called a *polyhedron*. By Weyl-Minkowski’s theorem *polytopes* are the same as bounded polyhedra.

The boundary of \mathbf{P} is the union of its proper faces (equivalently, the union of its facets). The rest is the *relative interior* of \mathbf{P} . Every polytope is the disjoint union of the relative interiors of all its faces. Observe that the relative interior of a vertex is the vertex itself. The *carrier* in \mathbf{P} of a point $\mathbf{x} \in \mathbf{P}$ or of a subset $\mathbf{X} \subseteq \mathbf{P}$ is the minimal face of \mathbf{P} containing \mathbf{x} or \mathbf{X} , respectively. Equivalently, the carrier of a point is the unique face having \mathbf{x} in its relative interior.

A set of points is *affinely independent* (or *independent* for short) if none of them is an affine combination of the rest. It is called *dependent* otherwise. Equivalently, k points are independent if their convex hull has dimension $k - 1$. An affinely independent set is also called a *basis* of its affine span. The convex hull of an affinely independent set of $k + 1$ points is a *k -simplex*. Equivalently, a *k -simplex* is any polytope of dimension k with $k + 1$ vertices. Every face of a k -simplex is a simplex and it has 2^{k+1}

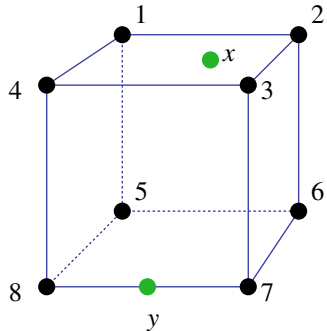


Figure 2.3: This polytope has 27 faces: 1 of dimension three, 6 of dimension 2 (facets), 12 of dimension 1 (edges), and 8 of dimension zero (vertices). Oh, and the empty face, which is usually said to have dimension -1 .
The carrier of x is the square $\text{conv}(1234)$. The carrier of y is the edge $\text{conv}(78)$.

possible faces. They are spanned by each of the possible subsets of points (the span of the empty set is the empty face). All k -simplices are affinely equivalent to one another. That is, if \mathbf{P} and \mathbf{Q} are simplices of the same dimension then there is an affine-linear bijection between $\text{aff}(\mathbf{P})$ and $\text{aff}(\mathbf{Q})$ sending \mathbf{P} to \mathbf{Q} .

So far we have been speaking about “affine” objects, but we will often need to consider the analogous objects in linear algebra. We now consider the elements of \mathbb{R}^m as “vectors” rather than “points”.

The *positive hull*, or *positive span*, of a finite set \mathbf{V} of vectors in \mathbb{R}^m is the set of vectors that can be obtained as non-negative linear combinations of our points.

$$\text{cone}(\mathbf{V}) := \left\{ \sum_{\mathbf{v} \in \mathbf{V}} \lambda_{\mathbf{v}} \mathbf{v} : \lambda_{\mathbf{v}} \geq 0 \quad \forall \mathbf{v} \in \mathbf{V} \right\}.$$

The sets of the form $\text{cone}(\mathbf{V})$ for a finite set of vectors \mathbf{V} is a *convex polyhedral cone*. Again, since we never deal with non-convex non-polyhedral cones, we simply call them *cones*. The *dimension* of a cone is the dimension of its *linear hull*, i.e., the linear subspace spanned by it. The *lineality space* of a cone is the largest linear subspace contained in it. A polyhedral cone is *pointed* if its lineality space is the zero subspace, or equivalently, if it does not contain any line.

As with polytopes, a *face* of a cone \mathbf{P} is the subset where a linear functional is maximized or minimized. The difference now is that when this happens the minimum, or maximum, must be zero. A *supporting hyperplane* for a face \mathbf{F} is a hyperplane that intersects \mathbf{P} exactly on \mathbf{F} , and the *relative interior* of a cone is the cone minus the union of its proper faces. We now collect some basic facts about cones. The first one is essentially Theorem 1.3 in [339].

Proposition 2.1.2. *A subset \mathbf{C} of \mathbb{R}^m is a polyhedral cone if and only if it is the intersection of finitely many linear halfspaces, i.e., there exists a finite index set I and $\psi_i \in (\mathbb{R}^m)^*$ for $i \in I$ such that*

$$\mathbf{C} = \left\{ \mathbf{x} \in \mathbb{R}^m : \psi_i(\mathbf{x}) \geq 0 \text{ for all } i \in I \right\}. \quad \square$$

Corollary 2.1.3. *Every linear hyperplane*

$$\left\{ \mathbf{x} \in \mathbb{R}^m : \psi(\mathbf{x}) = 0 \right\} = \left\{ \mathbf{x} \in \mathbb{R}^m : \psi(\mathbf{x}) \geq 0, -\psi(\mathbf{x}) \geq 0 \right\}$$

is a polyhedral cone. \square

Corollary 2.1.4. *The intersection of polyhedral cones is again a polyhedral cone.* \square

Recall that a (convex) polyhedron is any finite intersection of half-spaces. In particular, both polytopes and cones are polyhedra. Now we define polyhedral complexes:

Definition 2.1.5 (Polyhedral Complex). A set \mathcal{K} of polyhedra is a *polyhedral complex* if

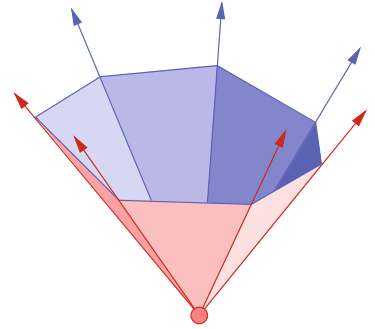


Figure 2.4: The positive hull of a finite set of vectors.

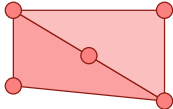


Figure 2.5: Is this a polyhedral complex?

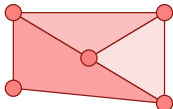
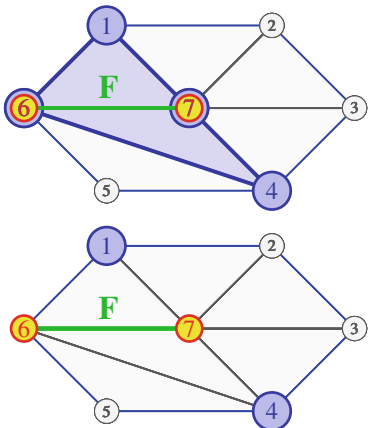
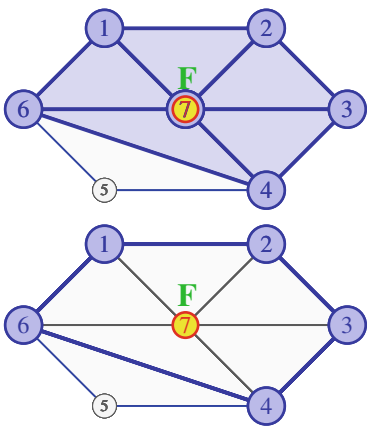


Figure 2.6: Not a polyhedral complex.

Figure 2.7: The star of the simplex $F = 67$ consists of the two triangles 167 and 467; the link consists of the two vertices 1 and 4.Figure 2.8: The star of the simplex $F = 7$ consists of the five triangles containing it; the link consists of their edges not containing 7.

(i) $\mathbf{P} \in \mathcal{K}$ and $\mathbf{F} \leq \mathbf{P}$ implies that $\mathbf{F} \in \mathcal{K}$.

(ii) $\mathbf{P} \cap \mathbf{Q} \leq \mathbf{P}$ and $\mathbf{P} \cap \mathbf{Q} \leq \mathbf{Q}$ for all $\mathbf{P}, \mathbf{Q} \in \mathcal{K}$.

The individual polyhedra in \mathcal{K} are called *cells* of the polyhedral complex. They are also sometimes called *faces* of the subdivision.

As an example, the set of all faces of a polytope, or of a polyhedron, is a polyhedral complex. The set of proper faces is another example called the *boundary complex*. Polyhedral subdivisions and triangulations of point sets, the central topic of this book, are also polyhedral complexes.

The dimension of a polyhedral complex is the highest among the dimensions of its cells. All cells of a polyhedral complex can be ordered by containment. A *maximal cell* is one that has no other cell containing it. A polyhedral complex is *pure* if all its maximal cells are of the same dimension. A (*geometric*) *simplicial complex* is one whose cells are all simplices. We will see more about (geometric and abstract) simplicial complexes in Section 2.6.1, but here are some important definitions.

Definition 2.1.6. • For any $\mathbf{F} \in \mathcal{K}$, the *star* of \mathbf{F} in \mathcal{K} , $\text{st}_{\mathcal{K}}(\mathbf{F})$, is the subcomplex of \mathcal{K} made up of all polyhedra of \mathcal{K} having \mathbf{F} as a face plus all their faces.

- The *link* of \mathbf{F} in \mathcal{K} is the polyhedral complex $\text{link}_{\mathcal{K}}(\mathbf{F}) = \{\mathbf{C} \in \mathcal{K} | \mathbf{F} \cap \mathbf{C} = \emptyset\}$. Note that the link of a $(k-1)$ -dimensional face \mathbf{F} , $\text{link}(\mathbf{F}, \mathcal{K})$, is a complex of dimension $d-k-1$.
- The *anti-star* of \mathbf{F} in \mathcal{K} is the polyhedral complex $\text{ast}_{\mathcal{K}}(\mathbf{F}) = \{\mathbf{C} \in \mathcal{K} | \mathbf{F} \cap \mathbf{C} = \emptyset\}$. Alternately:

$$\text{ast}_{\mathcal{K}}(\mathbf{F}) := (\mathcal{K} \setminus \text{st}_{\mathcal{K}}(\mathbf{F})) \cup \text{link}_{\mathcal{K}}(\mathbf{F})$$

- The *boundary* $\partial \mathcal{K}$ of a pure d -dimensional polyhedral complex \mathcal{K} is the polyhedral complex whose maximal faces consist of the $d-1$ faces contained in only one d -face. For example, the boundary of a simplicial ball is a simplicial sphere, and the boundary of a simplicial sphere is empty.

- We say that a polyhedral complex \mathcal{L} is a *subcomplex* of \mathcal{K} if $\mathcal{L} \subset \mathcal{K}$. The boundary of \mathcal{K} is an example of a subcomplex of \mathcal{K} .

Polyhedral complexes all of whose faces are cones are called fans:

Definition 2.1.7 (Fan). A *polyhedral fan* (or *fan* for short) in \mathbb{R}^m is a polyhedral complex consisting of polyhedral cones. A fan is *pointed* if all of its cones are pointed. A fan is *complete* if the union of all its cones is \mathbb{R}^m . \square

Observe that the face consisting of the origin must be the same in all the cones of a fan, and it coincides with the lineality space of them. So if a single cone in a fan is pointed, then all of the cones are.

Definition 2.1.8 (Normal Fan). Let \mathbf{P} be a polyhedron in \mathbb{R}^m . For a point $\mathbf{x} \in \mathbf{P}$ we define the *outer normal cone* of \mathbf{p} in \mathbf{P} in \mathbb{R}^m as

$$N_{\mathbf{P}}(\mathbf{x}) := \left\{ \psi \in (\mathbb{R}^m)^*: \langle \psi, \mathbf{x} \rangle \geq \langle \psi, \mathbf{y} \rangle \forall \mathbf{y} \in \mathbf{P} \right\}.$$

Put differently, $N_{\mathbf{P}}(\mathbf{x})$ consists of all the linear functionals whose maximum on \mathbf{P} is achieved at \mathbf{x} .

Similarly, for a face of \mathbf{P} , $\mathbf{F} \leq \mathbf{P}$ we say $N_{\mathbf{P}}(\mathbf{F})$ equals the cone $N_{\mathbf{P}}(\mathbf{x})$ for any \mathbf{x} in the relative interior of \mathbf{F} (this is clearly independent of the point chosen). $N_{\mathbf{P}}(\mathbf{F})$ is a polyhedral cone called the *outer normal cone* of \mathbf{F} in \mathbf{P} in \mathbb{R}^m .

The corresponding *inner normal cones* are defined as the negatives of the outer normal cones. The set

$$\mathcal{N}_{\mathbf{P}} := \left\{ N_{\mathbf{P}}(\mathbf{F}) : \mathbf{F} \leq \mathbf{P} \right\} = \left\{ N_{\mathbf{P}}(\mathbf{p}) : \mathbf{p} \in \mathbf{P} \right\}$$

is the *outer normal fan* of \mathbf{P} in \mathbb{R}^m .

Two polytopes \mathbf{P} and \mathbf{P}' are *normally equivalent* if their outer normal fans are the same:

$$\mathbf{P} \sim \mathbf{P}' \iff \mathcal{N}_{\mathbf{P}} = \mathcal{N}_{\mathbf{P}'} \quad \square$$

Proposition 2.1.9. Let \mathbf{P} be a polytope in \mathbb{R}^m , not necessarily full-dimensional. Then $N_{\mathbf{P}}(\mathbf{x})$ is full-dimensional (i.e., of dimension m), if and only if \mathbf{x} is a vertex of \mathbf{P} . \square

2.1.2 Point configurations

By a *point configuration* we mean a finite set of labeled points in real affine space \mathbb{R}^m , but we allow our set to have repeated points which receive different labels. To see why this may be useful, suppose for a moment that you project a 3-dimensional cube, as shown in Figure 2.11, in the direction of the diagonal line joining antipodal vertices a, b . Those two points are projected on top of each other. If you want to recall the top and bottom views of the cube (with respect to this direction) you get two similar but different two-dimensional pictures (see bottom of Figure 2.11). The issue is that the interior points used in the perspectives are different. It is then a good idea to remember that the plane of projection has, so to speak, two copies of the same point.

There are other fundamental operations that can be performed on point configurations which make repeated points natural and interesting. Among them are *Gale transforms* (see Section 4.1.3), the *contraction at a point* (see Section 4.2), and the *Minkowski sum* (see Section 9.2).

The best way to deal with repeated points is via labels. Every element of a point configuration will have a label, and all labels are assumed to be different. A repeated point will have several labels attached to it. Typically, but not necessarily, labels will be the first positive integer numbers. That is:

Definition 2.1.10. A *point configuration* in \mathbb{R}^m is a finite set of (perhaps repeated) points with (non-repeated) labels.

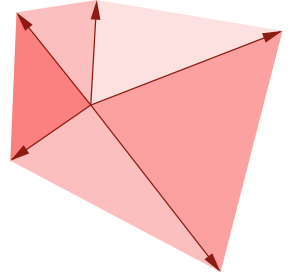


Figure 2.9: A complete pointed fan in dimension two.

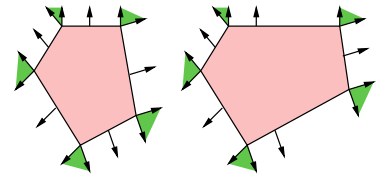


Figure 2.10: Two normally equivalent 5-gons.

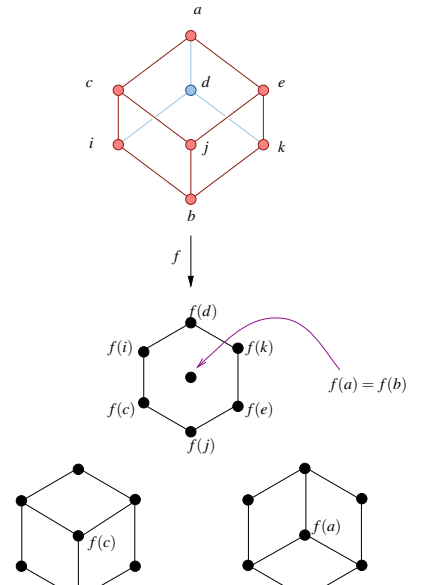


Figure 2.11: A situation when repeated points occur.

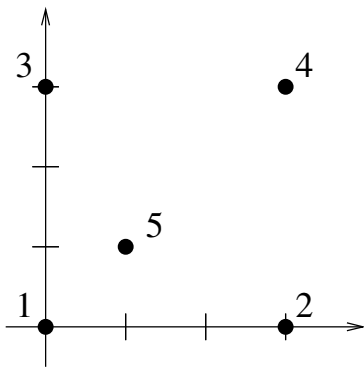


Figure 2.12: Five points in the plane.

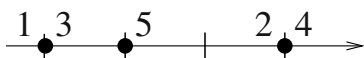


Figure 2.13: Five points along a line.

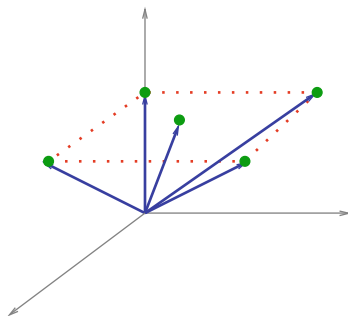


Figure 2.14: Homogenization of a five point planar configuration.

More formally, a point configuration in \mathbb{R}^m with set of labels J is a map $J \rightarrow \mathbb{R}^m$.

We will typically refer to elements of a configuration by their labels, not by their coordinates, saying, for example, that in Figure 2.12 the points 1, 5 and 4 are collinear. This takes care of ambiguities when we have repeated points, which are distinguished by their labels.

As a second advantage, we can carry labels from one configuration to another one, if the latter is obtained from the first by a geometric construction. For example, consider the projection of Figure 2.12 to Figure 2.13. This gives a different configuration \mathbf{A}' , but we can keep the same labels. In this way we can say things like: “2, 4, and 5 are independent in \mathbf{A} but dependent in \mathbf{A}' ”.

It is convenient to represent a configuration as the columns of a matrix. For example, the point configuration of Figure 2.12, consisting of the five points $(0,0)$, $(3,0)$, $(0,3)$, $(3,3)$, and $(1,1)$, would be represented as:

$$\begin{matrix} 1 & 2 & 3 & 4 & 5 \\ (0 & 3 & 0 & 3 & 1) \\ 0 & 0 & 3 & 3 & 1 \end{matrix}$$

The row above the matrix shows the labels we attach to the points. The matrix representation, among other things, makes repeated points familiar. They are just columns that happen to be equal.

But it is even more convenient to represent a point configuration in \mathbb{R}^d as a $(d+1) \times n$ matrix by adding a constant row. That is, the previous point configuration could be written instead as:

$$\mathbf{A} = \begin{pmatrix} 1 & 2 & 3 & 4 & 5 \\ 0 & 3 & 0 & 3 & 1 \\ 0 & 0 & 3 & 3 & 1 \\ 1 & 1 & 1 & 1 & 1 \end{pmatrix}$$

The addition of this extra coordinate is called *homogenization*. It is very helpful to use homogeneous coordinates in affine spaces, since it turns affine geometry into a special case of linear algebra. For example:

1. An affine dependence between the points $(0,0)$, $(3,0)$, $(0,3)$, $(3,3)$, and $(1,1)$ is any non-zero vector $\lambda = (\lambda_1, \dots, \lambda_5)$ with $\sum \lambda_i = 0$ and $\sum \lambda_i = 0$. Equivalently, it is a vector λ such that $\mathbf{A} \cdot \lambda = 0$, if \mathbf{A} is the homogeneous matrix of the point configuration.
2. Similarly, the fact that three points in \mathbf{A} are collinear, or the value area of the triangle they span in case they are not, are seen in the matrix as the vanishing, or the value, of the corresponding 3×3 determinant in the homogeneous matrix.

In Section 2.5 we will introduce triangulations of *vector*, rather than *point*, configurations. The use of homogeneous coordinates for point configurations will make this task seamless.

To represent a point configuration \mathbf{A} in homogeneous coordinates we do not really need to have a constant row. Homogeneous coordinates are based on the fact that the affine space \mathbb{R}^m can be naturally identified with *any* hyperplane of \mathbb{R}^{m+1} not passing through the origin. Hence, any matrix whose columns lie in such a hyperplane will do the job. We call such matrices *homogeneous*. Put differently, an $m \times n$ matrix \mathbf{A} is homogeneous if there is a row vector $\phi \in \mathbb{R}^m$ such that $\phi\mathbf{A}$ is a vector with all entries equal.

This freedom sometimes permits us to produce simpler coordinates, or coordinates that highlight symmetries. For example, the point configuration of Figure 2.15, consisting of the vertices of two concentric regular triangles, can be represented by the following matrix, whose columns all lie in the hyperplane $x_1 + x_2 + x_3 = 4$:

$$\begin{array}{cccccc} 1 & 2 & 3 & 4 & 5 & 6 \\ \left(\begin{array}{cccccc} 4 & 0 & 0 & 2 & 1 & 1 \\ 0 & 4 & 0 & 1 & 2 & 1 \\ 0 & 0 & 4 & 1 & 1 & 2 \end{array} \right) \end{array}$$

In this example, which we saw already in Section 1.2, each column gives the barycentric coordinates of the corresponding point with respect to the outer triangle, except that the barycentric coordinates have been normalized to add up to four, instead of one, for the convenience of getting integer numbers. Note that the coordinates can be changed via a rotation to have the points lying in the plane with coordinate $x_3 = 1$ instead of the plane $x_1 + x_2 + x_3 = 4$.

Summarizing what we have discussed:

A d -dimensional point configuration with n elements is represented as an $m \times n$ homogeneous matrix of rank $d + 1$. Usually, but not always, $m = d + 1$. Columns of the matrix are the elements of the configuration and will usually be identified by their labels.

Definition 2.1.11. The rank $d + 1$ of the matrix defining a point configuration is called the *rank* of the point configuration. The number $n - d + 1$, where n is the number of elements, is called the *corank* of the configuration. The *dimension* of a point configuration is the dimension of its convex hull. The dimension plus one is equal to the rank.

At this point let us make explicit some typesetting and notational conventions that we have been using so far and will keep using throughout the book:

- Subsets of \mathbb{R}^m (that is, polytopes, hyperplanes, cones, etc.) are denoted by upright boldface letters. This includes point configurations, as well as subconfigurations (submatrices made out from a subset of columns) ($\mathbf{A}, \mathbf{B}, \dots$), even if strictly speaking they are labeled subsets.

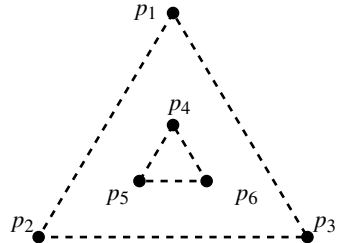


Figure 2.15: An interesting set of six points in the plane.

- Sets of labels are denoted by italic letters (J, I, Z). Our preference will be to use \mathbf{A} for the configuration and J for the label set.
- If C is a subset of the label set, then $\mathbf{A}|_C$ denotes the corresponding subconfiguration (the submatrix consisting of the columns labeled by C).
- Similarly, boldface lowercase letters ($\mathbf{p}, \mathbf{q}, \mathbf{z}$) will denote points or vectors in \mathbb{R}^m (e.g., the individual columns in a configuration) while italic lowercase letters represent individual labels (i, j, z).
- We will sometimes write matrices in abbreviated form. That is, $\mathbf{A} = (\mathbf{p}_1, \dots, \mathbf{p}_n)$ if $\{1, \dots, n\}$ is the set of labels or $\mathbf{A} = (\mathbf{p}_j)_{j \in J}$ for a general label set J .

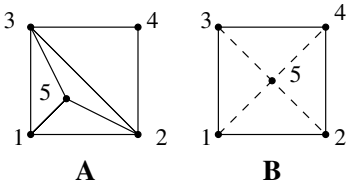


Figure 2.16: $\{125, 135, 325, 234\}$ is a triangulation of **A**, but not of **B**.

2.1.3 Geometry of point configurations

Let us look more closely at the consequences of our decision of referring to points by their labels. The left part of Figure 2.16 displays a triangulation of the point configuration **A** of the previous section. Triangles can be then referred to as triplets of labels, such as $\{1, 2, 5\}$, $\{1, 3, 5\}$, etc. To simplify notation, we sometimes abbreviate them as 125, 135, etc. As with point configurations, one advantage of this is that then we can also say things like “ \mathcal{T} is a triangulation of **A**, but not of **B**”, where **B** is the configuration on the right of the same figure, obtained from **A** by a perturbation.

If we accept this, then sentences like “ $\{1, 2\}$ is a facet of $\{1, 2, 5\}$ ” have to be allowed in our language. In this setup we can speak as if the sets of labels themselves were geometric objects, which have a convex hull, faces, etc. Thus when dealing with point configurations the convex set structure takes second place to the combinatorics.

Let us repeat most of the definitions of 2.1.1 in this new “labeled” setting.

Definition 2.1.12 (Convex hull, relative interior). Let $\mathbf{A} = (\mathbf{p}_j)_{j \in J}$ be a point configuration in \mathbb{R}^m , with set of labels J . For a subset C of J we define the *convex hull of C in \mathbf{A}* to be the following closed convex set:

$$\text{conv}_{\mathbf{A}}(C) := \left\{ \sum_{j \in C} \lambda_j \mathbf{p}_j : \lambda_j \geq 0 \text{ for all } j \in C, \text{ and } \sum_{j \in C} \lambda_j = 1 \right\}. \quad (2.1)$$

The *dimension* and *relative interior* of C are defined to be the dimension and relative interior of its convex hull. We recall that the latter is the following relatively open (i.e., open in its affine hull) convex set:

$$\text{relint}_{\mathbf{A}}(C) := \left\{ \sum_{j \in C} \lambda_j \mathbf{p}_j : \lambda_j > 0 \text{ for all } j \in C, \text{ and } \sum_{j \in C} \lambda_j = 1 \right\}. \quad (2.2)$$

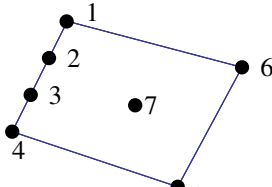


Figure 2.17: The relative interior of **A** is the rectangle without its border.

Remark 2.1.13. Every (nonempty) point configuration has a non-empty relative interior. For example, if C has only one element, that point is its relative interior (more precisely, $\text{relint}_{\mathbf{A}}(\{b\}) = \text{conv}_{\mathbf{A}}(\{b\}) = \{\mathbf{p}_b\}$).

Remark 2.1.14. Note that if \mathbf{A} is a point configuration with label set J and $R \subset C \subset J$, then $\text{conv}_{\mathbf{A}|_C}(C) = \text{conv}_{\mathbf{A}}(C)$. Thus, whenever the configuration to which the labels refer is clear, we will simply write $\text{conv}(R)$ and $\text{relint}(R)$. This applies to most of the notation introduced in this section.

Definition 2.1.15 (dependent, spanning, general and convex position). Let \mathbf{A} be a point configuration of dimension d with label set J . Let C be a subset of the label set J .

- (i) We say that C is *dependent* in \mathbf{A} if there is a non-zero vector $(\lambda_j)_{j \in C}$ such that

$$\sum_{j \in C} \lambda_j \mathbf{p}_j = 0 \text{ and } \sum_{j \in C} \lambda_j = 0.$$

It is called *independent* otherwise.

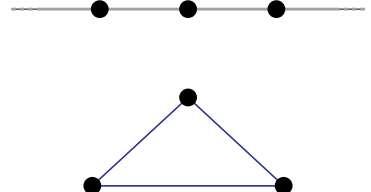


Figure 2.18: Three dependent points (top) and three independent points (bottom).

- (ii) We say that C is *spanning* if $\text{conv}(C)$ has the same dimension as $\text{conv}(J)$.
- (iii) C is *in general position* if each subset with at most $d + 1$ elements is independent. Equivalently, if every dependent set is spanning in $\mathbf{A}|_C$. If a set is not in general position we say it is in *special position*.
- (iv) An element $j \in J$ is *extremal* in \mathbf{A} if the corresponding point \mathbf{p}_j is not repeated in \mathbf{A} and is a vertex of $\text{conv}_{\mathbf{A}}(J)$. A point configuration is *in convex position* if all its elements are extremal.

Remark 2.1.16. Observe that if C has a repeated point (that is, two labels i and j pointing to the same point $\mathbf{p}_i = \mathbf{p}_j$), then C is necessarily dependent, since $\mathbf{p}_i - \mathbf{p}_j = 0$ is a dependence.

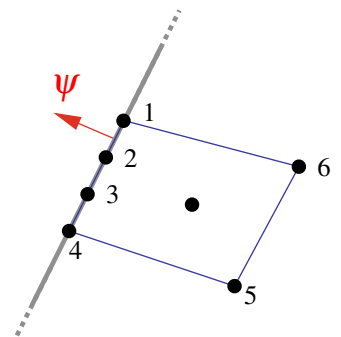


Figure 2.19: Face of C in the direction ψ is 1234.

Definition 2.1.17 (Face). Let $\mathbf{A} = (\mathbf{p}_1, \dots, \mathbf{p}_n)$ be a point configuration in \mathbb{R}^m , with set of labels J . Let $C \subset J$. For a linear functional $\psi \in (\mathbb{R}^m)^*$, the *face* of C in direction ψ is the following subset of C :

$$\text{face}_{\mathbf{A}}(C, \psi) := \left\{ j \in C : \psi(\mathbf{p}_j) = \max_{b \in C} (\psi(\mathbf{p}_b)) \right\}. \quad (2.3)$$

The affine hyperplane $\{ \mathbf{x} \in \mathbb{R}^m : \psi(\mathbf{x}) = \psi(\mathbf{p}_j), j \in F \} \subset \mathbb{R}^m$ is called a *supporting hyperplane* of the face F . The empty subset is considered a face and C is always a face of C , obtained with the zero functional. If F is a face of C , we write $F \leq_{\mathbf{A}} C$. If, moreover, $F \neq C$ then we write $F <_{\mathbf{A}} C$, and we say that F is a *proper face* of C . A *facet* of C is a face of dimension one less than the dimension of C , that is, it is a maximal proper face.

Remark 2.1.18. A face of a face of C is also a face of C , as is any intersection of faces.

Remark 2.1.19. $\text{relint}_{\mathbf{A}}(C) = \text{conv}_{\mathbf{A}}(C) \setminus \bigcup_{F < C} \text{conv}_{\mathbf{A}}(F)$. Thus, $\text{conv}_{\mathbf{A}}(C)$ equals $\bigcup_{F \leq C} \text{relint}_{\mathbf{A}}(F)$, where \bigcup denotes “disjoint union”.

Remark 2.1.20. We have the following connections to the corresponding concepts of convex geometry:

- (i) $\text{conv}_A(\text{face}_A(C, \psi))$ equals the face of the polytope $\text{conv}_A(C)$ in the direction of ψ .
- (ii) If $F <_A C$, then $\text{conv}_A(F) < \text{conv}_A(C)$, but in general the reverse implication is not true.
- (iii) If B is in general position, then $\text{conv}_A(F) < \text{conv}_A(C)$ implies $F <_A C$ too. This is because all proper faces are spanned by independent sub-configurations.
- (iv) $\bigcup_{F < C} \text{conv}_A(F) = \partial(\text{conv}_A(C))$.

Remark 2.1.21. A single element $\{j\}$ is a face of C if and only if \mathbf{p}_j is not repeated and is a vertex of $\text{conv}_A(C)$ in the usual sense. This is exactly what we defined as an *extremal point* of C .

Definition 2.1.22 (Carrier). Let A be a configuration in \mathbb{R}^m . Let C be a set of labels and let $\mathbf{X} \subseteq \text{conv}_A(C)$ and $R \subset C$. The *carrier* of \mathbf{X} in C is the smallest face of C whose convex hull contains \mathbf{X} . That is,

$$\text{carrier}_A(\mathbf{X}, C) := \bigcap_{\substack{\mathbf{X} \subseteq \text{conv}_A(F) \\ F \leq C}} F. \quad (2.4)$$

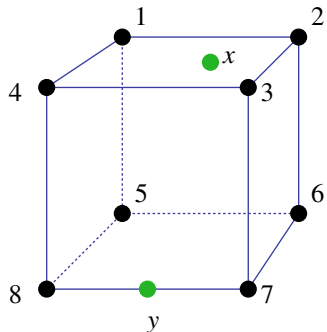


Figure 2.20: The carrier of x is $\{1, 2, 3, 4\}$. The carrier of y is $\{7, 8\}$.

The carrier of R in C is $\text{carrier}_A(R, C) := \bigcap_{R \subseteq F \leq C} F$. Clearly, $\text{carrier}_A(R, C)$ equals $\text{carrier}_{A|C}(R, C)$.

Sometimes the easiest way to prove that something is a face is to check that it coincides with its own carrier. For this trick, which will be applied several times in Section 4.5.1, the following lemma is useful.

Lemma 2.1.23. For every pair of subsets R, C of labels of a point configuration A that satisfy $R \subseteq C$ we have

$$\text{relint}_A(R) \subseteq \text{relint}_A(\text{carrier}_A(R, C)). \quad (2.5)$$

Remark 2.1.24. In fact, something more general is true: since different faces have disjoint relative interiors, the carrier of C is the unique face F with $\text{relint}_A(C) \subseteq \text{relint}_A(F)$. In particular, as in the geometric case, the carrier of a point \mathbf{x} in C is the unique (by Remark 2.1.19) face F of C with $\mathbf{x} \in \text{relint}_A(F)$.

Proof. We have to show that $\text{relint}_A(R) \cap \partial \text{conv}_A(\text{carrier}_A(R, C)) = \emptyset$.

Assume, for the sake of contradiction, that there exists a point \mathbf{x} in $\text{relint}_A(R) \cap \partial \text{conv}_A(\text{carrier}_A(R, C))$. Since \mathbf{x} is not in the boundary of $\text{conv}_A(R)$, each hyperplane $\mathbf{H} \subset \mathbb{R}^m$ through \mathbf{x} must either separate the points in $\text{conv}_A(R)$ (i.e., there are points in $\text{conv}_A(R)$ on both sides of \mathbf{H}) or \mathbf{H} must contain all of $\text{conv}_A(R)$. In particular, it must either separate the points in $A|_R$ or contain all points in A_R . Since $R \subseteq \text{carrier}_A(R, C)$ by definition of the carrier, each hyperplane through \mathbf{x} must either separate $\text{carrier}_A(R, C)$, or contain all points of $A|_R$. Since \mathbf{x} is in the boundary

of $\text{carrier}_{\mathbf{A}}(R, C)$, there is a hyperplane \mathbf{H} through \mathbf{x} neither separating $\text{carrier}_{\mathbf{A}}(R, C)$ nor containing all of $\text{carrier}_{\mathbf{A}}(R, C)$. Therefore, \mathbf{H} must contain $\mathbf{A}|_R$ completely. This, however, implies that $\mathbf{A}|_R$ is contained in $\text{carrier}_{\mathbf{A}}(R, C) \cap \mathbf{H} \neq \text{carrier}_{\mathbf{A}}(R, C)$, a contradiction with the minimality of the carrier. \square

Lemma 2.1.25. (i) For subsets $R \subseteq F \leq C$ of labels of a point configuration \mathbf{A} , we have

$$\text{carrier}_{\mathbf{A}}(R, F) = \text{carrier}_{\mathbf{A}}(R, C). \quad (2.6)$$

(ii) For subsets $F \leq C$ of labels of a point configuration \mathbf{A} and a point $\mathbf{x} \in \text{conv}_{\mathbf{A}}(F)$, we have

$$\text{carrier}_{\mathbf{A}}(\mathbf{x}, F) = \text{carrier}_{\mathbf{A}}(\mathbf{x}, C). \quad (2.7)$$

(iii) For subsets $F \leq C$ of labels of a point configuration \mathbf{A} and a subset $\mathbf{X} \subseteq \text{conv}_{\mathbf{A}}(F)$ we have

$$\text{carrier}_{\mathbf{A}}(\mathbf{X}, F) = \text{carrier}_{\mathbf{A}}(\mathbf{X}, C). \quad (2.8)$$

Proof. We only prove the first assertion; the remaining items are analogous and left to the reader. Let $R \subseteq F \leq C$ be subsets of labels of a point configuration \mathbf{A} . Then:

$$\begin{aligned} \text{carrier}_{\mathbf{A}}(R, F) &= \bigcap_{\substack{G \leq F \\ R \subseteq G}} G \\ &= F \cap \bigcap_{\substack{G \leq C \\ R \subseteq G}} G \\ &= \bigcap_{\substack{G \leq C \\ R \subseteq G}} G \\ &= \text{carrier}_{\mathbf{A}}(R, C). \end{aligned}$$

The second to last equality is true because $F \leq C$. \square

In words, this means that the carrier does not change if you (properly) enlarge the object in which the carrier is taken.

2.2 A closer look at the definition of triangulation

Here will demonstrate that the language developed in Section 2.1.3 is now adequate for our purposes. Nevertheless, let us first work with the probably more familiar language of Section 2.1.1 and pinpoint some of its limitations. We will discover that things actually become simpler by the use of a seemingly more abstract language.

We take as starting point the definition of triangulations given at the beginning of the book.

Definition 2.2.1. A *triangulation* of a point configuration \mathbf{A} is a collection \mathcal{T} of simplices, with vertices in \mathbf{A} , that satisfies the following properties:

1. All faces of simplices of \mathcal{T} are in \mathcal{T} . (*Closure Property*)
2. The intersection of any two simplices of \mathcal{T} is a (possibly empty) face of both. (*Intersection Property*.)
3. The union of all these simplices equals $\text{conv}(\mathbf{A})$. (*Union Property*)

Note that the first two properties are the definition of a (geometric) *simplicial complex*. In other words: a triangulation of \mathbf{A} is a *simplicial complex with vertex set contained in \mathbf{A} and which covers $\text{conv}(\mathbf{A})$* .

In our definition we do not assume $\text{conv}(\mathbf{A})$ to be full-dimensional. In particular, we may speak of triangulations of a single point (there is one!), or of triangulations of a face of $\text{conv}(\mathbf{A})$, as in the following statement, proved in Lemma 2.3.4 in a more general context.

Lemma 2.2.2. Let \mathcal{T} be a triangulation of a point configuration \mathbf{A} and let \mathbf{F} be a face of $\text{conv}(\mathbf{A})$. Then, the following is a triangulation of $\mathbf{A} \cap \mathbf{F}$:

$$\mathcal{T}_{\mathbf{F}} := \{ \sigma \in \mathcal{T} : \sigma \subset \mathbf{F} \}.$$

Observe that we do not require *all* the points of \mathbf{A} to be used as vertices in a triangulation. For example, the configuration of Figure 2.12 has the four triangulations shown in Figure 2.21. Two of them use the five points and have four triangles, and two use only four points and have two triangles. Similarly, the six points in Figure 2.15 have 18 triangulations, only 8 of which use all points. Of course, all vertices of $\text{conv}(\mathbf{A})$ are used in all triangulations.

2.2.1 There is always a triangulation

Our first goal is to show that every point configuration has at least one triangulation. The method we are going to use is conceptually the simplest way to compute triangulations of point configurations. It is surprisingly general and it is central to the structure of the set of all triangulations of \mathbf{A} . The process, illustrated in Figure 2.22, is as follows:

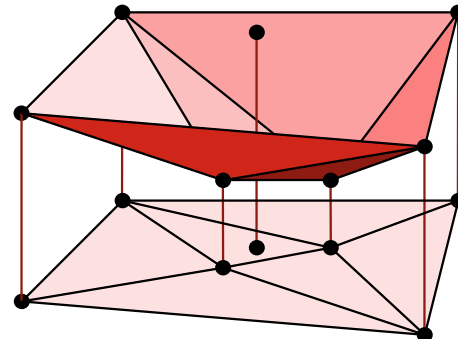


Figure 2.22: The lifting construction.

Let $\mathbf{A} = (\mathbf{p}_1, \dots, \mathbf{p}_n)$ be a point configuration in \mathbb{R}^m :

1. Pick a *height function* $\omega : \mathbf{A} \rightarrow \mathbb{R}$ (ω can be thought of as a vector $\omega = (\omega_1, \dots, \omega_n) \in \mathbb{R}^n$, with $\omega_i = \omega(\mathbf{p}_i)$), and consider the *lifted point configuration* in \mathbb{R}^{n+1}

$$\mathbf{A}^\omega := \begin{pmatrix} \mathbf{p}_1 & \dots & \mathbf{p}_n \\ \omega_1 & \dots & \omega_n \end{pmatrix}.$$

2. Compute the face structure of the polytope $\mathbf{P} = \text{conv}(\mathbf{A}^\omega)$. A *lower face* of \mathbf{P} is a face “visible from below”, that is, a face that can be defined by minimizing a linear functional ψ which is positive on the last coordinate (equivalently, a face that has a non-vertical supporting hyperplane \mathbf{H} and with \mathbf{P} above \mathbf{H}).
3. Lower faces, since they are not vertical, project bijectively to polytopes inside $\text{conv}(\mathbf{A})$. Moreover, as we will prove in a more general context in Lemma 2.3.11, the collection of projected lower faces always satisfies the three properties in the definition of triangulation. So, if all lower faces of \mathbf{P} are simplices, their projections form a triangulation of \mathbf{A} .

Definition 2.2.3 (Regular Triangulation). A triangulation of a point configuration \mathbf{A} in \mathbb{R}^m is called *regular* if it can be obtained by projecting the lower envelope of a lifting of \mathbf{A} to \mathbb{R}^{m+1} .

Regular triangulations have appeared in different mathematical contexts and have actually received different names, such as *convex*, *weighted Delaunay*, *Gale*, or *coherent* triangulations.

Proposition 2.2.4. *Every point configuration has regular triangulations.*

While reading the proof, observe that we profit from the use of homogeneous coordinates for our point configuration.

Proof. We need to check that for any given \mathbf{A} there are height functions ω for which \mathbf{A}^ω has the property that “all lower faces of $\text{conv}(\mathbf{A}^\omega)$ are simplices”. A sufficient condition for this to happen can be stated as: Every affine basis \mathbf{B} contained in \mathbf{A} is lifted so that the unique hyperplane containing the lifted point set \mathbf{B}^ω contains no other point \mathbf{p}^ω of \mathbf{A}^ω .

For a given basis $\mathbf{B} = \{\mathbf{p}_1, \dots, \mathbf{p}_{d+1}\} \subseteq \mathbf{A}$ and extra point $\mathbf{p} \in \mathbf{A} \setminus \mathbf{B}$ this condition is equivalent to the non-vanishing of the determinant

$$\left| \begin{array}{cccc} \mathbf{p}_1 & \dots & \mathbf{p}_{d+1} & \mathbf{p} \\ \omega(\mathbf{p}_1) & \dots & \omega(\mathbf{p}_{d+1}) & \omega(\mathbf{p}) \end{array} \right|.$$

This determinant is a linear equation on the ω 's with non-zero coefficient on (at least) $\omega(\mathbf{p})$, hence it is non-zero except on a certain hyperplane in the space \mathbb{R}^n of possible heights. As a conclusion, almost any choice satisfies the condition. More technically, there is an open dense subset of choices of ω in \mathbb{R}^n that satisfies the condition: any ω lying in the complement of a certain union of finitely many hyperplanes. \square

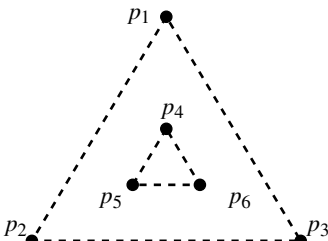


Figure 2.23: The mother of all examples and its six labeled points.

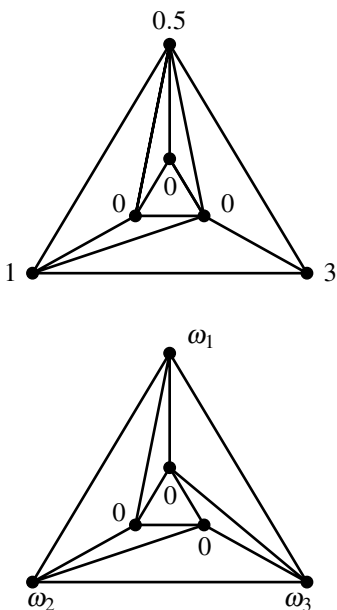


Figure 2.24: Two triangulations of the mother of all examples.

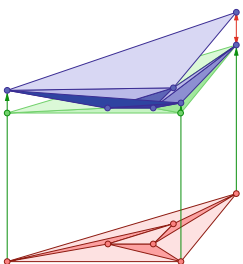


Figure 2.25: Fixing the height on the middle triangle and on the vertex in the background followed by tweaking the remaining heights (in order to “fold” along the missing diagonals) leads to a contradiction at the height of the vertex in the background.

The reader can verify without trouble that all the triangulations of (the vertex set of) a convex n -gon are regular. The same happens for the triangulations of our five-point example, displayed in Figure 2.21 (we will check this in detail in Section 2.2.3). But some point configurations have *non-regular triangulations*, which resemble Escher’s famous “impossible pictures”; they look like projections of something from a higher dimension, but they really are not. Here is a *very important example*:

Example 2.2.5 (The mother of all examples). Consider the two concentric triangles of Figure 2.23, whose coordinates we recall:

$$\mathbf{M} := \begin{pmatrix} 1 & 2 & 3 & 4 & 5 & 6 \\ 4 & 0 & 0 & 2 & 1 & 1 \\ 0 & 4 & 0 & 1 & 2 & 1 \\ 0 & 0 & 4 & 1 & 1 & 2 \end{pmatrix}$$

Figure 2.24 shows two triangulations of this configuration. The triangulation on top is produced by the heights shown in the picture. But the other one is not produced by any choice of heights, as we prove by contradiction. To simplify the argument, we first observe that there is no loss of generality in assuming that the three height values for the interior triangle are zero (see Exercise 2.1). The other three values must be strictly positive in order for the three interior points to be lower vertices of the lifted configuration.

Moreover, using the labels of Figure 2.23, the exact condition on ω_1 , ω_2 , and ω_3 that makes the edge 15 appear in the second triangulation is that $\omega_1 < \omega_2$. The same happens for the diagonals 26 and 34, giving rise to the following impossible sequence of inequalities.

$$\omega_1 < \omega_2 < \omega_3 < \omega_1.$$

See Figure 2.25 for an illustration of the lifting discussed.

2.2.2 A famous example: the Delaunay triangulation

Perhaps due to their easy construction, regular triangulations are often the prime examples of triangulations. Actually, special choices of the height vector ω produce some of the most studied and nicest triangulations. Here we study one of them, and more important examples will come in Section 4.3.

The *Delaunay triangulation* is arguably the most important triangulation of a point set for applications, and there is a vast literature about it (see, for example, [45, 129]). On the one hand, it is geometrically dual to the *Voronoi diagram* of the point set. The Voronoi cell of a point \mathbf{p} in a point configuration \mathbf{A} is the locus of points that are at least as close to \mathbf{p} as to any other point of \mathbf{A} . The Voronoi diagram of \mathbf{A} is the polyhedral complex whose maximal cells are the Voronoi cells. Clearly, Voronoi diagrams are important tools for solving proximity questions. This means Delaunay triangulations are useful too, since they carry exactly the same combinatorial information as Voronoi diagrams. As another example of usefulness, the set of edges of a Delaunay triangulation of any point set in the plane contains the minimum Euclidean spanning tree of the point set.

On the other hand, the Delaunay triangulation of a point set is considered to be one of the most uniform triangulations of it, meaning that its simplices are, on average, as close to regular simplices as possible. This makes a Delaunay triangulation a good candidate for meshing problems. For example, in two dimensions the Delaunay triangulation of \mathbf{A} has, for example, the following properties: It is the triangulation that minimizes both the maximum angle and the maximum circumradius of its triangles (it also maximizes the minimum circumradius). See Corollary 3.2.7 for the proofs of these and other properties.

Delaunay triangulations are also important examples of regular triangulations.

Definition 2.2.6. Let $\mathbf{A} \subset \mathbb{R}^d$ be a finite point set of dimension d . If the lifting procedure applied to the heights

$$\omega(i) = \|\mathbf{p}_i\|^2 = a_1^2 + a_2^2 + \cdots + a_d^2, \text{ for each } \mathbf{p}_i = (a_1, \dots, a_d) \in \mathbf{A},$$

produces a triangulation, then this triangulation is called the *Delaunay triangulation* of \mathbf{A} .

Put differently, we are lifting the points onto a paraboloid (as indicated in Figure 2.27). Let us further analyze this triangulation and see when it is well-defined. Observe that we are assuming that our configuration is full-dimensional. This simplifies some of the arguments in the following results.

Lemma 2.2.7. Let $\mathbf{C} \subset \mathbb{R}^{d+1}$ be the paraboloid given by the equation

$$x_{d+1} = x_1^2 + \cdots + x_d^2,$$

and let $\mathbf{H} \subset \mathbb{R}^{d+1}$ be a non-vertical hyperplane, that is, one whose normal vector has non-zero last coordinate. Let \mathbf{S} be the projection of $\mathbf{H} \cap \mathbf{C}$ into \mathbb{R}^d obtained by dropping the last coordinate. Then \mathbf{S} is either empty, a single point, or a sphere in \mathbb{R}^d . See Figure 2.28.

Proof. Since \mathbf{H} is not vertical, we can isolate the variable x_{d+1} in its defining equation. That is, \mathbf{H} is defined by an equation

$$x_{d+1} = \lambda_1 x_1 + \cdots + \lambda_d x_d + \lambda_0.$$

The intersection of \mathbf{H} and \mathbf{C} then satisfies the equation

$$x_1^2 + \cdots + x_d^2 = \lambda_1 x_1 + \cdots + \lambda_d x_d + \lambda_0,$$

which is equivalent to

$$(x_1 - \lambda_1/2)^2 + \cdots + (x_d - \lambda_d/2)^2 = (\lambda_1/2)^2 + \cdots + (\lambda_d/2)^2 + \lambda_0.$$

Since this equation does not involve the variable x_{d+1} , it is satisfied on the projection of $\mathbf{C} \cap \mathbf{H}$. Depending on whether the right-hand side is negative, zero or positive, it defines the empty set, a single point, or a sphere. \square

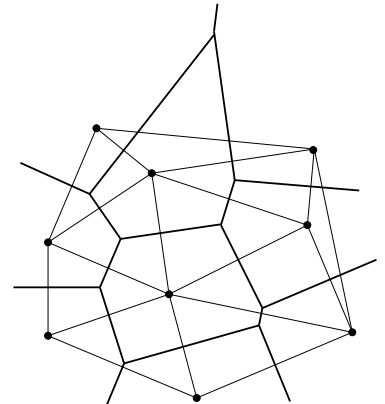


Figure 2.26: A Voronoi diagram and its dual Delaunay triangulation.

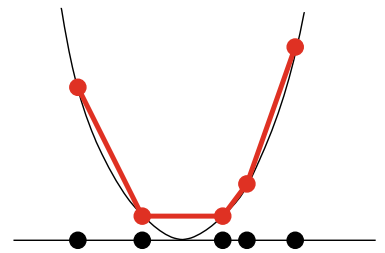


Figure 2.27: Delaunay triangulation of a 1-dimensional configuration.

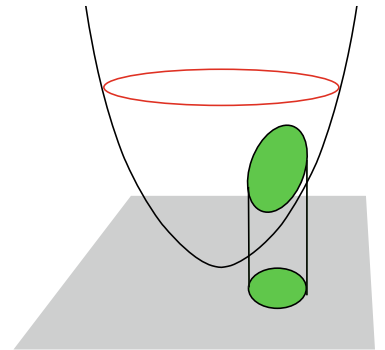


Figure 2.28: A hyperplane intersected with the paraboloid.

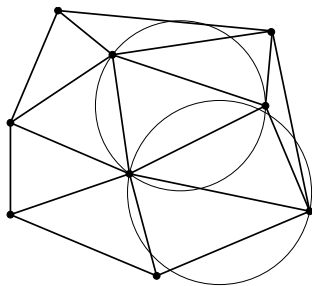


Figure 2.29: The empty-sphere property for an edge and a triangle in a Delaunay triangulation.

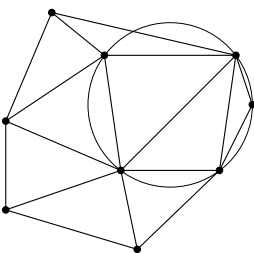
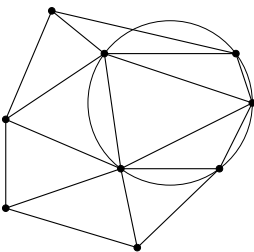


Figure 2.30: The empty sphere property of two Delaunay triangulations for a degenerate point configuration.

The following result indicates that the facets (highest dimension cells) of the Delaunay subdivision can be identified by a simple “empty sphere criterion”. That this is the case beyond two dimensional space was first observed in [204].

Corollary 2.2.8. *Let $\mathbf{A} \subset \mathbb{R}^d$ be a finite point set and let $\omega : \mathbf{A} \rightarrow \mathbb{R}$ be the height function*

$$\omega(i) = \|\mathbf{p}_i\|^2.$$

Let $\mathbf{B} \subset \mathbf{A}$ be a subset such that $\text{conv}(\mathbf{B})$ is full-dimensional. Then \mathbf{B} corresponds to the vertex set of a lower facet of the lifted point set if and only if there is a sphere passing through all points of \mathbf{B} and leaving all points of $\mathbf{A} \setminus \mathbf{B}$ outside.

Proof. Since \mathbf{B} is full-dimensional, there is at most one sphere passing through all points of \mathbf{B} . If there is no such sphere, then by Lemma 2.2.7, \mathbf{B} is not lifted to a hyperplane, hence it does not lie on a facet of the lifted point set. If there is such a sphere \mathbf{S} , then there is a hyperplane $\mathbf{H}_{\mathbf{B}}$ passing through the lifted point set. Points in the interior, on the surface and in the exterior of the sphere \mathbf{S} are lifted respectively to points below $\mathbf{H}_{\mathbf{B}}$, on $\mathbf{H}_{\mathbf{B}}$ or above $\mathbf{H}_{\mathbf{B}}$ (see Figure 2.28). Then \mathbf{B} is lifted to the vertex set of a lower facet if and only if there is no point in the interior of the sphere and the points on the surface are precisely those of \mathbf{B} . \square

In particular, simplices in the Delaunay triangulation are characterized by the “empty sphere” property: σ is a simplex in it if and only if there is a Euclidean sphere circumscribed to σ (i.e., with all vertices of σ on the surface of the sphere) with the rest of the points of \mathbf{A} outside; see Figure 2.29.

The corollary also gives a simple sufficient condition to guarantee that the Delaunay triangulation is uniquely defined: that no $d + 2$ points lie in the surface of any sphere. But, what if this is not the case and the lifting to the paraboloid does not produce a triangulation? In this case there are two approaches to defining a Delaunay triangulation. You can either

1. Give up uniqueness and call *Delaunay triangulations* all the triangulations that “refine” the projection of the lower envelope of the lifted point set, or
2. Give up simpliciality and call the projection that you get a *Delaunay subdivision*. This is indeed a subdivision of $\text{conv}(\mathbf{A})$ into convex polytopes that intersect face to face (that is, it is a *polyhedral complex*).

In applications, the first approach is what is usually used. After all, one of the reasons to construct the Delaunay triangulation is that one wants a triangulation in the first place! In this setting, a Delaunay triangulation is any triangulation \mathcal{T} whose simplices have the following “weak” empty sphere property: for any $\sigma \in \mathcal{T}$, there is a Euclidean sphere circumscribed to σ with no point of \mathbf{A} inside (but perhaps with extra points on its surface).

But, conceptually, the second approach is nicer. For example, the Delaunay subdivision is still dual to the corresponding Voronoi diagram; as

Figure 2.31 shows, its cells are characterized by the same empty sphere property as in the general position case: a polytope $\sigma \subset \text{conv}(\mathbf{A})$ with vertex set contained in \mathbf{A} is a cell in the complex if and only if there is a sphere circumscribed to σ with the rest of \mathbf{A} outside.

As a curious historical remark, although the spelling “Delaunay” is the standard one in Computational Geometry, the spelling “Delone” triangulations is also used in other areas. Both spellings honor the same Russian geometer Boris Nikolaevich Delone [123], who studied these triangulations mostly for infinite periodic point configurations (lattices) [103].

2.2.3 Regular subdivisions and their structure

Let a configuration \mathbf{A} be given. In Proposition 2.2.4 we have seen that for any sufficiently generic choice of a height function $\omega : \mathbf{A} \rightarrow \mathbb{R}$, the projection of the lower envelope of \mathbf{A}^ω is a regular triangulation.

What happens if we take a height vector ω for which the lifted point set \mathbf{A}^ω has some non-simplicial lower facets? As has been hinted in Figure 2.31 of the Delaunay subdivision of a degenerate point set, instead of being a triangulation, the projection of the lower envelope is a collection of more complicated polytopes, each with vertices in \mathbf{A} . This collection is called the *regular (polyhedral) subdivision* of \mathbf{A} , produced by the height vector ω . The different polytopes in it are called *cells* of the subdivision. Clearly, they still satisfy the three properties of Definition 2.2.1.

Polyhedral subdivisions play a fundamental role in this book; triangulations are nothing but particular cases of them. Even more, sometimes you need to understand general polyhedral subdivisions even if your ultimate goal is to work only with triangulations.

To justify the need for a more careful definition, other than just saying that a polyhedral subdivision is a *polyhedral complex that covers* $\text{conv}(\mathbf{A})$, let us look carefully at a particular example:

Example 2.2.9. Consider the configuration

$$\mathbf{A} = \begin{pmatrix} 1 & 2 & 3 & 4 & 5 \\ 0 & 3 & 0 & 3 & 1 \\ 0 & 0 & 3 & 3 & 1 \\ 1 & 1 & 1 & 1 & 1 \end{pmatrix}$$

of five points in the plane that appeared already in Figure 2.12. Figure 2.33 shows the six possible regular polyhedral subdivisions of it. Four of them are triangulations.

To check that these are indeed regular subdivisions and that the list is complete, we look at precisely what height vectors produce each of these six subdivisions. As in the previous section, there is no loss of generality in restricting attention to height vectors with $\omega_1 = \omega_2 = \omega_3 = 0$ (see Exercise 2.1). Hence, we do a case study depending on the values of ω_4 and ω_5 . The results can be represented in the plane. The exact conditions that produce the six subdivisions (a) to (f) are, respectively (check this!):

- (a) $\omega_5 \geq 0, \omega_4 = 0$.

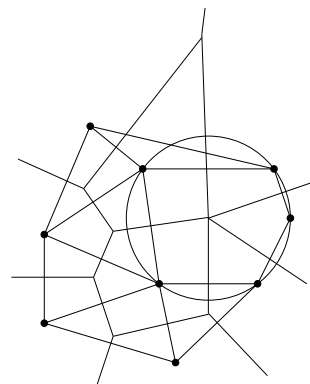


Figure 2.31: The Delaunay subdivision of a degenerate point set and its dual Voronoi diagram.

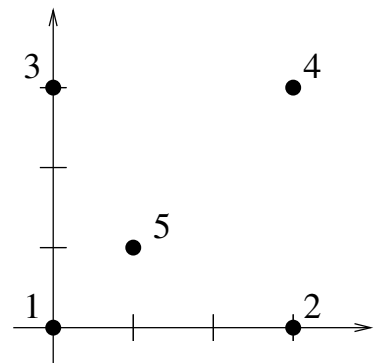


Figure 2.32: Five points in the plane.

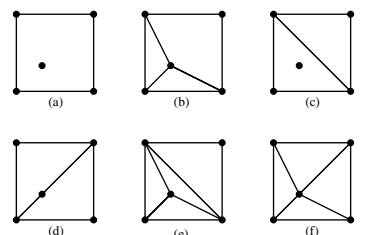


Figure 2.33: Subdivisions of the point set introduced in Figure 2.32.

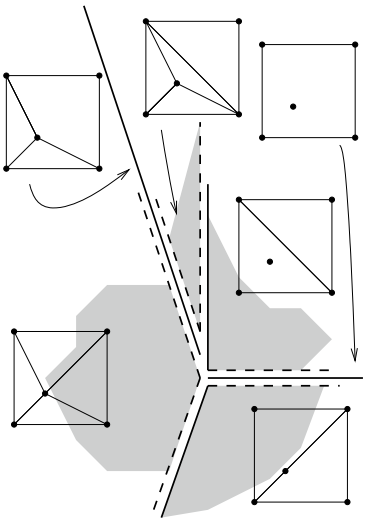


Figure 2.34: Stratification in the space of lifts.

- (b) $\omega_5 < 0, \omega_4 + 3\omega_5 = 0$.
- (c) $\omega_5 \geq 0, \omega_4 > 0$.
- (d) $\omega_4 < 0, \omega_4 \leq 3\omega_5$.
- (e) $\omega_5 < 0, \omega_4 + 3\omega_5 > 0$.
- (f) $\omega_5 < 0, \omega_4 + 3\omega_5 < 0, \omega_4 > 3\omega_5$.

Figure 2.34 shows these conditions pictorially. Height ω_5 is the horizontal coordinate and ω_4 is the vertical one.

One thing we observe is that the regions that produce triangulations are precisely the ones of full-dimension, in agreement with our assertion that sufficiently random heights produce triangulations.

But Figure 2.34 also shows that the stratification we obtain in the two-dimensional space of heights has defects. Some cones are neither open nor closed, but contain only one of their two boundary rays. This, and other unsatisfactory features come from the fact that our temporary definition of regular subdivision does not distinguish between the case where the interior point \mathbf{p}_5 is lifted to lie right *on* the lower envelope of the convex hull of the rest of the points (which should be considered a degenerate situation), and the case where it is lifted *above* the lower envelope of the rest.

To make this distinction, the language of Section 2.1.3 comes to the rescue. Instead of defining the regular subdivision by projecting the lower faces of the *polytope* $\text{conv}(\mathbf{A}^\omega)$, we project the lower faces of the *point configuration* \mathbf{A}^ω :

Definition 2.2.10. Let $\mathbf{A} \subset \mathbb{R}^m$ be a point configuration with n elements and let $\omega : J \rightarrow \mathbb{R}$ be a “height vector”. We use indistinctly $\omega(j)$ and ω_j to refer to the height given to j , although the latter is preferred.

Let \mathbf{A}^ω be the *lifted point configuration*, which has the same labels as \mathbf{A} and a point $\mathbf{p}_j^\omega := (\mathbf{p}_j, \omega_j) \in \mathbb{R}^{d+1}$ for each $j \in J$. A *lower face* of \mathbf{A}^ω is any face $F = \text{face}_{\mathbf{A}}(J, \psi)$ of \mathbf{A} in the direction of some functional ψ with last coordinate positive (put simply, a face that is visible from below).

The *regular subdivision* of \mathbf{A} produced by ω is the set of lower faces of the point configuration \mathbf{A}^ω . This regular subdivision will be denoted by $\mathcal{S}(\mathbf{A}, \omega)$.

Observe in this definition the convenience of using the same labels in \mathbf{A}^ω and in \mathbf{A} . This allows us to say that the lower faces of the former are cells in a subdivision of the latter. Also, observe that here (and in the rest of the book) our height function is defined on the labels rather than on the points. Aside from slightly simplifying notation (we write (\mathbf{p}_i, ω_i) instead of $(\mathbf{p}_i, \omega(\mathbf{p}_i))$ for the lifted points), this takes care of the possibility that \mathbf{A} may have repeated copies of a point and that we may want to lift them to different heights.

We now look at regular subdivisions of the point set of Example 2.2.9 in this new language. To give a subdivision we only list the full-dimensional cells, since the others are simply the faces of them (put differently, lower

faces of \mathbf{A}^ω are all the faces of lower facets). Also, as an abbreviation, we write 123, instead of $\{1, 2, 3\}$.

Example 2.2.11 (Example 2.2.9 continued). The triangulation (c) in the above list can be represented by the following list of subsets of \mathbf{A} :

$$\{123, 234\}.$$

But there is another regular subdivision with the same set of geometric cells, i.e., the same convex hulls. It is not a triangulation, since it contains cells with dependences. Its list of full-dimensional cells is:

$$\{1235, 234\}.$$

This subdivision is produced by heights lying in the positive vertical axis in the representation of Figure 2.34.

Let us work out the list of regular subdivisions of the five point example again, with this new definition, and with the same convention that $\omega_1 = \omega_2 = \omega_3 = 0$. Our point set now has exactly nine regular polyhedral subdivisions, namely:

- (a1) $\{12345\}$, obtained whenever $\omega_5 = 0, \omega_4 = 0$.
- (a2) $\{1234\}$, obtained whenever $\omega_5 > 0, \omega_4 = 0$.
- (b) $\{135, 125, 2345\}$, obtained whenever $\omega_5 < 0, \omega_4 + 3\omega_5 = 0$.
- (c1) $\{1235, 234\}$, obtained whenever $\omega_5 = 0, \omega_4 > 0$.
- (c2) $\{123, 234\}$, obtained whenever $\omega_5 > 0, \omega_4 > 0$.
- (d1) $\{1345, 1245\}$, obtained whenever $\omega_4 < 0, \omega_4 = 3\omega_5$.
- (d2) $\{134, 124\}$, obtained whenever $\omega_4 < 0, \omega_4 < 3\omega_5$.
- (e) $\{125, 135, 235, 234\}$, obtained whenever $\omega_5 < 0, \omega_4 + 3\omega_5 > 0$.
- (f) $\{125, 135, 245, 345\}$, obtained whenever $\omega_5 < 0, \omega_4 + 3\omega_5 < 0, \omega_4 > 3\omega_5$.

Figure 2.35 illustrates this catalogue. The difference between Figure 2.35 and Figure 2.34 is that each of the subdivisions (a), (c), and (d) of our first computation splits into two subdivisions, depending on whether the interior point \mathbf{p}_5 is lifted to lie in the lower envelope of $\text{conv}(\mathbf{A}^\omega)$ or above it. In the figures, we distinguish these two cases by drawing the point or not. Observe that there are two different subdivisions into a single cell, (a1) and (a2): (a1) is called the trivial subdivision because the cell is the whole of \mathbf{A} (Example 2.3.5).

To finish convincing the reader that this combinatorial framework gives a nicer set of regular subdivisions, let us look at the *refinement poset of regular subdivisions* of a point configuration. Given two regular subdivisions \mathcal{S}_1 and \mathcal{S}_2 of \mathbf{A} , we say that \mathcal{S}_1 refines \mathcal{S}_2 if every element of \mathcal{S}_1 is contained

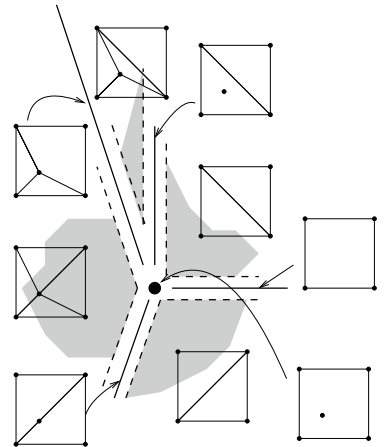


Figure 2.35: Stratification in the space of lifts, with the modified definition.

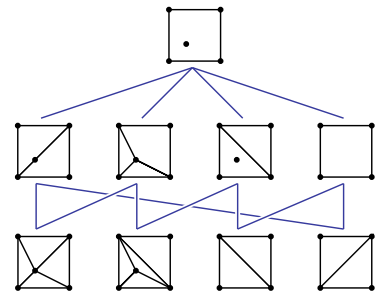


Figure 2.36: Poset of the subdivisions.

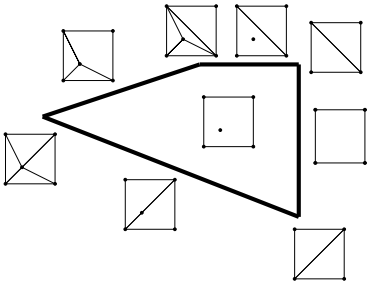


Figure 2.37: The poset of regular subdivisions, as the faces of a quadrilateral.

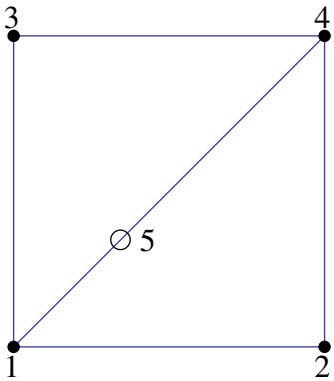


Figure 2.38: $\{1235, 234\}$ is not a subdivision while $\{1235, 2345\}$ is and $\{123, 234\}$ is another.

in some element of \mathcal{S}_2 . This relation induces a partial order; hence, the set of regular subdivisions is a partially ordered set, the *regular refinement poset* for short. Intuitively, if ω is a height vector and $\omega' = \omega + \varepsilon$ is a sufficiently small perturbation of it, then the regular subdivision $\mathcal{S}(\mathbf{A}, \omega')$ will be a refinement of $\mathcal{S}(\mathbf{A}, \omega)$. This is proved in Lemma 2.3.15.

With our temporary approach to regular polyhedral subdivisions, the refinement poset has three levels. On top, there is the trivial subdivision (a). Below this are (b), (c), and (d), which are incomparable to one another. Finally, (f) is the common refinement of (b) and (d), and (e) is the common refinement of (b) and (c). With the combinatorial definition, the poset has a different and a nicer structure in which, for example, the four triangulations are exactly the elements in the lower level (the minimal elements in the poset). Actually, the poset becomes isomorphic to the poset of non-empty faces of a quadrilateral. Furthermore Figure 2.35 shows the relative interiors of the normal cones of the quadrilateral of Figure 2.37. That the same happens for regular subdivisions of any point configuration is one of the fundamental results in this field.

2.3 A bullet-proof definition of polyhedral subdivisions

In this section we elaborate more on the idea of representing cells in triangulations and subdivisions of \mathbf{A} as subconfigurations of \mathbf{A} , rather than as convex hulls of subsets, which led to an unsatisfactory structure. We continue using geometric language to refer to those subsets of indices since we introduced the combinatorial framework in which, for example, faces of a configuration are subconfigurations. Faces, carriers, etc. were defined for configurations already.

2.3.1 Polyhedral subdivisions

We are finally ready to present our *master definition* that considers polyhedral subdivisions and triangulations of a point configuration \mathbf{A} with label set J as collections of subsets of J with certain properties, mimicking the ones in our “intuitive” definition of triangulations provided in Definition 2.2.1.

Definition 2.3.1 (Polyhedral subdivision). Let \mathbf{A} be a point configuration in \mathbb{R}^m , with a set of labels J . A collection \mathcal{S} of subsets of J is a *polyhedral subdivision* of \mathbf{A} if it satisfies the following conditions:

- (CP) If $C \in \mathcal{S}$ and $F \leq C$, then $F \in \mathcal{S}$ as well. (Closure Property)
- (UP) $\bigcup_{C \in \mathcal{S}} \text{conv}_{\mathbf{A}}(C) \supseteq \text{conv}_{\mathbf{A}}(J)$. (Union Property)
- (IP) If $C \neq C'$ are two cells in \mathcal{S} , then $\text{relint}_{\mathbf{A}}(C) \cap \text{relint}_{\mathbf{A}}(C') = \emptyset$. (Intersection Property)

The elements of a polyhedral subdivision \mathcal{S} are called *cells*. Cells of dimension k are called k -cells. Cells of the same dimension as \mathbf{A} are *full-dimensional* or *maximal*. Cells of dimension zero are called *vertices* of \mathcal{S} . Independent cells are called *simplices*. A *triangulation* of \mathbf{A} is a polyhedral subdivision all of whose cells are simplices. The set of polyhedral subdivisions of a point configuration \mathbf{A} will be denoted $\text{Subdivs}(\mathbf{A})$.

Sometimes we want to state (IP) for a cell and all of its faces. For this, we introduce a handy term.

Definition 2.3.2. Two subsets C and C' of J *intersect properly* if all their faces satisfy Property (IP) of Definition 2.3.1; they intersect *improperly* otherwise.

Remark 2.3.3. • Property (IP) can be reformulated as: All pairs of maximal cells intersect properly.

- The union property could have been written with an equality, since containment in the opposite direction is obvious.
- Similarly, Property (UP) could have been written with “relint” instead of “conv” in one or both sides, because Property (CP) implies that once a relative interior is covered, the convex hull is covered too.
- In property (UP), the restriction of the union to maximal cells is equivalent.

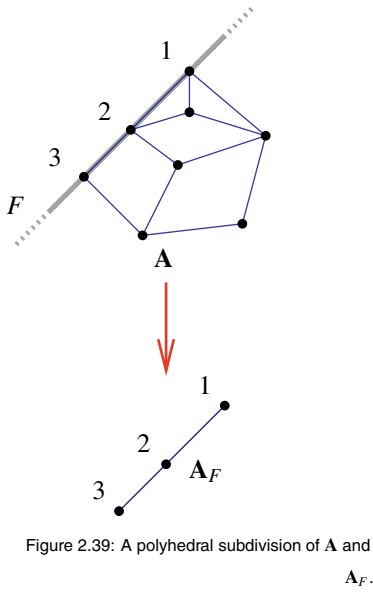
We now collect some facts in order to get used to the definition:

Lemma 2.3.4. Let \mathcal{S} be a polyhedral subdivision of a point configuration $\mathbf{A} \subset \mathbb{R}^m$ with a label set J . Then:

- (i) All maximal cells in \mathcal{S} are full-dimensional, i.e., their dimension equals the dimension of \mathbf{A} .
- (ii) For all $C, C' \in \mathcal{S}$, if $C \subseteq C'$ then $C \leq C'$.
- (iii) For all $C, C' \in \mathcal{S}$, if $C \subseteq C'$ then either $C = C'$ or $\dim C < \dim C'$.
- (iv) For any face F of \mathbf{A} , the set $\mathcal{S}|_F \subseteq \mathcal{S}$ of all cells C in \mathcal{S} with $C \subseteq F$ is a polyhedral subdivision of $\mathbf{A}|_F$.
- (v) If C and C' are cells of \mathcal{S} , then $C \cap C'$ is a face of both (and hence a cell in \mathcal{S}). Moreover;

$$\text{conv}_{\mathbf{A}}(C \cap C') = \text{conv}_{\mathbf{A}}(C) \cap \text{conv}_{\mathbf{A}}(C').$$

Proof. In order to prove Part (i), assume there is a maximal k -cell F with $k < \dim \mathbf{A} = d$. Pick an arbitrary point $\mathbf{x} \in \text{relint}(F)$, and consider a point $\mathbf{y} \in \text{conv}(\mathbf{A})$ very close to \mathbf{x} in general position, i.e., no point on the half-open segment $(\mathbf{x}, \mathbf{y}]$ from \mathbf{y} to \mathbf{x} is contained in any cell of dimension less than d . Then, by (UP), \mathbf{y} must be contained in the relative interior of a full-dimensional cell C_y . We claim that F is a face of C_y . First note that, because of (IP), \mathbf{x} cannot be in the relative interior of C_y . However, all points on $(\mathbf{x}, \mathbf{y}]$ must be in C_y as well because $(\mathbf{x}, \mathbf{y}]$ does not intersect any lower-dimensional face. Therefore, \mathbf{x} is in the boundary of C_y . Consider the carrier of point \mathbf{x} in C_y , $\text{carrier}_{\mathbf{A}}(\mathbf{x}, C_y)$. This is a face of C_y , thus it is in \mathcal{S} , and it contains \mathbf{x} in its relative interior. Since F contains \mathbf{x} in its relative interior as well, F must be equal to $\text{carrier}_{\mathbf{A}}(\mathbf{x}, C_y)$ by Property (IP). Thus F is a face of C_y , and we are done since we have reached a contradiction.



Part (ii) can be proved as follows: Let $C, C' \in \mathcal{S}$ with $C \neq C'$ and $C \subset C'$. Property (CP) implies that all faces of C' are in \mathcal{S} as well. In particular, the carrier of C in C' is in \mathcal{S} . Since the relative interior of C is contained in the relative interior of carrier(C, C') (in particular, the relative interiors of these subconfigurations have a non-empty intersection), Property (IP) implies that $C = \text{carrier}(C, C')$, which means $C \leq C'$.

Part (iii) is a direct consequence of Part (ii): The only face C of a point configuration C' with $\dim(C) = \dim(C')$ is C' itself. All other faces have strictly smaller dimensions.

In order to see Part (iv) we first note that (IP) is trivially fulfilled for all subsets of a polyhedral subdivision, in particular for $\mathcal{S}|_F$. Moreover, (CP) is satisfied because Property (CP) holds for \mathcal{S} , and whenever $C \subseteq F$, then $C' \subseteq F$ holds also for all faces C' of C .

It remains to show that $\text{conv}_{\mathbf{A}}(F)$ is covered by all cells contained in it (without loss of generality, F is a proper face). Since Property (UP) holds for \mathcal{S} , each point \mathbf{x} in $\text{conv}_{\mathbf{A}}(F)$ is contained in $\text{conv}_{\mathbf{A}}(C'_x)$ for some cell $C'_x \in \mathcal{S}$. Let $\text{carrier}_{\mathbf{A}}(\mathbf{x}, C'_x) \in \mathcal{S}$ be the carrier of \mathbf{x} in C'_x . Then, by Lemma 2.1.23, $\mathbf{x} \in \text{relint}(\text{carrier}_{\mathbf{A}}(\mathbf{x}, C'_x))$.

We claim that $\text{carrier}_{\mathbf{A}}(\mathbf{x}, C'_x)$ is in $\mathcal{S}|_F$. For this we simply need to show that $\text{carrier}_{\mathbf{A}}(\mathbf{x}, C'_x) \subseteq F$. Since $\mathbf{A}|_F = \mathbf{A} \cap \mathbf{H}_F$ for a supporting hyperplane \mathbf{H}_F of F , we know that $\mathbf{A}|_{\text{carrier}_{\mathbf{A}}(\mathbf{x}, C'_x)} \cap \mathbf{H}_F \subseteq \mathbf{A} \cap \mathbf{H}_F = \mathbf{A}|_F$.

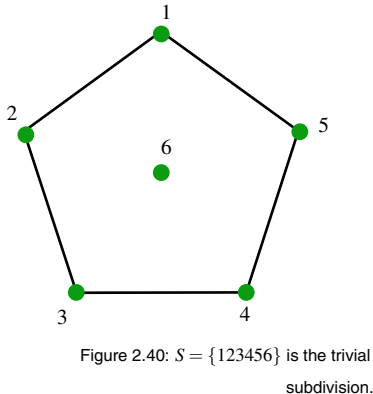
Since $\mathbf{A}|_{\text{carrier}_{\mathbf{A}}(\mathbf{x}, C'_x)} \cap \mathbf{H}_F$ is a face of $\mathbf{A}|_{\text{carrier}_{\mathbf{A}}(\mathbf{x}, C'_x)}$ that contains \mathbf{x} , we have, by the minimality of the carrier, that $\mathbf{A}|_{\text{carrier}_{\mathbf{A}}(\mathbf{x}, C'_x)} \subseteq \mathbf{H}_F$. Thus,

$$\mathbf{A}|_{\text{carrier}_{\mathbf{A}}(\mathbf{x}, C'_x)} \subseteq \mathbf{A}|_{\text{carrier}_{\mathbf{A}}(\mathbf{x}, C'_x)} \cap \mathbf{H}_F \subseteq \mathbf{A} \cap \mathbf{H}_F = \mathbf{A}|_F, \quad (2.9)$$

and $\text{carrier}_{\mathbf{A}}(\mathbf{x}, C'_x)$ is in $\mathcal{S}|_F$, as desired.

Part (v) is trivially true if $C \cap C'$ is empty. If it is not empty, let R and R' be the carriers of $C \cap C'$ in C and C' , respectively. R and R' are faces of C and C' , hence they are cells in \mathcal{S} , and have $C \cap C' \neq \emptyset$ in their relative interiors. Hence, by (IP), $R = R'$.

In the equation about convex hulls, the containment \subseteq is true for the convex hulls of arbitrary sets. So, let $\mathbf{x} \in \text{conv}(C) \cap \text{conv}(C')$ and let us see that \mathbf{x} is also in $\text{conv}(C \cap C')$. Let R and R' be the carriers of \mathbf{x} in C and C' , respectively. We again conclude that $R = R'$, hence $R \subseteq C \cap C'$ and $\mathbf{x} \in \text{conv}(R) \subset \text{conv}(C \cap C')$. \square



Example 2.3.5 (The trivial subdivision). Every point configuration \mathbf{A} has the *trivial subdivision*, consisting of all the faces of \mathbf{A} (including the non-proper one, that is, the full set J of labels). That this is indeed a subdivision according to Definition 2.3.1 is easy to show: (CP) follows from the fact that “a face of a face is a face”. (UP) is obvious since J is one of our cells, and (IP) follows from the fact that different faces of \mathbf{A} have disjoint relative interiors.

If \mathbf{A} is independent, then the trivial subdivision is the only polyhedral subdivision, and it is a triangulation.

Example 2.3.6 (0-dimensional point configurations). A configuration of dimension zero consists of several copies (say k) of a single point. By property (IP), a subdivision cannot have more than one (non-empty) cell. Conversely, any non-empty subconfiguration of \mathbf{A} (together with the empty set, which is its unique proper face) is a polyhedral subdivision. That is, \mathbf{A} has exactly $2^k - 1$ subdivisions in bijection with the non-empty subconfigurations of \mathbf{A} , labeled by subsets of \mathbf{A} 's label set J . Triangulations are the ones corresponding to one-element subconfigurations, and there are k of them.

Example 2.3.7 (1-dimensional point configurations, no repeated points). For a 1-dimensional point configuration, being in general position is equivalent to not having repeated points. The convex hull is a segment, and any subdivision \mathcal{S} is geometrically a chain of sub-segments going from one end to the other with the endpoints of sub-segments elements of \mathbf{A} . A sub-segment may also contain some points of \mathbf{A} in its interior. To get a polyhedral subdivision in the sense of Definition 2.3.1, we need to specify whether these interior points are part of the cell or not.

Put differently, if $\mathbf{A} = (\mathbf{p}_1, \dots, \mathbf{p}_n)$ is our point set (and the labels denote its ordering along the line \mathbb{R}), in a polyhedral subdivision \mathcal{S} of \mathbf{A} each of the $n - 2$ points \mathbf{p}_2 through \mathbf{p}_{n-1} will have one of the following three statuses: It may be an endpoint of two consecutive sub-segments of \mathcal{S} , it may belong to a cell of \mathcal{S} without being one of its endpoints, or it may not belong to any cell of \mathcal{S} . If we represent these three possibilities as the three signs “−”, “0”, and “+” respectively, we get:

Each polyhedral subdivision of \mathbf{A} has an associated string of length $n - 2$ on the alphabet $\{+, 0, -\}$.

We leave it to the reader to prove the following:

1. This correspondence is a bijection between the set of subdivisions of \mathbf{A} and the 3^{n-2} element set $\{+, 0, -\}^{n-2}$.
2. Triangulations correspond to the strings without zeroes, hence there are 2^{n-2} of them.

The most prominent structure on the set $\text{Subdivs}(\mathbf{A})$ of all polyhedral subdivisions of a point configuration \mathbf{A} is the *refinement poset*. It is often called the *Baues poset* of \mathbf{A} . Refinement of a polyhedral subdivision means roughly that some pieces of that subdivision are subdivided further. We have seen in Section 2.2.3 a restricted version using only the regular triangulations. Now we present a bigger more inclusive definition.

Definition 2.3.8 (Refinement). Let \mathcal{S} and \mathcal{S}' be two polyhedral subdivisions of a point configuration \mathbf{A} . Then, \mathcal{S} is a *refinement* of \mathcal{S}' —in brief notation: $\mathcal{S} \preceq \mathcal{S}'$ —if for each $C \in \mathcal{S}$, there is a $C' \in \mathcal{S}'$ with $C \subseteq C'$.

With the refinement relation, $\text{Subdivs}(\mathbf{A})$ is a *partially ordered set (poset)* for short). This means the following (by definition of a poset):

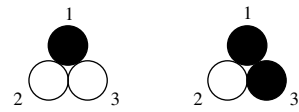


Figure 2.41: Two subdivisions of a zero-dimensional configuration with three copies of the same point. The one on the left, $\{1\}$, is a triangulation. The one on the right, $\{13\}$, is not.

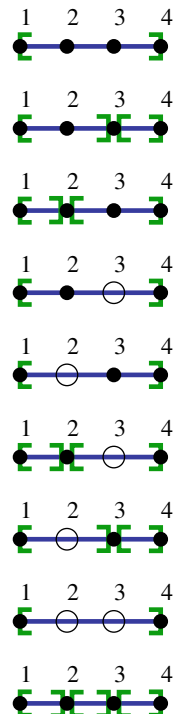


Figure 2.42: All subdivisions of four collinear points.

Lemma 2.3.9. *The refinement relation induces a partial order on the set of all polyhedral subdivisions of \mathbf{A} . That is, for every triple $\mathcal{S}, \mathcal{S}', \mathcal{S}''$ of polyhedral subdivisions of \mathbf{A} , one has:*

- (i) $\mathcal{S} \preceq \mathcal{S}$
- (ii) $\mathcal{S} \preceq \mathcal{S}'$ and $\mathcal{S}' \preceq \mathcal{S}$ imply $\mathcal{S} = \mathcal{S}'$
- (iii) $\mathcal{S} \preceq \mathcal{S}'$ and $\mathcal{S}' \preceq \mathcal{S}''$ imply $\mathcal{S} \preceq \mathcal{S}''$

Using the refinement we can say a subdivision is *coarsest* if it refines the trivial subdivision and no other. Triangulations are the *finest subdivisions*.

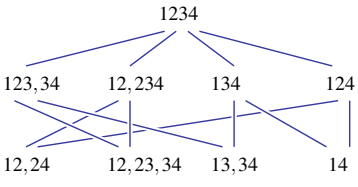


Figure 2.43: Refinement poset of four colinear points.

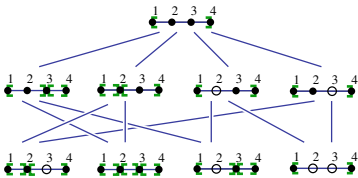


Figure 2.44: Refinement poset of four colinear points.

Proof. Part (i) is clear by the definition of “ \preceq ”. To prove Part (ii), let $\mathcal{S} \preceq \mathcal{S}'$ and $\mathcal{S}' \preceq \mathcal{S}$. Let C be an arbitrary maximal cell in \mathcal{S} . Since $\mathcal{S} \preceq \mathcal{S}'$, there is an $C' \in \mathcal{S}'$ with $C \subset C'$. Since $\mathcal{S}' \preceq \mathcal{S}$, there is a $C'' \in \mathcal{S}$ with $C' \subseteq C''$. Thus, $C \subseteq C''$, and, by Lemma 2.3.4(iii), either $C = C''$ or $\dim(C) < \dim(C'')$. Since C was chosen to be a maximal cell, only $C = C''$ is possible. This implies that in the chain $C \subseteq C' \subseteq C''$ we have equality everywhere. The remaining Part (iii) is again straightforward by definition of “ \preceq ”. \square

Recall that a maximal or minimal element in a poset is an element which is not strictly smaller or strictly greater, respectively, than any other one.

Lemma 2.3.10. *Let \mathbf{A} be a point configuration. Then:*

- (i) $\text{Subdivs}(\mathbf{A})$ has a unique maximal element, the trivial subdivision.
- (ii) A subdivision is a minimal element of $\text{Subdivs}(\mathbf{A})$ if and only if it is a triangulation.

Proof. For Part (i), observe simply that every cell of every subdivision is contained in the full-dimensional cell J of the trivial subdivision. Hence, every subdivision refines the trivial one.

For Part (ii), here we only prove that triangulations are minimal elements in the poset. The converse is Corollary 2.3.18 in the next section, and will be proved using regular triangulations.

Let \mathcal{S} be a triangulation and let \mathcal{S}' be a subdivision that refines \mathcal{S} . Every cell F' of \mathcal{S}' is contained in a cell F of \mathcal{S} and, since F is independent, F' is a face of it. Hence, by property (CP) F' is a cell of \mathcal{S} . Conversely, if F is a face of \mathcal{S} , let \mathbf{x} be a point in $\text{relint}(F')$. Then \mathbf{x} must also be in the relative interior of some face F' of \mathcal{S}' , by property (UP). By the previous argument, F' is a face of \mathcal{S} as well. Since F and F' intersect in their relative interiors, $F = F'$ by property (IP). \square

Let us close this section with a reassuring remark. The reader may wonder what parts of Section 2.2 need to be re-worked to match the combinatorial setting introduced in this one. The answer is “almost none”, for the following reason. In that section we were primarily interested in triangulations. With the new definition, cells in a triangulation are affinely

independent subsets and, hence, they are the vertex set of their convex hull. In particular, there is a one-to-one correspondence between the triangulations allowed by Definition 2.2.1 and those allowed by Definition 2.3.1, except in the following case: If the point configuration has repeated points, there will be several combinatorial representatives of each “geometric” triangulation. Indeed, each combinatorial triangulation will select a particular copy of each repeated point, since a cell with repeated points is not independent and two combinatorial simplices using different copies of a repeated point violate the intersection property (IP).

2.3.2 Regular subdivisions, again

We now look again at polyhedral subdivisions. The first thing to check is that they are indeed polyhedral subdivisions, according to our “bullet-proof” definition.

Lemma 2.3.11. $\mathcal{S}(\mathbf{A}, \omega)$ is a polyhedral subdivision of \mathbf{A} , for every ω .

Proof. Observe that every lower face F of \mathbf{A}^ω , by definition, lies in a non-vertical hyperplane (the one in which the functional ψ is constant). Hence, the projection $\pi : \mathbf{A}^\omega \rightarrow \mathbf{A}$ that forgets the last coordinate is an affine isomorphism between \mathbf{A}_F and \mathbf{A}_F^ω . In particular, the face structure of F is the same in \mathbf{A} and \mathbf{A}^ω .

The closure property (CP) then follows from the fact that if $F' < F \leq J$ are faces of \mathbf{A}^ω then every functional for the face F can be slightly perturbed to a functional of the face F' (for people familiar with polyhedral geometry, what we are saying is that the normal cone of F is a face of the normal cone of F'). In particular, if F is a lower face, then any $F' < F$ is a lower face as well. The intersection property for the projected faces follows from the intersection property of the faces of \mathbf{A}^ω [339].

For the union property, let \mathbf{x} be a point in the relative interior of \mathbf{A} . The intersection of $\mathbf{x} \times \mathbb{R}$ with $\text{conv}(\mathbf{A}^\omega)$ is a vertical segment from a bottom point \mathbf{x}_1 to a top point \mathbf{x}_2 . Let F be any proper face of \mathbf{A}^ω with $\mathbf{x}_1 \in \text{conv}_{\mathbf{A}^\omega} F$, which exists since \mathbf{x}_1 is in the boundary of $\text{conv}(\mathbf{A}^\omega)$. Let ψ be any linear functional selecting F as a face of \mathbf{A}^ω . We have that $\psi(\mathbf{x}_2) > \psi(\mathbf{x}_1)$, otherwise ψ would be constant in the whole segment from \mathbf{x}_1 to \mathbf{x}_2 , hence constant on $\text{conv}(\mathbf{A}^\omega)$, because this segment crosses its relative interior, contradicting the fact that F is a proper face.

But $\psi(\mathbf{x}_2) > \psi(\mathbf{x}_1)$ implies that ψ is positive on the last coordinate, so F must be a lower face. Its projection is a cell in $\mathcal{S}(\mathbf{A}, \omega)$ covering the point \mathbf{x} . \square

Example 2.3.12 (Example 2.3.5 continued). The trivial subdivision is the regular subdivision obtained with the zero height vector or, more generally, with any height vector that is the restriction to \mathbf{A} of an affine function $\mathbb{R}^m \rightarrow \mathbb{R}$. In this case, \mathbf{A}^ω has the same face structure as \mathbf{A} , since they are affinely equivalent configurations, and every face is a lower face.

Example 2.3.13 (Example 2.3.6 continued). Every subdivision of a zero-dimensional point configuration is regular. Remember that every subdivision

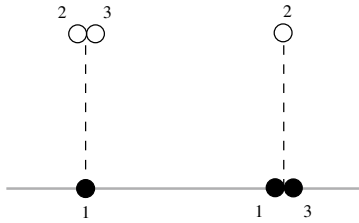


Figure 2.45: Heights that produce the regular subdivisions shown in Figure 2.41.

has a unique (non-empty) cell, say F . A height function that produces this subdivision is one that gives the same height to all points in F and greater height to the others.

Example 2.3.14 (Example 2.3.7 continued). In this case, all subdivisions are again regular. The proof is left to the reader as Exercise 5.1.

Lemma 2.3.15. *Let \mathbf{A} be a point configuration in \mathbb{R}^m and let $\omega : J \rightarrow \mathbb{R}$ be a height function. Let $\mathcal{S} = \mathcal{S}(\mathbf{A}, \omega)$ be the regular subdivision of \mathbf{A} produced by ω . Then,*

1. *If ω is sufficiently generic, then \mathcal{S} is a triangulation.*
2. *If F is a face of \mathbf{A} , then the restriction of \mathcal{S} to F equals the regular subdivision of \mathbf{A}_F obtained with ω . Symbolically:*

$$\mathcal{S}(\mathbf{A}, \omega)|_F = \mathcal{S}(\mathbf{A}_F, \omega|_F).$$

3. *There is an $\varepsilon > 0$ such that, for every height function $\omega' : J \rightarrow \mathbb{R}$ that is ε -close to ω , namely $|\omega(j) - \omega'(j)| < \varepsilon$ for all j , we have that $\mathcal{S}(\mathbf{A}, \omega') \preceq \mathcal{S}(\mathbf{A}, \omega)$.*

Proof. (1) Assume, without loss of generality, that \mathbf{A} is represented by a matrix of full rank. That is, that \mathbf{A} has dimension $m - 1$.

For every affine basis $C \subset J$ and every point $j \in J \setminus C$, there is a linear equation on the ω 's that expresses the fact that j is lifted to lie in the hyperplane containing the lift of C , namely the determinant of the lifted points. Since C is an affine basis, this equation has non-zero coefficient on, at least, $\omega(j)$ and, in particular it is not identically zero. Hence, it holds only on a hyperplane in \mathbb{R}^{m+1} . If ω does not lie in any of the hyperplanes obtained for the different choices of C and j , then ω must produce a triangulation: no lower facet, hence no lower face, projects to a dependent set.

(2) This follows from the fact that the lower faces of the lifted face $(\mathbf{A}_F)^{\omega|_F} = (\mathbf{A}^\omega)_F$ are just the lower faces of \mathbf{A}^ω contained in F .

(3) Recall that the determinant of $m + 2$ points in \mathbb{R}^{m+1} is zero if the points lie in a hyperplane and non-zero if they are independent. In this case the sign gives what is the relative position of each point with respect to the hyperplane determined by the other $m + 1$. Also, recall that the determinant is continuous with respect to the coordinates of the points.

Let \mathbf{A}^ω be the lifted point configuration for the original height function ω . By continuity of the determinant, for each independent subconfiguration C of $m + 2$ points in \mathbf{A}^ω there is an $\varepsilon_C > 0$ such that the determinant does not change sign under an ε_C -close perturbation of C . We take ε to be the minimum of all the ε_C 's for the different choices of C .

Let now ω' be an ε -close perturbation of ω and let F be a maximal cell in $\mathcal{S}(\mathbf{A}, \omega')$. Maximality means that \mathbf{A}_F is the projection of a facet $\mathbf{A}_F^{\omega'}$ of $\mathbf{A}^{\omega'}$, because every lower face is a face of a lower facet. In particular, the hyperplane \mathbf{H}' containing $\mathbf{A}_F^{\omega'}$ is not vertical and leaves the rest of $\mathbf{A}^{\omega'}$ above it. Let now C be a maximal independent subset in $\mathbf{A}_F^{\omega'}$, with $m + 1$ points.

Consider the corresponding set C^ω in \mathbf{A} and the hyperplane \mathbf{H} spanned by it. Our choice of ε implies that no point of \mathbf{A}^ω is below \mathbf{H} and that the points that are above \mathbf{H} have their corresponding points in $\mathbf{A}^{\omega'}$ above \mathbf{H}' . That is, \mathbf{H} is the supporting hyperplane of a lower facet of \mathbf{A}^ω and the projection of this facet contains (as a subconfiguration, as well as geometrically) the projection of F' . \square

Using regular subdivisions we can easily prove that a (regular or not) subdivision that cannot be refined further must be a triangulation. We need the following construction:

Lemma 2.3.16. *Let \mathcal{S} be a polyhedral subdivision of \mathbf{A} . Let $\omega : J \rightarrow \mathbb{R}$ be a height vector. Then the following is a polyhedral subdivision of \mathbf{A} that refines \mathcal{S} :*

$$\mathcal{S}_\omega := \cup_{C \in \mathcal{S}} \mathcal{S}(\mathbf{A}|_C, \omega|_C).$$

Moreover, if \mathcal{S} is regular, i.e., $\mathcal{S}(\mathbf{A}, \omega_0)$ for some ω_0 , then \mathcal{S}_ω is also regular and equals $\mathcal{S}(\mathbf{A}, \omega_0 + \varepsilon\omega)$ for any sufficiently small positive ε .

Recall that $\mathbf{A}|_C$ denotes C considered as a subconfiguration of \mathbf{A} . That is, \mathcal{S}_ω is obtained by refining each cell of \mathcal{S} in the regular way given by the height vector ω .

Proof. Our first goal is to prove that \mathcal{S}_ω is a subdivision of \mathbf{A} . That it refines \mathcal{S} is obvious.

Clearly, \mathcal{S}_ω satisfies (UP) since the cells in each $\mathcal{S}(\mathbf{A}|_C, \omega|_C)$ cover the convex hull of C , by the union property of $\mathcal{S}(\mathbf{A}|_C, \omega|_C)$. It also satisfies (CP), since each $\mathcal{S}(\mathbf{A}|_C, \omega|_C)$ does. So, we only need to prove (IP). To get a contradiction, let R_1 and R_2 be two different cells in \mathcal{S}_ω with $\mathbf{x} \in \text{relint}(R_1) \cap \text{relint}(R_2)$. By the intersection property of each $\mathcal{S}(\mathbf{A}|_C, \omega|_C)$, R_1 and R_2 come from two different regular subdivisions $\mathcal{S}(\mathbf{A}|_{C_1}, \omega|_{C_1})$ and $\mathcal{S}(\mathbf{A}|_{C_2}, \omega|_{C_2})$ of cells of \mathcal{S} . Then, $\mathbf{x} \in \text{conv}(C_1) \cap \text{conv}(C_2)$. Let F_1 and F_2 be the carriers of \mathbf{x} in C_1 and C_2 , so that $\mathbf{x} \in \text{relint}(F_1) \cap \text{relint}(F_2)$. By (CP) of \mathcal{S} , F_1 and F_2 are cells in \mathcal{S} . Then, by (IP), F_1 and F_2 are the same cell of \mathcal{S} . Let us call it simply F . Now, by Part (iv) of Lemma 2.3.4, the subdivision of F obtained via $\mathcal{S}(\mathbf{A}|_{C_2}, \omega|_{C_2})$ and $\mathcal{S}(\mathbf{A}|_{C_1}, \omega|_{C_1})$ are the same, namely $\mathcal{S}(\mathbf{A}|_C, \omega|_C)$. That is, R_1 and R_2 are both cells of $\mathcal{S}(\mathbf{A}|_C, \omega|_C)$, which contradicts the fact that they are different cells with non-empty common relative interiors.

We now prove regularity. By Lemma 2.3.15, $\mathcal{S}(\mathbf{A}, \omega_0 + \varepsilon\omega)$ refines \mathcal{S} if ε is sufficiently small. On the other hand, since ω_0 is a linear height vector on each cell $C \in \mathcal{S}$, the height vectors $\omega_0 + \varepsilon\omega$, $\varepsilon\omega$ and ω produce the same regular subdivision of that cell. Hence $\mathcal{S}_\omega = \mathcal{S}(\mathbf{A}, \omega_0 + \varepsilon\omega)$, as stated. \square

Definition 2.3.17. The polyhedral subdivision \mathcal{S}_ω of the previous lemma is called the *regular refinement* of \mathcal{S} for the height vector ω .

Observe that the regular refinement of a non-regular subdivision may be a non-regular subdivision itself. See three examples of regular refinements in Figure 2.46.

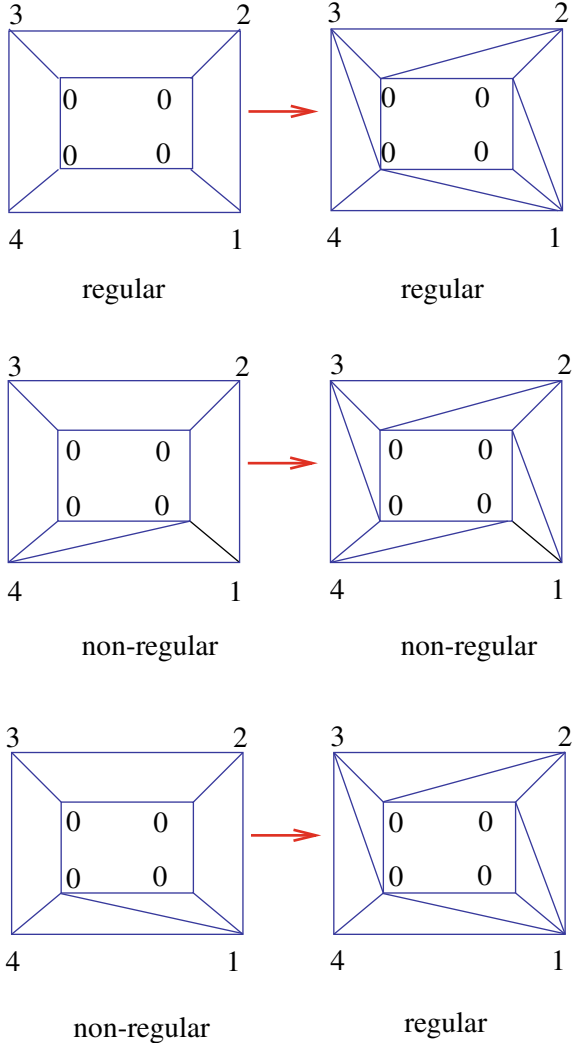


Figure 2.46: Subdivisions of a point configuration with heights and their regular refinements.

Corollary 2.3.18. *Every polyhedral subdivision of \mathbf{A} can be refined to a triangulation. Moreover, every regular subdivision of \mathbf{A} can be refined to a regular triangulation.*

Proof. For the first sentence, observe that if ω is sufficiently generic, then \mathcal{S}_ω is a triangulation since each $\mathcal{S}(\mathbf{A}|_C, \omega)$ is a triangulation. The second sentence follows from the last part of Lemma 2.3.16. \square

We now address the following question: if we are given a polyhedral subdivision \mathcal{S} of \mathbf{A} and a height vector ω , what is an easy way to check if $\mathcal{S} = \mathcal{S}(\mathbf{A}, \omega)$?

From the definition of regular subdivision we can certainly derive an algorithm to answer this question. Namely: $\mathcal{S} = \mathcal{S}(\mathbf{A}, \omega)$ if and only if every cell $C \in \mathcal{S}$ is lifted to lie in a hyperplane \mathbf{H}_C and every $j \notin C$ is lifted above that hyperplane. The decision question can be then phrased as the solvability of a system of linear inequalities (more about this later). What we want to show here is that this second part needs only be checked for some of the points $j \notin C$ determined by the cell adjacency (thus, giving a smaller system of inequalities).

Definition 2.3.19. A *wall* in a polyhedral subdivision of a point configuration \mathbf{A} is a cell C of codimension one that is a face of two maximal cells (equivalently, that does not lie in a facet of \mathbf{A}). We say that C *separates* those two cells.

Theorem 2.3.20. Let \mathcal{S} be a polyhedral subdivision of a point configuration $\mathbf{A} \in \mathbb{R}^m$, and let $\omega : J \rightarrow \mathbb{R}$ be a height function. Then, one has $\mathcal{S} = \mathcal{S}(\mathbf{A}, \omega)$ if and only if

- (i) For every full-dimensional cell $C \in \mathcal{S}$, the lifted subconfiguration $\mathbf{A}^\omega|_C$ lies in a hyperplane in \mathbb{R}^{m+1} (the coplanarity condition).
- (ii) For every wall $C_0 \in \mathcal{S}$, with incident full-dimensional cells C_1 and C_2 , all points in $\mathbf{A}_{C_1 \setminus C_0}^\omega$ lie above the hyperplane containing $\mathbf{A}^\omega|_{C_2}$ and vice versa (the local folding condition).

The coplanarity condition and the folding condition will play a crucial role in Chapter 5. Before going into the proof, observe that the “vice versa” in the second part is not an additional condition to be checked, but is equivalent to the stated condition. Also note that to verify the condition it is enough to check it for a single element of $C_1 \setminus C_2$. In fact, checking condition (ii) is equivalent to the computation of a certain $(d+2) \times (d+2)$ determinant. Condition (i), in turn, is equivalent to the vector $\omega|_C$ lying in the row span of the matrix $\mathbf{A}|_C$.

Proof. The “only-if”-direction is clear because we have taken a subset of the regularity conditions, and our result is implied by the definition of regularity.

Assume now that \mathcal{S} is some polyhedral subdivision of \mathbf{A} and $\omega : J \rightarrow \mathbb{R}$ is a height function satisfying the assumptions (i) and (ii).

We have to show that the remaining conditions are implied for ω : for every full-dimensional cell $C \in \mathcal{S}$ and every element $j \in J \setminus C$, point j is lifted above the hyperplane containing the lifted cell C^ω .

Let \mathbf{p}_j be an arbitrary point and let $C \in \mathcal{S}$ be an arbitrary cell not containing j . Choose a point \mathbf{x} in general position in $\text{conv}(C)$ and consider the straight line segment ℓ from \mathbf{p}_j to \mathbf{x} . This line segment intersects a sequence of full-dimensional cells $C_0, C_1, \dots, C_k = C$ with $C_i \in \mathcal{S}$ for $i = 0, 1, \dots, k$. Let \mathbf{H}_i be the hyperplane spanned by the lifted points in C_i for $i = 0, 1, \dots, k$.

If $k = 0$ then $j \in C$, contradicting the choice of C . Therefore, $k > 0$ and $j \in C_0 \setminus C_1$. We will now prove that for all $i = 1, \dots, k$ \mathbf{p}_j is lifted above \mathbf{H}_i .

For $i = 1$ the claim is literally Assumption (ii) in the Theorem. Let therefore $i > 1$, and let F_i be the wall between C_i and C_{i-1} . This wall is, by

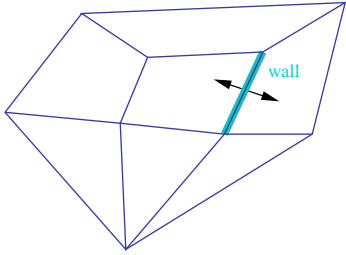


Figure 2.47: A wall in a two-dimensional point configuration.

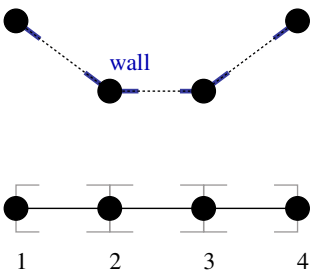


Figure 2.48: A wall in a one-dimensional point configuration.

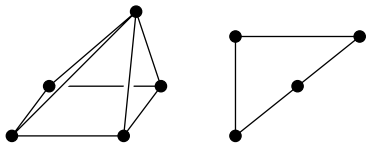


Figure 2.49: Two corank-one configurations.

construction, pierced by the segment ℓ . Therefore \mathbf{p}_j lies on the same side of the vertical hyperplane \mathbf{H}_{F_i} spanned by F_i as the points in $C_{i-1} \setminus C_i$.

Assumption (ii) for C_i and C_{i-1} says that the points in $C_{i-1} \setminus C_i$ are lifted above the hyperplane \mathbf{H}_i . In particular, the whole part of the hyperplane \mathbf{H}_{i-1} that is on the same side of \mathbf{H}_F as $C_{i-1} \setminus C_i$ is above \mathbf{H}_i . Moreover, by induction, \mathbf{p}_j is lifted above \mathbf{H}_{i-1} .

Putting everything together yields: \mathbf{p}_j is lifted above \mathbf{H}_{i-1} by induction, which in turn is lifted higher than \mathbf{H}_i on the side of \mathbf{p}_j by Assumption (ii), which proves that \mathbf{p}_j is lifted above \mathbf{H}_i as well.

Setting $i = k$ completes the proof, since $C_k = C$. \square

2.4 Flips and the graph of triangulations

Flips between triangulations are a central topic in this book. Flips are local changes that transform one triangulation into another. Reasons for introducing and understanding them come both from applications (they are a computationally simple way of searching for particular triangulations, or enumerating them) and theory (they highlight the rich structure to the set of all triangulations of a configuration). In Chapter 4, we will see how to technically deal with flips. Here, we simply introduce the concept. The core objects are configurations of corank one.

2.4.1 Corank-one configurations and circuits

Recall that the *corank* of a d -dimensional point configuration with n points is the number $n - d - 1$. Independent configurations are exactly the configurations of corank zero. Let \mathbf{A} be a configuration of corank one. Clearly, all non-trivial subdivisions of \mathbf{A} are triangulations, because every full-dimensional proper subconfiguration has corank zero and so is independent. Here we prove that there are exactly two such triangulations, and characterize them.

A configuration has *corank one* if and only if it has a unique affine dependence relation $\sum_{j \in J} \lambda_j \mathbf{p}_j = 0$, with $\sum_{j \in J} \lambda_j = 0$ (uniqueness is, of course, up to multiplication of all λ 's by the same constant). This affine dependence divides J into three subsets

$$J_+ := \{ j \in J : \lambda_j > 0 \}, J_0 := \{ j \in J : \lambda_j = 0 \}, J_- := \{ j \in J : \lambda_j < 0 \}.$$

J_+ and J_- are the only disjoint subsets of J with the property that their relative interiors intersect. They intersect at the point

$$\sum_{j \in J_+} \lambda_j \mathbf{p}_j = \sum_{j \in J_-} |\lambda_j| \mathbf{p}_j,$$

where the λ 's are assumed to be normalized so that

$$\sum_{j \in J_+} \lambda_j = \sum_{j \in J_-} |\lambda_j| = 1.$$

The set $J_+ \cup J_-$ containing the “relevant” part of the unique affine dependence is called a *circuit* in J . The pair (J_+, J_-) is classically called the

Radon partition of \mathbf{A} , or the *oriented circuit* of \mathbf{A} . Here is the formal definition, but much more will be said about circuits in Chapter 4:

Definition 2.4.1. Let \mathbf{A} be a point configuration, with index set J . A subset of J is called a *circuit*, Z , if it is a minimal dependent set (that is, it is dependent but every proper subset is independent).

The partition (Z_+, Z_-) of Z into two parts such that $\text{conv}(Z_+) \cap \text{conv}(Z_-)$ is non-empty (which exists and is unique except for the swap of Z_+ and Z_-) is called an *oriented circuit*, or *signed circuit*. We say that the circuit is of type $(|J_+|, |J_-|)$.

Since oriented circuits play a more prominent role than unoriented ones in this book, we will typically abuse language and drop the word “oriented” when referring to them. The underlying unoriented circuit Z will be called the *support* of (Z_+, Z_-) . Circuits are studied in a broader context in Section 4.1.

Candidates for full-dimensional simplices in a triangulation of \mathbf{A} are of the form $J \setminus \{j\}$ with $j \in J_+ \cup J_-$, since $j \in J_0$ means that $J \setminus \{j\}$ still has corank one.

Lemma 2.4.2. Let \mathbf{A} be a configuration of corank one and let $J = J_+ \cup J_0 \cup J_-$ be its label set, partitioned by the unique Radon partition of \mathbf{A} . Then the following are the only two triangulations of \mathbf{A} :

$$\mathcal{T}_+ = \{C \subset J : J_+ \not\subseteq C\}, \quad \text{and} \quad \mathcal{T}_- = \{C \subset J : J_- \not\subseteq C\}.$$

The two triangulations are regular.

Remark 2.4.3. The formulas given in this statement for \mathcal{T}_+ and \mathcal{T}_- are equivalent to saying that their sets of maximal simplices are, respectively,

$$\{J \setminus \{j\} : j \in J_+\}, \quad \text{and} \quad \{J \setminus \{j\} : j \in J_-\}.$$

These are actually the formulas we prove.

Proof. Clearly, no triangulation can simultaneously contain J_+ and J_- since their relative interiors intersect. That is, every triangulation is either contained in \mathcal{T}_+ or in \mathcal{T}_- . It then suffices to show that \mathcal{T}_+ and \mathcal{T}_- are indeed regular triangulations. For this, let $\omega : J \rightarrow \mathbb{R}$ be a height function and consider the quantity

$$\sum_{j \in J} \lambda_j \omega(j), \tag{2.10}$$

where the λ_j are the real coefficients of the unique (because of corank-one) dependence. If (2.10) equals zero, then the lifted point set lies in a hyperplane and $\mathcal{S}(\mathbf{A}, \omega)$ is the trivial subdivision. If (2.10) is not zero, then the lifted configuration is independent, because every affine dependence in the lifted configuration should be a dependence in \mathbf{A} too. Hence, $\mathcal{S}(\mathbf{A}, \omega)$ is a triangulation. Which triangulation we obtain is governed only by the sign of $\sum_{j \in J} \lambda_j \omega(j)$. More precisely, if it is positive, then each point in J_+

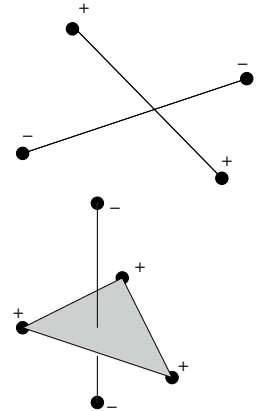


Figure 2.50: Two circuits represented as Radon partitions.

is lifted above the hyperplane spanned by the lift of the other points, which implies that the set of lower facets of the lifted point set is

$$\{J \setminus \{j\} : j \in J_+\}.$$

Similarly, if it is negative then the lower facets are

$$\{J \setminus \{j\} : j \in J_-\}.$$

□

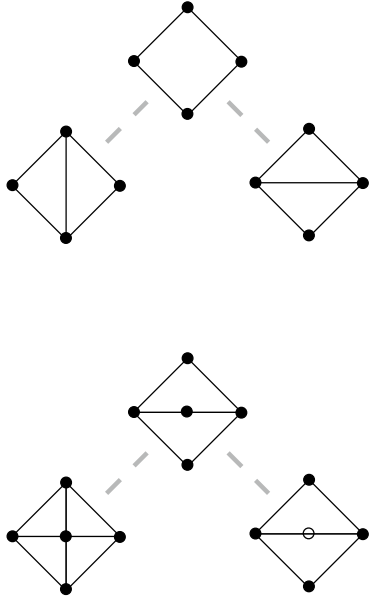


Figure 2.51: An almost-triangulation only has two triangulations that refine it.

Observe that all we have said is valid for the case where the corank one configuration J has a repeated point. In this case, \mathbf{A} is an independent set together with a second copy of one of its points, say \mathbf{p}_j . Then the affine dependence is $\mathbf{p}_j - \mathbf{p}_j = 0$ and J_+ and J_- have a single element each, the labels j and j' of the two copies of \mathbf{p}_j . In accordance with Lemma 2.4.2, \mathbf{A} has two triangulations, each with a unique maximal simplex $J \setminus \{j\}$ or $J \setminus \{j'\}$.

2.4.2 Almost-triangulations and flips

The poset of subdivisions gives a way to quantify how close to being a triangulation a subdivision is: for $\mathcal{S} \in \text{Subdiv}(\mathbf{A})$, let us call *height* of \mathcal{S} the maximal length of chains of proper refinements of \mathcal{S} . Triangulations are the subdivisions at height zero.

Definition 2.4.4. A subdivision \mathcal{S} is *almost a triangulation* (or an *almost-triangulation*) if it is at height one in the poset of subdivisions. That is, it is not a triangulation but all its proper refinements are triangulations.

As a first example, see Figure 2.51. We saw in Section 2.4.1 that the trivial subdivision of a corank-one configuration is an almost-triangulation: it has only two proper refinements, which are both triangulations. In what follows we show that this example is essentially unique. Every almost-triangulation is a triangulation except for a small part of it, where it is the almost-triangulation of a corank-one subconfiguration.

For this, observe that if \mathbf{A} has corank one and Z is its unique circuit, then for every $j \in J \setminus Z$ we have that $J \setminus \{j\}$ still has corank one, hence it must have dimension one less than \mathbf{A} , hence it is a face of it (the latter because there is a single point \mathbf{p}_j out of the hyperplane containing $J \setminus \{j\}$). In particular, the two triangulations of \mathbf{A} are the pyramids, with apex \mathbf{p}_j , over the two triangulations of $\mathbf{A} \setminus \{\mathbf{p}_j\}$ (a pyramid means that the face is constructed by taking the convex hull of each of the triangulation of $\mathbf{A} \setminus \{\mathbf{p}_j\}$ and the point \mathbf{p}_j). This is the only possibility to build full-dimensional cells. This fact follows also from the description of these triangulations given in Lemma 2.4.2. Together with the existence and properties of regular refinements, it is at the heart of the following characterization of almost-triangulations:

Lemma 2.4.5. Let \mathcal{S} be a polyhedral subdivision that is not a triangulation. \mathcal{S} is almost a triangulation if and only if:

- (i) All its cells have corank at most one, and
- (ii) All its cells of corank one contain the same circuit.

Proof. We start by proving necessity of the conditions: Condition (i) is easy with the ideas in the proof of Lemma 2.3.16. Suppose a cell $C \in \mathcal{S}$ has corank $k \geq 2$ and let $j \in C$ be such that $C \setminus \{j\}$ has at least corank one. Let $\omega : J \rightarrow \mathbb{R}$ be the height function that is everywhere zero except at j , where $\omega(j) > 0$. Then, the refinement \mathcal{S}_ω of \mathcal{S} is proper and is still not a triangulation, since it contains the cell $C \setminus \{j\}$. This means \mathcal{S} is not an almost-triangulation.

Similarly, if Condition (ii) fails this means there are two different minimal dependent cells C_1 and C_2 , both of corank one. Let $j \in C_1 \setminus C_2$. Minimality of C_1 implies that $C_1 \setminus \{j\}$ is independent thus of corank zero, thus of the same dimension as C_1 . In particular, it is not a facet of C_1 , and hence \mathcal{S}_ω , with ω exactly as before, again produces a proper refinement. Since $j \notin C_2$, this finer subdivision still has C_2 as a dependent cell, hence, it is not a triangulation.

Conversely, if Conditions (i) and (ii) hold, then \mathcal{S} has a unique minimal dependent cell Z , which is the circuit contained in all the dependent cells. Every proper refinement of \mathcal{S} will, in particular, refine Z to one of its two triangulations. Moreover, every proper refinement refines every dependent cell as a cone over this triangulation. In particular, every proper refinement is a triangulation, and is completely characterized by which of the two triangulations of Z it contains. \square

Corollary 2.4.6. *Every almost-triangulation has exactly two proper refinements, which are both triangulations.*

Proof. This follows from the ‘‘sufficiency’’ part of the proof of the previous lemma. Every proper refinement refines the unique circuit common to all dependent cells in one of the two possible ways, and the refinement of this circuit determines the refinement of every cell. \square

Corollary 2.4.6 suggests that we call the change from a triangulation \mathcal{T}_1 to another one \mathcal{T}_2 a *flip* if they are the two proper refinements of the same almost-triangulation \mathcal{S} . This is exactly what we do:

Definition 2.4.7 (Flip). Two triangulations of the same point configuration are *connected by a flip supported on the almost triangulation \mathcal{S}* if they are the only two triangulations refining \mathcal{S} .

In the literature, flips are defined in a more constructive way. The equivalence of our definition to that one will be the content of Theorem 4.4.1 in Chapter 4. For the time being we show some flips in action.

Figure 2.52 illustrates some examples of flips in the plane. The first is the traditional *diagonal-edge flip* common in computational geometry. The second is the insertion or deletion of a point in the interior of a triangle. There are other flips, not shown in the picture: the insertion or deletion of a point in the interior of an edge and the exchange between two copies of a repeated point.

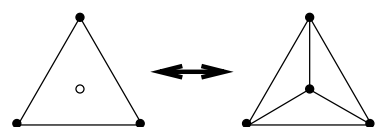
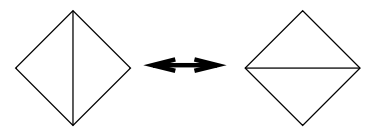


Figure 2.52: Some next-to-minimal subdivisions in the plane, each together with the two triangulations refining it.

The flip relation between triangulations of the same point configuration can be interpreted as an adjacency relation. The result of this is the graph of triangulations of a point configuration.

Definition 2.4.8. We call the *graph of triangulations* of \mathbf{A} the graph whose nodes are all the triangulations of \mathbf{A} and whose edges are flips between them. We denote it $\mathcal{G}_{\text{tri}} \mathbf{A}$.

Example 2.4.9 (Example 2.3.6 continued). The poset of subdivisions here is (isomorphic to) the Boolean lattice of all subsets of the label set J . The refinement poset is then the face lattice of a simplex with $|J|$ vertices. The graph of flips is the graph of this simplex, a complete graph.

Example 2.4.10 (Example 2.3.7 continued). By the description in Example 2.3.7, the poset of subdivisions is isomorphic to the face lattice of a cube. The graph of triangulations is the graph of this cube.

Our final result in this section extends Corollary 2.3.18. There we saw that triangulations are the minimal elements in the refinement poset. Here we see that almost triangulations are the “next-to-minimal” elements.

Proposition 2.4.11. *Every polyhedral subdivision \mathcal{S} other than a triangulation can be refined to an almost-triangulation. Moreover, if \mathcal{S} is regular, then it can be refined to a regular almost-triangulation.*

Proof. We use the regular refinements of Lemma 2.3.16. For this, let B be a cell of \mathcal{S} that is not a simplex (this exists because \mathcal{S} is not a triangulation). Let C be a circuit contained in B . Consider a height vector ω that is sufficiently generic except at C ; for example, let ω be zero on C and random in the rest of the elements of \mathbf{A} .

Then, \mathcal{S}_ω is an almost-triangulation since each $\mathcal{S}(\mathbf{A}|_D, \omega)$ is either a triangulation or an almost-triangulation with C as the unique circuit contained in some cell.

The sentence about regularity follows from the last part of Lemma 2.3.16. □

This result has a nice interpretation in the language of posets. A graph, as any simplicial complex, can be considered a poset. It has two levels, the bottom one consisting of the nodes of the graph and the top one consisting of the edges. Proposition 2.4.11 says that:

Corollary 2.4.12. *The graph of triangulations $\mathcal{G}_{\text{tri}} \mathbf{A}$, as a poset, consists of the lowest two levels of the refinement poset $\text{Subdivs}(\mathbf{A})$.*

Proof. This follows from the fact that edges in $\mathcal{G}_{\text{tri}} \mathbf{A}$ correspond to flips between triangulations, and a flip between two triangulations corresponds to an almost-triangulation. □

2.5 Vector configurations and their triangulations

The reader should now be prepared for a final generalization in our framework: the study of *vector configurations* instead of *point configurations* as

well as their triangulations and subdivisions. There are several immediate justifications for this: on the one hand, it is a harmless generalization; no extra complications are introduced, except perhaps for a slight need of “mental adjustment”. On the other hand, it is a case that arises naturally in several contexts: for example, the normal fan of a polytope is a polyhedral subdivision of the vector configuration consisting of facet normals. Also, we need vector configurations if we want to apply the contraction operation (to be introduced in Section 4.2.4) to non-extremal points in a point configuration.

But the most profound justification for the study of vector configurations is the Gale duality that exists between a point configuration and its *Gale transform*, which is a vector configuration. The study of this duality will be started in Chapter 4, but it will be taken much further in Chapters 5 and 8. Figure 2.53 shows two examples of vector configurations one of them a point configuration as well.

2.5.1 Vector configurations

A vector configuration is a finite collection of vectors in \mathbb{R}^m . We apply to vector configurations the same conventions that we used for point configurations: Repeated vectors are allowed, and distinguished by their labels, and we normally refer to vectors by their labels.

In fact, the homogeneous representation of a point configuration that we have been using so far is an example of a vector configuration. What we have called rank of a point configuration (its dimension plus one) is actually the rank of the linear space generated by the vectors. But there is no reason why we should not allow general, non-homogeneous vector configurations. One way to do this is to interpret what the concepts for a point configuration mean in a homogeneous vector configuration, and then apply them to non-homogeneous ones. For example:

Definition 2.5.1 (Vector configuration). A *vector configuration* in \mathbb{R}^m is a finite set $\mathbf{A} = (\mathbf{p}_j : j \in J)$ of labeled vectors $\mathbf{p}_j \in \mathbb{R}^m$. Its *rank* is its rank as a set of vectors. Its *corank* is $n - r$, where n is its number of elements and r is its rank. A *subconfiguration* is any (labeled) subset of it.

A vector (sub)configuration is *independent* if it does not have repeated vectors and its vectors are linearly independent. It is *dependent* otherwise. A vector configuration of rank r is *in general position* if each r -element subconfiguration is independent. Otherwise, it is *in special position*.

The *positive span*, or *conical hull*, of a subset $C \subseteq J$ of a vector configuration \mathbf{A} with label set J is the following closed polyhedral cone.

$$\text{cone}_{\mathbf{A}}(C) := \left\{ \sum_{j \in C} \lambda_j \mathbf{p}_j : \lambda_j \geq 0 \text{ for all } j \in C \right\}. \quad (2.11)$$

Its *relative interior* is

$$\text{relint}_{\mathbf{A}}(C) := \left\{ \sum_{j \in C} \lambda_j \mathbf{p}_j : \lambda_j > 0 \text{ for all } j \in C \right\}. \quad (2.12)$$

For a linear functional $\psi \in (\mathbb{R}^m)^*$ with the property that $\psi(\mathbf{p}_j) \geq 0$ for

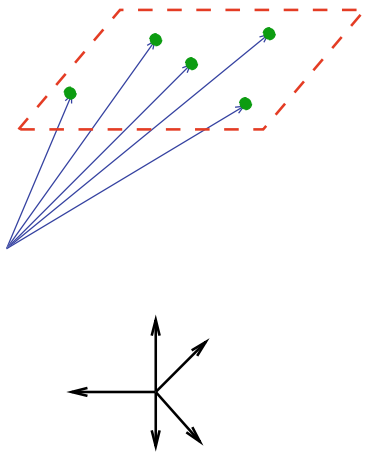


Figure 2.53: Miscellaneous vector configurations.

every $j \in C$, the *face of C in direction ψ* is the following set of labels:

$$\text{face}_{\mathbf{A}}(C, \psi) := \{ j \in C : \psi(\mathbf{p}_j) = 0 \} \quad (2.13)$$

If F is a face of C , we write $F \leq C$. Moreover, if $F \neq C$ then we write $F < C$, and we say that F is a *proper face* of C . Observe that C is always a face of C , obtained when ψ is the zero functional. However, the empty set is *not always* a face in a vector configuration. See Remark 2.5.6 below. A *facet* of C is a face of rank one less than the rank of C . That is, it is a maximal proper face. The linear hyperplane $\{\mathbf{x} \in \mathbb{R}^m : \psi(\mathbf{x}) = 0\} \subset \mathbb{R}^m$ is a *supporting hyperplane* of the face $\text{face}_{\mathbf{A}}(C, \psi)$. An element $j \in C$ is *extremal* if $\{j\}$ is a face. A configuration is *in convex position* if all its elements are extremal.

Remark 2.5.2. $\text{cone}_{\mathbf{A}} = \dot{\cup}_{F \leq J} \text{relint } F$, where $\dot{\cup}$ denotes “disjoint union”.

Definition 2.5.3 (Carrier). For a subconfiguration $S \subseteq \mathbf{A}$, the *carrier* of F in \mathbf{A} is the smallest face of \mathbf{A} containing S , i.e.,

$$\text{carrier}_{\mathbf{A}}(S) := \bigcap_{S \subseteq F \leq J} F \quad (2.14)$$

Remark 2.5.4 (Linearity space). Let \mathbf{L} be the maximal linear subspace contained in $\text{cone}(J)$, for a configuration \mathbf{A} . \mathbf{L} is usually called the *linearity space* of $\text{cone}(J)$. The linearity space of a cone is contained in every face, and since it is maximal, it equals the intersection of all faces of $\text{cone}(J)$. That is, it is the unique minimal face. For a vector configuration, its unique minimal face is the set of elements lying in the linearity space of its conical hull.

Here are two important, but more abstract, definitions:

Definition 2.5.5. A vector configuration \mathbf{A} with index set J is *acyclic* if there is a linear functional that is positive in all the elements of the configuration. It is *totally cyclic* if $\text{cone}_{\mathbf{A}}(J)$ is equal to the vector space spanned by \mathbf{A} .

In Section 2.1 we said we would *represent* point configurations as homogeneous matrices. In the same way, vector configurations will be represented by arbitrary matrices. In particular, a homogeneous matrix can be read both as a “homogeneous vector configuration” and as a point configuration. This is not a source of ambiguity; it simply that these two things are the same, for all the purposes of this book.

Furthermore, scaling the vectors of a configuration by positive scalars does not affect the face structure of the cone they span, or the set of subdivisions and triangulations of it (see next section). If a configuration is acyclic, by positive scaling we can make it homogeneous and thus equivalent to a point configuration. The bottom line is that acyclic vector configurations behave exactly as point configurations. Non-acyclic ones have a couple of strange new features. The first one is that they do not have an empty face:

Remark 2.5.6 (The empty face). In a point configuration, the empty set is considered a face because there is an affine functional that is positive

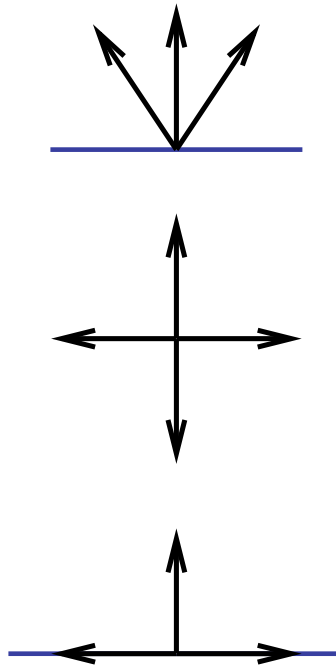


Figure 2.54: Three vector configurations: one acyclic, one totally cyclic, and one uninteresting (with three, four, and three vectors respectively).

at all points (for example, the constant functional $\psi(\mathbf{x}) = 1$). In vector configurations we only consider *linear* functionals and the existence of an always positive one is our definition of acyclic. That is, the empty set is a face of a vector configuration \mathbf{A} only if \mathbf{A} is acyclic. This agrees with the fact that the trivial subspace $\{0\}$ is a face of a cone only if the cone is *pointed* (that is, the positive span of an acyclic configuration). Observe that homogeneous vector configurations (also known as point configurations) are always acyclic.

Observe also that the zero vector may be an element in a vector configuration. In this case, the configuration cannot be independent, nor acyclic, nor in general position.

2.5.2 Polyhedral subdivisions of vector configurations

The definition of subdivision for a vector configuration is the same as for point configurations, except the role of the convex hull is now played by the positive hull (also called the positive span or the conic hull):

Definition 2.5.7 (Subdivision of a vector configuration). A collection \mathcal{S} of subconfigurations of a vector configuration \mathbf{A} in \mathbb{R}^m is a *polyhedral subdivision* of \mathbf{A} if it satisfies the following conditions:

- (CP) If $C \in \mathcal{S}$ and $F \leq C$ then $F \in \mathcal{S}$ as well. (Closure Property)
- (UP) $\bigcup_{C \in \mathcal{S}} \text{cone } C \supseteq \text{cone } \mathbf{A}$. (Union Property)
- (IP) $\text{relint } C \cap \text{relint } C' \neq \emptyset$ for $C, C' \in \mathcal{S}$ implies $C = C'$. (Intersection Property)

The elements of a polyhedral subdivision \mathcal{S} are called *cells*. Cells of the same rank as \mathbf{A} are *full-dimensional* or *maximal*. Cells of rank 1 are usually called *rays* of \mathcal{S} , but we will sometimes call them *vertices*, as if we were dealing with a point configuration. Independent cells are called *simplicial cells* or *simplices*.

Two subconfigurations *intersect properly* if they and all of their faces satisfy (IP); they intersect *improperly* otherwise.

A *triangulation* of \mathbf{A} is a polyhedral subdivision all of whose cells are simplices.

A subdivision \mathcal{S} *refines* another one \mathcal{S}' —symbolically: $\mathcal{S} \preceq \mathcal{S}'$ —if for each $C \in \mathcal{S}$ there is a $C' \in \mathcal{S}'$ with $C \subseteq C'$. The poset of polyhedral subdivisions of a vector configuration \mathbf{A} will be denoted $\text{Subdivs}(\mathbf{A})$.

Multiplying a vector (or more) of a vector configuration by a *positive* constant does not change its combinatorics (faces, positive spans, relative interiors, etc). In particular, it preserves the collection of subdivisions and triangulations of it. Since every acyclic vector configuration can be homogenized by normalizing each vector by the value that a certain positive functional ψ takes on it, acyclic vector configurations do not introduce extra complications into our picture. But non-acyclic ones may. Let us see two examples:

Example 2.5.8 (Four vectors in general position in rank 2). Consider the following four vectors in the plane

$$\mathbf{A} = \begin{pmatrix} 1 & 2 & 3 & 4 \\ 1 & -2 & 1 & 0 \\ 0 & 1 & -2 & 1 \end{pmatrix}.$$

We encourage the reader to check that \mathbf{A} has the eight subdivisions presented in Figure 2.55. We arranged them in a suggestive way to indicate the structure of the poset (without drawing the edges of a Hasse diagram) and, as usual, we only include the list of maximal cells in each. The top picture represents the trivial subdivision.

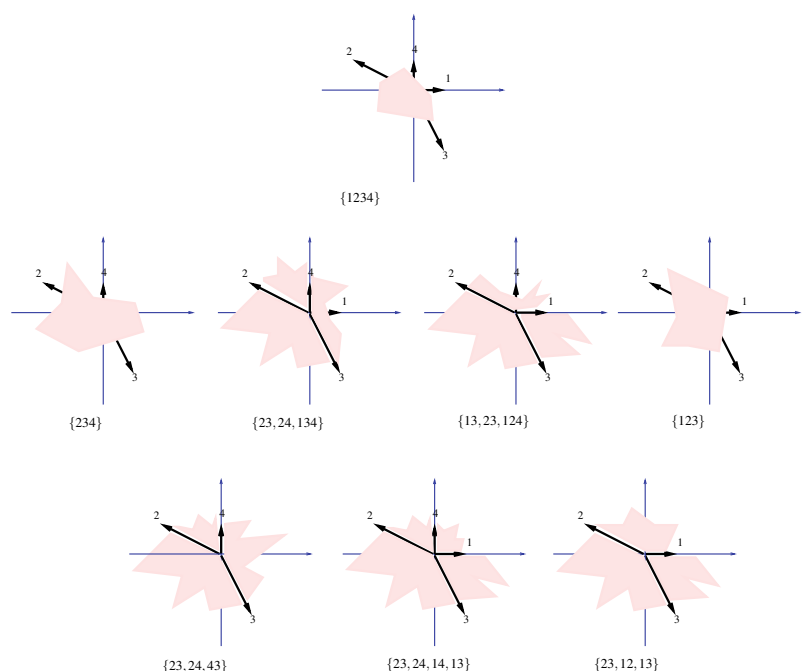


Figure 2.55: All subdivisions of four vectors in general (and non-acyclic) position in the plane.

Remark 2.5.9 (The empty set as a cell). We have said that the empty set is a face of a configuration only if the configuration is acyclic. Another feature of the empty set is that, by convention, its relative interior and hull form the zero cone $\{0\} \subseteq \mathbb{R}^m$ (a justification for this convention is that the result of an empty sum is zero).

In particular, if a subdivision contains a (non-empty, and necessarily not acyclic) cell with 0 in its relative interior, then the empty set is not a cell, or the intersection property would be violated. Conversely, if the empty set is not a cell, then the subdivision must contain a non-acyclic cell, then a unique minimal such one, in order for (UP) to hold: 0 is not in the relative interior of any acyclic set.

Summing up, a non-acyclic vector configuration has two types of subdivisions: those whose cells are all acyclic, which contain \emptyset as a cell, and those whose cells are all not acyclic, which contain a unique minimal non-empty cell. In the previous example there are three and five respective subdivisions of each type.

Example 2.5.10 (Five vectors in general position in the plane). We now let $\mathbf{A} \subset \mathbb{R}^2$ consist of five vectors of the same length, spaced equally (that is, pointing in the directions of the vertices of a regular pentagon). Each maximal simplex is a set of two vectors $\{i, j\}$, and a triangulation will just be a circular sequence of such pairs covering the circle of directions once. There are three possibilities, modulo the symmetries of the configuration:

1. The triangulation consisting of five cones $\{12, 23, 34, 45, 15\}$.
2. Five triangulations consisting of four cones, such as $\{13, 34, 45, 15\}$ and the ones obtained from it by symmetry.
3. Five triangulations consisting of three cones, such as $\{13, 35, 15\}$ and the ones obtained from it by symmetry.

There are six types of non-simplicial subdivisions. We encourage the reader to verify the definition for each, and check that the list is complete:

1. The trivial subdivision $\{12345\}$.
2. The non-trivial subdivisions with only one maximal cell, which come in two types: $\{1345\}$ and $\{135\}$ (observe that $\{123\}$, for example, is not a subdivision because it does not cover the whole positive span of \mathbf{A} , which is the whole plane).
3. The subdivisions whose cells are acyclic but still are not triangulations, which come in three types again: $\{123, 345, 15\}$, $\{13, 345, 15\}$ and $\{123, 34, 45, 15\}$.

2.5.3 Regular subdivisions of vector configurations

Again, for vector configurations we can take word for word the definition of regularity used for point configurations (see Definition 2.2.10). As an example, Figure 2.57 shows how the nine types of subdivisions of our last example arise as regular subdivisions. The lifting of vectors happens in \mathbb{R}^3 .

As expected, the zero height vector (first picture in the figure) produces the trivial subdivision. Triangulations (bottom row) are produced by sufficiently generic height vectors.

There is, however, one substantial difference with the case of point configurations. What would have happened if we took negative height vectors? In the case of point configurations this causes no trouble, since changing all entries of a height vector by a constant does not change the combinatorics. In particular, it does not change what the lower faces of the lifted point configuration are. The lifted point configuration lies below the hyperplane at height zero but the lower faces remain unchanged.

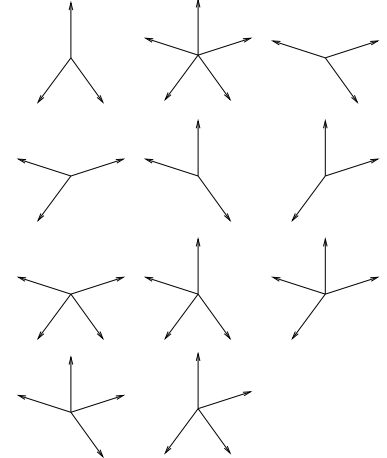


Figure 2.56: Triangulations of five vectors in general position in the plane.

In the case of a non-acyclic vector configuration, however, if the heights are negative then the lifted vector configuration *has no lower faces!* Indeed, a lower face is one for which there is a functional ψ with last coordinate positive and minimized at that face. In our “downwards lifted” vector configuration, however, such functionals do not achieve a minimum. For the time being let us be satisfied with just saying that *height vectors for vector configurations should better be taken with non-negative entries*, since this is sufficient (and essentially necessary) to obtain a regular subdivision from the height.

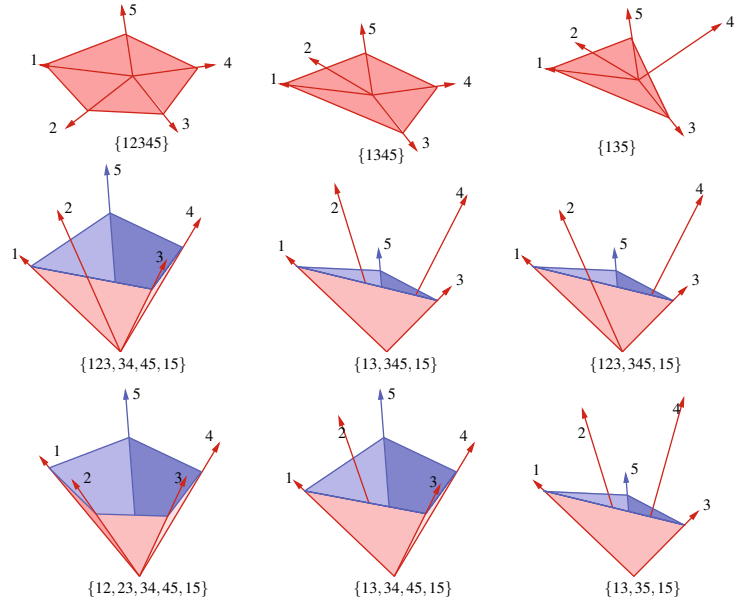


Figure 2.57: The subdivisions of Example 2.5.10, obtained as regular subdivisions. The three triangulations are in the bottom, the three subdivisions with a single cell are on top and the rest are in the middle.

Lemma 2.5.11. *Let \mathbf{A} be a vector configuration and let $\omega : J \rightarrow \mathbb{R}$. Then the set $\mathcal{S}(\mathbf{A}, \omega)$ of lower faces of \mathbf{A}^ω is a subdivision of \mathbf{A} if and only if ω differs from a nonnegative height only by a linear function.*

Proof. Let ω be a height function that differs from a nonnegative height $\omega' \leq 0$ only by a linear function. Then the set of lower faces of \mathbf{A}^ω and $\mathbf{A}^{\omega'}$ coincide. We prove that the set of lower faces of $\mathbf{A}^{\omega'}$ is a subdivision of \mathbf{P} by proving (CP), (IP), and (UP) for it. Conditions (CP) and (IP) again follow from elementary polyhedral geometry [339]; there is nothing new here. For nonnegative height functions, the proof of (UP) is completely analogous to the proof of (UP) for Theorem 2.3.11: For general heights ω and some $\mathbf{x} \in \text{cone}(\mathbf{A})$, the intersection of $\mathbf{x} \times \mathbb{R}$ with $\text{cone}(\mathbf{A}^\omega)$ (the *fiber over \mathbf{x}*) might not have a negative last coordinate, and such an \mathbf{x} would then not be contained in any lower face of $\text{cone}(\mathbf{A}^\omega)$. This may happen if \mathbf{A} is totally cyclic, as discussed before. However, if the heights are all nonnegative, then all fibers have lowest elements, and the proof of (UP) can proceed as before.

It remains to show that every regular subdivision is induced by a non-negative height function. For an arbitrary cell σ in such a regular subdivision, consider a supporting hyperplane of the corresponding lower face of cone(A^ω). Moreover, let ω_σ be the unique linear height function that lifts A to lie in that hyperplane. Then, $\omega - \omega_\sigma$ is a nonnegative height function with the desired properties. \square

In Section 4.1.3, Theorem 4.1.39, we will see why the restriction to non-negative heights is no loss of generality as far as the set of all regular subdivisions is concerned. A much more detailed look at the structure of the space of height vectors can be found in Section 5.4.1.

2.6 Triangulations as simplicial complexes

Triangulations of a point or vector configuration are, among other things, simplicial complexes. In this section, we review several basic notions regarding simplicial complexes and how they behave in triangulations of configurations. Most specifically, we are interested in the numbers of faces of various dimensions. A good reference for the contents of this section is [339].

2.6.1 Simplicial complexes

An *abstract simplicial complex* \mathcal{K} is a family of finite subsets of a label set J , such that, for every $F \in \mathcal{K}$, all subsets of F are also in \mathcal{K} . We will always assume that J is finite so that \mathcal{K} is finite too. In parallel to the geometric objects we studied earlier, the elements of a simplicial complex \mathcal{K} will be called *cells* or *simplices*. The dimension of a simplex is its cardinality minus one, and simplices of dimensions zero and one are called *vertices* and *edges* respectively. The maximal dimension among all cells is called the dimension of the complex, and the complex is called *pure* if all its maximal cells have the same dimension. In a pure complex of dimension d , the cells of dimensions d and $d - 1$ are called, respectively, facets and ridges. For example, the boundary of a simplicial polytope forms a simplicial complex whose facets and ridges correspond to those of the polytope.

There are good topological and combinatorial reasons to study abstract simplicial complexes on their own. We already defined a *geometric simplicial complex* as a polyhedral complex, all of whose faces are simplices. It is worth remarking that any abstract simplicial complex, which is just a set of sets, can in fact be effectively achieved as a geometric simplicial complex. For this we need a map $J \rightarrow \mathbb{R}^m$ that sends the set of labels into vectors of Euclidean space with the following properties: the image of every $F \in \mathcal{K}$ is affinely independent (that is, it is the vertex set of a simplex); and different (geometric) simplices of the complex only intersect in common faces. Indeed, any map $J \rightarrow \mathbb{R}^{|J|-1}$ with an affinely independent image satisfies these. In particular, we can study every simplicial complex as if it is embedded geometrically. It is not true that every simplicial complex of a certain dimension d can be embedded in that same \mathbb{R}^m . The theory of embeddability of complexes is quite rich (see [227]).

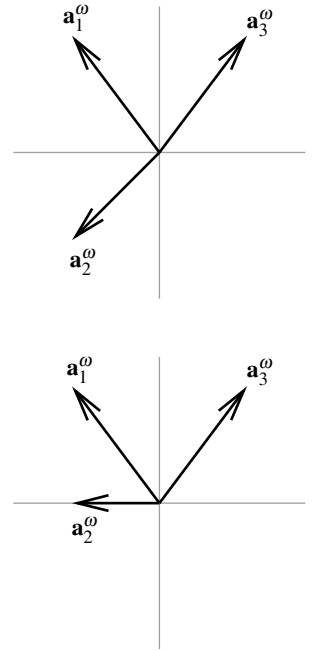


Figure 2.58: The one-dimensional vector configuration $(-1, -1, 1)$ and two of its liftings. When $\omega = (2, -1, 2)$ it has negative entries but it still defines a regular subdivision because $\omega + (1, 1, -1) = (3, 0, 1)$.

Let \mathcal{K} be a simplicial complex. For any $F \in \mathcal{K}$, the *star* of F in \mathcal{K} , $st_{\mathcal{K}}(F)$, is the subcomplex of \mathcal{K} induced by all simplices of \mathcal{K} that contain F as a face, plus all their faces (a word of caution: In the literature sometimes this is called the *closed star*). The *link* of F in \mathcal{K} is the simplicial complex $\text{link}_{\mathcal{K}}(F) = \{C \in st_{\mathcal{K}}(F) | F \cap C = \emptyset\}$. If \mathcal{K}, \mathcal{L} are simplicial complexes, their *join* is $K * L = \{F \cup G | F \in K, G \in L\}$. For a geometric simplicial complex \mathcal{K} we denote by $|\mathcal{K}|$ the underlying topological space, that is, the union of the geometric simplices. If $|\mathcal{K}|$ is homeomorphic to a ball or sphere we say that \mathcal{K} is a *simplicial ball* or *simplicial sphere*, respectively. Every triangulation of a point configuration is a simplicial ball, while triangulations of a vector configuration can be simplicial balls or simplicial spheres, the latter if and only if the configuration is totally cyclic.

2.6.2 The *f*-vector of a simplicial complex

In what follows the actual geometry is irrelevant. The notion of an *f-vector* of a simplicial complex has been central to the development of the combinatorial theory of polytopes [339]. The *f*-vector of an abstract simplicial complex \mathcal{K} of dimension d is the vector

$$f(\mathcal{K}) = (f_{-1}(\mathcal{K}), f_0(\mathcal{K}), f_1(\mathcal{K}), f_2(\mathcal{K}), \dots, f_d(\mathcal{K})),$$

where $f_i(\mathcal{K})$ denotes the number of simplices of dimension i in \mathcal{K} . As a convention, in this definition $f_{-1}(\mathcal{K}) = 1$ for the empty set. The top entry in the *f*-vector, that is, $f_d(\mathcal{K})$, is sometimes called the *size* of \mathcal{K} .

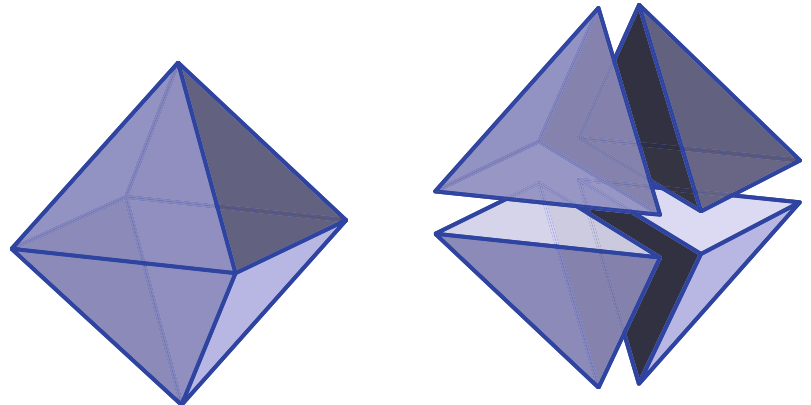


Figure 2.59: The *f*-vector of the boundary of the octahedron is $(1, 6, 12, 8)$; the *f*-vector of the triangulated regular octahedron is $(1, 6, 13, 12, 4)$ because there are four tetrahedra adding four interior triangles and one interior edge; the number of vertices remains unchanged.

Two of the most important questions about *f*-vectors of simplicial complexes are what constraints different entries of a same *f*-vector must satisfy and how big can the individual entries of *f*-vectors be for a given dimension and number of vertices. We will be interested in these questions only for simplicial balls and spheres. We first look at the smallest possible size.

On a simplicial ball or sphere, the *adjacency graph* or *dual graph* of \mathcal{K} is the graph whose nodes correspond to the maximal simplices in \mathcal{K} and

whose edges correspond to simplices intersecting in a common *ridge*, i.e., a simplex of dimension one less than the maximal simplex. Not much can be said in general about dual graphs of triangulations (see exercises), but they are useful to estimate a lower bound for the size of a triangulation:

Theorem 2.6.1 (Lower bound theorem for balls). *The size of a simplicial d -ball with n vertices is at least $n - d$. Moreover, the equality is achieved precisely if the following (equivalent) conditions occur:*

1. *The dual graph of the ball is a tree.*
2. *Every $(d - 2)$ -cell of the ball lies in the boundary of $\text{conv}(\mathcal{K})$.*

Proof. Observe that the dual graph of our ball \mathcal{K} is a connected graph. In particular, it is possible to order its nodes (the full-dimensional simplices $\sigma_1, \sigma_2, \dots$ of \mathcal{K}) in such a way that the first i of them form a connected subgraph, for every i .

We now imagine we are “building” \mathcal{K} from scratch by adding the simplices one by one. With the first simplex, σ_1 , we are inserting $d + 1$ vertices at the same time, but any subsequent simplex will either use only vertices that were already there or insert a single new one (because every σ_i , $i > 1$ shares at least one facet with one of the previous simplices). In particular, we need *at least* $n - d - 1$ simplices other than σ_1 to insert all vertices, which proves the first sentence:

$$f_d(\mathcal{K}) \geq 1 + (n - d - 1) = n - d.$$

Moreover, we get equality if and only if *every* simplex after σ_1 indeed inserts a new vertex, which is easily seen to be equivalent to not having cycles in the dual graph (if there is a cycle, the last simplex of the cycle that we insert has two facets in common with previous simplices, hence it introduces no new vertex).

We now prove that having a dual graph which is a tree is equivalent to excluding interior $(d - 2)$ -faces (interior edges in the case of three dimensions, for example). One direction is easy: if F is an interior $d - 2$ -cell, its link is itself a cycle, with nodes being the $(d - 1)$ -cells containing F and two consecutive nodes belonging to the same d -cell. This cycle is dual to a cycle in the adjacency graph of \mathcal{K} .

For the other direction (although the statement is valid for abstract simplicial complexes too), we will assume that our ball \mathcal{K} is a triangulation of a point configuration. That is, that we have it geometrically realized in \mathbb{R}^m and that $|\mathcal{K}|$ is a convex polytope. (If the reader is familiar with topological arguments, he or she can probably change the language in the proof to make it work for an abstract d -ball).

Assume that the dual graph of \mathcal{K} contains a cycle. Let $\sigma_0, \sigma_1, \dots, \sigma_k = \sigma_0$ denote the d -simplices forming the cycle, and let $\mathbf{p}_1, \dots, \mathbf{p}_k$ denote the barycenters of them. We consider the cycle geometrically embedded with the \mathbf{p}_i 's as nodes. Let \mathbf{p} be a point that “moves” along the cycle, starting at \mathbf{p}_1 and ending at \mathbf{p}_{k-1} . We look at what happens to the segment $\mathbf{p}_0\mathbf{p}$

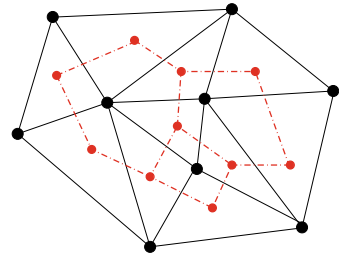


Figure 2.60: The dual graph of a triangulation appears in red.

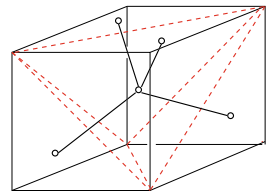


Figure 2.61: A triangulation of the 3-cube with 5 tetrahedra. Its dual graph is a tree.

during this motion. At the first and last moments, the segment crosses two different $(d-1)$ -faces of σ_0 . Since at every moment in time \mathbf{p} is outside σ_0 , there must be some instant when $\mathbf{p}_0\mathbf{p}$ intersects a $(d-2)$ -face of σ_0 . The intersection point must be in the interior of $|\mathcal{K}|$ by convexity, since both \mathbf{p}_0 and \mathbf{p} are in the interior. \square

Remark 2.6.2. What is the largest size of a triangulation? The answer is essentially given by the *Upper Bound Theorem* for spheres, that we state below. This theorem was first proved by Stanley in 1980 [306], and a detailed proof can be found in [339]. The cyclic d -polytope with n vertices, denoted by $\mathbf{C}(n, d)$, which appears in the statement, is the convex hull of n arbitrary points taken from the moment curve $\{(t, t^2, t^3, \dots, t^d) : t \in \mathbb{R}\} \subset \mathbb{R}^d$. The proper faces of this polytope form a simplicial $(d-1)$ -sphere that we still denote $\mathbf{C}(n, d)$. Cyclic polytopes are among the most important constructions in polytope theory. We will study them again in detail in Section 6.1 (and they make an appearance also in Section 3.6.1).

Theorem 2.6.3 (Upper Bound Theorem). *For any simplicial d -sphere \mathcal{K} with n vertices*

$$f_i(\mathcal{K}) \leq f_i(\mathbf{C}(n, d+1)), \quad 0 \leq i \leq d.$$

In order to adapt this statement to balls, we need to define the *deletion* of a vertex v in a simplicial complex \mathcal{K} . We denote it $\mathcal{K} \setminus v$ and by it we mean the subcomplex of \mathcal{K} consisting of the cells that do not contain v . A formula for it is

$$\mathcal{K} \setminus v = (\mathcal{K} \setminus \text{st}_{\mathcal{K}}(v)) \cup \text{link}_{\mathcal{K}}(v).$$

Lemma 2.6.4.

$$f_j(\mathcal{K}) = f_j(\mathcal{K} \setminus v) + f_{j-1}(\text{link}_{\mathcal{K}}(v)), \text{ for } -1 \leq j \leq d-1.$$

Proof. Suppose C is a cell of \mathcal{K} of dimension j . If $v \in C$ then C appears as a $(j-1)$ -face $C \setminus \{v\}$ in $\text{link}_{\mathcal{K}}(v)$. Otherwise, C is in $\mathcal{K} \setminus v$. In either case the presence of C is counted in exactly one summand of the formula. \square

Now we are ready to present the upper bound on the size of triangulations. This result is known to be tight, and the bound is achieved by the cyclic polytopes.

Corollary 2.6.5. *The size of a simplicial d -ball with n vertices is bounded above by $f_d(\mathbf{C}(n+1, d+1)) - (d+1)$.*

That is, the largest size of a triangulation is asymptotically $O(n^{\lceil(d+1)/2\rceil})$. Similar bounds hold for the i -th entry of the f -vector of a triangulation.

Proof. What we do is we embed the triangulation in question inside a simplicial d -sphere. For this, think of your d -ball as embedded in \mathbb{R}^d (here we do not really need it to be *geometrically* embedded; a topological embedding is enough, and it obviously exists since $|\mathcal{K}|$ is a d -ball).

Now, think of the “point at infinity” in \mathbb{R}^d as an extra $(n+1)$ -th vertex of your simplicial complex, joined to every boundary cell of \mathcal{K} . If you feel more comfortable being able to visualize this process, project \mathbb{R}^d stereographically to a d -sphere, as shown in Figure 2.62 so that the simplices of \mathcal{K} become spherical simplices in the sphere. Then use the center of the projection (the “north pole” in the figure) as the new vertex of your complex, joining it to all the boundary of \mathcal{K} .

In this way you get a simplicial d -sphere \mathcal{K}' which contains \mathcal{K} as a subcomplex, namely the subcomplex $\mathcal{K}' \setminus \{v\}$, where v is the new vertex.

In this situation, Lemma 2.6.4 reads

$$f_j(\mathcal{K}') = f_j(\mathcal{K}) + f_{j-1}(\partial \mathcal{K}), \quad -1 \leq j \leq d.$$

Hence,

$$f_d(\mathcal{K}) = f_d(\mathcal{K}') - f_{d-1}(\partial \mathcal{K}) \leq f_d(\mathbf{C}(n, d)) - (d+1),$$

as stated. In the last inequality we are using the upper bound theorem and the fact that $f_{d-1}(\partial \mathcal{K}) \geq d+1$ (since a simplicial $(d-1)$ -sphere needs at least $d+1$ vertices). \square

2.6.3 Linear constraints on the f -vector

We start this section by stating perhaps the most important formula involving the f -numbers, *Euler's formula*. Proofs of this result can be found in most sources in algebraic topology (see [237]). We will use Euler's formula heavily when we study the space of planar triangulations (in particular how they are connected).

Lemma 2.6.6. *For every simplicial d -ball \mathcal{K} :*

$$\sum_{j=0}^d (-1)^j f_j(\mathcal{K}) = 1.$$

For every simplicial d -sphere \mathcal{K} :

$$\sum_{j=0}^d (-1)^j f_j(\mathcal{K}) = 1 + (-1)^d.$$

The two versions of Euler's formula are easy to derive from one another. For example, if \mathcal{K}' is a d -sphere, removing the interior of any particular d -simplex from it gives a a simplicial d -ball \mathcal{K} , with the same f -vector except for $f_d(\mathcal{K}) = f_d(\mathcal{K}') - 1$. For the converse, the reader can use the same trick (stereographic projection) as in the proof of Corollary 2.6.5.

Can one characterize the f -vectors of triangulations of convex (simplicial) polytopes or point configurations? It turns out one can indeed, but in doing so it is convenient to first translate the f -vector into a different form, called the *h-vector*. Formally speaking, the transformation of f -vectors into h -vectors is just a linear change of coordinate system in the space \mathbb{R}^{d+2} where the f -vector $(f_{-1}, f_0, \dots, f_d)$ lies. Some benefits of this change are:

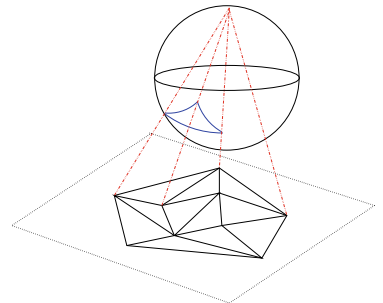


Figure 2.62: “Printing” a triangulation in the plane over the surface of the sphere.



Figure 2.63: Leonard Euler.

- (a) Complicated relations among entries of the f -vector become neat clean relations in terms of the entries of the h -vector,
- (b) The f_j are nonnegative linear combination of the h_i 's, therefore upper and lower bounds on the h_i imply upper and lower bounds on the f_j ,
- (c) The h -vector has a useful geometric meaning in terms of *shellings* of a simplicial complex [339] (we will come back to this in Section 9.5.2), and
- (d) The h -vector has also an amazing algebraic meaning in terms of the Stanley-Reisner rings [306].

Definition 2.6.7. Let \mathcal{K} be a $(d-1)$ -dimensional pure simplicial complex with f -vector $(f_{-1}(\mathcal{K}), f_0(\mathcal{K}), f_1(\mathcal{K}), \dots, f_{d-1}(\mathcal{K}))$. The *h-vector* of \mathcal{K} is the vector

$$h(\mathcal{K}) := (h_{-1}(\mathcal{K}), h_0(\mathcal{K}), h_1(\mathcal{K}), \dots, h_{d-1}(\mathcal{K})),$$

where:

$$h_k(\mathcal{K}) := \sum_{i=0}^k (-1)^{k-i} \binom{d-i}{k-i} f_{i-1}, \quad 0 \leq k \leq d.$$

A compact way of representing the f and h vector is as the coefficients of two univariate polynomials of degree d , written in reverse order. Namely:

$$F_{\mathcal{K}}(t) = \sum_{i=0}^d f_{i-1} t^{d-i}, \quad H_{\mathcal{K}}(t) = \sum_{i=0}^d h_i t^{d-i},$$

The reader can verify that in this notation the relation between the two is simply that:

$$H_{\mathcal{K}}(t) = F_{\mathcal{K}}(t-1),$$

from which

$$F_{\mathcal{K}}(t) = H_{\mathcal{K}}(t+1),$$

that is,

$$f_{k-1}(\mathcal{K}) := \sum_{i=0}^k \binom{d-i}{k-i} h_i, \quad 0 \leq k \leq d.$$

In the example of a triangulated regular octahedron of Figure 2.59 the h -vectors are $h(\mathcal{T}) = (1, 2, 1, 0, 0)$ and $h(\partial \mathcal{T}) = (1, 3, 3, 1)$. Observe also that $h_0 = f_{-1} = 1$. Euler's formula (Lemma 2.6.6) translates to the following simpler statement:

Corollary 2.6.8. For every simplicial d -ball, $h_d = 0$, while for every simplicial d -sphere, $h_d = 1$.

More generally, one has the following statements:

Lemma 2.6.9. Suppose \mathcal{K} is a $(d-1)$ -simplicial complex. Then

- $h_d(\mathcal{K}) = (-1)^d(1 - \chi(\mathcal{K}))$ where $\chi(\mathcal{K})$ is the Euler characteristic of the simplicial complex, i.e., $\chi(\mathcal{K}) = \sum_{j=0}^{d-1} f_j(\mathcal{K})$.
- $h_0(\mathcal{K}) = 1$.
- $h_1(\mathcal{K}) = f_0(\mathcal{K}) - d$.
- $f_{d-1}(\mathcal{K}) = \sum_{i=0}^d h_i(\mathcal{K})$.

It is easy to find other relations among the entries in the f -vector of a simplicial $(d-1)$ -sphere. For example, since every $(d-1)$ -cell has d facets and every $(d-2)$ -cells is a facet of precisely two $(d-1)$ -cells, one has that $df_{d-1} = 2f_{d-2}$. In a sense, this equation can be understood as Euler's formula summed over the links of every $(d-2)$ -cell. Indeed, such links are 0-spheres, and Euler's formula for the 0-sphere is “every 0-sphere has two vertices”. Similarly, the link of every $(d-2-k)$ -cell is going to be a k -sphere, so we will get one Euler's formula for each dimension k . Perhaps surprisingly, when written in terms of the h -vectors, all these relations are equivalent to the following beautiful and symmetric formulas:

Lemma 2.6.10 (Dehn-Sommerville equations). *The h -vector of any simplicial $(d-1)$ -sphere \mathcal{K} is symmetric, that is,*

$$h_i(\mathcal{K}) = h_{d-i}(\mathcal{K}) \quad 0 \leq i \leq d.$$

We now show another simple relation between the h -vectors of a ball and of its boundary. A proof for shellable balls will be sketched in Section 9.5.2.

Theorem 2.6.11 (McMullen and Walkup (1971)). *For any simplicial $(d-1)$ -ball \mathcal{K} we have:*

$$h_i(\partial\mathcal{K}) = \sum_{k=0}^i h_k(\mathcal{K}) - h_{d-k}(\mathcal{K}), \quad 0 \leq i \leq d-1.$$

Proof. We use the Dehn-Sommerville equations with two spheres: the $(d-2)$ -dimensional sphere $\partial\mathcal{K}$, and the $(d-1)$ -sphere \mathcal{K}' that we constructed for the proof of Corollary 2.6.5. The equation we settled there was

$$f_j(\mathcal{K}') = f_j(\mathcal{K}) + f_{j-1}(\partial\mathcal{K}), \quad -1 \leq j \leq d.$$

The above linear equation carries over to give

$$h_i(\mathcal{K}') = h_i(\mathcal{K}) + h_{i-1}(\partial\mathcal{K}).$$

Hence, we have $h_i(\mathcal{K}) = h_i(\mathcal{K}') - h_{i-1}(\partial\mathcal{K})$, where it is understood that $h_k(\mathcal{K}) = 0$ for $k < 0$. Therefore $h_i(\mathcal{K}) = h_{d-i}(\mathcal{K}') - h_{i-1}(\partial\mathcal{K})$ by the Dehn-Sommerville relations applied to \mathcal{K}' . Thus, $h_i(\mathcal{K}) - h_{d-i}(\mathcal{K}) = h_i(\partial\mathcal{K}) - h_{i-1}(\partial\mathcal{K})$, applying again the previous equation and the Dehn-Sommerville equations to $\partial\mathcal{K}$. Adding enough copies of this expression yields the desired result. \square

Intuitively, the above theorem says that the h -vector (equivalently, the f -vector) of the boundary of a simplicial ball is determined by the f -vector of the ball. We see two curious applications below.

Corollary 2.6.12. *A simplicial $(d - 1)$ -ball \mathcal{K} has no interior face of dimension $d - k - 1$ if and only if $h_i(\mathcal{T}) = 0$ for all $i \geq k$.*

Proof. Notice that due to the containments of faces, when \mathcal{K} has no interior face of dimension $d - k - 1$, then \mathcal{K} has no interior face of dimension less than that either. That is, $f_i(\mathcal{K})$ and $f_i(\partial\mathcal{K})$ are equal for all $0 \leq i \leq d - k$ and thus the same happens for the corresponding h -vector entries. On the other hand we saw in the proof of the McMullen-Walkup equations that $h_i(\mathcal{K}) - h_{d-i}(\mathcal{K}) = h_i(\partial\mathcal{K}) - h_{i-1}(\partial\mathcal{K})$. Hence $h_{d-i}(\mathcal{K}) = 0$ for $0 \leq i \leq d - k$. This means $h_i(\mathcal{K}) = 0$ for $k \leq i \leq d$. The converse implication is a reversal of the above arguments. \square

Exercises

Exercise 2.1. Let \mathbf{A} be a point configuration with label set J and consider two height functions $\omega, \omega' : J \rightarrow \mathbb{R}^n$ such that $\omega' - \omega$ is the restriction to \mathbf{A} of an affine map $\mathbb{R}^m \rightarrow \mathbb{R}$. Show that ω and ω' produce the same regular subdivision of \mathbf{A} . From this conclude that:

1. If \mathcal{S} is a regular subdivision and C is an affinely independent subset of \mathbf{A} , then there is a height function that produces \mathcal{S} and gives height zero to all points in C .
2. If ω is itself the restriction to \mathbf{A} of an affine map, then it produces the trivial subdivision.

Exercise 2.2. How many distinct circuits are there in the point configuration of the vertices of a regular hexagon? What happens if the points are not on a circle?

Exercise 2.3. Show that for a 1-dimensional point configuration without repeated points all subdivisions are regular.

Exercise 2.4. Let \mathbf{A} be a point configuration. Let C_1 be an affinely independent subset of points of \mathbf{A} . Show that there is a regular triangulation of \mathbf{A} in which C_1 is used as a simplex.

Exercise 2.5. Let \mathbf{A} be a point configuration. Let C_1 and C_2 be two subsets of points of \mathbf{A} . Suppose they are both affinely independent, and that they intersect properly. Show that there is a regular triangulation of \mathbf{A} in which both are used as simplices.

Exercise 2.6. Let \mathbf{A} be a point configuration. Let C_1, C_2 and C_3 be three subsets of points of \mathbf{A} . Suppose the three are affinely independent, and that they intersect properly to one another. Show by an example that there may not be any regular triangulation of \mathbf{A} in which the three are used as simplices.

Exercise 2.7. Let \mathbf{A} be a point configuration. Let C_1, C_2 and C_3 be three subsets of points of \mathbf{A} . Suppose the three are affinely independent, and that they intersect properly to one another. Show by an example that there may not be any triangulation, regular or not, of \mathbf{A} in which the three are used as simplices.

(Hint: Now you need to go to dimension three.)

Exercise 2.8. Find all subdivisions of the vector configuration

$$\mathbf{A} = \begin{pmatrix} 1 & 2 & 3 & 4 \\ 0 & 1 & 1 & 0 \\ 1 & 1 & -1 & -1 \end{pmatrix}.$$

Note that this example is neither totally cyclic nor acyclic.

Exercise 2.9. Let \mathcal{K} be a simplicial complex and let F_1 and F_2 be two of its faces. Suppose that $F_1 \cap F_2 = \emptyset$ and that $F_1 \cup F_2$ is a face of \mathcal{K} . Prove that $\text{link}(F_2, \text{link}(F_1, \mathcal{K})) = \text{link}(F_1 \cup F_2, \mathcal{K})$.

Exercise 2.10. Let \mathcal{K} be a simplicial d -ball with F a boundary face of \mathcal{K} such that it has dimension $k-1$ and $\text{link}(F, \mathcal{K})$ is a simplicial $d-k$ ball. Then $\text{link}(F, \partial \mathcal{K}) = \partial(\text{link}(F, \mathcal{K}))$.

Exercise 2.11. Let \mathcal{K} be the boundary complex of a simplicial d -polytope \mathbf{P} and \mathbf{v} a vertex of \mathbf{P} . Prove that $\partial(\mathcal{K} - \mathbf{v})$ equals $\text{link}(\mathbf{v}, \mathcal{K})$.

Exercise 2.12. Give a formula for the f and h -vectors and polynomials associated to a d -simplex. Do the same for the boundary of a d -simplex (this is a sphere now).

Exercise 2.13. Verify a couple of the properties of Lemma 2.6.9.

Exercise 2.14. Consider a simplicial complex \mathcal{K} which is the union or intersection of two other simplicial complexes. Can you write formulas for the h -vector of \mathcal{K} in terms of the h -vectors of its parts?

Exercise 2.15. What are the conditions that a vector with integer coordinates must satisfy to be the f -vector of a 3-dimensional convex polytope?

Exercise 2.16. Compute the f -vectors of triangulations of a regular 3-cube. What is the dimension of the convex hull of the f -vectors? Do you notice anything interesting?

Exercise 2.17. Can you find an example of a positive integral vector that satisfies the McMullen-Walkup equations but is not the f -vector of a triangulation of a simplicial polytope?

Exercise 2.18. Let \mathbf{A} be a point configuration of even dimension d , such that $\text{conv}(\mathbf{A})$ is a simplicial polytope. Prove that, for every pair of triangulations of \mathbf{A} , \mathcal{T}_1 and \mathcal{T}_2 , we have $f_d(\mathcal{T}_1) = f_d(\mathcal{T}_2)$ modulo 2. The parity of $f_d(\mathcal{T})$ is in fact determined by $\text{conv}(\mathbf{A})$ (Hint: you can prove this using the McMullen-Walkup equations, but there is also a very elementary way of doing it. Think spheres!).

Exercise 2.19. If two triangulations \mathcal{T}_1 and \mathcal{T}_2 differ by a flip, what can you say about their f -vectors? In other words, what are the f -vectors associated to flips? Investigate especially the case when the points are in general position.

Exercise 2.20. Prove that the dimension of the linear subspace spanned by the f -vectors of all full triangulations of a three-dimensional point configuration is one.

In this chapter, we focus on triangulations of point sets in the plane, with two goals in mind. On the one hand, dimension two is the first “non-trivial case” of study (triangulations of 1-dimensional point configurations were studied in the previous chapter; see Example 2.3.7). Looking at plane triangulations will prepare us for more complicated situations to come. But the reader must be cautious in thinking that all results about triangulations in dimension two remain true in higher dimensions; that this is not the case will be emphasized in Section 3.6, where we contrast two-dimensional results with three-dimensional analogues.

On the other hand, two-dimensional triangulations form by themselves a topic of study of strong presence in the computational geometry and the mesh generation literature. For this second reason, this chapter contains some repetition of things said more generally in the previous chapter or in later ones, which makes it, to a certain extent, self-contained.

In the spirit of this book, we are going to emphasize global problems, those that are referring to the *space of all triangulations* of a configuration. As we go along, we will touch some of the famous constructions in computational geometry. Much more on this topic can be found in the excellent books [93, 113], among others.

3.1 Some basic properties

Recall that a point configuration is a labeled set of points and that we say that a set of labels is independent (or collinear, or a face, etc.) meaning that the corresponding set of points is independent. The convenience of this language was emphasized in the previous chapter.

Let us start by recalling Definition 2.3.1, adapted to triangulations:

Definition 3.1.1 (Two dimensional triangulation). Let \mathbf{A} be a point configuration in dimension two, with set of labels J . A collection \mathcal{T} of affinely independent subsets of J is a *triangulation of \mathbf{A}* if it satisfies the following conditions:

- (CP) If $B \in \mathcal{T}$ and $F \subset B$, then $F \in \mathcal{T}$ as well. (Closure Property)
- (UP) $\bigcup_{B \in \mathcal{T}} \text{conv}(B) = \text{conv}(\mathbf{A})$. (Union Property)
- (IP) If $B \neq B'$ are two cells in \mathcal{T} , then $\text{relint}(B) \cap \text{relint}(B') = \emptyset$. (Intersection Property)

We want to stress that there are two aspects in which our definition deviates from the standard definition of triangulation in most of the 2-dimensional literature:

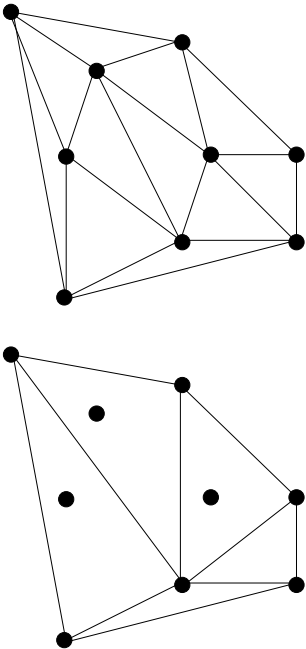


Figure 3.1: A full and a non-full triangulation of the same point set.

1. The standard convention in the literature is that a triangulation of \mathbf{A} uses all the elements of \mathbf{A} as vertices, while we allow some interior points to not be used. Recall Definition 1.0.2: We call a triangulation \mathcal{T} of a point set \mathbf{A} *full* if every element in \mathbf{A} appears in some cell of \mathcal{T} . See also Figure 3.1.
2. In higher dimension, we usually specify a triangulation via its list of maximal cells. In dimension two it is more usual, and sometimes more convenient, to define and represent triangulations via their sets of *edges*, rather than *triangles*. The following statement justifies why this works and gives a characterization of full triangulations in terms of their edges:

Lemma 3.1.2. *The edges of a full triangulation of \mathbf{A} are maximal sets of edges with the following properties:*

- (a) *Any two of them intersect properly. That is, their intersection is either empty or an end-point in both.*
- (b) *No point of the configuration is in the relative interior of one of the edges.*

Conversely, every maximal set of edges with these two properties is the set of edges of a unique full triangulation of \mathbf{A} .

In other words, full triangulations in dimension two are *maximal non-crossing plane graphs*, i.e., *planar graphs*, geometrically *embedded in the plane* with edges as straight lines and nodes at \mathbf{A} so that no two edges cross in their relative interiors.

Proof. That full triangulations satisfy Properties (a) and (b) should be obvious: no two edges in a triangulation can cross each other, since this violates property (IP) for those two edges; and no edge in a full triangulation can contain a point of \mathbf{A} in its interior, since that edge and that vertex would again violate property (IP) (here we use that our triangulation is full, so that every point of \mathbf{A} is used). To see that full triangulations are maximal with these properties, just observe that no edge can be added to a full triangulation without creating a crossing.

For the converse, let \mathcal{G} be a maximal set of edges with Properties (a) and (b), and let us show that \mathcal{G} is the set of edges in a full triangulation. First, it is clear that \mathcal{G} contains all the edges between consecutive points in the boundary of $\text{conv}(\mathbf{A})$, since otherwise adding the missing boundary edges does not violate the properties. This implies that \mathcal{G} divides $\text{conv}(\mathbf{A})$ into certain bounded regions. It suffices to show that these regions are triangles, each containing no point of \mathbf{A} other than its vertices. If this is so, then these triangles, together with the edges in \mathcal{G} and all the points in \mathbf{A} , form a full triangulation in the sense of Definition 3.1.1.

Let \mathbf{R} be one of these regions. If \mathbf{R} is convex but is not a triangle, then maximality of \mathcal{G} fails: the diagonal between two non-consecutive vertices of \mathbf{R} can be added to \mathcal{G} . The same happens if \mathbf{R} is a triangle but contains

a point of \mathbf{A} other than its three vertices: such point must be in the interior of \mathbf{R} (otherwise (b) is violated) and the edges joining it to the vertices of \mathbf{R} can be inserted. So, we only need to study the case of non-convex \mathbf{R} . In this case, \mathbf{R} must have a vertex \mathbf{p} that is “locally reflex”, meaning that the angle that \mathbf{R} spans in a neighborhood of \mathbf{p} is greater than 180 degrees. Let \mathbf{q} be one of the neighbors of \mathbf{p} along the boundary of \mathbf{R} and let \mathbf{r} be the second neighbor of \mathbf{q} . The edge \mathbf{pr} cannot be in \mathcal{G} , since \mathbf{p} was reflex. Now, imagine you are standing at \mathbf{p} and looking in the direction of \mathbf{q} , and start rotating towards the direction of \mathbf{r} until you first see a point \mathbf{s} of \mathbf{A} contained in \mathbf{R} . This must happen at the latest when you are looking towards \mathbf{r} (in which case you have $\mathbf{s} = \mathbf{r}$), because you will actually see \mathbf{r} unless you have hit another point before that. In any case, the edge \mathbf{ps} is not in \mathcal{G} (since \mathbf{p} was reflex and you have rotated less than 180 degrees) and it can be inserted, thus violating maximality of \mathcal{G} . \square

Observe that an implication of this proof is that every non-convex polygon can be triangulated. This is one of the points where the two-dimensional case differs from the higher-dimensional one (see Example 3.6.16). A second important difference is the next statement, which says that all full triangulations of a point set in the plane have the same number of triangles and the same number of edges. In contrast, triangulations of the three-dimensional cube may have five or six tetrahedra, as we saw in Figure 1.33 of Chapter 1 (see also Example 3.6.5 and Section 6.3).

Lemma 3.1.3. *Let \mathcal{T} be a full triangulation of a point set $\mathbf{A} \subset \mathbb{R}^2$. Let n be the number of points in \mathbf{A} and let n_b be the number of points in \mathbf{A} that lie on the boundary of $\text{conv } \mathbf{A}$. Then \mathcal{T} has exactly:*

- $3n - n_b - 3$ edges, and
- $2n - n_b - 2$ triangles.

Proof. Let e and t be the numbers of edges and triangles in \mathcal{T} . By Euler’s formula,

$$t - e + n = 1.$$

To eliminate one variable, we use double counting on the edges of \mathcal{T} . On the one hand, counting the edges of all triangles we clearly get $3t$, since each triangle has three edges. On the other hand, when we did this each interior edge was considered twice and each boundary edge only once. Since the number of boundary edges is precisely n_b , this gives

$$3t = 2e - n_b.$$

From these two equations we can eliminate either t or e and get the statement. \square

3.2 A few examples of triangulations in the plane

We saw in Chapter 2 several ways of constructing regular triangulations of a point set for arbitrary dimension. Here we revisit some of them and explore others inherent to dimension two, typically based on regarding a triangulation as a maximal set of non-crossing edges.

3.2.1 Placing and pulling triangulations

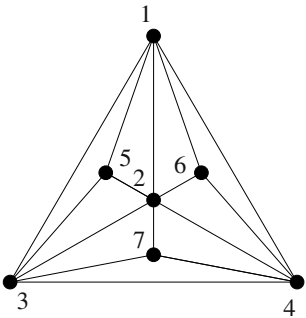


Figure 3.2: Is this the placing triangulation for the given ordering? And for some other ordering?

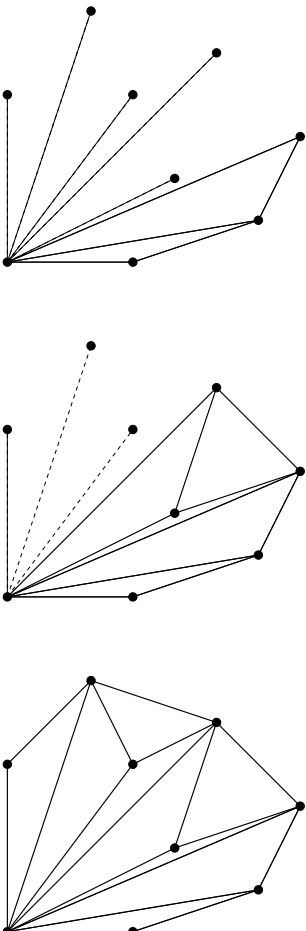


Figure 3.3: Two steps of Graham's convex hull algorithm constructing a placing triangulation.

The *placing triangulation* of a point set is probably the easiest to construct and to understand. We can think of it as a progressive construction that inserts (or, “places”) points one at a time, in a given order. To simplify the description we assume here that the points $\mathbf{p}_1, \mathbf{p}_2, \dots, \mathbf{p}_n$ are going to be added in the order indicated by their labels and let \mathbf{A}_i denote the configuration consisting of the first i points. We also assume that the first three points are not collinear, hence they form a triangle. Let $\mathcal{T}_3 = \{123\}$ be the triangulation of \mathbf{A}_3 consisting of just that triangle. Then, for each $i > 3$, \mathcal{T}_i is constructed from \mathcal{T}_{i-1} by adding the triangles that join \mathbf{p}_i to the part of the boundary of \mathcal{T}_{i-1} that is externally visible from \mathbf{p}_i . Visible means that the line segments connecting \mathbf{p}_i to those points in the boundary do not intersect $\text{conv}(\mathbf{A}_{i-1})$ except at the end-point.

It is important to observe that in our construction we join each new point \mathbf{p}_i to the ones that are *externally* visible from it. In particular, if \mathbf{p}_i is in the interior of the convex hull of the previous points, then it is not joined to anything and will not be used in our triangulation. For example, the answer to the first question in Figure 3.2 is “No. The placing triangulation for the given ordering is {123, 124, 234}”.

There is another iterative construction called *pulling points* that can be used to obtain triangulations (as it is the case for placing, the process has a higher-dimensional version).

Suppose now you have point configuration with n points of dimension d . Suppose so far you have a subdivision \mathcal{S}_k of the point subconfiguration using the first k points. We want to cleverly add the $(k+1)$ th point \mathbf{w} and enlarge the subdivision to include now $k+1$ points in a new subdivision \mathcal{S}_{k+1} . First, if S is one of the cells of \mathcal{S}_k which does not contain \mathbf{w} , then S remains as part of \mathcal{S}_{k+1} . Otherwise, if $\mathbf{w} \in S$ then \mathcal{S}_{k+1} contains all sets of the form $F \cup \{\mathbf{w}\}$, where F is a facet of S which does not contain \mathbf{w} .

Placing and pulling triangulations in arbitrary dimensions, and variations thereof, are studied in more detail in Section 4.3. In fact, as we show there they are a particular case of the regular triangulations studied in the previous chapter. Remember that *regular triangulations* of a d -dimensional configuration are those that can be geometrically obtained as the projection of the lower envelope of a $(d+1)$ -dimensional bounded polyhedron with simplicial faces. If $d=2$, these lower envelopes can be visualized as concave triangular terrains.

Let us mention a special case where placing triangulations make an appearance in one popular algorithm to compute the convex hull of a point configuration in the plane, the so-called *Graham scan* [145]. Given a point set \mathbf{A} , find the point \mathbf{p}_0 with smallest x -coordinate and sort the remaining points, say from largest to smallest, with respect to the slope of the line segments connecting \mathbf{p}_0 to \mathbf{p}_i , for $i > 0$. Once the convex hull \mathbf{C}_k of $\{\mathbf{p}_0, \mathbf{p}_1, \dots, \mathbf{p}_k\}$ has been found, the convex hull \mathbf{C}_{k+1} of $\{\mathbf{p}_0, \mathbf{p}_1, \dots, \mathbf{p}_{k+1}\}$ is obtained by drawing the line segments connecting \mathbf{p}_{k+1} to the visible points in \mathbf{C}_k . In other words, we construct the placing triangulation given by Graham’s order (see Figure 3.3).

3.2.2 Delaunay triangulations

Delaunay triangulations are another particular type of regular triangulations, and they were already introduced in arbitrary dimension in Section 2.2.2. Here we recall the definition, but then focus on special properties that the Delaunay triangulation has in two dimensions.

Definition 3.2.1. The *Delaunay subdivision* of a point configuration \mathbf{A} is the regular subdivision obtained by the choice of lifting heights given by $\omega(\mathbf{p}_i) = \|\mathbf{p}_i\|^2$. A *Delaunay triangulation* is any triangulation that refines it.

That is, the Delaunay subdivision is obtained by lifting the points to the paraboloid of equation $z = x^2 + y^2$. It is worth remarking that one does not, in general, have a *unique* Delaunay *triangulation*, but rather a Delaunay *subdivision* which sometimes is a triangulation itself and other times can be refined by several different triangulations. However, there is a simple sufficient condition that guarantees the Delaunay subdivision to be a triangulation; namely, that the lifted points contain no coplanar quadruple. As shown in Lemma 2.2.7, four points are lifted coplanarily to the paraboloid if and only if they are *cocircular* in the plane. For this reason, in the literature on Delaunay triangulations (and their duals, Voronoi diagrams) a point set is called *in general position* when it contains no four cocircular points, in addition to no three collinear.

Let us also recall here the “empty-sphere” characterization of the Delaunay triangulation (Corollary 2.2.8), directly adapted to the two-dimensional case:

Proposition 3.2.2. Let $\mathbf{A} \subset \mathbb{R}^2$ be a finite point set, with label set J . Let $B \subset J$ be a subset of its elements. Then B labels a cell in the Delaunay subdivision of \mathbf{A} if and only if there is a circle with no points of \mathbf{A} in its interior and with exactly the points of \mathbf{A} labeled by B on its boundary.

We want to emphasize that the above characterization is valid not only when B labels a two-dimensional cell, but also for the edges and vertices in the Delaunay subdivision (actually, the same characterization, with spheres instead of circles, works for the Delaunay subdivision of arbitrary dimensional point configurations).

Delaunay triangulations are so popular because they appear naturally in several applications. Sometimes this happens in a “dual way” as we mentioned in the previous chapter and we explain now. A *Voronoi cell* of a point \mathbf{p} in \mathbf{A} is the subset of all points of \mathbb{R}^2 for which \mathbf{p} is closest. Note that Voronoi cells are convex polygons due to the definition.

The *Voronoi diagram* of \mathbf{A} is the collection of all Voronoi cells, one for each of the points. It is a decomposition of the plane into polygonal regions, some possibly unbounded, as demonstrated in Figure 3.4. We can define a dual graph to the Voronoi diagram. The vertices are the input points and two are connected if their Voronoi cells share a common edge (see Figure 3.5).

Proposition 3.2.3. The dual graph of the Voronoi diagram of a point configuration \mathbf{A} consists precisely of the edges of the Delaunay subdivision.

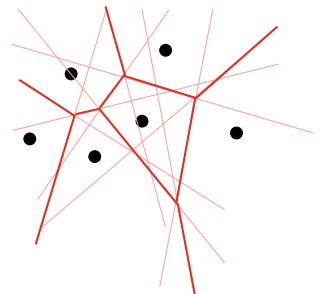


Figure 3.4: A Voronoi diagram traced with help of perpendicular bisectors.

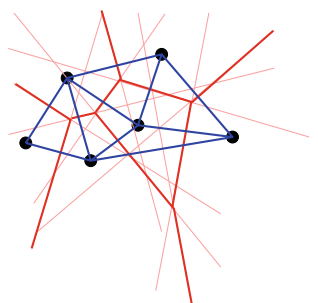


Figure 3.5: And the Delaunay triangulation as its dual graph.

Proof. Each edge of the Voronoi diagram is the bisector of the line segments between two points of \mathbf{A} . Moreover, a point \mathbf{x} in the relative interior of the Voronoi edge separating the regions of points \mathbf{p} and \mathbf{q} is closer to \mathbf{p} and \mathbf{q} than to any other point in the configuration. That is, the circle with center at \mathbf{x} and passing through \mathbf{p} and \mathbf{q} has no other point of \mathbf{A} on or inside it, which proves that \mathbf{pq} is an edge in the Delaunay subdivision, by Proposition 3.2.2. Conversely, if \mathbf{pq} is an edge in the Delaunay subdivision, Proposition 3.2.2 implies there is a point \mathbf{x} such that the circle with center \mathbf{x} and passing through \mathbf{p} and \mathbf{q} leaves every other point of \mathbf{A} outside, proving that there is a Voronoi edge passing through \mathbf{x} and separating the Voronoi regions of \mathbf{p} and \mathbf{q} . \square

With similar arguments, one can show that a Voronoi vertex \mathbf{x} is the center of a circle passing through precisely the points of \mathbf{p} whose Voronoi regions are incident to \mathbf{x} and leaving the rest of points outside, hence proving that Voronoi vertices are dual to the 2-dimensional cells in the Delaunay triangulation. Moreover, this duality of Voronoi diagrams and Delaunay subdivisions works in arbitrary dimension.

Now we come to the first property of the Delaunay subdivision that is special to dimension two, namely, that the “sphere test” stated in the above proposition has a very simple translation in terms of angles:

Proposition 3.2.4. *Let $\mathbf{A} \subset \mathbb{R}^2$ be a finite point set. A triangulation \mathcal{T} of \mathbf{A} is a Delaunay triangulation if and only if the opposite angles to every interior edge add up to at most 180 degrees.*

Moreover, the triangulation is the unique Delaunay triangulation of \mathbf{A} if and only if all these angle sums are strictly less than 180 degrees.

Let us clarify what we mean. Let \mathbf{pq} be an interior edge of \mathcal{T} , and let \mathbf{r} and \mathbf{s} be the two vertices that form triangles with it. We call “opposite angles to \mathbf{pq} ” the angle of \mathbf{r} in the triangle \mathbf{pqr} and the angle of \mathbf{s} in $\mathbf{pq}s$. See Figure 3.6.

Proof. Remember the following from Theorem 2.3.20: \mathcal{T} is the regular subdivision of \mathbf{A} corresponding to a certain height vector $\omega : J \rightarrow \mathbb{R}$ if and only if every “interior wall” (in the plane, every interior edge) is folded convex by this lift.

We also use the following elementary property of quadrilaterals in the plane: let $\mathbf{p}_1\mathbf{p}_2\mathbf{p}_3\mathbf{p}_4$ be a (perhaps non-convex) quadrilateral. Moreover, let $\angle_{\mathbf{p}_{i-1}\mathbf{p}_i\mathbf{p}_{i+1}}$ (with indices regarded modulo 4) denote the angle at the vertex \mathbf{p}_i . Then:

- The sum of the four angles equals 360 degrees,
- The quadrilateral can be inscribed in a circle if and only if $\angle_{\mathbf{p}_4\mathbf{p}_1\mathbf{p}_2} + \angle_{\mathbf{p}_2\mathbf{p}_3\mathbf{p}_4} = 180$ degrees (and hence $\angle_{\mathbf{p}_1\mathbf{p}_2\mathbf{p}_3} + \angle_{\mathbf{p}_3\mathbf{p}_4\mathbf{p}_1} = 180$ degrees as well), and
- If $\angle_{\mathbf{p}_{i-1}\mathbf{p}_i\mathbf{p}_{i+1}} + \angle_{\mathbf{p}_{i+1}\mathbf{p}_{i+2}\mathbf{p}_{i+3}} < 180$, then the point \mathbf{p}_i lies outside the circle passing through the other three vertices of the quadrilateral.

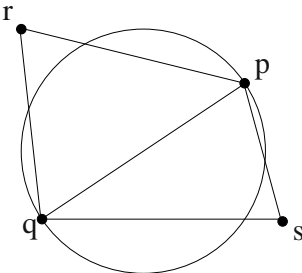


Figure 3.6: A characterization of Delaunay triangulations in terms of angles.

We already know that four points being cocircular is equivalent to their lifting to the paraboloid being coplanar. It follows from this that point \mathbf{p}_i being out of the circle through the other three is equivalent to the edge $\mathbf{p}_{i-1}\mathbf{p}_{i+1}$ lifting convex. This directly implies the statement at least in the generic case: if all the sums of opposite angles of interior edges are strictly less than 180 degrees, then all the edges are lifted convex to the paraboloid and, hence they are all walls, our triangulation is the Delaunay subdivision. The converse also holds trivially.

For the other case, first observe that if a sum of two opposite angles is bigger than 180 degrees then the corresponding edge is lifted concave, and the triangulation is not Delaunay. Finally, if all edges have opposite angles with sum 180 or smaller, those with equality are “lifted flat” and those with strict inequality are lifted convex. Hence, the triangulation in question refines the Delaunay subdivision, which is obtained by “erasing” all the edges that are lifted flat. \square

Definition 3.2.5. An edge \mathbf{pq} in a triangulation \mathcal{T} of A is called *locally Delaunay* if the sum of its opposite angles is at most 180 degrees, so that a triangulation is Delaunay if and only if all its edges are locally Delaunay.

Observe that checking whether a given edge is locally Delaunay amounts to computing the sign of a 4×4 determinant. Namely, if \mathbf{pq} is an interior edge with opposite vertices \mathbf{r} and \mathbf{s} and with the triple \mathbf{pqr} oriented positively (i.e., counter-clockwise) in the plane, the condition needed for the edge to be locally Delaunay is that

$$\begin{vmatrix} \mathbf{p}_x & \mathbf{q}_x & \mathbf{r}_x & \mathbf{s}_x \\ \mathbf{p}_y & \mathbf{q}_y & \mathbf{r}_y & \mathbf{s}_y \\ \|\mathbf{p}\|^2 & \|\mathbf{q}\|^2 & \|\mathbf{r}\|^2 & \|\mathbf{s}\|^2 \\ 1 & 1 & 1 & 1 \end{vmatrix} \geq 0,$$

where $(\mathbf{p}_x, \mathbf{p}_y)$ denote the coordinates of point \mathbf{p} , and so on.

It is rather curious that Delaunay triangulations turn out to be the optimal triangulations with respect to several interesting criteria. We present one here and leave others for the exercises. In what follows, for every three points \mathbf{p}, \mathbf{q} and \mathbf{r} in the plane, we denote by $R(\mathbf{p}, \mathbf{q}, \mathbf{r})$ the radius (in absolute value) of the circumcircle of the three points.

Lemma 3.2.6. Given a convex quadrilateral \mathbf{pqrs} as in Figure 3.7

with vertex \mathbf{p} exterior to (or lying on) the circle $C(\mathbf{q}, \mathbf{r}, \mathbf{s})$ (i.e., \mathbf{qs} is the locally Delaunay diagonal of the quadrilateral), then

1. $\max(R(\mathbf{p}, \mathbf{r}, \mathbf{s}), R(\mathbf{p}, \mathbf{q}, \mathbf{r})) \geq \max(R(\mathbf{q}, \mathbf{r}, \mathbf{s}), R(\mathbf{p}, \mathbf{q}, \mathbf{s}))$
2. $\min(R(\mathbf{p}, \mathbf{r}, \mathbf{s}), R(\mathbf{p}, \mathbf{q}, \mathbf{r})) \geq \min(R(\mathbf{q}, \mathbf{r}, \mathbf{s}), R(\mathbf{p}, \mathbf{q}, \mathbf{s}))$.
3. In particular, $R(\mathbf{p}, \mathbf{r}, \mathbf{s})^m + R(\mathbf{p}, \mathbf{q}, \mathbf{r})^m \geq R(\mathbf{q}, \mathbf{r}, \mathbf{s})^m + R(\mathbf{p}, \mathbf{q}, \mathbf{s})^m$.

Proof. Parts 1 and 2 follow from the following assertion: one of $R(\mathbf{p}, \mathbf{r}, \mathbf{s})$ or $R(\mathbf{p}, \mathbf{q}, \mathbf{r})$ is bigger than $R(\mathbf{q}, \mathbf{r}, \mathbf{s})$; the other one is bigger than $R(\mathbf{p}, \mathbf{q}, \mathbf{s})$. To prove this assertion we present a variation of the argument in [92].

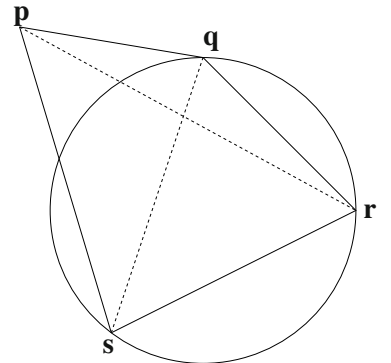


Figure 3.7: Auxiliary sketch for Lemma 3.2.6.

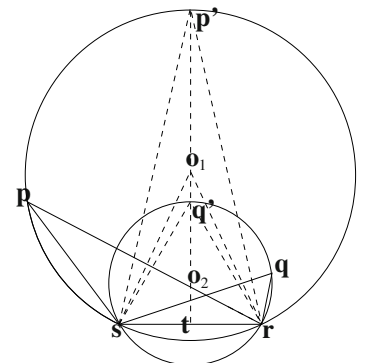


Figure 3.8: Auxiliary sketch for the proof of Lemma 3.2.6.

By elementary properties of angles and arcs of circle we know that the angles can be ordered in magnitude as follows:

$$\angle \text{rps} < \angle \text{rqs}, \quad \angle \text{qpr} < \angle \text{qsr}, \quad \angle \text{srp} < \angle \text{sqp}, \quad \angle \text{prq} < \angle \text{psq}.$$

It is sufficient to prove that either $R(\mathbf{p}, \mathbf{r}, \mathbf{s})$ or $R(\mathbf{p}, \mathbf{q}, \mathbf{r})$ are bigger than $R(\mathbf{q}, \mathbf{r}, \mathbf{s})$ as the other statement follows from identical properties.

In our argument we rely on Figure 3.8. We know that the sum of angles $\angle \text{sqr} + \angle \text{qsr} < \pi$, thus either one $\angle \text{sqr} \leq \pi/2$ or $\angle \text{qsr} \leq \pi/2$.

First consider what happens when $\angle \text{sqr} \leq \pi/2$. Let \mathbf{t} be the midpoint of \mathbf{rs} , and let $\mathbf{o}_1, \mathbf{o}_2$ be the centers of the circles $C(\mathbf{psr})$ and $C(\mathbf{qrs})$ respectively. It is well-known the points $\mathbf{o}_1, \mathbf{o}_2$ lie on the perpendicular bisector to \mathbf{sr} through the midpoint \mathbf{t} , therefore $\mathbf{o}_1, \mathbf{o}_2$, and \mathbf{t} are collinear. Denote by \mathbf{p}', \mathbf{q}' the points where this line meets the circles $C(\mathbf{psr})$ and $C(\mathbf{qrs})$. Note that we have divided two angles namely $\angle \mathbf{tp}'\mathbf{r} = (\angle \text{rps})/2$ and $\angle \mathbf{tq}'\mathbf{r} = (\angle \text{rqs})/2$ because two angles inscribed in the same circle that bound the same arc of circle are equal and the value of the angle is one half of the arc. Now

$$\tan(\angle \text{rqs}/2) = \frac{|\mathbf{tr}|}{|\mathbf{tq}'|} = \frac{|\mathbf{tr}|}{|\mathbf{to}_2| + |\mathbf{o}_2\mathbf{q}'|} = \frac{|\mathbf{tr}|}{|\mathbf{to}_2| + |\mathbf{o}_2\mathbf{r}|}.$$

From the right triangle $\mathbf{o}_2\mathbf{tr}$ we can rewrite the equation as

$$\tan(\angle \text{rqs}/2) = \frac{|\mathbf{tr}|}{(|\mathbf{o}_2\mathbf{r}| + (|\mathbf{o}_2\mathbf{r}|)^2 - (|\mathbf{tr}|)^2)^{1/2}}.$$

Similarly we have

$$\tan(\angle \text{rps}/2) = \frac{|\mathbf{tr}|}{(|\mathbf{o}_1\mathbf{r}| + (|\mathbf{o}_1\mathbf{r}|)^2 - (|\mathbf{tr}|)^2)^{1/2}}$$

and since $\angle \text{rps} \leq \angle \text{rqs} \leq \pi/2$, then $\tan(\angle \text{rps}/2) \leq \tan(\angle \text{rqs}/2)$ which is the same as

$$\frac{|\mathbf{tr}|}{(|\mathbf{o}_1\mathbf{r}| + (|\mathbf{o}_1\mathbf{r}|)^2 - (|\mathbf{tr}|)^2)^{1/2}} \leq \frac{|\mathbf{tr}|}{(|\mathbf{o}_2\mathbf{r}| + (|\mathbf{o}_2\mathbf{r}|)^2 - (|\mathbf{tr}|)^2)^{1/2}}.$$

Equivalently,

$$(|\mathbf{o}_1\mathbf{r}| + (|\mathbf{o}_1\mathbf{r}|)^2 - (|\mathbf{tr}|)^2)^{1/2} \geq (|\mathbf{o}_2\mathbf{r}| + (|\mathbf{o}_2\mathbf{r}|)^2 - (|\mathbf{tr}|)^2)^{1/2}.$$

Finally, because the function $x + (x^2 - a)^{1/2}$ is a monotone increasing function on x , we can safely conclude that $|\mathbf{o}_2\mathbf{r}| \leq |\mathbf{o}_1\mathbf{r}|$. Therefore the radius of the circumcircle $C(\mathbf{p}, \mathbf{s}, \mathbf{r})$ is larger than that of $C(\mathbf{q}, \mathbf{r}, \mathbf{s})$.

When $\angle \text{sqr} > \pi/2$ we have $\angle \text{qsr} \leq \pi/2$. Then, with the same argument as before, the radius of $C(\mathbf{p}, \mathbf{q}, \mathbf{r})$ is larger than the radius of $C(\mathbf{q}, \mathbf{r}, \mathbf{s})$. Thus we have concluded that either $R(\mathbf{p}, \mathbf{r}, \mathbf{s})$ or $R(\mathbf{p}, \mathbf{q}, \mathbf{r})$ are bigger than $R(\mathbf{q}, \mathbf{r}, \mathbf{s})$. Finally, the point \mathbf{r} is outside the circumcircle $C(\mathbf{p}, \mathbf{q}, \mathbf{s})$, so we can repeat the same arguments there and also conclude that either $R(\mathbf{p}, \mathbf{r}, \mathbf{s})$ or $R(\mathbf{p}, \mathbf{q}, \mathbf{r})$ are bigger than $R(\mathbf{p}, \mathbf{q}, \mathbf{s})$. \square

Corollary 3.2.7. Delaunay triangulations in the plane are optimal among triangulations of a fixed point set in the following senses:

1. They minimize the maximum circumradius of triangles in the triangulation.
2. They maximize the minimum circumradius of triangles in the triangulation.
3. For all real number powers $m > 0$, they minimize the functional $\sum_{\tau \in \mathcal{T}} R(\tau)^m$, where the sum is over all triangles τ in the triangulation.
4. They maximize the minimum angle in a triangulation.

It has to be mentioned that, in general, the Delaunay triangulation does not minimize the maximum angle. An algorithm to compute the triangulation that does this is described in [118].

Proof. We use the following important fact, that will be proved in Section 3.4.1: If a full triangulation \mathcal{T} is not a Delaunay triangulation, there is a locally non-Delaunay edge *that can be flipped*, meaning that its two adjacent triangles form a strictly convex quadrilateral.

The flipping of this edge strictly increases all the functionals in the statement. The ones in Parts (1), (2), and (3) are given by Lemma 3.2.6.

For the proof of Part (4), we refer again to Figure 3.7, where the locally non-Delaunay edge is **pr**. What we need to prove is that the minimum of the six angles formed when the edge **pr** is inserted is smaller than the minimum when the edge **qs** is inserted. Since the minimum of the twelve angles is clearly not one of the four angles of the quadrilateral **pqrq**, the statement follows from the following inequalities, already mentioned in the proof of Lemma 3.2.6:

$$\angle rps < \angle rqs, \quad \angle qpr < \angle qsr, \quad \angle srp < \angle sqp, \quad \angle prq < \angle psq.$$

□

Here is yet another reason to like Delaunay triangulations: A *minimum spanning tree* of a planar point configuration is a spanning tree with vertices on the points whose edges are straight-line segments connecting points with the property that the sum of the lengths of the edges is minimal. Note that, in principle, there are many possible trees and that the minimum length can be attained by many trees. It turns out that

Proposition 3.2.8. Every minimum spanning tree of a point configuration A is a subgraph of the Delaunay triangulation.

Proof. Let us recall *Prim's algorithm* for computing a minimum spanning tree. Order the points $\{\mathbf{p}_1, \dots, \mathbf{p}_n\}$. Begin by setting $\mathbf{T} = \{\mathbf{p}_1\}$. Then for each value i from 2 to n , find the shortest edge line segment among the segments of the form $\{\mathbf{s}\mathbf{u}\}$ where $\mathbf{s} \in \mathbf{T}$ and $\mathbf{u} \in A \setminus \mathbf{T}$. Add such a minimal edge to what is the evolving spanning tree and add \mathbf{u} to \mathbf{T} . It is well-known

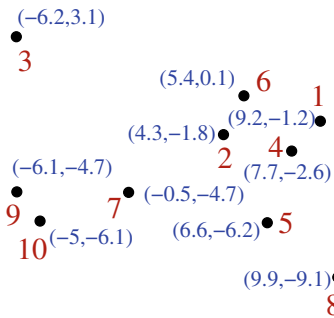


Figure 3.9: Ten random points in the plane.

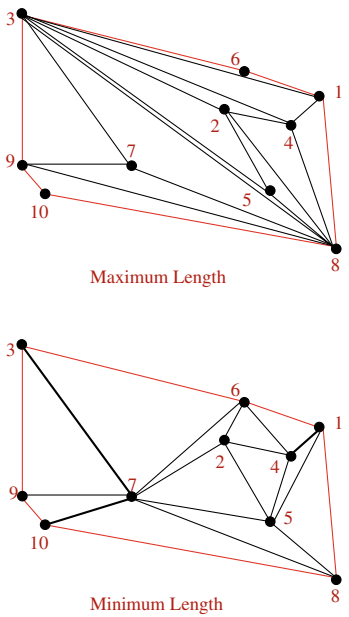


Figure 3.10: Their corresponding minimum and maximum length triangulations.

that the result is a minimum weight spanning tree and in fact all minimum spanning trees can be recovered this way for some ordering of the points and varying choices of equal-length edges.

Now, recall that when we chose $\{\mathbf{s}\mathbf{u}\}$, \mathbf{u} was the closest of $\mathbf{A} \setminus \mathbf{T}$ to \mathbf{s} and \mathbf{s} was a closest point in \mathbf{T} to \mathbf{u} . Therefore the interior of the disk centered at \mathbf{u} contains no points of \mathbf{T} and the interior of the disk centered at \mathbf{s} has no points of $\mathbf{A} \setminus \mathbf{T}$. This means the intersection of these two open disks contains no point from \mathbf{A} . This implies that the edge $\{\mathbf{s}\mathbf{u}\}$ must actually belong to a Delaunay triangulation because the circle with center at $\frac{\mathbf{u}+\mathbf{s}}{2}$ and radius half the length of $\{\mathbf{s}\mathbf{u}\}$ goes through the edge, but all other points of the configuration lie outside, thus it is locally Delaunay. \square

How do we compute Delaunay triangulations? Of course, straight from the definition, and valid in all dimensions, we have the *convex-hull-based algorithms* that compute the convex hull of the lifted points to a paraboloid. The Delaunay triangulation is obtained by simply looking at which faces of the convex hull are “lower”. This is not the most effective method in practice for point sets in the plane, but there are alternative algorithms available. There are *incremental insertion algorithms* that, starting with a triangle, insert the points in some order (e.g., random order) updating the triangulation at each step (to find the triangle(s) to be updated one needs good data structures such as a Quadtree; see for example [215]). There are also *divide-and-conquer* algorithms that subdivide the region into two partial regions, compute recursively the Delaunay triangulation of the parts, and finally merges both triangulations (e.g., [149]). Of similar $O(n \log(n))$ complexity as divide-and-conquer, we have the *planesweep* algorithm that computes Delaunay edges and Delaunay triangles by moving a sweep-line over the area (e.g., [128]). Sweeping and divide-and-conquer reach in fact the best possible complexity. We will not discuss the details of these algorithms here, but we suggest the references [45, 93]. For pointers to software, consult <http://www.geom.uiuc.edu/software/cglist/>. The only algorithm that we will discuss, later in this chapter, for its structural significance to the space of triangulations, is the flipping algorithm, which starts with an arbitrary triangulation and converts it into the Delaunay triangulation via flips.

3.2.3 Greedy and minimum weight triangulations

Let $\mathbf{A} = \{\mathbf{p}_1, \dots, \mathbf{p}_n\}$ be a point set in the plane. Suppose that for each pair of points $\mathbf{p}_i, \mathbf{p}_j \in \mathbb{R}^2$ we are given a certain “cost” or weight $w_{i,j} \in (0, \infty)$ of using the edge $\mathbf{p}_i\mathbf{p}_j$. The weights can in principle be arbitrary. But the natural choice, with several applications, is the Euclidean distance between points. Then we can call the *weight* of a triangulation the sum of weights of the edges used in it. The *minimum weight triangulation* (MWT for short) is the full triangulation of \mathbf{A} with the smallest possible weight. The problem of computing the minimum weight triangulation of a point set in the plane has received considerable attention, especially when the weights are simply the Euclidean lengths of the edges, which we will call the *minimum length triangulation problem*. This problem is often just called the MLT problem.

The first record we have of the MLT problem goes back to around 1975 [294]. In fact, MLT was, until recently, one of the items in the famous list, included in the seminal book by Garey and Johnson [134], of problems whose NP-completeness was not known. The list originally contained eleven problems, and MWT was one that remained open for a long time. Only in 2006, in a major breakthrough, Wolfgang Mulzer and Günter Rote [235] finally proved that finding the minimum length triangulation is NP-hard. In Chapter 8 we make a short sketch of their proof.

But life needs to go on, despite NP-hardness. What would be an effective method to actually find a minimum length triangulation or an approximation of it? Listing all triangulations and finding a MLT is beyond question. In Figures 3.9 and 3.10 we show a concrete example of a point set with 10 points and specific coordinates together with its maximum and minimum length triangulations. For this simple example there are over 2000 different triangulations.

A truly naive “algorithm” to try to compute the minimum weight triangulation goes as follows: order the $\binom{n}{2}$ possible edges by weight, then insert them one by one, choosing at every step the edge of smallest weight that does not cross any of the ones previously inserted. When no other edge can be inserted we have a full triangulation, by Lemma 3.1.2. Unfortunately, the triangulation obtained this way, which is called the *greedy triangulation*, is not always equal to the minimum weight triangulation [224]:

Lemma 3.2.9. *The minimum length triangulation (MLT) has in general different length than the greedy triangulation (GT) or than the Delaunay triangulation (DT). Moreover, there is no universal constant c satisfying*

$$\frac{\text{length}(DT(\mathbf{A}))}{\text{length}(MLT(\mathbf{A}))} \leq c, \text{ or } \frac{\text{length}(GT(\mathbf{A}))}{\text{length}(MLT(\mathbf{A}))} \leq c$$

for every point configuration \mathbf{A} .

In fact, the Delaunay triangulation may exceed the optimal length by a linear factor of the number of points [191].

Proof. We only present the proof for the case of the Delaunay triangulation, with a construction originally from [224]. See Figure 3.11. For each $n = 2^k + 1$, consider the configuration \mathbf{A}_k with n points, consisting of the vertices of the regular 2^k -gon of unit radius together with its center (or together with a generic point very close to the center, if you prefer a configuration in general position).

From the circumcircle description of the Delaunay triangulation it is clear that the Delaunay triangulation is a “wheel” consisting of the boundary edges of the 2^k -gon together with the 2^k radii joining the interior point to the boundary. The length of this triangulation is $\Theta(n)$ (more precisely, it is very close to $n + 2\pi$).

A better triangulation is constructed by taking the edges of the polygon, then a second layer of edges consisting of 2^{k-1} edges linking points at distance two, a third layer of edges consisting of edges linking points at

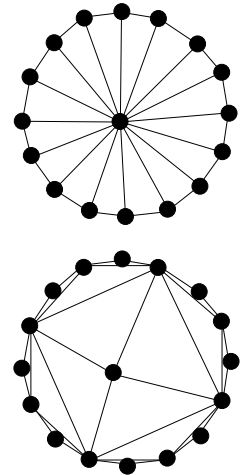


Figure 3.11: The Delaunay triangulation (top) does not approximate well minimum length triangulations. The bottom figure shows an asymptotically much better way of triangulating a 2^k -gon.

distance four, etc. In the final step, the interior point will be contained in a square and we join it to the four vertices of it. In this process, we have inserted $k - 1$ layers of edges plus the four final ones, and each layer has total length bounded by 2π . Hence, we have a triangulation of length less than $2(k - 1)\pi + 4 = \Theta(\log n)$.

In conclusion we have

$$\frac{\text{length}(DT(\mathbf{A}_k))}{\text{length}(MLT(\mathbf{A}_k))} \geq \Omega(2^k/k).$$

□

Finally observe that neither minimum length triangulations nor greedy triangulations are unique in general and they do not have to be regular either!

A very nice computational result, due to Klincsek [193], states that when triangulating simple polygons, i.e., polygonal regions without holes, one can find the minimum length triangulation efficiently. Klincsek's result is particularly nice and easy to explain, thus we present it here. He used the idea of dynamic programming in the following way:

Proposition 3.2.10. *Let $\mathbf{p}_1, \mathbf{p}_2, \dots, \mathbf{p}_n$ be the vertices of a (not-necessarily-convex) simple planar polygon \mathbf{P} listed in clockwise order (i.e., the points \mathbf{p}_{n+i} and \mathbf{p}_i are identical). The boundary edges of \mathbf{P} are precisely the edges of the form $\overline{\mathbf{p}_i \mathbf{p}_{i+1}}$. Then there is an $O(n^3)$ time algorithm to compute a triangulation of \mathbf{P} that minimizes the sum of the Euclidean lengths of the interior edges.*

Proof. Since the polygon \mathbf{P} is not necessarily convex we need to define a modified distance function to ensure that we use segments that are truly inside of \mathbf{P} . Let

$$d^*(\mathbf{p}_i, \mathbf{p}_j) = \begin{cases} d(\mathbf{p}_i, \mathbf{p}_j) & \text{if } j = i + 1 \text{ or if } \overline{\mathbf{p}_i \mathbf{p}_j} \text{ is interior to } \mathbf{P}. \\ \infty & \text{otherwise.} \end{cases}$$

Denote by $\text{optcost}(i, j)$ the minimum length of a triangulation for the sub-polygon whose boundary edges are $\mathbf{p}_i, \mathbf{p}_{i+1}, \dots, \mathbf{p}_j$. The key idea of the algorithm is that, because we are on a simple polygon, the equality

$$\text{optcost}(i, j) = d^*(\mathbf{p}_i, \mathbf{p}_j) + \min_{i < m < j} (\text{optcost}(i, m) + \text{optcost}(m, j)) \quad (3.1)$$

necessarily holds. Indeed, the m where the minimum is achieved is the third vertex of the unique triangle using i and j in the triangulation achieving $\text{optcost}(i, j)$ (see Figure 3.12). The algorithm proceeds as follows:

Step 1 Set $k = 1$, where k is the variable that keeps track of the level on which we operate to do the dynamic programming evaluations of Equation (3.1). In parallel, compute the values of $d^*(i, j)$.

Step 2 While $k < n - 1$, do the following:

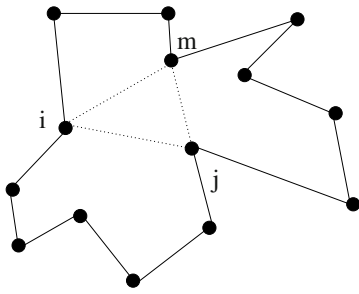


Figure 3.12: Dynamic programming at work: We can reduce the calculation of the minimum length of a triangulation of the polygon with edges $\mathbf{p}_i, \mathbf{p}_{i+1}, \dots, \mathbf{p}_j$ to m smaller calculations.

Increase $k = k + 1$, then using Equation (3.1), compute the values of $\text{optcost}(i, j)$ for $i = 1, \dots, n$ and $j = i + k$, using the known values of $\text{optcost}(i, j)$ for $|j - i| < k$.

Save in the auxiliary array $\text{opt}(i, j)$ the index m for which the minimum $\min_{i < m < j} (\text{optcost}(i, m) + \text{optcost}(m, j))$ is achieved in equation 3.1.

Step 3 Finally, when $n - 1 = k$, compute optimum length = cost(1, n) using Equation (3.1). To recover the edges involved in a minimal triangulation we use the array $\text{opt}(i, j)$: The edge $\overline{\mathbf{p}_1 \mathbf{p}_n}$ is in the minimum length triangulation. Then, for each $\overline{\mathbf{p}_i \mathbf{p}_j}$ currently in the triangulation, find the index $l = \text{opt}(i, j)$. By construction the edges $\overline{\mathbf{p}_i \mathbf{p}_l}$ and $\overline{\mathbf{p}_l \mathbf{p}_j}$ must also be present in the triangulation.

That the algorithm returns the correct answer follows from the validity of Equation (3.1). Step 2 of the algorithm above is the most costly. It requires $O(nk)$ operations for each $k = 1, 2, \dots, n - 1$, hence the running time is $O(n^3)$. The evaluation of the distance function d^* can be done beforehand and requires at most $O(n^3)$ steps. Detecting the intersection of the boundary edges $\overline{\mathbf{p}_i \mathbf{p}_{i+1}}$ with a segment $\overline{\mathbf{p}_i \mathbf{p}_j}$ with $j > i + 1$ can be done by solving a simple, constant size, system of equations. \square

The above algorithm was independently discovered by Gilbert [141]. The algorithm we described needs $O(n^2)$ space if applied to a convex polygon. Nobody knows whether the running time or memory space needed could be improved (see problems section).

For the minimum length triangulation of general point configurations the most successful practical approach for exact computation is what we call the *large MLT subgraph* or *skeleton* approach. The idea is to find as many edges as possible that must belong to a minimum length triangulation. If the resulting graph is connected, one can use Klincsek's algorithm to fill in the remaining holes. A similar idea was used in [117] to give a polynomial time algorithm for the problem of finding a triangulation that minimizes the length of the longest edge.

Perhaps the first ever attempt to find edges that must be inside a minimal triangulation was in Gilbert's 1979 thesis [141]. He proved that the shortest edges must belong to a minimum length triangulation. Later, the work by many authors [192, 184, 335, 79] led to the following important definition:

Definition 3.2.11. An edge is called a *light edge* if it is not crossed by another edge that is shorter.

Although the set of light edges does not always form a subgraph of a minimum weight triangulation, we have the following nice situation:

Theorem 3.2.12 (Aichholzer et al. [5]). *If the light edges form a triangulation, then the greedy triangulation is a minimum weight triangulation. In particular, the minimum length triangulation can be computed in polynomial time.*

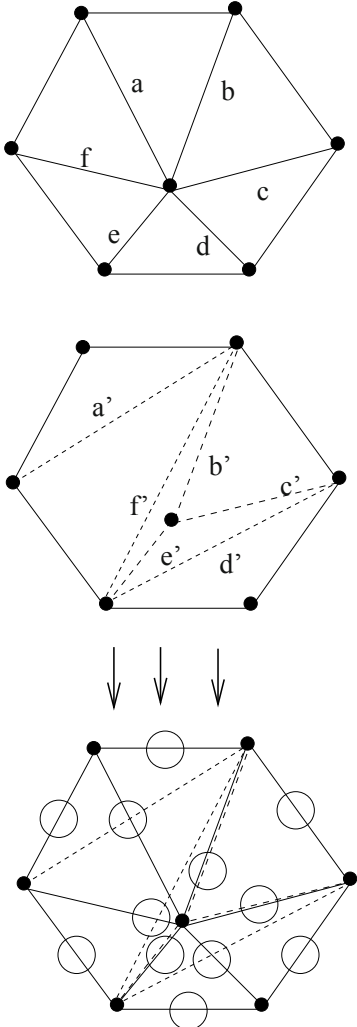


Figure 3.13: Two triangulations, their intersection and a matching of their edges (edges that match each other are marked with a circle).

The proof of this theorem relies on the following lemma, proved in [5]. See Figure 3.13 for an example.

Lemma 3.2.13 (Triangulations intersect nicely). *Consider \mathcal{T}_1 and \mathcal{T}_2 two full triangulations of a point configuration \mathbf{A} with n points. Let $E(\mathcal{T}_1)$ and $E(\mathcal{T}_2)$ be their sets of edges. Then there exist a perfect matching $\phi : E(\mathcal{T}_1) \rightarrow E(\mathcal{T}_2)$ such that every edge $e \in E(\mathcal{T}_1)$ either coincides with or crosses its matched edge $\phi(e)$.*

Proof. To prove that such a perfect matching exists we make use of the Hall's marriage theorem that states that a bipartite graph G , with bipartition X, Y , has a perfect matching if and only if, for any subset S of X , the number of neighbors of S in Y is larger or equal to the cardinality of S . The reader can find a proof in almost any graph theory book (e.g., [63]).

Now we construct an auxiliary bipartite graph G from the two triangulations $\mathcal{T}_1, \mathcal{T}_2$. The nodes of this graph are $X = E(\mathcal{T}_1)$ and $Y = E(\mathcal{T}_2)$. Two nodes are adjacent if the corresponding edges cross or coincide.

Let $S \subset X$ be any subset of edges in \mathcal{T}_1 , and let $N(S) \subset Y$ be its set of neighbors in G . We claim that $S \cup (Y \setminus N(S))$ is a non-crossing set of edges in \mathbf{A} . Indeed, since X, Y come from two triangulations, the only crossing could be between an edge $e_1 \in S$ and an edge $e_2 \in Y \setminus N(S)$, but then e_2 would be in $N(S)$ by definition, a contradiction. Since every non-crossing set of edges in the plane can be completed to a full triangulation (Lemma 3.1.2) and since all full triangulations have the same number of edges (Lemma 3.1.3) we have

$$|S \cup Y \setminus N(S)| \leq |X| = |Y|.$$

The same argument shows that no edge can be in both S and $Y \setminus N(S)$. Hence,

$$|S \cup Y \setminus N(S)| = |S| + |Y \setminus N(S)|.$$

Putting these two equations together we have

$$|N(S)| = |Y| - |Y \setminus N(S)| \geq |S|,$$

as desired. \square

Proof of Theorem 3.2.12. Call \mathcal{L} the triangulation all of whose edges are light. We want to prove that the length of \mathcal{L} is smaller than that of any other triangulation \mathcal{T} . Take the matching $\phi : \mathcal{L} \rightarrow \mathcal{T}$ of edges from Lemma 3.2.13. Then we have that $\text{length}(\phi(e))$ is bigger than $\text{length}(e)$, because e is light. \square

A major practical breakthrough for the computation of the planar MLT came with the introduction of the LMT-skeleton [107, 41].

Definition 3.2.14. A triangulation is *locally minimal* if there is no way to decrease the length by a flip. This means in particular that every convex quadrilateral contains the shorter of its diagonals and that any sub-polygon is optimally triangulated. We define the edge set of the *LMT-graph* as those edges belonging to the intersection of all locally minimal triangulations.

Minimum length triangulations are trivially locally minimal and thus the LMT-graph is a subgraph of all of them. The idea is to build a large subgraph of the LMT-graph, which we will call the *LMT-skeleton*. To achieve this, collect all edges except those that cannot be in a minimum length triangulation to begin with. For example, Das and Joseph [91] showed that it is necessary for an edge to belong to an MLT it must have a diamond point-free region like that shown in Figure 3.14. Even finer regions have been shown to be enough [108]. Thus to compute the LMT-skeleton, we can eliminate many edges using the diamond criterion or any of its relatives. Next, remove all edges that have a flip that decreases the length. We have now a list of *candidate edges* that may belong to the LMT-graph. We use the following lemma to extract candidate edges that are true LMT-graph edges:

Lemma 3.2.15. *Let \mathbf{A} be a point configuration and let $e \in E(\mathbf{A})$ be an edge of a locally minimal triangulation. If no other edge e' intersecting e is in a locally minimal triangulation, then e is in the LMT-graph.*

Proof. Any locally minimal triangulation not containing e must have an edge crossing it corresponding to triangles that cover a neighborhood of e . \square

Finally, the LMT-skeleton is constructed using Lemma 3.2.15: if an edge in our candidate list intersects no other edge in the candidate list, then e is in the LMT-graph and thus in all minimum length triangulations for sure. We add this edge to the LMT-skeleton.

Unfortunately, we show in Figure 3.15 that there are examples where the LMT-skeleton may not be large enough and has many connected components [41, 65]. The point set consists of points in a circle placed in such a way that any 60 degree angle sector contains 3 or more points plus a point in the center of the circle. The point in the center becomes isolated. Thus by pasting together many copies of the above point configuration we get a disconnected LMT-skeleton. One can of course try, as a solution, to add enough edges to connect them, but there are no bounds on how many components one can expect. In fact, the bad news is that although such configuration may appear artificial and rare, the paper [65] proved that the expected number of components on either the LMT-skeleton or the graph of light edges is linear in the number of vertices. It is also known that there are examples of point sets for which the LMT-skeleton is a proper subgraph of the LMT-graph. In [6] Aichholzer et al. showed an improved algorithm to compute the full LMT-graph for simple polygons and they studied when the graph is connected.

3.3 The set of all triangulations of a point set

The first global question about triangulations is: *How many triangulations are there?* Here we present a few results on the topic.

3.3.1 The exact number of triangulations

In general, it is impossible to have an explicit formula for the number of triangulations of a point set, but there are several families of point sets where

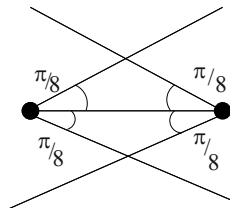


Figure 3.14: the $\pi/8$ -angular region must have no points inside.

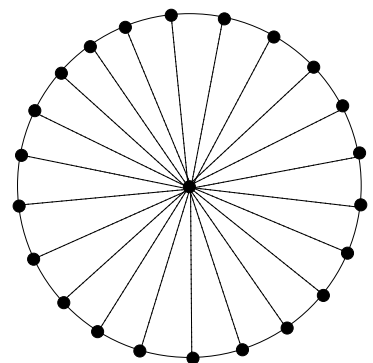


Figure 3.15: Diamond configurations obstruct the success of the LMT-skeleton heuristic.

this is possible. The first one is when the points are in *convex position*, that is, our configuration is the set of vertices of a convex polygon.

We already presented a proof of the following result in Section 1.1, but the result is important enough to present here another one (this proof was proposed as Exercise 1.5 in Chapter 1):

Theorem 3.3.1. *The number of triangulations of a convex n -gon is*

$$\frac{1}{n-1} \binom{2n-4}{n-2}.$$

The sequence

$$C_n := \frac{1}{n+1} \binom{2n}{n},$$

is called the *Catalan sequence*. That is to say, the number of triangulations of an n -gon is the $(n-2)$ -th Catalan number. From the formula the reader should see right away that $C_n \leq 4^n$ and, with some more attention, that $C_n \in \Theta(4^n n^{-3/2})$.

Proof. Throughout this proof let t_n denote the number of triangulations of the convex n -gon.

Consider the n -gon \mathbf{P} with its vertices labeled from 1 to n in cyclic order, and with a distinguished edge $\{1, n\}$ that we call the *base*. In every triangulation of \mathbf{P} the base is a side of one of the triangles, say $\{1, k, n\}$, and this triangle divides the rest of \mathbf{P} into two disjoint convex polygonal regions, S_1 with k vertices and S_2 with $n-k+1$. See Figure 3.16. The rest of the triangulation of \mathbf{P} is completed with some triangulation of the polygons S_1 and S_2 . Now, S_1 can be triangulated into t_k ways and S_2 into t_{n-k+1} ways. Hence, for a given choice of vertex k containing the edge $\{1, n\}$, there are $t_{k+1}t_{n-k}$ ways of triangulating \mathbf{P} and we have

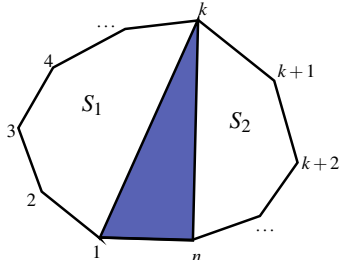


Figure 3.16: Setting up a recursion for t_n .

$$t_n = t_2 t_{n-1} + t_3 t_{n-2} + t_4 t_{n-3} + \cdots + t_{n-1} t_2.$$

Now we “only” need to solve this recurrence relation. It is slightly more convenient to shift the label n by one unit and call $s_{n-1} = t_n$ so that s_n is the number of triangulations of an $(n+1)$ -gon. We also set $s_1 = t_2 = 1$. The above recurrence relation becomes

$$s_{n-1} = s_1 s_{n-2} + s_2 s_{n-3} + \cdots + s_{n-2} s_1.$$

Now we use the method of formal power series: That is, we consider the expression

$$F(x) = \sum_{n=1}^{\infty} s_n x^n$$

and try to translate the recurrence on the s ’s to an algebraic identity on F .

For this, we multiply F by itself to get

$$\begin{aligned} F^2(x) &= (s_1)^2 x^2 + (s_1 s_2 + s_2 s_1) x^3 + \dots \\ &\quad + (s_1 s_{n-1} + s_2 s_{n-3} + \dots + s_{n-1} s_1) x^n + \dots \\ &= s_2 x^2 + s_3 x^3 + \dots + s_n x^n + \dots \\ &= F(x) - s_1 x \\ &= F(x) - x. \end{aligned}$$

Hence, F is a solution of the quadratic equation $F^2 - F + x = 0$. That is,

$$F(x) = (1 + \sqrt{1 - 4x})/2 \quad \text{or} \quad F(x) = (1 - \sqrt{1 - 4x})/2.$$

But we know that $F(0) = 0$ so the correct solution is the second one. We now use Newton's binomial theorem which in particular says that

$$(1+z)^{1/2} = \sum_{k=0}^{\infty} \binom{1/2}{k} z^k$$

where one defines $\binom{1/2}{k}$ as

$$\frac{[(1/2)(1/2-1)(1/2-2)\dots(1/2-k+1)]}{k!} = \frac{(-1)^{k-1}}{k 2^{2k-1}} \binom{2k-2}{k-1}.$$

Applying this to $z = -4x$ we get the formal power series expression of $(1 - \sqrt{1 - 4x})/2$ and, using that it must equal $F(x)$, we get the desired formula for t_n (don't forget to shift again by 1, because $s_n = t_{n+1}$). \square

There are a couple of variations of convex polygons where one can also determine the exact number of triangulations. We mention two important examples:

Example 3.3.2 (Double chain). Let \mathbf{A} consist of two convex chains of $k = n/2$ points each, facing one another and so that every pair of segments in different chains are visible from one another. See the bottom picture in Figure 3.17 for the case $k = 9$. The edges drawn in the figure are “unavoidable”, i.e., present in every full triangulation. They divide $\text{conv}(\mathbf{A})$ into two convex k -gons, with C_{k-2} triangulations each, and a non-convex $2k$ -gon which is easily seen to have $\binom{2k-2}{k-1}$ triangulations (see [133], and Example 3.3.2 below). Hence, the number of full triangulations of \mathbf{A} is:

$$\binom{2k-2}{k-1} C_{k-2}^2 = \Theta(64^k k^{-\frac{7}{2}}) = \Theta(8^n n^{-\frac{7}{2}}).$$

Example 3.3.3 (Double circle). Let now \mathbf{A} be a convex k -gon ($k = n/2$) together with k interior points, one sufficiently close to each boundary edge. See the top part of Figure 3.17 for the case $k = 9$. Again, the edges drawn are unavoidable, and triangulating \mathbf{A} is the same as triangulating the central

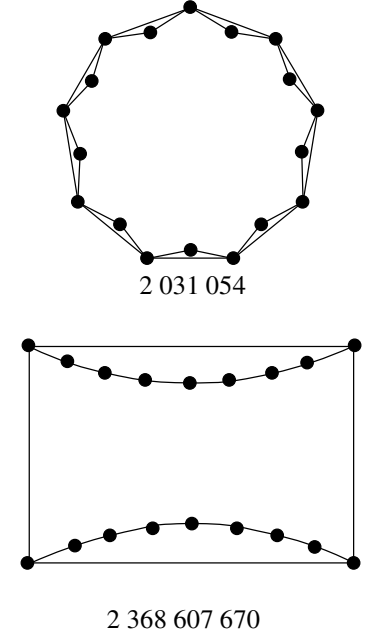


Figure 3.17: Some point sets in the plane whose numbers of triangulations are easy to compute exactly. The number of full triangulations of each, for $n = 18$, is shown.

non-convex n -gon. An inclusion-exclusion argument (see Proposition 1 in [171]) gives the exact number of triangulations of this polygon, which is

$$\sum_{i=0}^k (-1)^i \binom{k}{i} C_{k+i-2}.$$

Taking into account that C_i is essentially 4^i one gets that, neglecting a polynomial factor, this point set has

$$\sum_{i=0}^k (-1)^i \binom{k}{i} 4^{k+i} = 4^k \sum_{i=0}^k (-1)^i \binom{k}{i} 4^i = 4^k 3^k = 12^k = 12^{n/2}$$

triangulations.

Besides possessing nice combinatorial properties, the double circle and double chain are among the configurations with the smallest and the largest numbers of full triangulations. Actually:

- The double circle gives the exact minimum possible number of full triangulations for $n \leq 10$. (If n is even; for n odd the minimum number is given by a double circle with an extra interior point.) See [10, 9], where the conjecture is made that the same property holds for $n > 10$.
- On the other end, the double chain, with almost 8^n full triangulations and 9^n triangulations in total, was for some time the point set with asymptotically the largest number of triangulations known. But recently it was beaten by a simple variation of it, the so-called double zig-zag chain (see Figure 3.18). The double zig-zag produces about $(\sqrt{72})^n$ full triangulations [8]. For fixed and small n , the point sets which maximize the number of triangulations have been computed in [10] and they look like the right-side picture of Figure 3.17, which is self-explanatory. However, an analysis similar to the one we have done for the double chain shows that the number of triangulations of this “three-armed whirlpool” is “only” $\Theta(7.559^n n^{-5/2})$.

For arbitrary point configurations, counting their triangulations *exactly* is a tricky enterprise (at least empirically, although no one has proved it is hard in the complexity sense). Thus, we wish to at least *estimate* or *bound* the number of triangulations for an arbitrary point set in the plane.

Let T_n and t_n denote the maximum and minimum number of full triangulations among all point sets in the plane in general position and of cardinality n . For t_n to avoid trivialities we assume general position since $(n-1)$ points on a line, plus a point not on that line, produce a point set with only one triangulation. For T_n , however, general position is no loss of generality since “perturbing” a point set in the plane can only increase its number of triangulations.

The following table, taken from [10], gives T_n and t_n for $n = 3, \dots, 10$, and compares them to the number of triangulations of the convex n -gon C_n :

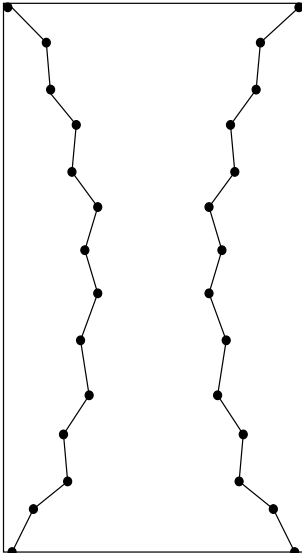


Figure 3.18: A double zigzag configuration.

| n | 3 | 4 | 5 | 6 | 7 | 8 | 9 | 10 |
|-------|---|---|---|----|----|-----|-----|------|
| t_n | 1 | 1 | 2 | 4 | 11 | 30 | 89 | 250 |
| C_n | 1 | 2 | 5 | 14 | 42 | 132 | 429 | 1430 |
| T_n | 1 | 2 | 5 | 14 | 42 | 150 | 780 | 4550 |

Concerning the asymptotic behavior of t_n and T_n it is known that:

$$\Omega^*(2.33^n) \leq t_n \leq O^*(12^{\frac{n}{2}}) = O(3.46^n), \quad (3.2)$$

$$\Omega^*(8.49^n) = \Omega^*(72^{\frac{n}{2}}) \leq T_n \leq O(43^n). \quad (3.3)$$

The “**” in the notations $\Omega^*(\cdot)$ is there to indicate that in the lower bounds a polynomial factor has been neglected. Compare these bounds with $C_{n-2} = \Theta^*(4^n)$ for the convex n -gon.

The upper bound for t_n comes from the “double circle” configuration, studied in Example 3.3.2. There we also studied the double chain, with about 8^n triangulations, which is close to the lower bound for T_n . The improved lower bound we give comes from [8]. The lower bound for t_n and the upper bound for T_n were established in [9] and [295], respectively. In what follows we prove the following slightly worse but easier to establish bounds:

$$\Omega^*(2^n) \leq t_n, \quad T_n \leq O(59^n).$$

The upper bound for T_n , the full triangulations, implies an upper bound for the number of all triangulations:

Theorem 3.3.4. *There is a constant c such that every point set in the plane with n points has at most c^n triangulations.*

Proof. Below we prove that $T_n \leq 59^n$. That is, every configuration with n points has at most 59^n full triangulations. Since every non-full triangulation of \mathbf{A} with label set J is a full triangulation of some sub-configuration of it, we conclude that \mathbf{A} has less than

$$\sum_{B \subseteq J} 59^{|B|} = \sum_{i=0}^n \binom{n}{i} 59^i = 60^n$$

triangulations. \square

In Section 7.2.2 we will show that this is not true in higher dimensions. For instance, we will construct point sets in dimension four with $\Omega(c^{n^2})$ triangulations (Theorem 7.2.10).

To conclude let us discuss another exact formula, but this time not on triangulations, but instead for *topological triangulations* in the plane. A plane graph is a topological triangulation if all its facets are triangles. Such triangulations are considered to be isomorphic modulo mappings which conserve all boundary vertices, adjacency, and triangles. If we assume that the graph is drawn in the plane with a triangular face as its outer boundary, we can distinguish two of those graphs to be isomorphic if they are isomorphic

as graphs. In this case we say the graphs are *rooted*. The number of non-isomorphic rooted topological triangulations was determined *exactly* by W. Tutte [323].

Theorem 3.3.5 (Tutte's formula). *Denote by TT_n the number of rooted topological triangulations with n vertices, then*

$$TT_n = \psi_{n,0} = \frac{2(4n+1)!}{(3n+2)!(n+1)!} \sim \frac{1}{16} \left(\frac{3}{2\pi}\right)^{1/2} n^{-5/2} \left(\frac{256}{27}\right)^{n+1}.$$

The study of topological triangulations and how to compute with them has been the focus of several papers (see [259] and the references therein).

We emphasize that the triangulations in this book have labeled vertices which makes isomorphic graphs different. Similarly, the coordinates of the vertices matter, e.g., it is clearly not the same to have seven points with six of the points collinear as having all seven points in general position! Thus two topologically identical triangulations, which are equal as graphs, can still be different in our context. This is something to keep in mind! Be careful.

3.3.2 The maximum possible number of triangulations

The first proof that the number of triangulations of a point set in the plane is $2^{\Theta(n)}$ is in [12], which actually bounds the number of non-crossing graphs that can be embedded in \mathbf{A} . Currently the best upper bound known for T_n , as of 2006, is that of M. Sharir and E. Welzl [295] improving on a result by F. Santos and R. Seidel [287]. Since the former uses the latter proof as a starting point, here we will present this one, which is also simpler. The precise statement that we want to prove is:

Theorem 3.3.6. *The number of full triangulations of \mathbf{A} is bounded above by*

$$\frac{59^v \cdot 7^b}{\binom{v+b+6}{6}},$$

where v and b denote the numbers of interior and boundary points of \mathbf{A} , respectively, meaning by this points of \mathbf{A} lying in the interior and the boundary of $\text{conv}(\mathbf{A})$.

We will assume that \mathbf{A} is in general position, i.e., that no three of its points are collinear. There is no loss of generality; if \mathbf{A} is not in general position, perturb it to a point set \mathbf{A}' in general position without making boundary points go to the interior. In this case every triangulation of \mathbf{A} is a triangulation of \mathbf{A}' as well. In particular, the maximum number of triangulations among point configurations in the plane of given cardinality is achieved by points in general position. The same result is not known in higher dimension.

Lemma 3.3.7. *Let \mathcal{T} be a full triangulation of \mathbf{A} . For each integer $i \geq 3$, let v_i denote the number of interior vertices of degree i in \mathcal{T} . For each*

integer $j \geq 2$, let b_j denote the number of boundary vertices of degree j in \mathcal{T} . Then,

$$\sum_{i \geq 3} (6 - i)v_i + \sum_{j \geq 2} (4 - j)b_j = 6.$$

In particular,

$$3v_3 + 2v_4 + v_5 + 2b_2 + b_3 \geq 6 + \sum_{i \geq 7} v_i + \sum_{j \geq 5} b_j.$$

Proof. Let v and b be the numbers of interior and boundary points of \mathbf{A} , respectively. Let e and t be the numbers of edges and triangles in \mathcal{T} . Counting the edges of \mathcal{T} according to their incidences to triangles shows that $3t = 2e - b$. Euler's formula says that $t - e + b + v = 1$. These two equations give:

$$6v + 4b = 6 + 2e.$$

On the other hand, counting the edges of \mathcal{T} according to their incidences to vertices shows that

$$2e = \sum_{i \geq 3} iv_i + \sum_{j \geq 2} jb_j.$$

Substituting this into the previous equality gives the first claimed equation, and the second one follows trivially. \square

Let \mathcal{T} be a full triangulation of \mathbf{A} and $\mathbf{p} \in \mathbf{A}$ be one of its points. We say that a triangulation \mathcal{T}' of $\mathbf{A} \setminus \{\mathbf{p}\}$ is obtained by *deleting \mathbf{p} in \mathcal{T}* if all the triangles of \mathcal{T} not incident to \mathbf{p} appear in \mathcal{T}' . In the same conditions we also say that \mathcal{T} is obtained by *inserting \mathbf{p} in \mathcal{T}'* . Observe that neither the deletion nor the insertion of a point in a triangulation is a unique process.

Lemma 3.3.8. *Let \mathcal{T}' be a full triangulation of $\mathbf{A} \setminus \{\mathbf{p}\}$. For each $i \in \mathbb{N}$, let h_i be the number of triangulations of \mathbf{A} in which \mathbf{p} has degree i and which can be obtained by inserting \mathbf{p} in \mathcal{T}' .*

- If \mathbf{p} is an interior point of \mathbf{A} , then $h_3 = 1$, $h_4 \leq 3$, $h_5 \leq 9$, and $h_6 \leq 28$.
- If \mathbf{p} is a boundary point of \mathbf{A} , then $h_2 \leq 1$, $h_3 \leq 1$, and $h_4 \leq 2$.

Proof. A bit of terminology first. For a star-shaped polygon its kernel is the set of points in its interior from which every point is visible. Let us first assume that \mathbf{p} is interior, and call Δ the unique triangle of \mathcal{T}' that contains \mathbf{p} . Inserting \mathbf{p} with degree i in \mathcal{T}' is done by first removing $i - 3$ edges of \mathcal{T}' with the requirement that a star-shaped i -gon with \mathbf{p} in its kernel is formed, and then joining \mathbf{p} to all the vertices of this polygon (see Figure 3.19 for an example of this process). If $i = 3$ no edge has to be removed and the insertion consists simply in joining \mathbf{p} to the three vertices of Δ . This proves $h_3 = 1$. If $i = 4$, then exactly one of the three edges of Δ has to be removed. Some or all of the three edges of Δ might produce polygons with \mathbf{p} not in the kernel, hence $h_4 \leq 3$. If $i = 5$, then we have to remove either two edges of Δ (three possibilities) or an edge of Δ and a second edge of the another triangle incident to the first edge removed (six possibilities). This proves $h_5 \leq 9$. A similar case study, which we leave to the reader, shows $h_6 \leq 28$.

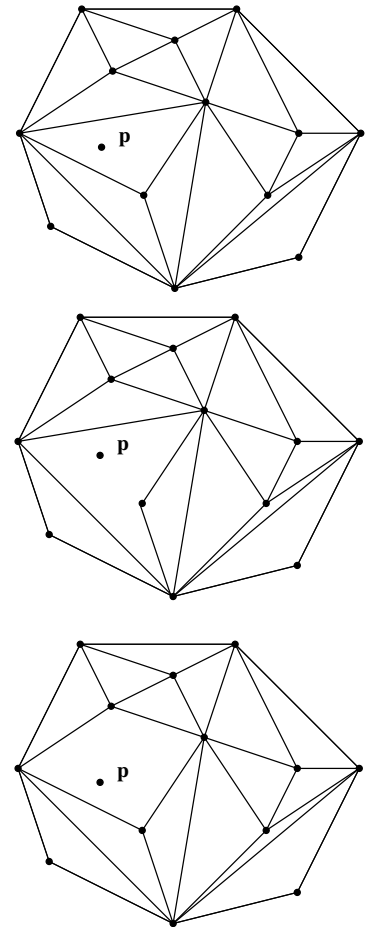


Figure 3.19: A triangulation and the two possible 4-gons that can be used to insert point \mathbf{p} .

Suppose now that \mathbf{p} is a boundary point. After its insertion in \mathcal{T}' , \mathbf{p} will at least be joined to the vertices of $\text{conv}(\mathbf{A} \setminus \{\mathbf{p}\})$ visible from \mathbf{p} . Let $b_{\mathbf{p}}$ be the number of such vertices, so that we must have $2 \leq b_{\mathbf{p}} \leq i$ in order to insert \mathbf{p} with degree i . The insertion consists of removing $i - b_{\mathbf{p}}$ edges from \mathcal{T}' , each of them making visible from \mathbf{p} a new vertex of the remaining non-convex triangulated polygon, and then joining \mathbf{p} to these $i - b_{\mathbf{p}}$ vertices and the $b_{\mathbf{p}}$ original ones. In particular, if $i = b_{\mathbf{p}}$ no edge has to be removed and only one insertion is possible. If $i = b_{\mathbf{p}} + 1$ then one of the $b_{\mathbf{p}} - 1$ edges of \mathcal{T}' visible from \mathbf{p} has to be removed. If $i = b_{\mathbf{p}} + 2$ then either two of these $b_{\mathbf{p}} - 1$ edges or one of them and one of the other two of the triangle incident to it have to be removed, which gives $\binom{b_{\mathbf{p}}-1}{2} + 2(b_{\mathbf{p}}-1)$ possibilities. With this, whenever $2 \leq b_{\mathbf{p}} \leq i \leq 4$ we have $h_2 \leq 1$, $h_3 \leq 1$, and $h_4 \leq 2$, as desired. \square

Proof of Theorem 3.3.6. Let $T_{v',b'}$ denote, for every pair of integers $v' \geq 0$ and $b' \geq 3$, the maximum number of triangulations among all point configurations with $v' + b'$ points and with at most v' of them interior. We will prove by induction on $v' + b'$ that $T_{v',b'} \leq 59^{v'} \cdot 7^{b'} / \binom{v'+b'+6}{6}$. The induction starts with $b' = 3$ and $v' = 0$, which gives $59^0 \cdot 7^3 / \binom{0+3+6}{6} = 49/12$.

Now let \mathbf{A} be a point configuration. For each $i \geq 3$, let V_i denote the sum over all triangulations of \mathbf{A} of the numbers of interior vertices of degree i . For each $j \geq 2$, let B_j denote the sum over all triangulations of \mathbf{A} of the numbers of boundary vertices of degree j . Let $T_{\mathbf{A}}$ be the number of triangulations of \mathbf{A} . Observe that deleting an interior point from \mathbf{A} gives a point configuration with b boundary points and $v - 1$ interior points, while deleting a boundary point gives a point configuration with $v + b - 1$ points, *at most* v of which are interior.

The number of triangulations of \mathbf{A} in which a certain vertex \mathbf{p} has degree i is at most equal to the number of ways of inserting \mathbf{p} with degree i in triangulations of $\mathbf{A} \setminus \{\mathbf{p}\}$. The inequality is in general strict since insertions from different triangulations of $\mathbf{A} \setminus \{\mathbf{p}\}$ can lead to the same triangulation of \mathbf{A} . Then Lemma 3.3.8 implies that

$$\begin{aligned} V_3 &\leq vT_{v-1,b}, & V_4 &\leq 3vT_{v-1,b}, \\ V_5 &\leq 9vT_{v-1,b}, & V_6 &\leq 28vT_{v-1,b}, \\ B_2 &\leq bT_{v,b-1}, & B_3 &\leq bT_{v,b-1} \quad \text{and} \quad B_4 &\leq 2bT_{v,b-1}. \end{aligned}$$

On the other hand, from Lemma 3.3.7 we have that

$$\begin{aligned} 6T_{\mathbf{A}} + \sum_{i \geq 7} V_i + \sum_{j \geq 5} B_j &\leq \\ 3V_3 + 2V_4 + V_5 + 2B_2 + B_3 &\leq \\ 18vT_{v-1,b} + 3bT_{v,b-1}. \end{aligned}$$

Adding these inequalities together we get

$$(6 + v + b)T_{\mathbf{A}} = 6T_{\mathbf{A}} + \sum_{i \geq 3} V_i + \sum_{j \geq 2} B_j \leq 59vT_{v-1,b} + 7bT_{v,b-1}.$$

By inductive hypothesis, $T_{v-1,b} \leq \frac{59^{v-1} \cdot 7^b}{\binom{v+b+5}{6}}$ and $T_{v,b-1} \leq \frac{59^v \cdot 7^{b-1}}{\binom{v+b+5}{6}}$. Hence,

$$(6+v+b)T_A \leq (v+b)\frac{59^v \cdot 7^b}{\binom{v+b+5}{6}} = (6+v+b)\frac{59^v \cdot 7^b}{\binom{v+b+6}{6}}.$$

This implies the desired result. \square

3.3.3 The minimum possible number of triangulations

What is the minimum number of triangulations that *every* n point configuration must have? Aichholzer et al. [9] proved the following result, which corroborates the suspicion that there are always exponentially many triangulations:

Theorem 3.3.9. *Let t_n denote the minimum number of full triangulations that any set of n points in general position exhibits. Then $t_n \geq \Theta(2.33^n)$.*

As before, instead of proving the best-known bound we present instead a shorter, less-technical proof of a slightly worse lower bound:

Proposition 3.3.10. *Every point set in general position in the plane has at least*

$$C_{b-2}2^{v-b+2} = \Theta(2^b b^{-3/2})\Theta(2^v) = \Omega(2^n n^{-3/2})$$

full triangulations, where b and v are the numbers of boundary and interior points, respectively, $n = v + b$, and C_k is the k -th Catalan number.

Proof. Let us denote by $t_{b,v}$ the minimum number of triangulations among all point sets in general position with b boundary and v interior points.

We first prove that $t_{3,v} \geq 2^{v-1}$, by induction on v . The cases $v \leq 7$ can be dealt via direct arguments, and are covered by the computational results in [10]. So, we assume $v \geq 8$.

For each interior point \mathbf{p} one can form triangulations joining \mathbf{p} to the three boundary vertices and then triangulating the three sub-triangles. The triangulations obtained in this way for each choice of \mathbf{p} are at least

$$t_{3,v_1} t_{3,v_2} t_{3,v_3} \geq 2^{v_1-1} 2^{v_2-1} 2^{v_3-1} = 2^{v-4},$$

where v_1 , v_2 , and v_3 are the numbers of interior points in the three sub-triangles, and the inequality comes from inductive hypothesis. Since different choices of interior points cannot produce repeated triangulations, we have $t_{3,v} \geq v 2^{v-4} \geq 2^{v-1}$.

If $b > 3$, just observe that each triangulation \mathcal{T} of the boundary points can be refined (by the previous case) to at least

$$2^{v_1-1} 2^{v_2-1} \dots 2^{v_{b-2}-1} = 2^{v-b+2}$$

triangulations, where v_1, \dots, v_{b-2} represent the number of interior points in the different triangles of \mathcal{T} . \square

3.3.4 The poset of subdivisions

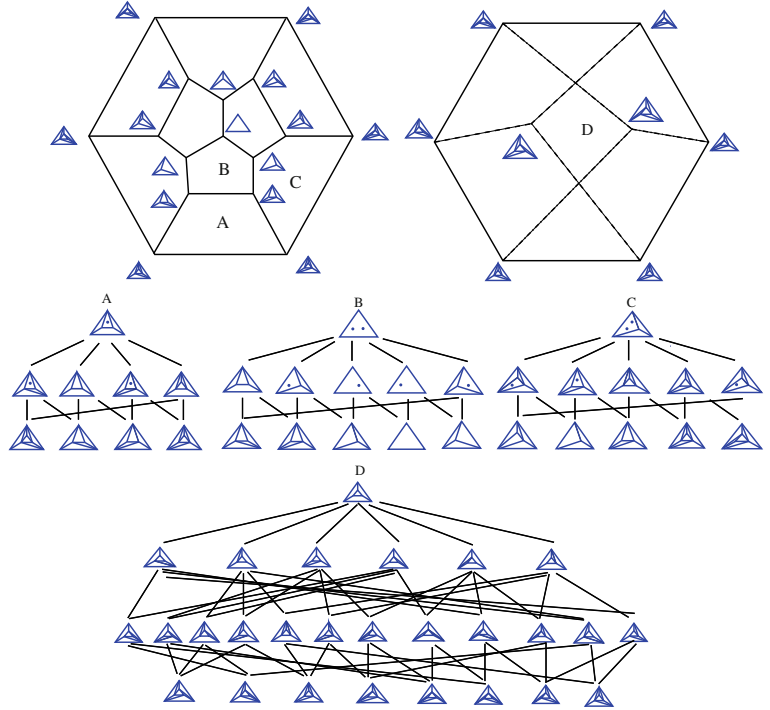


Figure 3.20: Four examples of poset of subdivisions. The biggest poset, poset D, is associated to all subdivisions refining eight triangulations of Example 2.2.5. Two of them were non-coherent triangulations. The full poset of all subdivisions will be presented in Chapter 5.

We have seen in Chapter 2 the definition of subdivisions, and of the poset that they induce via refinements. We will provide now some examples that aim to explain the extra topological structure we mentioned before. We will briefly introduce the space of all subdivisions and discuss the first example of the so called *Baues poset*. Further theory will be discussed in later chapters.

Now we explain a way to associate to each poset a topological space which is obtained by pasting simplices together, i.e., a *simplicial complex* as in Section 2.6.1. It is called the *order complex* of a poset. All we have to explain is what are the maximal simplices. Then all subsets of them will be lower-dimensional simplices. They consists of the maximal chains of the poset, namely chains of poset elements $x_0 < x_1 < \dots < x_k$. If the chain has length $k + 1$, we associate to it a k -dimensional simplex. For example, a chain of length three will be a triangle, a chain of length four will be a tetrahedron, etc. After we do this for every chain we recover a collection of simplices. Some share vertices precisely when their chains share poset elements. (See Remark 9.1.17 for a famous question about the order complex.)

As a running example we use the famous point configuration from Example 2.2.5.

Example 3.3.11 (A poset of subdivisions). In Figure 3.20 we show all its triangulations (top layer), all flips, and then we show the posets of

subdivisions refining four chosen subsets among all triangulations. Subposets (A), (B), (C) in Figure 3.20 have three levels (height three) while poset (D) has four levels.

Now let us apply the operation that associates the order complex to the poset, to this example. From the two posets of subdivisions shown in Figure 3.21 one of the simplicial complexes (right top part of the figure) is a triangulated pentagon. It is a 2-dimensional simplicial complex because the poset has three levels. On the other hand, the second bigger poset yields a triangulated solid cube (right bottom part of figure). We have officially given a topological-geometric structure to all the subdivisions of a point configuration.

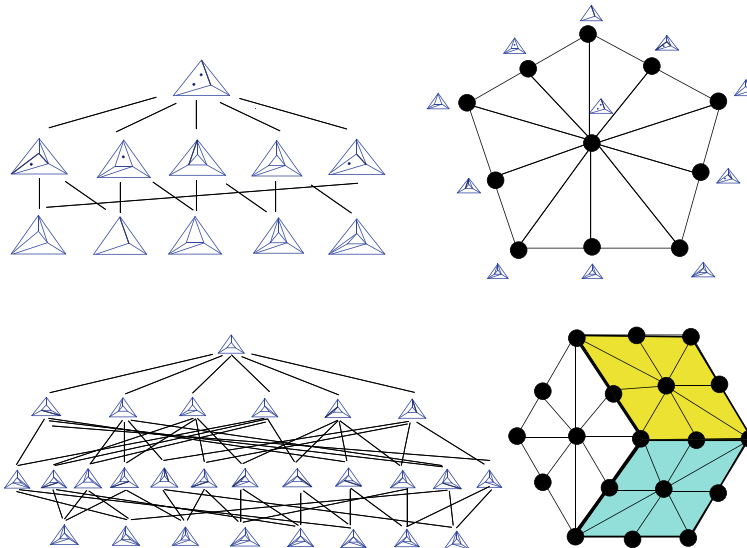


Figure 3.21: The simplicial complexes corresponding to two of the posets in Figure 3.20.

We would like to investigate properties of the poset of subdivisions and their geometric consequences. For example, the *height* of an element x in a poset is the maximum length k of a chain $x_0 < x_1 < \dots < x_k = x$, finishing in x . The height of the poset itself is the maximum height of its elements. The refinement poset of *regular* subdivisions of any configuration with n elements and dimension d has height exactly $n - d - 1$, since it is the face poset of a certain polytope of that dimension, as we will see in Chapter 5. But the poset of *all* subdivisions can have height larger than that, as the following example shows.

Example 3.3.12. (Several concentric triangles) Let A_k consist of $k + 1$ concentric triangles, as in Figure 3.22. The case $k = 1$ is the “mother of all examples”, Example 2.2.5, and the key observation is that this configuration has a sequence of four, instead of three, refinements. In the general case of $k > 1$ we can make a sequence consisting of k subsequences of length

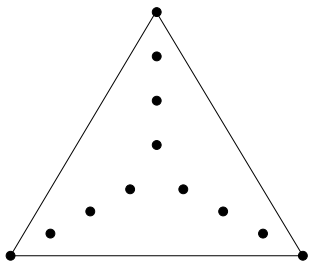


Figure 3.22: The configuration that maximizes the height of the refinement poset in the plane.

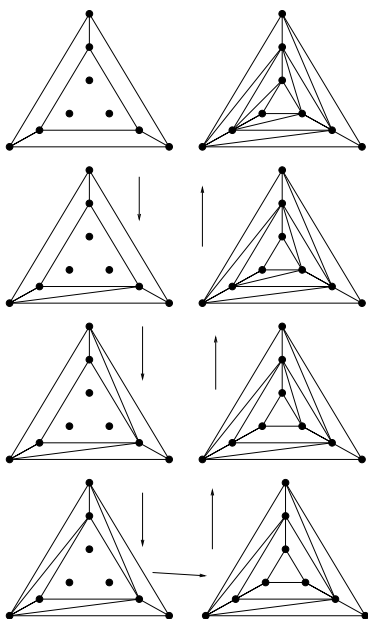


Figure 3.23: The maximal sequence of refinements.

four, triangulating first the region between the two outermost triangles, then the next one, and so on. Figure 3.23 shows the complete sequence of eight refinements for $k = 2$ (the sequence appears to have length seven, because the trivial subdivision is not shown).

Example 3.3.13. (Cutting a vertex) Let \mathcal{T} be a subdivision of a point configuration \mathbf{A} in general position in which all the points of \mathbf{A} are used as vertices. The height of this subdivision is clearly the sum of heights of the individual convex polygons forming it, and the height of a b -gon is $b - 3$. Hence, if the subdivision consists of k faces with b_1, \dots, b_f faces each, its height equals

$$\text{height}(\mathcal{T}) = \sum_{i=1}^k (b_i - 3) = \sum_{i=1}^k b_i - 3k = 2e - b - 3k,$$

where e is the number of edges, and b the number of boundary points. The equality $\sum_{i=1}^k b_i = 2e - b$ is obtained by double counting.

In particular, if \mathbf{a} is an interior vertex of degree three and we cut it by inserting a small triangle in its place, we increase the height by three (we add three to e and one to k) by adding two to the number of vertices. Obviously, if this process is iterated, we get a subdivision with, asymptotically, height equal to $3/2$ the number of interior points. More concretely, if we start with a subdivision having a single interior point, of degree three, the starting subdivision has height $b - 3$, where b is the number of boundary points (check this). Hence, the final subdivision has height

$$b - 3 + \frac{3(v-1)}{2},$$

where b and v are its number of boundary and interior points.

The following statement shows that the previous example is best possible.

Theorem 3.3.14. *Let \mathbf{A} be a point configuration in the plane, with b boundary points and v interior points. If $v \leq 1$, then all subdivisions are regular, and the poset of subdivisions has height $b + v - 3$. If $v \geq 1$, then every non-trivial subdivision has height bounded above by*

$$b - 3 + \left\lfloor \frac{3(v-1)}{2} \right\rfloor.$$

In particular, the poset of all subdivisions has height at most

$$b - 2 + \left\lfloor \frac{3(v-1)}{2} \right\rfloor.$$

Moreover, for every $b \geq 3$ and $v \leq 0$ there is a point configuration for which the bound is exact.

Proof. To prove the upper bound, let \mathcal{T} be a non-trivial subdivision of a point configuration \mathbf{A} . Of course, there is no loss of generality in assuming

that \mathcal{T} uses all the elements of \mathbf{A} , although some of them may appear in the interior of cells. Let $k > 1$ be the number of 2-dimensional cells. Let b_1, \dots, b_k be their numbers of boundary points and v_1, \dots, v_k be their numbers of interior points. By inductive hypothesis on the number of interior points, the height of the i -th cell (considered as a trivial subdivision) is at most $b_i + 3v_i/2 - 7/2$. Hence, the total height of \mathcal{T} is at most

$$\text{height}(\mathcal{T}) \leq \sum_{i=1}^k \left(b_i + \frac{3v_i}{2} - \frac{7}{2} \right) = \sum_{i=1}^k b_i + \frac{3}{2} \sum_{i=1}^k v_i - \frac{7}{2} k.$$

The first term $\sum_{i=1}^k b_i$ equals $2e - b$, by double counting. Also, by Euler's formula, k equals $e - n_{\mathcal{T}} + 1$, where $n_{\mathcal{T}}$ is the number of vertices of \mathcal{T} (that is, the number of points of \mathbf{A} that are used in \mathcal{T}). On the other hand, $\sum_{i=1}^k v_i$ clearly equals $v + b - n_{\mathcal{T}}$, the number of points not used as vertices. Hence, the previous inequality gives:

$$\begin{aligned} \text{height}(\mathcal{T}) &\leq 2e - b + \frac{3}{2}(v + b - n_{\mathcal{T}}) - \frac{7}{2}(e - n_{\mathcal{T}} + 1) \\ &= \frac{1}{2}b + \frac{3}{2}v + 2n_{\mathcal{T}} - \frac{3}{2}e - \frac{7}{2}. \end{aligned}$$

Comparing this with what we want to show, namely that $\text{height}(\mathcal{T}) \leq b - \frac{9}{2} + 3v/2$, we conclude it suffices to establish that

$$2n_{\mathcal{T}} - \frac{3}{2}e \leq b - 1$$

or

$$3e \geq 4n_{\mathcal{T}} - 2b + 1.$$

This holds, since $2e$ is the sum of all degrees of vertices, which is at least equal to $3n_{\mathcal{T}} - b$ (interior vertices have degree at most three, while boundary vertices may have degree two). In particular, $e \geq n_{\mathcal{T}}$. Hence,

$$3e = 2e + 2e \geq (3n_{\mathcal{T}} - b) + n_{\mathcal{T}} = 4n_{\mathcal{T}} - b > 4n_{\mathcal{T}} - 2b + 1.$$

□

3.4 Flips in triangulations

In the previous chapter we introduced the flip operation between triangulations. Our definition was a bit abstract, and our first goal here is to describe flips more explicitly, in the 2-dimensional case.

Let us recall our definition of flip: two triangulations are related by a flip if they are the only two refinements of a polyhedral subdivision that can only be refined by triangulations. We called such a subdivision an *almost-triangulation* and we gave, in Lemma 2.4.5, the following characterization of “almost-triangulations”: a polyhedral subdivision of a configuration \mathbf{A} that is not a triangulation is an almost-triangulation if and only if all its cells are either simplices or have corank one (that is, they have two more

elements than their affine dimension), and all the cells which are not simplices share one and the same circuit.

That is to say, every flip “happens” on a circuit, where a circuit is a minimal affinely dependent subset of points, and splits in a unique way into a pair (Z_+, Z_-) with the property that $\text{conv}(Z_+) \cap \text{conv}(Z_-) \neq \emptyset$. In the plane, there are the following three possibilities, depending on the type of circuit in question. Remember that the *type* of a circuit (Z_+, Z_-) is the pair $(|Z_+|, |Z_-|)$:

1. If the circuit is of type $(2, 2)$, that is, it consists of the four vertices of a convex quadrilateral, then the almost triangulation \mathcal{S} has a unique non-simplicial cell, consisting of these four points, because a cell strictly containing this circuit has corank greater than one. Hence, the two refinements of \mathcal{S} are obtained by inserting one or the other diagonal of this quadrilateral. The flip is normally called a *diagonal edge flip*, and an example of it is depicted at the top part of Figure 3.24.
2. If the circuit is of type $(3, 1)$, that is, it consists of a point \mathbf{a} in the interior of the triangle with vertices the other three $\{\mathbf{b}, \mathbf{c}, \mathbf{d}\}$, then again the almost triangulation \mathcal{S} has a unique non-simplicial cell, consisting of these four points. Its two refinements are obtained by “forgetting the interior point \mathbf{a} ” (which produces a non-full triangulation) and inserting \mathbf{a} as a new vertex incident to the three triangles $\{\mathbf{a}, \mathbf{b}, \mathbf{c}\}$, $\{\mathbf{a}, \mathbf{c}, \mathbf{d}\}$, and $\{\mathbf{a}, \mathbf{b}, \mathbf{d}\}$. The flip is called an *insertion-deletion flip* because it inserts or deletes a vertex from the triangulation. Find this situation in Figure 3.24.
3. If the circuit is of type $(2, 1)$, that is, it consists of three collinear points, then one or two cells of \mathcal{S} will contain it, depending whether the collinearity lies in the boundary or the interior of $\text{conv}(\mathbf{A})$. In any case, the two refinements are obtained by forgetting the central point of the collinearity, or by inserting it (which removes one or two triangles of the triangulation and inserts two or four new ones). The bottom of Figure 3.24 shows this flip in the case of an interior collinearity.

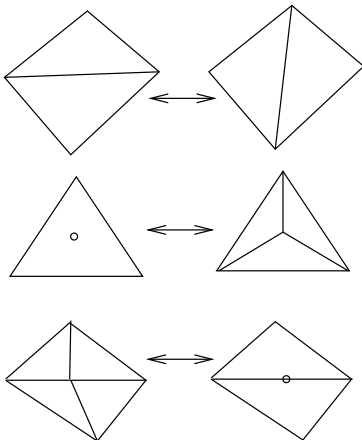


Figure 3.24: Types of flips in the plane.

Strictly speaking there is a fourth type of flip that can happen, but we do not need to care much about it. If we consider a configuration \mathbf{A} with a repeated point, the two copies of this point form a $(1, 1)$ -circuit. The flip on this circuit consists merely in changing our mind as to what copy of this point we want to consider a vertex in our triangulation.

3.4.1 All triangulations of a point set in the plane are connected by flips

The most natural question to ask about flips is whether any pair of triangulations of a configuration \mathbf{A} can be connected to one another by a finite sequence of flips. One may also wonder about the diameter of the graph of flips, or its maximum or minimum degree. In this section we discuss these questions.

Historically, the connectivity and diameter questions were first answered in the 1970's by Lawson [202, 203], who answered them with respect to the graph of $(2, 2)$ flips. We give three proofs of this fact because they have independent interest:

Theorem 3.4.1. *Let the points $\mathbf{p}_1, \dots, \mathbf{p}_n$ be given in an order such that $\mathbf{p}_i \notin \text{conv}(\mathbf{p}_1, \dots, \mathbf{p}_{i-1})$ for every i , so that the pushing triangulation $\mathcal{T}_{\text{push}}$ for this ordering is a full triangulation.*

Then any other triangulation \mathcal{T} of \mathbf{A} can be transformed to the pushing triangulation using at most $\binom{n-2}{2}$ flips, all of type $(2, 2)$.

Proof. We use induction on n , the number of points in the configuration. We will show that with at most $n - 3$ flips, all of type $(2, 2)$, we can arrive from our original triangulation $\mathcal{T} = \mathcal{T}_n$ to one consisting of a triangulation \mathcal{T}_{n-1} of $\mathbf{A} \setminus \{\mathbf{p}_n\}$ together with \mathbf{p}_n joined to the part of $\text{conv}(\mathbf{A} \setminus \{\mathbf{p}_n\})$ visible from it. This is represented in Figure 3.25. By inductive hypothesis, with at most $\binom{n-3}{2}$ additional flips we can go from \mathcal{T}_{n-1} to the pushing triangulation of $\mathbf{A} \setminus \{\mathbf{p}_n\}$, which produces the pushing triangulation of \mathbf{A} with a total of at most

$$(n-3) + \binom{n-3}{2} = \binom{n-2}{2}$$

flips.

Remember that the star of a vertex \mathbf{p} in a triangulation is the region obtained as the union of the triangles incident to it. The fact that our triangulation is full implies that, unless our triangulation is already of the desired form (that is, one that contains a triangulation of $\mathbf{A} \setminus \{\mathbf{p}_n\}$), the star of \mathbf{p}_n includes a flippable edge incident to \mathbf{p}_n . See Figure 3.26. Clearly, flipping that edge decreases the area covered by the star of \mathbf{p}_n . Hence, in a finite number of steps we must arrive to a triangulation in which the star of \mathbf{p}_n cannot be decrease further. Since each such flip also decreases the degree of \mathbf{p}_n , the number of steps needed is at most the number of interior edges incident to \mathbf{p}_n in the initial triangulation, which cannot exceed $n - 3$.

This finishes the proof. \square

A second proof of connectivity uses properties of the Delaunay triangulation. Indeed, Proposition 3.2.4 suggests that one can compute the Delaunay triangulation by first computing any triangulation and then flipping the edges that are *not* locally Delaunay until we have no such bad edges left. Will we always succeed with this process or can it get stuck? For triangulations in the plane one never gets stuck, as follows from the next “simplex filling” argument. Later we will see that for 3-dimensional point configurations the same process sometimes gets stuck in local optima that are not even regular!

Theorem 3.4.2. *If a triangulation \mathcal{T} of a set of points \mathbf{A} in the plane is not the Delaunay triangulation, then it contains a locally non-Delaunay edge which admits a diagonal-edge flip.*

In particular, every triangulation can be transformed into a Delaunay triangulation in a sequence of at most $\binom{n}{2}$ flips of type $(2, 2)$ on locally non-Delaunay edges.

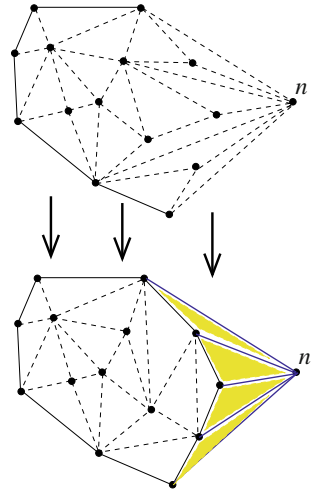


Figure 3.25: The desired transformation for \mathcal{T}_i .

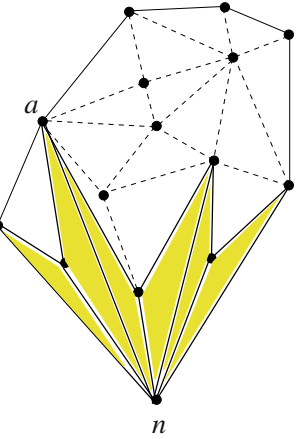


Figure 3.26: The link of n and some flippable inner diagonals.

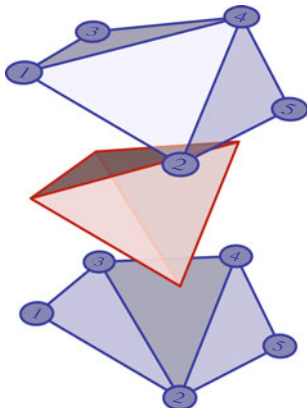


Figure 3.27: Doing a flip is the same as gluing the lower surface of a tetrahedron into the triangulated surface. When we see the upper surface of the tetrahedron we see the new diagonal.

Proof. The first assertion is actually a direct consequence of the following two facts:

- Every non-Delaunay triangulation has an edge which is not locally Delaunay (Proposition 3.2.4).
- Every edge which is not locally Delaunay is flippable. Indeed, if the quadrilateral consisting of the two triangles incident to the edge is not convex, then the Delaunay triangulation of those four points must contain that edge.

The second assertion comes from looking at flips in the configuration as lifted to the paraboloid. In the 3-dimensional lifting to a paraboloid we observed that an edge-flip amounts to gluing a tetrahedron underneath (if the flip is towards the locally Delaunay edge) or above (otherwise) two triangles that share a dihedral angle. See Figure 3.27. In particular, if we flip only on edges that are not locally Delaunay, we get surfaces which are always lower and lower (point-wise) so that the process must eventually terminate. It must terminate in at most $\binom{n}{2}$ steps, because the monotonicity implies that an edge that is removed by a flip in the sequence does not reappear again. When the sequence terminates we must be in the Delaunay triangulation, by the first part in the statement. Since the total number of edges removed cannot exceed $\binom{n}{2}$ we get the desired bound. \square

In the two proofs of connectivity we have looked at so far, we only allow for $(2, 2)$ -flips and, in particular, strictly speaking we have only proved connectivity of the graph of full triangulations. Connectivity of these two non-full triangulations is trivial, since every non-full triangulation can be connected to a full one by a sequence of (at most n) flips that insert points. However, if we allow for flips other than $(2, 2)$ we can get a much better bound on the total number of flips needed to go from one triangulation to another:

Theorem 3.4.3. *Let the points $\mathbf{p}_1, \dots, \mathbf{p}_n$ be given in any order in which \mathbf{p}_n is an extremal point (i.e., a vertex of the convex hull). Then any triangulation \mathcal{T} of \mathbf{A} can be transformed to the pulling triangulation of \mathbf{A} in at most $2n$ flips.*

Proof. We first consider the subgraph of triangulations in which every triangle is incident to \mathbf{p}_n . Clearly, the pulling triangulation is one of them.

If \mathbf{A} is in general position there is only one such triangulation, that joins \mathbf{p}_n to every convex hull edge not containing \mathbf{p}_n ; but if \mathbf{A} has collinear triples in its boundary then there can be more: points in the relative interior of edges of $\text{conv}(\mathbf{A})$ may be used or unused in a specific triangulation. However, (for the same reason as in the 1-dimensional case), the diameter of the graph of flips between these triangulations is bounded above by the number n_b of points of \mathbf{A} in the boundary of $\text{conv}(\mathbf{A})$ (more precisely, the diameter equals the number of them which are not extremal).

Now let \mathcal{T} be an arbitrary triangulation. If \mathcal{T} has triangles not incident to \mathbf{p}_n , then there is at least a flip that decreases the number of them (proof

left to the reader). Since the number of triangles in a triangulation with v_i interior vertices and v_b boundary ones is exactly $2v_i + v_b - 2$ (by Euler's formula) we can flip from any triangulation to one with every triangle incident to \mathbf{p}_n in at most $2v_i + v_b - 3 < 2|\mathbf{A}| - n_b$ flips. \square

Corollary 3.4.4. *The graph of triangulations of a point configuration in the plane with n points has diameter at most $4n$.*

We close this section with an example that shows that in order to get a graph of flips of linear diameter, you need to allow for insertion/deletion flips and, in particular, for non-full triangulations.

Example 3.4.5 (Example 3.3.2 continued). We consider again the *double chain* configuration of Section 3.3.2, consisting of two convex non-regular $(n/2)$ -gons, facing one another in such a way that every edge except one in the first polygon sees every edge except one in the second polygon (see Figure 3.17 again). As we saw before, in order to obtain a full triangulation of this configuration we must triangulate both the two convex $(n/2)$ -gons and the non-convex n -gon formed between them. In particular, the diameter of the graph of $(2, 2)$ -flips of the whole configuration is at least as large as the diameter of the graph of $(2, 2)$ -flips in triangulations of this non-convex polygon.

Now, it is easy to set up a bijection between triangulations of this non-convex n -gon and bit sequences of length $n - 2$: For a given triangulation, we read its triangles from left to right and use a 0 for triangles with two vertices in the bottom chain and a 1 for triangles with two vertices in the top chain. A $(2, 2)$ -flip amounts to changing a subsequence 01 to 10 or vice versa. This bijection proves our previous assertion that the number of triangulations of this polygon equals $\binom{n-2}{n/2-1}$. But what interests us now is that it also gives a quadratic lower bound to the diameter of the graph of flips. Indeed, if to each bit sequence we associate the sum of the positions where the 1's lie, we get that the bit sequence 1111...0000 gets weight about $n^2/8$ while the sequence 0000...1111 gets about $3n^2/8$. Since each flip changes the weight by exactly one unit, we need about $n^2/4$ flips to go from the first triangulation in Figure 3.28 to the second one, or vice versa.

3.4.2 Effective enumeration of triangulations

There is also the practical problem of computing *exactly* the number of distinct triangulations for concrete instances of point configurations. A way to list all triangulations is via a depth-first search or breadth-first search traversal of the graph of flips. By the connectivity results we have just seen, we are guaranteed to visit all triangulations. The trouble with this approach is that we may need a large amount of storage during these search traversals (saving all triangulations that have been visited). But there is a memory-efficient method of listing all triangulations of a point set in the plane: the *reverse search enumeration* of Avis and Fukuda [23, 24].

Reverse-search is in fact a very general method of listing all vertices of some directed graphs, under certain special assumptions. The amount of memory used for book-keeping is very small and it is independent of the

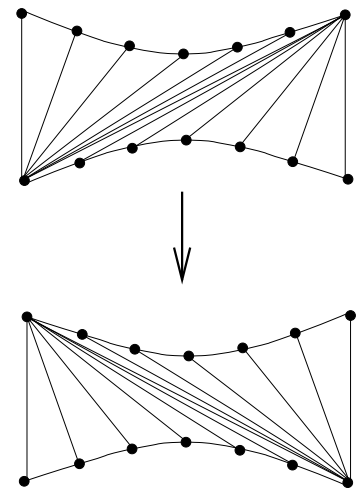


Figure 3.28: The flip distance from one triangulation to another is quadratic.

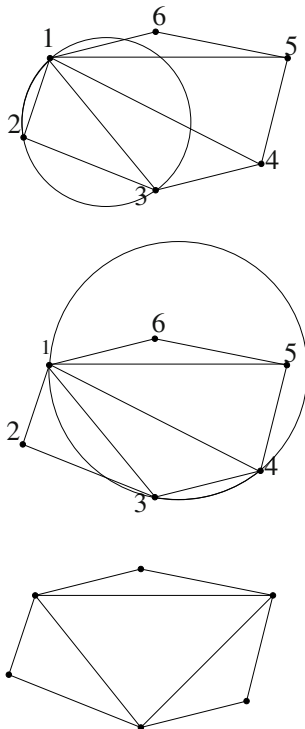


Figure 3.29: Finding a successor. First edge is locally Delaunay, second edge is not and the flip gives a new triangulation closer to being Delaunay.

size of the graph. The actual visit to the nodes is done in a depth-first search order and the running time of the reverse-search enumeration is polynomial on the number of triangulations. Thus the algorithm has a good output-sensitive complexity. For brevity we will not present reverse-search in full generality here, but only outline it for the graph of triangulations of point configurations in the plane. We assume the reader is familiar with depth-first search enumeration in graphs as in any introductory computer science course.

The main point of the algorithm is that, for point configurations in general position and with no co-circular points, the graph of flips can be oriented in such a way that it becomes an acyclic graph with a unique sink, the sink being at the Delaunay triangulation (which is unique under the non-cocircularity assumption). From any other triangulation we can reverse back to a parent triangulation by an oriented flip.

For each triangulation we have an *adjacency oracle* that tells us its flip neighbors. We can also define a *successor oracle* that given a triangulation \mathcal{T} assigns a unique successor. This should be another triangulation, closer to becoming a Delaunay triangulation. We saw that a triangulation is the Delaunay triangulation if each edge is locally Delaunay. Order all possible edges of the point configuration in some way, for instance lexicographically. From a triangulation \mathcal{T} its successor is \mathcal{T}' if \mathcal{T}' is obtained from \mathcal{T} by flipping the first (in our ordering) flippable edge which is not locally Delaunay (see Figure 3.29). Note that such successor \mathcal{T}' exists unless \mathcal{T} is already the Delaunay triangulation. In Figure 3.30 all triangulations of a generic hexagon with their successors are shown.

Now to generate all triangulations, start at the Delaunay triangulation, make it the root of the depth-first search (DFS) tree and the first parent node. Traverse the graph in the usual depth-first manner. Normally a depth-first search relies on a memory stack data structure to walk up and down the tree, but now this is no longer necessary. Walking up toward the root is done by following the successor function. For the current parent triangulation \mathcal{T} all its candidate children can be generated via flips in the order induced by the ordering of edges (i.e., we first try to flip edge 1, if it fails try to flip edge 2, etc). But we only accept \mathcal{T}' as a legitimate child of the DFS tree if the successor of \mathcal{T}' is \mathcal{T} .

No data structure is needed to mark or remember visited triangulations anymore. This can be deduced from the acyclic order defined in the set of triangulations and from two memory variables, one that marks the current parent and its immediate predecessor in the depth-first search traversal. Now we illustrate the algorithm with a simple example. The generic hexagonal point configuration has coordinates, given in the order we labeled the points, $(4, 2)$, $(5, -1)$, $(0, -3)$, $(4, -2)$, $(5, 2)$, $(0, 3)$. The reader can use these coordinates to compute the circumcircles of triangles and decide whether particular edges are locally Delaunay or not.

On top of Figure 3.30 we show its Delaunay triangulation and a labeling of the vertices. We use the labeling of the vertices to set a lexicographic order on the edges (i.e., edge $\{1,2\}$ comes before $\{1,3\}$, etc). In order for

the reader to find a successor it is necessary to draw the many circumcircles of triangles and decide which edges are locally Delaunay. In Figure 3.29 we show the sequence of circle checks that find the smallest edge ($\{1,4\}$) to be flipped.

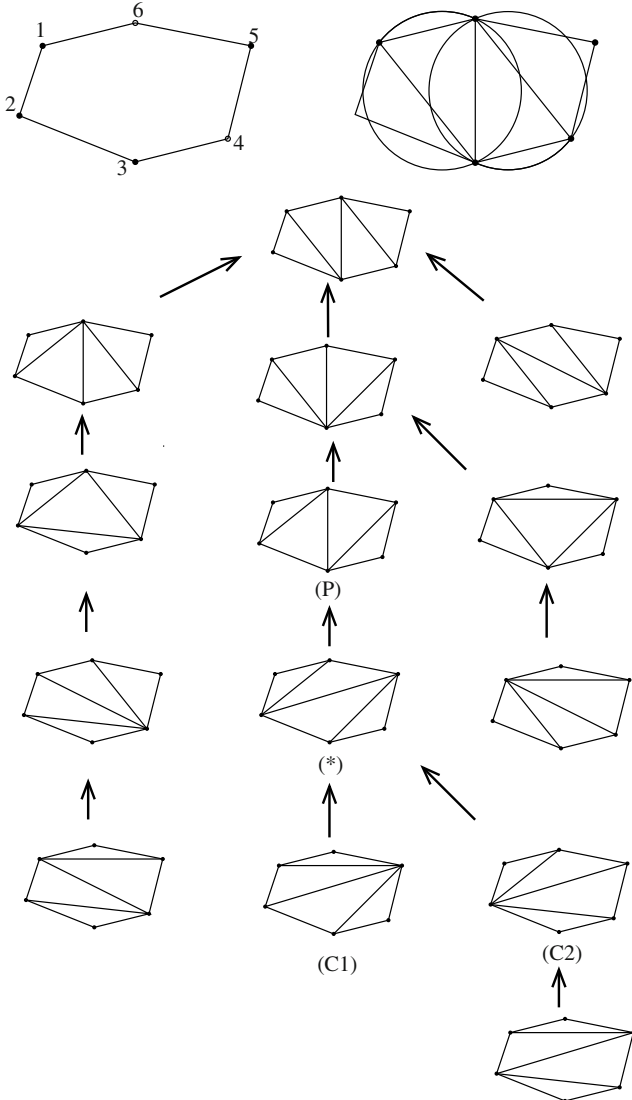


Figure 3.30: The DFS tree generated by reverse search.

Let us follow a few steps of the algorithm using the example of Figure 3.30. Suppose the search arrives at node (*). The adjacency oracle tells us all three adjacent triangulations. The successor function applied to these three neighbors checks that there are two legal children for the DFS tree, labeled (C1), (C2). The parent (P) of (*) is found by the successor function.

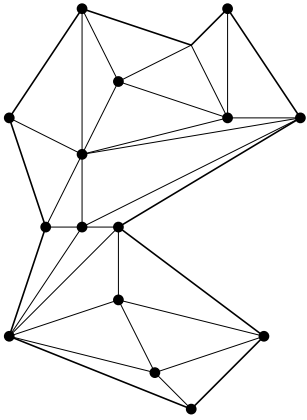
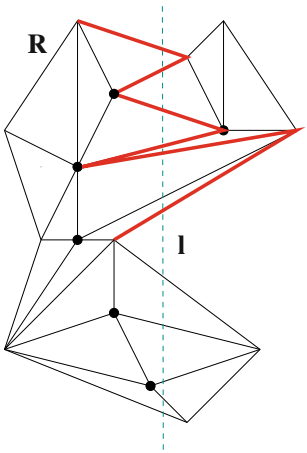
Figure 3.31: An \mathbf{A} -polygon.

Figure 3.32: A path.

How to decide whether to move forward to $(C1)$ or backtrack to (P) ? For this, recall that we keep a variable that marks the immediate predecessor of $(*)$. If the predecessor is (P) then the search is on the way down and moves to $(C1)$. On the other hand if the predecessor is $(C1)$ then it is on the way up and backtracks to $(*)$. If the predecessor is $(*)$ then it has to visit its next child $(C2)$ and if the predecessor is $(C2)$ we have visited all children of $(*)$ so that branch has been completely traversed. Finally, if the predecessor marker is *null* we are at the Delaunay triangulation.

A more recent alternative approach for enumeration, that does not use flips, was proposed by O. Aichholzer [2]. He introduced the so called *t-path* (or “triangulation path”) method which yields a fast divide-and-conquer enumeration scheme to enumerate all triangulations of a point configuration. To explain the algorithm it is necessary to consider triangulations of non-convex objects, but still related to a point configuration \mathbf{A} . Given a region \mathbf{R} of \mathbb{R}^2 we say it is \mathbf{A} -*triangulable* if \mathbf{R} has a triangulation whose vertices are a subset of \mathbf{A} . More precisely, there is a simplicial complex with vertices contained in \mathbf{A} with a geometric realization equal to \mathbf{R} . The most useful example of \mathbf{A} -triangulable sets are \mathbf{A} -polygons, namely a non-convex simple polygon whose vertices are contained in the configuration \mathbf{A} . For example see Figures 3.31 and 3.32. The point configuration \mathbf{A} is marked by black dots, and a triangulation of the polygon is shown. Observe that any \mathbf{A} -polygon is contained inside the convex hull of \mathbf{A} . Thus all triangulations of an \mathbf{A} -polygon appear in at least one triangulation of \mathbf{A} since any \mathbf{A} -polygon triangulation can be completed to a triangulation of \mathbf{A} .

Definition 3.4.6. Consider a point configuration in the plane \mathbf{A} and an \mathbf{A} -polygon \mathbf{R} . Let \mathcal{T} be a triangulation of \mathbf{R} and \mathbf{I} a line that intersects \mathcal{T} properly, meaning it cuts through the interior of edges.

We define the *path* of \mathcal{T} along \mathbf{I} , and denote it $\text{path}_{\mathbf{I}}(\mathcal{T})$, as the unique chain of edges from the triangulation \mathcal{T} , such that

- (a) \mathbf{I} properly intersects all edges in the chain,
- (b) The chain starts and ends at two boundary edges of \mathbf{R} such that the segment of \mathbf{I} between the two intersection points lies in the interior of \mathbf{R} ,
- (c) alternating vertices on the chain lie in opposite sides of \mathbf{I} , and
- (d) the area bounded by the chain and \mathbf{I} has no other points of the configuration.

See Figure 3.32 for an example.

The main property of paths is that they allow us to “identify” all triangulations by their paths coming from line \mathbf{I} and thus we can apply a divide-and-conquer enumeration strategy. See Theorems 1 and 3 of [2]:

Lemma 3.4.7. (a) Given a point configuration in the plane \mathbf{A} , a triangulation \mathcal{T} of an \mathbf{A} -polygon \mathbf{R} , and a line \mathbf{I} that intersects properly \mathcal{T} , there always exists a path $\text{path}_{\mathbf{I}}(\mathcal{T})$.

- (b) Given a point configuration in the plane \mathbf{A} , triangulations $\mathcal{T}_1, \mathcal{T}_2$ of an \mathbf{A} -polygon \mathbf{R} , and a line \mathbf{l} that intersects properly \mathcal{T}_1 , any two paths $\text{path}_{\mathbf{l}}(\mathcal{T}_1)$ and $\text{path}_{\mathbf{l}}(\mathcal{T}_2)$ with same start and end edges are either identical or properly intersect each other.

Proof. We can assume that \mathbf{l} is a vertical line, otherwise a rotation can be applied. To construct a path, we proceed inductively, starting with the top boundary edge \mathbf{e}_1 where \mathbf{l} first enters the interior of \mathbf{R} . Let T_1 be the triangle containing \mathbf{e}_1 and let \mathbf{e}_2 be the other edge of T_1 crossed by \mathbf{l} . Let the vertices of T_1 be called $\mathbf{p}_0, \mathbf{p}_1$ and \mathbf{p}_2 in such a way that $\mathbf{e}_1 = \mathbf{p}_0\mathbf{p}_1$ and $\mathbf{e}_2 = \mathbf{p}_0\mathbf{p}_2$.

In the general inductive step, assume that we have already constructed a path $\mathbf{e}_1 = \mathbf{p}_0\mathbf{p}_1, \mathbf{e}_2 = \mathbf{p}_1\mathbf{p}_2, \dots, \mathbf{e}_i = \mathbf{p}_{i-1}\mathbf{p}_i$ in the desired conditions. If \mathbf{e}_i is a bottom boundary edge of R we have finished, otherwise let us show how to continue the process.

Let \mathbf{p}' be the third vertex of the triangle in \mathcal{T} based on \mathbf{e}_i and below it. Either \mathbf{p}' lies on the opposite side of \mathbf{l} from \mathbf{p}_i , in which case we can continue the path with $\mathbf{e}_{i+1} = \mathbf{p}_i\mathbf{p}'$, or \mathbf{p}' is in the same side as \mathbf{p}_i in which case we abandon the last edge $\mathbf{e}_i = \mathbf{p}_{i-1}\mathbf{p}_i$ of our provisional path and make $\mathbf{p}_{i-1}\mathbf{p}'$ be the new i -th edge. This does not increase the number of edges of the path, but it makes the path reach lower along \mathbf{l} as before, so that the process eventually terminates, once we hit the boundary of \mathbf{R} again to exit (the edge by construction has its extremes in opposite sides; See Figure 3.33).

To prove the second part of the lemma we proceed by contradiction. Assume we have two different paths $\text{path}_{\mathbf{l}}(\mathcal{T}_1)$ and $\text{path}_{\mathbf{l}}(\mathcal{T}_2)$ which do not properly intersect. Thus if they do not have common vertices then path $\text{path}_{\mathbf{l}}(\mathcal{T}_1)$ lies entirely to the left of path $\text{path}_{\mathbf{l}}(\mathcal{T}_2)$. But since $\text{path}_{\mathbf{l}}(\mathcal{T}_2)$ is a path, no edge of $\text{path}_{\mathbf{l}}(\mathcal{T}_1)$ can intersect \mathbf{l} . This is a contradiction. Next, suppose the two paths have indeed a common vertex \mathbf{p} , but the successor of \mathbf{p} is different in each of the paths, say $\mathbf{p}', \mathbf{p}''$, as we show in Figure 3.34. The main point is that now the point \mathbf{p}' cannot be placed anywhere without violating part (d) of the definition or forcing a proper intersection between the two paths. \square

We can use Lemma 3.4.7 to count all triangulations recursively. First, separate the point set \mathbf{A} in two parts by a line \mathbf{l} . Compute all possible paths associated to \mathbf{l} , for each such path we recover several \mathbf{A} -polygons in which the triangulations can be counted separately, and the product of the numbers of triangulations of these subproblems gives the triangulations that have that concrete path. The total number of triangulations of \mathbf{A} is given by the sum of the numbers obtained for all paths, since different paths of \mathbf{A} and \mathbf{l} cannot be present in the same triangulation and since any triangulation of \mathbf{A} contains exactly one path for \mathbf{l} .

Experimental evidence shows that the algorithm runs in time sub-linear in the number of triangulations being counted. Nevertheless a detailed worst-case complexity analysis has not yet been derived. However, this highlights the difference between *enumerating* and *counting*. The reverse search method needs to *enumerate* all the triangulations (that is, to list them one by one) and hence its running time is at least proportional to the number

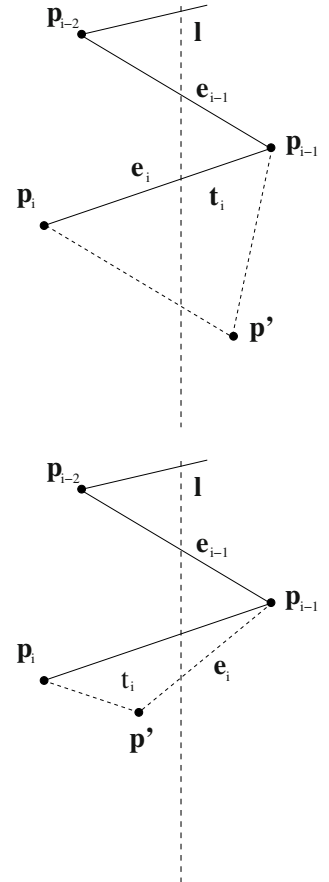


Figure 3.33: The process of constructing a path.

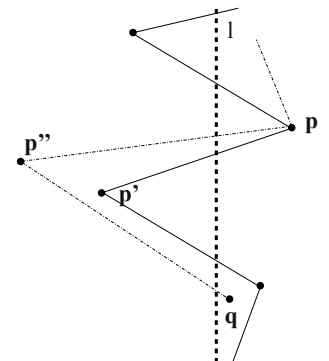


Figure 3.34: The uniqueness of the path.

of triangulations. The path method can, in principle, *count* triangulations (that is, compute their exact number) without listing them all.

Another counting algorithm has recently been proposed in [270]. Unfortunately, neither of these methods works without first doing major modifications in dimension three or higher.

3.4.3 Further properties of the graph of flips

We have seen that the graph of triangulations of a point set in the plane is connected, but how connected is it? What is the diameter of the graph of flips? In this section we will look at the diameter, number of neighbors and other properties of the graph of flips.

In the connected graph of flips, given two triangulations, it is natural to ask what is the smallest number of flips needed to go from one triangulation to the other? We begin with the following theorem due to S. Hanke, T. Ottmann, and S. Schuierer [155].

Theorem 3.4.8. *Let \mathcal{T}_1 and \mathcal{T}_2 be two full triangulations (i.e., using all the vertices) of a point configuration with n points in general position. Let $\text{cr}(\mathcal{T}_1, \mathcal{T}_2)$ be the number of crossings between edges of \mathcal{T}_1 and \mathcal{T}_2 , then*

1. $\text{cr}(\mathcal{T}_1, \mathcal{T}_2) \leq (3n - 2n_b - 3)^2$,
2. \mathcal{T}_1 can be transformed into \mathcal{T}_2 in at most $\text{cr}(\mathcal{T}_1, \mathcal{T}_2)$ flips of type (2,2).

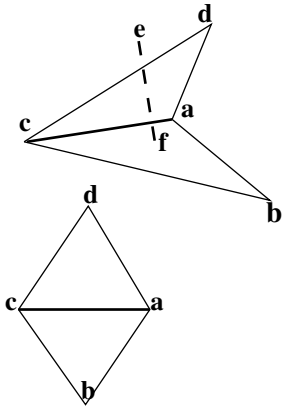


Figure 3.35: All maximal edges are flippable.

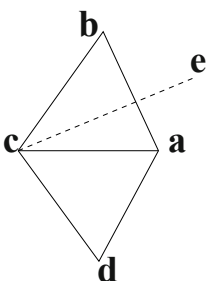


Figure 3.36: all maximal edges are flippable.

Proof. In what follows we call maximal edges of \mathcal{T}_1 those with the maximum number of crossings with \mathcal{T}_2 . We claim first that all maximal edges are flippable. For the justification of this claim we refer to Figure 3.35.

Suppose ac is a maximal but non-flippable edge of \mathcal{T}_1 . This means that one of the vertices, say a , is a reflex point of the quadrilateral $abcd$ (see Figure 3.35). Consider the edge ef of \mathcal{T}_2 that crosses ac and is closest possible to vertex a . This edge either crosses cd or cb or both (otherwise \mathcal{T}_1 or \mathcal{T}_2 are not full triangulations). Observe that aef must be a triangle in \mathcal{T}_2 because otherwise there would be an edge crossing ac and closer to a . Say ef crosses cd (the other cases are similar), then note that every edge crossing ac crosses cd because there are no other vertices inside the region bounded by acd . In particular, ae crosses cd as well, but this means that cd has at least one more edge crossing cd than ac , which is a contradiction to the assumption that ac was maximal. Now we know for sure that every maximal edge is the diagonal of a convex quadrilateral $abcd$ as in the lower part of Figure 3.35.

Next we claim there is some maximal edge whose flipping reduces the number of crossings. More precisely, if \mathcal{T}_2 has an edge which crosses the sides of the quadrilateral $abcd$ (present in \mathcal{T}_1) and of which at least one of its two vertices is a, b, c , or d , then flipping ac in \mathcal{T}_1 decreases the number $\text{cr}(\mathcal{T}_1, \mathcal{T}_2)$. See Figure 3.36. If the edge in question is actually bd the claim is obvious. If the edge ce crosses ab , then, once more, all edges that cross ac must cross ab , but this contradicts the maximality of ac since ce crosses ab as well. By symmetry, the same happens when the crossing edge is

ae. The final possibility is that the crossing edge is either **be** or **de**. Then all the edges of \mathcal{T}_2 crossing **bd** and edge **be**, cross **ad**. This means **bd** crosses less edges of \mathcal{T}_2 than **ad** and, by maximality of **ac**, less edges of \mathcal{T}_2 than **ac**. This proves the second claim.

The proof of the theorem will now use the two claims above and proceed by contradiction. If the theorem is not true no maximal edge can satisfy the conditions of the second claim (i.e., there is an edge intersecting the sides of **abcd** with one vertex being **a, b, c, d**). The four corners of **a, b, c, d** are vertices of some triangles of \mathcal{T}_2 , which “cut through” those corners. We call north and south the edges cutting **db** and east and west those edges cutting **ac**. Moreover there has to be one or more edges of \mathcal{T}_2 that connect the vertices corner cutting edges (see Figure 3.37).

Now let us make a count of the edges of \mathcal{T}_2 intersecting elements of **abcd**. We abbreviate D, N, S, E, W the number of diagonal, north, south, etc. edges in \mathcal{T}_2 intersecting the sides of **abcd**. Thus $\text{cr}(\mathbf{ac}, \mathcal{T}_2) = W + D + E$, $\text{cr}(\mathbf{ab}, \mathcal{T}_2) = N + D + E$, $\text{cr}(\mathbf{cd}, \mathcal{T}_2) = W + D + S$, $\text{cr}(\mathbf{bd}, \mathcal{T}_2) = N + D + S$. By the maximality of **ac** we have that $W \geq N$, $E \geq S$. Since we are assuming that flipping **ac** does not decrease the number of crossings $N + S \geq W + E$. These two facts together imply that $W = N$, $E = S$. This implies that **ab** and **bc** are also maximal edges. This means that every maximal edge is part of a “zig-zag” of 3 maximal edges (see Figure 3.38). Since the path cannot continue forever and cannot end at a boundary edge (no edges of \mathcal{T}_2 cross a boundary edge of \mathcal{T}_1 , they are shared) then the only possibility is that a cycle appears. This leads to a contradiction because for a cycle to exist it has a reflex vertex. But this reflex vertex is used by two consecutive quadrilaterals of the path. Thus the “cutting through” edges of \mathcal{T}_2 for these quadrilaterals intersect improperly. This is the desired contradiction.

Finally, since $3n - 2n_b - 3$ is the number of interior edges of both \mathcal{T}_1 and \mathcal{T}_2 , it is clear that the number of intersections $\text{cr}(\mathcal{T}_1, \mathcal{T}_2)$ is no more than $(3n - 2n_b - 3)^2$. □

Here is another nice property of the graph of triangulations of a point set in the plane:

Theorem 3.4.9. *Every triangulation of an n point configuration in the plane has at least $n - 3$ geometric bistellar flips. In other words, the graph of triangulations of a point set in the plane with n points has minimum degree $n - 3$.*

Proof. Let \mathcal{T} be a triangulation of an n point configuration \mathbf{A} in \mathbb{R}^2 . If there is a flip that inserts a point \mathbf{p} , then \mathcal{T} can be considered as a triangulation of $\mathbf{A} \setminus \{\mathbf{p}\}$ and induction on n shows that it has at least other $n - 4$ flips. Hence we assume that the triangulation uses all the points of \mathbf{A} .

We say that an edge of \mathcal{T} is flippable if it is interior (not contained in the boundary of \mathbf{A}) and the two triangles incident to it form either a strictly convex quadrilateral or a quadrilateral with two consecutive edges whose union is a straight line segment contained in the boundary of the convex hull of \mathbf{A} . In the first case there is a flip of type (2,2) which removes the flippable edge and inserts the other diagonal of the quadrilateral, and in the second

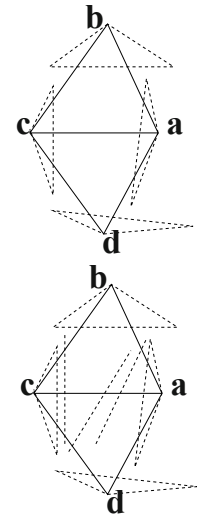


Figure 3.37: Edges of \mathcal{T}_2 cutting through **abcd** appear in dotted lines.

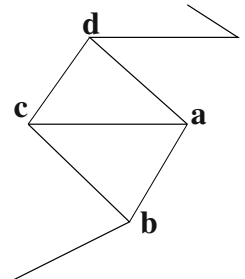


Figure 3.38: The darker edges mark a zig-zag path of maximal edges in \mathcal{T}_1 .

case there is a flip of type (2,1) which removes the interior edge and joins the two consecutive collinear edges into one (corresponding to the lowest part of Figure 3.24).

Let e_b be the number of boundary edges (note that e_b also equals the number of boundary points of \mathbf{A}). Denote by e_i the number of interior edges and by f the number of triangles. Euler's formula for the disk gives $n - e_i - e_b + f = 1$ and a counting argument shows that $3f = 2e_i + e_b$. With these two equalities we obtain:

$$e_i = 3n - 3 - 2e_b.$$

For an interior non-flippable edge \mathbf{e} , the union of the two triangles sharing \mathbf{e} is a quadrangle with a concave or flat vertex which we will call the vertex associated to \mathbf{e} . If a vertex \mathbf{p} is associated to four interior edges, then the four edges form two pairs of collinear edges with \mathbf{p} as a common end and there are two flips of type (2,1) which make \mathbf{p} disappear. If \mathbf{p} is associated to three interior edges, then the star of \mathbf{p} looks like either the center or lower parts of Figure 3.24, and there is one flip (of types (3,1) or (2,1)) which makes the point \mathbf{p} disappear.

Hence, the number of interior non-flippable edges is no greater than twice the number of interior points plus the number of flips which make a point disappear. In other words, the total number e_i of interior edges is no greater than the total number of flips plus twice the number $n - e_b$ of interior points. Thus the number of flips is at least $e_i - 2(n - e_b) = n - 3$, as desired. \square

Remark 3.4.10 (Variations on the theme of flips). Planar flips are very natural operations. As we saw they may have important algorithmic consequences too (e.g., enumeration). It is perhaps not surprising that there are similar definitions that have been studied in the computational geometry and graph theory literature. Because triangulations are examples of graphs (linearly embedded planar graphs), one can think of a flip for abstract graphs as an operation that deletes one edge and adds another one, with the condition that the new graph is still within “the same class” as the original graph. Some classes for which flips are studied belong to topological graph theory, e.g., maximal planar graphs or graphs embeddable in a certain surface, etc (see e.g., [195, 239, 328]). One can ask for more geometric examples (i.e., coordinates matter), such as triangulations of polygons, flips on pseudo-triangulations, etc. The literature on the topic is abundant, but here we would like to discuss a few results about some variations related to the flips defined here.

The most popular case, which we have actually already studied, is when one restricts attention to the graph of (2,2)-flips among full-triangulations of a point set. But we can also change the setting and study triangulations of, for example, a simple non-convex n -gon. In this case all we have said so far remains essentially true: the diameter of the graph of flips has a quadratic upper bound, and some polygons (see the double chain in Example 3.4.5) actually have a flip-graph with quadratic diameter. But one can give more precise statements, such as the following one from Hurtado et al. [172].

Theorem 3.4.11. *The graph of edge-flips among triangulations of a non-convex n -gon has diameter bounded above by $O(n + k^2)$, where k is the number of reflex vertices.*

This is in contrast to the case of convex n -gons where, as we saw in Chapter 1, the hyperbolic geometric arguments of Sleator et al. [300] demonstrated that the diameter is linear.

An extended flip notion, introduced by Galtier et al. [132], is that of *simultaneous flips*. A simultaneous flip (sometimes called *parallel flip*) is a set of edges that can be flipped simultaneously without interfering with each other (see Figure 3.39 for a simultaneous flip with seven edges).

Galtier et al. proved that $\Omega(n)$ flips are sometimes necessary to move from one triangulation to another and $O(n)$ simultaneous flips suffice. Another of their results is that $(n - 4)/6$ edges can always be simultaneously flipped but there are triangulations where at most $(n - 4)/5$ can be flipped simultaneously. One can see that there are at least $(n - 4)/2$ simple edge-flips of full triangulations, about a third of those can be argued to be disjoint from each other and thus can be flipped simultaneously. For a convex n -gon we have seen the flip distance is linear in n . In contrast, Galtier et al. have proved that $O(\log(n))$ simultaneous flips suffice to go from one triangulation the other.

3.5 Pseudo-triangulations

Another generalization of triangulations in the plane and their flips comes from pseudo-triangulations. These objects were first introduced in the context of visibility (see [257, 256]). They also appeared under the name of *geodesic triangulations* [78] as a data structure suitable for *ray shooting* in non-convex polygons. Later they have found applications as *kinetic data structures* for detecting collisions between a set of polygons that are not only moving but whose shapes can also change continuously with time [1], and as a tool to solve the Carpenter’s Rule Problem [310], among other topics. See [276] for more details.

So, what exactly is a pseudo-triangulation? Let A be a finite point set in the Euclidean plane, which we assume is in general position. A *pseudo-triangle* in the plane is a simple polygon with exactly three convex angles. For the computer graphics applications, a pseudo-triangle is a shape sufficiently flexible to allow extensive deformation, yet structured enough to make detection of self-collisions easy! See Figure 3.40. A *pseudo-triangulation* of A is a geometric (i.e., with straight edges), non-crossing graph with vertex set A , containing the convex hull edges of A and in which every bounded region is a pseudo-triangle. See Figure 3.41 for an example. A vertex v in a geometric graph G is called *pointed* if all the edges of G lie in a half-plane supported at v or, equivalently, if one of the angles incident to v is greater than 180° . A pseudo-triangulation is called *pointed* if all its vertices are pointed. Here is one numerical result that is helpful for a reader to practice some of the definitions above and which is used to prove properties of pseudo-triangulations:

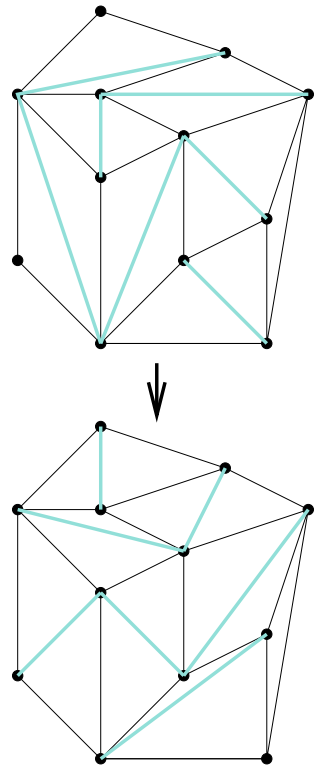


Figure 3.39: A simultaneous flip on the marked edges.

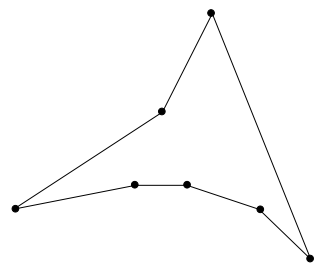


Figure 3.40: One pseudo-triangle.

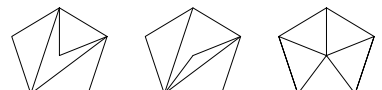


Figure 3.41: Three pseudo-triangulations of a point configuration with six points.

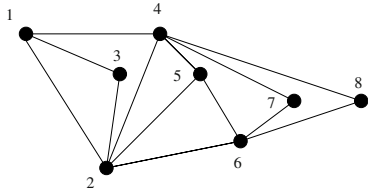


Figure 3.42: An example of a pointed pseudo-triangulation.

Lemma 3.5.1. Let \mathbf{G} be a non-crossing straight-line embedding of a connected graph in the plane. Let e , x and y denote the numbers of edges, non-pointed vertices and pointed vertices in \mathbf{G} . Then $e \leq 3x + 2y - 3$, with equality if and only if the embedding is a pseudo-triangulation.

Proof. Let f be the number of bounded faces of the embedding. By Euler's formula, $x + y + f = e + 1$. We now double-count the number of “big” and “small” angles in the embedding (that is, angles bigger and smaller than 180 degrees, respectively). The total number of angles equals $2e$. The number of big angles equals y , and the number of small angles is at least $3f$ (every bounded face has at least three corners) with equality if and only if the embedding is a pseudo-triangulation. These equations give the statement. \square

Just as in the case of triangulations, one can define flips between pseudo-triangulations. In fact, pseudo-triangulations are even nicer than triangulations in this respect: every interior edge in a pseudo-triangulation can be flipped, if flips are defined appropriately, and there is a polytope whose vertices are *all* the pseudo-triangulations of a point set and whose edges are the flips between them [7, 275, 247].

Some of the nice properties of pseudo-triangulations come from their beautiful relation to *rigidity theory*. Rigidity theory is the study of when structures made of linkages and bars are rigid. For example a graph is *generically rigid* in the plane, if any “random” embedded bar and joint framework corresponding to the graph has only trivial motions (e.g., translations). Generic rigidity is a property of the graph, and not of any particular embedding. It turns out that edge-minimal generically rigid graphs on a given number n of vertices are characterized by the so called *Laman’s Condition*: they have exactly $2n - 3$ edges and every subset of k vertices spans a subgraph with at most $2k - 3$ edges. Generically rigid graphs with $2n - 3$ edges are also known as *Laman graphs*. The connection between rigidity and pseudo-triangulations was first pointed out by I. Streinu [310], who proved that the graphs of pointed pseudo-triangulations are Laman graphs. Later D. Orden et al. [248] proved the following very general characterization of generically rigid graphs. A *plane graph* is a graph drawn without crossings in the plane.

Theorem 3.5.2. For a plane graph \mathbf{G} , the following conditions are equivalent:

1. \mathbf{G} is generically rigid.
2. \mathbf{G} can be stretched to become a pseudo-triangulation of a point set, with changing its topological embedding.

The same is true if *edge-minimal generically rigid* is put in part 1 and *pointed pseudo-triangulation* is put in part 2.

3.6 Life in three dimensions

In this section we take a quick look at what happens when we move up just one dimension. The conclusion is that most of the very simple proofs and nice results that we have for the plane do not apply anymore.

Many of the differences come from the following: Every non-convex polygon in the plane can be triangulated without extra vertices (see Exercise 3.13). In contrast, in dimension three (or higher), *there are non-triangulable non-convex polytopes*. The following example is not the first one in the literature (see [208]), but arguably the nicest one with the largest impact.

Example 3.6.1 (Schönhardt's polyhedron (see [290])). Let \mathbf{A} consist of the following six points, where ε is a small positive number (any $\varepsilon \in (0, 1/2)$ would work for this example):

$$\mathbf{A} = \begin{pmatrix} \mathbf{p}_1 & \mathbf{p}_2 & \mathbf{p}_3 & \mathbf{q}_1 & \mathbf{q}_2 & \mathbf{q}_3 \\ 1 - \varepsilon & 0 & \varepsilon & 1 & 0 & 0 \\ \varepsilon & 1 - \varepsilon & 0 & 0 & 1 & 0 \\ 0 & \varepsilon & 1 - \varepsilon & 0 & 0 & 1 \\ 0 & 0 & 0 & 1 & 1 & 1 \end{pmatrix},$$

When ε tends to zero, the six points in \mathbf{A} tend to a triangular prism with facets

$$\{\mathbf{q}_1, \mathbf{q}_2, \mathbf{p}_1, \mathbf{p}_2\}, \quad \{\mathbf{q}_2, \mathbf{q}_3, \mathbf{p}_2, \mathbf{p}_3\}, \quad \{\mathbf{q}_3, \mathbf{q}_1, \mathbf{p}_3, \mathbf{p}_1\}, \\ \{\mathbf{q}_1, \mathbf{q}_2, \mathbf{q}_3\}, \quad \{\mathbf{p}_1, \mathbf{p}_2, \mathbf{p}_3\}.$$

When ε is positive (and small), the bottom triangular face of the prism is rotated (and, in our choice of coordinates, slightly rotated) so that the three former quadrilateral facets of $\text{conv}(\mathbf{A})$ break into two triangles each, via the insertion of the diagonal $\{\mathbf{q}_{i+1} \mathbf{p}_i\}$ (where $i \in \{1, 2, 3\}$ and $i + 1$ is considered modulo three). The *Schönhardt polyhedron* is the non-convex 3-polytope formed by inserting the opposite diagonals. That is, the polyhedron's boundary consists of the following eight triangles. See Figure 3.43:

$$\{\mathbf{q}_1, \mathbf{p}_1, \mathbf{p}_2\}, \quad \{\mathbf{q}_1, \mathbf{q}_2, \mathbf{p}_2\}, \quad \{\mathbf{q}_2, \mathbf{p}_2, \mathbf{p}_3\}, \quad \{\mathbf{q}_2, \mathbf{q}_3, \mathbf{p}_3\}, \\ \{\mathbf{q}_3, \mathbf{p}_3, \mathbf{p}_1\}, \quad \{\mathbf{q}_3, \mathbf{q}_1, \mathbf{p}_1\}, \quad \{\mathbf{q}_1, \mathbf{q}_2, \mathbf{q}_3\}, \quad \{\mathbf{p}_1, \mathbf{p}_2, \mathbf{p}_3\}.$$

We leave it to the reader (Exercise 3.16) to check that:

Lemma 3.6.2 ([290]). *There is no tetrahedron contained in the Schönhardt polyhedron with vertices in \mathbf{A} . In particular, the polyhedron cannot be triangulated without extra vertices.*

As another consequence, suppose that you want to triangulate the point configuration and you start throwing in tetrahedra one by one, checking at every step that the new one intersects properly with the previous ones. In dimension two this process always terminates in a triangulation, but in dimension three it does not:

Lemma 3.6.3. *The three tetrahedra $\{\mathbf{q}_1, \mathbf{q}_2, \mathbf{p}_1, \mathbf{p}_2\}$, $\{\mathbf{q}_1, \mathbf{q}_3, \mathbf{p}_1, \mathbf{p}_3\}$ and $\{\mathbf{q}_2, \mathbf{q}_3, \mathbf{p}_3, \mathbf{p}_1\}$ intersect properly, but no triangulation of \mathbf{A} contains the three of them.*

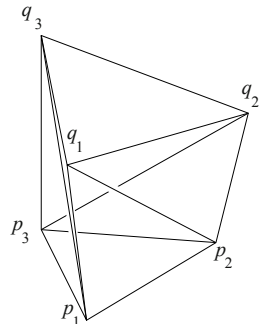
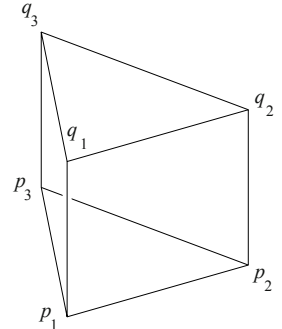


Figure 3.43: Schönhardt's non-triangulable polyhedron (bottom), constructed from a triangular prism (top).

Proof. The tetrahedra intersect properly because the intersection of two of them is a common edge (think of these three tetrahedra as lying in the three facets of the original prism, except these facets are slightly “inflated”. They do not belong to any triangulation of \mathbf{A} because the part of $\text{conv}(\mathbf{A})$ not covered by them is precisely Schönhardt’s polyhedron. \square

Schönhardt’s polyhedron is a very classical and important example in polytope theory, that we will encounter several times in this book. It is crucial, for example, in the results of Section 8.6 (computing minimum size triangulations is NP-hard, in particular the construction of Theorem 8.6.9) and also in the following related result (Note: if you are not familiar with NP-hardness, do not worry, basic complexity notions will be reviewed in Chapter 8):

Theorem 3.6.4 (Ruppert and Seidel [277]). *It is NP-complete to decide whether a 3-dimensional non-convex polytope can be triangulated without extra vertices.*

A natural generalization of Schönhardt’s polyhedron is the non-convex twisted prism over an n -gon. It was conjectured by most people in the area that this polyhedron has no triangulation without new vertices either. In [266] this was finally proved for the case of sufficiently small twists; for twists that are too large, all of a sudden triangulations emerge. The main tool to understand this is the Cayley trick, presented in Section 9.2.

3.6.1 The number of tetrahedra

The other fundamental difference between dimension two and higher dimensions is that in dimension two the number of triangles in all the full triangulations of a point set \mathbf{A} is constant. The same is not true in dimension three, even for a point configuration in convex position! In other words, full triangulations of three-dimensional configurations have different sizes. The best known example of this behavior is the 3-cube, which we already encountered in Chapter 1, in particular, Figure 1.33:

Example 3.6.5 (Triangulations of the 3-cube). Let \mathbf{I}^3 denote the vertex set of the 3-cube. That is, the following point configuration:

$$\begin{array}{ccccccc} 0 & 1 & 2 & 3 & 4 & 5 & 6 & 7 \\ \left(\begin{array}{ccccccc} 0 & 0 & 0 & 0 & 1 & 1 & 1 & 1 \\ 0 & 0 & 1 & 1 & 0 & 0 & 1 & 1 \\ 0 & 1 & 0 & 1 & 0 & 1 & 0 & 1 \\ 1 & 1 & 1 & 1 & 1 & 1 & 1 & 1 \end{array} \right) \end{array}$$

One easy way to classify the triangulations of the cube is by looking at what simplex contains the barycenter in its relative interior. A little thought will convince the reader that there are only two possibilities:

- An edge joining two opposite vertices of the cube (a “diagonal of the cube”), or
- A regular tetrahedron, either $\{0356\}$ or $\{1247\}$.

As we will show in more detail in Section 6.3, these two possibilities produce, respectively, triangulations of the 3-cube with six or with five tetrahedra. In the first case there are five possibilities, modulo the symmetries of the cube. In the second case there is only one. See a picture of each symmetry class in Figure 1.33 of Chapter 1.

If we look at bigger examples, the differences in sizes among various triangulations is more drastic. Essentially, every point configuration has triangulations with a linear number of tetrahedra, and some point configurations have even triangulations with quadratically many tetrahedra. Let us look at these two properties in more detail.

Lemma 3.6.6. *Let \mathbf{A} be a 3-dimensional point configuration. Then there is a triangulation of \mathbf{A} with no more than $2v - 7$ tetrahedra, where v is the number of vertices of $\text{conv}(\mathbf{A})$.*

If \mathbf{A} is in general position, there is a full triangulation with at most $3n - 7 - v$ tetrahedra, where n is the total number of elements in \mathbf{A} .

Proof. Consider any triangulation \mathcal{T}_0 of the boundary of $\text{conv}(\mathbf{A})$ using only its v vertices. By Euler's formula ($2 + e = v + t$) plus the double counting formula ($2e = 3t$), \mathcal{T}_0 has exactly $e = 3v - 6$ edges and $t = 2v - 4$ triangles.

Now, let \mathbf{p} be any vertex of \mathcal{T}_0 and let $\delta \geq 3$ be the degree of \mathbf{p} in \mathcal{T}_0 . Consider the triangulation \mathcal{T} of \mathbf{A} obtained by joining \mathbf{p} to each triangle of \mathcal{T}_0 not incident to \mathbf{p} . This triangulation has exactly $2v - 4 - \delta \leq 2v - 7 \leq 2n - 7$ tetrahedra.

Also, if \mathbf{A} is in general position we can add one by one the $n - v$ interior points by subdividing an old tetrahedra into four new ones, thus adding 3 to the total number of tetrahedra. We thus get a full triangulation of \mathbf{A} with $2v - 4 - \delta + 3(n - v) \leq 3n - 7 - v$ tetrahedra. \square

Remark 3.6.7. Observe that:

- Some point configurations have triangulations with much less than $2v - 7$ tetrahedra. In fact, by Theorem 2.6.1, full triangulations in three dimensions can have as few as $v - 3$ tetrahedra. Algorithmically, it is an NP-complete problem to decide where, between $v - 3$ and $2v - 7$, the exact minimum number of tetrahedra in triangulations of an input 3-dimensional polytope with v vertices lies (see Section 8.6).
- Interior points can be inserted in any triangulation, even if the configuration is not in general position. But in non-general position the insertion can add more than three to the number of tetrahedra. Indeed, if we add a point lying in the relative interior of an edge surrounded by k tetrahedra, these k tetrahedra become $2k$. This is an example of a $(1, 2)$ -flip. An important consequence is that, in three or more dimensions, flips cannot be considered “constant time operations” for algorithmic purposes, unless we restrict ourselves to point sets in general position.

The formula $2v - 7$ can be straightened a little bit. What the proof actually gives is $2v - 4 - \delta$, where δ is the degree of the chosen vertex \mathbf{p} . To

lower the number of tetrahedra we should take a vertex of maximum degree. Since every triangulation of the sphere with more than 12 vertices has a vertex of degree at least six (this follows from the formula $e = 3v - 6$ that we have used in the previous proof), we conclude that:

Corollary 3.6.8. *Every 3-dimensional polytope with $n \geq 13$ vertices has a triangulation with at most $2n - 10$ tetrahedra.*

It is no coincidence that the number $2n - 10$ in this statement equals the diameter of the $(n - 3)$ -dimensional associahedron. In fact, the proof of the formula for the diameter of the associahedron would follow easily from the following conjecture (Exercise 3.15):

Conjecture 3.6.9. *For every $n \geq 13$ there is a 3-dimensional polytope with n vertices and the following properties:*

1. *It has no (combinatorial) triangulation with less than $2n - 10$ tetrahedra.*
2. *Its graph has a Hamiltonian cycle.*

We now look at triangulations with quadratically many tetrahedra. In a sense, they have been already mentioned in Section 2.6. Indeed, there we mentioned cyclic polytopes, and said that the cyclic polytope of dimension four with n vertices has $O(n^2)$ facets. Taking a *Schlegel diagram* of a cyclic 4-polytope (see [339] for this concept) produces a triangulation in \mathbb{R}^3 with exactly the same number of tetrahedra, minus one. But let us see here a direct way of constructing them.

Example 3.6.10 (Cyclic 3-polytopes have neighborly triangulations). We start with the vertices of a convex n -gon in the plane, a configuration that we denote C_n . Let its vertices be denoted $\mathbf{p}_1, \mathbf{p}_n$, in cyclic order. We are now going to consider a lift of this configuration, meaning by this the same as what we meant in the definition of regular triangulations. That is, let $\omega : \{1, \dots, n\} \rightarrow \mathbb{R}$ be a height function and consider, for each point \mathbf{p}_i , the lifted point $\tilde{\mathbf{p}}_i = (\mathbf{p}_i, \omega(i)) \in \mathbb{R}^3$.

But we pose a condition to ω : that $\omega(1) > 0$ and each $\omega(i + 1)$ is *sufficiently higher* than the previous ones. What we exactly need is that $\tilde{\mathbf{p}}_{i+1}$ sees the whole upper envelope of the polytope $\text{conv}(\{\tilde{\mathbf{p}}_1, \tilde{\mathbf{p}}_2, \dots, \tilde{\mathbf{p}}_{i+1}\})$.

We now consider the placing triangulation of the lifted point set \mathbf{A}^ω for the given order. The first four points give us one tetrahedron and each subsequent point $\tilde{\mathbf{p}}_{i+1}$ we place introduces $i - 2$ tetrahedra. Hence, in total we have

$$1 + 2 + \dots + (n - 3) = \binom{n-2}{2}$$

tetrahedra in the triangulation.

Another interesting property is that this triangulation is *neighborly*, that is, its graph is a complete graph on the n vertices, hence with $\binom{n}{2}$ edges.

Let us finish this section with an important, for us, remark: the fact that triangulations in \mathbb{R}^3 do not have a constant number of tetrahedra is closely

related to the notion of flip. In dimension two, the only flips that do not make vertices appear or disappear are those of type (2, 2) and, as their name suggests, they leave the number of triangles invariant (two are removed, two are inserted). In dimension three, however, we have flips of type (2, 3), which remove two tetrahedra and insert three, or vice versa, as in Figure 3.44. These flips increase or decrease the number of tetrahedra.

3.6.2 Monotone flipping does not (always) work

Another difference between the situations in two and three dimensions concerns the graph of flips. In dimension two we have seen several easy proofs of the fact that the graph of triangulations of every point configuration is connected. However, in dimension three, there is currently no known proof of the similar property, which could in fact be false! Our goal in this section is to show why the proofs we have in dimension two do not work in dimension three. For this, let us introduce the concept of *monotone flipping*.

Let \mathbf{A} be a point configuration (in arbitrary dimension) with label set J and let $\omega : J \rightarrow \mathbb{R}$ be a heights function. Let us assume that ω is *sufficiently generic*, by which we mean that no $d + 1$ points are lifted to lie in a non-vertical hyperplane in $\mathbf{A}^\omega \subset \mathbb{R}^{d+1}$. (Observe that we cannot in general get rid of vertical hyperplanes unless we ask for \mathbf{A} itself to be generic, since co-hyperplanar elements of \mathbf{A} will necessarily be co-hyperplanar in \mathbf{A}^ω too).

Now, to every triangulation \mathcal{T} of \mathbf{A} we associate the following hypersurface in \mathbb{R}^{d+1} :

$$G_{\omega, \mathcal{T}} := \cup_{B \in \mathcal{T}} \text{conv}_{\mathbf{A}^\omega}(B) \subset \mathbb{R}^{d+1}$$

That is to say, we lift \mathcal{T} to \mathbb{R}^{d+1} by lifting the elements of \mathbf{A} as indicated by ω and then interpolating linearly on every simplex of \mathcal{T} . We call $G_{\omega, \mathcal{T}}$ the lifting graph of \mathcal{T} with respect to ω .

We now consider ω fixed, and look at what happens for different choices of \mathcal{T} . An example of this situation was already described in Theorem 3.4.2 when we flipped “monotonically” towards the Delaunay triangulation: we said there that a flip changed the lifting graph by stacking a tetrahedron above or below the surface obtained by lifting the points to the paraboloid. At least if we restrict ourselves to the case when \mathbf{A} is in general position, this is the general situation. We omit the proof of the following, which will be proved in more generality in Chapter 5:

Lemma 3.6.11. *In the above situation, suppose that \mathbf{A} and ω are both sufficiently generic, so that \mathbf{A}^ω is in general position.*

Let \mathcal{T} and \mathcal{T}' be two triangulations differing by a flip. Then $G_{\omega, \mathcal{T}}$ and $G_{\omega, \mathcal{T}'}$ differ by changing the lower envelope of a certain $(d + 1)$ -simplex to the upper envelope, or vice versa.

Definition 3.6.12. We say that the flip from \mathcal{T} to \mathcal{T}' is *decreasing with respect to the height function ω* if in the above lemma the upper envelope of a simplex is removed and the lower envelope inserted.

We say that a sequence of flips is *monotone towards ω* if all the flips are decreasing with respect to ω .

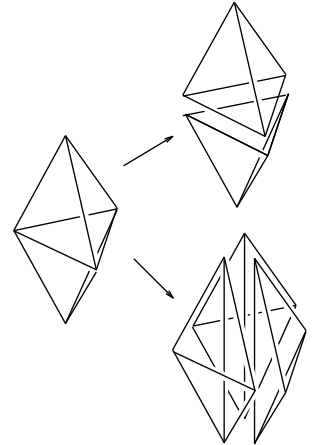


Figure 3.44: A triangular bi-pyramid can be triangulated with two or with three tetrahedra which implies a flip that adds or subtracts one to the number of tetrahedra.

Sometimes we will abuse language and say that the flip or the sequence goes towards $\mathcal{S}(\mathbf{A}, \omega)$, when the height function ω is understood. The three most important cases are:

- When we say that a sequence of flips is monotone towards the Delaunay triangulation, we mean monotone with respect to the height function that lifts \mathbf{A} to the paraboloid.
- Monotone towards the pushing triangulation means with respect to any height function that has $\omega(i+1) \gg \omega(i) > 0$.
- Monotone towards the pulling triangulation means with respect to any height function that has $\omega(i+1) \ll \omega(i) < 0$.

Monotone flipping towards the pulling and the pushing triangulations has a very simple interpretation in terms of which vertices get the volumes of their stars increased or decreased. Recall that the star of a vertex in a triangulation is the union of the simplices containing it. Then:

Lemma 3.6.13. *Let \mathbf{A} be a point configuration with its elements labeled by the numbers $\{1, \dots, n\}$. Let \mathcal{T}_1 and \mathcal{T}_2 be two triangulations of \mathbf{A} related by a flip. Let i be the last element whose star increases or decreases in volume during the flip.*

If the volume of the star of i increases, then the flip is towards the pulling triangulation. If it decreases, it is towards the pushing triangulation.

We leave this proof as an exercise for the reader.

In this language of monotone flipping, Theorems 3.4.1, 3.4.2, and 3.4.3 can be rephrased as:

Corollary 3.6.14. *In a 2-dimensional point configuration it is always possible to monotonically flip from any triangulation to either the pushing (for any ordering), the Delaunay, or the pulling (for any ordering ending in an extremal element of \mathbf{A}) triangulation.*

Moreover, monotone flipping to the pulling triangulation finishes in a linear number of steps, while flipping to the Delaunay or pushing may require quadratically many, by Example 3.4.5.

As we will see later in Chapter 5, a fundamental fact exploited in computational geometry is that one can actually flip between *regular* triangulations *monotonically*, in a generalization of Lawson's result for Delaunay triangulations in the plane. However, the same is not true for non-regular triangulations, in dimensions three and higher.

Indeed, the interpretation of flipping towards the pushing triangulation in terms of the star of the last vertex has the following immediate consequence: Any monotone sequence of flips from a triangulation \mathcal{T} to the pushing triangulation induces a triangulation of the following perhaps-non-convex polyhedron with vertices in $\mathbf{A} \setminus \{n\}$:

$$\text{st}_{\mathcal{T}}(n) \cap \text{conv}_{\mathbf{A}}(1, \dots, n-1).$$

Indeed, every flip that decreases the star of n introduces one (or more, if the points are not in general position) new simplex in this region, until the region is fully triangulated. This allows to easily construct non-pushing triangulations that are local optima for the “flipping to the pushing triangulation” criterion. The following example does this, and is also a local optimum for monotone Delaunay flipping. The first such example was constructed by B. Joe [178].

Example 3.6.15 (Example 3.6.1 continued). Consider the configuration consisting of the six vertices of a Schönhardt polyhedron together with an exterior point on its symmetry axis. For example, let

$$\mathbf{A} = \begin{pmatrix} \mathbf{p}_1 & \mathbf{p}_2 & \mathbf{p}_3 & \mathbf{q}_1 & \mathbf{q}_2 & \mathbf{q}_3 & \mathbf{r} \\ 1-\varepsilon & 0 & \varepsilon & 1 & 0 & 0 & 1/3 \\ \varepsilon & 1-\varepsilon & 0 & 0 & 1 & 0 & 1/3 \\ 0 & \varepsilon & 1-\varepsilon & 0 & 0 & 1 & 1/3 \\ 0 & 0 & 0 & 1 & 1 & 1 & \alpha \end{pmatrix},$$

where $\varepsilon > 0$ is small and $\alpha > 1$ is arbitrary (later we will put constraints on α). Observe that this point set is in general and convex position.

Let \mathcal{T} be the triangulation of \mathbf{A} consisting of the following 10 tetrahedra:

$$\begin{aligned} &\{\mathbf{q}_1, \mathbf{q}_2, \mathbf{p}_1, \mathbf{p}_2\}, \quad \{\mathbf{q}_2, \mathbf{q}_3, \mathbf{p}_2, \mathbf{p}_3\}, \quad \{\mathbf{q}_3, \mathbf{q}_1, \mathbf{p}_3, \mathbf{p}_1\}, \\ &\{\mathbf{r}, \mathbf{q}_1, \mathbf{p}_1, \mathbf{p}_2\}, \quad \{\mathbf{r}, \mathbf{q}_1, \mathbf{q}_2, \mathbf{p}_2\}, \quad \{\mathbf{r}, \mathbf{q}_2, \mathbf{p}_2, \mathbf{p}_3\}, \\ &\{\mathbf{r}, \mathbf{q}_2, \mathbf{q}_3, \mathbf{p}_3\}, \quad \{\mathbf{r}, \mathbf{q}_3, \mathbf{p}_3, \mathbf{p}_1\}, \quad \{\mathbf{r}, \mathbf{q}_3, \mathbf{q}_1, \mathbf{p}_1\}, \\ &\{\mathbf{r}, \mathbf{p}_1, \mathbf{p}_2, \mathbf{p}_3\}. \end{aligned}$$

That is to say, we are triangulating $\text{conv}(\mathbf{A})$ by coning \mathbf{r} to the boundary of Schönhardt’s polyhedron, without the triangle $\{\mathbf{q}_1, \mathbf{q}_2, \mathbf{q}_3\}$, and adding the three “almost flat” tetrahedra exterior to it. In particular, the region $\text{st}_{\mathcal{T}}(\mathbf{r}) \cap \text{conv}(\mathbf{A} \setminus \{\mathbf{r}\})$ is precisely Schönhardt’s polyhedron and cannot be triangulated. So, there is no monotone sequence of flips from \mathcal{T} to the pushing triangulation.

For the same property in the Delaunay case we observe that the vertices of the Schönhardt polyhedron, with the coordinates we have given to them, lie on a sphere. We now assume that \mathbf{r} lies outside this sphere, for which (when ε is small) $\alpha > 2$ is more than enough. If the reader wishes, the whole point set can be further perturbed by amounts that are sufficiently small compared with ε , so that the point configuration is generic in the Delaunay sense. But, if the perturbation is sufficiently small, we will still have the following property: the point \mathbf{r} lies outside the sphere circumscribed to any four of the other six points.

This implies that our triangulation \mathcal{T} is locally Delaunay: Since no flip in it decreases the star of \mathbf{r} , every flip must make one of the three tetrahedra not in this star, that is, one of the three almost flat tetrahedra, $\{\mathbf{q}_i, \mathbf{q}_{i+1}, \mathbf{p}_i, \mathbf{p}_{i+1}\}$, disappear. The circuit on which the flip is supported must consist of these four points together with \mathbf{r} . But then the flip is against the local Delaunay criterion, since the Delaunay triangulation of the five points $\{\mathbf{q}_i, \mathbf{q}_{i+1}, \mathbf{p}_i, \mathbf{p}_{i+1}, \mathbf{r}\}$ contains that almost flat tetrahedron.

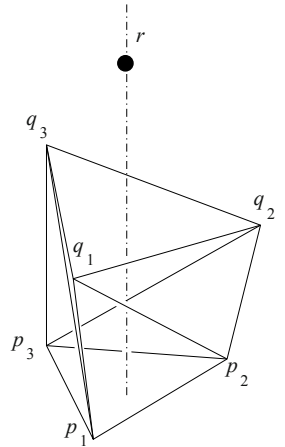


Figure 3.45: A point set where flipping monotonically towards the pushing or the Delaunay triangulation does not work.

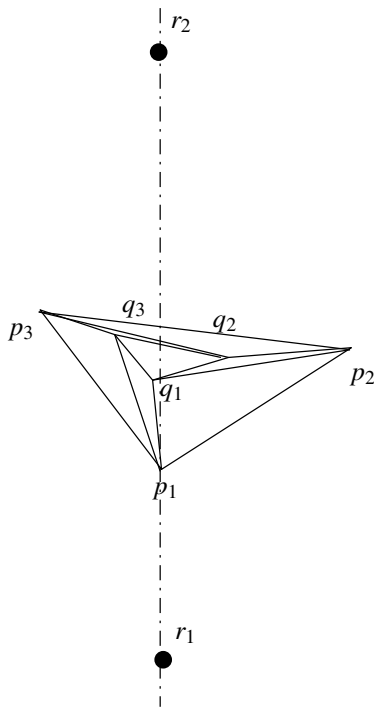


Figure 3.46: A point set where flipping monotonically towards the pulling triangulation

does not work.

For the pulling triangulation, the argument of Lemma 3.6.13 would say that it is enough to find a triangulation \mathcal{T} for which the complement of the star of n cannot be triangulated. Of course, this is impossible because the complement of the star of n is triangulated in \mathcal{T} . For this reason we need some extra work, and one extra point:

Example 3.6.16. Let A consist of the following eight points in dimension three:

$$A = \begin{pmatrix} \mathbf{p}_1 & \mathbf{p}_2 & \mathbf{p}_3 & \mathbf{q}_1 & \mathbf{q}_2 & \mathbf{q}_3 & \mathbf{r}_1 & \mathbf{r}_2 \\ 4-\varepsilon & 0 & \varepsilon & 2 & 1 & 1 & 4/3 & 4/3 \\ \varepsilon & 4-\varepsilon & 0 & 1 & 2 & 1 & 4/3 & 4/3 \\ 0 & \varepsilon & 4-\varepsilon & 1 & 1 & 2 & 4/3 & 4/3 \\ 0 & 0 & 0 & 1 & 1 & 1 & -10 & 10 \end{pmatrix}.$$

The first six points are an oblique version of Schönhardt's polyhedron (which, as it turns out, projects to a perturbed version of "the mother of all examples", Example 2.2.5, see also Figure 1.26 in Chapter 1). The last two lie on the symmetry axis of the Schönhardt, on opposite sides and "very far". \mathbf{r}_2 sees every face of the Schönhardt except the big triangle $\{\mathbf{p}_1, \mathbf{p}_2, \mathbf{p}_3\}$, while \mathbf{r}_1 sees only this triangle. Figure 3.46 shows the configuration.

We triangulate this point configuration as follows: insert three tetrahedra around the axis $\mathbf{r}_1\mathbf{r}_2$ (first three tetrahedra in the following list); then cone both \mathbf{r}_1 and \mathbf{r}_2 to the six relevant triangles in the boundary of the Schönhardt polyhedron. That is, our triangulation \mathcal{T} consists of the following fifteen tetrahedra:

$$\begin{aligned} &\{\mathbf{r}_1, \mathbf{r}_2, \mathbf{q}_1, \mathbf{q}_2\}, \quad \{\mathbf{r}_1, \mathbf{r}_2, \mathbf{q}_1, \mathbf{q}_3\}, \quad \{\mathbf{r}_1, \mathbf{r}_2, \mathbf{q}_2, \mathbf{q}_3\}, \\ &\{\mathbf{r}_1, \mathbf{q}_1, \mathbf{q}_2, \mathbf{p}_2\}, \quad \{\mathbf{r}_1, \mathbf{q}_1, \mathbf{p}_1, \mathbf{p}_2\}, \quad \{\mathbf{r}_2, \mathbf{q}_1, \mathbf{q}_2, \mathbf{p}_2\}, \quad \{\mathbf{r}_2, \mathbf{q}_1, \mathbf{p}_1, \mathbf{p}_2\}, \\ &\{\mathbf{r}_1, \mathbf{q}_2, \mathbf{q}_3, \mathbf{p}_3\}, \quad \{\mathbf{r}_1, \mathbf{q}_2, \mathbf{p}_2, \mathbf{p}_3\}, \quad \{\mathbf{r}_2, \mathbf{q}_2, \mathbf{q}_3, \mathbf{p}_3\}, \quad \{\mathbf{r}_2, \mathbf{q}_2, \mathbf{p}_2, \mathbf{p}_3\}, \\ &\{\mathbf{r}_1, \mathbf{q}_3, \mathbf{q}_1, \mathbf{p}_1\}, \quad \{\mathbf{r}_1, \mathbf{q}_3, \mathbf{p}_3, \mathbf{p}_1\}, \quad \{\mathbf{r}_2, \mathbf{q}_3, \mathbf{q}_1, \mathbf{p}_1\}, \quad \{\mathbf{r}_2, \mathbf{q}_3, \mathbf{p}_3, \mathbf{p}_1\}. \end{aligned}$$

We leave it to the reader (or wait until Section 4.2.4) to check that this triangulation has exactly four flips, supported on the following circuits. As we usually do, the first (positive) part of the circuit indicates the simplex that is inserted, the second part the one that is removed. For example, the first flip in the list removes the axis $\mathbf{r}_1\mathbf{r}_2$ (and its three incident tetrahedra) and inserts the two tetrahedra $\{\mathbf{r}_i, \mathbf{q}_1, \mathbf{q}_2, \mathbf{q}_3\}$ instead:

$$(\{\mathbf{q}_1, \mathbf{q}_2, \mathbf{q}_3\}, \{\mathbf{r}_1, \mathbf{r}_2\}), \quad (\{\mathbf{p}_1, \mathbf{q}_2\}, \{\mathbf{r}_2, \mathbf{q}_1, \mathbf{p}_2\}), \\ (\{\mathbf{p}_2, \mathbf{q}_3\}, \{\mathbf{r}_2, \mathbf{q}_2, \mathbf{p}_3\}), \quad (\{\mathbf{p}_3, \mathbf{q}_1\}, \{\mathbf{r}_2, \mathbf{q}_3, \mathbf{p}_1\}).$$

The important fact, for us, is that all these flips decrease the star of the last point in the ordering, r_2 (this comes from the fact that \mathbf{r}_2 is in their negative part). Hence, all flips go in the direction opposite to the pulling triangulation.

Another negative flipping result in dimension three using a variation of Schönhardt's polyhedron, is as follows. Instead of considering triangulations of a point set, consider polyhedral surfaces with vertex set on it, and with a fixed boundary. A flip consists in gluing a tetrahedron to the surface with two triangles in common, removing those two triangles and inserting the other two triangles of the same tetrahedron.

The connectivity of the flip-graph in dimension two can be interpreted as the fact that *if you restrict to surfaces that intersect every vertical line at most once* (these are sometimes called *polyhedral terrains*) the flip-graph is connected. If you, however, remove this constraint, there are disconnected flip-graphs [3].

3.6.3 The number of flips

We saw earlier that any triangulation of a point configuration in the plane has at least $n - 3$ distinct flips. In Chapter 5 we develop machinery that, in particular, implies that regular triangulations of point configurations of dimension d with n elements always have at least $n - d - 1$ flips. But non-regular triangulations may have fewer flips than that, and this already occurs in dimension three. The smallest example where this occurs has eight elements and will be presented in Section 7.1. Here we present an example that has more points, but also more symmetry:

Example 3.6.17 (The cube-octahedron). The *cube-octahedron* is the 3-dimensional polytope whose vertices are the mid-points of the twelve edges of a regular cube. You get the same polytope if you use the mid-points of the twelve edges of a regular octahedron instead. The cube-octahedron has 14 facets: 6 of them are squares (coming from facets of the cube) and 8 are triangles (coming from the octahedron). Every edge is incident to a triangle and a square. You can see a picture of this polytope in Figure 3.47.

As you can see in Figure 3.47, we have labeled the twelve vertices of the cube-octahedron with the twelve possible ordered pairs of different numbers from 1 to 4. The vertices of each triangle all have the same first label or the same second label. The vertices of each square are the four pairs ik , il , jk , jl , for some permutation (i, j, k, l) of $(1, 2, 3, 4)$. The reader can take this just as a very symmetric way of labeling vertices, but it actually comes from the fact that the cube-octahedron can be embedded in \mathbb{R}^4 having the following vertex set, where $\mathbf{e}_1, \dots, \mathbf{e}_4$ are the standard basis:

$$\{\mathbf{e}_i - \mathbf{e}_j : i, j \in \{1, 2, 3, 4\}, i \neq j\} \subset \mathbb{R}^4.$$

In the figure, the vertex labeled ij represents the point $\mathbf{e}_i - \mathbf{e}_j$.

Our point configuration consists of the twelve vertices of the cube-octahedron, together with its centroid as a thirteenth point, that we label O . In coordinates, we have the following thirteen points in \mathbb{R}^3 :

$$\begin{pmatrix} O & 12 & 21 & 13 & 31 & 14 & 41 & 23 & 32 & 24 & 42 & 34 & 43 \\ 1 & 1 & 1 & 1 & 1 & 1 & 1 & 1 & 1 & 1 & 1 & 1 & 1 \\ 0 & 1 & -1 & 1 & -1 & 1 & -1 & 0 & 0 & 0 & 0 & 0 & 0 \\ 0 & -1 & 1 & 0 & 0 & 0 & 0 & 1 & -1 & 1 & -1 & 0 & 0 \\ 0 & 0 & 0 & -1 & 1 & 0 & 0 & -1 & 1 & 0 & 0 & 1 & -1 \\ 0 & 0 & 0 & 0 & 0 & -1 & 1 & 0 & 0 & -1 & 1 & -1 & 1 \end{pmatrix}$$

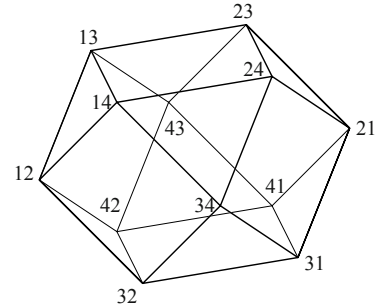


Figure 3.47: A regular cube-octahedron.

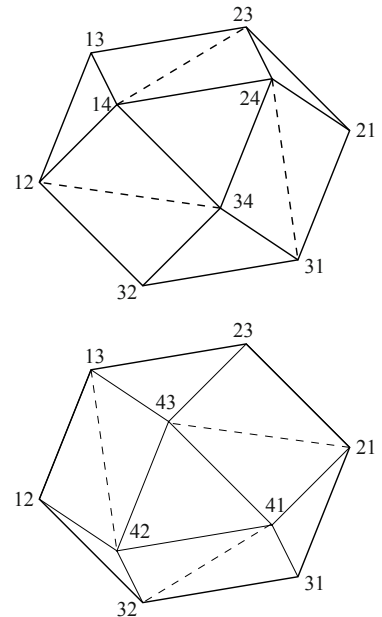


Figure 3.48: A triangulation of the boundary of the cube-octahedron.

Table 3.1: The matrix representing the cube-octahedron.

One easy way to triangulate this configuration is: triangulate the boundary by inserting one of the two diagonals of each square facet, then cone the centroid to the triangulated boundary. There are 64 triangulations that can be obtained in this way, because we have two choices in each square. We choose to triangulate the six squares in such a way that each of the twelve vertices is incident to one of the six diagonals inserted. This means we only have freedom to choose the diagonal in one of the squares and the rest of the triangulation is determined by this choice. One of the two possibilities, is to use the following six diagonals:

$$\{12,34\}, \{31,24\}, \{14,23\}, \{21,43\}, \{13,42\}, \{41,32\}.$$

This is displayed in Figure 3.48, where we have drawn the two halves of the boundary of the cube-octahedron separately to make the picture clearer.

Proposition 3.6.18. *The triangulation so obtained has only six geometric bistellar flips.*

Proof. To check the number of flips, the symmetries of the triangulation will help. Indeed, in Figure 3.48 one can check that the triangulation is symmetric under rotation of order three around the axis of every triangle, and rotation of order two around the axis of every square. There are also mirror symmetries on the planes through parallel diagonals of any pair of opposite squares of the cube-octahedron. These symmetries make the twelve half-squares equivalent to one another, and the eight triangular facets too. The 24 edges of the cube-octahedron are also equivalent.

There are then only two adjacent pairs of tetrahedra where we have to check for flips: a pair adjacent along a square diagonal and the centroid, and a pair adjacent along an edge of the cube-octahedron and the centroid.

The first case produces the six flips claimed in the statement: The two adjacent tetrahedra form a square pyramid, and there is a flip exchanging this triangulation to the other triangulation of this square pyramid (that is, a flip exchanging the diagonal chosen in that square facet to the opposite diagonal).

For the second case let us pick up a concrete pair. For example, the pair formed by the tetrahedra $\{O, 14, 24, 34\}$ and $\{O, 14, 24, 23\}$. In the four dimensional embedding we mentioned above, in which ij represents the point $e_i - e_j$ and O is the origin of coordinates, we clearly have $23 + 34 = O + 24$. Hence, the circuit contained in that pair is $(\{23, 34\}, \{O, 24\})$, and the triangulation of it is $\{O, 23, 34\}, \{O, 34, 24\}$. This triangulated circuit does not produce a flip, because the link of the first triangle are points 14 and 21 while the link of the second triangle are points 14 and 31. \square

As we said before, the fact that this triangulation is flip-deficient implies its non-regularity (this will be a consequence of results in Chapter 5). But the reader may want to see an explicit proof that this triangulation is not regular. Suppose, by way of contradiction, that it is regular and we can get lifting heights ω_O and ω_{ij} for the origin and the twelve vertices of the cube-octahedron. At every square facet ik, il, jk, jl we have the circuit

$ik + jl = il + jk$. If the diagonal chosen on that square is, say, the one joining ik and jl , the condition for a convex lift at the two tetrahedra incident to that square is

$$\omega_{ik} + \omega_{jl} < \omega_{il} + \omega_{jk}.$$

In our triangulation this gives the following six inequalities, which do not have a common solution because the sum of left-hand sides equals the sum of right hand sides:

$$\begin{aligned} \omega_{12} + \omega_{34} &< \omega_{14} + \omega_{32}, \\ \omega_{23} + \omega_{14} &< \omega_{24} + \omega_{13}, \\ \omega_{31} + \omega_{24} &< \omega_{34} + \omega_{21}, \\ \omega_{21} + \omega_{43} &< \omega_{23} + \omega_{41}, \\ \omega_{32} + \omega_{41} &< \omega_{31} + \omega_{42}, \\ \omega_{13} + \omega_{42} &< \omega_{12} + \omega_{43}. \end{aligned} \tag{3.4}$$

Still, if the point configuration is in *convex position*, that is, if no point is in the interior of the convex hull, flip-deficient triangulations do not exist in dimension three:

Proposition 3.6.19. *When the point configuration with n points in \mathbb{R}^3 is in convex position without collinearities, every triangulation has at least $n - 4$ flips.*

Proof. Let \mathcal{T} be a triangulation of an n point configuration \mathbf{A} in \mathbb{R}^3 , in convex position. If \mathcal{T} does not use a certain point $\mathbf{p} \in \mathbf{A}$, then we inductively assume that it has at least $n - 5$ flips as a triangulation of $\mathbf{A} \setminus \{\mathbf{p}\}$, plus the flip which inserts the point \mathbf{p} . Thus, we can assume without loss of generality that \mathcal{T} is a full triangulation.

Let t denote the number of tetrahedra and let f_i and f_b (respectively e_i and e_b) be the numbers of interior and boundary triangles (respectively edges).

Euler's formulas for the 3-ball and the 2-sphere imply:

$$f_i + f_b + n = t + e_i + e_b + 1, \quad f_b + n = e_b + 2.$$

We also have, by double counting, that

$$2f_i + f_b = 4t, \quad 2e_b = 3f_b.$$

Putting these equations together we obtain

$$e_i = t - n + 3, \quad f_i = 2t - n + 2.$$

As a consequence, we have the following important relation:

$$f_i - 2e_i = n - 4.$$

We will associate the interior non-flippable triangles of \mathcal{T} to certain interior edges of \mathcal{T} and then use a counting argument to conclude that the number of flips is at least $n - 4$. To formalize this, we consider each non-flippable interior triangle as having a “unit of charge”, which we will transfer to one of its three edges. Observe that if τ is a non-flippable interior triangle and σ_1 and σ_2 are the tetrahedra sharing it, then at least one of the edges of τ is flat or concave in $\sigma_1 \cup \sigma_2$. There are two cases:

1. If one of the edges of τ is concave in $\sigma_1 \cup \sigma_2$, then it is interior and is the only concave edge of the pair (σ_1, σ_2) , because if there are two concave edges their common end point cannot be in the boundary of $\text{conv}(\mathbf{A})$. We give the charge of τ to this concave edge.
2. Otherwise there is a unique non-convex edge of c which is flat for the pair (σ_1, σ_2) . Two flat edges would imply the existence of three collinear points. Moreover, the flat edge is interior because otherwise τ is flippable according to the discussion above. We give the charge of τ to the unique flat edge.

We claim that the total charge of the interior edges is at most twice the number of interior edges plus the number of edge-flips. From the claim it follows that the total number of interior triangles f_i is at most the total number of flips plus twice the number of interior edges e_i . Thus, the number of flips is at least $f_i - 2e_i = n - 4$, as desired.

To prove our claim, we only need to analyze interior edges with charge greater than two:

1. If an interior edge \mathbf{pq} is a non-convex edge for at least four pairs of consecutive tetrahedra in its star, then the star has precisely four tetrahedra and the sum of any two consecutive dihedral angles is 180. Let $\mathbf{a}, \mathbf{b}, \mathbf{c}$, and \mathbf{d} be the four points in the link of \mathbf{pq} , in circular order. The quadrilaterals \mathbf{apcq} and \mathbf{bpdq} are strictly convex; otherwise one of the points \mathbf{p} or \mathbf{q} would either be collinear with two of $\mathbf{a}, \mathbf{b}, \mathbf{c}$, and \mathbf{d} , or \mathbf{p} or \mathbf{q} would be contained in the convex hull of the other 5 points (violating the convexity assumption). Thus, the star of \mathbf{pq} forms a convex octahedron. The charge associated to \mathbf{pq} is four (the four triangles containing \mathbf{pq} are as in part (2) above) and there are two edge-flips of type (2,2) which make the edge \mathbf{pq} disappear, supported in the circuits $(\{\mathbf{p}, \mathbf{q}\}, \{\mathbf{a}, \mathbf{c}\})$ and $(\{\mathbf{p}, \mathbf{q}\}, \{\mathbf{b}, \mathbf{d}\})$.
2. If an interior edge \mathbf{pq} is non-convex for exactly three pairs of consecutive tetrahedra in its star, then there can be three or four tetrahedra in the star of \mathbf{pq} .

If there are three, then \mathbf{pq} is a concave edge associated to the three interior triangles incident to it. Let \mathbf{a}, \mathbf{b} and \mathbf{c} be the three vertices in the link of \mathbf{p}, \mathbf{q} . Then either $(\{\mathbf{a}, \mathbf{b}, \mathbf{c}\}, \{\mathbf{p}, \mathbf{q}\})$ is a (3,2) circuit or one of $(\{\mathbf{a}, \mathbf{b}, \mathbf{c}\}, \{\mathbf{p}\})$ and $(\{\mathbf{a}, \mathbf{b}, \mathbf{c}\}, \{\mathbf{q}\})$ is a (3,1) circuit with \mathbf{a}, \mathbf{b} , and \mathbf{c} lying in a facet of \mathbf{A} . In either case, there is an edge-flip supported in the circuit which makes \mathbf{pq} disappear.

If there are four, then let $\mathbf{a}, \mathbf{b}, \mathbf{c}$ and \mathbf{d} be the four points in the link of \mathbf{p}, \mathbf{q} in circular order. Two of them (say \mathbf{a} and \mathbf{c}) are coplanar with $\mathbf{p}, \mathbf{q}, \mathbf{q}$. \mathbf{p}, \mathbf{q} is a concave edge associated with one of the triangles $\mathbf{p}, \mathbf{q}, \mathbf{a}$ or $\mathbf{p}, \mathbf{q}, \mathbf{c}$ and an edge for the triangles $\mathbf{p}, \mathbf{q}, \mathbf{b}$ and $\mathbf{p}, \mathbf{q}, \mathbf{d}$. Note that the triangles $\mathbf{p}, \mathbf{q}, \mathbf{b}$ and $\mathbf{p}, \mathbf{q}, \mathbf{d}$ are in the situation of (2) above, with their charges associated to \mathbf{p}, \mathbf{q} . Then \mathbf{p}, \mathbf{q} has a charge of three, but $(\{\mathbf{a}, \mathbf{c}\}, \{\mathbf{p}, \mathbf{q}\})$ is a (2,2) circuit and there is an edge-flip supported on it which makes \mathbf{p}, \mathbf{q} disappear.

3. If an interior edge \mathbf{p}, \mathbf{q} is non-convex for at most two pairs of consecutive tetrahedra in its star, then the charge of \mathbf{p}, \mathbf{q} is at most two.

□

In forthcoming chapters we will show even more interesting pathologies that can occur in higher dimensions. Most strikingly, for some time it was not known whether flip connectivity held in higher dimensions. This changed when F. Santos constructed a disconnected 6-dimensional example in 2000 [278], and a simpler and smaller one in dimension five later [283]. We will describe these constructions in Chapter 7.

3.7 Notes and References

The concept of Voronoi diagram has been rediscovered in many different applications (each time using a different name) such as geographic studies (Thiessen polygons), Crystallography (Dirichlet tessellations), Pattern recognition (Blum’s transforms). See [20] for a really extensive list of references and applications.

There are even more surprising properties of Delaunay triangulations, besides those mentioned before. Examples include the fact that they also maximize the sum of radii of *inscribed* circles to each triangle [200], and minimize certain integral operators that characterize the drastic changes of surfaces [273].

Because of their optimality Delaunay triangulations are not just useful, they are *extremely* useful! In topics such as mesh generation and computer aided design the “roundedness” of triangles is important for simulations, e.g. small angles are bad. One important variation is that sometimes to assure optimal conditions of the triangles, extra points need to be added, i.e., we find a *refinement* of the set of points and recalculate the Delaunay triangulation. Also sometimes one is demanded to *constrain* a triangulation; thus, some edges or triangles are fixed in advance, and we must fill the rest, guaranteeing to be close to the Delaunay quality [45, 296]. The range and depth of applications of Delaunay triangulations is nothing that one can describe in a few pages, it certainly merits a whole book on its own. Many more pointers to applications can be found at <http://www.ics.uci.edu/~eppstein/geom.html>.

The graph of flips between triangulations of a *convex lattice point set* in the plane has some remarkable properties, as we will see in Section 9.3.1. By a convex lattice point set we mean the intersection of \mathbb{Z}^2 with a convex body. For example, there is a bijection between edges and “half-lattice” points lying in $\text{conv}(\mathbf{A})$. With some care it can be proved that this bijection induces an embedding of the graph of flips into the graph of a hypercube of dimension equal to this number of interior edges. Sharir and Welzl use this property to give a good upper bound for the number of triangulations, as well as a good enumeration algorithm. Eppstein generalizes this property to point sets without empty pentagons.

Exercises

Exercise 3.1. Consider a 1-dimensional configuration with n points. How many different triangulations are there? What is the poset of subdivisions? What is the connectivity of the graph? What is the diameter of the graph?

Exercise 3.2. Write proof for the following consequences of Lemma 3.1.3, that we list below.

1. The three numbers n , e , and t of vertices, edges, and triangles of a triangulation are always of similar magnitude in a plane triangulation. More precisely:

$$2n - 3 \leq e \leq \frac{3}{2}t \leq 3n.$$

2. Every triangulation has some vertex of degree at most five (remember the *degree* of a vertex is the number of edges incident to it). Moreover, every triangulation has some boundary vertex of degree at most three or some interior vertex of degree at most five (or both).

Exercise 3.3. Let \mathbf{A} be a point configuration in the plane. Show that if \mathbf{A} has less than three interior points then all its triangulations are regular.

Exercise 3.4. Suppose you have hexagon in the plane. Can you somehow add enough points to the interior of the hexagon so that the new point set has a triangulation with an *odd* number of triangles?

Exercise 3.5. Let \mathbf{abcd} form a convex quadrilateral, thus it contains two triangulations. Prove that the one that has the largest minimum angle is the Delaunay triangulation of the quadrilateral.

Exercise 3.6. Prove every minimum spanning tree of a point set in the plane in general position is a subgraph of the Delaunay triangulation.

Exercise 3.7. Given two triangulations $\mathcal{T}_1, \mathcal{T}_2$ of the same point set in the plane, that touch all the points, both have t many triangles. Thus we have $3t$ different angles. To each triangulation associate a vector of its angles ordered increasingly by size. We say $\mathcal{T}_1 < \mathcal{T}_2$ if their two sequences of angles are equal up to some index $j - 1$ and the j -th angle of \mathcal{T}_1 is smaller than the j -angle of \mathcal{T}_2 . Prove that the Delaunay triangulation is the largest triangulation in the angle ordering (i.e., intuitively, that it avoids small angles).

Exercise 3.8. Prove that the angle ordering on triangulations we discussed in the previous exercise is an antisymmetric total ordering.

Exercise 3.9. Every full triangulation of $n \geq 5$ points in \mathbb{R}^2 , no 3 collinear, contains two adjacent triangles that form a convex quadrilateral.

Exercise 3.10. Let \mathbf{A} be a point configuration and $\mathbf{p} \in \mathbf{A}$. Let \mathcal{T}' be a triangulation of $\mathbf{A} \setminus \mathbf{p}$. For each $i \in \mathbb{N}$, denote by h_i the number of full

triangulations of \mathbf{A} in which \mathbf{p} has degree i and which can be obtained by inserting \mathbf{p} in \mathcal{T}' . Prove that

$$h_i \leq C_{i-1} - C_{i-2}$$

where $C_n = \frac{1}{n+1} \binom{2n}{n}$ is the n th Catalan number.

Exercise 3.11. Find a pair of full triangulations of a point configuration in the plane where a shortest sequence of flips taking one triangulation into the other requires that the number of edge intersections increases at some moment.

Exercise 3.12. Is there a constant c such that for any 2-dimensional point configuration \mathbf{A} with n points, the number $T(\mathbf{A})$ of triangulations of \mathbf{A} is bounded by $2^{cn} \leq T(\mathbf{A}) \leq 2^{(c+1)n}$

Exercise 3.13. Let \mathbf{P} be a non-convex polygon, and let \mathbf{v} be a vertex of it. Prove that there is an edge \mathbf{pq} of \mathbf{P} not incident to \mathbf{v} such that the triangle $\text{conv}(\mathbf{v}, \mathbf{p}, \mathbf{q})$ is contained in \mathbf{P} . Conclude, inductively, that \mathbf{P} can be triangulated without extra vertices.

Exercise 3.14. You are given a planar polygon (not necessarily convex). To compute its area you could triangulate it and add the areas of its triangles. Unfortunately today you cannot triangulate it. Can you think of a way to calculate the area of the polygon without using a triangulation? Hint: You only know the boundary of the polygon and the coordinates of its vertices.

Exercise 3.15. Assuming Conjecture 3.6.9, prove that for every $n \geq 13$ there are two triangulations of the n -gon which need at least $2n - 10$ flips to be joined to one another. Hint: look at Exercises 1.9 and 1.10.

Exercise 3.16. Prove that Schönhardt's non-convex polyhedron has no triangulation (this is Lemma 3.6.2).

Exercise 3.17. Prove that a triangulation of n points in convex position inside \mathbb{R}^3 has no more than $\binom{n}{2} + n - 3$ tetrahedra and no less than $n - 3$.

Exercise 3.18. (Open) What is a good algorithm for, given two triangulations, describing how far apart they are in the flip-graph? Is there a polynomial time algorithm that finds a shortest path between any two triangulations?

Exercise 3.19. (Open) Can one find the minimum length triangulation in polynomial time if one knows beforehand the optimal length value?

Exercise 3.20. (Open) Can you say anything more about the general structure of the graph of flips of a point set in the plane: Independence number, Hamiltonicity, etc?

Exercise 3.21. (Open) Can you characterize the graphs of flips of nice families of point configurations (e.g. grid points, concentric families of identical n -gons)?

Exercise 3.22. (Open) Give a polynomial-time algorithm that computes the number of triangulations of a given set of points in \mathbb{R}^2 .

Exercise 3.23. (Open) Prove or disprove: The graph of triangulations of a point set in the plane is always $(n - 3)$ -connected.

Exercise 3.24. (Open) For a point configuration \mathbf{A} in general position in \mathbb{R}^3 , define $\mu(\mathbf{A})$ as the maximum number of tetrahedra of any triangulation of \mathbf{A} . What can be said of the growth of the function $f(n) = \min_{\mathbf{A}} \mu(\mathbf{A})$, where the minimum is taken among all possible such configurations? See [22, 115] for more information on the problem and its variations.

Exercise 3.25. (Open) Are there 3-dimensional point configurations with pairs of triangulations that cannot be connected by finitely many flips?

Exercise 3.26. (Open) Let \mathcal{T} be a triangulation of a point configuration in \mathbb{R}^3 . A *triangle coloring* of \mathcal{T} is a 4-coloring of its triangles so that each tetrahedron of \mathcal{T} has four different colored triangles. Is it true that every triangulation \mathcal{T} has a triangle coloring?

Exercise 3.27. (Open) We say a triangulation is *dually Hamiltonian* when the associated dual graph (edges connect adjacent maxima simplices) has a hamiltonian cycle. Is it true that every point configuration in \mathbb{R}^3 has a dually Hamiltonian triangulation? This problem was first studied in [17].

Exercise 3.28 (Compatible triangulations [4]). (Open) Let \mathbf{A}_1 and \mathbf{A}_2 be two arbitrary point sets in general position in the plane, with the same numbers of boundary and interior points. Is it true that they must have a full triangulation in common? (That is to say, that there is a $\mathcal{T} \subseteq \binom{[n]}{3}$ that is a full triangulation for some labeling of the two sets).

Exercise 3.29. Prove that the previous property is true if one of the point sets consists of:

1. The vertices of a convex $(n - 1)$ -gon together with an extra vertex in the exterior of it, or
2. It has at most three interior points.

4

A Tool Box

The definitions of triangulation and subdivision given in Chapter 2 are nice for theoretic reasoning, but they present a fundamental problem for computations. How can one check Definition 2.3.1 on a computer? Let \mathbf{A} be a point configuration in \mathbb{R}^m , with set of labels J . Recall that a collection \mathcal{S} of subsets of J is a *polyhedral subdivision* of \mathbf{A} if it satisfies the following conditions:

- (CP) If $C \in \mathcal{S}$ and $F \leq C$, then $F \in \mathcal{S}$ as well. (Closure Property)
- (UP) $\bigcup_{C \in \mathcal{S}} \text{conv}_{\mathbf{A}}(C) \supseteq \text{conv}_{\mathbf{A}}(J)$. (Union Property)
- (IP) If $C \neq C'$ are two cells in \mathcal{S} , then $\text{relint}_{\mathbf{A}}(C) \cap \text{relint}_{\mathbf{A}}(C') = \emptyset$. (Intersection Property)

For instance, how can we prove that a given family of convex sets covers another convex set (Property (UP))? It is a non-trivial computational challenge, one that we have to solve in practice. A key goal of this chapter is to develop the computational tools to test conditions (CP), (UP) and (IP).

In this chapter, we give an overview of the most frequently used tools and concepts for manipulating and investigating triangulations and polyhedral subdivisions. We begin by developing combinatorial tools and concepts that lead to a fully algorithmic definition of a triangulation. The foundations are the oriented matroid notions of *circuits*, *cocircuits*, and *Gale transforms*. A more detailed introduction into these concepts can be found in [339, Chapter 6] and the comprehensive books [55, 61]. After a thorough look at some natural constructions, like deletion and contraction, we encounter the need to deal with vector configurations. We describe special regular triangulations in Section 4.3, such as pulling and placing triangulations. We discuss what happens to triangulations and polyhedral subdivisions during those processes. Finally, we present several equivalent characterizations of flips and of polyhedral subdivisions that may come in handy in different contexts. Some of them are aimed for use in computer programs for the enumeration of all triangulations of a point set (see, e. g., [265]).

4.1 Combinatorics of configurations

The basic idea in this section is that, in order to compute or characterize triangulations, the fundamental primitives needed are vectors of signs arising from affine/linear functionals, dependences, and determinants. To give a uniform treatment of them we introduce the following notation.

Definition 4.1.1. A *signature* on a finite set J is a partition of J into three subsets, V_- , V_0 and V_+ . A signature is called *positive* if V_- is empty, and *negative* if V_+ is empty. Given a signature V_+, V_0, V_- on J , the set $V = V_- \cup V_+$ is called its *support*.

If $J = \{1, \dots, n\}$, then we can think of a signature as a vector of length n with entries in $\{-1, 0, +1\}$, and call it a *sign vector*. Reciprocally, every vector in \mathbb{R}^n (or, more formally, every map $J \rightarrow \mathbb{R}$) induces a signature, consisting of the preimages of $(-\infty, 0)$, $\{0\}$, and $(0, \infty)$. An equivalent, and sometimes more convenient, way of representing signatures is as the ordered pair (V_+, V_-) . This will be our preferred representation.

Definition 4.1.2. Let (V_+, V_-) and (U_+, U_-) be two signatures on a set J . We say that (V_+, V_-) and (U_+, U_-) are *conformal* if $V_+ \cap U_- = V_- \cap U_+ = \emptyset$.

Put differently, (V_+, V_-) and (U_+, U_-) are conformal if the *coordinate-wise* product of their representations as vectors does not have negative elements.

The *conformal sum* of two conformal signatures (V_+, V_-) and (U_+, U_-) is the signature $(V_+ \cup U_+, V_- \cup U_-)$. Observe this is not a signature if (V_+, V_-) and (U_+, U_-) are not conformal, since then the unions of positive and negative parts will not be disjoint. This is a reflection of the fact that the signature associated to a sum $v + \omega$ of two vectors $v, \omega \in \mathbb{R}^n$ can only be deduced from the signatures of v and ω if they are conformal.

4.1.1 Dependences, circuits, and the intersection property

Definition 4.1.3 (Dependence signatures). Let $\mathbf{A} = (\mathbf{p}_i)_{i \in J}$ be a vector configuration with label set J . Let $\sum_{i \in J} \lambda_i \mathbf{p}_i = 0$ be an (affine or linear) dependence. That is, $(\lambda_i)_{i \in J}$ is a vector in the kernel of the matrix representing \mathbf{A} . The signature of this vector is called a *dependence signature* of \mathbf{A} .

Example 4.1.4 (Five points in the plane). We use the five planar point configuration of Example 2.2.9. Our choices of homogeneous coordinates and label set are

$$\mathbf{A} = \begin{pmatrix} 1 & 2 & 3 & 4 & 5 \\ 0 & 3 & 0 & 3 & 1 \\ 0 & 0 & 3 & 3 & 1 \\ 1 & 1 & 1 & 1 & 1 \end{pmatrix}.$$

We also display a picture of the points with a different dependent signatures that is not a circuit (see Figure 4.2). The full list of circuits for the configuration is given, in short notation, by $(23, 45), (123, 5), (14, 5), (14, 23)$.

One interesting property of dependence signatures is that the relative interiors of their positive and negative parts intersect.

Lemma 4.1.5. Let V_+ and V_- be two disjoint subsets of the label set J of a vector configuration \mathbf{A} . Then the following are equivalent:

(i) (V_+, V_-) is a dependence signature on \mathbf{A} .

(ii) $\text{relint}(V_+) \cap \text{relint}(V_-) \neq \emptyset$.

$(+, +, 0, -, 0, -, +, -, -)$
 $(+, 0, 0, -, +, -, +, 0, -)$
 $(-, -, +, +, +, 0)$
 $(-, +, -, 0, -, -)$

Figure 4.1: Two pairs of sign vectors. The top pair is conformal and the second pair is not.

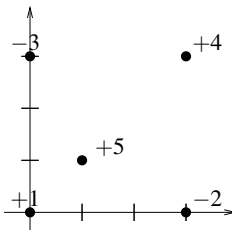


Figure 4.2: A dependence (affine) on a set of five points.

This lemma is true regardless of whether V_+ or V_- are empty. If V_+ is empty, then its relative interior is considered to be the zero cone $\{0\}$, which lies in the relative interior of a non-empty V_- if and only if there is a strictly positive linear dependence among its elements. In this case, (\emptyset, V_-) is a dependence signature, as well as (\emptyset, \emptyset) .

Proof. The statement that (V_+, V_-) is the dependence signature for the dependence $(\lambda_i)_{i \in J}$ is equivalent to the following with $\lambda := \sum_{i \in V_+} \lambda_i = \sum_{i \in V_-} -\lambda_i$:

$$\begin{aligned} \sum_{i \in V_+} \lambda_i \mathbf{p}_i + \sum_{i \in V_-} \lambda_i \mathbf{p}_i = 0 &\iff \sum_{i \in V_+} \lambda_i \mathbf{p}_i = \sum_{i \in V_-} -\lambda_i \mathbf{p}_i \\ &\iff \sum_{i \in V_+} \frac{\lambda_i}{\lambda} \mathbf{p}_i = \sum_{i \in V_-} -\frac{\lambda_i}{\lambda} \mathbf{p}_i. \end{aligned}$$

Since all λ_i are non-zero, the left hand side and the right hand side are convex combinations in the relative interiors of both V_+ and V_- , respectively. \square

An example of this is the case of a circuit Z , of \mathbf{A} , i.e., a minimal dependent subconfiguration. Then, there is a unique dependence with support in Z , hence there is a unique dependence signature (Z_+, Z_-) with support Z (up to exchanging Z_+ and Z_-). These minimal dependence signatures get a special treatment.

Definition 4.1.6 (Oriented Circuit). A minimally dependent subconfiguration Z of \mathbf{A} is called a *circuit in \mathbf{A}* . A dependence signature with support on Z is also called a *circuit signature* or an *oriented circuit of \mathbf{A}* .

Lemma 4.1.7 (Uniqueness of Circuit Signatures). *Let Z be a circuit in a point configuration \mathbf{A} with signature (Z_+, Z_-) . Then (Z_-, Z_+) is the only other possible circuit signature with support Z .*

Proof. There is only one dependence equation among the elements of Z (modulo a scalar factor) because if there were two, they could be used to get another one with smaller support, hence Z would not be minimally dependent. If the scalar factor is positive then it does not change the signature; if it is negative it exchanges the positive and negative parts of it. \square

Remark 4.1.8. In concrete examples, it is easy to compute the signature of a circuit in matrix form. Let $\mathbf{p}_1, \dots, \mathbf{p}_k$ be minimally dependent vectors, so that the matrix \mathbf{Z} having them as columns has rank $k - 1$. The unique dependence is the unique (modulo a scalar constant) element in the kernel of this matrix. To compute it, assume without loss of generality that the number of coordinates of your points is exactly $k - 1$ (if there are more coordinates, just choose a subset of $k - 1$ independent rows in your matrix) so that deleting the i -th column gives a square matrix. Let ω_i denote the determinant of the square matrix obtained by deleting the i -th column. Then the vector

$$\boldsymbol{\omega} = (\omega_1, -\omega_2, \dots, (-1)^k \omega_k)$$

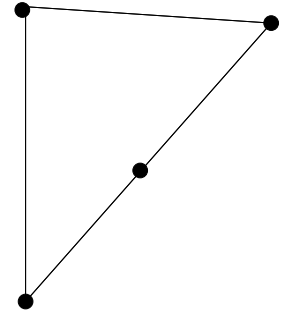


Figure 4.3: A dependence of four points which is not a circuit.

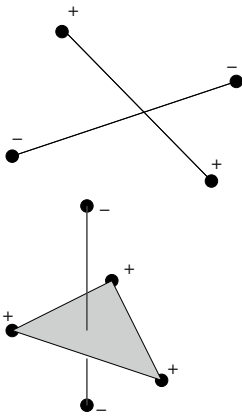


Figure 4.4: Two circuits represented as Radon partitions.

is in the kernel, as the following standard argument shows:

Consider the square $k \times k$ matrix obtained repeating the j -th row, for any j . Since it has a repeated row, this matrix is clearly singular. But its determinant, developed at the repeated row, is simply the scalar product of that row and the vector ω that we just defined. Hence, ω is orthogonal to every row of \mathbf{Z} .

One interesting property of circuits is that the relative interiors of the positive and negative parts intersect in a unique point. More interesting is the fact that this property essentially characterizes circuits.

Lemma 4.1.9. *Let Z_+ and Z_- be two non-empty subsets of the label set J of a vector configuration \mathbf{A} . Then the following are equivalent:*

- (i) (Z_+, Z_-) is a circuit signature.
- (ii) Z_+ and Z_- are independent and $\text{relint}(Z_+) \cap \text{relint}(Z_-)$ is a single point (for a point configuration) or a ray (for a vector configuration).

Remark 4.1.10. Here Z_+ and Z_- are required to be non-empty because in a non-acyclic configuration there are *positive circuits*, with signature (Z_+, \emptyset) , to which this lemma does not apply: Z_+ is not independent and $\text{relint}(Z_+) \cap \text{relint}(\emptyset)$ is not a ray.

Proof. For (i) \Rightarrow (ii), the uniqueness of the dependence, Lemma 4.1.7, implies that the intersection of the relative interiors is a unique point or ray. The fact that Z_+ is not empty implies that Z_- is independent, and vice versa.

For the other implication, let Z_+ and Z_- be independent and $\text{relint}(Z_+) \cap \text{relint}(Z_-)$ be a single point or ray. Lemma 4.1.5 says that (Z_+, Z_-) is a dependence signature. Let λ be the vector of coefficients in this dependence. We need to show that there is no proper subset of $Z_+ \cup Z_-$ supporting another dependence signature. If there was one, let μ be the vector of coefficients in this new dependence, and let $\lambda' = \lambda + \varepsilon\mu$ with ε sufficiently small. Since the support of μ is strictly contained in that of λ , λ' has the same signature Z as λ . But then we have that the following are points (or rays) in the relative interior of both Z_+ and Z_- :

$$\mathbf{x} = \sum_{i \in Z_+} \lambda_i \mathbf{p}_i = - \sum_{i \in Z_-} \lambda_i \mathbf{p}_i, \quad \mathbf{y} = \sum_{i \in Z_+} \lambda'_i \mathbf{p}_i = - \sum_{i \in Z_-} \lambda'_i \mathbf{p}_i.$$

By assumption, \mathbf{x} and \mathbf{y} must be the same point (for a point configuration) or lie in the same ray (for a vector configuration). But then the fact that Z_+ and Z_- are independent implies that λ' and λ are proportional, which contradicts the construction of λ' . \square

There is an important consequence of this characterization of interior intersection: we have an algorithm to tell whether or not a point is in the convex hull or the relative interior of a subconfiguration.

Lemma 4.1.11 (Circuits and convex hulls). *Let $i \in J$ and $B \subset J$. Let \mathbf{p}_i be the vector labeled by i . Then,*

- $\mathbf{p}_i \in \text{conv}_{\mathbf{A}}(B)$ if and only if there is a circuit $(Z_+, \{i\})$ with $Z_+ \subseteq B$.
- $\mathbf{p}_i \in \text{relint}_{\mathbf{A}}(B)$ if and only if $(B, \{i\})$ is a dependence signature.

In order to provide another application of circuits, we continue this section with a closer look at the exact relation between circuit signatures and other dependence signatures.

Lemma 4.1.12. *For every dependence signature (V_+, V_-) with non-empty support there is a circuit (Z_+, Z_-) with $Z_+ \subseteq V_+$ and $Z_- \subseteq V_-$.*

Proof. The proof proceeds by contradiction. Suppose $V_+ \cup V_-$ is dependent but does not contain a circuit as claimed. Assume that the cardinality of $V_+ \cup V_-$ is smallest possible. Since (V_+, V_-) is not a circuit, there are at least two independent dependences $(\lambda_i)_{i \in J}$ and $(\mu_i)_{i \in J}$ with support contained in $V_+ \cup V_-$. We let $(\lambda_i)_{i \in J}$ be one with signature (V_+, V_-) . Then, for every $\varepsilon \in \mathbb{R}$, $(\lambda_i + \varepsilon \mu_i)_{i \in J}$ is also a dependence. Let ε_0 be the biggest (necessarily negative) value for which there is an i with $\lambda_i \neq 0$ and $\lambda_i + \varepsilon \mu_i = 0$. For every bigger ε we have that $(\lambda_i + \varepsilon \mu_i)_{i \in J}$ has signature (V_+, V_-) , while for ε_0 it has signature (W_+, W_-) with $W_- \subseteq V_-$, $W_+ \subseteq V_+$, and with one of the containments strict. We reach a contradiction with the assumed minimality of (V_+, V_-) . \square

The following corollary implies that the set of circuit signatures and the set of all dependence signatures can be recovered from one another. Observe also that the circuits in the statement must necessarily be conformal, since V_+ and V_- are disjoint.

Corollary 4.1.13. *Every dependence signature can be written as a conformal sum of signed circuits. That is, for every dependence signature (V_+, V_-) with non-empty support there is a finite collection of signed circuits (Z_+^i, Z_-^i) , $i = 1, \dots, k$, with $V_+ = \bigcup_i Z_+^i$ and $V_- = \bigcup_i Z_-^i$.*

Proof. This follows easily from the previous lemma, by induction on the cardinality of $V_+ \cup V_-$. Indeed, let $(\lambda_i)_{i \in J}$ be a dependence giving the signature (V_+, V_-) and let $(\mu_i)_{i \in J}$ be one giving a circuit (Z_+, Z_-) with $Z_+ \subseteq V_+$ and $Z_- \subseteq V_-$.

As in the previous proof, for every $\varepsilon \in \mathbb{R}$, $(\lambda_i + \varepsilon \mu_i)_{i \in J}$ is also a dependence and a ε exists for which this dependence has signature (W_+, W_-) with $W_- \subseteq V_-$, $W_+ \subseteq V_+$, and with one of the containments strict. We apply the inductive hypothesis to (W_+, W_-) and add (Z_+, Z_-) to the set of circuits obtained for it. \square

Finally, we are in a position to present the promised most useful application of Lemma 4.1.9: whenever two cells intersect improperly there is a circuit as a certificate for this intersection:

Theorem 4.1.14. *Let \mathcal{S} be a family of subsets of the label set J of a configuration \mathbf{A} . Assume that \mathcal{S} satisfies the closure property (CP). Then, the following two properties are equivalent:*

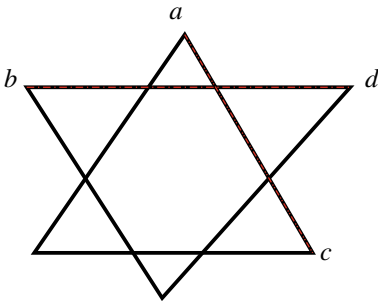


Figure 4.5: A dependence with six points contains a circuit with four points a, b, c, d .

(IP) If $B \neq B'$ are two cells in \mathcal{S} , then $\text{relint}(B) \cap \text{relint}(B') = \emptyset$. (Intersection Property)

(CiP) For each circuit (Z_+, Z_-) such that $Z_+ \subseteq B \in \mathcal{S}$ for some B , either there is no cell in \mathcal{S} containing Z_- , or every cell containing Z_+ contains Z_- too. (Circuit Property)

Proof. For (IP) \Rightarrow (CiP), assume that $Z_+ \subseteq B \in \mathcal{S}$ and $Z_- \subseteq B' \in \mathcal{S}$. Our goal is to prove that $Z_- \subseteq B$ (and that $Z_+ \subseteq B'$, but this is the same proof).

Let $F = \text{carrier}(Z_+, B)$ and $F' = \text{carrier}(Z_-, B')$ be the carrier faces of Z_+ and Z_- in B and B' respectively. By Lemmas 4.1.5 and 2.1.23,

$$\emptyset \neq \text{relint}(Z_+) \cap \text{relint}(Z_-) \subseteq \text{relint}(F) \cap \text{relint}(F'),$$

and then by (IP) $F = F'$. So $Z_- \subseteq F' \subseteq B$.

For the converse, suppose (CiP) and let $B, B' \in \mathcal{S}$ be different cells such that $\text{relint}(B) \cap \text{relint}(B') \neq \emptyset$. If $B \cap B' = \emptyset$, then Lemma 4.1.5 implies that (B, B') is a dependence signature. If $B \cap B' \neq \emptyset$, our condition implies that there is an expression

$$\sum_{i \in B} \lambda_i \mathbf{p}_i = \sum_{j \in B'} \mu_j \mathbf{p}_j$$

with all λ 's and μ 's positive. Subtracting $\sum_{i \in B \cap B'} \min\{\lambda_i, \mu_i\} \mathbf{p}_i$ on both sides we conclude that there are $V \subseteq B$ and $V' \subseteq B'$ disjoint and not both empty such that (V, V') is a dependence signature. Lemma 4.1.12 then gives the circuit we are looking for. \square

Before continuing, observe that the circuit property admits a simpler statement if we are interested only in the case where all cells of \mathcal{S} are independent (for example, if we want to check whether \mathcal{S} is a triangulation): no independent cell can contain a circuit, and every subset of an independent cell is a cell (by the closure property), so the circuit property can be relaxed for triangulations:

Theorem 4.1.15. Let \mathcal{T} be a family of independent subsets of the label set J of a configuration \mathbf{A} satisfying (CP). Then the following two properties are equivalent:

(CiP) For each circuit (Z_+, Z_-) such that $Z_+ \subseteq B \in \mathcal{T}$ for some B , either there is no cell in \mathcal{T} containing Z_- or every cell containing Z_+ contains Z_- , too. (Circuit property)

(TriangCiP) There is no circuit (Z_+, Z_-) with $Z_+, Z_- \in \mathcal{T}$ (Circuit property for triangulations).

In particular, if we want to check whether or not two cells B, B' intersect properly or not, we simply need to look at all circuits of \mathbf{A} that are not completely contained in at least one of B and B' and check whether one of them has its positive part completely in B and negative part completely in B' , or vice versa. This is a substantial progress in checking the intersection property (IP). Let us briefly think about how many circuits there are in a

point configuration with n points in dimension d . Each spanning $(d+2)$ -element contains a unique circuit and every circuit can be extended to a spanning $(d+2)$ -element. Hence, if worse comes to worst, then every $(d+2)$ -element subconfiguration is a circuit, and we have $\binom{n}{d+2}$ of them. This happens if and only if the configuration is in general position.

4.1.2 Evaluations, cocircuits, and the union property

In general it is an extremely difficult task to check whether a collection of simplices covers a polytope. Since (IP) is now easy to check (as we have learned in the previous section), we only need to check (UP) for collections that already satisfy (IP) and (CP). Our starting point is the following result:

Lemma 4.1.16. *Let \mathcal{S} be a family of subsets of the label set J of a configuration \mathbf{A} . Assume that \mathcal{S} satisfies the closure and intersection properties (CP) and (IP), and that all maximal elements in \mathcal{S} have full dimension. Then, the following properties are equivalent:*

(UP) $\bigcup_{B \in \mathcal{S}} \text{conv}(B) \supseteq \text{conv}(\mathbf{A})$ (Union Property).

(MaxMP) *For each facet F of a maximal cell B in \mathcal{S} , either F is contained in a facet of \mathbf{A} , or there is another maximal cell B' in \mathcal{S} that contains F as a facet (Pseudo-Manifold Property; see Figure 4.6).*

The “Max” in the abbreviation of the Pseudo-Manifold Property is there to remind us that this property needs to be checked only for maximal cells in a subdivision.

Proof. Assume (UP) and let F be a facet of a maximal cell B in \mathcal{S} that is not contained in a facet of \mathbf{A} . Pick a point \mathbf{x} in the relative interior of F and another point \mathbf{y} in general position, very close to \mathbf{x} but away from $\text{conv}(B)$, i.e., so that $\text{conv}(F)$ separates \mathbf{y} from $\text{relint } B$. Since F is not in a facet of \mathbf{A} , it is possible to do so with \mathbf{y} still in the interior of $\text{conv}(\mathbf{A})$.

Since (UP) holds, there is a B' in \mathcal{S} with $\mathbf{y} \in \text{conv}(B')$ which must be different from B . Since \mathbf{y} is in general position, \mathbf{y} must be in the relative interior of B' and B' must be full-dimensional. Since \mathbf{y} is very close to \mathbf{x} , each point on the open segment (\mathbf{x}, \mathbf{y}) must be also in $\text{relint}(B')$, so that $\mathbf{x} \in \text{conv}(B')$. By (IP) and (CP), the carriers of \mathbf{x} in B' and in F must be the same, and the latter is F itself. So, $F < B'$, as desired.

Now assume that (MaxMP) holds. Let $\mathbf{x} \in \text{conv}(\mathbf{A})$ and, for the sake of contradiction, assume that there is no cell in \mathcal{S} with \mathbf{x} in its convex hull. Pick a point \mathbf{y} in general position, meaning that no hyperplane contains a dependent subset of $\mathbf{A} \cup \{\mathbf{x}, \mathbf{y}\}$. For this it suffices to pick \mathbf{y} outside all of the (finite set of) hyperplanes spanned by points of $\mathbf{A} \cup \{\mathbf{x}\}$. Suppose also that \mathbf{y} does lie in the convex hull of some cell of \mathcal{S} . Consider the segment $[\mathbf{x}, \mathbf{y}]$ and let $\mathbf{z} \in [\mathbf{x}, \mathbf{y}]$ be the point closest to \mathbf{x} and that is in the convex hull of some cell of \mathcal{S} . This point exists because each $\text{conv}(B)$ intersects $[\mathbf{x}, \mathbf{y}]$ in either a point or a segment. Let B be a full-dimensional cell with $\mathbf{z} \in \text{conv}(B)$. The general position assumption on \mathbf{y} implies that the carrier of \mathbf{z} in B is a facet F of B . Since \mathbf{x} and \mathbf{y} lie on opposite sides of it, F is not contained in a facet of \mathbf{A} . Hence, (MaxMP) implies that there is a second

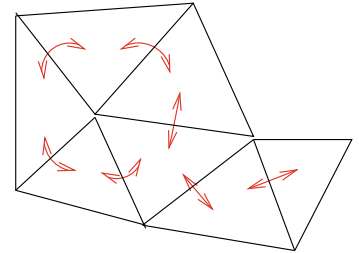


Figure 4.6: The pseudomanifold property.

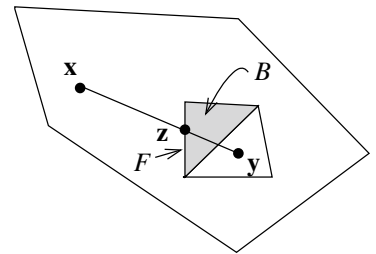


Figure 4.7: Proof of Lemma 4.1.16.

maximal cell B' with $F < B'$ and in particular $z \in \text{conv}(B')$. The intersection property (IP) then implies that $\text{conv}(B)$ and $\text{conv}(B')$ lie on opposite sides of $\text{conv}(F)$, which contradicts our assumption that no point in $[\mathbf{x}, \mathbf{z}]$ lies in the convex hull of a cell of \mathcal{S} . \square

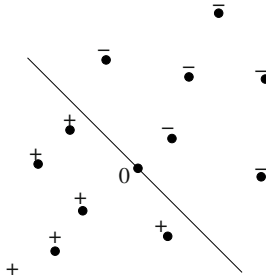


Figure 4.8: An evaluation signature.

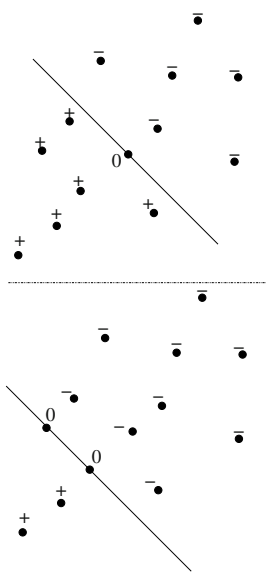


Figure 4.9: On top, an evaluation signature, but not a cocircuit. Below an honest cocircuit.

For triangulations, Condition (MaxMP) is already a “combinatorial property”, since the facets of a simplicial d -cell are just its d -subsets. Thus, for triangulations, (MaxMP) is easy to check computationally, so that Lemma 4.1.16 implies that *we can check whether a set of cells is a triangulation*. This is great news! Still, for general subdivisions we need to elaborate on the property. The key idea is to rewrite it in the language of signatures. Since faces are defined by linear functionals, the following seems the right tool for it:

Definition 4.1.17 (Evaluation signatures). Let \mathbf{A} be a vector configuration with label set J . An *evaluation signature* on \mathbf{A} is the signature of the vector $(\text{sign}(\psi(p_i)) : i \in J)$ where $\psi : J \rightarrow \mathbb{R}$ is a linear functional.

To mimic the situation with dependence signatures, we give a special name to the evaluation signatures with minimal support. The reason for the name chosen will be apparent in the next section.

Definition 4.1.18 (Cocircuits). A *cocircuit signature* is an evaluation signature with minimal support. Its support is a *cocircuit*.

Equivalently, the above definitions can be given in the sometimes more intuitive language of *oriented hyperplanes*:

Definition 4.1.19. For a linear functional $\psi \in (\mathbb{R}^d)^*$, let the *oriented hyperplane* \mathbf{H}^ψ defined by ψ be given by $\mathbf{H} = \{x \in \mathbb{R}^d : \psi(x) = 0\}$.

The *positive open halfspace* \mathbf{H}_+^ψ induced by \mathbf{H}^ψ is defined as $\mathbf{H}_+^\psi := \{x \in \mathbb{R}^d : \psi(x) > 0\}$. Similarly, the *negative open halfspace* \mathbf{H}_-^ψ induced by \mathbf{H}^ψ is defined as $\mathbf{H}_-^\psi := \{x \in \mathbb{R}^d : \psi(x) < 0\}$.

The closures of the open halfspaces are denoted by $\overline{\mathbf{H}}_+^\psi$ and $\overline{\mathbf{H}}_-^\psi$, respectively.

Example 4.1.20 (Example 4.1.4 continued). We list all covectors of our running example of five points in the plane (see Example 4.1.4) $(245, \emptyset), (1, 34), (125, \emptyset), (2, 3), (15, 4), (345, \emptyset), (135, \emptyset), (1, 24)$. As always, the “negative” of each of these cocircuits is also a cocircuit.

Lemma 4.1.21. Let \mathbf{A} be a full-dimensional configuration. Let V_+ and V_- be disjoint subsets of the label set of \mathbf{A} , not both empty. Then:

- (i) (V_+, V_-) is an evaluation signature if and only if there is an oriented hyperplane \mathbf{H} such that

$$V_+ = \{i : \mathbf{p}_i \in \mathbf{H}_+^\psi\}, \quad V_- = \{i : \mathbf{p}_i \in \mathbf{H}_-^\psi\}.$$

- (ii) (V_+, V_-) is a cocircuit signature if \mathbf{H} is spanned by a subset of elements of \mathbf{A} , or equivalently, if \mathbf{H} is unique.

Proof. Part (i) follows from the fact that every hyperplane is the zero set of a (non-zero) linear functional ψ , and the two half-spaces defined by \mathbf{H} are $\psi^{-1}(0, \infty)$ and $\psi^{-1}(-\infty, 0)$.

For part (ii), it is clear that uniqueness is equivalent to \mathbf{H} being spanned by $J \setminus (V_+ \cup V_-)$. If \mathbf{H} is not spanned we can rotate it slightly without changing its associated signature, and two different hyperplanes \mathbf{H}_1 and \mathbf{H}_2 exist, then the elements in $J \setminus (V_+ \cup V_-)$ span, at most, their intersection $\mathbf{H}_1 \cap \mathbf{H}_2$.

So, let us prove that these two properties are equivalent to being a cocircuit. If ψ_1 and ψ_2 define two different hyperplanes producing the signature (V_+, V_-) , then any linear combination $\alpha\psi_1 + \beta\psi_2$ has signature with support contained in $V_+ \cup V_-$. Choosing α and β appropriately we can make the functional be zero in any particular element, in particular obtaining an evaluation signature with support strictly contained in $V_+ \cup V_-$.

Conversely, if \mathbf{H} is not spanned by elements of \mathbf{A} , let L be the sub-linear space of \mathbf{H} spanned by $\mathbf{H} \cap \mathbf{A}$. As before, we can rotate \mathbf{H} around L and get a hyperplane whose signature is zero on any particular element, in particular one with support strictly contained in $V_+ \cup V_-$. \square

Remark 4.1.22 (Oriented hyperplanes for point configurations). As usual, \mathbf{A} is thought of as either a vector configuration or as a point configuration in homogeneous coordinates. In both cases, by a hyperplane we mean a linear hyperplane (one containing the origin). If \mathbf{A} is a d -dimensional point configuration and you prefer to think of it as embedded in \mathbb{R}^d , then in this lemma (and elsewhere) you need to consider *affine* hyperplanes.

Corollary 4.1.23. Let V_0 be a subset of the label set of a configuration \mathbf{A} . Then,

- (i) V_0 is the zero set (that is, the complement of the support) of an evaluation signature if and only if it equals the intersection of \mathbf{A} with a subspace.
- (ii) V_0 is the complement of a cocircuit if and only if it is not spanning and is maximal with this property.

Proof. For Part (i), the zero set of an evaluation signature is, by definition, the intersection of \mathbf{A} with a hyperplane. For the converse, if V_0 equals the intersection of \mathbf{A} with a subspace \mathbf{L} , let \mathbf{H} be a hyperplane containing \mathbf{L} and “sufficiently generic”. Then $\mathbf{L} \cap \mathbf{A} = \mathbf{H} \cap \mathbf{A}$.

For Part (ii), Part (i) implies that if V_0 is the complement of a cocircuit, then it is not spanning. By minimality of cocircuits, V_0 must span a hyperplane. The converse is clear. \square

Important for us is the following relation between evaluation signatures and faces of a configuration. Simply put: faces are the same as non-negative evaluation circuits:

Lemma 4.1.24. Let (V_+, V_-) be an evaluation signature of \mathbf{A} , with zero set $V_0 = J \setminus (V_+ \cup V_-)$. Then the following are equivalent:

- (i) Either $V_+ = \emptyset$ or $V_- = \emptyset$.

(ii) V_0 is a face of \mathbf{A} .

Proof. This follows directly from the properties of supporting hyperplanes of faces. \square

The following characterization of facets of point configurations will directly go into one of the combinatorial characterizations in Section 4.5.2.

Lemma 4.1.25. *Let (Z_+, Z_-) be a signed cocircuit of \mathbf{A} . Then the following are equivalent:*

- (i) Z_0 is a facet of \mathbf{A} .
- (ii) Either $Z_+ = \emptyset$ or $Z_- = \emptyset$.

Proof. Minimal evaluation signatures simply correspond to maximal zero-sets. These correspond to maximal proper faces, i.e., facets. \square

The following three statements say that the relation of cocircuits to evaluation signatures is the same we had for circuits and dependence signatures:

Lemma 4.1.26 (Uniqueness of Cocircuit Signatures). *Let Z be a cocircuit in a point configuration \mathbf{A} with signature (Z_+, Z_-) . Then (Z_-, Z_+) is the only other possible circuit signature on Z .*

Proof. By the previous lemma, there is a unique hyperplane containing Z_0 , and any two linear functionals vanishing on that hyperplane have to be multiples of each other. This implies that any induced signature is either identical or opposite. \square

Lemma 4.1.27 (Conformal decomposition of evaluations). *For every evaluation signature (V_+, V_-) whose support is non-empty there is a cocircuit (Z_+, Z_-) with $Z_+ \subseteq V_+$ and $Z_- \subseteq V_-$.*

Proof. If the codimension of V_0 is more than 1, the orthogonal complement of V_0 in \mathbb{R}^m contains at least one two-dimensional subspace that contains ψ . Now, turn around ψ in this subspace. This will generate a family of hyperplanes that covers \mathbb{R}^m . Now, we perform this process continuously, starting at ψ , and we stop at the first time when one or more new points are contained in the moving hyperplane. We remove this point from V , and either the resulting covector is already a cocircuit, or we repeat the process. See Figure 4.11. \square

As with circuits, this has the following corollary, whose proof we omit.

Corollary 4.1.28 (Conformal decomposition of evaluations). *For every evaluation signature (V_+, V_-) with non-empty support there is a collection of signed cocircuits (Z_+^i, Z_-^i) , $i = 1, \dots, k$, with $V_+ = \cup_i Z_+^i$ and $V_- = \cup_i Z_-^i$.*

In particular, cocircuits and evaluation signatures carry the same information on the configuration \mathbf{A} .

The punch line of our study of circuits was that we can use them to check for improper intersections (Property (IP) of subdivisions). Now similarly,

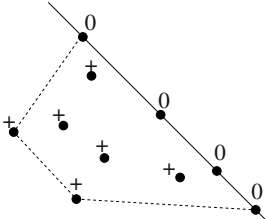


Figure 4.10: A positive cocircuit and the face it determines on the convex hull.

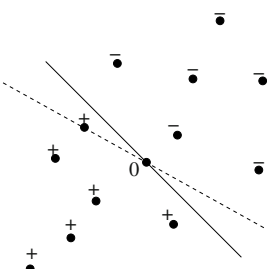


Figure 4.11: An evaluation and its conformally contained cocircuit (the dotted line).

in order to check (UP), we can utilize cocircuits, which we show next. Variations on this are given in Section 4.5.2. In order to check (UP) for \mathcal{S} , in Lemma 4.1.16 we provided Condition (MaxMP). If \mathcal{S} is of pure dimension and satisfies (IP) and (CP) already, then condition (UP) is fulfilled if every interior facet of a maximal cell is a facet of some other maximal cell in \mathcal{S} . Because of Lemma 4.1.25, we can now check this by looking at cocircuits of \mathbf{A} . Because of the importance of this observation we formulate it as a theorem.

Theorem 4.1.29. *Let \mathcal{S} be a set of cells in a point configuration \mathbf{A} labeled by J satisfying (CP) and (IP). Then the following are equivalent:*

- (UP) $\bigcup_{B \in \mathcal{S}} \text{conv}(B) \supseteq \text{conv}(\mathbf{A})$ (Union Property).
- (CoP) For each d -cell $B \in \mathcal{S}$ and for all cocircuits Z^* that are positive cocircuits on B but not positive on J , there is another d -cell $B' \in \mathcal{S}$ with $B \cap B' = Z_0^* \cap B$ (Cocircuit Property).

Again, the situation is simpler for triangulations since all facets of d -cells are obtained by deleting one single label from the cell.

Theorem 4.1.30. *Let \mathcal{T} be a set of independent subsets in a point configuration \mathbf{A} labeled by J , satisfying (CP) and (IP). Then the following are equivalent:*

- (UP) $\bigcup_{B \in \mathcal{T}} \text{conv}(B) \supseteq \text{conv}(\mathbf{A})$ (Union Property).
- (TriangCoP) For every d -subset F of a d -cell $B \in \mathcal{T}$, if one cocircuit Z^* spanned by F in \mathbf{A} is neither positive nor negative on J , then there is another d -cell $B' \in \mathcal{T}$ with $B \cap B' = Z_0^* \cap B$ (Cocircuit Property for Triangulations).

And how many cocircuits are there? Well, as many as there are hyperplanes spanned by subsets of elements of \mathbf{A} . If worse comes to worst, each subconfiguration of d elements spans a different hyperplane, which makes up for $\binom{n}{d}$ different cocircuits (up to sign reversal) in a point configuration consisting of n elements in dimension d .

Let us summarize the findings of this and the previous section in terms of a fully combinatorial characterization of polyhedral subdivisions. Here is a characterization that is crucial for the investigations in Chapter 6. It follows directly from Theorems 4.1.14 and 4.1.29.

Theorem 4.1.31. *A set \mathcal{S} of d -dimensional subconfigurations of a point configuration \mathbf{A} in \mathbb{R}^d labeled by J is the set of maximal cells of a polyhedral subdivision of \mathbf{A} if and only if it satisfies the following two conditions:*

- (CoP) For each d -cell $B \in \mathcal{S}$, and for all cocircuits Z^* that are positive cocircuits on B but not positive on J , there is another d -cell $B' \in \mathcal{S}$ with $B \cap B' = Z_0^* \cap B$ (Cocircuit Property).
- (CiP) For each circuit (Z_+, Z_-) such that $Z_+ \subseteq B \in \mathcal{S}$ for some B , either there is no cell in \mathcal{S} containing Z_- or every cell containing Z_+ contains Z_- too. (Circuit Property)

□

If we restrict ourselves to triangulations, then things become easier (see Theorems 4.1.15 and 4.1.30).

Corollary 4.1.32. *A set \mathcal{T} of d -dimensional independent subconfigurations of a point configuration \mathbf{A} in \mathbb{R}^d is the set of maximal cells of a triangulation of \mathbf{A} if and only if it satisfies the following two conditions:*

(TriangCoP) *For every d -subset F of a d -cell $B \in \mathcal{T}$, if one cocircuit Z^* spanned by F in \mathbf{A} is neither positive nor negative on J , then there is another d -cell $B' \in \mathcal{T}$ with $B \cap B' = Z_0^* \cap B$. (Cocircuit Property for Triangulations).*

(TriangCiP) *For each pair of cells $B, B' \in \mathcal{T}$, there is no signed circuit (Z_+, Z_-) in \mathbf{A} with $Z_+ \subseteq B$ and $Z_- \subseteq B'$ (Circuit Property for Triangulations). □*

4.1.3 Gale transforms and the duality between circuits and cocircuits

In this section we introduce the reader to a rather useful construction and duality notion used very frequently in discrete geometry, the *Gale transform*. Let $\mathbf{A} \in \mathbb{R}^{m \times n}$ be a vector configuration of rank k (for example, a point configuration, in a homogenized version) with n elements.

Definition 4.1.33. We call *linear dependences* the vectors of coefficients of dependences on \mathbf{A} . A *linear evaluation* is the restriction to \mathbf{A} of a linear function $\mathbb{R}^m \rightarrow \mathbb{R}$.

In other words, linear dependences and linear evaluations are the vectors whose signatures define dependence signatures and evaluation signatures. These two objects are closely related.

Lemma 4.1.34. *Linear dependences and linear evaluations of \mathbf{A} form two orthogonal complementary linear subspaces of \mathbb{R}^n , of ranks $n - k$ and k respectively.*

Proof. Linear evaluations are the row span of the matrix \mathbf{A} (because every linear functional is a linear combination of the coordinate functionals and vice versa) and linear dependences are, by definition, the orthogonal complement of it. □

Definition 4.1.35. A *Gale transform* of a configuration \mathbf{A} is a configuration \mathbf{B} such that the linear dependences of \mathbf{A} are the linear evaluations on \mathbf{B} and vice versa. The set of all Gale transforms of \mathbf{A} is denoted by $\text{Gale}(\mathbf{A})$. Nevertheless, in the future, we will often abuse notation and denote by $\text{Gale}(\mathbf{A})$ an explicitly or implicitly chosen Gale transform for \mathbf{A} .

Lemma 4.1.36. *Every configuration \mathbf{A} has at least one Gale transform.*

Proof. Compute the orthogonal complement of the row span of \mathbf{A} (that is, the kernel of \mathbf{A}) and take any basis of it as the rows of a matrix for the configuration \mathbf{B} . Moreover, all Gale transforms of \mathbf{A} are linearly isomorphic vector configurations. □

Example 4.1.37. Continuing the running Example 4.1.4, from the given coordinates we can easily calculate the affine dependences among the five points as the kernel of the matrix

$$\mathbf{A} = \begin{pmatrix} 1 & 2 & 3 & 4 & 5 \\ 0 & 3 & 0 & 3 & 1 \\ 0 & 0 & 3 & 3 & 1 \\ 1 & 1 & 1 & 1 & 1 \end{pmatrix}.$$

This gives, for instance, a Gale transform

$$\begin{pmatrix} 1 & 2 & 3 & 4 & 5 \\ 1 & 1 & 1 & 0 & -3 \\ 2 & 0 & 0 & 1 & -3 \end{pmatrix}.$$

These five vectors are represented in Figure 4.12. Of course, a basis for the kernel is not unique and thus the Gale transform is not unique either. An alternative would be

$$\begin{pmatrix} 1 & 2 & 3 & 4 & 5 \\ -\frac{1}{3} & -\frac{1}{3} & -\frac{1}{3} & 0 & 1 \\ 1 & -1 & -1 & 1 & 0 \end{pmatrix}.$$

Precisely this Gale transform was used for drawing Figures 2.34 and 2.35: the horizontal and vertical unit vectors represent, respectively, the height vectors ω_5 and ω_4 Gale dual to the elements 5 and 4 of \mathbf{A} , respectively.

Observe that in the definition of a Gale transform, the two configurations are implicitly assumed to be labeled by the same set, so that we can use the same symbol to refer to subsets of elements in both. Moreover, there are the following relations among the properties of the same subset in both configurations. See also Figures 4.14, 4.15, and 4.16:

Lemma 4.1.38. *Let $\mathbf{B} \in \text{Gale}(\mathbf{A})$. Then:*

- (i) *The dependence signatures of \mathbf{A} are the evaluation signatures of \mathbf{B} , and vice versa.*
- (ii) *The circuit signatures of \mathbf{A} are the cocircuits of any \mathbf{B} , and vice versa.*
- (iii) *The faces of \mathbf{A} are the complements of positive dependence signatures of any \mathbf{B} , and vice versa.*
- (iv) *The independent subconfigurations of \mathbf{A} are the complements of the full-dimensional subconfigurations of any \mathbf{B} , and vice versa.*

Proof. Part (i) is straightforward from the definition, and the rest of properties follow easily from what we said in the previous sections: Minimal dependences are circuits while evaluations with minimal support are cocircuits; faces are the complements of positive evaluation signatures, and circuits [cocircuits] are minimal dependent sets [complements of maximal non-spanning sets]. \square

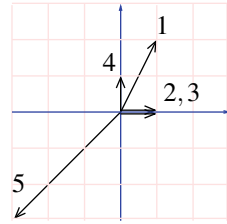


Figure 4.12: A Gale transform for the five-point planar configuration.

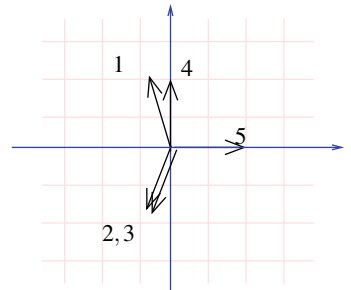


Figure 4.13: Another Gale transform for Example 4.1.4.

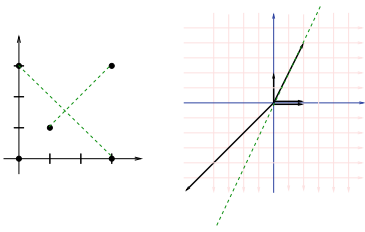


Figure 4.14: Circuits in \mathbf{A} correspond to cocircuits in $\mathbf{B} \in \text{Gale}(\mathbf{A})$.

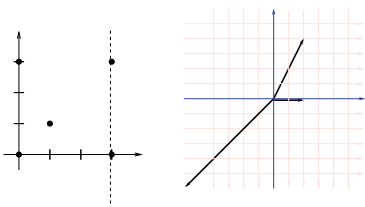


Figure 4.15: Cocircuits in \mathbf{A} correspond to circuits in $\mathbf{B} \in \text{Gale}(\mathbf{A})$.

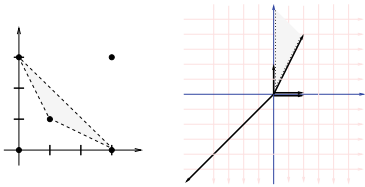


Figure 4.16: Independent sets in \mathbf{A} correspond to complements of independent sets in $\mathbf{B} \in \text{Gale}(\mathbf{A})$.

Why are Gale transforms interesting for studying subdivisions and triangulations? The main reason has to do with the fact that two height vectors $\omega, \omega' : \mathbf{A} \rightarrow \mathbb{R}$ whose difference is an affine [a linear] function on the coordinates of the point [vector] configuration, i.e., a linear evaluation, produce the same regular subdivision (more precisely, they produce lifted configurations that are linearly equivalent and with the same notion of “lower” face). This will be discussed in detail in Section 5.4.1. However, there is one fact we wish to reveal right away: Heights that produce subdivisions for vector configurations can be characterized very nicely using a Gale transform.

Theorem 4.1.39. *Let \mathbf{A} be a vector configuration with Gale transform $\mathbf{B} \in \text{Gale}(\mathbf{A})$. Let $\omega : J \rightarrow \mathbb{R}$ be a height vector. Then the following conditions are equivalent:*

1. ω produces a regular subdivision of \mathbf{A} , that is, the lifted configuration \mathbf{A}^ω has lower faces.
2. For every non-negative linear dependence λ of \mathbf{A} , we have $\omega \cdot \lambda \geq 0$.
3. $\omega \mathbf{B}^T \in \text{cone}(\mathbf{B})$.
4. ω is, modulo addition of a linear evaluation to it, non-negative.

Proof. The implication from (1) to (2) is by contradiction. Suppose that there is a linear dependence λ with $\omega \cdot \lambda = c < 0$. This implies that the vector $(0, \dots, 0, c)$ is in $\text{cone}(\mathbf{A}^\omega)$, so the whole ray in the negative direction of the lifting coordinate is in the cone. This implies that the cone cannot have a lower face.

For the implication from (2) to (3), contradiction works too: if $\omega \mathbf{B}^T \notin \text{cone}(\mathbf{B})$ then, by Farkas’ lemma, there is a linear functional ϕ that separates $\omega \mathbf{B}^T$ from $\text{cone}(\mathbf{B})$. That is, $\phi(\omega \mathbf{B}^T) < 0$, but ϕ is non-negative on every element of \mathbf{B} . Let λ be the evaluation vector corresponding to that functional. By Gale duality, λ is a dependence in \mathbf{A} , and by construction it is non-negative. Its scalar product with ω equals $\phi(\omega)$. This is a contradiction.

For the implication from (3) to (1), observe first that:

$$\begin{aligned} \omega \mathbf{B}^T \in \text{cone}(\mathbf{B}) &\iff \omega \mathbf{B}^T = \mu \mathbf{B}^T \text{ for some } \mu \in \mathbb{R}^n, \mu \geq 0 \\ &\iff \omega \mathbf{B}^T - \mu \mathbf{B}^T = 0 \text{ for some } \mu \in \mathbb{R}^n, \mu \geq 0 \\ &\iff (\omega - \mu) \mathbf{B}^T = 0 \text{ for some } \mu \in \mathbb{R}^n, \mu \geq 0 \\ &\iff (\omega - \mu) \in \ker(\mathbf{B}^T) \text{ for some } \mu \in \mathbb{R}^n, \mu \geq 0. \end{aligned}$$

This means that there is a nonnegative $\mu : J \rightarrow \mathbb{R}$ for which $(\omega - \mu)$ is a dependence of \mathbf{B} . By the definition of a Gale transform, $(\omega - \mu)$ is a linear evaluation of \mathbf{A} . Thus:

$$\omega \mathbf{B}^T \in \text{cone}(\mathbf{B}) \iff (\omega - \mu) = c^T \mathbf{A} \text{ for some } \mu \in \mathbb{R}^n, \mu \geq 0.$$

In words: A height vector maps via \mathbf{B} into the conical hull of \mathbf{B} if and only if ω plus some linear height function is a nonnegative height function, i.e., ω

produces the same set of lower faces as some nonnegative height function. That the nonnegative height functions induce all regular subdivisions was already proven in Lemma 2.5.11.

Finally (3) is clearly equivalent to (4). \square

That is:

The space of “allowable” height functions to obtain a regular subdivision of a vector configuration \mathbf{A} with $\mathbf{B} \in \text{Gale}(\mathbf{A})$ is naturally identified with $\text{cone}(\mathbf{B})$.

Now, if \mathbf{B} is not totally cyclic, the above identification sends some particular heights functions to lie in the boundary of $\text{cone}(\mathbf{B})$. What is special about the regular subdivisions defined by them? The following result gives the answer. Its proof, similar to that of Theorem 4.1.39, is left to the reader.

Theorem 4.1.40. *Let \mathbf{A} be a vector configuration with Gale transform $\mathbf{B} \in \text{Gale}(\mathbf{A})$. Let $\omega : J \rightarrow \mathbb{R}$ be a height vector. Then, the following conditions are equivalent:*

1. ω produces a regular subdivision of \mathbf{A} with all its cells acyclic. That is, the lifted configuration \mathbf{A}^ω has lower faces and all of them are acyclic.
2. For every non-negative linear dependence λ of \mathbf{A} , we have $\omega \cdot \lambda > 0$.
3. $\omega \mathbf{B}^T \in \text{relint}(\mathbf{B})$.
4. ω is, modulo addition of a linear evaluation to it, strictly positive.

Example 4.1.41 (The regular pentagon). Let \mathbf{C}_5 be the vertex set of a regular pentagon. We leave it to the reader to check that one of its Gale transform is precisely the configuration of five vectors in the plane that appeared in Example 2.5.10 (but be careful with the bijection between the points in one and the vectors in the transform; it is not the one you would expect). The five rays in the Gale transform correspond to the heights ω_i , which produce a subdivision of a pentagon into a quadrilateral and a triangle. The cone between the two rays represents the set of heights that produce a specific triangulation of the pentagon, with the ray between two adjacent cones corresponding to a flip.

We can also look at this example backwards. The regular subdivisions of the configuration dual to \mathbf{C}_5 were all depicted in Figure 2.57. The two bottom rows in the figure are the “acyclic” subdivisions appearing in Theorem 4.1.40, which somehow correspond to choices of ω lying in the interior of $\text{conv}(\mathbf{C}_5)$. The three on the top row, reproduced in Figure 4.18 correspond to choices in $\partial \text{conv}(\mathbf{C}_5)$. More precisely, the first one corresponds to the zero height vector (observe that \mathbf{C}_5 has to be understood as a vector configuration, and $\text{conv}(\mathbf{C}_5)$ as a pointed cone, to take full advantage of Gale duality), the second one to a choice in one of the vertices of $\text{conv}(\mathbf{C}_5)$, and the third one to a choice in the relative interior of an edge.

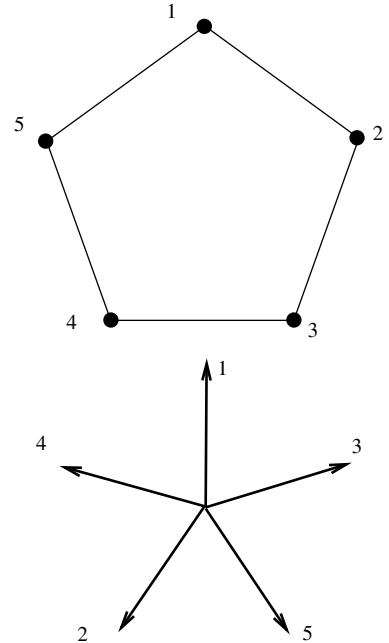


Figure 4.17: Five vertices of a regular pentagon and a Gale transform of it.

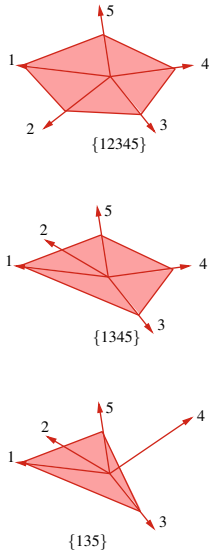


Figure 4.18: The three regular subdivisions of the Gale transform of C_5 containing some non-acyclic cells. They correspond to lifting heights “lying” in the boundary of $\text{conv } C_5$.

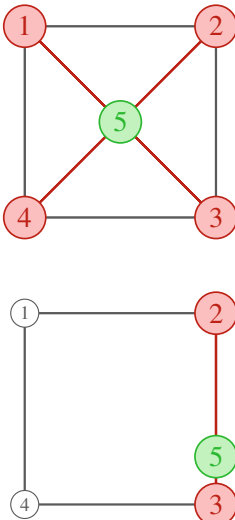


Figure 4.19: These two point configurations have different oriented matroids, since one of them contains a pair of circuits $(5, 13)$ and $(5, 24)$ with identical positive element 5, and the other does not. Another reason: one contains a positive cocircuit with three zero-elements, the other does not. Thus, there is no relabelling that maps (co-)circuits bijectively to (co-)circuits.

Example 4.1.42. (Four vectors in general position) We now turn our attention to the configuration of Example 2.5.8:

$$\mathbf{A} = \begin{pmatrix} 1 & 2 & 3 & 4 \\ 1 & -2 & 1 & 0 \\ 0 & 1 & -2 & 1 \end{pmatrix}, \quad \text{Gale}(\mathbf{A}) \ni \mathbf{B} = \begin{pmatrix} 1 & 2 & 3 & 4 \\ 0 & 1 & 2 & 3 \\ 1 & 1 & 1 & 1 \end{pmatrix}.$$

The indicated Gale transform is (a homogenized version of) a point configuration consisting on four points along a line. Its decomposition into the four points and the three open intervals is in bijection with the seven non-trivial subdivisions of \mathbf{A} .

We have seen that combinatorial structures of a point configuration carry all the information relevant to their subdivisions, except for regularity. That means we can consider any two point configurations \mathbf{A} and \mathbf{A}' equivalent if and only if they have identical sets of signed circuits and, thus, cocircuits. The following is common language in combinatorial geometry. See [55] for a full exposition of the theory of oriented matroids:

Definition 4.1.43 (Oriented Matroid). Two (point or vector) configurations are *combinatorially equivalent* if they have (up to relabeling) identical sets of circuits (and thus identical sets of cocircuits, identical dependence signatures, and identical evaluation signatures).

This is an equivalence relation on the set of all (point and vector) configurations. The equivalence class of a configuration with respect to this equivalence relation is called its *oriented matroid*.

One can give a more general definition of oriented matroid (or orientable matroids), one without any reference to a point or a vector configuration. One can specify various set of axioms that describe how a set of, e.g., circuits should look like (see the authoritative reference [55] for details). Within this more general framework, some oriented matroids may not be given by point or vector configuration with the same sets of circuits. Such oriented matroids are called *non-realizable* oriented matroids. In this book we are only directly interested in realizable oriented matroids, thus we can get away with the definition above. See Figure 4.19 for an example of two distinct realizable oriented matroids.

That oriented matroids are crucial to the study of triangulations and subdivisions of point configurations follows from the following corollary of Theorem 4.1.31.

Corollary 4.1.44. Two combinatorially equivalent configurations have the same (up to relabelling) poset of polyhedral subdivisions, in particular the same set and graph of triangulations.

It is important to observe, however, that regularity of triangulations and subdivisions *cannot* be deduced from the oriented matroid alone. It is an exercise for the reader to think of an example!

4.2 Manipulating vector configurations

We now define various operations on *point* or *vector* configurations and study their behavior with respect to triangulations and subdivisions. We begin with *joins* and *products*, both very easy operations on the level of point configurations. The easiest examples are, respectively, pyramids and prisms. For both joins and products there are easy and natural ways to produce canonical subdivisions of the new configuration from the original subdivisions of the operands. If we are after triangulations, however, joins turn out to be much more natural than products because they preserve affine independence. Later on we discuss *deletion* and *contraction* operations, which provide proof techniques in combinatorics because they maintain complementary information of an object. We conclude with the operation of *one-point suspension*.

4.2.1 Pyramids and joins

Consider a d -dimensional point configuration \mathbf{A} embedded into \mathbb{R}^m . Put a point \mathbf{p} outside the hyperplane spanned by \mathbf{A} . The resulting new point configuration is *the pyramid of \mathbf{A} with apex \mathbf{p}* . Since it really does not matter (as we will see) where we put the point \mathbf{p} , there is a standard model of the pyramid construction that we will use. More specifically:

Definition 4.2.1 (Pyramid). Let \mathbf{A} be a point configuration labeled by J . Then

$$\text{pyram}(\mathbf{A}) := \begin{pmatrix} J & * \\ \mathbf{A} & \mathbf{0} \\ 0 & 1 \end{pmatrix}$$

is *the standard pyramid over \mathbf{A}* .

Each point configuration combinatorially equivalent to the standard pyramid over \mathbf{A} is called a *pyramid over \mathbf{A}* . The new point $\mathbf{p}_* = \begin{pmatrix} \mathbf{0} \\ 1 \end{pmatrix}$ is called the *apex* of the pyramid, the old point configuration, augmented with a row of zeroes, is called the *base* of the pyramid. By abuse of notation, we will denote the base in the pyramid again by \mathbf{A} .

What does the set of all subdivisions of a pyramid look like? Let \mathcal{S}^* be a subdivision of $\text{pyram}(\mathbf{A})$. Since \mathbf{A} is a face of $\text{pyram}(\mathbf{A})$, it certainly restricts to a subdivision \mathcal{S} of \mathbf{A} . This subdivision is obtained by removing all cells in \mathcal{S}^* that contain $*$.

Now let \mathcal{S} be a subdivision of \mathbf{A} . No circuit in $\text{pyram}(\mathbf{A})$ can contain $*$, since \mathbf{p}_* is the only point with a one in the last row. Therefore, any set of cells that intersect properly in the base will intersect properly after the addition of $*$ to each cell, by the equivalence of (IP) and (CiP). Thus, adding a cell $C \cup \{*\}$ for each cell $C \in \mathcal{S}$ yields a collection of cells in $\text{pyram}(\mathbf{A})$ that satisfies (CiP) and, obviously, (CP).

Moreover, each point \mathbf{x} in the convex hull of the pyramid induces a unique point \mathbf{y} in the base by taking the intersection of the line through the apex and \mathbf{x} with the base. Since \mathcal{S} satisfies (UP), there is a cell C having \mathbf{y} in its convex hull. Therefore, \mathbf{p}_* and \mathbf{y} , and hence by convexity also \mathbf{x} , are

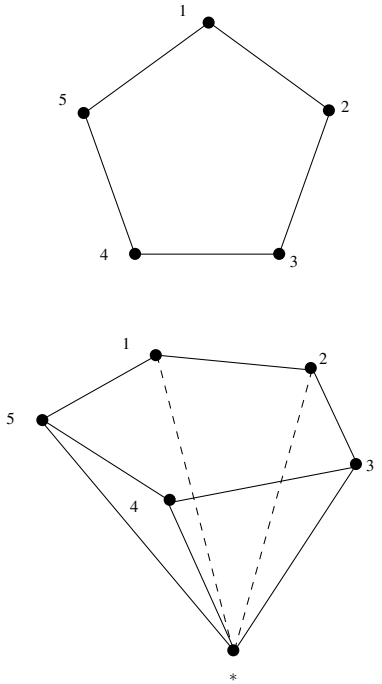


Figure 4.20: Five vertices of a regular pentagon and a pyramid over it.

contained in the convex hull of $C \cup \{*\}$. Therefore, adding a cell $C \cup \{*\}$ for each cell $C \in \mathcal{S}$ yields a collection of cells that satisfies (UP) as well.

This means that the set of maximal cells that is obtained by adding $*$ to every maximal cell of a subdivision of \mathbf{A} is the set of maximal cells of a subdivision of $\text{pyram}(\mathbf{A})$. Conversely, removing $*$ from every cell in a subdivision of $\text{pyram}(\mathbf{A})$ gives a subdivision of \mathbf{A} . This motivates the following definition:

Definition 4.2.2 (Pyramid over a Subdivision). Let \mathcal{S} be a subdivision of a point configuration \mathbf{A} labeled by J . Then the collection of cells

$$\text{pyram}(\mathcal{S}) := \mathcal{S} \cup \{C \cup \{*\} : C \in \mathcal{S}\}$$

is the *pyramid over \mathcal{S}* , which is a subdivision of $\text{pyram}(\mathbf{A})$.

The considerations above can be summarized now as follows.

Observation 4.2.3. For all subdivisions \mathcal{S} of \mathbf{A} , the set $\text{pyram}(\mathcal{S})$ is a subdivision of $\text{pyram}(\mathbf{A})$, and it is regular if and only if \mathcal{S} is regular. Moreover, all subdivisions of $\text{pyram}(\mathbf{A})$ arise in this way. \square

The pyramid construction has a natural generalization. The underlying geometric operation is called the *join*, and it is a binary operation on two complexes that reside in skew affine subspaces. We again give a standard model of this operation for point configurations:

Definition 4.2.4 (Join). Let \mathbf{A} and \mathbf{B} be point configurations labeled by J and K , respectively. Then

$$\mathbf{A} * \mathbf{B} := \begin{pmatrix} J \times \{1\} & K \times \{2\} \\ \mathbf{A} & \mathbf{0} \\ \mathbf{0} & \mathbf{B} \end{pmatrix}$$

is the *standard join of \mathbf{A} and \mathbf{B}* , where a label $(j, 1)$ or $(k, 2)$ is sometimes written j_1 or k_2 , respectively. If J and K are disjoint, then the join can be labeled by $J \cup K$ in the obvious way.

A point configuration combinatorially equivalent to the standard join of \mathbf{A} and \mathbf{B} is called a *join of \mathbf{A} and \mathbf{B}* . The natural embeddings of \mathbf{A} and \mathbf{B} into $\mathbf{A} * \mathbf{B}$ will, by abuse of notation, again be denoted by \mathbf{A} and \mathbf{B} , respectively.

Example 4.2.5. In Figure 4.21 we represent the join of two subdivided line segments, $\{a_1, a_2\}$ and $\{b_1, b_2, b_3, b_4\}$, and one of their resulting triangulations.

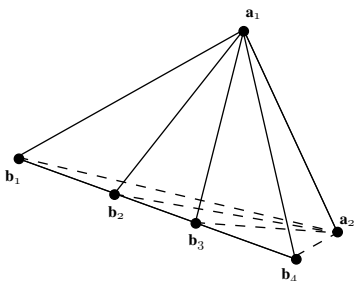


Figure 4.21: The join of two subdivisions is a subdivision of the join.

Of course, the pyramid is a special case of a join. The interesting thing about joins is that, similar to the pyramid, the set of all subdivisions of a join is completely determined by the sets of subdivisions of the operands. The construction for triangulations is similar to what is usually called the *simplicial join* of simplicial complexes.

Definition 4.2.6 (Join of Subdivisions). Let \mathcal{S} and \mathcal{R} be subdivisions of \mathbf{A} and \mathbf{B} , respectively. Then, the *join* of \mathcal{S} and \mathcal{R} is the collection of cells

$$\mathcal{S} * \mathcal{R} := \{(C \times \{1\}) \cup (B \times \{2\}) : C \in \mathcal{S}, B \in \mathcal{R}\}.$$

Again, if \mathbf{A} and \mathbf{B} are labeled by disjoint label sets J and K , then the labeling of the cells need not be modified.

The main property of join subdivisions is that they are the only subdivisions of the join.

Theorem 4.2.7. *The join of any two subdivisions of point configurations \mathbf{A} and \mathbf{B} is a subdivision of $\mathbf{A} * \mathbf{B}$. Moreover, every subdivision of $\mathbf{A} * \mathbf{B}$ arises in this way.*

Proof. Since both \mathbf{A} and \mathbf{B} are not full-dimensional, there can be no circuit of $\mathbf{A} * \mathbf{B}$ containing points of both pieces. Thus, the join of two subdivisions satisfies condition (CiP) (see Theorem 4.1.14) if and only if both operands satisfy (CiP). Property (CP) for the join of two subdivisions is also equivalent to (CP) for both operands, by construction.

Each point \mathbf{x} in $\text{conv}(\mathbf{A} * \mathbf{B})$ has a representation as a convex combination of a point \mathbf{u} in $\text{conv}_{\mathbf{A} * \mathbf{B}}(J)$ and a point $\mathbf{v} \in \text{conv}_{\mathbf{A} * \mathbf{B}}(K)$. Therefore, if \mathcal{S} and \mathcal{R} are subdivisions of \mathbf{A} and \mathbf{B} , respectively, then \mathbf{u} lies in the convex hull of a cell C of \mathcal{S} and \mathbf{v} lies in the convex hull of a cell B of \mathcal{R} . This implies that \mathbf{x} lies in the convex hull of $C \cup B$, which is a cell of $\mathcal{S} * \mathcal{R}$. Thus, (UP) is satisfied for the join subdivision.

In summary, each join of valid subdivisions is a subdivision of the join. Now let \mathcal{S} be any subdivision of $\mathbf{A} * \mathbf{B}$. This subdivision induces, by Lemma 2.3.4(iv), subdivisions of both \mathbf{A} and \mathbf{B} because both configurations are faces of $\mathbf{A} * \mathbf{B}$. Moreover, each cell in \mathcal{S} is exactly the union of the cells in the two restrictions. But that means that it is the join of the two restrictions, which proves the second claim. \square

In summary, the composition of join and restriction to the operands as well as the composition of restriction to the operands and join yields the identity. Obviously both maps are order preserving.

Corollary 4.2.8. *There is a bijection of posets between $\text{Subdivs}(\mathbf{A} * \mathbf{B})$ and $\text{Subdivs}(\mathbf{A}) \times \text{Subdivs}(\mathbf{B})$. This bijection is order preserving with respect to the refinement order.*

4.2.2 Prisms and products

Consider a d -dimensional point configuration \mathbf{A} embedded into \mathbb{R}^{d+1} at ‘height’ zero. If we put a parallel copy at height one, then we obtain what is called the *prism* over \mathbf{A} . On the level of convex hulls the prism is the product with an interval. As in the previous section, we want to give a standard model of a prism.

Definition 4.2.9 (Prism). Let \mathbf{A} be a point configuration labeled by J . Then

$$\text{prism}(\mathbf{A}) := \begin{pmatrix} J \times \{1\} & J \times \{2\} \\ \mathbf{A} & \mathbf{A} \\ 1 & 0 \end{pmatrix}$$

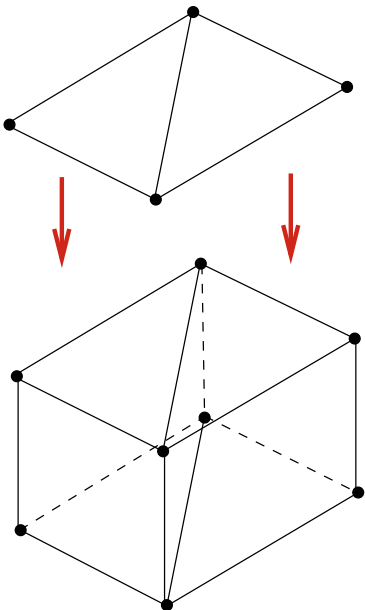


Figure 4.22: The prism over a square (a cube) is subdivided. The subdivision is obtained from a triangulation of the square.

is the standard prism over \mathbf{A} .

A point configuration combinatorially equivalent to the standard prism over \mathbf{A} is called a *prism over \mathbf{A}* .

There are two direct observations: first, every cell in a subdivision \mathcal{S} of \mathbf{A} labels a subconfiguration over which we may take the prism. For a maximal cell in \mathcal{S} this prism is a full-dimensional subconfiguration in the prism. However, a prism over an independent cell does not yield an independent subconfiguration in the prism. So, the prism over a subdivision that we define below cannot be expected to give all possible subdivisions of the prism; it does not even yield a single triangulation.

Definition 4.2.10 (Prism of a Subdivision). Let \mathcal{S} be a subdivision of a point configuration \mathbf{A} that is labeled by J . Then the collection of cells

$$\text{prism}(\mathcal{S}) := \bigcup_{C \in \mathcal{S}} \{C \times \{1\}, C \times \{2\}, C \times \{1, 2\}\}$$

of all prisms over cells in \mathcal{S} is the *prism over \mathcal{S}* .

Our considerations can be summarized as follows (see Figure 4.22).

Observation 4.2.11. For every subdivision \mathcal{S} of \mathbf{A} the collection of cells $\text{prism}(\mathcal{S})$ forms a subdivision of $\text{prism}(\mathbf{A})$. \square

Prisms can be generalized by products in a similar way as pyramids by joins. The Cartesian product of Euclidean point sets is a standard construction in geometry. For completeness we now give our standard representation of a product for labeled point configurations.

Definition 4.2.12 (Product). Let $\mathbf{A} = (\mathbf{p}_j)_{j \in J}$ and $\mathbf{B} = (\mathbf{q}_k)_{k \in K}$ be point configurations labeled by J and K , respectively. Then

$$\mathbf{A} \times \mathbf{B} := \left(\begin{array}{c} \mathbf{p}_j \\ \mathbf{q}_k \end{array} \right)_{j \in J, k \in K}^{(j, k)}$$

is the standard product of \mathbf{A} and \mathbf{B} .

A point configuration combinatorially equivalent to the standard product of \mathbf{A} and \mathbf{B} is called a *product of \mathbf{A} and \mathbf{B}* .

As before, we define an operation on subdivisions that yields subdivisions of the product. It is no surprise that this is the product of cells.

Definition 4.2.13 (Product of Subdivisions). Let \mathcal{S} and \mathcal{R} be subdivisions of \mathbf{A} and \mathbf{B} , respectively. Then, the *product of \mathcal{S} and \mathcal{R}* is the collection of cells

$$\mathcal{S} \times \mathcal{R} := \{C \times B : C \in \mathcal{S}, B \in \mathcal{R}\}.$$

The admittedly obvious result reads as follows.

Remark 4.2.14. The product of any two subdivisions of point configurations \mathbf{A} and \mathbf{B} is a subdivision of $\mathbf{A} \times \mathbf{B}$. Not every subdivision of $\mathbf{A} \times \mathbf{B}$ arises in this way. In particular, whenever both \mathbf{A} and \mathbf{B} have more than one point, then the product of two subdivisions is never a triangulation.

Any subdivision of $\mathbf{A} \times \mathbf{B}$ yields a subdivision of \mathbf{A} for every extreme point \mathbf{q} of \mathbf{B} via the restriction to the face $\mathbf{A} \times \mathbf{q}$ of $\mathbf{A} \times \mathbf{B}$. Similarly, we get a subdivision of \mathbf{B} for every extreme point of \mathbf{A} .

This means that whereas subdivisions of a join of two point configurations is completely determined by the subdivisions of the two operands, forming the product may result in a much more interesting set of subdivisions. The fact that triangulations of cubes (products of segments) are far from being understood today is partly explained by this pathology. Another example of how products yield rich structures can be found in Chapter 7.3. This is in contrast to other situations where products only lead to trivial objects.

4.2.3 Deletion

Definition 4.2.15. Let \mathbf{A} be a configuration with label set J and let $i \in J$ be one of its elements. The deletion of i in \mathbf{A} is the subconfiguration obtained by removing the corresponding element from the labeled set \mathbf{A} (that is, removing the corresponding column from the matrix of \mathbf{A}). Slightly abusing notation, we denote it $\mathbf{A} \setminus i$.

Thus, deleting a point means just “forgetting it”. Not every subdivision or triangulation of \mathbf{A} is compatible with one of $\mathbf{A} \setminus i$, as the following example shows.

Example 4.2.16. Consider Example 3.6.15, the configuration consisting of the six vertices of a Schönhardt polyhedron, the important non-convex polyhedron of Example 3.6.1, together with an exterior point along its axis of symmetry. We use again the coordinates

$$\mathbf{A} = \begin{pmatrix} \mathbf{p}_1 & \mathbf{p}_2 & \mathbf{p}_3 & \mathbf{q}_1 & \mathbf{q}_2 & \mathbf{q}_3 & \mathbf{r} \\ 1-\varepsilon & 0 & \varepsilon & 1 & 0 & 0 & 1/3 \\ \varepsilon & 1-\varepsilon & 0 & 0 & 1 & 0 & 1/3 \\ 0 & \varepsilon & 1-\varepsilon & 0 & 0 & 1 & 1/3 \\ 0 & 0 & 0 & 1 & 1 & 1 & 10 \end{pmatrix},$$

where $\varepsilon > 0$ is small. Figure 4.23 shows the profile of this point set. Consider again the triangulation \mathcal{T} of \mathbf{A} consisting of the ten tetrahedra:

$$\begin{aligned} &\{\mathbf{q}_1, \mathbf{q}_2, \mathbf{p}_1, \mathbf{p}_2\}, \quad \{\mathbf{q}_2, \mathbf{q}_3, \mathbf{p}_2, \mathbf{p}_3\}, \quad \{\mathbf{q}_3, \mathbf{q}_1, \mathbf{p}_3, \mathbf{p}_1\}, \\ &\{\mathbf{r}, \mathbf{q}_1, \mathbf{p}_1, \mathbf{p}_2\}, \quad \{\mathbf{r}, \mathbf{q}_1, \mathbf{q}_2, \mathbf{p}_2\}, \quad \{\mathbf{r}, \mathbf{q}_2, \mathbf{p}_2, \mathbf{p}_3\}, \\ &\{\mathbf{r}, \mathbf{q}_2, \mathbf{q}_3, \mathbf{p}_3\}, \quad \{\mathbf{r}, \mathbf{q}_3, \mathbf{p}_3, \mathbf{p}_1\}, \quad \{\mathbf{r}, \mathbf{q}_3, \mathbf{q}_1, \mathbf{p}_1\}, \\ &\{\mathbf{r}, \mathbf{p}_1, \mathbf{p}_2, \mathbf{p}_3\}. \end{aligned}$$

See Figure 4.23 for a view of the triangulation where the tetrahedron $\mathbf{p}_1 \mathbf{p}_2 \mathbf{q}_1 \mathbf{q}_2$ has been detached. If we delete point r and all the simplices of \mathcal{T} using it, we are left with only the tetrahedra $\mathbf{p}_1 \mathbf{p}_2 \mathbf{q}_1 \mathbf{q}_2$, $\mathbf{p}_2 \mathbf{p}_3 \mathbf{q}_2 \mathbf{q}_3$ and

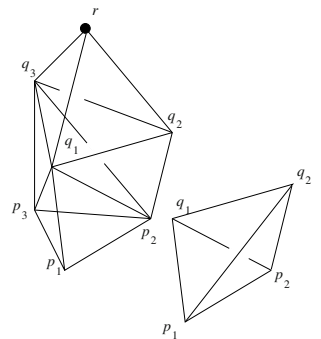


Figure 4.23: Triangulation \mathcal{T} shown with a detached tetrahedron $\mathbf{p}_1 \mathbf{p}_2 \mathbf{q}_1 \mathbf{q}_2$.

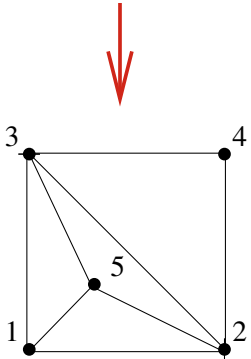
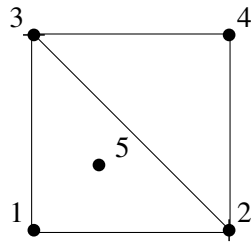


Figure 4.24: A regular triangulation of $\mathbf{A} \setminus 5$ extends to a regular triangulation of \mathbf{A} .

p₁p₃q₁q₃. The resulting object comes from twisting a prism, thus these tetrahedra are almost flat as they were rectangles before the twisting. The non-convex subregion of $\text{conv}(\mathbf{A})$ that is not covered by these tetrahedra is the *Schönhardt polyhedron*. As we discussed in Chapter 3, it is famous for not having any triangulation (unless you allow yourself to insert additional vertices). That is to say:

There is no triangulation of $\mathbf{A} \setminus \mathbf{r}$ that extends the subcomplex of \mathcal{T} not using \mathbf{r} .

Thus the deletion will, in general, yield only a canonical partial subdivision that may not be a subset of any full subdivision. This is a big difference to the two-dimensional case where all partial subdivisions can be completed.

The reader probably has noticed the similarity of Figures 4.23 and 2.24. This indicates that non-regularity plays a role in Example 4.2.16. This is indeed the case, as the following lemma shows:

Lemma 4.2.17. *If \mathcal{S} is a regular subdivision of \mathbf{A} and $i \in \mathbf{A}$ is one of its points (meaning that there is a cell in \mathcal{S} with i in it), then*

- *there is a subdivision of $\mathbf{A} \setminus i$ that uses all the cells of \mathcal{S} that do not contain i .*
- *If \mathcal{S} is a regular triangulation, the same statement holds with a regular triangulation of $\mathbf{A} \setminus i$.*

Proof. If ω is a height vector that produces \mathcal{S} , forgetting the entry of ω corresponding to point i gives a height vector that produces the desired regular subdivision of \mathbf{A} . If \mathcal{S} is a triangulation, assume ω sufficiently generic and this gives a triangulation of $\mathbf{A} \setminus i$. Details are left to the reader. \square

Observe, however, that, even in the case of regular subdivisions the deletion process is not unique: different choices of ω in the proof of the lemma may give different subdivisions of $\mathbf{A} \setminus i$ even if they give the same one in \mathbf{A} . For an extreme example, suppose that \mathbf{A} is in general position in the plane and that \mathcal{S} is the regular triangulation obtained by “pulling” i in the trivial subdivision of \mathbf{A} . Then, *all* the subdivisions of $\mathbf{A} \setminus i$ will do the job.

Please observe that, in some special situations, the assumption of regularity in Lemma 4.2.17 is not necessary. For instance, in dimension two, the extended validity of Lemma 4.2.17 actually plays a crucial role in the proof of Theorem 3.3.6. Similarly, for *cyclic polytopes*, in Section 6.1.5 we will discuss a canonical way to obtain a triangulation of the deletion from any triangulation of the whole cyclic point configuration.

Example 4.2.18. Looking again at Example 4.1.4, we can compute all circuits and cocircuits of $\mathbf{A} \setminus 5$. The only circuit remaining is $(14, 23)$. While the cocircuits are now $(24, \emptyset), (12, \emptyset), (2, 3), (1, 4), (34, \emptyset), (13, \emptyset)$.

4.2.4 Contraction

By contracting \mathbf{A} at a point or vector $\mathbf{p}_i \in \mathbf{A}$ we essentially mean “projecting towards \mathbf{p}_i ”. We begin with a very general definition.

Definition 4.2.19. Let $\mathbf{A} \subset \mathbb{R}^m$ be a vector configuration (or a point configuration, but in homogeneous coordinates). Let i be one of its elements, and \mathbf{p}_i be the corresponding column of \mathbf{A} , assumed not to be zero.

Let $\pi : \mathbb{R}^m \rightarrow \mathbb{R}^{m-1}$ be any linear surjective map that sends \mathbf{p}_i to zero. We call the configuration

$$\mathbf{A}/i := (\pi(\mathbf{p}_j))_{j \in J \setminus \{i\}}.$$

the *contraction of \mathbf{A} at i* , and denote it by \mathbf{A}/i (see Figure 4.25 for an example of a contraction). That is, in matrix notation, \mathbf{A}/i equals $\pi\mathbf{A}$, with the (now zero) column corresponding to i deleted.

The properties of the contraction operation are sort of opposite to those in the deletion case. (Almost) every subdivision of \mathbf{A} produces a subdivision of \mathbf{A}/i by taking the link at i , while only regular subdivisions of \mathbf{A}/i are guaranteed to be links of some subdivision of \mathbf{A} in general.

Lemma 4.2.20. Let \mathcal{S} be a subdivision of \mathbf{A} that uses the element $i \in J$ (meaning that there is a cell $B \in \mathcal{S}$ with $i \in B \in \mathcal{S}$). Then:

1. $\text{link}_{\mathcal{S}}(i)$ is a subdivision of \mathbf{A}/i .
2. If \mathcal{S} is regular, then $\text{link}_{\mathcal{S}}(i)$ is regular.
3. If \mathcal{S} is a triangulation, then $\text{link}_{\mathcal{S}}(i)$ is a triangulation.

Proof. Again, all statements are easy. For the regularity, the same height function that gives \mathcal{S} on \mathbf{A} gives $\text{link}_{\mathcal{S}}(i)$ in \mathbf{A}/i , as long as we take $\omega(i) = 0$ in the former. \square

Corollary 4.2.21. The operation “take the link at point i ” is a well-defined and order-preserving map from the subposet of $\text{Subdivs}(\mathbf{A})$ consisting of subdivisions that use i to the poset $\text{Subdivs}(\mathbf{A}/i)$.

Observe that if i is extremal (that is, a vertex of $\text{conv}(\mathbf{A})$ and not repeated as an element of \mathbf{A}), then the subposet referred to in the statement is the whole $\text{Subdivs}(\mathbf{A})$.

Corollary 4.2.22. Let i be an element of \mathbf{A} , then every flip between two triangulations \mathcal{T}_1 and \mathcal{T}_2 does one and only one of the following things:

1. Makes the element i appear or disappear.
2. Preserves the link at i , or
3. Produces a flip between the triangulations $\text{link}_{\mathcal{T}_1}(i)$ and $\text{link}_{\mathcal{T}_2}(i)$ of \mathbf{A}/i .

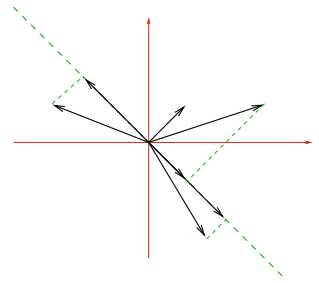


Figure 4.25: The contraction at point i consists of 3 collinear vectors.

Proof. We assume that $\text{link}_{\mathcal{T}_1}(i) \neq \text{link}_{\mathcal{T}_2}(i)$ and that neither of the two are empty, or otherwise we are clearly in one (and only one) of the first two cases. By the previous corollary, $\text{link}_{\mathcal{T}_1}(i)$ and $\text{link}_{\mathcal{T}_2}(i)$ are two different triangulations of \mathbf{A}/i . Now, let \mathcal{T} be the “flip”, that is, the subdivision of \mathbf{A} that is only refined by \mathcal{T}_1 and \mathcal{T}_2 . Again by the previous corollary, $\text{link}_{\mathcal{T}}(i)$ is a subdivision of \mathbf{A}/i only refined by $\text{link}_{\mathcal{T}_1}(i)$ and $\text{link}_{\mathcal{T}_2}(i)$, so it is a flip between them. \square

Example 4.2.23 (Example 3.6.16 continued). We wish to illustrate how to use the contraction to count flips. Let us explicitly compute the flips in the triangulation of Example 3.6.16. Recall that our point set and triangulation were:

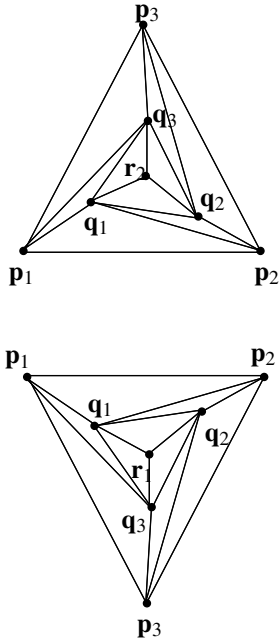


Figure 4.26: The links of r_1 (bottom) and r_2 (top).

$$\mathbf{A} = \begin{pmatrix} \mathbf{p}_1 & \mathbf{p}_2 & \mathbf{p}_3 & \mathbf{q}_1 & \mathbf{q}_2 & \mathbf{q}_3 & \mathbf{r}_1 & \mathbf{r}_2 \\ 4-\varepsilon & 0 & \varepsilon & 2 & 1 & 1 & 4/3 & 4/3 \\ \varepsilon & 4-\varepsilon & 0 & 1 & 2 & 1 & 4/3 & 4/3 \\ 0 & \varepsilon & 4-\varepsilon & 1 & 1 & 2 & 4/3 & 4/3 \\ 0 & 0 & 0 & 1 & 1 & 1 & -10 & 10 \end{pmatrix}.$$

and

$$\mathcal{T} = \left\{ \begin{array}{l} \{\mathbf{r}_1, \mathbf{r}_2, \mathbf{q}_1, \mathbf{q}_2\}, \{\mathbf{r}_1, \mathbf{r}_2, \mathbf{q}_1, \mathbf{q}_3\}, \{\mathbf{r}_1, \mathbf{r}_2, \mathbf{q}_2, \mathbf{q}_3\}, \\ \{\mathbf{r}_1, \mathbf{q}_1, \mathbf{q}_2, \mathbf{p}_2\}, \{\mathbf{r}_1, \mathbf{q}_1, \mathbf{p}_1, \mathbf{p}_2\}, \{\mathbf{r}_2, \mathbf{q}_1, \mathbf{q}_2, \mathbf{p}_2\}, \{\mathbf{r}_2, \mathbf{q}_1, \mathbf{p}_1, \mathbf{p}_2\} \\ \{\mathbf{r}_1, \mathbf{q}_2, \mathbf{q}_3, \mathbf{p}_3\}, \{\mathbf{r}_1, \mathbf{q}_2, \mathbf{p}_2, \mathbf{p}_3\}, \{\mathbf{r}_2, \mathbf{q}_2, \mathbf{q}_3, \mathbf{p}_3\}, \{\mathbf{r}_2, \mathbf{q}_2, \mathbf{p}_2, \mathbf{p}_3\} \\ \{\mathbf{r}_1, \mathbf{q}_3, \mathbf{q}_1, \mathbf{p}_1\}, \{\mathbf{r}_1, \mathbf{q}_3, \mathbf{p}_3, \mathbf{p}_1\}, \{\mathbf{r}_2, \mathbf{q}_3, \mathbf{q}_1, \mathbf{p}_1\}, \{\mathbf{r}_2, \mathbf{q}_3, \mathbf{p}_3, \mathbf{p}_1\} \end{array} \right\}.$$

Now, every flip removes at least one tetrahedron from the list. Since every tetrahedron uses one (or both) of \mathbf{r}_1 and \mathbf{r}_2 , every flip will appear as a flip in one (or both) of the two links $\text{link}_{\mathcal{T}}(\mathbf{r}_1)$, $\text{link}_{\mathcal{T}}(\mathbf{r}_2)$. To draw the links we recall the observation that the six points \mathbf{p}_i and \mathbf{q}_i project vertically to a perturbation of “the mother of all examples” with one of its two parallel triangles slightly rotated. Since \mathbf{r}_1 and \mathbf{r}_2 are relatively far along the axis of this projection, the same is true for the contractions at them. That is, the contractions look like the top and bottom parts of Figures 4.26 respectively. There we see that each of the links has exactly four flips: one that removes the central point and three edge flips on the three sides. We only need to check which of them are contractions of flips in \mathcal{T} . For this let us list the circuits involved in these flips (remark: each circuit C in \mathbf{A}/i gives either C or $C \cup i$ as an unoriented circuit in \mathbf{A} . Moreover, the former can only happen if \mathbf{A} is not in general position). The list contains seven instead of eight circuits because the first one gives a flip in both links:

$$\begin{aligned} & (\{\mathbf{r}_1, \mathbf{r}_2\}, \{\mathbf{q}_1, \mathbf{q}_2, \mathbf{q}_3\}), \\ & (\{\mathbf{q}_1, \mathbf{p}_2\}, \{\mathbf{r}_2, \mathbf{p}_1, \mathbf{q}_2\}), \quad (\{\mathbf{r}_1, \mathbf{q}_1, \mathbf{p}_2\}, \{\mathbf{p}_1, \mathbf{q}_2\}), \\ & (\{\mathbf{q}_2, \mathbf{p}_3\}, \{\mathbf{r}_2, \mathbf{p}_2, \mathbf{q}_3\}), \quad (\{\mathbf{r}_1, \mathbf{q}_2, \mathbf{p}_3\}, \{\mathbf{p}_2, \mathbf{q}_3\}), \\ & (\{\mathbf{q}_3, \mathbf{p}_1\}, \{\mathbf{r}_2, \mathbf{p}_2, \mathbf{q}_1\}), \quad (\{\mathbf{r}_1, \mathbf{q}_3, \mathbf{p}_1\}, \{\mathbf{p}_2, \mathbf{q}_1\}). \end{aligned}$$

The first and second columns differ only in that \mathbf{r}_1 appears on the positive part of the circuit while \mathbf{r}_2 lies on the negative part. This reflects the fact that the triangles $\{\mathbf{q}_i, \mathbf{q}_{i+1}, \mathbf{p}_{i+1}\}$ and $\{\mathbf{q}_i, \mathbf{p}_i, \mathbf{p}_{i+1}\}$ in their common link

are folded convex when seen from \mathbf{r}_2 and concave from \mathbf{r}_1 . This difference makes the circuits in the right column not support flips in \mathcal{T} , since the almost-flat tetrahedra $\{\mathbf{q}_i, \mathbf{q}_{i+1}, \mathbf{p}_i, \mathbf{p}_{i+1}\}$ would need to be in \mathcal{T} for that. So, as we claimed in Example 3.6.16, only the four circuits in the left column support flips.

Lemma 4.2.24. *If \mathcal{S} is a regular subdivision of \mathbf{A}/i , then there is a regular subdivision of \mathbf{A} that has \mathcal{S} as its link at i .*

Proof. Consider the height function ω that defines the regular subdivision \mathcal{S} of \mathbf{A}/i . Lift the configuration $\mathbf{A} \setminus i \subset \mathbb{R}^d$ to \mathbb{R}^{d+1} using exactly the same heights. Finally, lift the point i to a point i^0 at height zero. We claim that the regular subdivision we produced from these values has its link at i equal to \mathcal{S} . Indeed, a face \mathbf{F} in the link of i must be supported by a hyperplane \mathbf{H} with normal vector f . Now, for each point $b \in \mathbf{F}$ its lifting b^ω is projected, by the projection orthogonal to i , onto its lift $\pi(b)^\omega$, while f is still projected onto itself because f is perpendicular to i^0 . Thus the normal vectors inducing supporting hyperplanes are all still supporting hyperplanes in the orthogonal projection. \square

To show that regularity is needed in this result, we use essentially the same example as in the case of the deletion.

Example 4.2.25. Let \mathbf{A} be the point configuration of Example 4.2.23 (the continuation of Example 3.6.16). We delete the point \mathbf{r}_1 from the configuration

$$\mathbf{B} = \mathbf{A} \setminus \mathbf{r}_1 = \begin{pmatrix} \mathbf{p}_1 & \mathbf{p}_2 & \mathbf{p}_3 & \mathbf{q}_1 & \mathbf{q}_2 & \mathbf{q}_3 & \mathbf{r}_2 \\ 4 - \varepsilon & 0 & \varepsilon & 2 & 1 & 1 & 4/3 \\ \varepsilon & 4 - \varepsilon & 0 & 1 & 2 & 1 & 4/3 \\ 0 & \varepsilon & 4 - \varepsilon & 1 & 1 & 2 & 4/3 \\ 0 & 0 & 0 & 1 & 1 & 1 & 10 \end{pmatrix}.$$

The first six points of \mathbf{B} define the vertices of the prism obtained by truncating, at point $(2, 2, 2)$, the triangle-based pyramid that results as the convex hull of the first six points above and $(2, 2, 2)$. Since point r_2 is further above this apex, the contraction of this configuration is exactly “the mother of all examples”, that is, the vertex set of two concentric triangles in a plane. We consider the following simplices with vertices among the points of $\mathbf{B} \setminus \mathbf{r}_2$:

$$\mathcal{T} = \{\mathbf{q}_1 \mathbf{q}_2 \mathbf{q}_3, \mathbf{p}_1 \mathbf{p}_2 \mathbf{q}_1, \mathbf{p}_2 \mathbf{q}_1 \mathbf{q}_2, \mathbf{p}_2 \mathbf{p}_3 \mathbf{q}_2, \mathbf{p}_3 \mathbf{q}_2 \mathbf{q}_3, \mathbf{p}_1 \mathbf{p}_3 \mathbf{q}_3, \mathbf{p}_1 \mathbf{q}_1 \mathbf{q}_3\}.$$

If this was the correct link of a certain triangulation (or subdivision) \mathcal{S} of \mathbf{B} , \mathcal{S} would consist of $\mathcal{T} * \mathbf{r}_2$ plus a certain triangulation (or subdivision) of the prism $\text{conv}(\{\mathbf{B} \setminus \mathbf{r}_2\})$ with the property of using the three diagonals $\mathbf{p}_2 \mathbf{q}_1$, $\mathbf{p}_3 \mathbf{q}_2$, and $\mathbf{p}_1 \mathbf{q}_3$ of the prism. But the prism does not have any triangulation using this cyclic set of diagonals. Hence:

There is no triangulation of \mathbf{B} that extends the triangulation \mathcal{T} of the link at \mathbf{r}_2 .

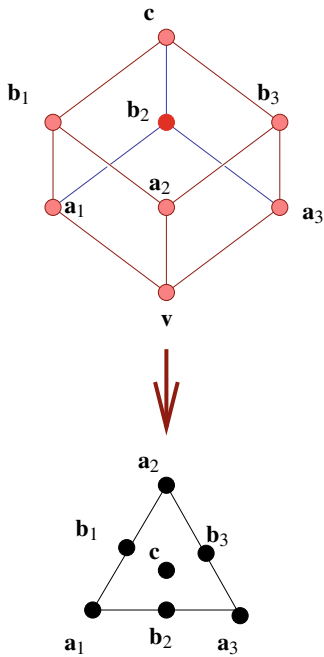


Figure 4.27: The homogeneous contraction of vertex v of a regular cube.

To better appreciate the concept of contraction it is worth looking at a related construction.

Definition 4.2.26. Let $\mathbf{A} = (\mathbf{p}_j)_{j \in J}$ be a point configuration in \mathbb{R}^d and let i be one of its extreme elements. That is, assume that $\{i\}$ is a face of \mathbf{A} .

Let \mathbf{H} be any hyperplane that separates \mathbf{p}_i from the rest of the configuration. Let $\pi : J \setminus \{i\} \rightarrow \mathbf{H}$ be the central projection that sends each element $j \in J \setminus \{i\}$ to \mathbf{H} . That is, geometrically, $\pi(j) = \mathbf{H} \cap [\mathbf{p}_i \mathbf{p}_j]$, for each j ; but recall that \mathbf{A} may have repeated points, which will still be repeated by π .

We call the *homogeneous contraction* of \mathbf{A} at i the resulting point configuration

$$\mathbf{A}/\!/i := (\pi(j))_{j \in J \setminus \{i\}}.$$

Remark 4.2.27. $\mathbf{A}/\!/i$ has one less element and rank one less than \mathbf{A} . Even if \mathbf{A} does not have multiple points, $\mathbf{A}/\!/i$ may have them (for instance, points of \mathbf{A} lying on the same ray from i).

Example 4.2.28. If we do the homogeneous contraction of the point configuration formed by the vertices of a regular cube at any one of its vertices, say vertex v in Figure 4.27, we will obtain a point configuration bounded by a triangle, with a point in its center representing the point antipodal to v and three more vertices along the edges representing vertices of the cube opposite to v along each of the three facets containing v .

Strictly speaking, the definition of the homogeneous contraction is not unique, since the point configuration obtained depends on the choice of the hyperplane \mathbf{H} . But different choices produce configurations which are projectively equivalent and, in particular, have the same subdivisions and triangulations (See Appendix 2.6 of [339] for a description of projective transformations and projective equivalence). Also, readers familiar with polytope theory should keep in mind that the homogeneous contraction is a generalization of the *vertex figures* (see Lecture 2 in [339]).

Now we explain what the homogeneous contraction has to do with the contraction we defined at the beginning.

Remark 4.2.29. Assume that \mathbf{A} is configuration of points in \mathbb{R}^d , given in homogeneous coordinates as a $(d+1) \times n$ matrix via the addition of a constant row of 1's to the coordinates of the points. Let $\pi : \mathbb{R}^{d+1} \rightarrow \mathbb{R}^d$ be the projection with matrix

$$\pi = (\mathbf{I} \quad -\mathbf{p}_i),$$

where \mathbf{I} is the identity $d \times d$ matrix and \mathbf{p}_i is the point at which we want to take the contraction, without its last homogenization coordinate.

The contraction $\mathbf{A}/i := \pi\mathbf{A}$ has as columns

$$\{ \mathbf{p}_j - \mathbf{p}_i : j \in J \setminus \{i\} \},$$

where \mathbf{p}_j denotes the j -th point of \mathbf{A} . Then, the homogeneous contraction of \mathbf{A} , considered as a homogeneous configuration, is obtained from the linear contraction \mathbf{A}/i by just scaling each column by a positive scalar λ_i in such a way that the scaled points $\lambda_i(\mathbf{p}_j - \mathbf{p}_i)$ are coplanar.

Finally, there is a rather useful duality relation between the deletion and contraction operations:

Lemma 4.2.30. *Let $\mathbf{A} \in \mathbb{R}^{m \times n}$ be a vector configuration of rank k with n elements. Suppose \mathbf{p} is a vector of the configuration. Then $\text{Gale}(\mathbf{A}/\mathbf{p})$ is equal to $\text{Gale}(\mathbf{A}) \setminus \mathbf{p}$.*

Proof. By construction, any Gale transform of \mathbf{A} consists of the rows of a matrix \mathbf{B} , such that $\mathbf{AB} = 0$, while the contraction of \mathbf{p} is given by a matrix π projecting \mathbf{A} where \mathbf{p} is projected to the origin. This means that \mathbf{B} minus the row corresponding to \mathbf{p} is still a Gale transform for $\pi\mathbf{A}$. \square

Corollary 4.2.31. *The circuits (cocircuits) of the contraction \mathbf{A}/\mathbf{p} are the cocircuits (circuits) of any element of $\text{Gale}(\mathbf{A}) \setminus \mathbf{p}$.*

4.2.5 One-point suspension

In this section we will meet another operation that behaves quite well with respect to the space of all subdivisions.

Definition 4.2.32. Let \mathbf{A} be a configuration in \mathbb{R}^m with label set J . Let $i \in J$ be an element, whose corresponding column is \mathbf{p}_i .

Then the *standard one-point suspension* $\mathbf{A} \uparrow_i^i$ of \mathbf{A} over i is given as

$$\mathbf{A} \uparrow_i^i := \begin{pmatrix} J \setminus i & i_1 & i_2 \\ \mathbf{A} \setminus \mathbf{p}_i & \mathbf{p}_i & \mathbf{p}_i \\ \mathbf{0} & 1 & -1 \end{pmatrix}.$$

Any point configuration combinatorially equivalent to the standard one-point suspension of \mathbf{A} will be called a *one-point suspension* of \mathbf{A} .

The general picture for a one-point suspension is as follows: Suppose that \mathbf{A} lies in a linear hyperplane \mathbf{H} . Let \mathbf{q} and \mathbf{r} be vectors outside \mathbf{H} with

$$\mathbf{p}_i \in \text{relint}(\{\mathbf{q}, \mathbf{r}\}).$$

The *one-point suspension* of \mathbf{A} over the element i , denoted by $\mathbf{A} \uparrow_i^i$ is the following configuration:

$$\mathbf{A} \uparrow_i^i := \begin{pmatrix} J \setminus i & i_1 & i_2 \\ \mathbf{A} \setminus \mathbf{p}_i & \mathbf{q} & \mathbf{r} \end{pmatrix}.$$

See Figure 4.28 for an example. Observe that in the general definition i need not be an interior point. The assumption that \mathbf{A} lies in a hyperplane is not relevant, since we can always embed \mathbb{R}^d as a hyperplane in \mathbb{R}^{d+1} .

This operation is, in a sense, an inverse of the contraction: contracting either of the two new points i_1 or i_2 in $\mathbf{A} \uparrow_i^i$ we recover exactly the configuration \mathbf{A} (check it!). Even if the operation seems too specific and perhaps less natural than both deletion and contraction, it has the following very nice feature:

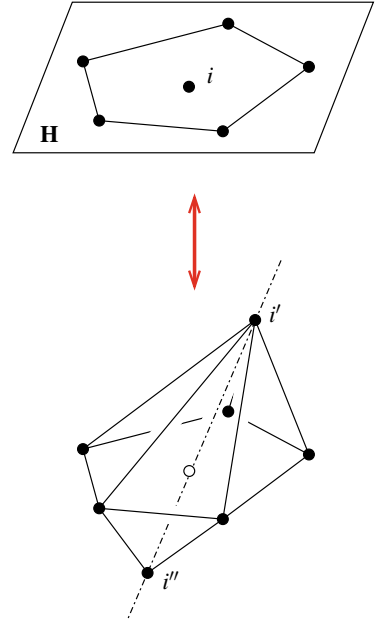


Figure 4.28: The one-point suspension construction.

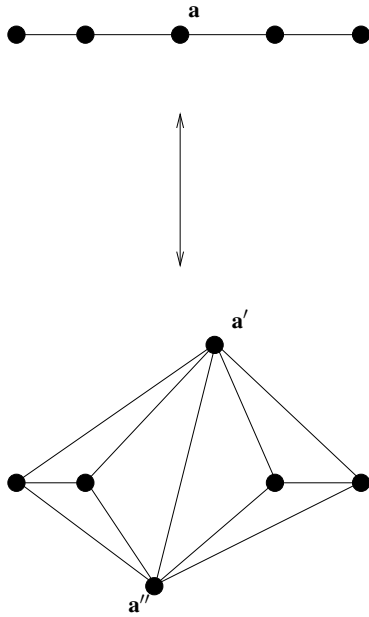


Figure 4.29: The one-point suspension construction.

Theorem 4.2.33. *The posets $\text{Subdiv}(\mathbf{A})$ and $\text{Subdiv}(\mathbf{A}_{\downarrow i}^i)$ are isomorphic. The isomorphism always maps triangulations to triangulations, lexicographic ones to lexicographic ones, and regular subdivisions to regular subdivisions.*

Proof. The isomorphism sends each subdivision \mathcal{S} of \mathbf{A} to the subdivision $\mathcal{S}_{\downarrow i}^i$ consisting of the following cells:

- The cells $B \cup \{i_1\}$ and $B \cup \{i_2\}$ for every cell $B \in \mathcal{S}$ with $i \notin B$.
- The cell $B \cup \{i_1, i_2\}$ for each cell $B \cup \{i\} \in \mathcal{S}$ containing i .

Said differently: $\mathcal{S}_{\downarrow i}^i$ consists of the link of i in \mathcal{S} joined to the segment $\{i_1, i_2\}$, together with the anti-star of i in \mathcal{S} joined to the vertices $\{i_1\}$ and $\{i_2\}$. See Figure 4.29 for an example. It is easy, and left to the reader, to check that $\mathcal{S}_{\downarrow i}^i$ is a polyhedral subdivision of $\mathbf{A}_{\downarrow i}^i$. That this process induces a bijection, preserving order in both directions, follows from the fact that taking the link at i_1 in a subdivision of $\mathbf{A}_{\downarrow i}^i$ can always be done and is the inverse operation.

That the bijection preserves regularity can be easily proved if we restrict our attention to height functions on \mathbf{A} and $\mathbf{A}_{\downarrow i}^i$ that give height zero to the three special points i, i_1 and i_2 . In this way the spaces of height functions on both configurations are identified to one another, and the height functions producing a regular subdivision \mathcal{S} on \mathbf{A} will produce the regular subdivision $\mathcal{S}_{\downarrow i}^i$ on $\mathbf{A}_{\downarrow i}^i$.

Finally, that triangulations are sent to triangulations is straightforward from the definition of $\mathcal{S}_{\downarrow i}^i$. \square

In fact, there is an easier way to see that the one-point suspension does not change the refinement poset of *regular* subdivisions. This, however, requires tools from Chapter 5 that utilize the Gale transformation (see Section 4.1.3). At this point, we prepare this by investigating what a Gale transform of the one-point suspension $\mathbf{A}_{\downarrow i}^i$ of \mathbf{A} at point $i \in J$ looks like. The result will be strikingly simple.

The following considerations provide an excellent example for computing Gale transforms without calculating: We only use Lemma 4.1.38 in our reasoning. First of all, the one-point suspension contains two versions i_1 and i_2 of point i with the following property (you prove this in Exercise 4.11):

- Whenever i is in a dependence vector V of \mathbf{A} with $i \in V_+$, then there is a dependence vector $V_{\downarrow i}^i$ in $\mathbf{A}_{\downarrow i}^i$ with $i_1, i_2 \in (V_{\downarrow i}^i)_+$.
- There are no other dependence vectors containing i_1 or i_2 .

This means that, by Lemma 4.1.38, in any Gale transform of $\mathbf{A}_{\downarrow i}^i$, any cocircuit with i_1 or i_2 in its zero-set has both i_1 and i_2 in its zero-set. In other words, every hyperplane that contains one of i_1 or i_2 contains both. This means that there is no hyperplane separating i_1 and i_2 . This is only possible when i_1 and i_2 are parallel vectors in the Gale transform. Therefore, we can assume, without loss of generality on oriented matroid level, that i_1 and i_2 is a repeated element.

We summarize:

Proposition 4.2.34. *A Gale transform of the one-point suspension $\mathbf{A} \uparrow_i^j$ is, up to combinatorial equivalence, obtained by doubling element i in a Gale transform of \mathbf{A} and labeling the repeated element by i_1 and i_2 , respectively.*

□

In Exercise 5.21 you will apply this together with the tools of Chapter 5 to obtain an almost obvious proof of the bijection of Theorem 4.2.33 in the regular case.

As said at the beginning, although in our examples so far we apply the one point suspension to an interior point, it can be applied to any point in the configuration. See Figure 4.30.

Moreover, iterating the construction gives rise to the following nice examples, the details of which will be subject of Exercise 4.12:

- If the one-point suspension is applied three times to the configuration consisting on three copies of the same point (one time on each of the original points), the result is the vertex set of an octahedron. More generally, if it is applied d times to d copies of the same point, it gives the configuration $\{\pm \mathbf{e}_1, \dots, \pm \mathbf{e}_d\}$ in \mathbb{R}^d . This is the vertex set of the so-called *cross-polytope* of dimension d . In the exercise you will—among other things—show that the (regular) cross-polytope has exactly d triangulations, each using a different diameter (edge joining two opposite vertices) of it.
- If it is applied to the interior point in the configuration of Example 4.1.4 it produces a non-regular octahedron. Hence, this non-regular octahedron has four triangulations (as opposed to the regular octahedron, which has three). There are octahedra with six triangulations, but no more; see Section 5.5.
- If it is applied to an independent configuration, it produces an independent configuration of one more dimension. No surprise, since both have exactly one triangulation. Similarly, when applied to a circuit it produces a circuit of one dimension more.

More interestingly, when the one-point suspension is applied to a non-extreme element of an acyclic configuration, it produces a configuration with one less non-extreme element (since i_1 and i_2 are extreme elements of $\mathbf{A} \uparrow_i^j$). In particular, the one-point suspension applied to all the non-extreme points of an arbitrary point configuration \mathbf{A} one by one produces a configuration in convex position (the vertex set of a polytope) with exactly the same set of triangulations and subdivisions as \mathbf{A} . That is to say:

Theorem 4.2.35. *Let \mathbf{A} be an arbitrary point configuration, of dimension d and with n elements. Let v be the number of elements of \mathbf{A} that are extremal.*

Then there is a point configuration $\tilde{\mathbf{A}}$ in convex position, of dimension $d + n - v$ and with $2n - v$ elements such that $\text{Subdivs}(\mathbf{A})$ and $\text{Subdivs}(\tilde{\mathbf{A}})$ are isomorphic as posets. The bijection between them preserves regularity.

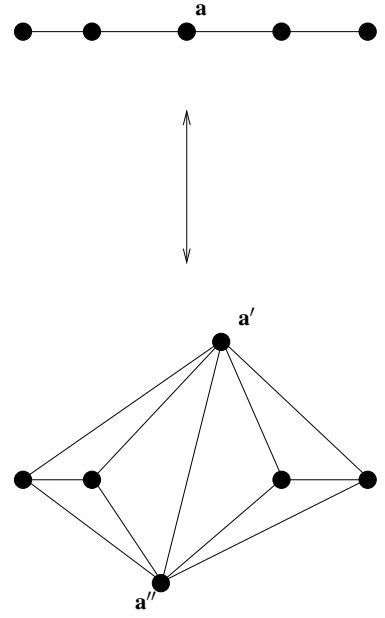


Figure 4.30: A one-point suspension of an extreme point.

Put differently: Unless you are interested in a fixed dimension, the study of subdivisions of point configurations in convex position cannot be considered to be simpler than the same for arbitrary point configurations.

Observe that a point configuration in convex position cannot have repeated points (see Remark 2.1.21). Also, note that in convex position the “bullet-proof” definition of subdivision via labeled cells is equivalent to the more geometric one of Section 2.2. Thus, Theorem 4.2.35 is a new justification for the conceptual approach used in this book: Without this approach, sets in non-convex position would give rise to new, more complicated, spaces of subdivisions.

4.3 Generating polyhedral subdivisions

The concept of regular subdivision allows us to easily construct triangulations of any (point or vector) configuration: Given a configuration \mathbf{A} with label set J , choose a random height function $\omega : J \rightarrow \mathbb{R}$ and compute the convex hull of the lifted point set to extract from it the regular subdivision $\mathcal{S}(\mathbf{A}, \omega)$. Typically, the subdivision will be a triangulation (see Part 1 of Lemma 2.3.15). If it is not, you can still “perturb” the height vector ω (as in part 3 of the same Lemma). In this section, we revisit two combinatorial ways of constructing triangulations. We saw already particular cases in Chapter 3, but here we present their general definition valid in all dimensions:

4.3.1 The placing (or pushing) triangulation

Let \mathbf{A} be a configuration of dimension d and $i \in J$ be one of its elements. In these conditions, we say that a face F of $J \setminus \{i\}$ is *visible* from i if there is a linear functional which is zero on F , positive on i and negative on the rest of J . Put differently, visible faces are those that have a supporting hyperplane \mathbf{H} separating the point \mathbf{p}_i labeled by i from $\text{relint}(J \setminus i)$. We say that a set $B \subset J \setminus i$ is visible from i if it is contained in some face visible from i . Since faces of visible faces are visible, this is equivalent to saying that the carrier of B is visible from i . Another characterization more related to our definition of subdivisions is:

Lemma 4.3.1. *Let F be a face of $J \setminus i$ and let point \mathbf{x} be in the relative interior of F . Then F is visible from a point \mathbf{p}_i if and only if the segment $[\mathbf{x}, \mathbf{p}_i]$ intersects $\text{conv}(J \setminus i)$ only at \mathbf{x} .*

Observe in particular that if $\mathbf{p}_i \in \text{conv}(J \setminus i)$ then no face is considered visible. That is, when we say “visible” we mean “externally visible”.

Proof. For Part (i), when F is visible from i then, for any point \mathbf{x} in its relative interior, the line segment $[\mathbf{x}, \mathbf{p}_i]$ is also separated by a supporting hyperplane. Thus the one-point intersection condition is necessary. For the converse, let us proceed by contradiction. Suppose F is not visible from i , then consider that the intersection \mathbf{M} of all supporting half-spaces whose hyperplane supports F must contain the point \mathbf{p}_i . But then any line segment $[\mathbf{x}, \mathbf{p}_i]$ must cross the interior of $\text{conv}(J \setminus i)$, a contradiction.

Part (ii) follows easily from Part (i) because the intersection

$$\text{relint}(\text{conv}(B \cup \{i\})) \cap \text{conv}(J \setminus i) = \emptyset$$

is non-empty precisely when, for some \mathbf{x} , the line segment $[\mathbf{x}, \mathbf{p}_i]$ intersects $\text{conv}(J \setminus i)$ at a point other than \mathbf{x} . \square

Lemma 4.3.2. Let $\mathbf{A} \setminus i$ denote the configuration obtained by deleting the element i from \mathbf{A} (that is, by deleting the column labeled i , if \mathbf{A} is represented as a matrix). Let \mathcal{T} be a subdivision of $\mathbf{A} \setminus i$.

Then, the following is a subdivision of \mathbf{A} and it is the only one that extends (i.e., contains) \mathcal{T} .

$$\mathcal{T}' := \mathcal{T} \cup \{B \cup \{i\} : B \in \mathcal{T} \text{ and is visible from } i\}.$$

Observe that another description is that the new subdivision \mathcal{T}' is equal to \mathcal{T} together with the join of i and the subcomplex of \mathcal{T} visible from i . Observe also that if \mathcal{T} is a triangulation then \mathcal{T}' is a triangulation too.

Proof. If i lies in $\text{conv}(J \setminus i)$, then \mathcal{T} is already a subdivision of \mathbf{A} and we cannot add anything to it without violating the proper intersection property of subdivisions. If $J \setminus i$ has smaller rank than i then every subdivision of \mathbf{A} is obtained by joining a subdivision of $\mathbf{A} \setminus i$ to i , by Lemma 2.2.2, and the result is also true.

In the general case, it is intuitively clear that \mathcal{T}' is indeed a subdivision of \mathbf{A} , but we postpone a formal proof of it until Section 4.3.4 (Lemma 4.3.10), where this statement is generalized. What is easy to prove is that no other subdivision satisfies the required properties. Indeed, any such subdivision must consist of all of \mathcal{T} plus some sets of the form $B \cup \{i\}$. The closure property implies that the set $B \subseteq J \setminus \{i\}$ is then a simplex in \mathcal{T} , and for \mathcal{T}' to satisfy the intersection property, B must be visible from i , by Lemma 4.3.1. \square

Definition 4.3.3 (Placing, or pushing, subdivision). The subdivision \mathcal{T}' of the previous lemma is said to be obtained by *placing* i in the subdivision \mathcal{T} of $\mathbf{A} \setminus i$. The triangulation of \mathbf{A} obtained by placing its points one by one in a certain order is called the *placing*, or *pushing* triangulation of \mathbf{A} for that order. (The starting step is the unique “triangulation of the first point”).

The insertion ordering of the points in the placing process can be given by some geometric property (e.g., a “sweep-hyperplane ordering” is the ordering by a linear functional), or it may be completely arbitrary. Figure 4.31 shows an example of the process.

Lemma 4.3.4. Let \mathbf{A} be a configuration, with labels $J = \{1, \dots, n\}$. There is a constant $c_0 > 0$ such that the pushing triangulation of \mathbf{A} (for the ordering given by the labels) equals the regular triangulation obtained by taking any height vector $\omega : J \rightarrow \mathbb{R}$ with $\omega(i+1) > \omega(i)c_0 > 0$ for all i .

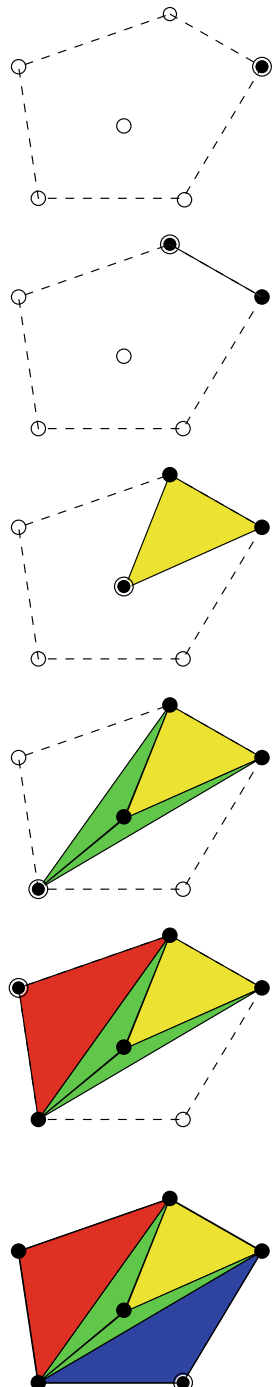


Figure 4.31: A placing triangulation. At each step we mark the new point being placed.

Loosely speaking, this statement can be rephrased as “the pushing triangulation is the regular triangulation obtained by lifting the points in a certain order, with each newly lifted point sufficiently higher than the previous ones”.

Proof. Let \mathcal{T}_2 be a regular subdivision of \mathbf{A} obtained as in the statement, for a certain constant. We will present a particular c that makes \mathcal{T}_2 equal to the placing triangulation. We proceed by induction on the number of vertices. The statement holds for dimension many vertices. By the inductive hypothesis on the number of vertices, we assume that there is a constant $c_0 > 0$ such that, if $c > c_0$, then the placing triangulation \mathcal{T} of $\mathbf{A} \setminus \mathbf{p}_n$ equals the regular triangulation for the heights $(\omega(1), \dots, \omega(n-1))$ that satisfy $\omega(i+1) > \omega(i)c > 0$ for all i .

For each maximal simplex $B \in \mathcal{T}$, we claim that there is a constant c_B such that, if $c > c_B$, then B is a simplex in \mathcal{T}_2 . This implies that for any c bigger than c_0 and the maximum of all the c_B 's, the triangulation \mathcal{T}_2 extends \mathcal{T} . This indeed proves that \mathcal{T}_2 is the placing triangulation, by the uniqueness part in Lemma 4.3.2.

To prove the claim, consider a particular $B = \{i_1, \dots, i_k\}$. Since B is maximal, it is a basis of the linear span of \mathbf{A} (or an affine basis of the affine span if \mathbf{A} is a *point* configuration). Write \mathbf{p}_n as a linear combination of B , that is, write $\mathbf{p}_n = \sum \lambda_k \mathbf{p}_{i_k}$. The hyperplane containing the lifted simplex B^ω contains the point $(\mathbf{p}_n, \sum \lambda_k \omega(k))$. It is enough to choose $c_B > \sum |\lambda_k|$. This suffices, since then

$$\sum \lambda_k \omega(k) \leq \sum |\lambda_k| \omega(n)/c_B \leq \omega(n).$$

□

Lemma 4.3.5. *The placing of i in subdivisions of $\mathbf{A} \setminus i$ is a well-defined and order-preserving map from $\text{Subdivs}(\mathbf{A} \setminus i)$ to $\text{Subdivs}(\mathbf{A})$, with the following properties:*

1. *Placing i in a triangulation produces a triangulation.*
2. *Placing i in a regular subdivision produces a regular subdivision.*
3. *Placing i in a non-regular triangulation produces a non-regular triangulation.*

We recall that a map $f : (P, \leq) \rightarrow (Q, \leq)$ between posets is order preserving if $a \leq b$ implies $f(a) \leq f(b)$.

Proof. All the statements are easy, and left to the reader. For the part about regular subdivisions see perhaps the proof of Lemma 4.3.4. For the part about non-regular ones, observe that if heights exist for the triangulation after placing the point i , then the same heights (restricted to the rest of points) work before the placing. □

However, as strange as it may seem, there is no (natural) map in the other direction. See again Example 4.2.16.

4.3.2 The pulling triangulation

We now define the “opposite” triangulation to a placing triangulation. One way of doing it is to just take the opposite lifting heights. That is, we take heights with $\omega(i+1) < c\omega(i) < 0$, with c positive and large. Remember, however, that negative lifting heights are only allowed for point configurations (or, equivalently, for acyclic vector configurations). So, we assume in this subsection that \mathbf{A} is acyclic.

Lemma 4.3.6. *Let \mathbf{A} be an acyclic configuration, labeled by $J = \{1, \dots, n\}$.*

1. *There is a constant c_0 such that every height vector $\omega : J \rightarrow \mathbb{R}$ satisfying $\omega(i+1) < c_0\omega(i) < 0$ for all i produces a triangulation \mathcal{T} , and the triangulation is unique.*
2. *In this triangulation, every maximal simplex contains n .*
3. *For each facet F of J , let \mathcal{T}_F denote the triangulation obtained in this way for the restricted configuration $\mathbf{A}|_F$ (and with the restricted lifting). Then, the simplices of \mathcal{T} are precisely the ones obtained by joining n to all the simplices in all the \mathcal{T}_F 's such that $n \notin F$.*

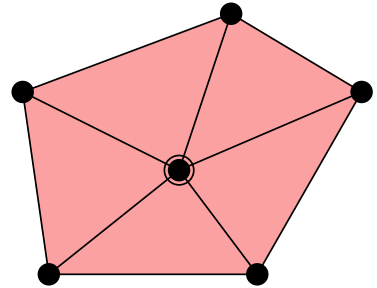


Figure 4.32: A pulling triangulation.

Proof. The proof uses induction on the dimension of the point configuration. In particular, we assume parts (1) and (2) hold for the triangulations of the facets of J and use this to prove the three statements for \mathbf{A} itself.

Actually, the first and third statements follow from the second one. For statement (3), we proved in Lemma 2.3.15 that the restriction to a face F of $\text{conv}(\mathbf{A})$ of a regular triangulation of \mathbf{A} equals the regular triangulation of \mathbf{A}_F obtained with the same heights. In particular, if (2) holds, there is only one possibility for the triangulation \mathcal{T} , namely the one stated in part (3). This also proves part (1).

To prove part (2), we need to prove that for any particular potential full-dimensional simplex $B \subseteq J \setminus \{n\}$ there is a constant c_B such that, for any lifting with $c > c_B$, the point n is lifted below the hyperplane passing through the lifted vertices of B . This prevents B from being in the regular triangulation produced by the lifting. Taking c_0 to be greater than the maximum of the c_B 's (which are a finite set) any triangulation obtained satisfies part (2). If c_0 is also greater than the constant needed for obtaining the desired triangulation \mathcal{T}_F on every facet, then the triangulation also satisfies part (3).

It remains to prove the claim for each B , but this is exactly the same computation we did in Lemma 4.3.4, except now the sign of the lifting heights is reversed and we get the opposite conclusion. \square

Definition 4.3.7 (Pulling triangulation). The *pulling triangulation* of an acyclic point configuration \mathbf{A} , with respect to a given ordering of the labels, is the regular triangulation obtained by taking heights $\omega(i+1) < c_0\omega(i) < 0$ for every i and for a positive and *sufficiently big* positive constant c_0 .

The combinatorial description of the pulling triangulation as the join of the last point to “the pulling triangulations on the faces of \mathbf{A} that do not contain the last point” gives another reason why the triangulation is not well-defined for non-acyclic configurations. In a non-acyclic configuration, there may not be any “face that does not contain the last point”. For example, if $\text{conv}(J) = \mathbb{R}^d$ (that is, if \mathbf{A} is totally cyclic), then J itself is the only face of $J!$

Finally, we can make two simple, but useful, observations about the pulling triangulation of a point set: (1) It always uses the last point as a vertex, but no other interior point, and (2) If the point set is in general position (more generally, if there is no affinely dependent subset of \mathbf{A} contained in a facet of $\text{conv}(J)$) then the pulling triangulation depends only on which is the last point and not on the rest of the ordering.

4.3.3 Lexicographic triangulations

Lexicographic triangulations are the combination of pushing and pulling triangulations. We again assume the point set to be ordered, but additionally we prescribe a direction (a sign) to lift each point.

Observe that a more explicit way of describing height functions that produce the pushing and the pulling triangulation is $\omega(i) = c^i$ for the pushing and $\omega(i) = -c^i$ for the pulling, where in both cases c is positive and sufficiently big. As in the case of the pulling triangulation, we here assume that our configurations are acyclic.

Definition 4.3.8 (Lexicographic triangulation). Let \mathbf{A} be an acyclic configuration with label set $J = \{1, \dots, n\}$.

The *lexicographic triangulation* of \mathbf{A} for the given ordering and a choice of signs $(\varepsilon_1, \dots, \varepsilon_n) \in \{-1, +1\}^n$ is the regular triangulation $\mathcal{S}(\mathbf{A}, \omega)$ obtained by taking $\omega_i = \varepsilon_i c^i$ for every i , and for a positive and sufficiently big positive constant c .

The proof that this triangulation is well-defined, in the sense that there is a c_0 such that the regular triangulation $\mathcal{S}(\mathbf{A}, \omega)$ is the same for all $c > c_0$, as well as a description of this triangulation, can be obtained by combining the proofs of Lemmas 4.3.4 and 4.3.6. Indeed:

Lemma 4.3.9. *Under the conditions of Definition 4.3.8:*

- If $\varepsilon_n = +1$, then the lexicographic triangulation of \mathbf{A} equals the triangulation obtained as the union of the lexicographic triangulation of $\mathbf{A} \setminus n$ and the simplices joining n to the (triangulated) faces of $\mathbf{A} \setminus i$ visible from it.
- If $\varepsilon_n = -1$, then the lexicographic triangulation of \mathbf{A} equals the unique triangulation in which every maximal simplex contains the last point n and which, restricted to each proper face F of \mathbf{A} , coincides with the lexicographic triangulation of that face.

Proof. We can proceed by induction on n . Clearly the statements are true for $n = 1$.

If $\varepsilon_n = +1$, the same proof of Lemma 4.3.2 shows that there is a c_n such that, for every $c > c_n$, the regular triangulation $\mathcal{S}(\mathbf{A}, \omega)$ contains a triangulation of $\mathbf{A} \setminus n$. This triangulation must be the regular triangulation of $\mathbf{A} \setminus n$ for the restricted height function (which we assume to be the same for all sufficiently big c by inductive hypothesis). By Lemma 4.3.4, $\mathcal{S}(\mathbf{A}, \omega)$ is as stated.

If $\varepsilon_n = -1$, then there is a c_n such that for every $c > c_n$ the regular triangulation in question has all maximal simplices containing n . Since restricted to each facet of $\text{conv}(\mathbf{A})$ the triangulation must coincide with the lexicographic triangulation of that facet, we get the statement by induction. \square

As before, these descriptions tell us how to recursively construct the lexicographic triangulation without knowing exactly how big the height constant c needs to be. In the next section we come back to lexicographic triangulations and give a different description of them which will explain the reason for the names “pushing” and “pulling” that we used. The intuitive image is that in the lifted point set, in a first approximation all points can be considered “almost coplanar” except for the last point n which has been “pushed up” or “pulled down”. See Figure 4.33.

4.3.4 Pushing and pulling refinements

We know that the simplest height vector, the all-zero function, produces the simplest regular subdivision, the trivial one. What subdivisions are produced by the next simplest height vectors, which are zero in all but one of the points?

Lemma 4.3.10. *Let $i \in J$ be an element of our configuration and let $\omega : J \rightarrow \mathbb{R}$ be a height vector with $\omega(j) = 0$ for all $j \in J \setminus \{i\}$. Let $\mathcal{S} = \mathcal{S}(\mathbf{A}, \omega)$ be the regular subdivision produced by ω :*

- If $\omega(i) > 0$, then

$$\mathcal{S} = \{F : F \leq J \setminus i\} \cup \{F \cup \{i\} : F \leq J \setminus i \text{ and } F \text{ is visible from } i\}.$$

- If $\omega(i) < 0$ (and we assume that \mathbf{A} is acyclic), then

$$\mathcal{S} = \{\emptyset\} \cup \{F \cup \{i\} : a \notin F \leq \mathbf{A}\}.$$

Proof. (i) Suppose $\omega(i) > 0$. Then $J \setminus i$ is clearly a cell in \mathcal{S} (projection of the horizontal lower face of \mathbf{A}^ω).

If $i \in \text{conv}(J \setminus i)$ then $J \setminus i$ together with all its faces is already a subdivision of \mathbf{A} . The statement holds because in this case no face of $J \setminus i$ is visible.

If $i \notin \text{conv}(J \setminus i)$, that is, if i is extremal in \mathbf{A} , then let F be a face of $J \setminus i$ visible from i , and let \mathbf{H} be a supporting hyperplane of F , not containing i . The hyperplane of \mathbb{R}^{d+1} containing $\mathbf{H} \times \{0\}$ and the lifted point \mathbf{p}_a^ω contains the lift of $F \cup \{i\}$ and leaves the rest of \mathbf{A}^ω above. Hence, $F \cup \{i\}$ is also a cell in \mathcal{S} . To see that this is the full list of cells in \mathcal{S} , it suffices to show

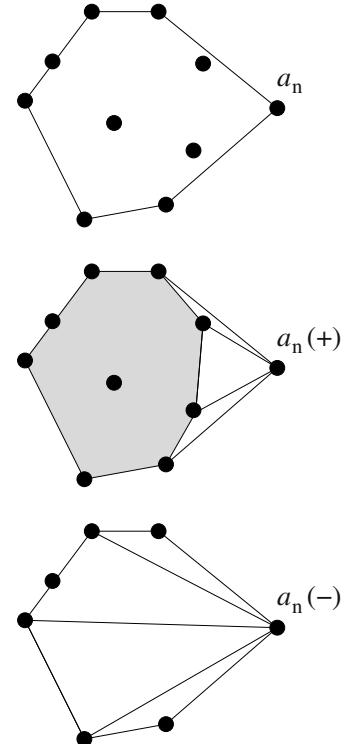


Figure 4.33: Pushing (middle) and pulling (bottom) a point in a point set (top).

that the relative interiors of these cells already cover $\text{conv}(J)$, and observe that Property (IP) prevents any other cell to appear, or otherwise some point would be covered by two relative interiors.

Clearly, $\text{conv}(J \setminus i)$ is already covered by the relative interior of $J \setminus i$ and its faces. So, let $\mathbf{x} \in \text{conv}(J)$ and assume $\mathbf{x} \notin \text{conv}(J \setminus i)$, and that $\mathbf{x} \neq \mathbf{p}_i$.

Consider the ray, or half-line, \mathbf{l} starting at \mathbf{p}_i and passing through \mathbf{x} . This ray must intersect the polytope $\text{conv}(J \setminus i)$ because otherwise \mathbf{x} cannot be written as a convex combination of i and a point in $\text{conv}(J \setminus i)$. Let \mathbf{x}' be the first point where the ray \mathbf{l} hits $\text{conv}(J \setminus i)$ and let F be the carrier face of point \mathbf{x}' in $\text{conv}(J \setminus i)$. By Lemma 4.3.1 F is visible from \mathbf{p}_i . By construction \mathbf{x} is in the convex hull of $F \cup i$.

(ii) If $\omega(i) < 0$, then let F be a face of \mathbf{A} not containing i . Since F must be a proper face, let \mathbf{H} be a supporting hyperplane. Again, the hyperplane of \mathbb{R}^{d+1} containing $\mathbf{H} \times \{0\}$ and i^ω contains $F^\omega \cup \{i^\omega\}$ and leaves the rest of \mathbf{A}^ω above. Hence, $F \cup \{i\}$ is a cell in \mathcal{S} . We claim that this (together with the empty face!) is the full list of cells in \mathcal{S} . That is:

$$T = \{\emptyset\} \cup \{F \cup \{i\} : i \notin F < \mathbf{A}\}.$$

The proof that the list is complete is left to the reader. \square

The regular subdivisions described in these two paragraphs is called the *pushing* (or *pulling*, respectively) of i in the trivial subdivision of \mathbf{A} . The idea is that we start with (a height vector that produces) the trivial subdivision and then “push” i up or “pull” it down slightly.

Using the notion of *regular refinement* introduced in Definition 2.3.17 and studied in Lemma 2.3.16 we can apply the pushing or pulling to subdivisions other than the trivial one. Recall that the regular refinement of a subdivision \mathcal{S} with respect to a height function $\omega : J \rightarrow \mathbb{R}$ is the polyhedral subdivision

$$\mathcal{S}_\omega := \bigcup_{B \in \mathcal{S}} \mathcal{S}(\mathbf{A}|_B, \omega).$$

Definition 4.3.11. Let \mathcal{S} be a subdivision of a point configuration \mathbf{A} . Let $i \in J$ be an element in the label set. Let $\omega : J \rightarrow \mathbb{R}$ be a height function that is zero on $J \setminus \{i\}$ and ± 1 at i . We call the subdivision \mathcal{S}_ω the

1. *Pushing refinement* of i in \mathcal{S} if $\omega_i = +1$, or the
2. *Pulling refinement* of i in \mathcal{S} if $\omega_i = -1$, and every cell of \mathcal{S} that contains i is acyclic.

Observe that the pulling refinement is not well-defined if i lies in some non-acyclic cell of \mathcal{S} .

Lemma 4.3.12. Let \mathcal{S} be a polyhedral subdivision of \mathbf{A} and let $i \in \mathbf{A}$. Then, the pushing (respectively, pulling) of i in \mathcal{S} is the subdivision of \mathbf{A} obtained by pushing (respectively, pulling) i in each cell B of \mathcal{S} .

In particular, the pushing and pulling refinements of a regular subdivision are regular.

Proof. The first part is just Lemma 2.3.16.

For the regularity, observe that the pushing or pulling of a single element in a subdivision \mathcal{S} produces, by Lemma 4.3.10, the regular refinement \mathcal{S}_ω , for the height function ω specified there. By Lemma 2.3.16, the regular refinement of a regular subdivision is regular. \square

We now relate the pushing-pulling operation to the pushing and pulling triangulations (more generally, to the lexicographic triangulations) introduced in Sections 4.3.1, 4.3.2, and 4.3.3. We recall that in the more general form, there is a lexicographic triangulation associated to each ordering of the points of \mathbf{A} and the choice of one sign, $+$ or $-$, for each point.

Proposition 4.3.13. *The lexicographic triangulation of \mathbf{A} for a given ordering and string of signs is the one obtained by starting with the trivial subdivision and pushing or pulling the points, as indicated by their signs (positive for pushing, negative for pulling), in the reverse order.*

Proof. We prove this by induction on the number n of points in \mathbf{A} . The base case $n = 1$ is trivial and for the inductive step we distinguish the cases where the sign given to the last element n is positive or negative.

- If the sign is positive, the lexicographic triangulation is, by definition, the only one that extends the lexicographic triangulation of $\mathbf{A} \setminus n$ for the given ordering and signs. By inductive hypothesis, the latter is obtained from the trivial subdivision of $\mathbf{A} \setminus n$ by the corresponding reverse sequence of pushings and pullings on $\mathbf{A} \setminus n$. On the other hand, the sequence of pullings and pushings applied to \mathbf{A} starting with n , first creates the cell $\mathbf{A} \setminus n$ (among others) and then refines it in the lexicographic manner. Hence, it extends the lexicographic triangulation of $\mathbf{A} \setminus n$.
- If the sign is negative the lexicographic triangulation, by definition, refines the subdivision \mathcal{S} obtained from the trivial one by pulling n , and agrees with the lexicographic triangulation (for the restricted ordering and signs) on each facet F not containing n . By inductive hypothesis, the lexicographic triangulation on F is the one obtained by pushing and pulling the points in these facets in the restricted (reverse) orderings, and by Lemma 4.3.12 it agrees with the subdivision obtained by pushing and pulling directly in $F \cup \{n\}$ (observe that F is also a facet of this). Hence, the two triangulations coincide.

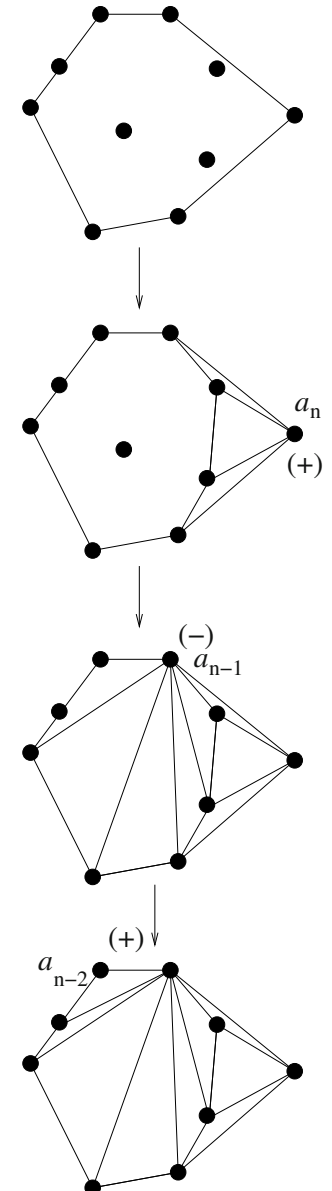


Figure 4.34: A lexicographic triangulation obtained by first pushing the point n , then pulling $n - 1$ and finally pushing $n - 2$. You have to imagine you are looking at the lifted point set from below.

4.4 Two equivalent characterizations of flips

The definition of a flip we gave in Section 2.4 is conceptually easy. However, in proofs and in computer calculations it is not very useful: Given a triangulation \mathcal{T} , in order to find a flip, we need to find an almost triangulation that \mathcal{T} refines. We have seen that signed circuits played a fundamental role in combinatorial characterizations of subdivisions; here they are useful again

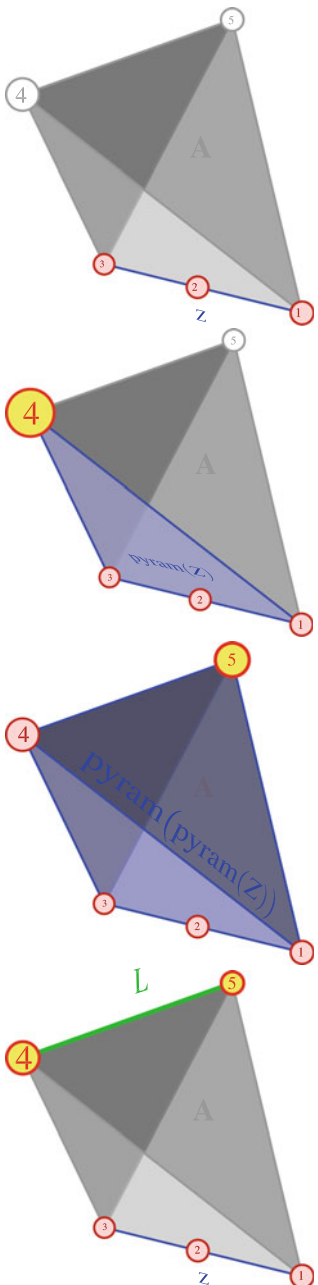


Figure 4.35: How a corank-one configuration with five points in three-space arises from the one-dimensional circuit $Z = 123$ by a repeated pyramid and by joining it to the link-simplex

$$L = 45.$$

for a characterization of flips. This is no surprise, since circuit signatures were already used to specify the two possible triangulations of a corank-1 configuration, and this was the starting idea for flips in the first place.

4.4.1 Flips via circuits

The closure Property (CP) of triangulations can be rephrased by saying that a triangulation is an (abstract) simplicial complex. In particular, we can apply constructions on simplicial complexes to them, like the link and the join (see Sections 2.6.1 and 4.2.1).

When we defined flips in Section 2.4, we saw that any corank-1 configuration that is not minimal is a pyramid over a corank-1 configuration with one less point, the deleted point being the apex of that pyramid. Thus, the two possible triangulations of any corank-1 configuration are repeated pyramids over the two possible triangulations of the unique circuit contained in it. A repeated pyramid (pyramid of the pyramid of ... of the pyramid over ... etc.) can be expressed as a join with the simplex formed by all the apices, i.e., those points inserted when doing a pyramid construction. Let us call this simplex the *link simplex* (see Figure 4.35). Since all corank-one cells in an almost-triangulation contain the same circuit, any of the two possible triangulations of this almost-triangulation contain the join of a triangulation of the circuit with the simplicial complex of all link-simplices, one for each corank-one cell. Conversely, each maximal cell in a triangulation of the unique circuit in an almost-triangulation has the same link in the almost-triangulation. This observation can be used to characterize flips combinatorially.

Theorem 4.4.1. *Let \mathcal{T}_1 and \mathcal{T}_2 be two triangulations of the same point configuration \mathbf{A} . Then: \mathcal{T}_1 and \mathcal{T}_2 differ by a flip if and only if there is circuit Z of \mathbf{A} such that*

- (i) *They contain, respectively, the two triangulations \mathcal{T}_Z^+ and \mathcal{T}_Z^- of Z .*
- (ii) *All the maximal simplices of \mathcal{T}_Z^+ and \mathcal{T}_Z^- have the same link, \mathcal{L} , in \mathcal{T}_1 .*
- (iii) *This is the only difference between \mathcal{T}_1 and \mathcal{T}_2 . That is, removing the subcomplex $\mathcal{T}_Z^+ * \mathcal{L}$ from \mathcal{T}_1 and putting $\mathcal{T}_Z^- * \mathcal{L}$ instead produces \mathcal{T}_2 .*

Definition 4.4.2. A flip is supported at the circuit Z if Z is the circuit as in the statement of Theorem 4.4.1.

Before we prove Theorem 4.4.1, note that if Z is a full-dimensional circuit, then the link condition is void. The link of a full-dimensional simplex in a triangulation is the empty complex $\{\emptyset\}$. This happens, for example, for point configurations in general position, all of whose circuits are full-dimensional.

Proof. Let \mathcal{T}_1 and \mathcal{T}_2 be the two triangulations in question. If they are the two refinements of an almost triangulation \mathcal{T} , their description in the paragraph prior to Theorem 4.4.1 of the proof of part (ii) shows that indeed they differ by a flip.

Conversely, suppose they differ by a flip on a certain circuit Z . Let \mathcal{T}_Z^+ and \mathcal{T}_Z^- be the two triangulations of Z . The second condition in the definition of circuit implies that we can remove $\mathcal{T}_Z^+ * \mathcal{L}$ from \mathcal{T}_1 and insert $\{Z\} * \mathcal{L}$, to get a subdivision that is refined by \mathcal{T}_1 . This subdivision is an almost triangulation since its unique minimal dependent cell is Z . We can do the same in \mathcal{T}_2 . The third condition implies that the almost triangulation obtained is the same one. \square

Example 4.4.3 (Dimension zero). If \mathbf{A} has dimension zero, then it consists of k copies of a single point. Each triangulations is the selection of one of the copies and the exchange of one copy to another is a flip. $\mathcal{G}_{\text{tri}} \mathbf{A}$ is the complete graph K_n .

Example 4.4.4 (Example 2.2.11 continued). Let \mathbf{A} be the point configuration of Examples 4.1.4 and 2.2.11. The whole poset of subdivisions is isomorphic to a quadrilateral, and shown in Figure 2.37. (There we only said that this is the poset of regular subdivisions, but all subdivisions are regular in this example. The reader can check this on his/her own or wait until Section 5.5).

From the poset structure we conclude that the graph of flips is a square. The reader is encouraged to verify this via Definition 4.4.2.

Example 4.4.5 (1-dimensional configurations in general position). If \mathbf{A} consists of n distinct points along a line, then to specify a triangulation we just need to say which among the $n - 2$ interior points are used as vertices. Flips correspond to insertion or deletion of a single point in the choice. $\mathcal{G}_{\text{tri}} \mathbf{A}$ is the graph of the $(n - 2)$ -dimensional cube, as in Figure 4.37.

Example 4.4.6 (The octahedron). Let

$$\mathbf{A} = \begin{pmatrix} 1 & 2 & 3 & 4 & 5 & 6 \\ 1 & 0 & 0 & -1 & 0 & 0 \\ 0 & 1 & 0 & 0 & -1 & 0 \\ 0 & 0 & 1 & 0 & 0 & -1 \\ 1 & 1 & 1 & 1 & 1 & 1 \end{pmatrix}.$$

This is the vertex set of a regular octahedron, with indices given so that i and $i + 3$ are opposite, for $i = 1, 2, 3$.

\mathbf{A} has three triangulations, and three circuits. Each triangulation \mathcal{T}_i consists of the axis $\{i, i + 3\}$ joined to the edges of the boundary square passing through the other four vertices. The circuit Z_i consists of these four vertices, and is actually the only one of the three circuits in which \mathcal{T}_i does not have a flip. The link condition is clearly satisfied. Hence, the graph of triangulations is a triangle.

Another proof of this fact is that the octahedron is obtained by applying the one-point-suspension (see Section 4.2.5) three times to a zero-dimensional point-configuration $\mathbf{A}_0 = (1, 1, 1)$. By 4.2.33, the two configurations have the same poset of subdivisions. This implies they also have the same graph of flips.

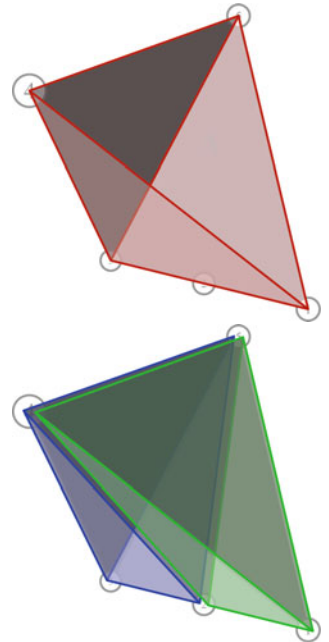
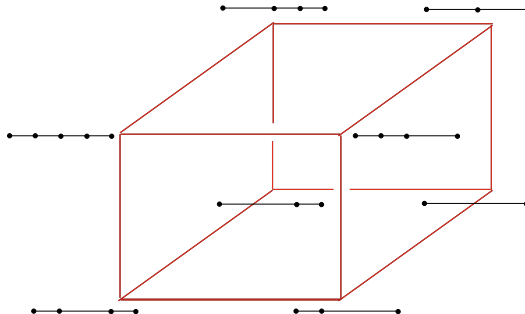


Figure 4.36: The two possible triangulations of a corank-one configuration: in both of them, all maximal simplices contain the link simplex; more specifically, both triangulations arise as joins of the two possible triangulations of the circuit with the common link simplex.

Figure 4.37: The graph of triangulations of a 5 point configuration in the real line.



Example 4.4.7 (Insertion flip). If a triangulation \mathcal{T} of \mathbf{A} does not use a certain point $i \in J$, let B be the unique simplex of \mathcal{T} with $i \in \text{relint}(B)$ (the *carrier* of i). Clearly, $B \cup \{i\}$ is a circuit and B alone is one of its two triangulations (the other one is the stellar subdivision of it). In particular, the link conditions in the definition of flip are satisfied and there is a flip on this circuit. This flip inserts i , subdividing B (and its link) in a stellar way.

Moreover, this is the only flip of \mathcal{T} that involves the element i . Indeed, if Z is a circuit containing i and one of its two triangulations is contained in \mathcal{T} , then this triangulation must have $Z \setminus \{i\}$ as its unique maximal simplex. This implies $\mathbf{p}_i \in \text{conv}(Z)$ and, in particular, there is a face B' of Z with $i \in \text{relint}(B')$. Since i cannot be contained in two relative interiors of cells of \mathcal{T} , $B = B'$ and $B \cup \{i\} \subseteq Z$. Since a circuit cannot be properly contained in another, $Z = B \cup \{i\}$.

For yet another nice example of the graph of flips, see Figure 1.15.

4.4.2 Flips via walls

In a typical situation, we will be given a triangulation \mathcal{T} of a point configuration and be asked to find all the possible flips in it (or, maybe, to find one flip that improves some criterion that we want to optimize). In this situation it may not be a good idea to apply Definition 4.4.2 directly by searching on all possible circuits. For example, n points in general position in the plane have $\binom{n}{4}$ circuits, while the flips of a particular planar triangulation can be found much more easily by inspecting which edges can be diagonally flipped and which vertices can be inserted or removed by a flip.

In this section we generalize this method to arbitrary dimension, introducing the concept of “witness wall”. Remember that by a *wall* in a polyhedral subdivision we mean an interior codimension one cell. That is, a cell of codimension one that is a face of two maximal cells.

Definition 4.4.8. Let Z be a circuit and \mathcal{T} a triangulation such that \mathcal{T} has a flip supported at Z . (That is, such that there is a triangulation \mathcal{T}' that differs from \mathcal{T} by a flip in Z). We say that a wall B *witnesses* a flip in a triangulation \mathcal{T} if Z is contained in the union of the two maximal simplices separated by B .

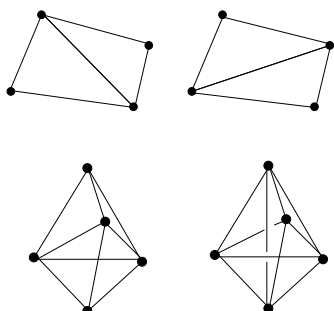


Figure 4.38: Two pairs of triangulations with a common circuit. On top, a planar configuration and below it a three-dimensional circuits.

Observe that the union of the two simplices separated by B is a corank-1 configuration and, in particular, it contains a unique circuit. That is to say, the same wall cannot witness two different flips.

The insertion flips described in Example 4.4.7 clearly do not have any insertion walls, simply because one of the points in the circuit is the one to be inserted. The next result shows that this is the only case.

Lemma 4.4.9. *Let \mathcal{T} be a triangulation of a point configuration that has a flip supported at the circuit Z . If all the elements of Z are used in \mathcal{T} (that is, “unless the flip is an insertion flip”) then the flip has some witness wall.*

Proof. If the flip is not an insertion flip, the triangulation \mathcal{T}_Z^+ of Z contained in \mathcal{T} has at least two maximal simplices. This is so because if \mathcal{T} has a single maximal simplex B , then the unique point i in $Z \setminus B$ would be in the convex hull of B (because $\{B\}$ is a triangulation of $Z = B \cup \{i\}$) which implies i is not used in \mathcal{T} . The flip would then be the insertion flip of i .

So, let B_1 and B_2 be two maximal simplices in \mathcal{T} . Let B' be any maximal simplex in the link \mathcal{L} of both B_1 and B_2 (it is the same by the definition of a flip). Then, $B_0 := B_1 \cap B_2$ is a wall in \mathcal{T}_Z^+ and $B_0 \cup B'$ is a wall in \mathcal{T} , separating $B_1 \cup B'$ and $B_2 \cup B'$. Since $Z = B_1 \cup B_2$, $B_0 \cup B'$ is a witness wall for the flip. \square

What is then a good algorithm for finding all the flips in a triangulation \mathcal{T} ? First, \mathcal{T} will have an insertion flip for each point that it does not use (if any). Second, check each wall in \mathcal{T} to see if it witnesses a flip, and on which circuit (this is important because, in general, a flip has more than one witness wall). For doing this in practice, recall that the sets of maximal simplices in the two possible triangulations of a circuit Z are, by Lemma 2.4.2,

$$\mathcal{T}_Z^+ = \{Z \setminus i : i \in Z_+\}, \quad \text{and} \quad \mathcal{T}_Z^- = \{Z \setminus i : i \in Z_-\}.$$

Let us go back to our situation of interest. We have a triangulation \mathcal{T} of a point configuration \mathbf{A} and want to check if a certain wall B_0 between two maximal simplices $B_1 = B_0 \cup \{i_1\}$ and $B_2 = B_0 \cup \{i_2\}$ is a witness for a flip. For this:

1. Compute the signed circuit (Z_+, Z_-) contained in the label set $B_1 \cup B_2 = \{i_1, \dots, i_{d+2}\}$. In concrete examples this is easy to do by inspection. Computationally, it can be done as shown in Remark 4.1.8 (it reduces to computing the kernel of a $(d+1) \times (d+2)$ matrix).
2. Automatically, we get that the two elements i_1 and i_2 belong to the circuit Z and are on the same part of it. Indeed, if ψ is the affine functional vanishing on B_0 , the functional ψ vanishes on all the circuit except for those two points, and then

$$\psi\left(\sum_{i \in Z} \lambda_i \mathbf{p}_i\right) = \sum \lambda_i \psi(\mathbf{p}_i) = \lambda_1 \psi(\mathbf{p}_{i_1}) + \lambda_2 \psi(\mathbf{p}_{i_2}) = 0$$

implies that λ_1 and λ_2 have opposite signs (they cannot be both zero because then the circuit would be contained in B_0 , which is independent). Without loss of generality, we assume that $i_1, i_2 \in Z_+$. The

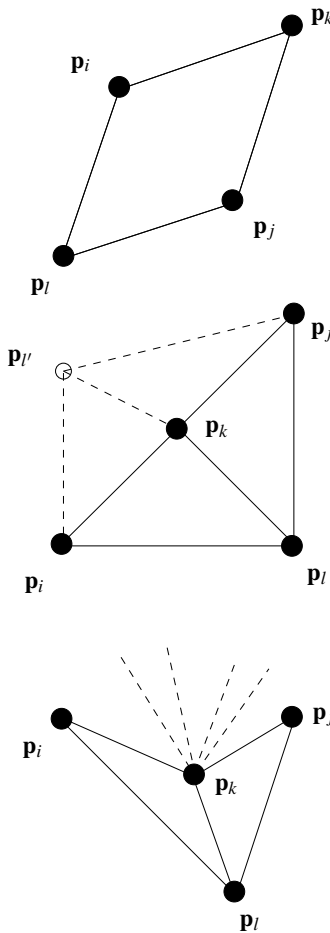


Figure 4.39: Possible ways in which a wall corresponds to a two-dimensional flip.

triangulation of Z that is a candidate to be contained in \mathcal{T} is \mathcal{T}_Z^+ , because we already have two of its maximal simplices, namely $Z \setminus \{i_1\}$ and $Z \setminus \{i_2\}$.

3. If the circuit is full-dimensional (that is, if $Z = B_1 \cup B_2$), then checking that \mathcal{T}_Z^+ is a subcomplex of \mathcal{T} is equivalent to checking that $Z \setminus i$ is a simplex, for every $i \in Z_+$. If the circuit is lower dimensional, we need to, in addition, to check that all the links of the maximal simplices in \mathcal{T}_Z^+ are the same (for which a necessary, but not sufficient, condition is that $Z \setminus i$ is a simplex, for every $i \in Z_+$).

To clarify this process, and to complement our discussion in Chapter 3, let us analyze the possible cases in dimension two in detail.

Example 4.4.10 (Flips in dimension two). Let $E = \{k, l\}$ be a wall (that is, an interior edge) between two triangles of a triangulation \mathcal{T} in the plane. Let i and j be the two points joined to E . Then:

1. If the quadrilateral $p_i p_k p_j p_l$ is strictly convex, then the circuit has $Z_+ = \{i, j\}$ and $Z_- = \{k, l\}$. It is full-dimensional and the two triangles in question are its positive triangulation. $\{k, l\}$ is a witness (and the unique witness) for the flip that removes the diagonal $\{k, l\}$ and inserts $\{i, j\}$.
2. If one of the angles of the quadrilateral (say the one at k) is flat, then the circuit has $Z_+ = \{i, j\}$ and $Z_- = \{k\}$. The two triangles in question are its positive triangulation, but the circuit is not full-dimensional. The link condition is equivalent to saying that either $\{i, k\}$ and $\{k, j\}$ are boundary edges or they are joined to the same vertex $\{l'\}$ on the side opposite to l . The flip merges $\{i, k\}$ and $\{k, j\}$ into a single edge deleting $E = \{k, l\}$ and (if it exists) $\{k, l'\}$. In the first case E is the only witness and in the second $\{k, l'\}$ is a second one.
3. If one of the angles of the quadrilateral (say the one at k) is reflex (greater than 180 degrees), then the circuit has $Z_+ = \{i, j, l\}$ and $Z_- = \{k\}$. It is a full-dimensional circuit and produces a flip if and only if $\{i, j, k\}$ is also a triangle. In this case the three edges $\{i, j\}$, $\{i, l\}$, and $\{j, l\}$ are witnesses for the flip.

The reader can check that the three possibilities arise in Example 4.1.4.

4.5 More characterizations of triangulations and subdivisions

In this section, we present a wealth of different characterizations of triangulations and polyhedral subdivisions that the reader may find useful in proving that something is a triangulation. Sometimes, using one of the non-standard characterizations saves substantial work. One example is the use of the characterization in Theorem 4.5.17 in Chapter 6. The first part on geometric characterizations aims at giving tools for proofs. The second part on purely combinatorial characterizations is intended for implementation into computer programs.

4.5.1 Geometric characterizations

In this section, polyhedral subdivisions of point configurations will be revisited using notions from convex geometry of point configurations. Triangulations are a special case in which all the cells are simplices.

The following theorem states that polyhedral subdivisions of \mathbf{A} are geometric polytopal complexes [339, Def. 5.1] that cover $\text{conv}(\mathbf{A})$ and that contain no distinct cells with identical convex hulls. The latter condition is trivially missing in common polyhedral subdivisions in a purely geometric context, where cells are uniquely determined as subsets of the Euclidean space. In Section 2.2 we argued that this is not enough to obtain the nice structures arising from a more combinatorial view. The need for Condition (MF) in the following characterization shows that the additional combinatorial structure requires some care.

Theorem 4.5.1. *A set \mathcal{S} of subconfigurations of a point configuration \mathbf{A} in \mathbb{R}^d labeled by J is a polyhedral subdivision of \mathbf{A} if and only if it satisfies the following conditions:*

- (CP) *If $B \in \mathcal{S}$ and $F \leq B$, then $F \in \mathcal{S}$ as well.*
- (UP) $\bigcup_{B \in \mathcal{S}} \text{conv}(B) \supseteq \text{conv}(\mathbf{A})$.
- (FP) $\text{conv}(B) \cap \text{conv}(B')$ is a face of both $\text{conv}(B)$ and $\text{conv}(B')$ for all $B, B' \in \mathcal{S}$. (*Face Property*).
- (MF) *For every two different cells $B \neq B'$ in \mathcal{S} , $\text{conv}(B) \neq \text{conv}(B')$. (*Multiple Face Property*)*

More specifically, (CP), (FP) and (MF) together are equivalent to (CP) and (IP).

The consequence of this is that non-incident cells intersect properly if and only if they intersect in a proper common face, possibly empty. Moreover, no distinct cells with identical convex hulls can coexist in a polyhedral subdivision.

Proof. We first prove that (FP) and (MF) are necessary for (IP). For (MF) this is clear because $\text{conv}(B) = \text{conv}(B')$ implies, in particular, $\text{relint}(B) = \text{relint}(B')$, and thus (IP) implies $B = B'$.

For (FP), assume \mathcal{S} is a polyhedral subdivision of \mathbf{A} . Then, in particular, (IP) holds for \mathcal{S} . Consider two cells $B, B' \in \mathcal{S}$. Let $F := \text{carrier}(\text{conv}(B) \cap \text{conv}(B'), \text{conv}(B))$ and $F' := \text{carrier}(\text{conv}(B) \cap \text{conv}(B'), \text{conv}(B'))$, both cells in \mathcal{S} because of (CP). Then, by Lemma 2.1.23,

$$\text{relint}(\text{conv}(B) \cap \text{conv}(B')) \subseteq \text{relint}(F) \cap \text{relint}(F'). \quad (4.1)$$

By (IP), this implies either $\text{relint}(\text{conv}(B) \cap \text{conv}(B')) = \emptyset$, thus $\text{conv}(B) \cap \text{conv}(B') = \emptyset$, or $F = F'$. In the first case, (FP) is trivially fulfilled for B, B' . In the second case, we have

$$\text{conv}(B) \cap \text{conv}(B') \subseteq F \cap F' \subseteq \text{conv}(B) \cap \text{conv}(B'). \quad (4.2)$$

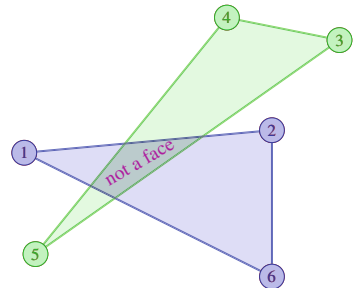


Figure 4.40: Two cells whose convex hulls intersect in something that is not a face at all.

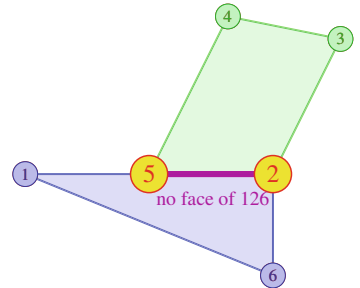


Figure 4.41: Two cells whose convex hulls intersect in something that is only a face of one of them but not of the other.

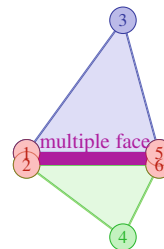


Figure 4.42: Two cells whose convex hulls intersect in something that is a face of both convex hulls; however, if 135 and 246 were together in a subdivision, (CP) would imply that both 15 and 26 were in the subdivision, too; however, they have identical convex hulls, violating (MF).

Hence, $\text{conv}(B) \cap \text{conv}(B') = F \cap F' = F = F'$, and this is a face of both $\text{conv}(B)$ and $\text{conv}(B')$, by the carrier construction. This proves (FP).

In order to prove that (FP) and (MF) are sufficient for (IP), we consider a set \mathcal{S} of subconfigurations of \mathbf{A} satisfying (FP) and (MF).

Let $B, B' \in \mathcal{S}$ and assume that there is a point $\mathbf{x} \in \text{relint}(B) \cap \text{relint}(B')$. We show that this implies $B = B'$, so that (IP) holds. Clearly, $\mathbf{x} \in \text{conv}(B) \cap \text{conv}(B')$, which is a face of both B and B' by (FP). But the fact that \mathbf{x} is in the relative interiors of B and B' implies that this face is the whole of $\text{conv}(B)$ and $\text{conv}(B')$, respectively. Hence, $\text{conv}(B) = \text{conv}(B')$ and, by (MF), $B = B'$. \square

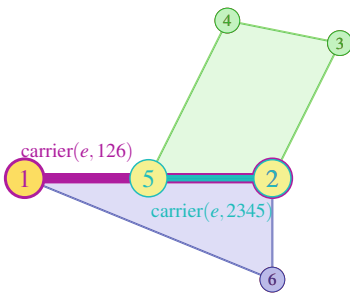


Figure 4.43: How to find a violation of (IP) from a violation of (FP)? The carrier of the segment $e = \text{conv}(126) \cap \text{conv}(2345)$ in 126 is 12; the carrier of e in 2345 is 25. If 126 and 2345 were in a polyhedral subdivision, then, because of (CP), so were the two carriers 12 and 25. However, the relative interiors of 12 and 25 intersect because both contain the relative interior of e , by Lemma 2.1.23.

Lemma 2.1.23.

For triangulations, Condition (MF) can be relaxed to a new condition (MP) requiring that the triangulation does not contain distinct versions of a multiple point as vertices.

Theorem 4.5.2. *A set \mathcal{T} of independent subconfigurations of a point configuration \mathbf{A} in \mathbb{R}^d labeled by J is a triangulation of \mathbf{A} if and only if it satisfies the following conditions:*

(CP) *If $B \in \mathcal{T}$ and $F \leq B$, then $F \in \mathcal{T}$ as well.*

(UP) $\bigcup_{B \in \mathcal{T}} \text{conv}(B) \supseteq \text{conv}(\mathbf{A})$.

(FP) *$\text{conv}(B) \cap \text{conv}(B')$ is a face of both $\text{conv}(B)$ and $\text{conv}(B')$ for all $B, B' \in \mathcal{T}$ (Face Property).*

(MP) *\mathcal{T} does not use two copies of the same point (Multiple Point Property).*

More specifically, (CP), (FP) and (MP) together are equivalent to (CP) and (IP).

In other words, a triangulation of a point configuration \mathbf{A} is an abstract simplicial complex (CP) properly embedded into \mathbb{R}^d (FP & MP) so that the union of its simplices equals the convex hull of \mathbf{A} (UP).

Proof. Clearly (MP) is weaker than (MF). Hence, it suffices to show the converse: for independent cells (MP) (together with the other properties) implies (MF).

If (MF) fails, let B and B' be two cells with the same convex hull. Let $i \in B \setminus B'$. Since every subset of an independent set is a face of it, $\{i\}$ is a cell in \mathcal{T} by (CP). But since B and B' have the same convex hull, $\text{conv}(i)$ is a vertex of $\text{conv}(B')$. Since i itself is not in B' , there is a $j \in B'$ not equal to i with $\text{conv}(i) = \text{conv}(j)$. Then i and j are different copies of a repeated point, in violation of (MP). \square

We present an alternative characterization that contains another common characterization of proper intersection in Condition (HP). In that characterization, only the general case of polyhedral subdivisions requires the additional combinatorial condition (LP). For triangulations things are again easier: (LP) can be dropped, as we will show below.

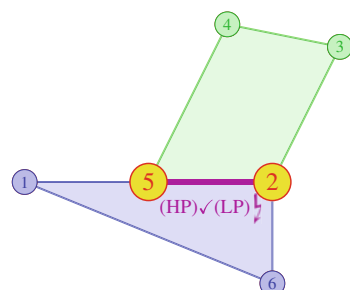


Figure 4.44: (HP) holds for 1256 and 2345, since their convex hulls intersect in the convex hull of $25 = 1256 \cap 2345$; however, (LP) is violated, since 25 is not a face of 1256.

Theorem 4.5.3. A set \mathcal{S} of subconfigurations of a point configuration \mathbf{A} labeled by J in \mathbb{R}^d is a polyhedral subdivision of \mathbf{A} if and only if it satisfies the following conditions:

(CP) If $B \in \mathcal{S}$ and $F \leq B$, then $F \in \mathcal{S}$ as well.

(UP) $\bigcup_{B \in \mathcal{S}} \text{conv}(B) \supseteq \text{conv}(\mathbf{A})$.

(HP) $\text{conv}(B) \cap \text{conv}(B') = \text{conv}(B \cap B')$ for all $B, B' \in \mathcal{S}$. (Hull Property)

(LP) $B \cap B'$ is a face of both B and B' for all $B, B' \in \mathcal{S}$. (Label Property)

More specifically, (CP), (HP), and (LP) together are equivalent to (CP) and (IP).

Proof. We first show that (HP) and (LP) are implied by (CP) and (IP). To this end, assume that \mathcal{S} is a polyhedral subdivision of \mathbf{A} .

We prove now (HP) for two arbitrary cells B, B' in \mathcal{S} . From the definition of convex hull it is immediate that $\text{conv}(B) \cap \text{conv}(B') \supseteq \text{conv}(B \cap B')$. It remains to show that $\text{conv}(B) \cap \text{conv}(B') \subseteq \text{conv}(B \cap B')$.

If $\text{conv}(B) \cap \text{conv}(B') = \emptyset$, we are fine. In the other case, let \mathbf{x} be in $\text{conv}(B) \cap \text{conv}(B')$. Let $F := \text{carrier}(\mathbf{x}, B)$ and $F' := \text{carrier}(\mathbf{x}, B')$. By (CP), these are cells in \mathcal{S} . By Lemma 2.1.23, we know that $\mathbf{x} \in \text{relint}(\mathbf{x}) \subseteq \text{relint}(F)$ and $\mathbf{x} \in \text{relint}(\mathbf{x}) \subseteq \text{relint}(F')$. Consequently, $\mathbf{x} \in \text{relint}(F) \cap \text{relint}(F')$. Since (IP) holds in particular for F and F' , we must have $F = F' =: G$. Moreover, $F \leq B$ and $F' \leq B'$, in particular, $F \subseteq B$ and $F' \subseteq B'$. Hence, $G \subseteq B \cap B'$. Thus, $\mathbf{x} \in \text{relint}(F) \cap \text{relint}(F') = \text{relint}(G) \subseteq \text{conv}(G) \subseteq \text{conv}(B \cap B')$.

We next prove (LP) for B, B' . If $B \cap B' = \emptyset$, we are fine. Let F be the carrier of $B \cap B'$ in B , and let F' be the carrier of $B \cap B'$ in B' . Both F and F' are cells in \mathcal{S} because of (CP). Moreover, by Lemma 2.1.23, we have

$$\text{relint}(B \cap B') \subseteq \text{relint}(F) \cap \text{relint}(F'). \quad (4.3)$$

Therefore, $F = F'$ by (IP), and thus

$$B \cap B' \subseteq F = F' \subseteq B \cap B'. \quad (4.4)$$

This means that

$$B \cap B' = F = F', \quad (4.5)$$

which, by construction of F and F' , is a face of both B and B' .

Now, we prove that (CP), (HP), and (LP) imply (IP).

To this end, let \mathcal{S} be a set of subconfigurations of \mathbf{A} satisfying (CP), (HP), and (LP). Let $B, B' \in \mathcal{S}$ and consider a point $\mathbf{x} \in \text{relint}(B) \cap \text{relint}(B')$. We have to show, that then $B = B'$ must hold. By Condition (LP), we know $B \cap B' \leq B$ and $B \cap B' \leq B'$. If $B \cap B' = B$ and $B \cap B' = B'$ then $B = B'$, and we are done. Assume, for the sake of contradiction, that equality does not hold in both cases, that is, without loss of generality, $B \cap B' < B$. Then $\text{conv}(B \cap B') < \text{conv}(B')$ (compare Remark 2.1.20) holds as well. We

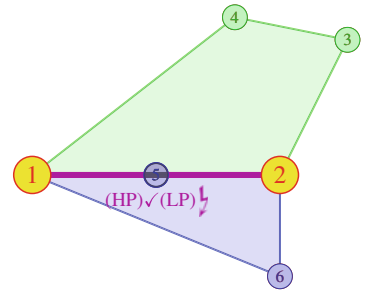


Figure 4.45: (HP) holds for 1256 and 1234, since their convex hulls intersect in the convex hull of 12 = 1256 ∩ 1234; however, (LP) is violated, since 12 is not a face of 1256; note that $\text{conv}(12)$ is a face of $\text{conv}(1256)$, so that, again, the combinatorial framework is necessary!

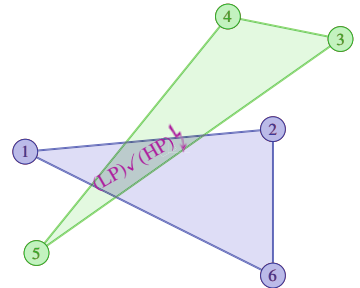


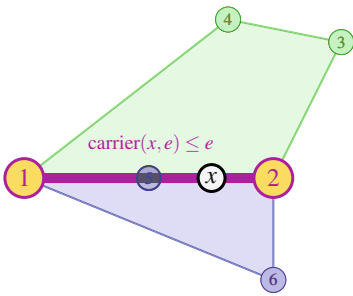
Figure 4.46: (LP) holds, but (HP) does not: the cells have empty intersection while their convex hulls do not.

conclude, since $\mathbf{x} \in \text{relint}(B) \cap \text{relint}(B') \subseteq \text{conv}(B) \cap \text{conv}(B')$:

$$\begin{aligned}\mathbf{x} &\in \text{carrier}(\mathbf{x}, \text{conv}(B) \cap \text{conv}(B')) \\ &\stackrel{(\text{HP})}{=} \text{carrier}(\mathbf{x}, \text{conv}(B \cap B')) \\ &\leq \text{conv}(B \cap B') \\ &< \text{conv}(B).\end{aligned}$$

In words: \mathbf{x} lies in a proper face of $\text{conv}(B)$, contradicting the fact that $\mathbf{x} \in \text{relint}(B)$. \square

Figure 4.47: How to find a violation of (LP) from a violation of (IP) in the presence of (HP)? The point x is in the intersection of the relative interiors of $125 < 1256$ and $12 < 1234$, respectively: a violation of (IP). The carrier of x in $e = \text{conv}(1256) \cap \text{conv}(1234)$, which equals $\text{conv}(12)$ by (HP), is by definition a face of e . If (LP) were satisfied, then $12 = 125 \cap 12$ would be a face of 125 —proper, since not equal. (We see in the picture that this is not the case, but we want to illustrate the formal argument.) Therefore, $\text{conv}(12)$ would also be a proper face of $\text{conv}(125)$. But since x is in the proper face of $\text{conv}(125)$, and at the same time in $\text{relint}(125)$, we have a contradiction.



Note that, in fact, proper intersection of any set of cells in the sense of (IP) follows from (HP) and (LP) alone, without the help of (CP). This contrasts the other characterizations above and will be useful soon.

Again, we have a simpler version for triangulations: (LP) is redundant, since every subset of an independent set is a face of it. This time we don't even need to exclude multiple points.

Theorem 4.5.4. *A set \mathcal{T} of independent subconfigurations of a point configuration \mathbf{A} in \mathbb{R}^d labeled by J is a triangulation of \mathbf{A} if and only if it satisfies the following conditions:*

(CP) *If $B \in \mathcal{T}$ and $F \leq B$ then $F \in \mathcal{T}$ as well.*

(UP) $\bigcup_{B \in \mathcal{T}} \text{conv}(B) \supseteq \text{conv}(\mathbf{A})$.

(HP) $\text{conv}(B) \cap \text{conv}(B') = \text{conv}(B \cap B')$ for all $B, B' \in \mathcal{T}$. (Hull Property).

This seems to be the most elegant characterization for triangulations, and it is used quite frequently in the literature: (HP) says that the combinatorial intersection (vertex sets) must be compatible with the geometric intersection (convex hulls of vertex sets).

Proof. We show that (HP) implies (LP) for triangulations. This is the case because each independent point configuration is uniquely determined by its convex hull. The independent point configuration is simply the set of vertices of its convex hull. But then (LP) follows from general polytope theory by considering vertices of cells. \square

So far, we have used conditions on cells in all dimensions in polyhedral subdivisions. However, each polyhedral complex is determined by the set of its maximal faces (just add all faces of the maximal faces to recover the complex). In our case—cf. Lemma 2.3.4(i)—, maximal faces are always full-dimensional: polyhedral subdivisions are of pure dimension d . Therefore, it makes sense to ask what the set of maximal cells of a polyhedral subdivision looks like. Essentially, we have to express a union property and an intersection property in terms of maximal faces so that the original (UP) and (IP) follow for all faces.

Recall that a trivial reformulation of (CP) and (IP) in terms of maximal cells is given by the term “proper intersection” (see Definition 2.3.2 and Remark 2.3.3). We repeat this here as a starting point.

Theorem 4.5.5. A set \mathcal{S} of d -dimensional subconfigurations of a point configuration \mathbf{A} in \mathbb{R}^d labeled by J is the set of maximal cells of a polyhedral subdivision of \mathbf{A} if and only if it satisfies the following conditions:

(MaxUP) $\bigcup_{B \in \mathcal{S}} \text{conv}(B) \supseteq \text{conv}(\mathbf{A})$ (Union Property for Maximal Cells).

(MaxPI) For all cells $B, B' \in \mathcal{S}$, it holds that B and B' intersect properly (Proper Intersection for Maximal Cells). \square

Of course: this does not save work, because for the check of proper intersection according to the definition we must touch all faces. We will, however, develop necessary and sufficient conditions for proper intersection that can be checked on the maximal cells alone.

The first attempt in this direction may be to just copy (UP) and (IP) and hope for the best. This essentially works whenever the point configuration is in general position. However, in special position, even two triangles might have empty interior intersection although two of their edges have non-empty interior intersection at the same time. Here is the result for general position:

Theorem 4.5.6. A set \mathcal{S} of d -dimensional subconfigurations of a point configuration \mathbf{A} in general position in \mathbb{R}^d labeled by J is the set of maximal cells of a polyhedral subdivision of \mathbf{A} if and only if it satisfies the following conditions:

(MaxUP) $\bigcup_{B \in \mathcal{S}} \text{conv}(B) \supseteq \text{conv}(\mathbf{A})$ (Union Property for Maximal Cells).

(MaxIP) If $B \neq B'$ are two different cells in \mathcal{S} , then $\text{relint}(B) \cap \text{relint}(B')$ is empty (Intersection Property for Maximal Cells).

More specifically: In general position, (MaxPI) is equivalent to (MaxIP).

In order to switch between maximal-faces descriptions and all-faces descriptions of polyhedral subdivisions, we introduce the following notation: For a set \mathcal{S} of label subsets of a point configuration \mathbf{A} , the set of all maximal cells of \mathcal{S} is denoted by $\hat{\mathcal{S}}$ and the set of all faces of cells in \mathcal{S} is denoted by $\bar{\mathcal{S}}$.

Proof. It is clear that (MaxUP) and (MaxIP) are necessary. We will now show that they are sufficient as well. We will use the characterization (CP), (UP), (IP).

Consider a set \mathcal{S} of d -cells satisfying (MaxUP) and (MaxIP). Then (UP) is fulfilled for the closure $\hat{\mathcal{S}}$ of \mathcal{S} , since the convex hull of any d -cell contains the convex hulls of all its faces.

Now, let B and B' be cells in $\hat{\mathcal{S}}$ of arbitrary dimension so that there is an $\mathbf{x} \in \text{relint}(B) \cap \text{relint}(B')$. If $B \neq B'$, this means that $B \cup B'$ is a dependent subconfiguration, and we conclude from the general position assumption that $|B \cup B'| \geq d + 2$ and that $\text{conv}(B \cup B')$ is full-dimensional.

Let R be a d -cell in \mathcal{S} containing B as a face, and let R' be a d -cell in \mathcal{S} containing B' as a face. First, no d -cell can have both B and B' as a face. Therefore, $R \neq R'$. We claim that $\text{relint}(R) \cap \text{relint}(R') \neq \emptyset$. If $R = B$ and $R' = B'$, then this is clear. Thus, we assume, without loss of generality, that

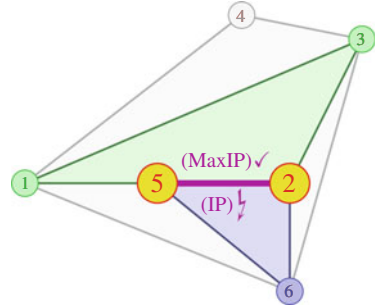


Figure 4.48: In non-general position, (MaxIP) cannot guarantee proper intersection of cells, not even for triangulations: the simplices 123 and 256 do not intersect properly (e.g., because they do not intersect in a common face of both), but (MaxIP) is satisfied. We see that $\{123, 256, 156, 134, 236\}$ satisfies both (MaxIP) and (MaxUP), but fails to be a triangulation.

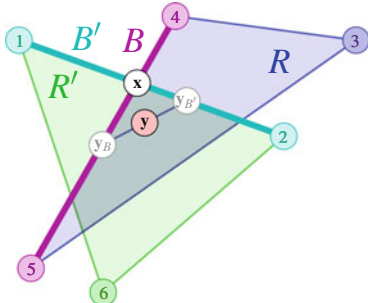


Figure 4.49: From a point x in the intersection of the relative interiors of lower dimensional cells B and B' we construct a point y in the intersection of the relative interiors of the incident full-dimensional cells R and R' , respectively. This is only possible because the general position assumption guarantees that intersections are transversal: here, this means that the points 1 and 2 are separated by a hyperplane containing B .

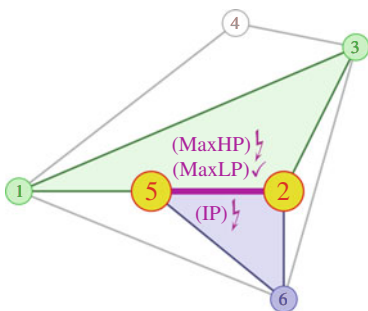


Figure 4.50: This example with (IP) violated by 12 and 25 showed the non-sufficiency of (MaxIP) in non-general position; we see that (MaxLP) is fulfilled because $123 \cap 256 = 2$, which is a vertex of both 123 and 256. (MaxHP) is, however, violated, since the intersection of convex hulls yields the convex hull of 25, whereas the convex hull of the intersection is 2 alone.

$R \neq B$, and thus $B < R$. Let \mathbf{H}_B be a supporting hyperplane of some facet of R that contains B . Since $\mathbf{x} \in \text{relint}(B)$, it follows that $\mathbf{x} \in \mathbf{H}_B$.

Not all points in B' can lie on \mathbf{H}_B (remember: $B \cup B'$ is full-dimensional), and since $\mathbf{x} \in \text{relint}(B')$ there must be points in B' , and thus in $F' \supseteq B'$, on both sides of \mathbf{H}_B , i.e., B' is strictly separated by \mathbf{H}_B . (Keep this in mind; we will use conclusions of this type in the next section in a combinatorial language.) In particular, $\text{relint}(B')$ intersects both open halfspaces generated by \mathbf{H}_B .

Pick a point $\mathbf{y}_{B'}$ on $\text{relint}(B')$ very close to \mathbf{x} that lies on the side of \mathbf{H}_B containing R . If $B' = R'$, then we are done, since $\mathbf{y}_{B'}$ is then in $\text{relint}(R) \cap \text{relint}(R')$.

Otherwise, we can analogously pick a point \mathbf{y}_B on $\text{relint}(B)$ very close to \mathbf{x} that lies on the side of $\mathbf{H}_{B'}$ containing R' .

By construction, $\mathbf{y}_{B'}$ lies in the relative interior of R and \mathbf{y}_B in the relative interior of R' . (This is similar to the “beneath/beyond”-concept in polytope theory, cf. [339].) Now, pick another point \mathbf{y} on the open segment $(\mathbf{y}_{B'}, \mathbf{y}_B)$. Since all distances are very small, this point \mathbf{y} will still be in $\text{relint}(R)$, but also in $\text{relint}(R')$. Thus, (MaxIP) is violated, and we are done. \square

What we actually used in the proof is the so-called orthogonality between dependences and linear functions. We will not elaborate on these concepts here.

Also the restriction of (FP) and (MF) to maximal faces does not suffice in general to guarantee proper intersection in a polyhedral subdivision (it does in general position, though; see exercises). Therefore, we resort to the characterization in Theorem 4.5.3: The reader may have noticed that (HP) and (LP) yield the only characterization of proper intersection that do not need (CP) for the proof of their sufficiency.

Theorem 4.5.7. *A set \mathcal{S} of d -dimensional subconfigurations of a point configuration \mathbf{A} in \mathbb{R}^d labeled by J is the set of maximal cells of a polyhedral subdivision of \mathbf{A} if and only if it satisfies the following conditions:*

- (MaxUP) $\bigcup_{B \in \mathcal{S}} \text{conv}(B) \supseteq \text{conv}(\mathbf{A})$ (*Union Property for Maximal Cells*).
- (MaxHP) $\text{conv}(B) \cap \text{conv}(B') = \text{conv}(B \cap B')$ for all $B, B' \in \mathcal{S}$. (*Hull Property for Maximal Cells*)
- (MaxLP) $B \cap B'$ is a face of both B and B' for all $B, B' \in \mathcal{S}$. (*Label Property for Maximal Cells*).

More specifically, (MaxHP) and (MaxLP) for \mathcal{S} together are equivalent to (CP) and (IP) for $\bar{\mathcal{S}}$, in particular, they are sufficient for proper intersection of \mathcal{S} .

We remark that this characterization was used as the definition of polyhedral subdivisions in [165].

Proof. Since (MaxHP) and (MaxLP) are weaker than (HP) and (LP), we only have to show sufficiency, i.e., that (MaxHP) and (MaxLP) for \mathcal{S} together imply (IP) for $\bar{\mathcal{S}}$, where (CP) is trivially fulfilled in $\bar{\mathcal{S}}$.

Let F and F' be cells in \mathcal{T} , and let $\mathbf{x} \in \text{relint}(F) \cap \text{relint}(F')$. We have to show once again that this is only possible when $F = F'$. Let B and B' be cells in \mathcal{S} with $F \leq B$ and $F' \leq B'$.

From (MaxLP), we know that $B \cap B'$ is a face of both B and B' . Moreover, $\mathbf{x} \in \text{relint}(F) \cap \text{relint}(F') \subseteq \text{conv}(B) \cap \text{conv}(B') = \text{conv}(B \cap B')$, the latter equality by (MaxHP). So we can apply Lemma 2.1.25 to obtain:

$$\text{carrier}(\mathbf{x}, B) = \text{carrier}(\mathbf{x}, B \cap B') = \text{carrier}(\mathbf{x}, B'). \quad (4.6)$$

Since $\mathbf{x} \in \text{relint}(F)$ and $F \leq B$ we know that $F = \text{carrier}(\mathbf{x}, B)$ by Remark 2.1.24. Similarly, $F' = \text{carrier}(\mathbf{x}, B')$. Putting everything together we obtain

$$F = \text{carrier}(\mathbf{x}, B) = \text{carrier}(\mathbf{x}, B \cap B') = \text{carrier}(\mathbf{x}, B') = F', \quad (4.7)$$

as desired. \square

Again, Condition (MaxLP) is trivially satisfied for independent cells. Thus, we state the simplified version for triangulations:

Theorem 4.5.8. *A set \mathcal{T} of d -dimensional independent subconfigurations of a point configuration \mathbf{A} in \mathbb{R}^d labeled by J is the set of maximal cells of a triangulation of \mathbf{A} if and only if it satisfies the following conditions:*

(MaxUP) $\bigcup_{B \in \mathcal{T}} \text{conv}(B) \supseteq \text{conv}(\mathbf{A})$ (*Union Property for Maximal Cells*).

(MaxHP) $\text{conv}(B) \cap \text{conv}(B') = \text{conv}(B \cap B')$ for all $B, B' \in \mathcal{T}$. (*Hull Property for Maximal Cells*)

More specifically, (MaxHP) for \mathcal{T} is equivalent to (CP) and (IP) for $\bar{\mathcal{T}}$, in particular, it is sufficient for proper intersection of \mathcal{T} .

So far, we have replaced the original (IP)-condition by many other constraints. We now turn our attention to find something handy to replace (UP). To this end, let \mathcal{S} be a polyhedral subdivision of \mathbf{A} . Now, imagine there is a cell B in \mathcal{S} that has a facet $F < B$ that is not contained in any facet of \mathbf{A} . Then, since (IP) and (UP) hold, it is intuitive that there must be another cell in \mathcal{S} sharing that facet with B . This is indeed the right idea, which works whenever \mathcal{S} is non-empty in the first place. Since (MaxHP) and (MaxLP) work more generally to enforce proper intersection, we combine the new condition with (MaxHP) and (MaxLP) instead of (MaxIP), which works only in general position.

Theorem 4.5.9. *A non-empty set \mathcal{S} of d -dimensional subconfigurations of a point configuration \mathbf{A} in \mathbb{R}^d is the set of maximal cells of a polyhedral subdivision of \mathbf{A} if and only if it satisfies the following conditions:*

(MaxMP) *For each facet F of a d -cell B in \mathcal{S} , either F is contained in a facet of \mathbf{A} or there is another d -cell B' in \mathcal{S} that contains F as a facet (Pseudo-Manifold Property for Maximal Cells).*

(MaxHP) $\text{conv}(B) \cap \text{conv}(B') = \text{conv}(B \cap B')$ for all $B, B' \in \mathcal{S}$. (*Hull Property for Maximal Cells*)

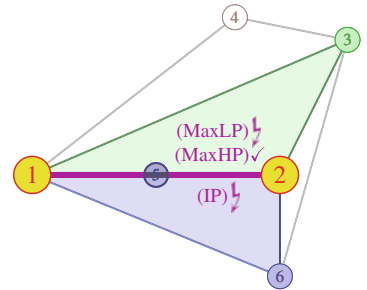


Figure 4.51: This example with (IP) violated by 12 and 125 shows once more the non-sufficiency of (MaxIP) in non-general position; we see that this time (MaxHP) is fulfilled because the convex hulls of 123 and 1526 intersect in the convex hull of 12, which is the convex hull of the intersection of 123 and 1256. (MaxLP) is, however, violated, since the intersection of 123 and 1526 is 12, which is not a face of 1526.

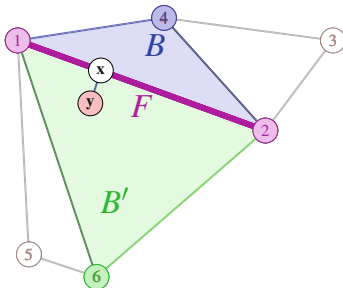


Figure 4.52: Given a facet F of a cell B in a subdivision that is not in a facet of the point configuration, how can we find a cell B' in the subdivision having F as a facet as well? From a point $x \in \text{relint}(F)$ in general position we can step away from B (since x is not in a facet of the point configuration!), obtaining y . By (MaxUP), there is a maximal cell B' containing y —in its relative interior because y can be chosen in general position. Then F must be a facet of B' : since y can be chosen arbitrarily close to x , the point x in $\text{conv}(B')$. Since by (IP) the carrier of a point must be the same in every cell of a subdivision, F must be the carrier of x in B' because it is the carrier of x in F .

(MaxLP) $B \cap B'$ is a face of both B and B' for all $B, B' \in \mathcal{S}$. (Label Property for Maximal Cells)

Moreover, (MaxMP) together with (MaxHP) and (MaxLP) for adjacent maximal cells already imply (MaxUP).

Proof. First of all, let \mathcal{S} be the set of maximal cells of a polyhedral subdivision of \mathbf{A} , in particular, (MaxUP), (MaxHP), and (MaxLP) hold for \mathcal{S} . We will show that then (MaxMP) must hold as well.

To this end, let F be a facet of a d -cell B in \mathcal{S} that is not contained in a facet of \mathbf{A} . Pick a point x in the relative interior of $\text{conv}(F)$ and another point y in general position very close to x and away from B , i.e., so that $\text{conv}(F)$ separates y from B . This is possible because F is not a facet of \mathbf{A} .

Since (MaxUP) holds there is a d -cell B' in \mathcal{S} with $y \in \text{conv}(B')$, which must be different from B , since y is separated from B by $\text{conv}F$. Since y is in general position, y must be in the relative interior of B' . Since y can be chosen arbitrarily close to x , each point on the open segment (x, y) must be also in $\text{relint}(B')$. This implies that point x must be in $\text{conv}(B')$. Proper intersection, i.e., (IP) for all faces of B and B' , implies that the carrier of x in B' must be equal to its carrier F in B , which implies that F is also a facet of B' .

Now assume that (MaxMP), (MaxHP), and (MaxLP) hold for $\mathcal{S} \neq \emptyset$. Pick an arbitrary $x \in \text{conv}(\mathbf{A})$ and a d -cell B in \mathcal{S} . Choose a point y in $\text{relint}(B)$ in general position and consider the segment $[x, y]$. Either this segment is completely contained in $\text{conv}(B)$ (done: $y \in \text{conv}(B)$), or the segment intersects a facet F of B in a point z . Since $[x, y]$ is not contained in $\text{conv}(B)$, the facet F of B cannot be a facet of \mathbf{A} . Thus, by (MaxMP), there is another d -cell B' having F as a facet. Because (MaxHP) and (MaxLP) imply in particular (MaxIP), B and B' must be separated by F . (Otherwise $\text{relint}(B)$ and $\text{relint}(B')$ have non-empty intersection.) Pick a point y' in $\text{relint}(B')$ in general position on the segment $[x, y]$. Note that the distance between x and y' is strictly smaller than the distance from x to y . Therefore, if we repeat the process, we finally find a d -cell that contains x in its convex hull, so that (MaxUP) holds. Because (MaxUP), (MaxHP), and (MaxLP) are sufficient by Theorem 4.5.7, so are (MaxMP), (MaxHP), and (MaxLP).

Since we have used (MaxHP) and (MaxLP) only for adjacent maximal cells to derive (MaxUP) from (MaxMP), the final assertion of the theorem is proved as well. \square

Only (MaxUP)—and hence (UP)—can be derived from (MaxMP) in the presence of (MaxHP) and (MaxLP) for adjacent cells; the proof of proper intersection used Theorem 4.5.7, whose proof required (MaxHP) and (MaxLP) in full generality.

At first glance, one is tempted to think that, since the new condition (MaxMP) is equivalent to (MaxUP) in the presence of proper intersection (which is true), it has nothing to contribute to proper intersection itself (which is false). In fact, in the presence of (MaxMP) instead of (MaxUP), the conditions for proper intersection can be further simplified so that the

effort to check the conditions is reduced drastically: At the expense of one additional condition, we can indeed restrict ourselves to adjacent maximal cells. For the proof, a tool is needed that will be also useful later.

Definition 4.5.10 (Segment Adjacency Graph). Let \mathcal{S} be a collection of d -cells of a point configuration \mathbf{A} in \mathbb{R}^d . The *adjacency graph* or *dual graph* of \mathcal{S} is the graph with nodes corresponding to the d -cells in \mathcal{S} and edges corresponding to d -cells sharing a common facet.

For a segment $[x, y] \subseteq \text{conv}(\mathbf{A})$ in general position (i.e., it does not intersect any $(d-2)$ -face of \mathcal{S}) the *segment adjacency graph* or—more specifically—the $[x, y]$ -*adjacency graph* of \mathcal{S} is the subgraph of the adjacency graph of \mathcal{S} with nodes corresponding to all d -cells in \mathcal{S} whose convex hulls intersect the open segment (x, y) and edges corresponding to pairs of d -cells that share a common facet intersecting (x, y) as well.

Walls whose convex hulls intersect the open segment are called *interior walls* of the segment adjacency graph.

Note that there may be additional edges between nodes if the intersection of the common facet of two nodes with the segment is not required (exercise). That is, the segment adjacency graph is not necessarily an *induced subgraph* of the adjacency graph.

Lemma 4.5.11 (Segment Adjacency Graph Lemma). Let \mathcal{S} be a collection of d -cells of a point configuration \mathbf{A} in \mathbb{R}^d . Moreover, let $[x, y] \subseteq \text{conv}(\mathbf{A})$ be a segment in general position.

Assume that every pair of d -cells adjacent in the $[x, y]$ -adjacency graph of \mathcal{S} intersects properly. Then the $[x, y]$ -adjacency graph of \mathcal{S} consists of disjoint paths (some of them maybe isolated points) only.

If, moreover, every interior facet of the segment adjacency graph is contained in at least two d -cells of \mathcal{S} , then the $[x, y]$ -adjacency graph of \mathcal{S} is a union of disjoint paths, each from a node containing x in its convex hull to a node containing y in its convex hull.

If moreover, there is a point on $[x, y]$ that is contained in exactly one d -cell of \mathcal{S} then the $[x, y]$ -adjacency graph of \mathcal{S} is a single path from a node containing x in its convex hull to a node containing y in its convex hull.

Proof. In order to show the first assertion, we show that each node in the segment adjacency graph has degree zero, one, or two, and that there are no cycles.

We start with the degree. Let B be a node in the segment adjacency graph, i.e., a d -cell intersecting $[x, y]$. The segment intersects $\partial \text{conv}(B)$ in at most two points. Since the segment is in general position, these points lie in unique facets of $\text{conv}(B)$. Only for each such facet there can exist at most one neighbor, since adjacent cells that are properly intersecting must be on different sides of their common facet.

If we “drive” on the segment from x to y , we can number all cells in the segment adjacency graph in the order of appearance. This yields a total order on all nodes in the segment adjacency graph. Assume that there is a cycle. The maximal and the minimal element have both of their neighbors on

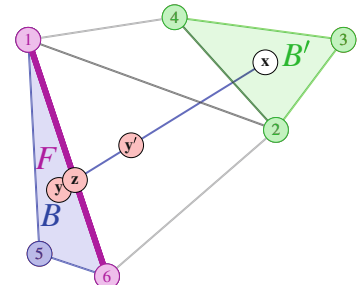


Figure 4.53: With the help of a straight line segment from an arbitrary point x to an interior point y of a full-dimensional cell we find a cell covering x provided (MaxMP) holds.

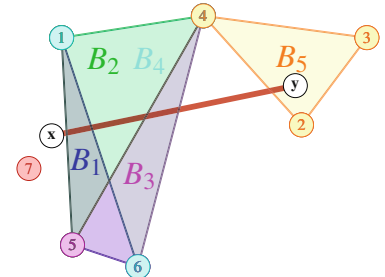


Figure 4.54: The set of cells 156, 145, 456, 146, 234 contains improper intersections among cells adjacent in the segment adjacency graph; ...

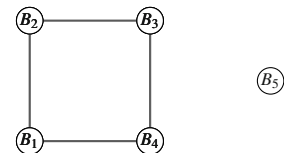


Figure 4.55: ... while its segment adjacency graph contains a cycle.

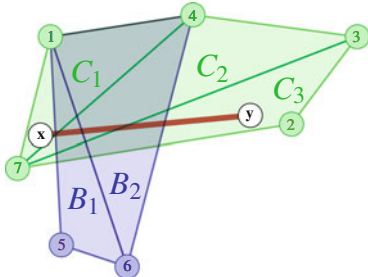


Figure 4.56: If all cells adjacent in the segment adjacency graph intersect properly (observe that B_2 and C_1 are adjacent and intersect improperly, however they are not adjacent in the segment adjacency graph!), ...

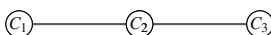


Figure 4.57: ... cycles are impossible.

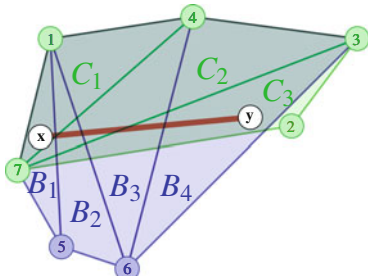


Figure 4.58: If, moreover, every facet pierced by the segment is in exactly two cells, ...

the same side of the common facet: a contradiction to the assumed proper intersection.

If every interior facet is a facet of at least two d -cells in \mathcal{S} , then every node not containing \mathbf{x} or \mathbf{y} in its convex hull has degree two. Since there are no cycles, the statement follows.

If, in this union of paths, one point of the segment lies in a unique node, then all paths must contain this node. This is only possible if there is only one path in the first place. \square

We can now state and prove the simplification of the conditions ensuring proper intersection because (MaxMP) helps. One additional condition (IPP) is required, though. The good thing about (IPP) is that it ensures non-emptiness for free.

Theorem 4.5.12. *A set \mathcal{S} of d -dimensional subconfigurations of a point configuration \mathbf{A} in \mathbb{R}^d is the set of maximal cells of a polyhedral subdivision of \mathbf{A} if and only if it satisfies the following conditions:*

(MaxMP) *For each facet F of a d -cell B in \mathcal{S} , either F is contained in a facet of \mathbf{A} or there is another d -cell B' in \mathcal{S} that contains F as a facet (Pseudo-Manifold Property for Maximal Cells).*

(MaxAdjPI) *Every two adjacent maximal cells intersect properly (Proper Intersection of Adjacent Maximal Cells).*

(IPP) *There is a point $\mathbf{x} \in \text{conv}(\mathbf{A})$ in general position that is contained in the convex hull of exactly one d -cell (Interior Point Property).*

More specifically, (MaxAdjPI) and (IPP) for \mathcal{S} together are equivalent to (IP) and (CP) for \mathcal{S} .

Proof. Condition (IPP) is necessary for polyhedral subdivisions since any point in general position lies in the relative interior of some d -cell, which must be unique because of (IP). Condition (MaxAdjPI) is weaker than (MaxPI), so it is necessary as well.

It remains to prove sufficiency. Assume that there are cells F and F' in \mathcal{S} and a point $\mathbf{x} \in \text{relint}(F) \cap \text{relint}(F')$. Once more, we want to show that $F = F'$ must hold. Since (IPP) holds, there is a point \mathbf{p} in general position that is in the relative interior of a unique cell. Consider the line segment $[\mathbf{p}, \mathbf{x}]$. Because \mathbf{p} is in general position, this segment intersects no $(d-2)$ -cell.

Now, consider arbitrary d -cells B and B' in \mathcal{S} with $F < B$ and $F' < B'$. We want to argue with the segment adjacency graph, i.e., we need d -cells in \mathcal{S} that intersect the open segment (\mathbf{p}, \mathbf{x}) and have F and F' , respectively, as faces. However, B and B' may indeed have empty intersection with (\mathbf{p}, \mathbf{x}) . Therefore, we must construct the d -cells we need. The key is another application of the segment adjacency graph.

To summarize: We want to find d -cells R and R' intersecting the open segment (\mathbf{p}, \mathbf{x}) that have F and F' , respectively, as faces.

Pick points \mathbf{y} and \mathbf{y}' in $\text{relint}(B)$ and $\text{relint}(B')$, respectively, very close to \mathbf{x} . Moreover, pick a point \mathbf{z} on the open segment (\mathbf{p}, \mathbf{x}) very close to \mathbf{x} in general position. This is possible because the segment is in general position. The $[\mathbf{z}, \mathbf{y}]$ -adjacency graph and the $[\mathbf{z}, \mathbf{y}']$ -adjacency graph contain paths connecting d -cells containing the respective end points of the segments in their convex hulls (this holds by (MaxMP), (MaxAdjPI), and Lemma 4.5.11).

Let R and R' be the cells corresponding to the end nodes of one of the paths containing \mathbf{z} . Each of them contains \mathbf{z} in its relative interior, since \mathbf{z} is in general position. Moreover, since \mathbf{z} and point \mathbf{y} can be chosen to lie arbitrarily close to \mathbf{x} , all points on the segment $[\mathbf{z}, \mathbf{y}]$ can be forced to lie arbitrarily close to \mathbf{x} . Thus, each d -cell in the $[\mathbf{z}, \mathbf{y}]$ -adjacency graph contains \mathbf{x} in its convex hull. If this d -cell equals B , then $R = B$ contains F as a face.

Otherwise, consider the first d -cell B_1 in the $[\mathbf{z}, \mathbf{y}]$ -adjacency graph that does not contain F as a face. Moreover, let B_0 be the previous adjacent d -cell in the $[\mathbf{z}, \mathbf{y}]$ -adjacency graph. Since $\mathbf{x} \in \text{conv}(B_1)$, we can compute the carrier F_1 of \mathbf{x} in B_1 , which is a face of B_1 containing \mathbf{x} in its relative interior. The fact that $\mathbf{x} \in \text{relint}(F) \cap \text{relint}(F_1)$ with $F \leq B_0$ and $F_1 \leq B_1$ means that the adjacent d -cells B_0 and B_1 do not intersect properly: contradiction to (MaxAdjPI).

Consequently, such a B_1 can not exist, and thus all d -cells on the $[\mathbf{z}, \mathbf{y}]$ -adjacency graph contain F as a face, in particular R . Similarly, R' contains F' as a face.

This time, by (MaxMP), (MaxAdjPI), (IPP), and Lemma 4.5.11, the $[\mathbf{p}, \mathbf{x}]$ -adjacency graph of \mathcal{S} is a unique path. That means, in particular, there is a unique cell on it containing \mathbf{x} in its convex hull. Translated to geometry, this means that there is only one unique d -cell whose convex hull intersects the open segment (\mathbf{p}, \mathbf{x}) and contains \mathbf{x} .

Thus, $R = R'$, and since this d -cell contains both F and F' as faces with non-empty interior intersection \mathbf{x} , we conclude that $F = F'$, as desired. \square

We know that a check of (MaxAdjPI) along the definition would require a check of interior intersections for all pairs of faces of cells. But for this, we already have provided a solution: proper intersection of maximal cells can be checked via (MaxHP) and (MaxLP) without any reference to all faces. Thus, we receive the following characterization that reduces intersection checks to maximal adjacent cells.

Corollary 4.5.13. *A set \mathcal{S} of d -dimensional subconfigurations of a point configuration \mathbf{A} in \mathbb{R}^d is the set of maximal cells of a polyhedral subdivision of \mathbf{A} if and only if it satisfies the following conditions:*

(MaxMP) *For each facet F of a d -cell B in \mathcal{S} , either F is contained in a facet of \mathbf{A} or there is another d -cell B' in \mathcal{S} that contains F as a facet (Pseudo-Manifold Property for Maximal Cells).*

(MaxAdjHP) $\text{conv}(B) \cap \text{conv}(B') = \text{conv}(B \cap B')$ for all adjacent $B, B' \in \mathcal{S}$.
(Hull Property for Adjacent Maximal Cells)

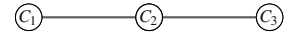


Figure 4.59: ... then the segment adjacency graph is a collection of paths, each from a cell whose convex hull contains x to a cell whose convex hull contains y .

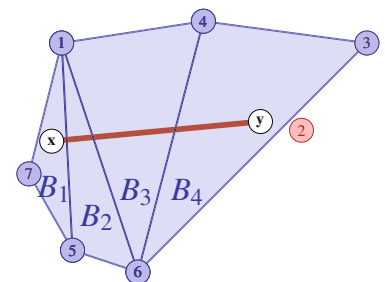


Figure 4.60: If, finally, there is a point in the segment that is in the convex hull of exactly one cell, ...



Figure 4.61: ... then the segment adjacency graph must be a unique path from a cell whose convex hull contains x to a cell whose convex hull contains y .

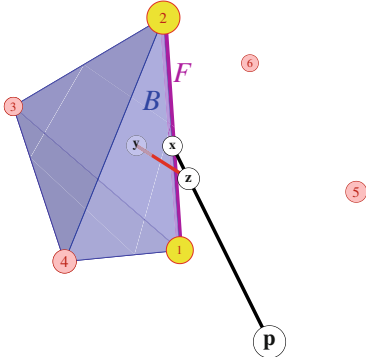


Figure 4.62: All d -cells intersecting the segment $[y, z]$ (which can be as close to x as we wish) contain F as a face, in particular the one containing z , which exists because of the Segment Adjacency Graph Lemma 4.5.11.

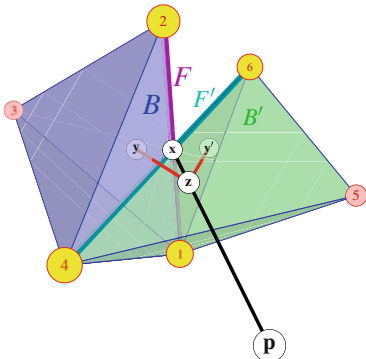


Figure 4.63: Via the $[y, z]$ -adjacency graph and the $[y', z]$ -adjacency graph together with (MaxMP) and (MaxAdjPI), we can construct cells that contain F respectively F' as faces and contain z ; the $[x, p]$ -adjacency graph together with (MaxMP), (MaxAdjPI), and (IPP) for p shows that z is covered by a unique d -cell, all of whose faces, in particular, F and F' , must be properly intersecting: thus, $F = F'$, i.e., the situation in the picture is impossible provided (MaxMP), (MaxAdjPI), and (IPP) hold.

(MaxAdjLP) $B \cap B'$ is a face of both B and B' for all adjacent $B, B' \in \mathcal{S}$.
 (Label Property for Adjacent Maximal Cells).

(IPP) There is a point $\mathbf{x} \in \text{conv}(\mathbf{A})$ in general position that is contained in the convex hull of exactly one d -cell (Interior Point Property).

More specifically, (MaxAdjHP), (MaxAdjLP), and (IPP) for \mathcal{S} together are equivalent to (IP) and (CP) for \mathcal{S} . \square

Remark 4.5.14. The theorem and its corollary is wrong with (MaxMP) replaced by (MaxUP): Consider a segment with unique end points 1 and 2 and a repeated interior point 3 and 4. Then $\{12, 34\}$ is not a valid polyhedral subdivision but (MaxUP) is satisfied, and (MaxAdjPI) as well as (MaxAdjHP) and (MaxAdjLP) are void because there are no adjacent cells. However, (MaxMP) is violated (see Figure 4.64). Thus, (MaxMP) contributes to proper intersection in the sense that it *enforces adjacencies between d -cells* to feed (MaxAdjPI).

We remark that there are other conditions that can replace (IPP) in the above characterization (Exercise 4.15).

If A happens to have a facet that is a simplex, it can be shown that the extra condition can be dropped [96], which leads to the following theorem.

Theorem 4.5.15. A set \mathcal{S} of d -dimensional subconfigurations of a point configuration \mathbf{A} in \mathbb{R}^d with a simplicial facet is the set of maximal cells of a polyhedral subdivision of \mathbf{A} if and only if it satisfies the following conditions:

(MaxMP) For each facet F of a d -cell B in \mathcal{S} , either F is contained in a facet of \mathbf{A} or there is another d -cell B' in \mathcal{S} that contains F as a facet (Pseudo-Manifold Property for Maximal Cells).

(MaxAdjPI) Every two adjacent maximal cells intersect properly (Proper Intersection of Adjacent Maximal Cells).

Proof. Only sufficiency must be proved. Let \mathcal{S} satisfy (MaxMP) and (MaxAdjPI). Consider the simplicial facet F : any two cells having a facet inside F are in fact adjacent. Thus, they must intersect properly by (MaxAdjPI). Since there are only points on one side of a facet, in any \mathcal{S} satisfying (MaxMP), (MaxAdjPI) there can be only one unique cell B having a facet inside F . Now take a point p very close to $\text{conv}(F)$ in the interior of B in general position. If the convex hull of a d -cell of \mathcal{S} contains p , then that cell inevitably also contains F as a facet as well. Thus, among the cells in \mathcal{S} only B contains p in its convex hull. This proves that (IPP) holds for \mathcal{S} , and thus, by Theorem 4.5.12, that \mathcal{S} is the set of maximal cells of a subdivision. \square

For completeness, we state the respective corollary:

Corollary 4.5.16. A set \mathcal{S} of d -dimensional subconfigurations of a point configuration \mathbf{A} in \mathbb{R}^d with a simplicial facet is the set of maximal cells of a polyhedral subdivision of \mathbf{A} if and only if it satisfies the following conditions:

- (MaxMP) For each facet F of a d -cell B in \mathcal{S} , either F is contained in a facet of \mathbf{A} or there is another d -cell B' in \mathcal{S} that contains F as a facet (Pseudo-Manifold Property for Maximal Cells).
- (MaxAdjHP) $\text{conv}(B) \cap \text{conv}(B') = \text{conv}(B \cap B')$ for all adjacent $B, B' \in \mathcal{S}$. (Hull Property for Adjacent Maximal Cells)
- (MaxAdjLP) $B \cap B'$ is a face of both B and B' for all adjacent $B, B' \in \mathcal{S}$. (Label Property for Adjacent Maximal Cells) \square

If our configuration is in general position, then there is a nice geometric characterization of polyhedral subdivisions, of a completely different flavor. Basically, it rewrites (MaxUP) and (MaxIP) in Theorem 4.5.6 in terms of volumes. This will be of use in Section 6.1.

Theorem 4.5.17. A set \mathcal{S} of full-dimensional subconfigurations of a point configuration \mathbf{A} in \mathbb{R}^d in general position is the set of maximal cells of a polyhedral subdivision of \mathbf{A} if and only if it satisfies the following conditions:

- (MaxUVP) The d -dimensional volume of the set of points $\mathbf{x} \in \text{conv}(\mathbf{A})$ for which there is no $B \in \mathcal{S}$ with $\mathbf{x} \in \text{conv}(B)$ is zero (Uncovered Volume Property).
- (MaxMVP) The d -dimensional volume of the set of points $\mathbf{x} \in \text{conv}(\mathbf{A})$ for which there is more than one $B \in \mathcal{S}$ with $\mathbf{x} \in \text{conv}(B)$ is zero (Multiply-Covered Volume Property).

We remark that this characterization was exploited in [112] for the vertex sets of cyclic polytopes.

Proof. It is clear that both (MaxUVP) and (MaxMVP) are necessary. In the following we show that (MaxUVP) and (MaxMVP) are sufficient as well. We will show that “not (MaxUP)” implies “not (MaxUVP)” and “not (MaxIP)” implies “not (MaxMVP)”.

Assume first that (MaxUP) is violated, i.e., there is a point $\mathbf{x} \in \text{conv}(\mathbf{A})$ for which there is no $B \in \mathcal{S}$ with $\mathbf{x} \in \text{conv}(B)$. Then, since the convex hull is a closed subset of $\text{conv}(\mathbf{A})$, the set $\text{conv}(\mathbf{A}) \setminus \bigcup_{B \in \mathcal{S}} \text{conv}(B)$ is an open, non-empty subset of \mathbb{R}^d , and any open subset of \mathbb{R}^d has non-zero d -dimensional volume. Therefore, (MaxUVP) is violated.

Assume now that (MaxIP) is violated, i.e., there are d -cells $B, B' \in \mathcal{S}$ with $B \neq B'$ and $\text{relint}(B) \cap \text{relint}(B') \neq \emptyset$. Then $\text{relint}(B) \cap \text{relint}(B')$ is the intersection of full-dimensional open subsets of \mathbb{R}^d , hence open, and thus the d -dimensional volume of $\text{relint}(B) \cap \text{relint}(B')$ is non-zero. But this is exactly the volume of all those points in $\text{conv}(\mathbf{A})$ that are in both $\text{conv}(B)$ and $\text{conv}(B')$. Therefore, the total d -dimensional volume of the set of points $\mathbf{x} \in \text{conv}(\mathbf{A})$ for which there is more than one $B \in \mathcal{S}$ with $\mathbf{x} \in \text{conv}(B)$ is non-zero, i.e., (MaxMVP) does not hold. \square

4.5.2 Combinatorial characterizations

The key of this section is that the properties of a point configuration \mathbf{A} that are relevant for its polyhedral subdivisions can be encoded completely in

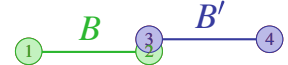


Figure 4.64: B and B' are not a triangulation. However, (MaxUP) and (IPP) are obvious, and, since B and B' are not adjacent, (MaxAdjPI) is trivially fulfilled as well. Hence, (MaxUP), (MaxAdjPI), and (IPP) are not sufficient for being a subdivision, not even in the case of triangulations in dimension one. (MaxMP) is violated because the interior facet 2 is contained only in one cell.

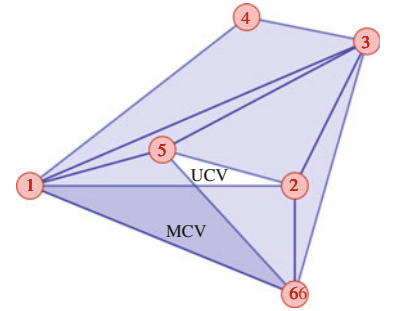


Figure 4.65: The uncovered as well as the multiply covered volumes are non-zero: no subdivision.

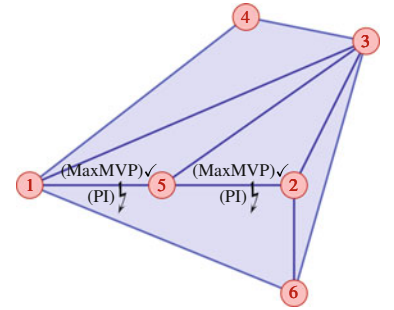


Figure 4.66: In special position, the multiply covered volume maybe zero although there are cells that are not intersecting properly because lower-dimensional intersections are not measured.

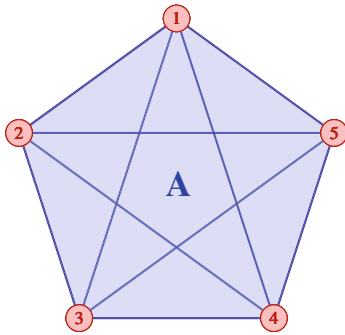


Figure 4.67: We illustrate the lexicographic extension with respect to the permutation

$(5, 2, 3)$ in the five-gon. Indicated is the stratification by all possible hyperplanes spanned by the points, illustrating the so-called discriminantal hyperplane arrangement. Its cells are regions of constant cocircuit signature.

the combinatorial data introduced in Section 4.1 (circuits and cocircuits, basically).

Theorem 4.1.31 in Section 4.1 already provided us with a purely combinatorial characterization of polyhedral subdivisions.

We want to present further combinatorial characterizations that take into account that the check of conditions should be as efficient as possible. We restrict ourselves to characterizations in terms of maximal cells because one goal of the combinatorial framework is to make the description as compact as possible.

The following characterization is an improvement in the sense that it reduces the effort of checking for proper intersection of pairs of adjacent maximal cells, like in the geometric characterization in Theorem 4.5.13. And again, this comes at a cost: some combinatorial version of (IPP) has to be checked.

In order to argue why this can be done purely combinatorially, we consider a very special new interior point in general position. This special point is useful because it has a predictable signature in each cocircuit of the point configuration extended by it. The special point is called a *lexicographic extension* of the point configuration, and its oriented matroid is called a *lexicographic extension* of the original oriented matroid (see [55] for a more detailed treatment).

Let the n points in \mathbf{A} , as usual, be denoted by \mathbf{p}_i with $j \in J$, and let \mathcal{S} be a set of cells that we want to check for (IPP).

In order to construct a special point for \mathcal{S} , we pick a full-dimensional cell C from \mathcal{S} and fix a permutation $\pi = (c_1, c_2, \dots, c_r, \dots, c_k)$ on the indices of C . For example, if the labels are totally ordered in a canonical way, e.g., like natural numbers, one can choose a order so that $c_1 < c_2 < \dots < c_r < \dots < c_k$, where r denotes the rank of \mathbf{A} , as usual.

The new special point \mathbf{p}_{n+1} is now constructed in r steps. First, place \mathbf{p}_{n+1} directly on top of \mathbf{p}_{c_1} . This way, in every cocircuit of the resulting point configuration, \mathbf{p}_{n+1} will have the same sign as \mathbf{p}_{c_1} . We could say that \mathbf{p}_{n+1} lies in the relative interior of the “cell” $\{c_1\}$. In the next step, we move \mathbf{p}_{n+1} directly towards \mathbf{p}_{c_2} , just enough to leave \mathbf{p}_{c_1} , but so that no new hyperplane spanned by points in \mathbf{A} is reached. This way, the sign of \mathbf{p}_{n+1} in all cocircuits that are zero on \mathbf{p}_{c_1} becomes non-zero, namely the same sign as the sign of \mathbf{p}_{c_2} in that cocircuit. Moreover, the new point now lies in the relative interior of the cell $\{c_1, c_2\}$ and in general position. Repeat this process until we have moved \mathbf{p}_{n+1} slightly towards \mathbf{p}_{c_r} . At that moment, \mathbf{p}_{n+1} is in the relative interior of C in general position and has the property, that in every cocircuit Z^* of the extended configuration $\mathbf{A} \cup \mathbf{p}_{n+1}$ it has the same sign as the minimal index in C that is non-zero in Z^* .

This special point should now lie in at most one cell. First of all, by construction, it lies in the relative interior of C . Therefore, if \mathcal{S} is to be a valid subdivision, it should have no other cell containing \mathbf{p}_{n+1} . This can be expressed in terms of dependence vectors as in Lemma 4.1.11. Since we have the full control over the cocircuits of the extended configuration, we would rather use a characterization in terms of cocircuits. The following

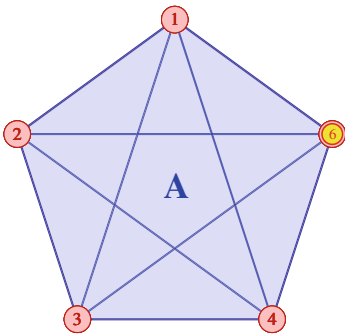


Figure 4.68: First, place Point \mathbf{p}_6 on top of \mathbf{p}_5 .

geometric reasoning leads to this: point \mathbf{p}_{n+1} is not in the convex hull of a full-dimensional cell C' if and only if there is a facet defining hyperplane separating it from the cell, or, expressed in terms of cocircuits, if and only if in one of the facet defining cocircuits Z of C' with zero set Z_0^* the new point \mathbf{p}_{n+1} has a different sign than the points in the (non-empty) set $C' \setminus Z_0^*$.

We can even remove the point \mathbf{p}_{n+1} from the reasoning, since we know that its sign in all cocircuits is given by the sign of the π -minimal element in C that is non-zero in that cocircuit. Thus, we end up with the following more efficient combinatorial characterization, in which (IPP) is implicitly expressed by the unique covering of a lexicographic extension in one of the cells.

Theorem 4.5.18. *A set \mathcal{S} of d -dimensional subconfigurations of a point configuration \mathbf{A} in \mathbb{R}^d labeled by J with n points is the set of maximal cells of a polyhedral subdivision of \mathbf{A} if and only if it satisfies the following conditions:*

- (CoP) *For each d -cell $B \in \mathcal{S}$ and for all cocircuits Z^* that are positive cocircuits on B but not positive on \mathbf{A} there is another d -cell $B' \in \mathcal{S}$ with $B \cap B' = Z_0^* \cap B$ (Cocircuit Property).*
- (AdjCiP) *For each circuit (Z_+, Z_-) such that $Z_+ \subseteq B \in \mathcal{S}$ for some B , either there is no cell in \mathcal{S} adjacent to B containing Z_- or every cell adjacent to B containing Z_+ contains Z_- too (Circuit Property).*
- (ExP) *There is a cell C of \mathcal{S} and a permutation π of its elements such that for all other cells $C' \in \mathcal{S}$ at least one cocircuit Z^* spanned by a facet of C' has different signs on the π -minimal index in $C \setminus Z_0^*$ and on $C' \setminus Z_0^*$ (Extension Property).*

Proof. From (AdjCiP) we easily conclude (MaxAdjHP) and (MaxAdjLP), which proves the assertion by Corollary 4.5.13, since (ExP) has the same geometric meaning as (IPP), as explained before the theorem. We leave the details as an exercise for the reader. \square

The combinatorial formulation (CoP) of (MaxMP) again simplifies when we restrict ourselves to triangulations, since in that case a facet of a cell is just the cell with one element removed, i.e., (MaxMP) is already a combinatorial condition, as in Lemma 4.1.16. Moreover, Condition (AdjCiP) can be merged with (CoP), since the proper intersection of adjacent cells meeting in a wall is equivalent to the following: the points in the cells not in the common wall must be on different sides of the common wall. Thus, we have proved (see also [96]):

Corollary 4.5.19. *A set \mathcal{T} of d -dimensional independent subconfigurations of a point configuration \mathbf{A} in \mathbb{R}^d labeled by J with n points is the set of maximal cells of a triangulation of \mathbf{A} if and only if it satisfies the following conditions:*

- (ICoP) *For every facet F of a d -cell in \mathcal{T} that is not in a facet of \mathbf{A} , there are exactly two simplices $F \cup s$ and $F \cup s'$ in \mathcal{T} such that s and*

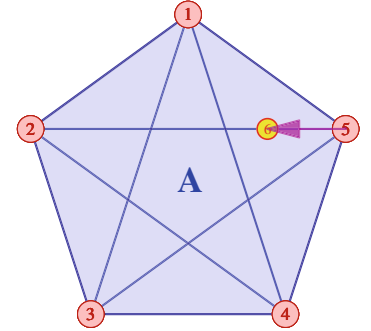


Figure 4.69: Then, move it towards \mathbf{p}_2 a little, but do not cross any hyperplane.

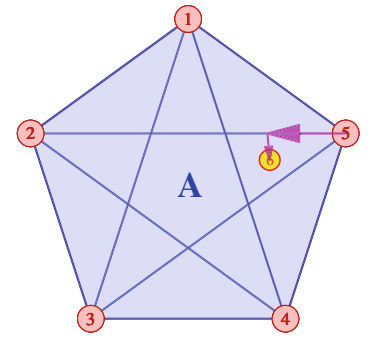


Figure 4.70: Finally, move it towards \mathbf{p}_3 a little, but do not cross any hyperplane. We see that such a procedure will never define a point in the central cell in the chamber complex, that means not every extension is lexicographic!

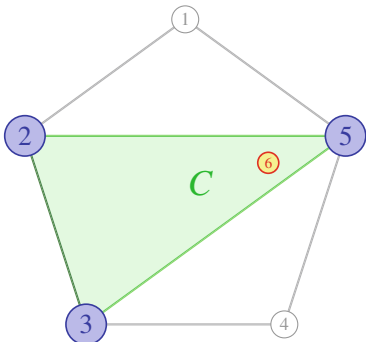


Figure 4.71: Illustration of (ExP): The lexicographic extension 6 w.r.t. $\pi = (523)$ is in the relative interior of the cell $C = 235$.

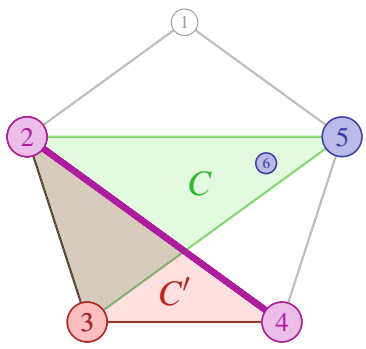


Figure 4.72: Point 6 is not in $\text{conv}(C') = \text{conv}(234)$ because the facet 24 of C' spans a cocircuit that has opposite signs on 6 and $C' \setminus 24$. By definition of the lexicographic extension, this is the case because the π -minimal index 5 in $C \setminus 24$ (w.r.t. the permutation $(5, 2, 3)$) and $C' \setminus 24$ have opposite signs in that cocircuit.

s' have different signs in the cocircuit spanned by F (Intersection Cocircuit Property).

(ExP) There is a cell C of \mathcal{S} and a permutation π of its elements such that for all other cells $C' \in \mathcal{S}$ at least one cocircuit Z^* spanned by a facet of C' has different signs on the π -minimal index in $C \setminus Z_0^*$ and on $C' \setminus Z_0^*$ (Extension Property).

□

Admittedly, (ExP) is still clumsy, but it is compatible with computer calculations.

The power of (ICoP) is further shown by our final statement. We list in it several properties any of which, in addition to (ICoP), are enough to guarantee that \mathcal{T} is a triangulation. Some of them assume particular properties of the point configuration.

Corollary 4.5.20. Let \mathcal{T} be a collection of bases of a configuration \mathbf{A} in \mathbb{R}^d labeled by J with n points. Assume that \mathcal{T} satisfies (ICoP). Then, any of the following conditions is sufficient for \mathcal{T} to be a triangulation of \mathbf{A} .

(IPP) There is a point $\mathbf{x} \in \text{conv}(\mathbf{A})$ in general position that is contained in the convex hull of exactly one d -cell (Interior Point Property).

(SFP) \mathbf{A} has a face that is a simplex and is contained in only one cell of \mathcal{T} (Simplicial Facet Property).

(GFP) \mathbf{A} has a facet F such that \mathcal{T} restricted to F is a triangulation and no $(d-1)$ -simplex in this restriction is part of two different d -simplices of \mathcal{T} (General Facet Property).

(LinkP) \mathbf{A} has an element i that is a vertex and such that the link $\text{link}_{\mathcal{T}}(i)$ is a triangulation of the contraction (Link Property).

(TVP) The total volume of the simplices spanned by the elements of \mathcal{T} equals the volume of $\text{conv}(\mathbf{A})$ (Total volume property).

Proof. (IPP) is equivalent to (ExP), so the fact that it is sufficient follows from Theorem 4.5.19. For the rest, it is easy to prove that any of them implies (IPP). □

This closes our discussion of various characterizations of polyhedral subdivisions. Some versions become much easier if restricted to triangulations because the face structures of their cells does not depend on the underlying geometry. Although at first glance the combinatorial characterizations do not allow for a very elegant language, they are very useful when one is concerned with the development of computer programs to actually compute subdivisions.

Corollary 4.5.19, e.g., has proved very useful for computer checks already: it is actually used in the computer program TOPCOM [265] to check the correctness of triangulations. More about this in Chapter 8.

Interestingly enough, the computational complications that arise when we are dealing with general polyhedral subdivisions may have prevented

the development of a corresponding computer program up to now. The combinatorial characterizations of this section may be a good starting point. Finally, there is another reason why the combinatorial characterizations in this section are important: they show that polyhedral subdivisions only depend on the combinatorial data appearing in the characterizations: Circuits and cocircuits of the point configuration, known as its oriented matroid.

Exercises

Exercise 4.1. Write a proof for Lemma 4.1.11.

Exercise 4.2. Compute all the circuits and cocircuits of the nine-point configuration given by the vertices of the three-dimensional regular cube plus its centroid. List all the facets as cocircuits and show, using the circuits, the centroid lies in the relative interior.

What happens to the circuits and cocircuits if we add as a tenth point the centroid of one of the facets?

Exercise 4.3. Compute the Gale transform of the nine-point configuration given by the vertices of the three-dimensional regular cube minus the origin. Verify the validity of Corollary 4.2.31 in this example.

Exercise 4.4. In this book we use Gale transforms for triangulations, but they have been used quite a bit to describe faces of polytopes. Let \mathbf{A} , labeled by J , be the set of vertices of a polytope \mathbf{P} . A subset $C \subseteq J$ is called a *coface* if $\text{conv}(\mathbf{A}(J \setminus C))$ is a face. Prove the following useful lemma:

If \mathbf{B} is some Gale transform of \mathbf{A} , then $C \subseteq J$ is a coface of $\mathbf{P} \Leftrightarrow 0 \in \text{relint}(\text{cone}_{\mathbf{B}}(C))$.

Exercise 4.5. Provide an example of two combinatorially equivalent point configurations \mathbf{A}_1 and \mathbf{A}_2 in which the same triangulation (given by its sets of labels) is regular for \mathbf{A}_1 but nonregular for \mathbf{A}_2 .

Exercise 4.6. Write a proof for Remark 4.2.14 about products of point configurations and their triangulations.

Exercise 4.7. Write a proof for Lemma 4.2.17.

Exercise 4.8. Show by an example that taking the link at i , of a triangulation constructed by placing i in the last place, may not produce a lexicographic triangulation of \mathbf{A}/i (although it produces a regular one).

Exercise 4.9. Using what you learned about deletion and contraction prove that any triangulation of $\mathbf{A} \setminus a$ (deletion) extends to a triangulation of \mathbf{A} . Similarly, prove that any regular triangulation of \mathbf{A}/a where a is a boundary point can be extended to a regular triangulation of \mathbf{A} . Prove that regularity is necessary (hint: think of the mother of all examples).

Exercise 4.10. Show that the union of a point configuration \mathbf{A} and a point not in the affine span of \mathbf{A} is a pyramid over \mathbf{A} .

Exercise 4.11. Compute the circuits of the one-point suspension $\mathbf{A} \uparrow_i^i$ in terms of the circuits of \mathbf{A} .

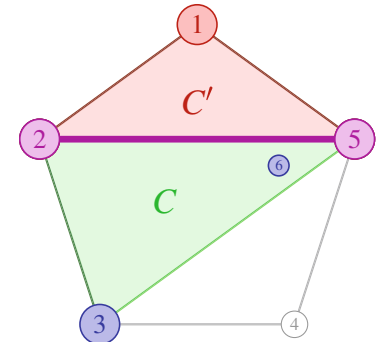


Figure 4.73: Here, $C' = 125$ is checked: the separating facet is 25, and the π -minimal index in $C \setminus 25$ is 3, which has a sign opposite to that of $1 = C' \setminus 25$.

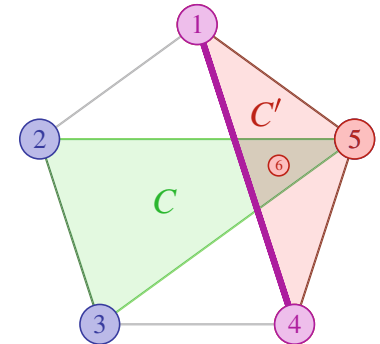


Figure 4.74: This time, for $C' = 145$, we see that no facet of 145 separates 6 from 145 without that facet. This is clear for the two facets of 145 that are facets of \mathbf{A} ; even Facet 14 spans a cocircuit for which the sign of the π -minimal index 5 of $C \setminus 14$ equals the sign of $C' \setminus 14 = 5$. Consequently, 6 is also in 145, which can be seen directly from the picture.

Exercise 4.12. Investigate the triangulations of one-point suspensions. In particular, show:

- (i) The (regular) cross-polytope has exactly d triangulations, each using a different diameter (edge joining two opposite vertices) of it. Moreover, show that each triangulation of the regular cross-polytope is determined by prescribing a single simplex. In particular, all triangulations of the regular cross-polytope are disjoint.
- (ii) If a one-point suspension is applied to the interior point in the configuration of Example 4.1.4 it produces a non-regular octahedron. Hence, this non-regular octahedron has four triangulations (as opposed to the regular octahedron, which has three). There are octahedra with six triangulations, but no more; see Section 5.5.
- (iii) If a one-point suspension is applied to an independent configuration, it produces an independent configuration of one more dimension. Similarly, when applied to a circuit it produces a circuit of one dimension more.

Exercise 4.13. Write a proof of Lemma 4.3.5 about placing triangulations.

Exercise 4.14. Show all triangulations of an n -gon are lexicographic.

Exercise 4.15. Try to find other conditions that can replace (IPP) in Corollary 4.5.13 so as to characterize polyhedral subdivisions of a point set in the general case. Try to find simplifications for triangulations and/or for general position.

Exercise 4.16. Prove the following characterization of polyhedral subdivisions:

(MaxMP) For each facet F of a d -cell B in \mathcal{S} , either F is contained in a facet of \mathbf{A} or there is another d -cell B' in \mathcal{S} that contains F as a facet (Pseudo-Manifold Property for Maximal Cells).

(MaxAdjSP) For every pair of adjacent cells $C, C' \in \mathcal{S}$ sharing a common facet F , the points in $C \setminus F$ and the points in $C' \setminus F$ lie on different sides of the hyperplane spanned by F (Separation Property for Adjacent Maximal Cells).

(IPP) There is a point $\mathbf{x} \in \text{conv}(\mathbf{A})$ in general position that is contained in the convex hull of exactly one d -cell (Interior Point Property).

(This was utilized in [165].)

5

Regular Triangulations and Secondary Polytopes

In this chapter we unveil the beautiful structure of the set of all regular subdivisions and, in particular, of all regular triangulations of a point or vector configuration. The two main ingredients for this are the definitions of *regular subdivisions* and of the *refinement poset* (see Section 2.2.3 and Definition 2.3.8, respectively), that we now recall:

Let \mathbf{A} be a configuration with elements \mathbf{p}_j labeled by $j \in J$. We have already seen that a height function $\omega \in \mathbb{R}^J$ on \mathbf{A} induces a polyhedral subdivision consisting of the projection of the lower faces of the set $\mathbf{A}^\omega := \{ (\mathbf{p}_j)_{\omega_j} : j \in J \}$ of lifted points. Whenever ω is in general position, i.e., no $d+2$ lifted points are on a common non-vertical hyperplane, then we obtain a regular triangulation. As usual, let us denote the polyhedral subdivision induced by such a height ω by $\mathcal{S}(\mathbf{A}, \omega)$.

Recall also from Section 2.3 the notion of refinement: for two polyhedral subdivisions $\mathcal{S}, \mathcal{S}'$ of a point configuration \mathbf{A} , we say \mathcal{S} refines \mathcal{S}' , in formula $\mathcal{S} \preceq \mathcal{S}'$, if, for every cell $C \in \mathcal{S}$, there is a cell $C' \in \mathcal{S}'$ with $C \subseteq C'$. The *refinement poset of all polyhedral subdivisions of \mathbf{A}* , denoted by $\text{Subdivs}(\mathbf{A})$, is the set of all polyhedral subdivisions of \mathbf{A} , partially ordered by refinement. The subposet of all regular polyhedral subdivisions of \mathbf{A} is denoted by $\text{Subdivs}_{\text{reg}}(\mathbf{A})$.

We will find out in this chapter that the subposet $\text{Subdivs}_{\text{reg}}(\mathbf{A})$ is remarkably better behaved than the poset $\text{Subdivs}(\mathbf{A})$. More precisely, if \mathbf{A} is a point configuration (or, equivalently, an acyclic vector configuration), then $\text{Subdivs}_{\text{reg}}(\mathbf{A})$ is the same as the poset of faces of a certain polytope naturally associated to \mathbf{A} , called the secondary polytope. The graph of flips between regular triangulations will be shown to be connected. This will be a consequence of the fact that it contains, as a spanning subgraph, the graph of the secondary polytope. In drastic contrast, we will see in Chapter 7 that the graph of flips between all triangulations is, in general, not connected.

One word about the case of *non-acyclic* vector configurations: Most of what we do in this chapter works for them, with the notable exception of the definition of the secondary polytope itself. A different, slightly more abstract, definition of the secondary polytope was developed in [48], and that definition does generalize to vector configurations, as shown in [49], and leads to the result that $\text{Subdivs}_{\text{reg}}(\mathbf{A})$ is the poset of faces of an unbounded *polyhedron*. We do not cover this second definition, but we do study the normal fan of this secondary polyhedron in Section 5.2.



Figure 5.1: Example $\mathbf{L}_4 \subset \mathbb{R}^4$.

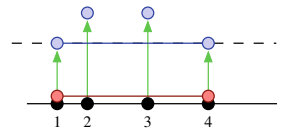


Figure 5.2: Alternative heights for \mathcal{T}_1 in \mathbf{L}_4 .

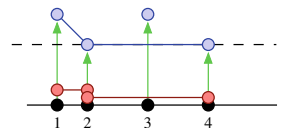


Figure 5.3: Alternative heights for \mathcal{T}_2 in \mathbf{L}_4 .

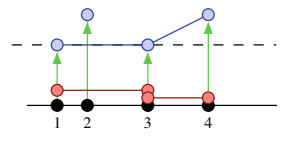


Figure 5.4: Alternative heights for \mathcal{T}_3 in \mathbf{L}_4 .

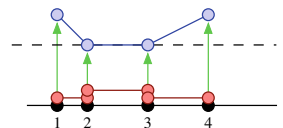
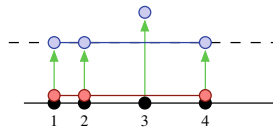
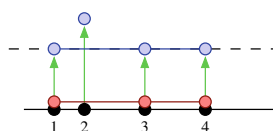
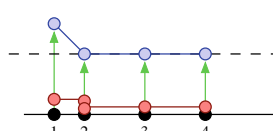
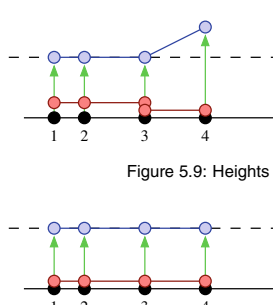


Figure 5.5: Alternative heights for \mathcal{T}_4 in \mathbf{L}_4 .

Figure 5.6: Heights for \mathcal{T}_{12} in L_4 .Figure 5.7: Heights for \mathcal{T}_{13} in L_4 .Figure 5.8: Heights for \mathcal{T}_{24} in L_4 .Figure 5.9: Heights for \mathcal{T}_{34} in L_4 .Figure 5.10: Heights for \mathcal{T}_{1234} in L_4 .

5.1 The secondary polytope

We are about to introduce the important concept of *secondary polytope* of a point configuration. Before we do that, we will motivate the “right” definition with a few examples that will hopefully illustrate the subtleties of the concept.

5.1.1 Motivating examples

Let us develop a better feeling of how regular triangulations relate to their defining height vectors by looking at some examples.

Example 5.1.1 (Four points on a line). Consider the point configuration L_4 consisting of four points 1, 2, 4, 6 on the real line, labeled 1, 2, 3, 4 from left to right. Here is a list of its four triangulations, where the cell $\{i, j\}$ is denoted by ij for $i, j = 1, 2, 3, 4$:

$$\begin{aligned}\mathcal{T}_1 &:= \{14\}, \\ \mathcal{T}_2 &:= \{12, 24\}, \\ \mathcal{T}_3 &:= \{13, 34\}, \\ \mathcal{T}_4 &:= \{12, 23, 34\}.\end{aligned}$$

Although it is not a complete coincidence that the number of triangulations equals the number of points (see Section 5.5.1), the way we have numbered them is arbitrary.

The flip graph of this point configuration is a four-gon, where only \mathcal{T}_1 and \mathcal{T}_4 and \mathcal{T}_2 and \mathcal{T}_3 are not connected by a flip. All these triangulations are regular. Corresponding heights $\omega_{\mathcal{T}_i}$ are given in the following list:

$$\begin{aligned}\omega_{\mathcal{T}_1} &= (1, 2, 2, 1), \\ \omega_{\mathcal{T}_2} &= (2, 1, 2, 2), \\ \omega_{\mathcal{T}_3} &= (2, 2, 1, 2), \\ \omega_{\mathcal{T}_4} &= (2, 1, 1, 2).\end{aligned}$$

You will actually prove in Exercise 5.1 that all one-dimensional polyhedral subdivisions are regular.

The list of all proper polyhedral subdivisions that are not triangulations reads as follows, where the indices indicate which triangulations refine them:

$$\begin{aligned}\mathcal{T}_{12} &:= \{124\}, \\ \mathcal{T}_{13} &:= \{134\}, \\ \mathcal{T}_{24} &:= \{12, 234\}, \\ \mathcal{T}_{34} &:= \{123, 34\}, \\ \mathcal{T}_{1234} &:= \{1234\}.\end{aligned}$$

Again, all of these polyhedral subdivisions are regular. Suitable heights

include the following (see also Figures 5.6 to 5.10):

$$\begin{aligned}\omega_{\mathcal{T}_{12}} &:= (0, 0, 1, 0), \\ \omega_{\mathcal{T}_{13}} &:= (0, 1, 0, 0), \\ \omega_{\mathcal{T}_{24}} &:= (1, 0, 0, 0), \\ \omega_{\mathcal{T}_{34}} &:= (0, 0, 0, 1), \\ \omega_{\mathcal{T}_{1234}} &:= (0, 0, 0, 0).\end{aligned}$$

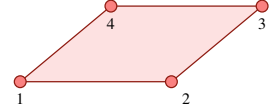


Figure 5.11: Point configuration \mathbf{C}_4

Note that we could have chosen the following alternative heights for the triangulations \mathcal{T}_1 , \mathcal{T}_2 , \mathcal{T}_3 , and \mathcal{T}_4 : for each triangulation, pick the coarsest non-trivial polyhedral subdivisions that are strictly refined by it, and sum up their heights.

$$\begin{aligned}\omega'_{\mathcal{T}_1} &= \omega_{\mathcal{T}_{12}} + \omega_{\mathcal{T}_{13}} = (0, 1, 1, 0), \\ \omega'_{\mathcal{T}_2} &= \omega_{\mathcal{T}_{12}} + \omega_{\mathcal{T}_{24}} = (1, 0, 1, 0), \\ \omega'_{\mathcal{T}_3} &= \omega_{\mathcal{T}_{13}} + \omega_{\mathcal{T}_{34}} = (0, 1, 0, 1), \\ \omega'_{\mathcal{T}_4} &= \omega_{\mathcal{T}_{24}} + \omega_{\mathcal{T}_{34}} = (1, 0, 0, 1).\end{aligned}$$

These heights are illustrated in Figures 5.2 to 5.5. That this is a general principle will be the content of Exercise 5.12. \square

Example 5.1.2 (A square). Consider the point configuration \mathbf{C}_4 consisting of the vertices of a square, labeled 1, 2, 3, 4 counter-clockwise (see Figure 5.11).

We find the following polyhedral subdivisions:

$$\begin{aligned}\mathcal{T}_1 &:= \{123, 134\}, \\ \mathcal{T}_2 &:= \{124, 234\}, \\ \mathcal{S}_{12} &:= \{1234\}.\end{aligned}$$

For $\varepsilon > 0$, possible heights are (see Figures 5.12 and 5.13):

$$\begin{aligned}\omega_1 &:= (1 - \varepsilon, 1, 1, 1), \\ \omega_2 &:= (1 + \varepsilon, 1, 1, 1), \\ \omega_{12} &:= (1, 1, 1, 1).\end{aligned}$$

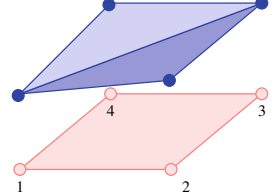


Figure 5.12: Heights for \mathcal{T}_1 in \mathbf{C}_4 .

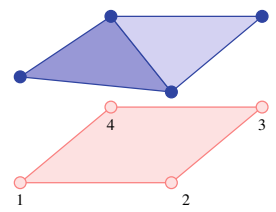


Figure 5.13: Heights for \mathcal{T}_2 in \mathbf{C}_4 .

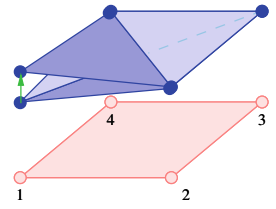
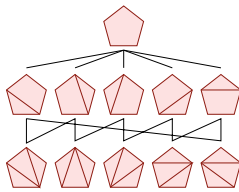
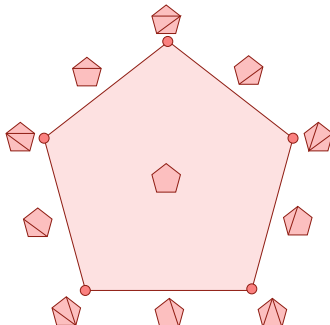
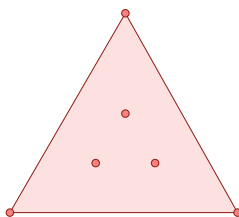
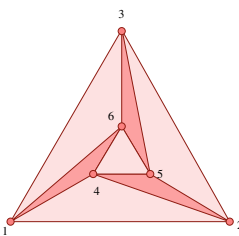
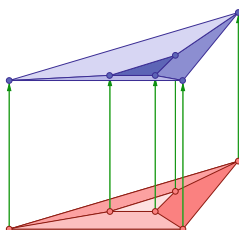


Figure 5.14: A “height homotopy” simulating a flip in \mathbf{C}_4 .

\mathcal{T}_1 and \mathcal{T}_2 are connected by a flip. Consider the “height homotopy” (see Figure 5.14):

$$\omega : \begin{cases} J \times [0, 1] &\rightarrow \mathbb{R}, \\ (j, t) &\mapsto (1 - t)\omega_{1j} + t\omega_{2j}. \end{cases}$$

Then, $\omega(j, 0) = \omega_{1j}$ and $\omega(j, 1) = \omega_{2j}$. Moreover, $\omega(j, \frac{1}{2}) = \omega_{12j}$. That means, when we are moving the heights as t ranges from 0 to 1, the lower convex hull moves through a singular configuration where the flip region becomes flat. More specifically, in order to obtain \mathcal{T}_1 , the lifted point 1 must

Figure 5.15: The Hasse-diagram of Subdivs(C_5).Figure 5.16: The face lattice of a five-gon is isomorphic to Subdivs(C_5).Figure 5.17: The mother of all examples M .Figure 5.18: A non-regular triangulation of M .Figure 5.19: Heights for a coarsening of \mathcal{T}_1 .

be strictly below the hyperplane spanned by the other three lifted points; in order to obtain \mathcal{T}_2 , point 1 must be lifted strictly above that hyperplane. In between it will be on that hyperplane. This suggests that flips can somehow be recovered from “sliding” the height vector across a certain border, at which the height induces a slightly coarser polyhedral subdivision. You have to wait until Section 5.4.2 for a more specific treatment of this. \square

Example 5.1.3 (A pentagon). Let us be brave and add another point to the configuration. Let C_5 be the point configuration of the vertices of a convex five-gon. If we lift one of the points very high up, then this will get us a polyhedral subdivision with one triangle and an adjacent four-gon. In other words, we have inserted an edge in the 5-gon. These subdivisions are almost-triangulations in the sense of Section 2.4.2. So the whole list of subdivisions of C_5 is: the trivial subdivision, these five almost-triangulations, and the five triangulations that refine them. (There are as many triangulations as almost-triangulations because each of the former refines two of the latter and each of the latter is refined by two of the former.)

If we draw the Hasse-diagram of Subdivs(C_5) (see Figure 5.15), then we see it equals the Hasse-diagram of the face lattice of another five-gon (see Figure 5.16). Is this a coincidence? Is the reason for this behaviour convexity, dimension two, or the fact that all the polyhedral subdivisions are regular? (solve Exercise 5.2 for a generalization of this fact to arbitrary n -gons.) Stay tuned until Section 5.2, where this question is answered.

Another feature of this example is that every triangulation of the five-gon contains a triangle that is contained in no other triangulation. It is the one that has just one edge in the boundary. Once we fix such a triangle, there is a unique triangulation containing it. This is proved to be a general property of configurations with no more than $d + 3$ elements in Section 5.5.

Example 5.1.4 (The Mother of All Examples (again)). Consider now the point configuration $M \subset \mathbb{R}^2$ consisting of two nested congruent triangles with parallel edges (see Figure 5.18). It has already appeared in Example 2.2.5 and in Section 3.3.4, and you can be sure it will show up later in the book!

In homogeneous coordinates, normalized so that the coordinate sum is four, we can describe M as follows:

$$M := \begin{pmatrix} 1 & 2 & 3 & 4 & 5 & 6 \\ 4 & 0 & 0 & 2 & 1 & 1 \\ 0 & 4 & 0 & 1 & 2 & 1 \\ 0 & 0 & 0 & 1 & 1 & 2 \end{pmatrix}$$

The first thing to notice is that M has two non-regular triangulations, as proved in Example 2.2.5 (\mathcal{T}_1 is shown in Figure 5.18):

$$\begin{aligned} \mathcal{T}_1 &:= \{124, 245, 235, 356, 346, 146, 456\}, \\ \mathcal{T}_2 &:= \{125, 145, 236, 256, 134, 136, 456\}. \end{aligned}$$

Moreover, if we look closely at the refinement poset of all polyhedral subdivisions of M , we observe something peculiar. Different portions of

the poset were drawn in Chapter 3, Figure 3.20. More precisely, this configuration has thirteen coarsest subdivisions, which fall into four types under the triangular symmetry of the configuration. The posets A, B, C and D of Figure 3.20 show one refinement of each type. Especially interesting is the subdivision of type D, consisting of the inner triangle 456, plus three quadrilaterals, 1245, 2356, 1346 filling the space between the inner and outer triangle. Its refinements form a poset isomorphic to that of a 3-cube, since in each of the three quadrilaterals we can independently decide to insert one diagonal, or the other, or none. In the 3-cube $[0, 1]^3$, to specify a face we choose to fix each coordinate to be zero, or one, or do not fix it at all. This subdivision itself is regular (as shown in Figure 5.19), but its poset of refinements contains the 2 non-regular triangulations of \mathbf{M} and 12 non-regular polyhedral subdivisions that are not triangulations.

With a little patience, you can see how the 13 subposets of refinements of coarsest subdivisions glue together in the poset of subdivisions of the whole configuration, or at least count how many subdivisions you get in total. The result is there are 18 triangulations and 47 polyhedral subdivisions that are not triangulations (including the trivial one). Moreover, there are 2 non-regular triangulations and 12 non-regular polyhedral subdivisions that are not triangulations. All of them are shown with an schematic rendition of the whole poset in Figure 5.20 (although it is impossible to draw most lines of the Hasse diagram).

But there is one important fact that can be read right away from Figure 3.20 (which is a microscope view of the full poset in Figure 5.20). The poset of subdivisions of \mathbf{M} has maximal chains of different lengths. Remember that a chain in a poset is a set of elements that are totally ordered. For example, in the poset of non-empty faces of a d -polytope, maximal chains have length d (which means that they contain $d + 2$ elements, with $d + 1$ cover relations relating them): they consist of one face of each dimension from 0 to d , each contained in the next one. In the poset of subdivisions of \mathbf{M} , the maximal chains that go through the coarsest subdivisions of types A, B, or C have length three. Those that go through the subdivision of type D have length four. Moreover, all of them contain at least one non-regular subdivision.

Summing up: in all previous examples the poset of subdivisions was isomorphic to the face poset of some polytope. But not here, since this contradicts the existence of maximal chains of different lengths (in technical terms, one says this poset is *not graded*). What is different here? Are the interior points the culprits? Or is it the fault of the non-regular polyhedral subdivisions? The fact that all chains of length four contain non-regular subdivisions seems to indicate the latter. In fact, if you remove from the poset D of Figure 3.20 the non-regular subdivisions what remains is the poset of faces of a hexagon. It is not hard to believe that this hexagon, glued with three copies of each of the other three sub-posets (which are all pentagons and quadrilaterals), makes the refinement poset $\text{Subdiv}_{\text{reg}}(\mathbf{M})$ of all regular polyhedral subdivisions of \mathbf{M} be isomorphic to the face poset of a nice three-dimensional polytope. \square

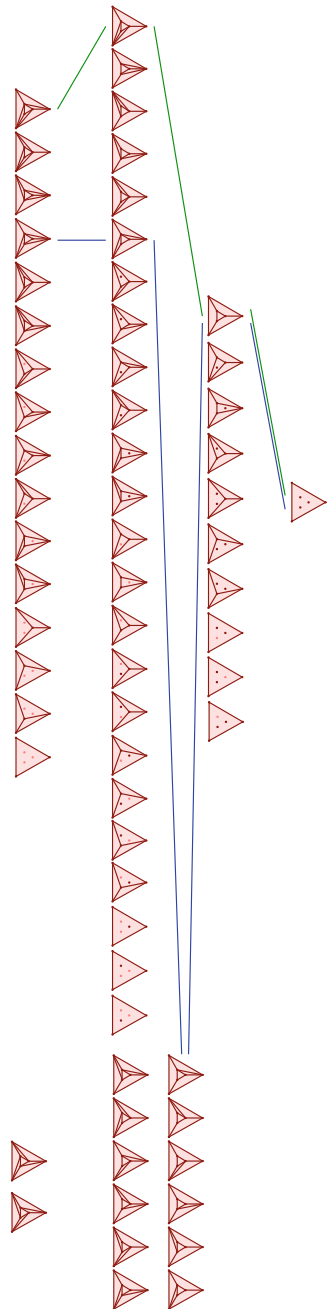


Figure 5.20: The refinement poset of the mother of all examples \mathbf{M} (rotated by 90 degrees and without most covering-relations; darker points are considered members of the enclosing cell); it contains chains of length three and four.

Example 5.1.5 (Five vectors in the plane). Let us now study regular subdivisions of a *vector configuration*. We consider five vectors of the same length, and regularly distributed, as in Example 2.56. As said there, there are three types (modulo pentagonal symmetry) of triangulations, and six types of non-simplicial subdivisions, all of them regular. See Figures 2.56 and 2.57.

The whole poset of subdivisions turns out to have a very nice structure (as usual!): forgetting the trivial subdivision, it is equal to the poset of faces of a decomposition of the whole plane into some bounded and some unbounded polyhedral regions. See Figure 5.21. The 11 vertices correspond to the 11 triangulations, shown in the picture. The 20 edges (15 bounded, 5 unbounded) and ten regions (5 bounded, 5 unbounded) correspond to subdivisions in which one or more vertices are considered used but not extremal in their respective cells. Observe that unbounded regions correspond to subdivisions into a single cell. This cell may consist of three or four elements, the case of five elements being the trivial subdivision that we are omitting in the picture.

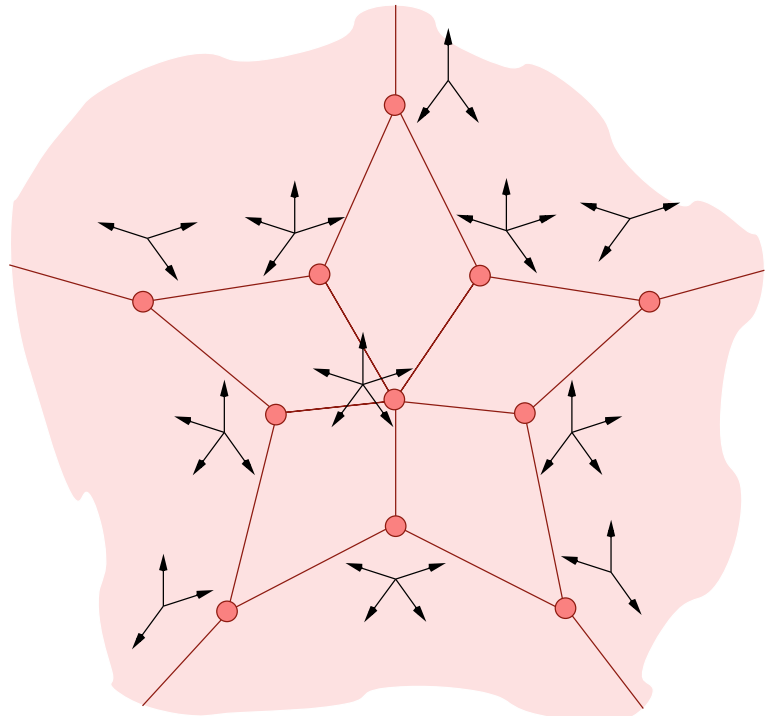


Figure 5.21: The poset of regular subdivisions of five vectors in the plane.

So, we hope by now you have enough reasons to further study this chapter.

5.1.2 Statement of the main theorem

We now come to a crucial point for understanding the space of triangulations of a point configuration. We introduce *secondary polytopes*. Most of

what we present here was first conceived and described by I.M. Gelfand, M. Kapranov, and A. Zelevinsky around the year 1989. Their fundamental original work can be found in [138, 139] and Chapter Seven of [140]. Two other important sources in the history of the subject are the papers [48, 49].

We now introduce a fundamental construction by which, to each triangulation of a *point configuration* with n elements, we associate a sequence of n numbers, that is, a vector in $\mathbb{R}^J \cong \mathbb{R}^n$. For now, this may seem like a mysterious definition, but it will be crucial later on. We denote by e_j the standard basis vector in \mathbb{R}^J corresponding to the j -th coordinate. Recall also that $\text{st}_{\mathcal{T}}(j)$ denotes the star of j in \mathcal{T} , that is, the subcomplex of simplices containing j .

In the following formula, $\text{vol}(\cdot)$ represents the usual Euclidean volume of a body in d -space. If \mathbf{A} is represented by a $(d+1) \times n$ homogeneous matrix of rank $d+1$, then the volume of each simplex is (modulo a normalization constant) equal to the absolute value of the determinant of the corresponding columns.

Definition 5.1.6 (GKZ-Vector). Let \mathbf{A} be a point configuration. Let \mathcal{T} be a triangulation of \mathbf{A} . Then set

$$\begin{aligned}\phi_{\mathbf{A}}(\mathcal{T}) &:= \sum_{j \in J} \text{vol}(\text{st}_{\mathcal{T}}(j)) e_j \\ &= \sum_{j \in J} \sum_{C \in \mathcal{T}: j \in C} \text{vol}(C) e_j \subset \mathbb{R}^J \cong \mathbb{R}^n.\end{aligned}$$

This is the *Gelfand-Kapranov-Zelevinsky* vector of \mathcal{T} . For brevity, it is most often referred as the *GKZ vector* of a triangulation.

This way we have a bunch of vectors in \mathbb{R}^J associated to our point configuration \mathbf{A} , one for each triangulation. We consider their convex hull.

Definition 5.1.7 (Secondary Polytope). The polytope

$$\Sigma\text{-poly}(\mathbf{A}) := \text{conv} \left\{ \phi_{\mathbf{A}}(\mathcal{T}) : \mathcal{T} \text{ triangulation of } \mathbf{A} \right\} \subset \mathbb{R}^J \cong \mathbb{R}^n$$

is the *secondary polytope* of \mathbf{A} in \mathbb{R}^n . □

Why is this polytope interesting? Let us look at our easiest example and see what happens.

Example 5.1.8 (5.1.1 continued). Let us compute the secondary polytope $\Sigma\text{-poly}(\mathbf{L}_4)$ of the point configuration \mathbf{L}_4 of Example 5.1.1. The volumes of all possible simplices can be read off of Figures 5.22 through 5.25.

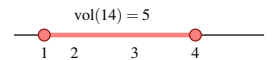


Figure 5.22: The volumes of simplices in \mathcal{T}_1 .



Figure 5.23: The volumes of simplices in \mathcal{T}_2 .

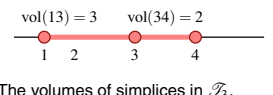


Figure 5.24: The volumes of simplices in \mathcal{T}_3 .

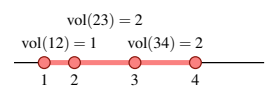


Figure 5.25: The volumes of simplices in \mathcal{T}_4 .

The GKZ-vectors of the four triangulations are:

$$\begin{aligned}\phi_{\mathbf{L}_4}(\mathcal{T}_1) &:= \begin{pmatrix} \text{vol}(14) \\ 0 \\ 0 \\ \text{vol}(14) \end{pmatrix} = \begin{pmatrix} 5 \\ 0 \\ 0 \\ 5 \end{pmatrix}, \\ \phi_{\mathbf{L}_4}(\mathcal{T}_2) &:= \begin{pmatrix} \text{vol}(12) \\ \text{vol}(12) + \text{vol}(24) \\ 0 \\ \text{vol}(24) \end{pmatrix} = \begin{pmatrix} 1 \\ 5 \\ 0 \\ 4 \end{pmatrix}, \\ \phi_{\mathbf{L}_4}(\mathcal{T}_3) &:= \begin{pmatrix} \text{vol}(13) \\ 0 \\ \text{vol}(13) + \text{vol}(34) \\ \text{vol}(34) \end{pmatrix} = \begin{pmatrix} 3 \\ 0 \\ 5 \\ 2 \end{pmatrix}, \\ \phi_{\mathbf{L}_4}(\mathcal{T}_4) &:= \begin{pmatrix} \text{vol}(12) \\ \text{vol}(12) + \text{vol}(23) \\ \text{vol}(23) + \text{vol}(34) \\ \text{vol}(34) \end{pmatrix} = \begin{pmatrix} 1 \\ 3 \\ 4 \\ 2 \end{pmatrix}.\end{aligned}$$

Therefore, $\Sigma\text{-poly}(\mathbf{L}_4)$ is the following convex hull:

$$\Sigma\text{-poly}(\mathbf{L}_4) = \text{conv}\left\{\begin{pmatrix} 5 \\ 0 \\ 0 \\ 5 \end{pmatrix}, \begin{pmatrix} 1 \\ 5 \\ 0 \\ 4 \end{pmatrix}, \begin{pmatrix} 3 \\ 0 \\ 5 \\ 2 \end{pmatrix}, \begin{pmatrix} 1 \\ 3 \\ 4 \\ 2 \end{pmatrix}\right\}.$$

Note that the coordinate sum in every column is ten. This comes as no surprise, because the volumes of the simplices in any triangulation must add up to the volume of the point configuration. Every volume of a simplex is counted in the GKZ-vector as many times as its number of vertices, and this number is dimension plus one for all simplices in all triangulations. In the example, every volume is counted twice for each triangulation. Since the volume of \mathbf{L}_4 is five, the coordinate sum of every GKZ-vector must be equal to ten. In Exercise 5.5, you will find d more affine relations among the coordinates of GKZ-vectors.

Can you guess the dimension and the combinatorics of $\Sigma\text{-poly}(\mathbf{L}_4)$? Note that we can arrange all the polyhedral subdivisions so that they label the faces of a four-gon and so that refinement of polyhedral subdivisions corresponds to face inclusion (see Figure 5.26). Could it be that the GKZ-vectors define a four-gon?

Let us elaborate on this a little bit. One can calculate by hand or with the help of a computer algebra system that the Gauss-Jordan normal form of the homogeneous coordinates

$$\begin{pmatrix} 5 & 1 & 3 & 1 \\ 0 & 5 & 0 & 3 \\ 0 & 0 & 5 & 4 \\ 5 & 4 & 2 & 2 \\ 1 & 1 & 1 & 1 \end{pmatrix}$$

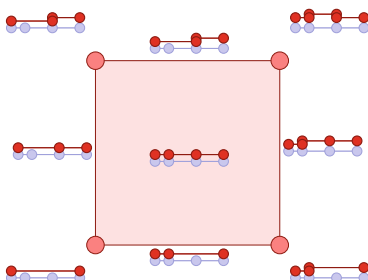


Figure 5.26: The refinement poset of \mathbf{L}_4 is isomorphic to the face lattice of a four-gon.

of $\Sigma\text{-poly}(\mathbf{L}_4)$ is

$$\begin{pmatrix} 1 & 0 & 0 & -\frac{2}{5} \\ 0 & 1 & 0 & \frac{3}{5} \\ 0 & 0 & 1 & \frac{4}{5} \\ 0 & 0 & 0 & 0 \\ 0 & 0 & 0 & 0 \end{pmatrix}.$$

The rank of this matrix is three. Hence, the affine dimension of $\Sigma\text{-poly}(\mathbf{L}_4)$ is two. All transformed column vectors already lie in a common hyperplane: they all have coordinate sum equal to one. Moreover, the fourth column is not in the positive hull of the first three, since its first coordinate is negative. From this it follows that $\Sigma\text{-poly}(\mathbf{L}_4)$ is indeed a two-dimensional four-gon embedded in \mathbb{R}^4 (see Figure 5.27 for an illustration of the vectors in the Gauss-Jordan normal form, canonically projected into \mathbb{R}^3). In other words: In this example, the face lattice of $\Sigma\text{-poly}(\mathbf{L}_4)$ is isomorphic to the refinement poset $\text{Subdivs}(\mathbf{L}_4) = \text{Subdivs}_{\text{reg}}(\mathbf{L}_4)$.

We will find another description of $\Sigma\text{-poly}(\mathbf{L}_4)$ in Section 5.4.1 that makes answering this question without any linear algebra almost trivial. Stay tuned!

It turns out that what we have seen in Example 5.1.8 is the general situation: the secondary polytope of \mathbf{A} has a face lattice isomorphic to the regular refinement poset $\text{Subdivs}_{\text{reg}}(\mathbf{A})$ of \mathbf{A} . This is one of the main theorems in this book, proved by I. M. Gelfand, M. M. Kapranov, and A. V. Zelevinsky in 1989 [138]. Remember that we have learned from Example 5.1.4 that such a thing cannot be true for the larger poset $\text{Subdivs}(\mathbf{A})$.

Theorem 5.1.9. *Let \mathbf{A} be a point configuration. Then:*

- *Vertices of $\Sigma\text{-poly}(\mathbf{A})$ are in one-to-one correspondence with the regular triangulations of \mathbf{A} . That is, the GKZ-coordinates $\phi_{\mathbf{A}}(\mathcal{T})$ of a triangulation \mathcal{T} are extremal in the set of all GKZ-coordinates of triangulations of \mathbf{A} if and only if \mathcal{T} is regular.*
- *Furthermore, the face lattice of $\Sigma\text{-poly}(\mathbf{A})$ is isomorphic to the refinement poset of regular polyhedral subdivisions of \mathbf{A} .*

The proof of this theorem is indirect. We will first construct a complete polyhedral fan with its cones in bijection to regular subdivisions of \mathbf{A} and then show that it is actually the normal fan of the secondary polytope. The whole of Section 5.2 is essentially devoted to these two tasks. But before doing that, let us at least determine the dimension of the secondary polytope.

5.1.3 Dimension and affine span of the secondary polytope

By definition, $\Sigma\text{-poly}(\mathbf{A})$ lives in \mathbb{R}^J , where $|J|$ is the number of elements in \mathbf{A} . But we saw in Example 5.1.8 that $\Sigma\text{-poly}(\mathbf{A})$ cannot be full-dimensional since, among other things, $\phi_{\mathbf{A}}(\mathcal{T})$ equals $(d+1)$ times the volume of the polytope $\text{conv}(\mathbf{A})$, for every \mathcal{T} .

For a more drastic example, consider the case of a corank-one configuration, that is, a configuration of dimension d with $d+2$ points. As we saw in

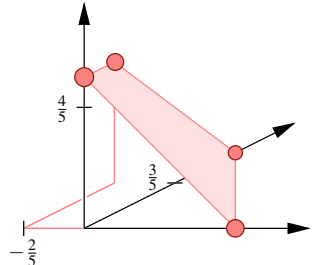


Figure 5.27: The Gauss-Jordan normal form of the non-zero homogeneous coordinates of $\Sigma\text{-poly}(\mathbf{L}_4)$ in the affine hyperplane with the sum of all coordinates equal to one.

Section 2.4, such configurations have only two triangulations, hence their secondary polytope cannot have dimension higher than one.

The main result in this section is:

Theorem 5.1.10. *Let \mathbf{A} be a point configuration. The linear subspaces of \mathbb{R}^J parallel and orthogonal to $\Sigma\text{-poly}(\mathbf{A})$ are the spaces of dependences and evaluations of \mathbf{A} .*

In particular,

$$\dim(\Sigma\text{-poly}(\mathbf{A})) = n - d - 1,$$

where d is the dimension of \mathbf{A} , (that is, $d + 1$ is its rank).

Remember that if \mathbf{A} is represented as an $m \times n$ homogeneous matrix, dependences and evaluations form, respectively, the kernel and the row span of the matrix. See Section 4.1.3. To prove Theorem 5.1.10, it suffices to show that dependences and evaluations are respectively parallel and orthogonal to $\Sigma\text{-poly}(\mathbf{A})$. Since they are, by definition, orthogonal complements in \mathbb{R}^J , this implies automatically that every vector parallel to $\Sigma\text{-poly}(\mathbf{A})$ is a dependence vector, and every vector orthogonal to it is an evaluation.

We start with linear evaluations. Remember that the linear evaluation associated to a linear function $\psi : \mathbb{R}^m \rightarrow \mathbb{R}$ is the vector $\omega \in \mathbb{R}^J$ obtained when restricting ψ to the columns of \mathbf{A} . Put differently, if we represent ψ as a row vector, we have

$$\omega = \psi \cdot \mathbf{A}.$$

Saying that ω is orthogonal to $\Sigma\text{-poly}(\mathbf{A})$ is the same as saying that its scalar product with the GKZ vector $\phi_{\mathbf{A}}(\mathcal{T})$ is independent of \mathcal{T} . Let us show that this is indeed the case:

Theorem 5.1.11. *If $\omega \in \mathbb{R}^J$ is the linear evaluation associated to a certain linear function $\psi : \mathbb{R}^m \rightarrow \mathbb{R}$ then, for every triangulation \mathcal{T} of \mathbf{A} , we have:*

$$\langle \omega, \phi_{\mathbf{A}}(\mathcal{T}) \rangle = (d + 1) \int_{\text{conv } \mathbf{A}} \psi(\mathbf{x}) d\mathbf{x}.$$

It may come as a surprise that integrals appear in a discrete mathematics book, but the reader should not forget that one of the principal uses of triangulations in applied mathematics is to approximately evaluate integrals or, more generally, solve partial differential equations. The main idea is that the integral over a complicated domain can be evaluated as a sum of integrals over simpler domains (simplices). That is exactly what we do to prove Theorem 5.1.11:

Proof. We prove the equality from right to left. Our first step is to use the triangulation \mathcal{T} to decompose the integral as:

$$(d + 1) \int_{\text{conv } \mathbf{A}} \psi(\mathbf{x}) d\mathbf{x} = (d + 1) \sum_{C \in \mathcal{T}} \int_{\text{conv } C} \psi(\mathbf{x}) d\mathbf{x}.$$

Now, we use the fact that the integral of a linear function on a domain \mathbf{X} equals the volume of the domain times the value at the barycenter. The

barycenter of a simplex is the average of its vertices and, since ψ is linear, its value at the barycenter is the average of its values at vertices, which are simply the coefficients of ω . That is:

$$\int_{\text{conv}C} \psi(\mathbf{x}) d\mathbf{x} = \frac{\text{vol}(C)}{d+1} \sum_{j \in C} \omega_j.$$

Putting both things together:

$$\begin{aligned} (d+1) \int_{\text{conv}\mathbf{A}} \psi(\mathbf{x}) d\mathbf{x} &= (d+1) \sum_{C \in \mathcal{T}} \int_{\text{conv}C} \psi(\mathbf{x}) d\mathbf{x} \\ &= \sum_{C \in \mathcal{T}} \text{vol}(C) \sum_{j \in C} \omega_j \\ &= \sum_{C \in \mathcal{T}} \sum_{j \in C} \omega_j \text{vol}(C) \\ &= \sum_{j \in J} \sum_{C \in \mathcal{T}: j \in C} \omega_j \text{vol}(C) \\ &= \sum_{j \in J} \omega_j \phi_{\mathbf{A}}(\mathcal{T})_j \quad = \langle \omega, \phi_{\mathbf{A}}(\mathcal{T}) \rangle. \end{aligned}$$

□

We now look at the linear space parallel to $\Sigma\text{-poly}(\mathbf{A})$ and show that it equals the space of dependences in \mathbf{A} . Remember that dependences are the vectors in the kernel of \mathbf{A} . More geometrically, if $\mathbf{p}_1, \dots, \mathbf{p}_n$ are the columns of \mathbf{A} , then a dependence is any vector $\lambda = (\lambda_1, \dots, \lambda_n)$ such that

$$\sum_{i=1}^n \lambda_i \mathbf{p}_i = 0.$$

Here we are assuming that the matrix \mathbf{A} is homogeneous, so the above equation contains in particular the equation $\sum \lambda_i = 0$.

Recall also that every circuit (Z_+, Z_-) has an associated dependence vector, defined uniquely up to a scalar factor. In what follows we prove that:

1. For every circuit (Z_+, Z_-) there is (at least) one pair of triangulations \mathcal{T}_1 and \mathcal{T}_2 that differ by a flip supported in that circuit.
2. The GKZ vectors $\phi_{\mathbf{A}}(\mathcal{T}_1)$ and $\phi_{\mathbf{A}}(\mathcal{T}_2)$ of those two triangulations differ by a scalar multiple of the dependence vector associated to the circuit.
3. The space of dependence vectors of \mathbf{A} is generated, as a vector space, by the dependence vectors of circuits.

Parts 1 and 2 imply that the dependence vectors of circuits are parallel to $\Sigma\text{-poly}(\mathbf{A})$. Part 3 implies that all dependence vectors are linear combinations of circuits. We prove these three statements in reverse.

Lemma 5.1.12. *Dependences produced by circuits span the vector space of all dependences of \mathbf{A} .*

Proof. Let B be a basis of \mathbf{A} . That is, a set of $d + 1$ independent columns, where $d + 1$ is the rank of \mathbf{A} . For each element $i \notin B$, there is one dependence with its support contained in $B \cup \{i\}$. Since B is independent we can normalize this dependence to have a coefficient of 1 in the i -th coordinate. Then these $n - d - 1$ dependences are independent, because the $(n - d - 1) \times m$ matrix formed by them contains the identity $(n - d - 1) \times (n - d - 1)$ matrix as a minor (in the columns $J \setminus B$). We see then that the dependences we constructed span the kernel of \mathbf{A} .

To finish the proof, simply observe that $\mathbf{A}|_{B \cup \{i\}}$ is a corank-one configuration, hence its unique dependence is the dependence of its unique circuit. \square

Lemma 5.1.13. *Let (Z_+, Z_-) be a circuit in \mathbf{A} and let λ be the dependence supported on it (which is unique up to a scalar factor). Let \mathcal{T}_1 and \mathcal{T}_2 be two triangulations of \mathbf{A} that differ by a flip in this circuit. Then*

$$\phi_{\mathbf{A}}(\mathcal{T}_1) - \phi_{\mathbf{A}}(\mathcal{T}_2)$$

is parallel to λ .

Proof. Assume by now that both \mathbf{A} and (Z_+, Z_-) are full-dimensional. That is, the matrix \mathbf{A} has full rank $m = d + 1$ and $|Z| = d + 2$, where $Z = Z_+ \cup Z_-$ is the support of our circuit.

In these conditions, the unique dependence λ with support in Z has as coefficients the maximal minors of the matrix $\mathbf{A}|_Z$. Put differently, the coefficient at an element $i \in Z$ is simply the volume of the complementary simplex $Z \setminus \{i\}$, with plus or minus sign depending on whether i is in Z_+ or in Z_- . Let \mathcal{T}_+ and \mathcal{T}_- be the two triangulations of Z , that is:

$$\mathcal{T}_+ = \{Z \setminus \{j\} : j \in Z_+\} \quad \text{and} \quad \mathcal{T}_- = \{Z \setminus \{j\} : j \in Z_-\}.$$

Look now at $\phi_{\mathbf{A}}(\mathcal{T}_+)$ and $\phi_{\mathbf{A}}(\mathcal{T}_-)$. We have that:

- In \mathcal{T}_+ , $\phi_{\mathbf{A}}(\mathcal{T}_+)_i$ equals the volume of $\text{conv}(Z)$ if $i \in Z_-$, and it equals that volume minus the volume of $\text{conv}(Z \setminus \{i\})$ if $i \in Z_+$ (the latter because the simplex $Z \setminus \{i\}$ is not incident to i).
- In \mathcal{T}_- , the same happens, with the roles of Z_+ and Z_- interchanged.

Hence:

$$\phi_{\mathbf{A}}(\mathcal{T}_1) - \phi_{\mathbf{A}}(\mathcal{T}_2) = \phi_{\mathbf{A}}(\mathcal{T}_+) - \phi_{\mathbf{A}}(\mathcal{T}_-) = -\lambda.$$

If \mathbf{A} is not full-dimensional, delete from \mathbf{A} superfluous rows before computing the secondary polytope. The choice of which rows we decide to delete is not important, since all the volumes we get with different choices differ only by a normalization constant. Then we can repeat the above argument. The case when the circuit Z is not full-dimensional is treated in the exercises at the end of this chapter. \square

Lemma 5.1.14. *For every circuit Z of \mathbf{A} , there is at least a pair of triangulations of \mathbf{A} that differ by a flip on that circuit.*

Proof. We use induction on the corank of \mathbf{A} . If \mathbf{A} has corank one, then it has a unique circuit, and two triangulations that differ by a flip on it (see Section 2.4.1).

If \mathbf{A} has corank greater than one, then there is (at least) one element i not in the support of Z . This means that Z is also a circuit in $\mathbf{A} \setminus i$ and, by inductive hypothesis, there are triangulations \mathcal{T}_1 and \mathcal{T}_2 of $\mathbf{A} \setminus i$ that differ by a flip on that circuit. We leave it to the reader to check that, then, the triangulations \mathcal{T}'_1 and \mathcal{T}'_2 obtained by placing i in \mathcal{T}_1 and \mathcal{T}_2 (see Lemma 4.3.2) differ by a flip on Z , too. \square

Proof of Theorem 5.1.10. Let \mathbf{L} be the linear span of the secondary polytope. The previous results show that \mathbf{L} contains the space of dependences of \mathbf{A} , and is orthogonal to the space of linear evaluations in \mathbf{A} . Since dependences and evaluations are orthogonal complements in \mathbb{R}^J , the result follows. \square

5.2 The normal fan of the secondary polytope

How can we actually prove that $\Sigma\text{-poly}(\mathbf{A})$ always has the kind of structure shown in Example 5.1.8? We will partition the space of all height functions according to what regular subdivision they produce. Then we show that this partition is a polyhedral fan, and is the normal fan of the secondary polyhedron $\Sigma\text{-poly}(\mathbf{A})$. Even if we have defined secondary polytopes only for *point* configurations, the fan we define here makes sense and has (almost) the same properties without that assumption. So, unless otherwise specified, here we allow \mathbf{A} to be a *vector configuration*, acyclic or not.

5.2.1 Secondary cones

Recall that $\mathcal{T} \preceq \mathcal{T}'$ if \mathcal{T} refines or equals \mathcal{T}' . This means that every cell of \mathcal{T} is contained in some cell of \mathcal{T}' . Refinement will be at the core of our investigations. The following will be our main objects of study for quite some time.

Definition 5.2.1 (Secondary Cone). Let \mathbf{A} be a vector configuration. Then for a polyhedral subdivision \mathcal{T} of \mathbf{A} , let

$$\begin{aligned}\mathbf{C}(\mathbf{A}, \mathcal{T}) &:= \{ \omega \in \mathbb{R}^J : \mathcal{T} \preceq \mathcal{S}(\mathbf{A}, \omega) \}, \\ \mathbf{C}^\circ(\mathbf{A}, \mathcal{T}) &:= \{ \omega \in \mathbb{R}^J : \mathcal{T} = \mathcal{S}(\mathbf{A}, \omega) \}.\end{aligned}$$

$\mathbf{C}(\mathbf{A}, \mathcal{T})$ is called the *secondary cone of \mathcal{T} in \mathbf{A}* , and $\mathbf{C}^\circ(\mathbf{A}, \mathcal{T})$ is called the *relatively open secondary cone of \mathcal{T} in \mathbf{A}* .

Although it is not yet justified to call these sets cones, one fact is immediate from the definition:

Lemma 5.2.2. *Let \mathbf{A} be a vector configuration and let \mathcal{T} be a polyhedral subdivision of \mathbf{A} . Then*

$$\mathbf{C}(\mathbf{A}, \mathcal{T}) = \bigcup \{ \mathbf{C}^\circ(\mathbf{A}, \mathcal{T}') : \mathcal{T} \preceq \mathcal{T}' \}. \quad \square$$

Before going on, observe there is a difference between the acyclic and the non-acyclic case. If \mathbf{A} is acyclic (for example, if it is a point configuration),

then every $\omega \in \mathbb{R}^J$ is in some secondary cone, since it produces some regular subdivision. If \mathbf{A} is not acyclic, then Theorem 4.1.39 tells us, in two different ways, what condition ω needs to satisfy in order to produce a regular subdivision. In any case, it is clear that the set of valid height vectors is simply $\mathbf{C}(\mathbf{A}, \{J\})$, where $\{J\}$ is the trivial subdivision of \mathbf{A} .

We show now that the set $\mathbf{C}(\mathbf{A}, \mathcal{T})$ has a very nice description. In the following, we do not aim at the most economic way to present the main theorems of this section (Theorems 5.2.11 and 5.1.9). We rather want to prove various facts about secondary polytopes and fans, together with descriptions of their structures, that are as explicit as possible.

Let us prepare for this by investigating the following question: When is a given polyhedral subdivision \mathcal{T} a refinement of the regular subdivision $\mathcal{S}(\mathbf{A}, \omega)$? By definition of refinement, every cell $C \in \mathcal{T}$ must be contained in a cell $C' \in \mathcal{S}(\mathbf{A}, \omega)$. By definition of $\mathcal{S}(\mathbf{A}, \omega)$, this is the case if the cell C is contained in a cell C' that is a lower face of the lifted point configuration \mathbf{A}^ω . That means that C labels coplanar points in \mathbf{A}^ω , and all points in \mathbf{A}^ω lie weakly above the hyperplane \mathbf{H}_C spanned by the points labeled by C .

In order to express our geometric considerations in formulas, we need some algebraic expression for the position of points relative to a hyperplane in \mathbb{R}^{r+1} . Here the fact that we are dealing with vectors, rather than points, comes to our rescue. Since every linear hyperplane passes through the origin, the vector $(\mathbf{0}, 1)$ is above any non vertical hyperplane. Hence, a vector (\mathbf{x}_0, h_0) lies above a non-vertical linear hyperplane \mathbf{H} equal to $\{(\mathbf{x}, h) : \phi(\mathbf{x}, h) = 0\}$ if and only if $\phi(\mathbf{x}, h)/\phi(\mathbf{0}, 1) \geq 0$. Here, the fact that $\phi(\mathbf{0}, 1) \neq 0$ is equivalent to \mathbf{H} not being vertical. In order to stress the fact that $\phi(\mathbf{0}, 1)$ is only used to calibrate the orientation, we will use the equivalent condition $\text{sign}(\phi(\mathbf{0}, 1))\phi(\mathbf{x}, h) \geq 0$.

By standard linear algebra in homogeneous coordinates, ϕ can be expressed in terms of a determinant function. So, for every (affine, for point configurations, or linear, for vector configurations) basis $\{s_1, s_2, \dots, s_{d+1}\}$ of a cell $C \in \mathcal{T}$, the resulting constraint on ω for C being contained in a lower facet of \mathbf{A}^ω reads as follows:

$$\begin{aligned} & [\text{sign} \det \begin{pmatrix} \mathbf{p}_{s_1} & \dots & \mathbf{p}_{s_{d+1}} & \mathbf{0} \\ \omega_{s_1} & \dots & \omega_{s_{d+1}} & 1 \end{pmatrix}] \\ & \cdot \det \begin{pmatrix} \mathbf{p}_{s_1} & \dots & \mathbf{p}_{s_{d+1}} & \mathbf{p}_j \\ \omega_{s_1} & \dots & \omega_{s_{d+1}} & \omega_j \end{pmatrix} \\ & \quad \begin{cases} = 0 & \text{if } j \in C \\ \geq 0 & \text{otherwise} \end{cases} \end{aligned}$$

Remark 5.2.3. Let us reformulate the idea behind this equation for *point* configurations. Here, we cannot rely on a particular point and a particular height that is guaranteed to always be above a hyperplane. Rather, we should say that lying above is the same as lying on the same side as an arbitrary point (for example $\mathbf{0}$) lifted to infinite height. Now, infinite height seems hard to express in coordinates at first glance. But it is not that hard: remember that, for point configurations, we use homogeneous coordinates, so that we can

assume that all of the original points have their $(d+1)$ st coordinate equal to one and $(d+2)$ nd coordinate equal to their heights. Then the point 0 “at height $+\infty$ ” can be easily written as $(\mathbf{0}, 0, 1)^T$ (see Figure 5.28). This is the same as we have done with vector configurations, since the “point” $(\mathbf{0}, 0)$ represents here the same as the vector $\mathbf{0}$ represents there.

Let us call the equality condition the *coplanarity condition* and the inequality condition the *weak folding condition*. If we require that the height vector reproduces exactly the polyhedral subdivision we started with then it must satisfy the corresponding *strict folding condition*, i.e., strict inequality. Recall that we have used these conditions locally (i.e., for points in adjacent cells) already in Theorem 2.3.20.

Observe that, if we develop the first determinant on its last column, consisting of zeros on all but the last position, we have that

$$\det \begin{pmatrix} \mathbf{p}_{s_1} & \cdots & \mathbf{p}_{s_{d+1}} & \mathbf{0} \\ \omega_{s_1} & \cdots & \omega_{s_{d+1}} & 1 \end{pmatrix} = \det (\mathbf{p}_{s_1} \cdots \mathbf{p}_{s_{d+1}}).$$

This motivates the following definition.

Definition 5.2.4 (Folding Form). Let $B = \{r_1, \dots, r_{d+1}\}$ be a basis of \mathbf{A} . Then, for a $\mathbf{p}_j \in \mathbf{A}$, the linear form

$$\begin{aligned} \psi_{B,j}(\omega) &:= \psi_{r_1, \dots, r_{d+1}, j}(\omega) \\ &:= [\operatorname{sign} \det (\mathbf{p}_{r_1} \cdots \mathbf{p}_{r_{d+1}})] \\ &\quad \cdot \det \begin{pmatrix} \mathbf{p}_{r_1} & \cdots & \mathbf{p}_{r_{d+1}} & \mathbf{p}_j \\ \omega(r_1) & \cdots & \omega(r_{d+1}) & \omega_j \end{pmatrix} \end{aligned}$$

is called the *folding form of j with respect to B* .

The folding form $\psi_{B,j}$ has the following interpretation: Whenever this linear functional evaluates to zero on some $\omega \in \mathbb{R}^J$, then ω lifts the element j onto the hyperplane spanned by the liftings of r_1, \dots, r_{d+1} . In this case, $(\frac{\mathbf{p}_1}{\omega(r_1)}), \dots, (\frac{\mathbf{p}_{d+1}}{\omega(r_{d+1})}), (\frac{\mathbf{p}_j}{\omega_j})$ are coplanar. Whenever this linear functional evaluates to a positive number, then j is lifted above that hyperplane. Thus, we can use the folding forms to express both the coplanarity and the folding conditions.

Before we make this explicit, we mention that coplanarity conditions and folding conditions are independent of the choice of the basis. (See Figures 5.29 and 5.30 for an illustration.)

Lemma 5.2.5. Let \mathbf{A} be a vector configuration. Let $C \subseteq J$ be a full-dimensional cell of \mathbf{A} , and let B, B' be bases of C . Then the following hold:

(i) Let $\omega \in \mathbb{R}^J$. Then

$$\psi_{B,j}(\omega) = 0 \quad \forall j \in C \iff \psi_{B',j}(\omega) = 0 \quad \forall j \in C.$$

(ii) Let $\omega \in \mathbb{R}^J$ so that $\psi_{B,j}(\omega) = 0$ for all $j \in C$. Then

$$\psi_{B,j}(\omega) = \psi_{B',j}(\omega) \quad \forall j \in J.$$

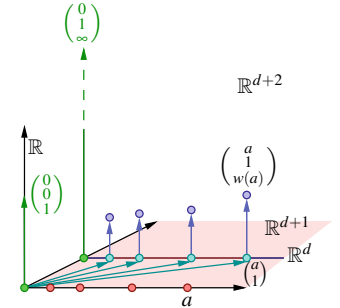


Figure 5.28: A point with infinite height like $\begin{pmatrix} 0 \\ 1 \\ \infty \end{pmatrix}$ can be equivalently expressed as $\begin{pmatrix} 0 \\ 0 \\ 1 \end{pmatrix}$ in homogeneous coordinates.

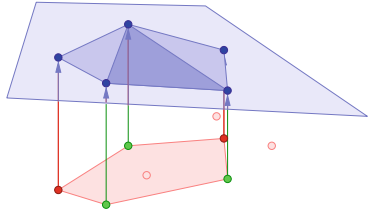


Figure 5.29: If a height vector satisfies the coplanarity conditions for a cell C ...

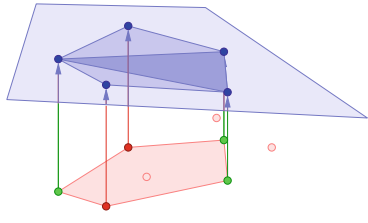


Figure 5.30: ... then the choice of another basis of C produces the same folding forms for all points.

Proof. The assertions follow from the fact that $\psi_{B,j}(\omega) = 0$ for all $j \in C$ means that all $j \in C$ lie on the hyperplane spanned by $\mathbf{A}^\omega|_B$. It then does not matter which basis we choose to describe that hyperplane. \square

Proposition 5.2.6. Let \mathbf{A} be a vector configuration. Let $\omega \in \mathbb{R}^J$. Then the following facts hold:

- (i) A cell C is in $\mathcal{S}(\mathbf{A}, \omega)$ if and only if for some (and hence for any) basis B of C , the coplanarity conditions and the strict folding conditions hold, i.e.,

$$\psi_{B,j}(\omega) \begin{cases} = 0 & \text{if } j \in C, \\ > 0 & \text{otherwise.} \end{cases}$$

- (ii) A cell C is contained in a cell C' in $\mathcal{S}(\mathbf{A}, \omega)$ if and only if for some (and hence for any) basis B of C , the coplanarity conditions and the weak folding conditions hold, i.e.,

$$\psi_{B,j}(\omega) \begin{cases} = 0 & \text{if } j \in C, \\ \geq 0 & \text{otherwise.} \end{cases}$$

- (iii) A cell C is strictly contained in a cell C' in $\mathcal{S}(\mathbf{A}, \omega)$ if and only if for some (and hence for any) basis B of C ,

$$\psi_{B,j}(\omega) \begin{cases} = 0 & \text{if } j \in C, \\ = 0 & \text{for at least one } j \in J \setminus C, \\ \geq 0 & \text{otherwise.} \end{cases}$$

Proof. The assertions are true by construction of the folding forms. (They are illustrated in Figures 5.31 to 5.34.) \square

Putting everything together yields the following polyhedral description of secondary cones.

Corollary 5.2.7. Let \mathcal{T} be an arbitrary polyhedral subdivision of \mathbf{A} . Then

- (i) The secondary cone of \mathcal{T} has the following description:

$$\begin{aligned} \mathbf{C}(\mathbf{A}, \mathcal{T}) = & \left\{ \omega \in \mathbb{R}^J : \begin{array}{l} \psi_{B,j}(\omega) = 0 \quad \forall j \in C, \\ \psi_{B,j}(\omega) \geq 0 \quad \forall j \in J \setminus C, \end{array} \right. \\ & \text{for all bases } B \text{ of } C, \\ & \forall C \in \mathcal{T} \} \\ = & \left\{ \omega \in \mathbb{R}^J : \begin{array}{l} \psi_{B,j}(\omega) = 0 \quad \forall j \in C, \\ \psi_{B,j}(\omega) \geq 0 \quad \forall j \in J \setminus C, \end{array} \right. \\ & \text{for some basis } B \text{ of } C, \\ & \forall C \in \mathcal{T} \}. \end{aligned}$$

- (ii) The relatively open secondary cone of \mathcal{T} has the following description:

$$\begin{aligned} \mathbf{C}^{\circ}(\mathbf{A}, \mathcal{T}) = & \left\{ \omega \in \mathbb{R}^J : \psi_{B,j}(\omega) = 0 \quad \forall j \in C, \right. \\ & \psi_{B,j}(\omega) > 0 \quad \forall j \in J \setminus C, \\ & \text{for all bases } B \text{ of } C, \\ & \left. \forall C \in \mathcal{T} \right\} \\ = & \left\{ \omega \in \mathbb{R}^J : \psi_{B,j}(\omega) = 0 \quad \forall j \in C, \right. \\ & \psi_{B,j}(\omega) > 0 \quad \forall j \in J \setminus C, \\ & \text{for some basis } B \text{ of } C, \\ & \left. \forall C \in \mathcal{T} \right\}. \end{aligned}$$

Proof. The assertions follow from Lemma 5.2.5 and Proposition 5.2.6. \square

The description above is terribly redundant; i.e., a lot of constraints are implied by sets of other constraints. In Theorem 2.3.20, we have already shown that the folding conditions on adjacent cells imply all the others. The redundant description above, however, is sometimes theoretically more convenient than the more efficient wall-based formulation in Theorem 2.3.20. In Chapter 8, we will come back to the wall-based description for the sake of computational efficiency.

Corollary 5.2.8. For all polyhedral subdivisions \mathcal{T} of \mathbf{A} the secondary cone $\mathbf{C}(\mathbf{A}, \mathcal{T})$ is a polyhedral convex cone.

5.2.2 The secondary fan

We now look at the set of all secondary cones. Our goal is to show that they form a polyhedral fan (remember Definition 2.1.7).

First, we compile some basic facts about secondary cones of regular polyhedral subdivisions. In Exercise 5.8, you will seek counterexamples to each assertion when the assumption of regularity is dropped. See Figure 5.35 for a (slightly misleading) illustration.

Proposition 5.2.9. Let $\mathcal{T}, \mathcal{T}'$ be regular polyhedral subdivisions of \mathbf{A} . Then:

- (i) $\mathbf{C}(\mathbf{A}, \mathcal{T}')$ is a proper face of $\mathbf{C}(\mathbf{A}, \mathcal{T})$ if and only if \mathcal{T} strictly refines \mathcal{T}' .
- (ii) $\mathbf{C}^{\circ}(\mathbf{A}, \mathcal{T})$ equals the relative interior of $\mathbf{C}(\mathbf{A}, \mathcal{T})$.
- (iii) $\mathbf{C}^{\circ}(\mathbf{A}, \mathcal{T})$ is non-empty.
- (iv) $\mathbf{C}(\mathbf{A}, \mathcal{T})$ is full-dimensional if and only if \mathcal{T} is a triangulation.
- (v) $\mathbf{C}(\mathbf{A}, \mathcal{T})$ has codimension one if and only if \mathcal{T} is an almost triangulation.

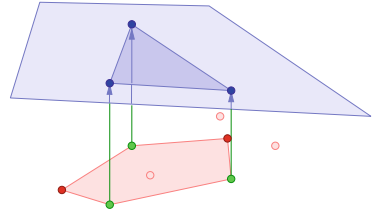


Figure 5.31: The heights on a basis of a cell define a hyperplane in \mathbb{R}^{d+1} .

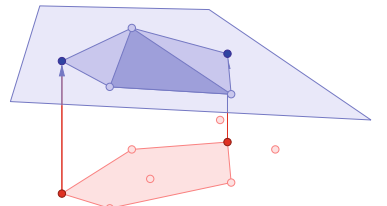


Figure 5.32: All other members of that cell must be lifted onto that hyperplane.

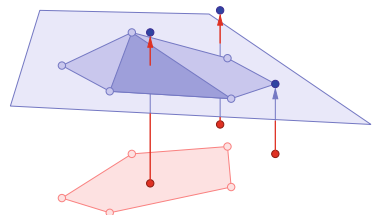


Figure 5.33: All non-members of that cell must be lifted weakly above that hyperplane; additional points on that hyperplane lead to refinement.

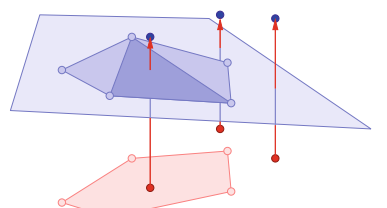


Figure 5.34: If all non-members are lifted strictly above that hyperplane then the heights induce exactly the cell we started with.

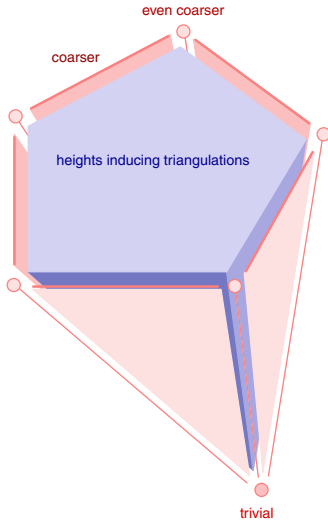


Figure 5.35: Refinement in a closed secondary cone. In one sense, this picture is misleading: the secondary cones in general contain non-trivial lineality spaces.

Proof. In order to prove one direction of (i), assume that \mathcal{T} and \mathcal{T}' are regular such that $\mathcal{T} \prec \mathcal{T}'$. We need to show that

$$\begin{aligned} \mathbf{C}(\mathbf{A}, \mathcal{T}') = \{ \omega' \in \mathbb{R}^J : & \quad \psi_{B',j}(\omega') = 0 \quad \forall j \in C' \\ & \psi_{B',j}(\omega') \geq 0 \quad \forall j \in J \setminus C' \\ & \text{for some basis } B' \text{ of } C', \\ & \forall C' \in \mathcal{T}' \} \end{aligned}$$

is a proper face of

$$\begin{aligned} \mathbf{C}(\mathbf{A}, \mathcal{T}) = \{ \omega \in \mathbb{R}^J : & \quad \psi_{B,j}(\omega) = 0 \quad \forall j \in C \\ & \psi_{B,j}(\omega) \geq 0 \quad \forall j \in J \setminus C \\ & \text{for some basis } B \text{ of } C, \\ & \forall C \in \mathcal{T} \}. \end{aligned}$$

By definition of the secondary cone, $\mathbf{C}(\mathbf{A}, \mathcal{T}') \subseteq \mathbf{C}(\mathbf{A}, \mathcal{T})$. Thus,

$$\begin{aligned} \mathbf{C}(\mathbf{A}, \mathcal{T}') = \{ \omega' \in \mathbf{C}(\mathbf{A}, \mathcal{T}) : & \quad \psi_{B',j}(\omega') = 0 \quad \forall j \in C' \\ & \psi_{B',j}(\omega') \geq 0 \quad \forall j \in J \setminus C' \\ & \text{for some basis } B' \text{ of } C', \\ & \forall C' \in \mathcal{T}' \}. \end{aligned}$$

Since $\mathcal{T} \prec \mathcal{T}'$, we can pick as a basis of C' a basis B of a cell $C \in \mathcal{T}$ with $C \subseteq C'$. But then all inequalities of the form $\psi_{B',j}(\omega) = \psi_{B,j}(\omega) \geq 0$ become redundant because all $\omega \in \mathbf{C}(\mathbf{A}, \mathcal{T})$ satisfy them. Therefore, we can define

$$\begin{aligned} \mathbf{H}_{\mathcal{T}'} := \{ \omega' \in \mathbb{R}^J : & \quad \psi_{B',j}(\omega') = 0 \quad \forall j \in C' \\ & \text{for some basis } B' \text{ of } C', \\ & \forall C' \in \mathcal{T}' \}, \end{aligned}$$

and $\mathbf{C}(\mathbf{A}, \mathcal{T}') = \mathbf{C}(\mathbf{A}, \mathcal{T}) \cap \mathbf{H}_{\mathcal{T}'}$. In words: $\mathbf{C}(\mathbf{A}, \mathcal{T}')$ just satisfies the additional coplanarity conditions for the cells in \mathcal{T}' that strictly contain cells of \mathcal{T} (see Figure 5.36). This proves that $\mathbf{C}(\mathbf{A}, \mathcal{T}')$ is a face of $\mathbf{C}(\mathbf{A}, \mathcal{T})$.

In order to show that it is a proper face, we need to show that it is neither empty nor equal to $\mathbf{C}(\mathbf{A}, \mathcal{T})$.

Since \mathcal{T}' is regular, there is a ω' in \mathbb{R}^J with $\mathcal{T}' = \mathcal{S}(\mathbf{A}, \omega')$. This ω' lies in $\mathbf{C}(\mathbf{A}, \mathcal{T}')$, by definition of the secondary cone, and thus $\mathbf{C}(\mathbf{A}, \mathcal{T}')$ is non-empty.

Since \mathcal{T} is regular, there is a height vector ω in $\mathbf{C}(\mathbf{A}, \mathcal{T})$ with $\mathcal{T} = \mathcal{S}(\mathbf{A}, \omega)$. Since $\mathcal{T} \prec \mathcal{T}'$, we have in particular $\mathcal{T}' \not\subseteq \mathcal{T}$. Therefore, ω is not in $\mathbf{C}(\mathbf{A}, \mathcal{T}')$, by definition of the secondary cone, and thus $\mathbf{C}(\mathbf{A}, \mathcal{T}') \neq \mathbf{C}(\mathbf{A}, \mathcal{T})$.

The reverse direction of the equivalence of Part (i) is obtained by reading the above argument the other way round.

From Part (i) we immediately get (ii), by definition of the relative interior. Assertion (iii) follows from the definition of $\mathbf{C}^\circ(\mathbf{A}, \mathcal{T})$.

Assertion (iv) follows from the fact that, for a regular triangulation, there are no coplanarity conditions, i.e., no non-trivial equations, because every cell itself is a basis. (Note that $\psi_{B,r}(\omega) \equiv 0$ for all $r \in B$, i.e., in the case of simplicial cells, all ω have coefficient zeros in the folding form, i.e., there is no coplanarity condition at all.)

Therefore, $\mathbf{C}^\circ(\mathbf{A}, \mathcal{T})$ is an intersection of finitely many open halfspaces. In particular, $\mathbf{C}^\circ(\mathbf{A}, \mathcal{T})$ is an open subset of \mathbb{R}^J . Moreover, it is non-empty since \mathcal{T} is regular. Thus, $\mathbf{C}^\circ(\mathbf{A}, \mathcal{T})$ is an open, non-empty subset in \mathbb{R}^J , thus full-dimensional, by elementary metric topology. If, in turn, \mathcal{T} is not a triangulation, then its secondary cone is a proper face of the secondary cone of a refinement of it, by Part (i). Therefore, it cannot be full-dimensional.

The proof of (v) is similar. Recall that an almost triangulation is a subdivision with the property that there is only one minimal dependent subset (circuit) contained in its cells. In particular, all the coplanarity conditions in the description of $\mathbf{C}^\circ(\mathbf{A}, \mathcal{T})$ boil down to one and the same condition: that ω lifts that dependent subset to be coplanar. In particular, $\mathbf{C}^\circ(\mathbf{A}, \mathcal{T})$ is the intersection of an open set with a single hyperplane. Since it is not empty (because \mathcal{T} is regular), and it is not full-dimensional (by part (iv)), it must have codimension one. Conversely, if \mathcal{T} is neither a triangulation nor an almost-triangulation, then there are two different circuits contained in (different or the same) cells of \mathcal{T} . Those two circuits provide at least two different equations in the description of $\mathbf{C}^\circ(\mathbf{A}, \mathcal{T})$, which then has codimension at least two. \square

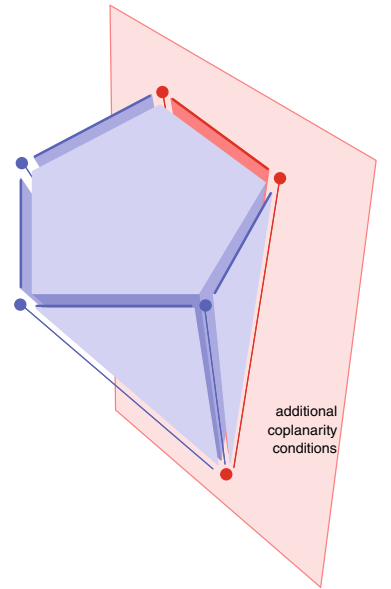


Figure 5.36: The supporting hyperplane for a face enforces the additional coplanarity conditions, producing coarser cells.

Example 5.2.10 (5.1.1 continued). We consider again the point configuration L_4 . We show the set of constraints for heights defining the triangulation $\mathcal{T}_2 = \{12, 24\}$. All cells are simplices, so there is no choice for the bases.

In order to find the simplex 12 in the set of lower facets of a lifting by ω_1 , ω_2 , ω_3 , and ω_4 , the following conditions must be fulfilled (see Figures 5.37 and 5.38):

$$\begin{aligned} \psi_{1,2,3}(\omega_1, \omega_2, \omega_3, \omega_4) \\ &= [\text{sign} \det \begin{pmatrix} 1 & 2 & 0 \\ 1 & 1 & 0 \\ \omega_1 & \omega_2 & 1 \end{pmatrix}] \det \begin{pmatrix} 1 & 2 & 4 \\ 1 & 1 & 1 \\ \omega_1 & \omega_2 & \omega_3 \end{pmatrix} \\ &= -(-2\omega_1 + 3\omega_2 - \omega_3) \\ &> 0, \end{aligned}$$

$$\begin{aligned} \psi_{1,2,4}(\omega_1, \omega_2, \omega_3, \omega_4) \\ &= [\text{sign} \det \begin{pmatrix} 1 & 2 & 0 \\ 1 & 1 & 0 \\ \omega_1 & \omega_2 & 1 \end{pmatrix}] \det \begin{pmatrix} 1 & 2 & 6 \\ 1 & 1 & 1 \\ \omega_1 & \omega_2 & \omega_4 \end{pmatrix} \\ &= -(-4\omega_1 + 5\omega_2 - \omega_4) \\ &> 0. \end{aligned}$$

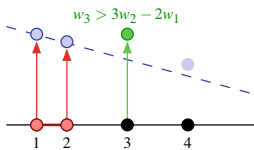


Figure 5.37: The condition $\omega_3 > 3\omega_2 - 2\omega_1$ ensures that the third point is lifted strictly above the line spanned by the lifted first two points; note how the geometric distances among the points in \mathbb{R} play an important role as coefficients in the line equations.

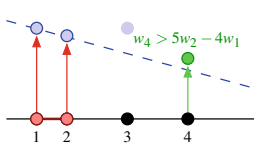


Figure 5.38: The condition $\omega_4 > 5\omega_2 - 4\omega_1$ ensures that the fourth point is lifted strictly above the line spanned by the lifted first two points.

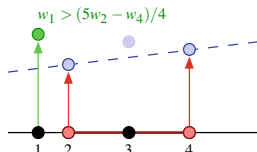


Figure 5.39: The condition $\omega_1 > (5\omega_2 - \omega_4)/4$ ensures that the first point is lifted strictly above the line spanned by the lifted second and fourth points.

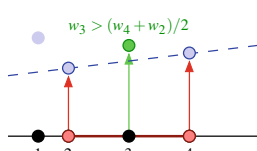


Figure 5.40: The condition $\omega_3 > (\omega_2 + \omega_4)/2$ ensures that the third point is lifted strictly above the line spanned by the lifted second and fourth point.

The simplex 24 is a lower facet if and only if the following linear constraints are satisfied (see Figures 5.39 and 5.40):

$$\begin{aligned} \psi_{2,4,1}(\omega_1, \omega_2, \omega_3, \omega_4) \\ = [\text{sign} \det \begin{pmatrix} 2 & 6 & 0 \\ 1 & 1 & 0 \\ \omega_2 & \omega_4 & 1 \end{pmatrix}] \det \begin{pmatrix} 2 & 6 & 1 \\ 1 & 1 & 1 \\ \omega_2 & \omega_4 & \omega_1 \end{pmatrix} \\ = -(5\omega_2 - \omega_4 - 4\omega_1) \\ > 0, \end{aligned}$$

$$\begin{aligned} \psi_{2,4,3}(\omega_1, \omega_2, \omega_3, \omega_4) \\ = [\text{sign} \det \begin{pmatrix} 2 & 6 & 0 \\ 1 & 1 & 0 \\ \omega_2 & \omega_4 & 1 \end{pmatrix}] \det \begin{pmatrix} 2 & 6 & 4 \\ 1 & 1 & 1 \\ \omega_2 & \omega_4 & \omega_3 \end{pmatrix} \\ = -(2\omega_2 + 2\omega_4 - 4\omega_3) \\ > 0. \end{aligned}$$

The complete system of linear equations and inequalities specifying the heights that induce \mathcal{T}_2 reads as follows (note that two of the above conditions are identical):

$$\begin{aligned} 2\omega_1 - 3\omega_2 + \omega_3 &> 0, \\ 4\omega_1 - 5\omega_2 + \omega_4 &> 0, \\ -2\omega_2 + 4\omega_3 - 2\omega_4 &> 0. \end{aligned}$$

Since this is the system for a regular triangulation, we have no coplanarity conditions. We see that both the height vectors $(2, 1, 2, 2)$ and $(1, 0, 1, 0)$ in Example 5.1.1 fulfill all the constraints.

The system of linear equations and equalities specifying the heights that induce subdivisions that are refined by \mathcal{T}_2 is the corresponding set of equations and weak inequalities:

$$\begin{aligned} 2\omega_1 - 3\omega_2 + \omega_3 &\geq 0, \\ 4\omega_1 - 5\omega_2 + \omega_4 &\geq 0, \\ -2\omega_2 + 4\omega_3 - 2\omega_4 &\geq 0. \end{aligned}$$

For example, the height vector $(0, 0, 0, 0)$ fulfills these non-strict inequalities with equality, meaning that \mathcal{T}_2 refines the polyhedral subdivision induced by $(0, 0, 0, 0)$, which is the trivial subdivision $\{1234\}$. (This is no surprise because every polyhedral subdivision refines the trivial one.) The height vector $(1, 2, 2, 1)$, which induces the triangulation $\mathcal{T}_1 = \{14\}$, violates all inequalities. Therefore, \mathcal{T}_2 does not refine \mathcal{T}_1 . Mind you, subdivisions and triangulations are not uniquely determined by the convex hulls of their cells; we need the point sets spanning the cells as well to specify a polyhedral subdivision.

The following theorem states the conclusion of all our work so far: *The collection of secondary cones forms a nice subdivision of the space of all possible heights* (see Figure 5.41 for a generic sketch).

Theorem 5.2.11. Let \mathbf{A} be a vector configuration, and let $\Sigma\text{-fan}(\mathbf{A})$ be the collection of all secondary cones $\mathbf{C}(\mathbf{A}, \mathcal{T})$ over all regular polyhedral subdivisions \mathcal{T} of \mathbf{A} . Then $\Sigma\text{-fan}(\mathbf{A})$ is a polyhedral fan in \mathbb{R}^d . The fan is complete if (and only if) \mathbf{A} is acyclic.

Moreover, the face lattice of $\Sigma\text{-fan}(\mathbf{A})$ is opposite to the refinement poset of regular polyhedral subdivisions of \mathbf{A} .

Proof. Recall that being a polyhedral fan (Definition 2.1.7) means that

- (i) For every regular polyhedral subdivision \mathcal{T} of \mathbf{A} , every face of the secondary cone $\mathbf{C}(\mathbf{A}, \mathcal{T})$ is a member of $\Sigma\text{-fan}(\mathbf{A})$.
- (ii) $\mathbf{C}(\mathbf{A}, \mathcal{T}) \cap \mathbf{C}(\mathbf{A}, \mathcal{T}')$ is a face of both $\mathbf{C}(\mathbf{A}, \mathcal{T})$ and $\mathbf{C}(\mathbf{A}, \mathcal{T}')$.

Being complete means that, in addition:

- (iii) The union of all $\mathbf{C}(\mathbf{A}, \mathcal{T})$ over all regular polyhedral subdivisions of \mathbf{A} covers \mathbb{R}^J .

Assertion (i) follows from Proposition 5.2.9(i). In order to prove (ii), consider the intersection of two cones $\mathbf{C}(\mathbf{A}, \mathcal{T}) \cap \mathbf{C}(\mathbf{A}, \mathcal{T}')$. By definition of the secondary cones, this intersection is the set of all heights $\omega \in \mathbb{R}^J$ such that $\mathcal{T} \preceq \mathcal{S}(\mathbf{A}, \omega)$ and $\mathcal{T}' \preceq \mathcal{S}(\mathbf{A}, \omega)$. By Proposition 5.2.9(i) again, this means that $\mathbf{C}(\mathbf{A}, \mathcal{T}) \cap \mathbf{C}(\mathbf{A}, \mathcal{T}')$ is a face of both $\mathbf{C}(\mathbf{A}, \mathcal{T})$ and $\mathbf{C}(\mathbf{A}, \mathcal{T}')$.

For Part (iii), observe that acyclic vector configurations are precisely those that do not have any non-negative dependence. Theorem 4.1.39 says that they coincide with those for which every $\omega \in \mathbb{R}^J$ belongs to some secondary cone.

Proposition 5.2.9(i) implies the order-reversing poset isomorphism. \square

5.2.3 Proof of the main theorem

A natural question to ask now is the following: Is the secondary fan polytopal? That is, does there exist a polytope whose normal fan coincides with the secondary fan? Of course, this can only happen if the fan is *complete*, that is to say, if its cones cover the whole \mathbb{R}^J . This happens if and only if \mathbf{A} is acyclic. In this case, we can think of it as a point configuration and, at last, the secondary polytope from Definition 5.2.1 enters the scene. In this section we will show that *the secondary fan is the normal fan of the secondary polytope*.

To further highlight the geometry behind the constructions, in this section we think of our point configuration as embedded in the affine space \mathbb{R}^d . If we have a geometric simplicial complex in \mathbb{R}^d and know the values that a certain function g takes on its vertices, it is natural to affinely interpolate g to the interior of the higher dimensional simplices. This is done, for example, in mesh generation or terrain modeling. Here, we do the same for any triangulation \mathcal{T} of our point configuration and any lifting heights $\omega \in \mathbb{R}^J$. See Figure 5.42 for an illustration.

Definition 5.2.12 (The characteristic section). Let \mathcal{T} be a triangulation of a point configuration \mathbf{A} , and let $\omega \in \mathbb{R}^J$ be a height function.

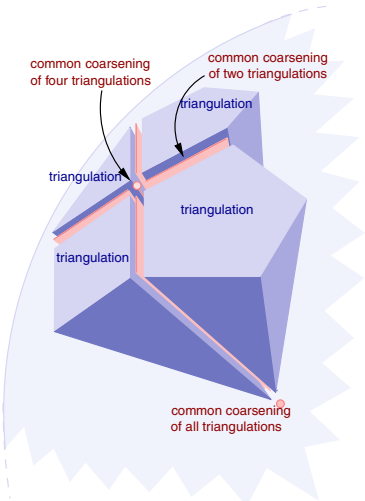


Figure 5.41: The structure of a piece of the secondary fan (intersected with a ball; lineality spaces not drawn): A height in a common face of two or more secondary cones induces a common coarsening of the respective polyhedral subdivisions.

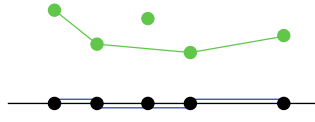


Figure 5.42: The graph of the piecewise affine function defined by a triangulation and a height vector. In this case, the function is “as convex as possible.” Thus, the height induces the given triangulation.

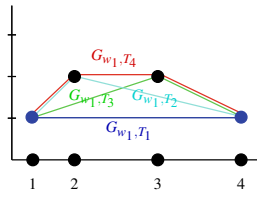


Figure 5.43: The characteristic sections corresponding to $\omega_1 = (1, 2, 2, 1)$: the one corresponding to \mathcal{T}_1 is minimal.

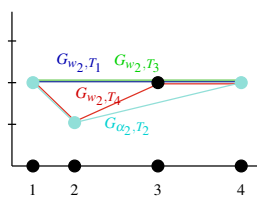


Figure 5.44: The characteristic sections corresponding to $\omega_2 = (2, 1, 2, 2)$: the one corresponding to \mathcal{T}_2 is minimal.

Then we can define a piecewise-linear function by

$$g_{\omega, \mathcal{T}} : \begin{cases} \text{conv}(\mathbf{A}) & \rightarrow \mathbb{R}^{d+1}, \\ \mathbf{p}_j & \mapsto g_{\omega, \mathcal{T}}(\mathbf{p}_j) := \omega_j, \end{cases}$$

and extended affinely on $\text{conv}(C)$ for each cell $C \in \mathcal{T}$. This function is called the *characteristic section* of \mathcal{T} with respect to ω .

We remark that this is well-defined on intersections of simplices, because of the intersection property of a polyhedral subdivision.

The following observation relates characteristic sections to things we already know:

Lemma 5.2.13. *Let \mathbf{A} be a point configuration, and let \mathcal{T} be any triangulation refining $\mathcal{S}(\mathbf{A}, \omega)$. The function graph*

$$G_{\omega, \mathcal{T}} := \left\{ \begin{pmatrix} \mathbf{x} \\ g_{\omega, \mathcal{T}}(\mathbf{x}) \end{pmatrix} : \mathbf{x} \in \text{conv} \mathbf{A} \right\} \subset \mathbb{R}^{d+1}$$

equals the union of lower facets of \mathbf{A}^ω .

More specifically,

$$G_{\omega, \mathcal{T}}(\text{conv}_{\mathbf{A}}(C)) = \text{conv}_{\mathbf{A}^\omega}(C) \quad \text{for all } C \in \mathcal{S}(\mathbf{A}, \omega).$$

□

So, if $\mathcal{T} = \mathcal{S}(\mathbf{A}, \omega)$ then we just get a formally different description of the definition of $\mathcal{S}(\mathbf{A}, \omega)$. Note, however, that in the definition of $g_{\omega, \mathcal{T}}$ we do not require ω to be the height function that induces \mathcal{T} . In fact, we want to find out what is special about $g_{\omega, \mathcal{T}}$ for $\mathcal{T} \preceq \mathcal{S}(\mathbf{A}, \omega)$. The following lemma describes what $g_{\omega, \mathcal{S}(\mathbf{A}, \omega)}$ looks like compared to the $g_{\omega, \mathcal{T}}$ induced by other polyhedral subdivisions \mathcal{T} .

Lemma 5.2.14 (Crucial Lifting Lemma). *Fix $\omega \in \mathbb{R}^J$ and let \mathcal{T} be an arbitrary triangulation of \mathbf{A} . Then the following are equivalent:*

$$(i) \quad \mathcal{T} \preceq \mathcal{S}(\mathbf{A}, \omega).$$

$$(ii) \quad g_{\omega, \mathcal{T}} \leq g_{\omega, \mathcal{T}'} \text{ for all triangulations } \mathcal{T}' \text{ of } \mathbf{A}.$$

Proof. First, we observe that, by definition of the convex hull, the lifted cell $g_{\omega, \mathcal{T}'}(\text{conv}(C))$ lies in the polytope $\text{conv}(\mathbf{A}^\omega)$ for all triangulations \mathcal{T}' of \mathbf{A} and all $C \in \mathcal{T}'$. Moreover, $\mathcal{T} \preceq \mathcal{S}(\mathbf{A}, \omega)$ if and only if the lifted cell $g_{\omega, \mathcal{T}}(C)$ lies in a lower facet of $\text{conv}(\mathbf{A}^\omega)$ for all $C \in \mathcal{T}'$.

Consider the fiber over $\mathbf{x} \in \text{conv}(\mathbf{A}^\omega)$, which is the set

$$\mathbf{F}_{\mathbf{x}} := \left\{ \mathbf{y} \in \text{conv}(\mathbf{A}^\omega) : y_i = x_i, i = 1, \dots, d \right\}.$$

This is a segment, because it is the intersection of the polytope $\text{conv}(\mathbf{A}^\omega)$ with a line, i.e., an affine subspace. Moreover, the line intersects the lower facets of $\text{conv}(\mathbf{A}^\omega)$ in the lowest point of $\mathbf{F}_{\mathbf{x}}$. This point equals $g_{\omega, \mathcal{T}}(\mathbf{x})$ for all $\mathbf{x} \in \text{conv} \mathbf{A}$ if and only if, for all $C \in \mathcal{T}'$, the lifted cell $g_{\omega, \mathcal{T}}(\text{conv}(C))$ lies in a lower facet of $\text{conv}(\mathbf{A}^\omega)$. This was shown to be equivalent to $\mathcal{T} \preceq \mathcal{S}(\mathbf{A}, \omega)$. □

Example 5.2.15 (5.1.1 continued). We show in Figures 5.43 through 5.46 the characteristic sections on $\text{conv}(\mathbf{L}_4)$ for all pairs of heights and triangulations in Example 5.1.1. Remember that all given triangulations are regular, and all of them were induced by one of the given heights. In the example it can be seen right away that the lifting according to the triangulation induced by a height is never above any other lifting. \square

We are now in a position to prove the main result in this section:

Theorem 5.2.16 (Gelfand, Kapranov, Zelevinsky 1989). *If \mathbf{A} is a point configuration, then $\Sigma\text{-fan}(\mathbf{A})$ is the inner normal fan of the secondary polytope $\Sigma\text{-poly}(\mathbf{A})$.*

Proof. Every polytope is determined by its vertices or, equivalently, by its full-dimensional normal cones. By definition of the convex hull the vertices of the secondary polytope $\Sigma\text{-poly}(\mathbf{A})$ are among the GKZ-vectors of triangulations, and thus it is sufficient to prove the following: For every triangulation \mathcal{T} , the normal cone $N_{\Sigma\text{-poly}(\mathbf{A})}(\phi_{\mathbf{A}}(\mathcal{T}))$ of the point $\phi_{\mathbf{A}}(\mathcal{T})$ in $\Sigma\text{-poly}(\mathbf{A})$ equals $\mathbf{C}(\mathbf{A}, \mathcal{T})$. This would also imply, by Proposition 5.2.9(iv), that $\phi_{\mathbf{A}}(\mathcal{T})$ is a vertex if and only if \mathcal{T} is regular.

We will first show the following:

$$\mathbf{C}(\mathbf{A}, \mathcal{T}) \stackrel{!}{\subseteq} N_{\Sigma\text{-poly}(\mathbf{A})}(\phi_{\mathbf{A}}(\mathcal{T}))$$

for all triangulations \mathcal{T} .

To this end, fix an arbitrary triangulation \mathcal{T} of \mathbf{A} , and let $\omega \in \mathbf{C}(\mathbf{A}, \mathcal{T})$. By definition of the secondary cone, $\mathcal{T} \preceq \mathcal{S}(\mathbf{A}, \omega)$, we need to show the following:

$$\langle \omega, \phi_{\mathbf{A}}(\mathcal{T}) \rangle \stackrel{!}{\leq} \langle \omega, \mathbf{x} \rangle \quad \text{for all } \mathbf{x} \in \Sigma\text{-poly}(\mathbf{A}).$$

Since on any polytope, every linear functional is minimized at one of its vertices, it is sufficient to check potential vertices of $\Sigma\text{-poly}(\mathbf{A})$ in place of a general \mathbf{x} . Again, the vertices of $\Sigma\text{-poly}(\mathbf{A})$ must be among the points defining its convex hull. Therefore, it is sufficient to prove

$$\langle \omega, \phi_{\mathbf{A}}(\mathcal{T}) \rangle \stackrel{!}{\leq} \langle \omega, \phi_{\mathbf{A}}(\mathcal{T}') \rangle \quad \text{for all triangulations } \mathcal{T}' \text{ of } \mathbf{A}.$$

For every triangulation \mathcal{T}' of \mathbf{A} , we have the following interpretation for

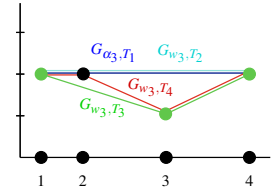


Figure 5.45: The characteristic sections corresponding to $\omega_3 = (2, 2, 1, 2)$: the one corresponding to \mathcal{T}_3 is minimal.

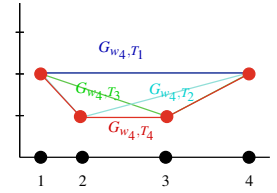


Figure 5.46: The characteristic sections corresponding to $\omega_4 = (2, 1, 1, 2)$: the one corresponding to \mathcal{T}_4 is minimal.

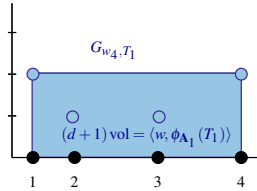


Figure 5.47: For the height vector ω_4 on \mathbf{L}_4 we see: for no triangulation of \mathbf{L}_4 ...

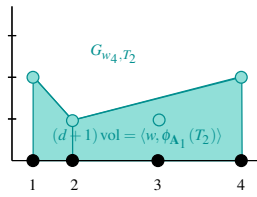


Figure 5.48: ... the volume under the graph of its characteristic section with respect to ω_4 —which is the sum of volumes of the “columns” between cells and their liftings—...

the multiplication of ω with the GKZ-coordinate of \mathcal{T}' :

$$\begin{aligned}
\langle \omega, \phi_{\mathbf{A}}(\mathcal{T}') \rangle &= \sum_{j \in J} \omega_j \phi_{\mathbf{A}}(\mathcal{T}')_j \\
&= \sum_{j \in J} \sum_{C \in \mathcal{T}' : j \in C} \omega_j \text{vol}(C) \\
&= \sum_{C \in \mathcal{T}'} \sum_{j \in C} \omega_j \text{vol}(C) \\
&= \sum_{C \in \mathcal{T}'} \text{vol}(C) \sum_{j \in C} \omega_j \\
&= (d+1) \sum_{C \in \mathcal{T}'} \text{vol}(C) \underbrace{\frac{1}{d+1} \left(\sum_{j \in C} \omega_j \right)}_{\substack{\text{avg. height over } C = \text{height over barycenter}}} \\
&\quad \underbrace{\text{volume of the “column” between } C \text{ and } C^{\omega}}_{\text{volume below the graph of } g_{\omega, \mathcal{T}'}} \\
&= (d+1) \int_{\text{conv} \mathbf{A}} g_{\omega, \mathcal{T}'}(\mathbf{x}) d\mathbf{x}.
\end{aligned}$$

By the Crucial Lifting Lemma (Lemma 5.2.14), the last expression is minimal for any \mathcal{T}' with $\mathcal{T}' \preceq \mathcal{S}(\mathbf{A}, \omega)$. In particular, it is minimized for $\mathcal{T}' = \mathcal{T}$ (see also Figures 5.47 through 5.50). Therefore, $\omega \in N_{\Sigma\text{-poly}(\mathbf{A})}(\phi_{\mathbf{A}}(\mathcal{T}))$, as desired.

The reverse set inclusion,

$$\mathbf{C}(\mathbf{A}, \mathcal{T}) \overset{!}{\supseteq} N_{\Sigma\text{-poly}(\mathbf{A})}(\phi_{\mathbf{A}}(\mathcal{T})),$$

is analogous: the Crucial Lifting Lemma luckily works in both directions. \square

This, in turn, finally gives the proof of Theorem 5.1.9:

Proof of Theorem 5.1.9. This is now an immediate consequence of Theorem 5.2.16 and Theorem 5.2.11, since the face lattice of any polytope is opposite to the face lattice of its normal fan. \square

Although there is still a lot to say about the structure of regular triangulations, one interesting consequence can be drawn: Whenever two triangulations share identical GKZ coordinates, then they are both non-regular. This is proved with the help of the following technical result:

Proposition 5.2.17. *Let \mathcal{T} be a non-regular polyhedral subdivision of \mathbf{A} . Then:*

- (i) $\mathbf{C}^{\circ}(\mathbf{A}, \mathcal{T})$ is empty.
- (ii) $\mathbf{C}(\mathbf{A}, \mathcal{T})$ is not full-dimensional.

Note that for Part (ii) we cannot use Proposition 5.2.9(ii), since we are talking about non-regular subdivisions.

Proof. Assertion (i) is by definition.

In order to prove Part (ii), we use Part (i) together with Lemma 5.2.2, where the latter gives us the link to regular subdivisions that we need to apply Proposition 5.2.9:

$$\begin{aligned}\mathbf{C}(\mathbf{A}, \mathcal{T}) &= \bigcup \{ \mathbf{C}^\circ(\mathbf{A}, \mathcal{T}') : \mathcal{T} \preceq \mathcal{T}' \} \\ &= \bigcup \{ \mathbf{C}^\circ(\mathbf{A}, \mathcal{T}') : \mathcal{T}' \text{ regular and } \mathcal{T} \prec \mathcal{T}' \}.\end{aligned}$$

No \mathcal{T}' with $\mathcal{T} \prec \mathcal{T}'$ can be a triangulation, since a triangulation cannot be strictly refined. Hence, by Part (i) and by Proposition 5.2.9(iv), no set in the union is full-dimensional. As a finite union of non-full-dimensional cones, $\mathbf{C}(\mathbf{A}, \mathcal{T})$ cannot be full-dimensional. \square

Corollary 5.2.18. *If two triangulations $\mathcal{T} \neq \mathcal{T}'$ of the same point configuration \mathbf{A} have the same GKZ-vector, then they are both non-regular.*

Proof. If one of the triangulations was regular, then both triangulations would correspond to the same vertex of $\Sigma\text{-poly}(\mathbf{A})$. In other words, their normal cones coincide and hence, according to Theorem 5.1.9, their secondary cones must coincide. Moreover, both secondary cones, as normal cones of vertices of a polytope, are full-dimensional, hence both triangulations must be regular by Proposition 5.2.17(ii). Therefore, we can apply Proposition 5.2.9(ii), and thus the relatively open secondary cones must coincide as well. By definition of the relatively open secondary cone, this means that $\mathcal{T} = \mathcal{T}'$, a contradiction. \square

5.3 Structure of the secondary polytope

The structure of the secondary polytope has interesting implications for regular subdivisions, regular triangulations, and their relations. Edges, paths, and facets correspond to structures in the space of regular subdivisions that we have discussed before.

5.3.1 Edges of the secondary polytope

One of the most important applications of Theorem 5.1.9 is to show that every two regular triangulations can be joined by a finite sequence of flips:

Theorem 5.3.1. *The edge graph of the secondary polytope $\Sigma\text{-poly}(\mathbf{A})$ of \mathbf{A} is contained in the flip graph of all regular triangulations of \mathbf{A} .*

Proof. In any polytope, adjacent full-dimensional normal cones correspond to adjacent vertices, i.e., vertices that are connected by an edge. Every edge of the secondary polytope represents an adjacency between two full-dimensional secondary cones. This corresponds, by Parts (iv) and (v) of Proposition 5.2.9 and Corollary 2.4.6, to a flip between two regular triangulations. \square

Corollary 5.3.2. *Every regular triangulation has at least $n - d - 1$ flips, where d is the dimension of \mathbf{A} , and the graph of all regular triangulations of \mathbf{A} is $(n - d - 1)$ -connected.*

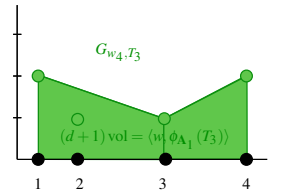


Figure 5.49: ... is strictly smaller ...

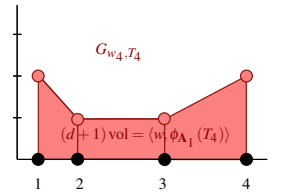


Figure 5.50: ... than the volume below the graph of the characteristic section of \mathcal{T}_4 .

Proof. As a graph of an $(n - d - 1)$ -dimensional polytope, this graph is $(n - d - 1)$ -connected, by Balinski's Theorem (see, e.g., [339, 148]). \square

The converse of Theorem 5.3.1 was generally believed to hold (see [140, Ch. 7, Theorem 2.10] and [280, Theorem 2.8]). But here we show it is in fact false: The graph of the secondary polytope is *not always equal* to the graph of flips between regular triangulations, because a *non-regular* almost-triangulation (a subdivision supporting the flip, see Subsection 2.4.2) can be refined by two *regular* triangulations. This situation produces flips between regular triangulations which do not appear as edges of the secondary polytope. Before showing an explicit example of this, let us see that such nasty examples cannot occur with points in general position or, more generally, for flips on circuits in general position (this is the content of Proposition 2.8 in [140]).

Theorem 5.3.3. *If two regular triangulations \mathcal{T}_1 and \mathcal{T}_2 differ by a flip on a full-dimensional circuit Z , then the almost-triangulation \mathcal{S} refined by \mathcal{T}_1 and \mathcal{T}_2 is regular too. That is, it is an edge in the secondary polytope.*

Proof. Let us assume that there is no element of \mathbf{A} in $\text{conv}(Z)$ other than those forming part of Z itself. This is no loss of generality, because such elements, if they exist, are not used in any of \mathcal{T}_1 , \mathcal{T}_2 and \mathcal{S} , so they do not affect their regularity.

If ω_1 and ω_2 are heights producing \mathcal{T}_1 and \mathcal{T}_2 respectively, then every positive combination of them gives a regular subdivision containing the subcomplex $\mathcal{T}_1 \cap \mathcal{T}_2$. In particular, there is a path on the secondary polytope going from \mathcal{T}_1 and \mathcal{T}_2 along only regular subdivisions that contain $\mathcal{T}_1 \cap \mathcal{T}_2$. (A more precise version of this argument will be given in Theorem 5.3.13).

Now, since Z is full-dimensional, $\mathcal{T}_1 \cap \mathcal{T}_2$ covers all of $\text{conv}(\mathbf{A})$ except for $\text{conv}(Z)$. Moreover, the boundary of $\text{conv}(Z)$ is simplicial (this holds for any circuit). So, the only subdivisions containing $\mathcal{T}_1 \cap \mathcal{T}_2$ are \mathcal{T}_1 , \mathcal{T}_2 , and \mathcal{S} , because the only subdivisions of a circuit are its two triangulations and the trivial one. This implies that the flip is an edge in the secondary polytope. \square

Example 5.3.4 (A non-regular flip between regular triangulations). Let \mathcal{A} be the following configuration of 10 points in dimension three (as usual, the last row is just for homogenization):

$$\mathcal{A} = \begin{pmatrix} 1 & 2 & 3 & 4 & 5 & 6 & 7 & 8 & 9 & 0 \\ 0 & 0 & 4 & -4 & 4 & -4 & 0 & 0 & 0 & 0 \\ 0 & 0 & 4 & -4 & -4 & 4 & 7 & -7 & 1 & -1 \\ 4 & -4 & 0 & 0 & 0 & 0 & 1 & -1 & 7 & -7 \\ 1 & 1 & 1 & 1 & 1 & 1 & 1 & 1 & 1 & 1 \end{pmatrix}.$$

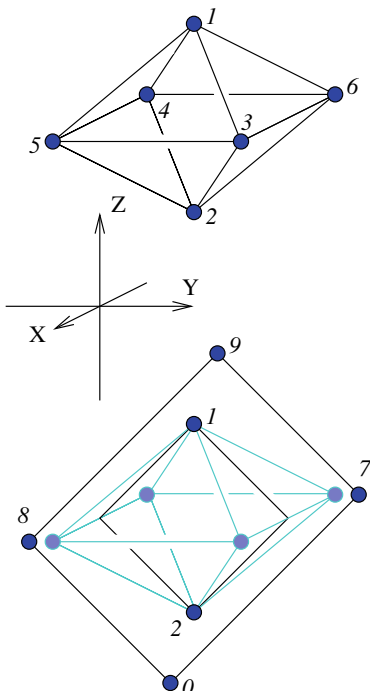


Figure 5.51: The configuration \mathcal{A} . The top picture shows the inner octahedron. The bottom picture shows the six points in the YZ-plane.

Figure 5.51 shows the configuration in two parts: the first six points form the vertices of an octahedron, affinely equivalent to a regular one. The last four vertices form a slanted rectangle with sides parallel to the square obtained by intersecting the octahedron the YZ-plane. Notice that the square is contained in the rectangle.

We are going to study the family of regular triangulations and subdivisions induced by the following 1-parameter family of height functions:

$$\omega(t) = \begin{pmatrix} 1 & 2 & 3 & 4 & 5 & 6 & 7 & 8 & 9 & 0 \\ 0 & 0 & 2+t & 2+t & 2-t & 2-t & 13.5 & 13.5 & 10 & 10 \end{pmatrix}.$$

Let \mathcal{T}_t be the regular subdivision obtained for a certain value of t . Observe that $\omega(t)$ does not depend on t at the six points of the YZ-plane. This makes it rather easy to compute the intersection of \mathcal{T}_t with that plane. We only need to take into account the four intersections of the edges 34, 36, 54, and 56, with that plane, and consider them as if they were four extra points of the configuration, with the following heights assigned to them:

$$\begin{aligned} \omega_{34}(t) &= \frac{\omega_3 + \omega_4}{2} = 2+t, & \omega_{36}(t) &= \frac{\omega_3 + \omega_6}{2} = 2, \\ \omega_{54}(t) &= \frac{\omega_5 + \omega_4}{2} = 2, & \omega_{56}(t) &= \frac{\omega_5 + \omega_6}{2} = 2-t. \end{aligned}$$

This is represented in Figure 5.52. The triangulation shown there is the one obtained as long as $t \in (-2, 2)$. It does not use the edges 34 and 56, and its only extension to the configuration consists of the following eighteen tetrahedra:

$$\mathcal{T}_0 = \left\{ \begin{array}{l} 1235, 1236, 1245, 1246, \\ 3619, 3679, 3627, 2370, 2670, \\ 4520, 4590, 4518, 1489, 1589, \\ 3519, 3520, 4619, 4620 \end{array} \right\}$$

The first row triangulates the central octahedron. The second and third triangulate the right and left regions around it, and the fourth triangulates the front and back.

When t gets out of the interval $(-2, 2)$, but not by too much, the only change is in the way the central octahedron is triangulated. More precisely, with $t \in (-11.5, -2)$ and $t \in (2, 11.5)$ we get, respectively, the following triangulations \mathcal{T}_{-5} and \mathcal{T}_{+5} :

$$\begin{aligned} \mathcal{T}_{-5} &= \mathcal{T}_0 \setminus \{1235, 1236, 1245, 1246\} \cup \{1356, 1456, 2356, 2456\}, \\ \mathcal{T}_{+5} &= \mathcal{T}_0 \setminus \{1235, 1236, 1245, 1246\} \cup \{1345, 1346, 2345, 2346\}. \end{aligned}$$

The important point so far is simply that these three triangulations, \mathcal{T}_0 , \mathcal{T}_{-5} and \mathcal{T}_{+5} are all regular, and they form a triangle in the graph of flips between triangulations of \mathbf{A} . (Every two triangulations of the regular octahedron are connected by a flip.)

Now, we are going to show that the almost-triangulation connecting \mathcal{T}_{-5} and \mathcal{T}_{+5} is not regular. This almost-triangulation has the exterior of the octahedron triangulated as \mathcal{T}_{-5} and \mathcal{T}_{+5} , but the octahedron itself subdivided into two square pyramids separated by the horizontal square 3456. That is to say:

$$\mathcal{S} := \mathcal{T}_0 \setminus \{1235, 1236, 1245, 1246\} \cup \{13456, 23456\}.$$

In particular, in the YZ-plane we should be able to get the regular subdivision of Figure 5.52 but with the middle edge flipped, as in Figure 5.53.

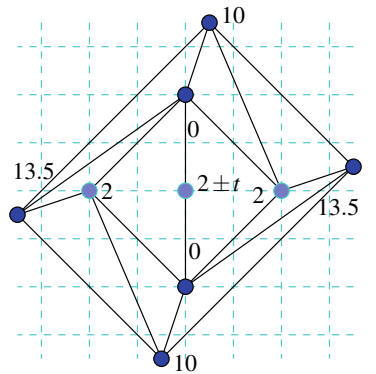


Figure 5.52: The heights induced by $\omega(t)$ on the YZ-plane are constant and produce this regular triangulation, for $t \in (-2, 2)$.

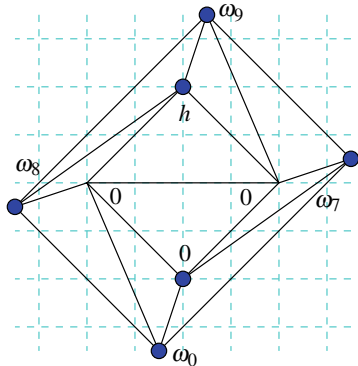


Figure 5.53: This subdivision is not regular.

This is impossible: Assuming, without loss of generality, height zero for the triangle below the middle edge and a positive height h for the second vertex joined to that edge, we get the following contradiction:

$$\omega_9 > \omega_8 + 2h \Rightarrow \omega_7 > \omega_9 - \frac{3}{2}h > \omega_8 + \frac{1}{2}h,$$

$$\Rightarrow \omega_8 > \omega_0 > \omega_7 > \omega_8 + \frac{1}{2}h.$$

Remark 5.3.5. The example above is minimal in terms of rank (see Exercise 5.24), but not in terms of number of points. In Exercise 5.23 and Example 5.4.16, we show two constructions, of rank four, but with only eight elements, one acyclic and one totally cyclic. In Theorem 5.4.15 we show that eight is indeed the minimum possible number of points, since examples with corank three cannot exist.

Observe that this example shows, in particular, that:

Corollary 5.3.6. *There are refinement-minimal non-regular subdivisions that are not triangulations.*

Most probably, there are even minimal non-regular subdivisions very high up in the refinement poset. Yet, we do not know the answer to the following question: Is there a configuration that has non-regular subdivisions, but only regular triangulations?

5.3.2 Monotone paths on the secondary polytope

In Chapter 3, we saw that, for two-dimensional problems one can flip monotonically from any triangulation to arrive, after finitely many steps, to the Delaunay triangulation. We also saw, in Example 3.6.15, that the same is false in dimension three. Nevertheless, the rich secondary polytope structure brings new hope. In this subsection, we show that one can still monotonically flip from any *regular* triangulation \mathcal{T} to any other target regular triangulation \mathcal{T}' (e.g., the Delaunay triangulation), guided by a height function ω that determines \mathcal{T}' . Effectively, the edges of the secondary polytope are oriented using ω to form an acyclic directed graph with a unique sink given by the triangulation \mathcal{T}' . (Note that the idea of orienting the edges of a polyhedron by a linear functional is rather common in linear programming and used by the simplex method.)

Theorem 5.3.7. *Let \mathbf{A} be a point configuration and let ω be a height vector determining its regular triangulation $\mathcal{T}' = \mathcal{S}(\mathbf{A}, \omega)$. Let \mathcal{T} be a different regular triangulation of \mathbf{A} . Then, there exists a finite sequence of regular triangulations, $\mathcal{S}_0, \mathcal{S}_1, \dots, \mathcal{S}_k$ from $\mathcal{S}_0 = \mathcal{T}$ to $\mathcal{S}_k = \mathcal{T}'$ such that*

1. *The inner product of ω with the GKZ vectors of consecutive triangulations satisfies $\langle \omega, \phi_{\mathbf{A}}(\mathcal{S}_i) \rangle > \langle \omega, \phi_{\mathbf{A}}(\mathcal{S}_{i+1}) \rangle$.*
2. *Two consecutive triangulations differ in a flip.*
3. *No circuit is used for two different flips in the sequence. Furthermore, no two circuits used can have the same positive part, or the same negative part.*

In part (3) we take our usual convention that the circuit $Z = (Z_-, Z_+)$ on which a flip is supported is always oriented so that Z_- disappears and Z_+ appears after the flip.

Proof. Consider the linear programming problem of minimizing a linear function with ω as its cost vector over the points of the secondary polytope $\Sigma\text{-poly}(\mathbf{A})$. By the proof of Theorem 5.2.16 and the theory of linear programming, the minimum must be attained at the vertex $\phi_{\mathbf{A}}(\mathcal{T}')$ of $\Sigma\text{-poly}(\mathbf{A})$. By linear programming optimality from the vertex corresponding to any other regular triangulation there exists an adjacent vertex, connected by an edge of the secondary polytope, whose inner product with ω strictly decreases its value. Hence, performing the corresponding flip, associated to that edge, a new triangulation with strictly smaller inner product value is obtained. Starting with \mathcal{T} and repeatedly applying this fact, we construct the desired sequence of triangulations from \mathcal{T} to \mathcal{T}' that satisfies Parts (2) and (1).

For Part 3, let us look at the piecewise linear functions $g_{\omega, \mathcal{S}_i}$ for the regular triangulations $\mathcal{S}_0, \dots, \mathcal{S}_k = \mathcal{T}'$ in our sequence. When we flip from \mathcal{S}_i to \mathcal{S}_{i+1} the function only changes in the simplices involved in the flip, that is, those containing the cells Z_+ (in \mathcal{S}_i) and Z_- (in \mathcal{S}_{i+1}). Since the convex hull of the lifted points corresponding to the circuit Z form a simplex, where the upper and lower envelopes are the two possible triangulations of the circuit induced by its parts, the change in the piecewise linear functions is everywhere the same: Either $g_{\omega, \mathcal{S}_i}(\mathbf{x}) \leq g_{\omega, \mathcal{S}_{i+1}}(\mathbf{x})$ for all \mathbf{x} or $g_{\omega, \mathcal{S}_i}(\mathbf{x}) \geq g_{\omega, \mathcal{S}_{i+1}}(\mathbf{x})$ for all \mathbf{x} . The interpretation of $\langle \omega, \phi_{\mathbf{A}}(\mathcal{S}_i) \rangle$ as the integral of $g_{\omega, \mathcal{S}_i}(\mathbf{x})$ (see the proof of Theorem 5.2.16), together with part (1) implies that the latter happens, so that the piecewise linear functions decrease at every step until reaching the convex function $g_{\omega, \mathcal{T}'}$. But then the same circuit Z cannot be flipped twice, for this would imply changing twice from the upper envelope to the lower envelope of a certain simplex (the lifting of Z). Furthermore, if a circuit (Z_-, Z_+) is flipped at a certain step, before that step the functions $g_{\omega, \mathcal{S}_i}$ lie all strictly above the lifting of Z_+ , and after that step they lie all strictly below the lifting of Z_- . This implies that the same positive or negative part cannot be used twice for a circuit. \square

Definition 5.3.8. A sequence of flips in the conditions of Theorem 5.3.7 is called *monotone towards ω* .

Remark 5.3.9. What we prove in part (3) of Theorem 5.3.7 is that the sequence of functions $g_{\omega, \mathcal{S}_0}, \dots, g_{\omega, \mathcal{S}_k}$ is point-wise monotonically decreasing. In particular, the associated hypersurfaces $G_{\omega, \mathcal{S}_0}, \dots, G_{\omega, \mathcal{S}_k}$, defined as in Lemma 5.2.13, are each below the previous one. Observe that the final hypersurface $G_{\omega, \mathcal{T}'}$ is, by definition of $\mathcal{T}' := \mathcal{S}(\mathbf{A}, \omega)$, the lower envelope of the lifted configuration \mathbf{A}^ω . That is, monotone flipping with respect to ω can be rephrased as *changing a triangulation by always decreasing the hypersurface (defined via ω) associated to it until the lower envelope of the lifted configuration is reached*.

In fact, what the monotone-flip sequence from \mathcal{T} to \mathcal{T}' gives is a triangulation of the region between $G_{\omega, \mathcal{T}}$ and $G_{\omega, \mathcal{T}'}$. Although this is true in general, it is especially easy to see in the case where \mathbf{A} is in general position.

In this case, each circuit has $d + 2$ points and is lifted to an affine basis in \mathbf{A}^ω . The region between the hypersurfaces $G_{\omega, \mathcal{S}_i}$ and $G_{\omega, \mathcal{S}_{i+1}}$ is just the simplex of \mathbf{A}^ω generated by those $d + 2$ points. This idea, which already appeared in Theorem 1.1.6, will also be fundamental in our study of the spaces of triangulations of cyclic polytopes, in Section 6.1.

Example 5.3.10 (Monotone flipping towards Delaunay and lexicographic triangulations). Let us see that the notion of monotone flipping of Theorem 5.3.7 agrees with the one mentioned for the Delaunay, pushing, and pulling triangulations in dimension two (Sections 3.4.1 and 3.6.2).

- If $\omega(a)$ is positive and much bigger in absolute value for a certain $a \in J$ than for every other element then, in a first approximation,

$$\langle \omega, \phi_{\mathbf{A}}(\mathcal{T}) \rangle \simeq \omega(a) \phi_{\mathbf{A}}(\mathcal{T})(a) = \omega(a) \text{vol}(\text{st}_{\mathcal{T}}(a)).$$

Hence, decreasing the value of $\langle \omega, \phi_{\mathbf{A}}(\mathcal{S}_i) \rangle$ is the same as decreasing the volume of the star of a . In particular, monotonically flipping towards a functional with

$$\omega(n) \gg \omega(n-1) \gg \cdots \gg \omega(1) > 0.$$

leads to the pushing (or placing) triangulation. Observe that these are the type of functionals described in Lemma 4.3.4, and that flipping to decrease, one by one, the stars of the elements $n, n-1$, etc. was what we did in Theorem 3.4.1.

- Similarly, flipping towards the pulling triangulation as we did in Theorem 3.4.3 corresponds to monotonically flipping with respect to a functional of the following type, which appeared in Lemma 4.3.6 (construction of the pulling triangulation):

$$\omega(n) \ll \omega(n-1) \ll \cdots \ll \omega(1) < 0.$$

- Finally, remember that the Delaunay triangulation of \mathbf{A} is the regular triangulation obtained when we lift \mathbf{A} to a paraboloid. Flipping to the Delaunay triangulation can be achieved by monotonically flipping with respect to that functional.

Observe, however, that in Theorems 3.4.1, 3.4.3 and 3.4.2 we prove that monotonically flipping towards the pushing, pulling, and Delaunay triangulations in dimension two works *even if the starting triangulation \mathcal{T} is not regular*. That is a special feature of these particular choices of the functional ω in dimension two. If a functional with that feature could be found for every three-dimensional configuration then we could conclude that graphs of triangulations in dimension three are connected by flips, too.

By the above theorem and a simple bound on the possible number of circuits, one can conclude:

Corollary 5.3.11. *Let \mathbf{A} be a configuration of dimension d in general position with n points. Then the diameter of the graph of $\Sigma\text{-poly}(\mathbf{A})$ cannot exceed*

$$\min \left\{ (d+2) \binom{n}{\lfloor \frac{d}{2} + 1 \rfloor}, \binom{n}{d+2} \right\}.$$

Proof. If our configuration is in general position, then its number of circuits is $\binom{n}{d+2}$. If it is not in general position, then the number of circuits is smaller. Indeed, every circuit is contained in a spanning set of $d+2$ points (of which there are at most $\binom{n}{d+2}$), and each such set is a corank-one configuration, hence contains a unique circuit. This proves the second bound.

For the first bound we use a similar argument: since the smaller side of each circuit has at most $(d+2)/2 = \frac{d}{2} + 1$ elements, the number of different “smaller parts” of circuits is at most

$$n + \binom{n}{1} + \cdots + \binom{n}{\lfloor \frac{d}{2} + 1 \rfloor} \leq \left(\frac{d}{2} + 1 \right) \binom{n}{\lfloor \frac{d}{2} + 1 \rfloor}.$$

In a monotone path, we can use at most two circuits with the same “smaller part”, one as its positive part and one as its negative part. \square

Observe that the first bound is better for small dimension d , but the second one is better for small number of points or, more precisely, for small dimension $n - d - 1$ of the secondary polytope. Indeed, the first is in $O(n^{\lfloor \frac{d}{2} + 1 \rfloor})$ when d is fixed and the second one is in $O(n^{r-1})$ when $r = n - d - 1$ is fixed. Both bounds are (essentially) tight: for the second one see Corollary 5.5.17, and for the first one, see parts (vi) and (vii) of Corollary 6.1.20.

Remark 5.3.12. If we agree that a disconnected graph has infinite diameter, then the existence of disconnected flip-graphs (see Chapter 7) implies that the bound of Corollary 5.3.11 does not hold for the graph of all triangulations of a point set. One can still ask about the diameter of individual connected components of that graph; there we do not know the answer, but we would expect them not to satisfy this bound, in general.

In the proof of Theorem 5.3.7, we rely on general properties of polytopes to show that a monotone flip sequence exists. But, in practice, one wants to find the sequence. One way to do it is as follows:

Theorem 5.3.13. *Let \mathbf{A} be a point configuration and let ω be a height vector determining its regular triangulation $\mathcal{T}' = \mathcal{S}(\mathbf{A}, \omega)$. Let \mathcal{T}_0 be a different regular triangulation of \mathbf{A} and let ω_0 be a height function producing \mathcal{T}_0 and “sufficiently generic”. For each $t \in [0, 1]$, let $\omega_t = (1-t)\omega_0 + t\omega$. Then:*

1. *For every $t \in [0, 1]$, the regular subdivision $\mathcal{T}_t := \mathcal{S}(\mathbf{A}, \omega_t)$ is either a triangulation or an almost-triangulation (i.e., a bistellar flip) between two of them.*
2. *The sequence of triangulations and bistellar flips obtained in this way is monotone in the sense of Theorem 5.3.7.*

3. All the intermediate subdivisions \mathcal{S}_i contain all simplices common to both \mathcal{T} and \mathcal{T}' .

Proof. Part (1) follows from the genericity assumption on ω : The cone spanned by ω_0 and ω will intersect only full-dimensional or codimension-1 cones of the secondary fan. Part (2) is also easy: whenever we cross a codimension-1 cone of the secondary fan we do so from the side of ω_0 to the side of ω . That is the condition for the flip to be monotone towards ω .

For part (3) we introduce the following notation: for each subset B of \mathbf{A} we let $\mathbf{C}(\mathbf{A}, -)_B$ be the set of all weights in such that the regular triangulation induced by them has B as a cell. The reader can verify as an exercise that this is a convex cone (the notion of chamber fan in the next section makes this almost self-evident). Since ω_0 and ω lie in $\mathbf{C}(\mathbf{A}, -)_B$ for every common cell B of \mathcal{T} and \mathcal{T}' , ω_t lies in it too. \square

Part 3 of this last statement was first observed in [260]. From it, the authors derived:

Corollary 5.3.14. *Let \mathbf{A} be a point configuration. The subgraph of the flip graph induced by all regular triangulations of \mathbf{A} that use the same vertices is connected.*

The first monotone flipping algorithm in arbitrary dimension was devised by Joe in 1993 [179] for the Delaunay triangulation. It uses an *incremental* strategy, that is, it constructs the desired triangulation by adding points one at a time, at each step updating the triangulation computed so far via monotone flipping. For the points that have not yet been introduced, the corresponding value of ω is replaced by ∞ . When a point is inserted, its correct value is put in ω and the “insertion-update” step consists of applying Theorem 5.3.13 for the new ω , taking as ω_0 the old ω . Edelsbrunner and Shah [116], already aware at least partially of the theory of secondary polytopes, generalized the algorithm to flipping towards any regular triangulation. A key point for analyzing the efficiency in both algorithms was to show that the sequence of flips can be found and performed, spending constant time per flip (in fixed dimension).

An exception to this time bound are the insertion steps. In theory, they are just another case of flip, one of type $(1, k)$ for some k . But in the algorithm they have a totally different treatment since they involve locating where the new points needs to be inserted in the old triangulation. To get good time bounds for the location step, the standard incremental algorithm is *randomized*: the ordering in which the points are inserted is considered random among the $n!$ possible orderings, and it is proved that the total *expected* time taken by the n insertion steps is bounded above by $O(n \log n)$ in the plane and $O(n^{\lceil d/2 \rceil})$ in higher dimension, which is close to optimal since the size of the Delaunay triangulation can be in $\Omega(n^{\lfloor d/2 \rfloor})$.

This incremental-randomized-flipping can be considered the standard algorithm for the Delaunay triangulation in current computational geometry. For example, it is the only one described in the textbooks [93] and [116]. In the survey [21], it is the first of four described in the plane, but the only one detailed in dimension three, as “the most intuitive and easy to implement.”

5.3.3 Facets of the secondary polytope

From Theorem 5.1.9, we see that the facets of the secondary polytope of a configuration \mathbf{A} correspond to those regular subdivisions of \mathbf{A} that can only be coarsened by the trivial subdivision; these are the *coarsest subdivisions*. In this subsection, we wish to quickly point out a few recent results about facets of secondary polytopes. This will include a brief look at the notion of *tight span*, which can be useful in studying arbitrary subdivisions. For more details, we refer the interested reader to the papers [29], [158], [157], [161], [160], [159], [162]. Let us begin with a special, but simple, kind of coarsest subdivision:

Definition 5.3.15. We call a coarsest subdivision \mathcal{S} of \mathbf{A} a *k-split* of \mathcal{S} if it has exactly k maximal faces and an interior face of codimension $k - 1$.

Interestingly, the notion of *k*-split was first introduced in phylogenetic analysis [29]. These authors initially only investigated 2-splits for special families of polytopes. Let us consider a few cases of *k*-splits. A 1-split of a point configuration \mathbf{A} is a subdivision of \mathbf{A} with exactly one maximal face containing all but one of the points in \mathbf{A} . Clearly, 1-splits are coarsest subdivisions, but they cannot exist for point configurations in convex position. If the points of \mathbf{A} are in convex position (i.e., they are the vertices of a polytope), a subdivision \mathbf{A} will be a 2-split if it has exactly two maximal dimensional cells. For general point configurations, it is only slightly more difficult to describe 2-splits; see Exercise 5.25.

Example 5.3.16. Let \mathbf{A} be the point configuration from Figure 5.54 (this configuration was studied in detail in Section 2.2). First of all, a 3-split of this configuration consists of the cell $\{1, 3, 5\}$, $\{1, 2, 5\}$, and $\{2, 3, 4, 5\}$. Moreover, consider the subdivision \mathcal{S}_1 with maximal cells $\{1, 2, 4, 5\}$ and $\{1, 3, 4, 5\}$, and the subdivision \mathcal{S}_2 whose maximal cells are $\{1, 2, 4\}$ and $\{1, 3, 4\}$. Only \mathcal{S}_1 is a 2-split of \mathbf{A} , since \mathcal{S}_2 is coarsened by \mathcal{S}_1 .

One important result of S. Hermann says that *k*-splits are good examples of facets for the secondary polytope.

Theorem 5.3.17. All *k*-splits of a point configurations are regular coarsest subdivisions.

Proof. Here we will only prove the theorem for $k = 1, 2$, and we do this explicitly by constructing weight functions that define 1-splits and 2-splits. For the rest of the proof, we refer the reader to [158, 157]. For a 1-split \mathcal{S}^p of \mathbf{A} , we define a height vector ω_p by $\omega_p(\mathbf{p}) = 1$ and $\omega_p(\mathbf{a}) = 0$ for all $\mathbf{a} \neq \mathbf{p} \in \mathbf{A}$. This obviously induces the subdivision \mathcal{S}^p . For a 2-split subdivision \mathcal{S} of \mathbf{A} , let $\mathbf{S}_1, \mathbf{S}_2$ be the two maximal faces and let

$H_{\mathcal{S}} = \{x \in \mathbb{R}^d : \langle \alpha, x \rangle = \beta\}$ be the corresponding 2-split (separating) hyperplane for normal vector $\alpha \in \mathbb{R}^d$, $\beta \in \mathbb{R}$. We define $\omega_{\mathcal{S}} : \mathbf{A} \rightarrow \mathbb{R}$ by

$$w_{\mathcal{S}}(v) := \begin{cases} |\langle \alpha, v \rangle - \beta| & \text{if } v \in \mathbf{S}_1, \\ 0 & \text{if } v \in \mathbf{S}_2. \end{cases}$$

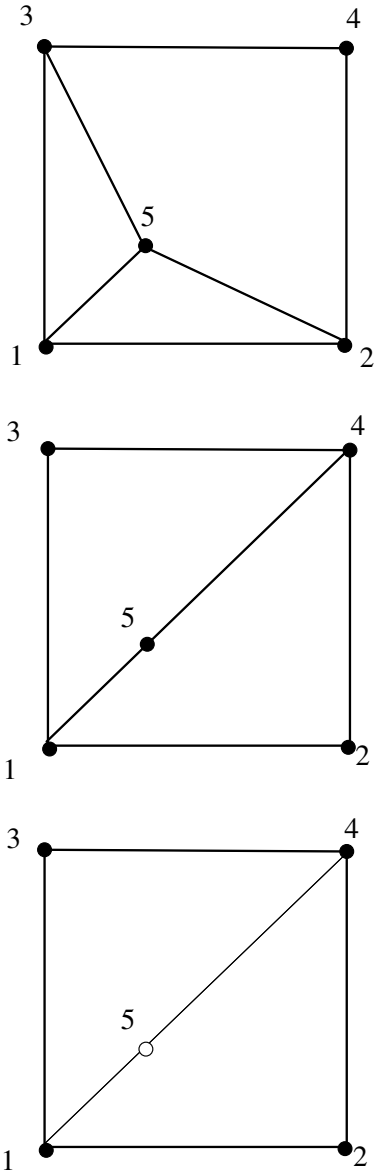


Figure 5.54: For a five point planar configuration, a 3-split, a 2-split, and a boring subdivision which is not the coarsest possible.

Note that this function is well-defined, since for $a \in H_{\mathcal{S}} = \text{aff}(\mathbf{S}_1 \cap \mathbf{S}_2)$ we have $\langle \alpha, v \rangle = \beta$. It is now obvious that ω induces the 2-split \mathcal{S} on \mathbf{A} . \square

From 1-splits and 2-splits, we get two kinds of facets of the secondary polytope. It is not difficult to write the explicit linear inequality that defines the facet of the secondary by using the cells of the subdivision (see Exercise 5.11 for a recipe!). We can define the *k-split polyhedron* $\text{Split-poly}(\mathbf{A})$ of a d -dimensional point configuration \mathbf{A} . It is the $(|\mathbf{A}| - d - 1)$ -dimensional polyhedron in $\mathbb{R}^{\mathbf{A}}$ defined by the inequalities for the k -splits, the inequalities for the j -splits for all $j \leq k$, and the equations defining the affine hull of the secondary polytope (see Section 5.1.3 and Exercise 5.5). Although, in general, the k -split polyhedron *properly* contains the secondary polytope, one can show the following (see [161] for a proof that makes generous use of Gale diagrams).

Theorem 5.3.18. *Let \mathbf{A} be a configuration consisting of the vertices of a polytope. The secondary polytope of \mathbf{A} equals the 2-split polyhedron if and only if \mathbf{A} has the same oriented matroid as a simplex, a cross polytope, a polygon, a prism over a simplex, or a (possibly multiple) join of these polytopes.*

Of course, not all coarsest subdivisions are k -splits. One nice methodology to try to understand general coarsest subdivisions is to look at their *tight span*. Roughly speaking, the tight span is the dual polyhedral complex to a subdivision; for example, the edges correspond to adjacents maximal cells on the subdivision (we have already seen the graph of the tight span, the *dual graph*, which appeared in Lemma 2.6.1). More generally, the tight span of a subdivision \mathcal{S} of dimension d is a polyhedral complex having a cell of dimension i for each *interior* cell of dimension $d - i$ of \mathcal{S} , with inclusions in the tight span reversed from those in \mathcal{S} . See [157] for more details.

It is easy to show that a subdivision is a k -split if and only if its tight span is the complex consisting of a $(k - 1)$ -dimensional simplex and all its faces. However, the tight spans of general coarsest subdivisions can be very complicated. See Figure 5.55 for an easy example in dimension 2. Still, tight spans of coarsest subdivisions have special properties that general tight spans do, in general, not have:

Theorem 5.3.19. *Let \mathbf{A} be a point configuration and \mathcal{S} a coarsest subdivision of \mathbf{A} with k maximal cells.*

1. *The graph of the tight span of \mathcal{S} is 2-connected, that is, it is still connected if one removes any vertex.*
2. *The tight span of \mathcal{S} is a contractible complex.*
3. *If \mathcal{S} is not a k -split, then $k \geq 4$.*
4. *The tight span of \mathcal{S} cannot be a k -gon, with $k \geq 4$, or a triangular prism.*

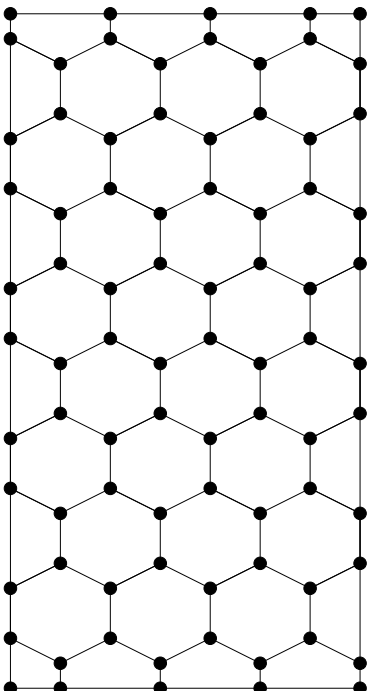


Figure 5.55: A complicated coarsest subdivision.

Proof. We only show a proof for Part 1. The proof for Parts (2) and (4) can be found in [162, 158]. Part (3) is an easy consequence of the first two.

We will show that if the graph of the tight span of the subdivision \mathcal{S} is not 2-connected, then \mathcal{S} could not have been a coarsest subdivision. Let \mathbf{R} be the graph of the tight span of \mathcal{S} . Take a vertex v of \mathbf{R} such that $\mathbf{R} \setminus \{v\}$ is not connected. Let V be the set of vertices of some connected component of $\mathbf{R} \setminus \{v\}$. For each vertex w of \mathbf{R} , let us denote by $\text{cell}(w)$ the corresponding maximal cell of \mathcal{S} . Define a coarser subdivision of \mathbf{A} by deleting all maximal cells, $\text{cell}(w)$ with $w \in V \cup \{v\}$, and replacing them with a single cell, defined as $\bigcup_{w \in V \cup \{v\}} \text{cell}(w)$ as a new maximal cell of the new subdivision. Of course, to be sure that this is indeed a subdivision we need to verify that the new cell we created is still a convex cell and that it intersects properly with the other cells.

For the first point, we just need to show that $\mathbf{C} = \bigcup_{w \in V \cup \{v\}} \text{conv}(\text{cell}(w))$. Assume that there exists $x, y \in \text{relint } \mathbf{C}$ such that the line segment l connecting x and y is not entirely contained in \mathbf{C} . Then l has to intersect (at least) two codimension-one-cells \mathbf{F}_1 and \mathbf{F}_2 among those original cells from \mathcal{S} . Note that codimension-one cells are edges of the graph of the tight span. By our assumption that V is the set of vertices of some connected component of the graph of the tight span minus v , the edges of the tight span of \mathcal{S} corresponding to those cells can only be connected to v . So \mathbf{F}_1 and \mathbf{F}_2 are facets of the $\text{conv}(\text{cell } v)$, and this implies that $\text{conv}(\text{cell } v)$ is not convex, a contradiction.

Finally, an improper intersection of cells cannot happen in the interior of $\text{conv } \mathbf{A}$ because all interior faces of \mathbf{C} are interior faces of $\text{cell}(v)$ by assumption. However, any improper intersection of faces $\mathbf{F}_1, \mathbf{F}_2$ in the boundary of $\text{conv } \mathbf{A}$ would yield an improper intersection of some interior faces $\mathbf{F}'_1, \mathbf{F}'_2$ with $\mathbf{F}_1 \subset \mathbf{F}'_1, \mathbf{F}_2 \subset \mathbf{F}'_2$. Thus, the new subdivision is a subdivision of \mathbf{A} that coarsens the original subdivision \mathcal{S} . \square

5.4 Chambers

We now know that the set of regular polyhedral subdivisions of a point configuration \mathbf{A} has a nice structure: its refinement poset is isomorphic to the face lattice of the secondary polytope $\Sigma\text{-poly}(\mathbf{A})$. We even know the vertices of this polytope. However, since our description is not full-dimensional, it is hard to get a feel for the face lattice of $\Sigma\text{-poly}(\mathbf{A})$. In other words, each cone in the secondary fan contains a non-trivial lineality space.

A very elegant way to get rid of these lineality spaces in the secondary fan, and thus to find a full-dimensional description of $\Sigma\text{-poly}(\mathbf{A})$, is described in this section.

5.4.1 The chamber fan

The lineality space in the normal fan of a polytope \mathbf{P} is the space of linear functions that are constant on \mathbf{P} , and is orthogonal to the affine hull of \mathbf{P} (see Figure 5.56). In the case of the secondary polytope $\Sigma\text{-poly}(\mathbf{A})$ of a point configuration, this, by Theorem 5.1.10, it is simply the space of linear evaluations on \mathbf{A} , that is, it is the space of lifting heights that are the

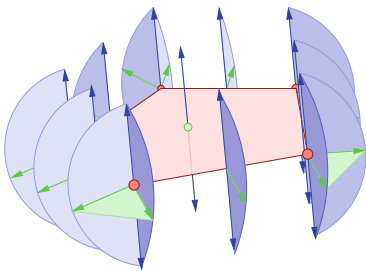


Figure 5.56: The normal fan of a five-gon in three-space is not pointed; the linearity spaces of the normal cones coincide and are equal to the normal cone of the polytope itself.

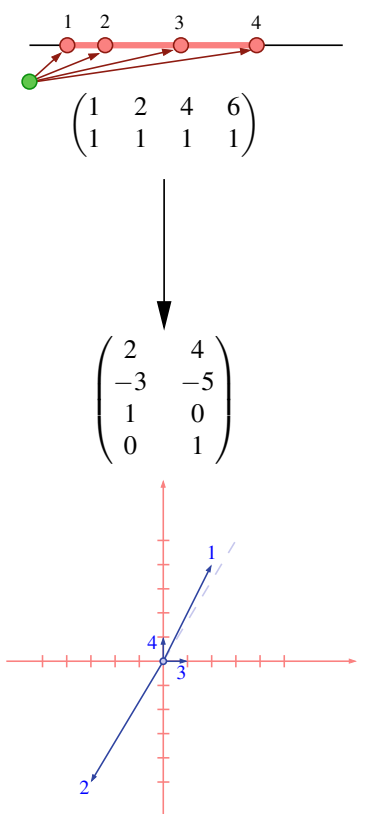


Figure 5.57: A Gale transform of \mathbf{L}_4 is a two-dimensional vector configuration.

restriction to \mathbf{A} of a linear function on \mathbb{R}^r . Theorem 5.1.11 can be rephrased as follows: *the linearity space of the secondary fan of a point configuration \mathbf{A} coincides with the space of linear evaluations on \mathbf{A} .* This is consistent with the observation that the addition of a linear function to a height vector does not change the induced regular polyhedral subdivision.

We start this section by proving this statement directly at the level of the secondary fan, so that it is also valid for vector configurations:

Proposition 5.4.1. *Let \mathbf{A} be a point or vector configuration of rank r . For every regular polyhedral subdivision \mathcal{S} of \mathbf{A} , the linearity space of the secondary cone $\mathbf{C}(\mathbf{A}, \mathcal{S})$ is the r -dimensional linear subspace of all linear evaluations of \mathbf{A} .*

Proof. Remember that, in any polyhedral fan, all the cones have the same linearity space, equal to the intersection of all the cones or, equivalently, to the unique minimal cone. By Theorem 5.2.11, the minimal cone is the secondary cone of the trivial subdivision. That is, ω is in the linearity space of $\Sigma\text{-fan}(\mathbf{A})$ if and only if $\mathcal{S}(\mathbf{A}, \omega)$ is the trivial subdivision, put differently, if and only if ω lifts all the elements of \mathbf{A} to lie in a hyperplane, which is exactly what it means to be a linear evaluation. \square

So, the secondary fan lives in a space of more dimensions than are actually needed (n versus $n - r$, where r is the rank of \mathbf{A}). It seems like a good idea to project its linearity space down to zero, so that we get a lower dimensional, yet complete, description of it. Here the Gale transform of \mathbf{A} plays a central role, as hinted at Theorem 4.1.39.

Recall that a *Gale transform* of \mathbf{A} is a vector configuration \mathbf{B} whose dependence vectors are exactly the evaluation vectors of \mathbf{A} and vice versa. In particular, \mathbf{B} is a vector configuration of rank $n - r$ consisting of n vectors, labeled by the same set J that indexes \mathbf{A} . We will denote these vectors (the columns of the matrix \mathbf{B}) by $(\mathbf{q}_j)_{j \in J}$. (See Figure 5.57 for an example.)

Fix such a Gale transform \mathbf{B} of \mathbf{A} . Proposition 5.4.1 now reads:

Lemma 5.4.2. *The linearity space of the secondary fan of \mathbf{A} equals the space of all the dependence vectors of \mathbf{B} .*

That is to say, the linearity space of the secondary fan is the kernel of the map $\beta : \mathbb{R}^{|J|} \rightarrow \mathbb{R}^{n-r}$ given by $\omega \mapsto \beta(\omega) := \omega \mathbf{B}^T$. When we project the secondary fan by this map, all evaluation heights are mapped to the zero height, and the linearity space of the projected fan will be trivial, as we intended. Since the image of β is spanned by the columns of \mathbf{B} , what we get is a description of the secondary fan living in the ambient space of the vector configuration \mathbf{B} . In the rest of this section, we show how this new version of the secondary fan can be easily described from the vector configuration \mathbf{B} .

Recall that Gale duality behaves very nicely by complementation of the set of vectors (see Section 4.1.3). More precisely, if \mathbf{A} and \mathbf{B} are Gale transforms of each other, hence they share the same index set J , then a subset $C \subseteq J$ is spanning in \mathbf{A} if and only if its complement $J \setminus C$ is independent in \mathbf{B} , and vice-versa. This suggests the following definition (see Figure 5.58).

Definition 5.4.3 (Dual Simplicial Cone). Let $C \subseteq J$ be a full-dimensional cell in \mathbf{A} . Then

$$C^* := J \setminus C$$

is called the *dual simplex* of C . The cone generated by C^* in \mathbf{B} is called the *dual simplicial cone* of C and is denoted, as usual, by $\text{cone}_{\mathbf{B}} C^*$. \square

Note that the name “dual simplex” is justified by the fact that cells that are full-dimensional in \mathbf{A} have complements that are independent in \mathbf{B} (see Lemma 4.1.38). Moreover, observe that in the special case of a cell that is a full-dimensional simplex in \mathbf{A} (that is, a basis), the dual simplex is again a basis in \mathbf{B} .

Lemma 5.4.4. Let \mathbf{B} be a Gale transform of \mathbf{A} . Let $\omega \in \mathbb{R}^J$ be any height function, and let $C \subseteq J$ be a full-dimensional subset in \mathbf{A} . Then,

$$C \in \mathcal{S}(\mathbf{A}, \omega) \Leftrightarrow \beta(\omega) \in \text{relint}_{\mathbf{B}}(C^*).$$

Proof. Suppose first that C is a cell of $\mathcal{S}(\mathbf{A}, \omega)$. The heights ω , restricted to any basis of \mathbf{A} contained in C , define a unique linear (or affine, for point configurations) function $f(\mathbf{x}) := \langle \psi, \mathbf{x} \rangle$ on \mathbb{R}^r , where $\psi \in \mathbb{R}^r$ is chosen such that $\langle \psi, \mathbf{p}_j \rangle = \omega_j$ for all $j \in C$. This means that there is another height vector $\omega^C \in \mathbb{R}^J$ defined by $\omega_j^C := \omega_j - f(\mathbf{p}_j)$, with $\mathcal{S}(\mathbf{A}, \omega) = \mathcal{S}(\mathbf{A}, \omega^C)$, according to Proposition 5.4.1 (see Figure 5.59), and with

$$\beta(\omega^C) = \beta(\omega - f) = \beta(\omega) - \beta(f) = \beta(\omega).$$

Now, $C \in \mathcal{S}(\mathbf{A}, \omega^C)$ translates to

$$\omega_j^C \begin{cases} = 0 & \text{for all } j \in C \\ > 0 & \text{for all } j \in J \setminus C, \end{cases}$$

which is equivalent to

$$\beta(\omega^C) = \omega^C \mathbf{B}^T \in \text{relint}_{\mathbf{B}}(C^*).$$

Conversely, if $\beta(\omega) \in \text{relint}_{\mathbf{B}}(C^*)$, let ω^C be the vector of coefficients of any expression giving $\beta(\omega)$ as a positive linear combination of the elements in C^* . That is, ω^C is zero on C , strictly positive on C^* , and

$$\beta(\omega) = \omega^C \mathbf{B}^T = \beta(\omega^C).$$

The sign pattern in ω^C implies that $\omega^C \in \mathcal{S}(\mathbf{A}, \omega^C)$, and the equality $\beta(\omega) = \beta(\omega^C)$ implies that $\mathcal{S}(\mathbf{A}, \omega^C) = \mathcal{S}(\mathbf{A}, \omega)$. \square

From this we get:

Theorem 5.4.5. Let \mathbf{A} be a vector configuration and let \mathbf{B} be a Gale transform of \mathbf{A} . Let \mathcal{T} be a polyhedral subdivision of \mathbf{A} . Then:

- (i) The projected cone $\beta(\mathbf{C}(\mathbf{A}, \mathcal{T}))$ of \mathcal{T} equals $\bigcap_{C \in \mathcal{T}} \text{cone}_{\mathbf{B}} C^*$, the intersection of all dual simplicial cones for all maximal cells C in \mathcal{T} .

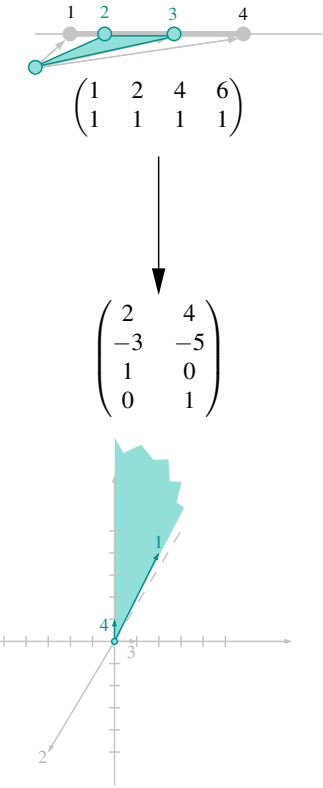


Figure 5.58: The dual cone of simplex 23 in a Gale transform of \mathbf{L}_4 .

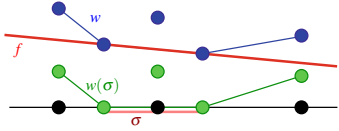


Figure 5.59: Each ω can be transformed to zero on every cell by subtraction of an affine function f .

- (ii) The relatively open projected cone $\beta(\mathbf{C}^\circ(\mathbf{A}, \mathcal{T}))$ equals the intersection $\bigcap_{C \in \mathcal{T}} \text{relint}_{\mathbf{B}} C^*$ of all relatively open, dual simplicial cones for all maximal cells C in \mathcal{T} .

Proof. We prove the second assertion; the first assertion can be proven analogously. (The technical details of it are left to the reader in Exercise 5.10).

The inclusion $\beta(\mathbf{C}^\circ(\mathbf{A}, \mathcal{T})) \subseteq \bigcap_{C \in \mathcal{T}} \text{relint}_{\mathbf{B}} C^*$ is directly implied by Lemma 5.4.4: if $\omega \in \mathbf{C}^\circ(\mathbf{A}, \mathcal{T})$, then $\mathcal{T} = \mathcal{S}(\mathbf{A}, \omega)$ and, by the lemma, $\beta(\omega) \in \text{relint}_{\mathbf{B}} C^*$ for all $C \in \mathcal{T}$.

To prove the reverse inclusion, consider a vector

$$\mathbf{y} \in \bigcap_{C \in \mathcal{T}} \text{relint}_{\mathbf{B}} C^*.$$

In order to show that \mathbf{y} is in $\beta(\mathbf{C}^\circ(\mathbf{A}, \mathcal{T}))$, we simply need to show that $\mathbf{y} = \omega \mathbf{B}^T$ for some $\omega \in \mathbb{R}^J$ with $\mathcal{T} = \mathcal{S}(\mathbf{A}, \omega)$. Since \mathbf{y} is in $\text{relint}_{\mathbf{B}} C^*$ for all $C \in \mathcal{T}$, it satisfies for all $C \in \mathcal{T}$ the equation

$$\mathbf{y} = \sum_{j \in J} \lambda_j^C \mathbf{q}_j = \beta(\lambda^C)$$

for unique non-negative coefficient vectors $\lambda^C \in \mathbb{R}^J$ with $\lambda_j^C = 0$ if $j \notin C$ and $\lambda_j^C > 0$ otherwise. In other words, the positive entries of λ^C form the barycentric coordinates of \mathbf{y} in the relatively open dual simplicial cone $\text{relint}_{\mathbf{B}} C^*$.

Then, in particular, we have

$$\beta(\lambda^C) = \beta(\lambda^{C'})$$

for all $C, C' \in \mathcal{T}$, which implies

$$\mathcal{S}(\mathbf{A}, \lambda^C) = \mathcal{S}(\mathbf{A}, \lambda^{C'}).$$

Since, obviously, we have $C \in \mathcal{S}(\mathbf{A}, \lambda^C)$ for each $C \in \mathcal{T}$, we conclude that $\mathcal{T} = \mathcal{S}(\mathbf{A}, \lambda^C)$ for any $C \in \mathcal{T}$, which implies

$$\mathbf{y} = \beta(\lambda^C) \in \beta(\mathbf{C}^\circ(\mathbf{A}, \mathcal{T})).$$

□

This implies that the projection under the map β of the secondary fan of \mathbf{A} is the polyhedral fan obtained by simultaneously “drawing” all the possible simplicial cones in the Gale transform \mathbf{B} . This fan is usually called the *chamber complex* or the *chamber fan* of \mathbf{B} :

Definition 5.4.6 (Chambers). Let \mathbf{B} be a vector configuration in \mathbb{R}^k , with index set J .

- Two vectors \mathbf{x} and \mathbf{y} are said to lie in the same *relatively open chamber* if, for every $C \subseteq J$, one has

$$\mathbf{y} \in \text{cone}_{\mathbf{B}}(C) \Leftrightarrow \mathbf{x} \in \text{cone}_{\mathbf{B}}(C).$$

Put differently, relatively open chambers are the minimal non-empty sets that can be obtained as intersections of relatively open cones spanned by subconfigurations in \mathbf{B} .

2. The closure of a relatively open chamber cone is a *closed chamber*.
3. The *chamber complex*, or *chamber fan*, of \mathbf{B} is the polyhedral fan consisting of the closed chambers of \mathbf{B} .

Theorem 5.4.7. Let \mathbf{A} and \mathbf{B} be vector configurations that are Gale transforms of one another, represented by matrices of sizes $r \times n$ and $k \times n$. (Typically, $k + r = n$; but not always, since one or both of the configurations might not be of full rank).

Let $\beta : \mathbb{R}^{|J|} \rightarrow \mathbb{R}^k$ be the projection given by $\omega \mapsto \beta(\omega) := \omega \mathbf{B}^T$.

Then, for each regular polyhedral subdivision \mathcal{T} of \mathbf{A} , one has that:

1. $\beta(C^\circ(\mathbf{A}, \mathcal{T}))$ is a relatively open chamber of \mathbf{B} .
2. $\beta(C(\mathbf{A}, \mathcal{T}))$ is a closed chamber of \mathbf{B} .

Hence, the projection β of the secondary fan of \mathbf{A} equals the chamber complex of \mathbf{B} .

This statement proves the claim, made in the definition of the chamber complex, that it is a polyhedral fan. An arbitrary projection of a polyhedral fan may not yield a polyhedral fan, since projected cones may overlap too much. In our case, this does not happen, because the projection β is along the lineality space of the secondary fan, hence vectors with the same projection were necessarily in the same secondary cone.

Proof. By definition, every vector in \mathbb{R}^k lies in a unique relatively open chamber of \mathbf{B} . Indeed, relatively open chambers are the equivalence classes of the equivalence relation “being contained in the same set of cones spanned by \mathbf{B} ”. Also, by Part 2 of Theorem 5.4.5, each relatively open chamber is contained in $\beta(C^\circ(\mathbf{A}, \mathcal{T}))$ for some \mathcal{T} . But, in principle, it could happen that $\beta(C^\circ(\mathbf{A}, \mathcal{T}))$ contains more than one relatively open chamber of \mathbf{B} .

That this is not the case follows from Lemma 5.4.4: If \mathbf{x} and \mathbf{y} both lie in $\beta(C^\circ(\mathbf{A}, \mathcal{T}))$, then the simplicial cones containing them in their relative interiors are the same, namely the cones dual to the full-dimensional cells in \mathcal{T} . \square

Remark 5.4.8. In the case of a point configuration, we can explicitly say how to modify $\Sigma\text{-poly}(\mathbf{A})$ to an affinely equivalent full-dimensional polytope in \mathbb{R}^{n-r} whose normal fan is the chamber fan of \mathbf{B} .

Without changing the normal fan, we can transform $\Sigma\text{-poly}(\mathbf{A})$ by a translation t so that its affine hull is a linear $(n-r)$ -dimensional subspace of \mathbb{R}^n , i.e., $\text{aff}(t(\Sigma\text{-poly}(\mathbf{A}))) = \text{lin}(t(\Sigma\text{-poly}(\mathbf{A}))) =: \mathbf{L}$. Since the kernel of \mathbf{B} equals \mathbf{L}^\perp , the projection β is one-to-one on the restriction of $\Sigma\text{-fan}(\mathbf{A})$ to \mathbf{L} . Thus, there is a linear map $\tilde{\beta}$ from \mathbb{R}^{n-r} into \mathbb{R}^n so that $\beta \tilde{\beta}$ is the identity on \mathbb{R}^{n-r} . Define $\tilde{\beta}^*$ to be the dual linear map to $\tilde{\beta}$. This is a map

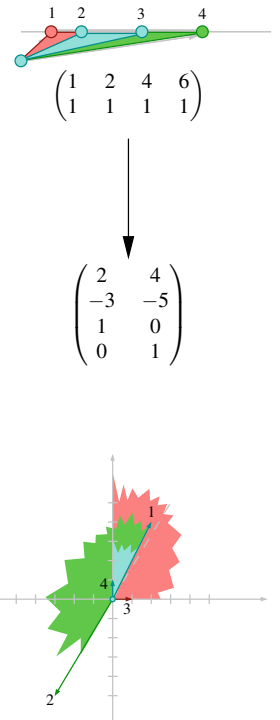


Figure 5.60: The intersection of dual cones over all simplices in the triangulation \mathcal{T}_4 of \mathbf{L}_4 is a chamber that is not subdivided by any other cone spanned by vectors in the Gale transform. This is the chamber cone corresponding to \mathcal{T}_4 . One can see that, in this case, the chamber cone of \mathcal{T}_4 equals the dual cone of one of the simplices in \mathcal{T}_4 ; this is a core simplex that already determines \mathcal{T}_4 (compare to Theorem 5.5.1).

from \mathbb{R}^n onto \mathbb{R}^{n-r} which restricts to an isomorphism on \mathbf{L} , and thus it maps $t(\Sigma\text{-poly}(\mathbf{A}))$ to an affinely isomorphic full-dimensional polytope in \mathbb{R}^{n-r} . The normal fan of this polytope is the chamber fan, because $\langle \beta(\omega), \bar{\beta}^*(\mathbf{x}) \rangle$ equals $\langle \bar{\beta}(\beta(\omega)), \mathbf{x} \rangle = \langle \omega, \mathbf{x} \rangle$ for all $\omega \in \mathbb{R}^n$ and all $\mathbf{x} \in \mathbb{R}^n$, and so the maximizing properties of normal vectors are maintained.

Let us interpret Theorem 5.4.5 for regular triangulations of \mathbf{A} : For every regular triangulation of \mathbf{A} , we find an open, full-dimensional chamber cone in its Gale transform \mathbf{B} . Such a chamber cone is the intersection of a set of simplicial cones given by the dual simplices of the given triangulation (see Figure 5.60). In turn, if we “draw” all possible simplicial cones in \mathbf{B} , then this dissects \mathbb{R}^k into smaller, perhaps non-simplicial, cones. Each full-dimensional cone in this dissection of \mathbf{B} corresponds to a regular triangulation \mathbf{A} . Lower dimensional cones arise as common coarsenings of the full-dimensional cones they are the intersection of. Therefore, \mathbf{B} contains the complete information about all regular polyhedral subdivisions of \mathbf{A} .

Since every simplicial cone in \mathbf{A} can be extended to a triangulation of \mathbf{B} , this dissection is exactly the common refinement of all triangulations of \mathbf{B} . Moreover, since \mathbf{A} is also a Gale transform of \mathbf{B} , its *chamber complex*, the common refinement of all its triangulations, contains the complete information about the regular polyhedral subdivisions of \mathbf{B} .

We finally mention that, since Gale duality is symmetric, the roles of \mathbf{A} and \mathbf{B} can be swapped: the chamber fan of \mathbf{A} equals (the lineality-free version of) the secondary fan of \mathbf{B} . As a conclusion:

Corollary 5.4.9. *Let \mathbf{A} and \mathbf{B} be configurations that are Gale transforms of each other.*

The face lattice of the chamber complex of \mathbf{B} , which is the common refinement of all triangulations of \mathbf{B} , is reverse-isomorphic to the refinement poset of all regular polyhedral subdivisions of \mathbf{A} , and vice versa.

Sometimes it is much easier to count or to estimate the number of full dimensional chamber cones or chambers than to count triangulations. Therefore, the correspondence in Theorem 5.4.5 can be exploited much more intuitively than the one in Theorem 5.1.9. This will be done, for example, in Section 5.5. Here let us only look at an example that will make this clear:

Example 5.4.10 (Examples 5.1.3 and 5.1.5 continued). The regular pentagon is a nice example, because we can draw both the point configuration and a Gale transform of it in dimension two.

Figure 5.62 shows the chamber of the unique triangulation (up to symmetry) of the pentagon.

In Figures 5.63 through 5.65, you see the three types of triangulations of the Gale transform, together with the corresponding chamber in the chamber complex of the pentagon (emerging as the darkest region).

5.4.2 Flips in the chamber fan

It follows from Theorem 5.3.1 that two adjacent full-dimensional chamber cones correspond to regular triangulations which differ by a flip. Such adjacencies represent regular subdivisions which can be refined only by two

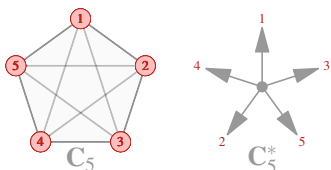


Figure 5.61: The regular five-vector configuration and a Gale dual of it, the regular pentagon.

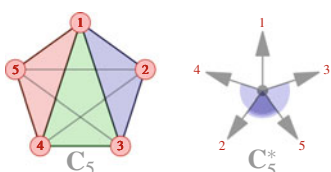


Figure 5.62: The up to symmetry unique triangulation of the pentagon, and its chamber in the Gale transform.

regular triangulations: They correspond to regular almost-triangulations. It will be instructive, however, to isolate the explicit data of such a flip in terms of the supporting circuit. This section will, therefore, provide a proof of this correspondence that can be used with the (more common) definition of flips via a supporting circuit.

We will use the following handy notation for k -element subsets.

Notation 5.4.11. For a set S and a $k \in \mathbb{N}$, let $\binom{S}{k} := \{R \subseteq S : |R| = k\}$. \square

For the following, let \mathbf{B} be a Gale transform of \mathbf{A} (homogeneous coordinates for affine spaces, as always). Consider two adjacent full-dimensional chamber cones $\beta(\mathbf{C}(\mathbf{A}, \mathcal{T}))$ and $\beta(\mathbf{C}(\mathbf{A}, \mathcal{T}'))$ in \mathbf{B} corresponding to two regular triangulations \mathcal{T} and \mathcal{T}' of \mathbf{A} .

We need to find a circuit Z of \mathbf{A} , that is, a cocircuit of \mathbf{B} with two properties: First, one of the triangulations of Z , say $\mathcal{T}_+(Z)$, is a subcomplex of \mathcal{T} and the other, say $\mathcal{T}_-(Z)$, is a subcomplex of \mathcal{T}' ; second, all maximal simplices in $\mathcal{T}_+(Z)$ have the same link \mathcal{L} in \mathcal{T} , and all maximal simplices in $\mathcal{T}_-(Z)$ have the same link \mathcal{L} in \mathcal{T}' . It turns out that the circuit-cocircuit duality yields the data of the flip—including the link—explicitly, albeit via some tedious juggling with dual simplicial cones.

One problem in formulating a rigorous proof is that the chamber cones are, in general, not spanned by vectors in \mathbf{B} . Therefore, we cannot describe facets of full-dimensional chamber cones by subsets of extreme rays. It is, however, sufficient for our purposes to use the description of chamber cones as intersections of dual simplicial cones, as we will see.

Let us now state the main theorem of this section (see Figure 5.66 for a motivating example and remember Theorem 5.3.1):

Theorem 5.4.12. *Let \mathcal{T} and \mathcal{T}' be two regular triangulations of \mathbf{A} whose chamber cones share a common facet spanned by (the complement of the support of) a cocircuit Z in a Gale transform \mathbf{B} of \mathbf{A} . Then the circuit Z in \mathbf{A} supports a flip between \mathcal{T} and \mathcal{T}' .*

Let us explain the last sentence in the statement. Recall that cocircuits of \mathbf{B} are the minimal evaluation signatures, i.e., the complement of a cocircuit has corank one and is the intersection of \mathbf{B} with a hyperplane. We say that a common facet (wall) between two chamber cones is spanned by Z if its complement is contained (and hence spans) that particular hyperplane.

Proof. Let Z be the cocircuit induced by the common facet of the chamber cones of \mathcal{T} and \mathcal{T}' . Let (Z_+, Z_-) be its signature, with orientation defined by the requirement that $\beta(\mathbf{C}(\mathbf{A}, \mathcal{T}))$ lies on its positive side. By the definition of a Gale transform, Z is at the same time a circuit in \mathbf{A} . We abbreviate

$$Z_0 := J \setminus Z := J \setminus (Z_+ \cup Z_-).$$

Since $\beta(\mathbf{C}(\mathbf{A}, \mathcal{T}))$ and $\beta(\mathbf{C}(\mathbf{A}, \mathcal{T}'))$ share a common facet F , they are contained in identical dual simplicial cones, except for those with a facet containing F . (That is the only way for vectors in the chamber cones very close to the common facet to be separated.) For a dual simplex C^* , let C_0^* be

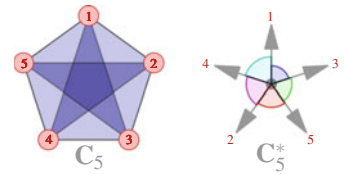


Figure 5.63: The unique triangulation using all vectors.

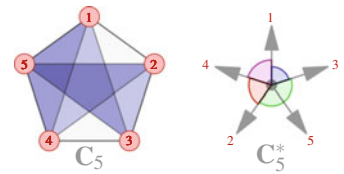


Figure 5.64: One of the five triangulations with one vector unused.

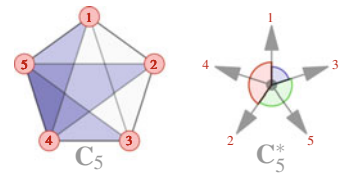


Figure 5.65: One of the five triangulations with two vectors unused.

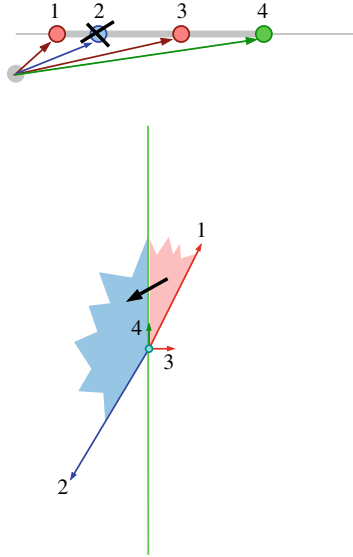


Figure 5.66: A flip supported at $Z = (2, 13)$ removes 2 from the triangulation \mathcal{T}_4 . In the Gale transform, this corresponds to the transition from

the chamber cone $\text{cone}\{1, 4\}$ of \mathcal{T}_4 —via the facet 4, spanned by Z_0 —to the adjacent chamber cone $\text{cone}\{2, 4\}$. Indeed, the triangulation corresponding to the chamber cone $\text{cone}\{2, 4\} = \text{cone}\{2, 4\} \cap \text{cone}\{1, 2\}$ is the intersection of simplicial cones dual to the simplices $\{1, 3\}$ and $\{3, 4\}$, and these simplices emerge when point 2 is flipped out of \mathcal{T}_4 .

that facet. Then, in particular, $C_0^* \subseteq Z_0$. The dual simplices corresponding to $\mathcal{T} \setminus \mathcal{T}'$ are then given by the following formula:

$$\begin{aligned} & \{ C^* \in \binom{A}{n-r} : C \in \mathcal{T} \setminus \mathcal{T}' \} \\ &= \{ C_0^* \cup a_+ : C_0^* \in \binom{Z_0}{n-r-1}, \text{cone}_{\mathbf{B}}(C_0^*) \supseteq \mathbf{F}, a_+ \in Z_+ \}. \end{aligned}$$

Note that $\text{cone } C_0^*$ must automatically be $(n-r-1)$ -dimensional, since C_0^* contains \mathbf{F} . Therefore, $C_0^* \cup a_+$ and $C_0^* \cup a_-$ span $(n-r)$ -dimensional cones. So the formula is plausible.

By forming complements of index sets, $\mathcal{T} \setminus \mathcal{T}'$ is therefore given by the following ugly but explicit description (see Figure 5.67 for an example in which all ingredients can be traced):

$$\begin{aligned} \mathcal{T} \setminus \mathcal{T}' &= \{ J \setminus (C_0^* \cup j_+) : j_+ \in Z_+, \\ &\quad C_0^* \in \binom{Z_0}{n-r-1}, \\ &\quad \text{cone}_{\mathbf{B}}(C_0^*) \supseteq \mathbf{F} \} \\ &= \{ (J \setminus (Z_0 \cup j_+)) \cup (Z_0 \setminus C_0^*) : j_+ \in Z_+, \\ &\quad C_0^* \in \binom{Z_0}{n-r-1}, \\ &\quad \text{cone}_{\mathbf{B}}(C_0^*) \supseteq \mathbf{F} \} \\ &= \{ (Z \setminus j_+) \cup (Z_0 \setminus C_0^*) : j_+ \in Z_+, \\ &\quad C_0^* \in \binom{Z_0}{n-r-1}, \\ &\quad \text{cone}_{\mathbf{B}}(C_0^*) \supseteq \mathbf{F} \}. \end{aligned}$$

Recall that

$$Z := Z_+ \cup Z_- = J \setminus Z_0$$

denotes the support of the circuit Z .

With the same reasoning, $\mathcal{T}' \setminus \mathcal{T}$ is given by:

$$\begin{aligned} \mathcal{T}' \setminus \mathcal{T} &= \{ (Z \setminus j_-) \cup (Z_0 \setminus C_0^*) : j_- \in Z_-, \\ &\quad C_0^* \in \binom{Z_0}{n-r-1}, \\ &\quad \text{cone}_{\mathbf{B}}(C_0^*) \supseteq \mathbf{F} \}. \end{aligned}$$

Define

$$\mathcal{L} := \{ Z_0 \setminus C_0^* : C_0^* \in \binom{Z_0}{n-r-1}, \text{cone}_{\mathbf{B}}(C_0^*) \supseteq \mathbf{F} \},$$

and recall that

$$\begin{aligned} \mathcal{T}_+(Z) &= \{ Z \setminus j_+ : j_+ \in Z_+ \}, \\ \mathcal{T}_-(Z) &= \{ Z \setminus j_- : j_- \in Z_- \}. \end{aligned}$$

Therefore, we can simplify the formula for $\mathcal{T} \setminus \mathcal{T}'$ and $\mathcal{T}' \setminus \mathcal{T}$, respectively, as follows:

$$\begin{aligned}\mathcal{T} \setminus \mathcal{T}' &= \mathcal{T}_+(Z) * \mathcal{L}, \\ \mathcal{T}' \setminus \mathcal{T} &= \mathcal{T}_-(Z) * \mathcal{L},\end{aligned}$$

which says that \mathcal{T} and \mathcal{T}' differ by a bistellar flip in the sense of Theorem 4.4.1. \square

In Section 5.3.1 we showed that the converse of Theorem 5.4.12 is false in general, (although true for flips supported on full-dimensional circuits), since regular triangulations connected by a flip may not have a regular almost-triangulation between them. The chamber complex gives another way of seeing what is wrong with this converse, and also allows us to show that

- The converse holds when the Gale transform has rank at most three.
- It may fail when the Gale transform has rank four.

For the rest of this section, let \mathbf{A} be a point or vector configuration labeled by J , and let \mathbf{B} be a Gale transform of it. Moreover, let \mathcal{T} and \mathcal{T}' be two regular triangulations of \mathbf{A} that are connected by a flip supported on a circuit $Z = (Z_+, Z_-)$.

By the characterization of flips via circuits (Theorem 4.4.1) that we already encountered in the previous proof, there is a subcomplex \mathcal{L} common to \mathcal{T} and \mathcal{T}' such that:

$$\begin{aligned}\mathcal{T} \setminus \mathcal{T}' &= \mathcal{T}_+(Z) * \mathcal{L}, \\ \mathcal{T}' \setminus \mathcal{T} &= \mathcal{T}_-(Z) * \mathcal{L},\end{aligned}$$

where $\mathcal{T}_+(Z)$ and $\mathcal{T}_-(Z)$ are the two triangulations of the subconfiguration $\mathbf{A}|_Z$ defined as

$$\begin{aligned}\mathcal{T}_+(Z) &= \{ Z \setminus j_+ : j_+ \in Z_+ \}, \\ \mathcal{T}_-(Z) &= \{ Z \setminus j_- : j_- \in Z_- \}.\end{aligned}$$

Remember also that the almost-triangulation \mathcal{S} refined by \mathcal{T} and \mathcal{T}' is obtained by removing from \mathcal{T} and \mathcal{T}' the subcomplexes $\mathcal{T}_+(Z) * \mathcal{L}$ and $\mathcal{T}_-(Z) * \mathcal{L}$ and putting $\{Z\} * \mathcal{L}$ instead. That is,

$$\mathcal{L} = \text{link}_{\mathcal{S}}(Z) = \text{link}_{\mathcal{T}}(Z \setminus j_+) = \text{link}_{\mathcal{T}'}(Z \setminus j_-),$$

for any $j_+ \in Z_+$ and for any $j_- \in Z_-$. This suggests the following definitions:

Definition 5.4.13. We call \mathcal{L} and $\mathcal{T} \cap \mathcal{T}'$ the *link* and *antistar* of the flip between \mathcal{T} and \mathcal{T}' .

We call *link cell* and *antistar cell* the following two intersections of dual simplicial cones:

$$\bigcap_{S \in \{Z\} * \mathcal{L}} \text{cone}_{\mathbf{B}}(S^*), \quad \bigcap_{S \in \mathcal{T} \cap \mathcal{T}'} \text{cone}_{\mathbf{B}}(S^*).$$

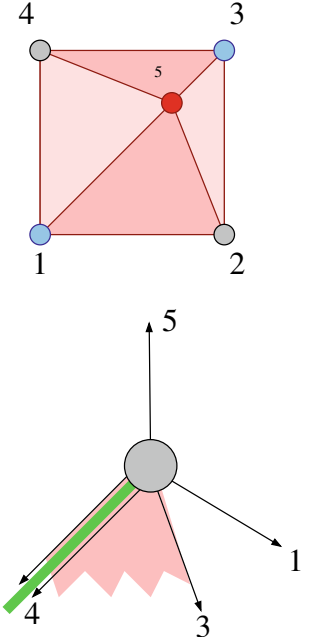


Figure 5.67: The proof of Theorem 5.4.12 illustrated in an example: The point configuration \mathbf{A}_5 contains four points in convex position together with one interior point 5. The points 1, 3, 5 are collinear. Thus, there is a circuit $(13, 5)$ in \mathbf{A}_5 . A possible Gale transform is depicted below the point configuration. The triangulation \mathcal{T} indicated in the point configuration corresponds to the chamber indicated in the Gale transform. This chamber is the intersection of the dual simplices $23, 34, 12$, and 14 . Consider the facet \mathbf{F} of that chamber that contains 2 and 4. The adjacent chamber in \mathbf{F} is the intersection of 25 and 45 and corresponds to another triangulation \mathcal{T}' . The dual simplices in which \mathcal{T} and \mathcal{T}' can differ must contain \mathbf{F} . In this case, they are all possible dual simplices, namely $23, 34, 12$, and 14 , which are all the union of either 2 or 4 with a vector on the positive side of the circuit $(13, 5)$. Their complements are therefore all unions of $24 \setminus 2$ respectively $24 \setminus 4$ with elements in $\mathcal{T}_+(Z) = \{13, 35\}$. This means that the maximal simplices 15 and 35 in $\mathcal{T}_+(Z)$ have the same link $\mathcal{L} := \{2, 4\}$ in \mathcal{T} . This shows that \mathcal{T} and \mathcal{T}' differ by a bistellar flip, which can be seen right away in this example by directly looking at \mathcal{T} and \mathcal{T}' .

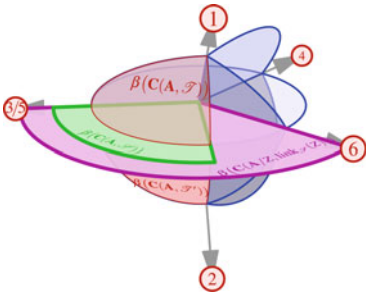


Figure 5.68: The objects of Proposition 5.4.14 in an example with six points in rank three, i.e., corank three.

Observe that \mathcal{L} is, by Lemma 4.2.20, a triangulation of \mathbf{A}/Z , and it is guaranteed to be regular as soon as one of \mathcal{T} , \mathcal{T}' , or \mathcal{L} is regular. Since a Gale transform of \mathbf{A}/Z is $\mathbf{B} \setminus Z$, it makes sense to speak of the link cell as a chamber in $\mathbf{B} \setminus Z$, that is, in $\mathbf{B}|_{Z_0}$.

We then have:

Proposition 5.4.14. *The intersection of the chambers of \mathcal{T} and \mathcal{T}' equals the chamber of \mathcal{L} , and it also equals the intersection of the link cell and the antistar cell:*

$$\begin{aligned}\beta(\mathbf{C}(\mathbf{A}, \mathcal{L})) &= \beta(\mathbf{C}(\mathbf{A}, \mathcal{T})) \cap \beta(\mathbf{C}(\mathbf{A}, \mathcal{T}')) \\ &= \bigcap_{S \in \{Z\} * \mathcal{L}} \text{cone}_{\mathbf{B}}(S^*) \cap \bigcap_{S \in \mathcal{T} \cap \mathcal{T}'} \text{cone}_{\mathbf{B}}(S^*).\end{aligned}$$

Proof. The following containments are immediate:

$$\beta(\mathbf{C}(\mathbf{A}, \mathcal{L})) \subseteq \beta(\mathbf{C}(\mathbf{A}, \mathcal{T})) \cap \beta(\mathbf{C}(\mathbf{A}, \mathcal{T}')) \subseteq \bigcap_{S \in \mathcal{T} \cap \mathcal{T}'} \text{cone}_{\mathbf{B}}(S^*),$$

the first by definition of secondary cone and the second by Theorem 5.4.5. The same theorem, together with the fact that

$$\mathcal{L} = (\mathcal{T} \cap \mathcal{T}') \cup (\{Z\} * \mathcal{L}),$$

implies the equality of the chamber of \mathcal{L} to the intersection of the link and antistar cells: So, only the following containment needs to be shown:

$$\beta(\mathbf{C}(\mathbf{A}, \mathcal{T})) \cap \beta(\mathbf{C}(\mathbf{A}, \mathcal{T}')) \subseteq \bigcap_{S \in \{Z\} * \mathcal{L}} \text{cone}_{\mathbf{B}}(S^*).$$

For this, observe that:

$$\beta(\mathbf{C}(\mathbf{A}, \mathcal{T})) \cap \beta(\mathbf{C}(\mathbf{A}, \mathcal{T}')) \quad (5.1)$$

$$\subseteq \bigcap_{S \in \mathcal{T} \setminus \mathcal{T}'} \text{cone}_{\mathbf{B}}(S^*) \cap \bigcap_{S \in \mathcal{T}' \setminus \mathcal{T}} \text{cone}_{\mathbf{B}}(S^*) \quad (5.2)$$

$$= \bigcap_{S \in \mathcal{T}_+(Z) * \mathcal{L}} \text{cone}_{\mathbf{B}}(S^*) \cap \bigcap_{S \in \mathcal{T}_-(Z) * \mathcal{L}} \text{cone}_{\mathbf{B}}(S^*) \quad (5.3)$$

$$= \bigcap_{\substack{S=S_0 \cup Z \setminus j \\ S_0 \in \mathcal{L}, j \in Z}} \text{cone}_{\mathbf{B}}(S^*) \quad (5.4)$$

$$= \bigcap_{S_0 \in \mathcal{L}, j \in Z} \text{cone}_{\mathbf{B}}((Z_0 \setminus S_0) \cup j) \quad (5.5)$$

$$= \bigcap_{S_0 \in \mathcal{L}} \text{cone}_{\mathbf{B}}((Z_0 \setminus S_0)) = \bigcap_{S \in \{Z\} * \mathcal{L}} \text{cone}_{\mathbf{B}}(S^*). \quad (5.6)$$

The next to last equality comes from

$$\text{cone}_{\mathbf{B}}((Z_0 \setminus S_0) \cup j_+) \cap \text{cone}_{\mathbf{B}}((Z_0 \setminus S_0) \cup j_-) = \text{cone}_{\mathbf{B}}(Z_0 \setminus S_0),$$

for any $j_+ \in Z_+$ and $j_- \in Z_-$, since j_+ and j_- lie in opposite sides of the hyperplane containing $\text{cone}_{\mathbf{B}}(Z_0)$. \square

As the proposition suggests, the link cell—although a chamber in $\mathbf{B} \setminus Z$ —is in general not a chamber in \mathbf{B} but a union of chambers. With this technical tool in our hands, we can prove the announced result.

As we will see in Theorem 5.5.1, in corank two or less all the subdivisions are regular.

Theorem 5.4.15. *Let \mathbf{A} be a point or vector configuration with corank three. If two regular triangulations \mathcal{T} and \mathcal{T}' are connected by a flip, supported on a certain circuit $Z = (Z_+, Z_-)$, then the intermediate almost triangulation \mathcal{S} is regular.*

That is, the chambers $\beta(\mathbf{C}(\mathbf{A}, \mathcal{T}))$ and $\beta(\mathbf{C}(\mathbf{A}, \mathcal{T}'))$ are adjacent in a common facet \mathbf{F} , supported by the hyperplane spanned by $\text{cone}_{\mathbf{B}}(Z_0)$.

Proof. The regularity assumption on \mathcal{T} and \mathcal{T}' implies that the antistar cell has full rank equal to three (that is, dimension two), since it contains the chambers of \mathcal{T} and \mathcal{T}' , and the link cell has codimension one, that is, dimension one, since it is a chamber of $\mathbf{B} \setminus Z$. Observe that, as usual, we call dimension of a cone or configuration its rank minus one. If you wish, we can think of the chamber complex of \mathbf{B} not as a rank three fan but as a geodesic cell complex drawn on a 2-sphere.

Let \mathbf{r} denote the rank two subspace containing $\text{cone}_{\mathbf{B}}(Z_0)$ and, in particular, the link cell. We think of \mathbf{r} as a great circle in this 2-sphere. Since chambers in a rank two configuration are delimited by two elements of it, we can write the link cell as $\text{cone}_{\mathbf{B}}(i_1 i_2)$ for certain elements $i_1, i_2 \in Z_0$. Since the link cell is a chamber in $\mathbf{B} \setminus Z$, there is no other element of \mathbf{B} contained in the link cell.

In the light of the previous proposition, all we need to prove is that the link cell and the antistar cell *overlap*, that is, that their intersection is one dimensional. We claim that, more strongly, at least one of the following two things happen:

1. Either every antistar dual triangle $\text{cone}_{\mathbf{B}}(C^*)$ (with $C \in \mathcal{T} \cap \mathcal{T}'$) contains the link cell, in which case the antistar cell contains the link cell, or
2. For every $\mathbf{x}_+ \in \beta(\mathbf{C}(\mathbf{A}, \mathcal{T}))$ and every $\mathbf{x}_- \in \beta(\mathbf{C}(\mathbf{A}, \mathcal{T}'))$ we have that the intersection point \mathbf{x}_0 of the (spherical) segment $\mathbf{x}_+ \mathbf{x}_-$ and the circle \mathbf{r} lies in the link cell. This finishes the proof since moving \mathbf{x}_+ and \mathbf{x}_- in their respective chambers, which are two-dimensional, produces a one-dimensional range of \mathbf{x}_0 's all lying in the intersection of the link cell and the antistar cell (observe that the antistar cell is a convex region containing both chambers).

So, let us assume that 1 does not hold and prove 2. Let $C \in \mathcal{T} \cap \mathcal{T}'$ be an antistar simplex whose antistar dual triangle $\text{cone}_{\mathbf{B}}(C^*)$ does not contain the link cell $\text{cone}_{\mathbf{B}}(i_1 i_2)$.

Since $\text{cone}_{\mathbf{B}}(C^*)$ contains both chambers, which lie on opposite sides of \mathbf{r} , the antistar triangle C^* contains at least one element of Z_+ and one of Z_- . Without loss of generality we assume that it contains *exactly* one

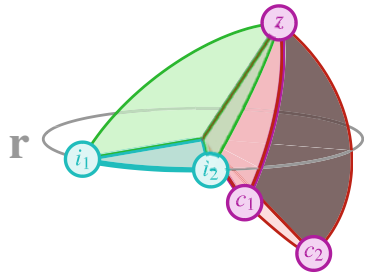


Figure 5.69: The following cannot occur: a dual antistar triangle $C^* = zc_1c_2$ does not intersect the link cell $\text{cone}_{\mathbf{B}}(i_1i_2)$.

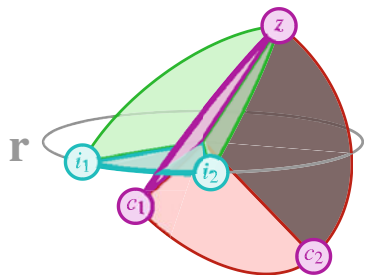


Figure 5.70: This situation must be like this: one edge of $\text{cone}_{\mathbf{B}}(zc_1)$ of a dual antistar triangle $C^* = zc_1c_2$ intersects the interior of the link cell $\text{cone}_{\mathbf{B}}(i_1i_2)$.

element z of Z_+ (if it contains two of Z_+ , then it contains one of Z_- and the same argument works). We will now exclude a situation like in Figure 5.69.

By definition of the link cell, i_1i_2z is a dual triangle for a simplex in \mathcal{T}_+ . This implies that both $\text{cone}_{\mathbf{B}}(i_1i_2z)$ and $\text{cone}_{\mathbf{B}}(C^*)$, which are triangles with a common vertex, contain the chamber $\beta(\mathbf{C}(\mathbf{A}, \mathcal{T}))$. In particular, they have a full-dimensional intersection.

Since z is the only vertex of $\text{cone}_{\mathbf{B}}(C^*)$ in Z_+ , both edges of $\text{cone}_{\mathbf{B}}(C^*)$ containing z intersect \mathbf{r} . If none of the intersections is in the relative interior of the link cell, then either $\text{cone}_{\mathbf{B}}(C^*)$ contains $\text{cone}_{\mathbf{B}}(i_1i_2z)$, and thus $\text{cone}_{\mathbf{B}}(i_1i_2)$, which is Case 1 and therefore excluded, or the intersection of $\text{cone}_{\mathbf{B}}(C^*)$ and $\text{cone}_{\mathbf{B}}(i_1i_2z)$ is not full-dimensional: contradiction to the fact that they contain the same full-dimensional chamber. Thus one edge $\text{cone}_{\mathbf{B}}(zc_1)$ intersects the link cell in its relative interior. Since the link cell has no elements of \mathbf{B} in its relative interior, this edge must intersect the link cell transversally, i.e., the cones $\text{cone}_{\mathbf{B}}(i_1i_2)$ and $\text{cone}_{\mathbf{B}}(zc_1)$ intersect in their relative interior. Thus, the situation is as in Figure 5.70.

This yields: The four elements z_+ , c_1 , i_1 and i_2 form a circuit of type $(2, 2)$ in \mathbf{B} and, in particular, $\mathbf{Q} = \text{cone}_{\mathbf{B}}(z_+c_1i_1i_2)$ is contained in an open half-space, and we can think of it as a convex spherical quadrilateral. Because i_1i_2z is a dual triangle of a simplex in \mathcal{T} and, in the same way, $i_1i_2c_1$ is a dual triangle of a simplex in \mathcal{T}' , the convex quadrilateral \mathbf{Q} contains the chambers of \mathcal{T} and \mathcal{T}' , separated by the link cell, which is one of its diagonals: this concludes the proof of 2. \square

Observe that case 2 in the proof implies that the union of the (closed) chambers of \mathcal{T} and \mathcal{T}' is convex. Already in corank 2 this is not always the case for two regular triangulations connected by a flip: see, e.g., Figure 2.35 in Chapter 2.

Example 5.4.16. Let \mathbf{A} and \mathbf{B} be the following configurations, Gale duals of each other. Their coordinates are

$$\mathbf{A} := \begin{pmatrix} 1 & 2 & 3 & 4 & 5 & 6 & 7 & 8 \\ 1 & -1 & 0 & 0 & 0 & 0 & 1 & -1 \\ 0 & 0 & 1 & -1 & 0 & 0 & 1 & -1 \\ 0 & 0 & 0 & 0 & -6 & 6 & 6 & -6 \\ 1 & 1 & 1 & 1 & 6 & 6 & -8 & -8 \end{pmatrix} \text{ and}$$

$$\mathbf{B} := \begin{pmatrix} 1 & 2 & 3 & 4 & 5 & 6 & 7 & 8 \\ -2 & -2 & -2 & -2 & 2 & 2 & 1 & 1 \\ 1 & 1 & -1 & -1 & 0 & 0 & 0 & 0 \\ -1 & 1 & -1 & 1 & 1 & -1 & 1 & -1 \\ 1 & 1 & 1 & 1 & 1 & 1 & 1 & 1 \end{pmatrix}.$$

\mathbf{A} is totally cyclic and \mathbf{B} is acyclic (actually, homogeneous). This allows to easily visualize \mathbf{B} and its chamber complex. We claim that the following

two triangulations of \mathbf{A} are regular and connected by a flip, but that their dual chambers do not share a facet:

$$\begin{aligned}\mathcal{T} = & \{\{0, 1, 2, 4\}, \{0, 1, 3, 4\}, \{0, 1, 2, 5\}, \{0, 1, 3, 5\}, \\& \{0, 2, 4, 6\}, \{1, 2, 5, 6\}, \{0, 2, 5, 6\}, \{0, 3, 5, 6\}, \\& \{1, 3, 4, 7\}, \{0, 3, 4, 7\}, \{1, 3, 5, 7\}, \{1, 2, 4, 7\}, \\& \{0, 4, 6, 7\}, \{0, 3, 6, 7\}, \{3, 5, 6, 7\}, \{1, 5, 6, 7\}, \{2, 4, 6, 7\}, \{1, 2, 6, 7\}\}. \\ \mathcal{T}' = & \{\{0, 2, 3, 4\}, \{0, 2, 3, 5\}, \{1, 2, 3, 4\}, \{1, 2, 3, 5\}, \\& \{0, 2, 4, 6\}, \{1, 2, 5, 6\}, \{0, 2, 5, 6\}, \{0, 3, 5, 6\}, \\& \{1, 3, 4, 7\}, \{0, 3, 4, 7\}, \{1, 3, 5, 7\}, \{1, 2, 4, 7\}, \\& \{0, 4, 6, 7\}, \{0, 3, 6, 7\}, \{3, 5, 6, 7\}, \{1, 5, 6, 7\}, \{2, 4, 6, 7\}, \{1, 2, 6, 7\}\}.\end{aligned}$$

A triangulation and regularity check in TOPCOM (for more about this software, see Chapter 8.2 and [265]) yields that both triangulations are valid and regular (in Exercise 5.22, you will prove this without a computer):

```
rambau$ checkregularity --heights --checktriang \
< chambers_regular-flips_3d_II_dual_reg.dat
Evaluating Commandline Options ...
--heights      : output of defining heights activated
--checktriangs : check seed triangulation activated
... done.
(15/4096,1/2048,105/4096,0,59/2048,0,0,0)
Checked 1 triangulations, 0 non-regular so far.
(97/2048,1/2048,15/2048,0,49/1024,0,0,0)
Checked 2 triangulations, 0 non-regular so far.
```

The output contains possible defining heights as rational numbers, coming from only exact arithmetic operations. Computing the corresponding points in the chamber complex yields:

$$\mathbf{x}_{\mathcal{T}} = \begin{pmatrix} \frac{1}{30} \\ -\frac{11}{30} \\ 0 \\ 1 \end{pmatrix}, \quad \mathbf{x}_{\mathcal{T}'} = \begin{pmatrix} -\frac{30}{211} \\ \frac{83}{211} \\ \frac{13}{211} \\ 1 \end{pmatrix}.$$

Of course, the configuration is symmetric with respect to reflection in the XZ -plane, but the LP solver `cdd` employed by TOPCOM computes the heights independently of each other. See Figure 5.71 for a sketch of the positions of these interior points in the chambers of \mathcal{T} and \mathcal{T}' , respectively.

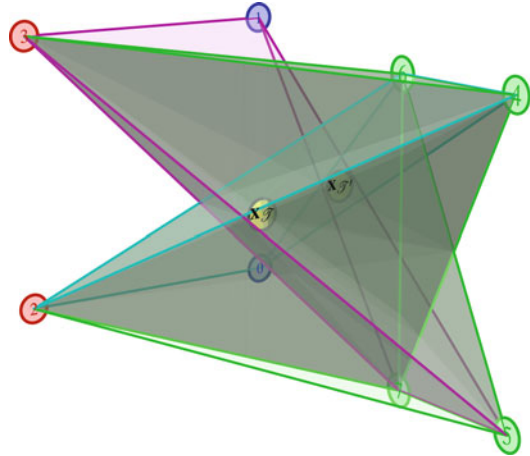


Figure 5.71: The two interior points in the chambers of \mathcal{T} and \mathcal{T}' induced by TOPCOM's height vectors; the four dual link simplices and the two crucial (see below) antistar simplices are also sketched.

Moreover:

$$\begin{aligned}\mathcal{T} \setminus \mathcal{T}' &= \{\{0, 1, 2, 4\}, \{0, 1, 3, 4\}, \{0, 1, 2, 5\}, \{0, 1, 3, 5\}\}, \\ \mathcal{T}' \setminus \mathcal{T} &= \{\{0, 2, 3, 4\}, \{0, 2, 3, 5\}, \{1, 2, 3, 4\}, \{1, 2, 3, 5\}\}.\end{aligned}$$

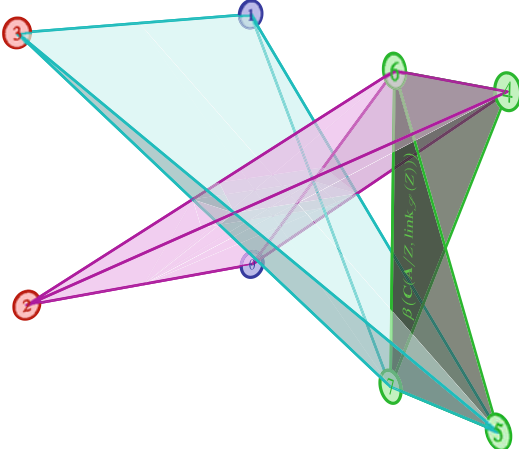


Figure 5.72: Two dual simplices (the two tetrahedra 1357 and 0246) in the common antistar cell of two triangulations joined by a flip, but their intersection does not meet the link cell (the darker vertical triangle).

That is, both triangulations are connected by the flip supported on the degenerate circuit $(01, 23)$ with link simplices 4 and 5. TOPCOM is currently not able to check regularity of flips. However, non-regularity of the flip can be seen more easily in a picture. Indeed, what happens is that, as shown in Figure 5.72, the intersection of the dual antistar simplices $\{0, 2, 4, 6\}$ and $\{1, 3, 5, 7\}$ common to \mathcal{T} and \mathcal{T}' does not intersect the link cell, even though each of them does individually.

In Chapter 8 we will encounter chambers again, as they provide equations for another polytope of triangulations: the universal polytope.

To conclude, let us say that Section 9.1 of Chapter 9 discusses *fiber polytope construction* by Billera and Sturmfels. This construction gives yet another way of thinking about the secondary polytope, this time as the average of fibers of the linear projection of a simplex.

5.5 Configurations with fixed corank

The minimum number of points that a point configuration of dimension d can have is $d + 1$. Its space of triangulations is then trivial: $d + 1$ points in dimension d are the vertices of a simplex, and that simplex alone is both the trivial subdivision of the point set and the unique triangulation of it. The next case, $d + 2$ points in dimension d , is what we have called a corank-one configuration and there is not much to add to what we said in Section 2.4.1: The set has exactly two triangulations, which are both regular and differ by a flip. The secondary polytope is a segment.

Here we study the next two cases, of configurations with $d + 3$ and $d + 4$ points respectively. These cases are at the limit of what can be considered “good” and “bad” behavior. Summing up:

- For $d + 3$ points, it is still true that all triangulations are regular. Hence, the graph of triangulations is a cycle (the graph of a polygon) and every triangulation has exactly two flip-neighbors. The total number of triangulations is linear in the number of elements of the configuration.
- With $d + 4$ points, non-regular triangulations arise for the first time (remember the “mother of all examples”). The number of regular triangulations grows quartically with the number of elements, but the number of non-regular ones can grow exponentially. Still, not all is lost. It is still true that every triangulation has *at least* three flips (the dimension of the secondary polytope) and the graph of flips is connected.

We also look at the numbers of regular and of all triangulations, as well as other complexity measures, for configurations of fixed corank. It turns out that the former has polynomial size while the latter can have exponential size.

5.5.1 Configurations with $d + 3$ points

The definition of flip (Section 2.4.1) is derived from the complete understanding of the triangulations of $d + 2$ points in dimension d , more precisely, from the fact that there are exactly two of them. In this section, we will completely describe the space of triangulations of $d + 3$ points: The graph of triangulations is a cycle. The reason for this is that all triangulations of $d + 3$ points in dimension d are regular, as was first proved by Lee [206], hence, the flip-graph is the graph of an $n - d - 1$ (that is, two) dimensional polytope (that is, a polygon).

With our knowledge up to here, we are in a position to present a very tidy proof of this fact, based on Gale transforms (as the original source), but with

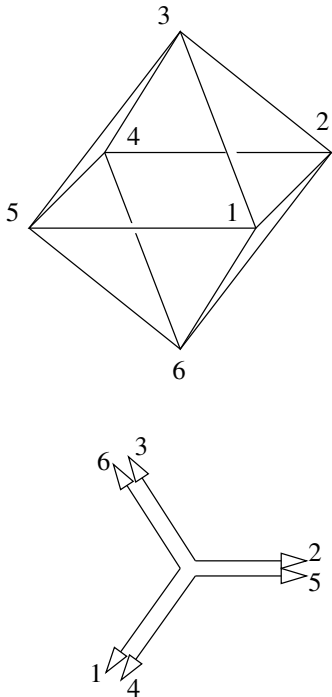


Figure 5.73: A regular octahedron and its Gale transform.

an extra twist that makes it easier: the fact that every triangulation of $d+3$ points contains a *core simplex* that is not used in any other triangulation of them. This was first noticed in [96].

Theorem 5.5.1. *All subdivisions of a d -dimensional point configuration \mathbf{A} with at most $n = d+3$ points are regular.*

Proof. We already know what happens if \mathbf{A} has less than $d+3$ points: If $n = d+1$ then \mathbf{A} is a simplex, and its only subdivision is the trivial one, which is regular. If $n = d+2$ then \mathbf{A} is a circuit, and its two triangulations are regular by Lemma 2.4.2.

So, let us turn our attention to the interesting case $n = d+3$. The subdivisions that are not triangulations are easy to prove to be regular (see Exercise 5.31), so we restrict our study to triangulations.

A Gale transform of \mathbf{A} is a rank 2 vector configuration \mathbf{B} consisting of n vectors. See in Figures 5.73 and 5.74 the Gale transforms of (the vertex sets of) an octahedron and a triangular prism. The first one consists of three pair of repeated vectors, the second one of three pairs of opposite vectors.

Every 2-dimensional chamber of \mathbf{B} corresponds to a regular triangulation of \mathbf{A} .

Look at the chambers in \mathbf{B} : they are the elementary ‘‘pieces’’ of the cake, i.e., the sectors that are not cut by any vector from \mathbf{B} . This shows a special property of two-dimensional vector configurations: all chambers are dual simplicial cones at the same time! Indeed, each chamber is the positive span of two vectors in \mathbf{B} .

As a consequence, each chamber corresponds to a certain dual simplex and hence to a certain simplex in \mathbf{A} . For example in Figure 5.73 chamber $\{2, 3\}$ corresponds to the 3-simplices $\{1, 4, 5, 6\}$ inside the octahedron. We call the simplices of \mathbf{A} corresponding to chambers in \mathbf{B} *core simplices*. Their defining property is that they are used in a single regular triangulation.

We will prove the following:

1. Every triangulation of \mathbf{A} contains at least one core simplex.
2. Every core simplex is contained in at most one triangulation, namely the regular one corresponding to it.

The second property implies that all triangulations containing some core simplex are regular. The first property says that this includes all possible triangulations, which proves the theorem.

Now, why does every triangulation of \mathbf{A} contain at least one core simplex? Let \mathcal{T} be an arbitrary triangulation of \mathbf{A} . It must certainly contain some simplex S . There are two possibilities: either S is a core simplex, and we are done, or the dual simplicial cone $\text{cone}(S^*)$ of S contains a vector \mathbf{v} of \mathbf{B} . Here, we use the fact that \mathbf{B} is 2-dimensional.

Pick a simplex S in \mathcal{T} that is not a core simplex such that its dual simplicial cone $\text{cone}(S^*)$ is inclusion-minimal. Since S is not a core simplex, $\text{cone}_{\mathbf{B}} S^*$ strictly contains a vector \mathbf{v} of \mathbf{B} , say the one labeled by $i \in J$. This means that (S^*, i) is a signed circuit in \mathbf{B} . By duality of circuits and cocircuits, (S^*, i) is a signed cocircuit in \mathbf{A} spanned by $F := S \setminus \mathbf{v}$. Because

of Property (CombMP) in Characterization 4.5.18, there must be another simplex R containing F and not containing i . Therefore, the corresponding dual simplex contains one element from S^* and i . Thus, $\text{cone}_{\mathbf{B}}(R^*)$ is strictly contained in $\text{cone}_{\mathbf{B}}(S^*)$, and, by the minimality of $\text{cone}_{\mathbf{B}}(S^*)$, the simplex R must be a core simplex contained in \mathcal{T} .

Finally, why is a core simplex only contained in the regular triangulation corresponding as a chamber to its dual simplicial cone? Look at an arbitrary core simplex S . We claim that any simplex R for which $\text{cone}_{\mathbf{B}}(R^*)$ does not contain $\text{cone}_{\mathbf{B}}(S^*)$ intersects improperly with S . Assume, $\text{cone}_{\mathbf{B}}(R^*)$ does not contain $\text{cone}_{\mathbf{B}}(S^*)$. Then, since S is a core simplex, the open cones $\text{cone}_{\mathbf{B}}(R^*)$ and $\text{cone}_{\mathbf{B}}(S^*)$ can be separated by a linear hyperplane in 2-space. Rotate this hyperplane until it is parallel to a vector in $S^* \cup R^*$ for the first time. Then the hyperplane still separates the two open cones, but it also spans a signed cocircuit (Z_+, Z_-) in \mathbf{B} . For this signed cocircuit we have $Z_+ \cap S^* = \emptyset$ and $Z_- \cap R^* = \emptyset$. That means, $Z_+ \subseteq \mathbf{A} \setminus S^* = S$ and $Z_- \subseteq \mathbf{A} \setminus R^* = R$. Since (Z_+, Z_-) is a circuit in \mathbf{A} , we have proved that R and S do not intersect properly. Therefore, the only simplices that can coexist with a core simplex are the ones that are in the regular triangulation defined by the chamber of the core simplex.

This completes the proof. \square

This proof of Lee's theorem suggests that core simplices are interesting objects. Curiously enough, we can extend their definition to point configurations with more than $d + 3$ vertices. The difference is that now not every triangulation will contain a core simplex.

Definition 5.5.2. Let \mathbf{A} be a d -dimensional point configuration. A *core simplex* of \mathbf{A} is a d -simplex that is contained in exactly one regular triangulation of \mathbf{A} .

The following theorem states that the second assertion in the proof of the previous theorem—"every core simplex is contained in at most one triangulation"—is true, and with essentially the same proof.

Theorem 5.5.3. A d -simplex S is a core simplex of \mathbf{A} if and only if its dual chamber cone is a chamber. In that case, the regular triangulation corresponding to that chamber is the only triangulation containing S .

Proof. Let us first assume that S is a core simplex of \mathbf{A} . Then it is contained in exactly one triangulation, in particular, it is contained in at most one regular triangulation. The number of regular triangulations it is contained in is the number of chambers in its dual simplicial cone. Therefore, its dual simplicial cone may only contain one chamber, i.e., it is actually a chamber.

Let us now assume that the dual simplicial cone of a d -simplex S is a chamber. Then we claim—as in the proof of Lee's theorem—that a simplex R intersects properly with S if and only if its dual simplicial cone contains the dual simplicial cone of S .

The proof is actually analogous: Let R be some other d -simplex in \mathbf{A} . Since $\text{cone}(S^*)$ is a chamber, the only way for $\text{cone}(R^*)$ to have a full-dimensional intersection with $\text{cone}(S^*)$ is to contain $\text{cone}(S^*)$. Therefore, without

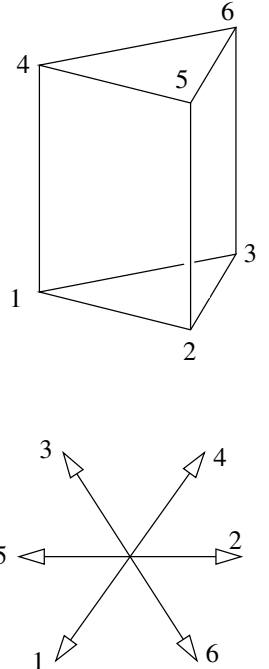


Figure 5.74: A triangular prism and its Gale transform.

loss of generality, $\text{cone } R^*$ and $\text{cone } S^*$ have empty interior intersection. Then there is a hyperplane that weakly separates S^* and R^* . Rotate this hyperplane until it hits a vector in $S^* \cup R^*$. Then turn it around that vector again until it hits another vector in $S^* \cup R^*$. Proceed this way until the hyperplane has no more degrees of freedom. At this point, the hyperplane spans a cocircuit (Z_+, Z_-) in a Gale transform with zero set $Z_0 \subseteq S^* \cup R^*$. Moreover, $Z_+ \cap S^* = \emptyset$ and $Z_- \cap R^* = \emptyset$. This cocircuit is a circuit in \mathbf{A} with $Z_+ \subseteq \mathbf{A} \setminus S^* = S$ and $Z_- \subseteq \mathbf{A} \setminus R^* = R$. Therefore, R does not intersect properly with S , and we are done. \square

Finally, let us derive a bound for the number of triangulations of a set of $d + 3$ points. This is much more explicit (and, actually, generically tight) than the general bound proved in Section 5.5.3.

Proposition 5.5.4. *A point configuration \mathbf{A} of dimension d and with $n = d + 3$ elements has at most n triangulations. If the points are in general position equality occurs.*

Proof. All triangulations are regular, hence they are chambers in the chamber complex of \mathbf{B} . Since the chambers form a cycle, with every two separated by an element of \mathbf{B} , the number of them is at most the same as the number n of elements of \mathbf{B} . Moreover, equality occurs unless an element of \mathbf{B} is zero or two elements of \mathbf{B} happen to be positive multiples of one another. Clearly, this can only happen if \mathbf{B} (and thus \mathbf{A}) is not in general position. \square

It is instructive to better understand Gale duality to analyze more closely the cases of point sets with $d + 3$ points not in general position and their Gale transforms. There are three ways in which the rank 2 vector configuration \mathbf{B} may not be in general position: it can contain the zero vector, or two vectors that are positive multiples of one another, or two that are negative multiples of one another. We can distinguish these cases looking at the circuits in \mathbf{B} : they correspond, respectively, to circuits of the form $(\{i\}, \emptyset)$, $(\{i\}, \{j\})$, or $(\{i, j\}, \emptyset)$.

In the above proof, the first two cases imply that the number of triangulations is strictly less than n , while the third case does not affect the number of triangulations. Using that circuits of \mathbf{B} are cocircuits in \mathbf{A} , this can be seen directly on \mathbf{A} , since these three cases correspond respectively to:

- All but the element i of \mathbf{A} lie in a hyperplane. That is, \mathbf{A} is a pyramid over the configuration $\mathbf{A} \setminus i = \mathbf{A}/i$. Hence, \mathbf{A} has as many triangulations as $\mathbf{A} \setminus i$, by observation 4.2.3 in Section 4.2.1. The latter is still a configuration of corank two, so Proposition 5.5.4 shows that the number of triangulations is less than n .
- All but the elements i and j of \mathbf{A} lie in a hyperplane, and these two elements lie on different sides of it. Then, the two contractions \mathbf{A}/i and \mathbf{A}/j coincide (modulo exchanging the roles of i and j), and \mathbf{A} has as many triangulations as any of them, by Theorem 4.2.33. Again, this implies that \mathbf{A} has less than n triangulations. This happens, for example, in the configuration of Example 2.2.9.

- All but the elements i and j of \mathbf{A} lie in a hyperplane, and these two elements lie on the same side of it. This does not a priori affect the number of triangulations.

5.5.2 Configurations with $d+4$ points

We now turn our attention to configurations with $n = d + 4$ points. We already know that they can have non-regular triangulations, since the “mother of all examples” is an instance (see Example 2.2.5).

We show in Theorem 5.5.19 that the number of regular triangulations grows polynomially with n , if $n - d = 4$ is fixed (in fact, it grows quartically). Here we show that, in contrast, the number of non-regular triangulations grows exponentially.

Again, we want to argue on the Gale transform \mathbf{B} of \mathbf{A} , which is a totally cyclic configuration of vectors in three dimensions. We could picture its elements on the surface of a sphere (since lengths of vectors are irrelevant for our purposes), but it is even better to use a trick, known as *affine Gale diagrams* (see [339, Chapter 6] for an introduction into that topic), that saves us one dimension while it allows using to represent vectors as points, for which usually our intuition is more reliable.

How does this trick work? For an acyclic vector configuration it is simply the inverse of a homogenization: we intersect the vector configuration with an affine hyperplane not containing the origin, but intersecting the positive span (ray) of every vector transversally. Such a hyperplane exists by the definition of acyclic. The points obtained as the intersections of the rays with that hyperplane represent the same dependence signatures and value signatures as the original vector configuration.

For not necessarily acyclic vector configurations (e.g., totally cyclic configurations), we again take a hyperplane not through the origin and not parallel to any of the vectors. This time, there may be vectors whose positive span does not intersect the hyperplane.

Still, whenever the positive span of a vector does not intersect our affine hyperplane, its negative span will, since the hyperplane is not parallel to the vector. So we still get a point in our hyperplane for each vector in the configuration. Of course, we have to encode somehow in the picture the fact that some of our points come from positive spans and some from negative spans. One common way to do it is to give the intersection points different colors: black if the positive span intersects the hyperplane, white if the negative span intersects the hyperplane.

The point configuration of all intersection points (ignoring the color) obviously has the same dependence and value signatures as the modified vector configuration in which each original vector corresponding to a white point is replaced by its negative. That means taking into account that color means reversing the sign of every white element in every sign vector derived from the modified point configuration. For an example of how an affine diagram of a two-dimensional vector configuration gives a one-dimensional colored point configuration, see Figure 5.75. Observe it is not completely straightforward to decide “by inspection” if two affine Gale diagrams come from the same vector configuration. Different choices of the

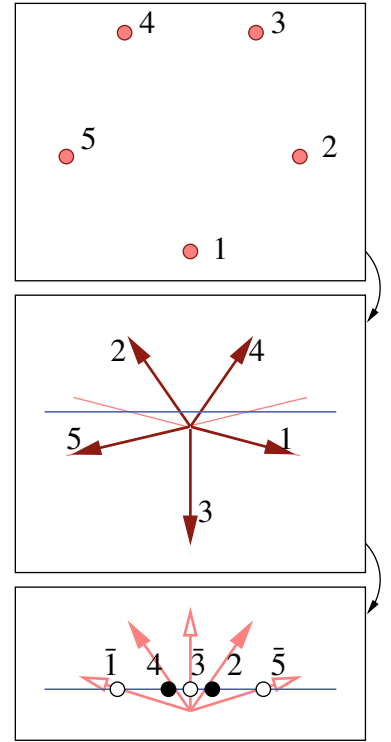


Figure 5.75: How an affine Gale diagram of the five-gon arises.

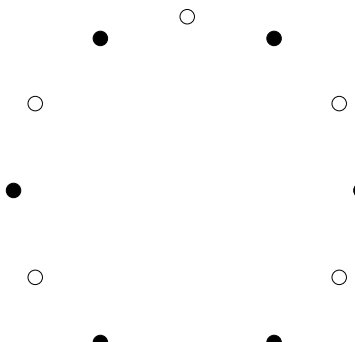


Figure 5.76: An affine Gale diagram of $\mathbf{C}(12,8)$.

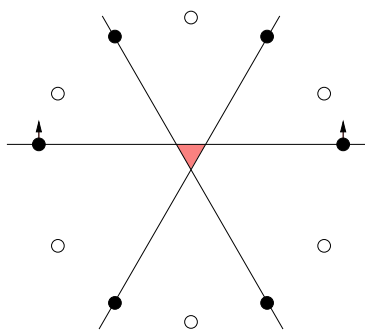


Figure 5.77: A perturbation of the points that translates one of the line segments lets a central full-dimensional chamber appear that was not present before. The triangulation corresponding to that chamber must also exist in the unperturbed configuration, albeit without a chamber; thus, in the unperturbed configuration, this triangulation is non-regular.

cutting hyperplane may give seemingly different configurations. But here we are only going to use Gale diagrams as a tool to understand the triangulations of a single corank 3 configuration that we now introduce.

Let $\mathbf{C}(d+4, d)$ be the point configuration of dimension d with $d+4$ elements whose Gale transform (totally cyclic of rank three) has the following affine Gale diagram: n points placed on a circle, with colors alternating (e.g., black in the odd indexed ones, white in the even indexed ones). If n is odd, this will give the same color to two cyclically consecutive points, but only to those). $\mathbf{C}(d+4, d)$ will reappear in more generality and with a different description in Section 6.1: it is the vertex set of a *cyclic polytope*.

Observe that these affine Gale diagrams are in general position: no three points in the diagram are collinear. That means if you move them only a little this will not affect the oriented matroid of the original vector configuration, hence it will not affect the set of triangulations of the polytope $\mathbf{C}(d+4, d)$.

It will affect, however, the regularity of the triangulations. To see this, look at the case $d = 8$ and $n = 12$. In Figure 5.76, we see twelve points on the circle, six of them black, six of them white. In our completely symmetric distribution of points on the circle, we find that the three lines spanned by opposite black points meet at the center. Since all points have the same color, we can interpret this intersection point as a zero-dimensional chamber in the chamber complex. By Theorem 5.4.9, this *central chamber* corresponds to a certain regular polyhedral subdivision of $\mathbf{C}(12,8)$. Let us call it the *central subdivision*. Now, if you move two of opposite points slightly into one direction, you find that a new full-dimensional chamber appears. This new chamber corresponds to a triangulation of the “modified $\mathbf{C}(12,8)$ ”. The perturbation does not change the oriented matroid, thus this was already a triangulation in the original, symmetric, $\mathbf{C}(12,8)$ (see Section 4.5.2 for all the characterizations of subdivisions that only depend on the oriented matroid). But it was not regular.

This shows two things: first, $\mathbf{C}(12,8)$ has a non-regular triangulation, and second, regularity of triangulations of $\mathbf{C}(12,8)$ depends on the specific coordinates, not only on the oriented matroid.

In Exercises 5.16 and 5.17 you will actually prove by this method that asymptotically there are, in fact, many more non-regular triangulations than regular triangulations of $\mathbf{C}(n, d)$ for $n = d + 4$:

Theorem 5.5.5. *Every configuration of $d+4$ points in dimension d has at most $O(d^4)$ regular triangulations. In contrast, the configuration $\mathbf{C}(4k+4, 4k)$ has at least 2^k non-regular triangulations.*

Using a more sophisticated version of this technique, Azaola and Santos [26] have proved that:

Theorem 5.5.6. *The number of triangulations of $C(n, n-4)$, the cyclic polytope of dimension $n-4$ and with n vertices, is*

- $(n+4)2^{\frac{n-4}{2}} - n$ if n is even, and
- $(\frac{3n+11}{2})2^{\frac{n-5}{2}} - n$, if n is odd.

- If the coordinatization is sufficiently generic, then the number of regular triangulations is $\frac{n^4}{64} \pm \Theta(n^3)$.

Thus the polytope $C(n, n - 4)$ has $\Theta(n2^{n/2})$ triangulations.

With the same ideas, Exercise 5.18 asks you to show that the number of flips in a triangulation, and the lengths of chains in the refinement poset, can be n and $n/2$ respectively, for a configuration with $d + 4$ points. This contrasts with the case $n = d + 3$, where these two parameters are at most 2.

Now, our proof that $C(12, 8)$ has non-regular triangulations, via the fact that its Gale transform can produce different chamber complexes with the same oriented matroid, raises the following question: Have all non-regular triangulations the property that they become regular in a different coordinatization of the same oriented matroid?

Affine Gale transforms also allow us to answer that question negatively.

Example 5.5.7 (A lift of the mother of all examples). Let \mathbf{M} be the familiar point configuration consisting of the vertices of two concentric triangles. Again, this is what we called the *mother of all examples*. The configuration and its Gale transform are pictured in Figure 5.80. We now lift \mathbf{M} to the configuration \mathbf{M}' whose Gale transform is obtained by placing a “white point” in the intersection of the three black meeting edges of the Gale transform of \mathbf{M} . We leave it to the reader to check that the configuration in question can be described as adding a point “slightly beyond” one of the triangular facets of a triangular prism, as in Figure 5.79.

The extra point added to the Gale transform makes the oriented matroid very “rigid”. In every coordinatization of the oriented matroid of \mathbf{M}' , the Gale transform will, for example, have a positive circuit $(147, \emptyset)$ and a co-circuit $(26, 35)$. Hence, the point configuration will have the quadrilateral 2365 as a facet. With the same argument, we get the other three quadrilateral facets so that $\mathbf{M}' \setminus 7$ must be, in every coordinatization, a triangular prism.

Let \mathcal{T} be the following triangulation of \mathbf{M}' , obtained, coning the new element 7 to a certain triangulation of the boundary of \mathbf{M}' (see Figure 5.81):

$$\mathcal{T} := \{1247, 2457, 2357, 3567, 1367, 1467, 4567\}.$$

We have that:

Proposition 5.5.8. \mathcal{T} is a non-regular triangulation of every point configuration with the oriented matroid of \mathbf{M}' .

Proof. If \mathcal{T} was regular, Lemma 4.2.17 would imply that $\mathbf{M}' \setminus 7$ would have a (regular) subdivision containing

$$\{124, 245, 235, 356, 136, 146, 456\}.$$

That is impossible, since $\mathbf{M}' \setminus 7$ is a triangular prism and the cyclic triangulation of its boundary cannot be extended to a triangulation of the whole prism. \square

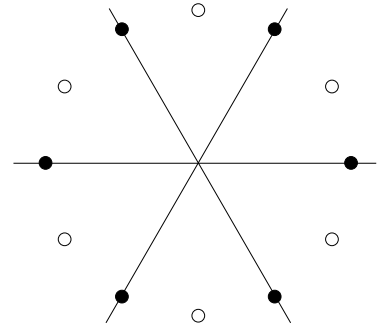


Figure 5.78: The central height vector corresponds to a zero-dimensional chamber of a Gale diagram of $C(12, 8)$; therefore, it induces a regular subdivision of $C(12, 8)$ but not a triangulation.

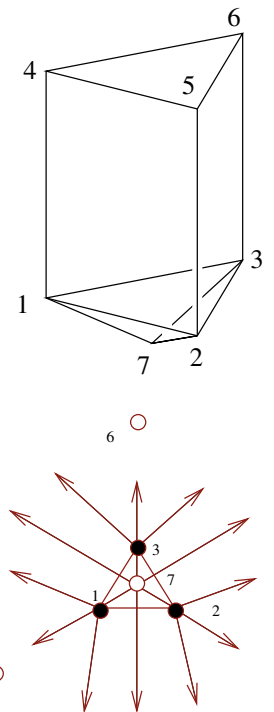


Figure 5.79: A lift \mathbf{M}' of the mother of all examples, and its affine Gale transform

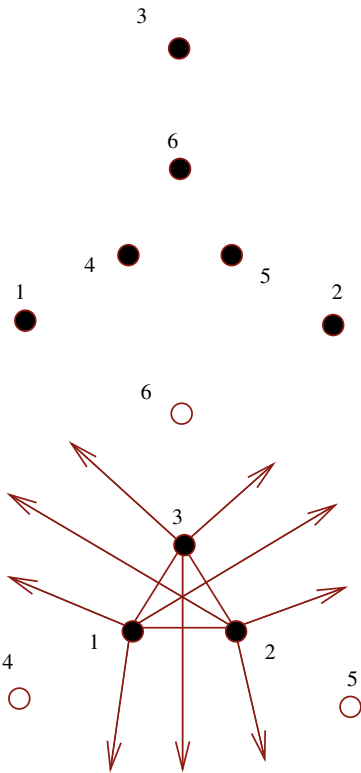


Figure 5.80: The mother of all examples, and its affine Gale transform.

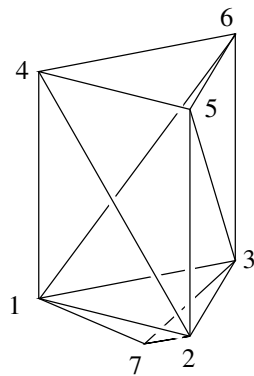


Figure 5.81: A non-regular triangulation of M' .

Still, in this example we *topologically* perturb the Gale transform of M' to make a small triangular “pseudo-chamber” appear in the center, opposite to the white dot in the back. Defining what “topologically perturb” means and, more importantly, checking that all the “topological chambers” obtained in the process have a meaning as triangulations of the Gale transform is delicate and we will not do it here. But, at least in rank three, it can be done. In [25], Azaola and Santos introduce the concept of a *pseudo-chamber complex* of a vector configuration and show that all the triangulations of a corank three configuration can be represented as pseudo-chambers in a rank three pseudo-chamber complex. As a consequence, they obtain that:

Theorem 5.5.9. *Let A be a point configuration of corank three. Then, the graph of flips between all triangulations of A is 3-connected. In particular, every triangulation has at least three flips.*

Proof (sketch). There are triangulations that appear as chambers in *every* pseudo-chamber complex, namely, the placing triangulations, which correspond to chambers incident to an element of the Gale transform. Consider three of them $\mathcal{T}_1, \mathcal{T}_2, \mathcal{T}_3$, fixed for all pseudo-chambers of the Gale transform.

Now, each pseudo-chamber complex forms a cell decomposition of the 2-sphere. By Balinski’s theorem, whose proof is topological, its (adjacency) graph is 3-connected. Hence, from every triangulation \mathcal{T} , since it can be represented as a pseudo-chamber, you can go to the three triangulations $\mathcal{T}_1, \mathcal{T}_2, \mathcal{T}_3$ by three vertex-disjoint paths. By a standard graph-theoretic argument, this implies that the whole graph is 3-connected. \square

This theorem does not generalize to arbitrary corank. On the one hand, there are point configurations with non-connected graphs of triangulations (the smallest one known has corank 10, and is described in Chapter 7, Section 7.4). On the other hand, even in corank 4 there are triangulations with only three flips (see again Chapter 7, Corollary 7.1.2). Those cannot possibly be represented as pseudo-chambers, unless one includes in the definition of pseudo-chamber complex some quite pathological objects.

5.5.3 Lawrence polytopes and the complexity of secondary polytopes

In Section 5.3.2, we saw the following upper bounds on the diameter of the secondary polytope: Let A be a configuration of n points in dimension d . Then, the diameter of $\Sigma\text{-poly}(A)$ cannot exceed

$$\min \left\{ (d+2) \binom{n}{\lfloor \frac{d}{2} + 1 \rfloor}, \binom{n}{d+2} \right\}.$$

Here we show, among other things, that the second bound is optimal in fixed corank. (The first bound is close to optimal, by Corollary 6.1.20, in fixed dimension).

The key to the proof is the following class of polytopes.

Definition 5.5.10. We say that a configuration L is a *Lawrence polytope* if its Gale transform $\text{Gale}(L)$ is centrally symmetric, that is to say, if, as a set of vectors, $\text{Gale}(L) = -\text{Gale}(L)$.

The Lawrence polytope $\Lambda(\mathbf{A})$ associated to a configuration \mathbf{A} is the Gale transform of the configuration $\text{Gale}(\mathbf{A}) \cup (-\text{Gale}(\mathbf{A}))$.

See [37] or the books [55, 339] for extra information on these polytopes. Implicit in the definition of a Lawrence configuration \mathbf{L} is the fact that its elements come in pairs, where a pair $\{a, \bar{a}\}$ consists of two opposite vectors in the Gale transform. Observe also that when we say “the” Lawrence polytope we are abusing language, since “the” Gale transform of a configuration is not unique. However, all the Lawrence polytopes associated to the same configuration \mathbf{A} are affinely equivalent.

Remarks 5.5.11. 1. It is easy to see that a Lawrence configuration \mathbf{L} is indeed “a polytope” in the sense that it is homogeneous (i.e., a point configuration) and in convex position (i.e., every element is a vertex).

Indeed, since $\text{Gale}(\mathbf{L})$ is centrally symmetric, the constant vector $(1, \dots, 1)$ is a linear dependence in it, hence it is a linear evaluation in \mathbf{L} , which is the definition of \mathbf{L} being homogeneous. Also, for each element a in \mathbf{L} let \bar{a} denote its companion element. Since $(\{a, \bar{a}\}, \emptyset)$ is a positive circuit in $\text{Gale}(\mathbf{L})$, there is a hyperplane in \mathbf{L} passing through every element other than a and \bar{a} and leaving these two on the same side. This implies that at least one of them is a vertex but, by the symmetry of $\text{Gale}(\mathbf{L})$, if one is a vertex then the other is a vertex too.

(There is a slight abuse in the last sentence: a and \bar{a} may turn to coincide as points, so that they are not “two vertices” of \mathbf{L} but a repeated one. In this case, \mathbf{L} is a cone over a one-dimension-less Lawrence configuration, with a double point at the apex).

2. The Lawrence construction is related to the one-point suspension. Remember that if i is an element of a point configuration \mathbf{A} , the one-point suspension $\mathbf{A} \uparrow_i^i$ is the configuration whose Gale transform $\text{Gale}(\mathbf{A} \uparrow_i^i)$ is the same as $\text{Gale}(\mathbf{A})$, except with the element a repeated. Similarly, we can define the *Lawrence lift* of \mathbf{A} , and denote it $\mathbf{A} \uparrow_i^i$ as the configuration whose Gale transform $\text{Gale}(\mathbf{A} \uparrow_i^i)$ is the same as $\text{Gale}(\mathbf{A})$ except with the vector opposite to the element a added to it. We would have that $\Lambda(\mathbf{A})$ is obtained from \mathbf{A} as an iterated Lawrence lift over all the elements.

From the perspective of \mathbf{A} , if \mathbf{p}_i is the point or vector of \mathbf{A} labelled by i , the one-point suspension $\mathbf{A} \uparrow_i^i$ is obtained by embedding \mathbf{A} in a hyperplane \mathbf{H} of one dimension more and substituting \mathbf{p}_i by two points or vectors \mathbf{q} and \mathbf{r} , one on each side of \mathbf{H} , with

$$\mathbf{p}_i \in \text{relint}(\{\mathbf{q}, \mathbf{r}\}).$$

Similarly, the Lawrence lift $\mathbf{A} \uparrow_i^i$ is obtained by embedding \mathbf{A} in a hyperplane \mathbf{H} in one dimension more and substituting \mathbf{p}_i by two points or vectors \mathbf{q} and \mathbf{r} , *on the same side* of \mathbf{H} , with

$$\mathbf{r} \in \text{relint}(\{\mathbf{p}_i, \mathbf{q}\}).$$

See Figure 5.83.

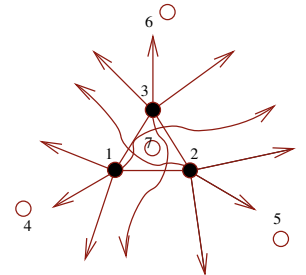


Figure 5.82: The non-regular triangulation \mathcal{T} can be represented as a “pseudo-chamber” in a “pseudo-chamber complex”

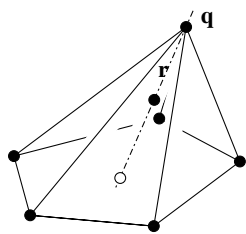
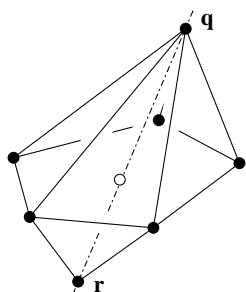
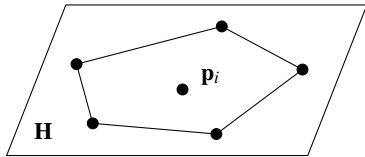


Figure 5.83: The Lawrence lift $A_{\mathbf{A}}^{\uparrow i}$ (bottom) versus the one-point suspension $A_{\mathbf{A}}^{\uparrow i}$ (middle) constructions. Both lift \mathbf{A} to lie in one dimension

more, with all elements except p_i lying in a hyperplane \mathbf{H} and with p_i replaced by two points

\mathbf{q} and \mathbf{r} away from that hyperplane. In the one-point suspension $A_{\mathbf{A}}^{\uparrow i}$, \mathbf{q} and \mathbf{r} lie in opposite sides of the hyperplane and play the same role.

In $A_{\mathbf{A}}^{\uparrow i}$, \mathbf{q} and \mathbf{r} lie in opposite sides of the hyperplane and have different roles.

The following is an easy matrix formula for the Lawrence polytope of a configuration \mathbf{A} . Its proof is left as an exercise:

Proposition 5.5.12. *A matrix representation of $\Lambda(\mathbf{A})$ is*

$$\Lambda(\mathbf{A}) = \begin{pmatrix} \mathbf{0} & \mathbf{A} \\ \mathbf{1} & \mathbf{1} \end{pmatrix},$$

Here, $\mathbf{1}$ and $\mathbf{0}$ denote the unit and the zero matrices of the appropriate dimensions ($n \times n$ and $r \times n$, respectively, if \mathbf{A} is represented by an $r \times n$ matrix).

The crucial property that we need from Lawrence polytopes is that their secondary fans come from hyperplane arrangements:

Definition 5.5.13. A (real, linear) *hyperplane arrangement* is a finite set of linear hyperplanes in the vector space \mathbb{R}^D . An arrangement is *simple* if the intersection of any D of the hyperplanes is the zero vector (that is, if the hyperplanes are in general position).

Every real linear hyperplane arrangement induces a complete polyhedral fan, whose (open) cells consist of vectors with the same relative position with respect to every hyperplane. Here, the relative position of a vector to a hyperplane is based on whether it lies on the hyperplane, on one side of it, or on the other side. We have the following result:

Theorem 5.5.14. *Let \mathbf{A} be a configuration with Gale transform \mathbf{B} . For each cocircuit Z of \mathbf{B} (i.e., circuit of \mathbf{A}), let \mathbf{H}_Z be the corresponding linear hyperplane (the hyperplane passing through all the elements of \mathbf{B} where Z vanishes). Let $\mathcal{H}_{\mathbf{B}}$ be the arrangement consisting of those hyperplanes for all cocircuits of \mathbf{B} . Then:*

1. *The fan induced by $\mathcal{H}_{\mathbf{B}}$ refines the chamber fan of \mathbf{B} (i.e., the secondary fan of \mathbf{A}).*
2. *If \mathbf{A} is a Lawrence configuration, then those two fans coincide.*
3. *In general, the fan of the hyperplane arrangement $\mathcal{H}_{\mathbf{B}}$ coincides with the secondary fan of $\Lambda(\mathbf{A})$.*

Proof. Part (1) can be proved in the language of the secondary fan \mathbf{A} or in that of the chamber fan of \mathbf{B} . We choose the latter. What we need to prove is that if two vectors \mathbf{v} and \mathbf{w} lie in the same cone of the fan of $\mathcal{H}_{\mathbf{B}}$, then they lie in the same (perhaps not full-dimensional) chamber. Suppose the latter is not the case, that is, there is a chamber containing \mathbf{v} but not containing \mathbf{w} . In particular, since every chamber is a certain intersection of dual simplicial cones, there is a dual simplicial cone $\text{relint}_{\mathbf{B}} C^*$ containing \mathbf{v} , but not containing \mathbf{w} . But every dual simplicial cone can easily be rewritten as an intersection of hyperplanes and halfspaces of the hyperplane arrangement $\mathcal{H}_{\mathbf{B}}$. So, there is a cone in the fan of $\mathcal{H}_{\mathbf{B}}$ containing \mathbf{v} but not containing \mathbf{w} , which finishes the proof.

For part (2), it is enough to prove the following: if \mathbf{A} is a Lawrence configuration, then every cocircuit hyperplane \mathbf{H}_Z of $\mathcal{H}_{\mathbf{B}}$ is a union of codimension one dual simplicial cones. If this is true, then the chamber fan of \mathbf{B} clearly refines the fan of $\mathcal{H}_{\mathbf{B}}$. To prove the claim, let $Z = (Z_+, Z_-)$ be a cocircuit of \mathbf{B} and let Z_0 be its complement. Let $C \subseteq Z_0$ be a maximal independent subset of Z_0 , so that $C = \{i_1, \dots, i_{r-1}\}$ is a basis of the hyperplane \mathbf{H}_Z (here $r = n - d - 1$ is the rank of \mathbf{B}). Let $\mathbf{v} \in \mathbf{H}_Z$ be an arbitrary vector in the hyperplane, which can be written uniquely as a linear combination of the elements of C . That is to say, if \mathbf{b}_a denotes the a -th column of \mathbf{B} :

$$\mathbf{v} = \lambda_1 \mathbf{b}_1 + \dots + \lambda_{r-1} \mathbf{b}_{r-1}.$$

Since \mathbf{B} is centrally symmetric, we can “reorient” C as follows:

$$C' := \{a \in C : \lambda_a > 0\} \cup \{\bar{a} : a \in C, \lambda_a < 0\}.$$

Here, \bar{a} denotes (the index of) the element of \mathbf{B} opposite to a . Then,

$$\mathbf{v} \in \text{conv}_{\mathbf{B}}(C') \subseteq \mathbf{H}_Z,$$

which proves the claim.

Part (3) follows from part (ii) if we prove that the hyperplane arrangements $\mathcal{H}_{\mathbf{B}}$ and $\mathcal{H}_{\mathbf{B} \cup (-\mathbf{B})}$ coincide, which is left as an exercise for the reader. \square

Remark 5.5.15. The hyperplane arrangement $\mathcal{H}_{\mathbf{B}}$ can be constructed from any point or vector configuration, and it has an interpretation in oriented matroid theory, where it is called the *adjoint* of \mathbf{B} [55]. Its *cells* represent different *oriented matroid extensions* of \mathbf{B} : two vectors are in the same cell if adding one as a new element of \mathbf{B} produces the same oriented matroid (that is, the same chirotope) as adding the other. Of course, not all extensions of the oriented matroid of \mathbf{B} arise in this way, for much the same reason why not all triangulations of its Gale transform \mathbf{A} arise as chambers; only the regular ones do.

Under the interpretation of vectors in (the ambient space of) \mathbf{B} as heights to lift the elements of \mathbf{A} , cells of $\mathcal{H}_{\mathbf{B}}$ correspond to lifts producing the same oriented matroid. (Except for one thing: the Gale transform of $\mathbf{B} \cup \omega$ is the lift of \mathbf{A} with an extra element “at infinity”, representing the lifting direction. For example, changing ω to its opposite $-\omega$ produces the same lift of \mathbf{A} except in the opposite direction: what was the “lower envelope” is now the “upper envelope” and vice-versa. This is in agreement with part (1) of Theorem 5.5.14: Heights lifting \mathbf{A} with the same chirotope (and the same direction to compute convex hulls) certainly produce the same regular subdivision).

To better understand these relations, observe that a height $\omega \in \mathbb{R}^J$ lies in a particular hyperplane \mathbf{H}_C of $\mathcal{H}_{\mathbf{B}}$ if it lifts the points in the circuit C of \mathbf{A} to a dependent position. (Remember that we have a hyperplane \mathbf{H}_C for each cocircuit of \mathbf{B} , i.e., for each circuit of \mathbf{B}).

Lawrence polytopes are interesting for several reasons. Several of their combinatorial properties are in the Exercises 5.28 and 5.30. They will

appear again in Chapter 9. Our interest in them right now is that they show that the diameter bound for the secondary polytope proved in Corollary 5.3.11 is essentially tight.

Theorem 5.5.16. *Let \mathbf{L} be a Lawrence configuration with n elements and dimension d . Then:*

1. *The diameter of the graph of $\Sigma\text{-poly}(\mathbf{L})$ is exactly the number of circuits of \mathbf{L} .*
2. *If \mathbf{L} is the Lawrence polytope of a configuration \mathbf{A} , then that number is the same as the number of circuits of \mathbf{A} .*

Proof. For the first part, one direction follows from Part (3) of Theorem 5.3.7, and the other from the fact that the secondary fan is the fan of a hyperplane arrangement: in order to go from one maximal chamber to the opposite one, we need to cross (at least once, and exactly once if the path is monotone) every hyperplane of the arrangement. The number of these is the number of cocircuits of $\text{Gale}(\mathbf{L})$, which is the number of circuits of \mathbf{L} .

The second part follows from Exercise 5.28. \square

Corollary 5.5.17. *For each pair of natural numbers $r < n$, let $\delta(n, r)$ denote the maximum diameter of the graphs of all secondary polytopes of configurations of n points in dimension $n - r - 1$ (so that r is the dimension of the secondary polytopes themselves). Then the following inequalities hold:*

$$\binom{\lfloor n/2 \rfloor}{r-1} \leq \delta(n, r) \leq \binom{n}{r-1}.$$

In particular, if r is considered fixed, then $\delta(n, r) \in \Theta(n^{r-1})$.

Proof. The upper bound follows from Corollary 5.3.11, since $\binom{n}{r-1}$ equals $\binom{n}{n-r+1}$. For the lower bound, assume without loss of generality that n is even. Let \mathbf{A} be a configuration of $n/2$ points in general position in dimension $n/2 - r - 1$, so that \mathbf{A} has exactly $\binom{n/2}{n/2-r+1} = \binom{n/2}{r-1}$ circuits. Its Lawrence polytope $\Lambda(\mathbf{A})$ has then n points and dimension $n - r - 1$. By Exercise 5.28, it has the same number of circuits as \mathbf{A} , and by Theorem 5.5.16, that number equals the diameter of the graph of $\Sigma\text{-poly}(\Lambda(\mathbf{A}))$. \square

After diameters, we now move to studying the number of regular triangulations that a point configuration can have when the corank is considered fixed, that to say, the maximum number of vertices of secondary polytopes of fixed dimension. Again, Lawrence polytopes will both give the ideas leading to a general upper bound and show that this bound is not far from optimal.

By Theorem 5.5.14 above, if \mathbf{L} is a Lawrence configuration then its secondary fan is the fan of the hyperplane arrangement $\mathcal{H}_{\text{Gale}(\mathbf{L})}$. Thus, the following classical lemma of R. Buck (see, for example, [337]) is relevant:

Lemma 5.5.18. *The number of full-dimensional regions defined by a linear arrangement of N hyperplanes in dimension D ($N \geq D$) is bounded above by*

$$2 \sum_{i=0}^{D-1} \binom{N-1}{i}.$$

Equality is achieved if the arrangement is simple.

Proof. Suppose first that we are dealing with a simple hyperplane arrangement \mathcal{H} . Recall that *simple* means that no $D+1$ hyperplanes have a common non-zero vector. We will prove by double induction on D and $N-D$ that the number of regions is exactly as predicted. Induction starts in the cases $D=1$ (where the number of regions is always two) and $N=D$ (where the number of regions is 2^D).

For the inductive step, we use the following notation. If $\mathbf{H} \in \mathcal{H}$ is any particular hyperplane in the arrangement, then $\mathcal{H} \setminus \mathbf{H}$ denotes the arrangement obtained by forgetting the hyperplane \mathbf{H} and \mathcal{H}/\mathbf{H} denotes the arrangement restricted to \mathbf{H} (\mathbf{H} is considered as a vector space itself, and each hyperplane of \mathcal{H} other than \mathbf{H} restricts to a hyperplane in it). Observe that both are simple if \mathcal{H} is.

It turns out that the number of full-dimensional regions in \mathcal{H} equals the sum of the numbers in $\mathcal{H} \setminus \mathbf{H}$ and in \mathcal{H}/\mathbf{H} . This is so because when \mathbf{H} is introduced in $\mathcal{H} \setminus \mathbf{H}$, each full-dimensional region of \mathcal{H}/\mathbf{H} divides a region of $\mathcal{H} \setminus \mathbf{H}$ in two. Then, using the notation $R(\mathcal{H})$ for the number of full-dimensional regions of an arrangement, we have:

$$\begin{aligned} R(\mathcal{H}) &= R(\mathcal{H}/\mathbf{H}) + R(\mathcal{H} \setminus \mathbf{H}) \\ &= 2 \sum_{i=0}^{D-1} \binom{N-2}{i} + 2 \sum_{i=0}^{D-2} \binom{N-2}{i} = 2 \sum_{i=0}^{D-1} \binom{N-1}{i}. \end{aligned}$$

In the case where \mathcal{H} is not simple, observe that \mathcal{H} can be perturbed into being simple. The perturbation process cannot make any region disappear, but it may make some appear. \square

Taking into account that when D is fixed, the number in this statement is in $\Theta(N^{D-1})$ we get:

Theorem 5.5.19 ([48]). *Let r be fixed.*

1. *The number of regular triangulations of any configuration of n points in dimension $n-r-1$ is in $O(n^{(r-1)^2})$.*
2. *The number of regular triangulations of a generic Lawrence polytope with n vertices in dimension $n-r-1$ is in $\Theta(n^{(r-1)^2})$.*

Proof. Let \mathbf{A} be an arbitrary configuration of dimension $n-r-1$, with Gale transform \mathbf{B} . Since the chamber fan of \mathbf{B} is refined by the fan of the hyperplane arrangement $\mathcal{H}_{\mathbf{B}}$, the number of regular triangulations of \mathbf{A} is at most the number of full-dimensional cells in that arrangement (refinement divides each full-dimensional cell into one or more cells). The arrangement

\mathcal{H}_B has dimension r , and its number of hyperplanes is the number of cocircuits in B , which is at most $\binom{n}{r-1}$. Hence, the number of regular triangulations of A is in

$$O\left(\binom{n}{r-1}^{r-1}\right) = O\left(n^{(r-1)^2}\right).$$

We omit the proof of the second part. See [48, Lemma 5.5]. \square

Exercises

Exercise 5.1. Prove that all polyhedral subdivisions of one-dimensional point configurations are regular.

Exercise 5.2. Prove that all polyhedral subdivisions of n -gons are regular.

Exercise 5.3. Make a large copy of Figure 5.20, and add all the remaining covering relations corresponding to refinement. (The picture will get cluttered, but never mind; doing this is important, not the resulting image.)

Exercise 5.4. State the relation among the coordinates of GKZ-vectors discussed in Example 5.1.8 for the GKZ-vector of a general point configuration.

Exercise 5.5. Consider a d -dimensional point configuration A . Show that the affine hull of $\Sigma\text{-poly}(A)$ is given by the $d+1$ equations

$$\begin{aligned} \sum_{a \in A} x_a &= d(d+1) \text{vol}(\text{conv } A), \text{ and} \\ \sum_{a \in A} x_a a &= ((d+1) \text{vol}(\text{conv } A)) \mathbf{c}_A, \end{aligned} \tag{5.7}$$

where \mathbf{c}_A denotes the centroid of $\text{conv } A$.

Exercise 5.6. Compute the systems of equations and inequalities constraining the heights for all polyhedral subdivisions of L_4 in Example 5.1.1.

Exercise 5.7. Let $C(A, -)_P$ be the set of all weights in \mathbb{R}^n such that the regular triangulation induced by them contains P as a polyhedral cell with vertices in A . Show that $C(A, -)_P$ is a convex cone.

Exercise 5.8. Find examples of non-regular polyhedral subdivisions, for which the assertions of Proposition 5.2.9 do not hold.

Exercise 5.9. Prove that \mathcal{H}_A is a refinement of $\Sigma\text{-fan}(A)$. Find an example where \mathcal{H}_A is a strict refinement of $\Sigma\text{-fan}(A)$.

Exercise 5.10. Work out the details of the proof of the first assertion in Theorem 5.4.5.

Exercise 5.11. For a height function $\omega : A \rightarrow \mathbb{R}$, prove that the linear inequality defining the facet of $\Sigma\text{-poly}(A)$ corresponding to the coarsest subdivision $\mathcal{S}(A, \omega)$ is given by

$$\sum_{a \in A} \omega(a) x_a \geq (d+1) \sum_{Q \in} \text{vol } Q \cdot g_{\omega, \mathcal{T}}(c_Q) \tag{5.8}$$

where $g_{\omega, \mathcal{T}} : \text{conv} \mathbf{A} \rightarrow \mathbb{R}$ denotes the characteristic section of \mathcal{T} (because \mathcal{T} is regular, then $g_{\omega, \mathcal{T}}$ is a piecewise-linear convex function)

Exercise 5.12. Prove or disprove the following: Let \mathcal{T} be an arbitrary polyhedral subdivision of \mathbf{A} . Then there is a unique finest regular polyhedral subdivision \mathcal{T}' with $\mathcal{T} \preceq \mathcal{T}'$.

Exercise 5.13. Are there point configurations with more than $d + 3$ points whose triangulations all contain a core simplex?

Exercise 5.14. Complete the proof of Lemma 5.1.13. For the missing case when the circuit Z is not full-dimensional, consider the following steps:

- Let \mathbf{B}_1 and \mathbf{B}_2 be simplices of the same dimension and spanning the same flat. Let \mathbf{C} be a simplex spanning a complementary affine space. Prove that: $\text{vol}(\mathbf{B}_1 * \mathbf{C}) / \text{vol}(\mathbf{B}_1) = \text{vol}(\mathbf{B}_2 * \mathbf{C}) / \text{vol}(\mathbf{B}_2)$.
- The flip based on Z now does not merely exchange two triangulations \mathcal{T}_+ for \mathcal{T}_- . It exchanges their joins with their (common) link \mathcal{L} , as explained in Section 4.4 (see Theorem 4.4.1). Prove that the fact that all the maximal simplices in \mathcal{T}_+ and \mathcal{T}_- have exactly the same link implies that there is a proportionality constant μ for which

$$\phi_{\mathbf{A}}(\mathcal{T}_1) - \phi_{\mathbf{A}}(\mathcal{T}_2) = \mu(\phi_{\mathbf{A}}(\mathcal{T}_+) - \phi_{\mathbf{A}}(\mathcal{T}_-)).$$

(Hint: μ is the sum over all maximal simplices in the link of the proportionality constants implicit in the previous step).

Exercise 5.15. Explicitly list the set of maximal simplices of a non-regular triangulation of $\mathbf{C}(10, 6)$ in Section 5.5.2.

Exercise 5.16. Show that every configuration \mathbf{A} of $d + 4$ points in dimension d has at most $O(d^4)$ regular triangulations. For this:

1. Think of their chamber complexes as cell decompositions of a 2-sphere.
2. Bound the number of vertices in these chamber complexes by $O(d^4)$, showing that every vertex corresponds (not uniquely, but that is not really a problem) to a pair of circuits of \mathbf{A} .
3. Using Euler's formula, show that any (polyhedral) cell decomposition of a 2-sphere has about as many vertices as it has 2-cells. More precisely, these two numbers are within a factor of two of each other.

Exercise 5.17. Use the ideas in Section 5.5.2 to show that the cyclic point configuration $\mathbf{C}(4k + 4, 4k)$ has at least $\frac{2^k}{4}$ many non-regular triangulations [96].

In order to do the count right, use the following hints:

1. Consider first the coordinatization that has a cyclically symmetric affine Gale diagram, in which k lines meet in a zero-dimensional chamber at the center.

2. Show that by perturbing the coordinates, each of these n lines can be moved towards one or the other side of it. Since the cyclic configuration is in general position, these perturbations produce different coordinatizations of the same oriented matroid, hence given the same set of triangulations.
3. Show that for all these perturbations the center of the Gale diagram corresponds to distinct triangulations. For this, use the description of a chamber as an intersection of the “dual simplicial cones” of the corresponding triangulation.

Exercise 5.18. With a variation of the same example, show that a triangulation of n points in dimension $d = n - 4$ can have $n - 1$ flips. Also, show that the poset of subdivisions can have chains of length $n/2$.

Exercise 5.19. Show that $\mathbf{C}(11, 7)$ (easy) and $\mathbf{C}(9, 5)$ (a bit more tricky) have non-regular triangulations. Is there a non-regular triangulation of $\mathbf{C}(8, 4)$?

Exercise 5.20. (Open) Let \mathcal{T} be a triangulation with k flips. Moreover, let $\mathcal{T}_1, \dots, \mathcal{T}_k$ be the triangulations obtained by these flips. Let $\mathbf{V}_1, \dots, \mathbf{V}_k$ be the GKZ-vectors of these flips. That is,

$$\mathbf{V}_i := \phi_{\mathbf{A}}(\mathcal{T}_i) - \phi_{\mathbf{A}}(\mathcal{T}).$$

Can it happen that the cone spanned by these vectors is the whole linear span of the secondary polytope?

Observe that, for a regular triangulation, the cone spanned by these vectors is the inner tangent cone at the vertex corresponding to \mathcal{T} , of the secondary polytope. Observe also that, in the non-regular triangulation of the mother of all examples, these vectors positively span a linear space rather than a pointed cone, but it is a proper linear subspace (of dimension two, instead of three) of the linear span of the secondary polytope.

Exercise 5.21. Show that the secondary polytopes of \mathbf{A} and a one-point suspension $\mathbf{A} \uparrow_i^t$ have identical face lattices. (*Hint:* Define a bijection between the sets of regular triangulations by relating the chamber complexes.)

Exercise 5.22. Show that both triangulations of the counterexample 5.4.16 are regular. (*Hint:* Look at the facets of all dual simplices and use on which side of them the missing point resides on.)

Exercise 5.23. Show that the following configuration has two regular triangulations connected by a non-regular flip, as in the case of Example 5.3.4:

$$\mathbf{A} := \begin{pmatrix} 1 & 2^+ & 2^- & 3 & 4 & 5 & 6^+ & 6^- \\ 4 & 0 & 0 & 0 & 2 & 1 & 1 & 1 \\ 0 & 4 & 4 & 0 & 1 & 2 & 1 & 1 \\ 0 & 0 & 0 & 4 & 1 & 1 & 2 & 2 \\ 0 & +4 & -4 & 0 & 0 & 0 & +1 & -1 \end{pmatrix}.$$

Hint: Observe that the mid-points of edges 2^+2^- and 6^+6^- lie in the plane containing points 1, 3, 4 and 5, and the six points together form the familiar ‘‘mother of all examples’’. Make one of its *non-regular* triangulations arise as the slice of the intermediate subdivision between two *regular* triangulations, with arguments similar to those used in Example 5.3.4.

Exercise 5.24 (Non-regular flips between regular triangulations need rank four). Let \mathcal{T}_1 and \mathcal{T}_2 be two regular triangulations of \mathbf{A} , joined by a flip on $Z = (Z_+, Z_-)$. Suppose that the intermediate almost-triangulation \mathcal{S} is not regular. Show that:

1. $|Z_+| \geq 2$ and $|Z_-| \geq 2$. Hint: use Theorem 5.3.3.
2. Conclude that \mathbf{A} needs to have at least rank four.

Exercise 5.25. Let \mathcal{S} be a subdivision of the configuration \mathbf{A} with exactly two maximal faces, \mathbf{S}_1 and \mathbf{S}_2 . Prove that the following statements are equivalent.

1. \mathcal{S} is a 2-split of \mathbf{A} ,
2. \mathcal{S} is a coarsest subdivision of \mathbf{A} ,
3. $\mathbf{S}_1 = \text{conv}(\mathbf{S}_1) \cap \mathbf{A}$ and $\mathbf{S}_2 = \text{conv}(\mathbf{S}_2) \cap \mathbf{A}$.

Exercise 5.26. Let \mathbf{A}_n denote the zero dimensional point configuration consisting of n copies of the same point. Show that its Lawrence polytope is the prism over an $(n - 1)$ -simplex (that is, the product of an $(n - 1)$ -simplex and a segment).

Exercise 5.27 (Matrix description of Lawrence polytopes). Prove Proposition 5.5.12.

Exercise 5.28 (Oriented matroid of Lawrence polytopes). Let \mathbf{A} be a point configuration of rank $d + 1$ with n elements and let \mathbf{B} be its Gale transform. Let $\Lambda(\mathbf{A})$ be its Lawrence polytope, with Gale transform $(\mathbf{B}, -\mathbf{B})$. For each index a of an element of \mathbf{A} and \mathbf{B} let a and \bar{a} denote the pair of elements of $\Lambda(\mathbf{A})$ and $(\mathbf{B}, -\mathbf{B})$ corresponding to it, so that the a -th column of \mathbf{B} and $(\mathbf{B}, -\mathbf{B})$ coincide, and the \bar{a} -th column of $(\mathbf{B}, -\mathbf{B})$ is the opposite of it. Prove the following facts about the oriented matroid of $\Lambda(\mathbf{A})$:

- For each basis C of \mathbf{A} , $\Lambda(\mathbf{A})$ has 2^{n-d-1} bases, each containing the two elements of every pair $\{a, \bar{a}\}$ for the elements a of C and exactly one element of each pair $\{a, \bar{a}\}$ for the elements $a \notin C$. These are all the bases of $\Lambda(\mathbf{A})$.
- \mathbf{A} and $\Lambda(\mathbf{A})$ have the same number of circuits. More precisely, for each circuit (Z_+, Z_-) of \mathbf{A} with k elements, $\Lambda(\mathbf{A})$ has the circuit $(Z_+ \cup \overline{Z_-}, Z_- \cup \overline{Z_+})$, and these are all the circuits of it.
- There are only the following two types of cocircuits in $\Lambda(\mathbf{A})$:
 - The cocircuit $(\{a\}, \{\bar{a}\})$ for each element a of \mathbf{A} .

- The 2^k cocircuits obtained by “reorienting in all possible ways” each cocircuit $Z = (Z_+, Z_-)$ of \mathbf{A} , where $k := |Z_+ \cup Z_-|$ and reorienting means choosing a certain subset $C \subseteq Z_+ \cup Z_-$. The reoriented circuit for a specific choice is

$$((Z_+ \cap C) \cup (Z_- \setminus C), (Z_- \cap C) \cup (Z_+ \setminus C)).$$

Exercise 5.29. Finish the proof of part (3) of Theorem 5.5.14. That is, show that the hyperplane arrangement fans of the Gale transforms of \mathbf{A} and $\Lambda(\mathbf{A})$ coincide. Hint: this is closely related to part (2) of the previous exercise.

Exercise 5.30 (Lawrence polytopes are equidecomposable). Prove that all triangulations of $\Lambda(\mathbf{A})$ have the same number of full-dimensional simplices. More precisely, every triangulation uses exactly one basis of the 2^{n-d-1} associated to each basis of \mathbf{A} .

Exercise 5.31. Prove that if a subdivision \mathcal{T} with $d+3$ points in dimension d is not trivial and is not a triangulation, then it equals the pushing refinement of the trivial subdivision at a certain element i (see Lemma 4.3.2 in Chapter 4). In particular, \mathcal{T} is regular and it is an almost-triangulation.

Some Interesting Configurations

We have seen in Section 3.4.1 that there is a friendly structure on the set of all triangulations of a planar point configuration: It is a connected graph with triangulations as nodes and flips between triangulations as edges. We also saw in Chapter 5 that, for arbitrary dimension, the *regular* triangulations are all connected by flips. In fact, we saw that all regular subdivisions correspond to faces of the secondary polytope. Nevertheless, as we will see in Chapter 7, for general triangulations in arbitrary point configurations of high dimension this needs not be true.

There is a way to partially extend the above “friendly structure” results to arbitrary dimensions, namely by restricting our attention to particular concrete nice classes of point configurations. This chapter has a collection of special configurations that, either because of their properties or because of their practical importance, play a very significant role in the theory of subdivisions.

6.1 Cyclic polytopes

Cyclic polytopes are a very interesting example of polytope. They have the maximum possible number of faces among polytopes of a given dimension and number of vertices. Their oriented matroids (that is, circuits, cocircuits, etc) admit a very nice combinatorial characterization. In even dimension they are (combinatorially) symmetric under cyclic permutation of vertices. In a sense, they are the best generalization of convex polygons to higher dimensions. For a detailed introduction to cyclic polytopes we recommend [148, 339].

The key to the main results in this chapter is to reveal a “friendly” poset structure on the set of all triangulations of cyclic polytopes. As we will see the Hasse diagram of this poset will be the graph of all triangulations, and we will show, among other things, that this graph is connected.

As we did in previous chapters, we start with a two-dimensional example to get a feeling for the additional structure of the space of triangulations of a cyclic polytope. Of course, in dimension two connectivity of the graph of all triangulations is nothing new, but while the known proofs in dimension two for general planar point configurations cannot be generalized to higher dimensions (see Section 3.6.2 if you have forgotten why), the additional structure developed for polygons in the following section can be generalized to arbitrary cyclic polytopes.

Before we go on, however, let us remind the reader that the space of triangulations of a cyclic polytope is not considered friendly because trivially *all* of its triangulations are regular. In fact, the opposite is true: Cyclic

polytopes, in general, have many more non-regular than regular triangulations, as we saw in Theorem 5.5.6.

6.1.1 Warm-up example: two dimensions

Let us have a closer look at flips in a convex polygon in dimension two. Every flip can be given a natural direction and, as we will see, the resulting directed graph of triangulations is acyclic. In other words, the space of triangulations of an n -gon is in fact a partially ordered set (a *poset* for short).

A flip in a triangulation \mathcal{T} of a convex n -gon (with vertices numbered counter-clock-wise) is given by two triangles forming a convex quadrilateral \mathbf{Q} with vertices labeled by $i < j < k < \ell \in [n]$. The boundary edges of \mathbf{Q} are $\{i, j\}, \{j, k\}, \{k, \ell\}$, and $\{\ell, i\}$. Exactly one of the diagonals $\{i, k\}$ and $\{j, \ell\}$ is also an edge in \mathcal{T} . A flip supported on \mathbf{Q} replaces the diagonal of \mathbf{Q} present in \mathcal{T} by the other possible one.

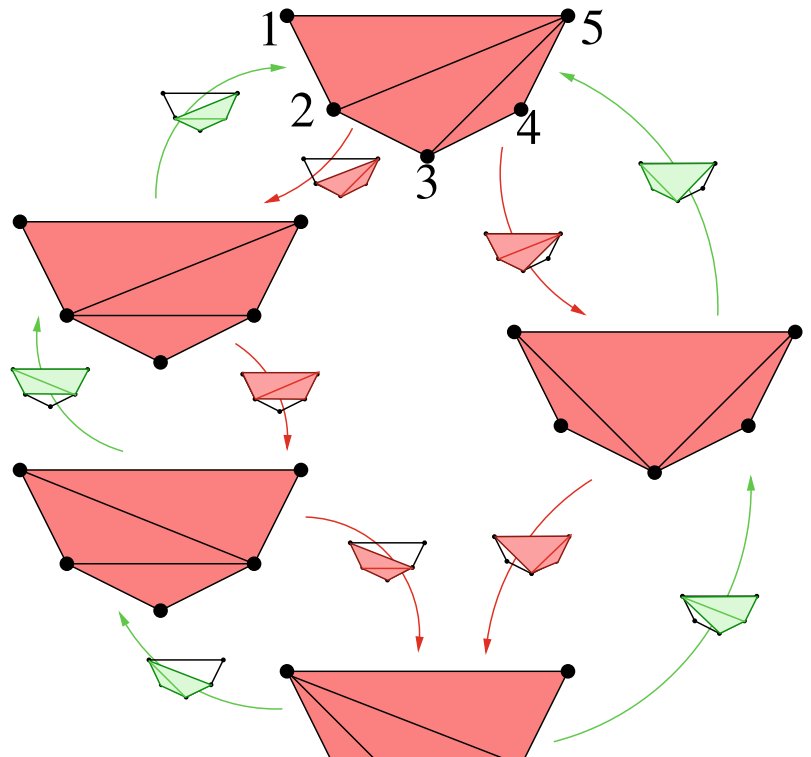


Figure 6.1: The (oriented) graph of triangulations of the 5-gon (with up and down flips) is the Hasse-diagram of a bounded poset.

Here is the definition that yields a direction on flips.

Definition 6.1.1 (Upflip/Downflip). A flip supported on $i < j < k < \ell$ in a triangulation of an n -gon is *upward* or an *upflip* if it replaces $\{i, k\}$ by $\{j, \ell\}$. It is *downward* or a *downflip* otherwise.

For triangulations $\mathcal{T}, \mathcal{T}'$ of an n -gon we say that $\mathcal{T} \leq_1 \mathcal{T}'$ when \mathcal{T}' can be produced from \mathcal{T} by a (possibly empty) sequence of upflips.

The notation “ \leq_1 ” will be explained in Section 6.1.4 in a more general framework.

We will now be even more concrete and restrict ourselves to the example of the 5-gon. We know already that the graph of triangulations of the 5-gon is connected. Now, what does the *directed* graph of triangulations look like? Figure 6.1 shows the result. From it we can read off the following:

- Neither upflips nor downflips produce directed cycles.
- There is a unique minimal triangulation $\hat{0}$ and a unique maximal triangulation $\hat{1}$.
- Every two triangulations $\mathcal{T}, \mathcal{T}'$ are connected via a sequence of upflips from \mathcal{T} to $\hat{1}$ and a sequence of downflips from $\hat{1}$ to \mathcal{T}' ; alternatively, they are connected by a sequence of downflips from \mathcal{T} to $\hat{0}$ and a sequence of upflips from $\hat{0}$ to \mathcal{T}' .

In summary: the graph of triangulations of a convex pentagon $\mathbf{C}(5,2)$ is a *bounded poset*. This additional structure implies that the graph of triangulations is connected—a fact that we already knew. The punch line is that the additional poset structure enables us to prove the stronger statement (triangulations form a bounded poset) for the general case of triangulations of the more general configurations $\mathbf{C}(n,d)$ that we are going to study, receiving connectedness of the graph for free—and in general dimension, this is new.

6.1.2 Combinatorial properties of cyclic polytopes

Cyclic polytopes form the (combinatorially) best understood class of polytopes with no bound on the number of vertices nor the dimension. In this section, we provide a definition and basic properties that we need in order to

- define a orientation on each flip of the cyclic polytope,
- construct new triangulations from old ones, and
- prove that the triangulations of the cyclic polytope form a bounded poset.

For a more detailed reference on properties of cyclic polytopes see [148, 339].

Definition 6.1.2 (Moment Curve). For $d \geq 0$, the curve

$$v_d : \begin{cases} \mathbb{R} & \rightarrow \mathbb{R}^d \\ t & \mapsto \begin{pmatrix} 1 \\ t \\ t^2 \\ \vdots \\ t^d \end{pmatrix} \end{cases} \quad (6.1)$$

is the d -dimensional *moment curve* (homogeneous coordinates, as it is our custom).

Cyclic point configurations are sometimes defined as a set of distinct points on the moment curve. This is neither the most general definition possible nor completely unambiguous. We prefer to introduce a well-defined, concrete *standard cyclic point configuration*, from which we derive general cyclic point configurations via their sets of circuits.

Definition 6.1.3 (Standard Cyclic Point Configuration). For $n > d \geq 0$, the d -dimensional *standard cyclic point configuration* with n points is the following point configuration:

$$\mathbf{C}(n, d) := \begin{pmatrix} 1 & 2 & \dots & n \\ v_d(1) & v_d(2) & \dots & v_d(n) \end{pmatrix} = \begin{pmatrix} 1 & 1 & \dots & 1 \\ 1 & 2 & \dots & n \\ \vdots & \vdots & & \vdots \\ 1 & 2^d & \dots & n^d \end{pmatrix} \quad (6.2)$$

For a subset $A \subseteq J = \{1, \dots, n\}$, the *standard cyclic subconfiguration* w.r.t. A is the subconfiguration $\mathbf{C}(n, d)|_A$. We denote it $\mathbf{C}(A, d)$. Of course, a *cyclic polytope* is the convex hull of the points of $\mathbf{C}(n, d)$.

Any d -dimensional point configuration with n points that is combinatorially equivalent to the standard cyclic point configuration is a *d -dimensional cyclic point configuration with n points*.

Here by *combinatorially equivalent*, we mean that the sets of signed circuits and cocircuits coincide in both configurations, i.e., they have the same *oriented matroid* (see Chapter 4 Definition 4.1.43).

Before we have a closer look at the circuits of $\mathbf{C}(n, d)$, we present some cyclic polytopes in small dimensions and codimensions.

The case $d = 0$: $\mathbf{C}(n, 0)$ is a multiset of n copies of the only point in \mathbb{R}^0 . Therefore, all zero-dimensional point configurations are cyclic.

The case $d = 1$: $\mathbf{C}(n, 1)$ consists of n points $1, 2, \dots, n$ in \mathbb{R} without repetitions. All one-dimensional point configurations without repeated points are cyclic.

The case $d = 2$: $\mathbf{C}(n, 2)$ consists of n points in strictly convex position, i.e., the vertices of an n -gon. All such point configurations are combinatorially equivalent, hence they are all cyclic.

The case $n - d = 1$: $\mathbf{C}(d + 1, d)$ is a d -simplex.

The case $n - d = 2$: $\mathbf{C}(d + 2, d)$ is a d -dimensional circuit.

The following lemma about the sign of the determinant of points on the moment curve is important for the combinatorial structure of cyclic point configurations.



Figure 6.2: The cyclic polytope $\text{conv}(\mathbf{C}(6,1))$ in dimension one, ...

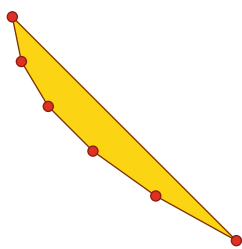


Figure 6.3: ... $\text{conv}(\mathbf{C}(6,2))$ in dimension two

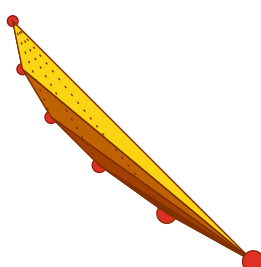


Figure 6.4: ... and $\text{conv}(\mathbf{C}(6,3))$ in dimension three.

Lemma 6.1.4. *For any $d + 1$ points, $v_d(t_1), \dots, v_d(t_{d+1})$, with $t_1 < t_2 < \dots < t_{d+1}$ on the moment curve, we have*

$$\operatorname{sign} \det(v_d(t_1), \dots, v_d(t_{d+1})) = 1.$$

Moreover, $v_d(t_{d+1})$ lies above (with respect to the last coordinate) every hyperplane spanned by the other points.

Proof. The determinant under consideration is the famous Vandermonde determinant, that can be explicitly computed as follows. Subtracting from each row, except the first, the previous row multiplied by t_1 gives a matrix in which the first column has a repeated non-zero entry, and the j -th column is a multiple of $t_j - t_1$. Taking those factors out of the determinant yields:

$$\begin{vmatrix} 1 & 1 & \dots & 1 \\ t_1 & t_2 & \dots & t_{d+1} \\ \vdots & \vdots & & \vdots \\ t_1^d & t_2^d & \dots & t_{d+1}^d \end{vmatrix} = \prod_{2 \leq j \leq d+1} (t_j - t_1) \begin{vmatrix} 1 & \dots & 1 \\ \vdots & & \vdots \\ t_2^{d-1} & \dots & t_{d+1}^{d-1} \end{vmatrix}.$$

Since the determinant on the right is also a Vandermonde determinant, induction on d gives:

$$\det(v_d(t_1), \dots, v_d(t_{d+1})) = \prod_{1 \leq i < j \leq d+1} (t_j - t_i) > 0.$$

From this, the first claim follows.

In order to prove the second claim, consider a point with “infinite height” w.r.t. to the last coordinate, represented as

$$\mathbf{p}_\infty := \begin{pmatrix} 0 \\ 0 \\ \vdots \\ 0 \\ 1 \end{pmatrix}$$

(Compare with Remark 5.2.3, where we did the same.)

The claim that the last point lies above all hyperplanes is therefore equivalent to saying that

$$\operatorname{sign} \det(v_d(t_1), \dots, v_d(t_{d+1})) = \operatorname{sign} \det(v_d(t_1), \dots, v_d(t_d), \mathbf{p}_\infty)$$

But the last determinant, developed in the last column, equals

$$\det(v_{d-1}(t_1), \dots, v_{d-1}(t_d)),$$

which is positive by part one. \square

From this we immediately conclude that $\mathbf{C}(n, d)$ is in general position:

Lemma 6.1.5. *No $d + 1$ points in $\mathbf{C}(n, d)$ lie on a common hyperplane in \mathbb{R}^d , i.e., $\mathbf{C}(n, d)$ is in general position.*

Proof. Being in general position is equivalent to the non-vanishing of the determinants in the previous lemma. \square

Moreover, we conclude that:

Corollary 6.1.6. *Every subconfiguration of a cyclic configuration of dimension d is itself a cyclic configuration of dimension d .*

Let us explain what we mean here more precisely. When we say that a configuration \mathbf{A} of dimension d on a label set J with k elements is *cyclic*, we mean that there is a bijection between J and the set $\{1, \dots, k\}$ under which the oriented matroids of \mathbf{A} and the standard cyclic configuration $\mathbf{C}(n, k)$ coincide. In the statement above, where $J = \{z_1, \dots, z_k\}$ is a subset of $\{1, \dots, n\}$ we, moreover, have that the bijection is given by the ordering of the elements of J .

Proof. One of the ways of characterizing the oriented matroid of a configuration of rank $d + 1$ is via its *chirotope*, that is, the map that assigns to each ordered $(d + 1)$ -tuple of elements the sign of the determinant they form. In the case of cyclic configurations, Lemma 6.1.4 says that the chirotope of a cyclic configuration is “the determinant of any $(d + 1)$ -tuple of elements is positive, when the elements are given in their canonical order”. This is inherited in all subconfigurations. \square

We will show that chirotopes are very useful later on in Section 8.1.1, but let us use them now for cyclic polytopes: As said in this proof, Lemma 6.1.4 gives us the chirotope of a cyclic configuration in a concise form, from which the signed circuits and cocircuits of it (or any other oriented matroid information) can be recovered. Let us show how to do this. For the cocircuits, the following concept is important:

Definition 6.1.7 (Gaps). For a cyclic configuration $\mathbf{C}(n, d)$ and a set $F \subseteq J = [n]$, a *gap* of F is an index $i \in J \setminus F$. A gap i of F is an *even gap* if the number of elements in F larger than i is even, and i is an *odd gap* otherwise.

Since cyclic configurations are in general position, each subset A of d elements defines a signed cocircuit: the partition of $J \setminus A$ into the elements on and the other side of the hyperplane spanned by A . The following statement, the *Gale’s evenness criterion*, says that points are on one side or the other depending simply on whether they are even or odd gaps:

Theorem 6.1.8 (Cocircuits of cyclic configurations). *Let $A \subseteq J = [n]$ be a set of d elements in the cyclic point configuration $\mathbf{C}(n, d)$. Let \mathbf{H} be the hyperplane spanned by the points labeled by A and let $i \in J \setminus A$. Then, the point labeled by i lies above (with respect to the last coordinate) \mathbf{H} if i is an even gap in A and it lies below if i is an odd gap.*

Proof. The linear equation defining \mathbf{H} is given by $\det(\mathbf{C}(A, d), \mathbf{x}) = 0$. A point \mathbf{x} lies above \mathbf{H} w.r.t. the last coordinate if and only if it lies on the same

side of \mathbf{H} as the point $v_d(n+1)$, by Lemma 6.1.4. This means that the point labeled by i is above \mathbf{H} if and only if

$$\operatorname{sign} \det(\mathbf{C}(A, d), v_d(i)) = \operatorname{sign} \det(\mathbf{C}(A, d), v_d(n+1)).$$

The determinant on the left is positive, by Lemma 6.1.4. The one on the right would become positive if the columns are reordered according to their labels, so its sign equals the parity of the permutation of $A \cup \{i\}$ that inserts i in its appropriate place. That permutation is even or odd depending on whether i is an even or an odd gap in A . \square

In particular, we can describe the facets of a cyclic configuration in terms of gaps, and even say what facets are lower and upper, with respect to the last coordinate. This statement is usually called Gale's evenness criterion (see, e.g., [339]).

Corollary 6.1.9 (Oriented Gale's Evenness Criterion). *A subset $F \subseteq [n]$ of a cyclic point configuration is a facet of it if and only if the gaps of F are either all even or all odd.*

If all gaps of F are odd then F is an upper facet of $\mathbf{C}(n, d)$ with respect to the last coordinate; it is a lower facet of $\mathbf{C}(n, d)$ with respect to the last coordinate, otherwise.

Proof. A set of d points defines a lower facet if the hyperplane spanned by them has the rest of the points above it, and an upper facet if it has all the points below. \square

From this we get exact numbers of upper and lower facets of $\mathbf{C}(n, d)$; this will be useful later. We leave the proof of this as an exercise to the reader.

Corollary 6.1.10. *For even d , the number of upper facets of $\mathbf{C}(n, d)$ is $\binom{n-(d/2+1)}{d/2-1}$; the number of lower facets of $\mathbf{C}(n, d)$ is $\binom{n-d/2}{d/2}$.*

For odd d , the numbers of upper and lower facets of $\mathbf{C}(n, d)$ coincide. They are both equal to $\binom{n-(d+1)/2}{(d-1)/2}$. \square

As a side remark, it will be essential later that in Figure 6.1 we observe:

- The minimal triangulation $\hat{0}$ of $\mathbf{C}(5, 2)$ is (labeled by) the set of lower facets of $\mathbf{C}(5, 3)$.
- The maximal triangulation $\hat{1}$ of $\mathbf{C}(5, 2)$ is the set of upper facets of $\mathbf{C}(5, 3)$.

Now we turn our attention to the circuits of cyclic point configurations.

Theorem 6.1.11 (Circuits of Cyclic Point Configurations). *The circuits Z of $\mathbf{C}(n, d)$ are exactly the sets $\{z_1, z_2, \dots, z_{d+2}\}$ with $z_1 < z_2 < \dots < z_{d+2}$.*

Their positive part $Z_+ = \{z_1, z_3, \dots\}$ consists of all elements with odd indices, and their negative part is given by the set $Z_- = \{z_2, z_4, \dots\}$ of elements with even indices, or vice versa.

Because of the structure of its circuits, the oriented matroid of a cyclic configuration is called the *alternating oriented matroid*: the (ordered) elements of a circuit Z are alternatingly in Z_+ and Z_- .

Proof. Since $\mathbf{C}(n, d)$ is in general position, every set of $d + 2$ points in $\mathbf{C}(n, d)$ forms a circuit. The circuit signature of a set $Z = \{z_1, z_2, \dots, z_{d+2}\}$ is given by the signs of the coefficients in the unique (modulo a scalar factor) dependence supported on it, that is, the generator of the kernel of Z when written as a matrix is:

$$\mathbf{C}(Z, d) = \begin{pmatrix} 1 & 2 & \dots & d+2 \\ z_1 & z_2 & \dots & z_{d+2} \\ \vdots & \vdots & & \vdots \\ z_1^d & z_2^d & \dots & z_{d+2}^d \end{pmatrix}.$$

As explained in Remark 4.1.8, one choice for the generator is to take as the i -th entry in it the determinant of the matrix obtained by deleting the i -th column in $\mathbf{C}(Z, d)$, multiplied by the sign $(-1)^i$. The determinants themselves are all positive, by Lemma 6.1.4, so multiplying the entries by $(-1)^i$ causes them to alternate in sign. \square

Example 6.1.12 (The affine Gale transform of $\mathbf{C}(d, d + 4)$). Let us show that the cyclic affine Gale transform introduced in Section 5.5.2 is, as claimed there, a Gale transform of $\mathbf{C}(d, d + 4)$. The alternating circuit property is a property on the cocircuits of the Gale transform, that is, on the way that lines spanned by pairs of points split the other ones. Having in mind that white points represent antipodal vectors to black points, the exact translation is as follows: For every line spanned by two arbitrary points in the affine diagram, the remaining points, taken in order of increasing labels, must in every step either change color or change to the other side of the line, but not both.

This is easily verified by looking at Figure 5.78: If the points chosen for the line are consecutive, at every increase in the label, we change colors and stay on the same side of the line. If they are not consecutive, the same happens, except when we pass over one of the chosen two points, at which step we change to the other side of the line but keep the same color.

Observe that we are not claiming that points in a circle form a geometric Gale transform of the cyclic polytope in its standard realization on the moment curve, only that they are a Gale transform of a polytope with the same oriented matroid, hence the same set of triangulations.

To finish the description of the oriented matroid of a cyclic configuration let us make a final remark. In arbitrary point configurations, the signatures of circuits and cocircuits are unique modulo an exchange of the positive and negative parts, and there is not, a priori, a canonical way of saying which is positive and which is negative, simultaneously for all of them. In cyclic configurations, however, we have a canonical way of orienting cocircuits

(call the upper part of them positive) and one of orienting circuits (postulate that the last element in them be in the positive part of the circuit). Since this convention will be crucial in what comes next, let us make it formal and explicit:

Definition 6.1.13 (Upward/Downward Circuit). Let $Z = \{z_1, z_2, \dots, z_{d+2}\}$ be a circuit in $\mathbf{C}(n, d)$.

As in Theorem 6.1.11, we assume that the z_i 's are given in increasing order and define $Z_+ := \{\dots, z_d, z_{d+2}\}$ and the $Z_- := \{\dots, z_{d-1}, z_{d+1}\}$.

Then, the *upward signature* on Z is the partition (Z_+, Z_-) . The circuit (Z_+, Z_-) is then an *upward (signed) circuit* of $\mathbf{C}(n, d)$.

Likewise, the *downward signature* on Z is given by the opposite signature (Z_-, Z_+) on Z : (Z_-, Z_+) is then a *downward (signed) circuit* of $\mathbf{C}(n, d)$.

The set of all upward circuits of $\mathbf{C}(n, d)$ is denoted by $\mathcal{Z}_+(n, d)$, and the set of all downward circuits is denoted by $\mathcal{Z}_-(n, d)$.

The existence of this canonical orientation is related to the fact that $\mathbf{C}(n, d)$ has $\mathbf{C}(n, d + 1)$ as its natural lift. Indeed, a circuit Z of $\mathbf{C}(n, d)$ becomes a basis, when regarded as a subset of $\mathbf{C}(n, d + 1)$, that is, its convex hull is a $(d + 1)$ simplex. The two subsets Z_- and Z_+ , being a Radon partition, have the property that their convex hulls intersect in a unique point when regarded in $\mathbf{C}(n, d)$. But in $\mathbf{C}(n, d + 1)$, Z_+ lies above Z_- . Moreover, we have

$$Z_+ = \bigcap_{F_+ \in \mathcal{F}_+(Z, d+1)} F_+, \quad (6.3)$$

$$Z_- = \bigcap_{F_- \in \mathcal{F}_-(Z, d+1)} F_- \quad (6.4)$$

where $\mathcal{F}_+(Z, d + 1)$ and $\mathcal{F}_-(Z, d + 1)$ are the sets of upper and lower facets of $\mathbf{C}(Z, d + 1)$, respectively.

6.1.3 Triangulations as sections of the canonical projection

A very useful connection between cyclic point configurations in different dimensions is provided by the *canonical projection*: we take the points in $\mathbf{C}(n, d)$ and forget their last coordinates, obtaining $\mathbf{C}(n, d - 1)$. We will soon see that we can interpret a triangulation \mathcal{T} of $\mathbf{C}(n, d - 1)$ as a geometric object sitting in $\mathbf{C}(n, d)$ that is mapped back onto \mathcal{T} by the canonical projection. The description of triangulations as *characteristic sections* of the canonical projection will allow for an enhanced geometric understanding of directed flips (see Figures 6.5 and 6.6 for an illustration).

Definition 6.1.14 (Canonical Projection). The *canonical projection* from $\text{conv}(\mathbf{C}(n, d))$ to $\text{conv}(\mathbf{C}(n, d - 1))$ is the map induced by forgetting the last

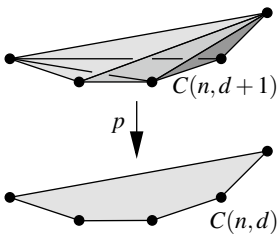


Figure 6.5: The canonical projection.

coordinate, i.e.,

$$p_{n,d} : \begin{cases} \text{conv}(\mathbf{C}(n, d)) & \rightarrow \text{conv}(\mathbf{C}(n, d-1)), \\ \begin{pmatrix} x_0 \\ x_1 \\ \vdots \\ x_d \end{pmatrix} & \mapsto \begin{pmatrix} x_0 \\ x_1 \\ \vdots \\ x_{d-1} \end{pmatrix} \end{cases} \quad (6.5)$$

In Chapter 5, we made extensive use of the *characteristic sections* associated to a triangulation from a lifting of its vertices (see Definition 5.2.12). We recall now the definition for the case of a cyclic polytope.

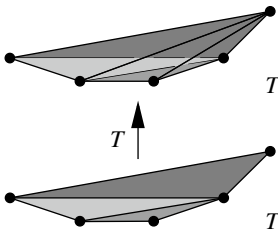


Figure 6.6: The characteristic section.

Definition 6.1.15 (Characteristic Section). Let \mathcal{T} be a triangulation of $\mathbf{C}(n, d)$. Then the *characteristic section* of \mathcal{T} is the unique piecewise affine map that is affine on each simplex of \mathcal{T} and that lifts the points in $\mathbf{C}(n, d)$ to the $(d+1)$ -dimensional moment curve, i.e.,

$$s_{\mathcal{T}} : \begin{cases} \text{conv}(\mathbf{C}(n, d)) & \rightarrow \text{conv}(\mathbf{C}(n, d+1)), \\ v_d(i) & \mapsto v_{d+1}(i), \\ & \text{affinely extended inside simplices of } \mathcal{T}. \end{cases} \quad (6.6)$$

To illustrate the use of characteristic sections, we first look at cyclic point configurations in dimension one. Recall that cyclic point configurations with n points in dimension one consist of n distinct points on the real line, labeled in the order of increasing coordinates.

Intuitively, a valid triangulation of $\mathbf{C}(n, 1)$ is a set of non-overlapping intervals covering the interval from 1 to n . Such a triangulation can be encoded by specifying the boundary points of the subdividing intervals. Since both 1 and n as faces of $\mathbf{C}(n, 1)$ need to be covered by an interval, it is enough to give the points among 2 through $n-1$ that bound an interval in the triangulation. This way, any subset of $[2, n-1] := \{2, 3, \dots, n-1\}$ induces a unique valid triangulation of $\mathbf{C}(n, 1)$. Therefore, the set of triangulations of $\mathbf{C}(n, 1)$ is in bijection to the set of subsets of $[2, n-1]$.

What do the characteristic sections look like? When we take a triangulation of $\mathbf{C}(n, 1)$ and lift the points to the two-dimensional moment curve, the segments between the points on the moment curve fold in a convex fashion. Moreover, when two triangulations $\mathcal{T}, \mathcal{T}'$ are such that the set of points used in \mathcal{T} contains the set of points used in \mathcal{T}' , then the characteristic section $s_{\mathcal{T}}$ of \mathcal{T} lies *weakly below* the characteristic section $s_{\mathcal{T}'}$ of \mathcal{T}' .

This means, that the last coordinate of the characteristic section of \mathcal{T} is nowhere higher than in the characteristic section of \mathcal{T}' . In formulas: $s_{\mathcal{T}}(\mathbf{x})_2 \leq s_{\mathcal{T}'}(\mathbf{x})_2$ for all $\mathbf{x} \in \mathbf{C}(n, 2)$. In Figure 6.7, all the triangulations of $\mathbf{C}(6, 1)$ are drawn as characteristic sections.

The relation “characteristic section is weakly lower” defines a partial order on the set of triangulations of $\mathbf{C}(n, 1)$, via $\mathcal{T} \leq_2 \mathcal{T}'$ if and only if $s_{\mathcal{T}}$ is weakly below $s_{\mathcal{T}'}$. The notation “ \leq_2 ” will be explained in the next section, when we will introduce the general case.

Let us look at a flip in a triangulation \mathcal{T} of $\mathbf{C}(n, 1)$, resulting in a new triangulation \mathcal{T}' . Flipping is equivalent to the insertion or the removal of exactly one point. A natural direction on flips can be given as follows: an upflip removes a subdivision point, a downflip inserts one. We get the poset structure $\mathcal{T} \leq_1 \mathcal{T}'$ if and only if \mathcal{T} can be changed into \mathcal{T}' by removing subdivision points. As this cannot produce any cycles, we get a poset structure like in the two-dimensional case. It is easy to see that the poset of triangulations of $\mathbf{C}(n, 1)$ is equivalent to the reversed Boolean lattice on $n - 2$ elements.

How are the two poset structures related? If we insert a point in \mathcal{T} , then $s_{\mathcal{T}'}$ lies below $s_{\mathcal{T}}$, and exactly one triangle fits in between. This triangle is the convex hull of the points supporting the flip (see Figure 6.8).

This shows at the same time that $\mathcal{T} \leq_1 \mathcal{T}'$ implies $\mathcal{T} \leq_2 \mathcal{T}'$. We say, “the poset \leq_1 ” is *coarser* than “ \leq_2 ” and “ \leq_2 ” is *finer* than “ \leq_1 ”.

There is another thing to observe in the one-dimensional case: Assume, we start with the minimal triangulation of $\mathbf{C}(n, 1)$ and flip upwards. On the level of characteristic sections, this corresponds to stacking a triangle t_1 somewhere on top of the lower facets and taking the upper envelope. We can interpret this as a continuous action of sliding up the characteristic section, thereby wiping exactly over t_1 . If we perform another upflip, the corresponding wiped triangle t_2 will intersect properly with t_1 . Eventually, we arrive at the maximal triangulation.

In the continuous process of sliding the lower facets all the way up to the upper facets we have wiped over the whole two-dimensional cyclic polytope $\mathbf{C}(n, 2)$. This means that the triangles corresponding to the upflips cover $\mathbf{C}(n, 2)$. Since they are intersecting properly and cover, they form a triangulation of $\mathbf{C}(n, 2)$. In other words: the sets of flips in maximal chains of the first poset structure correspond to triangulations.

Conversely, every triangulation of $\mathbf{C}(n, 2)$ gives rise to a sequence of flips in $\mathbf{C}(n, 1)$ from $\hat{0}$ to $\hat{1}$ (exercise).

6.1.4 Higher Stasheff-Tamari posets

In this section, we will define two poset structures on the set of triangulations of a cyclic point configuration. In our two-dimensional example, the first poset structure yields exactly the structure in Figure 6.1. It is a poset structure that is defined by means of its covering relations via a *direction on flips*. The second poset structure is defined for every pair of triangulations via the height of their *characteristic sections*, and yields the poset structure that we have seen in the previous section in dimension one.

Let us start with the second poset structure because it will help us to understand why the directed flips defined below do not produce directed cycles.

Definition 6.1.16 (Second Stasheff-Tamari Poset). For triangulations \mathcal{T} and \mathcal{T}' of $\mathbf{C}(n, d)$ define

$$\mathcal{T} \leq_2 \mathcal{T}' : \iff s_{\mathcal{T}}(\mathbf{x})_{d+1} \leq s_{\mathcal{T}'}(\mathbf{x})_{d+1} \quad \forall \mathbf{x} \in \text{conv}(\mathbf{C}(n, d)). \quad (6.7)$$

The poset induced by “ \leq_2 ” is the *Second Stasheff-Tamari Poset* and is

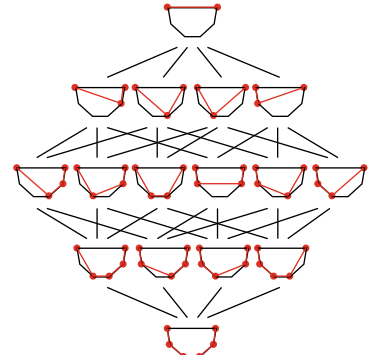


Figure 6.7: The height of a section defines a poset on all triangulations of $\mathbf{C}(6, 1)$.

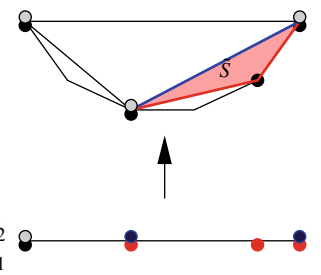


Figure 6.8: A flip can be interpreted as stacking a triangle on top of the characteristic section and taking the new upper envelope; this defines a covering relation among triangulations of $\mathbf{C}(6, 1)$.

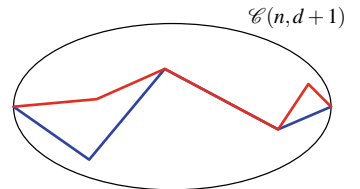


Figure 6.9: The brighter section is weakly higher than the darker section; therefore, the corresponding triangulations are ordered accordingly in $\text{HST}_2(n, d)$.

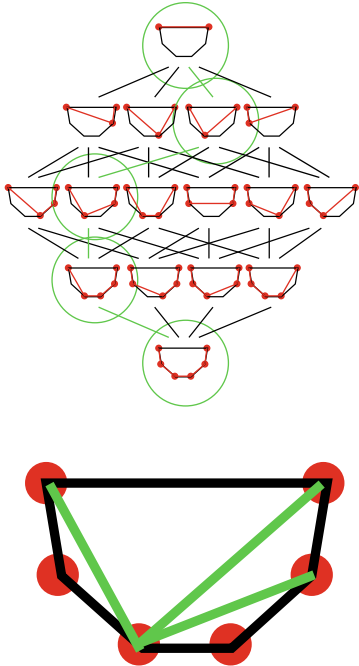


Figure 6.10: A maximal chain of triangulations of $C(6,1)$ induces via its set of flips a triangulation of $C(6,2)$.

denoted by $HST_2(n,d)$.

Next we want to make Definition 6.1.1 of upflips and downflips compatible with the general definition of flips in Section 2.4, as applied to the n -gon. In Section 2.4, we defined flips in general dimensions via flippable circuits. So what are the flippable circuits corresponding to the flips in a triangulation of an n -gon?

Every four-point set in $C(n,2)$ is a circuit, and every circuit contains four points. For $Z = \{i, j, k, \ell\}$, the canonical signature is as follows: The upper facets of $\{i, j, k, \ell\}$ (interpreted as a tetrahedron in $C(n,3)$) are $\{i, j, \ell\}$ and $\{j, k, \ell\}$; the lower facets are $\{i, j, k\}$ and $\{i, k, \ell\}$. Therefore, according to 6.1.13, $Z_+ = \{j, \ell\}$ and $Z_- = \{i, k\}$. The two possible triangulations of $C(Z,d)$ according to Section 2.4 are $\mathcal{T}_+(Z) = \{\{i, j, \ell\}, \{j, k, \ell\}\}$ and $\mathcal{T}_-(Z) = \{\{i, j, k\}, \{i, k, \ell\}\}$. In other words:

$$\mathcal{T}_+(Z) = \mathcal{F}_+(Z, d+1), \quad (6.8)$$

$$\mathcal{T}_-(Z) = \mathcal{F}_-(Z, d+1). \quad (6.9)$$

Note that $\mathcal{T}_+(Z)$ contains the diagonal $Z_+ = \{j, \ell\}$, and $\mathcal{T}_-(Z)$ contains the diagonal $Z_- = \{i, k\}$. If a triangulation contains, e.g., $\mathcal{T}_-(Z)$ as a subcomplex then the two triangles $\{i, j, k\}$ and $\{i, k, \ell\}$ form a convex quadrilateral triangulated by the diagonal $\{i, k\}$. Replacing $\mathcal{T}_-(Z)$ by $\mathcal{T}_+(Z)$ leaves the boundary of the quadrilateral alone, and the diagonal $\{i, k\}$ is replaced by $\{j, \ell\}$: we have an upflip as in Definition 6.1.1. Likewise, we obtain a downflip whenever $\mathcal{T}_+(Z)$ is replaced by $\mathcal{T}_-(Z)$ in some triangulation containing $\mathcal{T}_+(Z)$ as a subcomplex.

The description of flips via \mathcal{T}_+ and \mathcal{T}_- no longer relies on dimension two: we can use them to define a direction on flips in triangulations of $C(n,d)$.

Definition 6.1.17. Let \mathcal{T} be a triangulation of $C(n,d)$.

An *upflip* in \mathcal{T} is a flip that replaces the lower facets of a $(d+1)$ -simplex in $C(n,d+1)$ by its upper facets.

An *downflip* in \mathcal{T} is a flip that replaces the upper facets of a $(d+1)$ -simplex in $C(n,d+1)$ by its lower facets.

More specifically, let Z be a circuit of $C(n,d)$.

If $\mathcal{T}_-(Z)$ is a subcomplex of \mathcal{T} , we say that Z supports an *upward flip* or an *upflip*.

If $\mathcal{T}_+(Z)$ is a subcomplex of \mathcal{T} , we say that Z supports a *downward flip* or *downflip*.

With this direction or orientation on flips, the flip graph of triangulations of a cyclic polytope is a directed graph. Let us collect what we have found in dimensions one and two (at least in the examples):

- In dimensions one and two, neither upflips nor downflips produce directed cycles.
- In dimension one and two, there is a unique minimal triangulation $\hat{0}$ and a unique maximal element $\hat{1}$.

- In dimension one and two, $\hat{0}$ equals the set of lower facets of $\mathbf{C}(n, d + 1)$, and $\hat{1}$ equals the set of upper facets of $\mathbf{C}(n, d + 1)$.
- In dimensions one and two, every two triangulations $\mathcal{T}, \mathcal{T}'$ are connected via a sequence of upflips from \mathcal{T} to $\hat{1}$ and a sequence of downflips from $\hat{1}$ to \mathcal{T}' ; alternatively, they are connected by a sequence of downflips from \mathcal{T} to $\hat{0}$ and a sequence of upflips from $\hat{0}$ to \mathcal{T}' .
- In dimension one, any sequence of flips from $\hat{0}$ to $\hat{1}$ induces a triangulation of $\mathbf{C}(n, 2)$.

The goal is now to show that the limitation “in dimensions one and two” can be dropped.

Why are there no directed cycles? From the definition via the exchange of lower and upper facets of a $(d + 1)$ -simplex in $\mathbf{C}(n, d + 1)$, we see that an upflip weakly lifts the characteristic section. In other words: If \mathcal{T}' is obtained from \mathcal{T} by an upflip, then $\mathcal{T} <_2 \mathcal{T}'$. Since “ \leq_2 ” defines a poset, there can be no directed cycle of upflips. In other words: the directed graph of all triangulations of a cyclic point configuration is the Hasse diagram of a poset.

Definition 6.1.18. For triangulations \mathcal{T} and \mathcal{T}' of $\mathbf{C}(n, d)$ define

$$\mathcal{T} \leq_1 \mathcal{T}' : \iff \mathcal{T}' \text{ is obtained from } \mathcal{T} \text{ by a sequence of upflips. (6.10)}$$

The poset induced by \leq_1 is the *First Stasheff-Tamari Poset* and is denoted by $\text{HST}_1(n, d)$.

It takes a little more work to show boundedness of the poset and the correspondence between maximal chains and triangulations one dimension up. Therefore, we devote the entire next section to the statement and the proof of the structure theorem for triangulations of cyclic polytopes.

6.1.5 The structure theorem for the first Stasheff-Tamari poset

We have already announced that the results about one- and two-dimensional examples are true in the general case. Therefore, let us state the theorem and its implications first.

Theorem 6.1.19. *The first Stasheff-Tamari Poset $\text{HST}_1(n, d)$ is bounded. The unique minimal triangulation is the set of lower facets of $\mathbf{C}(n, d + 1)$ and the unique maximal triangulation is the set of upper facets of $\mathbf{C}(n, d + 1)$.*

Moreover, there is a one-to-one correspondence between maximal chains in $\text{HST}_1(n, d)$ and triangulations of $\mathbf{C}(n, d + 1)$. This correspondence is induced by mapping each flip in a maximal chain in $\text{HST}_1(n, d)$ to the corresponding $(d + 1)$ -simplex in $\mathbf{C}(n, d + 1)$.

This theorem has many remarkable consequences:

Corollary 6.1.20. *For all $n > d \geq 0$, we have that:*

- The flip graph of $\mathbf{C}(n, d)$ is connected.*

- (ii) The number of simplices in a triangulation of $\mathbf{C}(n, d)$ is bounded between the number of upper facets and the number lower facets of $\mathbf{C}(n, d + 1)$.
- (iii) The length of a maximal chain in $\text{HST}_1(n, d)$ is bounded between the number of upper facets and the number of lower facets of $\mathbf{C}(n, d + 2)$.
- (iv) For even d , all triangulations of $\mathbf{C}(n, d)$ have the same number of simplices.
- (v) For odd d , all maximal chains in $\text{HST}_1(n, d)$ have the same lengths.
- (vi) For even d , the diameter of the flip graph of $\mathbf{C}(n, d)$ is bounded between $\binom{n-d/2-2}{d/2}$ and $2\binom{n-d/2-2}{d/2}$.
- (vii) For odd d , the diameter of the flip graph of $\mathbf{C}(n, d)$ is $\binom{n-(d+1)/2-1}{(d+1)/2}$.

Proof. Assertion (i) is clear since all triangulations can be connected to the top element or the bottom element. Assertion (ii) follows from the fact that upflips cannot increase the number of simplices in a triangulation. Once we know this, Assertion (iii) follows from the one-to-one correspondence between flips in dimension d and simplices in dimension $d + 1$.

The remaining assertions follow from the formulas for the numbers of upper and lower facets of $\mathbf{C}(n, d)$ in Corollary 6.1.10, applied to the correct dimensions. \square

Remark 6.1.21. We can be more precise with respect to the number of simplices in triangulations of $\mathbf{C}(n, d)$. In even dimension, they all have $\binom{n-(d+2)/2}{d/2}$ maximal simplices. For odd d , the number goes from a minimum of $\binom{n-(d+3)/2}{(d-1)/2}$ to a maximum of $\binom{n-(d+1)/2}{(d+1)/2}$. The minimum is achieved by the maximum triangulation $\hat{1}$ and the maximum is achieved by the minimum one $\hat{0}$ in the Higher Stasheff-Tamari posets.

Also observe that, in the odd-dimensional case, all the intermediate numbers between the maximum and minimum are also achieved by some triangulation. One easy proof is that the graph of flips is connected and every flip changes the number of flips by exactly one, since all the circuits are of type $((d-1)/2, (d+1)/2)$.

We now prove Theorem 6.1.19. Sure enough, the interpretation of triangulations as characteristic sections one dimension up plays a crucial role. To avoid unnecessary notational overhead, we will make no distinction between a triangulation \mathcal{T} , its characteristic section $s_{\mathcal{T}}$, and the image $s_{\mathcal{T}}(\mathbf{C}(n, d))$ of $\text{conv}(\mathbf{C}(n, d))$ in $\text{conv}(\mathbf{C}(n, d + 1))$ under $s_{\mathcal{T}}$.

The proof will contain arguments of various types, some of them quite technical but others also appealingly simple. In order not to get lost in the environment of the proof, we start with a roadmap.

Let us start with the proof of the boundedness of $\text{HST}_1(n, d)$. We claim that the following assertions imply that $\text{HST}_1(n, d)$ has a unique minimal and a unique maximal element:

- (i) It suffices to show that in each triangulation $\mathcal{T} \neq \hat{1}$ [$\mathcal{T} \neq \hat{0}$] we can find an upflip [a downflip].
- (ii) For each triangulation \mathcal{T} of $\mathbf{C}(n, d)$, there is a triangulation $\delta(\mathcal{T})$ of $\mathbf{C}(n, d+1)$ containing \mathcal{T} .
- (iii) Every triangulation \mathcal{T} of $\mathbf{C}(n, d)$ is *stackable*: the stacking relation

$$S \prec S' : \iff S \cap S' \text{ is an upper facet of } S \quad (6.11)$$

does not produce any cycles.

Proof of Theorem 6.1.19 (boundedness) given the claims above.

By Claim (i), it suffices to show that there is an upflip in every triangulation \mathcal{T} of $\mathbf{C}(n, d)$ not equal to $\hat{1}$, and a downflip in every triangulation \mathcal{T} of $\mathbf{C}(n, d)$ not equal to $\hat{0}$. We prove the first case; the second case is analogous.

Let \mathcal{T} be a triangulation of $\mathbf{C}(n, d)$ not equal to $\hat{1}$. Consider the triangulation $\delta(\mathcal{T})$ of $\mathbf{C}(n, d+1)$ containing \mathcal{T} as a subcomplex (such a triangulation exists by Claim (ii)).

Since $\mathcal{T} \neq \hat{1}$, there are simplices in \mathcal{T} that are not upper facets of $\mathbf{C}(n, d+1)$. Therefore, since $\delta(\mathcal{T})$ covers $\mathbf{C}(n, d+1)$, it contains $(d+1)$ -simplices above \mathcal{T} , i.e., all points in their convex hull have last coordinate no smaller than those points in \mathcal{T} with the same image under the canonical projection. Since the stacking relation “ \prec ” on the $(d+1)$ -simplices in $\delta\mathcal{T}$ is cycle-free, we can pick the minimal simplex S in $\delta(\mathcal{T})$ above \mathcal{T} . If all lower facets of S are in \mathcal{T} , then S supports an upflip in \mathcal{T} , and we are done. If not, then there is a lower facet of S not in \mathcal{T} . This facet gives rise to an adjacent simplex $S' \prec S$ which is still above \mathcal{T} , which is a contradiction to the minimality of S . \square

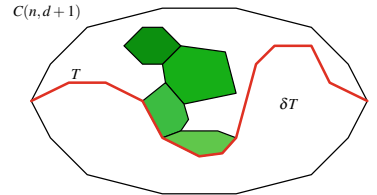


Figure 6.11: Finding an upflip by starting at a $(d+1)$ above \mathcal{T} and searching “downwards”.

It remains to show that Claims (i)–(iii) are correct.

- (i) Let \mathcal{T} be an arbitrary triangulation of $\mathbf{C}(n, d)$. Since there are only a finite number of different triangulations, and flipping upwards [downwards] does not create any cycles, we will find a sequence of upflips [downflips] to the top [bottom] element.
- (ii) In order to prove this part, we present two operations on triangulations: the *extension* and the *deletion*.

The extension $\hat{\mathcal{T}}$ and the deletion $\mathcal{T} \setminus n$ of \mathcal{T} are defined as follows in terms of maximal simplices:

$$\begin{aligned} \hat{\mathcal{T}} &:= \mathcal{T} * n \\ &\cup \{S \setminus \{n\} \cup \{j, j+1\} : S = \{s_1, \dots, s_n\} \in \mathcal{T}, \\ &\quad s_{n-1} < j < n+1\}, \\ \mathcal{T} \setminus n &:= \{S : S \in \mathcal{T}, n \notin S\} \\ &\cup \{S \setminus \{n\} \cup \{n-1\} : S \in \mathcal{T}, \\ &\quad n-1 \notin S, \\ &\quad n \in S\}. \end{aligned}$$

We claim that the extension of \mathcal{T} is a triangulation of $\mathbf{C}(n+1, d+1)$, and the deletion of \mathcal{T} is a triangulation of $\mathbf{C}(n-1, d)$.

Let us have a look at $\hat{\mathcal{T}}$ first. The part $\mathcal{T} * n$ triangulates the complete area of $\text{conv}((C(n+1, d+1))$ above the hypersurface $s_{\mathcal{T}}$: (MaxIP) holds because it holds for \mathcal{T} and coning does no harm; (MaxMP) modulo facets in $s_{\mathcal{T}}$ also follows immediately from (MaxMP) for \mathcal{T} . That the other, more complicated part triangulates the rest, is a tedious check of (CombAdjIP) and (CombMP) that we actually do not need. We refer to [264] for a proof.

The deletion $\mathcal{T} \setminus n$ is a triangulation of $\mathbf{C}(n, d)$ because of the following sliding argument: Assume that we slide point n continuously along the moment curve towards point $n-1$ in the time interval $[0, 1]$. Then, because the oriented matroid of the point configuration stays the same for all $t \in [0, 1]$, the simplices in \mathcal{T} will form a triangulation throughout. Therefore, (MaxUVP) and (MaxMVP) hold (see Theorem 4.5.17), i.e., the total uncovered volume and the total multiply covered volume are zero throughout $t \in [0, 1]$.

Since the volume is a continuous function of the coordinates of the points, the uncovered volume and the multiply-covered volume must also be zero for $t = 1$. Thus, the resulting d -simplices of this sliding procedure form a triangulation. The simplices that are still d -dimensional after this slide are exactly the ones in the formula of $\mathcal{T} \setminus n$.

- (iii) This can be proven by giving a linear extension of the relation. This is another nice application of the notion of the gap parity. Map each simplex $S \in \mathcal{T}$ to an n -letter string $\Gamma(S)$ on the alphabet $\{o, *, e\}$. The i -th letter $\Gamma_i(S)$ is defined as:

$$\Gamma_i(S) := \begin{cases} e & \text{if } i \text{ is an even gap of } S, \\ o & \text{if } i \text{ is an odd gap of } S, \text{ or} \\ * & \text{if } i \in S. \end{cases}$$

This is a bijection. Now, the following is easy to see: If we switch from a simplex $S \in T$ to a simplex $S' \in \mathcal{T}$ stacked on top of S then, because of (CombAdjIP), in the corresponding strings either an e switches to the left or an o switches to the right. That means, the lexicographic order w.r.t. $o < * < e$ is a linear extension of the stacking relation “ \prec ”, and thus the stacking relation does not produce cycles.

6.1.6 Cyclic polytopes have many triangulations

Cyclic polytopes are known to maximize the number of faces a polytope of given dimension and number of vertices can have. Not surprisingly, they also have *many triangulations*. The lower bound on the number of triangulations we show here follows the ideas from a paper of Kalai [181] where he uses the number of triangulations of a cyclic polytope as a lower bound for the number of combinatorial simplicial balls. From that bound he

derives the same for spheres. Put differently, the number of triangulations of $\mathbf{C}(n, d)$ is not significantly different from the total number of combinatorially different triangulations that exist, when we consider arbitrary point sets with n elements and dimension d . More precise information on this will be given in Sections 7.2.2 and 8.4.

The main result is:

Theorem 6.1.22 (Kalai [181]). *If d is considered fixed, the cyclic polytope $\mathbf{C}(n, d)$ has at least $\Omega(2^{n^{\lfloor d/2 \rfloor}})$ triangulations.*

Remark 6.1.23. The number of triangulations (respectively, regular triangulations) of a given point set cannot be larger than the number of simplicial spheres (respectively polytopal simplicial spheres) with one more vertex and the same dimension, modulo an $n!$ factor that accounts for possible combinatorially equal but geometrically different triangulations in a point configuration.

In arbitrary, but fixed, dimension $d \geq 3$, Dey and Shah [106] (see the proof in Theorem 8.4.2) showed that the number of combinatorial spheres is in $2^{\Omega(n^{cd/2})}$ for odd dimension (and a $\log n$ extra factor appears in the exponent of the proven bound for even dimension). Theorem 6.1.22 show that those bounds are not far from optimal.

In contrast, the number of polytopal spheres (that is, the number of regular triangulations) is in $2^{\Omega(n \log n)}$ by a classical result of Goodman and Pollack [143, 142]. In Theorem 7.2.10, we show point configurations which achieve this number of regular triangulations for every $d \geq 4$.

To simplify notation, let $k = \lfloor d/2 \rfloor$. The key to the proof is, as usual with triangulations of cyclic polytopes, to consider triangulations of $\mathbf{C}(n, d)$ as sections in $\mathbf{C}(n, d+1)$. We are only going to look at the sections that appear as a subcomplex in the minimum triangulation $\mathcal{T}_0 := \hat{0}$ of $\mathbf{C}(n, d+1)$. Remember that this triangulation equals the set of lower facets of $\mathbf{C}(n, d+2)$, which we can write as follows:

1. If $d = 2k$ is even, then

$$\begin{aligned} \mathcal{T}_0 := & \left\{ \{a_0, a_0 + 1, a_1, a_1 + 1, \dots, a_k, a_k + 1\} : \right. \\ & \left. 1 \leq a_0 < a_0 + 1 < a_1 < a_1 + 1 < \dots < a_k < a_k + 1 \leq n \right\}. \end{aligned} \quad (6.12)$$

2. If $d = 2k+1$ is odd, then

$$\begin{aligned} \mathcal{T}_0 := & \left\{ \{1, a_0, a_0 + 1, a_1, a_1 + 1, \dots, a_k, a_k + 1\} : \right. \\ & \left. 2 \leq a_0 < a_0 + 1 < a_1 < a_1 + 1 < \dots < a_k < a_k + 1 \leq n \right\}. \end{aligned} \quad (6.13)$$

We will consider the simplices of \mathcal{T}_0 partially ordered by the following relation. As usual, we assume that the labels z_i (respectively y_i) of our elements are listed in increasing order:

$$\{z_1, z_2, \dots, z_{d+2}\} \prec \{y_1, y_2, \dots, y_{d+2}\} \Leftrightarrow z_i \leq y_i \quad \forall i.$$

Lemma 6.1.24. *The order \prec in \mathcal{T}_0 is the transitive closure of the relation $B_1 \prec B_2$ if B_1 and B_2 share an upper facet of B_1 and a lower facet of B_2 .*

Proof. Let us first show that, if B_1 and B_2 share an upper facet of B_1 and a lower facet of B_2 then $B_1 \prec B_2$.

If B_1 and B_2 share a facet, then $B_1 \cup B_2 = \{z_1, z_2, \dots, z_{d+3}\}$. Since B_1 and B_2 are both lower facets of the cyclic polytope $C(d+3, d+2)$ defined by these indices, we have that the elements $z_i \in B_1 \setminus B_2$ and $z_j \in B_2 \setminus B_1$ are both even gaps in $B_1 \cup B_2$. Now, the fact that the common facet $B_1 \cap B_2$ is upper in B_1 and lower in B_2 implies that z_i is an odd gap in B_1 and z_j is an even gap in B_2 , which implies $j > i$. Thus, $B_1 \prec B_2$ as desired.

To finish the proof, let $B_1 = \{z_1, z_2, \dots, z_{d+2}\}$ and $B_2 = \{y_1, y_2, \dots, y_{d+2}\}$ in \mathcal{T}_0 be such that $B_1 \prec B_2$. Let i be the greatest index such that $z_i < y_i$. For B_1 and B_2 to be both in \mathcal{T}_0 we then need $z_{i-1} = z_i - 1$ (otherwise $z_i - 1$ is an odd gap in B_1 , because $z_i + 1$ is an even gap in it) and $y_{i-1} = y_i - 1$ (if $y_i - 1$ was not in B_2 , then it would be an odd gap, because y_i is an even gap in B_1). This means that we can get B_1 “closer” to B_2 by removing from it the pair $\{z_i - 1, z_i\}$ and inserting the pair $\{z_i, z_i + 1\}$, which changes B_1 to a B_1' in \mathcal{T}_0 that shares a lower facet with B_1 , as in the first part of the proof. Repeating this process, we eventually move from B_1 to B_2 . \square

Remark 6.1.25. Let A be an arbitrary configuration and let \mathcal{T}_0 be an arbitrary triangulation. Can we generalize the above construction and define a partial order on the set of full-dimensional simplices of \mathcal{T}_0 via the covering property “ $B_1 \prec B_2$ if B_1 and B_2 share an upper facet of B_1 and a lower facet of B_2 ”, with respect to a certain projection direction? The answer is, in general, no: the transitive closure of that relation may produce cycles.

A sufficient condition for the relation to be acyclic is that the triangulation \mathcal{T}_0 be regular. (This is related to the fact that polytopal simplicial complexes are *shellable*.) But it was proved in [267, Corollary 2.16] that, for the canonical projections of cyclic polytopes, the relation is acyclic, even if the triangulation is not assumed to be regular.

Corollary 6.1.26. *The triangulations of $C(n, d)$ that appear as sections in \mathcal{T}_0 are in bijection to the lower ideals of the order \prec in \mathcal{T}_0 .*

Let us look a bit at this poset. As a first remark, it follows right away from formulas 6.12 and 6.13 that the poset is the same in the even and odd cases. Moreover,

Lemma 6.1.27. *(\mathcal{T}_0, \prec) is isomorphic, as a poset, as the following subset of \mathbb{N}^{k+1} with the coordinate-wise partial order:*

$$S := \{(p_0, \dots, p_k) : 0 \leq p_0 \leq p_1 \leq \dots \leq p_k \leq n - 2k - 1\}.$$

Proof. Assume, without loss of generality that k is even. Then the following transformations give poset isomorphisms:

$$\mathcal{T}_0 \rightarrow S$$

$$\{a_0, a_0 + 1, a_1, a_1 + 1, \dots, a_k, a_k + 1\} \mapsto (a_0 - 1, a_1 - 3, \dots, a_k - 2k - 1),$$

and

$$\begin{aligned} S &\rightarrow \mathcal{T}_0 \\ (p_0, \dots, p_k) &\mapsto (p_0 + 1, p_0 + 2, \dots, p_k + 2k + 1, p_k + 2k + 2). \end{aligned}$$

□

So, we only need to find a lower bound on the number of poset ideals in the number set S . One easy way to do this is to find a big subset of incomparable elements. If R is a set of N incomparable elements in S then S has at least 2^N different ideals, one for each subset of R : the ideal $I(R)$ associated to each subset $R \subset S$ is defined by the set R together with all the elements that are below some element of R . These ideals are all different because $I(R) \cap S = R$ for each of them. Hence, the following finishes the proof of Theorem 6.1.22:

Theorem 6.1.28. *For fixed k , S has at least $\Omega(n^k)$ incomparable elements.*

Proof. Consider the subset

$$R := \{(p_0, \dots, p_k) \in S : \sum p_i = n - 2k - 1\} \subset S.$$

The condition that the sum of coordinates is constant in all vectors of R guarantees that its elements are incomparable. To develop a lower bound on the size of R , think of each vector in it as the exponent vector of a monomial of degree $n - 2k - 1$ in $k + 1$ variables. The total number of such monomials is well known to be $\binom{(n-2k-1)+k}{k} = \binom{n-k-1}{k}$.

Not every monomial gives an element in R ; only those in which the exponent vector satisfies $p_0 \leq p_1 \leq \dots \leq p_k$. But from every such monomial, we can get one in R by permuting its entries. This implies that R has at least as many elements as the total number of monomials divided by the number of permutations of $k + 1$ coordinates. That is to say:

$$|R| \geq \frac{1}{(k+1)!} \binom{n-k-1}{k} \geq \frac{n-2^{k^k}}{k!(k+1)!} \in \Omega(n^k).$$

□

Remark 6.1.29. The constant inside the $\Omega(n^k)$ in our proof is basically $\frac{1}{k!k!}$. One of the $k!$ can be removed with some work: It can be shown that if instead of putting $\sum p_i = n - 2k - 1$ in the definition of R we put $\sum p_i = (n - 2k - 1)(k + 1)/2$ (that is, half of the maximum it can be) then the bound gets multiplied by (essentially) the normalized volume of the middle hypersimplex $\mathbf{D}(k + 1, (k + 1)/2)$. This volume is (essentially) $k!$.

6.2 Products of two simplices

The *product of two simplices* is a particularly important point configuration. The study of its triangulations has connections to algebraic geometry (Segre varieties, tropical polytopes, flag varieties), optimization and game theory (transportation problems and n -person games), etc. See [282, 27, 104, 312, 15, 16, 97, 292]. Also, the product of two simplices is the natural building block for constructing triangulations of products of two polytopes. This is done, for example, in [154, 246] for triangulations of cubes, and in [278] to construct configurations with disconnected graphs of flips (see Chapter 7). Note also that the ubiquitous examples of Schönhardt's non-triangulable polyhedron (Example 3.6.1) and the planar mother of all examples (Example 2.2.5) are derived from the product of a triangle and a segment. We start by looking at the simplest case, the product of a simplex and a segment. Then we will look at the general case.

6.2.1 The prism over a simplex

In this section we are concerned with triangulations of prisms over a simplex. In dimension three, this is the ordinary triangular prism. In dimension two, it is a square.

Although we do not really use an explicit coordinatization, favoring a more combinatorial approach, the natural coordinatization to highlight the symmetry of this configuration (at the expense of using one more coordinate than needed) is the following one.

Definition 6.2.1. We call *n -th standard simplex* the configuration whose elements are the vertices of the standard simplex of dimension $n - 1$; that is, the following point configuration:

$$\mathbf{D}_n := \begin{pmatrix} 1 & 2 & \dots & n \\ 1 & 0 & \dots & 0 \\ 0 & 1 & \dots & 0 \\ \vdots & \vdots & \ddots & \vdots \\ 0 & 0 & \dots & 1 \end{pmatrix}.$$

In Definition 4.2.9 the prism over a point configuration was defined. In our concrete case, the prism over \mathbf{D}_n is an n -dimensional point configuration, which we represent by the following labeled $((n+2) \times 2n)$ -matrix:

$$\text{prism}(\mathbf{D}_n) = \mathbf{D}_n \times \mathbf{D}_2 = \begin{pmatrix} a_1 & a_2 & \dots & a_n & b_1 & b_2 & \dots & b_n \\ 1 & 0 & \dots & 0 & 1 & 0 & \dots & 0 \\ 0 & 1 & \dots & 0 & 0 & 1 & \dots & 0 \\ \vdots & \vdots & \ddots & \vdots & \vdots & \vdots & \ddots & \vdots \\ 0 & 0 & \dots & 1 & 0 & 0 & \dots & 1 \\ 1 & 1 & \dots & 1 & 0 & 0 & \dots & 0 \\ 0 & 0 & \dots & 0 & 1 & 1 & \dots & 1 \end{pmatrix}.$$

This polytope has $2n$ vertices, dimension n and it has $n + 2$ facets: the two embedded copies of \mathbf{D}_n , which we call the *top base* (labeled by the a 's)

and *bottom base* (labeled by the b 's), and n products of the form $\mathbf{D}_{n-1} \times \mathbf{D}_2$, which we call *vertical facets*.

The investigation of triangulations of these point configurations will be extended in Section 6.2, where we study products of two arbitrary simplices. This point configuration is actually also an instance of a *Cayley embedding* (as are all products of simplices), studied in Section 9.2. Triangulations of prisms over simplices have also been studied in [140, Section 7.3.C].

Figure 6.12 shows the familiar triangular prism, which is $\mathbf{D}_3 \times \mathbf{D}_2$.

Lemma 6.2.2. *A set of $n+1$ points of $\text{prism}(\mathbf{D}_n)$ is an affine basis if and only if it contains at least one from each pair $\{a_i, b_i\}$. Equivalently, if it contains only one such pair.*

Proof. The “only if” comes from the fact that every two pairs a_i, b_i, a_j and b_j form a quadrilateral face of $\text{prism}(\mathbf{D}_n)$. The “if” direction is easy by induction on n . \square

This statement tells us a lot about the structure of every triangulation of $\text{prism}(\mathbf{D}_n)$. Indeed, every basis B that we can use as a maximal simplex has n “vertical” facets (contained in the vertical facets of $\text{prism}(\mathbf{D}_n)$), which are not incident to any other maximal simplex of the triangulation. We can call the other two facets of B , opposite to the points a_i and b_i in the statement of Lemma 6.2.2, the *top and bottom facets* of B . As a consequence, every triangulation of $\text{prism}(\mathbf{D}_n)$ is a linearly ordered “sequence of bases”. Starting with a basis containing the top base of $\text{prism}(\mathbf{D}_n)$ and ending with one containing the bottom base of $\text{prism}(\mathbf{D}_n)$, where the bottom facet of each simplex coincides with the top of the next one. Moreover, at each step in the sequence the new affine basis contains one more element from the bottom base, so that the triangulation in total consists of n such bases.

As an example, consider the following triangulation of the triangular prism, depicted in Figure 6.13:

$$\{a_1, b_1, b_2, b_3\}, \{a_1, a_2, b_2, b_3\}, \{a_1, a_2, a_3, b_3\},$$

This gives the following bijection between triangulations of $\text{prism}(\mathbf{D}_n)$ and reorderings (that is, permutations) of the set $\{1, \dots, n\}$:

Proposition 6.2.3. (i) *Let $\sigma = (i_1, \dots, i_n)$ be a permutation of the numbers $1, \dots, n$. Then, the following n simplices form a triangulation of $\text{prism}(\mathbf{D}_n)$:*

$$\mathcal{T}_\sigma = \left\{ \{a_{i_1}, \dots, a_{i_k}, b_{i_k}, \dots, b_{i_n}\} : k = 1, \dots, n \right\}.$$

(ii) *All the triangulations of $\text{prism}(\mathbf{D}_n)$ have this form. In particular, they are all equivalent to one another by affine symmetries.*

(iii) *Two triangulations of $\text{prism}(\mathbf{D}_n)$ differ by a flip if and only if the corresponding permutations differ by the exchange (i.e., a transposition) of a pair of consecutive elements.*

In particular, $\text{prism}(\mathbf{D}_n)$ has exactly $n!$ triangulations.

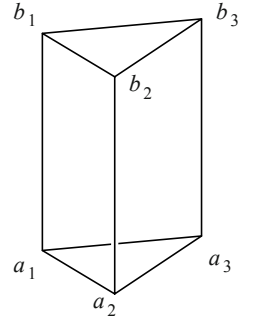


Figure 6.12: The triangular prism
 $\text{prism}(\mathbf{D}_3) = \mathbf{D}_3 \times \mathbf{D}_2$.

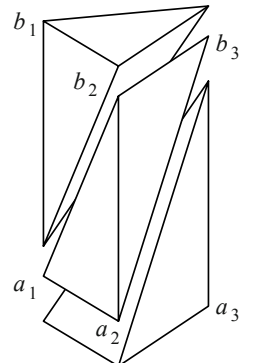


Figure 6.13: A triangulation of $\text{prism}(\mathbf{D}_3)$.

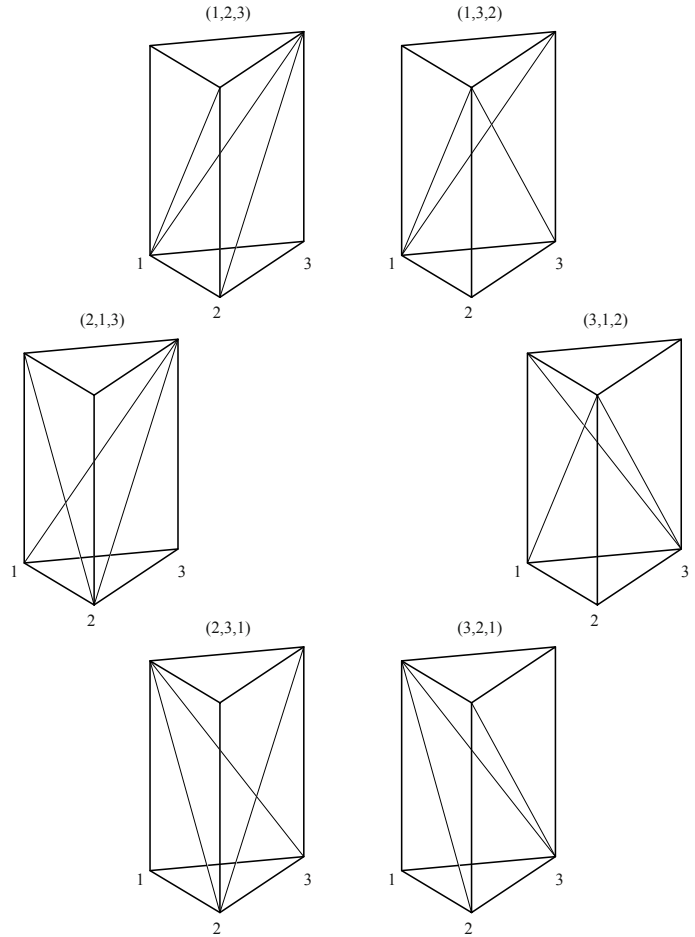


Figure 6.14: The six triangulations of prism(\mathbf{D}_4).

The secondary polytope is a hexagon.

Proof. We start with Part (ii) of the statement. Let \mathcal{T} be a triangulation of prism(\mathbf{D}_n). Let $B_1 \in \mathcal{T}$ be the only maximal simplex incident to the top base, and let $a_{i_1} \in B_1$ be the vertex opposite to the top base in B_1 .

The only facet of B_1 which is interior to the polytope is the bottom one. It must, by (MaxIFP), be the top facet of a second simplex B_2 , obtained by deleting b_1 from B_1 and inserting a second bottom vertex a_{i_2} .

Again, the bottom face of B_2 must be contained in another simplex B_3 containing a third bottom vertex a_{i_3} , and so on and so forth. The vertex set of the k -th simplex B_k in this process will be $\{a_{i_1}, \dots, a_{i_k}, b_{i_k}, \dots, b_{i_n}\}$. This proves Part (ii). Part (i) is proved with essentially the same arguments.

We now prove Part (iii). Any pair of adjacent simplices in a triangulation \mathcal{T} have the form

$$B_k = \{a_{i_1}, \dots, a_{i_k}, b_{i_k}, \dots, b_{i_n}\}$$

and

$$B_{k+1} = \{a_{i_1}, \dots, a_{i_{k+1}}, b_{i_{k+1}}, \dots, b_{i_n}\}.$$

The positive triangulation of the circuit involved is

$$\{a_{i_k}, b_{i_k}, b_{i_{k+1}}\}, \{a_{i_k}, a_{i_{k+1}}, b_{i_{k+1}}\}.$$

No other simplex in \mathcal{T} contains any of these two triangles, which implies that a flip on this circuit exists. Hence, \mathcal{T} has n flips, as claimed. Since the circuit affects only the k -th and $(k+1)$ -th simplices, it can affect only the k -th and $(k+1)$ -th elements in the permutation corresponding to \mathcal{T} . Hence, it produces a transposition of those two elements. \square

Remark 6.2.4. Since all the triangulations of $\text{prism}(\mathbf{D}_n)$ are affinely equivalent, they all have to be “pushing” and “pulling” triangulations, at the same time. The procedure in the previous proof actually associates to the permutation (i_1, \dots, i_n) the triangulation obtained by starting with the simplex $\{b_{i_1}, \dots, b_{i_n}, a_{i_1}\}$ and then “placing” the points $\{a_{i_2}, \dots, a_{i_n}\}$ in this order (i.e., the one obtained pushing these $n-1$ points in the reversed order). But it is also the triangulation obtained pushing $\{b_{i_1}, \dots, a_{i_{n-1}}\}$ in this order, or pulling $\{a_{i_1}, \dots, a_{i_{n-1}}\}$, or pulling $\{b_{i_n}, \dots, a_{i_2}\}$, etc.

We now wonder what the *secondary polytope* of $\text{prism}(\mathbf{D}_n)$ looks like. Of course, we know it will have $n!$ vertices and dimension $n-1$. For $n=3$ it is a hexagon, as Figure 6.14 shows. For the sake of simplicity, in this figure we have labeled the vertical edges of the prisms (as 1, 2, and 3) instead of the vertices. Above each triangulation, the figure shows the permutation corresponding to it. An easy way to get the triangulation from the permutation (or vice versa) is observing that the diagonal in the rectangle delimited by the vertical edges i and j will go from the bottom end of i to the top end of j if and only if i comes before j in the permutation.

The following observation will allow us to explicitly give coordinates for the vertices of the secondary polytope of $\text{prism}(\mathbf{D}_n)$:

Lemma 6.2.5. *All the bases of $\text{prism}(\mathbf{D}_n)$ span simplices with the same volume.*

Polytopes with this property (all the bases have the same volume) are called *unimodular* (see Definition 6.2.10). They play a very fundamental role within *lattice polytopes* (i.e., polytopes with integer vertices), which are studied in Section 9.3, and in the relations to algebraic geometry (Sections 1.3 and 9.4).

Proof. We will use induction on n . In the case $n=1$, our configuration is the two end-points of a segment, and the statement is true.

Let F be a vertical facet of $\text{prism}(\mathbf{D}_n)$, which is affinely isomorphic to $\text{prism}(\mathbf{D}_{n-1})$. By inductive hypothesis, all the bases of F have the same $(n-1)$ -dimensional volume. Moreover, the two elements a_i and b_i opposite to F have the same distance to the hyperplane containing F . Hence, any two bases having a facet in the same vertical facet of $\text{prism}(\mathbf{D}_n)$ have the same volume.

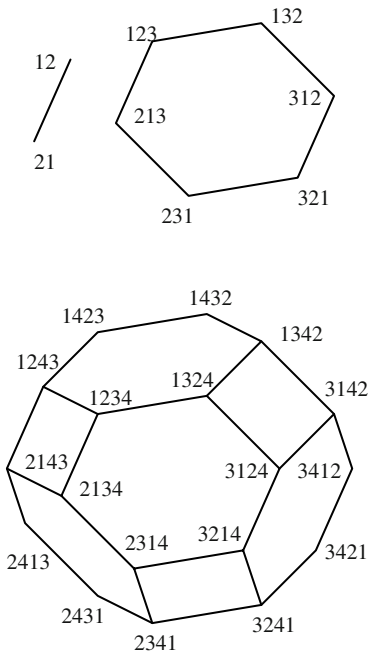


Figure 6.15: The permutohedra of dimensions 1, 2 and 3.

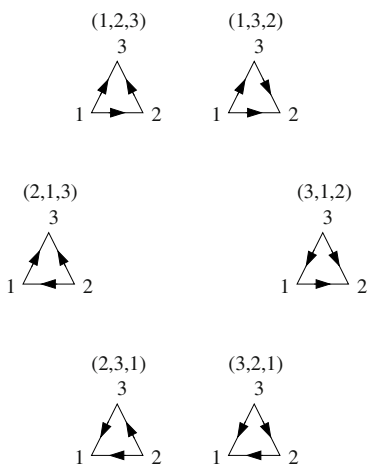


Figure 6.16: The six acyclic orientations of the complete graph K_3 represent the six triangulations of the triangular prism $\text{prism}(\mathbf{D}_3)$.

Compare with Figure 6.14.

But it turns out that every two bases have this property, because $n > 1$ and every full-dimensional simplex has vertical facets in all but one of the n vertical facets of $\text{prism}(\mathbf{D}_n)$. \square

The *permutohedron* appearing in the following theorem is a classical polytope, described, for example, in the very first pages of [339, Chapter 0] (see also [27]). Figure 6.15 shows examples of dimension 1, 2 and 3. Observe that the faces of a permutohedron are products of lower dimensional permutohedra. For example, the central hexagon in the 3-dimensional permutohedron of Figure 6.15 is the product of a 2-dimensional permutohedron on the label set $\{1, 2, 3\}$ and a 0-dimensional permutohedron on the label set $\{4\}$.

Theorem 6.2.6. *The secondary polytope of $\text{prism}(\mathbf{D}_n)$ is affinely isomorphic to the $(n-1)$ -dimensional permutohedron, i.e., the convex hull of the $n!$ points (i_1, \dots, i_n) whose coordinates are a permutation of $\{1, 2, \dots, n\}$.*

Proof. Let \mathbf{T} be one of the triangulations of $\text{prism}(\mathbf{D}_n)$, corresponding to a permutation $\sigma = (i_1, \dots, i_n)$ of $\{1, \dots, n\}$. Let $\phi_{\text{prism}(\mathbf{D}_n)}(\mathcal{T})$ be the GKZ-vector of \mathcal{T} , i.e., the vertex of the secondary polytope corresponding to \mathcal{T} . Let $\phi_{\text{prism}(\mathbf{D}_n)}(\mathcal{T})_p$ denote the coordinate of $\phi_{\text{prism}(\mathbf{D}_n)}(\mathcal{T})$ corresponding to a certain vertex labeled by p of $\text{prism}(\mathbf{D}_n)$.

Proposition 6.2.3 implies that

$$\phi_{\text{prism}(\mathbf{D}_n)}(\mathcal{T})_{a_i} = n + 1 - \phi_{\text{prism}(\mathbf{D}_n)}(\mathcal{T})_{b_i}, \quad \forall i = 1, \dots, n.$$

Since this is valid for all the triangulations, the projection of the secondary polytope to the n coordinates corresponding to the elements b_1, \dots, b_n does not decrease the dimension of the polytope, hence it gives an affinely equivalent polytope.

Now, from Proposition 6.2.3 we also conclude that the vertex b_{i_k} lies exactly in k simplices of \mathcal{T} . Hence, the restriction of $\phi_{\text{prism}(\mathbf{D}_n)}(\mathcal{T})$ to the coordinates b_1, \dots, b_n is the permutation of $\{1, \dots, n\}$ inverse to σ . \square

We finish this section with a reinterpretation of Proposition 6.2.3 which will be extremely useful in Chapter 7. It is based in the observation that the permutations of the n symbols $\{1, \dots, n\}$ can be represented as *acyclic orientations* of the complete graph K_n . Indeed, any permutation specifies an order on the vertices of K_n and hence a direction for its edges. Conversely, any orientation of the edges without cycles corresponds (uniquely, because the graph is complete) to an ordering.

In this sense, Figure 6.16 can be thought of as a more compact version of Figure 6.14. To visualize the triangulation of the prism corresponding to one of the six triangles of Figure 6.16, the reader just needs to imagine a prism sitting on the triangle, and think of the arrows as diagonals on the square faces of the prism, always pointing upwards. Flips appear in the figure as edges whose reversal does not produce a cycle, of which each triangulation has two.

Summing up:

Corollary 6.2.7. *Triangulations of prism(\mathbf{D}_n) are in bijection with acyclic orientations of the complete graph K_n . Flips in a triangulation correspond to the reversal of a single edge.*

6.2.2 The product of simplices

We come now to the general case of a product of two arbitrary simplices. This is the polytope $\mathbf{D}_n \times \mathbf{D}_m$. It has nm vertices and dimension $n+m-2$.

The following list summarizes the main results that we are going to encounter. The list may also give the reader a clue of how close or how far this case is from the one we have just left:

- $\mathbf{D}_n \times \mathbf{D}_m$ is still a unimodular polytope. In particular, all its triangulations have the same number of simplices, namely $\binom{n+m-2}{n-1}$.
- In contrast to $\mathbf{D}_n \times \mathbf{D}_2$, for any values $n, m > 2$, the polytope $\mathbf{D}_n \times \mathbf{D}_m$ has more than one symmetry class of triangulations.
- There is a particular symmetry class of triangulations of $\mathbf{D}_n \times \mathbf{D}_m$ whose representatives are associated with pairs of permutations of the elements of \mathbf{D}_n and of \mathbf{D}_m . This class contains $\frac{n!m!}{2}$ triangulations, because reversing both permutations leaves the triangulation unchanged.
- The only values of $n, m > 2$ for which all the triangulations of $\mathbf{D}_n \times \mathbf{D}_m$ are regular are $(3, 3)$, $(3, 4)$, $(3, 5)$, $(4, 3)$ and $(5, 3)$.

If $\mathbf{p}_1, \dots, \mathbf{p}_n$ and $\mathbf{q}_1, \dots, \mathbf{q}_m$ are the vertices of \mathbf{D}_m and \mathbf{D}_n respectively, then $\mathbf{D}_n \times \mathbf{D}_m$ has the nm vertices $(\mathbf{p}_i, \mathbf{q}_j)$, $i = 1, \dots, n$, $j = 1, \dots, m$. There are two nice ways of graphically representing this configuration:

The grid representation. The elements are represented as a grid with n columns, corresponding to the vertices of \mathbf{D}_n and m rows, corresponding to those of \mathbf{D}_m . See Figure 6.17 for the case $n = 6, m = 4$.

Each vertex of the product appears as the checker box in the intersection of the corresponding row and column. More generally, faces of the product correspond to the different minors, or sub-grids, that one can obtain by deleting some rows and/or columns. In particular, there are m “horizontal” facets obtained deleting a single row and n “vertical” facets obtained by deleting a single column.

To represent a subset of $\mathbf{D}_n \times \mathbf{D}_m$ we will mark with dots the corresponding boxes in the grid. For example, Figure 6.13 represents the three tetrahedra of the triangulation of $\mathbf{D}_3 \times \mathbf{D}_2$ displayed in Figure 6.13.

We will normally label the elements of \mathbf{D}_n and \mathbf{D}_m as $\{1, \dots, n\}$ and $\{1, \dots, m\}$ respectively. But sometimes we will use letters instead of numbers for one of the two sets. This is done for example in Figures 6.18 and 6.20, in order to keep the notation closer to the one used for prism(\mathbf{D}_n) in the previous section.

The bipartite graph representation. Now, the elements of $\mathbf{D}_n \times \mathbf{D}_m$ appear as the edges in the complete bipartite graph $K_{n,m}$. The two parts of nodes

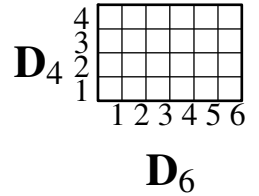


Figure 6.17: A grid representing $\mathbf{D}_6 \times \mathbf{D}_4$.

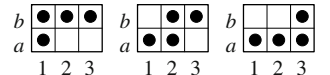


Figure 6.18: The same triangulation as in Figure 6.13, shown in a grid representation of $\mathbf{D}_3 \times \mathbf{D}_2$.

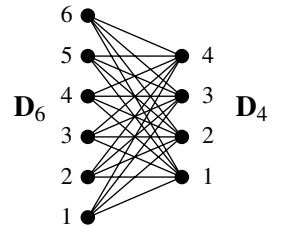


Figure 6.19: The bipartite graph $K_{6,4}$ representing the vertex set of $\mathbf{D}_6 \times \mathbf{D}_4$.

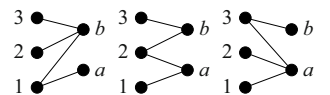
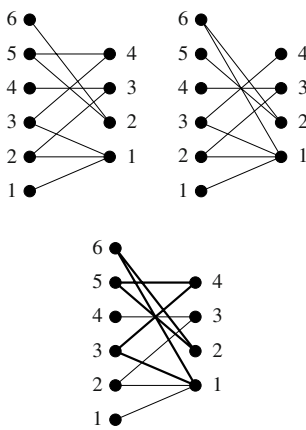


Figure 6.20: The same triangulation as in Figures 6.13 and 6.18, in a bipartite graph representation of $\mathbf{D}_3 \times \mathbf{D}_2$.

Figure 6.21: Two spanning trees in $K_{6,4}$,

representing two bases (full-dimensional simplices) in $\mathbf{D}_6 \times \mathbf{D}_4$ (above). The simplices differ only in one vertex and, hence, their union

contains a unique circuit, with positive and negative sides $(6, 2), (5, 4), (3, 1)$ and $(5, 2), (3, 4), (6, 1)$ (below). Since the edges missing from the circuit in one and the other are at distance three (odd) in the circuit, the two simplices lie in opposite sides of their common face.

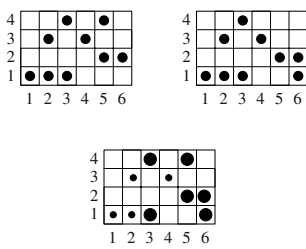


Figure 6.22: The same simplices and circuit of Figure 6.21, now in a grid representation. In the bottom grid, big dots represent the vertices involved in the circuit.

represent \mathbf{D}_n and \mathbf{D}_m , respectively. Faces of $\mathbf{D}_n \times \mathbf{D}_m$ are in bijection with induced subgraphs. In particular, the facets are the $n+m$ subgraphs obtained by deleting a single vertex in $K_{n,m}$. Figures 6.19 and 6.20 represent exactly the same graph as Figures 6.17 and 6.18.

Lemma 6.2.8. *In the bipartite graph representation:*

- (1) *A subset of $\mathbf{D}_n \times \mathbf{D}_m$ is affinely independent if and only if the corresponding subgraph has no cycles (i.e., it is a forest). In particular, affine bases correspond to spanning trees.*
- (2) *A subset of $\mathbf{D}_n \times \mathbf{D}_m$ is affinely spanning if and only if the corresponding subgraph is connected and spanning.*
- (3) *A subset of $\mathbf{D}_n \times \mathbf{D}_m$ is a circuit if and only if the corresponding subgraph is a cycle. The positive and negative elements of the circuit alternate along the cycle. In other words, two edges of the cycle have the same sign as elements in the circuit if and only if they are an even number of steps away from each other.*

Proof. Let G be a subgraph of $K_{n,m}$, and let C be the corresponding subset of elements of $\mathbf{D}_n \times \mathbf{D}_m$.

That a subgraph without cycles corresponds to an independent set of vertices is easy to establish by induction on the size (number of edges) of G : a graph without cycles must have some node of degree one. The induced subgraph of $K_{n,m}$ obtained by deleting this node corresponds to a facet of $\mathbf{D}_n \times \mathbf{D}_m$ which contains all but one of the points of C . By inductive hypothesis, C intersected with this facet is an independent set, which implies that C itself is independent. This proves one direction of Part (1).

The converse can be rephrased as: Any cycle in $K_{n,m}$ corresponds to an affinely dependent set. This is true because if we take the vertices of $\mathbf{D}_n \times \mathbf{D}_m$ corresponding to the cycle and give alternately coefficients +1 and -1 we get an affine dependence: for each node p_i involved in the cycle we will have a summand $+(p_i, *)$ and another $-(p_i, *)$, and for each q_j we will have a $+(*, q_j)$ and a $-(*, q_j)$, so that everything cancels out. This finishes the proof of part (1).

Parts (2) and (3) are easy consequences of Part (1). For Part (2), observe that a subset is affinely spanning if and only if it contains an affine basis (i.e., a full-dimensional simplex), and that a subgraph is connected and spanning if and only if it contains a spanning tree.

For Part (3), remember that circuits are the minimal dependent sets. That is, a circuit corresponds to a graph containing a cycle in which the removal of any edge gives a graph without cycles. This is only possible for a graph which is itself a cycle. \square

Lemma 6.2.9. *A subset of the grid corresponds to a spanning subset of $\mathbf{D}_n \times \mathbf{D}_m$ if and only if it meets all rows and columns of the grid.*

In particular, bases are the subsets of cardinality $n+m-1$ meeting every row and column.

Proof. By Lemma 6.2.8, a subset is spanning if and only if, in the bipartite graph representation, it gives a connected and spanning subgraph, i.e., a subgraph meeting every vertex of the graph. Vertices of the graph correspond to rows and columns of the grid. \square

One can also try to express the properties of being a circuit or an independent set in the grid representation, but it is difficult to find a description easier to state than the following: A circuit (respectively, an independent set) in the grid representation is a subset of boxes whose corresponding graph in the bipartite graph representation is a cycle (respectively, has no cycles).

We now explain a very important and useful property enjoyed by the product of two simplices.

Definition 6.2.10. We say that a point or vector configuration is a *unimodular configuration* if all full-dimensional simplices spanned by it have the same volume.

For an example of a configuration that is not unimodular consider the regular 3-dimensional cube, which has at least two simplices of volume $2/6$ while the rest have volume $1/6$. One example of unimodular configuration is the product of two simplices. This property is similar to that of Lemma 6.2.5 for the prism over a simplex.

Proposition 6.2.11. *The product of two simplices is unimodular.*

Proof. The product structure of $\mathbf{D}_n \times \mathbf{D}_m$ has as a consequence that for any facet of it, all the vertices not contained in that facet are at the same distance from the hyperplane containing the facet. As in Lemma 6.2.5 this together with inductive hypothesis implies that any two bases with facets contained in a common facet of $\mathbf{D}_n \times \mathbf{D}_m$ have the same volume. Unfortunately, it is not true that every pair of simplices have this property.

But we will prove the following weaker property, which is enough for our purposes: If $n, m > 2$ (the case $n = 2$ or $m = 2$ was proved in Lemma 6.2.5) then for any pair of bases B_1 and B_2 we can find a third basis B_3 which has a facet contained in the same facet of $\mathbf{D}_n \times \mathbf{D}_m$ as some facet of B_1 , and a facet contained in the same facet of $\mathbf{D}_n \times \mathbf{D}_m$ as some facet of B_2 .

Indeed, let us represent B_1 and B_2 as spanning trees of $K_{n,m}$, and consider a leaf (node of degree one) in each of the spanning trees. Our claim boils down to saying that there is a third spanning subgraph of $K_{n,m}$ which has degree one on both nodes. This is trivial: After removing these two nodes we still have two non-empty parts, and we can consider a spanning subgraph of their complete bipartite graph. Adding two edges, one incident to each of the nodes in question, we have the spanning subgraph we are looking for. \square

6.2.3 Staircase triangulations

Proposition 6.2.11 implies that all triangulations of $\mathbf{D}_n \times \mathbf{D}_m$ have the same number of simplices. To compute this number, we are going to explicitly construct one triangulation. The grid representation comes, especially handy for this.

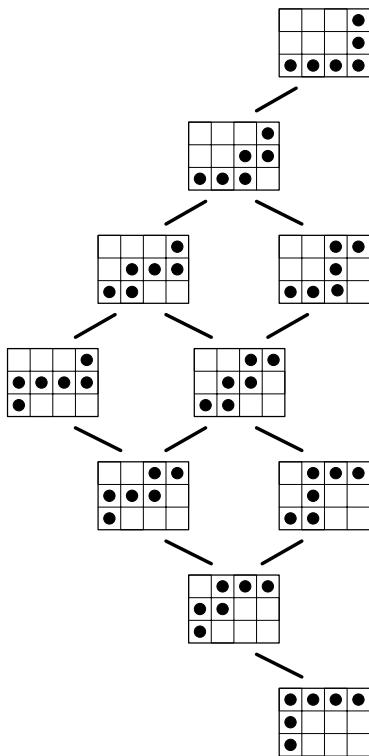


Figure 6.23: The ten staircases in the grid of size 4×3 . They form a triangulation of $\mathbf{D}_4 \times \mathbf{D}_3$. Adjacent grids in the picture represent adjacent simplices in the triangulation.

Definition 6.2.12. A *monotone staircase* in the grid of size $n \times m$ is a subset of $n + m - 1$ boxes, beginning with $(1, 1)$ and ending with (n, m) , such that each one is immediately above or to the right of the previous one.

It is easy to prove that there are exactly $\binom{n+m-2}{n-1}$ monotone staircases in the grid; for example, by induction on $n + m$: each monotone staircase either extends a staircase in the grid of size $n \times (m - 1)$, ending with $(n, m - 1)$ or one in the grid of size $(n - 1) \times m$, and not both. By inductive hypothesis the numbers of such staircases are $\binom{n+m-3}{n-2}$ and $\binom{n+m-3}{n-2}$, whose sum equals $\binom{n+m-2}{n-1}$.

Theorem 6.2.13. All the monotone staircases correspond to full-dimensional simplices in $\mathbf{D}_n \times \mathbf{D}_m$. The set of all monotone staircases is a triangulation of the polytope.

In particular, all triangulations of $\mathbf{D}_n \times \mathbf{D}_m$ have size $\binom{n+m-2}{n-1}$.

Proof. A monotone staircase has exactly $n + m - 1$ elements, and it goes through every row and column. Hence, it is indeed a full-dimensional simplex, by Lemma 6.2.9. It is a good exercise for the reader to explicitly check that staircases correspond to independent sets.

To prove that staircases form a triangulation, we will use one of the characterizations of triangulations from Corollary 4.5.20, via the Properties (ICoP) and (GFP). Translated to our language, these properties say:

(ICoP) For any staircase, and for any box of it, the removal of that box either gives a subset lying in a facet of $\mathbf{D}_n \times \mathbf{D}_m$, or there is another box that can be added in order to obtain another staircase. If the latter happens, the two staircases represent full-dimensional simplices in opposite sides of their common facet.

(GFP) There is a row or column of the grid (i.e., a facet of $\mathbf{D}_n \times \mathbf{D}_m$) such that the staircases containing a single element in it form a triangulation of the corresponding facet of $\mathbf{D}_n \times \mathbf{D}_m$ without repetition (that is, there are no two staircases in this list that differ only on the element of that row or column).

Property (GFP) is easy, by induction on $n + m$. Removing one row or column from the grid, every staircase can be restricted to a staircase and, conversely, every staircase of the restricted grid can be extended to one in the original grid. By inductive hypothesis, the set of all the staircases on this subgrid form a triangulation of the facet.

For (ICoP), we consider the several cases that removal of an element in a staircase can produce. Let B be a subset of $\mathbf{D}_n \times \mathbf{D}_m$ that is a staircase in the grid, and let (i, j) be an element that we remove from it. If (i, j) is the only element of B in the row or column we remove, then $B \setminus (i, j)$ is contained in a facet of $\mathbf{D}_n \times \mathbf{D}_m$. If neither of the two cases happens, that is, if there are two elements (i, j') and (i', j) in B with $i \neq i'$ and $j \neq j'$, then assume without loss of generality that $i' > i$. In order for B to be a staircase, it is then necessary that $j' < j$, and that all the elements $(i, j), (i+1, j), \dots, (i', j)$

are in B , as well as the elements (i, j') , $(i, j' + 1)$, \dots , (i, j) . In particular, replacing (i, j) by $(i + 1, j - 1)$ in B is still a staircase.

It only remains to be proved that the two staircases represent simplices lying in opposite sides of their common facets. The way to prove this is to identify the unique circuit contained in the union of the two simplices, and check that the two elements in which the simplices differ have the same sign in this circuit.

The circuit in question is $(\{(i, j), (i + 1, j - 1)\}, \{(i, j - 1), (j, i + 1)\})$, and, indeed, the two elements lying in only one of the two simplices are (i, j) and $(i + 1, j - 1)$, which have the same sign in the circuit. \square

Definition 6.2.14. The triangulation obtained in this way is called the *staircase triangulation* of the product of two simplices.

That the staircase triangulation is a triangulation admits a shorter proof, by induction. We now show that proof, which also shows that this triangulation is lexicographic:

Proposition 6.2.15. *The staircase triangulation of $\mathbf{D}_n \times \mathbf{D}_m$ is the pulling triangulation with respect to any ordering of the boxes in the grid that extends the partial order*

$$(i, j) < (i', j') \Leftrightarrow i < i' \text{ and } j < j'.$$

Proof. By the description in Lemma 4.3.6, the pulling triangulation is characterized as being the unique triangulation that is pulling when restricted to every facet of the configuration that does not contain the last point in the ordering. That this holds for the staircase triangulation is obvious. If we remove the last element (n, m) from each staircase, we obtain either a staircase in the $(n - 1) \times m$ subgrid or a staircase in the $n \times (m - 1)$ subgrid. These subgrids represent the two facets of $\mathbf{D}_n \times \mathbf{D}_m$ not containing that element. \square

It has to be noted that the staircase triangulation depends on the order chosen to represent the elements of \mathbf{D}_n as columns and the elements of \mathbf{D}_m as rows in the grid. In other words, there is a staircase triangulation associated to each pair of permutations, one of the numbers $(1, \dots, n)$ and one of the numbers $(1, \dots, m)$.

Proposition 6.2.16. *Two pairs of permutations produce the same staircase triangulation if and only if one is obtained from the other by reversing both permutations. In particular, $\mathbf{D}_n \times \mathbf{D}_m$ has exactly $n!m!/2$ staircase triangulations.*

In this statement, when we say *reversing a permutation* we mean that the permutation is read backwards. This is not the same as the *inverse* of the permutation, considered as a map. (For example, the identity permutation $(1, 2, \dots, n)$ is its own inverse; but its reversal is $(n, \dots, 2, 1)$.)

Proof. Reversing both permutations just rotates staircases 180 degrees, giving new staircases. Hence the old and the new staircase triangulation are the same.

Suppose now that we have two different pairs (σ_1, τ_1) and (σ_2, τ_2) of permutations. The σ 's are permutations of $(1, \dots, n)$ and the τ 's are permutations of $(1, \dots, m)$. We assume that the pairs are different and not obtained one from the other by reversing both permutations.

Two permutations are the same if and only if they produce the same relative order in every pair of indices, and they are opposite if they produce opposite relative orders in every pair of indices. Then our hypothesis is that there is a pair of indices $i, j \in \{1, \dots, n\}$ which appear in the same relative order in σ_1 and σ_2 and a pair of indices $k, l \in \{1, \dots, m\}$ which appear in the opposite relative order in τ_1 and τ_2 , or vice versa. We assume the first, without loss of generality. We further assume that i comes before j in σ_1 and k comes before l in τ_1 .

In the triangulation corresponding to (σ_1, τ_1) , the triangles given by the edges $\{(i, k), (j, k), (j, l)\}$ and $\{(i, k), (i, l), (j, l)\}$ appear, while the “opposite” pair of triangles of the same 2×2 subgrid appear in the triangulation of (σ_2, τ_2) . \square

Remark 6.2.17 (Staircase triangulations of products of more than two simplices). The product of three or more simplices (often called a *simplotope*) is slightly less well-behaved than the product of two. To start with, it is not unimodular anymore as the three dimensional cube (the product of three segments) shows. See Section 6.3.4. However, staircase triangulations still exist and have most of the same properties as in the case of two factors. Let us comment on the case of three factors, the general case being similar.

The nml vertices of the product $\mathbf{D}_n \times \mathbf{D}_m \times \mathbf{D}_l$ of three simplices can be represented as the boxes in the $n \times m \times l$ three-dimensional grid. A monotone staircase in this grid is any set of $n+m+l-2$ boxes, starting with the box $(1, 1, 1)$ and ending with the box (n, m, l) , with the property that each box has one, and only one, coordinate increased by one with respect to the previous box. Clearly, there are $(n+m+l-3)!/(n-1)!(m-1)!(l-1)!$ such staircases in the grid. With much the same ideas as in the case of two factors, one can prove that:

Theorem 6.2.18. *The following statements hold:*

1. *Monotone staircases form an affine basis in $\mathbf{D}_n \times \mathbf{D}_m \times \mathbf{D}_l$.*
2. *The simplices spanned by monotone staircases are all unimodular.*
3. *The family of all monotone staircases is a triangulation of $\mathbf{D}_n \times \mathbf{D}_m \times \mathbf{D}_l$.*
4. *In fact, the monotone staircases form the pulling triangulation with respect to any linear ordering of the boxes that extends the partial ordering given by coordinate-wise comparison of labels of boxes.*

6.2.4 Non-regular triangulations of products of simplices

Observe that in the case $n = 2$, Proposition 6.2.16 gives $m!$ staircase triangulations. This agrees with the results of the previous section, where we

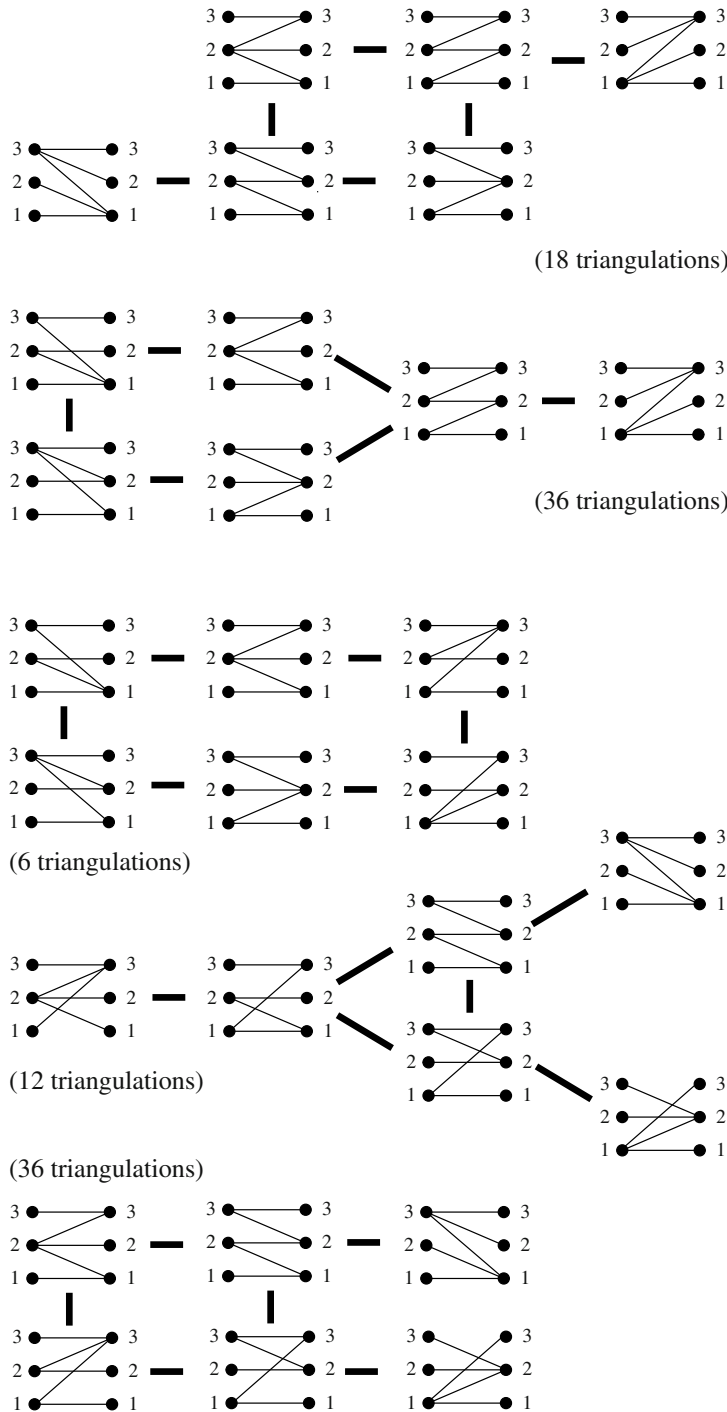


Figure 6.24: Representatives for all the triangulations of $D_3 \times D_3$, modulo the symmetries of the polytope. Next to each representative, the number of triangulations equivalent to this one is shown.

saw that $\mathbf{D}_2 \times \mathbf{D}_m$ has $m!$ triangulations, all affinely equivalent (hence they all staircase). For $n, m > 2$ the same is not true. To prove it, we only need to consider the case $n = m = 3$. If we find non-staircase triangulations for these parameters, then we can build triangulations for any other parameters starting with a non-staircase triangulation of a face isomorphic to $\mathbf{D}_3 \times \mathbf{D}_3$ and then *placing* the rest of points. The resulting triangulations will be non-staircase because, as shown in the proof of Lemma 6.2.8, restricting staircase triangulations to faces gives staircase triangulations.

We can actually give a complete list of triangulations of $\mathbf{D}_3 \times \mathbf{D}_3$. They are shown in Figure 6.24, in the bipartite graph representation. We only show a representative of each symmetry class, and there are 5 symmetry classes. The one on top is the staircase triangulation, and has 18 representatives, as stated in Proposition 6.2.16.

The symmetry classes do not all have the same number of elements. They have respectively, 18, 36, 6, 12, and 36, giving a total of 108 triangulations. The same figure, in a grid representation, appears in [140, page 250]. The reader can check that the five pictures indeed represent triangulations, but a direct proof that these are all the triangulations is not easy. We postpone this until much later in the book, in Section 9.2.4.

But triangulations of $\mathbf{D}_3 \times \mathbf{D}_3$ are all still regular. One has to check this by explicitly finding heights vectors, which we will not do here. The same is true for $\mathbf{D}_3 \times \mathbf{D}_4$ and for $\mathbf{D}_3 \times \mathbf{D}_5$, as was first shown by Jesús De Loera in [95].

In the rest of this section, we are going to prove that both $\mathbf{D}_4 \times \mathbf{D}_4$ and $\mathbf{D}_3 \times \mathbf{D}_6$ have non-regular triangulations. These results were first shown in [95] and [312], respectively. Together with the above statements, this gives:

Theorem 6.2.19. *The product of two simplices $\mathbf{D}_n \times \mathbf{D}_m$ has non-regular triangulations if and only if $(n - 2)(m - 2) \geq 4$.*

A non-regular triangulation of $\mathbf{D}_4 \times \mathbf{D}_4$

Let \mathcal{T} be the collection of 20 spanning subgraphs of $K_{4,4}$ displayed, in Figure 6.25. We are going to show that they are a non-regular triangulation of $\mathbf{D}_4 \times \mathbf{D}_4$.

It is worth noting that the family is symmetric under the exchange of the left and right vertices of the graph, and also by even permutations of the set of indices $\{1, 2, 3, 4\}$, when each permutation acts simultaneously over the two sides of the bipartite graph. These operations correspond to affine symmetries of $\mathbf{D}_4 \times \mathbf{D}_4$ which leave our triangulation invariant. (Remember that a permutation is even if it can be decomposed into an even number of pair exchanges. In the case of four elements, the even permutations are the cyclic permutations of three of the elements and the simultaneous exchanges of two pairs.)

Actually, there are only two symmetry classes of simplices under the action of these symmetries, the first two and last three rows in Figure 6.25.

Lemma 6.2.20. *\mathcal{T} is a triangulation of $\mathbf{D}_4 \times \mathbf{D}_4$.*

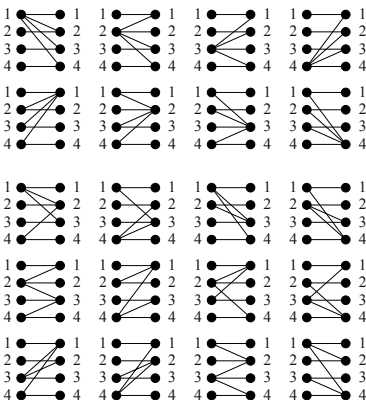


Figure 6.25: A non-regular triangulation of $\mathbf{D}_4 \times \mathbf{D}_4$, in its bipartite graph representation.

Proof. Having symmetries in mind in order to reduce the number of cases to deal with, it is easy to check property (ICoP), which amounts to the following: the removal of any edge from any of the trees in \mathcal{T} gives either something on a facet of $\mathbf{D}_4 \times \mathbf{D}_4$ (that happens when one of the end-points is a leaf of the tree) or something contained in exactly one of the other 19 trees. If the latter happens, it has to also be checked that the two trees represent simplices lying in opposite sides of their common facet.

We leave it as an exercise to actually do this check, but Figure 6.26 should help in this task. It shows the three neighbor simplices of one representative simplex from each symmetry class. The two representatives are the top two simplices and they are adjacent to one another and to two other simplices. The reader has to check that in each of the five adjacencies of the figure, the two edges which lie in only one of the two trees are at even distance along the unique cycle present in the union of the two trees. For example, the top two graphs of Figure 6.26 produce the cycle 12, 42, 44, 14, and the edges which appear in only one of the two graphs are 42 and 14. Here and in what follows, we write ij as an abbreviation of (i, j) to index the elements of $\mathbf{D}_4 \times \mathbf{D}_4$.

Once (ICoP) has been proved, any of the properties listed in Corollary 4.5.20 guarantees that \mathcal{T} is a triangulation. In our case, the simplest one is (TVP): the total volume of the simplices used in \mathcal{T} equals the volume of the convex hull of $\mathbf{D}_4 \times \mathbf{D}_4$. Indeed, this follows from the fact that $\mathbf{D}_4 \times \mathbf{D}_4$ that \mathcal{T} has the same number of simplices $20 - \binom{6}{3}$ as the staircase triangulation of $\mathbf{D}_4 \times \mathbf{D}_4$, since the product of two simplices is unimodular (all the full-dimensional simplices spanned by it have the same volume). \square

Lemma 6.2.21. \mathcal{T} has only six flips. Hence, it is not regular.

Proof. Let us check that only adjacency E of Figure 6.26 produces a flip:

- The circuit involved in adjacency A is $(\{42, 14\}, \{12, 44\})$, triangulated into the two triangles $\{42, 12, 44\}$ and $\{14, 12, 44\}$. The first is joined to $\{11, 22, 33, 32\}$ (second graph in the second row of Figure 6.25), and the second is joined to $\{11, 22, 33, 34\}$ instead. Hence, we do not have a flip.
- The adjacencies B and C are obtained from A by a cyclic permutation of the indices 2, 3 and 4. Hence, by symmetry, they do not produce flips.
- The adjacency D is obtained from A by switching left and right in the graphs, and then swapping indices 1 and 2, and 3 and 4. Hence, by symmetry, it does not produce a flip.
- The circuit involved in adjacency E is $(\{43, 12\}, \{13, 42\})$. It forms a square 2-face of $\mathbf{D}_4 \times \mathbf{D}_4$, which is triangulated into the two triangles $\{43, 13, 42\}$ and $\{12, 13, 42\}$). None of them is joined to any other simplex than the two in the adjacency. Hence, there is a flip which exchanges the diagonal of that square face.

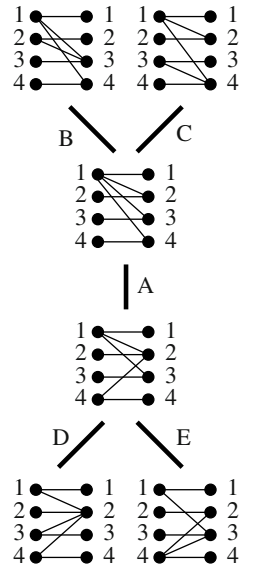


Figure 6.26: Some adjacencies between simplices in the triangulation of Figure 6.25.

The symmetries of the triangulation reproduce adjacency E six times (dividing the twelve bottom graphs of Figure 6.25 into six pairs of adjacent ones). Hence \mathcal{T} has only six flips, as claimed. \square

Remark 6.2.22 ($\mathbf{D}_4 \times \mathbf{D}_4$ and the cube-octahedron). Observe that the 20 full-dimensional simplices in this triangulation share the vertices 11, 22, 33, and 44 (the horizontal matching in the tree representation). The link $\text{link}_{\mathcal{T}}(\{11, 22, 33, 44\})$ of the tetrahedron spanned by these four points is a triangulation of the iterated contraction $\mathbf{D}_4 \times \mathbf{D}_4 / 11/22/33/44$. In principle, this triangulation could be regular. But, in our case, we can rely on Lemma 4.2.24 to conclude that it is not regular: if the link were regular, there should be a regular triangulation of $\mathbf{D}_4 \times \mathbf{D}_4$ extending it. But this cannot happen because the link uses all the full dimensional simplices of \mathcal{T} , which is non-regular.

What does $\mathbf{D}_4 \times \mathbf{D}_4 / 11/22/33/44$ look like? It must be a configuration of rank 3, since $\mathbf{D}_4 \times \mathbf{D}_4$ has rank equal to seven and $\{11, 22, 33, 44\}$ is independent. But since $\{11, 22, 33, 44\}$ intersects the interior of $\text{conv}(\mathbf{D}_4 \times \mathbf{D}_4)$ (it is not contained in any facet), the contracted configuration is totally cyclic. We leave it to the reader to check that $\mathbf{D}_4 \times \mathbf{D}_4 / 11/22/33/44$ equals, modulo linear equivalence, the configuration of twelve vectors of the form $\pm e_i \pm e_j$, with $i \neq j$ in $\{1, 2, 3\}$.

In fact, the link $\text{link}_{\mathcal{T}}(\{11, 22, 33, 44\})$ coincides with the link at the origin of the non-regular triangulation of the cube-octahedron studied in Section 3.47.

In particular, the same explicit proof of non-regularity that we carry out in Proposition 3.6.18 works here. If we give heights $\omega_{i,j}$, $i, j \in \{1, 2, 3, 4\}$, to the 16 vertices of $\mathbf{D}_4 \times \mathbf{D}_4$, the six triangulated squares that produce bistellar flips of \mathcal{T} produce, exactly, the same unfeasible system of six equations that we got there (3.4).

A non-regular triangulation of $\mathbf{D}_6 \times \mathbf{D}_3$

We are now going to exhibit a non-regular triangulation of $\mathbf{D}_6 \times \mathbf{D}_3$. We are going to slightly change our conventions to make the pictures and the notation more clear. The vertices of \mathbf{D}_6 are going to be labeled 1, 2, 3, 4, 5 and 6 and those of \mathbf{D}_3 are going to be labeled a, b and c . Put differently, our configuration $\mathbf{D}_6 \times \mathbf{D}_3$ is given by the following 8×18 labeled matrix:

$$\begin{array}{cccccccccccccccccc} & 1a & 2a & 3a & 4a & 5a & 6a & & 1b & 2b & 3b & 4b & 5b & 6b & & 1c & 2c & 3c & 4c & 5c & 6c \\ \left(\begin{array}{cccccccccccccccccc} 1 & 0 & 0 & 0 & 0 & 0 & 0 & & 1 & 0 & 0 & 0 & 0 & 0 & & 1 & 0 & 0 & 0 & 0 & 0 \\ 0 & 1 & 0 & 0 & 0 & 0 & 0 & & 0 & 1 & 0 & 0 & 0 & 0 & & 0 & 1 & 0 & 0 & 0 & 0 \\ 0 & 0 & 1 & 0 & 0 & 0 & 0 & & 0 & 0 & 1 & 0 & 0 & 0 & & 0 & 0 & 1 & 0 & 0 & 0 \\ 0 & 0 & 0 & 1 & 0 & 0 & 0 & & 0 & 0 & 0 & 1 & 0 & 0 & & 0 & 0 & 0 & 1 & 0 & 0 \\ 0 & 0 & 0 & 0 & 1 & 0 & 0 & & 0 & 0 & 0 & 0 & 1 & 0 & & 0 & 0 & 0 & 0 & 1 & 0 \\ 0 & 0 & 0 & 0 & 0 & 1 & 0 & & 0 & 0 & 0 & 0 & 0 & 1 & & 0 & 0 & 0 & 0 & 0 & 1 \\ \end{array} \right) \\ \left(\begin{array}{cccccccccccccccccc} 1 & 1 & 1 & 1 & 1 & 1 & 0 & 0 & 0 & 0 & 0 & 0 & 0 & 0 & 0 & 0 & 0 & 0 & 0 & 0 \\ 0 & 0 & 0 & 0 & 0 & 0 & 1 & 1 & 1 & 1 & 1 & 1 & 1 & 1 & 0 & 0 & 0 & 0 & 0 & 0 \\ 0 & 0 & 0 & 0 & 0 & 0 & 0 & 0 & 0 & 0 & 0 & 0 & 0 & 0 & 1 & 1 & 1 & 1 & 1 & 1 \end{array} \right) \end{array}$$

Table 6.1: The matrix representing $\mathbf{D}_6 \times \mathbf{D}_3$

Moreover, when using the bipartite graph representation, we will put 123, abc, and 456 in three columns (in this order). The full bipartite graph representing $\mathbf{D}_6 \times \mathbf{D}_3$ under these conventions is shown in Figure 6.27.

We will build our triangulation in two steps. First we consider a polyhedral subdivision \mathcal{S} of $\mathbf{D}_6 \times \mathbf{D}_3$ into seven cells, and then we will refine the cells into simplices to give a triangulation. The seven cells are shown as bipartite graphs in Figure 6.28. Some edges are drawn thicker than others to help in following later explanations.

Lemma 6.2.23. \mathcal{S} is the regular subdivision of $\mathbf{D}_6 \times \mathbf{D}_3$ produced by the following heights:

$$\begin{aligned} \omega_{1a} &= 1, \quad \omega_{2a} = 0, \quad \omega_{3a} = 0, \quad \omega_{4a} = 0, \quad \omega_{5a} = 1, \quad \omega_{6a} = 1, \\ \omega_{1b} &= 0, \quad \omega_{2b} = 1, \quad \omega_{3b} = 0, \quad \omega_{4b} = 1, \quad \omega_{5b} = 0, \quad \omega_{6b} = 1, \\ \omega_{1c} &= 0, \quad \omega_{2c} = 0, \quad \omega_{3c} = 1, \quad \omega_{4c} = 1, \quad \omega_{5c} = 1, \quad \omega_{6c} = 0. \end{aligned} \quad (6.14)$$

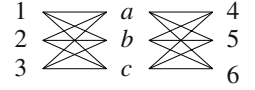


Figure 6.27: A modified bipartite graph representation of $\mathbf{D}_6 \times \mathbf{D}_3$.

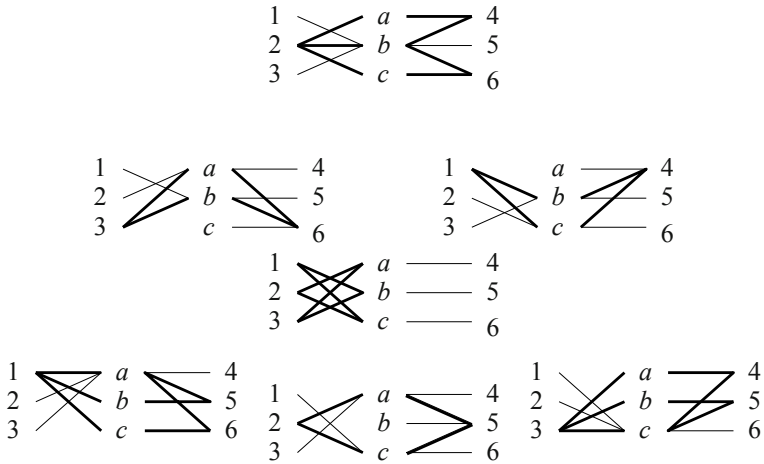


Figure 6.28: A polyhedral subdivision of $\mathbf{D}_6 \times \mathbf{D}_3$ into seven cells.

Proof. Let $\overline{\mathcal{S}}$ be the lifted configuration in \mathbb{R}^7 obtained from \mathcal{S} with the heights ω . The following list of seven functionals, applied to the lifted configuration, vanish each on one of the cells of \mathcal{S} , and are positive in the rest of elements. Since the coefficient of the lifting coordinate x_ω is positive in them, these seven cells are indeed lower facets in the lifted configuration. The functionals are displayed in a triangle-like manner, corresponding to the distribution of cells in Figure 6.28.

$$x_\omega + x_1 + x_3 + x_5 - x_b,$$

$$\begin{array}{ccc} x_\omega + x_c - x_6, & & x_\omega + x_a - x_4, \\ & 0 & \\ x_\omega + x_2 + x_3 + x_4 - x_a, & x_\omega + x_b - x_5, & x_\omega + x_1 + x_2 + x_6 - x_c. \end{array}$$

□

Before showing how to refine \mathcal{S} into a triangulation, let us concentrate in some of its properties.

First observe that any permutation of the three rows $1a4$, $2b5$ and $3c6$ leaves our set of seven cells invariant, and hence provides an affine symmetry of \mathcal{S} . The triangular disposition of the seven cells in Figure 6.28 has been devised to highlight these symmetries. Each of the three mirror symmetries of the triangle correspond to exchanging two of the rows $1a4$, $2b5$ and $3c6$ of the figure. The rotations of the triangle correspond to cyclic permutations of the rows.

A second observation is that if an edge in one of the graphs representing a cell C of \mathcal{S} has the property that the removal of that edge leaves the graph non-connected or non-spanning, then the corresponding element i of $\mathbf{D}_6 \times \mathbf{D}_3$ has the property that $C \setminus i$ is lower dimensional. In order to refine the cell C to a triangulation, those elements are irrelevant. These are the elements that appear as thin lines in Figure 6.28. The rest of the vertices, that is, those which lie in circuits contained in the cell, have been emphasized with thick lines in Figure 6.28.

As we see from the correspondence between circuits in the configuration and cycles in the graph (Lemma 6.2.8, part 3), in four of the cells there is a unique circuit, which implies that these cells have only two triangulations. Indeed, each of these cells is a corank one configuration, whose triangulations are repeated cones over the two triangulations of their unique circuit (cf. Section 2.4.1). The three cells in the corners of the figure are slightly more complicated.

The third, and most important, observation is that no cycle lies in more than one graph. That is, *the intersection of any two cells is independent*. This implies that in order to refine \mathcal{S} , we can triangulate each cell independently, and the different triangulations will automatically glue correctly to give a triangulation of $\mathbf{D}_6 \times \mathbf{D}_3$.

Lemma 6.2.24. *There are triangulations refining \mathcal{S} and containing the following six (not full-dimensional) cells:*

$$\{1c, 5b, 6a\}, \{2a, 6c, 4b\}, \{3b, 4a, 5c\}, \{1b, 4c\}, \{2c, 5a\}, \{3a, 6b\}.$$

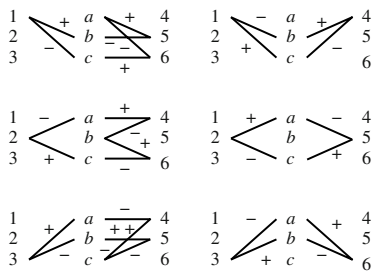


Figure 6.29: A choice of simplex in six of the cells of Figure 6.28.

Proof. The six cells are the negative parts of six circuits contained in six different cells of \mathcal{S} , as Figure 6.29 shows. Hence, we only need to triangulate each of these six cells in a way that makes that simplex occur, for example, by the placing procedure. □

Lemma 6.2.25. *No regular triangulation of $\mathbf{D}_6 \times \mathbf{D}_3$ can contain the six cells listed in Lemma 6.2.24.*

Proof. Let \mathcal{T} be such a triangulation. If \mathcal{T} were regular, the heights producing it should satisfy the following six equations, one for each circuit

of Figure 6.29:

$$\begin{aligned} \omega_{6a} + \omega_{5b} + \omega_{1c} &< \omega_{5a} + \omega_{1b} + \omega_{6c}, \\ \omega_{2a} + \omega_{4b} + \omega_{6c} &< \omega_{4a} + \omega_{6b} + \omega_{2c}, \\ \omega_{4a} + \omega_{3b} + \omega_{5c} &< \omega_{3a} + \omega_{5b} + \omega_{4c}, \\ \omega_{1b} + \omega_{4c} &< \omega_{4b} + \omega_{1c} \\ \omega_{5a} + \omega_{2c} &< \omega_{2a} + \omega_{5c}, \\ \omega_{3a} + \omega_{6b} &< \omega_{6a} + \omega_{3b}. \end{aligned}$$

The sum of left-hand sides equals the sum of right-hand sides. Hence, the equations cannot be satisfied simultaneously. \square

In Section 9.2.4 we will see a way of visualizing triangulations of $\mathbf{D}_n \times \mathbf{D}_3$ which will make the construction we have just finished, and its non-regularity, much more apparent.

Incidentally, before we move on, note that one can take the product of many simplices, not just two or three. The general term used by the people in economics and game theory for the product of simplices, with arbitrary number of factors, is *simplotope*; see [292].

6.3 Cubes and their subpolytopes

The cube of dimension d is the product of d copies of a segment, that is, the polytope

$$\mathbf{I}^d := \{(x_1, \dots, x_d) \in \mathbb{R}^d : 0 \leq x_i \leq 1 \ \forall i = 1, \dots, d\}.$$

Some people call this a hypercube. The cube is a fascinating polyhedron which is familiar to everyone since childhood (who has not played with building blocks?), and which appears in many theoretical and practical contexts, to the point that a whole book has recently been devoted to its exploration [342] (see also [341]). It is then surprising that its space of triangulations is not well understood. Heuristically, we can say the reason is that triangulations do not behave well under products (as we have seen in the previous sections). In this section we present what we know about the triangulations of the cube and of its subpolytopes.

Subpolytopes with 0/1 vertices are very important in combinatorial optimization and they come in rather different types and sizes (see [340]). In this section, we do a little tour of what is known about triangulations of 0/1 polytopes. We start with construction of non-regular triangulations of small size and dimension. Besides their pure beauty, cube triangulations have been studied for their applications, including calculations of fixed-points of continuous maps ([57, 322, 321] and references therein), and also through connections to the algebraic properties of the *hyperdeterminant* (see [140] and [167]), so we collect a few key results about them. In the rest of the section, we look at *slices* of cubes, known as *hypersimplices*. We conclude with a look at triangulations of the *Birkhoff polytope*.

6.3.1 Small 0/1 non-regular triangulations

Cubes, and products of simplices, are examples of 0/1 polytopes: polytopes whose vertices have entries all equal to zero or one. This class of polytopes

is extremely important in combinatorial optimization where, quite often, the best (biggest, smallest, nicest) subset of a finite set S needs to be found. One way to approach this is to consider the family of subsets of S as the set of 0/1 points in \mathbb{R}^S , and rephrase the optimization question as a geometric problem in its convex hull. This gives raise to a myriad of 0/1 polytopes that one can associate to, for example, a graph: the convex hull of its spanning trees, of its Hamiltonian cycles, of its matchings, etc.

In some respects, 0/1 polytopes are nicer than arbitrary polytopes. For example, there is only a finite number of combinatorially different 0/1 polytopes in each dimension, for obvious reasons. As another example, the graphs of 0/1 polytopes are known to have diameter bounded above by their number of facets minus their dimension [238]. Whether arbitrary polytopes have the same property is the famous Hirsch conjecture [339], recently disproved by Santos [286].

We already know that 0/1 polytopes can have non-regular triangulations, since products of simplices are examples of them. But products of simplices have non-regular triangulations only starting in dimension six. Here, we are going to show that 0/1 polytopes of dimension four can have non-regular triangulations. Those of dimension three cannot, since all triangulations of the 3-cube are regular, as we will see in Section 6.3.4.

Example 6.3.1 (The one point suspension of the barycenter in a 3-cube). The 3-cube has only regular triangulations if no interior points are used as vertices. But if we insert a single interior point, e.g., its barycenter, then non-regular triangulations arise. To make things precise, consider the following point configuration:

$$\overline{\mathbf{I}}^3 = \begin{pmatrix} 0 & 1 & 2 & 3 & 4 & 5 & 6 & 7 & 8 \\ 1 & 1 & 1 & 1 & 1 & 1 & 1 & 1 & 1 \\ 1/2 & 0 & 1 & 1 & 0 & 0 & 1 & 1 & 0 \\ 1/2 & 0 & 0 & 1 & 1 & 0 & 0 & 1 & 1 \\ 1/2 & 0 & 0 & 0 & 0 & 1 & 1 & 1 & 1 \end{pmatrix}.$$

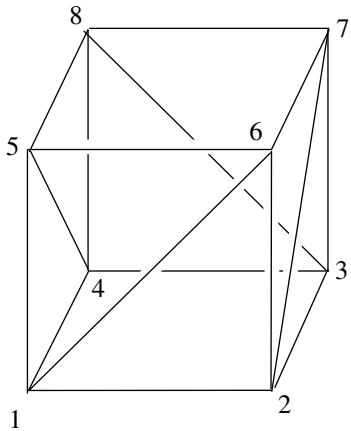


Figure 6.30: A cyclic way to triangulate the boundary of a 3-cube.

Consider any triangulation of the boundary of the 3-cube that uses four cyclically chosen diagonals, such as 16, 27, 38 and 45. See Figure 6.30. Now triangulate $\overline{\mathbf{I}}^3$ extending the triangulation of the boundary to the interior by coning at the centroid 0. That triangulation cannot be regular. Indeed, if ω is a height function producing that triangulation, then the four diagonals we have chosen to use in the square faces 1256, 2367, 3478 and 1458 have the following implications for its values:

$$\begin{aligned} \omega_1 + \omega_6 &< \omega_5 + \omega_2, \\ \omega_2 + \omega_7 &< \omega_6 + \omega_3, \\ \omega_3 + \omega_8 &< \omega_7 + \omega_4, \\ \omega_4 + \omega_5 &< \omega_8 + \omega_1. \end{aligned}$$

What does this have to do with 0/1 polytopes? Our configuration has a point with half-integer coordinates. Well, let us do a one-point suspension

at that point. Remember that the one point suspension (see Chapter 4, Section 4.2.5) consists of embedding our configuration in a hyperplane in one more dimension and substituting our point 0 by two points 0^+ and 0^- on both sides of that hyperplane. The actual coordinates chosen for these new points are irrelevant, as long as the segment joining them intersects the hyperplane containing all the other points precisely at the point where the old element 0 was. In particular, what follows is a one point suspension of $\overline{\mathbf{I}}^3$:

$$\overline{\mathbf{I}}^3 \uparrow_0^0 = \begin{pmatrix} 0^+ & 0^- & 1 & 2 & 3 & 4 & 5 & 6 & 7 & 8 \\ 1 & 1 & 1 & 1 & 1 & 1 & 1 & 1 & 1 & 1 \\ 1 & 0 & 0 & 1 & 1 & 0 & 0 & 1 & 1 & 0 \\ 1 & 0 & 0 & 0 & 1 & 1 & 0 & 0 & 1 & 1 \\ 0 & 1 & 0 & 0 & 0 & 0 & 1 & 1 & 1 & 1 \\ 0 & 1 & 1 & 1 & 1 & 1 & 0 & 0 & 0 & 0 \end{pmatrix}.$$

Indeed, all points except 0^+ and 0^- lie in the hyperplane where the sum of the last two coordinates equals one. 0^+ and 0^- lie on opposite sides of that hyperplane, and intersect it at Point $(1, 1/2, 1/2, 1/2, 1/2)$. We label this point 0. Deleting the last coordinate in the configuration consisting of this new point and the points 1 through 8 gives the configuration $\overline{\mathbf{I}}^3$.

Now, by Theorem 4.2.33, $\overline{\mathbf{I}}^3 \uparrow_0^0$ and $\overline{\mathbf{I}}^3$ have isomorphic sets of triangulations and the isomorphism preserves, among other things, regularity. Hence:

Proposition 6.3.2. *There are non-regular triangulations of the 4-dimensional 0/1-configuration $\overline{\mathbf{I}}^3 \uparrow_0^0$.*

This example is not the smallest possible, but the next one is. As said above, a 0/1 configuration with non-regular triangulations needs to have at least dimension 4. By the results in Section 5.5.1, it then needs to have at least eight elements. The following configuration satisfies both requirements.

Example 6.3.3 (The smallest 0/1 non-regular triangulation). Consider the following configuration:

$$\mathbf{A} = \begin{pmatrix} 1 & 2 & 3 & 4 & 5 & 6 & 7^+ & 7^- \\ 1 & 1 & 1 & 1 & 1 & 1 & 1 & 1 \\ 0 & 0 & 0 & 1 & 1 & 1 & 0 & 1 \\ 1 & 0 & 0 & 1 & 0 & 0 & 0 & 1 \\ 0 & 1 & 0 & 0 & 1 & 0 & 0 & 1 \\ 0 & 0 & 1 & 0 & 0 & 1 & 0 & 1 \end{pmatrix}.$$

The first six elements lie in the hyperplane “sum of last three coordinates equal to 1”. The last two points lie on opposite sides of that hyperplane, and the segment through them intersects that hyperplane at the point with coordinates $(1, 1/3, 1/3, 1/3, 1/3)$. Hence, \mathbf{A} is a one point suspension of

the following configuration:

$$\mathbf{A}_0 = \begin{pmatrix} 1 & 2 & 3 & 4 & 5 & 6 & 7 \\ 1 & 1 & 1 & 1 & 1 & 1 & 1 \\ 0 & 0 & 0 & 1 & 1 & 1 & 1/3 \\ 1 & 0 & 0 & 1 & 0 & 0 & 1/3 \\ 0 & 1 & 0 & 0 & 1 & 0 & 1/3 \\ 0 & 0 & 1 & 0 & 0 & 1 & 1/3 \end{pmatrix}.$$

Here, either the first or one of the last three coordinates is superfluous (the configuration has rank four, and dimension three). The first six points form a triangular prism, and the last point lies in the interior of it, along its symmetry axis. Triangulating the boundary of the prism in the cyclic way and joining that to the interior point we get a non-regular triangulation of \mathbf{A}_0 . By Theorem 4.2.33, this implies that the original configuration \mathbf{A} has a non-regular triangulation.

6.3.2 Two simple ways to triangulate any cube

Let us start with a widely canonical triangulation of the cube, which comes from orderings of variables (and is closely related to the *order polytopes* of Theorem 1.1.10). For each permutation $\sigma = (\sigma_1, \dots, \sigma_d)$ of the numbers $1, \dots, d$, consider the polytope defined by the following chain of inequalities:

$$\mathbf{P}_\sigma := \{ (x_1, \dots, x_d) : 0 \leq x_{\sigma(1)} \leq x_{\sigma(2)} \leq \dots \leq x_{\sigma(d)} \leq 1 \}.$$

\mathbf{P}_σ is contained in the cube, since each coordinate is bounded between 0 and 1. Moreover, it is a full-dimensional polytope in \mathbb{R}^d since (for example) the point with σ_i -th coordinate equal to $i/(d+1)$ is in its interior (none of the inequalities defining \mathbf{P}_σ are tight at this point). Since \mathbf{P}_σ is defined by $d+1$ constraints and it has dimension d , it must necessarily be a simplex. In fact, its vertices are the following $d+1$ vertices of the cube: for each $i \in \{0, \dots, d\}$, consider the point whose coordinates $\sigma_1, \dots, \sigma_i$ are 0 with the rest 1. Indeed, since these $d+1$ points are in \mathbf{P}_σ and are vertices of the cube containing it, they must be vertices of \mathbf{P}_σ as well.

We leave it to the reader to prove that the $d!$ simplices defined with different choices of σ form a triangulation of the cube (see Exercise 6.15). As a corollary we have:

Proposition 6.3.4. *The cube of dimension d has a triangulation with $d!$ simplices.*

This particular triangulation has the following interpretations:

1. It is the staircase triangulation of the cube, if we consider the cube as a product of d copies of the 1-simplex \mathbf{D}_2 .
2. As such, it is the pulling triangulation obtained with any order of the vertices that extends the coordinate-wise poset (the Boolean poset) formed by the vertices of the cube.

3. It is an example of the triangulations of order polytopes introduced in Chapter 1 (see Theorem 1.1.10). The poset in question is the trivial one, in which none of the d -elements in the poset are comparable to one another. So any of the $d!$ orderings of them is a linear extension.
 4. It is the subdivision of the cube, obtained by cutting it via the $\binom{d}{2}$ hyperplanes $x_i = x_j$. In this sense, this triangulation is important in the context of reflection groups and Coxeter groups.

Is this a good triangulation of the cube? In terms of its symmetries and ease of construction, yes. But if we are looking for a triangulation with as few simplices as possible then this triangulation is as bad as can be:

Proposition 6.3.5. *No triangulation of \mathbb{I}^d can have more than $d!$ simplices. Equality arises if all simplices are unimodular.*

In this statement we are using the word unimodular in a slightly stronger sense than before. We do not only mean that all simplices have the same volume, but also that their volume is $1/d!$, that is, the determinant formed by its vertices is ± 1 .

Proof. Of course, here it is important that we speak of triangulations of the point configuration \mathbb{I}^d , and do not allow extra points in the cube to be used as vertices. This makes every full-dimensional simplex have integer vertices, hence its Euclidean volume is a multiple of $1/d!$, with equality if and only if the simplex is unimodular. Since the total Euclidean volume of the cube is 1, the statement follows. \square

This proposition and the practical applications of small triangulations of the cube (e.g., see [321, 292]) motivate the problem of finding the smallest number of simplices *needed* to triangulate a d -cube. In Section 6.3.3 we say what is known about that. Here we show one way to construct smaller triangulations of arbitrary cubes.

Theorem 6.3.6. *There are triangulations of the regular d -cube with at most $(d! + 2^{d-1})/2$ full-dimensional simplices.*

When d grows, the exponential 2^{d-1} is much smaller than the factorial $d!$. So, the triangulations that we construct in this proof, called the *corner-cut* triangulations, have about half the size of the completely unimodular triangulation of Proposition 6.3.4.

Proof. The triangulations in this proof are called corner-cut because the key idea is to “cut” as many corners of the cube as possible. Cutting a corner means picking up any particular vertex of the d -cube and chopping off the simplex formed by it and its d -neighbors in the graph of the cube. Those simplices are called *cornered* simplices. Two or more cornered simplices can be used in the same triangulation of \mathbf{I}^d if and only if no two of the vertices they cut are adjacent in the graph of the cube. Then, what is the maximal number of vertices that can be cut simultaneously?

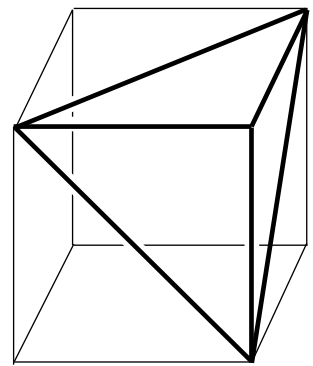


Figure 6.31: A cornered simplex.

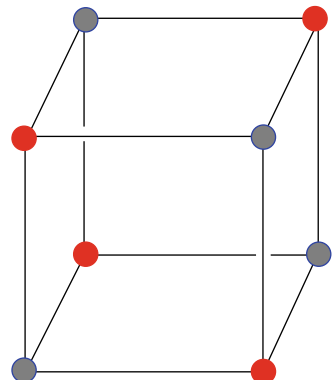


Figure 6.32: The coloring of vertices of \mathbf{I}^3 . \mathbf{H}^3 is a regular tetrahedron.

Observe that the graph of the d -cube is 2-colorable. One color consists of vertices with an even sum of coordinates, the other of the vertices with odd sum of coordinates. Hence, it is possible to cut simultaneously (that is, use in the same triangulation) 2^{d-1} cornered simplices of \mathbf{I}^d . Our claim is that any triangulation constructed by cutting those 2^{d-1} simplices and then triangulating what is left arbitrarily has (at most) the claimed number of full-dimensional simplices.

To see this, assume without loss of generality that we cut the vertices with an even sum of coordinates. Let \mathbf{H}^d be the configuration consisting of vertices with odd sum. The first remark is that the cornered simplices are unimodular, that is, they have volume $1/d!$. Hence, the volume of \mathbf{H}^d is $1 - 2^{d-1}/d! = (d! - 2^{d-1})/d!$. We now claim that the volume of any simplex with vertices in \mathbf{H}^d is a multiple not only of $1/d!$ (which follows from the fact that the vertices have integer coordinates), but also of $2/d!$. This follows from the fact that the $(d-1) \times (d-1)$ matrix \mathbf{B} representing the vertices of such a simplex has the property that the sum of entries in each column is even (the sum of coordinates is odd in each vertex, but we have to add 1 to it for the homogenization row). In particular, the following product is still an integer matrix:

$$\begin{pmatrix} 1/2 & 1/2 & \cdots & 1/2 \\ 0 & 1 & \cdots & 0 \\ \vdots & \vdots & \ddots & \vdots \\ 0 & 0 & \cdots & 1 \end{pmatrix} \cdot \mathbf{B}.$$

Since the determinant of the first factor is $1/2$, and the determinant of the product is integer, the determinant of the second factor is even.

Hence, any triangulation of \mathbf{H}^d has at most

$$\frac{(d! - 2^{d-1})/d!}{2/d!} = \frac{d! - 2^{d-1}}{2}$$

simplices. Adding the 2^{d-1} cornered simplices to this gives the result. \square

6.3.3 Triangulating high-dimensional cubes. State of the art

For $d = 3$ and $d = 4$, the corner cut triangulations that we have constructed have respectively 5 and 16 full-dimensional simplices. It turns out that, in both cases, this is the minimum possible size of a triangulation of the cube. In the case $d = 5$, corner cut triangulations are guaranteed to have at most $(120 + 16)/2 = 68$ full-dimensional simplices, but some other triangulations have fewer simplices. Indeed, it is easy to check that \mathbf{H}^5 has simplices of volume four (instead of two); for example, the one whose vertices are the standard basis vectors plus the point $(1, \dots, 1)$. Using any simplex like that, we can get triangulations of \mathbf{H}^5 with 51, instead of 52, full-dimensional simplices. That provides triangulations of \mathbf{I}^5 with 67 simplices, which is the minimal size of a triangulation of \mathbf{I}^5 .

But starting with \mathbf{I}^6 , the minimum size triangulations are not that easy to describe. In fact, the actual minimum possible size is only known up to \mathbf{I}^7 , and is shown in the following table:

| Dimension | 1 | 2 | 3 | 4 | 5 | 6 | 7 | 8 |
|---------------|---|---|---|----|----|-----|------|--------------|
| Smallest size | 1 | 2 | 5 | 16 | 67 | 308 | 1493 | ≤ 11944 |

Table 6.2: Smallest size and efficiency of triangulations of \mathbf{I}^d .

The last two entries were computed by Hughes and Anderson [169], with a method similar to that of the *universal polytope* that we will study in Section 8.5.1, but simplifying the system of equations via the symmetries of the cube. Still, this calculation was a computational *tour-de-force*, which involved an integer program with 1 456 318 variables and ad hoc ways of decomposing the system into smaller subsystems. Perhaps surprisingly, the minimum triangulations of \mathbf{I}^6 are not corner-cut. The minimum size of a corner-cut triangulation of \mathbf{I}^6 is 324 [168].

From the table, we see that the minimum size of a triangulation of \mathbf{I}^7 (1493) is much smaller than what can be guaranteed for corner-cut triangulations of the same cube (2552). How big is this discrepancy, asymptotically? The answer is: Huge! The following result of Haiman [154] shows that there is a constant $\rho < 1$ such that the cubes of sufficiently large dimension d can be triangulated with less than $\rho^d \cdot d!$ full-dimensional simplices. Finding the best value for this constant ρ is an open question. The best one that has been proved so far is $\rho = 0.8159$ [246].

Theorem 6.3.7 (Haiman). *If \mathcal{T}_1 and \mathcal{T}_2 are triangulations of \mathbf{I}^{d_1} and \mathbf{I}^{d_2} using N_1 and N_2 full-dimensional simplices respectively, then there is a triangulation of $\mathbf{I}^{d_1+d_2}$ using $\binom{d_1+d_2}{d_1} N_1 N_2$ full-dimensional simplices.*

As a consequence, if there is a triangulation of \mathbf{I}^d with $\rho^d d!$ simplices for a certain $\rho < 1$, then the same is true, with the same ρ for all dimensions that are a multiple of d .

Proof. Consider the product \mathcal{S} of the two triangulations \mathcal{T}_1 and \mathcal{T}_2 , which is a polyhedral subdivision of $\mathbf{I}^{d_1+d_2}$ into $N_1 \times N_2$ full-dimensional cells, each a product $\mathbf{D}_{d_1+1} \times \mathbf{D}_{d_2+1}$ of two simplices of dimensions d_1 and d_2 . Then refine \mathcal{S} to a triangulation arbitrarily (for example, via the regular refinements of Definition 2.3.17). By Theorem 6.2.13, in the refinement each cell is triangulated with $\binom{d_1+d_2}{d_1}$ simplices.

For the conclusion, consider a dimension kd and apply induction on k . If you assume that the cube of dimension $(k-1)d$ can be triangulated with $\rho^{(k-1)d}((k-1)d)!$ simplices, and apply the first part of the statement, you obtain triangulations of \mathbf{I}^{kd} with

$$\binom{kd}{d} \rho^{(k-1)d} ((k-1)d)! \rho^d d! = \rho^{kd} (kd)!$$

simplices. □

This result suggests that in order to compare the sizes of triangulations of cubes in different dimensions, the following normalization is natural. Observe, however, that its definition was proposed by Todd much before the previous theorem was proved:

Definition 6.3.8 (Todd [321]). The *efficiency* of a triangulation \mathcal{T} of the d -cube is the number $(|\mathcal{T}|/d!)^{\frac{1}{d}}$.

This number is at most 1, and equal to one if and only if \mathcal{T} is unimodular. On the other extreme, Hadamard's inequality for determinants of matrices with coefficients in $[-1, 1]$ implies that the volume of every d -simplex inscribed in the regular d -cube $\mathbf{I}^d = [0, 1]^d$ is at most $(d+1)^{(d+1)/2}/2^d d!$. Hence, every triangulation has size at least $2^d d!/(d+1)^{(d+1)/2}$ and efficiency at least $2/(d+1)^{\frac{d+1}{2d}} \approx 2/\sqrt{d+1}$.

Let \mathbf{P} be an n -dimensional polytope. Dissections are important variation of triangulations. A *dissection* is a finite set \mathcal{D} of n -simplices inside \mathbf{P} that satisfies $\bigcup_{\mathbf{T} \in \mathcal{D}} \mathbf{T} = \mathbf{P}$ and $\dim(\mathbf{T}_1 \cap \mathbf{T}_2) < n$ for any $\mathbf{T}_1, \mathbf{T}_2 \in \mathcal{D}$. Thus dissections are not necessarily simplicial complexes, but when they are, they become triangulations. Both objects are equally useful to compute volumes, but they can be quite different too. For example, it is known that any two dissections of a polytope are connected by finitely many *elementary moves*, which are local modifications that are similar to flips (see [221], or the forthcoming book [249], for details).

Denote by ϕ_d and ρ_d the smallest size and efficiency, respectively, of all dissections of the cube of dimension d . The number ϕ_d is known as *simplicity* of the d -cube. Obviously, $\rho_d = (\phi_d/d!)^{1/d}$. Haiman's result and the lower bound obtained from Hadamard's inequality have the following consequences:

Theorem 6.3.9. 1. The sequence $(\rho_i)_{i \in \mathbb{N}}$ converges and

$$\lim_{i \rightarrow \infty} \rho_i \leq \rho_d \quad \forall d \in \mathbb{N}.$$

$$2. \lim_{i \rightarrow \infty} \rho_i \sqrt{i} \geq 2.$$

Proof. Let us fix $d \in \mathbb{N}$ and $k \in \{1, \dots, d\}$. Haiman's theorem implies that, for every $i \in \mathbb{N}$,

$$\rho_{k+id} \leq \rho_k^{k/(k+id)} \rho_d^{id/(k+id)}.$$

Since the right-hand side converges to ρ^d when i grows, the d subsequences of indices modulo d , and hence the whole sequence $(\rho_i)_{i \in \mathbb{N}}$, have an upper limit bounded by ρ_d . An upper limit bounded by every term in the sequence must coincide with the lower limit. This proves part one. Part two follows from the Hadamard bound. \square

Both parts of this theorem have been improved with more sophisticated arguments, but the improvement is (asymptotically) only by a constant. Much work is left to be done!

- For the upper bound, D. Orden and F. Santos [246] have generalized the ideas of Haiman to efficient triangulations of a product polytope $\mathbf{P} \times \mathbf{Q}$, starting from a triangulation of \mathbf{Q} and another of $\mathbf{P} \times \mathbf{D}^{m+1}$, where \mathbf{D}^{m+1} denotes a simplex of relatively small dimension m . They

apply this to \mathbf{P} a small-dimensional cube and \mathbf{Q} a high-dimensional one iteratively. This allows to obtain asymptotically efficient triangulations of arbitrarily high-dimensional cubes from any (efficient) triangulation of $\mathbf{I}^l \times \mathbf{D}^{m+1}$. Of course, the asymptotic efficiency of the triangulations obtained depends on how good the triangulation of $\mathbf{I}^l \times \mathbf{D}^{m+1}$ is. Finding the triangulation of $\mathbf{I}^l \times \mathbf{D}^{m+1}$ which is optimal for this purpose reduces to an integer programming problem, similar to finding the smallest triangulation of that polytope (actually, it is the same system of linear equations, with a different objective function) and it can then be solved using once more the universal polytope. Using this method, Orden and Santos found that

$$\lim_{i \rightarrow \infty} \rho_i \leq \sqrt[3]{\frac{44/3}{27}} \approx 0.8159.$$

In other words, they proved that (asymptotically) the d -cube can be triangulated with $0.8159^d d!$ simplices, instead of the $0.840^d d!$ achievable before via the value of ρ_7 .

- For the lower bound, Smith [301] had the idea that using hyperbolic volumes instead of Euclidean ones could give better bounds. An intuition for why this is reasonable comes from the fact that in the hyperbolic setting the corner simplices are regular, hence they have the same volume as the Hadamard simplex. But actually computing the ratio between the hyperbolic volumes of the regular ideal cube and the regular ideal simplex is not an easy task. Smith did it, and improved the inequality in the lower bound to be

$$\lim_{i \rightarrow \infty} \rho_i \sqrt{i} \geq \sqrt{6}.$$

More recently, Bliss and Su [57] set up a simple (i.e., smaller than [169]) linear programming problem based on analysis of the number of exterior faces that a simplex in the cube can have of a specified dimension and volume, and a characterization of corner simplices in terms of their exterior faces. The lower bounds obtained are better than Smith's up to $d = 12$, but no asymptotic formula can be obtained from their method.

6.3.4 Cubes of three dimensions

There is not much to say about triangulations of the 2-cube, or, put differently, we have already said all there is. The configuration \mathbf{I}^2 has corank one, hence it has two triangulations, both regular and differing by a single flip.

To understand triangulations of the 3-cube, let us first look at the possible tetrahedra that can be made with vertices of it. Modulo the symmetries of the cube, there are the following four types:

1. The tetrahedron obtained with any 0/1 point, together with its three neighbors. This is usually called a *corner* tetrahedron.
2. The tetrahedron whose vertices form a monotone path between opposite vertices of the cube. This is the type of tetrahedron used in the *staircase* triangulation of Proposition 6.3.4.

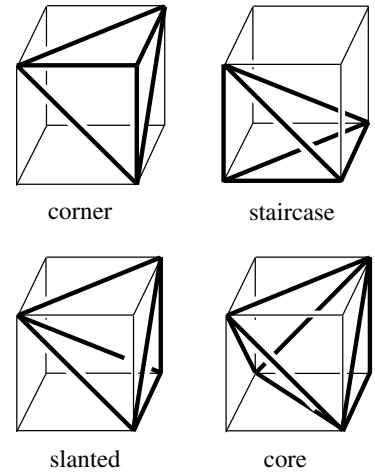


Figure 6.33: The four types of tetrahedra in the 3-cube.

3. The *slanted* tetrahedron, obtained with two opposite vertices of the cube and two neighbors of one of them.
4. The regular, or *core*, tetrahedron, obtained with all vertices with an odd sum of coordinates (or the one with an even sum of coordinates). Its vertices form the configuration \mathbf{H}^3 , obtained by cutting half of the corners in the cube.

We leave it as an exercise to the reader to check that the list is complete and irredundant. For the latter, it is enough to count how many faces each type of tetrahedron has in facets of the cube. One consequence of this classification is the following classification of triangulations of the 3-cube. As far as we know, the classification of triangulations of the 3-cube was first explicitly done by F. Bigdeli in her dissertation [47], although it is also implicit in the results of J. Böhm [59]. The classification is in terms of the number of corner tetrahedra used.

Theorem 6.3.10 (Classification of triangulations of the 3-cube).

1. *Every triangulation of the 3-cube contains either a regular tetrahedron or a diameter; that is, an edge joining two opposite vertices.*
2. *There are two triangulations of the first type, symmetric to one another. The triangulations of the second type are completely classified, modulo symmetries, by their link at the diameter.*
3. *That link can be one of the five shown in Figure 6.34. There are 4, 24, 24, 12, and 8 triangulations in each class.*

Hence, the 3-cube has 74 triangulations, all of them lexicographic (hence regular).

Proof. Let \mathcal{T} be a triangulation of the 3-cube. Let $B \in \mathcal{T}$ be the carrier of the barycenter $\mathbf{O} = (1/2, 1/2, 1/2)$ in \mathcal{T} . Remember that the carrier is the unique cell containing that point in its relative interior or, equivalently, the minimal cell containing that point.

By the classification of the tetrahedra in the 3-cube, the carrier of \mathbf{O} is either the regular tetrahedron or one of the four diameters. This proves part 1.

Now observe that the only type of tetrahedra in the list not containing \mathbf{O} are the corner tetrahedra. That is, once we know the list of tetrahedra in \mathcal{T} that contain \mathbf{O} (which is the core tetrahedra alone in the first case, and a diameter joined to its link in the second case), we can recover the rest of \mathcal{T} by adding the necessary corner tetrahedra. There is no choice in which corner tetrahedra are to be used: we need to use those, and only those, cornered at vertices of \mathbf{I}^3 that are not present in any other tetrahedron. This proves part two.

To prove part three, we need to first understand the contraction of \mathbf{I}^3 at the two end points of a diameter, say the points $(0, 0, 0)$ and $(1, 1, 1)$. We leave it to the reader to check that this is indeed the rank 2 vector configuration consisting of three pairs of opposite vectors (which particular vectors to use

is irrelevant for this discussion, and is actually dependent on the particular choices made when constructing a contraction). That the five possibilities of Figure 6.34 are the only triangulations of this configuration is easy to check, and that they can all be “lifted” to triangulations of the cube follows from the fact that they are all regular and Lemma 4.2.24, or by looking at the pictures of triangulations of the 3-cube in Figure 1.33.

So, only the conclusion (the number of triangulations and the fact that they are all lexicographic) needs to be proved. For the number, each symmetry class in Figure 6.34 produces four times the number of symmetric ways of triangulating the rank 2 vector configuration, the four coming from the choice of which diagonal is used.

For the fact that they are all lexicographic, observe first that the same triangulation may, in principle, be obtained by more than one pushing/pulling procedure. In our case, all the triangulations of the 3-cube except the one whose link is the first one in Figure 6.34 can be obtained with only pushings (that is, they are all placing triangulations). The one that is not placing is the *staircase* triangulation of Proposition 6.3.4. As said after that proposition, it can be obtained as a pulling triangulation. \square

As another way of visualizing the six different types of triangulations of the 3-cube, we can draw their dual complexes (or *tight spans*). In the dual complex, we put a vertex for each tetrahedron, and two vertices are connected by an edge if the corresponding tetrahedra share a triangle. A 2-cell of the dual complex corresponds to an interior edge of the triangulation (which, as we know, is unique and exists only in the triangulations that use a diameter). The six dual complexes are shown in Figure 6.35.

The secondary polytope of the regular unit 3-cube is still small enough to be computed entirely. It is 4-dimensional, so that a Schlegel diagram (projection to a facet) can be visualized in three dimensions. With a convex hull computation, e.g., PORTA [81], cdd [130], or polymake [135], we can use the GKZ-vectors and recover the f -vector $(74, 152, 100, 22)$ of the secondary polytope. The interested reader can find this and other nice interactive pictures of Schlegel diagrams of secondary polytopes constructed by Julian Pfeifle [252]. One finds that the secondary polytope of the 3-cube has the following irredundant presentation by linear equations and inequalities (note the variables are indexed by the 8 vertices of the 3-cube, as mandated by using GKZ coordinates):

$$\begin{aligned} \Sigma\text{-poly}(\mathbf{I}^3) = & \{(x_{000}, x_{001}, \dots, x_{111}) \in \mathbb{R}^8 : \\ & x_{000} + x_{001} + x_{010} + x_{011} = x_{000} + x_{001} + x_{100} + x_{101} = 12, \\ & x_{000} + x_{010} + x_{100} + x_{110} = x_{001} + x_{011} + x_{101} + x_{111} = 12, \\ & 1 \leq x_{000}, x_{001}, x_{010}, x_{011}, x_{100}, x_{101}, x_{110}, x_{111} \leq 6, \\ & x_{000} + x_{001} \geq 4, x_{000} + x_{010} \geq 4, x_{000} + x_{100} \geq 4, \\ & x_{001} + x_{011} \geq 4, x_{010} + x_{011} \geq 4, x_{001} + x_{101} \geq 4\}. \end{aligned} \quad (6.15)$$

The 22 facets of the secondary polytope correspond to proper subdivisions of the 3-cube which are as coarse as possible. The eight facet

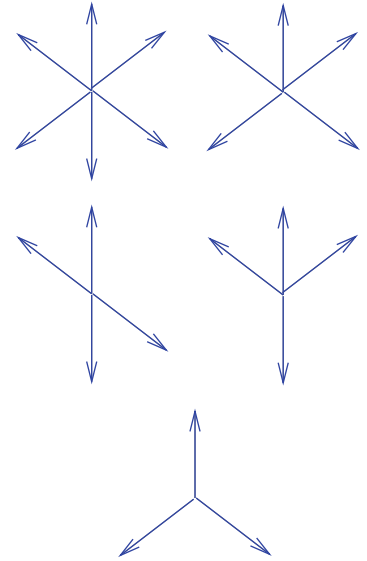


Figure 6.34: The five possible links at an interior edge, in triangulations of the 3-cube.

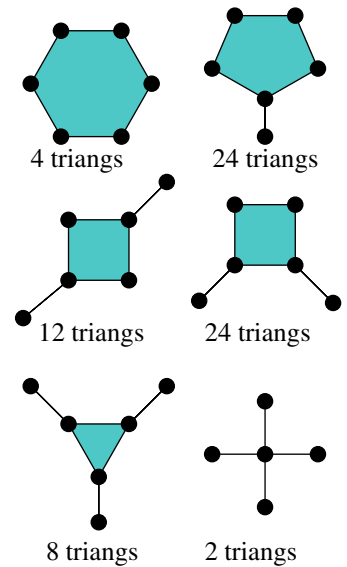


Figure 6.35: The dual complexes to the six types of triangulations of the 3-cube.

inequalities like $x_{000} \geq 1$ correspond to slicing off one vertex. The eight inequalities like $x_{000} \leq 6$ correspond to subdividing the 3-cube into three pyramids whose bases are the square facets disjoint from one vertex. The six inequalities like $x_{000} + x_{001} \geq 4$ correspond to subdividing the 3-cube into two triangular prisms.

6.3.5 Cubes of four dimensions

It is certainly not true in higher dimensions that all triangulations of cubes are lexicographic. In fact, they may not even be regular.

Theorem 6.3.11. *The d -cube \mathbf{I}^d has non-regular triangulations if and only if $d \geq 4$.*

Non-regular triangulations of the 4-cube were first found by De Loera [95]. Here we present a very explicit construction using what we saw in Section 6.3.1.

Proof. That cubes of dimension three have only regular triangulations was established in the previous section. Non-regular triangulations of the 4-cube can be obtained by extending any of the two non-regular triangulations of 0/1 configurations of dimension four constructed in Section 6.3.1. Indeed, if a subconfiguration of a configuration \mathbf{A} has a non-regular triangulation \mathcal{T} , then any triangulation of \mathbf{A} obtained by starting with \mathcal{T} and then placing the rest of points one by one (cf. Section 4.3.1) is non-regular as well (Lemma 4.3.5). \square

Although much more computational effort than was needed for the 4-cube, the complete classification of *regular* triangulations of the 4-cube was done in 2006 by Huggins et al. [167]. Their geometric results, which currently can be verified in about 20 minutes with the software TOPCOM [265], can be summarized as follows:

Theorem 6.3.12. *The 4-cube has 87959448 regular triangulations, partitioned in 235277 symmetry classes. The secondary polytope of the 4-cube has 80876 facets, distributed in 334 symmetry classes.*

The reader may be surprised that we do not give the results for the set of *all* triangulations. The fact is that they are not known. The only method for enumerating triangulations that is efficient enough to finish for the 4-cube is based on exploring the graph of triangulations. But this method only gives the triangulations that can be flipped to the regular ones. This includes some non-regular ones but, in principle, may not contain all of them. There are point sets with a disconnected graph of triangulations, and we do not know if \mathbf{I}^4 is one of them.

The following table lists how many orbits of regular triangulations of each possible size are there. The size of an orbit (or symmetry class) must always be a divisor of $4! \cdot 2^4 = 384$, since this is the order of the symmetry group of the 4-cube. But not all the divisors appear in the list. For example, there is no orbit of size 1, which means that no triangulation has the full symmetry group of the cube.

| orbit size | 8 | 16 | 24 | 32 | 48 | 64 | 96 | 192 | 384 |
|---------------|---|----|----|----|----|-----|-----|--------|---------|
| no. of orbits | 3 | 7 | 2 | 13 | 48 | 102 | 516 | 11 357 | 223 229 |

As seen in the table, most of the triangulations have no symmetry at all, since their orbits have the full size of the symmetry group of the cube. This may come as a surprise after we classified the triangulations of the 4-cube, in which *no orbit* has the size of the whole symmetry group (which is 48). Especially interesting are the most symmetric ones, which are the three whose orbit has size eight. Figures 6.36 and 6.37 show the dual complexes of two of them, which have the symmetries of a 3-cube. These two pictures are taken from [167], where triangulations of the 4-cube are analyzed with a method reminiscent of what we did for the 3-cube (classifying according to the carrier of the barycenter). The data they obtained can be accessed publicly at bio.math.berkeley.edu/4cube/.

Example 6.3.13 (The staircase triangulation of the 4-cube). One of the triangulations with orbit size 8 is the *staircase triangulation*. The description of it as having one full-dimensional simplex corresponding to each permutation makes it no surprise that its dual complex (by this we mean its *tight span*, as introduced in Section 5.3.3) is the *permutohedron* that we already encountered in Section 6.2.1. Its GKZ vector is $(4, 6, 6, 24, 6, 4, 4, 6, 6, 4, 4, 6, 24, 6, 6, 4)$. The orbit has size eight because the triangulation is characterized by which of the eight diameters of the 4-cube it uses (choosing a particular diameter corresponds to fixing the ordering in each factor modulo a reversal of all of them, as in Proposition 6.2.16).

Example 6.3.14 (The minimal triangulation of the 4-cube). Another triangulation is the corner-cut triangulation of Theorem 6.3.6. In the case of the 4-cube, the configuration \mathbf{H}^4 obtained by cutting half of the vertices of \mathbf{I}^4 turns out to be the set of vertices of a cross-polytope. The d -dimensional cross-polytope (d -fold one-point suspension of the configuration consisting of d repeated points) has d triangulations, all equivalent, and with 2^d full-dimensional simplices. In particular, the corner-cut triangulation of the 4-cube is unique, modulo symmetries. The size of its orbit is eight since there are two choices of how to cut half the corners (the even ones or the odd ones), and for each choice there are four triangulations of the resulting cross-polytope.

The dual complex of the triangulation of the d -cross-polytope is the face complex of a $d - 1$ cube. In the corner-cut triangulation, each of the eight vertices of that 3-cube is joined to a tentacle representing each of the eight cornered tetrahedra. This is what Figure 6.37 shows. It is known that the corner-cut triangulation of the 4-cube has the minimum possible size and that it is the unique one with this property (cf. [86]). Its GKZ vector is $(1, 12, 12, 1, 12, 1, 1, 20, 20, 1, 1, 12, 1, 12, 12, 1)$.

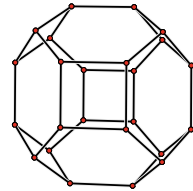


Figure 6.36: One of the most symmetric triangulations of the 4-cube; its *tight span* or dual complex is a permutohedron.



Figure 6.37: Symmetric triangulation of the 4-cube is the minimal one. Its tight span is a “cube with spikes”.

| # maximal simplices | # simplices of volume 1 | # simplices of volume 2 | # simplices of volume 3 | # \mathbf{I}^4 -orbits of triangulations |
|---------------------|-------------------------|-------------------------|-------------------------|--|
| 16 | 8 | 8 | 0 | 1 |
| 17 | 10 | 7 | 0 | 1 |
| 18 | 12 | 6 | 0 | 6 |
| 18 | 13 | 4 | 1 | 11 |
| 19 | 14 | 5 | 0 | 25 |
| 19 | 15 | 3 | 1 | 48 |
| 20 | 16 | 4 | 0 | 628 |
| 20 | 17 | 2 | 1 | 344 |
| 21 | 18 | 3 | 0 | 5 847 |
| 21 | 19 | 1 | 1 | 1 263 |
| 22 | 20 | 2 | 0 | 24 499 |
| 22 | 21 | 0 | 1 | 1 967 |
| 23 | 22 | 1 | 0 | 48 648 |
| 24 | 24 | 0 | 0 | 151 989 |

Table 6.3: Classification of regular triangulations of the 4-cube according to the number and volumes of maximal simplices.

We finish with some more data about $\Sigma\text{-poly}(\mathbf{I}^4)$, extracted from [167]. The reader can observe and extract patterns. For example, Table 6.3 shows the distributions of volumes of simplices in triangulations of the 4-cube. When we say that a simplex has volume i we mean $i/4!$ (put differently, we have normalized our volumes so that unimodular simplices have volume one).

The maximum volume of a simplex contained in the 4-cube is three. But, as seen in the table, no triangulation uses more than one such simplex. The reason is simply that all simplices of volume three in \mathbf{I}^4 contain the centroid in their interior!

In Table 6.4, we classify the f -vectors of (the dual complexes of) triangulations of \mathbf{I}^4 . The last entry in each f -vector, which is always zero or one, corresponds to the existence (or not) of a 3-dimensional cell in the dual complex, that is, to the appearance of an interior edge in the triangulation. If such an edge appears, it must be a diameter and, hence, unique.

As we have seen in Chapter 5, the facets of the secondary polytope correspond to the coarsest regular polyhedral subdivisions. Remember that a subdivision \mathcal{S} is coarsest if \mathcal{S} does not refine other proper subdivisions. Huggins et al. computed all such subdivisions for the 4-cube, finding that there are exactly 80876 of them. The distribution of the types of coarsest regular subdivisions according to orbit size is

| orbit size | 8 | 12 | 16 | 24 | 32 | 48 | 64 | 96 | 192 | 384 |
|---------------|---|----|----|----|----|----|----|----|-----|-----|
| no. of orbits | 2 | 1 | 4 | 2 | 4 | 14 | 16 | 26 | 132 | 133 |

A coarsest subdivision of the 4-cube can have up to 13 maximal cells. See Table 6.5.

| <i>f</i> -vector | {3} | {3,2} | {3,1} | {3,2,1} | {2} | {2,1} | total |
|------------------|------|--------|---------|---------|--------|--------|---------|
| (16, 20, 6, 1) | | | 1 | | | | 1 |
| (17, 22, 7, 1) | | | 1 | | | | 1 |
| (18, 24, 8, 1) | | | 4 | 2 | | | 6 |
| (18, 23, 6, 0) | | | | | 11 | | 11 |
| (19, 26, 9, 1) | | | 6 | 19 | | | 25 |
| (19, 25, 7, 0) | | | | | 48 | | 48 |
| (20, 28, 10, 1) | 1 | 23 | 209 | | | | 233 |
| (20, 27, 8, 0) | | | | 24 | 715 | | 739 |
| (21, 30, 11, 1) | 5 | 34 | 1 372 | | | | 1 411 |
| (21, 29, 9, 0) | | | | 392 | 5 307 | | 5 699 |
| (22, 32, 12, 1) | 112 | 84 | 9 342 | | | | 9 538 |
| (22, 31, 10, 0) | | | | 2 156 | 14 772 | | 16 928 |
| (23, 34, 13, 1) | 2116 | 100 | 46 432 | | | | 48 648 |
| (24, 36, 14, 1) | 125 | 27 054 | 124 810 | | | | 151 989 |
| total | 125 | 29 288 | 253 | 182 186 | 2 572 | 20 853 | 235 277 |

Table 6.4: Distribution of the 235 277 types of triangulations of \mathbf{I}^4 . Rows correspond to the *f*-vectors and columns correspond to the dimensions of maximal faces of the dual complex.

| # cells | {3} | {3,2} | {2} | {1} | total |
|---------|-----|-------|-----|-----|-------|
| 2 | | | 4 | | 4 |
| 3 | | | 5 | | 5 |
| 4 | 3 | | 7 | | 10 |
| 5 | 4 | 3 | 17 | | 24 |
| 6 | 5 | 14 | 12 | | 31 |
| 7 | 13 | 21 | 39 | | 73 |
| 8 | 7 | 31 | 51 | | 89 |
| 9 | 7 | 26 | 24 | | 57 |
| 10 | 2 | 14 | 21 | | 37 |
| 11 | 1 | 1 | | | 2 |
| 12 | 1 | | | | 1 |
| 13 | 1 | | | | 1 |
| total | 44 | 176 | 110 | 4 | 334 |

Table 6.5: Distribution of the 334 types of coarsest regular subdivisions of the 4-cube. Rows correspond to the number of maximal cells, and columns correspond to the dimensions of maximal faces of the dual complex.

6.3.6 Slices of cubes: triangulations of hypersimplices

The *k*-th hypersimplex of order *n* (or, of dimension *n* – 1) is the configuration $\mathbf{D}(n, k)$, consisting of the vertices of the *n*-cube \mathbf{I}^n in the hyperplane of all points whose sum of coordinates is equal to *k*. It is understood that $k \in \{1, \dots, n\}$. Clearly, the hypersimplex $\mathbf{D}(n, k)$ has $\binom{n}{k}$ vertices and the hypersimplex $\mathbf{D}(n, 1)$ is just the *n* – 1 simplex \mathbf{D}_n . As an example, the second hypersimplex of order 6, $\mathbf{D}(6, 2)$, is:

$$\begin{pmatrix} & 12 & 13 & 14 & 15 & 16 & 23 & 24 & 25 & 26 & 34 & 35 & 36 & 45 & 46 & 56 \\ \left(\begin{array}{cccccccccccccc} 1 & 1 & 1 & 1 & 1 & 0 & 0 & 0 & 0 & 0 & 0 & 0 & 0 & 0 & 0 & 0 \\ 1 & 0 & 0 & 0 & 0 & 1 & 1 & 1 & 1 & 0 & 0 & 0 & 0 & 0 & 0 & 0 \\ 0 & 1 & 0 & 0 & 0 & 1 & 0 & 0 & 0 & 1 & 1 & 1 & 0 & 0 & 0 & 0 \\ 0 & 0 & 1 & 0 & 0 & 0 & 1 & 0 & 0 & 0 & 1 & 0 & 0 & 1 & 1 & 0 \\ 0 & 0 & 0 & 1 & 0 & 0 & 0 & 1 & 0 & 0 & 0 & 1 & 0 & 1 & 0 & 1 \\ 0 & 0 & 0 & 0 & 1 & 0 & 0 & 0 & 1 & 0 & 0 & 1 & 0 & 1 & 0 & 1 \end{array} \right) \end{pmatrix}.$$

Observe that we do not write the customary homogenization row of ones. The reason is that the hypersimplex is already homogeneous, since the sum of coordinates is constant.

Hypersimplices appear very frequently in mathematical questions and have a long history, going back more than a hundred years (see [225] and the many references therein for a survey of results and various properties of $\mathbf{D}(n, k)$). For example, they appear in algebraic combinatorics in connection to enumeration and toric varieties [303], [137]. The matrix of the second hypersimplex $\mathbf{D}(n, 2)$ is the same as the vertex-edge incidence matrix of the complete graph K_n . Thus, one can investigate the second hypersimplex with the purpose of studying random graphs on n nodes, and more general hypersimplices to do the same for *uniform multigraphs*; this problem has been studied in [299]. In turn, the set of all multigraphs on n nodes with fixed vertex degrees is the set of feasible solutions of an important problem of combinatorial optimization, namely, the perfect f-matching problem. See [219] and [101]. But the list of applications continues, as hypersimplices are also studied in analysis and number theory, especially using bounds of their volumes (see [64] and the references therein). Yet another application of hypersimplices is their connection to tropical geometry and phylogenetics (see [29, 159]).

One curious property of hypersimplices is that $\mathbf{D}(n, k)$ is an identical copy of $\mathbf{D}(n, n - k)$ via the map that changes zeros for ones and vice versa. This is justified by the interpretation of $\mathbf{D}(n, k)$ as a slice of the cube. The slicing hyperplanes are orthogonal to the line segment joining the point $(0, 0, \dots, 0)$ with the point $(1, 1, \dots, 1)$. In this way, $\mathbf{D}(n, k)$ is at the same distance from $(0, 0, \dots, 0)$ as $\mathbf{D}(n, n - k)$ is from $(1, 1, \dots, 1)$; thus by the symmetry of the cube they must be identical isometric slices.

But other relations between hypersimplices arise:

Proposition 6.3.15. *The hypersimplex $\mathbf{D}(n, k)$, for $1 < k < n - 1$, has exactly $2n$ facets, which are all hypersimplices: n of them are isomorphic to $\mathbf{D}(n - 1, k - 1)$, and the other n to $\mathbf{D}(n - 1, k)$. In fact, the complement of each facet of one type is a facet of the other type.*

Proof. By definition, facets of the hypersimplex are defined by setting one coordinate equal to zero or to one. The former produces a hypersimplex $\mathbf{D}(n - 1, k)$ and the latter produces $\mathbf{D}(n - 1, k - 1)$. Every vertex of the original hypersimplex lies in exactly one of the facets obtained when fixing a particular coordinate. \square

Related to this last statement is an alternative way of thinking of $\mathbf{D}(n, k)$:

As the slice of the cube \mathbf{I}^{n-1} lying between the consecutive hypersimplices $\mathbf{D}(n-1, k-1)$ and $\mathbf{D}(n-1, k)$. For this, consider the matrix defining $\mathbf{D}(n, k)$ and add to a particular row (say, the first one) all the other ones. The combinatorics of the configuration does not change, but that particular row becomes constant, which means you can think of it as the homogenization coordinate. Forgetting that coordinate, the columns of the matrix defining $\mathbf{D}(n, k)$ are the union of the columns of $\mathbf{D}(n-1, k-1)$ and those of $\mathbf{D}(n-1, k)$. This has the interesting consequence that you can build a cube, \mathbf{I}^{n-1} , by gluing the different hypersimplices $\mathbf{D}(n-1, k)$, for $k = 1, \dots, n-1$. For example, the 3-cube is the union of a tetrahedron $\mathbf{D}(4, 1)$, an octahedron $\mathbf{D}(4, 2)$, and another tetrahedron $\mathbf{D}(4, 3)$. See Figure 6.38.

This has the consequence that the sum of the normalized volumes of the different hypersimplices must equal the volume of the cube \mathbf{I}^{n-1} . More precisely:

Proposition 6.3.16. *The normalized volumes of hypersimplices satisfy the following recurrence relation:*

$$\text{vol}(\mathbf{D}(n, k)) = k \text{vol}(\mathbf{D}(n-1, k)) + (n-k) \text{vol}(\mathbf{D}(n-1, k-1)).$$

Proof. To compute the volume we arbitrarily choose a vertex of $\mathbf{D}(n, k)$ and decompose $\mathbf{D}(n, k)$ as the unions of cones with apex at this vertex and with base at all the facets not using that vertex. Since our vertex has k coordinates equal to 1 and $n-k$ of them equal to zero, it lies on n facets of $\mathbf{D}(n, k)$: k of the form $\mathbf{D}(n-1, k)$ and $n-k$ of the form $\mathbf{D}(n-1, k)$. The height of all cones is 1, hence the formula follows. \square

The numbers obtained by this recursion are called the *Eulerian numbers* and have several different combinatorial interpretations. Most famously the numbers $E(n, k)$ record the number of permutations of the numbers $1, \dots, n$ having exactly k ascents, so $\pi(i) < \pi(i+1)$ for precisely k indices. (see [146, 303, 308]). It is instructive to compute the first few of these numbers. They can be nicely arranged in a fashion similar to Pascal's triangle, called *Eulerian numbers triangle*:

$$\begin{array}{ccccccc} & & & 1 & & & \\ & & & 1 & 1 & & \\ & & & 1 & 4 & 1 & \\ & & & 1 & 11 & 11 & 1 \\ & & & 1 & 26 & 66 & 26 & 1 \\ & & & 1 & 57 & 302 & 302 & 57 & 1 \end{array}$$

The first and last diagonals are 1 because that is the normalized volume of the simplex $\mathbf{D}(n, 1)$. The second diagonal admits the following simple formula:

$$\text{vol}(\mathbf{D}(n, 2)) = 2^{n-1} - n.$$

For example, the normalized volume of the octahedron $\mathbf{D}(4, 2)$ is $2^3 - 4 = 4$.

For the volume of hypersimplices, Vaaler [324] established a sharp lower bound on the volume of a central slice (passing through the origin) of at

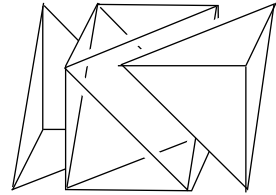


Figure 6.38: A 3-cube as the union of the hypersimplices $\mathbf{D}(4, 1)$, $\mathbf{D}(4, 2)$, and $\mathbf{D}(4, 3)$.

least one. Later K. Ball [28] proved that if H is a k -dimensional subspace, $1 \leq k < n$, intersects the cube \mathbf{I}^n , then $\text{vol}(H \cap \mathbf{I}^n) \leq (\sqrt{2})^{(n-k)}$, where vol is k -dimensional volume. This bound is the best possible and, in particular, gives a bound for the volume of hypersimplices. Let us study now triangulations of hypersimplices. First, we look at the pulling triangulations which corroborates that volume considerations and triangulations are indeed closely related:

Proposition 6.3.17. *Every pulling triangulation of $\mathbf{D}(n, k)$ is unimodular; hence it has $\text{vol}(\mathbf{D}(n, k))$ maximal simplices.*

Proof. This follows from the same arguments as in the previous proof. The pulling triangulation is obtained by coning the last vertex v (of the given order) to all the pulling triangulations of the facets that do not contain it. Since the facets are themselves hypersimplices, their pulling triangulations are unimodular. Since the vertex v is at distance one from each facet, the final triangulation is unimodular as well. \square

Proposition 6.3.18. *The hypersimplex $\mathbf{D}(6, 3)$ has non-regular triangulations.*

Proof. For $\mathbf{D}(6, 3)$, consider the following subconfiguration of it:

$$\mathbf{A} = \begin{pmatrix} 0^+ & 0^- & 1 & 2 & 3 & 4 & 5 & 6 & 7 & 8 \\ 0 & 1 & 1 & 1 & 1 & 1 & 0 & 0 & 0 & 0 \\ 1 & 0 & 0 & 0 & 0 & 0 & 1 & 1 & 1 & 1 \\ 1 & 0 & 0 & 0 & 1 & 1 & 0 & 0 & 1 & 1 \\ 0 & 1 & 0 & 1 & 0 & 1 & 0 & 1 & 0 & 1 \\ 0 & 1 & 1 & 0 & 1 & 0 & 1 & 0 & 1 & 0 \\ 1 & 0 & 1 & 1 & 0 & 0 & 1 & 1 & 0 & 0 \end{pmatrix}.$$

We claim that this subconfiguration has non-regular triangulations, from which non-regular triangulations of $\mathbf{D}(6, 3)$ can be constructed by placing the rest of points in an arbitrary order. To prove the claim, we show that \mathbf{A} is nothing but the configuration $\overline{\mathbf{I}}^3$ of Example 6.3.1 in disguise.

First, observe that \mathbf{A} has rank (at most) five, that is, dimension four. Indeed, the sum of the first two coordinates equals 1, and the sum of the last four equals two. In particular, we can erase the last row and have an affinely isomorphic configuration. If, after this is done, the second row of the matrix is added to the first one, our matrix becomes exactly the one in Example 6.3.1. \square

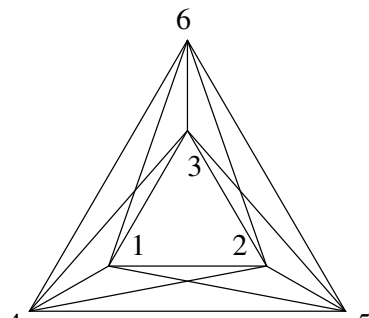


Figure 6.39: The complete graph K_6 , as a representation of $\mathbf{D}(6, 2)$.

In the rest of this section, we want to show that $\mathbf{D}(6, 2)$ also has non-regular triangulations. As we have done several times, we start by studying a certain regular subdivision, which we then show how to define. We are going to represent the elements of $\mathbf{D}(6, 2)$ as the edges in the complete graph K_6 . We draw the nodes of K_6 lying in two parallel triangles to highlight certain symmetries.

Let ω be the height vector that is zero on the elements 14, 25, and 36, and one on the other twelve elements of $\mathbf{D}(6, 2)$.

Proposition 6.3.19. *The regular subdivision $\mathcal{S}(\mathbf{D}(6,2), \omega)$ has the fourteen maximal cells drawn as subgraphs of K_6 in Figure 6.39. Eight of them are bases and the other six have corank one. Moreover, the intersection of any two of them is independent.*

Proof. This is left for the reader as an exercise (see a hint in Exercise 6.14). \square

Since no intersection of two cells contains a dependent subset, in order to refine $\mathcal{S}(\mathbf{D}(6,2), \omega)$ we can independently triangulate each of the six corank-one cells. Doing so is the same as choosing one of the two parts of their unique circuits to be simplices. We choose to use the six that are drawn in solid lines in Figure 6.41.

Proposition 6.3.20. *The triangulation of $\mathbf{D}(6,2)$ obtained in this way is not regular.*

Proof. Suppose that ω' was a height vector producing this triangulation as a regular triangulation. Then, the appearance of the six triangles we have selected in the six (3,3) circuits of Figure 6.41 implies the following six conditions on ω' :

$$\begin{aligned}\omega'_{14} + \omega'_{23} + \omega'_{35} &< \omega'_{25} + \omega'_{13} + \omega'_{34}, \\ \omega'_{36} + \omega'_{15} + \omega'_{45} &< \omega'_{14} + \omega'_{35} + \omega'_{56}, \\ \omega'_{25} + \omega'_{34} + \omega'_{46} &< \omega'_{36} + \omega'_{24} + \omega'_{45}, \\ \omega'_{25} + \omega'_{13} + \omega'_{16} &< \omega'_{36} + \omega'_{12} + \omega'_{15}, \\ \omega'_{36} + \omega'_{12} + \omega'_{24} &< \omega'_{14} + \omega'_{23} + \omega'_{26}, \\ \omega'_{14} + \omega'_{26} + \omega'_{56} &< \omega'_{25} + \omega'_{16} + \omega'_{46}.\end{aligned}$$

Since the sum of left-hand sides equals that of right-hand sides, this system of inequalities is infeasible. \square

Theorem 6.3.21. *The hypersimplex $\mathbf{D}(n,k)$ has a non-regular triangulation if and only if $k \geq 2$, $n - k \geq 2$ and $n \geq 6$.*

Proof. Every hypersimplex with $k \geq 2$ and $n - k \geq 4$ contains either $\mathbf{D}(6,2)$ or $\mathbf{D}(6,3)$ as a face. We have seen that those two hypersimplices have non-regular triangulations, hence those containing them have non-regular triangulations too. So, we only need to argue that the hypersimplices not satisfying those constraints do not have non-regular triangulations.

If k or $n - k$ equals 1, then our hypersimplex is a simplex. Among those with $k \geq 2$ and $n - k \geq 2$, the ones we need to discuss are $\mathbf{D}(4,2)$, $\mathbf{D}(5,2)$ and $\mathbf{D}(5,3)$. The first one is a regular octahedron, whose three triangulations are equivalent, hence regular.

The other two are isomorphic. The polytope $\mathbf{D}(5,2)$ has dimension four, 10 vertices and 10 facets (five tetrahedra and five octahedra). It is small enough that TOPCOM can compute all its triangulations, not just the regular ones. The result is that they are all regular. \square

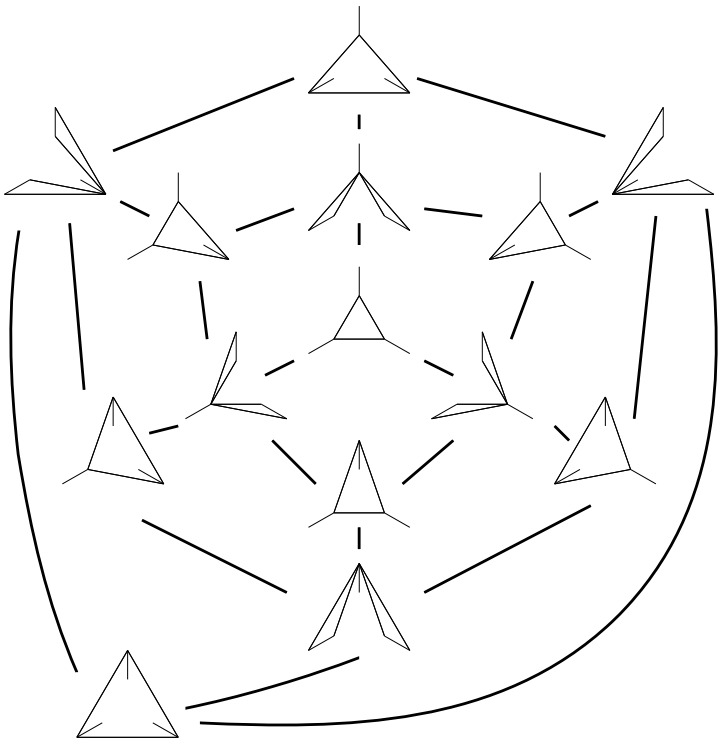


Figure 6.40: The regular subdivision $\mathcal{S}(\mathbf{D}(6,2), \omega)$.

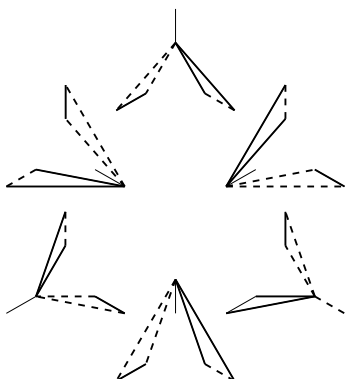


Figure 6.41: Specifying one side of each circuit,
in $\mathcal{S}(\mathbf{D}(6,2), \omega)$.

As additional information, the secondary polytope of $\mathbf{D}(5,2)$ is five dimensional and has 102 vertices, 255 edges, 240 two-faces, 105 three-faces, and 20 facets. Under the natural S_5 -action on the vertices of $\mathbf{D}(5,2)$, there are only three regular triangulations of it. See [101] and [242] for more on the second hypersimplex and its subpolytopes.

6.3.7 Birkhoff's polytope

A very important polytope in many applications is the polytope \mathbf{B}_n of all $n \times n$ doubly stochastic matrices; that is, the set of real nonnegative matrices with all row and column sums equal to one. This polytope is sometimes known as the *Birkhoff polytope*, the *Birkhoff-von Neumann polytope* or simply the *assignment polytope*. We will describe a few results about the triangulations of \mathbf{B}_n .

One interest in computing a triangulation of \mathbf{B}_n is to compute its volume which goes back to the problem of generating a doubly stochastic matrix uniformly at random. The search for a close formula for the volume (and thus of the size of a triangulation) of \mathbf{B}_n continues. Nevertheless, we still do not know a close (efficient) formula for the volume or for the size of a unimodular triangulation for all values of n . As of today the record for values computed is by Beck and Pixton [38] who computed the exact value of the volume and the Ehrhart polynomials for up to $n = 10$ and $n = 9$

respectively. The computations in [38] took several years of computer CPU (running in a parallel machine setup). A combinatorial formula appeared in [98] (although it is exponentially long and thus hard to evaluate). On the other hand, Canfield and McKay [71] provided simple fairly-accurate asymptotic approximation formulas for the volume of \mathbf{B}_n as well as for the number of lattice points of the dilated polytope $t\mathbf{B}_n$.

In what follows, we will make use of some well known properties of the face structure of \mathbf{B}_n (see [52] and [74] for further properties and references). A famous result of Birkhoff says that the vertices of \mathbf{B}_n are precisely the $n \times n$ permutation matrices. Permutation matrices are in bijection with matchings on the complete bipartite graph $K_{n,n}$, and this helps establish a graph theoretic interpretation of the faces of \mathbf{B}_n . The polytope \mathbf{B}_n lies in the n^2 -dimensional real space $\mathbb{R}^{n^2} = \{n \times n \text{ real matrices}\}$, and we use $M(i,j)$ to denote the (i,j) -entry of a matrix M in the space. The edges of \mathbf{B}_n correspond to the cycles in $K_{n,n}$. On the other hand, for each pair (i,j) with $1 \leq i, j \leq n$, the set of doubly-stochastic matrices with the (i,j) entry equal to 0 is a *facet* (a maximal proper face) of \mathbf{B}_n , and all facets arise in this way. It is also easy to see that the dimension of \mathbf{B}_n is $(n-1)^2$ (i.e., the volume of \mathbf{B}_n is the $(n-1)^2$ -volume of \mathbf{B}_n regarded as a subset of n^2 -dimensional Euclidean space).

Example 6.3.22. \mathbf{B}_2 consists of the line segment joining the matrices

$$\begin{pmatrix} 1 & 0 \\ 0 & 1 \end{pmatrix} \quad \text{and} \quad \begin{pmatrix} 0 & 1 \\ 1 & 0 \end{pmatrix},$$

and hence its volume is two.

In general, it is convenient to identify the faces of \mathbf{B}_n with certain $n \times n$ matrices of 0's and 1's, as follows: First, we identify a 0-1 matrix with the set of entries in the matrix that are 1's. Thus, for two 0-1 matrices M and N of the same size, we can define their union $M \cup N$ as the 0-1 matrix whose set of 1's is the union of the sets of 1's of M and N , e.g.,

$$\begin{pmatrix} 1 & 0 & 0 \\ 0 & 1 & 0 \\ 0 & 0 & 1 \end{pmatrix} \cup \begin{pmatrix} 0 & 1 & 0 \\ 1 & 0 & 0 \\ 0 & 0 & 1 \end{pmatrix} = \begin{pmatrix} 1 & 1 & 0 \\ 1 & 1 & 0 \\ 0 & 0 & 1 \end{pmatrix}.$$

Similarly we can speak of one 0-1 matrix containing another and so forth.

Now to each face \mathbf{F} of \mathbf{B}_n , we associate the matrix M which is the union of the vertices (permutation matrices) in \mathbf{F} . The facets of \mathbf{B}_n containing \mathbf{F} are precisely those associated with the zero entries of M . Since any face is the intersection of the facets containing it, any permutation matrix contained in M must be a vertex of \mathbf{F} . Thus, the vertices of \mathbf{F} are precisely the permutation matrices contained in M , so we can recover \mathbf{F} from M . In this way we identify the faces of \mathbf{B}_n with the set of 0-1 matrices which are unions of permutation matrices. This characterization is very useful for investigating the polytope. Note that not every 0-1 matrix corresponds to a face of \mathbf{B}_n . For example

$$\begin{pmatrix} 0 & 1 \\ 1 & 1 \end{pmatrix}$$

is not a union of permutation matrices, hence it is not a face of \mathbf{B}_2 .

The matrix representations of the faces of \mathbf{B}_n is useful for all sort of calculations and to prove properties, but one can also think of these matrices as specifying a bipartite graph, i.e., the bipartite graph on $2n$ nodes in which i is joined to j when the (i, j) entry of the matrix of \mathbf{F} is 1. This is used, for example, to calculate the dimension of a face of \mathbf{B}_n , since the dimension is equal to $e + k - 2n$, where e is the number of 1's in the matrix of \mathbf{F} and k the number of components in the graph corresponding to \mathbf{F} .

Example 6.3.23. Using this characterization of faces and their dimension, Billera and Sarangarajan (see Theorem 2.2 in [51] and more details in [52]) proved that:

Lemma 6.3.24. *Every pair of vertices of \mathbf{B}_n is contained in a cubical face of dimension at most $\lfloor n/2 \rfloor$.*

Proof. Think of each vertex of \mathbf{B}_n as a perfect matching in the complete bipartite graph on $2n$ vertices. Then the minimal face \mathbf{F} containing two given vertices has as an associated graph the union of two perfect matchings. The connected components of this graph are either isolated edges or cycles of even length. In each of the cycles, there are two choices of perfect matching, so that the vertices contained in \mathbf{F} are 2^p , where p is the number of such cycles. The face \mathbf{F} itself is a Minkowski sum of the segments corresponding to changing one matching to the other in a single component. \square

An $n \times n$ doubly stochastic matrix is determined by its upper left $(n-1) \times (n-1)$ submatrix. The set of $(n-1) \times (n-1)$ matrices obtained this way is the set \mathbf{A}_n of all nonnegative $(n-1) \times (n-1)$ matrices with row and column sums ≤ 1 such that the sum of all the entries is at least $n-2$. This is affinely isomorphic to \mathbf{B}_n .

There is a more natural unit for the volume of \mathbf{B}_n and its faces or simplices. This is based on the fact that the vertices of \mathbf{B}_n are integer matrices. Suppose that \mathbf{F} is a d -dimensional face of \mathbf{B}_n . Since its vertices have integer coordinates, the integer points in the affine span of \mathbf{F} comprise a d -dimensional affine lattice \mathbf{L} . Given such a lattice, there is a minimum volume of any d -simplex with vertices in \mathbf{L} . Lattice points $\mathbf{w}_0, \dots, \mathbf{w}_d$ are the vertices of one of these minimum volume simplices if and only if every point of \mathbf{L} is uniquely expressible in the form $\sum_{i=0}^d k_i \mathbf{w}_i$, where the k_i 's are integers whose sum is 1. The *relative volume* of a face \mathbf{F} is the volume of \mathbf{F} expressed in units equal to the volume of a minimal simplex in \mathbf{L} .

The relative volume of a face is the same, whether regarded as a face of \mathbf{B}_n or as a face of \mathbf{A}_n , since the mapping from \mathbf{B}_n to \mathbf{A}_n (by taking the upper left $(n-1) \times (n-1)$ minor) preserves integrality of points. To convert relative volumes to true volumes, we need to know the volume of a minimal simplex of \mathbf{A}_n , but the affine span of \mathbf{A}_n is all of $(n-1)^2$ -dimensional space. Hence, the volume of a minimal simplex in \mathbf{A}_n is $\frac{1}{((n-1)^2)!}$, and the volume of a minimal simplex in \mathbf{B}_n is $\frac{n^{n-1}}{((n-1)^2)!}$.

For \mathbf{B}_n , we use a standard pulling triangulation of \mathbf{B}_n into simplices (recall Section 4.3.2) The triangulation is constructed recursively (and at the same

time compute the volume). To get started we use the fact that the relative volume of any zero-dimensional face of \mathbf{B}_n is 1 and it is already triangulated. We produce a list of all faces of each dimension. Then, for each face \mathbf{F} of dimension d we select a vertex \mathbf{v} , determine the facets of \mathbf{F} opposite \mathbf{v} . Assuming recursively that their triangulations and relative volumes have already been computed, we now find the new triangulation of \mathbf{F} by pulling from the vertex to the opposite faces. Summing the relative volumes of the facets gives the relative volume of \mathbf{F} . The process continues until the triangulation of \mathbf{B}_n is then formed by joining a chosen vertex to each simplex in the triangulation of each of the facets. Of course, in practice it is naive to think that one can compute and store all faces of \mathbf{B}_n . Since many of the 2^{n^2} possible 0-1 matrices are actually faces of \mathbf{B}_n . One can nevertheless appeal to several tricks and symmetry to carry out the computation (see [74] for practical implementation details) The pulling triangulation of \mathbf{B}_n and its faces have an unusual property, given by R. P. Stanley in [304]:

Proposition 6.3.25. *In any lexicographic pulling triangulation of a face \mathbf{F} of \mathbf{B}_n , every simplex has minimal volume in the affine lattice determined by \mathbf{F} .*

Proof. Let \mathbf{F} be a d -dimensional face of \mathbf{B}_n , \mathbf{v}_0 any vertex in \mathbf{F} , and \mathbf{G} a facet of \mathbf{F} opposite \mathbf{v}_0 . Suppose that a simplex in a pulling triangulation of \mathbf{G} has vertices $\mathbf{v}_1, \mathbf{v}_2, \dots, \mathbf{v}_d$. We need to prove that the set of integer points of the affine space determined by \mathbf{F} is the same as the set of points $\sum_{i=0}^d k_i \mathbf{v}_i$, where the k_i are integers whose sum is 1.

Of course, all the integer combinations are in the affine span. The question is whether there are any other points. Any integral point of the affine span can be uniquely expressed in the form $\sum_{i=0}^d r_i \mathbf{v}_i$, where the r_i 's are real numbers with sum 1.

Since \mathbf{v}_0 is not in the face \mathbf{G} , there is a facet of \mathbf{B}_n containing \mathbf{G} but not \mathbf{v}_0 . Thus, \mathbf{v}_0 must have at least one entry equal to 1 in the same position where all \mathbf{v}_i , $i \geq 1$ have zeroes. Thus, in the hypothetical combination above, r_0 must be an integer. If we add $r_0(\mathbf{v}_1 - \mathbf{v}_0)$ to the combination above, we obtain another integral point in the affine span of \mathbf{G} . It follows, using induction, that $r_1 + r_0$, and r_2, \dots, r_d are integers and therefore all the r 's are integers, as desired. \square

Corollary 6.3.26. *In any pulling triangulation of a face of the \mathbf{B}_n , the number of simplices in the triangulation is equal to the relative volume and thus the triangulation is made of unimodular simplices. Moreover, given a face \mathbf{F} of \mathbf{B}_n and a vertex v of \mathbf{F} , the relative volume of \mathbf{F} is the sum of the relative volumes of facets of \mathbf{F} opposite v .*

It is worth noting that \mathbf{B}_n is then officially a member of the family of *compressed polytopes* that are characterized by having all its pulling triangulations to be unimodular, but this implies that they are “thin” in all facet directions. We will give details about this in Chapter 9, Definition 9.3.18. The same procedure works for computing a pulling triangulation of any face. This was done by Chan, Robbins, and Yuen [75] for the set of matrices for

which the set of zeroes of the matrix form a Young tableau in a corner of the matrix. More precisely, suppose that $n \geq 2$ and that \mathbf{F}_n is the $n \times n$ matrix whose (i, j) entry is 1 when $j \leq i + 1$, and 0 otherwise. Then \mathbf{F}_n is a union of permutation matrices, corresponding to a face of \mathbf{B}_n of dimension $\binom{n}{2}$ with 2^{n-1} vertices, and we have the following result, proved by D. Zeilberger in [338]

Proposition 6.3.27. *The relative volume of \mathbf{F}_n is the product*

$$\prod_{i=0}^{n-2} \frac{1}{i+1} \binom{2i}{i}$$

of the first $n - 1$ Catalan numbers.

To conclude, we investigate the existence of non-regular triangulations for \mathbf{B}_n .

Theorem 6.3.28. *For all $n \geq 4$, the Birkhoff polytope \mathbf{B}_n contains non-regular triangulations.*

Proof. The idea of the proof is that once one finds a subpolytope of \mathbf{B}_4 that has a non-regular triangulation, this can be extended to a non-regular triangulation of \mathbf{B}_4 via placings, in the sense of Section 4.3.1. In addition, since \mathbf{B}_n is isomorphic to a face of \mathbf{B}_{n+1} , the same argument guarantees that there exists a non-regular triangulation for all \mathbf{B}_n , $n \geq 4$.

In [190], E. Kim, found a non-regular triangulation of a subpolytope of \mathbf{B}_4 . We skip this more complicated triangulation, but let us show a simple argument implying that \mathbf{B}_6 has, indeed, a non-regular triangulation. Observe that \mathbf{B}_{n+m} contains as a face the product $\mathbf{B}_n \times \mathbf{B}_m$, given by the block diagonal matrix with an $n \times n$ and an $m \times m$ block of 1's. Now, any product of two polytopes of dimensions three or more has non-regular triangulations, because the product of two tetrahedra does (Section 6.2.4). We conclude that every \mathbf{B}_n , $n \geq 6$, has a face with non-regular triangulations. \square

To conclude this section, we leave it as an exercise to the reader to see that \mathbf{B}_3 has only regular triangulations.

Exercises

Exercise 6.1. Prove Lemma 6.1.10.

Exercise 6.2. Show that any consecutively labeled configuration of n points on the $n - d - 2$ -dimensional moment curve that is alternatingly colored black and white represents a Gale diagram of $\mathbf{C}(n, d)$. (*Hint:* use the signs of the Vandermonde-determinant to draw conclusions about circuits and cocircuits.)

Exercise 6.3. Find coordinates of a cyclic point configuration so that the cyclic group action on the points that preserves circuits up to reversing signs

can be represented by an isometric affine map. In other words, in these coordinates the point configuration is cyclically symmetric in the usual geometric sense. (*Hint:* try to use trigonometric monomials instead of ordinary monomials; if you are desperate, google for “Carathéodory’s curve.”)

Exercise 6.4. Show that for one-dimensional cyclic polytopes, the first and the second Higher Stasheff-Tamari posets coincide.

Exercise 6.5. Show that every triangulation of $\mathbf{C}(n, 2)$ gives rise to a sequence of flips in $\mathbf{C}(n, 1)$ from $\hat{0}$ to $\hat{1}$.

Exercise 6.6 (Open). Prove or disprove that the first and the second higher Stasheff-Tamari posets coincide in general.

Exercise 6.7. Show that the permutohedron of dimension $d - 1$ has $2^d - 2$ facets and $(d - 1)d!/2$ edges. (If you want more, show also that it has $3^d - 3 \cdot 2^d + 3$ ridges, $4^d - 4 \cdot 3^d + 6 \cdot 2^d - 4$ faces of codim 3, and so on).

Exercise 6.8. Prove the following extension of Corollary 6.2.7: Subdivisions of prism(\mathbf{D}_n) are in bijection with partial orientations of the complete graph K_n with the following property: In every triangle either zero, two, or all three edges are directed. If three, the orientation is acyclic. If two, they either have the same origin or the same destination.

Exercise 6.9. Characterize staircases of $\mathbf{D}_n \times \mathbf{D}_m$ in the bipartite graph representation.

Exercise 6.10. For the five symmetry classes of triangulations of $\mathbf{D}_3 \times \mathbf{D}_3$ (see Figure 6.24):

1. Say which ones are pushing and which ones are pulling. (*Hint:* three classes are pushing and pulling simultaneously. One is only pushing and another is only pulling)
2. Count how many flips there are (*Hint:* one of the symmetry classes has six. The rest all have four).

Exercise 6.11. Check property (ICoP) for the triangulation of Section 6.2.4 (that is, finish the proof of Lemma 6.2.20).

Exercise 6.12. Prove that the list of symmetry types of tetrahedra in \mathbf{I}^3 given at the beginning of Section 6.3.4 is complete.

Exercise 6.13. Using the interpretation of the points of $\mathbf{D}(n, 2)$ as the edges of the complete graph K_n prove the following properties

A subpolytope σ of $\mathbf{D}(n, 2)$ is an $(n - 1)$ -dimensional simplex if and only if the corresponding subgraph H satisfies the following properties.

- (i) H is a spanning subgraph with n edges.
- (ii) Each component contains at most one cycle.

(iii) All cycles in H have odd length

Furthermore the normalized volume of σ is $2^{q(H)-1}$ where $q(H)$ is the number of disjoint cycles in H .

Exercise 6.14. Prove Proposition 6.3.19.

Hint: You will save a lot of work if you observe that the subdivision $\mathcal{S}(\mathbf{D}(6,2), \omega)$ must inherit all the symmetries of $\mathbf{D}(6,2)$ that are preserved by ω . These form a group of order 48 consisting of all the permutations that send each of the pairs $\{1,4\}$, $\{2,5\}$ and $\{3,6\}$ to another, not necessarily in the same order. Modulo these symmetries, there are only two types of graphs in Figure 6.39.

Exercise 6.15. Consider the d -dimensional 0/1-cube and for each permutation $\sigma = (\sigma_1, \dots, \sigma_d)$ of the numbers $1, \dots, d$, consider the polytope defined by the following chain of inequalities:

$$\mathbf{P}_\sigma := \{ (x_1, \dots, x_d) : 0 \leq x_{\sigma(1)} \leq x_{\sigma(2)} \leq \dots \leq x_{\sigma(d)} \leq 1 \}$$

Prove that the $d!$ simplices defined by the different choices of σ form a triangulation of the cube. This will finish the proof of Proposition 6.3.4.

Exercise 6.16. Show that the list of four kinds of tetrahedra of a 3-cube presented in Subsection 6.3.4 contains all possible tetrahedra of a cube and it is irredundant.

Exercise 6.17. As a refinement of Theorem 6.3.10, prove that there are only two types of triangulations of the 3-cube that use the same number of corner tetrahedra

Exercise 6.18. • Show that the Birkhoff polytope \mathbf{B}_3 has only regular triangulations.

Some Interesting Triangulations

In previous chapters, we have seen examples of non-regular triangulations which had fewer flips than the number of flips that a regular triangulation must always have (e.g., the triangulation of the cube-octahedron in Proposition 3.6.18). This motivates a definition:

Definition 7.0.29. We say a triangulation of a point configuration with n points in dimension d is *flip-deficient* if it has less than $n - d - 1$ flips.

The term is a fair choice, because any regular triangulation with the same n and d must have at least $n - d - 1$ flips, the dimension of the secondary polytope. Balinski's theorem (see [148, 339]) states that the graph of a k -dimensional polytope must be k -connected. This means that the removal of any $k - 1$ or fewer points does not disconnect the graph and, moreover that the number of edges entering a vertex is at least k . Applied to the secondary polytope, this guarantees dimension many flips. In this chapter, we will see constructions of extremely deficient triangulations:

- Highly flip-deficient triangulations in dimensions 3 and 4. More precisely, triangulations with n vertices, for arbitrarily large n , and only $O(\sqrt{n})$ (in dimension 3) and $O(1)$ (in dimension 4) flips.
- Disconnected graphs of triangulations, in dimensions 5 and 6. The smallest example known has 17 points. Moreover, we will show that the number of connected components of the graph of triangulations can grow exponentially with the number of points.

All these examples were discovered by F. Santos [279, 283, 284], who also constructed a triangulation in dimension 6 without any flips at all [278].

The reader should not be frightened by the fact that some of these examples lie in dimensions higher than three. They can be understood by 3-dimensional geometric building blocks, after all, we have already studied 6-dimensional and 7-dimensional triangulations in Section 6.2, when studying products of simplices. In fact, the constructions in dimension four and higher that appear in this chapter will be formed by taking the products of lower dimensional objects. The basic idea is the understanding of triangulations of a triangular prism; or, rather, of many triangular prisms glued together.

Before going to these examples, we take a closer look at the most important example of a point configuration with non-regular triangulations, the one we have called the *mother of all examples*. Even if it is the smallest possible configuration in which non-regular triangulations arise, it is rich

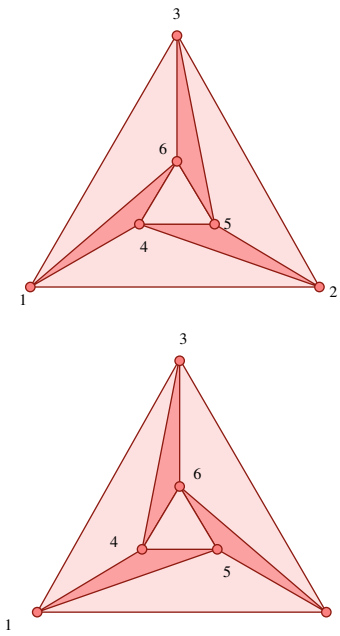


Figure 7.1: Two non-regular triangulations.

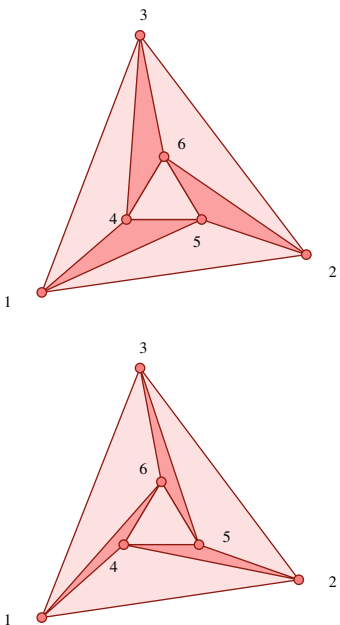


Figure 7.2: One regular and one non-regular triangulation.

enough to exhibit many of the features that non-regular triangulations have (or do not have) in general.

7.1 The mother of all examples, and some relatives

In this section, we are going to analyze in detail several variations of the *mother of all examples* (see Example 2.2.5 and its many subsequent sightings). This configuration appeared in print for the first time in the paper [83] by Connelly and Henderson, but it is closely related to Schönhardt's non-triangulable 3-polytope from 1928 [290] (see also Example 3.6.16), and Barnette's non-polytopal 3-sphere from 1970 [32].

The mother of all examples has appeared several times in the book, either in its original form (see Examples 2.2.5, 3.3.11, 5.1.4) or in several variations (Examples 4.2.23, 4.2.25 and 5.5.7). Our goal here is to understand the relations between the several variations of the same example. Gale transforms will be very useful for this purpose.

7.1.1 A theme with many variations

The mother of all examples is the following point configuration:

$$\mathbf{M} := \begin{pmatrix} 1 & 2 & 3 & 4 & 5 & 6 \\ 4 & 0 & 0 & 2 & 1 & 1 \\ 0 & 4 & 0 & 1 & 2 & 1 \\ 0 & 0 & 4 & 1 & 1 & 2 \end{pmatrix}$$

The first variation of it is that we can slightly perturb its coordinates in the following symmetric way:

$$\mathbf{M}_\varepsilon := \begin{pmatrix} 1 & 2 & 3 & 4 & 5 & 6 \\ 4 - \varepsilon & 0 & \varepsilon & 2 & 1 & 1 \\ \varepsilon & 4 - \varepsilon & 0 & 1 & 2 & 1 \\ 0 & \varepsilon & 4 - \varepsilon & 1 & 1 & 2 \end{pmatrix}$$

This *perturbation* should not have a major impact on the set of triangulations of the configuration. Observe that the original configuration \mathbf{M} is in general position (no three points are collinear), which implies that if ε is sufficiently small then \mathbf{M} and \mathbf{M}_ε have the same *oriented matroid*, that is, the same sets of affine bases, circuits, cocircuits, etc. In particular, they have the same poset of subdivisions and the same graph of triangulations (Corollary 4.1.44).

However, the perturbation affects the *regularity* of a particular subdivision, or triangulation. Consider the two non-regular triangulations of \mathbf{M} , displayed in Figure 7.1.

$$\mathcal{T}_1 = \{125, 145, 236, 256, 134, 346\}, \quad \mathcal{T}_2 = \{124, 245, 235, 356, 136, 146\}.$$

After the perturbation, \mathcal{T}_2 is still non-regular, but \mathcal{T}_1 is the regular triangulation obtained with (for example) the height vector $\omega = (1, 1, 1, 0, 0, 0)$.

Let us try to understand this phenomenon by considering *Gale transforms*. The following are Gale transforms of \mathbf{M} and \mathbf{M}_ε :

$$\text{Gale}(\mathbf{M}) := \begin{pmatrix} 1 & 2 & 3 & 4 & 5 & 6 \\ 2 & 1 & 1 & -4 & 0 & 0 \\ 1 & 2 & 1 & 0 & -4 & 0 \\ 1 & 1 & 2 & 0 & 0 & -4 \end{pmatrix},$$

$$\text{Gale}(\mathbf{M}_\varepsilon) := \begin{pmatrix} 1 & 2 & 3 & 4 & 5 & 6 \\ 2 & 1 & 1 & -4 + \varepsilon & -\varepsilon & 0 \\ 1 & 2 & 1 & 0 & -4 + \varepsilon & -\varepsilon \\ 1 & 1 & 2 & -\varepsilon & 0 & -4 + \varepsilon \end{pmatrix}.$$

It is a coincidence that these configurations have the same coordinates as their Gale transforms, modulo relabeling and changing the sign of some columns. Figure 7.3 shows the affine diagrams corresponding to these Gale transforms (see Section 5.5.2 if you do not remember what an affine Gale diagram is).

What we see in the picture is that, even if the oriented matroid of the configuration (hence that of the Gale transform) does not change when we pass from \mathbf{M} to \mathbf{M}_ε , the chamber complexes do change. In $\text{Gale}(\mathbf{M})$ there are three segments that meet at a point, while in $\text{Gale}(\mathbf{M}_\varepsilon)$ those three edges meet only pairwise, creating a new full-dimensional chamber. That new chamber is (dual to) the triangulation \mathcal{T}_1 , which was non-regular in \mathbf{M} and is now regular in \mathbf{M}_ε .

Figure 7.4 shows the same effect in the *secondary polytope*. In the unperturbed configuration \mathbf{M} , the secondary polytope has a hexagonal facet whose vertices are the GKZ vectors of six regular triangulations. The GKZ vectors of the two non-regular triangulations coincide, and lie at the barycenter of the hexagon. After the perturbation, all the GKZ vectors change slightly. Those of the two formerly non-regular triangulations move in opposite directions, inflating the former hexagon to become a 3-cube with three quadrilaterals still in the boundary of the secondary polytope and three in the interior. The former intersect in a new vertex of the secondary polytope, corresponding to the triangulation that has become regular. The other triangulation, which remains non-regular, lies in the interior of the secondary polytope.

We now look at several three-dimensional variations of the mother of all examples. The first one happens when we simply embed \mathbf{M} and \mathbf{M}_ε to lie in an affine hyperplane, and add a seventh point out of that hyperplane. That is to say:

$$\overline{\mathbf{M}} := \begin{pmatrix} 1 & 2 & 3 & 4 & 5 & 6 & 7 \\ 4 & 0 & 0 & 2 & 1 & 1 & 4/3 \\ 0 & 4 & 0 & 1 & 2 & 1 & 4/3 \\ 0 & 0 & 4 & 1 & 1 & 2 & 4/3 \\ 0 & 0 & 0 & 0 & 0 & 0 & 8 \end{pmatrix},$$

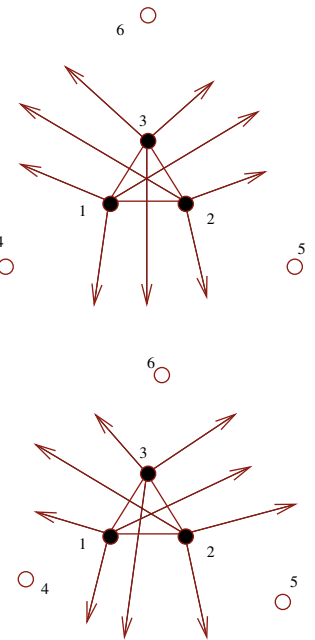


Figure 7.3: Affine Gale diagrams of the unperturbed and perturbed “mother of all examples”.

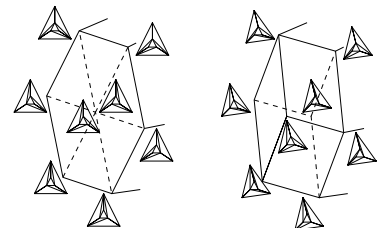


Figure 7.4: Secondary polytopes of the unperturbed and perturbed “mother of all examples”.

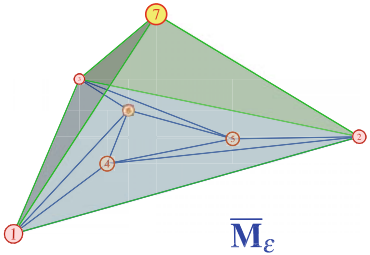


Figure 7.5: A pyramid over the twisted “mother of all examples”: no new revelations here.

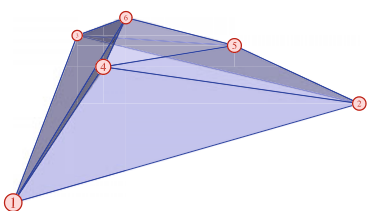


Figure 7.6: The twisted “mother of all examples” with the inner triangle lifted.

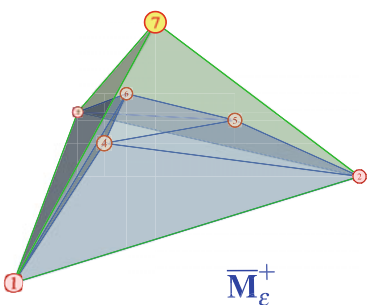


Figure 7.7: A pyramid on top of the “mother of all examples” with the inner triangle lifted: joining 7 to \mathcal{T}_2 cannot be completed to a triangulation of $\overline{\mathbf{M}}_e^+$, since the uncovered space equals the interior of the non-convex Schönhardt polyhedron.

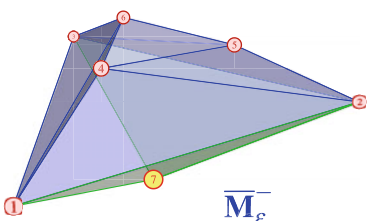


Figure 7.8: A pyramid below the twisted “mother of all examples” with the inner triangle lifted: this time, joining 7 to \mathcal{T}_2 can be completed to a triangulation of $\overline{\mathbf{M}}_e^-$, ...

$$\overline{\mathbf{M}}_\varepsilon := \begin{pmatrix} 1 & 2 & 3 & 4 & 5 & 6 & 7 \\ 4-\varepsilon & 0 & \varepsilon & 2 & 1 & 1 & 4/3 \\ \varepsilon & 4-\varepsilon & 0 & 1 & 2 & 1 & 4/3 \\ 0 & \varepsilon & 4-\varepsilon & 1 & 1 & 2 & 4/3 \\ 0 & 0 & 0 & 0 & 0 & 0 & 8 \end{pmatrix}.$$

This change does not affect the triangulations *or* their regularity. Indeed, $\overline{\mathbf{M}}$ is a pyramid over \mathbf{M} and $\overline{\mathbf{M}}_\varepsilon$ is one over \mathbf{M}_ε . See Observation 4.2.3. In the Gale transform, what happens is that the new element 7 appears as the zero vector, which has no effect in the chamber complex:

$$\text{Gale}(\overline{\mathbf{M}}) := \begin{pmatrix} 1 & 2 & 3 & 4 & 5 & 6 & 7 \\ 2 & 1 & 1 & -4 & 0 & 0 & 0 \\ 1 & 2 & 1 & 0 & -4 & 0 & 0 \\ 1 & 1 & 2 & 0 & 0 & -4 & 0 \end{pmatrix},$$

$$\text{Gale}(\overline{\mathbf{M}}_\varepsilon) := \begin{pmatrix} 1 & 2 & 3 & 4 & 5 & 6 & 7 \\ 2 & 1 & 1 & -4+\varepsilon & -\varepsilon & 0 & 0 \\ 1 & 2 & 1 & 0 & -4+\varepsilon & -\varepsilon & 0 \\ 1 & 1 & 2 & -\varepsilon & 0 & -4+\varepsilon & 0 \end{pmatrix}.$$

More interesting is what happens when we *lift* the two triangles of \mathbf{M} and \mathbf{M}_ε to lie in parallel planes. Let us only do this in the perturbed case of \mathbf{M}_ε , the unperturbed case being similar (and slightly less interesting). We consider the following two configurations:

$$\overline{\mathbf{M}}_\varepsilon^+ := \begin{pmatrix} 1 & 2 & 3 & 4 & 5 & 6 & 7 \\ 4-\varepsilon & 0 & \varepsilon & 2 & 1 & 1 & 4/3 \\ \varepsilon & 4-\varepsilon & 0 & 1 & 2 & 1 & 4/3 \\ 0 & \varepsilon & 4-\varepsilon & 1 & 1 & 2 & 4/3 \\ 0 & 0 & 0 & 1 & 1 & 1 & 8 \end{pmatrix},$$

$$\overline{\mathbf{M}}_\varepsilon^- := \begin{pmatrix} 1 & 2 & 3 & 4 & 5 & 6 & 7 \\ 4-\varepsilon & 0 & \varepsilon & 2 & 1 & 1 & 4/3 \\ \varepsilon & 4-\varepsilon & 0 & 1 & 2 & 1 & 4/3 \\ 0 & \varepsilon & 4-\varepsilon & 1 & 1 & 2 & 4/3 \\ 0 & 0 & 0 & 1 & 1 & 1 & -8 \end{pmatrix}.$$

The difference between them is that in $\overline{\mathbf{M}}_\varepsilon^+$ the small triangle $\{456\}$ lies between the big triangle $\{123\}$ and the new element 7, while in $\overline{\mathbf{M}}_\varepsilon^-$ the big triangle $\{123\}$ is the one in between. The following are Gale transforms of these two point configurations:

$$\text{Gale}(\overline{\mathbf{M}}_\varepsilon^+) := \begin{pmatrix} 1 & 2 & 3 & 4 & 5 & 6 & 7 \\ \frac{11}{6} & \frac{5}{6} & \frac{5}{6} & -4+\varepsilon & -\varepsilon & 0 & \frac{1}{2} \\ \frac{5}{6} & \frac{11}{6} & \frac{5}{6} & 0 & -4+\varepsilon & -\varepsilon & \frac{1}{2} \\ \frac{5}{6} & \frac{5}{6} & \frac{11}{6} & -\varepsilon & 0 & -4+\varepsilon & \frac{1}{2} \end{pmatrix},$$

$$\text{Gale}(\overline{\mathbf{M}}_{\varepsilon}^-) := \begin{pmatrix} 1 & 2 & 3 & 4 & 5 & 6 & 7 \\ \frac{13}{6} & \frac{7}{6} & \frac{7}{6} & -4 + \varepsilon & -\varepsilon & 0 & -\frac{1}{2} \\ \frac{7}{6} & \frac{13}{6} & \frac{7}{6} & 0 & -4 + \varepsilon & -\varepsilon & -\frac{1}{2} \\ \frac{7}{6} & \frac{7}{6} & \frac{13}{6} & -\varepsilon & 0 & -4 + \varepsilon & -\frac{1}{2} \end{pmatrix}.$$

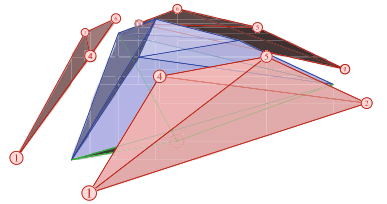


Figure 7.9: ... since the uncovered space can be filled with three tetrahedra touching each other at their vertical edges only.

Except for a dilation on the small triangle (whose coordinates change by $\pm 1/6$), the change in these Gale transforms with respect to that of \mathbf{M}_{ε} is the inclusion of a seventh element on one side of the Gale transform. See the pictures in Figure 7.10. Deleting this element in the Gale transform gives us back the Gale transform of \mathbf{M}_{ε} . This is not surprising, since deletion and contraction are dual operations, and the way that $\overline{\mathbf{M}}_{\varepsilon}^+$ and $\overline{\mathbf{M}}_{\varepsilon}^-$ are constructed shows that their contraction at the element 7 is essentially \mathbf{M}_{ε} .

How many non-regular triangulations do $\overline{\mathbf{M}}_{\varepsilon}^+$ and $\overline{\mathbf{M}}_{\varepsilon}^-$ have? It turns out that the latter has one, but the former has none. The triangulation \mathcal{T}_2 , which is the only non-regular triangulation of the contraction $\mathbf{M}_{\varepsilon} = \overline{\mathbf{M}}_{\varepsilon}^+ / 7 = \overline{\mathbf{M}}_{\varepsilon}^- / 7$, can be “lifted” to be a link in a (necessarily) non-regular triangulation of $\overline{\mathbf{M}}_{\varepsilon}^-$, by Lemma 4.2.24. Unfortunately, it cannot be lifted to $\overline{\mathbf{M}}_{\varepsilon}^+$. This was shown in Example 4.2.25. A Gale transform explanation can be done in terms of the *pseudo-chambers* briefly introduced as a tool for the proof of Theorem 5.5.9 in Section 5.5.2. In $\overline{\mathbf{M}}_{\varepsilon}^+$, as in \mathbf{M}_{ε} , the three edges of the chamber complex that prevent \mathcal{T}_1 to appear as a chamber can be topologically perturbed to create a pseudo-chamber corresponding to that triangulation. In $\overline{\mathbf{M}}_{\varepsilon}^-$, the same is not possible, because the element 7 blocks those edges from flipping to their alternate configuration (one or more of them would need to pass through the new element, drastically changing the chamber complex in forbidden ways).

Other relatives of the mother of all examples are interesting. In Examples 3.6.16 and 4.2.23, we considered one with eight elements, obtained as the union of $\overline{\mathbf{M}}_{\varepsilon}^+$ and $\overline{\mathbf{M}}_{\varepsilon}^-$. We finish this discussion by showing the smallest example of a triangulation with fewer than $n - d - 1$ flips, where n is its number of vertices and d its dimension.

Example 7.1.1 (The double tetrahedron). The point set consists of six points on a plane, forming the “mother of all examples”, plus two points on a half-line perpendicular to this configuration and originating at its barycenter. Coordinates for it may be as follows. See Figure 7.12.

$$\mathbf{A} := \begin{pmatrix} 1 & 2 & 3 & 4 & 5 & 6 & 7 & 8 \\ 4 & 0 & 0 & 2 & 1 & 1 & 4/3 & 4/3 \\ 0 & 4 & 0 & 1 & 2 & 1 & 4/3 & 4/3 \\ 0 & 0 & 4 & 1 & 1 & 2 & 4/3 & 4/3 \\ 0 & 0 & 0 & 0 & 0 & 0 & 4 & 8 \end{pmatrix}.$$

We consider the following triangulation:

$$\mathcal{T} = \{1247, 2457, 2357, 3567, 1367, 1467, 1278, 2378, 1378\}.$$

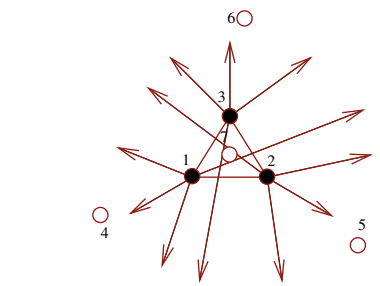
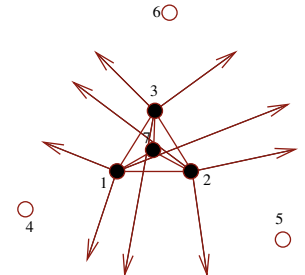


Figure 7.10: Affine Gale diagrams of the lifted versions of the “mother of all examples”.

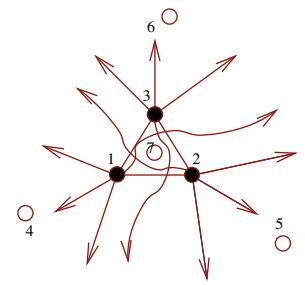


Figure 7.11: A pseudo-chamber complex for one of the lifted versions of the “mother of all examples”.

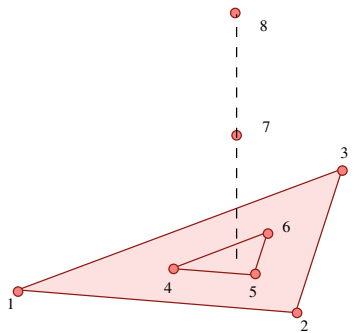


Figure 7.12: The smallest configuration with flip-deficient triangulations.

The first six tetrahedra cone the non-regular triangulation \mathcal{T}_1 of the mother of all examples to the element 7. The last three tetrahedra place (in the sense of Section 4.3.1) the final element 8 in the triangulation of $\mathbf{A} \setminus 8$ so obtained.

We count flips in \mathcal{T} as follows. Each flip is either a flip in the cone triangulation of $\mathbf{A} \setminus 8$, or it uses the last element 8. Flips of the first type are only the three flips already present in the planar triangulation \mathcal{T}_1 , supported in the circuits (15, 24), (16, 34), and (26, 35). The crucial point (proof left to the reader) is that the placing of point 8 does not add any new flips. Hence:

Corollary 7.1.2. \mathcal{T} is a triangulation of dimension three with eight vertices and only three flips.

This is again a flip-deficient triangulation, since $n - d - 1 = 4$ flips (the dimension of the secondary polytope). These values of n and d are the smallest possible for a flip-deficient triangulation, since triangulations in the plane and triangulations with $n \leq d + 4$ are never flip-deficient (Theorems 3.4.9 and 5.5.9).

This construction can be iterated by putting k concentric triangles in a plane and k collinear points along a transversal line through its barycenter. This way, one gets triangulations with $4k$ vertices and only $3k - 3$ flips. Triangulations with $5k$ points and $3k - 2$ flips can also be obtained. See Exercise 7.1.

7.1.2 Twelve proofs of non-regularity

We now list several different ways to show the existence of non-regularity in subdivisions of the mother of all examples, \mathbf{M} .

- (1) *Escher-like figure.* The first proof is to show by contradiction that no lifting heights exist that produce the triangulations of Figure 7.1. We did exactly that in Example 2.2.5 in Chapter 2. Suppose that there is a height vector giving the triangulation. Assume, without loss of generality, that the height vector $\omega \in \mathbb{R}^{\{1,2,3,4,5,6\}}$ gives height zero to the three interior points. Then the conditions needed to obtain the diagonals 16, 24 and 35 present in \mathcal{T}_1 are, respectively, $\omega_1 < \omega_3$, $\omega_3 < \omega_2$, and $\omega_2 < \omega_1$. This is impossible.
- (2) *Algebraic infeasibility.* A slight variation of the previous proof proceeds by looking at the circuits with supports in the 4-tuples 1245, 2356, and 1346. More precisely, if we denote by \mathbf{p}_i the i -th column of the matrix \mathbf{M} , we have that:

$$\begin{aligned}\mathbf{p}_1 + 4\mathbf{p}_5 &= \mathbf{p}_2 + 4\mathbf{p}_4, \\ \mathbf{p}_2 + 4\mathbf{p}_6 &= \mathbf{p}_3 + 4\mathbf{p}_5, \\ \mathbf{p}_3 + 4\mathbf{p}_4 &= \mathbf{p}_1 + 4\mathbf{p}_6.\end{aligned}$$

Each of these affine dependences implies a condition that ω needs to satisfy in order to force one of the diagonals to be lifted below the

other one. The three precise inequalities that force 24, 35, and 16 to be lifted below 15, 26, and 34 are, respectively:

$$\begin{aligned}\omega_1 + 4\omega_5 &> \omega_2 + 4\omega_4, \\ \omega_2 + 4\omega_6 &> \omega_3 + 4\omega_5, \\ \omega_3 + 4\omega_4 &> \omega_1 + 4\omega_6.\end{aligned}$$

These three inequalities cannot be satisfied simultaneously, since the three left-hand sides have the same sum as the three right-hand sides.

- (3) *Repeated GKZ vectors.* A third proof uses Corollary 5.2.18: no regular triangulation of a point configuration can have the same GKZ vector as any other triangulation. In our case, symmetry implies that the two triangulations \mathcal{T}_1 and \mathcal{T}_2 of \mathbf{M} have

$$\phi_{\mathbf{A}}(\mathcal{T}_1) = \phi_{\mathbf{A}}(\mathcal{T}_2).$$

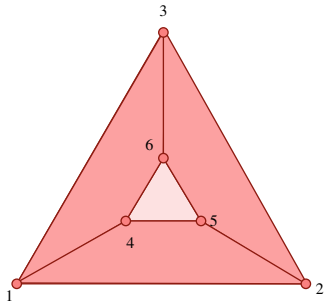
Hence, they are both non-regular.

- (4) *Monotone flipping.* We now use the idea of monotone flipping first presented in Section 5.3.2. Consider the height vector ω equal to $(0, 0, 0, 1, 1, 1)$ that lifts the inner triangle to height zero and the outer triangle to height one. Remember that we can think of ω as a linear functional on $\Sigma\text{-poly}(\mathbf{M})$ and, as such, it is minimized at the regular triangulation $\mathcal{S}(\mathbf{M}, \omega)$ (or at all the triangulations that refine it, if $\mathcal{S}(\mathbf{M}, \omega)$ was not a triangulation).

In our case, the functional adds together the last three coordinates in the GKZ vector of a triangulation. Since none of the three flips in the triangulation \mathcal{T}_1 changes that sum, \mathcal{T}_1 cannot be regular: *none of the flips in \mathcal{T} is monotone towards the opposite height's functional $-\omega$.*

- (5) *Non-triangulable lift.* Our next proof also uses flips. As before, consider the height function $\omega = (0, 0, 0, 1, 1, 1)$. A monotone sequence of flips from our triangulation \mathcal{T}_1 to the regular triangulation $\mathcal{S}(\mathbf{M}, \omega) = \{123\}$ would lift to produce a triangulation of the region between the lifting of \mathcal{T}_1 and the lifting of $\mathcal{S}(\mathbf{M}, \omega)$, that is, it would produce a triangulation of an oblique triangular prism with its boundary triangulated in the cyclic manner. This is impossible, by the same reasons why Schönhardt's polyhedron is not triangulable.

- (6) *Long chains in poset.* Consider $\mathcal{S}_0 = \{1245, 2356, 1346, 456\}$ (see Figure 7.13). The three quadrilaterals in it can be independently refined into a triangulation. Refining them one by one gives rise to a chain of four non-trivial subdivisions, $\mathcal{S}_0 \prec \mathcal{S}_1 \prec \mathcal{S}_2 \prec \mathcal{S}_3$, in $\text{Subdivs}(\mathbf{M})$. If all of them were regular, they would correspond to proper non-empty faces of different dimensions in the secondary polytope of \mathbf{M} . This is impossible, since $\Sigma\text{-poly}(\mathbf{M})$ has dimension

Figure 7.13: A subdivision of \mathbf{M}

three by the Theorem 5.1.10. So, at least one of the subdivisions in that chain has to be non-regular. Observe that which triangulation is non-regular may change, if we change the coordinates of \mathbf{M} while keeping its oriented matroid intact, but the fact that at least one of them is non-regular must hold in any point configuration with that oriented matroid.

- (7) *Common coarsening of flip-neighbors.* We can use a similar argument involving flips. All the flips in the triangulation \mathcal{T}_1 (or in \mathcal{T}_2) produce triangulations that refine the subdivision \mathcal{S}_0 (of Figure 7.13). This implies that either \mathcal{S}_0 , \mathcal{T}_1 , or one of its three flip-neighbors must be non-regular. Indeed, otherwise $\phi_{\mathbf{M}}(\mathcal{T}_1)$ would be a vertex in $\Sigma\text{-poly}(\mathbf{M})$ with the (impossible) property that all its neighbors are contained in the same proper face of the polytope.
- (8) *Flip-deficiency.* This proof is based on the flip-deficient triangulation constructed in Example 7.1.1. A flip-deficient triangulation can certainly not be regular. But, in our case, if the original triangulation \mathcal{T}_1 were regular, the final one would need to be regular too: it is obtained by first coning to a new point and then placing yet another point. Both operations preserve regularity.
- (9) *Non-extendable link.* Here we prove that \mathcal{T}_2 is not regular in the perturbed mother of all examples, \mathbf{M}_ε . The proof uses a lift to the configuration $\overline{\mathbf{M}}_\varepsilon^+$. If \mathcal{T}_2 were regular in $\mathbf{M}_\varepsilon = \overline{\mathbf{M}}_\varepsilon^+ / 7$, it would appear as the link at 7 in some (regular) triangulation of $\overline{\mathbf{M}}_\varepsilon^+$, by Lemma 4.2.24. But that cannot be the case, because what is left in $\text{conv}(\overline{\mathbf{M}}_\varepsilon^+)$ after inserting the tetrahedra that join \mathcal{T}_2 to the new element 7 is precisely (an oblique version of) the untriangulable Schönhardt's polyhedron.
- (10) *Non-extendable deletion.* We now use a somewhat similar proof for the point configuration $\overline{\mathbf{M}}_\varepsilon^-$. There is a triangulation of $\overline{\mathbf{M}}_\varepsilon^-$ that extends the join of \mathcal{T}_2 to 7. Indeed, after the join is inserted, the volume left is precisely the one that can be occupied by the tetrahedra 1245, 2356, and 1346. The problem is that, according to Lemma 4.2.24, the (unique) triangulation obtained in this way should be regular. Then, according to Lemma 4.2.17, there should be a (regular) triangulation of the configuration $\overline{\mathbf{M}}_\varepsilon^- \setminus 7$ using those three tetrahedra. That is impossible because, again, the part of $\text{conv}(\overline{\mathbf{M}}_\varepsilon^- \setminus 7)$ not covered by those three tetrahedra is a Schönhardt's polyhedron.
- (11) *Chamber complex.* Here we verify that the triangulation \mathcal{T}_1 does not correspond to a chamber in the Gale transform of Figure 7.3. Indeed, the intersection of the cells $\{346, 145, 256\}$, dual to the triangles $\{125, 236, 134\} \subset \mathcal{T}_1$, is not full-dimensional, in the unper- turbated version, and empty in the perturbed one.

(12) Your turn!

We want to emphasize that proofs (6) and (7) are combinatorial; they rely only on the oriented matroid of \mathbf{M} and not on the specific coordinates of its elements. As a consequence, they cannot tell us that a specific triangulation or subdivision is non-regular, because that is not a property of the oriented matroid. They only tell us that the configuration has *some* non-regular subdivision.

It is also worth remarking that proofs (7) to (10) happen in three dimensions. They involve a lifting of our configuration to 3D, and then studying the triangulations of the new configuration. In fact, the flip-deficiency and non-extendability that play a role in those proofs are properties that cannot happen in dimension two.

7.2 Highly flip-deficient triangulations

We know that regular triangulations and triangulations in dimension at most two (Section 3.4.3) or corank at most three (Section 5.5) always have at least $n - d - 1$ flips, where n is the number of elements and d is the dimension. We have also seen (Examples 3.6.17 and 7.1.1) that the same is not true for non-regular triangulations outside those parameters. Here we construct examples in dimensions three and four that are drastically flip-deficient. These examples seem to indicate that there are point configurations in these dimensions for which the graphs of flips are not connected, but this is still an open problem.

7.2.1 Dimension 3: A zig-zag grid

We start with a very simple (and not flip-deficient) triangulation that illustrates the crucial point in the flip-deficient triangulation we build later. Let k be a positive integer, and consider the point configuration with the $(k+1)^2$ points $(i, j, 0) \in \mathbb{R}^3$, with $i, j = 0, \dots, k$. Triangulate these points in a triangular-grid manner, using the $2k^2$ triangles with vertex sets

$$\{(i, j, 0), (i+1, j, 0), (i+1, j+1, 0)\}$$

and

$$\{(i, j, 0), (i, j+1, 0), (i+1, j+1, 0)\}.$$

See Figure 7.14, where $k = 6$.

All the interior edges in this triangulation are flippable, so we get a triangulation with about $3k^2$ flips, that is, about $3n$ flips, where n is the number of points. But there is a simple way to “kill” some of these flips using the third dimension: We add k more points with coordinates $(k/2, j, 1)$, for $j = 0, \dots, k-1$. We extend the triangulation of the grid to the third dimension by joining the point $(k/2, j-1, 1)$ to the i -th horizontal strip of the grid, and filling the intermediate space with tetrahedra of the form

$$\{(i, j, 0), (i+1, j, 0), (k/2, j, 1), (k/2, j+1, 1)\}.$$

(Remark: for the pictures in this section we will take as vertical direction the second coordinate of the plane containing the grid. The first and third coordinates are, hence, horizontal.)

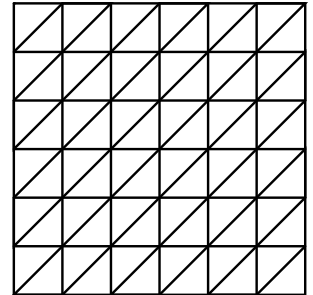


Figure 7.14: A triangular grid in the plane has about $3n$ flips, but...

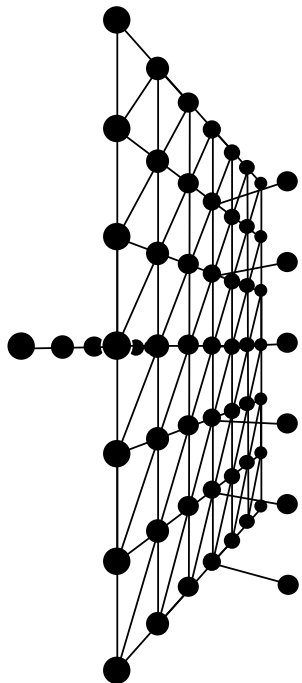


Figure 7.15: ... about $2n$ of them can be killed by the third dimension.

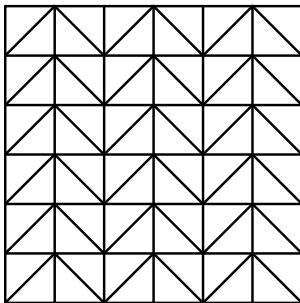


Figure 7.16: A zig-zag triangulation of the square grid in the plane has about $2n$ flips.

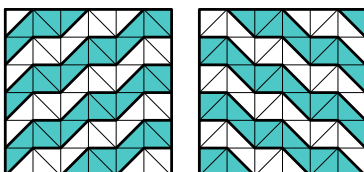


Figure 7.17: Strips to be joined to points in front of and behind the planar grid.

This trick makes the former flips on horizontal edges of the grid disappear. (When we say “flips on horizontal edges”, we now mean “flips on the circuits of the grid whose negative part is a horizontal edge”). Another k points can be added behind the grid, now on a horizontal line, and joined to vertical strips to kill the flips on vertical edges (see Figure 7.15). Now only the about n flips on the diagonal edges have survived. In particular, our triangulation is not flip deficient, or at least not highly so.

But, of course, we started with a very bad triangulation of the square grid. We should start with one that has fewer flips! For example, in the zig-zag triangulation of Figure 7.16, only the diagonal and horizontal edges can be flipped, and we get about $2n$ flips to start with, instead of $3n$. From now on we assume that k is even, to avoid annoying case studies.

Our task is to kill about $2n$ flips by joining the grid to auxiliary points lying in front and behind the hyperplane of the grid. The simplest thing to do would be to kill the flips of horizontal edges using horizontal strips as we did before, but then the diagonal edges would be difficult to deal with. What we will do, instead, is use zig-zag strips both for the front and the back, allowing each side to kill about $n/2$ horizontal and $n/2$ diagonal flips.

The two families of zig-zag strips to be used are shown in Figure 7.17. One part of the figure shows the strips to be joined to the points in front, and the other part (symmetric to the first one) shows the strips to be used for the back. Strips have alternately been colored grey and white, and thicker lines show their boundaries. Now, no pair of adjacent triangles of the grid are joined to the same point in the front and in the back half-spaces, except the ones separated by vertical edges, which cannot be flipped in the grid. What this gives is:

Lemma 7.2.1. *A triangulation constructed by joining these strips to different points will not have any flip supported on a circuit fully contained in the grid.* \square

Of course, we need to check for other flips that may appear. Before doing this in detail, let us point out three difficulties that we did not have in the warm-up construction, but that do exist here:

- The points on the back cannot be placed horizontally as before, or there will be bad intersections between the joins of consecutive strips to those points. We will place them in a vertical line parallel to the one containing the points in the front.
- We have more than k strips in each direction, precisely $\lfloor 3k/2 \rfloor$ of them. Hence, we need to add that number of points on each side of the grid. Also, we need to put them at a smaller distance to one another, so that the segment from any point in the front to any point in the back crosses the planar grid. In this way, a triangulation of the front half-space and a triangulation of the back can be done independently and will fill in the convex hull of our point set. For reasons that will become apparent later, we choose to put them very close to each other, all of them with a second coordinate strictly between 0 and 1. See Figure 7.18.

- In order to entirely fill in the convex hull of our point set, the strips to be joined to our points need to go all the way from the left side to the right side of the square grid. So the strips of Figure 7.17 are not enough. Figure 7.18 shows what we actually need to join to the $\lfloor 3 \cdot 6/2 \rfloor = 9$ points in the front for the case $k = 6$. The parts which degenerate to segments in the j -th strip do not produce tetrahedra when joined to the corresponding point in the front, but they have to be joined to the edges between two consecutive front points, just as with the other edges in the bottom and top boundaries of a strip.

Theorem 7.2.2. *The triangulation so obtained has less than $7k = O(\sqrt{n})$ flips.*

Proof. As usual, the best strategy for an exhaustive search of flips is to look at all the adjacent pairs of tetrahedra or, equivalently, at all interior triangles (walls, in the sense of Section 4.4.2) of our triangulation. There are the following three types of such triangles:

1) A triangle C contained in the planar grid. Such a triangle is joined to one element a in the front and one element b in the back. Since these two elements are not connected by an edge, in order to have a flip they have to be the only two positive elements in the circuit supporting that flip. In particular, the segment $\text{conv}(\{a, b\})$ and the triangle $\text{conv}(C)$ must intersect.

This gives only one possibility for a and b : they are the front and back elements joined to the unique strips containing the lowest segment in the middle vertical line of the grid (the segment $(k/2, 0, 0)(k/2, 1, 0)$). The only candidate circuit is the one having that segment in one part and the segment $\{a, b\}$ in the other.

All in all, walls of this type produce at most one flip.

2) A triangle C with an edge in the planar grid and the third vertex outside it. Without loss of generality, let us assume that the third vertex is in the front and denote it a . Let a^- and a^+ denote the front elements of the point configuration immediately below and above a .

There are three possibilities for the two vertices joined to this

- C is joined to both a^- and a^+ . Then the circuit contained in these two adjacent tetrahedra is $(\{a^-, a^+\}, \{a\})$. This circuit produces no flip because the segments $\{a^-, a\}$ and $\{a, a^+\}$ have different links (the lower and upper envelopes of a certain strip).
- C is joined to two points in the grid. Then the candidate circuit is contained in the grid. By construction, circuits contained in the grid do not produce flips.
- C is joined to one of a^- and a^+ and to a point in the grid. Assume it is joined to a^+ (the other case is similar). Then the five points contained in the two tetrahedra are one triangle from the grid and two consecutive points from the front. Since every triangle in the grid has a vertical edge, the circuit involves only four points: the vertical edge of the grid triangle plus the two points in the front. To fix notation,

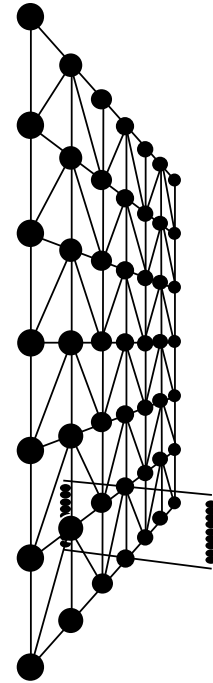


Figure 7.18: A point set with a triangulation with $O(\sqrt{n})$ flips.

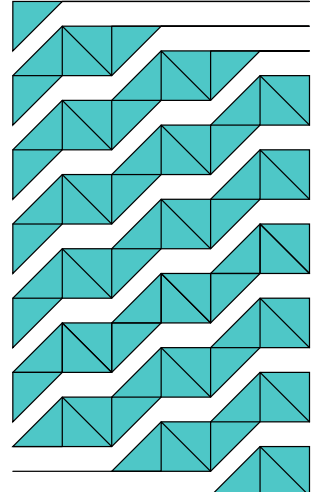


Figure 7.19: The true meaning of “strips” in the zig-zag construction.

let b and b^+ denote the elements of that vertical edge and let c be the third vertex in the grid triangle. So, our circuit is

$$\{(a, b^+), (b, a^+)\}.$$

If b and b^+ are either on the right or left ends of the grid (that is, if their first coordinate equals 0 or k), then there is clearly going to be a flip on that circuit. The triangulated circuit lies in the boundary of the triangulation, and by construction the two triangles in it are joined to the same vertex c . This gives us $2k$ flips, k of them on each side of the grid. We have to multiply by two because we have counted only flips in the front part of the triangulation. Hence we get $4k$ flips.

If the vertical edge $\{b, b^+\}$ is interior to the grid, then the condition to have a flip is that the two triangles in the grid that are incident to it be incident to the top boundary of the strip they lie in (if the second front vertex was a^- instead of a^+ we would say the lower boundary of the strip). The reader can check in Figure 7.19 that there are exactly $k - 1$ such vertical edges in the square grid; $k/2 - 1$ incident to the top and $k/2$ incident to the bottom. With another $k - 1$ flips to account for what happens in the back, this gives $2k - 2$ possible flips.

3) A triangle C with only one vertex b in the planar grid. The other two vertices are consecutive vertices in the front or the back. Denote them a and a^+ . The two adjacent tetrahedra appear in Figure 7.19 as consecutive segments in the common boundary of the consecutive strips joined to a and a^+ . Let c be the common end of these two segments, and denote the other two as c^- and c^+ . By construction of our strips, the first coordinates of c^- , c , and c^+ are consecutive integers. In particular, c^- and c^+ are not joined by an edge and, in order to have a flip, the two of them must form the positive part of the circuit involved. That is to say, the segment $\text{conv}(\{c^-, c^+\})$ must intersect the triangle $\text{conv}(\{c, a, a^+\})$. But since a and a^+ both lie in the front, the only possible intersection is the point c itself, meaning that c^- , c , and c^+ are collinear.

The only collinear segments in the boundary of a strip are the ones in the top or bottom boundary of the grid, and this condition alone gives a number of possible flips that are linear in k (exactly $2k - 2$). But something more can be said. In order to have a flip, we need $\{c^-, c\}$ and $\{c, c^+\}$ to have the same link. This eliminates about half of the candidates, leaving only the following $k - 1$ circuits to support flips:

$$\begin{aligned} & \left(\{(i-1, 0, 0), (i+1, 0, 0)\}, \{(i, 0, 0)\} \right), \quad i = 1, 3, \dots, k-1 \quad \text{and} \\ & \left(\{(i-1, k, 0), (i+1, k, 0)\}, \{(i, k, 0)\} \right), \quad i = 2, 4, \dots, k-2. \end{aligned}$$

Summing up, our triangulation has at most $1 + 4k + 2k - 2 + k - 1 = 7k - 2$ flips, as claimed. \square

Remark 7.2.3. In Exercise 7.12, we will see how to reduce the number of flips from about $7n$ to $4\sqrt{2}n$ without much effort. The paper [279] achieves

$4n$ by choosing a different shape for the boundary of the starting planar grid: the shape shown in Figure 7.20.

Observe that in this construction all the flips appear close to the boundary of the triangulation, which contains $O(\sqrt{n})$ of the points. The shape of the boundary can only modify the constant (as long as the perimeter is kept proportional to \sqrt{n}).

7.2.2 Locally acyclic orientations and triangulations of products

Let \mathbf{A} be a point configuration in dimension d and let \mathcal{S} be any subdivision of it. Consider the product $\mathbf{A} \times \mathbf{I}$ of \mathbf{A} with the vertices of a segment $\mathbf{I} = \mathbf{D}_2$.

Taking as a cell in $\mathbf{A} \times \mathbf{I}$ the product of a cell of \mathcal{S} with (the vertices of) the segment \mathbf{I} yields a polyhedral subdivision of $\mathbf{A} \times \mathbf{I}$ that we denote, $\text{prism}(\mathcal{S})$. We have encountered these objects when we studied triangulations of the cube in Section 6.3.7.

Lemma 7.2.4. $\mathcal{S} \times \mathbf{I}$ is regular if and only if \mathcal{S} is regular.

Proof. If $\text{prism}(\mathcal{S})$ is regular, then \mathcal{S} is regular because it is the restriction of $\text{prism}(\mathcal{S})$ to a facet (see Lemma 2.3.15).

Conversely, suppose $\omega : J \rightarrow \mathbb{R}$ is a height function that defines \mathcal{S} as a regular subdivision. Then $\text{prism}(\mathcal{S})$ is the regular subdivision obtained with the height function $\tilde{\omega} : J \times \{0, 1\} \rightarrow \mathbb{R}$ defined as $\tilde{\omega}(i, j) = \omega(i)$. \square

Suppose now that \mathcal{S} is a triangulation of \mathbf{A} . Of course, $\text{prism}(\mathcal{S})$ cannot be a triangulation, its cells are prisms over the simplices of \mathcal{S} . In order to refine $\text{prism}(\mathcal{S})$ to a triangulation, we need to specify a triangulation of each prism. As explained in Corollary 6.2.7, triangulating a prism over a simplex is equivalent to specifying an acyclic orientation of the graph of the simplex. So we need to specify an acyclic orientation for each simplex of \mathcal{S} . Now, each edge of \mathcal{S} will typically appear in several simplices. In order for the triangulations of adjacent prisms to agree in common faces, a necessary condition is that the orientation given to the edge is the same in all the simplices containing it. Indeed, the orientation given to the edge e specifies which of the two diagonals is inserted in the quadrilateral $e \times \mathbf{I}$ (with the convention made before Corollary 6.2.7, that the orientation $i \rightarrow j$ for an edge inserts the diagonal $\{(i, 0), (j, 1)\}$).

Since all the faces of a prism are either simplices or prisms, this necessary condition is also sufficient. Hence, we have the following natural definition:

Definition 7.2.5. Let \mathcal{K} be a simplicial complex. A *locally acyclic orientation* on \mathcal{K} (or l.a.o., for short) is an orientation of all the edges of its 1-skeleton which does not produce a cycle in any of the simplices.

A *reversible edge* in a locally acyclic orientation of \mathcal{K} is an edge whose reversal produces another locally acyclic orientation.

The *graph of l.a.o.'s* of \mathcal{K} is the graph whose vertices are all the locally acyclic orientations of \mathcal{K} and whose edges correspond to single-edge reversals in them. We denote it $\mathcal{G}_{\text{l.a.o.}}(\mathcal{K})$.

As an example, Figure 7.21 shows a locally acyclic orientation of a 2-dimensional complex consisting of 3 triangles. It has three reversible edges.

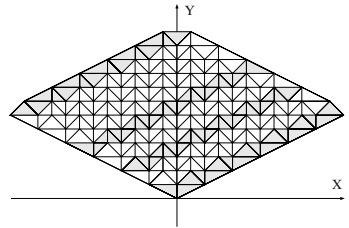


Figure 7.20: A shape giving triangulations with $4\sqrt{n} + O(1)$ flips in dimension 3.

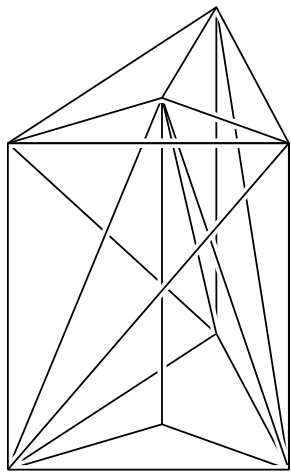
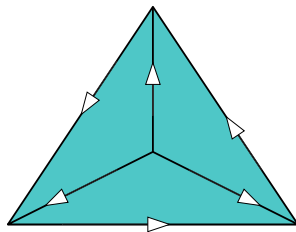


Figure 7.21: Top: a l.a.o. with a non-local cycle and three reversible edges. Below: the triangulation of eight points in dimension three induced by it.

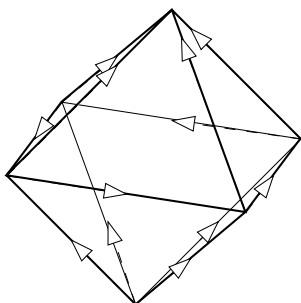


Figure 7.22: A locally acyclic orientation of the boundary of an octahedron.

Observe that it has a cycle, but this cycle is not contained in a simplex.

Example 7.2.6. A special case of locally acyclic orientations are *globally acyclic* ones, that is, orientations compatible with a total ordering of the vertices of \mathbf{A} .

Transposition of two consecutive elements in the total order of \mathbf{A} produces either no change in the locally acyclic orientation (if the elements were not joined by an edge in \mathcal{K}), or a single-edge reversal. Hence, *all globally acyclic orientations lie in the same connected component of $\mathcal{G}_{\text{l.a.o.}}(\mathcal{K})$* .

Example 7.2.7. Let us study in some detail the possible locally acyclic orientations of the boundary of an *octahedron*. Because of the previous remark, we can concentrate on orientations having at least one cycle. The only cycles which are not faces of the octahedron are the three cycles of length four which separate two opposite vertices. It can be easily checked that, once such a cycle is chosen, the other two vertices need to be either sinks or sources in order to get a locally acyclic orientation.

In other words, there are exactly 24 *locally acyclic orientations* of this complex which are not globally acyclic: we have 3 cycles to choose from with two orientations each, and for each cycle we have 4 possibilities; either sink/source for the two vertices that are not in the cycle. Figure 7.22 shows one of these orientations. In all of these orientations, the reversible edges are the four edges of the cycle, and any single reversal produces a globally acyclic orientation. In particular, the graph of locally acyclic orientations is connected.

Exercise 7.10 generalizes this example to show the following: if \mathbf{A} is 3-dimensional, any choice of simplicial subcomplex \mathcal{K} of the boundary of \mathbf{A} will have a connected graph $\mathcal{G}_{\text{l.a.o.}}(\mathcal{K})$ and at least $n - 2$ reversible edges (where n is the number of vertices in \mathcal{K} , which may be smaller than that of \mathbf{A}).

Remark 7.2.8. Only the 2-dimensional skeleton of \mathcal{K} is relevant when speaking of locally acyclic orientations: If \mathcal{K} has dimension greater than 2 and \mathcal{K}^2 denotes its 2-skeleton, then $\mathcal{G}_{\text{l.a.o.}}(\mathcal{K}) = \mathcal{G}_{\text{l.a.o.}}(\mathcal{K}^2)$ (Exercise 7.3).

Lemma 7.2.9. Let \mathcal{T} be a triangulation of \mathbf{A} . The triangulations of $\mathbf{A} \times \mathbf{I}$ that refine the subdivision prism(\mathcal{T}) are in bijection to the locally acyclic orientations of the graph of \mathcal{T} . The graph of flips between them equals $\mathcal{G}_{\text{l.a.o.}}(\mathcal{T})$.

Moreover, the refinement produced by a certain locally acyclic orientation is regular if and only if \mathcal{T} is regular and the orientation is globally acyclic (the graph contains no directed cycle).

Proof. We have already shown the bijection, let us look at flips of a triangulations that refine prism(\mathcal{T}). First, a flip in prism(\mathcal{T}) must restrict to either the identity or a flip in the triangulated prism over each simplex of \mathcal{T} . Flips in triangulations of prisms correspond to reversals of a single edge in the orientation (see Corollary 6.2.7 again), and the circuit involved is the quadrilateral over that edge. Hence, every flip in prism(\mathcal{T}) will be of that form.

Now let us look at regularity. Suppose first that a triangulation refining $\text{prism}(\mathcal{T})$ is regular. Then \mathcal{T} is regular, since it equals the restriction of $\text{prism}(\mathcal{T})$ to a facet. Also, the locally acyclic orientation is globally acyclic. Otherwise, let i_1, i_2, \dots, i_k be a set of elements of \mathbf{A} that form a cycle (in the order given). Then, the lifting heights producing $\text{prism}(\mathcal{T})$ as a regular triangulation satisfy:

$$\begin{aligned}\omega_{(i_1,0)} + \omega_{(i_2,1)} &< \omega_{(i_1,0)} + \omega_{(i_2,1)}, \\ \omega_{(i_2,0)} + \omega_{(i_3,1)} &< \omega_{(i_2,0)} + \omega_{(i_3,1)}, \\ &\vdots \\ \omega_{(i_k,0)} + \omega_{(i_1,1)} &< \omega_{(i_k,0)} + \omega_{(i_1,1)}.\end{aligned}$$

These inequalities give a contradiction, since the left hand sides and right hand sides have the same sum.

Conversely, suppose that \mathcal{T} is regular and that its skeleton is given by an acyclic orientation. Such an orientation is then compatible with a global order in the elements of \mathbf{A} . Without loss of generality, assume that the elements are labelled $1, 2, \dots, n$ with respect to that total order. Then, the refinement of $\text{prism}(\mathcal{T})$ produced is the lexicographic refinement in which we pull the vertices $(1,0), (2,0), \dots, (n,0)$, in this order. Lexicographic refinements of a regular subdivision are always regular (Lemma 4.3.12). \square

Application: Construction of point sets with many triangulations

Our main application of locally acyclic orientations will be the construction of point sets with arbitrarily many vertices and a constant number of flips in dimension four (Section 7.2.4) and of disconnected graphs of triangulations in dimension five (Section 7.3). But before doing that, let us use them to construct point configurations in dimension four with *many triangulations*. In the plane, there is a constant c such that every point configuration n points has at most c^n triangulations (Theorem 3.3.4). For higher dimensions, we saw in Theorem 6.1.22 that the cyclic polytope $\mathbf{C}(n,d)$ has $\Omega(2^{n^{\lfloor d/2 \rfloor}})$ triangulations, if d is considered fixed. Here we construct other examples of 4-dimensional configurations with $2^{\Omega(n^2)}$ triangulations; they are again based on cyclic polytopes, since the use of locally acyclic orientations makes the proof cleaner.

Theorem 7.2.10. *Let n be even and let \mathbf{A} be the vertex set of a cyclic polytope in dimension three with $n/2$ vertices. Let \mathbf{B} be the prism over \mathbf{A} (that is, its product with $\{0,1\}$). We claim that:*

1. \mathbf{B} has at least $(n/2)! = 2^{\Omega(n \log n)}$ regular triangulations.
2. \mathbf{B} has at least $2^{\Omega(n^2)}$ non-regular triangulations.
3. The poset of subdivisions of \mathbf{B} has chains of length at least $\Omega(n^2)$.

Proof. Parts one and two of Theorem 7.2.10 follow from Lemma 7.2.9 and the example presented in the following Lemma. Part three is left as an exercise (Exercise 1). \square

Lemma 7.2.11. Consider the regular neighborly triangulation \mathcal{T} of \mathbf{A} , consisting of the $\binom{(n/2)-2}{2}$ simplices $\{i-1, i, j, j+1\}$ over all $2 \leq i < j \leq (n/2) - 1$, described in Section 6.1. Then

1. \mathcal{T} has exactly $(n/2)!$ globally acyclic orientations.
2. \mathcal{T} has at least $2^{(n-1)/2}^2$ locally acyclic orientations.

Proof. Part one is trivial. Every ordering of the vertices provides an acyclic orientation of \mathcal{G} , and two orderings cannot provide the same orientation because the graph is complete.

For part (2), we consider the following family of orientations. For each edge ij :

1. If only one of i and j is even, we orient the edge from the odd vertex to the even vertex.
2. If both edges are even or odd, we give the edge an arbitrary orientation.

All orientations like this are locally acyclic, because each full-dimensional simplex $\{i-1, i, j, j+1\}$ of \mathcal{T} has two even and two odd vertices. It is clear that the number of such orientations is in $2^{\Omega(n^2)}$. More precisely, it equals

$$2^{\lfloor \frac{n}{4}(\frac{n}{4}-1) \rfloor}.$$

□

Remark 7.2.12. \mathbf{B} is in convex position, and if it is perturbed to general position, the lower bounds for regular triangulations and triangulations remain valid. For regular triangulations this is a general fact: perturbing into general position can only increase the number of regular triangulations, because every regular triangulation of the unperturbed point set can be extended to a regular triangulation of the perturbed point set. For non-regular triangulations, it is not a general fact, but, in our case, all the non-simplicial facets of \mathbf{B} are prisms over a triangle and all the triangulations we have constructed triangulate these prisms in a regular way. This regularity implies that the triangulation, after perturbation, can be extended to the uncovered space.

7.2.3 Locally acyclic orientations without reversible edges

Here we show two examples of locally acyclic orientations without reversible edges. In the light of Lemma 7.2.9, these constructions will be a good initial step to construct triangulations with very few flips or disconnected spaces of triangulations. Indeed, if \mathcal{T} is a triangulation that has a l.a.o. without reversible edges, then the refinement of $\text{prism}(\mathcal{T})$ given by this l.a.o. will not be connected by flips to any other refinement of $\text{prism}(\mathcal{T})$. Of course, it can in principle be connected to triangulations that do not refine $\text{prism}(\mathcal{T})$. We will address this issue later.

A locally acyclic orientation in the 2-skeleton of the 24-cell

The *24-cell* is one of the six *regular polytopes* existing in dimension four. Recall that a polytope is called regular if its symmetry group acts transitively over its flags, in more common language, if all its facets are regular polytopes equal to one another and equivalent to one another by symmetries of the polytope. The regular polytopes in dimension three are the well-known platonic solids.

The polytope we are interested in is called the 24-cell because it has 24 facets. All its facets are regular octahedra, and the polytope turns out to have 24 vertices, whose coordinates are as follows. The first line gives 16 vertices and the second one gives eight:

$$\begin{aligned} \mathbf{P} := \text{conv}\{ & (\pm 1, \pm 1, \pm 1, \pm 1), \\ & (\pm 2, 0, 0, 0), (0, \pm 2, 0, 0), (0, 0, \pm 2, 0), (0, 0, 0, \pm 2) \}. \end{aligned} \quad (7.1)$$

It is not clear at first sight why the polytope having these 24 vertices is regular. The vertex set rather looks like (and actually, is) the union of the vertex set of the 4-dimensional cube \mathbf{I}^4 and the scaled crosspolytope $2\text{conv}(\{\pm \mathbf{e}_1, \pm \mathbf{e}_2, \pm \mathbf{e}_3, \pm \mathbf{e}_4\})$. But the reader can check that the following list of 24 vectors, whose symmetry is more apparent, are the normals to the facets of \mathbf{P} . More precisely, for each of the vectors \mathbf{v} in formula (7.2) there are six vertices \mathbf{p} in (7.1) where the scalar product (\mathbf{v}, \mathbf{p}) is maximal and equal to 2. Conversely, each vertex \mathbf{p} maximizes exactly six of the functionals.

$$\begin{aligned} (\pm 1, \pm 1, 0, 0), \quad & (\pm 1, 0, \pm 1, 0), \quad (\pm 1, 0, 0, \pm 1), \\ (0, \pm 1, \pm 1, 0), \quad & (0, \pm 1, 0, \pm 1), \quad (0, 0, \pm 1, \pm 1). \end{aligned} \quad (7.2)$$

Actually, the 24-cell is a self-dual polytope. This means that by taking (7.2) as 24 vertices, we get combinatorially the same polytope, whose facet-normal vectors are given by (7.1).

Our goal is to show that the 2-skeleton of the 24-cell, which is simplicial, has a disconnected graph of locally acyclic orientations (observe that we defined locally acyclic orientations for arbitrary simplicial complexes, not necessarily triangulations). More precisely, we get a graph of locally acyclic orientations with at least 13 connected components, 12 of which are isolated vertices. In other words, there are (at least) 12 ways of locally acyclically orienting the 2-skeleton of the 24-cell without reversible edges.

Remark 7.2.13. The 24-cell has the same number of triangles and edges, 96 of each (check this!). Since each triangle in a complex prevents at most one edge from being reversed, it is especially surprising that it has l.a.o.'s without reversible edges. Any of them will provide a perfect matching between triangles and edges incident to them.

To describe these 12 locally acyclic orientations, let us first get a deeper understanding of the 24-cell.

According to (7.1) we can construct a 24-cell starting with the 16 vertices of the 4-dimensional cube, which has 8 facets, all of them 3-dimensional cubes. See a Schlegel diagram of it in Figure 7.23. The other 8 vertices

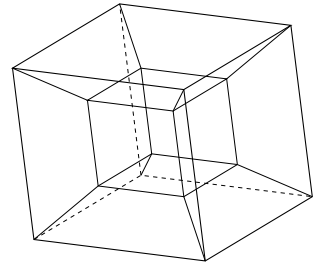


Figure 7.23: Schlegel diagram of the 4-dimensional cube.

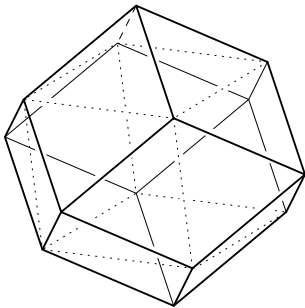
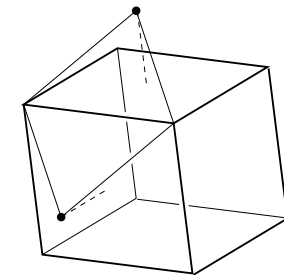


Figure 7.24: 3-dimensional analogy of the construction of a 24-cell from a 4-dimensional cube.

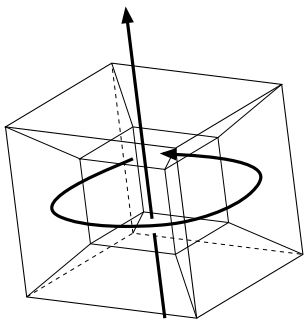


Figure 7.25: Two solid tori in the boundary of the 4-dimensional cube.

of the 24-cell are placed one “beyond” each of these 3-dimensional cubes. Individually, each new vertex would replace a 3-cube from the boundary by six square pyramids (in a Schlegel diagram, we would see the cube get centrally subdivided). But they are at exactly the right distance around the cube so that every two square pyramids adjacent to the base form the same facet, which indeed is an octahedron. The $8 \times 6 = 48$ squared pyramids grouped into 24 pairs form the eight octahedral facets of the 24-cell. Although this is a slight abuse of notation, we will say that the eight new vertices are each “inside” each of the 8 facets of the 4-cube, and that the square pyramids “subdivide” the eight 3-cubes.

To clarify this, Figure 7.24 shows the analogue starting with a 3-cube. In this case the outcome is not a regular polytope (one reason being that $\sqrt{1+1+1} \neq 2$). Instead, it is the so-called rhombic dodecahedron. Incidentally, this polytope is the polar of the cube-octahedron we found in Section 7.1.

One more feature of the 4-dimensional cube that we will benefit from is that its 8 facets can be divided into 2 cycles of 4 facets each, as Figure 7.25 shows in a Schlegel diagram of the 4-cube. Each cube belongs to one of the cycles and the other one goes around it (for the vertical cycle, “around” means “through infinity”, in Figure 7.25).

Once we have chosen a specific decomposition of the boundary of the 4-cube into two cycles and a specific orientation for those two cycles, there is an orientation of the whole 4-skeleton of the 24-cell which is “most compatible” with those choices: For the 32 edges that belong to the 4-cube, take the direction parallel to the two cycles (the edges get divided into eight cycles of length four). For the other 64 edges (eight inside each 3-cube) choose the direction closer to the cycle containing that 4-cube. See Figure 7.26, where we show the orientation in each of the eight 3-cubes of Figure 7.23 separately. We have that:

Proposition 7.2.14. *The orientation of edges shown in Figure 7.26 is locally acyclic and it has no reversible edges.*

Proof. Where are the 96 triangles of the 24-cell? Let us see. The decomposition of each 3-cube into six square pyramids creates 12 triangles (one joining each of the 12 edges of the 3-cube to the interior point). Since the only cycles in the orientation of each 3-cube are the cycles of length four coming from the 4-cube, no triangle gets a cycle.

To check edge reversals, first observe that the eight 3-cubes are equivalent. Hence, we only need to check one of them; for example, the “smaller” 3-cube on the top right corner of Figure 7.23. The twelve triangles interior to that 3-cube prevent the eight interior edges plus the four vertical edges from being reversed. Since all the original edges of the 4-cube are also equivalent under the symmetries of our construction, the eight horizontal edges cannot be reversed either. \square

Remark 7.2.15. As usual, we are taking advantage of symmetries to reduce the number of cases to be studied. As we have presented it, the construction of our l.a.o. has 32 symmetries (the product of the four rotations along each

cycle of 3-cubes multiplied by two, because there is a symmetry exchanging the two cycles). But there are more symmetries in the final l.a.o. than in the original 4-cube. In fact, the symmetry group of our l.a.o. has 96 elements, and makes all the 96 triangles and 96 edges of the 24-cell equivalent to one another.

The reader can check that the 24 octahedra of the 24-cell get exactly the l.a.o. displayed in Figure 7.22. For the eight octahedra along the two cycles of Figure 7.23, this is no surprise, but for the other 16 it is perhaps unexpected. The four symmetries of any single octahedron times the 24 octahedra present (which are also equivalent by the orientation) give the 96 symmetries of the orientation.

Corollary 7.2.16. *The graph of all locally acyclic orientations of the 2-skeleton of a 24-cell has (at least) 12 isolated vertices and 13 components.*

Proof. There are 12 different, but equivalent under symmetries of the 24-cell, ways of constructing the l.a.o. of Proposition 7.2.14: On any particular octahedron the orientation we have chosen has 4 symmetries and the octahedron itself has 48 symmetries, all of which are symmetries of the 24-cell. \square

L.a.o.'s of triangulations without reversible edges

For our application in the next section, we need a locally acyclic orientation of a *triangulation* of a point set. We can get one from the previous example by triangulating the 24-cell and extending the orientation of the previous example. Observe that in the l.a.o. of the 2-skeleton of the 24-cell, the boundary of each of the 24 octahedra has received precisely the non-globally acyclic orientation with one sink and one source that we depicted in Figure 7.22. This l.a.o. of the boundary of the octahedron can be extended to a l.a.o. of a triangulation of the whole octahedron as shown in Figure 7.28. Doing this in the 24 octahedra of the 24-cell, we get a l.a.o. of a triangulation of the boundary of it.

Let us now remark that this orientation does not have any global sinks or sources. Indeed, each individual octahedron has a source and a sink, but each vertex of the 24-cell is incident to six octahedra and it is a sink in one, a source in another one, and neither of the two in the other four. This is interesting for the following reason:

Lemma 7.2.17. *Let \mathcal{K} be a simplicial complex, and consider a locally acyclic orientation of it without reversible edges and without sinks (respectively, without sources). Consider a cone $\mathcal{K} * v$ over \mathcal{K} and orient every edge incident to v towards v (respectively, away from v). This gives a locally acyclic orientation of $\mathcal{K} * v$ without reversible edges.*

Proof. Assume, without loss of generality, that the orientation of \mathcal{K} has no sinks. We need to show that no edge of the form vw , with w in \mathcal{K} , can be reversed. Since w is not a sink, there is an edge ww' in \mathcal{K} oriented towards w' . Additionally, we have the edges wv and $w'v$ oriented towards v by construction. Then, the triangle $ww'w$ in $\mathcal{K} * v$ forces wv to be non-reversible. \square

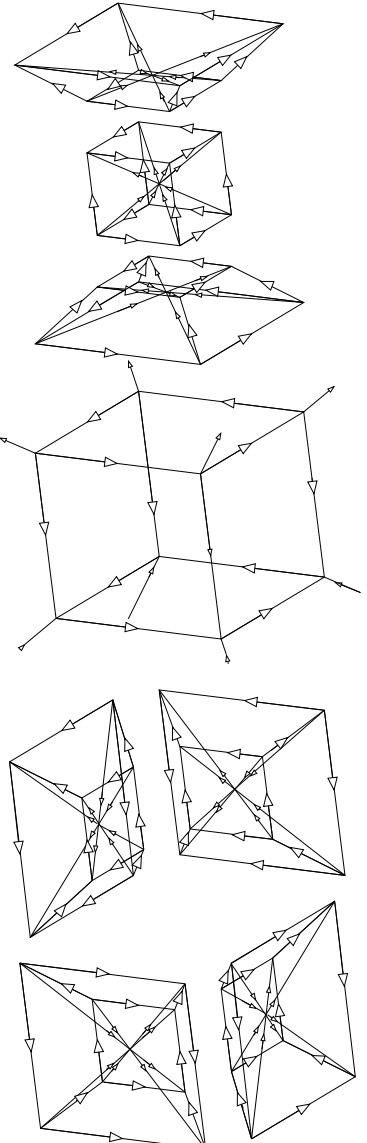


Figure 7.26: A locally acyclic orientation of the graph of a 24-cell.

Corollary 7.2.18. *Extending the previous triangulation of the boundary of the 24-cell to the interior by joining it to the centroid gives a triangulation of 25 points in dimension four with a locally acyclic orientation that has no reversible edges.*

Can we do better? Yes. In particular, we can get a construction in dimension three as follows: consider the Schlegel diagram of the 24-cell. This gives a polyhedral complex in \mathbb{R}^3 with 24 vertices and 23 maximal cells, all of them octahedra, and with the same 2-skeleton as the 24-cell. Apply to it the previous construction (including the step of triangulating the octahedra). This way we get:

Corollary 7.2.19. *There is a triangulation of 24 points in \mathbb{R}^3 with a locally acyclic orientation that has no reversible edges, sinks, or sources.*

This construction will be instrumental in the next section.

7.2.4 Dimension 4: Layers of prisms

Let \mathcal{T} be a triangulation of a d -dimensional point configuration \mathbf{B} with n elements. We are going to show how, from a locally acyclic orientation of \mathcal{T} without sources, sinks, or reversible edges, we can build triangulations in dimension $d+1$ with an arbitrarily large number of vertices and a constant number of flips.

We start with three copies of \mathbf{B} embedded in \mathbb{R}^{d+1} , parallel to one another. This is the point configuration $\mathbf{B} \times \{-1, 0, 1\}$. For reasons to be explained later, the points in $\mathbf{B} \times \{0\}$ need to be slightly moved up or down along the vertical lines passing through them, until the following genericity property holds for $\mathbf{B} \times \{0\}$: when we embed in it the triangulation \mathcal{T} of \mathbf{B} , no two adjacent maximal simplices lie in the same hyperplane. See Figure 7.27.

The union of the three copies will be denoted \mathbf{A}_0 and from it we construct, for any given $k \in \mathbb{N}$, a point configuration \mathbf{A}_k with $(k+2)n$ elements, as follows: Let $\mathbf{B}_{-1} := \mathbf{B} \times \{-1\}$ and let \mathbf{B}_0 be the perturbed version of $\mathbf{B} \times \{0\}$ contained in \mathbf{A}_0 . Let ε be a positive real number (we will later assume it to be small) and let \mathbf{B}_i , for each $i = 1, \dots, k$ be obtained by vertical translation of positive length εi of the middle point configuration \mathbf{B}_0 . Let $\mathbf{B}_{k+1} := \mathbf{B} \times \{1 + \varepsilon k\}$. Finally, let

$$\mathbf{A}_k := \mathbf{B}_{-1} \cup \mathbf{B}_0 \cup \dots \cup \mathbf{B}_k \cup \mathbf{B}_{k+1}.$$

In other words, \mathbf{A}_k is obtained by separating the upper and lower halves of \mathbf{A}_0 and inserting another $k-1$ (perturbed) copies of \mathbf{B} in between. See a picture in Figure 7.29. For each element a or subset C of \mathbf{B} , $a^{(i)}$, and $C^{(i)}$, $i = 0, \dots, k$ will denote their counterparts in \mathbf{B}_i .

In these conditions, the following is a polyhedral subdivision of \mathbf{A}_k , that we call \mathcal{S}_k : We embed the original triangulation \mathcal{T} in all the copies (perturbed or not) of \mathbf{B} and fill in the spaces between consecutive copies with prisms over the simplices of \mathcal{T} . Some of the prisms will not have parallel bases, but they are projectively equivalent to prisms with parallel bases and, in particular, they have exactly the same triangulations.

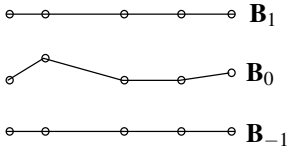


Figure 7.27: The starting point set \mathbf{A}_0 .

We call i -th layer of \mathcal{S}_k , for $i = 0, \dots, k+1$, the union of the prisms between \mathbf{B}_{i-1} and \mathbf{B}_i . There is a bottom or 0-th layer between \mathbf{B}_{-1} and \mathbf{B}_0 and a top or $k+1$ -th layer between \mathbf{B}_k and \mathbf{B}_{k+1} .

If we want to refine \mathcal{S}_k into a triangulation, we just need to triangulate each of the prisms in the layers. For each such prism, triangulations are in bijection with acyclic orientations of the 1-skeleton of its bottom base. As in Lemma 7.2.9, the necessary and sufficient condition for triangulations of adjacent prisms in the same layer to intersect properly is that acyclic orientations coincide on their common edges. That is, triangulations that refine \mathcal{S}_k are in bijection to $(k+2)$ -tuples of locally acyclic orientations of \mathcal{T} . Figure 7.30 shows how to triangulate the third layer in the example of Figure 7.29.

Theorem 7.2.20. Let G_0 denote a locally acyclic orientation of \mathcal{T} without sinks, sources, or reversible edges. Take G_i equal to G_0 for even i and opposite to G_0 for odd i . Let \mathcal{T}_k be the triangulation of \mathbf{A}_k obtained with this process. Then,

1. For every flip of \mathcal{T}_k , all the maximal simplices involved in the flip are either in the top or bottom layers.
2. \mathcal{T}_k has exactly the same number of flips as \mathcal{T}_0 , for every even k .

Proof. As usual, we count flips by looking at which walls (codimension 1 simplices) of \mathcal{T}_k support them. Let C be one such wall. If some maximal simplex of which C is a facet is not in the top or bottom layers, then C is contained in $\mathbf{B}_0 \cup \dots \cup \mathbf{B}_k$.

The following three cases cover all possibilities for C . The cases are illustrated in parts (a) through (c) of Figure 7.31, where the walls (edges, in the figure) under study are drawn thicker.

- (a) If C is contained in some \mathbf{B}_i , $i \in \{0, \dots, k\}$, then it cannot be flipped. Indeed, by our choice that the orientations given to consecutive layers are opposite, C is joined to the same point of the $(i-1)$ -th and $(i+1)$ -th layer, this point being the sink of the orientation given to C . The circuit involved is 1-dimensional, namely $(\{a^{(i+1)}, a^{(i-1)}\}, \{a^{(i)}\})$, where $a^{(i)}$ is the sink of C . But the two edges of this circuit cannot have the same link, because this common link should be contained in \mathbf{B}_i , which would imply that $a^{(i)}$ is a sink of the orientation given to the i -th layer. That orientation has no sinks, because G_0 has no sinks or sources.
- (b) If C is interior to a prism in some layer, then a flip in C corresponds to a single-edge reversal in the orientation of the bottom base of this prism. But this would also be a flip in the prisms over all other simplices containing that edge, which would imply that the edge should be reversible in G_i . This cannot happen since G_0 , hence G_i , has no reversible edges.

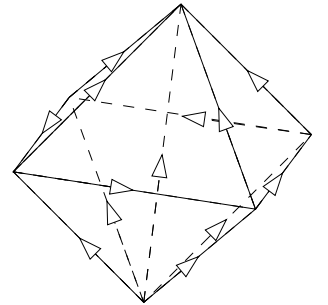


Figure 7.28: A locally acyclic orientation of a triangulation of an octahedron.

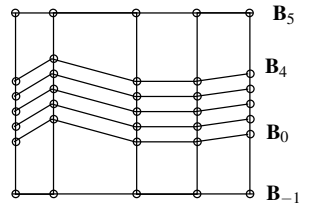


Figure 7.29: Insertion of 4 layers of prisms in a triangulation.

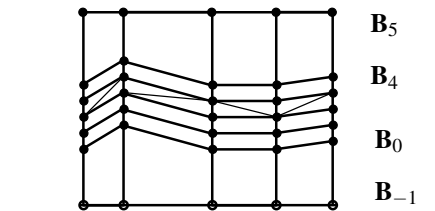
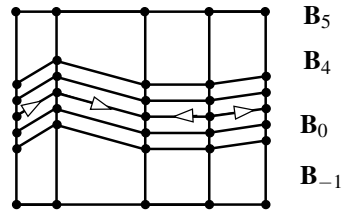


Figure 7.30: Orienting the edges in \mathbf{B}_2 we triangulate the third layer of Figure 7.29.

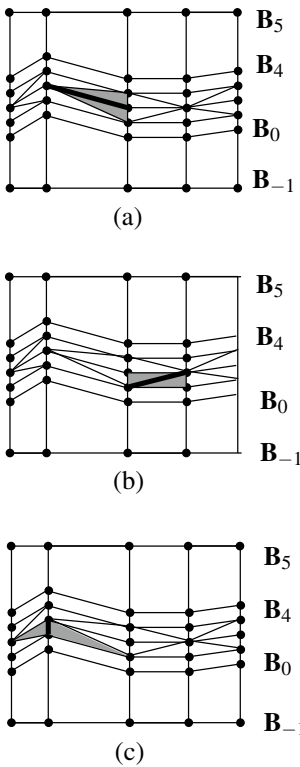


Figure 7.31: The four cases in the proof of Theorem 7.2.20.

- (c) Finally, suppose that C has vertices in two consecutive layers, \mathbf{B}_i and \mathbf{B}_{i-1} , for some $i \in \{1, \dots, n\}$, but it is not interior to a prism. That is to say, the two maximal simplices $C \cup a$ and $C \cup b$ sharing C belong to different prisms of the same layer. For the circuit contained in $C \cup \{a, b\}$ to be flippable, we need (among other things) \mathcal{T}_k to contain a triangulation of $C \cup \{a, b\}$.

But the assumption that the points in the intermediate copies of \mathbf{B} have generic heights implies that, if ε is sufficiently small, then the convex hull of $C \cup \{a, b\}$ is not contained in the layer containing C . We assume ε to fit these requirements. Then some maximal simplex involved in the flip is contained in one of the layers neighbor to i , which implies that one of the flippable walls is fully contained in the copy of \mathbf{B} between these two layers, a case we have already seen is impossible.

The above case study implies Part 1 of the Theorem. Part 2 is straightforward from it: if all the simplices involved in the flip lie in the first or last layer, then the flip was already present in \mathcal{T}_0 , because the first and last layers are just translations of the two layers in \mathcal{T}_0 . \square

Corollary 7.2.21. *There are triangulations in dimension 4 with arbitrarily many vertices and a constant number of flips.*

Proof. Consider the 3-dimensional triangulation of Corollary 7.2.19, with the locally acyclic orientation that we constructed there, which has neither reversible edges, sinks, nor sources. Apply to it Theorem 7.2.20. \square

Remark 7.2.22. The ideas in this section come from [279]. There, the original 3-dimensional triangulation used has 15 vertices, and the 4-dimensional arbitrarily large triangulations obtained are shown to have at most nine flips.

7.3 Dimension 5: A disconnected graph of triangulations with unimodular triangulations

The construction we present here is also based on layers of prisms, except:

- There will only be one layer.
- The key point is that we are not interested in the whole layer, but only in some faces of its convex hull. Put differently, we do not look at locally acyclic orientations of a whole triangulation, but just those of a certain subcomplex of it.

7.3.1 Locally acyclic orientations of boundary subcomplexes

Let \mathbf{A} be a point configuration and let F be a simplicial face of it. Remember that, as introduced in Chapter 2, by this we mean that $\text{conv}_{\mathbf{A}}(F)$ is a simplex and, moreover, no element of \mathbf{A} except those in F are contained in $\text{conv}_{\mathbf{A}}(F)$.

Then, $\text{prism}(F)$ is a face of $\text{prism}(\mathbf{A})$ and it is a prism over a simplex. Every triangulation of $\text{prism}(\mathbf{A})$ can be restricted to a triangulation of $\text{prism}(F)$, which in turn can be represented as an acyclic orientation of

the complete graph on F . Any flip in a triangulation of $\text{prism}(\mathbf{A})$ will either leave the triangulation of $\text{prism}(F)$ unchanged or will produce a flip. Summing up: *There is a map from the graph of triangulations of $\text{prism}(\mathbf{A})$ to the graph of acyclic orientations of B .* When we say we have a *map between two graphs* $f : \mathcal{G} \rightarrow \mathcal{G}'$, we mean that f maps vertices of \mathcal{G} to vertices of \mathcal{G}' , and the image of every edge of \mathcal{G} is either an edge or a single vertex in \mathcal{G}' .

Let us now consider a simplicial subcomplex \mathcal{K} of the boundary complex of \mathbf{A} ; that is, a collection of simplicial faces F_1, \dots, F_k of \mathbf{A} , closed under taking faces. As before, every triangulation \mathcal{T} of $\text{prism}(\mathbf{A})$ induces a triangulation in each of the products $\text{prism}(F_i)$, and hence an acyclic orientation of the edges of each F . If an edge e is common to two of the simplices F_i and F_j , then the orientation received by e from the two triangulated prisms is the same, because this orientation indicates only which of the two diagonals of $\text{prism}(e)$ appears in \mathcal{T} .

That is to say:

Lemma 7.3.1. *The above procedure induces a map from the graph $\mathcal{G}_{\text{tri}} \text{prism}(\mathbf{A})$ of triangulations of $\text{prism}(\mathbf{A})$ to the graph $\mathcal{G}_{\text{l.a.o.}}(\mathcal{K})$ of locally acyclic orientations of \mathcal{K} .*

Observe a difference between this lemma and Lemma 7.2.9: The statement of Lemma 7.2.9 can be thought of as giving a map in the opposite direction: if \mathcal{T} is a triangulation of \mathbf{A} , there is an injective map (an immersion) of the graph $\mathcal{G}_{\text{l.a.o.}}(\mathcal{T})$ into $\mathcal{G}_{\text{tri}} \text{prism}(\mathbf{A})$.

Proof. We know how to associate a locally acyclic orientation of \mathcal{K} to each triangulation. And we know that each bistellar flip in triangulations of \mathcal{K} corresponds to at most a single-edge reversal in each triangle of \mathcal{K} . Is it obvious that two edges of different simplices cannot be reversed by the same flip in triangulations of \mathbf{A} ? It is, because the flip which reverses a certain edge e is precisely the one supported on the circuit $\text{prism}(e)$. \square

Remark 7.3.2. The map of Lemma 7.3.1 need not be surjective. For example, Rambau [266] has shown that if \mathbf{P} is the vertex set of a convex (not necessarily regular) polygon and \mathcal{K} is its boundary complex, the cyclic orientation of \mathcal{K} is not in the image of the map of Lemma 7.3.1. Put differently, the helix-like triangulation of the vertical boundary $\text{prism}(\mathcal{K})$ of a prism cannot be extended to a triangulation of the prism (see Figure 7.32).

In particular, knowing that $\mathcal{G}_{\text{l.a.o.}}(\mathcal{K})$ is disconnected does not automatically imply that $\mathcal{G}_{\text{tri}}(\mathbf{A})$ is disconnected. It needs to be checked that locally acyclic orientations from at least two connected components of $\mathcal{G}_{\text{l.a.o.}}(\mathcal{K})$ are in the image of this map. Lemma 7.2.9 is useful for this purpose. It guarantees that orientations which can be extended to locally acyclic orientations of a triangulation of \mathbf{A} are in the image.

With this, we are ready to construct our first point set with a *disconnected graph of triangulations*. Remember that the 24-cell is a 4-dimensional polytope whose 2-skeleton is simplicial and which has locally acyclic orientations without reversible edges (Corollary 7.2.18).

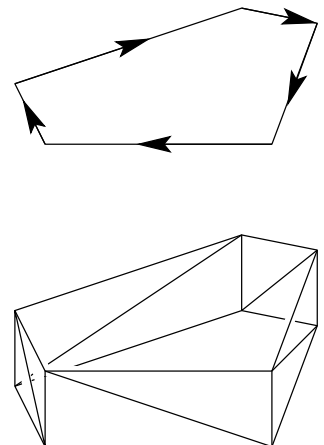


Figure 7.32: The cyclic orientation of a polygon (top) represents a triangulation of the vertical faces of a prism (bottom) that cannot be extended to a triangulation of the whole prism.

Theorem 7.3.3. *Let \mathbf{B} be the vertex set of a 24-cell and let \mathbf{o} be its centroid. Let $\mathbf{A} = \mathbf{B} \cup \{\mathbf{o}\}$. Then:*

1. *There are (at least 12) locally acyclic orientations of the 2-skeleton of \mathbf{A} that have no reversible edges and that can be extended to locally acyclic orientations of triangulations of \mathbf{A} .*
2. *Hence, the graph of triangulations of the 5-dimensional configuration $\mathbf{A} \times \mathbf{I}$ has at least 13 connected components.*

Proof. Part 1 is Corollary 7.2.18 and Part 2 follows from it by Lemma 7.3.1. The twelve locally acyclic orientations without reversible edges are in the image of the map of that lemma because they can be extended to triangulations. They are images of twelve different connected components of the graph of triangulations of $\text{prism}(\mathbf{A})$. The thirteenth component is the one containing regular triangulations. Observe that the component of $\mathcal{G}_{\text{l.a.o.}}(\mathcal{K})$ containing the image of the regular triangulations contains all the globally acyclic orientations of \mathcal{K} , hence it is different from the previous 12. \square

7.3.2 Unimodular triangulations in different components of the graph of triangulations

Recall that a triangulation of an integer point configuration is called *unimodular* if all its simplices have determinant equal to ± 1 . Unimodular triangulations have even stronger connections with algebraic geometry than non-unimodular ones. Hence, after the first example of a disconnected graph of triangulations was found [278], there was still interest in the following question: is there an integer point set that has unimodular triangulations in different components of the graph of flips? The locally acyclic orientation of the 24-cell that we have just shown was constructed in [283] to answer this question positively. This provided, in particular, an example of a non-connected *toric Hilbert scheme*, in the sense of [251], by a result of [223].

To show that the disconnected graph of triangulations of Theorem 7.3.3 has unimodular triangulations in different components, we use the coordinatization in which the vertices of the 24-cell are

$$\begin{aligned} (\pm 1, \pm 1, 0, 0), \quad & (\pm 1, 0, \pm 1, 0), \quad (\pm 1, 0, 0, \pm 1), \\ (0, \pm 1, \pm 1, 0), \quad & (0, \pm 1, 0, \pm 1), \quad (0, 0, \pm 1, \pm 1). \end{aligned} \quad (7.3)$$

We first compute the determinants of the simplices in the triangulation of Corollary 7.2.18. Each such simplex has as vertices the centroid $(0, 0, 0, 0)$ plus four of the six vertices of a facet of the 24-cell (regular octahedron). Being a regular polytope, which octahedron we look at is irrelevant, and it is easy to check that all the tetrahedra with vertices in a regular octahedron have the same volume, so we choose an arbitrary one. For example, we look at the octahedron whose facet-defining equation first coordinate equal to one and at the simplex $\{(1, -1, 0, 0), (1, 1, 0, 0), (1, 0, 1, 0), (1, 0, 0, 1)\}$. Adding the centroid and an extra coordinate equal to 1 to every point for

homogenization, the determinant we want to look at is:

$$\begin{vmatrix} 1 & 1 & 1 & 1 & 1 \\ 0 & 1 & 1 & 1 & 1 \\ 0 & -1 & 1 & 0 & 0 \\ 0 & 0 & 0 & 1 & 0 \\ 0 & 0 & 0 & 0 & 1 \end{vmatrix} = \begin{vmatrix} 1 & 1 & 1 & 1 \\ -1 & 1 & 0 & 0 \\ 0 & 0 & 1 & 0 \\ 0 & 0 & 0 & 1 \end{vmatrix} = \begin{vmatrix} 1 & 1 \\ -1 & 1 \end{vmatrix} = 2.$$

But wait, that is not unimodular! What happens is that all the points in our configuration (the hcentroid and the vertices of the octahedron) lie in a proper *sublattice* of \mathbb{Z}^4 ; namely, the sublattice consisting of all points with an even sum of coordinates. This means that there is an affine mapping that reduces volume and sends our point set to another one that still has integer coordinates. In our case, one such projection is

$$f(x_1, x_2, x_3, x_4) = (x_1, x_2, x_3, (x_1 + x_2 + x_3 + x_4)/2).$$

Since the determinant of this map is 1/2, it reduces all volumes by one half. See an analogue of this in Figure 7.33. So:

Lemma 7.3.4. *In the coordinatization obtained by the map f above, the triangulation \mathcal{T} of Corollary 7.2.18 is unimodular. Hence, all the refinements of $\text{prism}(\mathcal{T})$ are unimodular also.*

Proof. We have also shown that \mathcal{T} is unimodular. The second statement comes from the fact that all simplices in refinements of $\text{prism}(\mathcal{T})$ have vertices contained in the prism over a (unimodular) simplex. Since the prism over a simplex is totally unimodular (Lemma 6.2.5), our simplices are unimodular. \square

Corollary 7.3.5. *Let $\text{prism}(\mathbf{A})$ be as in Theorem 7.3.3.*

The thirteen connected components of the graph of triangulations of \mathbf{A} contain unimodular triangulations.

Proof. For the twelve non-regular components, the previous lemma proves this. These components contain refinements of $\text{prism}(\mathcal{T})$, for the \mathcal{T} in the lemma.

For the regular component, we can proceed similarly. Triangulate \mathbf{A} by first pulling the interior point (which gives a subdivision consisting of the 24 cones over the octahedral facets) and then refining this subdivision to a triangulation \mathcal{T}' in an arbitrary, but regular, way; for example, in a lexicographic way. All the simplices in this triangulation of \mathbf{A} consist of the centroid joined to a tetrahedron inscribed in an octahedral facet, hence they are unimodular, as we have seen above. With the same argument of Lemma 7.3.4, all the refinements of $\text{prism}(\mathcal{T}')$ are unimodular as well. The ones obtained with globally acyclic orientations of the graph of \mathcal{T}' are regular, by Lemma 7.2.9. \square

7.3.3 Exponential number of components in the graph of flips

Combining the construction we have just done with the idea of stacking layers of prisms that we used in Section 7.2.4, we can get examples of point

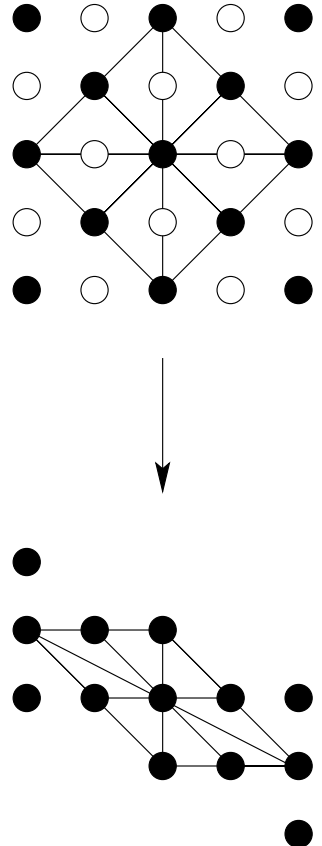


Figure 7.33: A triangulation of a point set in a proper sublattice of \mathbb{Z}^d may become unimodular when the sublattice is sent to \mathbb{Z}^d .

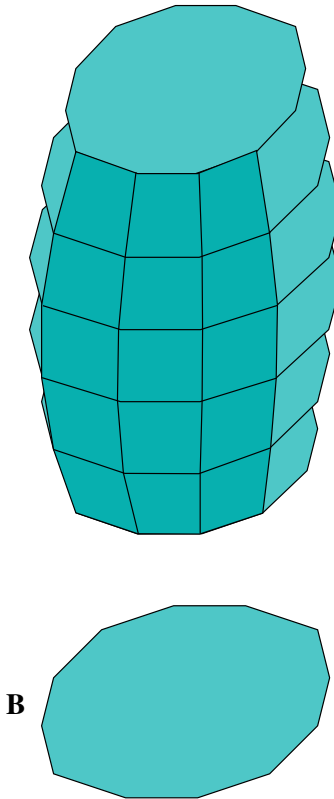


Figure 7.34: The “fattened product” construction.

configurations in dimension 5 in which the number of connected components in the graph of triangulations grows exponentially with the number of points.

We start with the 24-cell, and let \mathbf{B} be the configuration consisting of its 24-vertices plus its centroid, as in Theorem 7.3.3. We construct the following “fattened product” of it with a path: let $f(x)$ be a concave and positive function on the interval $[0, n]$, and let

$$\mathbf{A}_n := \bigcup_{i=0}^k f(i)\mathbf{B} \times \{i\},$$

where $f(i)\mathbf{B}$ denotes the dilation of \mathbf{B} by a factor of $f(i)$.

Figure 7.34 sketches the construction. The key idea is that the vertical part of the face complex of $\text{prism}(\mathbf{B})$ is repeated k times in \mathbf{A}_n and we know that the triangulations of that part provide (at least) 13 connected components in the graph. What we would like to do is say that these k copies of the relevant face complex can be triangulated independently, which would provide us with 13^k connected components. Unfortunately, that may not be true. The common boundary of every two layers is a triangulated 24-cell, and we cannot guarantee in principle that the two triangulations of it coming from the two adjacent layers match to one another...

... Unless we take *the same* triangulation for all the copies of the 24-cell. Observe that the 12 ways of constructing a special locally acyclic orientation mentioned in Corollary 7.2.18 come in 6 pairs of opposites. The triangulation used for one orientation and the opposite one is the same (remember that the triangulation of Figure 7.22 is based on how to triangulate the octahedron in a way compatible with the orientations given). Hence, even if we consider only triangulations that refine the product $\text{prism}(\mathcal{T})$ of a particular triangulation \mathcal{T} we can get three connected components in the graph of triangulations of the vertical boundary of $\text{prism}(\mathbf{B})$, which implies:

Theorem 7.3.6. *The fattened product \mathbf{A}_k , of dimension 5 and with $25(k+1)$ elements, has a disconnected graph of triangulations with at least 3^k connected components, for every $k \in \mathbb{N}$.*

7.4 Dimension 6: A disconnected graph of triangulations in general position

In this section we describe a point set in general position with a *disconnected graph of triangulations*. The example has seventeen points and lies in \mathbb{R}^6 .

There are several reasons why having an example of a disconnected graph of triangulations in *general position* is interesting. In engineering applications, the coordinates of points are sometimes approximate and there is no loss in perturbing them into general position, that is, the general position case is sometimes the only case. Even in a purely theoretical framework, point sets in general position have simpler properties than those in special position. For example, showing a disconnected graph of flips in general position served to disprove the so-called *Generalized Baues Conjecture* for subdivisions of point configurations (see Remark 9.1.17).

Moreover, only in general position are flips truly *local* operations: a flip in general position in dimension d involves $d+2$ points, while a flip in

non-general position may involve arbitrarily many points (those in the triangulated circuit plus those in the link of it). Probably for this reason, some computational geometry authors define flips only in general position. See, for example, [114].

7.4.1 The building block: Gale octagons

All throughout Section 7.4, \mathbf{A}_0 denotes the configuration consisting of the columns \mathbf{a}_j of the following matrix, labeled by $J_0 = \{1, 2, \dots, 8\}$:

$$\begin{array}{cccccccc} & 1 & 2 & 3 & 4 & 5 & 6 & 7 & 8 \\ x_1 & 1 & 0 & 0 & 0 & 1 & 0 & 0 & 0 \\ x_2 & 0 & 1 & 0 & 0 & 0 & 1 & 0 & 0 \\ x_3 & 0 & 0 & 1 & 0 & 0 & 0 & 1 & 0 \\ x_4 & 0 & 0 & 0 & 1 & 0 & 0 & 0 & 1 \\ x_5 & \sqrt{2} & 1 & 0 & -1 & -\sqrt{2} & -1 & 0 & 1 \\ x_6 & 0 & 1 & \sqrt{2} & 1 & 0 & -1 & -\sqrt{2} & -1 \end{array}.$$

This is a rank 6 homogeneous vector configuration or, equivalently, a point configuration in the 5-dimensional real affine space embedded in the hyperplane with equation $x_1 + x_2 + x_3 + x_4 = 1$ in \mathbb{R}^6 . The projection to the last two coordinates sends the eight points to the vertices of a regular octagon, keeping their order. In particular, the eight points of \mathbf{A}_0 are extremal (that is, vertices of $\text{conv}(\mathbf{A}_0)$). The projection to the first four coordinates sends each pair of opposite points $\{i, i+4\}$ to a different vertex of a tetrahedron. The affine symmetry group of the configuration is the dihedral group D_{16} of symmetries of the octagon.

To better understand the structure of \mathbf{A}_0 —and its triangulations—we construct a Gale transform of it:

$$\mathbf{A}_0^* := \begin{pmatrix} 1 & 2 & 3 & 4 & 5 & 6 & 7 & 8 \\ \sqrt{2} & -1 & 0 & 1 & -\sqrt{2} & 1 & 0 & -1 \\ 0 & -1 & \sqrt{2} & -1 & 0 & 1 & -\sqrt{2} & 1 \end{pmatrix}.$$

The elements \mathbf{a}_j^* of \mathbf{A}_0^* are again (in the directions of) the vertices of a regular octagon, except they are not in the same order (see Figure 7.35). Also, and more importantly, we now have to think of them as vectors, rather than points.

From this Gale transform we can read the face structure of the polytope $\text{conv}(\mathbf{A}_0)$. The set of vertices of each facet of \mathbf{A}_0 is the complement of a positive circuit in \mathbf{A}_0^* , and there are twelve of them:

- Eight with dependence $\mathbf{a}_{i-1}^* + \sqrt{2}\mathbf{a}_i^* + \mathbf{a}_{i+1}^* = 0$ (indices are regarded modulo 8). The corresponding facets in \mathbf{A}_0 are 4-dimensional simplices.
- Four of the form $\mathbf{a}_i^* + \mathbf{a}_{i+4}^* = 0$. The corresponding facet of \mathbf{A}_0 , that we denote $F_{i,i+4}$, has six vertices and dimension four. Hence, it is not a simplex. In fact, its six vertices form a circuit, whose affine dependence is

$$\mathbf{a}_{i+1} + \sqrt{2}\mathbf{a}_{i+6} + \mathbf{a}_{i+3} = \mathbf{a}_{i+5} + \sqrt{2}\mathbf{a}_{i+2} + \mathbf{a}_{i+7}.$$

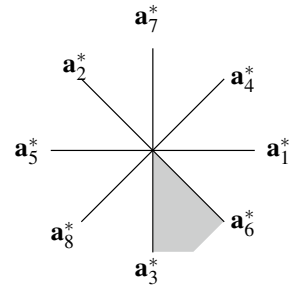


Figure 7.35: The Gale transform of \mathbf{A}_0 , with one chamber marked.

\mathbf{A}_0 has corank two, so all its triangulations are regular (Theorem 5.5.9). From the Gale transform we also read, via Theorem 5.4.7, that \mathbf{A}_0 has exactly eight regular triangulations, with the graph of bistellar flips being a cycle. More precisely, for each $i \in \{1, \dots, 8\}$, there is a unique triangulation of \mathbf{A}_0 that contains the simplex $J_0 \setminus \{i, i+3\}$. We denote this triangulation $\mathcal{T}_{i,i+3}$. For example, the chamber marked in Figure 7.35 corresponds to the triangulation $\mathcal{T}_{3,6}$ consisting of the following six 5-dimensional simplices and eight adjacencies among them:

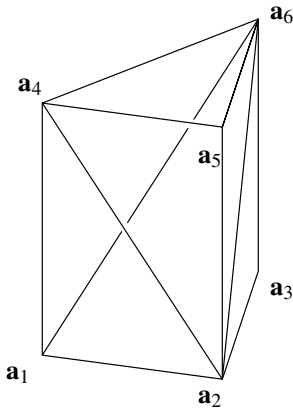
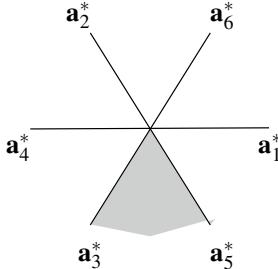


Figure 7.36: A “Gale hexagon” is the vertex set

of a triangular prism. Here we see its Gale transform with the chamber 35 marked (above).

This chamber corresponds to the triangulation $\{1236, 1246, 2456\}$ (below).

$$\begin{array}{c} \{1, 2, 5, 6, 7, 8\} — \{2, 4, 5, 6, 7, 8\} \\ \quad \backslash \qquad \quad / \qquad \quad \backslash \\ \quad \{1, 2, 4, 5, 7, 8\} \qquad \{2, 3, 4, 5, 6, 7\} \\ / \qquad \quad \backslash \qquad \quad / \\ \{1, 2, 3, 4, 7, 8\} — \{1, 2, 3, 4, 5, 7\} \end{array} \quad (7.4)$$

That \mathbf{A}_0 has *only* eight triangulations contrasts the fact that the boundary of $\text{conv}(\mathbf{A}_0)$ can be triangulated in sixteen ways. Indeed, since all ridges (codimension 2 faces) of $\text{conv}(\mathbf{A}_0)$ are simplices, to triangulate $\partial \text{conv}(\mathbf{A}_0)$ we can independently triangulate the four facets which are not simplices. Each of them is a circuit, hence it has two triangulations. It can be checked that different triangulations of \mathbf{A}_0 have distinct restrictions to $\partial(\text{conv}(\mathbf{A}_0))$, so that:

Lemma 7.4.1. *Exactly eight triangulations of the boundary $\partial(\text{conv}(\mathbf{A}_0))$ can be extended to triangulations of \mathbf{A}_0 , each in a unique way.*

Example 7.4.2. That triangulations of the boundary of a polytope may sometimes not be extendable to the whole polytope (without using additional interior points as vertices) is a well-known fact that occurs also in three-dimensional examples such as the cube or the triangular prism, as we have seen already in Chapter 6. Let us analyze the latter again. Matrices for the triangular prism and its Gale transform are, for example,

$$\begin{matrix} & 1 & 2 & 3 & 4 & 5 & 6 \\ \left(\begin{array}{cccccc} 1 & -\frac{1}{2} & -\frac{1}{2} & 1 & -\frac{1}{2} & -\frac{1}{2} \\ 0 & \frac{\sqrt{3}}{2} & -\frac{\sqrt{3}}{2} & 0 & \frac{\sqrt{3}}{2} & -\frac{\sqrt{3}}{2} \\ 0 & 0 & 0 & 1 & 1 & 1 \\ 1 & 1 & 1 & 1 & 1 & 1 \end{array} \right) \end{matrix}$$

and

$$\begin{matrix} & 1 & 2 & 3 & 4 & 5 & 6 \\ \left(\begin{array}{cccccc} 1 & -\frac{1}{2} & -\frac{1}{2} & -1 & \frac{1}{2} & \frac{1}{2} \\ 0 & \frac{\sqrt{3}}{2} & -\frac{\sqrt{3}}{2} & 0 & -\frac{\sqrt{3}}{2} & \frac{\sqrt{3}}{2} \end{array} \right). \end{matrix}$$

There are several properties in this example similar to those of the configuration \mathbf{A}_0 : The Gale transform consists of three pairs of opposite vectors; the prism has three special facets which are not simplices but instead support unique circuits; the boundary can be triangulated in $2^3 = 8$ ways, of which only six can be extended to the interior, etc.

A crucial point in order to understand what follows is how to read, in the Gale transform, which triangulation of the boundary is induced by a certain

triangulation of \mathbf{A}_0 . Let us explain this with the facet $F_{1,5} := \text{conv}(J_0 \setminus \{1,5\})$. Since the circuit formed by its six vertices is $(\{2,4,7\}, \{3,6,8\})$, the two triangulations of $F_{1,5}$ are

$$\begin{aligned}\mathcal{T}_+ &:= \{\{3,4,6,7,8\}, \{2,3,6,7,8\}, \{2,3,4,6,8\}\}, \\ \mathcal{T}_- &:= \{\{2,4,6,7,8\}, \{2,3,4,7,8\}, \{2,3,4,6,7\}\}.\end{aligned}$$

Let $\mathcal{T}_{i,i+3}$ be one of the triangulations of \mathbf{A}_0 , corresponding to the chamber between the rays i and $i+3$. Then, at least one of i and j , say i , is not in $\{1,5\}$. Also, exactly one of $\text{cone}(\{1,i\})$ and $\text{cone}(\{5,i\})$, say $\text{cone}(\{1,i\})$, contains the sector $\text{cone}(\{i,i+3\})$. Then, $J_0 \setminus \{1,i\}$ is a simplex in $\mathcal{T}_{i,i+3}$. Hence, the triangulation of $F_{1,5}$ is (in this case) the one that contains the simplex $J_0 \setminus \{1,5,i\}$. In other words:

Lemma 7.4.3. *The triangulation of $F_{1,5}$ induced by a triangulation $\mathcal{T}_{i,i+3}$ of \mathbf{A}_0 is \mathcal{T}_+ if and only if the chamber corresponding to $\mathcal{T}_{i,i+3}$ lies on the side of the line through $\{1,5\}$ that contains 2, 4 and 7.¹*

The following corollary is crucial for our construction.

Corollary 7.4.4. *The flip between the triangulations $\mathcal{T}_{i-3,i}$ and $\mathcal{T}_{i,i+3}$ of \mathbf{A}_0 preserves the triangulations induced in the facets $F_{i+1,i+5}$ and $F_{i+2,i+6}$ and switches the triangulations induced in the facets $F_{i,i+4}$ and $F_{i+3,i+7}$.*

7.4.2 Seventeen points in special position

Let \mathbf{A} be the point set defined by the columns \mathbf{a}_k of the matrix displayed in Figure 7.1, labeled by $K = \{0, 1^+, \dots, 8^+, 1^-, \dots, 8^-\}$. The matrix is written in two pieces for typographic reasons. \mathbf{A} is a configuration of 17 points in \mathbb{R}^6 (the first row in the matrix is, as usual, a homogenization coordinate) and consists of the origin and two copies of the configuration \mathbf{A}_0 of the previous section, placed centrally symmetrically around the origin. Observe that the point opposite to i^+ is $(i+4)^-$, rather than i^- . Our indexing is chosen so that i^+ and i^- go to the same vertex of a regular octagon via the projection onto the last two coordinates.

The affine symmetry group of \mathbf{A} is $\mathbb{Z}_2 \times \mathbb{Z}_2 \times \mathbb{Z}_2 \times \mathbb{Z}_2 \times D_{16}$, the last factor acting as the octagon symmetries on the last two coordinates (with the corresponding permutations of the first four coordinates) and the \mathbb{Z}_2 factors by sign reversal, one on each of the first four coordinates. In particular, \mathbf{A} contains 16 facets affinely equivalent to \mathbf{A}_0 , that we denote $F_{\delta_1, \delta_2, \delta_3, \delta_4}$, with $\delta_i \in \{+, -\}$. More precisely,

$$F_{\delta_1, \delta_2, \delta_3, \delta_4} := \{1^{\delta_1}, 2^{\delta_2}, 3^{\delta_3}, 4^{\delta_4}, 5^{\delta_1}, 6^{\delta_2}, 7^{\delta_3}, 8^{\delta_4}\}$$

is the label set of the facet defined by the equation

$$\delta_1 x_1 + \delta_2 x_2 + \delta_3 x_3 + \delta_4 x_4 = 1.$$

¹In oriented matroid language: a triangulation restricts to the positive triangulation of the circuit $(\{2,4,7\}, \{3,6,8\})$ if and only if the dual chamber lies in the positive side of the corresponding cocircuit $(\{2,4,7\}, \{3,6,8\})$.

| | 0 | I^+ | 2^+ | 3^+ | 4^+ | 5^+ | 6^+ | 7^+ | 8^+ | |
|---------------------|---------|------------|-------|------------|-------|-------------|-------|-------------|-------|-----|
| x_1 | 1 | 1 | 1 | 1 | 1 | 1 | 1 | 1 | 1 | ... |
| | 0 | 1 | 0 | 0 | 0 | 1 | 0 | 0 | 0 | ... |
| x_2 | 0 | 0 | 1 | 0 | 0 | 0 | 1 | 0 | 0 | ... |
| $\mathbf{A} := x_3$ | 0 | 0 | 0 | 1 | 0 | 0 | 0 | 1 | 0 | ... |
| x_4 | 0 | 0 | 0 | 0 | 1 | 0 | 0 | 0 | 1 | ... |
| x_5 | 0 | $\sqrt{2}$ | 1 | 0 | -1 | $-\sqrt{2}$ | -1 | 0 | 1 | ... |
| x_6 | 0 | 0 | 1 | $\sqrt{2}$ | 1 | 0 | -1 | $-\sqrt{2}$ | -1 | ... |
| | \dots | I^- | 2^- | 3^- | 4^- | 5^- | 6^- | 7^- | 8^- | |
| | \dots | 1 | 1 | 1 | 1 | 1 | 1 | 1 | 1 | 1 |
| | \dots | -1 | 0 | 0 | 0 | -1 | 0 | 0 | 0 | 0 |
| | \dots | 0 | -1 | 0 | 0 | 0 | -1 | 0 | 0 | 0 |
| | \dots | 0 | 0 | -1 | 0 | 0 | 0 | -1 | 0 | 0 |
| | \dots | 0 | 0 | 0 | -1 | 0 | 0 | 0 | 0 | -1 |
| | \dots | $\sqrt{2}$ | 1 | 0 | -1 | $-\sqrt{2}$ | -1 | 0 | 1 | |
| | \dots | 0 | 1 | $\sqrt{2}$ | 1 | 0 | -1 | $-\sqrt{2}$ | -1 | |

Table 7.1: A point configuration with a disconnected space of triangulations.

Each $F_{\delta_1, \delta_2, \delta_3, \delta_4}$ is adjacent to the other four, namely the ones whose labels differ from $(\delta_1, \delta_2, \delta_3, \delta_4)$ on a single δ_i . Their common face, a ridge of \mathbf{A} , is one of the non-simplicial ones denoted $F_{i,i+4}$ in the previous section. In other words, the adjacency graph among the sixteen $F_{\delta_1, \delta_2, \delta_3, \delta_4}$'s is that of a four-dimensional cube, and each adjacency happens on a 4-dimensional face with six vertices, hence containing a unique circuit. The full list of facets of the polytope $\text{conv}(\mathbf{A})$ consists of the 16 non-simplicial facets isomorphic to \mathbf{A}_0 , together with 96 five-dimensional simplices which fall into two orbits via the symmetry group. There are 64 simplices in one orbit and 32 in the second. The f -vector of $\text{conv}(\mathbf{A})$ is $(16, 112, 352, 528, 384, 112)$.

We now wish to fix a certain triangulation of the boundary of $\text{conv}(\mathbf{A})$. To this end, we only need to say which of the eight possible triangulations we use in each of the sixteen non-simplicial facets $F_{\delta_1, \delta_2, \delta_3, \delta_4}$. Since each such facet contains one member of every pair $\{i^+, i^-\}$, there is a canonical isomorphism from it to the configuration \mathbf{A}_0 , so we specify a triangulation of $F_{\delta_1, \delta_2, \delta_3, \delta_4}$ via a triangulation of \mathbf{A}_0 , that is, a chamber in the Gale transform \mathbf{A}_0^* . Our choice is to triangulate $F_{\delta_1, \delta_2, \delta_3, \delta_4}$ with:

- the chamber cone $(3, 6)$, if $\delta_1 = \delta_2$ and $\delta_3 = \delta_4$;
- the chamber cone $(1, 4)$, if $\delta_1 = \delta_2$ and $\delta_3 \neq \delta_4$;
- the chamber cone $(5, 8)$, if $\delta_1 \neq \delta_2$ and $\delta_3 = \delta_4$;
- the chamber cone $(7, 2)$, if $\delta_1 \neq \delta_2$ and $\delta_3 \neq \delta_4$.

Figure 7.37 shows this choice pictorially. Arrows represent adjacencies between different $F_{*,*,*,*}$'s. The arrow directions are convenient to follow the following proof.

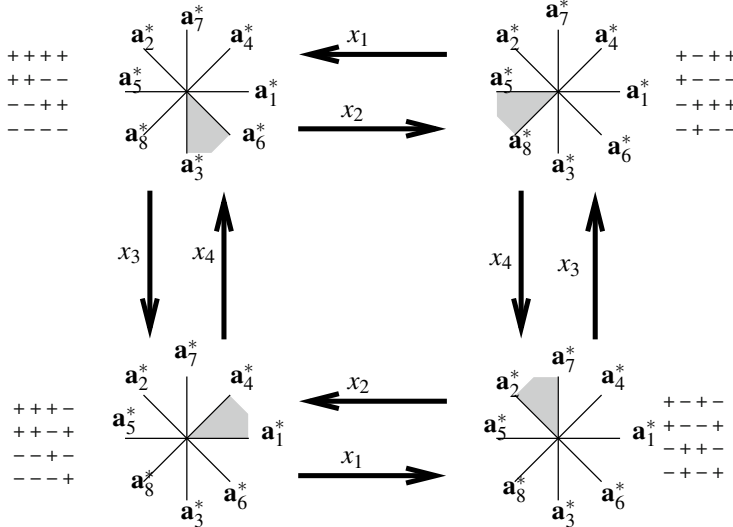


Figure 7.37: A schematic view of a certain triangulation of $\partial \text{conv}(\mathbf{A})$.

Lemma 7.4.5. 1. The triangulations in adjacent $F_{*,*,*,*}$'s are compatible, that is, this choice defines a triangulation \mathcal{K} of $\partial \text{conv}(\mathbf{A})$.

2. There are triangulations of \mathbf{A} inducing \mathcal{K} on the boundary.

3. If \mathcal{T} is a triangulation of \mathbf{A} inducing \mathcal{K} on the boundary, and \mathcal{T}' is obtained from \mathcal{T} by a flip, then \mathcal{T}' still induces \mathcal{K} on the boundary; that is, the subcomplex \mathcal{K} of a triangulation cannot be destroyed by flips.

Proof. 1. The compatibility condition for the triangulations chosen in different $F_{*,*,*,*}$'s is that if $F_{\delta_1, \delta_2, \delta_3, \delta_4}$ and $F_{\epsilon_1, \epsilon_2, \epsilon_3, \epsilon_4}$ are adjacent (that is, if $\delta_i = -\epsilon_i$ for some $i \in \{1, 2, 3, 4\}$ and $\delta_j = \epsilon_j$ for all $j \neq i$), then their triangulations induce the same triangulation on their common facet $F_{i, i+4}$. By Lemma 7.4.3, this is equivalent to saying that the chambers chosen to triangulate $F_{\delta_1, \delta_2, \delta_3, \delta_4}$ and $F_{\epsilon_1, \epsilon_2, \epsilon_3, \epsilon_4}$ lie on the same side of the line through i and $i+4$. That this holds can be readily checked in Figure 7.37, where each adjacency (arrow) is labeled by the coordinate in which the neighboring $F_{*,*,*,*}$'s differ.

2. This part is trivial. It suffices to cone \mathcal{K} to the origin 0, as we did in the 24-cell (Corollary 7.2.18).

3. If a flip changes \mathcal{K} , then the flip must happen on a circuit contained in a non-simplicial facet $A_{\delta_1, \delta_2, \delta_3, \delta_4}$, hence in the circuit common to two of them.

What is special about our triangulation \mathcal{K} of $\partial \text{conv}(\mathbf{A})$ is that, in every adjacency between two $F_{*,*,*,*}$'s, the triangulation on one side has the property that none of its two flips changes the triangulation induced in the common facet. In the picture, this is indicated by the arrows. Arrows are labeled x_1, x_2, x_3 , or x_4 indicating which of the first four coordinates is zero in the common facet of the corresponding $F_{*,*,*,*}$'s. The arrow labeled x_i points to the side where no chamber adjacent to the shaded one lies on the opposite side of the line through i and $i+4$, that is, no flip changes the triangulation in any of the 32 ridges between the $F_{*,*,*,*}$'s, and the triangulation of the ridges uniquely defines the triangulation of the $F_{*,*,*,*}$'s too. \square

As a consequence, the triangulations of \mathbf{A} that induce this boundary triangulation are not connected by flips to other triangulations of \mathbf{A} . We conclude that the graph of triangulations of \mathbf{A} is not connected. More precisely:

Theorem 7.4.6. *The graph of triangulations of \mathbf{A} has at least 9 connected components.*

Proof. There are eight triangulations of the boundary of $\text{conv}(\mathbf{A})$ affinely equivalent to the one we have described: first, there are two choices of how to pair the four coordinates x_1, x_2, x_3 and x_4 : we have chosen the pairing x_1-x_2, x_3-x_4 , but the pairing x_1-x_4, x_2-x_3 is equivalent to it since a cyclic permutation of the four coordinates, together with a 90-degree rotation on the plane x_5-x_6 , leaves \mathbf{A} invariant.

Second, once the pairing x_1-x_2, x_3-x_4 is chosen, we can switch our choice of triangulations for the $F_{*,*,*,*}$'s in two ways, giving a total of four choices. Indeed, we can switch the triangulations chosen for the cases where δ_1 and δ_2 are equal or different and, independently, those chosen for the cases where δ_3 and δ_4 are equal or different.

The previous lemma implies that triangulations of \mathbf{A} exist, inducing these 8 boundary triangulations, and that they lie in 8 different components of the graph of flips (or possibly more, the graph of triangulations of \mathbf{A} inducing a certain boundary triangulation could as well be not connected). To these 8, we have to add the component containing all the regular triangulations of \mathbf{A} . \square

Two final remarks concerning this construction are:

1. A different way of proving that “there are 8 boundary triangulations affinely equivalent to ours” is to observe that the symmetry group of \mathbf{A} has order 256, while the symmetry group of our triangulation has order 32. Table 7.2 in the next section describes four symmetries, which generate 16 of them, but there is a fifth generator, namely “change sign of first coordinate and rotate the plane $x_5-x_6 = 0$ by 90 degrees”.
2. Each of the 9 connected components mentioned above can be easily proved to contain at least 2^{16} triangulations, by an analysis of what flips are possible in the triangulation that cones the central point 0

to everything in the boundary. This triangulation has 32 flips, each involving 0 coned to six of the simplicial facets of $\text{conv}(\mathbf{A})$. Among them one can find 16 non-overlapping sets, which can be flipped independently.

7.4.3 A disconnected space of triangulations in general position

We now consider the following perturbation $\mathbf{A}(t)$ of \mathbf{A} , where t denotes a sufficiently small and positive real constant.

$$\begin{array}{cccccccccc} & 0 & I^+ & 2^+ & 3^+ & 4^+ & 5^+ & 6^+ & 7^+ & 8^+ & \dots \\ x_1 & \left(\begin{array}{cccccccccc} 1 & 1 & 1 & 1 & 1 & 1 & 1 & 1 & 1 & 1 & \dots \\ 0 & 1 & -t & 0 & 0 & 1 & t & 0 & 0 & 0 & \dots \\ x_2 & 0 & t & 1 & 0 & 0 & -t & 1 & 0 & 0 & \dots \\ x_3 & 0 & 0 & 0 & 1 & -t & 0 & 0 & 1 & t & \dots \\ x_4 & 0 & 0 & 0 & t & 1 & 0 & 0 & -t & 1 & \dots \\ x_5 & 0 & \sqrt{2} & 1 & 0 & -1 & -\sqrt{2} & -1 & 0 & 1 & \dots \\ x_6 & 0 & 0 & 1 & \sqrt{2} & 1 & 0 & -1 & -\sqrt{2} & -1 & \dots \\ \dots & I^- & 2^- & 3^- & 4^- & 5^- & 6^- & 7^- & 8^- & & \end{array} \right) \\ \dots & 1 & 1 & 1 & 1 & 1 & 1 & 1 & 1 & 1 & \dots \\ \dots & -1 & t & 0 & 0 & -1 & -t & 0 & 0 & 0 & \dots \\ \dots & -t & -1 & 0 & 0 & t & -1 & 0 & 0 & 0 & \dots \\ \dots & 0 & 0 & -1 & t & 0 & 0 & -1 & -t & & \dots \\ \dots & 0 & 0 & -t & -1 & 0 & 0 & t & -1 & & \dots \\ \dots & \sqrt{2} & 1 & 0 & -1 & -\sqrt{2} & -1 & 0 & 1 & & \dots \\ \dots & 0 & 1 & \sqrt{2} & 1 & 0 & -1 & -\sqrt{2} & -1 & & \dots \end{array}$$

By saying that $\mathbf{A}(t)$ is a perturbation of \mathbf{A} , we mean that every determinant which is non-zero in the oriented matroid of \mathbf{A} keeps its sign in the oriented matroid of $\mathbf{A}(t)$. This occurs when t is sufficiently small (and it can be taken as a definition of “sufficiently small”).

Observe that $\mathbf{A}(t)$ is not in general position. For example, for every $i = 1, 2, 3, 4$, we have the affine dependence

$$\mathbf{a}_{i^+}(t) + \mathbf{a}_{(i+4)^+}(t) + \mathbf{a}_{i^-}(t) + \mathbf{a}_{(i+4)^-}(t) = 4\mathbf{a}_0.$$

However, $\mathbf{A}(t)$ is in “sufficiently” general position for our purposes, in the sense that all properties needed in our proof will be preserved in any sufficiently small perturbation of $\mathbf{A}(t)$ into general position.

Our main new result, proved in the rest of this section, is:

Theorem 7.4.7. *Let t be a sufficiently small and positive constant.*

1. *There are triangulations of $\mathbf{A}(t)$ containing the simplicial complex \mathcal{K} introduced in the previous section.*

2. If \mathcal{T} is a triangulation of $\mathbf{A}(t)$ containing the simplicial complex \mathcal{K} , then every triangulation obtained from \mathcal{T} by a flip contains the simplicial complex \mathcal{K} . In particular, the graph of triangulations of $\mathbf{A}(t)$ is not connected.
3. The previous two statements remain true if $\mathbf{A}(t)$ is perturbed into general position in an arbitrary way.

We start by describing the affine symmetry group of $\mathbf{A}(t)$. It has order 16, and is generated by the four isometries displayed in Table 7.2. The action of each on the first four coordinates is indicated as a 4×4 matrix, while the action on the last two coordinates is described in words.

| Action on
(x_1, x_2, x_3, x_4) | Action on (x_5, x_6)
[octagon symmetry] |
|--|--|
| $\begin{pmatrix} -1 & 0 & 0 & 0 \\ 0 & -1 & 0 & 0 \\ 0 & 0 & 1 & 0 \\ 0 & 0 & 0 & 1 \end{pmatrix}$ | Identity |
| $\begin{pmatrix} 1 & 0 & 0 & 0 \\ 0 & 1 & 0 & 0 \\ 0 & 0 & -1 & 0 \\ 0 & 0 & 0 & -1 \end{pmatrix}$ | Identity |
| $\begin{pmatrix} -1 & 0 & 0 & 0 \\ 0 & 1 & 0 & 0 \\ 0 & 0 & -1 & 0 \\ 0 & 0 & 0 & 1 \end{pmatrix}$ | Rotation 180°
$1 \leftrightarrow 5, 2 \leftrightarrow 6$
$3 \leftrightarrow 7, 4 \leftrightarrow 8$ |
| $\begin{pmatrix} 0 & 1 & 0 & 0 \\ -1 & 0 & 0 & 0 \\ 0 & 0 & 0 & 1 \\ 0 & 0 & 1 & 0 \end{pmatrix}$ | Reflection
$1 \leftrightarrow 2, 8 \leftrightarrow 3$
$7 \leftrightarrow 4, 6 \leftrightarrow 5$ |

Table 7.2: Symmetries in the perturbed configuration $\mathbf{A}(t)$.

From this list it follows that:

Lemma 7.4.8. *The affine symmetry group of $\mathbf{A}(t)$ acts transitively over the sixteen subconfigurations $\mathbf{B}(t)|_{F_{\delta_1, \delta_2, \delta_3, \delta_4}}$ and preserves the simplicial complex \mathcal{K} .*

Proof. The first two symmetries transitively permute the four $F_{*,*,*,*}$'s on which we have chosen the same triangulation, while the third exchanges the groups of $F_{*,*,*,*}$'s diagonally opposite in Figure 7.37, and the fourth exchanges those in the same row of the figure. In both cases, the Gale octagon is transformed in a precise way as to preserve \mathcal{K} . \square

The lemma implies that we can focus on studying what the transformation does to one of the sixteen subconfigurations $F_{*,*,*,*}$, namely $F_{+,+,+,+}$. For this, we show a Gale transform of the nine points $\{0\} \cup F_{+,+,+,+}$. It is

as follows, where c equals the constant $\sqrt{2} - 1$; Figure 7.38 shows a picture of the transform.

$$\begin{array}{cccccccccc} 0 & 1^+ & 2^+ & 3^+ & 4^+ & 5^+ & 6^+ & 7^+ & 8^+ \\ \left(\begin{array}{cccccccc} 4t & 1-t & -1-t & c(1+t) & c(1-t) & -(1+t) & 1-t & -c(1-t) & -c(1+t) \\ -4t & c(1+t) & c(1-t) & -(1-t) & 1+t & -c(1-t) & -c(1+t) & 1+t & -(1-t) \end{array} \right). \end{array}$$

From this Gale transform we can determine the following properties:

Lemma 7.4.9. 1. $\{0\} \cup F_{+,+,+,+}$ is in general position. In particular, both $\text{conv}_{\mathbf{A}(t)}(F_{+,+,+,+})$ and $\text{conv}(\mathbf{A}(t))$ are simplicial polytopes.

2. $F_{+,+,+,+}$ is a circuit in $\mathbf{A}(t)$. The signed circuit is:

$$(\{1^+, 4^+, 6^+, 7^+\}, \{2^+, 3^+, 5^+, 8^+\}).$$

3. $F_{+,+,+,+}$ intersects any other $F_{\delta_1, \delta_2, \delta_3, \delta_4}$ in a common simplicial face, of dimension $2s - 1$, where s is the number of positive signs among the four δ 's.

4. The part of the boundary of $F_{+,+,+,+}$ visible from 0 contains precisely the triangulation $\mathcal{T}_{3,6}$ that we chose for $F_{+,+,+,+}$ in the previous section.

Proof. 1. $\{0\} \cup F_{+,+,+,+}$ is in general position, since its Gale transform is in general position. In particular, $\text{conv}_{\mathbf{A}(t)}(F_{+,+,+,+})$ is clearly simplicial, since it is in general position. For $\text{conv}(\mathbf{A}(t))$, observe that all its non-simplicial faces should be contained in non-simplicial faces of the unperturbed polytope $\text{conv}(\mathbf{A})$. Since the latter has the sixteen $F_{*,*,*,*}$'s as its only non-simplicial facets, and since these facets have been perturbed into general position, $\text{conv}(\mathbf{A}(t))$ is simplicial.

2. The two rows in the Gale transform of $\{0\} \cup F_{+,+,+,+}$ are the coefficient vectors of two affine dependences. Their sum, which is positive on $\{1^+, 4^+, 6^+, 7^+\}$ and negative on $\{2^+, 3^+, 5^+, 8^+\}$, is the unique affine dependence in $F_{+,+,+,+}$. Another way of proving this part is by looking at Figure 7.38: The hyperplane (line) passing through 0 leaves $\{1^+, 4^+, 6^+, 7^+\}$ and $\{2^+, 3^+, 5^+, 8^+\}$ on different sides. This is a cocircuit in $\text{Gale}(\{0\} \cup F_{+,+,+,+})$, hence a circuit in $\{0\} \cup F_{+,+,+,+}$.

3. The intersection of $F_{+,+,+,+}$ and $F_{\delta_1, \delta_2, \delta_3, \delta_4}$ has $2s$ elements, so we only need to show that these elements form a simplicial face. Now, since $F_{+,+,+,+}$ is a circuit, all proper subsets of it are independent, and the only ones that are not faces are those containing either the positive or the negative part of the circuit. In our case, both the positive and the negative parts contain one element of each pair $i^+, (i+4)^+$, so none of them is contained in the intersection of $F_{+,+,+,+}$ and $F_{\delta_1, \delta_2, \delta_3, \delta_4}$.

4. A facet F of $F_{+,+,+,+}$ visible from 0 corresponds to a cocircuit of the form $(F, 0)$ in $\{0\} \cup F_{+,+,+,+}$, that is to say, to a circuit $(F, \{0\})$ in the Gale transform. Hence, the statement follows from the fact that, after the perturbation, 0 lies in precisely the (perturbed) chamber of the Gale transform corresponding to $\mathcal{T}_{3,6}$. \square

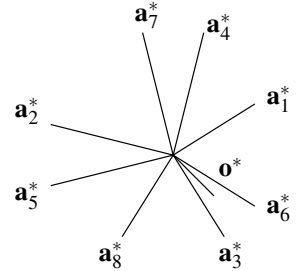


Figure 7.38: Gale transform of $\{0\} \cup F_{+,+,+,+}$ after perturbation.

Property 3 implies that the following is a triangulation of $\mathbf{A}(t)$: Consider an arbitrary triangulation of each perturbed $F_{*,*,*,*}$, and cone to 0 the parts of the boundaries of the $F_{*,*,*,*}$ visible from 0 and not common to any other $F_{*,*,*,*}$. Property 4 says that, in this triangulation, the link of 0 is precisely the simplicial complex \mathcal{K} . This proves Part 1 of Theorem 7.4.7. Since the proof is based solely in the properties of the subconfigurations $\{0\} \cup F_{*,*,*,*}$, which are already in general position, this also proves that Part 1 holds if $\mathbf{A}(t)$ is perturbed, arbitrarily, into general position.

For the proof of Part 2 of Theorem 7.4.7, we need to know certain signed circuits in $\mathbf{A}(t)$. That the following are indeed circuits can be easily checked with a computer, but we offer a computer-free (although not computation-free!) proof for the interested reader.

Lemma 7.4.10. *If t is positive and sufficiently small, then the following are signed circuits in $\mathbf{A}(t)$, for every $k \in K \setminus F_{+,+,+,+} = \{0\} \cup F_{-,-,-,-}$:*

$$(\{1^+, 4^+, 6^+, 7^+, k\}, \{2^+, 5^+, 8^+\}), \quad (7.5)$$

$$(\{2^+, 3^+, 5^+, 8^+, k\}, \{1^+, 4^+, 7^+\}). \quad (7.6)$$

$$\begin{aligned}\phi(0) &= -1 \\ \phi(1^+) &= 0 \\ \phi(2^+) &= 0 \\ \phi(3^+) &= \sqrt{2} + o(t) \\ \phi(4^+) &= 0 \\ \phi(5^+) &= 0 \\ \phi(6^+) &= 0 \\ \phi(7^+) &= \sqrt{2} + o(t) \\ \phi(8^+) &= 0 \\ \phi(1^-) &= -2 + o(t) \\ \phi(2^-) &= -2 + o(t) \\ \phi(3^-) &= -2 - \sqrt{2} + o(t) \\ \phi(4^-) &= -2 + o(t) \\ \phi(5^-) &= -2 + o(t) \\ \phi(6^-) &= -2 + o(t) \\ \phi(7^-) &= -2 - \sqrt{2} + o(t) \\ \phi(8^-) &= -2 + o(t)\end{aligned}$$

Proof. We concentrate first on the first circuit. Observe that, before the perturbation, $\{1^+, 2^+, 4^+, 5^+, 6^+, 7^+, 8^+\}$ spans the hyperplane $x_1 + x_2 + x_3 + x_4 = 1$, which does not contain any $k \in \{0\} \cup F_{-,-,-,-}$. Hence, the configuration $\{1^+, 2^+, 4^+, 5^+, 6^+, 7^+, 8^+, k\}$ is, both before and after the perturbation, full-dimensional and contains a unique circuit. Before the perturbation, this circuit is

$$(\{1^+, 4^+, 6^+\}, \{2^+, 5^+, 8^+\}),$$

as you can read from Figure 7.35 or from the following equality:

$$\sqrt{2}\mathbf{a}_{1+} + \mathbf{a}_{4+} + \mathbf{a}_{6+} = \sqrt{2}\mathbf{a}_{5+} + \mathbf{a}_{8+} + \mathbf{a}_{2+} = (1, \sqrt{2}, 1, 0, 1, 0, 0).$$

By continuity of the unique affine dependence among these eight points, the perturbed circuit still contains $\{1^+, 4^+, 6^+\}$ on one side and $\{2^+, 5^+, 8^+\}$ on the other. The only question is which side 7^+ and k lie on. The statement is that, no matter which k we choose in $\{0\} \cup F_{-,-,-,-}$, both 7^+ and k lie on the side of $\{1^+, 4^+, 6^+\}$. We prove this in two steps:

- (a) $(\{1^+, 4^+, 6^+, 7^+, 0\}, \{2^+, 5^+, 8^+\})$ is a circuit for the choice $k = 0$. This can be read in the Gale transform of $\mathbf{A}|_{\{0\} \cup F_{-,-,-,-}}$ (see Figure 7.38): The line containing 3^+ leaves the points $\{1^+, 4^+, 6^+, 7^+, 0\}$ and $\{2^+, 5^+, 8^+\}$ on different sides.
- (b) 7^+ and k lie on the same side of the circuit, for any choice of k . For this, we compute the linear functional that vanishes on the other six points $\{1^+, 2^+, 4^+, 5^+, 6^+, 8^+\}$. That functional is:

$$\phi(x_1, \dots, x_6; t) := x_1 + x_2 + (1 + \sqrt{2})x_3 + x_4 - \frac{t}{\sqrt{2}}x_5 + \frac{\sqrt{2} + 1}{\sqrt{2}}tx_6 - 1.$$

Figure 7.39: A functional for proving the first circuit of Lemma 7.4.10.

The values of ϕ on the 17 points of $\mathbf{A}(t)$ are those displayed in Figure 7.39 where, as usual, $o(t)$ denotes terms that tend to zero when t tends to zero. What is important here is that the sign at k is negative for every $k \in \{0\} \cup F_{-, -, -, -}$, while the sign at 7^+ is positive. By the orthogonality of linear dependences and linear evaluations (compare Lemma 4.1.34), if two elements of a circuit Z are separated by a hyperplane passing through the rest of the elements of Z , then those two elements must be on the same side of Z . This implies that 7^+ and k lie on the same side of the first circuit and finishes the proof of the lemma for that circuit.

The proof for the second circuit is the same, except using the linear functional:

$$\phi(x_1, \dots, x_6; t) := x_1 + (1 + \sqrt{2})x_2 + x_3 + x_4 - \frac{\sqrt{2} + 1}{\sqrt{2}}tx_5 - \frac{t}{\sqrt{2}}x_6 - 1,$$

The values it takes are shown in Figure 7.40. \square

Remark 7.4.11. For the case $k = 0$, the two circuits in question can directly be read from the Gale transform of $\{0\} \cup F_{+, +, +, +}$.

Proof of Part 2 of Theorem 7.4.7. Let \mathcal{T} be a triangulation of $\mathbf{A}(t)$ containing the pure five-dimensional simplicial complex \mathcal{K} . Certainly, no flip removes any of the 5-simplices of \mathcal{K} that were simplicial facets in $\text{conv}(\mathbf{A})$, since they are still simplicial facets in $\text{conv}(\mathbf{A}(t))$. So, we only need to look at the simplices contained in one of the $F_{*, *, *, *}$'s and, by symmetry, only at those contained in $F_{+, +, +, +}$. By Part 1 of Lemma 7.4.9, these six 5-simplices are in general position in the sense that the hyperplane spanned by each of them does not contain any other point of $\mathbf{A}(t)$.

Let B be one of these six simplices. The general position of B implies that a flip removes B from \mathcal{T} only if it is supported in the unique circuit $Z = (Z_+, Z_-)$ contained in the two full-dimensional simplices incident to B . So, let k and k' be the two vertices joined to B in \mathcal{T} . The sets of points on one and the other side of the hyperplane through B are $\{0\} \cup F_{-, -, -, -}$ and $F_{+, +, +, +} \setminus B$, by Property 4 in Lemma 7.4.9, and we assume without loss of generality that k is in the former and k' in the latter. As usual, we orient Z so that $k, k' \in Z_+$.

Observe that $B \cup \{k\}$ is already full-dimensional before the perturbation, since B spans the facet $F_{+, +, +, +}$ and k does not lie in it. In particular, the circuit Z of $\mathbf{A}(t)$ conforms to² the circuit $Z' = (Z'_+, Z'_-)$ contained in $B \cup \{k'\} \subset F_{+, +, +, +}$ before the perturbation.

Moreover, in order for Z to produce a flip, for each $k'' \in Z'_+ \subseteq Z_+$ the 6-dimensional simplex consisting of k joined to $B \cup \{k'\} \setminus \{k''\}$ needs to be a simplex in \mathcal{T} . In particular, Z' must be one of the two flippable circuits of the triangulation $\mathcal{T}_{3,6}$ of $F_{+, +, +, +}$, and $B \cup \{k'\}$ must equal the support of this circuit together with the vertex joined to a triangulation of it in $\mathcal{T}_{3,6}$.

| |
|------------------------------------|
| $\phi(0) = -1$ |
| $\phi(1^+) = 0$ |
| $\phi(2^+) = \sqrt{2} + o(t)$ |
| $\phi(3^+) = 0$ |
| $\phi(4^+) = 0$ |
| $\phi(5^+) = 0$ |
| $\phi(6^+) = \sqrt{2} + o(t)$ |
| $\phi(7^+) = 0$ |
| $\phi(8^+) = 0$ |
| $\phi(1^-) = -2 + o(t)$ |
| $\phi(2^-) = -2 - \sqrt{2} + o(t)$ |
| $\phi(3^-) = -2 + o(t)$ |
| $\phi(4^-) = -2 + o(t)$ |
| $\phi(5^-) = -2 + o(t)$ |
| $\phi(6^-) = -2 - \sqrt{2} + o(t)$ |
| $\phi(7^-) = -2 + o(t)$ |
| $\phi(8^-) = -2 + o(t)$ |

Figure 7.40: A functional for proving the second circuit of Lemma 7.4.10.

²By this we mean that $Z'_+ \subseteq Z_+$ and $Z'_- \subseteq Z_-$.

That is to say, Z is one of the two circuits

$$\begin{aligned} &(\{1^+, 4^+, 6^+, 7^+, k\}, \{2^+, 5^+, 8^+\}), \\ &(\{2^+, 3^+, 5^+, 8^+, k\}, \{1^+, 4^+, 7^+\}). \end{aligned}$$

studied in Lemma 7.4.10.

Suppose that Z equals the first circuit (the case of the second is similar). Then the following must be a simplex in \mathcal{T} in order for Z to be flippable:

$$C := \{1^+, 5^+, 2^+, 6^+, 4^+, 8^+, k\}.$$

Since $\{1^+, 5^+, 2^+, 6^+, 4^+, 8^+\}$ is the set of points in the common facet between $F_{+,+,+,+}$ and $F_{+,+,-,+}$, k must be one of 3^- and 7^- . Depending on which of them equals k , consider the following simplex, which must also be in \mathcal{T} :

$$C' := \{1^+, 5^+, 2^+, 6^+, 3^-, 8^+, 3^+\},$$

or

$$C'' := \{1^+, 5^+, 2^+, 7^-, 4^+, 8^+, 3^+\},$$

This simplex is 3^+ joined to a 5-simplex $B' := C' \setminus \{3^+\}$ or $B'' := C'' \setminus \{3^+\}$ contained in $F_{+,+,-,+}$. This implies that one of B' or B'' is in the triangulation $\mathcal{T}_{1,4}$ that we chose for $F_{+,+,-,+}$. But neither of them is. \square

Proof of Part 3 of Theorem 7.4.7. The proofs of Parts 1 and 2 are based solely in the structure of the subconfigurations $A|_{F_{*,*,*,*}}$ and the circuits stated in Lemma 7.4.10. Since both are already in general position, everything stated for them is preserved by a sufficiently small perturbation of $A(t)$. \square

Exercises

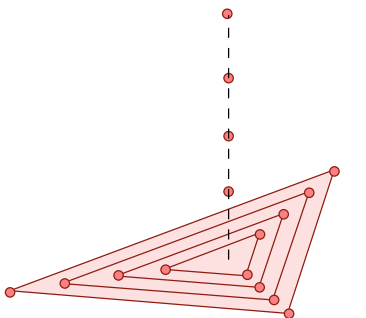


Figure 7.41: More flip-deficient triangulations.

Exercise 7.1. Show that the point configuration of Figure 7.41, with $4k$ vertices, has triangulations with only $3k - 3$ flips. Show that adding another k collinear points in the same transversal line but in the opposite direction produces triangulations with $5k$ vertices and $3k - 2$ flips (one flip arises in the innermost bipyramid).

Exercise 7.2. Find your own proof that the “mother of all examples” has non-regular triangulations.

Exercise 7.3. Prove that for every simplicial complex \mathcal{K} :

1. $\mathcal{G}_{\text{l.a.o.}}(\mathcal{K}) = \mathcal{G}_{\text{l.a.o.}}(\mathcal{K}^2)$, where \mathcal{K}^2 is the 2-skeleton of \mathcal{K} and $\mathcal{G}_{\text{l.a.o.}}(\mathcal{K})$ denotes the graph of locally acyclic orientations of \mathcal{K} .
2. If \mathcal{K} has more edges than triangles, every l.a.o. has at least as many reversible edges as the difference between these two numbers.

Exercise 7.4. Let \mathcal{T} be a regular triangulation of a point configuration A . Derive from Lemma 7.2.9 that there is a polytope of dimension $|A| - 1$ whose vertices are the acyclic orientations of the graph of \mathcal{T} and whose edges correspond to the reversal of a single edge in the graph.

Exercise 7.5. 1. Show the following extension of Lemma 7.2.9 (*Hint:* use Exercise 6.8):

Let \mathcal{T} be a triangulation of a point configuration. The polyhedral subdivisions that refine $\text{prism}(\mathcal{T})$ are in bijection to the partial orientations of the graph of \mathcal{T} which satisfy, in every triangle of \mathcal{T} , the conditions of Exercise 6.8.

2. Derive from this part three of Theorem 7.2.10.

Exercise 7.6. (Open) Are there disconnected graphs of triangulations for 3-dimensional point sets? How about 4-dimensional?

Exercise 7.7. Let \mathbf{A} be a 3-dimensional point set in general, convex position. Let $t_{\min}(\mathbf{A})$ be the minimum number of tetrahedra in a triangulation of \mathbf{A} and $t_{\max}(\mathbf{A})$ the maximum such number. Suppose that the graph of triangulations of \mathbf{A} is connected. Show that every integer value between $t_{\min}(\mathbf{A})$ and $t_{\max}(\mathbf{A})$ is the number of tetrahedra in some triangulation of \mathbf{A} .

Remark: Observe that the same is not always true in higher dimensions. Actually, it can never be true in even dimensions (unless $t_{\min}(\mathbf{A}) = t_{\max}(\mathbf{A})$). Why?

Exercise 7.8. (Open) Prove the previous exercise without the assumption that the graph of triangulations of \mathbf{A} is connected.

Exercise 7.9. Let \mathcal{G} be an arbitrary graph. Prove that the set of orientations of \mathcal{G} which have neither sinks nor sources is connected under single edge reversals.

Hint: Given two orientations of \mathcal{G} without sinks or sources, prove that either (1) there is an edge differently oriented in the two of them, that can be reversed in one of them, thus decreasing their distance from each other, or (2) the edges which are differently oriented in the two orientations are distributed in vertex-disjoint cycles. In this case, moreover, the edges incident to one of these cycles (and not belonging to the cycle) are oriented all towards or all away from the cycle. Use these properties to find a sequence of valid edge reversals whose final outcome is the reversal of one of these cycles, hence decreasing the distance too.

Exercise 7.10. Let \mathcal{K} be the boundary complex of a 3-dimensional simplicial polytope with n vertices. Prove that:

1. Every locally acyclic orientation of \mathcal{K} has at least $n - 2$ reversible edges (*hint:* Use Euler relation and the fact that each triangle prevents at most one edge from being reversible).
2. $\mathcal{G}_{\text{l.a.o.}}(\mathcal{K})$ is connected. *Hint:* Define the dual graph \mathcal{K}^* of this complex and identify orientations of the graph of \mathcal{K} and of \mathcal{K}^* by rotating all arrows in the same sense. Then apply Exercise 7.9!
3. Prove that the same holds when \mathcal{K} is a triangulation of a point configuration in dimension two, except the bound in part one is now $n - 1$. (*hint:* For part two, complete \mathcal{K} to be the boundary complex of a

3-polytope by adding a point at infinity joined to every edge of \mathcal{K} .

Exercise 7.11. Everything in the previous exercise is equally valid when \mathcal{K} is any *pseudo-surface* (a 2-dimensional simplicial complex in which every edge belongs to exactly 2-triangles), except:

1. The number $n - 2$ has to be replaced by something else (what?), which will always be greater or equal than $n - 2$ (why?).
2. The proof of connectivity only works as is if \mathcal{K} is *orientable* (why?). If you are familiar with the topological theory of covering spaces, you can easily extend the result to non-orientable pseudo-surfaces.

Exercise 7.12. Go through the proof of Theorem 7.2.2 to show that:

1. If the upper and lower boundary of the starting grid are modified as shown in Figure 7.42, then the number of flips is reduced by $k - 1$, giving a total of $6\sqrt{n} + O(1)$ flips.
2. If, moreover, a rectangular grid is chosen instead of the square one, the ratio between the number of flips and the square root of the number of points can be further decreased to $4\sqrt{2} = 5.6$.

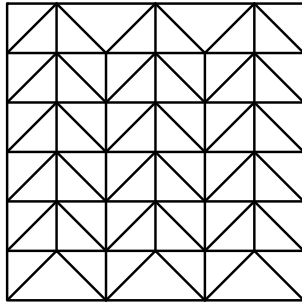


Figure 7.42: Modified version of Figure 7.42, which reduces the number of flips.

8

Algorithmic Issues

In previous chapters, we have not been directly concerned with how to actually carry on calculations required to investigate triangulations. For example, how can we efficiently verify whether a set of simplices forms a triangulation? How can we verify whether a triangulation is regular? We have already counted triangulations via formulas for a few well-structured instances, but we have not discussed how one could actually list or enumerate *all* triangulations of arbitrary dimensional configurations (though we did some of that in dimension two). Similarly, we have not addressed the issue of finding optimal or special triangulations explicitly. For instance, given a d -dimensional point configuration (e.g., the vertices of a d -cube), how can we find a triangulation with the smallest number of d -simplices? In this chapter, we deal with the computation and complexity of carrying through some natural computations on the space of triangulations.

8.1 Tools for computation

In the following, we denote by n the number of points in \mathbf{A} , by r the rank of \mathbf{A} , which equals the dimension (denoted by d) plus one, and by $c := n - r$ the corank of \mathbf{A} . In all practically solvable cases, you may think of n and r as small numbers compared to the total number of triangulations of \mathbf{A} . Often in our discussion we may refer to special, but standard, data structures that would allow efficient access or storage of data (e.g., heaps, hash tables, etc). For this, we refer unfamiliar readers to any good undergraduate level book, such as [85].

8.1.1 Chirotopes

A key question in analyzing algorithms concerning triangulations of point configurations is: How do you represent your point configuration during the calculations? We have learned in Section 4.5.2 that there are many purely combinatorial characterizations of polyhedral subdivisions and, in particular, triangulations. Although this is a big step towards efficient computations compared to geometric characterizations or even Definition 2.3.1, we still have to take into account that searching in the set of circuits or the like may be very inefficient. Let us therefore propose a unified interface from point configurations to their oriented matroids: the chiotope.

Definition 8.1.1. The *chiotope* χ of a point or vector configuration \mathbf{A} labeled by J is a function assigning a sign in $\{0, +, -\}$ to each r -element

sequence in J in the following way:

$$\chi_A : \begin{cases} J^r & \rightarrow \{+, -, 0\} \\ (i_1, i_2, \dots, i_r) & \mapsto \text{sign}(\det(a_{i_1}, a_{i_2}, \dots, a_{i_r})) \end{cases} \quad (8.1)$$

The word “chirotope” is derived from the word “chirality”, used to describe orientation and the relation to mirror images of molecules in chemistry, and was proposed by A. Dress.

The determinant is alternating. Thus, if (i_1, i_2, \dots, i_r) has a repeated element, then its chirotope vanishes. Also, that the chirotope of any permutation of a given sequence equals the chirotope of the original sequence multiplied by $+1$ or -1 , depending on the parity of the permutation. For this reason, if a canonical ordering is implicit in the label set J , as is usually the case, we can call or denote the chirotope function with a subset of J as argument, rather than a sequence; this simply means calling the chirotope with the sequence corresponding to the sorted set.

Example 8.1.2. Consider the two-dimensional configuration with five elements shown in Figure 8.1. Four of the points form the corners of a square centered at the origin. The list of all chirotope values is as follows:

$$\begin{aligned} \chi_A(1, 2, 3) &= -, & \chi_A(1, 2, 4) &= -, & \chi_A(1, 2, 5) &= -, & \chi_A(1, 3, 4) &= -, \\ \chi_A(1, 3, 5) &= +, & \chi_A(1, 4, 5) &= +, & \chi_A(2, 3, 4) &= -, & \chi_A(2, 3, 5) &= -, \\ \chi_A(2, 4, 5) &= -, & \chi_A(3, 4, 5) &= -. \end{aligned}$$

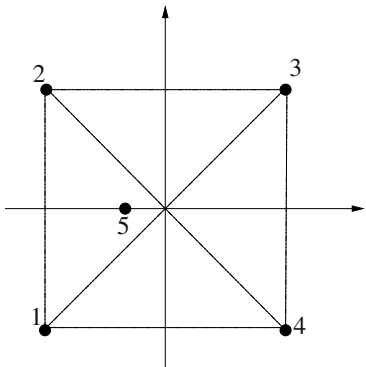


Figure 8.1: The chirotope of a five-point configuration in the plane is determined by

$${5 \choose 2} = 10 \text{ different values.}$$

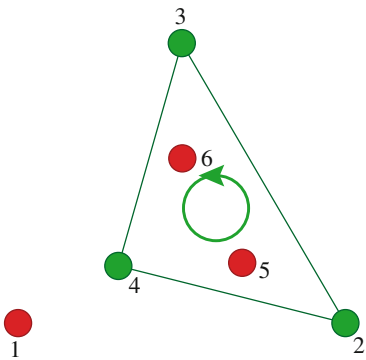


Figure 8.2: The chirotope value of $(2, 3, 4)$ in the mother of all examples is $+$: the chirotope value of a r -sequence can be interpreted as the orientation of the corresponding simplex; in dimension two, this can be indicated by rotation directions.

Figure 8.2 shows one of the values of the chirotope in the mother of all examples; we encourage the reader to compute all other missing values (see exercises).

All algorithms presented in the sequel will consider the input point configuration as given by the *chirotope oracle*: if we call the oracle with an r -subset, then the oracle returns the chirotope value of the ordered sequence corresponding to that subset. We will measure the asymptotic run-time complexity of algorithms in the number of elementary operations and oracle calls.

However, first we present how the chirotope oracle itself can be implemented cleverly in the case where all chirotope values can be stored in advance.

8.1.2 Computing the chirotope

Naïvely, to compute the chirotope of a point configuration, we would have to compute $\binom{n}{r}$ determinants of size r , each requiring $O(r^3)$ steps if we proceed by an elimination algorithm, which is quite reasonable since r will be typically a small number. We assume unit cost per arithmetic operation (see [182] for a related survey about what happens if more realistic computational models are investigated).

Instead of repeating unnecessary column reduction, we will organize the computation in a certain computation tree where we can reuse some column reduction operations to reduce the effort of computation substantially, especially when r is small and n is large compared to it. The leaves of the

computation tree will be all the possible $r \times r$ submatrices of \mathbf{A} in triangular form, thus their determinants and their signs can easily be computed.

In this tree, a child node in level $k + 1$ is obtained from a node A_k in level k by adding a column to the right of A_k and then performing column reduction operations until the resulting matrix is in column reduced form. Finally, the leaves of the tree will be all the possible $r \times r$ submatrices of \mathbf{A} set in triangular form. Thus their determinants, and especially their signs, can be computed in linear time.

Theorem 8.1.3. *The chirotope values of all the r -subsets of J ordered by labels can be computed in time $O\left(\frac{r+c}{1+c}r^2\right)$ per value.*

Proof. We now construct a rooted computation tree whose nodes are subsets of columns of the matrix containing \mathbf{A} as follows: The root node corresponds to the empty submatrix \mathbf{A}_0 . The nodes at level k of the rooted tree are matrices in column reduced form corresponding to a subset of k columns of \mathbf{A} . Now, let \mathbf{A}_k be one such node. We now show how a child node of \mathbf{A}_k is constructed: first, add to the right of \mathbf{A}_k a column of \mathbf{A} , then perform column elimination steps until a matrix \mathbf{A}_{k+1} in reduced column normal form is obtained. At the end, the leaves of the tree are all possible $(r \times r)$ -submatrices of \mathbf{A} in equivalent triangular form, and their determinants and thus their chirotope values can be computed easily in time $O(r)$ per value.

Note then that the bulk of the work lies in the generation of the computation tree. We need to count the total number of nodes and the time required to generate their children.

We first count the nodes in the levels of the computation tree as follows: Let $g(k, j) = \binom{j-1}{k-1}$ be the number of submatrices of \mathbf{A} with k columns and right-most column at index j . Then the number of nodes in level k of the tree is equal to $\sum_{j=k}^{n-r+k} g(k, j)$.

We claim that the number of operations in each node at level k is bounded by rk . In order to prove the claim, consider the matrix right after adding the k th column of \mathbf{A} . In order to obtain a matrix in column normal form, we have to get rid of at most $k - 1$ non-zeroes in the k th column. We start the elimination in row 1 and proceed from top to bottom. Assume the first $m - 1$ values in column k are already transformed to zero, $1 \leq m < k$. If the m th row in the (just added) k th column is already zero as well, then there is nothing to do. If the m th row of the m th column is non-zero, then we can eliminate (i.e., transform to zero) the non-zero in the m th row of the newly added k th column by computing $r - m \leq r - 1$ new numbers. If m is the smallest index such that the m th row of column k is non-zero but the m th row of column m is zero, we swap column k and column m , which can be done in constant time using appropriate matrix structures. The first $k - 1$ columns of the resulting matrix are again in column normal form, and row m of column k is zero now. In any case, we obtain a matrix where the m th row in the k th column is now zero, computing at most $(r - 1)(k - 1)$ numbers, which is no more than rk .

The total number of nodes in the tree is given by $\sum_{k=1}^r \sum_{j=k}^{c+k} g(k, j)$. Thus, the number of operations is at most $G(n, r) := \sum_{k=1}^r \sum_{j=k}^{c+k} g(k, j)kr$. The

amortized number of operations per determinant is then $G(n, r) / \binom{n}{r}$.

The following calculation shows the assertion; in it we use the following well-known formula for sums of binomial coefficients:

$$\sum_{k=0}^r \binom{a+k}{k} = \binom{a+k+1}{k}. \quad (8.2)$$

Using this we obtain (recall that $n = r + c$):

$$\begin{aligned} G(n, r) &= \sum_{k=1}^r \sum_{j=k}^{c+k} \binom{j-1}{k-1} kr \\ &= r \sum_{k=0}^{r-1} (k+1) \sum_{j=k}^{c+k} \binom{j}{k} \\ &= r \sum_{k=0}^{r-1} (k+1) \binom{k+c+1}{c} \\ &= r \sum_{k=0}^{r-1} (k+1) \frac{(k+c+1)!}{c!(k+1)!} \\ &= r \sum_{k=0}^{r-1} \frac{(k+c+1)!}{c!k!} \\ &= r \sum_{k=0}^{r-1} (c+1) \frac{(k+c+1)!}{(c+1)!k!} \\ &= r(c+1) \sum_{k=0}^{r-1} \binom{k+c+1}{k} \\ &= r(c+1) \binom{r+c+1}{r-1} \\ &= r(c+1) \frac{(r+c+1)!}{(r-1)!(c+2)!} \\ &= r^2 \frac{(r+c+1)}{c+2} \frac{(r+c)!}{r!c!} \\ &= r^2 \frac{(r+c+1)}{c+2} \binom{n}{r}. \end{aligned}$$

This expression divided by $\binom{n}{r}$ asymptotically has the claimed growth. \square

This proves that the computation tree yields savings of order r per determinant whenever the corank $n - r$ is not much smaller than the rank of the point configuration.

| Sub-set | Level 1:
4 nodes | Level 2:
10 nodes | Level 3:
15 nodes | χ |
|-------------|---|---|--|--------|
| $\{1,2,3\}$ | $+ \begin{vmatrix} 4 & * & * \\ 0 & * & * \\ 0 & * & * \end{vmatrix}$ | $+ \begin{vmatrix} 4 & 0 & * \\ 0 & 4 & * \\ 0 & 0 & * \end{vmatrix} \mapsto + \begin{vmatrix} 4 & 0 & * \\ 0 & 4 & * \\ 0 & 0 & * \end{vmatrix}$ | $+ \begin{vmatrix} 4 & 0 & 0 \\ 0 & 4 & 0 \\ 0 & 0 & 4 \end{vmatrix} \mapsto + \begin{vmatrix} 4 & 0 & 0 \\ 0 & 4 & 0 \\ 0 & 0 & 4 \end{vmatrix} \mapsto +64$ | + |
| $\{1,2,4\}$ | | | $+ \begin{vmatrix} 4 & 0 & 2 \\ 0 & 4 & 1 \\ 0 & 0 & 1 \end{vmatrix} \mapsto + \begin{vmatrix} 4 & 0 & 0 \\ 0 & 4 & 0 \\ 0 & 0 & 1 \end{vmatrix} \mapsto +16$ | + |
| $\{1,2,5\}$ | | | $+ \begin{vmatrix} 4 & 0 & 1 \\ 0 & 4 & 2 \\ 0 & 0 & 1 \end{vmatrix} \mapsto + \begin{vmatrix} 4 & 0 & 0 \\ 0 & 4 & 0 \\ 0 & 0 & 1 \end{vmatrix} \mapsto +16$ | + |
| $\{1,2,6\}$ | | | $+ \begin{vmatrix} 4 & 0 & 1 \\ 0 & 4 & 1 \\ 0 & 0 & 2 \end{vmatrix} \mapsto + \begin{vmatrix} 4 & 0 & 0 \\ 0 & 4 & 0 \\ 0 & 0 & 2 \end{vmatrix} \mapsto +32$ | + |
| $\{1,3,4\}$ | $+ \begin{vmatrix} 4 & 0 & * \\ 0 & 0 & * \\ 0 & 4 & * \end{vmatrix} \mapsto + \begin{vmatrix} 4 & 0 & * \\ 0 & 0 & * \\ 0 & 4 & * \end{vmatrix}$ | $+ \begin{vmatrix} 4 & 0 & 2 \\ 0 & 0 & 1 \\ 0 & 4 & 1 \end{vmatrix} \mapsto - \begin{vmatrix} 4 & 0 & 0 \\ 0 & 1 & 0 \\ 0 & 1 & 4 \end{vmatrix} \mapsto -16$ | - | |
| $\{1,3,5\}$ | | | $+ \begin{vmatrix} 4 & 0 & 1 \\ 0 & 0 & 2 \\ 0 & 4 & 1 \end{vmatrix} \mapsto - \begin{vmatrix} 4 & 0 & 0 \\ 0 & 2 & 0 \\ 0 & 1 & 4 \end{vmatrix} \mapsto -32$ | - |
| $\{1,3,6\}$ | | | $+ \begin{vmatrix} 4 & 0 & 1 \\ 0 & 0 & 1 \\ 0 & 4 & 2 \end{vmatrix} \mapsto - \begin{vmatrix} 4 & 0 & 0 \\ 0 & 1 & 0 \\ 0 & 2 & 4 \end{vmatrix} \mapsto -16$ | - |
| $\{1,4,5\}$ | $+ \begin{vmatrix} 4 & 2 & * \\ 0 & 1 & * \\ 0 & 1 & * \end{vmatrix} \mapsto + \begin{vmatrix} 4 & 0 & * \\ 0 & 1 & * \\ 0 & 1 & * \end{vmatrix}$ | $+ \begin{vmatrix} 4 & 0 & 1 \\ 0 & 1 & 2 \\ 0 & 1 & 1 \end{vmatrix} \mapsto + \begin{vmatrix} 4 & 0 & 0 \\ 0 & 1 & 0 \\ 0 & 1 & -1 \end{vmatrix} \mapsto -4$ | - | |
| $\{1,4,6\}$ | | | $+ \begin{vmatrix} 4 & 0 & 1 \\ 0 & 1 & 1 \\ 0 & 1 & 2 \end{vmatrix} \mapsto + \begin{vmatrix} 4 & 0 & 0 \\ 0 & 1 & 0 \\ 0 & 1 & 1 \end{vmatrix} \mapsto +4$ | + |
| $\{1,5,6\}$ | $+ \begin{vmatrix} 4 & 1 & * \\ 0 & 2 & * \\ 0 & 1 & * \end{vmatrix} \mapsto + \begin{vmatrix} 4 & 0 & * \\ 0 & 2 & * \\ 0 & 1 & * \end{vmatrix}$ | $+ \begin{vmatrix} 4 & 0 & 1 \\ 0 & 2 & 1 \\ 0 & 1 & 2 \end{vmatrix} \mapsto + \begin{vmatrix} 4 & 0 & 0 \\ 0 & 2 & 0 \\ 0 & 1 & \frac{3}{2} \end{vmatrix} \mapsto +12$ | + | |
| $\{2,3,4\}$ | $+ \begin{vmatrix} 0 & * & * \\ 4 & * & * \\ 0 & 4 & * \end{vmatrix} \mapsto + \begin{vmatrix} 0 & 0 & * \\ 4 & 0 & * \\ 0 & 4 & * \end{vmatrix}$ | $+ \begin{vmatrix} 0 & 0 & 2 \\ 4 & 0 & 1 \\ 0 & 4 & 1 \end{vmatrix} \mapsto + \begin{vmatrix} 2 & 0 & 0 \\ 1 & 4 & 0 \\ 1 & 0 & 4 \end{vmatrix} \mapsto +32$ | + | |
| $\{2,3,5\}$ | | | $+ \begin{vmatrix} 0 & 0 & 1 \\ 4 & 0 & 2 \\ 0 & 4 & 1 \end{vmatrix} \mapsto + \begin{vmatrix} 1 & 0 & 0 \\ 2 & 4 & 0 \\ 1 & 0 & 4 \end{vmatrix} \mapsto +16$ | + |
| $\{2,3,6\}$ | | | $+ \begin{vmatrix} 0 & 0 & 1 \\ 4 & 0 & 1 \\ 0 & 4 & 2 \end{vmatrix} \mapsto + \begin{vmatrix} 1 & 0 & 0 \\ 1 & 4 & 0 \\ 2 & 0 & 4 \end{vmatrix} \mapsto +16$ | + |
| $\{2,4,5\}$ | $+ \begin{vmatrix} 0 & 2 & * \\ 4 & 1 & * \\ 0 & 1 & * \end{vmatrix} \mapsto - \begin{vmatrix} 2 & 0 & * \\ 1 & 4 & * \\ 1 & 0 & * \end{vmatrix}$ | $+ \begin{vmatrix} 2 & 0 & 1 \\ 1 & 4 & 2 \\ 1 & 0 & 1 \end{vmatrix} \mapsto - \begin{vmatrix} 2 & 0 & 0 \\ 1 & 4 & 0 \\ 1 & 0 & \frac{1}{2} \end{vmatrix} \mapsto -4$ | - | |
| $\{2,4,6\}$ | | | $- \begin{vmatrix} 2 & 0 & 1 \\ 1 & 4 & 1 \\ 1 & 0 & 2 \end{vmatrix} \mapsto - \begin{vmatrix} 2 & 0 & 0 \\ 1 & 4 & 0 \\ 1 & 0 & \frac{3}{2} \end{vmatrix} \mapsto -12$ | - |
| $\{2,5,6\}$ | $+ \begin{vmatrix} 0 & 1 & * \\ 4 & 2 & * \\ 0 & 1 & * \end{vmatrix} \mapsto - \begin{vmatrix} 1 & 0 & * \\ 2 & 4 & * \\ 1 & 0 & * \end{vmatrix}$ | $- \begin{vmatrix} 1 & 0 & 1 \\ 2 & 4 & 1 \\ 1 & 0 & 2 \end{vmatrix} \mapsto - \begin{vmatrix} 1 & 0 & 0 \\ 2 & 4 & 0 \\ 1 & 0 & 1 \end{vmatrix} \mapsto -4$ | - | |
| $\{3,4,5\}$ | $+ \begin{vmatrix} 0 & * & * \\ 0 & * & * \\ 4 & * & * \end{vmatrix} \mapsto - \begin{vmatrix} 0 & 2 & * \\ 0 & 1 & * \\ 4 & 1 & * \end{vmatrix}$ | $- \begin{vmatrix} 1 & 0 & 2 \\ 1 & 0 & 1 \\ 1 & 4 & 1 \end{vmatrix} \mapsto + \begin{vmatrix} 2 & 0 & 0 \\ 1 & \frac{3}{2} & 0 \\ 1 & \frac{1}{2} & 4 \end{vmatrix} \mapsto +12$ | + | |
| $\{3,4,6\}$ | | | $- \begin{vmatrix} 1 & 0 & 1 \\ 1 & 4 & 2 \\ 1 & 4 & 2 \end{vmatrix} \mapsto + \begin{vmatrix} 2 & 0 & 0 \\ 1 & \frac{3}{2} & 0 \\ 1 & \frac{1}{2} & 4 \end{vmatrix} \mapsto +4$ | + |
| $\{3,5,6\}$ | $+ \begin{vmatrix} 0 & 1 & * \\ 0 & 2 & * \\ 4 & 1 & * \end{vmatrix} \mapsto - \begin{vmatrix} 1 & 0 & * \\ 2 & 0 & * \\ 1 & 4 & * \end{vmatrix}$ | $- \begin{vmatrix} 1 & 0 & 1 \\ 2 & 0 & 1 \\ 1 & 4 & 2 \end{vmatrix} \mapsto + \begin{vmatrix} 2 & -1 & 0 \\ 1 & 1 & 4 \end{vmatrix} \mapsto -4$ | - | |
| $\{4,5,6\}$ | $+ \begin{vmatrix} 2 & * & * \\ 1 & * & * \\ 1 & * & * \end{vmatrix}$ | $+ \begin{vmatrix} 2 & 1 & * \\ 1 & 2 & * \\ 1 & 1 & * \end{vmatrix} \mapsto + \begin{vmatrix} 2 & 0 & * \\ 1 & \frac{3}{2} & * \\ 1 & \frac{1}{2} & * \end{vmatrix}$ | $+ \begin{vmatrix} 2 & 0 & 1 \\ 1 & \frac{3}{2} & 1 \\ 1 & \frac{1}{2} & 2 \end{vmatrix} \mapsto + \begin{vmatrix} 2 & 0 & 0 \\ 1 & \frac{3}{2} & 0 \\ 1 & \frac{1}{2} & \frac{4}{3} \end{vmatrix} \mapsto +4$ | + |

Table 8.1: The computation tree for the chirotope of the mother of all examples: Every row corresponds to a chirotope value. In each cell of a row, the next column corresponding to the next element in the subset is added to the matrix on the left; the result is transformed into column normal form immediately. The empty cells in the table show the savings when column eliminations are reused. The method of computing all chirotope values as individual $r \times r$ determinant calculations (using the same elimination algorithm) corresponds to column additions and eliminations in every column of the table.

Example 8.1.4. Table 8.1 shows the computation tree for the chirotope of the mother of all examples (Example 2.2.5). Remember that the matrix of coordinates of it is:

$$\mathbf{M} := \begin{pmatrix} 1 & 2 & 3 & 4 & 5 & 6 \\ 4 & 0 & 0 & 2 & 1 & 1 \\ 0 & 4 & 0 & 1 & 2 & 1 \\ 0 & 0 & 4 & 1 & 1 & 2 \end{pmatrix}.$$

The computation proceeds from left to right and from top to bottom. This way we have four nodes on level 1, 10 nodes on level 2, and 15 nodes on level 3. In a node at level k we need at most $(r-1)(k-1)$ elementary operations, so that there are at most $4 \cdot 0 + 10 \cdot 2 + 15 \cdot 4 = 80$ eliminations to build the tree (data handling neglected). If we naively use 15 Gaussian elimination steps on the $(r \times r)$ -submatrices, then we need more. We can view one determinant calculation as computing the chirotope in rank r and corank 0, which leads to a total of $(2+4) \cdot 15 = 90$ elementary operations for the 15 determinants (bit complexity again not counted for simplicity). This shows that even in the case of tiny examples, the computation tree already pays off.

Thus, in the example, the chirotope output, listed as a string of signs corresponding to the chirotope values on the lexicographically sorted 3-subsets, would read as $+++ - - - + + + + - - + + - +$.

We saw in Chapter 4 that there is an important dual construction of point configurations, the Gale diagram construction. Remember that the Gale transform of a matrix of rank r will have rank $n-r$, thus one can ask about the relation between the chirotopes of a matrix and that of its Gale diagram. Similarly, one can wonder about the behavior of chirotopes with respect to the other manipulations that we saw in Chapter 4, such as deletion and contraction. Since we will not use it, we only state without proof a theorem that answers these questions (one can find a proof of this in [55, 61]):

Theorem 8.1.5. *Let \mathbf{A} be a point configuration with n points and rank r .*

1. *Let $\mathbf{B} \in \text{Gale}(\mathbf{A})$ be a Gale transform of \mathbf{A} , and let λ denote an ordered sequence $\lambda_1, \lambda_2, \dots, \lambda_{n-r}$ and λ^c the complementary ordered sequence $\{1, 2, \dots, n\} \setminus \lambda$, then the chirotope of \mathbf{B} is given by*

$$\chi_{\mathbf{B}}(\lambda) = \chi_{\mathbf{A}}(\lambda^c) (-1)^{\text{sign}(\lambda, \lambda^c)}.$$

2. *For the operation of deleting point \mathbf{i} ,*

$$\chi_{\mathbf{A} \setminus \mathbf{i}} = \chi_{\mathbf{A}}.$$

3. *For computing the chirotope after the contraction operation \mathbf{A}/\mathbf{i} , let $\mathbf{C} \in \text{Gale}(\mathbf{B} \setminus \mathbf{i})$, then*

$$\chi_{\mathbf{A}/\mathbf{i}} = \chi_{\mathbf{C}}.$$

8.1.3 Computing circuit and cocircuit signatures from the chirotope

We claim (and those familiar with oriented matroids know already) that this curious vector of signs, the chirotope, is enough to extract all the combinatorial data of a point configuration such as the circuits or cocircuits that were so useful in Section 4.5.2. In the following section we will present how to efficiently compute circuit and cocircuit signatures from chirotope values directly, without using the coordinates of the points. It is worth stressing that chirotopes have a distinguished history in computational geometry and convexity. We recommend the wonderful textbook [61] and the monograph [62] for a more in-depth discussion of applications of chirotopes and oriented matroids.

Theorem 8.1.6. *Let \mathbf{A} be a point or vector configuration of rank r labeled by J and let $\chi_{\mathbf{A}} : J^r \rightarrow \{+, -, 0\}$ be its chirotope. Let F be an independent $(r - 1)$ -subset of J .*

Then, F induces a unique (up to sign-reversal) cocircuit, whose signature (Z_+, Z_0, Z_-) in \mathbf{A} is given by the following formulas:

$$Z_+ = \{z \in J : \chi_{\mathbf{A}}(F, z) = +\}, \quad (8.3)$$

$$Z_- = \{z \in J : \chi_{\mathbf{A}}(F, z) = -\}, \quad (8.4)$$

$$Z_0 = \{z \in J : \chi_{\mathbf{A}}(F, z) = 0\}. \quad (8.5)$$

Moreover, all the cocircuits can be obtained this way.

The good thing about the formulas above is that the signs of individual elements can be extracted individually; whenever we only need part of the signature, we need fewer calls to the chirotope oracle. For example, if we only want to know whether a wall is interior, we can stop as soon as we have found one positive and one negative element of the corresponding cocircuit. The straightforward proof is included here, since it is difficult to find a good reference for it.

Proof. Since every point lying on the hyperplane \mathbf{H}_F spanned by F forms an affinely dependent family with F , the function $z \mapsto \chi_{\mathbf{A}}(F, z)$, which is a determinant, vanishes on all points on \mathbf{H}_F , and this is exactly what is required by the definition of a cocircuit spanned by F .

Two points \mathbf{x} and \mathbf{y} lie on the same side of \mathbf{H}_F if and only if the segment spanned by them does not intersect \mathbf{H}_F . Since $\mathbf{p} \mapsto \det(\mathbf{A}|_F, \mathbf{p})$ is linear and continuous in \mathbf{p} , this is the case if and only if $\det(\mathbf{A}|_F, \mathbf{p}_x)$ and $\det(\mathbf{A}|_F, \mathbf{p}_y)$ have identical signs, as claimed. \square

In particular, this means that given a subset of the given point configuration that spans a hyperplane, the corresponding signature of any point in the configuration can be computed by calling the chirotope oracle once. Whenever we need the complete signature, we have to call the chirotope oracle c many times.

Example 8.1.7. We continue with Example 8.1.2. In this case, if we wish to list all cocircuits spanned by two of these five points, we have to look

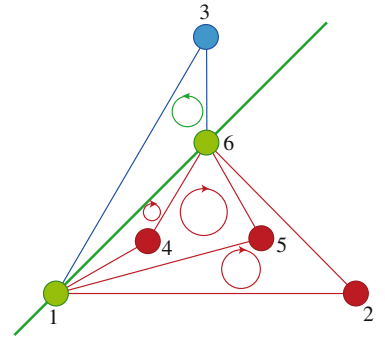


Figure 8.3: The hyperplane spanned by $\{1, 6\}$ induces the signed cocircuit $(\{3\}, \{2, 4, 5\})$; in concordance with the formula in Theorem 8.1.6, the chirotope values of $(1, 6, 2)$, $(1, 6, 4)$, and $(1, 6, 5)$ are negative, and the chirotope value of $(1, 6, 3)$ is positive.

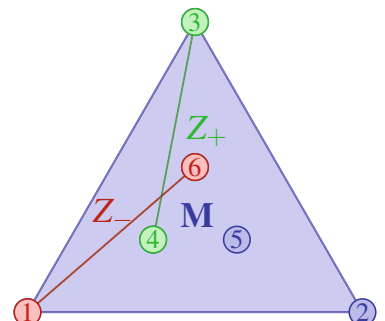


Figure 8.4: The circuit $(\{3, 4\}, \{1, 6\})$ in the mother of all examples; the signature matches with the assertion of Theorem 8.1.8, since ...

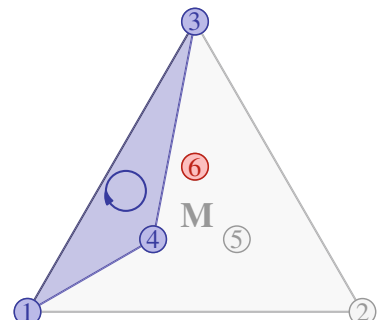


Figure 8.5: ... Basis 134 has clock-wise orientation, 6 is missing in an even position in 1346; the signature of 6 without loss of generality is fixed as - ...

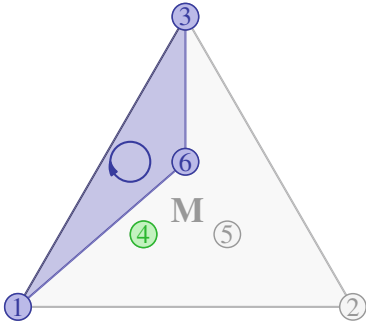


Figure 8.6: ... Basis 136 has clock-wise orientation as well, but 4 is missing in an odd position in 1346; thus, the signatures of 4 and 6 must differ, i.e., the signature of 4 is + as well ...

at ten possible pairs. Each pair will provide a cocircuit. For instance, for the independent set $F = \{2, 5\}$ we can recover the cocircuit by computing $\chi_A(F, z)$ for $z \in \{3, 4, 1\}$. Thus Z_- equals $\{1\}$, while Z_+ equals $\{3, 4\}$.

What about circuits? The formulas turn out to be a bit more complicated, but the proof is just a clever application of Cramer's rule.

Theorem 8.1.8. *Let A be a point or vector configuration of rank r labeled by J , and let $\chi_A : J^r \rightarrow \{+, -, 0\}$ be its chirotope. Let $F = \{z_0, \dots, z_r\}$ with $z_i < z_j$ for all $i < j$ be any full-dimensional $(r+1)$ -subset of J .*

Then, the unique (up to sign-reversal) circuit signature (Z_+, Z_-) in A with $Z_+ \cup Z_- \subseteq F$ is given by the following formulas:

$$Z_+ = \{z_i \in F : (-1)^i \chi_A(F \setminus z_i) > 0\}, \quad (8.6)$$

$$Z_- = \{z_i \in F : (-1)^i \chi_A(F \setminus z_i) < 0\}, \quad (8.7)$$

$$Z_0 = \{z \in F : \chi_A(F \setminus z) = 0\} \cup J \setminus F. \quad (8.8)$$

Moreover, all circuits can be obtained this way.

Proof. To simplify notation, we assume without loss of generality that $z_i = i$ for $i = 0, 1, \dots, r$. In order to find a circuit signature on a dependent set, we need to sort out what the signs in a minimal affine dependence are. More specifically, we must find out when i and j must have identical signs. To this end, we first find a normalizing element. Since F is a full-dimensional $(r+1)$ -subset, the complement of at least one point in it is an affine basis. Therefore, this point cannot have a zero coefficient in any non-trivial affine dependence. Let us also assume without loss of generality that this point is \mathbf{a}_0 that its coefficient in the affine dependence is λ_0 . We now compute the signs of all the other points in F with respect to the reference point \mathbf{a}_0 . This can be done as follows: The coefficients λ_i , $i = 0, \dots, r$ of an affine dependence on F have to fulfill the following equation:

$$-\lambda_0 \mathbf{a}_0 = \lambda_1 \mathbf{a}_1 + \dots + \lambda_r \mathbf{a}_r \quad (8.9)$$

$$\iff -\mathbf{a}_0 = \frac{\lambda_1}{\lambda_0} \mathbf{a}_1 + \dots + \frac{\lambda_r}{\lambda_0} \mathbf{a}_r. \quad (8.10)$$

When we now inspect the signs of $\frac{\lambda_i}{\lambda_0}$ in a solution, we know whether or not λ_i has the same sign as λ_0 .

Now, how can we discover the sign of such a solution on the basis of chirotope information? Chirotope information is essentially based on determinants, and determinants determine the unique solution of a square system of linear equations by Cramer's Rule.

$$\frac{\lambda_i}{\lambda_0} = \frac{\det(\mathbf{a}_1, \dots, \mathbf{a}_{i-1}, -\mathbf{a}_0, \mathbf{a}_{i+1}, \dots, \mathbf{a}_r)}{\det(\mathbf{a}_1, \dots, \mathbf{a}_{i-1}, \mathbf{a}_i, \mathbf{a}_{i+1}, \dots, \mathbf{a}_r)}. \quad (8.11)$$

This means for signs:

$$\text{sign} \left(\frac{\lambda_i}{\lambda_0} \right) = \frac{-\chi_{\mathbf{A}}(1, \dots, i-1, 0, i+1, \dots, r)}{\chi_{\mathbf{A}}(1, \dots, i-1, i, i+1, \dots, r)} \quad (8.12)$$

$$= \frac{-(-1)^{i-1} \chi_{\mathbf{A}}(0, 1, \dots, i-1, i+1, \dots, r)}{\chi_{\mathbf{A}}(1, \dots, i-1, i, i+1, \dots, r)} \quad (8.13)$$

$$= \frac{(-1)^i \chi_{\mathbf{A}}(0, 1, \dots, i-1, i+1, \dots, r)}{(-1)^0 \chi_{\mathbf{A}}(1, \dots, i-1, i, i+1, \dots, r)} \quad (8.14)$$

$$= \frac{(-1)^i \chi_{\mathbf{A}}(Z \setminus z_i)}{(-1)^0 \chi_{\mathbf{A}}(Z \setminus z_0)}. \quad (8.15)$$

The only signatures with this property are those in the assertion and their sign-opposites; thus, we are done. \square

Example 8.1.9. Using the point configuration of Example 8.1.2 again, we can search circuits by looking at subsets of four points in the configuration that contain at least three non-collinear points and, applying formula 8.6, recover the signature vector. For instance, for the set $F = \{1, 2, 3, 5\}$, we would compute $(-1)^i \chi_{\mathbf{A}}(F \setminus z)$ for $z \in F$. In this case, we obtain $Z_+ = \{1, 2, 3\}$ and $Z_- = \{5\}$.

8.2 Verification and realizability

As said before, we assume that the chirotope of \mathbf{A} is given by an oracle. For example, it has been preprocessed and stored in a *hash table*, so that the sign of a r -subset can be accessed in amortized constant time.

From the combinatorial characterizations of triangulations, checking that something is a triangulation is, in principle, straightforward. The only issue is efficiency. To analyze this we use here the characterization of triangulations provided by Corollary 4.5.19. Recall that two properties need to be verified: (ICoP) and (ExP). The following result shows how many steps this may take. By the way, Figure 8.9 shows that Condition (ExP), the most abstract of the two, cannot be dropped:

Theorem 8.2.1. *Deciding whether a subset \mathcal{T} of r -simplices in \mathbf{A} is a triangulation of \mathbf{A} can be verified in time $O(\max\{c, r\}r|\mathcal{T}|)$.*

Proof. The check of Characterization 4.5.19 has two parts: (ICoP) and (ExP).

- (ICoP) can be checked as follows: first, compute the link of all d -walls in \mathcal{T} . The computation of all links can be accomplished in $O(r|\mathcal{T}|)$ operations by traversing all the simplices in \mathcal{T} and collecting their contributions to the links of their facets in a hash map (this a well-known data structure that allows search and insertion in amortized constant time). Next, check whether the link of some facet F contains only one point. In this case, we need to check whether F is in the boundary of \mathbf{A} ; if no, we return ‘invalid’. This can be done

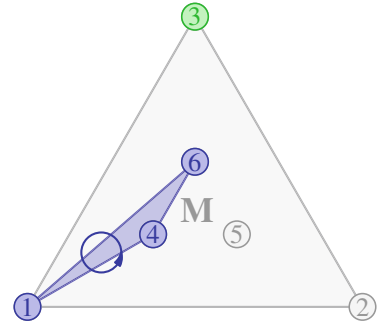


Figure 8.7: ... Basis 146 has counter-clock-wise orientation, 3 is missing in an even position in 1346; thus, the signatures of 3 and 6 must differ, i.e., the signature of 3 is +; ...

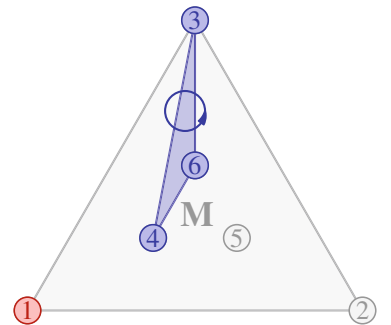


Figure 8.8: ... Basis 346 has counter-clock-wise orientation, 1 is missing in an odd position in 1346; thus, the signatures of 1 and 6 must coincide, i.e., the signature of 1 is -.

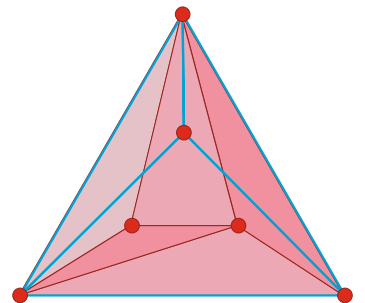


Figure 8.9: The thicker lines and the filled areas indicate two triangulations of the mother of all examples whose union satisfies property (ICoP), but not property (ExP).

by retrieving at most c chirotope values. In case the link has more than two elements, we output ‘invalid’ immediately. In the case that there are two elements in the link of a facet, the orientations of the two points in the corresponding cocircuit can be checked by retrieving two chirotope values. Summarizing, the number of operations needed to check (ICoP) is $O(c r |\mathcal{T}|)$.

- Property (ExP) can be checked by utilizing a lexicographic extension p in the interior of a some simplex in \mathcal{T} . The formula for the chirotope values involving p requires the retrieval of at most r other chirotope values (only one if \mathbf{A} is in general position) [55]. For each simplex in \mathcal{T} we need to check if p is in its interior. This can be done by retrieving r chirotope values involving p . Thus, for the whole procedure we need at most $O(r^2 |\mathcal{T}|)$ steps.

Thus, in at most $O(\max\{c, r\} r |\mathcal{T}|)$, we can check the validity of a triangulation. \square

8.2.1 Constructing regular triangulations in practice

An important computational problem is to generate all regular triangulations of a point configuration. For this, one relies on finding an initial “seed” triangulation from which one uses flips to generate the rest of the triangulations.

We begin by addressing the problem of constructing the first regular triangulation. As we saw in Section 4.3.1, the construction of a placing triangulation is an incremental process. During the process, we maintain in the k -th step:

- the set of points \mathbf{A}_k that is currently triangulated,
- a placing triangulation \mathcal{T}_k of \mathbf{A}_k , and
- a set \mathcal{F}_k of all boundary facets of \mathcal{T}_k that are interior in \mathbf{A} , i.e., those facets
 - that are facets of exactly one simplex in \mathcal{T}_k
 - that are not in the boundary of \mathbf{A} , i.e., the corresponding cocircuits are neither positive nor negative in \mathbf{A} .

The first r points to be added have to form a valid (i.e., full-dimensional) simplex. Finding such a simplex can be integrated in the computation of the chirotope at the cost of storing a simplex B with non-zero chirotope. Consequently, \mathbf{A}_r equals B , the triangulation \mathcal{T}_r consists of the simplex B , and \mathcal{F}_r contains those facets of B that are not in the boundary of \mathbf{A} .

Adding a new point \mathbf{a}_{k+1} to \mathbf{A}_k , yielding \mathbf{A}_{k+1} , for some $k \geq r$ will add all simplices $F \cup a_{k+1}$ to \mathcal{T}_k for which $F \in \mathcal{F}_k$ is visible from \mathbf{a}_{k+1} , i.e., the sign of \mathbf{a}_{k+1} in the cocircuit defined by F is opposite to those signs of the points in \mathbf{A}_k that are non-zero: this yields \mathcal{T}_{k+1} (there are points in \mathbf{A} with non-zero sign, since \mathbf{A}_k is full-dimensional for all $k \geq r$). The visible facets

in \mathcal{F}_k are removed and the new non-boundary facets of the new simplices are added to \mathcal{F}_k ; this yields \mathcal{F}_{k+1} .

The process stops as soon as \mathcal{F}_k is empty for some $k \geq r$. This happens at the latest when $k = n$, but can occur earlier, in which case not all points are used for the placing triangulation. If one wants a triangulation that uses all the points, the missing points are added one by one by performing stellar subdivisions inside existing simplices; the points are “flipped-in”.

The number of operations on the sets \mathcal{F}_k is bounded by the number of all $(d - 1)$ -faces of the resulting placing triangulation \mathcal{T} , which is at most $O(r|\mathcal{T}|)$. The use of universal hashing facilitates unique insertion and deletion in amortized constant time. For one visibility check, we need to retrieve at most c chiropope values (if \mathbf{A} is in general position, two values suffice). Each facet occurring in some \mathcal{F}_k may have to be checked for visibility in each but one step of the construction.

Thus, we need at most $O(rc^2|\mathcal{T}|)$ operations (respectively $O(rc|\mathcal{T}|)$ operations if \mathbf{A} is in general position) for all visibility checks. This dominates the computation of a placing triangulation. In conclusion, we have:

Lemma 8.2.2. *An initial placing triangulation \mathcal{T} for a point configuration of n points of rank r can be computed in no more than $O(rc^2|\mathcal{T}|)$ operations.*

8.2.2 Checking regularity of a triangulation

As we saw in Chapter 5, regularity of a subdivision is equivalent to the feasibility of a certain linear program (see Section 5.2). Here we will deal with triangulations only, so there are no non-trivial coplanarity conditions in the system.

However, the set of strict folding conditions presented in Theorem 5.2.6(i) is too redundant to be useful in a computer program. Thus, we make use of Theorem 2.3.20 instead. We need to impose a strict folding condition only for each interior facet, or *wall*, F in our triangulation \mathcal{T} . Recall that the constraint induced by an F adjacent to the simplices B and B' in \mathcal{T} expresses that B and B' can be folded at F , such that the resulting signed volume spanned by B and B' is positive.

Recall that this strict folding condition can be expressed as a condition on the determinant of the homogeneous coordinate vectors of the points in $B \cup B'$. This determinant develops into a linear constraint in the height variables for each point. The coefficients turn out to be the same determinants that specify the signs for the chiropope values on all subsets of $B \cup B'$. If we therefore save the determinants rather than the signs in the chiropope, then we can form each constraint in time $O(r)$, resulting in a time complexity of $O(r^2|\mathcal{T}|)$ for setting up the complete linear program. Summarized:

Lemma 8.2.3. *The regularity of a triangulation can be checked in time $O(r^2|\mathcal{T}|)$ times the time to solve a linear program with at most $r|\mathcal{T}|$ constraints and $|\mathbf{A}|$ variables.* □

Example 8.2.4. We end with an example that shows again that regularity is totally dependent on the actual coordinates of the vertices in the

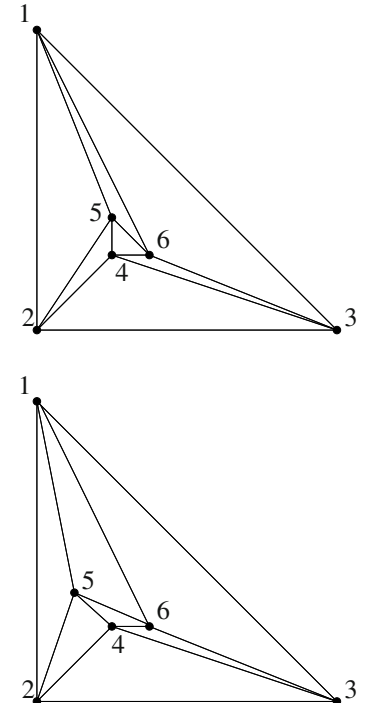


Figure 8.10: Two coordinates for the same triangulation: one is regular (bottom), the other is not (top).

triangulation, and not just on the combinatorics of the simplices involved. Is the reader surprised to see yet again the mother of all examples? (See Section 7.1 and all the prehistoric material going all the way to Example 3.6.16.) Our coordinates now are just a minor variation of those presented there; our proof is computational.

Consider the point configuration \mathbf{A} with coordinates: $a_1 = (0, 8), a_2 = (0, 0), a_3 = (8, 0), a_4 = (2, 2), a_5 = (2, 3), a_6 = (3, 2)$ (The reader may notice this is a “cousin” of the mother of all examples, so this can be called the aunt of all examples). At the same time, we have an alternative configuration \mathbf{A}' obtained by moving a_5 be $(1, 3)$. Now we will see that the triangulation consisting of triangles $\{1, 2, 5\}, \{4, 5, 6\}, \{2, 3, 4\}, \{2, 4, 5\}, \{3, 4, 6\}, \{1, 5, 6\}$, and $\{1, 3, 6\}$ is regular or non-regular, depending on whether we use \mathbf{A} or \mathbf{A}' .

For the configuration \mathbf{A} (top side of Figure 8.10) the system of inequalities defined by the triangulation has nine inequality constraints. By using a linear programming solver, we can check that three of them form an infeasible subsystem. The inequality $-16\lambda_4 - 2\lambda_1 + 16\lambda_5 + 2\lambda_2 < 0$ is defined by the simplex $\{1, 2, 5\}$ and the point a_4 along the wall $\{2, 5\}$. The point a_6 and the simplex $\{2, 3, 4\}$ along the wall $\{3, 4\}$ give the inequality $-2\lambda_2 + 2\lambda_3 - 16\lambda_6 + 16\lambda_4 < 0$. Finally, $-3\lambda_3 + 24\lambda_6 + 3\lambda_1 - 24\lambda_5 < 0$, comes from simplex $\{1, 5, 6\}$ and the point a_3 along the wall $\{1, 6\}$. To see that the whole system of inequalities has no solution, it suffices to show that these three inequalities are inconsistent. Multiply these inequalities by $3/8, 3/8$ and $1/4$ respectively. Adding these multiples of the constraints to the linear combination gives $0 < 0$, a contradiction.

On the other hand, the reader is invited to verify (see exercises and bottom of Figure 8.10) that if we set new coordinates for \mathbf{A}' , now with a value $(1, 3)$ for a_5 , then the triangulation is regular. Concrete heights that induce the triangulation shown are $\lambda_6 = 0, \lambda_5 = 1/2, \lambda_4 = 0, \lambda_3 = 0, \lambda_2 = 1/2, \lambda_1 = 4$, but of course there are many others.

8.3 Listing and enumerating triangulations

In this section, we turn our attention to the computer-aided enumeration of triangulations. Essentially two ideas come to mind:

- We can enumerate all regular triangulations of a point configuration \mathbf{A} by exploring the graph of flips via, e.g., a breadth-first-search algorithm, flipping away from a seed triangulation. This is justified by the results of Chapter 5: the graph of flips among regular triangulations of \mathbf{A} is connected. Since flips in a regular triangulation may produce non-regular triangulations (in some situations with annoying frequency), we need to check whether an output triangulation is regular or not, unless we want to enumerate the whole connected component of the graph of flips.
- If we really want to enumerate *all* triangulations, an approach would be to try to build them from scratch by inserting maximal simplices one-by-one in all possible ways, in each step checking proper intersection, until we arrive to a triangulation or to a dead-end complex

that cannot be extended further. (This process is reminiscent of building a puzzle.)

8.3.1 Exploring a flip-graph component

In this section, we analyze a standard Breadth-First-Search (BFS) procedure to explore a connected component of the flip graph [85]. Since the graph is not given explicitly, we need to construct edges dynamically during the exploration. To this end, we maintain for each triangulation a node containing its set of flips, i.e., a set of edges leading out of this node. A flip in a triangulation can be seen as a pair of two sets of simplices, namely, those simplices to be removed, the flip-out set, and simplices to be added, the flip-in set. We can compute the resulting triangulation in amortized time $O(r)$ by using some data structure that allows for unique insertion and deletion in amortized constant time (e.g., hash tables with universal hashing, or something derived thereof; this is well-known and explained in [85]).

All flips can be found quickly using the chirotope as follows: Assume \mathcal{F} is the set of flips in \mathcal{T} , and we have used one of those flips, $f \in \mathcal{F}$, to discover a new triangulation \mathcal{T}' . We now want to compute the family \mathcal{F}' of flips of \mathcal{T}' . Let $|\mathcal{T}|$ and $|\mathcal{T}'|$ be the number of maximal simplices in \mathcal{T} and \mathcal{T}' , respectively. Similarly, let $|f|$ be the number of maximal simplices in f . Then, the set \mathcal{F}' of flips of \mathcal{T}' consists of the remaining old flips already in \mathcal{F} , not destroyed by f , and flips newly generated by f .

The undestroyed old flips in \mathcal{F}' are those flips in \mathcal{F} whose flip-out sets are disjoint from f 's flip-out set. Computing the undestroyed flips from \mathcal{F} takes time $O(|f||\mathcal{F}|)$ by testing membership of each simplex in the flip-out set of f in the flip-out sets of the flips in \mathcal{F} , where each membership test can be carried out in amortized constant time by hashing techniques.

Now we compute the new flips. Their flip-out sets always have a non-empty intersection with the flip-in set of f . Thus, to find new flips we can restrict ourselves to potential flips containing simplices of f 's flip-in set. To this end, we first build all potential supports (sets of involved vertices) of flips by collecting all $(r+1)$ -supersets of simplices in the flip-in set that might support a flip.

Note that the number of unused points in \mathcal{T} is at most the corank c . One can find all possible new flip supports in $O(|f|(c + |\mathcal{T}'|))$ by first testing all non-used points for containment in all possible simplices in the flip-in set of f and, second, checking all simplices in \mathcal{T}' for adjacency to the simplices in f . This results in at most $O(r|f| + c)$ many distinct supports of potential new flips, because no more than $r|f|$ distinct simplices in \mathcal{T}' can be adjacent to a simplex in the flip-in set of f .

Lemma 8.3.1. *Let \mathcal{T}' be generated by flipping f in $(\mathcal{T}, \mathcal{F})$. Then the number of new potential supports of flips in \mathcal{T}' , i.e., those not supporting a flip in \mathcal{F} , is in $O(r|f| + c)$, and all these supports can be computed in time $O(|f|(c + |\mathcal{T}'|))$. \square*

To check the flippability of an $(r+1)$ -set, we first compute its circuit signature $Z = (Z_+, Z_-)$ by retrieving $r+1$ chirotope values. The two possible triangulations $\mathcal{T}_+(Z)$ and $\mathcal{T}_-(Z)$ can be computed from this data in time

$O(r)$. Then we need to check whether one, say $\mathcal{T}_+(Z)$, of the two possible circuit triangulations is a sub-complex of \mathcal{T}' .

If Z is in general position (no chiropode value is zero), then we need to check containment in \mathcal{T}' for all the at most $O(r)$ simplices in $\mathcal{T}_+(Z)$. This can be done in amortized time $O(r)$ by using a special data structure for triangulations that allows for membership test in amortized constant time.

If Z is not in general position, then we need to compute the links of all the (maximal) simplices in $\mathcal{T}_+(Z)$ in \mathcal{T}' . This takes at most time $O(r|\mathcal{T}'|)$ by collecting the contributions of all facets of simplices to this link. If all simplices in $\mathcal{T}_+(Z)$ have the same non-empty link, then Z is indeed flippable, and the flip-out and flip-in sets are the unions of the $O(r)$ maximal simplices in $\mathcal{T}_+(Z)$, respectively $\mathcal{T}_-(Z)$, with the $O(|f|)$ maximal simplices in the common link; they can therefore be deduced in time $O(r|f|) \subseteq O(r|\mathcal{T}'|)$, i.e., the whole computation is dominated by computing the link.

Lemma 8.3.2. *Let \mathcal{T}' be generated by flipping f in $(\mathcal{T}, \mathcal{F})$, and let Z be a potential support of a new flip in \mathcal{T}' ; then, we can check the flippability of Z in time $O(r|\mathcal{T}'|)$. \square*

Since there are at most $O(r|\mathcal{T}|)$ many walls in \mathcal{T} and, thus, at most that many flips in \mathcal{F} , we obtain a total effort to compute new flips of

$$\begin{aligned} O\left(\underbrace{|f| \cdot r|\mathcal{T}|}_{\text{check old flips}} + \underbrace{|f|(c + |\mathcal{T}'|)}_{\text{compute candidate supports}} + \underbrace{(r|f| + c)r|\mathcal{T}'|}_{\text{check flippability of all candidates}}\right) \\ = O(r(r|f| + c) \cdot \max\{|\mathcal{T}|, |\mathcal{T}'|\}). \quad (8.16) \end{aligned}$$

Summarized, we obtain:

Theorem 8.3.3. *Generating a new node $(\mathcal{T}', \mathcal{F}')$ from flipping $f \in \mathcal{F}$ in the node $(\mathcal{T}, \mathcal{F})$ in the flip exploration graph of \mathbf{A} can be implemented in time $O(r(r|f| + c) \cdot \max\{|\mathcal{T}|, |\mathcal{T}'|\})$.*

Remark 8.3.4. Note that computing flips from scratch for each node would yield a time complexity of $\Omega((r|\mathcal{T}'| + c)r|\mathcal{T}'|)$ —assuming the same algorithm is used for checking flippability of a potential support of a flip, which is substantially more whenever the triangulation \mathcal{T}' contains substantially more maximal simplices than the flip f .

Using a data structure for triangulations that allows to retrieve an adjacent simplex in constant time (the adjacency graph [319]) can reduce the time complexity in the non-general-position case. This, however, would result in a higher complexity when computing an adjacent node, a higher complexity for equality checks for triangulations, and—most importantly—in a substantially higher memory consumption.

8.3.2 Enumeration of all triangulations

Since we know that not all triangulations are connected by flips and can even have no flips at all (see Chapter 7), we need to offer a method to list all triangulations. We build up triangulations by adding one simplex at a time. Slowly a partial triangulation grows until we either reach a dead-end

or we have completed a triangulation. The process can be seen as a standard Depth-First-Search (DFS) in the Hasse-diagram of all partial triangulations, partially ordered by inclusion. We call *partial triangulation* any set of full-dimensional simplices that intersect properly. Every node in the DFS-tree contains a partial triangulation \mathcal{T} , a set of simplices $\mathcal{A}(\mathcal{T})$ (admissibles) that can be added to \mathcal{T} without violating (IP), and the set $\mathcal{F}(\mathcal{T})$ of facets of simplices in the boundary of \mathcal{T} that are in the interior of \mathbf{A} . The leaves in the DFS-tree are the non-extendable partial triangulations, and some of them are in fact triangulations, namely those \mathcal{T} with $\mathcal{F}(\mathcal{T}) = \emptyset$.

In our generation, new simplices are explored in lexicographic order. Consider a node $(\mathcal{T}, \mathcal{A}(\mathcal{T}))$ and add a simplex $B \in \mathcal{A}(\mathcal{T})$ to \mathcal{T} in order to discover node $(\mathcal{T}', \mathcal{A}(\mathcal{T}'))$. Then $\mathcal{A}(\mathcal{T})$ is updated to $\mathcal{A}(\mathcal{T}) \setminus B$, so that none of the other branches above $(\mathcal{T}, \mathcal{A}(\mathcal{T}))$ can ever reach a partial triangulation with subcomplex $\mathcal{T}' = \mathcal{T} \cup \{B\}$.

This way, we only need the memory to store one complete path to the leaf in the DFS-tree. If M is the maximal number of simplices in a triangulation of \mathbf{A} , then storing $O(M)$ simplices on a stack for the partial triangulations plus $O(M \binom{n}{r})$ simplices in the admissibles fields suffice. It is important to observe that the memory requirements do not depend on the number of triangulations of \mathbf{A} .

One can use a preprocessed hash table with all possible $\binom{n}{r}$ simplices as keys. The value $\mathcal{A}(B)$ of a simplex B is the set of all simplices B' such that B and B' intersect properly. This preprocessing takes time $O(\binom{n}{r}^2)$. The table allows for the following fast update algorithm: if \mathcal{T}' is discovered by adding simplex B to \mathcal{T} , then $\mathcal{A}(\mathcal{T}') = \mathcal{A}(\mathcal{T}) \cap \mathcal{A}(S)$. This step can be accomplished in time $O(|\mathcal{A}(\mathcal{T})|)$, which is—crudely estimated—in $O(\binom{n}{r})$.

The set of all interior facets of \mathbf{A} is also preprocessed by checking for each $(r-1)$ -subset the facet property. This needs time $O(r \binom{n}{r-1})$. The set $\mathcal{F}(\mathcal{T})$ can be updated by adding the interior boundary facets of B to $\mathcal{F}(\mathcal{T})$ modulo 2. This can be done in time $O(r |\mathcal{F}(\mathcal{T})|)$, which is in $O(r^2 M)$.

In total, we need time $O(\binom{n}{r}^2)$ preprocessing time and time $O(r \binom{n}{r})$ per output node. The time needed per triangulation is much higher, because there are a lot more partial triangulations than triangulations.

Theorem 8.3.5. *All triangulations of a rank- r point configuration with n points and N maximal partial triangulations can be computed in time $O(\binom{n}{r}^2 + N r \binom{n}{r})$.* \square

We can explain the above notions using graph theory. The *intersection graph* of a d -dimensional configuration \mathbf{A} , $OBS(\mathbf{A})$, is the graph whose vertices are all the full dimensional simplices in \mathbf{A} , and two simplices B_1, B_2 are adjacent if there exists a circuit (Z_+, Z_-) such that Z_+ is a face of B_1 and Z_- is a face of B_2 . In this way, a triangulation of \mathbf{A} corresponds to a unique maximal stable set of $OBS(\mathbf{A})$ (i.e., a set of vertices with no two adjacent by an edge). This setup was used in [319] to enumerate all triangulations. Here we have presented an improved version: first, we do not proceed via adjacent simplices only, and, second, we use the chirotope for checking proper intersections of simplices. The basic method goes back to 1980 [201].

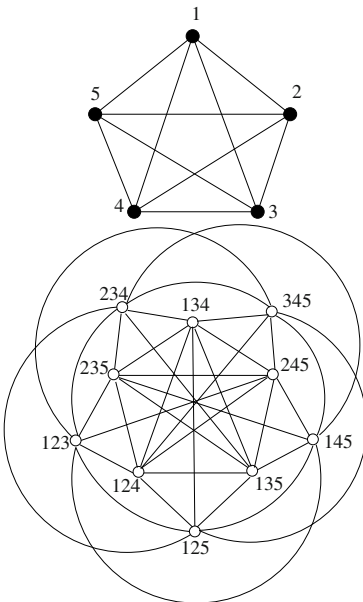


Figure 8.11: The bottom part of the figure shows the intersection graph of all simplices in a pentagon (on the top). Triangulations are maximal stable sets.

Not all the maximal stable set of $OBS(\mathbf{A})$ correspond to triangulations as we can see from the next example. Nevertheless, if we associate with every node of $OBS(\mathbf{A})$ the volume of the corresponding simplex, the triangulations of \mathbf{A} are in bijection with the maximum weight stable sets of $OBS(\mathbf{A})$. Unfortunately, the problem of enumerating all the maximal stable sets of a graph is a $\#P$ -hard problem [147].

Example 8.3.6. Consider the point configuration of Example 3.6.15, with exactly those coordinates. Consider also the following simplicial complex: $\{\mathbf{r}, \mathbf{p}_1, \mathbf{p}_2, \mathbf{p}_3\}$, $\{\mathbf{q}_1, \mathbf{q}_2, \mathbf{p}_1, \mathbf{p}_2\}$, $\{\mathbf{q}_2, \mathbf{q}_3, \mathbf{p}_2, \mathbf{p}_3\}$, and $\{\mathbf{q}_3, \mathbf{q}_1, \mathbf{p}_3, \mathbf{p}_1\}$. This simplicial complex leaves a hole to be covered; namely, the boundary of this simplicial complex is missing the face $\{\mathbf{p}_1, \mathbf{p}_2, \mathbf{p}_3\}$. Every other tetrahedron with vertices on $\{\mathbf{q}_1, \mathbf{q}_2, \mathbf{q}_3\}$ intersects improperly one of the four listed above, hence the simplicial complex is maximal, but still not a triangulation.

8.3.3 Enumeration with symmetry

Often we are interested in triangulations for point sets with large numbers of symmetries (e.g., the vertices of a regular d -cube). The good news that we can do a breadth-first-search (BFS) generation of combinatorial symmetry classes of triangulations connected by flips.

Let us assume that we are given not only the chirotope of the configuration, but also a set of symmetry permutations of the points that generate all symmetries. In the BFS procedure there are always three kinds of nodes [85]: unknown nodes (white nodes), nodes that have been discovered but may have unknown neighbors (gray nodes), and discovered nodes, all of whose neighbors have also been discovered (black nodes). Black nodes can be removed from memory.

The BFS procedure behaves well with respect to symmetries. It is possible (by an equivalent-edge marking procedure) to store only one representative per symmetry class and to remove the black nodes from memory. This works without ever discovering a white node equivalent to a black one [253]. We also do not want to store the complete orbit of a triangulation. For every new triangulation, we check whether one of the stored representatives is in the orbit of the new triangulation. Using the symmetries that leave a triangulation unchanged, one can reduce the effort of finding flips.

Of course, it is not clear whether we re-enter an orbit symmetry class whose representative triangulation we have forgotten already when we marked it black. The solution to this problem is to also carefully monitor the symmetry of flips: whenever we find, via the flip f , a triangulation \mathcal{T} with $\pi(\mathcal{T}) = \mathcal{T}'$ for some already stored representative \mathcal{T}' and some combinatorial symmetry π , we mark $\pi(f^{-1})$ in \mathcal{T}' . One can prove that, this way, we can mark black all nodes whose edges have been processed completely, since we will not enter their symmetry class again. Finally, symmetries can also be taken into account when checking (CombIFP) in a potential triangulation. In contrast to this, (ExP) has to be checked for all simplices—not only for all symmetry classes of simplices.

8.3.4 Implementation issues

The ideas discussed earlier have been implemented in the software package TOPCOM [265]. TOPCOM was inspired by the Maple package PUNTOS [94], which was probably the first triangulation program based on oriented matroid machinery. By now, TOPCOM can be used from inside polymake [135], which is—among other useful things—a command center for polyhedral transformations and computations.

In this section, we informally explain a selection of low level, but useful, details in the current implementation of TOPCOM. Our intention is to give some guidance to people who may need to implement their own programs.

We make some remarks now about the different data structures that need to be implemented.

- *Simplicial complexes:* Simplicial complexes are regarded as the sets of their maximal simplices. TOPCOM aims at using set data structures that perform fast on the following tasks: equality check, membership test, unique insertion, deletion, intersection, and union. For this reason, simplices are implemented as dynamic bitsets. The largest number of points ever handled in TOPCOM was 324 in dimension six (the Santos triangulation). This still requires only 41 bytes per simplex, as opposed to $7 \cdot 4 = 28$ bytes for an array representation. For all potentially accessible enumeration problems the number of points must be much smaller: in most applications 32 bits suffice, in which case the memory consumption is larger for arrays.

Note that in this structure equality check needs $\lceil n/32 \rceil$ integer equality checks. Membership test, unique insertion, and deletion just need a single (very fast) bit operation each. Intersections and unions are linear in n ; however, on a normal PC, 32 bits can be processed at a time, thus this is practically very fast for reasonable values of n .

Simplicial complexes are based on dynamic bitsets, where each bit represents a simplex. The assignment of bit positions to simplices remains fixed during one complete run of the program. When a simplex occurs for the first time, it gets the next free bit assigned; this assignment is stored in a dictionary. Retrieving the simplex corresponding to a bit is implemented via an array indexed by integers; getting the bit position of a simplex is accomplished by a hash table look-up. Both can be done (theoretically and practically) in amortized constant time.

This way, operations on simplicial complexes can work fast via bitset operations. Another advantage is the excellent behavior in terms of memory cache misses (a main bottleneck on nowadays computers): retrieving even a long bitstring from memory is very fast whenever the bits are stored consecutively. If we enumerate a flip graph component, then for each possible simplex there is at least one triangulation (usually many) that contains that simplex. Thus, we need to store each possible simplex at least once, from which the use of the simplex dictionary does not harm memory-wise.

The main draw-back of this structure is that equality checks take time $O(\binom{n}{r})$, although with small constants. The plausible observation is that for dense simplicial complexes (the number of simplices is of order $\binom{n}{r}$), the structure is performing very well; for very sparse complexes, one should use an ordinary representation.

When the sizes of accessible problems grow, TOPCOM will probably switch to an asymptotically faster data structure. For (most) instances solvable on nowadays computers, the bitstring technique works fastest.

- *Chirotopes:* The chirotope values are stored in a hash table so that they can be retrieved in amortized constant time. Alternatively, one could compute the lexicographic index of each simplex and store its value in an array, yielding access to each chirotope value in constant time by computing the lexicographic index. The chirotope values for simplices are stored in a hash map, allowing for amortized constant time retrieval. If the problem is very large, the table can be assigned a fixed size and works as a cache with random eviction.
- *Nodes in the flip-graph:* TOPCOM stores the triangulation \mathcal{T} as a simplicial complex and the flips of \mathcal{T} as a hash-map, assigning marked or unmarked to the representation of the flip. In this way, a flip's internal representation is simply a dependent set with $r+1$ points, which is stored as a simplex. By deleting $r+1$ bits and retrieving $r+1$ chirotope values, one can obtain from this a flip represented by a pair of simplicial complexes: the flip-in and the flip-out simplices. Thus, deleting the flip-out set from and adding the flip-in set to a triangulation works on bitset level. Marking of a particular flip would work in amortized constant time in hash maps. Because the set of flips assigned to one triangulation is not that large, TOPCOM now rather uses sorted maps for flips (logarithmic time for marking, but less overhead).
- *Node in the tree of partial triangulations:* The triangulation \mathcal{T} , the set $\mathcal{A}(\mathcal{T})$ of admissible simplices, and the set of uncovered interior facets $\mathcal{F}(\mathcal{T})$ are all stored as simplicial complexes. This way, computing the intersection of admissible sets is a bitset operation. Moreover, adding interior facets modulo two means an xor-operation on bitset level, which is also very fast in practice.
- *Symmetries:* Symmetries are stored as arrays σ of integers, where $\sigma[i]$ is the image of vertex i under the symmetry σ . The images of simplices and simplicial complexes are computed vertex by vertex. Here, there is certainly potential for improvement by using more sophisticated structures.

To conclude, we present some performance results of TOPCOM-0.16.3. In Table 8.2, we compare CPU times required for certain operations with different data structures. Note that equality checks in STL sets are fast when

the cardinalities of the operands differ, as was the case in the equality-false test instances in the table; the genuine equality checks for TOPCOM's simplicial complexes are much faster, but cannot take advantage of the cardinality function.

| Relative CPU-times for different data structures for simplicial complexes | | | |
|---|-------------------|------------------|--------|
| operation | STL set(vec(int)) | STL set(bitstr.) | TOPCOM |
| insert 99 simplices | 100% | 58% | 50% |
| assignment | 100% | 49% | 0.3% |
| delete 89 simplices | 100% | 57% | 40% |
| intersect (~ 50 simpl.) | 100% | 56% | 4.7% |
| lex. compare (~ 50 simpl.) | 100% | 53% | 64% |
| equality false (~ 50 simpl.) | 100% | 100% | 600% |
| equality true (w.r.t. above) | 72 100% | 39 250% | 750% |

Table 8.2: Operations in simplicial complexes (2.8 GHz Quad Core Intel Xeon 64bit, 22 GB RAM, Darwin 10.3.0, MacOSX 10.6.3, simplices chosen randomly) using three different data structures for simplicial complexes: STL (= C++ Standard Template Library) set(vec(int)) = STL set, based on red-black trees, of arrays of integers; STL set(bitstr.) = STL set of TOPCOM's dynamic bitstrings; TOPCOM = TOPCOM's bitstrings specifying simplex indices with respect to a table of essentially all possible simplices; parameters comparable to triangulations of the 4-cube.

| configuration | what | result | CPU-time/s |
|--------------------------------------|------------------------|-----------|------------|
| C(12,5) | # triangulations | 5049932 | 1073 |
| C(13,3) | # triangulations | 16384508 | 3711 |
| C(13,4) | # triangulations | 116447760 | 8478 |
| C(13,6) | # triangulations | 132943239 | 15265 |
| C(13,7) | # triangulations | 6429428 | 1855 |
| (4 × 5)-grid | # full triangulations | 2822648 | 263 |
| D₄ × D₄ | # flip graph component | 4533408 | 266 |
| I⁴ | # flip graph component | 92487256 | 4801 |
| Santos triang. | check (ICoP) & (ExP) | okay | 30 |
| Santos triang. | # flips | 0 | 10 |

Table 8.3: Some actual computations done with TOPCOM for the first time (MacBook 2.8 GHz Intel Core 2 Duo 64bit, 8 GB RAM, Darwin 10.3.0, MacOSX 10.6.3).

In Table 8.3, we update a table from [253] containing the output and computation times of some large enumeration problems solved for the first time (to the best of our knowledge) by TOPCOM. The first six configurations (five cyclic polytopes and a two-dimensional point set) are known to have connected flip-graphs (Corollary 6.1.20 and, e.g., Theorem 3.4.3), so the enumeration via flips gives all triangulations. In the case of the (4 × 5)-grid we only enumerated *full* triangulations, meaning those that use all vertices. In the next two examples (product of two tetrahedra and 4-dimensional cube) only the component containing regular triangulations is enumerated. The last two rows are computations checking that the triangulation constructed in [278] (with 324 points in dimension six) is indeed a triangulation and has no flips.

8.4 Bounding the number of triangulations

When we are listing or enumerating triangulations, it is desirable to have an upper bound on their total number in order to estimate the running time of a computer program. We have seen in Chapter 3 that in the plane there are constants c_1, c_2 such that every point configuration in the plane with n points has at least $2^{c_1 n}$ triangulations and at most $2^{c_2 n}$ triangulations. It is natural to ask whether the same is true in higher dimensions. Unfortunately, Theorem 7.2.10 showed that the answer is no for dimension four. So what is the correct bound for arbitrary dimension? Before we state the main theorem, we need some preparation.

Lemma 8.4.1 (T. Dey [105]).

1. *For $k_1 + k_2 \geq d$, let B_1 be a k_1 -dimensional simplex that intersects improperly a k_2 -simplex B_2 . Then there must be an l_1 -face of B_1 that intersects improperly an l_2 -face of B_2 with $l_1 + l_2 \leq d$.*
2. *All simplices of a triangulation of a point configuration in d -dimensional space are completely determined from its $\lfloor d/2 \rfloor$ -skeleton, i.e., the collection of all faces of dimension less than or equal to $\lfloor d/2 \rfloor$.*

Proof. For Part 1, simply note that when two simplices intersect improperly there is a circuit (C_+, C_-) such that $C_+ \subset B_1$ and $C_- \subset B_2$. Of course, C_+ and C_- form faces of B_1, B_2 respectively, and we let m_1, m_2 be their dimension. Now, any circuit in \mathbb{R}^d has no more than $d + 2$ elements, thus $(m_1 + 1) + (m_2 + 1) \leq d + 2$.

For Part 2, let us show that if we are given the $\lfloor d/2 \rfloor$ -skeleton \mathcal{K} of a triangulation \mathcal{T} then we have that a simplex B is in \mathcal{T} if and only if it meets the following two properties: (a) its $\lfloor d/2 \rfloor$ -skeleton is contained in \mathcal{K} , and (b) it intersects properly every $C \in \mathcal{K}$.

The “only if” direction is trivial. For the “if” direction, let C be a simplex not in \mathcal{T} . Then, it intersects improperly some simplex C' in \mathcal{T} and, by Part 1, we have faces $F \subset C$ and $F' \subset C'$ that intersect improperly and with sum of dimensions at most d . Hence, one of them has dimension at most $\lfloor d/2 \rfloor$. If F' has dimension at most $\lfloor d/2 \rfloor$, then C fails to satisfy Condition (b). If F has dimension at most $\lfloor d/2 \rfloor$, then it fails to satisfy Condition (a). \square

Theorem 8.4.2. *Let d be a given positive integer dimension and let \mathbf{A} be a point configuration of n points inside \mathbb{R}^d .*

1. *There is an upper bound of $2^{O(n^{\lceil d/2 \rceil} \log(n))}$ for the number of triangulations of \mathbf{A} .*
2. *The number of regular triangulations of \mathbf{A} has a tight upper bound of $2^{\Theta(n \log(n))}$. More strongly, the same asymptotic bound holds for the number of regular subdivisions of \mathbf{A} .*
3. *When d is an odd number, one can improve the bound on the number of triangulations of \mathbf{A} to $2^{O(n^{\lceil d/2 \rceil})}$.*

Proof. For Part 1: From the upper bound theorem (see Theorem 2.6.3 and its Corollary 2.6.5) we know that the size of a triangulation of the configuration is no more than $O(n^{\lceil d/2 \rceil})$. Thus, since a triangulation is a set of no more than $O(n^{\lceil d/2 \rceil})$ d -simplices selected from a set of $\binom{n}{d+1}$ possibilities, the total number of triangulations is no more than $O(n^{d+1})^{O(n^{\lceil d/2 \rceil})}$ or $O(n^{O((d+1)n^{\lceil d/2 \rceil})})$. This is the same as $2^{O(n^{\lceil d/2 \rceil} \log(n))}$ for fixed d .

For Part 2: The number of regular triangulations of a given point set cannot be larger than the number of *polytopal simplicial spheres* with one more vertex and the same dimension, modulo an $n!$ factor that accounts for possible combinatorially symmetric but geometrically different triangulations of a point configuration. To see this we refer the reader again to the construction of stereographic or central projection as used in Section 2.6.2 to obtain Corollary 2.6.5 for balls from the upper bound theorem for spheres. Recall that a polytopal simplicial sphere is a simplicial complex, homeomorphic to the d -sphere that admits coordinatizations realizing it as a simplicial polytope (see [62] for a nice discussion about polytopality of simplicial spheres).

The number of combinatorially different polytopal spheres is in $2^{\Omega(n \log(n))}$ by a classical result of Goodman and Pollack [143, 142]. The bound is achieved, for example, by the construction in Theorem 7.2.10.

For Part 3: From Lemma 8.4.1 any triangulation of n points in \mathbb{R}^d can be completely determined by the set of its $\lfloor d/2 \rfloor$ -faces. A $\lfloor d/2 \rfloor$ -face has $\lfloor d/2 \rfloor + 1 = \lceil d/2 \rceil$ elements (note we are using that d is odd in the last equality). Thus one can construct up to $\binom{n}{\lceil d/2 \rceil}$ such cells; which means that there are $2^{\binom{n}{\lceil d/2 \rceil}}$ possible triangulations. \square

Note that for even d , the argument for Part 3 unfortunately does not provide a better bound than the one we obtained in Part 1 already. Still, T. Dey observed that with a reasonable assumption one can achieve more (see [105]): We say that a set \mathcal{F} of crossing-free u -dimensional simplices with n vertices in the sphere S^d is *cf-small* if the cardinality of \mathcal{F} is no more than $O(n^u)$. Dey proved that, with the assumption that \mathcal{F} is cf-small, Part 3 of Theorem 8.4.2 can also be attained for dimension d even. For instance, in dimension four, the number of triangulations is known to be between $2^{\Omega(n^2)}$ and $2^{O(n^2 \log n)}$, but the construction in Theorem 7.2.10 may be the “best possible” if the condition of cf-smallness is always true. So far, we only know it always holds true for dimension $d = 2$.

As for lower bounds, we recall here the construction of many triangulations of cyclic polytopes that we did in Chapter 6 (Theorem 6.1.22):

Theorem 8.4.3 (Kalai [181]). *If d is considered fixed, the cyclic polytope $C(n, d)$ has at least $\Omega(2^{n^{\lfloor d/2 \rfloor}})$ triangulations.*

So, the difference between the upper bound and the lower bound given by cyclic polytopes is “only” a factor of n or $\log n$ in the exponent, depending on whether d is odd or even. In particular, for $d = 3$, the cyclic polytope construction gives only c^n triangulations while the upper bound is c^{n^2} . This raises the following question:

Is there a constant c such that every three-dimensional point configuration has at most c^n triangulations?

It is interesting to observe that if we ask for three-dimensional simplicial balls without any geometric constraint, the answer is a big “no”. Pfeifle and Ziegler [254] have shown that there are at least $2^{\Omega(n^{5/4})}$ combinatorially different 3-balls with n vertices. However, their construction is extremely “twisted” in the geometric sense (it uses as a starting point triangulations of surfaces with large genus and few vertices), which probably implies that they cannot be realized in a straight manner, as geometric triangulations.

8.5 Optimization

We have seen already in Chapter 3 that for two-dimensional point configurations there is a huge zoo of “optimal” triangulations (Delaunay triangulations, minimum-weight triangulations, etc). But, how about other optimization problems in higher dimensions? Suppose there is a way of assigning a weight or a price μ_B to each of the possible d -simplices of a d -dimensional point configuration. The weight of a simplex could be its volume, area, diameter, etc. In what follows, we present a powerful method to study two kinds of optimization problems.

1. *Linear optimization problems*: We intend to minimize the sum of the weights of the d -simplices present in the triangulation.
2. *MinMax optimization problems*: We intend to minimize the maximum weight among d -simplices present in the triangulation.

One of the main goals of this section is to present a very general framework that contains these two optimization problems on the space of triangulations of a point configuration. The power of the method stems from being able to use popular techniques in discrete optimization and integer programming [291] to solve and classify these problems.

Let us look at some examples in dimension two. Take, for instance, that the weight of each triangle is equal to a constant, say 1. Then, from Euler’s formula, the linear minimization problem is easily solved by a triangulation that only uses boundary vertices and the corresponding maximization problem is solved by any triangulation that uses all points. Both are solved trivially in polynomial time! But what is the behavior of the problem as we change the weights? Say, for example, that all $\binom{n}{2}$ edges possible for a planar point set have weight either with a 0 or a 1. You can think of the edges that have weight 0 as the most desirable (perhaps because they are very cheap). Define then the weight of a triangle to be the sum of the weights of its edges, thus the weights of triangles range from 0 to 3. As we will see later, it is NP -complete to decide whether whether a triangulation of cost 0 is possible [216].

Another more famous example, which we encountered already in Chapter 3, is when one takes as weights of a triangle the sum of the Euclidean lengths of its edges. The corresponding linear minimization problem is that

of finding *minimum length triangulation* (MLT for short). Now we know this problem is *NP-hard*. The moral is that, as the weights assigned to simplices change, the complexity of finding an optimal triangulation can be rather variable. We will more carefully discuss the complexity of triangulations later in this chapter.

Similar optimization problems can be stated for higher dimensions, for example, in 3-dimensional space, computer graphics applications make it interesting to find a triangulation that minimizes the total surface area of the tetrahedra used. Why? Suppose you have ray of light and polyhedral 3-dimensional obstacles. Two essential queries of many computer graphic algorithms are *ray-shooting*, which means to report the first obstacle hit by a ray of light, and *line-stabbing*, which is to report which objects are hit by an *x-ray* that stabs through some objects. The idea to respond to such queries is to construct a triangulation of the environment space compatible with the obstacles and “walk” along the ray reporting the triangles encountered. The walk takes time proportional to the number of triangles crossed, therefore the walk can be very long when we have a triangulation that has lots of tetrahedra along the ray direction. But we do not know in advance which ray direction will be necessary for analysis. Thus, the following question arises: given a triangulation, what is the average-case cost of ray-shooting or line-stabbing? It turns out that the average walk length for line-stabbing or ray-shooting is proportional to the area of the triangles used in the triangulation. This means it is best for us to use a triangulation that minimizes the sum of tetrahedral areas. See [18] for details and algorithms for approximating the minimum total area triangulation in three dimensions.

Another important high-dimensional optimization question refers to minimizing or maximizing *the number of simplices* present in the triangulation. For instance, given a convex polytope \mathbf{P} inside Euclidean d -space represented by its vertices or facets, or both, we want to find a triangulation of \mathbf{P} that uses the *smallest (largest)* possible number of d -simplices. Each d -simplex receives weight one, and we are solving a linear optimization problem. For lattice polytopes and their relation to algebraic geometry, finding unimodular triangulations (which certainly maximize the number of simplices present) is an important step necessary for obtaining de-singularizations of toric varieties [89]. Finding triangulations that minimize the number of simplices appear in the context of hyperbolic geometry and its applications, most notably, we saw in the proof of Theorem 1.1.6 that this is useful for bounding the diameter of the secondary polytope of an n -gon, the associahedron. Finally, in Sections 1.2 and 6.3, we encountered the very famous problem of minimally triangulating d -cubes in connection to algorithms that find fixed points of continuous maps. We will learn about solving such optimization problems in this chapter.

In the next section, we explain how to use the techniques of linear integer programming and combinatorial optimization to attack linear optimization or minmax optimization over triangulations (we recommend [240, 291] as references). These techniques will provide us with a single unifying framework that works for arbitrary dimension and arbitrary weights chosen for

the simplices.

8.5.1 A linear optimization approach: the universal polytope

From now on we think of triangulations as long vectors of zeros and ones. For a point configuration \mathbf{A} , let $\mathcal{B}(\mathbf{A})$ denote the set of all its bases. If \mathbf{A} is in general position then $\mathcal{B}(\mathbf{A})$ will have $\binom{n}{d+1}$ elements, one for each subset of $d+1$ points in \mathbf{A} . But sometimes there will be far fewer bases (i.e., possible d -simplices) if the points of the configuration have collinearities, coplanarities, etc. (as happens, for example, in a regular cube).

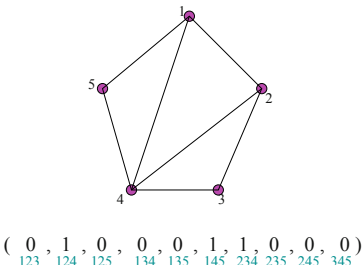


Figure 8.12: For each triangulation, one has a 0/1 vector whether each of the $\binom{n}{d+1}$ d -simplices is used or not. The picture gives a triangulation of the pentagon and its corresponding incidence vector.

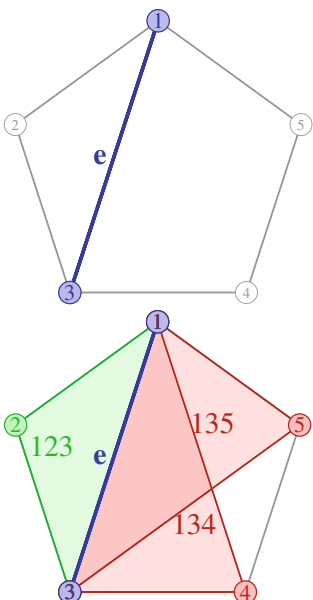


Figure 8.13: In a triangulation, each interior edge e lies in no simplex or exactly two simplices, one on each side; in particular, it lies in an identical number of simplices on each of its sides; thus, it defines a homogeneous linear equation among the incidence vectors of triangulations of the pentagon; for example, for the edge 13 we get the equation $x_{123} - x_{134} - x_{135} = 0$.

Definition 8.5.1. For a triangulation \mathcal{T} of \mathbf{A} the *incidence vector* $v_{\mathcal{T}} \in \{0, 1\}^{\mathcal{B}(\mathbf{A})}$ has coordinates $(v_{\mathcal{T}})_B = 1$ if $B \in \mathcal{T}$ and $(v_{\mathcal{T}})_B = 0$ if $B \notin \mathcal{T}$.

For example, a pentagon has ten possible 2-simplices, hence, the vectors encoding triangulations will have length ten. Each triangulation of a pentagon has exactly three triangles, thus, there are only three non-zero entries on display in each of these vectors. In this example, we have five different vectors, one for each triangulation. See Figure 8.12.

Definition 8.5.2. We define the *universal polytope* of a configuration \mathbf{A} of dimension d with n elements to be

$$\text{U-poly}(\mathbf{A}) := \text{conv}\{x \in \{0, 1\}^{\mathcal{B}(\mathbf{A})} : x = v_{\mathcal{T}} \text{ for a triangulation } \mathcal{T} \text{ of } \mathbf{A}\}.$$

We begin by showing that the minmax optimization problems can, in fact, be reduced to optimization of linear functionals over the simplices.

Lemma 8.5.3. 1. *The linear optimization problem of triangulations reduces to optimizing the linear functional $\sum_{d\text{-simplex } B \in \mathbf{A}} \mu_B x_B$ over the polytope $\text{U-poly}(\mathbf{A})$.*

2. *The minmax optimization problem for triangulations reduces to minimizing the value of an auxiliary variable y over the polyhedron with linear constraints those of $\text{U-poly}(\mathbf{A})$ together with the inequalities $y \geq \mu_B x_B$ for all d -simplices B of the point configuration \mathbf{A} .*

Proof. For the first statement, simply observe that all the incidence vectors of triangulations appear as vertices of the universal polytope, because the vectors are vertices of the cube. A linear functional achieves optimal values (either maximum or minimum) at a vertex of the polytope [291]. For the second statement, the optimal integral solution of the minimization problem, restricted to the x_B 's, is an incidence vector of a triangulation. The optimal value is indeed the largest weight possible. \square

Remark 8.5.4. Observe that in the definition of the universal polytope we only have coordinates to represent the *full-dimensional* simplices. But is that enough? Among our motivating examples we included the minimum total length of edges in the plane and the minimum tetrahedral area in dimension three. In those problems we want to minimize a sum of weights given to lower dimensional simplices. The following result shows that we can also

treat this type of problems with the universal polytope. For example, we can use the universal polytope not only to maximize/minimize the number of d -simplices in a triangulation, but also any other entry in the f -vector.

Lemma 8.5.5. *Let $\mathcal{I}(\mathbf{A})$ be the set of all independent subsets of a point configuration \mathbf{A} . Let $v : \mathcal{I}(\mathbf{A}) \rightarrow \mathbb{R}$ be an assignment of weights to all the elements of $\mathcal{I}(\mathbf{A})$. Then, there is an assignment $\mu : \mathcal{B}(\mathbf{A}) \rightarrow \mathbb{R}$ of weights to the bases of \mathbf{A} that perfectly mimicks v in the following sense: For every triangulation \mathcal{T} of \mathbf{A} , one has*

$$\sum_{B \text{ a } d\text{-simplex of } \mathcal{T}} \mu_B = \sum_{C \text{ a simplex of } \mathcal{T}} v_C.$$

Proof. Let $F \in \mathcal{I}(\mathbf{A})$ be a certain independent subset of \mathbf{A} and consider the v that gives weight one to F and weight zero to every other element of $\mathcal{I}(\mathbf{A})$. Knowing how to mimic weights of this form is enough, since any other weight is a linear combination of them.

To mimic this particular v , let $\mathbf{x}_0 \in \text{relint}_{\mathbf{A}}(F)$ and let \mathbf{x} be a point that is

- In the interior of $\text{conv}(\mathbf{A})$,
- In general position with respect to \mathbf{A} (that is, not in the convex hull of any non-full-dimensional subset of \mathbf{A}), and
- Sufficiently close to \mathbf{x}_0 so that for every subset B of \mathbf{A} one has

$$\mathbf{x} \in \text{conv}(B) \Rightarrow \mathbf{x}_0 \in \text{conv}(B).$$

Such points clearly always exist. We now define for each basis $B \in \mathcal{B}(\mathbf{A})$:

$$\mu_B = \begin{cases} 1 & \text{if } \mathbf{x} \in \text{conv}(B) \text{ and } F \text{ is a face of } B \\ 0 & \text{otherwise.} \end{cases}$$

We claim that μ satisfies what we want. Indeed:

- Since \mathbf{x} is in general position and in the interior of \mathbf{A} , for every triangulation \mathcal{T} there is a unique d -simplex $B \in \mathcal{T}$ with $\mathbf{x} \in \text{conv}(B)$: the carrier of \mathbf{x} in \mathcal{T} .
- By the third assumption on \mathbf{x} , we have $\mathbf{x}_0 \in \text{conv}(B)$ for that B .
- B either contains F as a face or it intersects F improperly, since both have \mathbf{x}_0 in their convex hulls and since $\mathbf{x}_0 \in \text{relint}(F)$ is not in a proper face of F .

In particular: if F is a face of some simplex of \mathcal{T} then both μ and v give weight 1 to \mathcal{T} . If not, then both give it weight zero. \square

Observe that the μ in the above result is not unique. For example, different choices of the points \mathbf{x} close to each independent set C produce different

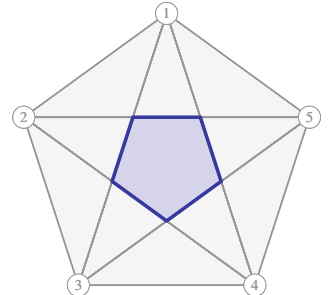


Figure 8.14: Each of the eleven chambers of the pentagon defines a non-homogeneous equation; the equation for the shaded central chamber is $x_{245} + x_{134} + x_{135} + x_{124} + x_{235} = 1$, meaning that a triangulation must contain exactly one of the simplices containing the central chamber.

weights μ . The reason behind this lack of uniqueness is that the universal polytope is not full dimensional (as we will soon show).

We typically do not know explicitly the 0/1 vectors of triangulations, i.e., the vertices of $U\text{-poly}(\mathbf{A})$. Among other things, there are sometimes too many, as seen in Section 8.4. But we still want to tackle the linear and minmax optimization problems. Following a classical method in combinatorial optimization (see, e.g., [240, 291]), we will instead try to find a linear inequality description of $U\text{-poly}(\mathbf{A})$. Once we have a full description of the facet inequalities and equations defining $U\text{-poly}(\mathbf{A})$, we could use linear programming [291] to find an optimal solution for our problems. Although, in general, we only have a partial description, we will see that this suffices to do useful calculations.

The idea of using polyhedral optimization to study triangulations had an origin with the 1985 work of Dantzig, Hoffman and Hu [90]. They studied the case of convex polygons deriving essentially a particular case of what we presented. In the 1990's Billera, Filliman, and Sturmfels [48] introduced a general definition valid in arbitrary dimension and explained algebraic properties using the language of multilinear algebra. They also proved that the secondary polytope is a linear projection of the universal polytope. Finally, it was developed explicitly and for general point sets in [96].

Recall that the dimension of a convex polytope is the dimension of the smallest affine linear space that contains it. This is the affine hull of \mathbf{P} . Clearly, we need to find out which equations, if any, are satisfied by all triangulations when we think of triangulations in terms of their 0/1 incidence vectors. In Figures 8.13 and 8.14 we show a pair of equations that work for convex polygons (illustrated there in the case of a pentagon). The reader should notice that the equations seem to be related to cocircuits of the pentagon. This will give us a general answer.

We first present the linear equations of the affine hull $\text{aff}(U\text{-poly}(\mathbf{A}))$ of $U\text{-poly}(\mathbf{A})$. As in the example, the linear equations involve the cocircuits of the point configuration. For any F which is a $(d-1)$ -simplex of \mathbf{A} , let \mathbf{H}_F be the hyperplane that contains F and let \mathbf{H}_F^+ and \mathbf{H}_F^- denote the two open halfspaces defined by \mathbf{H}_F . We recall that the cocircuits of \mathbf{A} are the resulting partitions $(\mathbf{A} \cap \mathbf{H}_F^+, \mathbf{A} \cap \mathbf{H}_F^0, \mathbf{A} \cap \mathbf{H}_F^-)$ of \mathbf{A} . If $\text{conv}(F)$ meets the interior of $\text{conv}(\mathbf{A})$, we say that F is an *interior* $(d-1)$ -simplex. Observe that this is equivalent to $\mathbf{A} \cap \mathbf{H}_F^-$ and $\mathbf{A} \cap \mathbf{H}_F^+$ both being non-empty. For each interior simplex, we can consider the following homogeneous linear equation,

$$0 = \sum_{B=F \cup \{a\}, a \in \mathbf{A} \cap \mathbf{H}_F^+} x_B - \sum_{B=F \cup \{a\}, a \in \mathbf{A} \cap \mathbf{H}_F^-} x_B. \quad (8.17)$$

We call this the *interior cocircuit equation* associated with the $(d-1)$ -simplex F . Note that in this case neither of the two sums in the interior cocircuit equation is void. Moreover, every triangulation \mathcal{T} of \mathbf{A} contains either no d -simplex containing F or exactly two, one in the first sum and one in the second. Thus the equation is satisfied by the incidence vector $v_{\mathcal{T}}$ of every triangulation of \mathbf{A} (even those triangulations not having F as

a face!), and hence, all points in $\text{aff}(\text{U-poly}(\mathbf{A}))$ satisfy the equation as well. In fact, this equation is essentially a form of condition (ICoP) from Corollary 4.5.19. See an example in Figure 8.15.

Theorem 8.5.6. *Let \mathbf{A} be a point configuration.*

1. *The affine span of $\text{U-poly}(\mathbf{A})$ is defined by all interior cocircuit equations, one for each interior $(d-1)$ -simplex F , plus a single non-homogeneous linear equation valid on $\text{U-poly}(\mathbf{A})$.*
2. *The affine span of $\text{U-poly}(\mathbf{A})$ is spanned by the incidence vectors of regular triangulations.*

Example 8.5.7. Let us consider an example to illustrate Theorem 8.5.6. We can again consider “the mother of all examples”, the point configuration of Example 2.2.5 consisting of two nested equilateral triangles with parallel sides. We saw in Figure 1.30 that there are 18 triangulations, of which all but two are regular. The reader can easily compute all the 0/1 incidence vectors of triangulations. Now in this case, Figure 8.16 shows all edges. From them, we can recover the homogeneous cocircuit equations.

$$\begin{aligned} x[2,3,6] + x[3,5,6] - x[1,3,6] - x[3,4,6] &= 0, \\ x[1,2,5] + x[2,4,5] - x[2,3,5] - x[2,5,6] &= 0, \\ x[1,4,5] + x[2,4,5] - x[3,4,5] - x[4,5,6] &= 0, \\ x[2,5,6] + x[3,5,6] - x[1,5,6] - x[4,5,6] &= 0, \\ x[2,3,6] - x[1,2,6] - x[2,5,6] - x[2,5,6] &= 0, \\ x[1,3,5] + x[1,4,5] + x[1,5,6] - x[1,2,5] &= 0, \\ x[1,2,4] - x[2,3,4] - x[2,4,5] - x[2,5,6] &= 0, \\ x[1,3,4] - x[2,3,4] - x[3,4,5] - x[3,4,6] &= 0, \\ x[2,5,6] + x[4,5,6] - x[1,4,6] - x[3,4,6] &= 0, \\ x[1,3,5] + x[3,4,5] + x[3,5,6] - x[2,3,5] &= 0, \\ x[1,2,6] + x[1,4,6] + x[1,5,6] - x[1,3,6] &= 0, \\ x[1,2,4] + x[1,4,5] - x[1,3,4] - x[1,4,6] &= 0. \end{aligned}$$

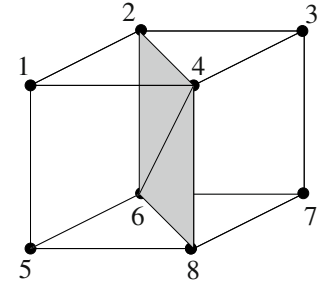


Figure 8.15: the interior cocircuit equation for the regular cube associated with $\{2, 4, 6\}$ is $x_{1246} + x_{2456} - x_{2346} - x_{2467}$, which is different from the interior cocircuit equation associated with $\{4, 6, 8\}$ or any of the other triangles in the plane $\{2, 4, 6, 8\}$.

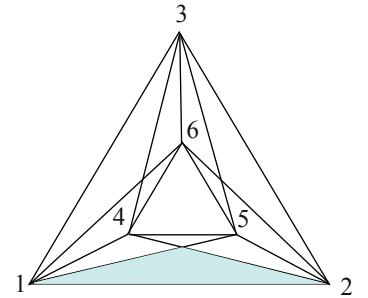


Figure 8.16: From the list of edges of \mathbf{A} we can recover the cocircuit equations and any chamber. We have shaded one chamber.

The reader can verify that the eighteen 0/1 vectors he or she found satisfy the above equations and, as the theorem predicted, the affine hull of the 18 points is already defined by the 16 vectors associated to regular triangulations (i.e., the two associated to the non-regular triangulations are affine combinations of the other 16 incidence vectors).

The proof of Theorem 8.5.6 follows easily from the next lemma.

Lemma 8.5.8. *Let $0 = \sum_B \text{a } d\text{-simplex of } \mathbf{A} c_B x_B$ ($c_B \in \mathbb{R}$) be a homogeneous linear equation on $|\mathcal{B}(\mathbf{A})|$ variables labeled by bases of \mathbf{A} . The following properties are equivalent:*

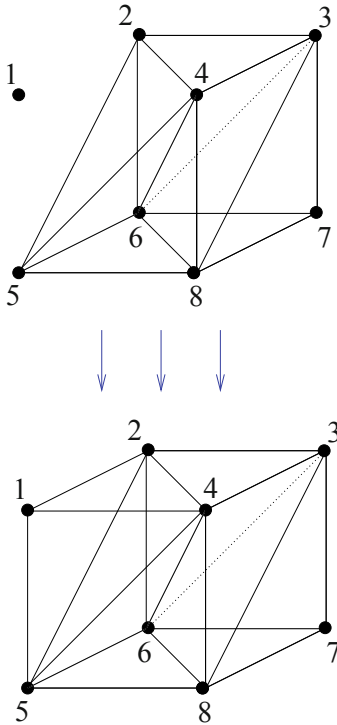


Figure 8.17: Any triangulation of $\mathbf{A} \setminus 1$ (the deletion of point 1) extends to a triangulation of \mathbf{A} .

1. The equation is a linear combination of the interior cocircuit equations.
2. The equation vanishes on (the incidence vector of) every triangulation of \mathbf{A} .
3. The equation vanishes on (the incidence vector of) every regular triangulation of \mathbf{A} .

Proof of Theorem 8.5.6. From (1) \Rightarrow (2) in Lemma 8.5.8 we have that all homogeneous equations are linear combinations of the cocircuit equations. If we have two non-homogeneous equations q_1 and q_2 , multiplying q_1 by a suitable non-zero number and subtracting it from q_2 produces a homogeneous equation. This shows that the cocircuits equations plus q_1 can be used to write any other non-homogeneous q_2 . Thus, Part 1 of the theorem follows. Part 2 follows from the implication (2) \Rightarrow (3) in Lemma 8.5.8. \square

Proof of Lemma 8.5.8. The implications (1) \Rightarrow (2) \Rightarrow (3) are obvious. We prove (3) \Rightarrow (1): Let $U\text{-poly}^{\text{reg}}(\mathbf{A})$ denote the convex hull of all incidence 0/1-vectors $v_{\mathcal{T}}$ where \mathcal{T} is a regular triangulation of \mathbf{A} . Thus $U\text{-poly}^{\text{reg}}(\mathbf{A}) \subset U\text{-poly}(\mathbf{A})$. Let $h = \sum c_B x_B$ be any linear form vanishing on $U\text{-poly}^{\text{reg}}(\mathbf{A})$. We shall prove that h is a linear combination of the interior cocircuit equations and the equations $x_F = 0$ for degenerate sets of $d+1$ points. We use a double induction on $n = |\mathbf{A}|$ and $d = \dim(\mathbf{A})$. When $n = d+1$, the smallest case, there is only one variable x_B associated to the only d -simplex. Linear forms are just multiples of this variable and would be equal to zero if $x_B = 0$. This happens when the simplex is degenerated. Assume that the statement is true for any configuration of cardinality smaller than n or dimension smaller than d .

Let a_1 be a vertex of $\text{conv}(\mathbf{A})$. Let us suppose that $\mathbf{A} \setminus a_1$ still spans \mathbb{R}^d . Otherwise \mathbf{A} is a cone over $\mathbf{A} \setminus a_1$, so that $U\text{-poly}^{\text{reg}}(\mathbf{A})$ and $U\text{-poly}^{\text{reg}}(\mathbf{A} \setminus a_1)$ are affinely isomorphic (see Chapter 4, in particular Remark 4.2.3) and the theorem follows by induction. Recall that the interior cocircuit equations vanish on $U\text{-poly}^{\text{reg}}(\mathbf{A})$. Denote by Cof_F the interior cocircuit equation associated with the $(d-1)$ -simplex F . If $a_1 \notin F$, then Cof_F involves at most one d -simplex of the form $B = \{a_1\} \cup F$. Subtracting appropriate multiples of those Cof_F from h , we get another linear form h_1 in which the variables x_B corresponding to these simplices do not appear. That is,

$$h_1 = \sum_{\substack{B: a_1 \in B \\ \text{conv}(B \setminus a_1) \subset \partial(\text{conv}(\mathbf{A}))}} c_B x_B + \sum_{B: a_1 \notin B} c'_B x_B.$$

We claim the second part of the sum, $h_2 = \sum_{B: a_1 \notin B} c'_B x_B$, is a linear form vanishing on $U\text{-poly}^{\text{reg}}(\mathbf{A} \setminus a_1)$. Indeed, let \mathcal{T}' be any regular triangulation of $\mathbf{A} \setminus a_1$. We can now pick a regular triangulation \mathcal{T} of \mathbf{A} that extends \mathcal{T}' (see Lemma 4.2.17 and Figure 8.17). Since a_1 is a vertex of $\text{conv}(\mathbf{A})$, the triangulation \mathcal{T} cannot contain a simplex B of the form $\{a_1\} \cup F$ where $\text{conv}(F)$ is in the boundary of $\text{conv}(\mathbf{A})$. This fact together with $h_1(v_{\mathcal{T}}) = 0$

implies $h_2(v_{\mathcal{T}}) = 0$ (as well as the other summand too), and consequently $h_2(v_{\mathcal{T}'} = 0$, because the simplices that touch a_1 are not present in the formula.

Every cocircuit equation Co_F of $\mathbf{A} \setminus a_1$ is either a cocircuit equation of \mathbf{A} as well or can be extended to a cocircuit of \mathbf{A} by adding a single variable $x_{\{a_1\} \cup F}$ with the appropriate sign. By induction hypothesis, h_2 is a linear combination of the cocircuit forms of $\mathbf{A} \setminus a_1$. We extend this presentation to a linear combination of cocircuit forms of \mathbf{A} , which vanishes on $U\text{-poly}^{\text{reg}}(\mathbf{A})$. We subtract it from h_1 to get a new form h_3 which vanishes on $U\text{-poly}^{\text{reg}}(\mathbf{A})$ and involves only d -simplices B of the form $a_1 \cup F$:

$$h_3 = \sum_{B: a_1 \in B} c''_B x_B.$$

The assignment $F \rightarrow \{a_1\} \cup F$ defines a bijection between the simplices of the contraction \mathbf{A}/a_1 and the simplices of \mathbf{A} containing a_1 . Therefore we can interpret h_3 as a linear form on $U\text{-poly}^{\text{reg}}(\mathbf{A}/a_1)$. The main fact we need is that any *regular* triangulation \mathcal{T}' of \mathbf{A}/a_1 can be extended to a regular triangulation \mathcal{T} of \mathbf{A} (Lemma 4.2.24). The hypothesis of coherence is really necessary (see Example 4.2.25 and Figure 8.18). This guarantees that h_3 vanishes on $U\text{-poly}^{\text{reg}}(\mathbf{A}/a_1)$. By the induction hypothesis, h_3 is a linear combination of cocircuit forms Co_F of \mathbf{A}/a_1 . We replace each variable x_F in this linear combination by the corresponding variable $x_{\{a_1\} \cup F}$. This transforms cocircuit forms of \mathbf{A}/a_1 into cocircuit forms $Co_{\{a_1\} \cup F}$ of \mathbf{A} . Therefore, h_3 is a linear combination of cocircuit forms of \mathbf{A} . This proves Lemma 8.5.8. \square

Corollary 8.5.9. *The linear subspace of $\mathbb{R}^{\mathcal{B}(\mathbf{A})}$ parallel to $\text{aff}(U\text{-poly}(\mathbf{A}))$ is spanned by all vectors $v_{\mathcal{T}} - v_{\mathcal{T}'}$ where \mathcal{T} and \mathcal{T}' are regular triangulations of \mathbf{A} differing by a bistellar flip.*

Proof. It follows from Lemma 8.5.8 that the linear subspace in question is spanned by all vectors $v_{\mathcal{T}} - v_{\mathcal{T}'}$ where \mathcal{T} and \mathcal{T}' are regular triangulations. Since every pair of regular triangulations is connected by a sequence of bistellar flips, the corollary follows. \square

In general, the dimension of the universal polytope of \mathbf{A} does not depend on the number of elements and the dimension of \mathbf{A} alone; but if \mathbf{A} is in general position, then it does:

Corollary 8.5.10. *When the point configuration is in general position the universal polytope has dimension $\binom{n-1}{d+1}$.*

Thus, coming back to our example of a pentagon, the dimension of its universal polytope is equal to $\binom{4}{3}$, thus it is 4-dimensional and it has 5 points. The only polytope with this property is a simplex!

Proof. $\dim(U\text{-poly}(\mathbf{A})) = \binom{n}{d+1} - R - 1$, where R is the rank of the interior cocircuit forms. The cocircuit forms Co_F for the $(d-1)$ -simplices F not containing a_1 are linearly independent, because each simplex B containing

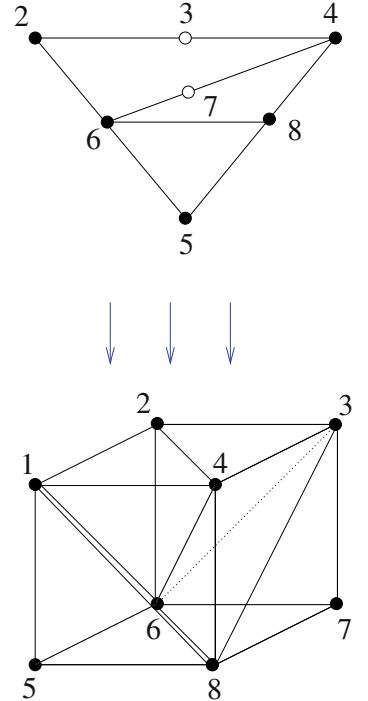


Figure 8.18: While not all triangulations of $\mathbf{A}/1$ (the contraction by point 1) extend to a triangulation of \mathbf{A} , a regular triangulation of $\mathbf{A}/1$ always extend to a regular triangulation of \mathbf{A} . See Lemma 4.2.24 for details. In the top part of the figure we show a triangulation of the contraction of a cube by point 1 (points 3, 7 are not used in the triangulation). For more information on deletion contraction properties see Chapter 4.

a_1 appears in exactly one of them. Thus, $R + 1 \geq \binom{n-1}{d}$. Note also that the vector $v_{\mathcal{T}} - v_{\mathcal{T}'}$, where \mathcal{T} and \mathcal{T}' are regular triangulations of \mathbf{A} differing by a bistellar flip, equals the vector $v_{\mathcal{T}_+} - v_{\mathcal{T}_-}$, where \mathcal{T}_+ and \mathcal{T}_- are the two unique triangulations of the circuit Z on which the bistellar flip is supported. Likewise the vectors $v_{\mathcal{T}_+} - v_{\mathcal{T}_-}$ for the circuit Z containing a_1 are linearly independent, because each simplex B not containing a_1 appears in exactly one of them. Thus $\dim(\text{U-poly}(\mathbf{A})) \geq \binom{n-1}{d+1}$. This together with the formula $\dim(\text{U-poly}(\mathbf{A})) = \binom{n}{d+1} - R - 1$ finishes the proof. \square

Here are two possible choices of non-homogeneous equations that may be used to complete the description of $\text{aff}(\text{U-poly}(\mathbf{A}))$ given in Theorem 8.5.6: Let $\mathbf{p} \in \text{conv}(\mathbf{A})$ be a point not lying in the convex hull of any $(d-1)$ -simplex of \mathbf{A} , then every triangulation of \mathbf{A} satisfies a *chamber equation*:

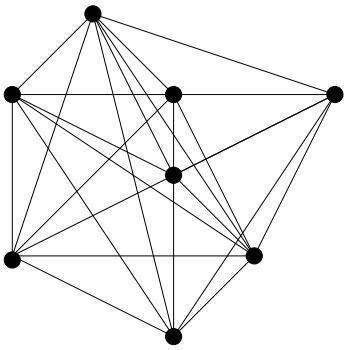


Figure 8.19: The chamber complex of 8 points.
How many chambers are there?

$$\sum_{\substack{B \text{ full-dimensional simplex in } \mathbf{A}, \\ \text{with } \mathbf{p} \in \text{conv}(B)}} x_B = 1. \quad (8.18)$$

The name of the equation comes from the fact that the simplices being considered, when intersected, define a chamber in the sense of Section 5.4. Note that two such points define the same chamber equation if and only if they lie in the same chamber.

Continuing Example 8.5.7 of two nested equilateral triangles with labels as in Figure 8.16; we shaded one such chamber, out of 13 possible. Its associated equation is $x[1, 2, 3] + x[1, 2, 4] + x[1, 2, 5] + x[1, 2, 6] = 1$.

Recall that we studied in Chapter 5, the *chamber complex* of \mathbf{A} is the common refinement of all triangulations of \mathbf{A} (see Figure 8.19). We call the equations of type (3) *chamber equations*, because the simplices in the sum only depend on the chamber in which p lies. Finally, if we denote by $\text{vol}(\cdot)$ the standard volume form in \mathbb{R}^d , the following *volume equation* is satisfied by every triangulation of \mathbf{A} :

$$\sum_{B \in \Delta(\mathbf{A})} \text{vol}(\text{conv}(B)) x_B = \text{vol}(\text{conv}(\mathbf{A})). \quad (8.19)$$

8.5.2 Relaxations of the universal polytope and its edges

With the knowledge we acquired in the previous section, we can construct a polyhedron that approximates the universal polytope fairly well. Although this is unfortunately not always an equality, it has some rather pleasant properties as the graphs of the universal polytope is an induced-subgraph of this larger polyhedron, which has some tantalizing consequences.

Definition 8.5.11. Given a point configuration \mathbf{A} with n points and dimension d , denote by $\text{Q-poly}(\mathbf{A})$ the intersection of the linear affine space of the universal polytope with the cube $[0, 1]^{\mathcal{P}(\mathbf{A})}$. We call the *support of an incidence vector* v , whose entries are labeled by the set of all full-dimensional d -simplices, the collection of all d -simplices B for which $v_B \neq 0$. We will denote it $\text{supp}(v)$. Thus $\text{supp}(v)$ records the non-zero entries of v .

Clearly, since every vertex of $U\text{-poly}(\mathbf{A})$ is also a vertex of $Q\text{-poly}(\mathbf{A})$, we have $U\text{-poly}(\mathbf{A}) \subset Q\text{-poly}(\mathbf{A})$. Here is the crucial result for practical computations.

Lemma 8.5.12. *1. Let v be a vertex of $Q\text{-poly}(\mathbf{A})$. Then v is a vertex of $U\text{-poly}(\mathbf{A})$ if and only if its support contains a triangulation.*

2. If v is any vertex in $Q\text{-poly}(\mathbf{A})$, then the simplices indexed by $\text{supp}(v)$ cover $\text{conv}(\mathbf{A})$, i.e.,

$$\bigcup_{B:B \in \text{supp}(v)} \text{conv}(B) = \text{conv}(\mathbf{A}).$$

3. Every lattice point of $Q\text{-poly}(\mathbf{A})$ is the incidence vector of a triangulation of \mathbf{A} ; i.e., the universal polytope $U\text{-poly}(\mathbf{A})$ is the integer hull of $Q\text{-poly}(\mathbf{A})$, i.e., the convex hull of the lattice points of $Q\text{-poly}(\mathbf{A})$, is precisely $U\text{-poly}(\mathbf{A})$. See Figure 8.20.

Remark 8.5.13. Part 3 of Lemma 8.5.12 contains implicit a new characterization of triangulations, that can be added to those in Section 4.5: a triangulation is simply a set of full-dimensional simplices whose incidence vector satisfies the equations defining the affine span of $U\text{-poly}(\mathbf{A})$: the interior cocircuit equations plus any non-homogeneous linear equation valid on $U\text{-poly}(\mathbf{A})$, such as a chamber equation.

Proof. Part 1: The only-if-direction of (1) is obvious. For the if-direction; We assume $\text{supp}(v)$ contains a triangulations. If any of the entries of the vector v is equal to one, e.g., $v_j = 1$, Because v satisfies all the chambers equalities all non-zero entries of v must also be one. Thus, we can assume the entries of v are all less than one, and thus it strictly contains a triangulation \mathcal{T} (i.e., the support has more simplices than those of a triangulation \mathcal{T}). With this, we reach a contradiction with the fact v is vertex of $Q\text{-poly}(\mathbf{A})$ because $v_\varepsilon := \frac{v - \varepsilon v_{\mathcal{T}}}{1-\varepsilon}$ is still a point in $Q\text{-poly}(\mathbf{A})$, for a sufficiently small positive ε (essentially, take ε small enough to make $v_i + \varepsilon \leq 1$). But then $v = (1 - \varepsilon)v_\varepsilon + \varepsilon v_{\mathcal{T}}$ is not a vertex of $Q\text{-poly}(\mathbf{A})$ (vertices cannot be convex combinations of other points). In conclusion, the support of a vertex, if it contains a triangulation, equals the support of a triangulation. Finally if $\text{supp}(v)$ is the support of a triangulation \mathcal{T} , then again the chamber equations imply that v is exactly the incidence vector of \mathcal{T} because it must be filled with zeros and ones. Hence it is a vertex of $U\text{-poly}(\mathbf{A})$.

Part 2: The chamber equations are satisfied by any point, not necessarily a vertex, of $Q\text{-poly}(\mathbf{A})$. This implies that any point is covered as stated.

Part 3: Let v be an integral point of $Q\text{-poly}(\mathbf{A})$. By Part 2 we only need to prove that any two simplices in $\text{supp}(v)$ intersect properly. Suppose this is not the case for two simplices B_1 and B_2 in $\text{supp}(v)$, i.e.:

$$\text{conv}(B_1 \cap B_2) \neq \text{conv}(B_1) \cap \text{conv}(B_2).$$

Take a point a in $(\text{conv}(B_1) \cap \text{conv}(B_2)) \setminus \text{conv}(B_1 \cap B_2)$. Then the minimal face (subset) F of B_1 with $a \in \text{conv}(F)$ is not a face of B_2 . For each

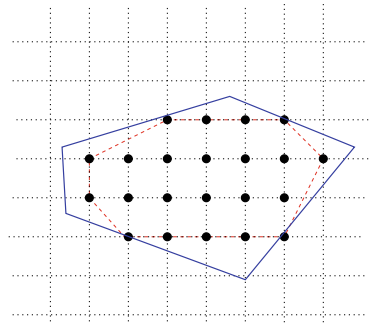


Figure 8.20: For most polytopes, the vertices of the integer hull are quite separate from the vertices of the polytope. The polytope $Q\text{-poly}(\mathbf{A})$ is very special!

simplex B of $\text{supp}(v)$ having F as a face, consider the convex polyhedral cone

$$c(B) := a + \text{pos}(\text{conv}(B) - a) = \{\lambda p + (1-\lambda)a : p \in \text{conv}(B), \lambda \geq 0\}.$$

Note that the facets of $c(B)$ are in 1-to-1 correspondence with the facets of B which contain F . We claim that $\text{conv}(\mathbf{A})$ is contained in the union of such cones. Suppose a point b of $\text{conv}(\mathbf{A})$ lies outside their union. Then b “sees” a facet of some cone $c(B)$, where $B \in \text{supp}(v)$. Let F be the corresponding facet of B , which contains F . By the choice of F , there is no d -simplex in $\text{supp}(v)$ having F as a facet and lying in the halfspace containing b . This violates the interior cocircuit equation $C_{\text{of}}(v) = 0$, since $v \geq 0$. Therefore an open neighborhood of a in $\text{conv}(\mathbf{A})$ is covered by those simplices in $\text{supp}(v)$ which have F as a face. The interior of one of these simplices intersects the interior of $\text{conv}(B_2)$. This violates the chamber equations for v . \square

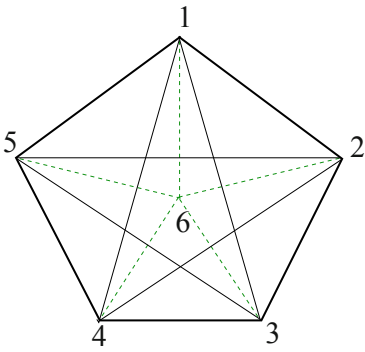


Figure 8.21: A covering that is a vertex of $\text{Q-poly}(\mathbf{A})$, but not of $\text{U-poly}(\mathbf{A})$.

Corollary 8.5.14. *Let $\mathbf{A} \subset \mathbb{R}^2$ be a planar configuration of n points in convex position, then the equality $\text{U-poly}(\mathbf{A}) = \text{Q-poly}(\mathbf{A})$ holds. In general, $\text{U-poly}(\mathbf{A})$ is strictly contained in $\text{Q-poly}(\mathbf{A})$.*

Proof. Let v be a vertex of $\text{Q-poly}(\mathbf{A})$. Let S be a subset of $\text{supp}(v)$ where all triangles in S intersect properly and cover a convex subpolygon of $\text{conv}(\mathbf{A})$. Suppose that S is maximal with these two properties. Let e be an edge of the subpolygon covered by S . Then S is contained in one of the two half-planes defined by e . By maximality of S and the interior cocircuit equations, e must be a segment on the boundary of $\text{conv}(\mathbf{A})$. This proves that S covers $\text{conv}(\mathbf{A})$ and hence is a triangulation. Lemma 8.5.12 Part 1 implies that v is a vertex of $\text{U-poly}(\mathbf{A})$. In Figure 8.21, we illustrate a planar point set with six points (a pentagon and its centroid). This configuration is in general position and has 20 triangles and 16 possible triangulations. Consider the vector $v \in \mathbb{R}^{20}$ with coordinates $v_{\{123\}} = v_{\{234\}} = v_{\{345\}} = v_{\{145\}} = v_{\{125\}} = v_{\{013\}} = v_{\{024\}} = v_{\{035\}} = v_{\{014\}} = v_{\{025\}} = 1/2$ and all other coordinates zero. It satisfies the interior and boundary cocircuit equations. Therefore v lies in $\text{Q-poly}(\mathbf{A})$. Since $\text{supp}(v)$ does not contain any triangulation, $\text{U-poly}(\mathbf{A}) \neq \text{Q-poly}(\mathbf{A})$. This fractional point is the only vertex of $\text{Q-poly}(\mathbf{A})$ which is not in $\text{U-poly}(\mathbf{A})$. \square

We close this section by observing that there is a nice connection between the edges of $\text{U-poly}(\mathbf{A})$ and those of $\text{Q-poly}(\mathbf{A})$. It is in fact a consequence of more general results about 0/1 polytopes and packing polytopes due to Matsui and Tamura [228]. See also [96] for an ad hoc proof using triangulations.

Theorem 8.5.15. *Let \mathcal{T}_1 and \mathcal{T}_2 be two distinct triangulations of \mathbf{A} . The following statements are equivalent:*

1. $v_{\mathcal{T}_1}$ and $v_{\mathcal{T}_2}$ are not neighbors in $\text{Q-poly}(\mathbf{A})$.
2. $v_{\mathcal{T}_1}$ and $v_{\mathcal{T}_2}$ are not neighbors in $\text{U-poly}(\mathbf{A})$.

3. There exist two triangulations \mathcal{T}_3 and \mathcal{T}_4 of \mathbf{A} (different from \mathcal{T}_1 and \mathcal{T}_2) such that $v_{\mathcal{T}_1} + v_{\mathcal{T}_2} = v_{\mathcal{T}_3} + v_{\mathcal{T}_4}$.
4. There exist partitions $\mathcal{T}_1 = R_1 \cup L_1$ and $\mathcal{T}_2 = R_2 \cup L_2$ such that $L_1 \cup R_2$ and $R_1 \cup L_2$ are two other triangulations of \mathbf{A} , different from \mathcal{T}_1 and \mathcal{T}_2 .

We close the section with several comments about how to use the universal polytope as the integer programming formulation in other not direct cases. In computational geometry authors often refer to triangulations of a point configuration \mathbf{A} as those that touch *all* the points of the configuration (in this book called *full triangulations*). Our theory allows more triangulations to have more structure (e.g., secondary polytopes are only possible in that case), but to optimize only over full triangulations we need to add some more constraints. In the case of the planar point set, a single condition equation suffices, namely $\sum x_B = 3n - 3 - b$, which says exactly how many triangles must be present in terms of the vertices and those on the boundary. In d -dimension space the following equations suffice, one for each point a_i in the configuration:

$$\sum_{B \text{ } d\text{-simplex: } a_i \in B} x_B \geq 1.$$

Note also that we can force any simplex, of any dimension, that we wish to be present in an optimization problem by adding a similar equation that forces at least one of the top-dimensional simplices that contain it to be included. Therefore, given a planar point configuration and an specific simple polygon supported on this point set we only need to add n many such inequalities and we can optimize over the space of all triangulations of the simple non-convex polygon.

There are other authors who have considered the optimization of triangulations as linear or integer programs. For example, following [198], if we denote by c_i the length of edge e_i , then one can easily set up a linear program (what in optimization would be called a set packing formulation) to solve the planar minimum length triangulation where there is one variable x_i for the edge e_i (no more than $\binom{n}{2}$ variables altogether). So the objective is

$$\text{minimize } \sum_{e_i \text{ edge}} c_i x_i, \text{ subject to}$$

$$0 \leq x_i \leq 1,$$

$$x_i + x_j \leq 1 \text{ if the edges } e_i, e_j \text{ intersect, and}$$

$$\sum_{e_i \text{ edge}} x_i = 3n - 3 - b,$$

where $3n - 3 - b$ is the number of edges of a triangulation that uses all the points of a configuration by Euler's formula (see Lemma 3.1.3). The integer optimal solution of such constrained problem would give us a minimum

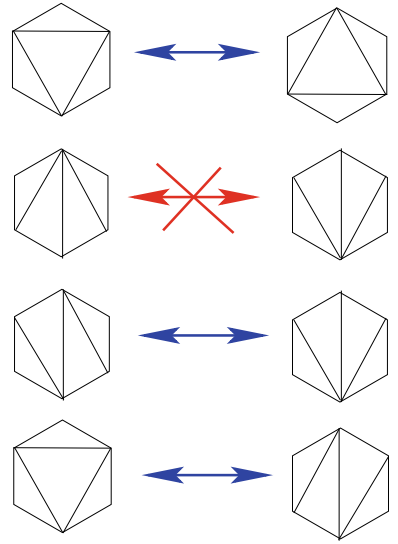


Figure 8.22: Adjacencies in the universal of a hexagon.

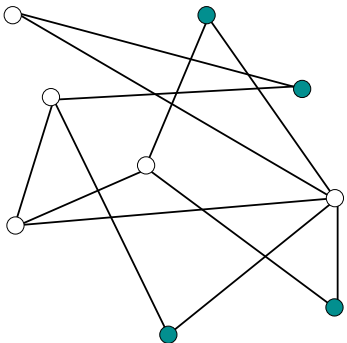


Figure 8.23: One gray stable set of a graph.

length triangulation. Abstractly, planar triangulations are maximal independent set of vertices of a combinatorial graph whose vertices are edge segments in \mathbf{A} and two vertices are adjacent when the corresponding edges cross. Thus we want a maximal size *stable set*, a set of vertices that are not pairwise adjacent in the auxiliary graph 8.23. The *maximal stable set* problem is one of the most studied problems in combinatorial optimization and known linear inequalities can be added to the present description for eliminating non-integral vertices. For example, the cliques of the graph, which geometrically represent set of edges pairwise crossing each other, define *clique inequalities*:

$$\sum_{\text{clique of edges}} x_e \leq 1.$$

For some abstract graphs, e.g., perfect graphs, there is a full characterization of facets for describing the convex hull of the 0/1 incidence vectors. Odd-cycle inequalities are also popular inequalities that help to remove fractional solutions and speed up the solution of integer programs. Intersection graphs of crossing edges and their independent sets have been studied in [196]. The above polyhedral formulation of optimization for triangulations is specific to dimension two. Even there, it does not give a complete description of the polyhedron of triangulations because several of its vertices are not integral.

The experimental comparison made by A. Tajima [317] indicates that the universal polytope is the most effective formulation. It is also clear of course that the inequalities $x_i + x_j \leq 1$ are weaker than and implied by the chamber equations. The universal polytope approach gives of course provably exact solutions to the MLT problem too. It has the advantage of being the only method available for optimization problems of arbitrary dimension. For the planar case the polyhedral approach is not as powerful as ad hoc methods, it works practically for up to a few hundred points. Other authors have reported the current limit is between 300 [318] and 500 points [73]. But the fact that we have a planar problem affords many other heuristics and simplifications.

8.5.3 Equidecomposable and weakly neighborly polytopes

Here we show that the universal polytope, somewhat surprisingly, sheds new light on an almost twenty year old question. We want to answer the following: *what point configurations have the property that all their triangulations have the same number of simplices?*

Definition 8.5.16. We say that a configuration \mathbf{A} is *equidecomposable* if all its triangulations have the same number of full-dimensional simplices.

Remark 8.5.17. The standard definition of equidecomposable (cf. [36], or Section 17.4.2 in the survey paper [207]) is stronger than ours: it requires all triangulations of \mathbf{A} to have the same f -vector. That is, all triangulations need to share not only the number of d -simplices, but also the number of $(d-1)$ -simplices, $(d-2)$ -simplices, etc. For example, the vertices of a

convex n -gon form an equidecomposable configuration in this strong sense, since every triangulation of them has f -vector $(n, 2n - 3, n - 2)$.

We show here (Theorem 8.5.19) that the weak definition, based only on d -simplices, is equivalent to the strong one. We prefer to use the weak one as a starting point because it readily shows that the following configurations that we have already encountered are equidecomposable: Lawrence polytopes (Exercise 5.30), unimodular configurations such as the product of two simplices (Proposition 6.2.11), and cyclic polytopes in even dimension (Theorem 6.1.20, part (iv)).

What do all these configurations have in common? The theory of regular triangulations gives us the following simple, necessary condition for a configuration to be equidecomposable:

Lemma 8.5.18. *If \mathbf{A} is equidecomposable, then all its signed circuits are balanced; that is, for every circuit (Z_+, Z_-) one has $|Z_+| = |Z_-|$.*

Proof. For every circuit Z of \mathbf{A} , there exists a pair of regular triangulations \mathcal{T}_1 and \mathcal{T}_2 that differ by a flip on that circuit (Lemma 5.1.14). The characterization of flips via circuits implies that, for a flip not to change the number of simplices in a triangulation, it is necessary and sufficient that $|Z_+| = |Z_-|$. \square

In particular, an equidecomposable configuration must be *acyclic* (that is, we can think of it as a point configuration) and in convex position: if an element a of \mathbf{A} is not a vertex, then there is a circuit of the form $(\{a\}, C)$ (take as C any minimal subset of $\mathbf{A} \setminus a$ having a in its convex hull), which cannot be a balanced circuit (unless we allow \mathbf{A} to have repeated points). For this reason one can speak of equidecomposable *polytopes*, rather than configurations. The main result in this section is the following strong converse of Lemma 8.5.18.

Theorem 8.5.19. *The following properties are equivalent for a configuration \mathbf{A} .*

- (i) *All triangulations of \mathbf{A} have the same f -vector.*
- (ii) *All triangulations of \mathbf{A} have the same number of d -simplices (\mathbf{A} is equidecomposable).*
- (iii) *All regular triangulations of \mathbf{A} have the same number of d -simplices.*
- (iv) *For every signed circuit (Z_+, Z_-) of \mathbf{A} one has $|Z_+| = |Z_-|$.*

Proof. The implications (i) \Rightarrow (ii) \Rightarrow (iii) are obvious. Lemma 8.5.18 states (ii) \Rightarrow (iv) but, in fact, its proof shows (iii) \Rightarrow (iv) since the triangulations used in it can be chosen to be regular.

For the final implication (iv) \Rightarrow (i), the universal polytope comes to our rescue. It is a consequence of Lemma 8.5.5 that each entry of the f -vector can be computed as the value of a linear functional over the universal polytope: the i -th entry of the f -vector is obtained by the choice of weight $v_C = 1$ for every i -simplex and $v_C = 0$ for every other independent set. Since

the affine span of the whole universal polytope is spanned by the regular triangulations alone (Theorem 8.5.6), to prove that an f -vector entry is constant on all triangulations, it suffices to show it is constant on regular triangulations. This can be done via flips.

That is, all we need to show is that *a flip supported on a balanced circuit does not change the f -vector*. This is true by the characterization of flips via circuits (Theorem 4.4.1): a flip consists in removing a subcomplex $\mathcal{T}_Z^+ * \mathcal{L}$ from a triangulation and putting $\mathcal{T}_Z^- * \mathcal{L}$ instead, where \mathcal{T}_Z^+ and \mathcal{T}_Z^- are the two triangulations of the circuit and \mathcal{L} is a certain complex. If the circuit is balanced then \mathcal{T}_Z^+ and \mathcal{T}_Z^- have the same f -vector (they are combinatorially equivalent), hence $\mathcal{T}_Z^+ * \mathcal{L}$ and $\mathcal{T}_Z^- * \mathcal{L}$ have the same f -vector, hence the two triangulations joined by the flip have the same f -vector. \square

Equidecomposable polytopes were studied by M. Bayer in [36]. (See also Section 17.4.2 in the survey paper [207] by Lee). There, among other things, the implications $(\text{i}) \Rightarrow (\text{ii}) \Rightarrow (\text{iii}) \Leftrightarrow (\text{iv})$ of Theorem 8.5.19 were proved, but the other direction was left as an open question. Bayer also noticed the relation of equidecomposability to the following concepts:

Definition 8.5.20. • We say that a configuration \mathbf{A} is *weakly neighborly* if every subset C of $i + 1$ elements is contained in a face of $\text{conv } \mathbf{A}$ of dimension at most $2i$, for all i .

- We say that a triangulation \mathcal{T} of \mathbf{A} is *shallow* if every i -simplex of \mathcal{T} is contained in a face of $\text{conv } \mathbf{A}$ of dimension at most $2i$, for every i .

Remarks 8.5.21. If the convex hull of \mathbf{A} is simplicial, then being weakly neighborly is equivalent to every set of $\lfloor (d + 1)/2 \rfloor$ elements being the vertex set of a face. That is, to the $\lfloor (d + 1)/2 \rfloor$ -skeleton of \mathbf{A} being the complete simplicial complex of dimension $\lfloor (d + 1)/2 \rfloor$. This is the usual definition of a *neighborly* polytope [339].

It is easy to show that:

Lemma 8.5.22. *A configuration \mathbf{A} is weakly neighborly if and only if all its triangulations are shallow.*

Proof. This follows from the fact that in the definition of weakly neighborly there is no loss of generality in assuming that the subset C of size $i + 1$ is independent, and that every independent subset of $i + 1$ elements appears as an i -simplex in some triangulation of \mathbf{A} . \square

Bayer proved the following by showing that the f -vector of any shallow triangulation of a given polytope can be recovered from the f -vector of the polytope itself. (In particular, all shallow triangulations of a polytope have the same f -vector). Here we use Theorem 8.5.19 to give a shorter proof:

Theorem 8.5.23 (Bayer [36]). *Weakly neighborly configurations are equidecomposable.*

Proof. Assume that \mathbf{A} is not equidecomposable. In particular, it has an unbalanced circuit Z . Suppose for example that $|Z_-| < |Z_+|$ and let $i = |Z_-| - 1$. Then, Z_- is a set of $i + 1$ elements whose carrier face in $\text{conv}\mathbf{A}$ contains the whole circuit because

$$\text{relint}_{\mathbf{A}}(Z_-) \cap \text{relint}_{\mathbf{A}}(Z_+) \neq \emptyset.$$

But the dimension spanned by $Z_- \cup Z_+$ equals $|Z_-| + |Z_+| - 2 > 2|Z_-| - 2 = 2i$. This finishes the proof. \square

The converse of Theorem 8.5.23 is not true. For example, the vertex set of a regular octahedron is equidecomposable but not weakly neighborly.

8.6 Computational complexity of triangulation problems

It is a central concern to investigate the amount of time, number of iterations, or memory requirements for algorithms of specific triangulation problems. We have been doing that in this chapter, but another important aspect of the theory of computation is to classify computational problems and algorithms into *complexity classes*. Such a classification provides a useful differentiation between those problems that can be approached efficiently and those that will unfortunately require heuristics, approximations, or ad hoc methods. In what follows we will discuss this classification for computational triangulation problems with regard to the *time complexity* of a problem.

8.6.1 A very quick review of complexity classes

Our review will be necessarily short. We hope it will suffice for people that do not know about complexity, although we definitely rely on informal intuitive notions for ease of presentation. We highly recommend that you read a proper formal account of complexity theory such as the classic book [134]).

A *problem* is a generic computational question with unspecified data such as what is the determinant of a matrix? Or given a graph and an integer k , does the graph have a clique of size k ? An *instance* of a problem is a particular specification of the data defining the problem. An *algorithm* is a finite set of instructions for performing basic operations on an input to produce an output. An algorithm *solves a problem* P if given a *representation* of each instance I of P as input it supplies as output the solution of instance I . Note that an instance can have more than one representation, for example, polytopes can be described by either their facets or their vertices (to define this rigorously one uses Turing machines, formal languages, and other constructions). We also note that when an algorithm involves a random choice (e.g., picking a point at random), then the algorithm is randomized or probabilistic. Otherwise, we say it is *deterministic*.

How do we measure the efficiency of an algorithm A ? We do this based on *running time*, a count of the number of elementary operations needed to run the algorithm. The number of operations depends on the *size* of the input instance. For example, the size of a graph can be measured by the number of vertices and edges. On a polytope things are a bit more complicated

because they are defined, say, by a system of inequalities $Ax \leq b$ or by its vertices. The numeric data helps determine the size of the input. Thus the size of the polytope is given by the number of variables, the number of rows involved, and the size of the numbers involved. An integer n is encoded in binary, thus its size is simply the number of bits necessary, $\log_2 n$ bits. What is the size of a rational number? $\text{size}\left(\frac{p}{q}\right) = \max(\text{size}(p), \text{size}(q))$. All these have been taken into account in our prior analysis.

When we study how difficult a problem is we will discuss the worst case analysis, i.e., the worst possible instance one can have. Of course, another type of conclusion can be reached from the average-case analysis but we will not discuss this here. We say that an algorithm is *polynomial time* if the number of operations needed in its running time is bounded above by a polynomial function in the size of the input. As a simple example, suppose you are given a list \mathcal{L} of n numbers. A silly algorithm requires around $\binom{n}{2}$ comparisons to re-order the whole list. This is not the best algorithm, but it shows that this is a polynomial-time solvable problem.

We discuss *decision problems*, namely problems where the answer is always yes or no (e.g., is the graph G 3-colorable?). Of course, most problems can be formulated in this way, thus it is not a very serious restriction. The complexity class P is the set of decision problems that can be solved by a deterministic algorithm in polynomial time in the input size. A decision problem is in the class NP if there exists an algorithm to verify a solution of the problem in time $O(n^k)$ for some constant k . Note that if the problem L belongs to the class P , it automatically belongs to the class NP , thus $P \subset NP$. A problem L is *NP-hard* if every instance of any problem $\tilde{L} \in NP$ is polynomial-time reducible to an instance L that when solved produces a solution of the original problem. We will see a detailed example of such polynomial reductions in the next subsection. We say a problem is *NP-complete* if it is *NP-hard* and is also a member of NP . The question whether $P = NP$ remains open, but since it is widely believed that the classes P and NP are different, *NP*-complete problems are the ones most likely not to be in P , i.e., finding an *NP*-complete problem that can be solved in polynomial time would mean that $P = NP$.

The “first” *NP*-Complete problem is the logic *satisfiability problem* or SAT: Input: A Boolean expression f in conjunctive normal form.

Output: YES or NO depending on whether there is an assignment of TRUE or FALSE values to the variables such that all clauses in f are simultaneously satisfied. That is, a truth assignment that makes the formula TRUE. Let us explain what *conjunctive normal form* means. A *literal* in a Boolean formula is an occurrence of a variable, or of its negation. A *clause* is a subset of literals joined by OR connectors. A formula in conjunctive normal form is a formula that is a conjunction of finitely many clauses. Observe that any Boolean formula can be rewritten in conjunctive normal form, but to study the complexity of SAT, we restrict ourselves to conjunctive normal formulas of a certain size.

Example 8.6.1. One simple conjunctive form Boolean expression with

three clauses and four variables is

$$f = (X_1 \vee \neg X_2 \vee X_3) \wedge (\neg X_1 \vee X_4) \wedge (\neg X_1 \vee \neg X_2 \vee \neg X_3 \vee \neg X_4).$$

which has a satisfying truth assignment $X_1 = X_2 = X_4 = \text{TRUE}$, $X_3 = \text{FALSE}$.

On the other hand, the following two logical formulas are not in conjunctive normal form: $\neg(X_1 \vee X_3)$, $X_2 \wedge (X_1 \vee (X_4 \wedge X_2))$. But they can be easily rewritten into conjunctive normal form, respectively, as $\neg X_1 \wedge \neg X_3$ and $X_2 \wedge (X_1 \vee X_4) \wedge (X_1 \wedge X_2)$.

Although there are many other *NP*-complete problems available we focus our attention on SAT and some of its variations. A Boolean formula is in *3-conjunctive normal form* (3-CNF) if each clause has exactly three distinct literals.

Example 8.6.2. Here is one example of a 3-CNF formula $(x_1 \vee \neg x_1 \vee \neg x_2) \wedge (x_3 \vee x_2 \vee x_4) \wedge (\neg x_1 \vee \neg x_3 \vee \neg x_4)$.

The 3-SAT problem is the same as SAT but restricted to 3-CNF formulas. That is, decide if a 3-CNF formula has an assignment of variables such that the Boolean statement evaluates to true. Even this special case of SAT is known to be an *NP*-complete problem (see [134]).

Definition 8.6.3. Let Φ be a Boolean formula in 3-CNF. The associated graph of Φ , $G(\Phi)$, has one vertex for each variable x in Φ and one vertex for each clause C in Φ . There is an edge between a variable-vertex x and a clause-vertex C if and only if x or $\neg x$ appears in C . A formula Φ is called *planar* if and only if its associated graph $G(\Phi)$ is a planar graph. See Figure 8.24 for an example.

Lichtenstein showed in [211] that the 3-SAT remains *NP*-complete even if the input is restricted to planar formulas. This is called the PLANAR-3-SAT problem. More strongly, Mulzer and Rote [235, 236] proved that the PLANAR-1-IN-3-SAT is *NP*-complete. In the PLANAR-1-IN-3-SAT problem, we are given a collection Φ of clauses containing exactly three variables together with a planar embedding of the associated graph $G(\Phi)$. The problem is to decide whether there exists an assignment of values to the variables of Φ such that exactly one literal in each clause is true.

In what follows, we discuss the reduction of SAT and 3-SAT to three different problems about triangulations in dimensions two and three. To help the reader getting acquainted with the essential steps of an *NP*-hardness proof we will discuss most of the details of the proof of the first problem (the easiest to describe) and from then on just highlight the essential geometric building blocks in the other two hardness proofs.

8.6.2 The hardness of the planar constrained triangulation problem

The planar constrained triangulation problem is as follows: Given a planar point configuration \mathbf{A} and a set \mathcal{H} of edges connecting pairs of points in \mathbf{A} , we would like to know whether there is a subset $\mathcal{E} \subset \mathcal{H}$ such that \mathcal{E} defines a triangulation. We will prove now that this problem is *NP*-complete. We

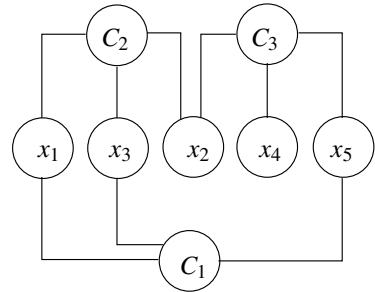


Figure 8.24: Planar embedding of the Boolean formula

$$(x_1 \vee \neg x_3 \vee x_5) \wedge (\neg x_1 \vee x_2 \vee x_3) \wedge (x_2 \vee x_4 \vee \neg x_5).$$

first show that this problem is *NP*-hard and then show that it is in *NP*. Our presentation will follow closely the elegant proof of E. Lloyd [216], which provides a reduction of SAT into the constrained triangulation problem.

The proof is an excellent example of how *NP*-completeness proofs are normally constructed. Since we are modeling logical formulas we need geometric devices that can be “switched” between states that represent TRUE vs. FALSE assignments.

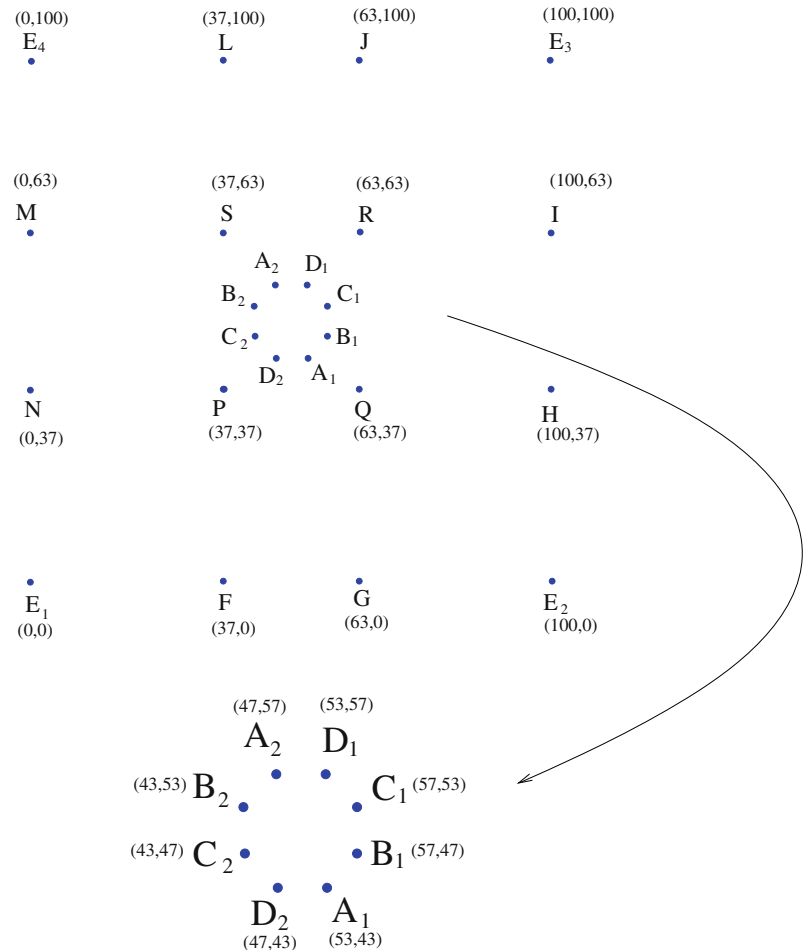


Figure 8.25: A view of the point configuration of a switch.

The switch: The key building block in our construction will be a set of vertices and edges that we call a *switch*. Each switch consists of 24 vertices with very specific integer coordinates and a large set of edges. First, Figure 8.25 describes the coordinates and labeling of the points and should be kept in mind for later reference. Note that opposite points in the central octagon appear with the same letter.

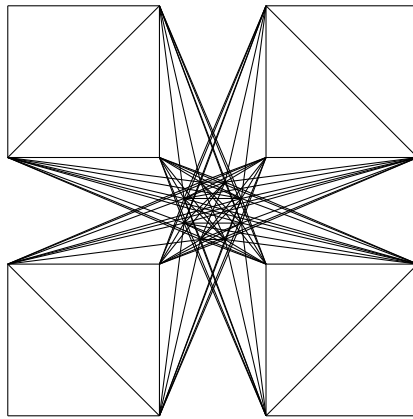


Figure 8.26: A view of the relevant edges of a switch.

Next, Figure 8.26 shows a picture of a switch with all its edges drawn. All switches will be translated copies of each other. The vertices of each switch will be in two important groups (please refer to Figure 8.25):

- *Frame vertices* (points $E_1, E_2, E_3, E_4, F, G, H, I, J, L, M, N, P, Q, R, S$, and
- *Terminals* (points $A_1, A_2, B_1, B_2, C_1, C_2, D_1, D_2$).

The pairs of points (A_1, A_2) , (B_1, B_2) , (C_1, C_2) , (D_1, D_2) will be called *matched pairs of terminals*.

The edges present will also be divided into two kinds (now see Figure 8.26 where all the edges are shown together).

- The *frame edges*: $E_1F, E_1N, FP, FN, NP, E_2G, E_2H, GH, GQ, HQ, E_3I, E_3J, IJ, IR, JR, E_4L, E_4M, LM, LS, MS$) and
- The *non-frame edges*: $FR, GS, HM, HS, IN, IP, JP, LQ, MQ, NR, A_1G, A_1Q, A_1H, A_1I, A_1C_1, A_1A_2, A_1C_2, A_1D_2, A_1P, A_1F, B_1G, B_1Q, B_1H, B_1I, B_1R, B_1L, B_1D_1, B_1A_2, B_1M, B_1C_2, B_1N, B_1D_2, B_1P, B_1F, C_1Q, C_1H, C_1I, C_1R, C_1J, C_1L, C_1S, C_1A_2, C_1M, C_1B_2, C_1N, C_1D_2, C_1F, D_1H, D_1I, D_1R, D_1J, D_1L, D_1S, D_1A_2, D_1B_2, D_1C_2, D_1P, D_1D_2, A_2Q, A_2R, A_2J, A_2L, A_2S, A_2M, A_2N, A_2C_2, B_2H, B_2I, B_2R, B_2J, B_2L, B_2S, B_2M, B_2N, B_2P, B_2G, B_2D_2, C_2Q, C_2H, C_2I, C_2J, C_2S, C_2M, C_2N, C_2P, C_2F, C_2G, D_2G, D_2Q, D_2R, D_2M, D_2N, D_2P, D_2F$.

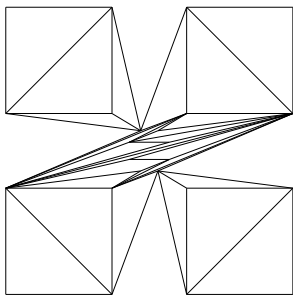


Figure 8.27: A triangulation contained in the switch transmitting information horizontally.

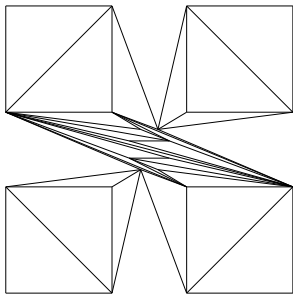


Figure 8.28: A triangulation contained in the switch transmitting information horizontally.

From a Boolean formula in conjunctive normal form C_1, C_2, \dots, C_k in the variables x_1, \dots, x_n we will construct a set of points in the plane and a set of edges (many of them crossing each other). The construction resembles the experience of building an electric circuit of some kind, where wires are attached to electric outlets. We are laying out many switches in a circuit board, and the final structure will be called a *network*. The reader should keep track and check that the point configuration \mathbf{V} and the edge set \mathcal{E} will be constructed in $O(n \cdot k)$ steps.

We will now need to copy the switch we described above many times with identical translation copies. For this reason, we will use superscripts on the labeling of the points to denote points from different switches but that are translations from the original switch. For example, A_2^{ij} is the translation of point A_2 inside the switch S_{ij} . It is worth remarking that the switches are symmetric along the middle vertical and horizontal lines. See Figure 8.26.

Now, consider a finite collection of logical formulas C_1, C_2, \dots, C_k , each of which is disjunction of logical variables. We are going to set up a rectangular array of switches, with one switch for each clause-variable pair. Denote as S_{ij} the switch for variable x_i and clause C_j . Each switch S_{ij} will be of one of three types depending on whether (a) x_i is in C_j , (b) $\neg x_i$ is in C_j , or (c) neither is in C_j . In our construction, adjacent switches will share appropriate frame vertices and point E_1^{ij} , the lower left corner of S_{ij} , will have coordinates $(100 \cdot (i - 1)), 100 \cdot (j - 1))$. At this moment, the set of vertices consists of all vertices in each of the switches and the set of edges \mathcal{E} . The arrangement of switches resembles a grid.

In what follows, we add edges to \mathcal{E} , in addition to those edges coming already associated with each switch. First, we need to add edges that go in between adjacent switches. They will be called *interswitch edges*. Only terminal points will be endpoints of interswitch edges and these nodes will be assigned meanings. The notation $Q \times R$ will denote the set of all edges of the form $[q, r]$ with $q \in Q$ and $r \in R$.

The idea for the vertical interswitch edges is that they carry the information about the truth values of variables in the vertical direction. Vertical switch edges are as follows: For each pair i, j the following edges are placed in \mathcal{E} :

$$(A_2^{ij}, C_1^{ij}) \times (A_1^{i,j+1}, C_2^{i,j+1}) \text{ and } (B_2^{ij}, D_1^{ij}) \times (B_1^{i,j+1}, D_2^{i,j+1}).$$

The $A - C$ edges will carry the “FALSE” value, while the $B - D$ edges transport “TRUE” in the variable x_i .

The horizontal interswitch edges between S_{ij} and $S_{i+1,j}$ are more complicated, they will depend on the type of switch S_{ij} . First, we say S_{ij} is a *neutral switch* if x_i is not C_j and $\neg x_i$ is not in C_j either. The switch S_{ij} is a *positive switch* if x_i is in clause C_j . Finally, S_{ij} is a *negative switch* if $\neg x_i$ is in clause C_j . The interswitch edges will transmit information about the clauses horizontally, and this information will be read from some terminal endpoints. The end points of interswitch edges will be labeled as *clause-FALSE* or *clause-TRUE* depending on whether the message they transmit to us is “clause not satisfied” or “clause satisfied”.

When S_{ij} is neutral, one needs to add the following edges to the set \mathcal{E} :

$$(A_1^{ij}, B_1^{ij}) \times (A_2^{i+1,j}, B_2^{i+1,j}) \text{ and } (C_1^{ij}, D_1^{ij}) \times (C_2^{i+1,j}, D_2^{i+1,j}).$$

In this case we define terminal points A_1, B_1 to be *clause-FALSE* and terminals C_1, D_1 to be *clause-TRUE*. For a positive switch we add to \mathcal{E} the edges

$$(A_1^{ij}) \times (A_2^{i+1,j}, B_2^{i+1,j}) \text{ and } (B_1^{ij}, C_1^{ij}, D_1^{ij}) \times (C_2^{i+1,j}, D_2^{i+1,j}).$$

In this case we define terminal A_1 to be clause-FALSE and the terminals B_1, C_1, D_1 to be clause-TRUE in a positive switch. Then, in the case that we have a negative switch we add to \mathcal{E} the edges

$$(B_1^{ij}) \times (A_2^{i+1,j}, B_2^{i+1,j}) \text{ and } (A_1^{ij}, C_1^{ij}, D_1^{ij}) \times (C_2^{i+1,j}, D_2^{i+1,j}).$$

We say that terminal B_1 is a clause-FALSE point and terminals A_1, C_1, D_1 are clause-TRUE in the negative switch.

Finally, we have to be careful about what happens with the switches on the boundary, namely those switches of the form $S_{1j}, S_{i1}, S_{nj}, S_{ik}$. To insure that the edges of the convex hull of the point configuration \mathbf{V} are included in \mathcal{E} , we modify the switches of these boundary rows and columns of switches. They will have additional *special boundary vertices and edges* following the rules: Each switch S_{1j} , contains a special vertex, T^{1j} with coordinates $(0, 100 \cdot (j-1) + 50)$ and the set of edges $(T^{1j}) \times (M^{1j}, N^{1j}, A_2^{1j}, B_2^{1j})$. Each switch S_{i1} has an special point U_{i1} with coordinates $(100 \cdot (i-1) + 50, 0)$ and the edges $(U^{i1}) \times (F^{i1}, G^{i1}, A_1^{i1}, B_1^{i1}, C_2^{i1}, D_2^{i1})$. A switch of the form S_{nj} contains a special vertex V^{nj} of coordinates $(100n, 100(j-1) + 50)$ and the following edges are added to \mathcal{E} : $(V^{nj}) \times (H^{nj}, I^{nj}, C_1^{nj}, D_1^{nj})$. Finally, for switches of the form S_{ik} we have a special point $W^{ik} = (100(i-1) + 50, 100k)$ as well as new edges $(W^{ik}) \times (J^{ik}, L^{ik}, A_2^{ik}, B_2^{ik}, C_1^{ik}, D_1^{ik})$. Additionally, based on the type of the switch S_{nj} (neutral, positive, or negative), we include the following edges: For positive S_{nj} , we add edge V^{nj}, B_1^{nj} , and if the switch is negative, we add V_{nj}, A_1^{nj} .

The *frame* consists of the frame edges of each switch in the network as well as edges, which have a frame vertex as one endpoint and a special boundary vertex as the other end point. Note that this way, no edge with a terminal as an endpoint is included in the frame.

From a triangulation recover a Boolean assignment and vice versa: Suppose \mathcal{T} is a triangulation of the point configuration \mathbf{V} that uses only edges of \mathcal{E} . We need to prove that from \mathcal{T} we can recover a TRUE-FALSE value assignment to the variables x_1, \dots, x_n that makes the logical formula TRUE. First of all, note that the frame is included in \mathcal{E} , but no edge intersects any of its edges. Thus, any triangulation \mathcal{T} of \mathbf{V} using edges in \mathcal{E} must use all edges in the frame. The non-frame edges in \mathcal{T} must complete the triangulation of each switch in the network, and connect adjacent switches together too.

In any triangulation of the array of switches we note there will be two “streams” of information passing through it. To fully understand this we

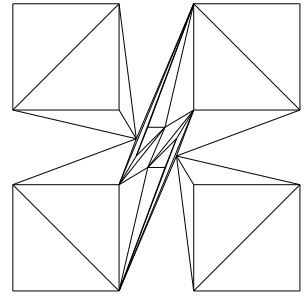


Figure 8.29: A triangulation contained in the switch transmitting information vertically.

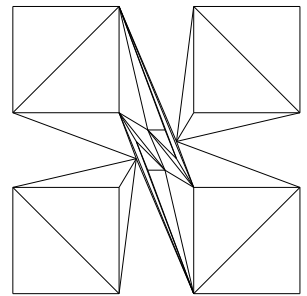


Figure 8.30: A triangulation contained in the switch transmitting information vertically.

recommend the reader takes a look at the pair of Figures 8.27 and 8.28 as well as the symmetric Figures 8.29 and 8.30. Through each switch one stream flows vertically and another horizontally. The vertical stream flows through S_{ij} carrying a truth assignment for variable x_i . For each variable x_i its truth assignment must be spread north through each switch $S_{i,j}$, with $1 \leq j \leq k$. The horizontal stream of information leaving switch S_{ij} on the right indicates whether or not clause C_j is satisfied by the assignment of truth values to the variables x_1, x_2, \dots, x_n . One key point is that the construction forces the stream of information flowing into the left side of a switch S_{ij} to be “not satisfied” and the information flowing out of the right side to be “satisfied”.

Inside each switch S_{ij} , a terminal A is *east-connected* in triangulation \mathcal{T} if there exists an edge AB that properly intersects the edge I^{ij}, H^{ij} . Since the edge I^{ij}, H^{ij} is not in \mathcal{E} , and thus not in \mathcal{T} , there must be an edge of \mathcal{T} which properly intersects it. By construction, each such edge has a terminal of S_{ij} as an endpoint. This means that there must be at least one east-connected terminal per switch. We have the same situation for *west-connected*, *north-connected*, and *south-connected* terminals. A *connected terminal* will be one that is connected in either direction. From the construction, the reader can verify the following lemma

Lemma 8.6.4. *Given any triangulation \mathcal{T} of the point configuration \mathbf{V} that uses only edges from the set \mathcal{E} there are exactly two connected terminals in each switch and furthermore for each switch those two terminals are a matched pair of terminals.*

The following corollary follows from Lemma 8.6.4 and the construction:

Corollary 8.6.5. *If S_1 and S_2 are adjacent switches in the network and \mathcal{T} is a triangulation of \mathbf{V} using only edges from the set \mathcal{E} , then there is exactly one interswitch edge in \mathcal{T} whose endpoints are a terminal in S_1 and a terminal in S_2 .*

Now we are ready to make an assignment of TRUE or FALSE to each variable from the edges in the triangulation.

Theorem 8.6.6. *Given the triangulation \mathcal{T} of \mathbf{V} , set variable x_i to be TRUE if the south connected terminal in S_{i1} is B_1 or D_2 , else set x_i to FALSE if the south-connected terminal in S_{i1} is A_1 or C_2 . With this assignment each clause C_j is satisfied*

Proof. It follows from the construction, Lemma 8.6.4, Corollary 8.6.5 that in any given triangulation of \mathbf{V} for each j there is exists an i between 1 and n such that the east-connected terminal of S_{ij} is either A_1 or B_1 and it is clause-TRUE. Similarly we also have that in any triangulation \mathbf{V} , for each i , either the connected terminals are B 's and D 's for all S_{ij} , or the connected terminals are A 's and C 's for all S_{ij} .

In the case that the connected terminal in switch S_{ij} is B_1 , since it is clause-TRUE, this must be a positive switch, thus x_i is in C_j . But then B_1 is the south-connected terminal. This mean that the south-connected termina

of S_{i1} is B_1 or D_2 . Then by our assignment x_i is TRUE and thus C_j is a satisfied clause. Similarly, in the case that the connected terminal in S_{ij} is A_1 , since it is clause-TRUE this must be a negative switch. Thus $\neg x_i$ is in C_j . But then A_1 is the south connected terminal. Hence the south-connected terminal of S_{i1} is A_1 or C_2 . Then, by our assignment x_i is false and C_j is satisfied. \square

Now we describe what is needed to go from a Boolean assignment to a proper triangulation (i.e., which edges will be selected from those in \mathcal{E}). Assume now that we have a truth assignment to x_1, \dots, x_n such that each of the clauses C_1, \dots, C_k is satisfied. We will show that there is a subset of the edges \mathcal{T} of \mathcal{E} that defines a triangulation.

To begin we include in \mathcal{T} all edges that form the frame. No edge of \mathcal{E} intersects the edges of \mathcal{T} so far. For each clause, C_j , we define μ_j to be the smallest index i such that either x_i or $\neg x_i$ are in C_j and the truth assignment H_i to x_i causes C_j to be satisfied. From this we triangulate the switch S_{ij} as follows: For $i \leq \mu_j$, if H_i is true, then S_{ij} is a triangulated using the triangulation depicted in Figure 8.29. Otherwise use the triangulation in Figure 8.27. For $i > \mu_j$, if H_i is true, then S_{ij} is triangulated using the triangulation depicted in Figure 8.28, otherwise, use the triangulation in Figure 8.30.

Some of the terminal points will be exposed or reachable from outside the switch S_{ij} after this construction and they will be used to connect adjacent switches. From the construction so far, for each pair i, j with $1 \leq i \leq n$ and $1 \leq j \leq k - 1$, there is an edge in \mathcal{E} whose endpoints are the north-exposed of terminal point of S_{ij} and the south-exposed terminal of $S_{i,j+1}$. Similarly one can prove (left as exercise), that, for each pair i, j with $1 \leq i \leq n$ and $1 \leq j \leq k - 1$, there is an edge in \mathcal{E} whose endpoints are the east-exposed terminal point of S_{ij} and the west-exposed terminal point of $S_{i+1,j}$.

Thus, for each pair of adjacent switches there is an edge of \mathcal{E} whose endpoints are the appropriate exposed points of these switches. We add those edges to the current \mathcal{E} . We can also verify what happens to switches on the boundary, and their connection to the special boundary vertices U^{il} , W^{ik} , T^{1j} , and V^{nj} , but it is easy to see those available edges in \mathcal{E} suffice to form a triangulation. \mathcal{T} will contain the edges in the frame and the edges in a triangulation of each switch in the network.

Verifying the problem belongs to NP: Consider an instance of the constrained triangulation problem, which is specified by the sets of vertices \mathbf{V} and edges \mathcal{E} . We know that a set of edges $\mathcal{T} \subset \mathcal{E}$ is a triangulation if and only if no two edges cross and the set of edges is maximal with this property (see Lemma 3.1.2). Hence, we have to check that these two conditions hold. The first one can be verified pair by pair, in $O(|\mathcal{T}|^2)$ and testing for the second property can be done in no more than $O(|\mathbf{V}|^2|\mathcal{T}|)$. Therefore the problem is in NP . This final step completes a proof of the next theorem.

Theorem 8.6.7. *The following decision problem is NP-complete:*

Input: A point configuration \mathbf{V} in the plane and a set \mathcal{E} of edges connecting certain pairs

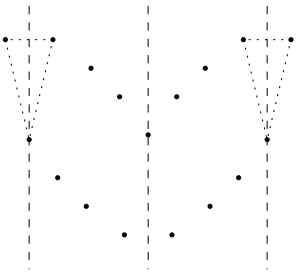


Figure 8.31: The points of a wire block.

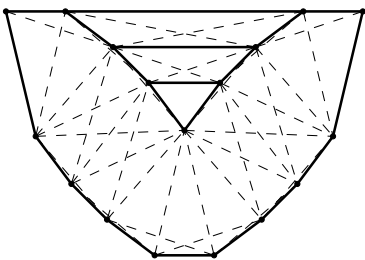


Figure 8.32: The LMT-skeleton of a wire piece.
The solid edges are skeleton edges, dashed edges are candidate edges.

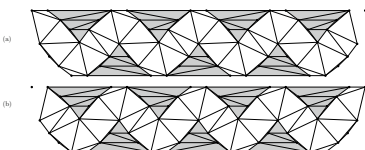


Figure 8.33: The two states of a wire piece.

Problem: Is there a triangulation of \mathbf{V} using only edges from \mathcal{E} ?

Finally, it is worth mentioning that, based on Lloyd's result, Heath and Pemmaraju [156] proved that the constrained problem of computing a minimum weight triangulation, from a pre-specified set of edges (that forms a triangulation) is *NP*-hard.

8.6.3 Hardness of minimum length triangulations in the plane

After almost 30 years in the famous (and short) list of open problems of undetermined complexity in Garey and Johnson's book on computational complexity [134], the question what is the complexity of finding a minimum length triangulation was only recently settled by Mulzer and Rote [235, 236]. They have proved the problem is *NP*-hard. We will sketch now a few key geometric ideas of this major breakthrough.

In their solution, Mulzer and Rote used the LMT skeleton, which we introduced in Chapter 3 (see Definition 3.2.14). The *NP*-complete problem PLANAR-1-IN-3-SAT is then reduced to the minimum length triangulation problem using some "wire gadgets" to simulate Boolean formulas. We focus now on the wires, the main geometric gadgets of the proof.

The wires were first constructed by Beirouti and Snoeyink from their work on the LMT algorithm [40]. They are extended arbitrarily by mirroring along the dashed lines of the basic point set shown in Figure 8.31. One can find, via direct calculation, the LMT-skeleton of a wire piece, as is shown in Figure 8.32. Because of their properties, wires can be used as building blocks. First of all, they provide a mean to transport information across the plane because there are only *two* possible MLT triangulations of a wire piece (e.g., TRUE or FALSE values). See Figure 8.33. The wires can be elongated and bended with great flexibility, for example, in Figure 8.34, we see a wire can be curved to make turns of ninety degrees. The wires can then be used to create variables, clauses and connections between them so they can represent a PLANAR-1-IN-3-SAT instance.

Let us look at variables. The main block stores a TRUE or FALSE state. This is shown in Figure 8.35, this storage loop has exactly two optimal triangulations. This kind of gadgets can then be glued together to create variables and clauses.

Glueing together the gadgets made of bent wires one can represent a Boolean Formula: First Mulzer and Rote showed that an embedding of a PLANAR-1-IN-3-SAT instance Φ can be constructed on a grid of size $O(n) \times O(n)$, where n is the size of the input. They showed that no negations of variables are necessary. Edges, variables, and clauses of Φ are replaced by the appropriate geometric gadgets yielding a point set S . The boundaries of all wire pieces belong to the MLT of S . The faces outside the wires are simple polygons and can be triangulated using Klincsek's dynamic programming ([193], see also Proposition 3.2.10 in Chapter 3). Via computation, for each gadget we know the "ideal triangulation". Adding this to the face calculations we have a target weight W . Φ is 1-IN-3 satisfiable if and only if the MWT of S is W .

To conclude, let us comment that their proof only shows that the problem is *NP*-hard, but it is not known whether it is in *NP*. This is due to the difficulty of checking an identity between sums of radicals (this is, after all,

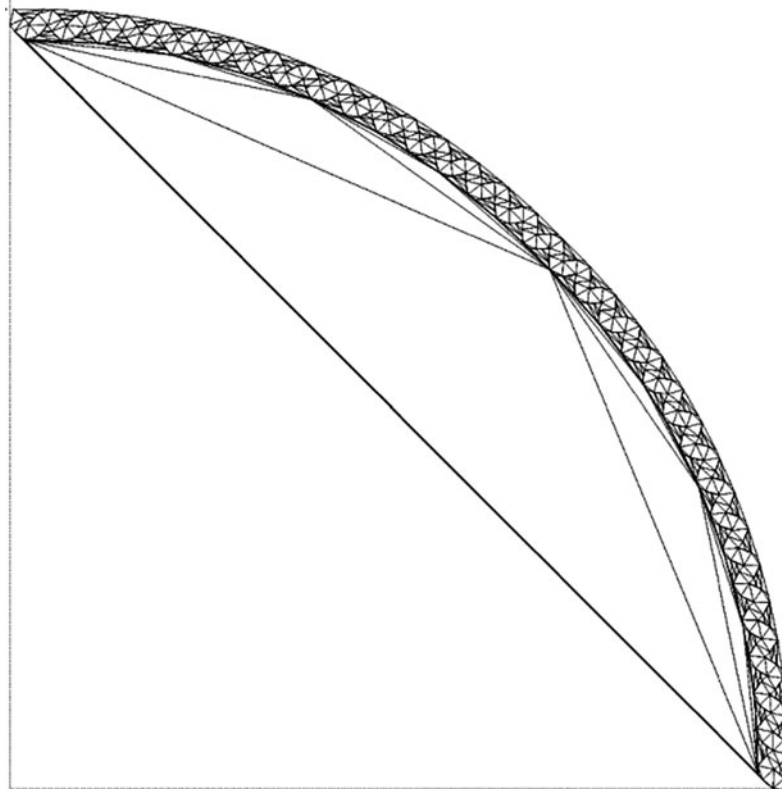


Figure 8.34: A wire can be curved to make 90° turns.

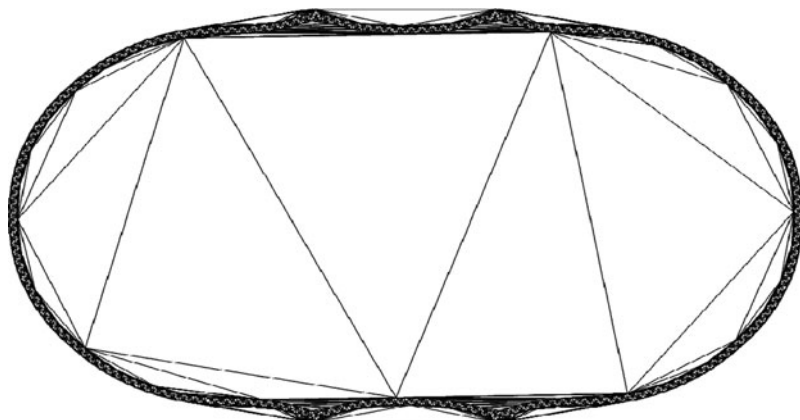


Figure 8.35: A gadget which has two uniform minimum triangulations, hence two states.

the Euclidean distance). The other interesting point is that, to verify that

some of the gadgets have indeed the desired properties, it was necessary to use computers. See [236] for details and more history of the MLT problem.

As of today there are a few known polynomial-time instances of the MLT problem, besides Klincsek's algorithm for simple polygons. It was proved in [13] that when the points are arranged in a constant number of nested convex polygons one can also provide an efficient algorithm. More recently Hoffmann and Okamoto [163] have generalized Klincsek's result by showing that when the number of points in the interior of the convex hull is assumed to be constant, there is a polynomial time solution. More strongly they can prove this is also the case when only a logarithm of the total points lies inside. Another curiosities is that finding a *maximal length* triangulation does not seem to be any easier than the minimal length triangulation, but not much work exist about this topic, see [331].

In this chapter, we concentrated mostly on how to find *exact* solutions to the MLT problem but one can instead try to *approximate* the optimal solution or to look at its average behavior. Some authors have tried to look at average or probabilistic behavior of the problem. We can mention Yukich's work [336], who has studied the asymptotic behavior, as the number of points increases, of the total edge length of the minimal triangulation for points which are independently and identically distributed on the unit square. He showed that, asymptotically, the length of the MWT is equal to a constant times the length of the optimal traveling salesman tour. On the other hand, Lingas [213] proved that for uniformly distributed points both the Delaunay and the greedy triangulations yield satisfactory approximations. Some of the first approximation algorithms were those by Lingas [214], Plaisted and Hong [255]. The idea to find a good approximation is again to partition the convex hull of the points as the union of polygons, not necessarily convex, and then apply Klincsek's algorithm to fill in the empty holes. To construct such a partition, one can use edges coming from the Greedy triangulation (or similarly from the Delaunay triangulation).

A “dynamic” variation of the minimum length triangulation problem happens when one allows the freedom of introducing new points at will in the calculations, the so called *Steiner points*. Can these extra “free” points reduce the length of the minimum length of a triangulation? Eppstein has showed that the weight of the minimum length Steiner triangulation (MLST) for an original point configuration with n points may be $\Omega(n)$ times *smaller* than the true length of the MLT (adding points actually decreases the length!). See the example in Figure 8.36. Although the MLST can be approximated to a constant factor in polynomial time [122], we still do not know whether a MLST can be computed *exactly* in polynomial time. For a long time, it was not known whether a polynomial time algorithm that always produces a triangulation whose length is within a constant factor from the minimum length was possible. This problem was solved by Lev-copoulos and Krznaric [209] using a slight modification of an $O(n \log n)$ algorithm for the greedy triangulation.

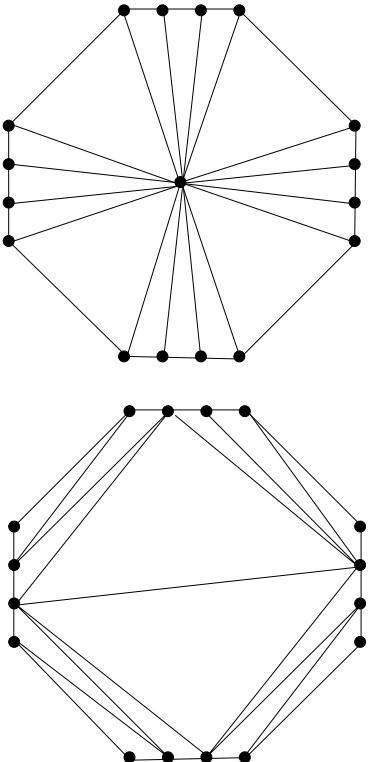


Figure 8.36: The effect of Steiner points, length of minimal triangulation decreases. The points are symmetrically placed on the sides of a square. The top triangulation is shorter even though it has one more point in the center than the bottom triangulation. This cute example is due to Cindy Traub.

8.6.4 Hardness of minimal size triangulations of convex polytopes

In this section, we focus on the problem of finding triangulations that minimize or maximize the size (i.e., the number of top-dimensional simplices) while assuming the points are the vertices of a convex polytope. What makes this problem so challenging is that even though the points are in convex position, it is not a combinatorial problem as it was for polygons (e.g., Klincsek's algorithm from Chapter 3, Proposition 3.2.10, also mentioned in the previous section). It is highly dependent on the coordinates of the points. We first show that the size of minimal or maximal triangulations does not depend on the face lattice of the polytope alone, but that the coordinates influence the outcome too. This is even the case when the polyhedron is simplicial.

The simplest example is given by the combinatorial 3-polytope with 10 vertices shown in Figure 8.37. If the points A, B, C, D are coplanar then the edges AB or CD cannot be in a triangulation at the same time. Any triangulation has at least 10 simplices. The reader can check that, on the other hand, one can arrange the z -coordinates of A, B, C and D in such a way that the edge AB is above the edge CD . This way it has a unique minimal triangulation with 9 simplices.

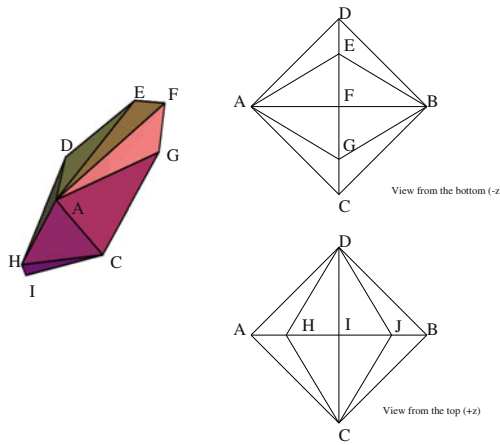


Figure 8.37: A view of the polyhedron with variable minimal triangulation.

We saw in Chapter 2, Theorem 2.6.1, that the size of a triangulation of a convex d -polytope P with n vertices, lies between $n - d$ and an upper bound of $O(n^{\lfloor(d+1)/2\rfloor})$. Since the size of 2-dimensional triangulations is settled easily by Euler's formula, the next frontier is to say something about the size of triangulations in 3-dimensions. Again, remember that in this section we assume the points are in convex position.

Proposition 8.6.8. *Any convex 3-polytope P with n vertices can be triangulated in $O(n \log(n))$ time with a triangulation that has at most $2n - 7$ tetrahedra. Hence, for 3-polytopes, the size of minimal triangulation is between $n - 3$ and $2n - 7$. The upper bound can be improved when $n \geq 12$ to be $2n - 10$.*

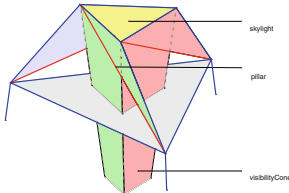


Figure 8.38: The visibility cone of Schönhardt polytope with the skylight and their bounding planes marked.

Proof. We have seen in Chapter 2 that all triangulations must have at least $n - 3$ tetrahedra. For the upper bound, we claim this is achieved by a pulling triangulation. Find a vertex v on the boundary of P with highest degree. This will be the last vertex pulled in the polytope. Pull all others in an arbitrary order; this induces a triangulation of the facets of \mathbf{P} that do not touch v . By Euler's relation, there are $2n - 4 - \deg(v)$ triangles on the boundary which will be turned into tetrahedra once we pull v to cover \mathbf{P} . Finally note that $2n - 4 - \deg(v) \leq 2n - 7$. If $n \geq 12$, the maximum degree of a vertex is at least 6, thus we have the improvement. \square

As a consequence, we know that minimum size triangulations of convex 3-polytopes with n vertices have size between $n - 3$ and $2n - 7$. But presented with a particular 3-polytope, *how could we find a small triangulation, e.g., one of size less than $2n - 7$?* And what is the computational complexity of finding a small triangulation? These questions were presented in 1992 in the survey [45]. The answer was found in [43, 44]:

Theorem 8.6.9. *The following problem is NP-complete and it has a polynomial transformation to the SAT problem:*

Input: Vertices of a convex 3-polytope \mathbf{P} , and a number k .

Problem: Is there a triangulation of \mathbf{P} of size $\leq k$?

The transformation we present will map any Boolean formula f into a certain convex 3-polytope \mathbf{P}_f and an integer k_f such that f is satisfiable precisely when \mathbf{P}_f can be triangulated with no more than k_f tetrahedra. The proof is long (see [44] for all details), but we will at least sketch the proof trying to emphasize the main geometric and combinatorial ideas.

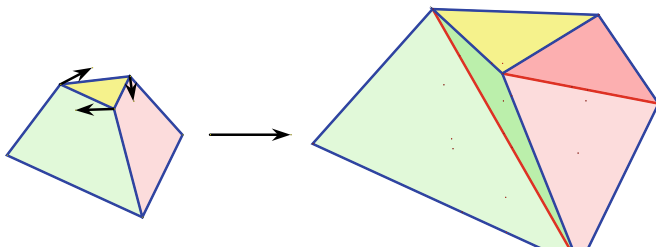


Figure 8.39: Schönhardt's polytope as a deformation of a prism.

As we did in the previous subsection, we need to build gadgets that encode Boolean formulas. Perhaps the most important object our old friend from Chapter 3, Example 3.6.1, the Schönhardt's polytope [290]. Recall this is a non-convex polytope which, roughly speaking, is obtained by twisting the top of a normal triangular prism to create three non-convexities along the former three diagonals of the prism. See Figure 8.39 for another view of the object. Its fundamental property is that its interior cannot be triangulated without first adding at least one extra point. This extra auxiliary point is what we will use to create Boolean switches. Of course, the

seventh point p needed for triangulation cannot really be placed at random; if one traces segments from p to the top or bottom triangle of Schönhardt's polytope, which we call the *skylight*, its points must be visible from p . This is determined by three of the diagonals of the Schönhardt polytope and the chosen skylight. See Figure 8.38.

Our plan is to glue Schönhardt polytopes along the bottom face of a bigger *frame polytope*. This will momentarily give us a non-convex polytope simply because the Schönhardt's are non-convex. Recall that each Schönhardt polytope has a skylight. Triangulating this non-convex polytope is only possible if there are vertices that are visible to each of the skylights; they must be in the visibility cones. So two main issues are (1) how to patch the non-convexities of the glued Schönhardt's, and (2) how to design the frame to satisfy the visibility conditions. We tackle problem (1) with the following lemma [42]:

Lemma 8.6.10. *Let \mathbf{P} be a convex 3-polytope with n vertices. Assume \mathbf{P} satisfies the following two conditions depicted in Figure 8.41:*

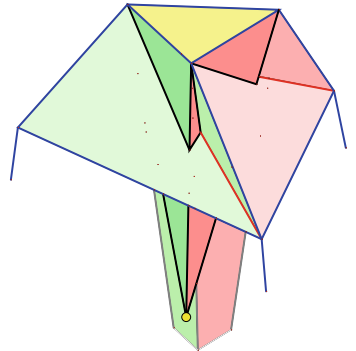


Figure 8.40: A point (tiny circle) which is not inside the visibility cone cannot be used to triangulate since it cannot see all points of the skylight.

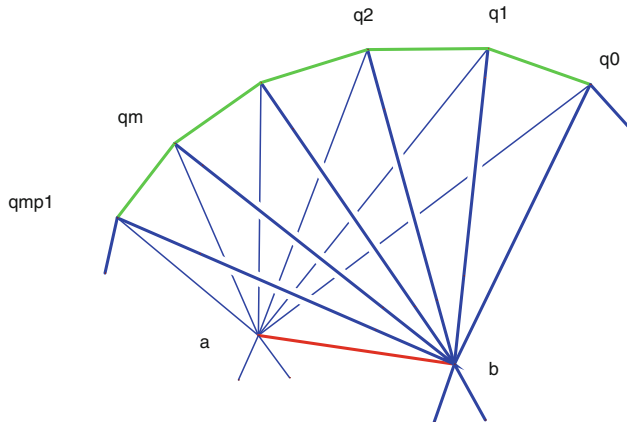


Figure 8.41: A chain of edges connected to two points (a, b) give a chain structure.

1. *The facets of \mathbf{P} contain the triangles $[a, q_i, q_{i+1}]$ and $[b, q_i, q_{i+1}]$ (for $i = 0, \dots, m$); and*
2. *The interior segment $[a, b]$ does not intersect $\text{conv}(\{q_0, \dots, q_{m+1}\})$.*

Then for each triangulation \mathcal{T} of \mathbf{P} that does not use the interior edge $[a, b]$, the number of simplices of T is greater than or equal to $n + m - 3$.

Proof. Since $\text{conv}\{q_0, q_{m+1}\}$ is in the interior of \mathbf{P} , we obtain the following simple fact: For all $|i - j| \geq 2$, if $q_i q_j$ is an edge of a triangulation, it will be also an interior edge. The proof of the lemma proceeds by induction on m . The lemma is clearly true for $m = 1$. Call (*) the assumption that all vertices q_i , with $1 \leq i \leq m$, are incident to at least one interior edge

of the triangulation \mathcal{T} . We now show how to invoke induction in case (*) does not hold: A vertex q_i untouched by an interior edge belongs to the tetrahedra $\sigma_{i,a} = (a, q_{i-1}, q_i, q_{i+1})$ and $\sigma_{i,b} = (b, q_{i-1}, q_i, q_{i+1})$. This is because the triangle (a, q_i, q_{i+1}) is in some simplex, and if the fourth point is some other vertex besides q_{i-1} or b we have an interior edge touching q_i . Furthermore, the fourth point cannot be b since in this case the edge ab would be present. By chopping off these two tetrahedra together with the vertex q_i (i.e., considering the convex hull of all of \mathbf{P} 's vertices except q_i) we can apply induction to guarantee that the remaining triangulation $\mathcal{T} \setminus \sigma_{i,a}, \sigma_{i,b}$ has at least $m - 1$ interior edges. Together with the edge $q_{i-1}q_{i+1}$ they amount for m interior edges in \mathcal{T} .

If (*) holds, we will show the claim directly; we set up a one-to-one map from the set $\{q_1, \dots, q_m\}$ to a subset of the interior edges that touch them: The vertices q_i come along a polygonal curve in a canonical order which is reflected by their indices. We mark or orient the interior edges q_iv that touch a vertex q_i as follows: If $v \notin \{q_0, \dots, q_{m+1}\}$, we call the edge q_iv *special*, otherwise we orient it from smaller to larger index. For the vertices q_i with special edges incident to them, we map q_i to one of those special edges. If a vertex q_i has no special edges, but has outgoing interior edges, we map it to the outgoing edge q_iq_k with the smallest index k . We are left with the case of those vertices q_i that have only incoming interior edges incident to q_i . Consider the triangle (a, q_i, q_{i+1}) . It has to be in some tetrahedron of \mathcal{T} whose fourth point is bound to be a q_{j_a} with $j_a < i$. Likewise (b, q_i, q_{i+1}) is in a tetrahedron with fourth point q_{j_b} with $j_b < i$. If both $j_a = j_b = i - 1$, there can be no interior edges incident to q_i (see above), a contradiction to (*). Let j be any of j_a, j_b such that $j < i - 1$. Map q_i to q_jq_{i+1} .

We claim that the given map is one-to-one. If some vertex q_i maps to the special edge q_jv , then necessarily $i = j$. There are potentially two vertices that can be mapped to an interior edge q_jq_k with $j < k$: q_j when q_jq_k is the chosen outgoing edge of q_j and q_{k-1} , in case q_{k-1} has only incoming edges. In the latter case, one of the tetrahedra (a, q_j, q_{k-1}, q_k) and (b, q_j, q_{k-1}, q_k) has to be in the triangulation, and q_j will be mapped to the smaller indexed edge q_jq_{k-1} . This is an interior edge since $j < k - 2$, so q_j cannot also be mapped to q_jq_k . The injectivity of the map is proven. \square

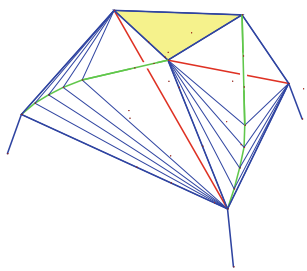


Figure 8.42: A cupola.

The moral of this lemma is that, if this special chain structure is present on the polytope, all the small triangulations must necessarily use the edge $[a, b]$. Otherwise the size of the triangulations not using $[a, b]$ grows with the length of the chain. We next patch the non-convex parts of the Schönhardt polytopes we have glued to the frame polytope. We call these new subpolytopes *cupolas*. See Figure 8.42. More precisely, a cupola is what you obtain when you attach the vertex-edge chains of Lemma 8.6.10 to a Schönhardt polytope in opposite direction to the pillars, with the vertices of the chain low right above the bottom face, m of vertices are in each chain, for m sufficiently large. Thus the pillars of the Schönhardt polytopes will work as the edges $[a, b]$ in Lemma 8.6.10. Hence:

Corollary 8.6.11. *Let \mathbf{P} be a frame polytope and C a cupola. In a triangulation*

lation \mathcal{T} of $\mathbf{P} \cup C$, let v be the auxiliary vertex needed for triangulating the skylight of C . If v is not in C 's visibility cone, then $|\mathcal{T}| \geq \#\text{vert}(\mathbf{P}) + 3m + m$.

If v is in the visibility cone, it is conceivable that order of $3m + \text{constant}$ many tetrahedra will suffice.

Now let us say a few words about the frame polytope where we are gluing the cupolas (starting by gluing the Schönhardt polytopes and patching the vertex-chain structure to make them convex). The shape will be of a wedge, as an orange wedge, where there will be special facets for each Boolean variable and each Boolean clause. Without more detail, we look at an example. See Figure 8.43.

$$\begin{aligned} f = & (X_1 \vee \neg X_2 \vee X_3) \wedge (\neg X_1 \vee X_4) \\ & \wedge (\neg X_1 \vee X_2 \vee \neg X_3 \vee \neg X_4) \end{aligned} \quad (8.20)$$

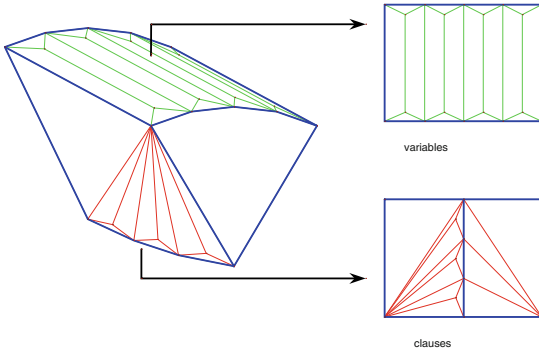


Figure 8.43: an example of frame polytope corresponding to Boolean formula 8.20.

We conclude this section with two remarks: as a corollary of Theorem 8.6.9, the problem of finding minimum size triangulations of convex d -polytopes is NP -hard. To see this, simply build pyramids over the constructed polytope. The same hardness property extends to the minimal size triangulations of the boundary of a convex polytope. In work by Chin et al. [80], there is a discussion on how to give an approximation to the minimum size triangulation of a convex 3-polytope of ratio $2 - \Omega(1/\sqrt{n})$. In fact, given only the face lattice of the polytope, one cannot do better. It follows easily from the theory of universal polytopes that when the point set has $d+2$ or $d+3$ points, finding the minimal triangulation can be done in polynomial time.

Exercises

Exercise 8.1. Determine all the values of the chirotope for the mother-of-all-examples, as presented in Example 8.1.2. Then, apply Theorem 8.1.6 and Theorem 8.1.8 to recover all cocircuits and circuits.

Exercise 8.2. Consider the following rank 3 chirotope on four points: $+-+ -$ (where the bases are listed lexicographically). Find all the circuits and all cocircuits. Can you find a point configuration with precisely that chirotope?

Once you finish the above challenge, solve the same challenges for the following rank 3 chirotope on seven points:

$$+++++0++--++0-----++----++00++-$$

Here again the list of signs refers to bases in lexicographic order, e.g., $\chi(123) = +$, $\chi(124) = +$, ..., $\chi(456) = 0$, $\chi(457) = +$, $\chi(467) = +$, and $\chi(567) = -$.

Exercise 8.3. Prove Formula 8.2 for sums of binomial coefficients.

Exercise 8.4. Finish the calculations of Example 8.2.4 and show that regularity depends on the actual coordinates and not on the combinatorial type of the triangulation.

Exercise 8.5. Familiarize yourself with TOPCOM, software for computing triangulations and secondary polytopes.

Exercise 8.6. Find a complete description of the universal polytopes of a planar point set with 5 points in the boundary and a sixth the barycenter of the others.

Exercise 8.7. Can a simplex of the 3-cube ever have exterior faces in parallel facets of the cube? How about the 4-cube?

Exercise 8.8. Find the graph of the universal polytope of the point configuration whose points are the vertices of the product of a segment and a simplex.

Exercise 8.9. Show that the universal polytope of a point configuration in \mathbb{R}^d with up to $d + 3$ points is a simplex.

Exercise 8.10. Find an algorithm to compute the triangulation of a set of points in the plane that minimizes the maximum edge length.

Exercise 8.11. Find your own planar point configuration for which there is a Steiner point that decreases the length of a minimal triangulation.

Exercise 8.12. Given a point configuration \mathbf{A} in the plane, consider the problem of finding a non-trivial subdivision of \mathbf{A} , with each point of \mathbf{A} appearing as a vertex, which is minimal under inclusion of edge sets. In other words, these correspond to coarsest subdivisions of \mathbf{A} . Can you give a lower bound on the number of pieces you will need if there are i interior points?

Exercise 8.13. Using the fact that it is NP -hard to minimally partition a polygon with holes (see [212] for the proof), prove that it is an NP -hard problem to find a minimal partition of simple non-convex 3-d polyhedra into convex pieces.

Exercise 8.14. (Open) It is easy to see that the largest size of a triangulation of the regular 3-cube is 6, on the other hand, one can find a combinatorial 3-cube where the largest number of tetrahedra is seven. See Figure 8.44.

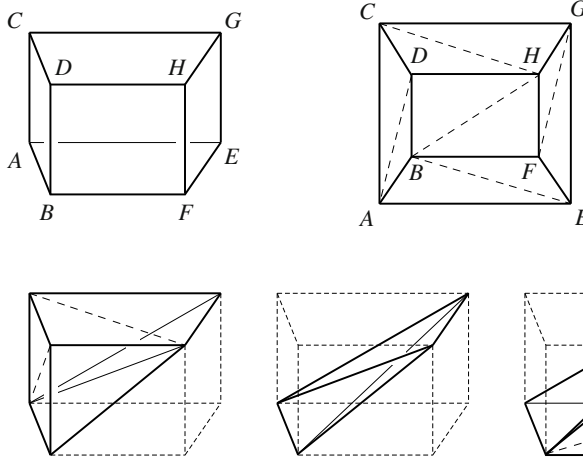


Figure 8.44: The maximal triangulation depends on the coordinates of cube, not just its face lattice.

What is the largest possible number of simplices in a triangulation of some combinatorial d -dimensional cube? This is a very “generic” cube!

Exercise 8.15. (Open) Suppose the input polytopes are given in terms of their vertices. How hard is it to compute the size of the largest triangulation in that case? (*Hint:* The construction in [109] will not help you).

Exercise 8.16. (Open) What is the computational complexity of *counting* all triangulations of a point configuration? It has been conjectured that even for fixed dimension two the problem is $\#P$ -hard.

Exercise 8.17. (Open) Recall that for a Let \mathbf{P} be an n -dimensional polytope. A *dissection* is a finite set \mathcal{D} of n -simplices inside \mathbf{P} that satisfies $\bigcup_{\mathbf{T} \in \mathcal{D}} \mathbf{T} = \mathbf{P}$ and $\dim(\mathbf{T}_1 \cap \mathbf{T}_2) < n$ for any $\mathbf{T}_1, \mathbf{T}_2 \in \mathcal{D}$.

It is known that dissections can be smaller than the smallest of triangulations (see [42]). Do high dimensional cubes admit dissections with fewer simplices than are needed in a triangulation? The minimal size dissections of dimensions three and four are the same as minimal triangulations. Beyond dimension four, not much is known.

Exercise 8.18. (Open) A *simplicial cover* of a n -dimensional polytope is a finite set \mathcal{D} of n -simplices inside \mathbf{P} that satisfies $\bigcup_{\mathbf{T} \in \mathcal{D}} \mathbf{T} = \mathbf{P}$. This is an even weaker notion than dissection.

Is there a cover of the 5-cube strictly smaller than its minimal triangulation? Is there a d -cube for which using a point in the interior in the triangulation produces a smaller triangulation? (See [57] for more information.)

Exercise 8.19. (Open) Find a full inequality description of the universal polytope of an interesting family of point sets (e.g., cyclic polytopes, product of simplices).

Exercise 8.20. (Open) We saw that Klincsek's dynamic programming algorithm finds the minimum length triangulation of a convex n -gon in $O(n^3)$ time. Can one improve this complexity?

Exercise 8.21. (Open) Related to the possible sizes of triangulations of point sets in \mathbb{R}^3 . Let s_{\min} and s_{\max} be the sizes of minimal and maximal triangulations of a convex 3-polytope, is it true that for any number K , $s_{\min} < K < s_{\max}$ there is a triangulation with K tetrahedra?

Exercise 8.22. (Open) Let \mathbf{P} be a polytope in \mathbb{R}^3 . Let $\sigma(\mathbf{P})$ be the minimum number of tetrahedra required to decompose \mathbf{P} and $\tau(\mathbf{P})$ be the minimum number of tetrahedra used in a triangulation of \mathbf{P} . Clearly $\sigma(\mathbf{P}) \leq \tau(\mathbf{P})$ and we have seen the inequality can be strict. Is there a constant c such that $\tau(\mathbf{P}) \leq c \cdot \sigma(\mathbf{P})$?

9

Further Topics

In this chapter, we present a selection of topics that further show the beauty, potential, and richness of this field:

To begin, in Section 9.1, we will see how the *fiber polytope* construction by Billera and Sturmfels provides a unified view on seemingly different phenomena and generalizes the notion of secondary polytope. Next, in Section 9.2, we discuss what the *Cayley trick*—originally a method in sparse elimination theory of equations—means in the context of polyhedral subdivisions, and we illustrate its power with one nice application. Section 9.3 introduces the active field of *lattice triangulations*, which is related to lattice points in polytopes. These are important objects, as they correspond to solutions of integer linear programs and have fascinating connections to algebraic geometry and number theory. Section 9.4 discusses further the fascinating connections of triangulations and algebra. We show how to encode triangulations through Gröbner bases and connections to toric ideals. To conclude the chapter, in Section 9.5, we show how triangulations, as the duals of polyhedral complexes, can be used to answer topological questions such as polytopality of spheres or to offer a new look at face numbers of polytopes.

9.1 Fiber polytopes

Here we start by discussing three interesting phenomena in polytope theory that do not seem to be related at first glance. Then we will learn about a beautiful construction which shows that they are all incarnations of the very same principle: fiber polytopes, which generalize secondary polytopes.

9.1.1 Monotone paths

Let \mathbf{P} be a d -polytope in \mathbb{R}^d , and consider some linear functional $\psi : \mathbb{R}^d \rightarrow \mathbb{R}$. Assume ψ is generic on each edge of \mathbf{P} , i.e., $\psi(v) \neq \psi(w)$ for each edge vw of \mathbf{P} . This situation is exactly what we encounter in linear programming, where we want to find a maximal or a minimal vertex w.r.t. ψ . Since ψ is generic on edges, there is a unique optimal vertex, of course (see Figure 9.1 for the setup).

One famous method to find, say, the maximal vertex in \mathbf{P} , is the *simplex algorithm* for solving linear programs (recall Section 1.2 in Chapter 1). Starting from an arbitrary vertex, this method finds a path along edges of \mathbf{P} to the maximal vertex, and while we are walking along this path we never see ψ decreasing. In our case, ψ is generic on edges, so ψ will be actually increasing all the time.

Assume we are starting from the unique minimal vertex v_m . We are now

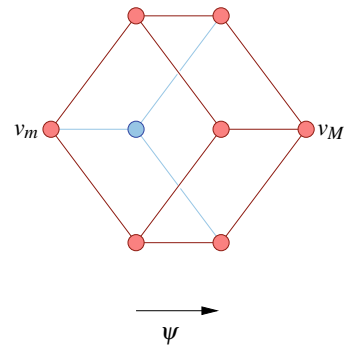
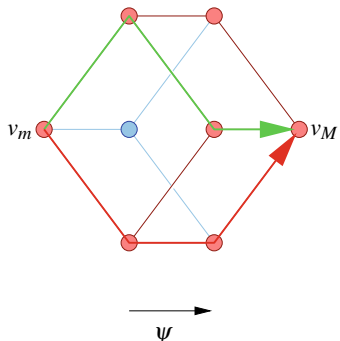


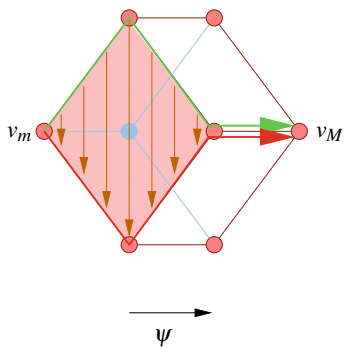
Figure 9.1: A polytope and a linear functional.

Figure 9.2: Two monotone paths w.r.t. ψ .

interested in the set of all ψ -monotone paths on \mathbf{P} (see Figure 9.2) that might occur when we are going to the maximal vertex v_M along edges of \mathbf{P} . In other words, we ask: what are the possible paths the simplex algorithm may generate on \mathbf{P} while walking from the minimal to the maximal vertex?

Monotone paths always exist (that is what makes the simplex method work), and there are typically a lot of them. For example, if \mathbf{P} is a d -simplex with its $d + 1$ vertices labeled $1, 2, \dots, d + 1$ according to values of ψ , each ordered subset of the intermediate vertices $2, 3, \dots, d$ yields a monotone path (since every pair of vertices forms an edge in the simplex). Therefore, we have 2^{d-1} many distinct monotone paths on the d -simplex: exponentially many. (Note that 2^{d-1} happens to be the number of vertices of the $(d - 1)$ -cube, is this a coincidence?)

So we have a large set of objects, and, as we have been doing throughout this book, we are looking for a nice structure on this complicated set. We are not claiming that the following really helps you in linear programming (it does not), but we are talking about important objects here. For example, one of the most famous open problems in polytope theory is the following *monotone Hirsch conjecture*, cf. [339]: for any d -polytope with n facets and any generic linear functional, there is always a *short monotone path* from the minimal to the maximal vertex, where short means that it uses at most $n - d$ edges. Although the conjecture was disproved by Santos recently, a nice structure on the set of monotone paths will come in handy to investigate the principle situation. Moreover, monotone paths can be viewed as a kind of a extremal path from the minimal to the maximal vertex in a certain topological space of paths. Some of the concepts we are presenting also have applications in algebraic topology [34, 50, 263].

Figure 9.3: A face flip between two monotone paths w.r.t. ψ .

As a first way method of giving structure to the set of monotone paths we can look at what are the natural ‘‘elementary moves’’ that change one monotone path into another, very much as we defined flips for triangulations. There is such a notion, and it is called a *face flip*. Remember that the starting point for flips in triangulations of general dimensions was the fact that a minimally dependent point configuration always has exactly two triangulations. Let us look at the case when \mathbf{P} is a two-dimensional polytope, i.e., a polygon. Then there are exactly two paths from v_m to v_M . Now, every polytope of larger dimension has two-dimensional faces. So, the intuitive idea is that a face flip changes a monotone path only on a two-dimensional face of \mathbf{P} (see Figure 9.3).

To summarize:

Definition 9.1.1. Let \mathbf{P} be a polytope and let ψ be a generic linear functional (that is, one that is not constant along any edge of \mathbf{P}). Let v_m and v_M be the minimal and maximal vertices of \mathbf{P} with respect to ψ .

- A ψ -monotone path is a path of edges of \mathbf{P} going from v_m to v_M and along which ψ is always increasing.
- Two ψ -monotone paths differ by a *face flip* if their symmetric difference is the boundary of a two-dimensional face of \mathbf{P} .

- The graph of ψ -monotone paths on \mathbf{P} is the graph whose vertices are all the ψ -monotone paths and whose edges are the face flips between them.

Remark 9.1.2. The assumption that ψ is generic on edges is not substantial for the following. Most of it is still true for general functionals ψ , but a more sophisticated notion of face flip may be needed; see [271] for a thorough discussion of the subtleties.

Let us go back to the polygon again and look for a special property of the two possible monotone paths. If the polygon \mathbf{P} is drawn in the plane with ψ increasing horizontally to the right, then v_m is the left most and v_M is the right most vertex of \mathbf{P} . This suggests a nice way of finding many monotone paths in an arbitrary polytope:

Lemma 9.1.3. Let ψ be a generic linear functional on a polytope $\mathbf{P} \subset \mathbb{R}^d$, and let $\pi : \mathbb{R}^d \rightarrow \mathbb{R}^2$ be a linear projection such that:

- ψ is constant along the projection direction (that is, ψ , as a projection $\mathbb{R}^d \rightarrow \mathbb{R}$, factors by π , i.e., $\psi(x) = pr(\pi(x))$, where $pr : \mathbb{R}^2 \rightarrow \mathbb{R}$ is a coordinate projection), and
- π is generic enough for every edge of $\pi(\mathbf{P})$ to be the projection of an edge of \mathbf{P} , and not of a higher dimensional face.

Then, the two monotone paths of $\pi(\mathbf{P})$ are the projections of two ψ -monotone paths of \mathbf{P} .

But can all ψ -monotone paths be obtained this way? No: consider a 3-polytope that looks like the convex hull of a DNA helix, so that there is a monotone path along the helix, i.e., one that wraps around \mathbf{P} several times. No matter which side you look at it, the path will always switch from top to bottom as the winding of a screw does. (It is easy to explicitly build such a polytope (see Exercise 9.2).) If you take a photo of such “screw-like” polytope from a generic direction, then you discover that the resulting polygon contains, of course, the two monotone paths in its boundary that we have been talking about already. Since the photo was taken from a generic direction, the preimage any of these two paths is also a monotone path in \mathbf{P} : a path that does not wrap around \mathbf{P} .

We are going to call *coherent monotone paths* in \mathbf{P} the ones that can be obtained as in Lemma 9.1.3: those that are part of the boundary of a two-dimensional projection of \mathbf{P} (see Figure 9.4). In an analogous way, *coherent face flips* are defined. A concrete example of a non-coherent monotone path appears in Figure 9.5.

Now there is the following amazing theorem about the graph of all coherent monotone paths on a polytope. Note that it is reminiscent of Theorem 5.1.9:

Theorem 9.1.4 ([53]). *The graph of all coherent ψ -monotone paths and coherent face flips on a d -polytope \mathbf{P} with n vertices is the edge graph of a $(d-1)$ -polytope, the monotone path polytope of \mathbf{P} and ψ , denoted by $\Sigma(\mathbf{P}, \psi)$.*

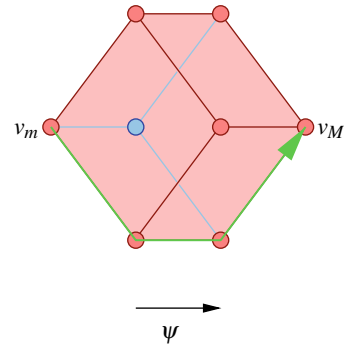


Figure 9.4: This monotone path is coherent.

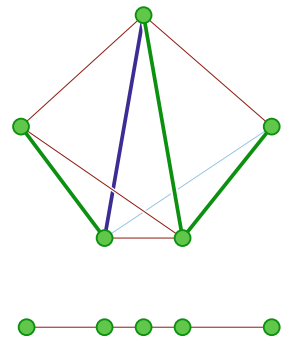


Figure 9.5: The indicated monotone path, visiting all the vertices of the bipyramid over a triangle, is not coherent.

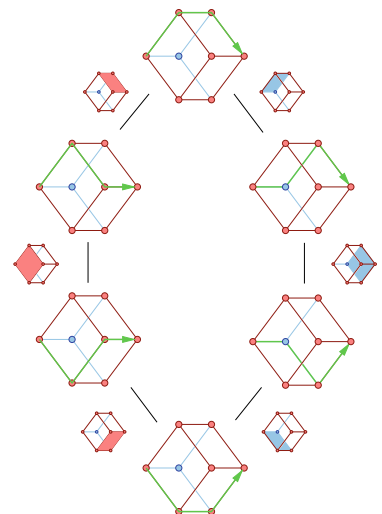


Figure 9.6: Monotone path polytope of the cube.

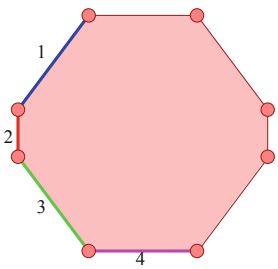


Figure 9.7: A zonotope in dimension two is just a centrally symmetric n -gon; the segments 1, 2, 3, 4 sum up to this zonotope.

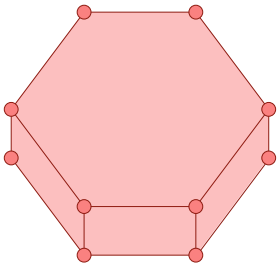


Figure 9.8: A non-tight zonotopal tiling of a two-dimensional zonotope; note that there are vertices in the tiling that are not vertices of the tiled zonotope.

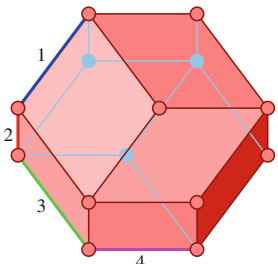


Figure 9.9: A zonotope in dimension three, a Minkowski sum of four segments in three-space.

In other words: coherent ψ -monotone paths on \mathbf{P} are in one-to-one correspondence with vertices of the monotone path polytope of \mathbf{P} and ψ . Two ψ -monotone paths are connected by a coherent face flip if and only if the corresponding vertices share an edge in the monotone path polytope.

We will not prove this here; since it will turn out to be a special case of a much more general theorem, stay tuned! As an example, the monotone path polytope of the cube is shown in 9.6.

9.1.2 Zonotopal tilings

We now look at *zonotopes*, a special, very important class of polytopes with close connections to the theory of hyperplane arrangements and oriented matroids. So what is a *zonotope*? In dimension two, zonotopes are the centrally symmetric n -gons. In general dimension, a d -zonotope $Z \subset \mathbb{R}^d$ with n zones is the *Minkowski sum* of n line segments. The set of line segments out of which the zonotope was produced is considered part of the data of Z . More precisely, a zone consist of all faces of the zonotope whose supporting hyperplanes have normals perpendicular to one of the defining line segments. The edges of faces in the zone are parallel to the other line segments. When the zonotope is not defined using parallel line segments, then its faces will be divided into n -zones.

There is another way of looking at zonotopes. For example, imagine you take a photo of a regular three-cube from a generic point of view. Then the boundary of what you see on the photograph is a centrally symmetric six-gon. So the six-gon is the projection of a three-cube. In general, d -zonotopes with n zones are projections of the regular n -cube $[-1, 1]^n$ in \mathbb{R}^d to \mathbb{R}^d . (We use the cube $[-1, 1]^n$ as opposed to $[0, 1]^n$ in order to stress the fact that all zonotopes are centrally symmetric.)

A *zonotopal tiling* of Z is a dissection of Z into a set of non-overlapping zonotopes made from the same set of line segments. A zonotopal tiling is *tight* if no cell in the tiling has a non-trivial zonotopal tiling itself.

You can find a wealth of information about zonotopes and zonotopal tilings in the books [339, 55] and also in the recent work by Chavalon and Rémy [77]. For example (to mention just a few connections), the combinatorics of the faces of a zonotope are equivalent to those of an arrangement of hyperplanes. Readers with background in the theory of oriented matroids will probably know the celebrated Bohne-Dress Theorem: the set of all one-element lifts of a realizable oriented matroid is in bijection to the set of all zonotopal tilings of the oriented matroid's zonotope, and the lift is realizable if and only if the corresponding zonotopal tiling is *coherent*—see definition of coherent below. Crystallographers also use zonotopes in their work. Moreover, several seemingly distant combinatorial objects are related to zonotopal tilings in a surprising way. For example, the number of spanning trees in a graph is the same as the number of tiles in some zonotopal tiling (we will also elaborate on this in Section 9.2).

Clearly, zonotopal tilings are a special class of polyhedral subdivisions, that contains only zonotopes as cells, but it is not clear exactly what point configuration we are subdividing. We will make that exact a little later.

(The vertices of the zonotope are not enough, obviously.)

Again, we would like to understand the set of all zonotopal tilings of a zonotope. For this, let us use the same trick and look at small zonotopes that have only two distinct tight zonotopal tilings. One example is a centrally symmetric six-gon. There are two tight zonotopal tilings of it, namely the two that have edges incident with every other vertex on the boundary—see Figures 9.10 and 9.11, where these two tilings of a hexagon appear as substructures in tilings of a larger zonotope. This picture illustrates the notion of flip we want to arrive at.

How does this look in general? We consider a d -zonotope with $d+1$ zones. Look again at the photo of the three-cube: we see the boundary, which is a hexagon, but we also see a tight zonotopal tiling consisting of the projection of the three facets of that cube that were visible from the camera. Now, if we had taken the photograph from the opposite side, we would have seen a second tight zonotopal tiling. This principle holds in general, but at this point we do not elaborate on this any further. The important thing is that we can again define an adjacency structure using this fact by changing a tight zonotopal tiling on just a d -subzonotope with $d+1$ zones.

Definition 9.1.5. We say that two tight zonotopal tilings of Z differ by a (*cubical*) *flip*, if they are equal except on a d sub-zonotope of Z with $d+1$ zones.

The *graph of zonotopal tilings* of Z has as vertices all the tight zonotopal tilings and as edges the cubical flips between them.

Are there coherent zonotopal tilings, just like there were special coherent monotone paths? Yes, although we have not yet explained exactly in which sense zonotopal tilings are polyhedral subdivisions, we can use the *lifting principle* to define them: A zonotopal tiling T of Z is *coherent* if, in one dimension higher, there are slopes for all the segments of Z such that T is the set of projections of all lower facets of the Minkowski sum of the sloped segments down to Z . Analogously, a cubical flip is *coherent* if such slopes exist except that they have to be “flat” on the respective sub-zonotope. In particular, a coherent zonotopal tiling is regular when regarded as a subdivision. This allows us to easily construct non-coherent zonotopal tilings, such as the ones in Figures 9.12 and 9.13.

Interestingly enough, we have a very similar theorem here to that for monotone paths:

Theorem 9.1.6. *The graph of all coherent zonotopal tilings and coherent cubical flips of a d -zonotope Z with n zones is the edge graph of an $(n-d)$ -polytope $\Sigma(Z)$.*

In other words: coherent zonotopal tilings of Z are in one-to-one correspondence with vertices of a polytope and two coherent zonotopal tilings are connected by a coherent cubical flip if the corresponding vertices share an edge in $\Sigma(Z)$.

Again, we do not prove the theorem here, and something more general is about to come.

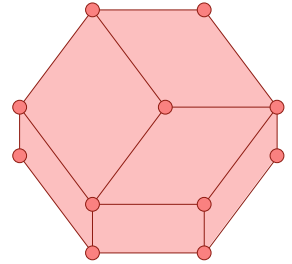


Figure 9.10: A tight zonotopal tiling of a two-dimensional zonotope ...

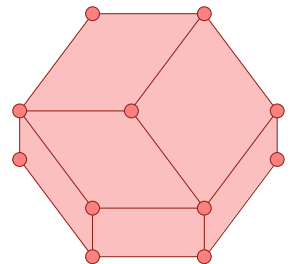


Figure 9.11: ... and flipped to another tight zonotopal tiling.

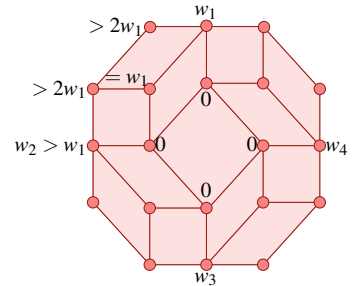


Figure 9.12: A non-coherent tight zonotopal tiling of a zonotope with six zones of four different directions; the data indicated in the figure yields a contradiction like in the mother of all examples, since every height function inducing this tiling must obey $w_1 < w_2 < w_3 < w_4 < w_1$, which is impossible.

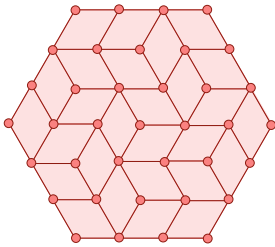


Figure 9.13: A non-coherent tight zonotopal tiling, this time with nine zones but only of three different directions.

9.1.3 Polyhedral subdivisions

This is what the book is about, and this is Chapter 9. So by now you know a lot, and it may have occurred to you that the concepts in the previous two sections are very much reminiscent of the graph of all *regular* triangulations of a point configuration that was constructed by flips (cf. Chapter 1). Recall that not all triangulations are regular. We restate the main theorem one can extract from our work in Chapter 5 (presented here by emphasizing the analogy with our previous examples):

Theorem 9.1.7 ([139]). *The graph of all regular triangulations and regular flips of a d -dimensional point configuration \mathbf{A} with n points is the edge graph of an $(n - d - 1)$ -dimensional polytope, the secondary polytope $\Sigma\text{-poly}(\mathbf{A})$.*

In other words: regular triangulations of \mathbf{A} are in one-to-one correspondence with vertices of $\Sigma\text{-poly}(\mathbf{A})$, and two regular triangulations differ by a regular flip if the corresponding vertices share an edge in $\Sigma\text{-poly}(\mathbf{A})$.

Note: Because of Examples 5.3.4 and 5.4.16, we need to restrict ourselves to regular flips.

As Figure 9.15 suggests, the secondary polytope of the prism over a triangle is a six-gon. Incidentally the same polytope is the monotone path polytope of a cube (see Figure 9.6). In Section 9.2, we will discuss this in somewhat more detail.

Now, we have three theorems that are saying almost exactly the same about seemingly different objects. There must be some general concept behind this. The following section gives the answer.

9.1.4 Compatible subdivisions and the fiber polytope

We have already described zonotopes as projections of cubes. More specifically, let $I_i = [-a_i, +a_i]$ be the line segments of Z in \mathbb{R}^d for $i = 1, 2, \dots, n$. (We are enforcing here central symmetry around the origin again.) Then consider the following affine map:

$$\pi : \begin{cases} \mathbb{R}^n & \rightarrow \mathbb{R}^d \\ \begin{pmatrix} t_1 \\ t_2 \\ \vdots \\ t_n \end{pmatrix} & \mapsto \sum_{i=1}^d t_i a_i \end{cases}$$

Since the point $t_i a_i$ lies in $[-a_i, +a_i]$ for all $t_i \in [-1, 1]$ ($i = 1, 2, \dots, n$), the zonotope $\sum_{i=1}^n [-a_i, +a_i]$ is the image of $[-1, 1]^n$ under π .

Now comes the catch: We do not consider π as a projection of polytopes, but as a projection of point configurations. We consider the *zonotopal* point configuration of all possible sums of segment boundary points; in formula:

$$\begin{aligned} \mathbf{Z} &:= \{\pi(v) : v \text{ is a vertex of } [-1, 1]^n\} \\ &= \left\{ \sum_{i=1}^n \varepsilon^{(i)} a_i : \varepsilon^{(i)} \in \{-1, +1\}, i = 1, 2, \dots, n \right\} \end{aligned}$$

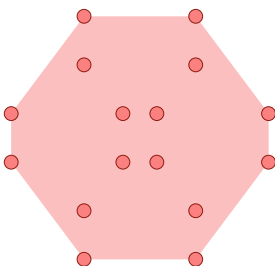


Figure 9.14: A zonotopal point configuration in dimension two; note that it automatically contains all the points that might occur as vertices of a zonotopal tiling.

Obviously, the zonotope Z is the convex hull of the point configuration \mathbf{Z} . But \mathbf{Z} is not in convex position, and it may contain repeated points. Already when Z is the regular six-gon, the point configuration \mathbf{Z} contains the barycenter of it twice, and the six-gon also shows that it may happen that no zonotopal tiling (we know the two possible by now) uses all points in the configuration. We have not actually introduced formally what a zonotopal subdivision is, but now that we have polyhedral subdivisions at hand, we can easily define them as special polyhedral subdivisions that have cells that are themselves zonotopal subconfigurations.

Observe that the cubes that project into the cells of a zonotopal subdivision are faces of the big cube $[-1, 1]^n$. Thus, another way to phrase the definition of a zonotopal tiling is the following:

Lemma 9.1.8. *Let \mathbf{I}^n be the point configuration of vertices of the n -dimensional regular cube $[-1, 1]^n$. The zonotopal tilings of a zonotope $Z = \pi([-1, 1]^n)$ are exactly those polyhedral subdivision of the corresponding zonotopal point configuration $\mathbf{Z} = \pi(\mathbf{I}^n)$, all of whose cells are faces of \mathbf{I}^n .*

A tight zonotopal tiling is a zonotopal tiling, all of whose k -cells ($k = 0, \dots, d$) are k -dimensional faces of \mathbf{I}^n . In particular, all cells of a tight zonotopal tiling are combinatorially cubes.

Analogous things can be done for the case of monotone paths and even for the general polyhedral subdivisions. Any linear functional on a polytope \mathbf{P} can be reinterpreted as a projection π of \mathbf{P} into \mathbb{R} . The projections of the vertices of \mathbf{P} induce a point configuration \mathbf{A} in \mathbb{R} . It is easy to see that the strict monotonicity of paths translates into the following: the set of faces in a monotone path induces a triangulation of \mathbf{A} . However, not every triangulation corresponds to a monotone path in \mathbf{P} . For example, all monotone paths on the cube have three edges, whereas there are triangulations of the projection \mathbf{A} with one, two, and three cells. So, monotone paths correspond to those triangulations all of whose cells are labeled projections of faces of \mathbf{P} . Keeping track of the labels is important, since several vertices may project to the same geometric point, and we need to distinguish between them.

Using this, we can actually define monotone paths via triangulations. Because we allow for multiple points, ψ need not even be generic.

Lemma 9.1.9. *The ψ -monotone paths in a polytope \mathbf{P} with vertices \mathbf{V} are exactly those triangulations of the point configuration $\mathbf{A} := \pi(\mathbf{V})$, all of whose cells are edges of \mathbf{P} .*

This can now easily be generalized to higher dimensional objects:

Definition 9.1.10. An ψ -monotone cellular string in \mathbf{P} is a polyhedral subdivision of \mathbf{A} , all of whose cells are faces of \mathbf{P} (see Figure 9.17).

Can we fit the general polyhedral subdivisions of previous chapters in this context? Where is the projection in the theory of unrestricted polyhedral subdivisions? Well, not imposing any restriction on what is accepted as a cell means that each subset of the vertices is allowed, and this can be

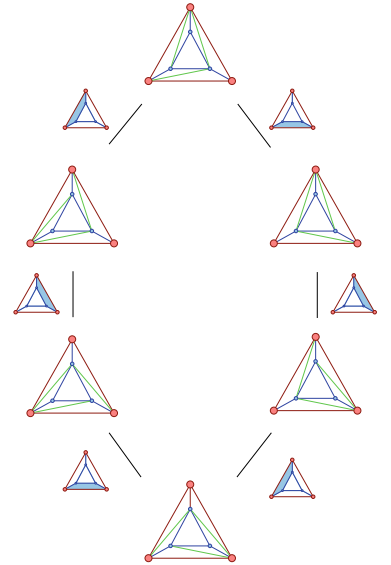


Figure 9.15: The graph of all triangulations of the prism over a triangle; we show the corresponding triangulations on the boundary, that can be seen if one removes the upper triangular face of the prism and looks inside the prism from above (this yields actually a Schlegel-diagram of the triangulated boundary of the prism).

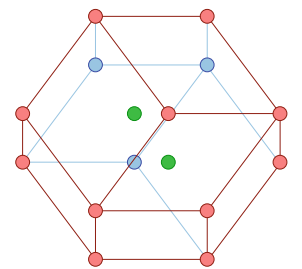


Figure 9.16: A zonotopal point configuration in dimension three; it has two interior points (those not on any edge).

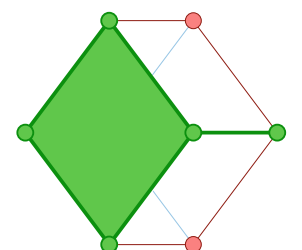


Figure 9.17: An ψ -monotone cellular string.

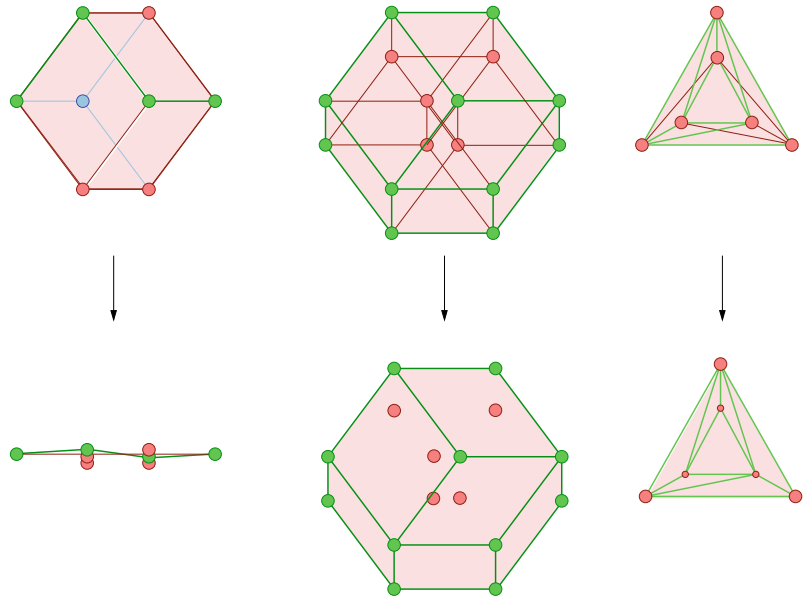
artificially expressed by a projection of a simplex with the same number of points as the configuration. For completeness we state:

Lemma 9.1.11. *Let \mathbf{D}_n be the point configuration of vertices of the $(n-1)$ -dimensional standard simplex \mathbf{D}_{n-1} . Then all the cells of any polyhedral subdivision of a point configuration $\mathbf{A} = \pi(\mathbf{D}_n)$ are projections of faces of \mathbf{D}_n .*

The triangulations of \mathbf{A} are exactly those polyhedral subdivisions whose maximal cells are projections of d -faces of \mathbf{D}_n .

So, in all cases we have a projection π of the vertices \mathbf{V} of a polytope \mathbf{P} that yields a point configuration $\mathbf{A} = \pi(\mathbf{V})$ in lower dimension. Then we are after polyhedral subdivisions of \mathbf{A} that contain *only* cells that label faces of \mathbf{V} . (See Figure 9.18 for a sketch of the projections corresponding to monotone paths, zonotopal tilings, and polyhedral subdivision, respectively.)

Figure 9.18: A monotone path in a 3-cube (left); a zonotopal tiling in an octagon (center); and a triangulation of six points in the plane (right). All three phenomena can be described via projections of polytopes: projections of monotone paths are special triangulations of a segment; a zonotopal tiling of a zonotope with n summands is a special polyhedral subdivision where all cells are projections of faces of the n -cube; polyhedral subdivisions fit into this framework because every cell in a subdivision of n points is the projection of a face of the $(n-1)$ -simplex with n vertices.



The general concepts behind all three examples above, deserve their own name:

Definition 9.1.12. Let \mathbf{P} be a D -polytope in \mathbb{R}^D with vertex set $\mathbf{V} = \text{vert } \mathbf{P}$. Moreover, let $\pi : \mathbb{R}^D \rightarrow \mathbb{R}^d$ with $d < D$ be an affine map, and let $\mathbf{A} := \pi(\mathbf{V})$ (labeling inherited).

- A π -compatible subdivision of \mathbf{A} is a polyhedral subdivision of \mathbf{A} all of whose cells label faces of \mathbf{V} .
- A π -compatible subdivision is *tight* if all its cells label d -faces of \mathbf{V} .

- A π -compatible subdivision \mathcal{T} is *coherent* if there is a lifting for the points in \mathbf{A} that is an affine image of \mathbf{V} such that \mathcal{T} labels the set of lower faces of the lifted point configuration.
- The set of faces of \mathbf{V} that induces a π -compatible subdivision is called a *locally coherent string* in \mathbf{P} .
- If a locally coherent string induces a tight subdivision, it is called *tight*, if it induces a regular subdivision, it is called *globally coherent*.
- Two tight π -compatible subdivisions $\mathcal{T}, \mathcal{T}'$ of \mathbf{A} differ by a *flip* if and only if there is a π -compatible subdivision that is refined by only \mathcal{T} and \mathcal{T}' .
- The *graph of all tight π -compatible subdivisions of \mathbf{A}* is the graph, where the nodes are the π -compatible subdivisions of \mathbf{A} and where two π -compatible subdivisions are connected by an edge if and only if they differ by a flip.

The original name in [53] for π -compatible subdivision is *π -induced subdivision*. We chose to use *compatible* rather than *induced* since a π -compatible subdivision is not uniquely determined by π , it is just satisfying an additional restriction. Note, that distinct locally coherent strings can project to the same geometric cells, so that in a purely geometric notion of polyhedral subdivision the strings cannot be recovered from the subdivisions. In our combinatorial setting, distinct strings yield distinct subdivisions, and working with either object will give the same results.

The exciting fact about this concept is that everything that has been claimed in the theorems of this section (and some more) can be proved for arbitrary compatible subdivisions.

Theorem 9.1.13 ([53]). *The refinement poset of all coherent π -compatible subdivisions of \mathbf{A} is isomorphic to the face lattice of a $(D-d)$ -dimensional polytope, the fiber polytope $\Sigma(\mathbf{P}, \pi)$ of \mathbf{P} and π .*

In particular: the graph of all tight coherent π -compatible subdivisions of \mathbf{A} and all coherent flips is the edge graph of $\Sigma(\mathbf{P}, \pi)$.

The notation for the fiber polytope varies in the literature. Sometimes, people start from a projection of polytopes $\pi : \mathbf{P} \rightarrow \mathbf{Q}$ and call the fiber polytope $\Sigma(\mathbf{P}, \mathbf{Q})$. Others include the information about the projection map π into the notation and call the fiber polytope $\Sigma(\mathbf{P} \xrightarrow{\pi} \mathbf{Q})$. Another possibility is to regard π as implicitly denoting not only the projection but also its domain and its image, so that $\Sigma(\pi)$ is enough to uniquely specify the fiber polytope. Our notation $\Sigma(\mathbf{P}, \pi)$ is kind of a compromise that we propose because the image as a polytope is not really the important object: it is the point configuration emerging as the projection of vertices of the polytope \mathbf{P} that counts.

But how can the fiber polytope be constructed? We will sketch one construction. There is no loss of generality if we assume that the projection π

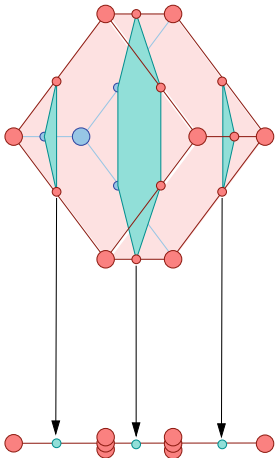


Figure 9.19: Some fibers in the projection of the cube to a segment.

forgets the last $D - d$ coordinates. That is, $\pi(\mathbf{p}) = \pi(\mathbf{x}, \mathbf{q}) = \mathbf{q} \in \mathbb{R}^d$ with $\mathbf{x} \in \mathbb{R}^{D-d}$.

In order to construct a π -compatible subdivision of \mathbf{A} , we must specify a set of faces of \mathbf{P} that yields a valid subdivision of \mathbf{A} . This can be synthetically done as follows.

For each $\mathbf{q} \in \text{conv}(\mathbf{A})$, consider the set $\mathbf{P}_\mathbf{q} := \{\mathbf{x} \in \mathbb{R}^{D-d} : (\mathbf{x}, \mathbf{q}) \in \mathbf{P}\}$, i.e., the set of all $\mathbf{p} \in \mathbf{P}$ that project to \mathbf{q} , embedded into \mathbb{R}^{D-d} . This set is called the *fiber of π over \mathbf{q}* , and it is a polytope in \mathbb{R}^{D-d} , which is guaranteed to be of full dimension $D - d$ whenever \mathbf{q} is in $\text{relint}(\mathbf{A})$, i.e., for almost all $\mathbf{q} \in \text{conv}(\mathbf{A})$.

The crucial observation now is that every face \mathbf{F} of the fiber $\mathbf{P}_\mathbf{q}$ lies in a unique minimal face $\mathbf{F}_\mathbf{P}$ of \mathbf{P} containing \mathbf{F} . Why? Just take for $\mathbf{F}_\mathbf{P}$ the carrier of \mathbf{F} in the face lattice of \mathbf{P} . So, by picking a face in $\mathbf{P}_\mathbf{q}$ for all $\mathbf{q} \in \text{conv}(\mathbf{A})$, we can pick a set of faces in \mathbf{P} .

When does such a set of faces label a valid subdivision of \mathbf{A} ? First of all, the choice should be *locally coherent on the projection of a face of \mathbf{P}* . If we chose the face \mathbf{F} in $\mathbf{P}_\mathbf{q}$, then for all points $\mathbf{q}' \in \text{relint}(\pi(\mathbf{F}_\mathbf{P}))$ we should choose an \mathbf{F}' in $\mathbf{P}_{\mathbf{q}'}$ such that $\mathbf{F}'_\mathbf{P} = \mathbf{F}_\mathbf{P}$, because otherwise we would violate (IP) in Definition 2.3.1.

How can this be done? Well, the unique choice of \mathbf{F}' with that property is $\mathbf{F}' = \mathbf{F}_\mathbf{P} \cap \mathbf{P}_{\mathbf{q}'}$. Furthermore, the choice should be *locally coherent on the boundary of a projected face of \mathbf{P}* . That means that for all points $\mathbf{q}' \in \partial(\pi(\mathbf{F}_\mathbf{P}))$, we should choose \mathbf{G} in $\mathbf{P}_{\mathbf{q}'}$ such that $\pi(\text{vert}(\mathbf{G}))$ is a face of $\pi(\mathbf{F}_\mathbf{P})$, because otherwise we would either violate (CP) or (IP) in Definition 2.3.1. Again, the unique choice is $\mathbf{G} = \mathbf{F}_\mathbf{P} \cap \mathbf{P}_{\mathbf{q}'}$. A choice of a face in $\mathbf{P}_\mathbf{q}$ for all $\mathbf{q} \in \text{conv}(\mathbf{A})$ would give us trivially (UP). The local coherence immediately gives us (CP), (FP), and (MF) in Characterization 4.5.1.

Why does there exist a locally coherent choice of faces in the fibers? Here the coherent compatible subdivisions come into play. Choose a vector ψ in the space $(\mathbb{R}^{D-d})^*$ of linear functionals on \mathbb{R}^{D-d} . Then we simply choose the face $\mathbf{P}_\mathbf{q}^\psi$ in $\mathbf{P}_\mathbf{q}$ for all $\mathbf{q} \in \text{conv}(\mathbf{A})$. This can be checked to be locally coherent using the following observation: if \mathbf{q}' is in the boundary of $\pi(\mathbf{F}_\mathbf{P})$, then the normal fan of $\mathbf{P}_\mathbf{q}'$ in $(\mathbb{R}^{D-d})^*$ is a refinement of the normal fan of $\mathbf{P}_\mathbf{q}'$ in $(\mathbb{R}^{D-d})^*$ for all \mathbf{q} in the interior of $\pi(\mathbf{F}_\mathbf{P})$. It can also be seen that this construction yields a coherent compatible subdivision according to the definition with heights $\omega(\mathbf{a}) := \psi(\mathbf{x}_\mathbf{a})$ for some $\mathbf{x}_\mathbf{a} \in \mathbf{P}_\mathbf{a}^\psi$, for all $\mathbf{a} \in \mathbf{A}$.

Imagine now that we are moving around ψ in $(\mathbb{R}^{D-d})^*$. When does the compatible subdivision specified by the choice of ψ change? It changes whenever ψ changes the normal cone in the normal fan of at least one fiber $\mathbf{P}_\mathbf{q}$. In other words: if it moves to another cone in the common refinement of all normal fans of fibers. Therefore, every coherent compatible subdivision corresponds to a cone in the common refinement of all normal fans of the fibers. It is known from basic polytope theory that the common refinement of normal fans of polytopes is the normal fan of the Minkowski sum of the polytopes (see, e.g., [339]). Thus, every coherent compatible subdivision corresponds to a face of the Minkowski sum of all fibers. But what is the Minkowski sum of a continuous number of fibers, one for each

$\mathbf{x} \in \text{conv}(\mathbf{A})$? It is tempting to write an integral over all $\mathbf{x} \in \text{conv}(\mathbf{A})$ instead of a Minkowski sum. This can indeed be done, and it yields a potential definition of the fiber polytope:

$$\Sigma(\mathbf{P}, \pi) := \int_{\text{conv}(\pi(\mathbf{P}))} \mathbf{P}_q d\mathbf{q} \quad (9.1)$$

However, because the inventors of the fiber polytope wanted $\Sigma(\mathbf{P}, \pi)$ to be a subset of \mathbf{P} , they introduced a normalizing factor $\frac{1}{\text{vol}(\pi(\mathbf{P}))}$. So, here is the original definition by Billera and Sturmfels[53]:

Definition 9.1.14. The fiber polytope $\Sigma(\mathbf{P}, \pi)$ is defined as the following Minkowski integral:

$$\Sigma(\mathbf{P}, \pi) := \frac{1}{\text{vol}(\pi(\mathbf{P}))} \int_{\pi(\mathbf{P})} \mathbf{P}_q d\mathbf{q}. \quad (9.2)$$

We can describe the fiber polytope in terms of a finite Minkowski sum. The following observations lead to the right formula.

Let the *chamber* σ_q of $\mathbf{q} \in \pi(\mathbf{P})$ be the intersection of all $\pi(F_p)$ that contain \mathbf{q} , where F_p is a face of \mathbf{P} . Chambers in Chapter 5 can be regarded as coming from a projection of a simplex. It is easy to see that the collection of chambers of \mathbf{q} for all $\mathbf{q} \in \pi(\mathbf{P})$ forms a polyhedral complex, the *chamber complex* $\Gamma(\mathbf{P}, \pi)$. The normal fans of the fibers over an open chamber coincide, because, by the very definition of a chamber, identical sets of faces of \mathbf{P} live above all points in an open chamber.

That means that all fibers \mathbf{P}_q above the relative interior of a chamber σ_q are normally equivalent. Furthermore, for \mathbf{q} in an open chamber, the set-valued fiber function $\mathbf{q} \rightarrow \mathbf{P}_q$ is linear, since the union of all fiber faces in a certain direction over an open chamber is contained in a face of \mathbf{P} . Therefore, we simply pick for every chamber σ its barycenter \mathbf{q}_σ and sum up the fibers over these points. Note that, since values over lower dimensional subsets of $\pi(\mathbf{P})$ are unimportant anyway in the Minkowski integral (they are sets of measure zero), we can restrict ourselves to full-dimensional chambers. This way, we end up with a formula for the fiber polytope as a scaled finite Minkowski sum of fibers over full-dimensional chambers (see Figure 9.21).

Theorem 9.1.15. The fiber polytope $\Sigma(\mathbf{P}, \pi)$ is given by the following formula:

$$\Sigma(\mathbf{P}, \pi) = \sum_{\substack{\sigma \in \Gamma(\mathbf{P}, \pi) \\ \dim(\sigma)=d}} \frac{\text{vol}(\sigma)}{\text{vol}(\pi(\mathbf{P}))} \mathbf{P}_{\mathbf{q}_\sigma} \quad (9.3)$$

Our arguments from above can in fact be turned into a rigorous proof of Theorem 9.1.13. This is left as an exercise to the reader. Consult [53] if you get stuck. It pays off to study the examples in [339, Chapter 9].

Of course, from the above description as the Minkowski sum of finitely many fibers of the projection, the fiber polytope $\Sigma(\mathbf{P}, \pi)$ can be computed explicitly. Nevertheless, there is another way to do it which in some way might be more convenient if you already have good software to compute

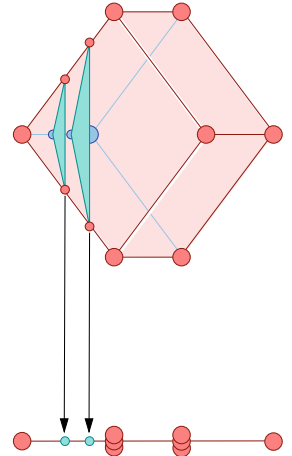


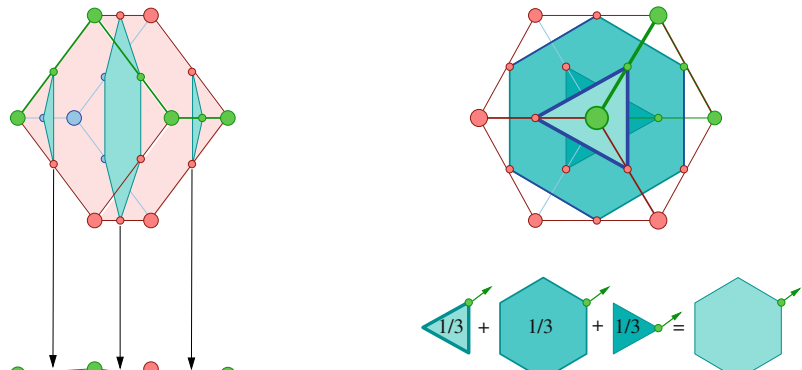
Figure 9.20: On an open chamber, the function that assigns to each x the fiber of π over x is linear.

triangulations (e.g., TOPCOM [265]). In [53] they also showed that the fiber polytope can be very conveniently computed from the knowledge of the vertices of the secondary polytope of \mathbf{P} . We need the following lemma

Lemma 9.1.16. *Let $\theta : \mathbf{P} \rightarrow \mathbf{P}$ and $\pi : \mathbf{P} \rightarrow \mathbf{R}$ surjective linear maps. Then the fiber polytope $\Sigma(\mathbf{P}, \pi)$ is equal to $\theta(\Sigma(\mathbf{P}, \theta(\pi)))$.*

Thus, if we take \mathbf{P} to be a simplex we know that $\Sigma(\mathbf{P}, \theta(\pi))$ is the secondary polytope of \mathbf{R} . Thus, one can simply use TOPCOM to find the GKZ coordinates of the vertices of the secondary and then project them to find the potential vertices of the fiber polytope (we are then required to do a convex hull computation). See Lemma 2.3 and Corollary 2.6 in [53].

Figure 9.21: How the monotone path polytope of the cube emerges as a fiber polytope: To the left, we see the fibers over the barycenters of the full-dimensional chambers; to the right and above, the cube and the fibers are shown from an orthogonal perspective; below, the scaled Minkowski sum of the fibers and a normal vector that chooses exactly the indicated monotone path.



Remark 9.1.17 (The Generalized Baues Problem). For any given poset P one can define the *order complex* of P to be the following simplicial complex (compare Section 3.3.4, where this construction already popped up):

$$\mathcal{O}(P) := \{S \subset P : S \text{ is linearly ordered}\}.$$

Put differently, $\mathcal{O}(P)$ has a vertex for each element of P and a simplex for each chain in P . For example, if P is the complex of proper faces of a polytope \mathbf{P} then $\mathcal{O}(P)$ is isomorphic to the barycentric subdivision of the boundary of \mathbf{P} . Order complexes are a natural way of thinking of a poset as a topological space and their *homotopy type* is of special interest [54].

In 1994, Billera et al. [50] posed the problem whether or not the poset of proper π -compatible subdivisions for a d -dimensional projection of a D -dimensional polytope \mathbf{P} was homotopy equivalent to a $(D - d - 1)$ -sphere. Put differently, they asked whether the non-coherent subdivisions changed the topological type but not the homotopy type of the face poset of the fiber polytope. They gave an affirmative answer for $d = 1$ (the case of monotone paths), which had previously been conjectured by Baues in his study of loop spaces [34]. For this reason, their question became known as the *Generalized Baues Problem*, or GBP [271].

Subsequently, the GBP was answered in the affirmative for $D - d \leq 2$ but in the negative in general by Rambau and Ziegler [268, 263] with a counterexample having the minimal possible $D = 5$ and $d = 2$. Still, the problem remained of interest for the special cases where \mathbf{P} is a simplex or a cube and for special classes of projections $\pi : \mathbf{P} \rightarrow \pi(\mathbf{P})$.

For example, for all projections between cyclic polytopes, the answer is affirmative [267, 19]. The simplex case, however, was disproved, when F. Santos constructed a disconnected graph of triangulations in general position (see Exercise 9.3). The cube case is still open. By the Cayley trick (see the next section, in particular Corollary 9.2.19) this cube case is equivalent to the projection from a simplex to a Lawrence polytope. It is also equivalent to the *extension space conjecture* of oriented matroid theory [55].

9.2 Mixed subdivisions and the Cayley trick

We have seen in Section 1.3, Theorem 1.3.6 that mixed subdivisions play a fundamental role in counting the number of common roots of a system of polynomial equations via Bernstein's Theorem. In this section, we will see that the set of all mixed subdivisions of the Minkowski sum of point configurations is in one-to-one correspondence to the set of all subdivisions of another object: the *Cayley embedding* of the point configurations. Of course, this makes things easier, since now we may use everything that we already know about subdivisions. In particular, in order to find and/or enumerate fine mixed subdivisions, we can use methods that find and/or enumerate triangulations, e.g., TOPCOM (see Chapter 8, especially Sections 8.2 and 8.3). But also the other direction of this correspondence is useful, as we will see. The name of this magic correspondence is the *Cayley trick*.

9.2.1 An example

Let us start with an example. Let $\mathbf{A}^{(1)}$ and $\mathbf{A}^{(2)}$ be the following two 2-dimensional point configurations (in homogeneous coordinates), labeled by $J^{(1)} = \{1, 2, 3, 4\}$ and $J^{(2)} = \{1, 2, 3\}$, respectively:

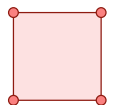


Figure 9.22: Example configuration $\mathbf{A}^{(1)}$.

$$\mathbf{A}^{(1)} = \begin{pmatrix} 1 & 2 & 3 & 4 \\ 0 & 1 & 0 & 1 \\ 0 & 0 & 1 & 1 \\ 1 & 1 & 1 & 1 \end{pmatrix} \quad (9.4)$$

$$\mathbf{A}^{(2)} = \begin{pmatrix} 1 & 2 & 3 \\ 0 & 1 & 2 \\ 0 & 0 & 1 \\ 1 & 1 & 1 \end{pmatrix} \quad (9.5)$$

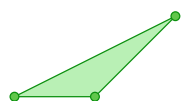
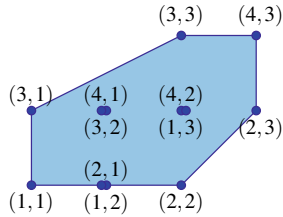


Figure 9.23: Example configuration $\mathbf{A}^{(2)}$.

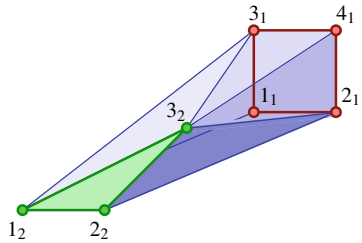
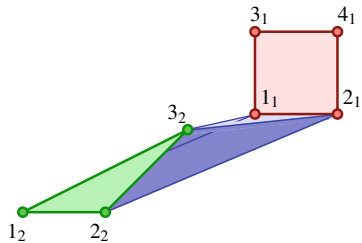
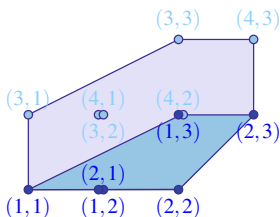
The (affine) *Minkowski sum* of $\mathbf{A}^{(1)}$ and $\mathbf{A}^{(2)}$ is the 2-dimensional point configuration $\mathbf{A}^{(1)} + \mathbf{A}^{(2)}$ consisting of all points that are affine sums of a point in $\mathbf{A}^{(1)}$ and a point in $\mathbf{A}^{(2)}$, naturally labeled by $J^{(1)} \times J^{(2)}$. The homogeneous coordinates of the resulting points are as follows:

Figure 9.24: The configuration $\mathbf{A}^{(1)} + \mathbf{A}^{(2)}$.

$$\mathbf{A}^{(1)} + \mathbf{A}^{(2)} := \begin{pmatrix} (I, I) & (I, 2) & (I, 3) & (2, I) & (2, 2) & (2, 3) & \dots \\ 0 & 1 & 2 & 1 & 2 & 3 & \dots \\ 0 & 0 & 1 & 0 & 0 & 1 & \dots \\ 1 & 1 & 1 & 1 & 1 & 1 & \dots \\ \dots & (3, 1) & (3, 2) & (3, 3) & (4, 1) & (4, 2) & (4, 3) \\ \dots & 0 & 1 & 2 & 1 & 2 & 3 \\ \dots & 1 & 1 & 2 & 1 & 1 & 2 \\ \dots & 1 & 1 & 1 & 1 & 1 & 1 \end{pmatrix} \quad (9.6)$$

The resulting point configuration has $4 \cdot 3 = 12$ points with repeated points at $(1, 0, 1)^T$, $(1, 1, 1)^T$, and $(2, 1, 1)^T$.

The (affine) Cayley embedding of $\mathbf{A}^{(1)}$ and $\mathbf{A}^{(2)}$ is the following 3-dimensional point configuration $\text{Cayley}(\mathbf{A}^{(1)}, \mathbf{A}^{(2)})$ that contains $\mathbf{A}^{(1)}$ and $\mathbf{A}^{(2)}$ in parallel affine spaces:

Figure 9.25: The configuration $\text{Cayley}(\mathbf{A}^{(1)}, \mathbf{A}^{(2)})$.Figure 9.26: A cell in $\text{Cayley}(\mathbf{A}^{(1)}, \mathbf{A}^{(2)})$.Figure 9.27: The corresponding cell in $\text{Cayley}(\mathbf{A}^{(1)}, \mathbf{A}^{(2)})$.

$$\text{Cayley}(\mathbf{A}^{(1)}, \mathbf{A}^{(2)}) :=$$

$$\begin{pmatrix} I_1 & 2_1 & 3_1 & 4_1 & I_2 & 2_2 & 3_2 \\ 0 & 1 & 0 & 1 & 0 & 1 & 2 \\ 0 & 0 & 1 & 1 & 0 & 0 & 1 \\ 1 & 1 & 1 & 1 & 1 & 1 & 1 \\ 1 & 1 & 1 & 1 & 0 & 0 & 0 \\ 0 & 0 & 0 & 0 & 1 & 1 & 1 \end{pmatrix} \quad (9.7)$$

The resulting point configuration is 3-dimensional and has $4 + 3 = 7$ points with no multiple points. The description is not full-dimensional, but that does no harm here.

Let us discover what connects these seemingly unrelated constructions: Consider a 3-dimensional cell in $\text{Cayley}(\mathbf{A}^{(1)}, \mathbf{A}^{(2)})$. Let us call this a full-dimensional Cayley cell. Since both $\mathbf{A}^{(1)}$ and $\mathbf{A}^{(2)}$ are 2-dimensional, this cell must contain points from both $\mathbf{A}^{(1)}$ and $\mathbf{A}^{(2)}$. One Cayley cell is, e.g., given by the label set

$$S := \{1_1, 2_1, 1_2, 2_2, 3_2\}. \quad (9.8)$$

Now, produce all pairs of labels $(j_1^{(1)}, j_2^{(2)})$, with $j^{(1)} \in J^{(1)}$ and $j^{(2)} \in J^{(2)}$. This yields for our Cayley cell:

$$\hat{S} := \{(1, 1), (1, 2), (1, 3), (2, 1), (2, 2), (2, 3)\} = \{1, 2\} \times \{1, 2, 3\}. \quad (9.9)$$

This obviously labels a 2-dimensional cell in the Minkowski sum that is labeled by a product. We call such a cell a full-dimensional *Minkowski cell*.

Even better, we can see from the product description from which Cayley cell we started: Just put subscript 1 to the elements of the first factor and subscript 2 to the elements of the second factor. This means that for our example:

Observation 9.2.1. *Cayley cells are in one-to-one correspondence with Minkowski cells.*

Now, look at the following polyhedral subdivision of Cayley($\mathbf{A}^{(1)}, \mathbf{A}^{(2)}$) (that this is actually a polyhedral subdivision can be seen by drawing a picture):

$$\mathcal{S} := \left\{ \{1_1, 2_1, 1_2, 2_2, 3_2\}, \right. \quad (9.10)$$

$$\{1_1, 3_1, 1_2, 3_2\}, \quad (9.11)$$

$$\left. \{1_1, 2_1, 3_1, 4_1, 3_2\} \right\}. \quad (9.12)$$

According to our observation, this collection of cells corresponds to the following collection of cells:

$$\hat{\mathcal{S}} := \left\{ \begin{array}{l} \{1, 2\} \times \{1, 2, 3\}, \\ \{1, 3\} \times \{1, 3\}, \end{array} \right. \quad (9.13)$$

$$\left. \{1, 2, 3, 4\} \times \{3\} \right\}. \quad (9.14)$$

$$(9.15)$$

Consulting Figures 9.26 through 9.32, we see that this is a valid polyhedral subdivision of $\mathbf{A}^{(1)} + \mathbf{A}^{(2)}$!

We could play the same game in the other direction and we could check all possible subdivisions with the same result. Therefore, in our example we have:

Observation 9.2.2. *Polyhedral subdivisions of the Cayley embedding are in one-to-one correspondence with polyhedral subdivisions of the Minkowski sum by cells that are labeled by products.*

The goal of the following sections is to sketch a prove of this correspondence in general. And this is surprisingly easy with the tools that we have already.

9.2.2 Mixed subdivisions and the Minkowski projection

For the ease of exposition, we will in the following restrict ourselves to the case of two summands. The case of an arbitrary number of summands produces no extra difficulties. So, let $\mathbf{A}^{(1)}$ and $\mathbf{A}^{(2)}$ be arbitrary point configurations in the same ambient space \mathbb{R}^d .

Definition 9.2.3 (Minkowski Sum). The *Minkowski sum* $\mathbf{A}^{(1)} + \mathbf{A}^{(2)}$ of $\mathbf{A}^{(1)}$ and $\mathbf{A}^{(2)}$ in \mathbb{R}^d labeled by $J^{(1)}$ and $J^{(2)}$, respectively, is the following point configuration:

$$\mathbf{A}^{(1)} + \mathbf{A}^{(2)} := \left(\mathbf{a}_{j^{(1)}}^{(1)} + \mathbf{a}_{j^{(2)}}^{(2)} \right)_{j^{(1)} \in J^{(1)}, j^{(2)} \in J^{(2)}}, \quad (9.16)$$

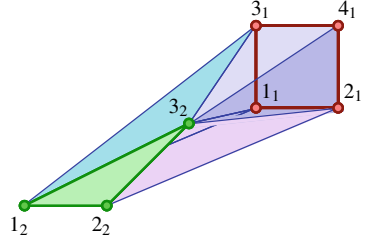


Figure 9.28: A subdivision \mathcal{S} of the Cayley embedding.

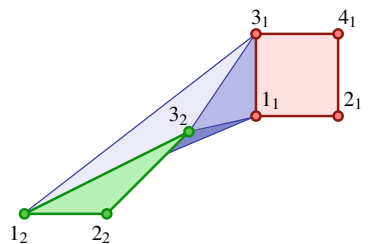
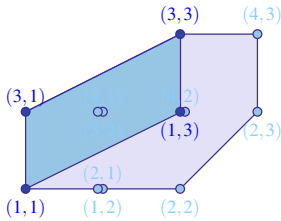
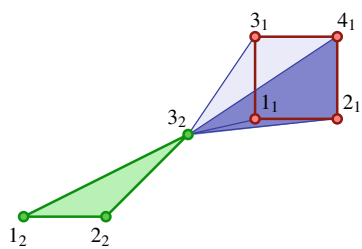
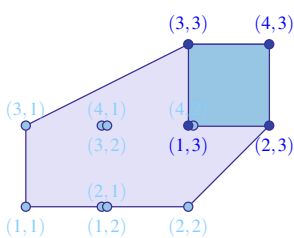
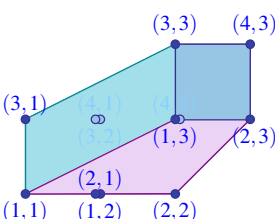


Figure 9.29: The second cell in \mathcal{S} .

Figure 9.30: The corresponding cell in $\hat{\mathcal{S}}$.Figure 9.31: The last cell in \mathcal{S} .Figure 9.32: The corresponding cell in $\hat{\mathcal{S}}$.Figure 9.33: We obtain a subdivision \mathcal{S} of the Minkowski sum.

where $\mathbf{a}_{j^{(1)}}^{(1)} + \mathbf{a}_{j^{(2)}}^{(2)}$ denotes the affine sum of $\mathbf{a}_{j^{(1)}}^{(1)}$ and $\mathbf{a}_{j^{(2)}}^{(2)}$, i.e., addition inside the common affine space. The Minkowski sum is labeled by $J^{(1)} \times J^{(2)}$.

The Minkowski sum of more than two point configurations can be defined analogously.

It is not essential to prefer the affine sum over the homogeneous sum, but it is in concordance with the literature.

Definition 9.2.4 (Mixed Cells). A subset B of labels in $J^{(1)} \times J^{(2)}$ is a *mixed cell* if it is the product of a label set $B^{(1)} \subseteq J^{(1)}$ and a label set $B^{(2)} \subseteq J^{(2)}$. A subconfiguration of $\mathbf{A}^{(1)} + \mathbf{A}^{(2)}$ is *mixed* if it is labeled by a mixed cell.

Let us look at our example:

- $\{(1,1)\} \times \{(1,1)\} = \{(1,1)\}$ is a mixed cell; the corresponding point configuration is

$$\begin{pmatrix} (1,1) \\ 0 \\ 0 \\ 1 \end{pmatrix}. \quad (9.17)$$

- $\{(1,2,3,4)\} \times \{(1,2,3)\}$ is a mixed cell; the corresponding point configuration is $\mathbf{A}^{(1)} + \mathbf{A}^{(2)}$.
- $\{(1,2)\} \times \{(1,2)\} = \{(1,1), (1,2), (2,1), (2,2)\}$ is a mixed cell that is one-dimensional, since the summands are parallel segments; the resulting point configuration has a double point:

$$\begin{pmatrix} (1,1) & (1,2) & (2,1) & (2,2) \\ 0 & 1 & 1 & 2 \\ 0 & 0 & 0 & 0 \\ 1 & 1 & 1 & 1 \end{pmatrix}. \quad (9.18)$$

- $\{(1,2)\} \times \{(1,3)\} = \{(1,1), (1,3), (2,1), (2,3)\}$ is a mixed cell that is a parallelogram. The resulting point configuration is:

$$\begin{pmatrix} (1,1) & (1,3) & (2,1) & (2,3) \\ 0 & 2 & 1 & 3 \\ 0 & 1 & 0 & 1 \\ 1 & 1 & 1 & 1 \end{pmatrix} \quad (9.19)$$

- The set of labels $\{(1,1), (2,2)\}$, leading to the configuration

$$\begin{pmatrix} (1,1) & (2,2) \\ 0 & 2 \\ 0 & 0 \\ 1 & 1 \end{pmatrix} \quad (9.20)$$

does not form a mixed cell because it is not a product. Note that its convex hull is a facet of the convex hull of $\mathbf{A}^{(1)} + \mathbf{A}^{(2)}$. The cell itself, however, is not, according to our Definition 2.1.17. This shows again that our combinatorial model for a point configuration is more powerful than plain geometry.

- The configuration

$$\begin{array}{cccc} (1,1) & (1,3) & (1,2) & (2,3) \\ \left(\begin{array}{cccc} 0 & 2 & 1 & 3 \\ 0 & 1 & 0 & 1 \\ 1 & 1 & 1 & 1 \end{array} \right) \end{array} \quad (9.21)$$

has the same coordinates as the one in Equation (9.19). It is, however, not a mixed cell, since it contains the “wrong” copy of $(1,0,1)^T$, namely the one labeled by $(1,2)$ as opposed to $(2,1)$. This way, the label set is not a product and thus the cell is not mixed. If we had defined mixed cells only as Minkowski sums of subsets (with no reference to labels), then we could not distinguish the cell in Equation (9.21) from the one in Equation (9.19), and then the Cayley trick would simply not be true. Sometimes you have got to be picky with the definitions in order to obtain the most beautiful results!

Definition 9.2.5 (Mixed Subdivision). A polyhedral subdivision of $\mathbf{A}^{(1)} + \mathbf{A}^{(2)}$ is *mixed* if all its cells are mixed cells.

Now we can simply check whether a collection \mathcal{S} of subsets of $J^{(1)} \times J^{(2)}$ forms a mixed subdivision: if all cells are products, then the subdivision is mixed. Here are examples for our special configuration:

- The subdivision

$$\mathcal{S}_0 := \{ \{(1,1), (1,2), (1,3), (2,1), (2,2), (2,3), \} \quad (9.22)$$

$$(3,1), (3,2), (3,3), (4,1), (4,2), (4,3)\} \quad (9.23)$$

is the trivial subdivision. Its only cell is $J^{(1)} \times J^{(2)}$.

- The subdivision

$$\mathcal{S}_1 := \{ \{(1,1), (1,3), (2,1), (2,3)\}, \quad (9.24)$$

$$\{(2,1), (2,2), (2,3)\}, \quad (9.25)$$

$$\{(1,3), (2,3), (3,3), (4,3)\}, \quad (9.26)$$

$$\{(1,1), (3,1), (1,3), (3,3)\} \}. \quad (9.27)$$

is mixed because it can be written as

$$\mathcal{S}_1 = \{ \{1,2\} \times \{1,3\}, \quad (9.28)$$

$$\{2\} \times \{1,2,3\}, \quad (9.29)$$

$$\{1,2,3,4\} \times \{3\}, \quad (9.30)$$

$$\{1,3\} \times \{1,3\} \}. \quad (9.31)$$

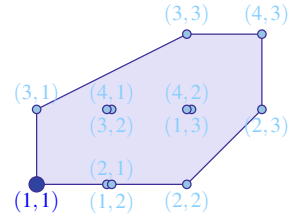


Figure 9.34: A cell with a single point.

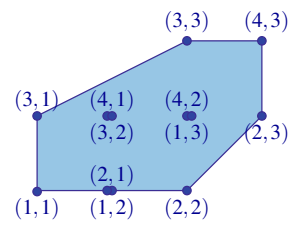


Figure 9.35: A cell with all points.

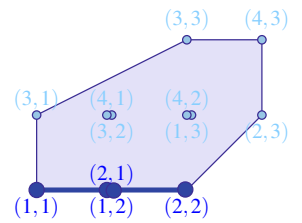


Figure 9.36: A cell with a multiple point.

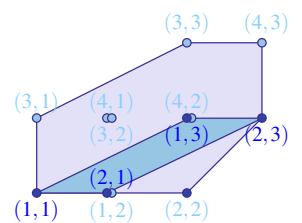


Figure 9.37: A cell with the “right” copy of a multiple point.

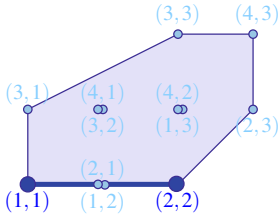


Figure 9.38: Not a cell.

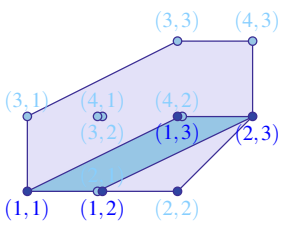


Figure 9.39: A non-cell with the "wrong" copy of a multiple point.

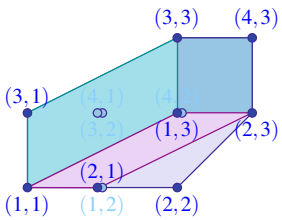


Figure 9.40: A mixed subdivision.

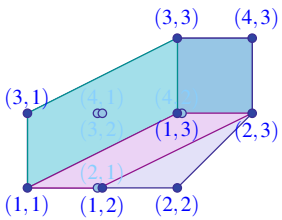


Figure 9.41: A non-mixed subdivision with the same geometric cells.

- The subdivision

$$\mathcal{S}_2 := \{(1,1), (1,3), (1,2), (2,3)\}, \quad (9.32)$$

$$\{(1,2), (2,2), (2,3)\}, \quad (9.33)$$

$$\{(1,3), (2,3), (3,3), (4,3)\}, \quad (9.34)$$

$$\{(1,1), (3,1), (1,3), (3,3)\}\} \quad (9.35)$$

is not mixed because it contains the non-mixed cell from Equation 9.21. It is a valid subdivision of $\mathbf{A}^{(1)} + \mathbf{A}^{(2)}$ though, because the only difference to the mixed subdivision in Equation 9.32 is the replacement of $(2,1)$ by $(1,2)$ in every cell, which does not affect any of our characterizations of polyhedral subdivisions in Section 4.5.

We want to look at this from a different point of view. Let $n^{(i)}$ be the number of points in $\mathbf{A}^{(i)}$. Consider the standard simplices with $n^{(1)}$ and $n^{(2)}$ vertices, respectively. In our example, these simplices are given as follows:

$$\mathbf{D}_4 = \begin{pmatrix} 1 & 2 & 3 & 4 \\ 1 & 0 & 0 & 0 \\ 0 & 1 & 0 & 0 \\ 0 & 0 & 1 & 0 \\ 0 & 0 & 0 & 1 \end{pmatrix}, \quad (9.36)$$

$$\mathbf{D}_3 = \begin{pmatrix} 1 & 0 & 0 \\ 0 & 1 & 0 \\ 0 & 0 & 1 \end{pmatrix}. \quad (9.37)$$

$\mathbf{D}_{n^{(1)}}$ projects to $\mathbf{A}^{(1)}$ in a natural way: each vertex of the simplex projects to the point in $\mathbf{A}^{(1)}$ with the same label, similarly for $\mathbf{D}_{n^{(2)}}$ and $\mathbf{A}^{(2)}$. Let us call these projections $\pi^{(1)}$ and $\pi^{(2)}$, respectively.

Now let us look at the product of the two simplices. In our example, it is the following point configuration (it does not matter that the product configuration is not full-dimensional in the following coordinatization):

$$\mathbf{D}_4 \times \mathbf{D}_3 := \left(\begin{array}{ccccccc} (I, I) & (I, 2) & (I, 3) & (2, I) & (2, 2) & (2, 3) & \dots \\ 1 & 1 & 1 & 0 & 0 & 0 & \dots \\ 0 & 0 & 0 & 1 & 1 & 1 & \dots \\ 0 & 0 & 0 & 0 & 0 & 0 & \dots \\ 0 & 0 & 0 & 0 & 0 & 0 & \dots \\ 1 & 0 & 0 & 1 & 0 & 0 & \dots \\ 0 & 1 & 0 & 0 & 1 & 0 & \dots \\ 0 & 0 & 1 & 0 & 0 & 1 & \dots \\ \dots & (3, 1) & (3, 2) & (3, 3) & (4, 1) & (4, 2) & (4, 3) \\ \dots & 0 & 0 & 0 & 0 & 0 & 0 \\ \dots & 0 & 0 & 0 & 0 & 0 & 0 \\ \dots & 1 & 1 & 1 & 0 & 0 & 0 \\ \dots & 0 & 0 & 0 & 1 & 1 & 1 \\ \dots & 1 & 0 & 0 & 1 & 0 & 0 \\ \dots & 0 & 1 & 0 & 0 & 1 & 0 \\ \dots & 0 & 0 & 1 & 0 & 0 & 1 \end{array} \right) \quad (9.38)$$

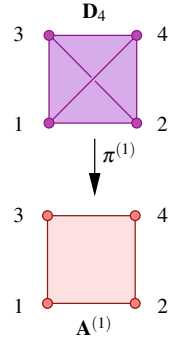


Figure 9.42: The projection $\pi^{(1)}$ of the vertices of the standard 3-simplex (with 4 points) onto $A^{(1)}$.

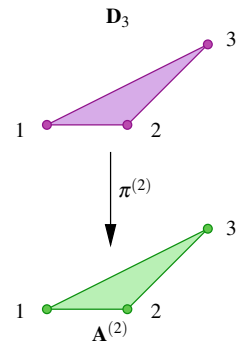


Figure 9.43: The projection $\pi^{(2)}$ of the vertices of the standard 2-simplex (with 3 points) onto $A^{(2)}$.

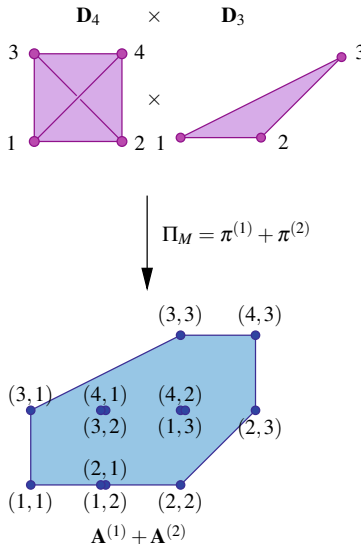
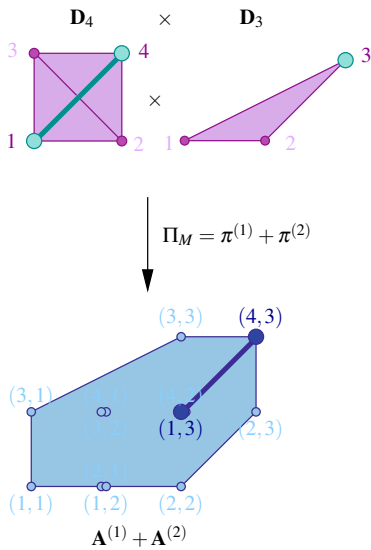
Consider the following *Minkowski projection*, given by mapping points in the product of the two simplices to points in the Minkowski sum with the same labels:

$$\Pi_M : \left\{ \begin{array}{l} \mathbf{D}_{n^{(1)}} \times \mathbf{D}_{n^{(2)}} \rightarrow A^{(1)} + A^{(2)} \\ \left(\begin{array}{c} (j^{(1)}, j^{(2)}) \\ \mathbf{d}_{j^{(1)}}^{(1)} \\ \mathbf{d}_{j^{(2)}}^{(2)} \end{array} \right) \mapsto \left(\pi^{(1)}(\mathbf{d}_{j^{(1)}}^{(1)}) + \pi^{(2)}(\mathbf{d}_{j^{(2)}}^{(2)}) \right) \end{array} \right. \quad (9.39)$$

We claim that Mixed subdivisions can be characterized as follows:

Observation 9.2.6 (Mixed = Π_M -compatible). *A subdivision of $A^{(1)} + A^{(2)}$ is a mixed subdivision if and only if it is Π_M -compatible.*

Proof. To prove this let us discuss what a cell $B \subseteq J^{(1)} \times J^{(2)}$ in a mixed Π_M -compatible subdivision must look like. B must, by the definition of Π_M -compatible, label a face of the product of simplices $\mathbf{D}_{n^{(1)}} \times \mathbf{D}_{n^{(2)}}$. That means, it must label a product of non-empty faces $S^{(1)} \times S^{(2)}$ with $S^{(1)} \leq \mathbf{D}_{n^{(1)}}$ and $S^{(2)} \leq \mathbf{D}_{n^{(2)}}$. Therefore, B is the label set $B^{(1)} \times B^{(2)}$ of $S^{(1)} \times S^{(2)}$. Since all non-empty subconfiguration of simplices are non-empty faces, each $R^{(1)} \times R^{(2)} \subset J^{(1)} \times J^{(2)}$ with $R^{(1)}, R^{(2)}$ non-empty is a mixed cell. In a nutshell: a subset of $J^{(1)} \times J^{(2)}$ is a mixed cell Π_M -compatible if and only if it is a product, i.e., mixed. \square

Figure 9.44: The Minkowski projection Π_M .Figure 9.45: A cell is Π_M -compatible if and only if it is mixed.

By the virtue of this characterization, we get some additional concepts for free:

Definition 9.2.7. A mixed subdivision is *fine* if it is Π_M -tight. It is *coherent* if it is Π_M -coherent.

Remark 9.2.8. Here is what happens geometrically: The cell $\mathbf{S} = \Pi_M(\mathbf{S}^{(1)} \times \mathbf{S}^{(2)})$ as a point configuration is just a Minkowski sum $\mathbf{B}^{(1)} + \mathbf{B}^{(2)}$ of a non-empty subconfiguration $\mathbf{B}^{(1)} = \pi^{(1)}(\mathbf{S}^{(1)})$ of $\mathbf{A}^{(1)}$ and a non-empty subconfiguration $\mathbf{B}^{(2)} = \pi^{(2)}(\mathbf{S}^{(2)})$ of $\mathbf{A}^{(2)}$. Note that in the case of multiple points the copy with the right label must be chosen so that the label set of the mixed cell is a product.

Remark 9.2.9 (Zonotopes). Recall that a *zonotope* \mathbf{Z} is any Minkowski sum of line segments, and that its *zonotopal tilings* are, by Lemma 9.1.8, the subdivisions compatible with the natural projection $\pi : \mathbf{I}^n \rightarrow \mathbf{Z}$. Since \mathbf{I}^n is simply the product of n copies of the “simplex” \mathbf{D}_2 , we have that:

Lemma 9.2.10. Let the zonotope \mathbf{Z} be the Minkowski sum $\mathbf{A}^{(1)} + \cdots + \mathbf{A}^{(n)}$ of n segments. Then, the zonotopal tilings of \mathbf{Z} are the same as the mixed subdivisions of the Minkowski sum $\mathbf{A}^{(1)} + \cdots + \mathbf{A}^{(n)}$. Subdivisions that are coherent in one sense are also coherent in the other, and tight zonotopal tilings correspond to fine mixed subdivisions.

9.2.3 Subdivisions in the Cayley embedding and the Cayley projection

This time, we describe the general construction of the Cayley embedding of two point configurations $\mathbf{A}^{(1)}$ and $\mathbf{A}^{(2)}$. The easiest way to think about Cayley embeddings would be to put $\mathbf{A}^{(1)}$ and $\mathbf{A}^{(2)}$ into parallel affine spaces by using an extra coordinate 0 for the points in $\mathbf{A}^{(1)}$ and 1 for the points in $\mathbf{A}^{(2)}$. But this would break the symmetry between $\mathbf{A}^{(1)}$ and $\mathbf{A}^{(2)}$: there is no natural way of deciding who should receive the extra 0 and who should receive the extra 1. Essentially, we would like to see that an exchange of $\mathbf{A}^{(1)}$ and $\mathbf{A}^{(2)}$ in $\text{Cayley}(\mathbf{A}^{(1)}, \mathbf{A}^{(2)})$ will result in at most a reordering of coordinates. This can be achieved by the following definition that in addition has the most intuitive generalization to more than two starting configurations.

Definition 9.2.11 (Cayley Embedding). The Cayley embedding of $\mathbf{A}^{(1)}$ and $\mathbf{A}^{(2)}$, denoted by $\text{Cayley}(\mathbf{A}^{(1)}, \mathbf{A}^{(2)})$, is the following $d+1$ -dimensional point configuration:

$$\text{Cayley}(\mathbf{A}^{(1)}, \mathbf{A}^{(2)}) := \begin{pmatrix} (j^{(1)}, 1) & (j^{(2)}, 2) \\ \mathbf{a}_{j^{(1)}}^{(1)} & \mathbf{a}_{j^{(2)}}^{(2)} \\ 1 & 0 \\ 0 & 1 \end{pmatrix}_{j^{(1)} \in J^{(1)}, j^{(2)} \in J^{(2)}} \quad (9.40)$$

It is labeled by $J^{(1)} \times \{1\} \cup J^{(2)} \times \{2\}$, where we occasionally use the subscript notation $j_i^{(i)}$ for each $(j^{(i)}, i)$. The Cayley embedding of more than

two summands can be defined analogously. Each summand adds one to the dimension.

The cumbersome generic label notation comes from the fact that very frequently we want to label the starting point configurations $\mathbf{A}^{(i)}$ with the numbers from 1 to $n^{(i)}$. That means, there are identical labels in $J^{(1)}$ and $J^{(2)}$. In the Cayley embedding we need to distinguish them, so they receive an extra marker. You can see this in the example in Section 9.2.1.

In the same example all subdivisions of the Cayley embedding correspond to mixed subdivisions in the Minkowski sum. So, there is nothing special about the subdivisions we are looking at in the Cayley embedding. Nevertheless, we will take the projection view from above again.

In Section 9.1.3, we have seen that every polyhedral subdivision of a point configuration is compatible to a projection of a simplex to the point configuration. We are now doing exactly the same thing here. As above, let $\pi^{(1)}$ and $\pi^{(2)}$ be projections from $\mathbf{D}_{n^{(1)}}$ to $\mathbf{A}^{(2)}$ and $\mathbf{D}_{n^{(2)}}$ to $\mathbf{A}^{(2)}$, respectively.

Now let us look at the *simplicial join* of the two simplices. In our example, it is the following point configuration (it again does not matter that the join configuration is not full-dimensional in the following coordinatization):

$$\mathbf{D}_4 * \mathbf{D}_3 := \begin{pmatrix} I_1 & 2_1 & 3_1 & 4_1 & I_2 & 2_2 & 3_2 \\ 1 & 0 & 0 & 0 & 0 & 0 & 0 \\ 0 & 1 & 0 & 0 & 0 & 0 & 0 \\ 0 & 0 & 1 & 0 & 0 & 0 & 0 \\ 0 & 0 & 0 & 1 & 0 & 0 & 0 \\ 0 & 0 & 0 & 0 & 1 & 0 & 0 \\ 0 & 0 & 0 & 0 & 0 & 1 & 0 \\ 0 & 0 & 0 & 0 & 0 & 0 & 1 \end{pmatrix} \quad (9.41)$$

Essentially, the matrix of the join is the block-diagonal formed by the matrices of the operands. That means, in particular, that joins of standard simplices are standard simplices again.

Consider the following *Cayley projection*, where—similarly to the Minkowski projection—a point in the join of the two simplices is mapped to the point in the Cayley embedding with the same labels:

$$\Pi_C : \left\{ \begin{array}{l} \mathbf{D}_{n^{(1)}+n^{(2)}} = \mathbf{D}_{n^{(1)}} * \mathbf{D}_{n^{(2)}} \rightarrow \text{Cayley}(\mathbf{A}^{(1)}, \mathbf{A}^{(2)}) \\ \left(\begin{array}{c} (j^{(1)}, 1) \\ \mathbf{d}_{j^{(1)}} \\ \mathbf{0} \end{array} \right) \mapsto \left(\begin{array}{c} (j^{(1)}, 1) \\ \pi^{(1)}(\mathbf{d}_{j^{(1)}}) \\ 1 \\ 0 \end{array} \right) \\ \left(\begin{array}{c} (j^{(2)}, 2) \\ \mathbf{0} \\ \mathbf{d}_{j^{(2)}} \end{array} \right) \mapsto \left(\begin{array}{c} (j^{(2)}, 2) \\ \pi^{(2)}(\mathbf{d}_{j^{(2)}}) \\ 0 \\ 1 \end{array} \right) \end{array} \right. \quad (9.42)$$

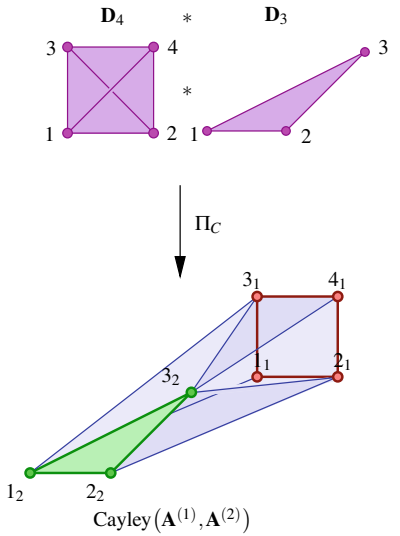


Figure 9.46: The Cayley projection Π_C .

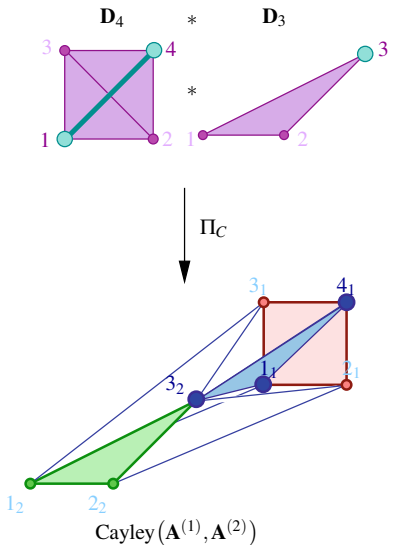


Figure 9.47: Any cell is Π_C -compatible, and any full-dimensional cell contains non-empty subsets of both operands of the Cayley embedding.

Then, it is clear by the considerations in Section 9.1.3 that the following holds.

Observation 9.2.12 (Cayley subdivision = Π_C -compatible). *Any subdivision of Cayley($\mathbf{A}^{(1)}, \mathbf{A}^{(2)}$) is Π_C -compatible.*

Remark 9.2.13 (Lawrence polytopes). We recall here the *Lawrence polytopes* introduced in Section 5.5.3. Remember that the Lawrence polytope $\Lambda(\mathbf{A})$ of a configuration \mathbf{A} is defined as the configuration having as its Gale transform the union of $\text{Gale}(\mathbf{A})$ and its opposite. That is:

$$\text{Gale}(\Lambda(\mathbf{A})) = \text{Gale}(\mathbf{A}) \cup (-\text{Gale}(\mathbf{A}))$$

But a more direct definition in matrix form was found in Proposition 5.5.12

$$\Lambda(\mathbf{A}) = \begin{pmatrix} \mathbf{0} & \mathbf{A} \\ \mathbf{1} & \mathbf{1} \end{pmatrix}, \quad (9.43)$$

where $\mathbf{1}$ and $\mathbf{0}$ denote the unit and the zero matrices of the appropriate dimensions ($n \times n$ and $r \times n$, respectively, if \mathbf{A} is represented by an $r \times n$ matrix).

Let $\mathbf{a}_1, \dots, \mathbf{a}_n$ denote the elements of \mathbf{A} ; that is to say, the columns of \mathbf{A} as a matrix. Reordering the columns of the right hand side of equation (9.43) we see that $\Lambda(\mathbf{A})$ is also represented by the matrix

$$\begin{pmatrix} \mathbf{0} & \mathbf{a}_1 & \mathbf{0} & \mathbf{a}_2 & \dots & \mathbf{0} & \mathbf{a}_n \\ 1 & 1 & 0 & 0 & \dots & 0 & 0 \\ 0 & 0 & 1 & 1 & \dots & 0 & 0 \\ \vdots & \vdots & \vdots & \vdots & \ddots & \vdots & \vdots \\ 0 & 0 & 0 & 0 & \dots & 1 & 1 \end{pmatrix},$$

where $\mathbf{0} \in \mathbb{R}^r$ is the zero vector. But this is simply the Cayley embedding of the n segments $[\mathbf{0}\mathbf{a}_i]$, $i = 1, \dots, n$. Thus:

Lemma 9.2.14. *The Lawrence polytope of a configuration \mathbf{A} with points $(\mathbf{a}_1, \mathbf{a}_2, \dots, \mathbf{a}_n)$ equals the Cayley embedding of the segments $\{[\mathbf{0}\mathbf{a}_i]\}_{i=1, \dots, n}$.*

9.2.4 The Cayley trick

With our explicit labeling of points in the Minkowski sum and the Cayley embedding, respectively, we are in a position to state the Cayley trick very easily. Consider the following map from cells in the Cayley embedding to cells in the Minkowski sum.

Definition 9.2.15 (Cayley Map). The *Cayley map* is the following map that associates to every cell in Cayley($\mathbf{A}^{(1)}, \mathbf{A}^{(2)}$) a mixed cell in $\mathbf{A}^{(1)} + \mathbf{A}^{(2)}$ via

$$\Phi_C : \begin{cases} 2^{J^{(1)} \times \{1\} \cup J^{(2)} \times \{2\}} & \rightarrow 2^{J^{(1)} \times J^{(2)}} \\ (B^{(1)}, 1) \cup (B^{(2)}, 2) & \mapsto B^{(1)} \times B^{(2)} \end{cases} \quad (9.44)$$

where, by convention, any product with the empty set is the empty set.

Since any collection of cells in the Cayley embedding is mapped by Φ_C to a collection of mixed cells in the Minkowski embedding, it is interesting to ask whether subdivisions of the Cayley embedding map to mixed subdivisions in the Minkowski sum. This is indeed the case, and this is the content of the *Cayley trick without restrictions*.

Theorem 9.2.16 (Cayley Trick without Restrictions). *The Cayley map induces a poset isomorphism from the refinement poset of all Π_C -compatible subdivisions of $\text{Cayley}(\mathbf{A}^{(1)}, \mathbf{A}^{(2)})$ to the refinement poset of all Π_M -compatible subdivisions of $\mathbf{A}^{(1)} + \mathbf{A}^{(2)}$.*

We do not prove this here because something even more general is true. So far, we started out from projections of simplices. This led to arbitrary polyhedral subdivisions in the Cayley embedding. We can equally well just fix more general projections of vertices of polytopes $\pi^{(1)} : \text{vert}(\mathbf{P}) \rightarrow \mathbf{A}^{(1)}$ and $\pi^{(2)} : \text{vert}(\mathbf{P}) \rightarrow \mathbf{A}^{(2)}$ and look at Π_C -compatible and Π_M -compatible subdivisions, respectively. The crucial thing: although now the set of possible cells is restricted, the restrictions in both the Cayley embedding and the Minkowski sum are identical!

For the largest generality of the Cayley trick, we need the notion of a weighted Minkowski sum.

Definition 9.2.17 (Weighted Minkowski Sum). Let $\lambda = (\lambda_1, \dots, \lambda_k)$ be a vector with $\lambda_1, \dots, \lambda_k > 0$ and $\sum_{i=1}^k \lambda_i = 1$.

The Minkowski sum of $\mathbf{A}^{(1)}, \dots, \mathbf{A}^{(k)}$ scaled by λ is the following point configuration:

$$\sum_{i=1}^k \lambda_i \mathbf{A}^{(i)} := \left(\begin{array}{c} (j^{(1)}, \dots, j^{(k)}) \\ \sum_{i=1}^k \lambda_i \mathbf{a}_{j^{(i)}}^{(i)} \end{array} \right)_{j^{(1)} \in J^{(1)}, \dots, j^{(k)} \in J^{(k)}}, \quad (9.45)$$

This time, the sum may be taken directly from the homogeneous coordinates, since the condition $\sum_{i=1}^k \lambda_i = 1$ ensures that the affine space of the operands is not left out.

We now are proud to state the following beautiful discovery in full generality; it was first proved in [165].

Theorem 9.2.18 (Cayley Trick with Restrictions). *Let $\mathbf{P}^{(i)}$, $i = 1, \dots, k$, be polytopes with vertex sets $\mathbf{V}^{(i)}$ labeled by $J^{(i)}$, each $\mathbf{v}_{j^{(i)}}^{(i)}$ having $p^{(i)}$ homogeneous coordinates. Moreover, let*

$$\pi^{(i)} : \begin{cases} \mathbf{V}^{(i)} & \rightarrow \mathbf{A}^{(i)} \\ \left(\mathbf{v}_{j^{(i)}}^{(i)} \right) & \mapsto \left(\pi^{(i)}(\mathbf{v}_{j^{(i)}}^{(i)}) =: \mathbf{a}_{j^{(i)}}^{(i)} \right) \end{cases} \quad (9.46)$$

be arbitrary projections to \mathbb{R}^d , image points labeled with the labels of their

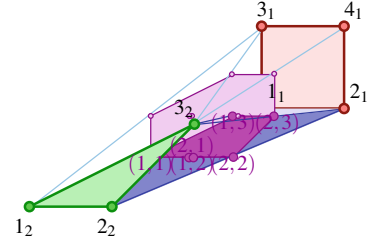


Figure 9.48: The image of the first cell in our example subdivision \mathcal{S} under the Cayley map Φ_C , viewed as a subset of the Cayley embedding: Its convex hull is obtained by intersecting the cell in the Cayley embedding with the affine subspace W ; other weightings are obtained by sliding W back and forth between the copies of $\mathbf{A}^{(1)}$ and $\mathbf{A}^{(2)}$.

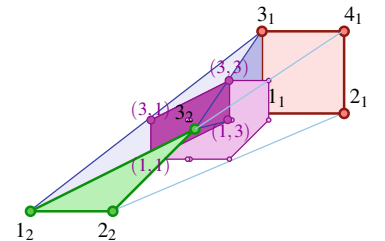


Figure 9.49: The image of the second cell in \mathcal{S} under the Cayley map Φ_C .

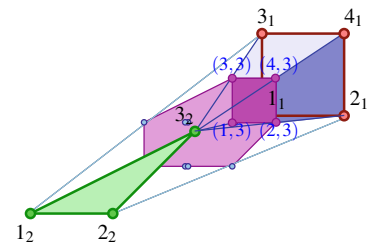


Figure 9.50: The image of the third cell in \mathcal{S} under the Cayley map Φ_C .

preimages. Let

$$\Pi_M := \lambda_1 \pi^{(1)} + \cdots + \lambda_k \pi^{(k)} : \begin{cases} \mathbf{V}^{(1)} \times \cdots \times \mathbf{V}^{(k)} & \rightarrow \quad \lambda_1 \mathbf{A}^{(1)} + \cdots + \lambda_k \mathbf{A}^{(k)} \\ \left(\begin{array}{c} (j^{(1)}, \dots, j^{(k)}) \\ \mathbf{v}_{j^{(1)}}^{(1)} \\ \vdots \\ \mathbf{v}_{j^{(k)}}^{(k)} \end{array} \right) & \mapsto \quad \left(\begin{array}{c} (j^{(1)}, \dots, j^{(k)}) \\ \lambda_1 \pi^{(1)}(\mathbf{v}_{j^{(1)}}^{(1)}) + \cdots + \lambda_k \pi^{(k)}(\mathbf{v}_{j^{(k)}}^{(k)}) \end{array} \right) \end{cases} \quad (9.47)$$

be the associated Minkowski projection and

$$\Pi_C := \text{Cayley}(\pi^{(1)}, \dots, \pi^{(k)}) : \begin{cases} \mathbf{V}^{(1)} * \cdots * \mathbf{V}^{(k)} & \rightarrow \quad \text{Cayley}(\mathbf{A}^{(1)}, \dots, \mathbf{A}^{(k)}) \\ (j^{(i)}, i) & \mapsto \quad (j^{(i)}, i) \\ \left(\begin{array}{c} \mathbf{0}^{p^{(1)}} \\ \vdots \\ \mathbf{0}^{p^{(i-1)}} \\ \mathbf{v}_{j^{(i)}}^{(i)} \\ \mathbf{0}^{p^{(i+1)}} \\ \vdots \\ \mathbf{0}^{p^{(k)}} \end{array} \right) & \mapsto \quad \left(\begin{array}{c} \pi^{(i)}(\mathbf{v}_{j^{(i)}}^{(i)}) \\ 0 \\ \vdots \\ 0 \\ 1 \\ 0 \\ \vdots \\ 0 \end{array} \right) \end{cases} \quad (9.48)$$

be the associated Cayley projection.

Then the Cayley map Φ_C that maps cells in the Cayley embedding to cells in the weighted Minkowski sum via

$$\Phi_C((B^{(1)}, 1) \cup \cdots \cup (B^{(k)}, k)) := B^{(1)} \times \cdots \times B^{(k)} \quad (9.49)$$

induces a poset isomorphism from the refinement poset of all Π_C -compatible subdivisions of the Cayley embedding $\text{Cayley}(\mathbf{A}^{(i)})_{i=1,\dots,k}$ to the refinement poset of Π_M -compatible subdivisions of the scaled Minkowski sum $\sum_{i=1}^k \lambda_i \mathbf{A}^{(i)}$ for all $\lambda = (\lambda_i)_{i=1,\dots,k}$ with $\lambda_i > 0$ and $\sum_{i=1}^k \lambda_i = 1$.

In this poset isomorphism, tight subdivisions correspond to tight subdivisions, and Π_C -coherent subdivisions correspond to Π_M -coherent subdivisions.

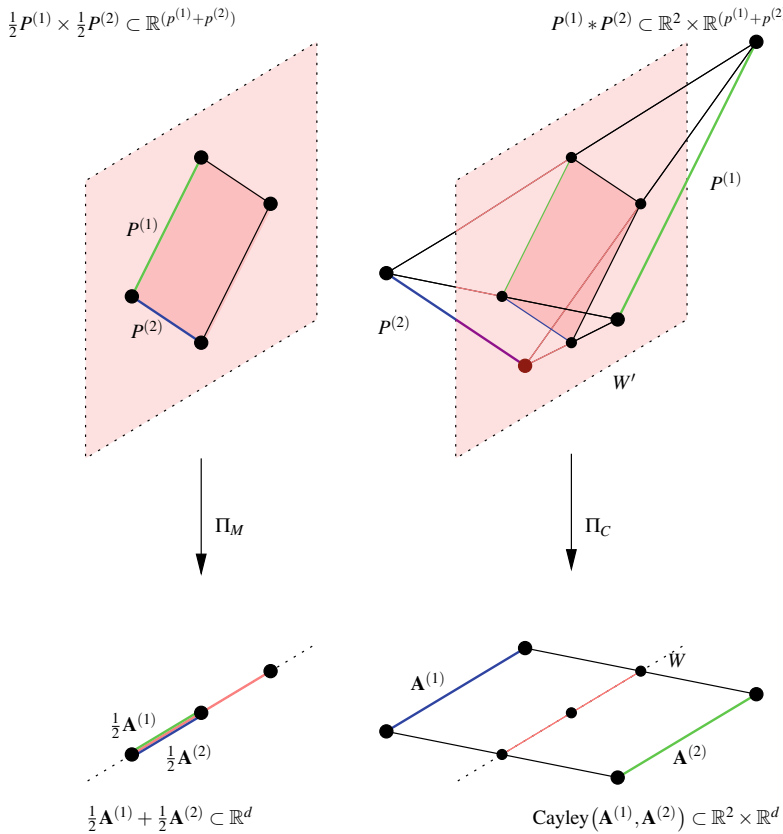


Figure 9.51: A sketch in which all relevant objects in the Cayley trick with restrictions can be seen; the product has scaled factors because that way the visualized projection is an orthogonal projection.

Figure 9.51 is an attempt to sketch the general situation in the smallest non-trivial example.

We just present a set of plausible observations and claims as a proof sketch. A formal check does not reveal more; it is, however, recommended as an exercise, since many concepts of this book can be revisited.

Proof Sketch. First note that it is sufficient to consider full-dimensional cells. On these cells, the Cayley map is bijective with an obvious inverse map. The key observation is that the Cayley map on cells has a geometric meaning: The image of any cell (including the trivial one) labels the intersection of the point configuration of the cell with an affine subspace of dimension d , namely

$$W := \left\{ \mathbf{x} \in \mathbb{R}^{d+k} : \mathbf{x}_{d+i} = \lambda_i, i = 1, \dots, k \right\}. \quad (9.50)$$

We list a couple of observations that together prove the theorem:

1. If we intersect the convex hull of the Cayley embedding with W , then we obtain the convex hull of the weighted Minkowski sum.

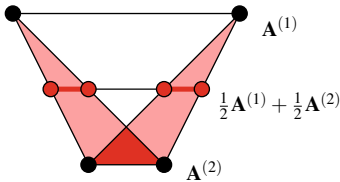


Figure 9.52: Two properly intersecting Minkowski cells whose corresponding Cayley cells intersect improperly; this cannot happen when the cells are full-dimensional and adjacent because, then the unique hyperplane separating the Minkowski cells, spanned by the common facet, induces a unique separating hyperplane separating the Cayley cells, spanned by the Cayley cell corresponding to that facet.

2. If we intersect the convex hull of any of the cells with W , then we obtain the convex hull of the corresponding mixed cell.
3. If two cells in the Cayley embedding are intersecting properly, then the corresponding cells in the weighted Minkowski sum are.
4. If two adjacent cells in the Cayley embedding are intersecting improperly, then the corresponding cells in the weighted Minkowski sum are adjacent and intersect improperly as well. (This statement is *not* true for general non-adjacent pairs of cells, though (see Figure 9.52).)
5. If in a subdivision of the weighted Minkowski sum there is a point in general position that is contained in the interior of exactly one full-dimensional cell then this very same point is contained in the relative interior of exactly one cell of the corresponding subdivision of the Cayley embedding.

Because of the first observation, the union of the convex hulls of a collection of cells in the Cayley embedding equals the convex hull of the Cayley embedding if and only if the corresponding union of convex hulls of the corresponding cells equals the convex hull of the weighted Minkowski sum. This shows that (UP) from Definition 2.3.1 holds in the Cayley embedding if and only if it holds in the weighted Minkowski sum.

Looking at our definition of polyhedral subdivisions via (CP), (UP), and (IP) in Definition 2.3.1 and the second observation, we see that every Π_C -compatible subdivision of the Cayley embedding maps to a valid mixed subdivision of the weighted Minkowski sum, since intersection with an affine subspace cannot

- destroy closedness under taking faces; therefore, (CP) must hold
- create uncovered points; therefore, (UP) must hold
- create interior intersections; therefore, (IP) must hold

This valid subdivision is Π_M -compatible because the corresponding restrictions are literally equivalent to the ones posed by Π_C -compatible.

For the other direction, we need the characterization by (MaxMP), (MaxAdjHP), (MaxAdjLP), and (IPP) in Theorem 4.5.13. The last two observations from above show that every Π_M -compatible subdivision of the weighted Minkowski sum corresponds to a valid subdivision of the Cayley embedding, since (MaxAdjHP) and (MaxAdjLP), because of the second-to-last observation, as well as (IPP), because of the last observation, are preserved. Π_C -compatibility is again literally equivalent to Π_M -compatibility.

The correspondence is order preserving because the intersection with an affine subspace preserves set inclusion. The correspondence preserves coherence because the fibers of Π_C and Π_M are isomorphic individually, and so are the fiber polytopes. \square

The Cayley trick as above is now a fairly general theorem. What can you do with it? One nice application of it relates zonotopal tilings of a zonotopal

to subdivisions of a Lawrence polytope. Remember that a zonotope is a Minkowski sum of segments and, by Lemma 9.2.10, zonotopal tilings of $\mathbf{Z} = [\mathbf{0}\mathbf{a}_1] + \cdots + [\mathbf{0}\mathbf{a}_n]$ are the same as the Π_M -compatible subdivisions for the natural projection

$$\Pi_M : \mathbf{I} \times \cdots \times \mathbf{I} \rightarrow \mathbf{Z},$$

where $\mathbf{I} \times \cdots \times \mathbf{I} = \mathbf{I}^n$ is the n -cube.

On the other hand, if we consider the vectors $\mathbf{a}_1, \dots, \mathbf{a}_n$ as the elements of a (point or vector) configuration \mathbf{A} , by Lemma 9.2.14 the Lawrence polytope $\Lambda(\mathbf{A})$ equals the Cayley embedding of the same segments $[\mathbf{0}\mathbf{a}_1], \dots, [\mathbf{0}\mathbf{a}_n]$. So, the Cayley trick implies the following nice result that, together with a result of Santos in [281], yields a new proof [165] of the famous Bohne-Dress Theorem [60].

Corollary 9.2.19. *The refinement poset of all zonotopal tilings of a zonotope is isomorphic to the refinement poset of all polyhedral subdivision of the corresponding Lawrence polytope. The correspondence preserves coherence (a.k.a. regularity), flips, etc.* \square

Example 9.2.20 (The permutohedron). Probably the simplest, yet one of the nicest examples where the Cayley trick applies is the permutohedron. Remember that the product $\mathbf{I} \times \mathbf{D}_n$ of a segment and an $(n - 1)$ -simplex has $n!$ triangulations, all of them regular, and the associated secondary polytope is the *permutohedron* (cf. Section 6.2.1, in particular Theorem 6.2.6). But $\mathbf{I} \times \mathbf{D}_n$ is the Cayley embedding of n parallel copies of the segment \mathbf{I} . By the Cayley trick, its secondary polytope must coincide with the fiber polytope of the natural projection

$$\Pi_M : \mathbf{I}^n \rightarrow \mathbf{I} + \cdots + \mathbf{I}.$$

Since this is a projection into dimension one (all copies of the segment are parallel), the Π_M -compatible subdivisions are the monotone paths on the cube \mathbf{I}^n , with respect to the functional $(1, \dots, 1)$. Hence:

Corollary 9.2.21. *The monotone path polytope of a regular cube with respect to the functional $(1, \dots, 1)$ is a regular permutohedron.*

In fact, the same is true for any functional on the cube, as long as it is generic in the sense of Section 9.1.1

9.2.5 Product of a triangle and k -simplex

Counting triangulations is in general very complicated, but one nice application of the above ideas can be used to detect non-regular triangulations and to count triangulations of the product of simplices.

In Section 6.2, we investigated products of simplices. It turns out that if one of the simplices involved is of much smaller dimension than the other one, the Cayley trick can help us.

According to the Cayley trick, the refinement poset of all polyhedral subdivisions of $\mathbf{D}_m \times \mathbf{D}_n = \text{Cayley}(\mathbf{D}_m, \dots, \mathbf{D}_m)$ (n operands) is isomorphic to the refinement poset of all mixed subdivision of $\mathbf{D}_m + \cdots + \mathbf{D}_m$

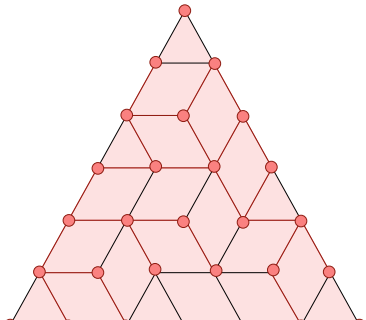


Figure 9.53: A non-coherent mixed subdivision of $6 \cdot \mathbf{D}_3$.

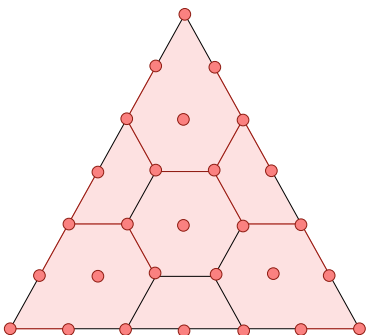


Figure 9.54: A coherent, but not fine, mixed subdivision of $6 \cdot \mathbf{D}_3$.

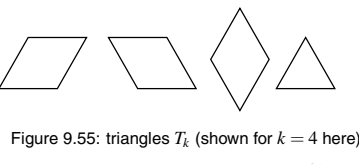
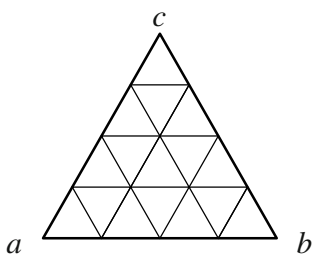


Figure 9.55: triangles T_k (shown for $k = 4$ here) will be subdivided by three types of “tiles”.

(n summands). This is especially useful if one of the factors has small dimension. Moreover, non-coherent mixed subdivisions correspond to non-regular triangulations, as was proved in [166].

For example, if $m = 3$, instead of investigating the product $\mathbf{D}_3 \times \mathbf{D}_n$, which is $n + 1$ -dimensional, one can investigate the n -fold Minkowski sum of the triangle, which is a 2-dimensional configuration. In general, we have the following:

Corollary 9.2.22. *The refinement poset of all polyhedral subdivisions $\mathbf{D}_p \times \mathbf{D}_q$ is isomorphic to the refinement poset of all mixed subdivisions of $\sum_{i=1}^q \mathbf{D}_p$. \square*

Applied to our small example $\mathbf{D}_3 \times \mathbf{D}_6$, we recover the fact that $\mathbf{D}_3 \times \mathbf{D}_6$ has non-regular subdivisions. The triangulation of the following corollary is actually the same as the one we constructed in Section 6.25 for Theorem 6.2.19. There we constructed it as a refinement of a regular subdivision with seven cells. Figure 9.54 shows that subdivision in a Cayley trick picture.

Corollary 9.2.23. *$\mathbf{D}_3 \times \mathbf{D}_6$ has a non-regular triangulation.*

Remark 9.2.24. The triangulation of the previous corollary is actually the same one we constructed in Section 6.25. There we constructed it as a refinement of a regular subdivision with seven cells. Figure 9.54 shows that subdivision in a Cayley trick picture.

Sketch of a Proof. Look at Figure 9.53: it shows a non-coherent (Exercise 9.4) mixed subdivision of the Minkowski sum. The corresponding triangulation of $\mathbf{D}_3 \times \mathbf{D}_6$ is non-regular because of the Cayley trick. \square

We can also try to picture the non-regular triangulation of $\mathbf{D}_4 \times \mathbf{D}_4$ via the Cayley trick. We now need to study mixed subdivisions of the four-fold sum of a tetrahedron \mathbf{D}_4 . Figure 9.56 shows one of them, obtained by cutting $4 \cdot \mathbf{D}_4$ via the four planes parallel to its facets and meeting at the barycenter. We leave it to the reader to check that this is the regular mixed subdivision obtained using the heights $\omega_{ii} = 0$, $i = 1, \dots, 4$ and $\omega_{ij} = 1$ if $i \neq j$. This mixed subdivision is not fine, that is, it corresponds to a regular subdivision of $\mathbf{D}_4 \times \mathbf{D}_4$ that is not a triangulation. But its only non-simplicial cells have corank 1 and can be triangulated independently. They correspond to the six cells that go “along the edges” of the tetrahedron in Figure 9.56. The figure also shows with dashed lines how to split each of them into two pieces, so that we get 20 pieces in total. That is the normalized volume of $\mathbf{D}_4 \times \mathbf{D}_4$, so that this refinement represents now a triangulations. We leave it to the reader to check that this triangulation is actually the non-regular triangulation of $\mathbf{D}_4 \times \mathbf{D}_4$ described in Section 6.2.4.

We begin looking at the case of $\mathbf{D}^2 \times \mathbf{D}^k$, i.e., the product of a triangle with a k -dimensional simplex. The main idea from [282] is that the triangulations of polytope $\mathbf{D}^2 \times \mathbf{D}^k$ can be pictured as 2-dimensional pictures of subdivisions of a rather symmetric planar point set whose cells are of very special kind. From that a simple and effective recursion formula will be

derived. More precisely consider the equilateral triangle T_k of side k ; in homogeneous coordinates its underlying point configuration consists of points (r, s, t) with $r + s + t = k$. See Figure 9.55. The polyhedral subdivisions we need use exactly k unit-one regular triangles and $(k^2 - k)/2$ “lozenge” cells that come in three orientations (up, left, right). Following common usage, we call these subdivisions *lozenge tilings*. See Figure 9.57 for an example. We will use the following lemma:

Lemma 9.2.25. *The number of triangulations of $\mathbf{D}^2 \times \mathbf{D}^{k-1}$ equals $k!$ times the number of lozenge tilings of T_k .*

We do not present the formal proof the lemma here. As a “proof by example” consider the case of $\mathbf{D}^2 \times \mathbf{D}^1$. Figure 9.58 shows all triangulations of this polytope. Observe that when you slice each of them through the middle by a horizontal plane, the resulting intersections will give exactly six different triangles which are subdivided by two triangles and a lozenge, as in Figure 9.58. The triangles are the “traces” of the intersection of the plane with the tetrahedra covering the top and bottom triangles of the prism, while the lozenge tile is a trace of the intersection with a mixed tetrahedron, namely two points on the top, two on the bottom.

In the figure, the letters T , B are used to denote such triangles. As predicted by Lemma 9.2.25 you can see that each tiling appears twice, with interchanged labeling.

The number of lozenge tilings of T_k can be computed in the following way. Let k be fixed, and let S be a subset of $\{1, 2, \dots, k\}$. We classify the lozenge tilings of T_k according to what triangles they have in the bottom line. More precisely, let $f_k(S)$ denote the number of lozenge tilings of T_k which have triangles exactly in the positions of the bottom line given by S . Similarly, let $g_k(S)$ denote the number of lozenge tilings of T_k which have triangles at least in the positions of the bottom line given by S . Clearly,

$$g_k(S) = \sum_{S' \subseteq S} f_k(S'). \quad (9.51)$$

But, moreover:

Proposition 9.2.26. *Let $S = \{s_1, \dots, s_j\} \neq \emptyset$, where $1 \leq s_1 < \dots < s_j \leq k$. If $j = 1$, then $f_k(S) = g_{k-1}(\emptyset)$. If $j > 1$, then:*

$$f_k(S) = \sum_{\substack{s_1 \leq s'_1 < s_2 \\ \vdots \\ s_{j-1} \leq s'_{j-1} < s_j}} g_{k-1}(\{s'_1, \dots, s'_{j-1}\}). \quad (9.52)$$

Proof. Between every two triangles of the bottom row there must be one and only one vertical lozenge. Once we fixed the positions s'_1, \dots, s'_{j-1} of these vertical lozenges, the ways to complete the lozenge tiling are exactly the same as the lozenge tilings of T_{k-1} containing triangles in (at least) the positions s'_1, \dots, s'_{j-1} of the bottom row. \square

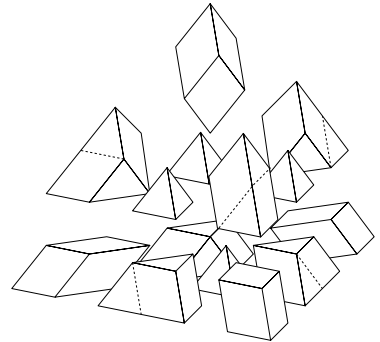


Figure 9.56: A non-coherent mixed subdivision of $4 \cdot \mathbf{D}_4$.

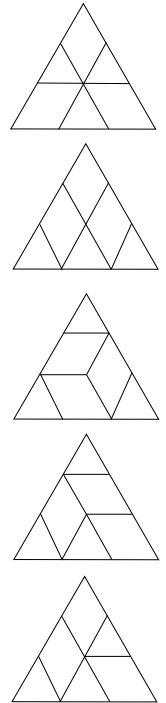


Figure 9.57: All combinatorial types of triangulations of $\mathbf{D}^2 \times \mathbf{D}^2$ shown here in their tiling representation.

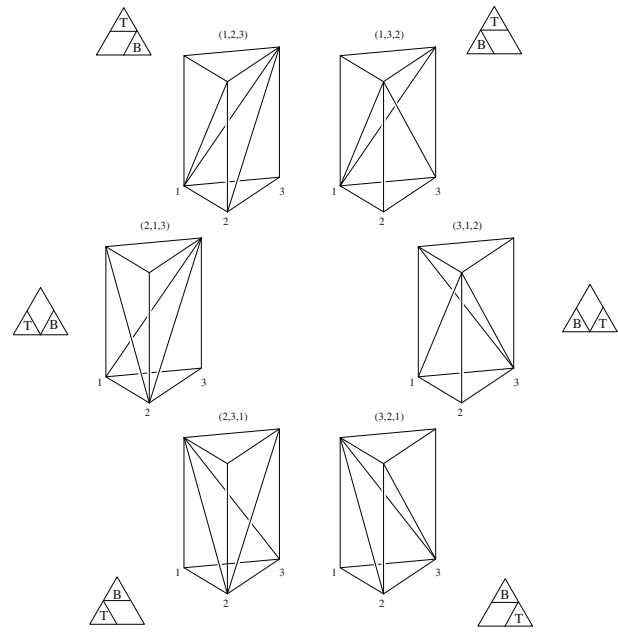


Figure 9.58: All triangulations of $\mathbf{D}^2 \times \mathbf{D}^1$ shown here together with their “slices”. Intuitively, this gives the correspondence between tilings and triangulations.

Example 9.2.27. Table 9.1 shows all the values of $f_k(S)$ and $g_k(S)$ with $k = 1, 2, 3$, as well as the values of $f_4(S)$, computed using the recursive equations (9.51) and (9.52). Adding all the entries of $f_4(S)$ we get the number of lozenge tilings of T_4 , which is $g_4(\emptyset) = 187$. Hence, the number of triangulations of $\mathbf{D}^2 \times \mathbf{D}^3$ is $187 \times 4! = 4488$.

| S | \emptyset | 1 | 2 | 1, 2 | 3 | 1, 3 | 2, 3 | 1, 2, 3 |
|---------------------|-------------|-----------------|------------------|----------------|----|-----------------|------|---------|
| $f_1(S)$ | 0 | 1 | | | | | | |
| $g_1(S)$ | 1 | 1 | | | | | | |
| $f_2(S)$ | 0 | 1 | 1 | 1 | | | | |
| $g_2(S)$ | 3 | 2 | 2 | 1 | | | | |
| $f_3(S)$ | 0 | 3 | 3 | 2 | 3 | $+\frac{2}{4}$ | 2 | 1 |
| $g_3(S)$ | 18 | 10 | 8 | 3 | 10 | 5 | 3 | 1 |
| $f_4(S)$ | 0 | 18 | 18 | 10 | 18 | $+\frac{8}{18}$ | 8 | 3 |
| $f_4(S \cup \{4\})$ | 18 | $+\frac{8}{10}$ | $+\frac{10}{18}$ | $+\frac{5}{8}$ | 10 | $+\frac{3}{8}$ | 3 | 1 |

Table 9.1: The number of triangulations of $\mathbf{D}^2 \times \mathbf{D}^3$ computed by hand. It is $4!$ times the sum of entries in the last two rows

The numbers of lozenge tilings shown in Table 9.2 below were computed with an implementation of the recursive formulas in Maple. The computation is clearly exponential in time, since we need to compute 2^k values of $f_k(S)$ and $g_k(S)$ for each k . The number of triangulations of $\mathbf{D}^2 \times \mathbf{D}^{k-1}$, for $k = 1, \dots, 16$, is $k!$ times the number shown in the table.

| k | lozenge tilings of $k\mathbf{D}^2$ | k | lozenge tilings of $k\mathbf{D}^2$ |
|-----|------------------------------------|-----|--|
| 1 | 1 | 9 | 15 952 438 877 |
| 2 | 3 | 10 | 1 983 341 709 785 |
| 3 | 18 | 11 | 355 891 356 876 534 |
| 4 | 187 | 12 | 91 655 826 195 854 811 |
| 5 | 3135 | 13 | 33 726 014 269 095 727 260 |
| 6 | 81 462 | 14 | 17 665 249 123 640 876 125 464 |
| 7 | 3 198 404 | 15 | 13 130 399 067 698 641 838 496 272 |
| 8 | 186 498 819 | 16 | 13 813 411 778 618 644 581 617 635 925 |

Table 9.2: Number of tilings of $k\mathbf{D}^2$ into k triangles and $\binom{k}{2}$ lozenges. Multiplied by $k!$, these numbers give the number of triangulations of $\mathbf{D}^2 \times \mathbf{D}^{k-1}$

A closed formula seems to be tricky to obtain, but if we denote by l_k the number of lozenge tilings of T_k , it is easy to show that l_k is of order $e^{\Theta(k^2)}$. First, since a lozenge tiling can be specified by which of the three upward neighbors of each of the $(k^2 - k)/2$ downward triangles forms a lozenge with it, $l_k \leq 3^{(k^2-k)/2} < 3^{\frac{k^2}{2}}$. Second, assume k is a multiple of 3. T_k can be tiled into $3 \binom{k/3}{2} = \frac{k^2-3k}{6}$ hexagons plus k boundary trapezoids (see Figure 9.59), each of which can independently be refined in two different ways. Hence, $l_k \geq 2^{(k^2+3k)/6}$.

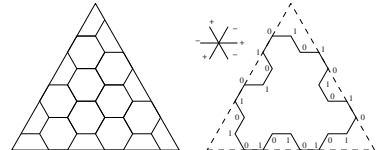


Figure 9.59: Proof of a quadratic lower bound for $\log(l_k)$ (left) and a lozenge tileable region of nearly constant boundary height (right).

9.3 Lattice polytopes and unimodular triangulations

Definition 9.3.1. Let $\mathbf{v}_0, \dots, \mathbf{v}_m$ be affinely independent points in \mathbb{R}^d . The set of integer affine combinations of them is called an *affine lattice*. That is, the lattice generated by $\mathbf{v}_0, \dots, \mathbf{v}_m$ is

$$\Lambda = \left\{ \sum_i \lambda_i \mathbf{v}_i : \lambda_i \in \mathbb{Z}, \sum_i \lambda_i = 1 \right\}.$$

The set of points $\mathbf{v}_0, \dots, \mathbf{v}_m$ is called a *basis* for the lattice Λ .

If Λ contains the origin then it is a finitely generated free abelian group, isomorphic to \mathbb{Z}^k , and we call it a *linear lattice*. Every affine lattice is a translation of a linear lattice, in the same way as an affine subspace is a translation of a linear subspace.

The basis of a lattice is of course not unique. If \mathbf{A} is the $(d+1) \times (m+1)$ matrix whose columns are the basis $\{\mathbf{v}_i\}_i$ (in homogeneous coordinates, as usual) and \mathbf{B} is any $(m+1) \times (m+1)$ integer matrix with determinant equal to 1 or -1 , then the columns of $\mathbf{A}' := \mathbf{A} \cdot \mathbf{B}$ are again integer, independent, and span the same lattice; for the latter observe that the determinant of \mathbf{B} being ± 1 implies that \mathbf{B}^{-1} is an integer matrix, so that $\mathbf{A}' := \mathbf{A}' \cdot \mathbf{B}^{-1}$. The

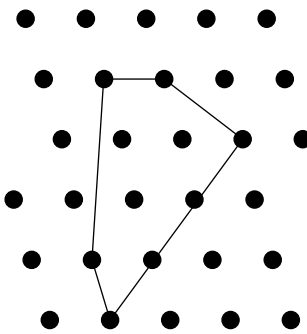


Figure 9.60: A lattice polygon.

affine transformation \mathbf{B} is called a *unimodular transformation*. Put differently: a unimodular transformation of a lattice is an affine transformation that sends the lattice to itself and preserves volumes. It also sends lattice bases to lattice bases.

Not every point configuration is contained in a lattice. For example, if you consider the three numbers $0, 1$ and $\sqrt{2}$ as points on the real line, their integer affine combinations form a dense subset of the line, which can never be contained in an affine lattice (in our definition, all lattices are *discrete*). This suggests the following definition:

Definition 9.3.2. A *lattice polytope* \mathbf{P} or *lattice point configuration* \mathbf{A} is one all of whose vertices or elements belong to a certain lattice Λ .

Lattice polytopes appear in several areas, from algebraic geometry (e.g., toric varieties) to integer programming (e.g., notion of total unimodularity and submodularity). The purpose of this section is to outline some interesting properties of the triangulations of lattice polytopes or, more generally, of point configurations with integer coordinates. We will also touch upon some of its applications. From now on we will state most results just for lattices of the form $\Lambda = \mathbf{W} \cap \mathbb{Z}^d$ where \mathbf{W} is an affine subspace of \mathbb{R}^d , since the generalization to arbitrary lattices is mostly a matter of notation.

In this section, a special kind of “maximal” triangulations, the *unimodular triangulations*, will play a key role. For an affine subspace \mathbf{W} , there is a well-defined notion of volume, but we would like to normalize it with respect to the lattice $\mathbf{W} \cap \mathbb{Z}^d$ in such a way that the volumes of lattice polytopes become integer numbers. For instance, the normalized volume of the m -dimensional unit cube will be $m!$.

Definition 9.3.3. A lattice simplex \mathbf{S} with vertices $\mathbf{v}_0, \dots, \mathbf{v}_m$ is *unimodular* if the vectors $\mathbf{v}_m - \mathbf{v}_0, \mathbf{v}_{m-1} - \mathbf{v}_0, \dots, \mathbf{v}_1 - \mathbf{v}_0$ form a basis for the lattice $\text{aff}(\mathbf{S}) \cap \mathbb{Z}^d$. A triangulation of a lattice polytope is a *unimodular triangulation* if all its maximal dimensional simplices are unimodular. Consider the example displayed in Figure 9.61.

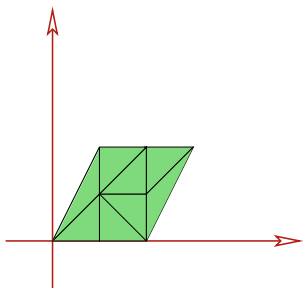


Figure 9.61: A unimodular planar triangulation.

When triangulating a lattice polytope, one is usually allowed to use all the lattice points in it. Put differently, if we have a lattice polytope \mathbf{P} , we are interested in triangulations of the point configuration $\mathbf{A} := \mathbf{P} \cap \mathbb{Z}^d$. The concept of unimodular triangulations is interesting in this context:

Lemma 9.3.4. Let \mathbf{P} be a lattice polytope of volume k (normalized to the lattice). Then, every lattice triangulation of \mathbf{P} has at most k full-dimensional simplices, with equality if and only if the triangulation is unimodular.

Proof. Unimodular simplices are the smallest possible lattice simplices, and k of them will suffice to triangulate \mathbf{P} . \square

We have encountered unimodular triangulations already, when we studied triangulations of cubes, products of simplices, and Birkhoff polytopes in Sections 6.2 and 6.3. Observe, however, that not all lattice polytopes have unimodular triangulations. For example, the regular tetrahedron inscribed

in a three dimensional unit cube (Figure 9.62) is not unimodular, and it does not contain any lattice point other than its vertices. Hence, it has no unimodular triangulation. In Section 9.3.2 we will look more closely at the question of whether a given polytope has unimodular triangulations.

9.3.1 Triangulations of lattice polygons

In what follows, a *lattice polygon* \mathbf{P} is a (perhaps non-convex) simple polygon with vertices in \mathbb{Z}^2 . A *lattice triangulation* of it is a simplicial complex covering it and using only points of $\mathbf{P} \cap \mathbb{Z}^2$ as vertices.

The first nice property of lattice polygons is that they can all be unimodularly triangulated, even non-convex ones. This follows from the fact that all non-unimodular triangles have extra lattice points apart from their vertices, by the following famous result (see [39] for a proof):

Theorem 9.3.5 (Pick's Theorem). *The (normalized) area of a lattice polygon \mathbf{P} equals $2i + b - 2$, where b and i are the numbers of lattice points in the boundary and the interior of \mathbf{P} , respectively.*

As a consequence, if a two-dimensional lattice triangulation is not unimodular, then there are necessarily lattice points that have not been used. Inserting them we reduce the area of some triangles, and the process can continue until all triangles are unimodular. Thus:

Corollary 9.3.6. *A lattice triangulation of \mathbf{P} is unimodular if and only if it uses all the lattice points on \mathbf{P} .*

An interesting question about two-dimensional lattice configurations is: How many triangulations can they have? For general point configurations in the plane, we saw in Section 3.3.2 a bound of $O(43^n)$, where n is the number of points. But, what happens if the coordinates of the points are all *integer*? Here we present a result of E. Anclin [14] which significantly improves the bound:

Theorem 9.3.7. *The number of unimodular triangulations of a (perhaps non-convex) lattice polygon \mathbf{P} is bounded by 2^{3i+b-3} , where i and b are the numbers of interior and boundary lattice points in \mathbf{P} .*

Before going into details, let us show where the number $k = 3i + b - 3$ comes from:

Lemma 9.3.8. *Let \mathbf{P} be a lattice polygon, and let i and b be the numbers of interior and boundary lattice points in it. Let $k = 3i + b - 3$. Then:*

1. *k equals the number of interior edges in any unimodular triangulation of \mathbf{P} .*
2. *k equals the number of half-integer lattice points in the interior of \mathbf{P} . That is:*

$$k = \left| \left(\frac{1}{2} \mathbb{Z}^2 \setminus \mathbb{Z}^2 \right) \cap \text{int}(\mathbf{P}) \right|$$

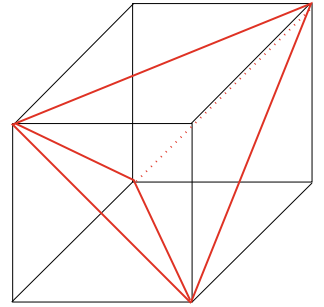


Figure 9.62: The fat central tetrahedron of a cube has no unimodular triangulations.

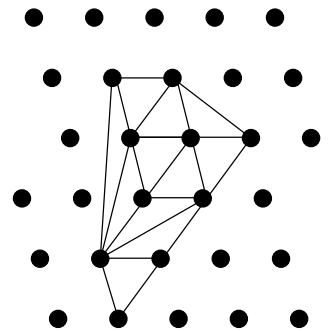


Figure 9.63: This triangulation must be unimodular, since it uses all the lattice points.

Proof. By Pick's Theorem, our lattice polygon has area $2i + b - 2$. That is also the number of triangles in every unimodular triangulation of it. By double counting, the number of interior edges is $3/2$ the number of triangles minus $1/2$ the number of boundary edges, which is the same as the number of boundary points. That finishes the proof of the first assertion.

For the second, observe that taking the lattice $\frac{1}{2}\mathbb{Z}^2$ instead of \mathbb{Z}^2 is the same as considering the lattice polygon $2\mathbf{P}$ in the original lattice. This operation clearly multiplies the volume by four and the number of boundary lattice points by two (we get exactly one boundary point in between two old ones). Hence, Pick's Theorem gives the following equality, where i' is the number of interior lattice points in $2\mathbf{P}$:

$$4(2i + b - 2) = 2i' + 2b - 2.$$

From this, $2i' = 8i + 2b - 6 = 2k + 2i$, which gives $k = i' - i$, as stated. \square

This lemma has the following consequence: every unimodular triangulation of \mathbf{P} has an edge centered at each interior half-integer point in the interior of \mathbf{P} . Indeed, an edge in a unimodular lattice triangulation cannot contain any lattice points other than its vertices, so its center is always a half-integer point. There are no other half-integer points since we have the same number of interior edges as half-integer interior points.

So, one way of reading Anclin's result is that, when building our triangulation, there are (on average) two choices of which edge to use to cover each half-integer point. That is basically how the result is proved. For the proof, we introduce the following concepts:

Definition 9.3.9. Let $\mathbf{M} := (\frac{1}{2}\mathbb{Z}^2 \setminus \mathbb{Z}^2) \cap \text{int}(\mathbf{P})$ be the set of half-integer interior points in \mathbf{P} . We consider it ordered with the lexicographic order $(x_1, y_1) \prec (x_2, y_2) \iff [y_1 < y_2] \text{ or } [y_1 = y_2 \text{ and } x_1 < x_2]$.

An *edge-stack* \mathcal{S} with respect to some $\mathbf{r} \in \mathbf{I}$ is a subcomplex of a triangulation of \mathbf{P} , with an edge through $\mathbf{r}' \in \mathbf{M}$ if and only if $\mathbf{r}' \prec \mathbf{r}$.

Proof of Theorem 9.3.7. A triangulation \mathcal{S} in the plane is uniquely determined by its interior edges. By Lemma 9.3.8, there is one interior edge centered at each point \mathbf{r} of \mathbf{M} . We denote this edge $e_{\mathcal{S}}(\mathbf{r})$, and extend this notation to the case where \mathcal{S} is a subcomplex of a triangulation instead of a full triangulation.

We are now going to build a triangulation \mathcal{T} by inserting the edges $e_{\mathcal{T}}(\mathbf{r})$ one by one, with the points \mathbf{r} ordered lexicographically, so at each step what we have is a stack \mathcal{S} . The crucial claim is that in each step there are at most two possibilities to insert the edge through the next \mathbf{r} , i.e., the number of edge-stacks with respect to some $\mathbf{r} \in \mathbf{M}$ is $\leq 2^{e_{\mathbf{r}}}$ where $e_{\mathbf{r}}$ is the number of predecessors of \mathbf{r} in \mathbf{M} . Thus, after the final step (that is, after processing the largest \mathbf{r} in (\mathbf{M}, \prec)), we have the desired result: there are at most $2^{|\mathbf{M}|}$ unimodular triangulations of \mathbf{P} .

You can see in Figure 9.64 an example of a partial subcomplex \mathcal{S} .

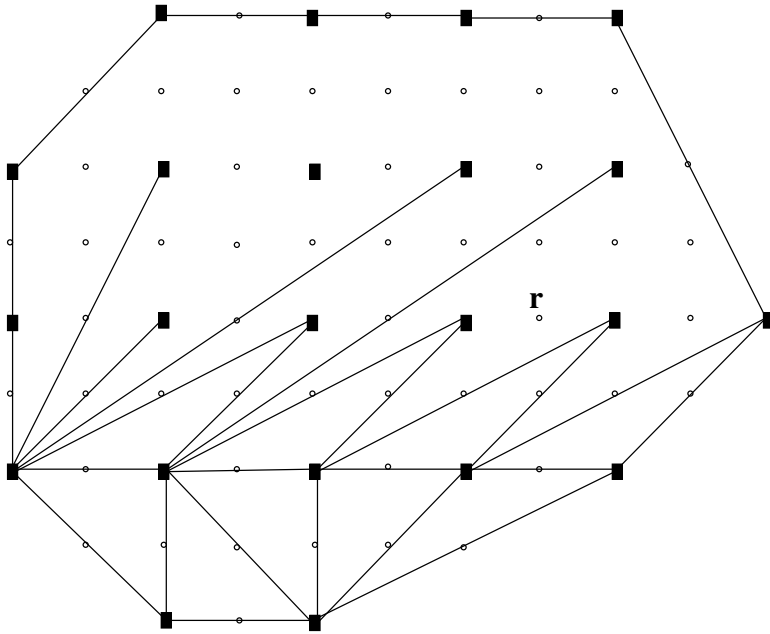


Figure 9.64: An example of edge-stack with respect to \mathbf{r} . Note that we use two different symbols: normal dot for a point in \mathbf{M} , squared dot for an integer point.

Consider now the current edge-stack \mathcal{S} with respect to $\mathbf{r} \in \mathbf{M}$. We want to add an edge to our edge-stack so that the resulting subcomplex will again be an edge-stack. Since each edge through \mathbf{r} has exactly one endpoint \mathbf{v} with $\mathbf{v} \prec \mathbf{r}$, counting possible edges is the same as counting those possible endpoints. Thus, we let:

$$\mathbf{A}_{\mathbf{r}} := \{\mathbf{v} \in \mathbb{Z}^2 \mid \mathbf{v} \prec \mathbf{r} \text{ and } \mathcal{S} \cup \{[\mathbf{v}, \mathbf{v} + 2\vec{\mathbf{v}\mathbf{r}}]\} \text{ is an edge-stack}\}.$$

Our task is to prove that $|\mathbf{A}_{\mathbf{r}}| \leq 2$.

We say that \mathbf{v} is *visible* from \mathbf{r} if the half-edge $[\mathbf{v}, \mathbf{r}]$ crosses no other edge or integral point already in the stack. Consider also

$$\mathbf{A}^{\mathbf{r}} := \{\mathbf{v} \in \text{conv}(\{\mathbf{r}\} \cup \mathbf{A}_{\mathbf{r}}) \cap \mathbb{Z}^2 \mid \mathbf{v} \text{ is visible from } \mathbf{r}\}.$$

As any $\mathbf{v} \in \mathbf{A}_{\mathbf{r}}$ is visible from \mathbf{r} , we have $\mathbf{A}^{\mathbf{r}} \supseteq \mathbf{A}_{\mathbf{r}}$. Furthermore $\mathbf{v} \prec \mathbf{r}$ holds for all $\mathbf{v} \in \mathbf{A}^{\mathbf{r}}$. (See Figure 9.65).

Order $\mathbf{A}^{\mathbf{r}}$ by the angles $\alpha(\mathbf{v})$ of $\vec{\mathbf{rv}}$ with the x-axis turning counter-clockwise and starting by π , so that we have $\alpha_i = \alpha(\mathbf{v}_i)$, $\alpha_1 < \alpha_2 < \dots < \alpha_k$. Indeed, we never have $\alpha_i = \alpha_j$, otherwise $\mathbf{r}, \mathbf{v}_i, \mathbf{v}_j$ would lie on a line, but then one of the two points $\mathbf{v}_i, \mathbf{v}_j$ would not be visible from \mathbf{r} , because both are $\prec \mathbf{r}$. At this point all points of $\mathbf{A}^{\mathbf{r}}$ are labeled in such a way that $\alpha(\mathbf{v}_i) = \alpha_i$.

Observe that we must have $\mathbf{v}_1 \in \mathbf{A}_{\mathbf{r}}$. The reason is $\mathbf{v} \prec \mathbf{r}$ for all $\mathbf{v} \in \mathbf{A}^{\mathbf{r}}$, so a point \mathbf{v} with a smaller angle to the x-axis than the first one in $\mathbf{A}_{\mathbf{r}}$ cannot belong to $\text{conv}(\mathbf{A}_{\mathbf{r}} \cup \{\mathbf{r}\})$. This is a contradiction because $\mathbf{A}^{\mathbf{r}}$ is contained in $\text{conv}(\mathbf{A}_{\mathbf{r}} \cup \{\mathbf{r}\})$ by definition.

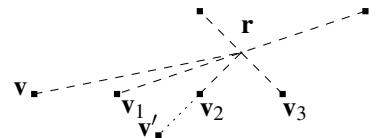


Figure 9.65: An example showing $\mathbf{A}_{\mathbf{r}} = \{\mathbf{v}_1, \mathbf{v}_3\}$, $\mathbf{A}^{\mathbf{r}} = \{\mathbf{v}_1, \mathbf{v}_2, \mathbf{v}_3\}$. In the example the points $\mathbf{v}, \mathbf{v}' \notin \mathbf{A}^{\mathbf{r}}$ and the angles satisfy $\alpha_1 < \alpha_2 < \alpha_3$.

We say that a triangle $[\mathbf{v}_i, \mathbf{v}_{i+1}, \mathbf{r}]$ is *empty* if there is no edge through it and no $\frac{1}{2}\mathbb{Z}^2$ -points in its interior. The triangle $[\mathbf{v}_i, \mathbf{v}_{i+1}, \mathbf{r}]$ is empty as A contains all points in $\text{conv}(\mathbf{A}_\mathbf{r} \cup \{\mathbf{r}\}) \supset [\mathbf{v}_i, \mathbf{v}_{i+1}, \mathbf{r}]$ visible from \mathbf{r} . The midpoint $\mathbf{s}_i := \frac{1}{2}(\mathbf{v}_i + \mathbf{v}_{i+1})$ is half-integer, $\mathbf{s}_i \in \mathbf{M}$, as $[\mathbf{v}_i, \mathbf{v}_{i+1}, \mathbf{r}]$ is empty. We also have $\mathbf{s}_i \prec \mathbf{r}$, and so $e_{\mathcal{S}}(\mathbf{s}_i) = [\mathbf{v}_i, \mathbf{v}_{i+1}]$, since the triangle $[\mathbf{v}_i, \mathbf{v}_{i+1}, \mathbf{r}]$ is empty. Additionally it has area $\frac{1}{4}$, otherwise the triangle wouldn't be empty.

Define $\mathbf{w}_i := \mathbf{r} + \vec{\mathbf{v}_i}\mathbf{r}$ and $\mathbf{r}' := \frac{1}{2}(\mathbf{v}_1 + \mathbf{w}_2)$, $\mathbf{r}'' := \frac{1}{2}(\mathbf{v}_2 + \mathbf{w}_1)$. Then $\mathbf{v}_1, \mathbf{w}_2, \mathbf{v}_2, \mathbf{w}_1$ form a parallelogram with center \mathbf{r} , and $\mathbf{r}, \mathbf{r}', \mathbf{r}''$ are on a line (parallel to $(\mathbf{v}_1 \mathbf{v}_2)$). So either $\mathbf{r}' \prec \mathbf{r}$ or $\mathbf{r}'' \prec \mathbf{r}$.

Case 1: Suppose first that $\mathbf{r}' \prec \mathbf{r}$.

The triangle $\Delta = [\mathbf{v}_1, \mathbf{v}_2, \mathbf{w}_2]$ is unimodular as $\text{area}(\Delta) = 2\text{area}[\mathbf{v}_1, \mathbf{v}_2, \mathbf{r}] = \frac{1}{2}$; so there are no integer points between the line $(\mathbf{w}_1 \mathbf{w}_2)$ and the line $(\mathbf{v}_1 \mathbf{v}_2)$. The edge $e_{\mathcal{S}}(\mathbf{r}')$ has nonempty intersection with these two lines (but doesn't cross $[\mathbf{v}_1, \mathbf{w}_1]$, since $\mathbf{v}_1 \in \mathbf{A}_\mathbf{r}$). See Figure 9.66.

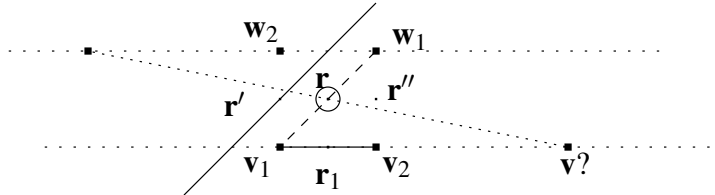


Figure 9.66: Case 1, line set up.

We will look at the possible positions of third point $\mathbf{v} \in \mathbf{A}_\mathbf{r}$ (other than $\mathbf{v}_1, \mathbf{v}_2$). We will conclude it is impossible to have such point. The line $(\mathbf{r}' \mathbf{r})$ is parallel to $(\mathbf{v}_1 \mathbf{v}_2)$, we have $\alpha(\mathbf{r}') < \alpha_1 \leq \alpha_i$; and $\mathbf{r}' \prec \mathbf{r}$, $\mathbf{v} \prec \mathbf{r}$ for all $\mathbf{v} \in \mathbf{A}_\mathbf{r}$. So all points of A are on the same side of $(\mathbf{r}' \mathbf{r})$ as \mathbf{v}_1 and \mathbf{v}_2 . So \mathbf{v} is on or beyond the line $(\mathbf{v}_1 \mathbf{v}_2)$ and hence the edge through \mathbf{r} starting at \mathbf{v} would necessarily cross the edge $e_{\mathcal{S}}(\mathbf{r}')$. So there can be no other point \mathbf{v} in $\mathbf{A}_\mathbf{r}$, that is, $|\mathbf{A}_\mathbf{r}| \leq 2$.

Case 2: The situation for $\mathbf{r}'' \prec \mathbf{r}$ is similar:

The edge through \mathbf{r}'' must be $e(\mathbf{r}'') = [\mathbf{v}_2, \mathbf{w}_1]$, otherwise it would cut $[\mathbf{v}_1, \mathbf{w}_1]$ or $[\mathbf{v}_1, \mathbf{v}_2]$; in the first case we would have $\mathbf{v}_1 \notin \mathbf{A}_\mathbf{r}$ and in the second case \mathbf{v}_2 wouldn't be visible from \mathbf{r} . And $[\mathbf{v}_1, \mathbf{v}_2, \mathbf{w}_1]$ is again unimodular, so there is no possibility for a third $\mathbf{v} \in \mathbf{A}_\mathbf{r}$. \square

Example 9.3.10. Consider the concrete problem of counting the triangulation of a finite $n \times m$ grid $\mathbf{P}_{n,m} = \text{conv}(\{0, 1, \dots, n\} \times \{0, 1, \dots, m\})$. Note that all triangulations will have $2nm$ triangles. From Theorem 9.3.7 we get:

Corollary 9.3.11. *The number of unimodular triangulations of the grid $\mathbf{P}_{m,n}$ is bounded by*

$$f(m, n) \leq 2^{3mn-m-n} < 2^{3mn}.$$

How good is this bound? For $m = 1$, one can easily compute that

$$f(1, n) = \binom{2n}{n} \sim 2^{2n}/\sqrt{n}.$$

Similarly, since $f(m+1, n) \geq f(m, n)f(1, n)$ one has

$$f(m, n) \geq \binom{2n}{n}^m \sim 2^{2mn}/n^{m/2}.$$

Kaibel and Ziegler [180] derived finer recursion formulas for $(n \times 2)$ and $(n \times 3)$ grids and were able to show a lower bound $f(m, n) \geq 2^{2.055mn}$. Many other interesting aspects were thoroughly developed in that article including a fast dynamic programming algorithm to generate all triangulations of a grid faster than the general methods we saw in Chapter 3.

9.3.2 Existence of unimodular triangulations

Remember that not all lattice polytopes in dimension three or higher have unimodular triangulations. The simplest example is the regular “fat” central tetrahedron inside the regular 3-cube that we saw in Figure 9.62. Since this tetrahedron does not contain any lattice point other than its vertices, it has only one triangulation, the tetrahedron itself, which is not unimodular. We call a simplex with this same property (that its only lattice points are its vertices) *lattice-free*. The first surprising result is that in dimension three lattice-free tetrahedra can have arbitrarily large volume. In fact, the classification of lattice-free tetrahedra modulo unimodular equivalence is known and relatively simple. It was proven in 1964 by G. K. White [332].

Theorem 9.3.12. *Every lattice-free lattice tetrahedron in dimension three is unimodularly equivalent to the lattice-free simplex $\Delta_{p,q}$ whose vertices are the columns of the following matrix, Here, $0 \leq p \leq q$ are arbitrary coprime positive integers.*

$$\begin{pmatrix} 0 & 1 & 0 & p \\ 0 & 0 & 0 & q \\ 0 & 0 & 1 & 1 \\ 1 & 1 & 1 & 1 \end{pmatrix}$$

Moreover, two such tetrahedra $\Delta_{p,q}$ and $\Delta_{p',q'}$ are unimodularly equivalent if and only if $q = q'$ and $p' \in \{\pm p, \pm p^{-1}\} \pmod{q}$.

The parameter q in $\Delta_{p,q}$ is its (normalized) volume, which is clearly invariant under unimodular transformations. The parameter p is a bit more subtle and carries arithmetic information. For example, Exercise 9.10 asks you to show that the lattice-free simplices with $p = \pm 1 \pmod{q}$ have more unimodular automorphisms than arbitrary lattice-free simplices, namely eight. For this reason we will call them *symmetric* lattice-free simplices. (Of course, unimodular tetrahedra have even more automorphisms: any of the 24 permutations of their vertices induce unimodular transformations; less trivially, the same happens for the lattice-free tetrahedra of volume two).

One way to visualize $\Delta_{p,q}$ is to consider the dilated tetrahedron $2\Delta_{p,q}$. Apart from its vertices and the mid-points of edges, $2\Delta_{p,q}$ contains other

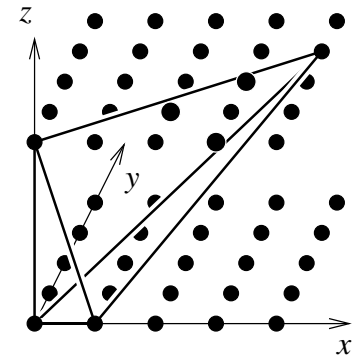


Figure 9.67: The lattice-free tetrahedron $\Delta_{4,3}$.

The vertical coordinate has been dilated for better view.

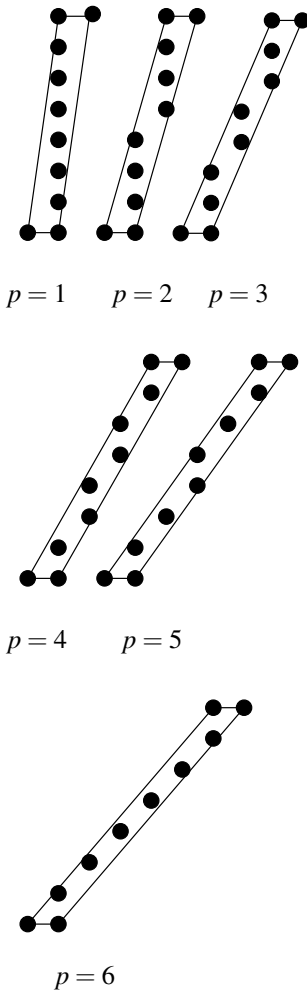


Figure 9.68: The lattice-free tetrahedra of volume 7, $\Delta_{p,7}$. For each of them, the intersection of $2\Delta_{p,7}$ with the middle horizontal hyperplane is shown.

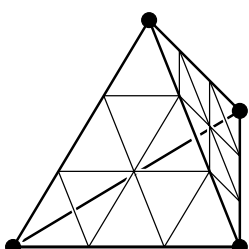


Figure 9.69: The standard boundary triangulation of the third dilation of a tetrahedron.

lattice points, all in its intersection with the horizontal plane at height one. Figure 9.68 shows this intersection for all the empty simplices with $q = 7$. From the pictures it is clear that those with $p \in \{1, 6\}$ are not equivalent to those with $p \in \{2, 3, 4, 5\}$, since the first group has all its interior lattice points collinear, while the others do not. Less obvious but still true is the fact that those in the same group are equivalent to one another.

Observe that Theorem 9.3.12 implies that every empty 3-simplex has width equal to 1 with respect to a certain integer functional; that is, there is an integer functional for which the difference between the maximum and minimum value is one. Compare with Definition 9.3.18. In dimension four an *almost complete* classification has recently been announced in [31], and it implies that all but a finite number of unimodular equivalence classes of empty 4-simplices have width 1 or 2. But in dimension higher not much is known. Clearly, there have to be a finite number of empty simplices for each fixed volume and dimension. Bárány and Kantor [30] have shown that the number of them of dimension d and volume bounded by v is about v^{d-1} . So, there are also many polytopes without unimodular triangulations. However, Kempf et al. [185] have proved the following nice result:

Theorem 9.3.13. *For any lattice polytope \mathbf{P} there is a nonnegative integer $k = k(\mathbf{P})$ such that $k\mathbf{P}$ (the k th dilation of \mathbf{P}) has a unimodular triangulation.*

A tantalizing question arises: If we fix a certain dimension d , is there a dilation factor k that works for *all* lattice d -polytopes? Clearly, in the plane $k = 1$ works; every lattice polygon has a unimodular triangulation. In dimension 4 and higher we do not know the answer, but at least in dimension three we know that the answer is yes, as was first proved by Kantor and Sarkaria. Their proof is based in the following fact:

Lemma 9.3.14 (Kantor-Sarkaria [183]). *Let $\Delta_{p,q}$ be an empty lattice tetrahedron. Then:*

1. $2\Delta_{p,q}$ has a unimodular triangulation if and only if $p = \pm 1 \pmod{q}$ (that is, if $\Delta_{p,q}$ is a symmetric empty tetrahedron).
2. $2\Delta_{p,q}$ always has a triangulation into symmetric empty tetrahedra (those of the types $p' = \pm 1 \pmod{q}'$).

Moreover, in both cases the stated triangulations can be chosen to restrict, in each boundary facet, to the standard triangulation of a dilated unimodular triangle.

Let us explain the boundary condition: Each facet of a lattice-free tetrahedron Δ is a lattice-free triangle, hence a unimodular triangle in the lattice obtained as the integer points in the facet-defining hyperplane. The standard triangulation of $k\Delta$ is the unimodular triangulation whose edges are all the translated copies of the edges of Δ into $k\Delta$. The fact our triangulations of dilated tetrahedra are standard on the boundary guarantees that they glue together nicely, if we dilate not a tetrahedron but a triangulation consisting of lattice-free tetrahedra. Hence, the above lemma has the following consequence:

Theorem 9.3.15 (Kantor-Sarkaria [183]). *Let \mathbf{P} be any lattice polytope in \mathbb{R}^3 . Then, $4\mathbf{P}$ has a unimodular triangulation.*

Observe that it is not trivial, and probably not true (although explicit counter-examples are not known) that once a certain dilation $k\mathbf{P}$ of a lattice polytope has a unimodular triangulation then the same happens for all $k'\mathbf{P}$, $k' > k$. In particular, the following strengthening of the previous result is not automatic:

Theorem 9.3.16 (Santos [285]). *Let \mathbf{P} be any lattice polytope in \mathbb{R}^3 . then, $k\mathbf{P}$ has a unimodular triangulation for all $k > 1$ except perhaps for $k \in \{2, 3, 5, 7, 11\}$.*

Concerning $k = 2$, it follows from Lemma 9.3.14 that $2\mathbf{P}$ does not always have a unimodular triangulation. But for $k = 3$ and 5 the question is open.

In arbitrary dimension the only general positive result that seems to be known about unimodular triangulability is the following:

Theorem 9.3.17. *If a lattice polytope \mathbf{P} has a unimodular triangulation \mathcal{T} , then every integer dilation $k\mathbf{P}$ of it has a unimodular triangulation too. Is, moreover, \mathcal{T} is regular, then $k\mathbf{P}$ has a regular unimodular triangulation.*

For the proof we need the following concept:

Definition 9.3.18. Let \mathbf{P} be a lattice polytope and let \mathbf{F} be a facet of it. The *width* of \mathbf{P} with respect to \mathbf{F} is the maximum lattice distance from points of \mathbf{P} to \mathbf{F} , where the lattice distance from a point \mathbf{x} to a lattice hyperplane \mathbf{H} is one plus the number of lattice hyperplanes parallel to \mathbf{H} that separate \mathbf{x} from \mathbf{H} . See Figure 9.70.

A lattice polytope is called *compressed* if its width with respect to every facet equals one. Compressed polytopes are sometimes called *facet-width one* polytopes.

We have seen in Section 6.3.7 that the Birkhoff polytope is compressed. In fact compressed polytopes seem to play a key role in combinatorial optimization (especially in connection to semidefinite programming relaxations) and stable set polytopes of perfect graphs yield other examples of compressed polytopes (see [144] and references therein).

Lemma 9.3.19. 1. All faces of a compressed lattice polytope are compressed.

2. All pulling triangulations of a facet-width one lattice polytope are unimodular.

Observe that faces of a lattice polytopes are lattice polytopes. One we say that a face \mathbf{F} of \mathbf{P} is compressed, we mean with respect to the lattice obtained by intersecting \mathbb{Z}^d with the affine span of \mathbf{F} .

Proof. By induction on the codimension of faces, part one only needs to be shown for facets. Let \mathbf{F} be a facet of \mathbf{P} , and let \mathbf{C} be a facet of \mathbf{F} . Then, there is a second facet \mathbf{F}' of \mathbf{P} such that $\mathbf{C} = \mathbf{F} \cap \mathbf{F}'$. Now, the assertion

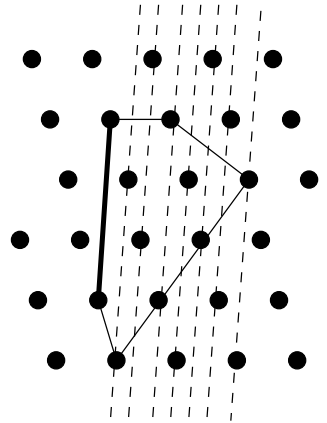


Figure 9.70: The lattice width of this polygon with respect to the highlighted size is 7. Show that the widths with respect to the other sides are 3, 3, 6, and 4.

follows from the fact that the width of \mathbf{F} with respect to \mathbf{C} cannot exceed that of \mathbf{F}' with respect to \mathbf{F}' : every lattice hyperplane parallel to \mathbf{F} intersects the affine span of \mathbf{F}' in a lattice hyperplane parallel to \mathbf{C} .

For part two the crucial observation is the following: if Δ is a lattice simplex (empty or not) and \mathbf{F} is a facet of it, then the normalized volume of Δ equals that of \mathbf{F} times the facet width of Δ with respect to \mathbf{F} . For a proof of this, assume without loss of generality that the hyperplane spanned by \mathbf{F} is $x_d = 0$ and relate the determinants that compute the volumes of Δ and \mathbf{F} . Once we have this, the result about pulling triangulations is trivial by induction on the dimension: Any pulling triangulation of \mathbf{P} is obtained by coning to a lattice point \mathbf{v} certain pulling triangulations of facets of \mathbf{P} . By inductive hypothesis those facet-triangulations are unimodular, and since all the facet widths are 1 the whole pulling triangulation is itself unimodular.

□

Proof of Theorem 9.3.17. We triangulate $k\mathbf{P}$ in three steps. First, dilating a unimodular triangulation \mathcal{T} of \mathbf{P} we construct a triangulation of $k\mathbf{P}$ into k -th dilations of unimodular simplices. Second, we refine each dilated unimodular simplex by cutting it with all the lattice translations of its facets. Doing this in dimension two produces what we called the *standard triangulation* of a dilated unimodular triangle (see Figure 9.69). In higher dimension this procedure does not produce simplices, but it certainly produces a subdivision into compressed polytopes. There is, however, a non-trivial statement here: we are claiming that all d -tuples of lattice-translated copies of the facets of a unimodular simplex are lattice points. The same would not be true if our simplices were not unimodular. In the third step, we refine the subdivision of step two by pulling all the lattice points one by one, in any arbitrary order. This produces a triangulation that restrict to a pulling triangulation of each of the cells obtained in step two. By the previous lemma all these triangulations are unimodular.

We now show that if the initial triangulation \mathcal{T} was regular, then the three steps above preserve regularity. For step one this is trivial: after dilation, the same height function that produced \mathcal{T} still produces the new triangulation. For step three we rely on Lemma 4.3.12: every pulling refinement of a regular triangulation is regular. So, only step two remains to be shown.

For this we first look at the dilation $k\Delta$ of a unimodular simplex Δ . We consider the lattice regular triangulation obtained by assigning to each lattice point \mathbf{p} the height:

$$\omega_{\mathbf{p}} = \sum_{\mathbf{F} \text{ a facet of } \Delta} -\text{dist}(\mathbf{F}, \mathbf{p})^2.$$

We claim (Exercise 9.11) that this regular subdivision coincides with the one obtained by cutting $k\Delta$ via all the lattice translations of the facets. In particular, step two preserves regularity “within each simplex”. It also preserves regularity globally, since whenever a point \mathbf{p} lies in the intersection of two adjacent dilated unimodular simplices Δ_1 and Δ_2 , the lattice distances of \mathbf{p} to the facets of $k\Delta_1$ and $k\Delta_2$ are the same: Zero for the common

facet, and equal to k times the barycentric coordinates of \mathbf{p} in that facet for the other facets.

So, in step two, we start with the height function for the regular triangulation $k\mathcal{T}$ of step one, and we add to it a small multiple of the height function $(\omega_{\mathbf{p}})_{\mathbf{p}}$ defined above. By Lemma 2.3.16 this refines $k\mathcal{T}$ so that, restricted to each cell of it, it produces the regular triangulation given by the height function $(\omega_{\mathbf{p}})_{\mathbf{p}}$. \square

We have seen that unimodular triangulations are useful but hard to come by. We would like to offer a hierarchy of properties that provide possible weakenings or strengthenings of the condition of having unimodular triangulation. At the bottom of this hierarchy we have the notion of *normality*. A lattice polytope $\mathbf{P} \subset \mathbb{R}^d$ is *normal* if $n\mathbf{P} \cap \mathbb{Z}^d = n(\mathbf{P} \cap \mathbb{Z}^d)$ for every $n \in \mathbb{N}$. Normal polytopes arise naturally in algebraic geometry and in combinatorial optimization [69, 312]. Starting with [293, 124, 243], it has been repeatedly observed that normality of a polytope is closely related to being covered by unimodular simplices. More precisely, from [293, 124] one can extract the following sequence of properties, each of which implies the next one. In all of them, $\mathbf{A} = \mathbf{P} \cap \mathbb{Z}^d$. In what follows we say a triangulation or simplicial cover is unimodular if all its simplices are.

Proposition 9.3.20. *In the following list of statements, the i -th property implies the $(i+1)$ -th property:*

- (1) *All simplices with vertices in \mathbf{A} are unimodular. (\mathbf{P} is totally unimodular).*
- (2) *\mathbf{P} is compressed, this means that all its pulling triangulations are unimodular.*
- (3) *\mathbf{P} has a unimodular regular triangulation.*
- (4) *\mathbf{P} has a unimodular triangulation.*
- (5) *\mathbf{P} has a unimodular binary cover. This is a property introduced by Firla and Ziegler [124], whose significance comes from the fact that it is much easier to check algorithmically than any of the other properties (3) through (8).*
- (6) *\mathbf{P} has a unimodular cover. (Every $\mathbf{x} \in \mathbf{P}$ lies in some unimodular simplex.)*
- (7) *For every n , every integer point in $n\mathbf{P}$ is an integer positive combination of an affinely independent subset of points of \mathbf{A} . (This is called the Free Hilbert Cover Property in [67].)*
- (8) *For every n , every integer point in $n\mathbf{P}$ is an integer positive combination of at most $d+1$ points of \mathbf{A} . (The Integral Carathéodory Property of [124].)*
- (9) *For every n , every integer point in $n\mathbf{P}$ is an integer positive combination of an affinely independent subset of points of \mathbf{A} . (\mathbf{P} is normal.)*

It is very easy to find examples that prove $3 \not\Rightarrow 2$ and $2 \not\Rightarrow 1$, but not so easy for any of the other implications. Ohsugi and Hibi [243] found the first normal polytope without regular unimodular triangulations, which turned out to give $4 \not\Rightarrow 3$. Later Ohsugi [241] even found an infinite family of such polytopes. Then Bruns and Gubeladze [67] proved $8 \Leftrightarrow 7$ and found an example for $9 \not\Rightarrow 8$ [68]. The implications from 7 to 4 remain open. (There is an example of a *cone*, not a polytope, disproving $5 \Rightarrow 4$ in [124]).

We have a few more remarks on the above hierarchy of properties. Santos proved that a polytope \mathbf{P} is compressed if and only if \mathbf{P} has a *facet width* one. One says that a polytope has facet width one if when $\mathbf{P} = \{x : Ax \leq b\}$ then $Ax \geq b - 1$ for all points $x \in \mathbf{P}$. It is worthwhile to note that there is an equivalent algebraic characterization for compressed polytopes. the toric ideal $I_{\mathbf{P}} \subset \mathbb{K}[y_1, \dots, y_q]$, generated by the binomials that encode the affine dependencies between the vertices $\delta_1, \dots, \delta_q$, satisfies the condition: the initial ideal of $I_{\mathbf{P}}$ with respect to any reverse lexicographic monomial order on $\mathbb{K}[y_1, \dots, y_q]$ is generated by squarefree monomials. (Here \mathbb{K} is a field and the y are variables.) We will see more of this later in this chapter. Let us conclude with a historical reference to R. P. Stanley's paper [304] where this family of polytopes was introduced and he first showed that the convex polytope of all $n \times n$ doubly stochastic matrices is compressed (see Subsection 6.3.7).

The best examples of polytopes that are more than just normal are those polytopes that have regular unimodular triangulations. Let us mention some families of such polytopes:

- All polytopes with totally unimodular collection of facet normals (e.g., transportation/flow polytopes). This follows easily from the algebraic techniques of Gröbner bases applied to triangulations introduced by Sturmfels in the 1990's (more on this in the next section).
- Order polytopes, hypersimplices, and stable polytopes of perfect graphs are in fact compressed. This was showed by Hibi and Ohsugi in [244].
- Let Φ be a root system with corresponding positive system Φ^+ , where Φ is one of the types A_n , B_n , C_n , D_n , and BC_n . Let $\tilde{\Phi}^+ = \Phi^+ \cup (0, 0, \dots, 0)$, where $(0, 0, \dots, 0)$ is the origin of \mathbb{R}^n . In [245], Hibi and Ohsugi showed the existence of a regular unimodular triangulation of the configuration $\tilde{\Phi}^+$ in \mathbb{R}^n .

One of the exceptional cases for which we can easily characterize normality is that of the *edge polytope* \mathbf{P}_G of a connected graph G with d vertices and n edges. This is the convex hull of the n points $\{e_i + e_j : ij \in G\} \subset \mathbb{R}^d$. Note that edge polytopes are subpolytopes of the second hypersimplex $\mathbf{D}(n, 2)$ (see Subsection 6.3.6). They lie in an affine hyperplane and in a lattice of index 2. It has dimension $d - 1$, unless G is bipartite, in which case it has dimension $d - 2$ and is totally unimodular (this was found independently by Hibi-Ohsugi [242] and Simis-Vasconcelos-Villarreal [298]).

Theorem 9.3.21 ([242]). *The following properties are equivalent for a graph G :*

- (a) *Every two vertex-disjoint cycles in G are joined by an edge.*
- (b) \mathbf{P}_G *is normal.*
- (c) \mathbf{P}_G *has a unimodular binary cover.*

For a more complete account of the topics of this section see [153].

9.3.3 Ehrhart polynomials and unimodular triangulations

Given a convex polytope \mathbf{P} and for a positive integer t , let

$$i_{\mathbf{P}}(t) = \#(t\mathbf{P} \cap \mathbb{Z}^d) \quad \text{and} \quad i_{\mathbf{P}}^\circ(t) = \#(t\mathbf{P}^\circ \cap \mathbb{Z}^d)$$

denote the number of integer points (“lattice points”) in the dilated polytope $t\mathbf{P} = \{tx : x \in \mathbf{P}\}$ and its interior, respectively. In Figure 9.72 we present an example of what we mean by a dilation.

The main structure theorem about these counting functions for lattice convex polytopes is due to Eugène Ehrhart [119] (see also [222, 229, 302] and the book [39] for extensions and details).

Theorem 9.3.22 (Ehrhart). *If \mathbf{P} is a convex lattice polytope, then:*

- *The functions $i_{\mathbf{P}}(t)$ and $i_{\mathbf{P}}^\circ(t)$ are polynomials in t whose degree is the dimension of \mathbf{P} . Let us denote it δ .*
- *The leading term of $i_{\mathbf{P}}(t)$ (and $i_{\mathbf{P}}^\circ(t)$) equals $\delta!$ times the volume of \mathbf{P} , normalized with respect to the sublattice $\mathbb{Z}^d \cap \text{aff}(\mathbf{P})$. The constant term is equal to one.*
- *The reciprocity formula $i_{\mathbf{P}}(-t) = (-1)^\delta i_{\mathbf{P}}^\circ(t)$ holds.*

Example 9.3.23. Here are two easy examples. What is the Ehrhart polynomial of a d -dimensional cube, say the cube with 0/1 vertices? Lattice points essentially are given by the length of sides; the reader can easily verify that $i_{I^d} = (n+1)^d$. For the interior lattice points of the dilations of the cube we obtain $i_{I^d}^\circ = (n-1)^d$. This agrees with the reciprocity formula.

Consider next the pentagon in Figure 9.73, with coordinates $(-1, -1)$, $(2, 0)$, $(0, 2)$, $(3, 2)$, and $(2, 3)$. From Theorem 9.3.22 it is expected that the Ehrhart polynomial of a two dimensional lattice polygon is a quadratic polynomial whose leading term is the area (in our case $17/2$), and constant equal one. The linear term coefficient turns out to be half the perimeter measured in terms of the number of lattice points in the boundary of the pentagon. Thus the final Ehrhart polynomial for this pentagon is $\frac{17t^2}{2} + \frac{5t}{2} + 1$. A general formula for all lattice polygons, here only in the special case of a pentagon, is given by the celebrated Pick’s theorem [39].

Triangulations enter the proof of Theorem 9.3.22 because they help to reduce the proof to the case of simplices.



Figure 9.71: Eugène Ehrhart circa 1940.

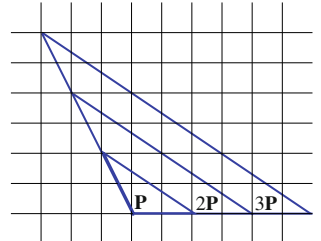


Figure 9.72: The first three dilations of a triangle.

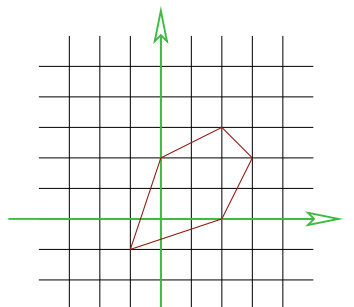
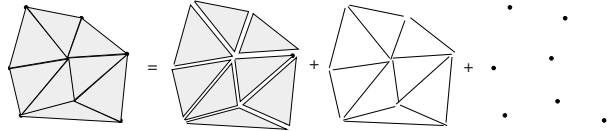


Figure 9.73: A lattice pentagon.

Proof. We will only prove the first two claims here. For a proof of the reciprocity theory see [39].

First we prove that the Ehrhart function $i_{\mathbf{P}}$ is a polynomial. Triangulate the polytope $\mathbf{P} \subset \mathbb{R}^d$ using all integral points (including some possibly not vertices of \mathbf{P}). Then, every lattice point of \mathbf{P} or its dilations clearly belongs to the relative interior of one, and only one, of the simplices (of all possible dimensions of this triangulation \mathcal{T}) (see Figure 9.74).

Figure 9.74: Decompose a polytope as the union of interiors of lattice simplices.



Thus we have the following formula

$$i_{\mathbf{P}}(n) = \sum_{\mathbf{F} \text{ face of } \mathcal{T}} i_{\mathbf{F}}^{\circ}(n)$$

and thus it is enough to prove the statement for the interior of simplices.

What we will do is to write an explicit formula for simplices. Here is the outline of the proof, with the reader invited to fill in the missing details (see Exercise 9.9). Let $\mathbf{a}_0, \dots, \mathbf{a}_k$ be the vertices of a lattice simplex \mathbf{S} of dimension k which, without loss of generality, we assume to lie in \mathbb{R}^k . We consider the cone $C_{\mathbf{S}} \subset \mathbb{R}^{k+1}$ of nonnegative integer combinations of $(\mathbf{a}_1, 0), \dots, (\mathbf{a}_k, 1)$, so that $i_{\mathbf{S}}(n)$ and $i_{\mathbf{S}}^{\circ}(n)$ are the numbers of lattice points in $C_{\mathbf{S}}$ and in the interior of $C_{\mathbf{S}}$ “at level n ”. Here, and in what follows, the *level* of a lattice point in $C_{\mathbf{S}}$ is the value of its last coordinate.

We consider also the half-open parallelepiped (see Figure 9.75)

$$\Pi_{\mathbf{S}} = \{\mathbf{x} : \lambda_0(\mathbf{a}_0, 1) + \lambda_2(\mathbf{a}_2, 1) + \dots + \lambda_k(\mathbf{a}_k, 1), \text{ with } 0 < \lambda_i \leq 1\}.$$

Tiling $C_{\mathbf{S}}$ by translated copies of $\Pi_{\mathbf{S}}$ you will notice that each integer lattice point \mathbf{v} in the interior of $C_{\mathbf{S}}$ can be written uniquely as

$$\mathbf{v} = \sum_{i=0}^k c_i(\mathbf{a}_i, 1) + \mathbf{u},$$

for some nonnegative integer coefficients (c_0, \dots, c_k) and some lattice point $\mathbf{u} \in \Pi_{\mathbf{S}}$.

Now, each $\mathbf{u} \in \Pi_{\mathbf{S}}$ of a certain level i produces exactly $\binom{n-i+k}{k}$ interior points $\Pi_{\mathbf{S}}$ in this form at level n . Thus,

$$i_{\mathbf{S}}(n) = \sum_{\mathbf{u} \in \Pi_{\mathbf{S}}} \binom{n - \text{level}(\mathbf{u}) + k}{k} = \sum_{i=1}^{k+1} \delta_i \binom{n - i + k}{k},$$

where δ_i is the number of lattice points in $\Pi_{\mathbf{S}}$ at level i . This formula is a polynomial of degree d in n , describing the Ehrhart counting function

for the interior lattice points of a simplex. Going back to our triangulated lattice polytope \mathbf{P} , we get that $i_{\mathbf{P}}(n)$ is a sum of one such polynomial for each simplex in its triangulation \mathcal{T} , with $k \in \{0, \dots, \dim(\mathbf{P})\}$ being the dimension of each such simplex.

For a proof of the second claim simply observe that for the coefficient of degree $\dim(\mathbf{P})$ in this polynomial

- Only full-dimensional simplices contribute to it, and
- The contribution of a simplex \mathbf{S} of full dimension equals the number of lattice points in the half-open parallelepiped $\Pi_{\mathbf{S}}$. Again by the fact that translated copies of $\Pi_{\mathbf{S}}$ tile the space covering every point exactly once we have that the number of lattice points in $\Pi_{\mathbf{S}}$ equals its (Euclidean, non-normalized) volume.

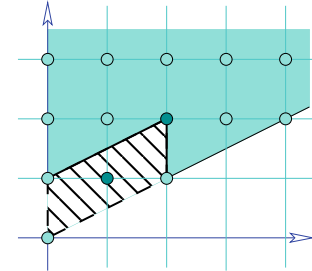


Figure 9.75: The parallelepiped for the associated cone over a simplex (one dimensional $[0, 2]$).

□

Example 9.3.24. Suppose \mathbf{S} is the 1-dimensional simplex $[0, 2]$ (just as in our Figure 9.75). We can see that there are two lattice points in the parallelepiped Π (in this case this is a parallelogram in the plane), $(1, 1)$ and $(2, 2)$. Thus i_{σ}° is $\binom{n}{1} + \binom{n-1}{1} = 2n - 1$, as expected.

The importance of Ehrhart polynomials in commutative algebra and algebraic geometry is demonstrated by the fact that these polynomials are essentially the Hilbert functions of semi-group rings (see the chapter on toric varieties of [312]). It turns out that from a unimodular triangulation one can actually recover the Ehrhart polynomial.

Theorem 9.3.25. *If a convex d -dimensional lattice polytope \mathbf{P} has a unimodular triangulation \mathcal{T} with f -vector (f_0, \dots, f_d) , then*

$$i_{\mathbf{P}}(n) = \sum_{k=0}^d \binom{n-1}{k} f_k.$$

In particular, one can get the coefficients of $i_{\mathbf{P}}(n)$ from the f -vector of \mathcal{T} and vice-versa.

Proof. For a unimodular simplex \mathbf{S} of dimension k , the parallelepiped Π_k of the previous proof has only one lattice point, at level $k+1$, so the Ehrhart polynomial of its interior is

$$i_{\mathbf{S}}^{\circ}(n) = \sum_{i=1}^{k+1} \delta_i \binom{n-i+k}{k} = \binom{n-1}{k}.$$

Now, if \mathcal{T} is a unimodular triangulation then we have that

$$i_{\mathbf{P}}(n) = \sum_{\mathbf{S} \text{ a face in } \mathcal{T}} i_{\mathbf{S}}^{\circ}(n) = \sum_{k=0}^d \binom{n-1}{k} f_k.$$

To get the f -vector of \mathcal{T} from the coefficients of $i_{\mathbf{P}}(n)$, think of $i_{\mathbf{P}}$ as a vector of length $d+1$ (its coefficients) and of the above equation as a matrix

equation of the form $i_{\mathbf{P}} = \mathbf{M}f$ relating the vectors $i_{\mathbf{P}}$ and f -vector. Since the k -th coefficient of the Ehrhart polynomial is expressed as a combination of only the entries (f_k, \dots, f_d) of the f -vector, the linear system relating the two vectors is triangular, and can be inverted. \square

Example 9.3.26. For example, if \mathcal{T} is a unimodular triangulation of a convex 3-polytope \mathbf{P} , and (f_0, f_1, f_2, f_3) is the f -vector, then we have that the Ehrhart polynomial is equal to

$$i_{\mathbf{P}}(n) = \frac{1}{6}f_3n^3 + \left(\frac{1}{2}f_2 - f_3\right)n^2 + \left(f_1 - \frac{3}{2}f_2 + \frac{11}{6}f_3\right)n + (f_0 - f_1 + f_2 - f_3).$$

The bad news is that not all lattice polytopes have unimodular triangulations. We already addressed this issue in Section 9.3.2. Still, for the purpose of computing the Ehrhart polynomial from a triangulation, there is a generalization of Theorem 9.3.25 for any triangulation due to S. Payne [250]. It expresses the multivariate generating function for lattice points in a rational polyhedral cone using the f -vector of an arbitrary triangulation but, this time, in terms of multivariate analogues of the h -polynomials of the triangulation and extra “local contributions” of the links of its nonunimodular faces. This has many applications. For example, Payne computes examples of nonunimodal Ehrhart h -vectors (the numerator of the generating function of an Ehrhart polynomial, which counts lattice points in integer dilates of a lattice polytope) for reflexive polytopes.

The relationship between Ehrhart’s lattice point counting and triangulations of the lattice polytope is indeed close and there are also examples where the information of how many points are at each dilation of \mathbf{P} can help extract information about the triangulations of \mathbf{P} . For example in [33] the authors provided a complete classification of lattice polytopes \mathbf{P} such that $k\mathbf{P}$ has no interior points for $1 \leq k < n$. This corresponds to the h^* polynomial (the numerator of the Ehrhart series) having degree at most one. They prove that the degree of $h^*(\mathbf{P})$ is less than 1 if and only if \mathbf{P} is either an exceptional simplex or a Lawrence prism. The triangulations, secondary polytopes and principal A -determinants are computed for these polytopes. The authors also prove that the corresponding secondary polytope is always simple.

9.4 Triangulations and Gröbner bases

We have seen already in Chapter 1 that triangulations and subdivisions appear naturally in algebraic geometry. The interaction between triangulations, toric geometry, and Gröbner bases is one of the richest examples of this, and it shows that the relation is mutually beneficial: triangulations not only help in attacking algebra problems, but also the algebraic encoding can be used to prove deep results about triangulations and polytopes. Among other things, the ideas in this section provide a method to construct triangulations of a given configuration. The method revolves around the concepts of Gröbner bases of toric ideals and their relation to minimal *non-faces* of triangulations. We will illustrate it with examples.

We do not assume that the reader is an expert in algebraic geometry, but we do assume that the reader is not afraid of algebra! Several excellent

references for the concepts we use are the books [87], [88], [312]. We encourage you to look for more details there; here we only show the tip of a big iceberg!

9.4.1 Gröbner bases and toric ideals

Let $\mathbb{C}[x_1, \dots, x_n]$ be the ring of polynomials with complex coefficients. (Most of what we say works with respect to any field, not necessarily \mathbb{C} , but we use \mathbb{C} to make things more concrete and because it is the most common case). An *ideal* of $\mathbb{C}[x_1, \dots, x_n]$ is a subset I that is closed under addition and has the property that if $f \in I$, then the product gf is in I too, for all $g \in \mathbb{C}[x_1, \dots, x_n]$. In short, $I + I \subseteq I$ and $I\mathbb{C}[x_1, \dots, x_n] \subseteq I$.

One way to get an ideal is to consider all possible linear combinations $f_1g_1 + f_2g_2 + \dots + f_kg_k$ of a fixed finite set of polynomials g_1, g_2, \dots, g_k , where the f_i 's are arbitrary polynomials. This set is the *ideal generated by* g_1, \dots, g_k , denoted $\langle g_1, g_2, \dots, g_k \rangle$. A fundamental theorem in algebraic geometry (Hilbert's basis theorem) says that every ideal I in the ring of polynomials is *finitely generated* in this sense.

Given a real vector $\omega = (\omega_1, \dots, \omega_d)$ in \mathbb{R}^n we can define a total order $>_\omega$ in the set of all monomials as follows: we declare $x^\mathbf{u} >_\omega x^\mathbf{v}$ if $\langle \mathbf{u}, \omega \rangle > \langle \mathbf{v}, \omega \rangle$, with ties broken via the lexicographic order. (This means that, in the case of equality, we declare $x^\mathbf{u} >_\omega x^\mathbf{v}$ if $u_1 > v_1$, or if $u_1 = v_1$ but $u_2 > v_2$, or if $u_1 = v_1$ and $u_2 = v_2$ but $u_3 > v_3$, etc.) Here, as usual, if $\mathbf{u} = (u_1, u_2, \dots, u_d) \in \mathbb{Z}^n$ is an integer point, $x^\mathbf{u}$ denotes the monomial $x_1^{u_1} x_2^{u_2} \cdots x_d^{u_d}$.

This total order is called the *monomial order* or *term order* associated to ω . With it we define the *initial monomial* or *initial term* of each polynomial f , which will be denoted by $\text{in}_{>_\omega}(f)$, as the maximum of the monomials of f .

Definition 9.4.1. • The *initial ideal* of an ideal I in $\mathbb{C}[x_1, \dots, x_n]$ with respect to a certain term order $>_\omega$ is the ideal $\text{in}_{>_\omega}(I)$ generated by the initial monomials of all its polynomials.

- A finite subset of polynomials $G = \{g_1, \dots, g_k\}$ of I is a *Gröbner basis* with respect to $>_\omega$ if $\text{in}_{>_\omega}(I)$ is generated by $\{\text{in}_{>_\omega}(g_1), \dots, \text{in}_{>_\omega}(g_k)\}$.
- We say the monomials $m \notin \text{in}_{>_\omega}(I)$ are called *standard*.

In other words, G is a Gröbner basis for I if the initial monomial of any f in I is divisible by one of the monomials $\text{in}_{>_\omega}(g_i)$. Through Gröbner bases many questions about general ideals in polynomial rings can be reduced to questions about ideals generated by monomials, which are far easier. For example, one can prove that any Gröbner basis is a generating set of I (see Exercise 9.13). In fact the problem of deciding whether a polynomial belongs to the ideal can be solved using Gröbner bases.

Given an ideal I and any monomial order $>_\omega$, it is known that the set of standard monomials forms a \mathbb{C} -vector space basis for the *residue ring* $\mathbb{C}[x_1, \dots, x_n]/I$. Gröbner bases theory provides a *division algorithm* for computing the *residue* or *normal form* of a polynomial f modulo the ideal I . First compute a Gröbner basis G for I with respect to $>_\omega$. Iterate the

following process: Check whether all monomials in f are standard. If so, we have a residue for f . Otherwise consider the highest non-standard monomial m in f . Find $g \in G$ such that $\text{in}_{>\omega}(g)$ divides m , thus for some monomial q we have $m = \text{in}_{>\omega}(g)q$. Replace f by $f - gq$. Repeat this process until all monomials in f are standard (this will happen eventually but it is not obvious). We remark that the normal form obtained by the division algorithm using the Gröbner basis is unique. One can prove that f belongs to I if and only if the normal form of f is zero.

When I is a linear ideal (generated by polynomials of degree one) computing a Gröbner basis with respect to a lexicographic term order is the same as doing Gaussian elimination in the linear system of equations. Actually, the whole idea behind Gröbner bases is that they generalize Gaussian elimination to arbitrary systems of polynomial equations. See [314] for a short, informal introduction to them, or [87] for a more in-depth treatment. Gröbner bases can be computed via *Buchberger's algorithm* which is implemented by several computer algebra systems. Its details are beyond the interest of this book, so we will use it as a black box.

What relates Gröbner bases to the world of triangulations of point configurations is what happens when we vary the term order $>_{\omega}$. If we fix a polynomial f , the space \mathbb{R}^n of possible weights ω is divided into a finite number of regions in each of which we get the same initial term for f . You can easily convince yourself that this decomposition is simply the normal fan of the *Newton polytope* of f (Definition 1.3.2): the polytope whose vertices are the exponents of the monomials of f , considered as integer points in \mathbb{Z}^n as in the definition of term orders.)

So, Gröbner bases and initial ideals should decompose \mathbb{R}^n into some polyhedral fan too, by intersecting the fans of the individual polynomials. One problem with this is that there are infinitely many Newton polytopes of polynomials in I so, in principle, we might get an infinite number of possible initial ideals. But Hilbert's basis theorem comes to the rescue: since the initial ideals are finitely generated, to compute them we will only need to compare monomials up to a certain degree, and the number of those is finite. The regions where the initial ideal stays the same are then clearly convex polyhedral cones, and they form a polyhedral fan called the *Gröbner fan* of I . The Gröbner fan is, just like the secondary polytope fan, the normal fan of a polytope, the *state polytope* (these notions were investigated by algebraists in the 1980's [35, 234], and recently there has been an effort for fast computation [131]). Note that the existence of this polyhedral fan has the implication that if we take the union of one Gröbner basis for each possible initial ideal we get a finite set of polynomials in I that is a Gröbner basis for all the possible term orders at the same time. This is called a *universal Gröbner basis*.

We now introduce *toric ideals*, in which the relation to point configurations is more apparent. Given an integer matrix \mathbf{A} of size $d \times n$ with columns $\mathbf{a}_1, \dots, \mathbf{a}_n$, for any vector $\mathbf{u} = (u_1, u_2, \dots, u_n) \in \mathbb{Z}^n$, we let, as usual

$$\mathbf{A}\mathbf{u} := u_1\mathbf{a}_1 + u_2\mathbf{a}_2 + \cdots + u_n\mathbf{a}_n.$$

For any $\mathbf{u} \in \mathbb{Z}^n$, we denote by $\text{supp}(\mathbf{u}) := \{i : u_i \neq 0\}$ the *support* of \mathbf{u} . Note that every \mathbf{u} can be written uniquely as $\mathbf{u} = \mathbf{u}^+ - \mathbf{u}^-$, where \mathbf{u}^+ and \mathbf{u}^- are nonnegative and have disjoint support.

Definition 9.4.2. The *toric ideal* of \mathbf{A} is the ideal generated by the binomials

$$I_{\mathbf{A}} := \langle x^{\mathbf{u}^+} - x^{\mathbf{u}^-} : \mathbf{A}\mathbf{u} = 0 \rangle.$$

That is to say, if we think of \mathbf{A} as representing a point or vector configuration, the binomials $x^{\mathbf{u}^+} - x^{\mathbf{u}^-}$ in $I_{\mathbf{A}}$ are those for which $\mathbf{u} = \mathbf{u}^+ - \mathbf{u}^-$ is a dependence in \mathbf{A} .

Usually, homogeneous, or at least acyclic, configurations are used. Acyclic implies that $I_{\mathbf{A}}$ contains no monomials, and homogeneous that $I_{\mathbf{A}}$ is a homogeneous ideal in the standard algebraic geometry sense, i.e., it is generated by homogeneous polynomials.

To make the analogy more apparent, a *circuit* of $I_{\mathbf{A}}$ is a binomial $x^{\mathbf{u}^+} - x^{\mathbf{u}^-}$ for which \mathbf{u} is (the linear dependence associated to) a circuit of \mathbf{A} . That is to say, $x^{\mathbf{u}^+} - x^{\mathbf{u}^-}$ is a circuit if it cannot be written as combination of other binomials in $I_{\mathbf{A}}$ and it has minimal support under inclusion.

Gröbner bases of toric ideals have beautiful geometric interpretations in terms of the lattice points of the polyhedra of the form $\mathbf{A}\mathbf{u} = \mathbf{b}, \mathbf{u} \geq 0$. For example, it is known, and important for us, that the standard monomials with respect to the monomial order $>_{\omega}$ coincide with the possible optimal solutions of the integer linear programs of the form

$$\text{minimize } \mathbf{u} \cdot \boldsymbol{\omega} \text{ subject to } u_1\mathbf{a}_1 + u_2\mathbf{a}_2 + \cdots + u_n\mathbf{a}_n = \mathbf{b}, \quad u_i \geq 0 \quad u_i \in \mathbb{Z}.$$

where \mathbf{b} ranges over an arbitrary integer lattice point inside the cone generated by the columns of \mathbf{A} . Another important geometric result is the following. Remember that a *totally unimodular* matrix is one in which every minor is 0, +1, or -1. As an example, we saw in Section 6.2 that the (vertices of) a product of two simplices are totally unimodular.

Lemma 9.4.3. Circuits form a system of generators of the toric ideal $I_{\mathbf{A}}$. If \mathbf{A} is a totally unimodular matrix, then circuits form a universal Gröbner basis. \square

9.4.2 Sturmfels' correspondence

Here we show that each Gröbner basis of a toric ideal $I_{\mathbf{A}}$ yields a *regular triangulation* of \mathbf{A} . In order to precisely state this, a representation of triangulations, different from the one we are accustomed to, will be introduced now. We usually represent a simplicial complex by its simplices, and most commonly by the maximal-dimensional ones. Nevertheless, there is a complementary representation of simplicial complexes in terms of *minimal non-faces*. A *non-face* of a simplicial complex \mathcal{K} is any subset of vertices that is not a face. See Figure 9.76 for an example. Non-faces, the just as faces, are partially ordered by inclusion. Clearly, if we know the minimal non-faces we can list all the non-faces, and from them all the faces. But the

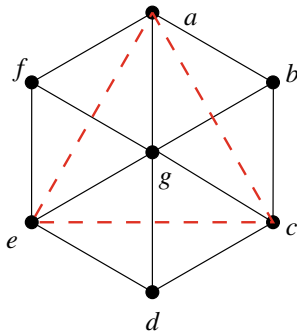


Figure 9.76:

In the complex $\{abg, bcg, cdg, deg, efg, afg\}$, the triangle ace is a non-face of the triangulated hexagon, but it is not a minimal non-face, while the edges ac , ae and ce are. In fact, in this example the minimal non-faces are precisely the six missing edges.

following characterization allows to go from facets to minimal non-faces and vice-versa in a shorter way. Let $MNF(\mathcal{K}) = \{C_1, C_2, \dots, C_t\}$ be the non-faces of a simplicial complex \mathcal{K} . A *transversal* for $MNF(\mathcal{K})$ is any minimal set of vertices S such that $S \cap C_i \neq \emptyset$, for every i .

Lemma 9.4.4. *The complement of every transversal S for the set of minimal non-faces of \mathcal{K} is a maximal face of \mathcal{K} . Conversely, the complement of every maximal face is a transversal of $MNF(\mathcal{K})$.*

Proof. Denote by J the set of vertices of \mathcal{K} .

Let us prove by contradiction that $J \setminus S$ is a face, for every transversal S of $MNF(\mathcal{K})$. If not, $J \setminus S$ contains one of the minimal non-faces C_i . This means $S \cap C_i = \emptyset$, contradicting the definition of transversal. To see that $J \setminus S$ is a *maximal* face, assume the contrary and let F be a facet properly containing it. Then, $J \setminus F$ is also properly contained in S and, since S is minimal with respect to transversality, there is at least one minimal non-face (C_i) such that $C_i \cap (J \setminus F) = \emptyset$, which is the same as saying $C_i \subset F$, a contradiction.

The argument for the converse (the complement of any facet is a transversal for $MNF(\mathcal{K})$) is similar and left to the reader. \square

One more algebraic definition: By the *radical of a monomial ideal I* we mean the ideal resulting from deleting all powers of monomials in I . For example, for the ideal $\langle x^2y^3, xy^2, z^2, x^{100} \rangle$ its radical is $\langle xy, z, x \rangle$. That is, a monomial ideal is its own radical if it can be generated by square-free monomials.

We are now ready to state the main result of this subsection that relates regular triangulations and Gröbner bases.

Theorem 9.4.5 (Sturmfels' correspondence). *Let \mathbf{A} be a $d \times n$ matrix with integer entries.*

Let $I_{\mathbf{A}}$ be the toric ideal defined by \mathbf{A} . Then:

- *The regular triangulations of \mathbf{A} are in one-to-one correspondence with the radicals of the monomial initial ideals of $I_{\mathbf{A}}$. More precisely, for the monomial order $>_{\omega}$, the generators of the radical of $in_{>_{\omega}}(I_{\mathbf{A}})$ have as exponent vectors the minimal non-faces of the regular triangulation $\mathcal{S}(\mathbf{A}, \omega)$.*
- *An initial ideal $in_{>_{\omega}}(I_{\mathbf{A}})$ is square-free (that is, it equals its own radical) if and only if the regular triangulation $\mathcal{S}(\mathbf{A}, \omega)$ is unimodular (all simplices have normalized volume equal to one).*

Proof. We will prove the first claim of Sturmfels' correspondence following the presentation in [312]. The steps tie rather well with what we saw in Chapter 1 about linear programming and the complementary slackness principle (see in particular Lemma 1.2.1 and Theorem 1.2.1).

First of all, by definition of regular triangulation, a subset J is a face of $\mathcal{S}(\mathbf{A}, \omega)$ if there exist a vector \mathbf{c} , the normal vector to the supporting hyperplane of the face, such that $\mathbf{a}_j \cdot \mathbf{c} = \omega_j$ for $j \in J$ and yet, at the same

time, $\mathbf{a}_j \cdot \mathbf{c} < \omega_j$ when $j \notin J$. Because of this condition it make sense to consider, for an arbitrary $\mathbf{b} \in \mathbb{R}^n$, the following type of linear programs

$$\text{minimize } \mathbf{u} \cdot \omega \text{ subject to } u_1\mathbf{a}_1 + u_2\mathbf{a}_2 + \cdots + u_n\mathbf{a}_n = \mathbf{b}, \text{ and } u_i \geq 0, \quad (9.53)$$

and its dual linear program, is given by

$$\text{maximize } \mathbf{c} \cdot \mathbf{b} \text{ subject to } \mathbf{a}_1 \cdot \mathbf{c} \leq \omega_1, \dots, \mathbf{a}_n \cdot \mathbf{c} \leq \omega_n. \quad (9.54)$$

The reader can see the face conditions of regular subdivisions appear as equations in the inequalities within the dual linear programs. Now consider an indexing set J . We claim the following statements are equivalent:

1. J labels a face of the regular subdivision $\mathcal{S}(\mathbf{A}, \omega)$ of \mathbf{A} induced by ω .
2. There exist a feasible solution \mathbf{c} of the dual LP (9.54) that satisfies $J = \{j : \mathbf{a}_j \cdot \mathbf{c} = \omega_j\}$.
3. There exist $\mathbf{b} \in \mathbb{Z}^d$ such that an optimal solution for the dual LP (9.54) satisfies $J = \{j : \mathbf{a}_j \cdot \mathbf{c} = \omega_j\}$.
4. There exist $\mathbf{b} \in \mathbb{Z}^d$ such that an optimal solution \mathbf{u} for the primal LP (9.53) satisfies its support is precisely the set of indices J .
5. There exist $\mathbf{b} \in \mathbb{Z}^d$ such that an optimal solution \mathbf{u} for the primal LP 9.53 satisfies its support $\text{supp}(\mathbf{u})$ equals the set of indices J and is integral.
6. There exist a monomial $x^\mathbf{u}$ such that $J = \text{supp}(\mathbf{u})$ and every power of $x^\mathbf{u}$ is a standard monomial.
7. J is a face of the simplicial complex whose non-faces are the generators of the radical of $\text{in}_{>\omega}(I_{\mathbf{A}})$.

The equivalence of Parts 1 and 2 is a direct consequence of the notion of regular subdivision. The equivalence of Parts 2 and 3 holds because every point \mathbf{c} in the dual polyhedron will lie in the relative interior of some face. The equivalence of Parts 3 and 4 holds by complementary slackness (see Lemma 1.2.1). The equivalence of Parts 4 and 5 holds because we can replace \mathbf{b} with an integer multiple of \mathbf{b} if necessary. The equivalence of Parts 5 and 6 holds because, as we stated at the end of the past subsection, standard monomials are precisely the optimal solutions of the integer programs of type (9.53) with varying \mathbf{b} . Thus, all powers of $x^\mathbf{u}$ are standard if and only if all integer multiples of \mathbf{u} are optima of the corresponding linear program. Finally, Parts 6 and 7 are equivalent because standard monomials with respect to K , the radical of $\text{in}_{>\omega}(I_{\mathbf{A}})$, are index sets that are supports of faces of the simplicial complex whose non-faces are in the monomial ideal K .

The chain of equivalences proves the first statement in the theorem. For a proof of the second part we refer the reader to Corollary 8.9 in [312]. \square

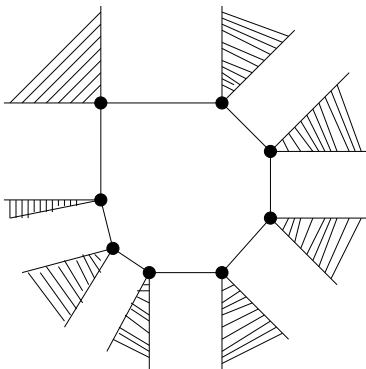


Figure 9.77: The eight initial ideals do correspond to the vertices of an eight-gon.

Sturmfels' correspondence has the following consequence:

Corollary 9.4.6. *The Gröbner fan of I_A refines the secondary fan of \mathbf{A} . The two fans coincide if and only if \mathbf{A} is totally unimodular.*

We will now work through some examples to illustrate it in three well-structured families of point configurations. It is really a very useful technique to prove that a set of simplices is a triangulation.

Example 9.4.7. Let \mathbf{A} be the 2×4 matrix

$$\begin{matrix} a & b & c & d \\ \left(\begin{array}{cccc} 1 & 1 & 1 & 1 \\ 0 & 1 & 2 & 3 \end{array} \right). \end{matrix}$$

It can be calculated, using your favorite computer algebra package (e.g., COCOA, Macaulay2, Singular, MAPLE, etc.) or a special software for it (Jensen's Gfan [177]), that there are all together eight initial ideals as we vary the weight vector for the toric I_A . Indeed, if two weight vectors give the same initial ideal, then they are found inside the same of the eight polyhedral cones represented in Fig 9.77. In the table below we show the eight initial ideals with a sample weight vector that determines each.

Table 9.3: The eight initial ideals, with a term order producing each.

| Term order ω | initial ideal |
|---------------------|-------------------------------------|
| $(0, 0, 1, 3)$ | $\langle ad, bd, ac \rangle$ |
| $(0, 0, -4, -3)$ | $\langle ad, b^2, bd \rangle$ |
| $(0, 0, -4, -5)$ | $\langle ad^2, b^2, bc, bd \rangle$ |
| $(0, 0, -4, -7)$ | $\langle b^2, bc, bd, c^3 \rangle$ |
| $(0, 0, -4, -9)$ | $\langle b^2, bc, c^2 \rangle$ |
| $(0, 0, 1, -1)$ | $\langle ac, b^3, bc, c^2 \rangle$ |
| $(0, 0, 2, 1)$ | $\langle a^2d, ac, bc, c^2 \rangle$ |
| $(0, 0, 2, 3)$ | $\langle ac, ad, c^2 \rangle$ |

Now: the point configuration for the matrix \mathbf{A} consists of four collinear points. The triangulations are subdivisions of the length four segment into smaller segments that use the four given points. It is clear that all such triangulations are regular and only four are possible (by choosing or not choosing a combination of the two interior points on the segment). The reason why there are eight initial ideals and only four triangulations is that some ideals have the same radical. The radicals of the eight initial monomial ideals are $\langle ac, ad, bd \rangle$, $\langle b, ad \rangle$, $\langle b, c \rangle$, $\langle c, ad \rangle$. They are, precisely, labelings for the minimal non-faces of the four triangulations of four points on a line.

For example, $\langle b, c \rangle$ being non-faces means that b and c do not appear in the triangulation, so the segment is triangulated with a single cell, ad . In the other extreme, if the minimal non-faces are $\langle ac, ad, bd \rangle$, all the elements are used as vertices (none is a non-face) and the edges are the pairs that are

not non-faces, namely ab , bc and bd . We let the reader apply Lemma 9.4.4 to the four sets of minimal non-faces.

Example 9.4.8. Now let \mathbf{A} to be the vertex-edge incidence matrix of the complete graph K_4 . This is a 4×6 matrix with two ones in each column. In Figure 9.78 we show how this configuration consists of the vertices of a regular octahedron (embedded in four-dimensional space), and we label its elements by the variables of the ideal (columns are labeled by the edge of the graph K_4 , thus we use a bi-index). The three binomials

$$y[1,2]y[3,4] - y[1,3]y[2,4],$$

$$y[1,2]y[3,4] - y[1,4]y[2,3],$$

$$y[1,3]y[2,4] - y[1,4]y[2,3],$$

correspond to cycles of length four in K_4 , form a *universal Gröbner basis* for the toric ideal $I_{\mathbf{A}}$; this means it is a Gröbner basis with respect to any possible monomial order.

There are three distinct initial ideals, depicted in Figure 9.78, where we have also listed the three initial ideals. Observe that the generators in each are precisely the minimal non-faces of a triangulation of the octahedron (the vertices of the octahedron are labeled by the six edges of the complete graph K_4).

An example related to arborescences

To conclude we do a more sophisticated application of the Gröbner bases technology. This time we wish to find, for each n , a triangulation of the point configuration $\mathbf{M}_n = \{\mathbf{m}_{i,j}\}_{1 \leq i,j \leq n, i \neq j}$, where $\mathbf{m}_{i,j}$ is the $(n-1)$ by $(n-1)$ matrix such that

- (i) If $i \neq n \neq j$, then $\mathbf{m}_{i,j}$ has a single non-zero entry, in position (i,j) .
- (ii) In $\mathbf{m}_{i,n}$, the entries on the i th row are all -1 and all other entries equal zero.
- (iii) In $\mathbf{m}_{n,j}$, the entries on the j th column are all -1 and all other entries equal zero.

For example, the following is the list of the six elements of \mathbf{M}_3 , where each 2 by 2 matrix $\mathbf{m}_{i,j}$ appears as a row vector:

$$\begin{aligned} \mathbf{m}_{1,3} &= \begin{pmatrix} -1 & -1 \\ 0 & 0 \end{pmatrix}, & \mathbf{m}_{2,3} &= \begin{pmatrix} 0 & 0 \\ -1 & -1 \end{pmatrix}, & \mathbf{m}_{3,1} &= \begin{pmatrix} -1 & 0 \\ -1 & 0 \end{pmatrix}, \\ \mathbf{m}_{3,2} &= \begin{pmatrix} 0 & -1 \\ 0 & -1 \end{pmatrix}, & \mathbf{m}_{1,2} &= \begin{pmatrix} 0 & 1 \\ 0 & 0 \end{pmatrix}, & \mathbf{m}_{2,1} &= \begin{pmatrix} 0 & 0 \\ 1 & 0 \end{pmatrix}. \end{aligned}$$

We consider \mathbf{M}_n as a big $(n-1)^2 \times n(n-1)$ matrix, representing a certain configuration labeled by the set $J_n := \{(i,j) : i, j \in [n], i \neq j\}$. A nice way of representing J_n is as the set of all edges in the doubly directed complete graph with n nodes. See Figure 9.79.

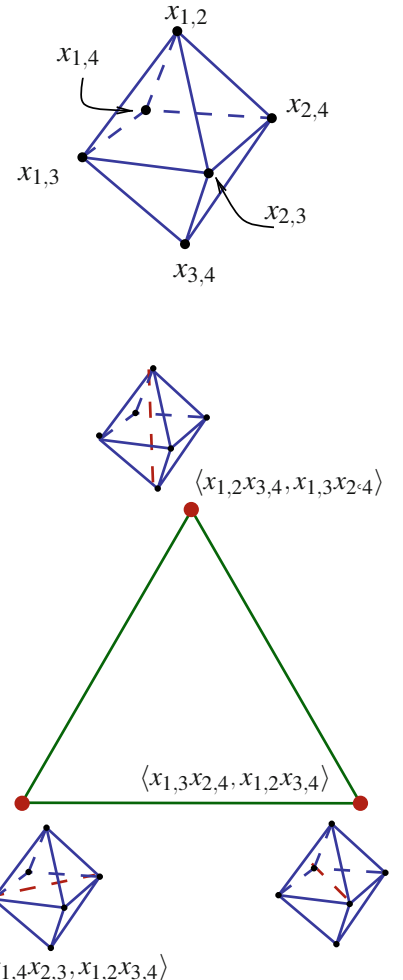


Figure 9.78: Initial ideals for the toric ideal of K_4 .

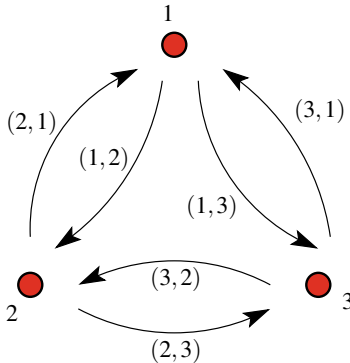


Figure 9.79: The doubly directed complete graph on 3 nodes.

We wish to study its triangulations via Sturmfels' correspondence. For this, we consider the toric ideal

$$I_{\mathbf{M}_n} := \langle x^{\mathbf{u}^+} - x^{\mathbf{u}^-} : \mathbf{M}_n \mathbf{u} = 0 \rangle$$

of \mathbf{M}_n in the polynomial ring $\mathbb{C}[x_{i,j} : 1 \leq i, j \leq n, i \neq j]$. The key property is that the configuration is totally unimodular.

Lemma 9.4.9. *The matrix \mathbf{M}_n is homogeneous and totally unimodular. Hence, all triangulations of the point set \mathbf{M}_n have the same number of full-dimensional simplices.*

Proof. To check the configuration is homogeneous, observe that some of the matrices have trace zero and sum of entries equal to 1 and the rest have trace -1 and sum of entries equal to $1 - n$. Hence, the functional “sum of entries minus n times the trace” evaluates to 1 at every element of \mathbf{M}_n .

For the unimodularity, observe that up to a rearrangement of rows and columns, \mathbf{M}_n will look as follows: The first few rows are the negatives of the vertex-edge incidence matrix of the complete bipartite graph $K_{n-1,n-1}$, then under that we have $n-1$ cyclically arranged copies of an $(n-2) \times (n-2)$ identity matrix. It is well-known that the vertex-edge incidence matrix of any bipartite graph is totally unimodular. It is also known, see e.g., Theorem 19.3 in [291], that a matrix \mathbf{A} is totally unimodular if each collection of columns of \mathbf{A} can be split into two parts so that the sum of the columns in one part minus the sum of the columns in the other part is a vector with entries only 0, +1, and -1. This characterization of totally unimodular matrices is easy to verify in our matrix \mathbf{M}_n : whatever partition works for the columns of the vertex-edge incidence matrix of the complete bipartite $K_{n-1,n-1}$ also works for the corresponding columns of \mathbf{M}_n , because of the diagonal structure of the rows below it. \square

Thus we conclude:

Corollary 9.4.10. *The set $C_{\mathbf{M}_n}$ of circuits of the homogeneous toric ideal $I_{\mathbf{M}_n}$ is a universal Gröbner basis for $I_{\mathbf{M}_n}$.*

Moreover, we can read the minimal non-faces of each triangulation from the generators of the universal Gröbner basis. So, we now look at who the circuits of $I_{\mathbf{M}_n}$ are. The answer will be pleasing for people who like combinatorics: Essentially they consist of *bi-partitions* or *cuts* of $[n] = 1, 2, \dots, n$.

For any partition of $[n] = S \cup T$, we denote by $\mathbf{u}_{S,T} \in \mathbb{Z}^{n(n-1)}$ the $n(n-1)$ dimensional vector, where

$$\mathbf{u}_{S,T}(i, j) = \begin{cases} 1, & \text{if } i \in S, j \in T, \\ -1, & \text{if } i \in T, j \in S, \\ 0, & \text{otherwise.} \end{cases}$$

That is to say, $\mathbf{u}_{S,T}(i, j)$ is a 0/1 vector with 1's on the edges corresponding to the complete bipartite graph with all edges directed from S to T and

-1 's on the complete bipartite graph with edges from T to S . With this description it easily follows that

$$\mathbf{u}_{S,T}(i,j) + \mathbf{u}_{S,T}(j,i) = 0 \text{ for any } i \neq j. \quad (9.55)$$

$$\mathbf{u}_{S,T}(i,j) + \mathbf{u}_{S,T}(j,k) + \mathbf{u}_{S,T}(k,i) = 0 \text{ for any distinct } i, j \text{ and } k. \quad (9.56)$$

We define

$$P_{S,T} := x^{u_{S,T}^+} - x^{u_{S,T}^-} = \prod_{s \in S, t \in T} x_{s,t} - \prod_{s \in S, t \in T} x_{t,s}.$$

Proposition 9.4.11. *The set of circuits of $I_{\mathbf{M}_n}$ consists of all the binomials $P_{S,T}$:*

$$C_{\mathbf{M}_n} = \{P_{S,T} : S \cup T \text{ is a partition of } [n]\}.$$

Here is the example for $n = 3$.

$$\begin{aligned} C_{\mathbf{M}_n} &= \{P_{\{1\}, \{2,3\}} = x_{1,2}x_{1,3} - x_{2,1}x_{3,1}, \\ &\quad P_{\{2,3\}, \{1\}} = x_{2,1}x_{3,1} - x_{1,2}x_{1,3}, \\ &\quad P_{\{2\}, \{1,3\}} = x_{2,1}x_{2,3} - x_{1,2}x_{3,2}, \\ &\quad P_{\{1,3\}, \{2\}} = x_{1,2}x_{3,2} - x_{2,1}x_{2,3}, \\ &\quad P_{\{3\}, \{1,2\}} = x_{3,1}x_{3,2} - x_{1,3}x_{2,3}, \\ &\quad P_{\{1,2\}, \{3\}} = x_{1,3}x_{2,3} - x_{3,1}x_{3,2}\}. \end{aligned}$$

Corollary 9.4.12. *For any $\ell \in [n]$,*

$$G_\ell := \{P_{S,T} : S \cup T \text{ is a partition of } [n] \text{ s.t. } \ell \in S\}$$

is a Gröbner basis of $I_{\mathbf{M}_n}$ with respect to any term order $>_\ell$ satisfying $x_{\ell,j} >_\ell x_{i,k}$, for any $i \neq \ell$. Thus, the set of initial monomials of the elements in G_ℓ are

$$in_{>_\ell}(I_{\mathbf{M}_n}) := \left\{ \prod_{s \in S, t \in T} x_{s,t} : S \cup T \text{ is a partition of } [n] \text{ s.t. } \ell \in S \right\}.$$

We call the supports of the monomials appearing in this corollary ℓ -cuts, since they correspond to complete directed bipartite graphs with edges directed away from the part S containing ℓ .

For example, for $n = 3, \ell = 3$ we have:

$$\begin{aligned} G_\ell &= \{P_{\{2,3\}, \{1\}} = x_{2,1}x_{3,1} - x_{1,2}x_{1,3}, \\ &\quad P_{\{1,3\}, \{2\}} = x_{1,2}x_{3,2} - x_{2,1}x_{2,3}, \\ &\quad P_{\{3\}, \{1,2\}} = x_{3,1}x_{3,2} - x_{1,3}x_{2,3}\} \end{aligned}$$

and

$$in_{>_\ell}(I_{\mathbf{M}_n}) = \{x_{2,1}x_{3,1}, x_{1,2}x_{3,2}, x_{3,1}x_{3,2}\}.$$

A directed spanning tree with all arcs pointing away from the root is an *arborescence*. We denote arb_ℓ the set of all arborescences with a certain

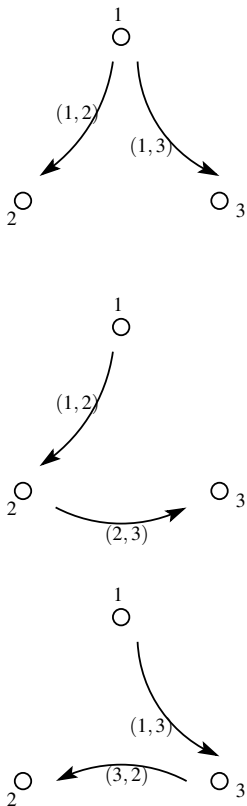


Figure 9.80: The three arborescences on three nodes and rooted at 1.

root $\ell \in [n]$, which we call ℓ -arborescences. Since every tree can be rooted at any of its vertices, the number of ℓ -arborescences for a fixed ℓ equals the number of labeled rooted trees on n nodes, which equals n^{n-2} . This result is available in most combinatorics textbooks or, for example, in [11].

Of course, we think of each arborescence as its set of edges, that is, as a subset of the label set J_n of \mathbf{M}_n .

Proposition 9.4.13. *For each $\ell \in [n]$, any term order as described in Corollary 9.4.12, gives as Gröbner basis a triangulation \mathcal{T}_ℓ of \mathbf{M}_n whose maximal simplices are labeled by the (complements of) the ℓ -arborescences,*

$$\mathcal{T}_\ell := \{J_n \setminus B : B \in \text{arb}_\ell\}.$$

Proof. We have discussed how to recover maximal faces from the minimal non-faces via transversals. Since the initial monomials are in bijection to the ℓ -cuts, we need to show that the transversals of this set are precisely all possible ℓ -arborescences.

One direction is easy: given any ℓ -arborescence B on $[n]$ with root ℓ , each ℓ -cut $P_{S,T}$ with $\ell \in S$ clearly contains at least one edge of B : any one joining S to T in B . Moreover, the arborescence B is minimal with that property because removing any single edge from it we get a graph with two components and letting S and T denote the vertices of those components, with $\ell \in S$, we have an ℓ -cut using no edge of B .

We show the other direction: Let B be a transversal of the set of all ℓ -cuts and consider B as a directed graph. We let S be the set of vertices that can be reached from ℓ by a directed path on B . S must be the whole $[n]$ since otherwise $(S, [n] \setminus S)$ is an ℓ -cut with no edge of B . Therefore, for any vertex i , there exists a directed path from ℓ to i which implies B contains an arborescence. By minimality of B as a transversal to all ℓ -cuts, B equals this arborescence. \square

9.5 Polytopal complexes and regular triangulations

Most of the structural results of Chapters 2, 4, 5, and 8 are valid for both point and for vector configurations, but when we speak about concrete examples in the rest of the chapters they are typically *point configurations*. The reader may get the impression that *vector configurations* are here only to make the theory more “consistent”, namely:

- It is convenient to be able to apply without any restriction the *contraction* operation to a configuration, because it is the natural way of studying *links* in triangulations. When we do so we sometimes get vector configurations from point configurations.
- Gale duality, which is fundamental for understanding secondary polytopes, transforms point configurations to totally cyclic vector configurations. If we want Gale duality to work both ways (and it does) we need to consider triangulations of those vector configurations as natural objects in the theory.

This section is devoted to show that, even if those two arguments are already powerful reasons to study triangulations and subdivisions of vector configurations, there is an even more important one: triangulations and subdivisions of vector configurations arise naturally in polytope theory and are actually ubiquitous in it; except they do not appear not under that explicit name! Consider the following situations:

1. The *normal fan* of a polytope \mathbf{P} (recall Definition 2.1.8) is a regular subdivision of the vector configuration consisting of the facet normals of \mathbf{P} . If \mathbf{P} is simple then this subdivision is a triangulation.
2. If \mathbf{P} contains the origin in its interior, then the complex of proper faces of \mathbf{P} is a regular subdivision of the totally cyclic vector configuration \mathbf{A}/\mathbf{o} , where \mathbf{A} consists of the vertices of \mathbf{P} together with the origin \mathbf{o} . If \mathbf{P} is simplicial polytope then its face complex is a triangulation.
3. *Line shellings*, the natural way to shell the boundary of a polytope, is an instance of monotone flipping sequences. Noticing this is the key to adapting the concept to arbitrary triangulations, and show that regular triangulations of point or vector configurations are always shellable.
4. The *g-vector* of a polytope, is an extremely important way of rewriting its *f*-vector. Basically, it counts how many bistellar flips in different types of circuits are needed to get the boundary complex of \mathbf{P} from the boundary complex of a simplex.

This final section will discuss these four situations, viewed as problems on subdivisions of vector configurations, and show a few interesting results.

9.5.1 Central and normal fans as regular triangulations

Let \mathbf{P} be a polytope in \mathbb{R}^m with the origin \mathbf{o} in its interior. Let \mathbf{A} be the point configuration consisting of the vertices of \mathbf{P} , and let $\mathbf{A} \cup \{\mathbf{o}\}$ denote the configuration obtained adding the origin as an extra element of \mathbf{A} . Let $\mathbf{V} = \mathbf{A} \cup \{\mathbf{o}\}/\mathbf{o}$ be the contraction of $\mathbf{A} \cup \{\mathbf{o}\}$ at the origin. By construction, \mathbf{V} is a totally cyclic configuration labeled by the same set of labels J as \mathbf{A} . Remember that totally cyclic means that the cone hull of \mathbf{V} , that we denote by $\text{conv}_{\mathbf{V}}(J)$, is the whole of \mathbb{R}^m .

Let now \mathcal{S} denote the complex of proper faces of \mathbf{P} . As an abstract cell complex, \mathcal{S} has its cells labeled by subsets of J . It makes sense, then, to ask whether \mathcal{S} is a polyhedral subdivision of the configuration \mathbf{V} . You can see an example in Figure 9.81:

Lemma 9.5.1. *With the notations above, the proper face complex \mathcal{S} of \mathbf{P} equals the regular polyhedral subdivision of \mathbf{V} obtained with the constant height function $\omega = (1, 1, \dots, 1)$.*

Proof. The proof basically consists in tracking down the construction \mathbf{V} in matrix form.

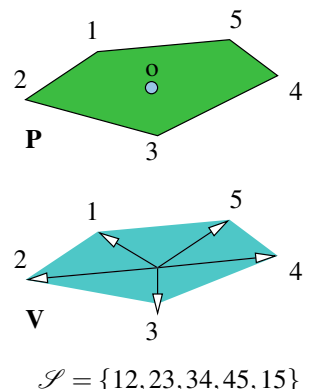
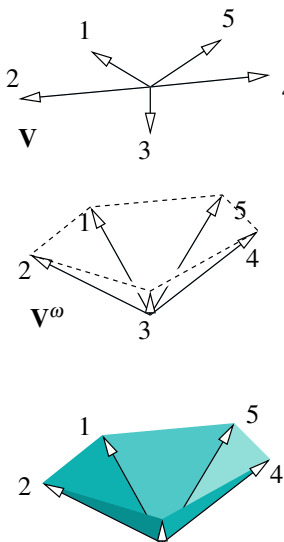


Figure 9.81: The central fan of a polytope.



$$\mathcal{S}(\mathbf{V}, \omega) = \{12, 23, 34, 45, 15\}$$

Figure 9.82: The central fan, as a regular subdivision.

Suppose that \mathbf{A} is, as usual, represented as a homogeneous matrix with its last row constantly 1 for homogenization. $\mathbf{A} \cup \{\mathbf{o}\}$ is represented as the same matrix, with an extra column equal to the vector $(0, \dots, 0, 1)$. Contracting at this element \mathbf{o} can simply be done by deleting the last row of the matrix. So: \mathbf{V} is obtained from \mathbf{A} by deleting its homogenization row.

Now, let us look at the construction of the regular subdivision $\mathcal{S}(\mathbf{A}, \omega)$ for the height function $\omega = (1, 1, \dots, 1)$. We have to lift our vectors to a configuration

$$\mathbf{V}^\omega := ((\mathbf{v}_i, \omega_i))_{i \in J},$$

and then consider as cells of $\mathcal{S}(\mathbf{V}, \omega)$ the lower facets of $\text{conv}(\mathbf{V}^\omega)$. Two things happen:

1. When lifting our vectors we are simply reinserting the homogenization row that we previously inserted. That is: $\mathbf{V}^\omega = \mathbf{A}$, even if we tend to think of the former as a vector configuration and the latter as a point configuration!
2. If \mathbf{V} is a totally cyclic configuration and ω is a valid height function, then all proper faces of \mathbf{V}^ω are lower faces.

Thus, we have that the lower faces of \mathbf{V}^ω coincide with the faces of the original point configuration \mathbf{A} , as desired. \square

Definition 9.5.2. The subdivision $\mathcal{S}(\mathbf{V}, \omega)$ of \mathbf{V} is the *central subdivision* of the polytope \mathbf{P} .

The central subdivision is (in the language of subdivisions of configurations) the same as the *central fan* of a polytope (in the language of polyhedral fans): the central fan of a polytope \mathbf{P} containing the origin is the complete polyhedral fan whose cells are the linear cones over the faces of \mathbf{P} .

Of course, the central subdivision \mathcal{S} is a triangulation of \mathbf{V} if and only if the original polytope \mathbf{P} is simplicial.

Let us generalize Lemma 9.5.1 a bit: for a totally cyclic vector configuration \mathbf{V} with index set J , there are two ways in which an arbitrary assignment of positive scalars to the elements of \mathbf{V} (i.e., a function $J \rightarrow [0, \infty)$) gives rise to a subdivision of \mathbf{V} :

1. The usual notion of regular triangulation. Use a function $\omega : J \rightarrow (0, \infty)$ to lift \mathbf{V} to a configuration

$$\mathbf{V}^\omega := \{(\mathbf{v}_i, \omega_i) \in \mathbb{R}^{m+1} : i \in J\},$$

where \mathbf{v}_i is the i -th vector in \mathbf{V} for each $i \in J$. Then consider the subdivision $\mathcal{S}(\mathbf{V}, \omega)$ whose cells are the lower facets of $\text{conv}(\mathbf{V}^\omega)$.

2. The following generalization of the central subdivision: use a function $\rho : J \rightarrow (0, \infty)$ to scale the vectors of \mathbf{V} , and then add a homogenization coordinate to consider the elements as *points* rather than vectors. That is, if the i -th element of \mathbf{V} is the vector \mathbf{v}_i , let \mathbf{A} be the configuration having as i -th element the point $(\rho_i \mathbf{v}_i, 1)$. Let $\mathbf{P} := \text{conv}_{\mathbf{A}}(J)$ and consider the face lattice of \mathbf{P} as a subdivision of \mathbf{V} , as in Lemma 9.5.1.

After seeing the proof of Lemma 9.5.1 it should be easy for you to derive that:

Corollary 9.5.3. *These two procedures give the same family of subdivisions of \mathbf{V} . More precisely, the subdivision of \mathbf{V} obtained by the second procedure for a certain ρ equals the regular subdivision $\mathcal{S}(\mathbf{S}, \omega)$ with*

$$\omega_i = 1/\rho_i, \quad \forall i \in J.$$

Remark 9.5.4. Readers may be puzzled by the fact that in this construction only the regular subdivisions of \mathbf{V} obtained with *strictly positive* choices of ω arise. This has to do with Theorems 4.1.39 and 4.1.40. The first theorem says that to construct all regular subdivisions of a vector configuration \mathbf{V} , non-negative choices of height vectors are enough. The second one says that the strictly positive ones suffice if we are only interested in subdivisions having only acyclic cells. That is, if we allowed for zero choices of some of the ω_i we might get regular subdivisions whose cones have a non-trivial linearity space. Those can certainly not be interpreted as central fans of polytopes.

We now look at polarity, in its usual polytope theory sense [339]. Remember that the *polar* of a certain polytope $\mathbf{P} \subset \mathbb{R}^m$ with vertices (in homogeneous coordinates)

$$\mathbf{A} = \begin{pmatrix} & 1 & 2 & \dots & n \\ \mathbf{p}_1 & & \mathbf{p}_2 & \cdots & \mathbf{p}_n \\ 1 & & 1 & \dots & 1 \end{pmatrix}$$

is the polytope \mathbf{P}^\vee with the following inequality description:

$$\mathbf{P}^\vee := \{\mathbf{x} \in \mathbb{R}^m : \langle \mathbf{p}_i, \mathbf{x} \rangle \leq 1, \forall i\}.$$

We state without proof the following basic results from polytope theory:

Theorem 9.5.5. 1. *Polarity is an involution: $(\mathbf{P}^\vee)^\vee = \mathbf{P}$.*

2. *The central fan of \mathbf{P} equals the outer normal fan of \mathbf{P}^\vee , and vice-versa.*

As usual, the (outer) normal fan of a polytope \mathbf{P} is defined as having, for each face $\mathbf{F} \leq \mathbf{P}$, the following cone, called the *normal cone* of \mathbf{F} :

$$N_{\mathbf{P}}(\mathbf{F}) := \{\mathbf{x} \in \mathbb{R}^m : \langle \mathbf{x}, \mathbf{y} \rangle \geq \langle \mathbf{x}, \mathbf{z} \rangle, \forall \mathbf{y} \in \mathbf{F}, \mathbf{z} \in \mathbf{P}\}.$$

Let us see what Corollary 9.5.3 gives under polar duality:

Theorem 9.5.6. *Let \mathbf{P} be a polytope with facets indexed by a set J . Let \mathbf{V} be the vector configuration of facet outer normal vectors of \mathbf{P} . For each possible (positive) right-hand side vector $\omega : J \rightarrow (0, \infty)$ define*

$$\mathbf{P}^\omega := \{\mathbf{x} \in \mathbb{R}^m : \langle \mathbf{p}_i, \mathbf{x} \rangle \leq \omega_i, \forall i\},$$

so that $\mathbf{P} = \mathbf{P}^{(1, \dots, 1)}$.

Then: for every choice of ω , the normal fan of \mathbf{P}^ω equals the regular subdivision $\mathcal{S}(\mathbf{V}, \omega)$.

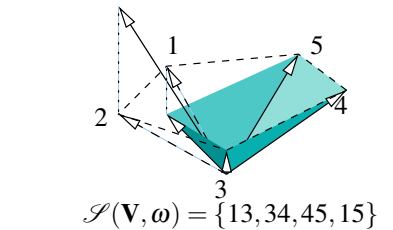
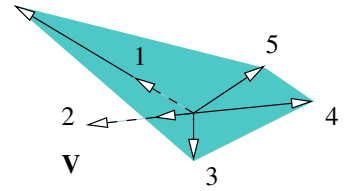


Figure 9.83: Moving vertices away from or towards the origin (top, where $\rho = (3, 1/3, 1, 1, 1)$) has the same effect on the central subdivision as changing in the opposite way the lift for the regular subdivision of \mathbf{V} (bottom, where $\omega = (1/3, 3, 1, 1, 1)$).

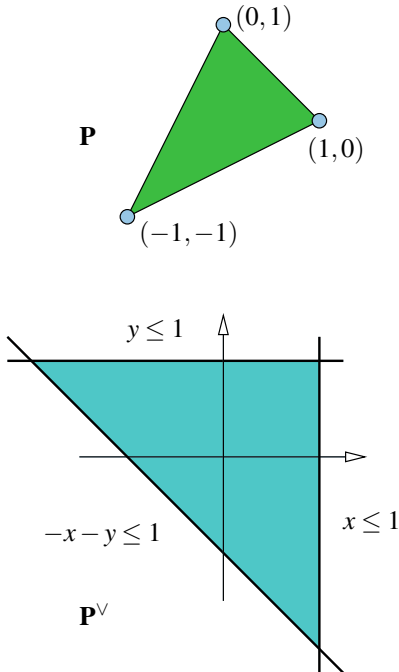


Figure 9.84: A polytope \mathbf{P} , with its three vertices, and its polar \mathbf{P}^\vee , with its three defining inequalities. Moving away from or towards the origin the vertices of \mathbf{P} will have the effect of translating the facets of \mathbf{P}^\vee in the opposite direction.

Proof. Fix a choice of ω and let ρ be defined by

$$\rho_i = 1/\omega, \quad \forall i.$$

Clearly, we have that

$$\mathbf{P}^\omega := \{\mathbf{x} \in \mathbb{R}^m : \langle \rho_i \mathbf{p}_i, \mathbf{x} \rangle \leq 1, \forall i\}.$$

That is, \mathbf{P}^ω is the polar to the polytope whose central fan is given by the configuration \mathbf{V} with its elements weighted by ρ . By Corollary 9.5.3, that polytope has as central fan the regular subdivision $\mathcal{S}(\mathbf{V}, \omega)$. \square

The above result is at the heart of the relation between parametric linear programming and chambers, that we discussed in Section 1.2. Let us see the precise connection.

Suppose we want to study the family of polytopes \mathbf{P}^ω of Theorem 9.5.6, for a certain $m \times n$ matrix \mathbf{V} . Let us first do a change of variables. Instead of the m variables \mathbf{x} we use n variables $\mathbf{y} = (y_1, \dots, y_n)$ defined as:

$$y_i = \omega_i - \langle \mathbf{p}_i, \mathbf{x} \rangle.$$

Under this change of variables we have that $\mathbf{x} \in \mathbf{P}^\omega$ is equivalent to $\mathbf{y} \geq 0$. In a sense, the n entries of \mathbf{y} measure how far is \mathbf{x} from each of the n facets of \mathbf{P}^ω , with a negative y_i indicating that it is “beyond” the i -th facet. Now, since \mathbf{y} has more entries than \mathbf{x} , its entries are not independent. In fact, for each linear dependence λ of \mathbf{V} we have that:

$$\langle \lambda, \mathbf{y} \rangle = \sum_i \lambda_i \omega_i - \sum_i \lambda_i \langle \mathbf{p}_i, \mathbf{x} \rangle = \sum_i \lambda_i \omega_i - \langle \sum_i \lambda_i \mathbf{p}_i, \mathbf{x} \rangle = \sum_i \lambda_i \omega_i = \langle \lambda, \omega \rangle.$$

Let now \mathbf{B} be a Gale transform of \mathbf{V} . Since the rows of \mathbf{B} are a basis for the space of dependences of \mathbf{V} , the set of valid vectors \mathbf{y} are those satisfying the matrix equation $\mathbf{B} \cdot \mathbf{y} = \mathbf{B}\omega$. That is to say:

Corollary 9.5.7. *Let $d = n - m$, let \mathbf{B} be a Gale transform of \mathbf{V} and, for each $\omega \in \mathbb{R}^n$ let $b := \mathbf{B}\omega \in \mathbb{R}^d$. Then, the polytope \mathbf{P}^ω is linearly isomorphic to the polytope*

$$\mathbf{P}_b := \{\mathbf{y} : \mathbf{B} \cdot \mathbf{y} = b, \mathbf{y} \geq 0\}.$$

This is the standard LP-tableaux formulation of parametric linear programming (refer to [291]). In it, the right hand side $b \in \mathbb{R}^d$ plays the same role of our usual ω , but with the advantage that b is not “redundant”. (Remember that choices of ω differing by an evaluation of \mathbf{V} represent essentially the same polytope). In fact, the passage from ω to b is nothing but the projection that gave the chamber complex from the secondary fan in Section 5.4.1 of Chapter 5.

In particular, as we change the right-hand side defining our feasibility region \mathbf{P}_b we get the same effect as changing ω in Theorem 9.5.6, polar to the effect of changing the height function for a regular subdivision of \mathbf{V} : the normal fan stays constant for some time until a “flip” occurs. The

stratification of the space of right hand sides into what we called “chambers” in Section 1.2 is simply the *chamber complex*, in the sense of Section 5.4, of \mathbf{B} .

Recall that in the LP setting, *basic feasible solutions* are the vertices of \mathbf{P}_b (assuming b is generic, so that \mathbf{P}_b is simple). If not, each vertex represents several basic solutions). At each vertex (again, assuming genericity) exactly d coordinates of \mathbf{y} vanish, and their labels from a basis of \mathbf{V} . Put differently, the non-vanishing coordinates form a basis of \mathbf{B} . The collection of all basic solutions for a given b form a regular triangulation of \mathbf{V} so that, for example, two adjacent simplices correspond to basic solutions that differ by a single element (this is a *pivot* in the simplex method).

For any two vectors b_1 and b_2 in the same chamber of \mathbf{B} the corresponding triangulations of \mathbf{V} are the same, which means that \mathbf{P}_{b_1} and \mathbf{P}_{b_2} are *normally equivalent* (same normal fan), hence of the same combinatorial type, the same graph, etc. This point of view might be of interest to study properties of the graph of \mathbf{P}_b , for example, the diameter of \mathbf{P}_b as the vector b changes.

More importantly for the simplex method, in this case \mathbf{P}_{b_1} and \mathbf{P}_{b_2} produce the same optimal basic solution for every cost vector. “The same” means that its zeroes are at the same positions; the non-zero values vary but each can be computed by simply evaluating a certain $d \times d$ determinant.

9.5.2 Shellings, flips, and face vectors

Although shellings can be defined for more general cell complexes (see, e.g., [339]), we concentrate here on shellings of simplicial complexes. Remember that *facets* of a simplicial complex are its maximal simplices, and that a simplicial complex is *pure* if all facets have the same dimension d ; that is, if they all have the same number of vertices $d + 1$. A pure simplicial complex is *shellable* if there is a nice ordering of its facets.

Let us be more precise: Let \mathcal{K} be a pure simplicial complex of dimension d and let s be its number of facets. An ordering F_1, \dots, F_s of its facets induces an incremental way of constructing \mathcal{K} : for each $i = 1, \dots, m$ we call \mathcal{K}_i the pure d -dimensional simplicial complex whose facets are F_1, \dots, F_i :

Definition 9.5.8. An ordering F_1, \dots, F_s of the facets of \mathcal{K} is a *shelling order* or a *shelling* of \mathcal{K} if, for every $k = 1, \dots, s - 1$, the intersection of each new facet ∂F_{i+1} with the previously constructed complex \mathcal{K}_i is a pure simplicial complex of dimension $d - 1$.

Here, ∂F_{i+1} denotes the simplicial complex of all proper faces of the simplex F_{i+1} .

Example 9.5.9. Let us see this concept in action in the small examples of Figure 9.85.

- Let \mathcal{K} be the simplicial complex on four vertices with maximal simplices 123, 134 and 124. Each of the six possible orderings of these three triangles is a shelling order, since the first will always intersect the second in an edge, and the third will intersect the union of the first two in two edges.

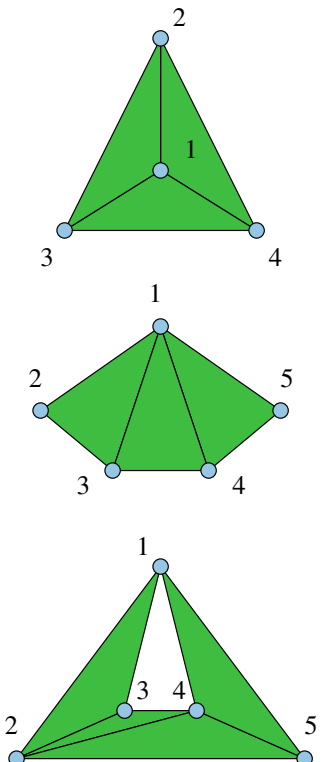


Figure 9.85: Three pure simplicial complexes of dimension two. In the top one, every order is a shelling. In the middle one some orderings are shellings and some are not. The bottom complex is unshellable.

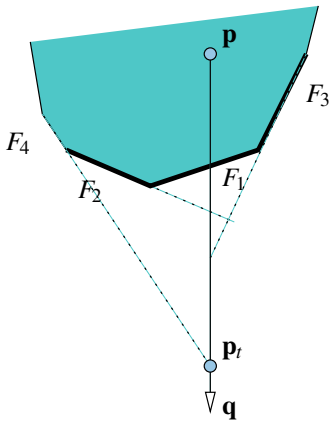


Figure 9.86: The line-shelling idea.

2. Let now \mathcal{K} be the simplicial complex on five vertices with maximal simplices 123, 134 and 145. Only four of the six possible orderings are shelling orders; the two ending with 134 are not, because in them the first and second triangles intersect in a vertex, which is not a “pure simplicial complex of dimension 1”.

3. Finally, let \mathcal{K} be the simplicial complex on five vertices with maximal simplices 123, 234, 245 and 145. Now no ordering of the triangles is a shelling order; this is an example of an *unshellable* complex. To convince yourself, assume without loss of generality that 123 comes before 145 in the ordering. Then, when 145 enters in the complex, its intersection with the previously inserted simplices will necessarily contain the isolated vertex 1 (plus, perhaps, some other things). In particular, this intersection will not be pure 1-dimensional.

The main result we want to prove is that regular triangulations (of point or vector configurations) are always shellable. For triangulations of totally cyclic configurations (which are the same, according to Corollary 9.5.3, as boundary complexes of simplicial polytopes) this is a classical result of Bruggesser and Mani [339]. For the general case the proof follows the same ideas:

Theorem 9.5.10 (Line shellings of a regular triangulations). *Let \mathbf{A} be a (point or vector) configuration, and let \mathcal{T} be a regular triangulation of it. Then, as a simplicial complex, \mathcal{T} is shellable.*

Proof. We follow the classical proof of Bruggesser and Mani, based on the concept of *line shelling*, except we adapt the language of it to the framework of regular triangulations of vector configurations, which have point configurations as a special case. In our pictures, however, we draw \mathbf{A} as a point configuration.

Let $\omega : J \rightarrow \mathbb{R}$ be a height function. Here J , as usual, is the set of labels of \mathbf{A} . Let \mathbf{A}^ω denote the lifted configuration.

We now introduce two new vectors in the space \mathbb{R}^{m+1} where \mathbf{A}^ω lives: Let \mathbf{q} denote the vector $(0, \dots, 0, -1)$. In a “point configuration picture”, \mathbf{q} denotes the negative direction of the lift. And let \mathbf{p} denote any vector in the interior of $\text{conv}(\mathbf{A}^\omega)$, different from \mathbf{q} (which is in the interior of $\text{conv}(\mathbf{A}^\omega)$ when \mathbf{A} is totally cyclic) and sufficiently generic. Finally, let \mathbf{l} denote the subspace spanned by \mathbf{q} and \mathbf{p} . It is a 2-dimensional linear subspace but, in a “point configuration picture” it appears as the vertical line passing through \mathbf{p} . See Figure 9.87.

The key of the proof is to move monotonically along \mathbf{l} from \mathbf{p} to \mathbf{q} . That is, let $\mathbf{p}_t = \mathbf{p} + t\mathbf{q}$, for each $t \in [0, \infty)$. In the “point configuration picture”, we are moving a point along a half-line, in the vector configuration picture we are rotating a vector in a linear plane (and changing its length at the same time, but that is not relevant for the process; in fact we can think of $\lim_{t \rightarrow \infty} \mathbf{p}_t$ as being just \mathbf{q}). See Figure 9.86.

Since \mathbf{p} is interior to $\text{conv}(\mathbf{A}^\omega)$ no facet of $\text{conv}(\mathbf{A}^\omega)$ is “seen from \mathbf{p} ”. As usual, we say a facet is “seen from a point or vector” if its exterior side

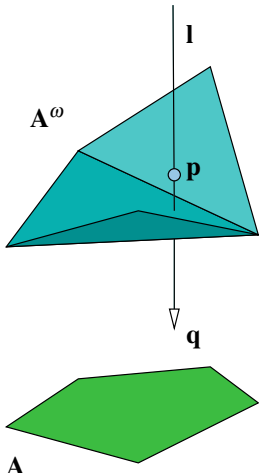


Figure 9.87: The setting for the proof of Theorem 9.5.10 (line shellings).

is seen. Also, by definition of regular triangulation, the full-dimensional simplices in \mathcal{T} are the facets of $\text{conv}(\mathbf{A}^\omega)$ “seen from \mathbf{q} ”. So, when moving from \mathbf{p} to \mathbf{q} we cross exactly once the hyperplane spanned by each full-dimensional simplex of \mathcal{T} . We claim that the order in which those hyperplanes are crossed is a shelling order on \mathcal{T} . To see this observe that:

- The genericity assumption in the choice of \mathbf{p} implies that no two of those hyperplanes will be crossed at the same time: the intersection of two of those hyperplanes has codimension two and does not contain \mathbf{q} (the hyperplanes we are interested in are never vertical with respect to the lift), so a generic choice of \mathbf{p} prevents \mathbf{l} (the subspace spanned by \mathbf{p} and \mathbf{q}) from meeting any of those intersections.
- The first facet F_1 in the shelling is the carrier of the intersection of the ray $[\mathbf{pq}]$ and the boundary of $\text{conv}(\mathbf{A}^\omega)$. Right after we cross this boundary, F_1 is the only facet of $\text{conv}(\mathbf{A}^\omega)$ seen from \mathbf{p}_t . See Figure 9.86 again.
- When the hyperplane spanned by a new facet F_{i+1} is crossed by \mathbf{p}_t , the part of $\partial \text{conv}(F_{i+1})$ already in the complex $\mathcal{T}_i = \{F_1, \dots, F_i\}$ is precisely the part seen from \mathbf{p}_t which implies it is indeed a pure $(d-1)$ -dimensional complex.

□

What is the difference between the cases where \mathbf{A} was totally cyclic or acyclic (or anything in between) in this *line shelling* procedure? The answer is in Figure 9.88. This is a “vector configuration picture” where \mathbf{l} appears as a truly two-dimensional linear space. Observe that in the totally cyclic case the shelling finishes when $-\mathbf{p}_t$ enters again the interior of $\text{conv}(\mathbf{A}^\omega)$ through a certain facet F_s . This is the last facet in the shelling, with index $d+1$, and it “closes” the triangulation \mathcal{T} , which is topologically a sphere. In the acyclic case \mathcal{T} is a ball.

Line shellings and monotone flipping

Shellings play a role in polytope theory and geometric combinatorics similar to that of flips in the theory of triangulations: They give a way of changing a simplicial complex in a controlled and step-by-step manner. In fact, our next goal is to use the central fan construction of the previous section to show that a line shelling as the one in the proof of Theorem 9.5.10 can be regarded as a monotone sequence of flips in the space of triangulations of a certain vector configuration. We briefly recall all the notation in that proof:

- \mathbf{A} is a configuration in \mathbb{R}^m with label set J , lifted to a configuration \mathbf{A}^ω via a height function ω .
- \mathbf{p} and \mathbf{q} are two extra points/vectors in the space \mathbb{R}^{m+1} where \mathbf{A}^ω lives: \mathbf{p} is generic and in the interior of $\text{conv}(\mathbf{A}^\omega)$, and $\mathbf{q} = (0, \dots, 0, -1)$ represents the lifting direction.

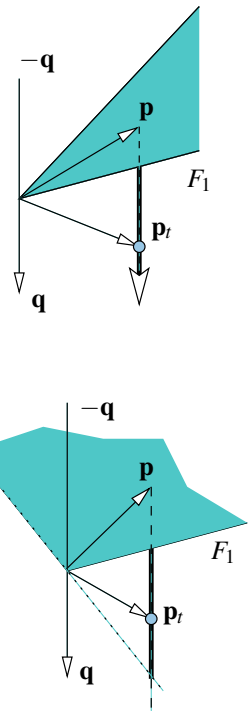


Figure 9.88: When \mathbf{A} is acyclic (top), $\text{conv}(\mathbf{A}^\omega)$ lies to one side of the vector \mathbf{q} , so that only part of its boundary is visible from it. When \mathbf{A} is totally cyclic (bottom), $-\mathbf{q}$ lies in the interior of $\text{conv}(\mathbf{A}^\omega)$, so that the whole boundary of $\text{conv}(\mathbf{A}^\omega)$ is visible from \mathbf{q} . The thick ray (top) and segment (bottom) indicate the interval when the shelling takes place.

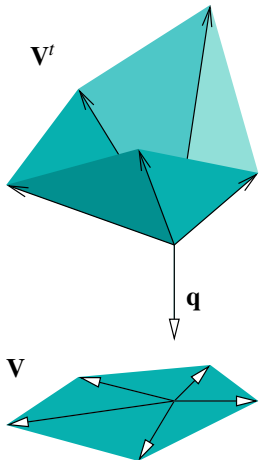
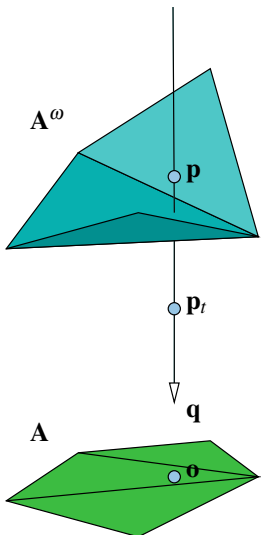


Figure 9.89: The configurations used in the proof of Theorem 9.5.10 (top) and some contractions of them (bottom). In both parts we have a base configuration (A and V) and a lift of it (A^ω and V^t)

which induces a regular subdivision (the triangulation \mathcal{T} and the subdivision \mathcal{S}_t). The figure depends on the parameter t , which in the top part moves the point p_t from p towards q and in the bottom part changes the whole subdivision.

- For each $t \in [0, \infty)$ we denote $\mathbf{p}_t = \mathbf{p} + t\mathbf{q}$.

We now introduce a couple more elements into the picture. See Figure 9.89:

- Let \mathbf{o} be the projection of \mathbf{p} to \mathbb{R}^m . More formally, \mathbf{o} is the element corresponding to \mathbf{p} in the contraction $A^\omega \cup \{\mathbf{p}, \mathbf{q}\}/\mathbf{q}$.
- Let \mathbf{V} be the vector configuration obtained by the central projection of A from \mathbf{o} . Equivalently,

$$\mathbf{V} := A^\omega \cup \{\mathbf{p}, \mathbf{q}\}/\mathbf{pq}.$$

- For each t , let \mathbf{V}^t denote the vector configuration

$$\mathbf{V}^t := A^\omega \cup \{\mathbf{p}_t\}/\mathbf{p}_t.$$

This notation is consistent with the fact that if \mathbf{V} is projected along the direction of \mathbf{q} we recover the configuration \mathbf{V} : since \mathbf{p}_t lies in the linear span of \mathbf{p} and \mathbf{q} and it is different from \mathbf{q} . We have:

$$\mathbf{V}^t \cup \{\mathbf{q}\}/\mathbf{q} = A^\omega \cup \{\mathbf{p}_t, \mathbf{q}\}/\mathbf{p}_t \mathbf{q} = A^\omega \cup \{\mathbf{p}, \mathbf{q}\}/\mathbf{pq} = \mathbf{V}.$$

In particular, whenever \mathbf{V}^t has any lower facets, so that it is a *valid* lift of \mathbf{V} in the conditions of Theorem 4.1.39, the lower hull of \mathbf{V}^t is the regular subdivision of the vector configuration \mathbf{V} given by the height function

$$\omega_t := \omega + (t, \dots, t) - (c, \dots, c),$$

where the constant c denotes the height of the initial point \mathbf{p} . We denote this subdivision by \mathcal{S}^t .

There is always an interval of values of t for which \mathbf{V}^t has lower facets. It starts when \mathbf{p}_t gets out of $\text{conv}(A^\omega)$ through the first facet F_1 in the shelling and it finishes differently in the acyclic and totally cyclic cases: in the acyclic case it goes all the way up to $t = \infty$, but in the totally cyclic case it finishes when $-\mathbf{p}_t$ enters again in $\text{conv}(A^\omega)$ through the last facet F_s of the shelling. See Figure 9.88 again.

This description shows that the different subdivisions \mathcal{S}_t obtained in this process from a monotone flip sequence in the space of triangulations of \mathbf{V} :

Theorem 9.5.11. *The subdivision \mathcal{S}_t is always a triangulation except when \mathbf{p}_t crosses a facet defining hyperplane of $\text{conv}(A^\omega)$. In this case it is a non-degenerate (that is, supported in a full-dimensional circuit) bistellar flip. Moreover:*

1. *The sequence of triangulations is monotone in the sense of Theorems 5.3.7 and, more specifically, 5.3.13.*
2. *If we call t_k ($k = 1, \dots, s$) the value of t at which the k -th facet is introduced in the shelling, and \mathcal{T}_k the partial complex given by the shelling at that stage, we have the following equality of simplicial complexes:*

$$\mathcal{S}_t = \partial \mathcal{T}_k, \quad \forall t \in (t_k, t_{k+1}).$$

3. When $t \rightarrow \infty$, \mathcal{S}_t is the central subdivision of $\text{conv}(\mathbf{A})$ in the sense of Definition 9.5.2.

In Part 2 we say that the equality is only of simplicial complexes in the same sense as we said the “the central subdivision of a polytope \mathbf{P} equals the boundary complex of it”. The central subdivision is made out of cones but, as an abstract cell complex, it equals the face complex of \mathbf{P} .

Proof. Lower facets of $\mathbf{V}^t = \mathbf{A}^\omega \cup \{\mathbf{p}_t\}/\mathbf{p}_t$ are the same as lower facets of $\mathbf{A}^\omega \cup \{\mathbf{p}_t\}$ containing \mathbf{p}_t . They are all simplicial except at the moments when \mathbf{p}_t crosses the hyperplane defined by a certain facet F_k in the shelling. In this case $F_k \cup \{\mathbf{p}_t\}$ is the only non-simplicial facet, and it is a non-degenerate circuit. This proves the first sentence, and part (1) follows from the specific form of ω_t (compare it with the statement of Theorem 5.3.13).

To prove Part 2 observe that, actually, all the facets of $\mathbf{A}^\omega \cup \{\mathbf{p}_t\}$ containing \mathbf{p}_t are lower. So, $\mathbf{V}^t = \mathbf{A}^\omega \cup \{\mathbf{p}_t\}/\mathbf{p}_t$ is the link of \mathbf{p}_t in the boundary complex of $\mathbf{A}^\omega \cup \{\mathbf{p}_t\}$. This equals the boundary of the complex of faces of \mathbf{A}^ω visible from \mathbf{p}_t , which is precisely the definition of \mathcal{T}_k via the shelling order.

When t goes to infinity \mathbf{p}_t tends to \mathbf{q} so that \mathbf{V}^t tends to $\mathbf{A}^\omega \cup \{\mathbf{q}\}/\mathbf{q} = \mathbf{A}$ and ω_t , suitably normalized, tends to $(1,;1)$. Thus, we are exactly in the situation of Lemma 9.5.1. \square

Summing up: as we build a regular triangulation simplex by simplex via a line shelling, all the intermediate simplicial complexes that we get are star-shaped with respect to the origin (where we call “origin” \mathbf{o} in the ambient space of \mathbf{A} the projection of the line \mathbf{l} used for the shelling). The central fans, with respect to the origin, of the boundaries of these intermediate complexes, form a monotone sequence of flips. Figure 9.90 illustrates this.

h-vectors, g-vectors, and flips

In Section 2.6 we encountered f -vectors and h -vectors. The following definition and lemma state in a precise way how the f -vector of a shellable complex changes when the complex is built up step by step via a shelling.

Definition 9.5.12. Let \mathcal{K} be a shellable simplicial complex of dimension d and let F_1, \dots, F_s denote the facets of \mathcal{K} , labeled according to the shelling order.

1. We say that a certain facet F_{i+1} has *index* k in the shelling if exactly k facets of F_{i+1} were already present in \mathcal{K}_i . By convention, F_1 has index 0.
2. We define the *h-vector* (h_0, \dots, h_{d+1}) of the shelling as the vector counting the number of facets introduced with each index $k \in \{0, \dots, d+1\}$. That is to say:

$$h_k = |\{F_i : F_i \text{ has index } k\}|.$$

Remember that the f -vector $(f_{-1}, f_0, \dots, f_d)$ of a d -dimensional complex has each f_k equal to the number of cells of dimension k . By convention,

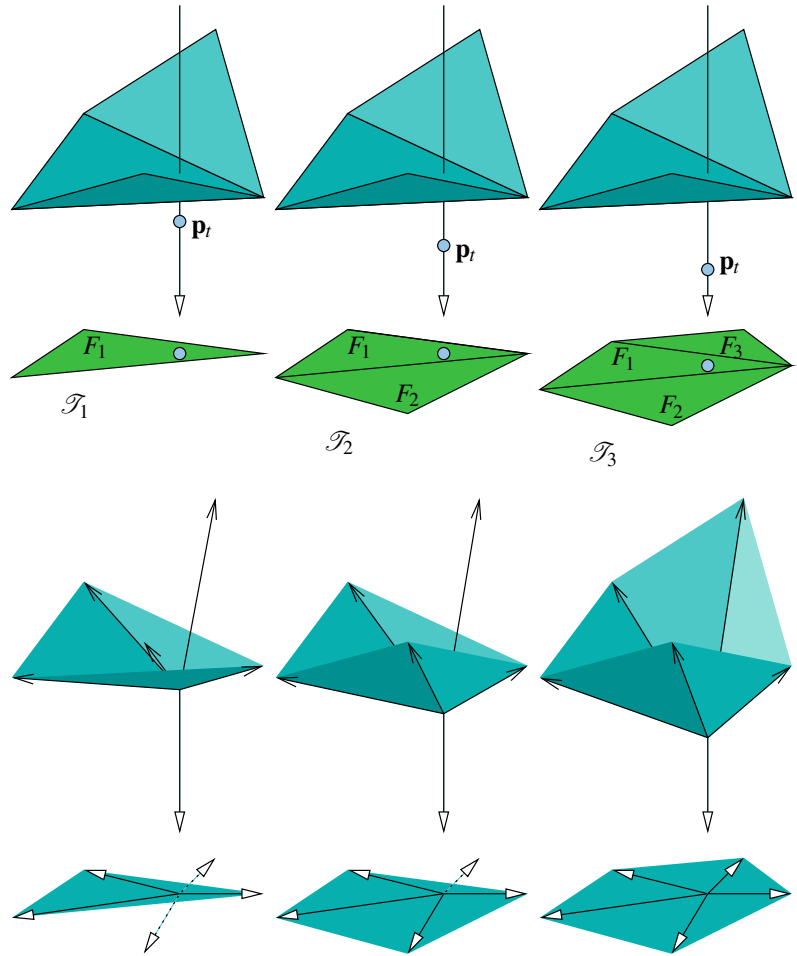


Figure 9.90: The shelling (top) and bistellar flip sequence (bottom). The shelling process goes from left to right

$f_{-1} = 1$ for every complex, since the “empty cell” is in every complex, and it is considered to have dimension -1 .

The following lemma proves that what we saw in Chapter 2 in Section 2.6 is indeed the same h -vector obtained from a shelling!

Lemma 9.5.13. *For every shelling of a shellable complex \mathcal{K} of dimension d , its h -vector and f -vector are related by the following linear relation:*

$$\begin{pmatrix} f_{-1} \\ f_0 \\ f_1 \\ \vdots \\ f_{d-1} \\ f_d \end{pmatrix} = \begin{pmatrix} \binom{d+1}{0} & 0 & 0 & \dots & 0 & 0 \\ \binom{d+1}{1} & \binom{d}{0} & 0 & \dots & 0 & 0 \\ \binom{d+1}{2} & \binom{d}{1} & \binom{d-1}{0} & \dots & 0 & 0 \\ \vdots & \vdots & \vdots & \ddots & \vdots & \vdots \\ \binom{d+1}{d} & \binom{d}{d-1} & \binom{d-1}{d-2} & \dots & \binom{1}{0} & 0 \\ \binom{d+1}{d+1} & \binom{d}{d} & \binom{d-1}{d-1} & \dots & \binom{1}{1} & \binom{0}{0} \end{pmatrix} \cdot \begin{pmatrix} h_0 \\ h_1 \\ h_2 \\ \vdots \\ h_d \\ h_{d+1} \end{pmatrix}$$

Proof. Check that when a d -simplex is inserted in the shelling process with index k the change in the f -vector is exactly as given in the $(k+1)$ -th column of the matrix. For example, a simplex with index 0 introduces its whole face complex, adding $\binom{d+1}{k+1}$ to each f_k , and a simplex with index $d+1$ adds 1 to f_d and nothing to the rest, since its boundary complex was already in the complex.

We leave details to the reader, but let us discuss the value of f_{-1} . The statement says that h_0 equals f_{-1} ; that is to say, that h_0 is 1. This is true because:

1. The first simplex in the shelling is always added with index zero.
2. No other simplex can be added with index zero. That would mean it is added without gluing it to anything already present, which is against the definition of shelling; the intersection would be the complex whose only cell is the empty simplex, which is not “pure $(d-1)$ -dimensional”.

□

The matrix in the statement is clearly invertible: It has 1's in the diagonal and 0's above it. Thus, the formula can be inverted to give an expression for the h -vector in terms of the f -vector. We leave it to the reader (Exercise 9.14) to prove that the formula is as follows. Observe it is the same matrix of Lemma 9.5.13 except with alternating signs. See also Section 2.6.

Lemma 9.5.14. *For every shellable complex \mathcal{K} of dimension d , its f -vector and h -vector are related by the following linear relation. In particular, the h -vector does not depend on the particular shelling of \mathcal{K} chosen.*

$$\begin{pmatrix} h_0 \\ h_1 \\ h_2 \\ \vdots \\ h_d \\ h_{d+1} \end{pmatrix} = \begin{pmatrix} +\binom{d+1}{0} & 0 & \dots & 0 & 0 \\ -\binom{d+1}{1} & +\binom{d}{0} & \dots & 0 & 0 \\ +\binom{d+1}{2} & -\binom{d}{1} & \dots & 0 & 0 \\ \vdots & \vdots & \ddots & \vdots & \vdots \\ (-1)^d \binom{d+1}{d} & (-1)^{d-1} \binom{d}{d-1} & \dots & +\binom{1}{0} & 0 \\ (-1)^{d+1} \binom{d+1}{d+1} & (-1)^d \binom{d}{d} & \dots & -\binom{1}{1} & +\binom{0}{0} \end{pmatrix} \cdot \begin{pmatrix} f_{-1} \\ f_0 \\ f_1 \\ \vdots \\ f_{d-1} \\ f_d \end{pmatrix}$$

This suggests the following definition. Check that it is consistent with Definition 2.6.7 in Chapter 2.

Definition 9.5.15. The h -vector $h(\mathcal{K})$ of a pure simplicial complex \mathcal{K} of dimension d is defined via the formula in Lemma 9.5.14 applied to its f -vector.

Remark 9.5.16. Apart from its relation to shellability, the h -vector has very nice properties which make it a useful way of looking at the f -vector of an arbitrary pure complex. For example:

1. According to Lemma 9.5.14, h_{d+1} is the alternating sum of the numbers of simplices of each dimension. This is the same as the Euler

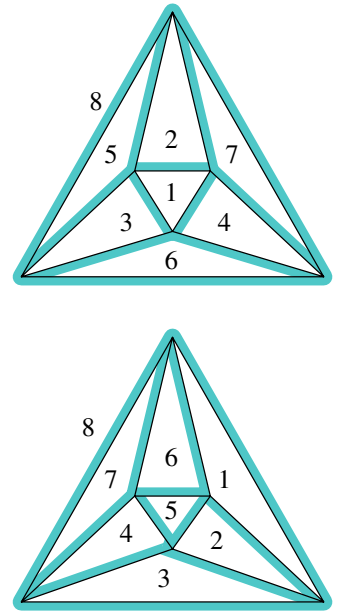


Figure 9.91: Two shellings in the boundary complex of an octahedron. The index of each triangle is its number of shaded sides. The h -vector is $(1, 3, 3, 1)$ in both.

characteristic $\chi(\mathcal{K})$ of the complex, except for the fact that the h -vector includes the empty face in the count and that there is a global change of sign for odd-dimensional complexes. That is, we always have:

$$h_{d+1}(\mathcal{K}) = (-1)^d (\chi(\mathcal{K}) - 1).$$

2. If \mathcal{K} is a shellable d -manifold, then the opposite of any shelling order is also a shelling order (prove it!). A simplex of index k in the first shelling has index $d + 1 - k$ in the second shelling (as should follow from your proof). Hence, the h -vector of any shellable d -manifold is palindromic:

$$h_k = h_{d+1-k}, \quad \forall k \in \{0, \dots, d+1\}.$$

These formulae are called the *Dehn-Sommerville relations*. They are valid (with a different proof, based on applying Euler's relation to all the links of simplices of all dimensions) for arbitrary simplicial manifolds. We already stated them in Chapter 2 (Definition 2.6.10).

3. The h -vector of a simplex is $(1, \dots, 1)$ and the h -vector of the boundary of the cyclic polytope $\mathbf{C}(n, d)$ is

$$h_k(\partial \text{conv}(\mathbf{C}(n, d))) = \binom{n-d-1+k}{k}, \quad \forall k \leq d/2.$$

The h -vector of any simplicial sphere lies coordinate-wise between these two extreme cases. (This is a generalization of the Upper and Lower Bound Theorems of Section 2.6.2.)

Let us now look at how the h -vector of a triangulation \mathcal{T} changes when a flip is applied to it.

Lemma 9.5.17. *Let \mathcal{T} be a triangulation of a d -dimensional configuration, and let \mathcal{T}' be obtained from \mathcal{T} by a flip on a circuit of type (i, j) with $i + j = d + 2$ (that is to say, a non-degenerate flip). Then:*

$$h_k(\mathcal{T}') - h_k(\mathcal{T}) = \begin{cases} +1 & \text{if } i \leq k < j, \\ -1 & \text{if } j \leq k < i, \\ 0 & \text{otherwise.} \end{cases}$$

Proof. Let \mathcal{T}_Z^+ and \mathcal{T}_Z^- be the positive and negative triangulations of the circuit. Since \mathcal{T} and \mathcal{T}' differ only in those subcomplexes, we have

$$f(\mathcal{T}) - f(\mathcal{T}_Z^+) = f(\mathcal{T}') - f(\mathcal{T}_Z^-).$$

Since all the complexes in the formula are pure of the same dimension, we can apply to all of them the linear transformation sending f -vectors to h -vectors, and get:

$$h(\mathcal{T}) - h(\mathcal{T}_Z^+) = h(\mathcal{T}') - h(\mathcal{T}_Z^-).$$

We leave it to the reader to check that

$$h_k(\mathcal{T}_Z^+) = \begin{cases} 1 & \text{if } k < i, \\ 0 & \text{otherwise,} \end{cases} \quad \text{and} \quad h_k(\mathcal{T}_Z^-) = \begin{cases} 1 & \text{if } k < j, \\ 0 & \text{otherwise.} \end{cases}$$

From this the statement follows. \square

This suggests the following definition and corollary:

Definition 9.5.18. The g -vector $g(\mathcal{K}) = (g_0, \dots, g_{d+2})$ of a pure simplicial complex \mathcal{K} of dimension d is defined as:

$$g_i := h_i - h_{i-1}, \quad \forall i \in \{0, \dots, d+2\}$$

where (h_0, \dots, h_{d+1}) is the h -vector of \mathcal{K} and with the convention that $h_{-1} = h_{d+2} = 0$.

Corollary 9.5.19. Let \mathcal{T} be a triangulation of a d -dimensional configuration, and let \mathcal{T}' be obtained from \mathcal{T} by a flip on a circuit of type (i, j) with $i + j = d + 2$. Then, \mathcal{T} and \mathcal{T}' have the same g -vector except for the entries

$$g_i(\mathcal{T}') = g_i(\mathcal{T}) + 1, \quad g_j(\mathcal{T}') = g_j(\mathcal{T}) - 1.$$

The g -vector is especially interesting for simplicial spheres, so we assume from now on that \mathbf{A} is totally cyclic. Some properties of the g -vectors of spheres are:

- The g -vector of any manifold is anti-palindromic: $g_i = -g_{d+2-i}$ (Dehn-Sommerville relations).
- The first half of the g -vector of a *polytope* is non-negative. This is equivalent to saying that the h -vector is unimodal: it increases up to the middle and then it decreases. It is important to notice that no purely combinatorial proof of this fact is known, the existing proofs being algebraic (they interpret the entries of the g -vector as the dimensions of the cohomology groups of certain varieties). The same result for spheres is open.
- The g -vector of the boundary of a $(d+1)$ -simplex has $g_0 = 1, g_{d+2} = -1$ and no other non-zero entry.

Because of the first two properties most authors define the g -vector of a simplicial sphere as having only the first half of the entries; that is, $g = (g_0, \dots, g_{\lfloor(d+2)/2\rfloor})$ (see, e.g., [339]): the second half is just the negative of the first half, in reverse order, and the first half is more interesting since it is non-negative. But we follow Peter McMullen's convention (the inventor of the g -theorem) of writing it in full. See, e.g., [230, 231].

The third property, together with Corollary 9.5.19, has the following interesting consequence: the g -vector basically counts the number of flips needed to get a given triangulation of the sphere from one that is combinatorially the boundary of a simplex:

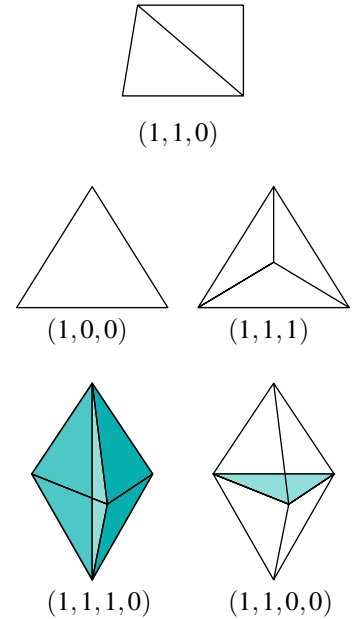


Figure 9.92: h -vectors of triangulations of circuits are always of the form $(1, \dots, 1, 0, \dots, 0)$, with a 1 for each facet.

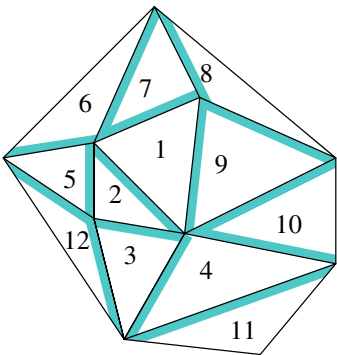


Figure 9.93: A 2-dimensional ball with h -vector $(1, 7, 4, 0)$ (a shelling of it is indicated). Its boundary is a hexagon, with h -vector $(1, 4, 1)$ and g -vector $(1, 3, -3, -1)$. As predicted by Theorem 9.5.21 we have:

$$(1, 3, -3, -1) = (1, 7, 4, 0) - (0, 4, 7, 1).$$

Corollary 9.5.20. Let \mathcal{T} be a triangulation of a totally cyclic vector configuration \mathbf{V} of dimension d . Let $\mathcal{T}_0, \mathcal{T}_1, \dots, \mathcal{T}_s$ be a sequence of triangulations of \mathbf{V} , such that:

1. \mathcal{T}_0 is isomorphic to the boundary of a $(d+1)$ -simplex and $\mathcal{T}_s = \mathcal{T}$.
2. Each \mathcal{T}_k obtained from the previous one by a flip in a non-degenerate circuit Z_k .

Then, $g_0(\mathcal{T}) = -g_{d+2}(\mathcal{T}) = 1$ and for every $i \in \{1, \dots, d+1\}$, $g_i(\mathcal{T})$ equals the number of circuits of type $(i, d+2-i)$ minus the number of circuits of type $(d+2-i, i)$ that have been used in the sequence.

A sequence of triangulations such as the one in the statement may look as an unusual thing, but actually the monotone sequences obtained via line shellings in Theorem 9.5.11 are of this type. After the very first facet F_1 in the shelling is introduced, the central subdivision of it that we get is combinatorially the boundary of the simplex $\text{conv}(F_1)!$

Another use of g -vectors is that they allow for a more compact statement of the McMullen-Walkup Theorem that we mentioned in Section 2.6.2. The reader can verify that the following is equivalent to Theorem 2.6.11:

Theorem 9.5.21 (McMullen and Walkup (1971)). *For any simplicial $(d+1)$ -ball \mathcal{K} we have:*

$$g(\partial \mathcal{K}) = h(\mathcal{K}) - \bar{h}(\mathcal{K}),$$

where $\bar{h}(\mathcal{K}) = (h_{d+1}, \dots, h_1, h_0)$ denotes the h -vector read backwards.

Observe that the sphere $\partial \mathcal{K}$ has one dimension less than the ball \mathcal{K} . This is compensated by the fact that g -vectors get an extra coordinate with respect to h -vectors. Let us show that shellings provide a nice proof of this theorem, at least for regular triangulations of polytopes:

Proof. We prove the theorem only for the case where \mathcal{K} is shellable. As we know, every time we add a facet to \mathcal{K} with index i , the i -th entry of the h -vector increases by one and the others remain the same. We also know what adding a simplex with index i to \mathcal{K} does to the boundary $\partial \mathcal{K}$: it amounts to a flip of type $(i, d+2-i)$, which increases $g_i(\partial \mathcal{K})$ and decreases $g_{d+2-i}(\partial \mathcal{K})$ by one and leaves the rest of the g -vector unchanged. \square

9.5.3 Polytopality via regular triangulations

In this last section we show that the theory of regular subdivisions is a useful tool to prove and study polytopality of a given abstract simplicial or polyhedral complex. For ease of exposition, we restrict our treatment to *simplicial* complexes although the main ideas work also for non-simplicial ones. We illustrate the method showing an explicit realization of the associahedron as an *alcoved polytope* for the root system of type A . That is to say, we show that the polar complex of the associahedron is a regular triangulation of the root system of type A .

Let \mathcal{K} be a pure simplicial complex of a certain dimension d . If \mathcal{K} is topologically a sphere you may have reasons to believe that it is the face complex of a simplicial polytope of dimension $d + 1$. Of course, it is not necessarily so, since there exist non-polytopal spheres (see [62, 272] for a discussion of polytopality of spheres and possible realizations of polytopes). But if your complex was obtained by some “natural” combinatorial procedure chances are that it will be polytopal and, more importantly, realizing it as a polytope may help you get insight into the problem from which you got your complex in the first place.

Remark 9.5.22. Non-polytopal spheres do not only exist; they are much more abundant than polytopal ones. For a fixed given dimension $d \geq 3$ and varying number of vertices n , the number of combinatorially different polytopal d -spheres with n -vertices is bounded above by $2^{\Omega(n \log(n))}$ while the number of non-polytopal ones is bounded below by $\Omega(2^{n^{\lfloor d/2 \rfloor}})$. These bounds were found respectively in [142] and [181] and are closely related to Theorems 8.4.2 and 8.4.3 of Section 8.4, on the number of regular and non-regular triangulations that a given configuration may have.

Example 9.5.23 (Barnette’s sphere). The smallest possible non-polytopal spheres happen in dimension 3 (Steinitz’s Theorem implies that every simplicial 2-sphere is polytopal) and with 8 vertices. An example is *Barnette’s sphere*, closely related to Schönhardt’s polyhedron and the mother of all examples. Its set of maximal facets is:

$$\begin{aligned} & 1245, 2356, 1346, \\ & 1237, 4567, 1247, 2457, 2357, 3567, 3167, 1647, \\ & 1238, 4568, 1258, 1458, 2368, 2568, 3148, 3648. \end{aligned}$$

See some hints on proving non-polytopality of this configuration in Exercise 9.15.

Saying that a pure simplicial complex \mathcal{K} of dimension d is polytopal is equivalent to saying that it is a regular triangulation of a certain totally cyclic configuration \mathbf{V} of rank $d + 1$. This simple reformulation of Lemma 9.5.1 allows to break polytopality proofs into two steps:

1. Find a vector configuration \mathbf{V} on which \mathcal{K} is a triangulation, and:
2. Prove that the triangulation \mathcal{K} of \mathbf{V} is regular.

In the first step the most difficult part is to *guess* the right configuration \mathbf{V} to embed your complex. In principle there is nothing we can say about it except that you should try vector configurations that seem natural, taking into account where your complex came from. Of course, one can consider the $n \times (d + 1)$ entries in a matrix representing \mathbf{V} as unknowns; if we already know that \mathcal{K} is a d -sphere then being a triangulation of \mathbf{V} is equivalent to saying that the chirotope of \mathbf{V} has the same sign on every facet of \mathcal{K} . But this is not our point here. What we want to stress is that once you have the right configuration \mathbf{V} the rest of the politopality proof gets simplified by breaking it into these two steps: one more combinatorial and one more geometric.

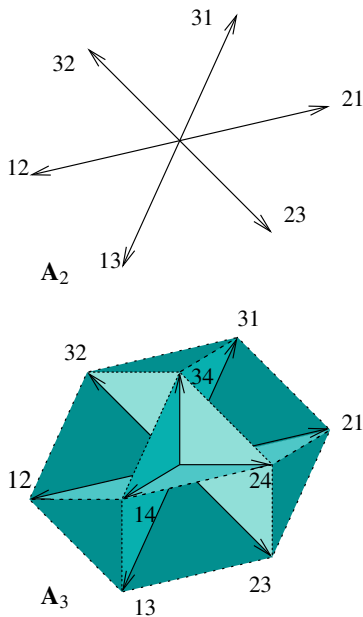


Figure 9.94: The root systems A_2 and A_3 . In the latter the vectors labeled 41 , 42 and 43 are not visible. Observe that $\mathbf{a}_{ij} = -\mathbf{a}_{ji}$ and that $\mathbf{a}_{ij} + \mathbf{a}_{jk} = \mathbf{a}_{ik}$.

The associahedron as a regular triangulation of a root system

We started this book speaking about the associahedron (Section 1.1) and we are going to finish it in the same way. In its usual setting, the associahedron is a simple polytope. In order to profit from what we know about triangulations, what we construct is its polar; put differently, we realize its normal fan as a triangulation of a vector configuration. The vector configuration in question is a root system of type A and the construction shows that the associahedron is an *alcoved polytope* in the sense Lam and Postnikov [199] (see Section 1.48).

Let us start by precisely introducing the key elements:

Definition 9.5.24. For each pair of numbers $i \neq j$ in $\{1, \dots, n\}$ we denote \mathbf{a}_{ij} the vector $\mathbf{e}_i - \mathbf{e}_j$, where $\{\mathbf{e}_1, \dots, \mathbf{e}_n\}$ is the standard basis in \mathbb{R}^n .

The *root system of type A* and rank $n-1$ is the vector configuration \mathbf{A}_{n-1} of these $n(n-1)$ vectors. The *positive roots* are the subconfiguration \mathbf{A}_{n-1}^+ consisting of the $\binom{n}{2}$ vectors \mathbf{a}_{ij} with $i < j$.

Both the whole root system and the positive root system are configurations of rank $n-1$, since they span the linear hyperplane $\sum x_i = 0$ in \mathbb{R}^n . \mathbf{A}_{n-1} is totally cyclic (and centrally symmetric) while \mathbf{A}_{n-1}^+ is acyclic: it consists of the elements where the functional $\phi(x_1, \dots, x_n) = -\sum ix_i$ is positive. \mathbf{A}_{n-1}^+ is not homogeneous but, being acyclic, we can think of it as if it was a point configuration of dimension $n-2$.

We use the following notation for their natural sets of labels:

$$J_{n-1} := \{ij : 1 \leq i, j \leq n, i \neq j\}, \quad J_{n-1}^+ := \{ij : 1 \leq i < j \leq n\}.$$

It is obvious that each root system is a subconfiguration of the next one:

$$\cdots \subset \mathbf{A}_{n-1} \subset \mathbf{A}_n \subset \cdots, \quad \cdots \subset \mathbf{A}_{n-1}^+ \subset \mathbf{A}_n^+ \subset \cdots.$$

But we are here more interested in the following natural projection:

Lemma 9.5.25. *The following map of labels induces a vector isomorphism of $\mathbf{A}_{n-1}^+/\{1n\}$ to a subconfiguration of \mathbf{A}_{n-2} :*

$$\begin{aligned} J_{n-1}^+ &\rightarrow J_{n-2} \\ ij &\mapsto \begin{cases} ij, & \text{if } j \neq n \\ il, & \text{if } j = n \end{cases} \end{aligned}$$

Proof. The following matrix sends $\mathbf{a}_{1n} \mapsto 0$, $\mathbf{a}_{in} \mapsto \mathbf{a}_{i1}$, and $\mathbf{a}_{ij} \mapsto \mathbf{a}_{ij}$ if $i, j < n$:

$$\begin{pmatrix} \frac{1}{2} & -\frac{1}{2} & \cdots & -\frac{1}{2} & \frac{1}{2} \\ 0 & 1 & \cdots & 0 & 0 \\ \vdots & \vdots & \ddots & \vdots & \vdots \\ 0 & 0 & \cdots & 1 & 0 \end{pmatrix}.$$

□

How can we relate the associahedron to the root system of type A ? One way is to describe each triangulation of a polygon by its edges rather than its triangles. Each edge joins two vertices of the polygon, say, the ones labeled i and j , so we can associate a positive \mathbf{a}_{ij} root to it. This allows us to think of each triangulation of the polygon as a subset of positive roots. But to save one dimension in the root system we label the possible interior edges not by the vertices they join but by the first and last boundary edges they cover. More precisely:

- Let \mathbf{C}_{n+1} denote a convex $(n+1)$ -gon. Mark one of its boundary edges as a reference edge, and label the other n edges with the numbers 1 to n , in their boundary order.
- We label the interior diagonals with J_{n-1}^+ using ij to label the diagonal covering the boundary edges i to j . Observe that we even get a label $1n$ for the reference edge. We do not need labels for the other boundary edges.

See Figure 9.95 for the case $n = 5$, where the reference edge appears as the only upper envelope edge. The “reference edge” idea appeared already in Section 1.1, to prove the bijection between triangulations of the polygon and binary trees (Theorem 1.1.3). The particular way of drawing polygons with a unique upper edge was also used in Section 6.1.

Try not to get confused by our use of the index $n+1$, $n-1$, etc. For the root system, we use the canonical convention that A_{n-1} denotes a system of rank $n-1$ (which, for us, means dimension $n-2$). The labels i and j of its elements go from 1 to n , so they correspond to labelling the diagonals of an $(n+1)$ -gon. That is why the diagonals of an $(n+1)$ -gon label the elements of the configuration A_{n-1}^+ .

We now introduce the simplicial complex we want to realize.

Definition 9.5.26. To each triangulation \mathcal{T} of the $(n+1)$ -gon we associate the susbet of J_{n-1}^+ consisting of the diagonals used by it. We call *associahedral complex*, and denote it \mathcal{K}_{n-1} , the simplicial complex whose facets are the subsets of J_{n-1} so obtained. We call *extended associahedral complex* the complex $\mathcal{K}_{n-1} := \mathcal{K}_{n-1} * \{1n\}$.

Example 9.5.27 (The associahedral complex of a pentagon). As seen in Figure 9.96, the five triangulations of a pentagon make \mathcal{K}_3 consist of five edges $\{12, 13\}, \{12, 34\}, \{13, 23\}, \{23, 24\}, \{24, 34\}$ so it is a cycle of length five. The extended complex consists of five triangles, obtained joining the cycle to a sixth vertex labeled 14.

We are now ready to state the main result we want to prove in this section:

Theorem 9.5.28. 1. The extended associahedral complex $\overline{\mathcal{K}_{n-1}}$ is a regular triangulation of the positive root system A_{n-1}^+ .

2. The associahedral complex \mathcal{K}_{n-1} is, under the inclusion $\mathbf{A}_{n-2} \subset A_{n-1}^+/1n$ mentioned in Lemma 9.5.25, a regular triangulation of the root system \mathbf{A}_{n-2} .

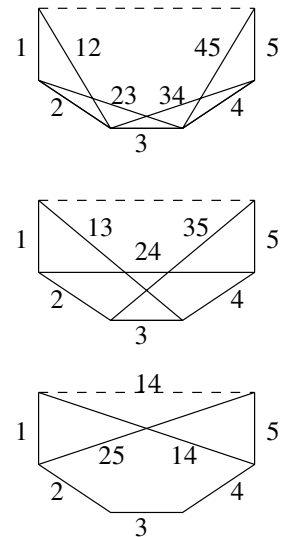


Figure 9.95: Labelling of the nine interior diagonals of a hexagon.

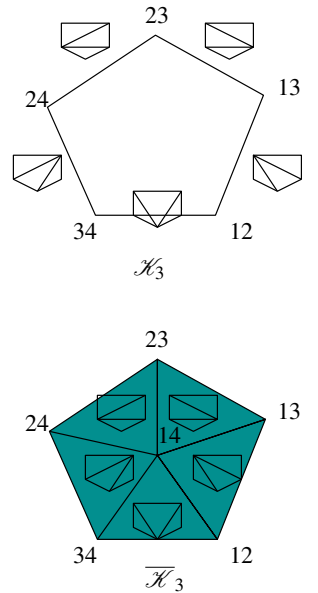


Figure 9.96: The non-extended (top) and extended (bottom) associahedral complexes \mathcal{K}_3 and $\mathcal{K}_3 * \{14\}$.

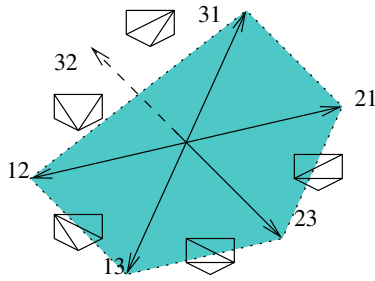


Figure 9.97: The extended associahedral complex $\overline{\mathcal{K}_3}$ as a triangulation of the positive root system A_2 .

Observe that in Part 2 the triangulation in question does not use all the elements of A_{n-2} , since the inclusion is not surjective. See Figure 9.97 for an example.

The second statement follows from the first one and Lemma 9.5.25, since $\text{link}_{\mathcal{T}}(i)$ is a regular triangulation of A/i for every regular triangulation \mathcal{T} of A . So, we only need to prove Part 1. For this we first prove that $\overline{\mathcal{K}_{n-1}}$ is a triangulation and then that it is regular.

Lemma 9.5.29. $\overline{\mathcal{K}_{n-1}}$ is a triangulation of the positive root system A_{n-1}^+ .

Proof. According to Corollary 4.5.20, to prove that $\overline{\mathcal{K}_{n-1}}$ is a triangulation of A_{n-1}^+ it suffices to check the following two properties (ICoP) and (SFP).

(ICoP) There are exactly two full-dimensional simplices $F \cup s$ and $F \cup s'$ in $\overline{\mathcal{K}_{n-1}}$ containing every codimension-one simplex (ridge) F in $\overline{\mathcal{K}_{n-1}}$ not contained in a facet of $\text{conv } A_{n-1}^+$. Moreover, they lie on opposite sides of the hyperplane spanned by F (Intersection Co-circuit Property).

(SFP) There is a codimension-one simplex F in $\overline{\mathcal{K}_{n-1}}$ that is a facet of A_{n-1}^+ and contained in a unique full-dimensional simplex of $\overline{\mathcal{K}_{n-1}}$ (Simplicial Facet Property).

We start with (ICoP), for which we show that:

- If a ridge F does not contain the element $1n$ then it lies in a facet of $\text{conv } A_{n-1}^+$. In this case, F “is” a triangulation of C_{n+1} in which we have removed the reference edge $1n$. We look at the third vertex v of the triangle containing the reference edge, which separates two boundary edges j and $j+1$, for some $j \in \{1, \dots, n-1\}$. Then, F is contained in the facet of $\text{conv } A_{n-1}^+$ defined by the inequality

$$\sum_{i=1}^j x_i - \sum_{i=j+1}^n x_i \geq 0.$$

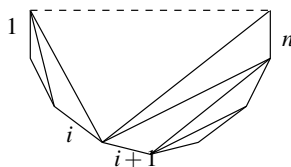


Figure 9.98: A ridge F in $\overline{\mathcal{K}_{n-1}}$ not containing $1n$ is a triangulation of C_{n+1} considered without its reference edge. It is divided in two by a vertex v , which we use to show that F lies in a facet of $\text{conv } A_{n-1}^+$.

Indeed, this functional vanishes on all diagonals not covering v (which is the case for those in F) and it equals 2 on the diagonals covering v . See Figure 9.98.

- If a ridge F contains $1n$ then it is contained in two full-dimensional simplices of $\overline{\mathcal{K}_{n-1}}$, and these two lie in opposite sides of F .

Now F is obtained by removing an interior edge from a triangulation. The first part of (ICoP) is then obvious: there are exactly two ways in which a diagonal can be inserted back: the diagonal we removed, and the one obtained by a flip. The rest of (ICoP) is stating that

The two simplices T_1 and T_2 of $\overline{\mathcal{K}_{n-1}}$ corresponding to two triangulations that differ by a flip lie, when realized on A_{n-1}^+ , on opposite sides of their common facet F .

Proving this can be done via the unique circuit contained in the union of T_1 and T_2 . The simplices lie on opposite sides of F if and only if the elements s and s' not in the F are on the same side of the circuit. Figure 9.100 shows the six diagonals of the n -gon involved in the flip. Four of them alone give us the desired circuit. Namely:

$$\mathbf{a}_{i+1,k} + \mathbf{a}_{j+1,l} = \mathbf{a}_{i+1,l} + \mathbf{a}_{j+1,k}.$$

Observe that the bottom edge $\mathbf{a}_{j+1,k}$ might not be a diagonal but a boundary edge of the polygon, if $k = j + 1$. In this case the circuit becomes $\mathbf{a}_{i+1,k} + \mathbf{a}_{k,l} = \mathbf{a}_{i+1,l}$.

For (SFP), we consider the facet of \mathbf{A}_{n-1}^+ defined by the inequality

$$x_1 - \sum_{i=2}^n x_i \leq 2.$$

This inequality is tight exactly on the elements \mathbf{a}_{1i} . Since the diagonals $\{1i : i = 1, \dots, n-1\}$ form a triangulation of \mathbf{C}_{n+1} and are clearly independent as elements of \mathbf{A}_{n-1}^+ , the property is fulfilled. \square

Lemma 9.5.30. $\overline{\mathcal{K}_{n-1}}$ is the regular triangulation of \mathbf{A}_{n-1}^+ induced by the height vector $(\omega_{ij})_{1 \leq i < j \leq n}$ defined as

$$\omega_{ij} = -(i-j)^2.$$

Proof. Once we know that $\overline{\mathcal{K}_{n-1}}$ is a triangulation, to prove regularity we simply need to check that every pair of adjacent full-dimensional simplices are lifted “convex” by ω . As before, such a pair of simplices corresponds to two triangulations that differ by a flip, for which we recall that the circuit contained in them is

$$\mathbf{a}_{i+1,k} + \mathbf{a}_{j+1,l} = \mathbf{a}_{i+1,l} + \mathbf{a}_{j+1,k},$$

where, if $i < j < k < l$, $\{\mathbf{a}_{i+1,k}, \mathbf{a}_{j+1,l}\}$ are the “positive part” of the circuit, that is, the one not contained in the common facet. Saying that ω lifts this particular ridge convex is the same as saying that

$$\omega_{i+1,k} + \omega_{j+1,l} > \omega_{i+1,l} + \omega_{j+1,k}, \quad \forall i < j < k < l, \quad (9.57)$$

$$\omega_{i+1,k} + \omega_{k,l} > \omega_{i+1,l} \quad \forall i < k < l. \quad (9.58)$$

(The second equation is there for the degenerate case when $j+1 = k$). If we let $a = j-i$, $b = k-j-1$, and $c = l-k$, so that $l-i-1 = a+b+c$, $l-j-1 = c+b$ and $k-i-1 = b+c$, we have:

$$\begin{aligned} \omega_{i+1,k} + \omega_{j+1,l} &= -(b+c)^2 - (a+b)^2 \\ &> -(a+b+c)^2 - b^2 = \omega_{i+1,l} + \omega_{j+1,k}. \end{aligned}$$

Observe that since \mathbf{A}_{n-1}^+ is acyclic, we are allowed to use negative heights for our lifts. If you, however, prefer positive ones, change the definition of ω to $\omega_{ij} = n^2 - (i-j)^2$, for example. \square

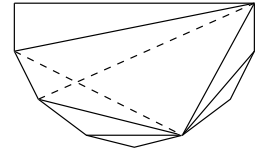


Figure 9.99: A ridge F in $\overline{\mathcal{K}_{n-1}}$ containing $1n$ is a triangulation of \mathbf{C}_{n+1} without an edge. It is contained in exactly two full-dimensional simplices T_1 and T_2 , corresponding to triangulations joined by diagonal flip.

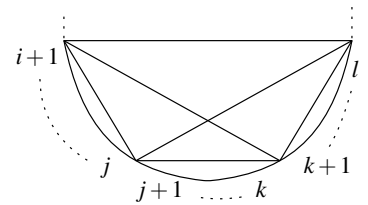


Figure 9.100: The six diagonals involved in a flip between triangulations of \mathbf{C}_{n+1} .

Remark 9.5.31. From the proof of Lemma 9.5.30 it follows that in fact we can choose different values of the heights ω_{ij} . The only conditions we need them to satisfy are equations (9.57) and (9.58).

We finish with the explicit statement of how the associahedron is an alcoved polytope. For this we need to take Theorem 9.5.6 into account. Remember that in that theorem the heights ω_i chosen for a regular triangulation of a vector configuration were the same as the right hand sides for the facet-defining inequalities of the polar polytope. We need to translate equations (9.57) and (9.58) that produce heights giving $\overline{\mathcal{K}_{n-1}}$ as a regular triangulation of \mathbf{A}_{n-1}^+ into conditions for heights giving $\mathcal{K}_{n-1} = \text{link}_{\overline{\mathcal{K}_{n-1}}}(1n)$ as a regular triangulation of \mathbf{A}_{n-2} . Lemmas 4.2.20 and 4.2.24 solve the problem: the same heights work, as long as we take $\omega_{1n} = 0$. Hence:

Corollary 9.5.32. *Let $(\omega_{ij})_{1 \leq i < j \leq n}$ be real numbers satisfying equations (9.57) and (9.58) and with $\omega_{1n} = 0$. Then, the following system of inequalities defines a $(n-2)$ -dimensional simple polytope in \mathbb{R}^{n-2} combinatorially isomorphic to the associahedron:*

$$\begin{aligned} \langle \mathbf{a}_{ij}, \mathbf{x} \rangle &\leq \omega_{ij}, & \forall 1 < i < j < n, \\ -\omega_{in} &\leq \langle \mathbf{a}_{1i}, \mathbf{x} \rangle \leq \omega_{1i}, & \forall 1 < i < n, \end{aligned}$$

Example 9.5.33. If we let $n = 4$, the system of inequalities we need for our heights (already taking $\omega_{14} = 0$) is

$$\begin{aligned} \omega_{12} + \omega_{24} &> 0, \\ \omega_{13} + \omega_{34} &> 0, \\ \omega_{12} + \omega_{23} &> \omega_{23}, \\ \omega_{23} + \omega_{34} &> \omega_{24}, \\ \omega_{13} + \omega_{24} &> \omega_{23}. \end{aligned}$$

A simple solution is to take the five heights equal to 1. This gives as our associahedron precisely the polar of the shaded region of Figure 9.97.

The associahedral *complex* was first constructed by Stasheff in 1963 [309] in the context of homotopy theory. The associahedron as a polytope was first realized by Haiman (unpublished, 1984), then by Lee in 1989 [205]. The first construction of it related to the root system of type A is probably in [136], where Gelfand et al. prove Part 1 of Theorem 9.5.28 and derive from it that the volume of the convex hull of the positive root system \mathbf{A}_n^+ is the *Catalan number* $C_n = \frac{1}{n+1} \binom{2n}{n}$. Fomin and Zelevinsky [126] have later introduced an “associahedral complex” for every root system of any type and, together with Chapoton, [76] they proved it to be polytopal. Another generalization was introduced by Carr and Devadoss in 2006 [72]. They construct a *graph associahedron* by considering connected subgraphs of any given graph G , and retrieve the standard associahedron for the case of a path. A different, simple construction of the associahedron was given by

Loday [217] and generalized by Hohlweg and Lange [164]. Ultimately, all these associahedra and their generalizations fit into the theory of *generalized permutohedra* introduced by Postnikov [258].

Exercises

Exercise 9.1. Compute explicitly the fiber polytope of an octahedron projected to a hexagon. Use either the Minkowski sum of finitely many fibers or use the method outlined from Lemma 9.1.16 where one first computes the secondary polytope of a hexagon and then projects.

Exercise 9.2. Construct a 3-dimensional “screw-like” polytope, i.e., a 3-dimensional polytope such that some of its ψ -monotone paths are not coherent (see Lemma 9.1.3).

Exercise 9.3. For a point configuration \mathbf{A} we call *Baues complex* of \mathbf{A} the order complex of the poset of proper subdivisions of \mathbf{A} (by proper we mean that the trivial subdivision is excluded). Prove:

1. If the graph of triangulations of \mathbf{A} is connected, then the Baues complex of \mathbf{A} is connected.
2. If \mathbf{A} is in general position and its graph of triangulations is not connected, then the Baues complex of either \mathbf{A} or a subconfiguration of it is not connected.

Exercise 9.4. Show That Figure 9.101 represents nonregular subdivision of $\mathbf{D}_3 \times \mathbf{D}_6$.

Exercise 9.5. Show how Figure 9.102 represents a coarsest nonregular subdivision of $\mathbf{D}_3 \times \mathbf{D}_7$.

Exercise 9.6. Consider the Cayley embedding \mathbf{P} of a rectangle \mathbf{abcd} and a 90-degree-rotated copy $\mathbf{a'b'c'd'}$ of it. Show by using the Cayley trick that there is a triangulation of \mathbf{P} without new vertices using the cyclic set of diagonals $\{\mathbf{aa'}, \mathbf{bb'}, \mathbf{cc'}, \mathbf{dd'}\}$ if and only if the rectangle is not a square (compare [266]).

Exercise 9.7. List all the combinatorially different fine mixed subdivisions of the Minkowski sum of two equal squares. There are nine of them. Taking into account that the Cayley trick makes these objects correspond to triangulations of the 3-cube, why are there only six combinatorially different triangulations of the latter?

Exercise 9.8. Find a formula for the number of all the unimodular triangulations of a $2 \times n$ grid.

Exercise 9.9. For a simplex \mathbf{S} with vertices $\mathbf{a}_0, \dots, \mathbf{a}_d$, consider the cone of all nonnegative integer combinations of $(\mathbf{a}_0, 1), \dots, (\mathbf{a}_d, 1)$ and the parallelepiped $\Pi = \{\mathbf{x} : \lambda_1(\mathbf{a}_1, 1) + \lambda_2(\mathbf{a}_2, 1) + \dots + \lambda_d(\mathbf{a}_d, 1) \text{ with } 0 \leq \lambda_i < 1\}$ (half-open). Prove that the Ehrhart function of the σ is equal to $i_\sigma(n) = \sum_{i=0}^d \delta_i \binom{n-i+d}{d}$, where δ_i is the number of lattice points in Π at level i .

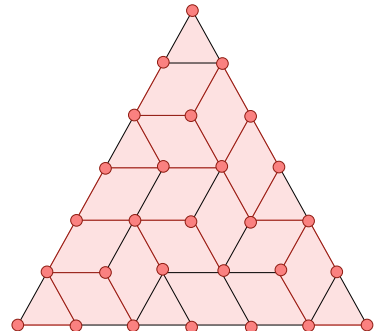


Figure 9.101: A non-coherent mixed subdivision of $6 \cdot \mathbf{D}_3$.

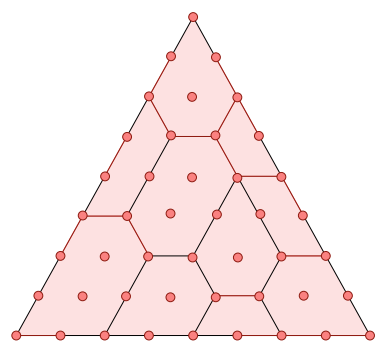


Figure 9.102: A coarsest non-regular subdivision of $\mathbf{D}_3 \times \mathbf{D}_7$.

Exercise 9.10. Consider the lattice-free simplices $\Delta_{p,q}$ in dimension three, classified in Theorem 9.3.12.

1. Find explicitly an unimodular transformation that sends $\Delta_{p,q}$ to $\Delta_{p',q}$, assuming that $p' = \pm p^{\pm 1} \pmod{q}$.
2. Show that the group of unimodular symmetries (lattice transformations) that send $\Delta_{p,q}$ to itself has the following order. (Hint, look at Figure 9.68):
 - Twenty four, if $q \leq 2$.
 - Eight, if $p = \pm 1 \pmod{q}$ and $q \geq 3$.
 - Either four or two, otherwise. You can even try to show that the case of order four arises if and only if $p^2 = \pm 1 \pmod{q}$.

Exercise 9.11. Let Δ be a lattice unimodular simplex. Consider the lattice regular subdivision of $k\Delta$ obtained assigning to each lattice point \mathbf{p} the height:

$$\omega_{\mathbf{p}} = \sum_{\mathbf{F} \text{ a facet of } \Delta} -\text{dist}(\mathbf{F}, \mathbf{p})^2.$$

Prove that this subdivision coincides with the subdivision obtained cutting $k\Delta$ with all the lattice translations of the facets.

Exercise 9.12. (Open) Prove that all matroid polytopes have a unimodular regular triangulation. This would be implied by a proof of N. White's open conjecture that the toric ideal of a matroid polytope has a quadratic square-free Gröbner bases [333]. See also [56] and references therein.

Exercise 9.13. Prove that a Gröbner basis of an ideal I is always a generating set for I .

Exercise 9.14. 1. Finish the proof of Lemma 9.5.13.

2. Prove that the inverse relation, giving the h -vector from the f -vector, is the one in Lemma 9.5.14.

Exercise 9.15. Show that Barnette's sphere, described in Remark 9.5.22, is indeed a 4-sphere and that it is not polytopal. Use the following ideas:

1. To show that it is sphere, start with the boundary complex \mathcal{L} of a triangular prism with facets 123, 456, 1245, 2356, 1346, and consider the *suspension* of it on two new elements 7 and 8. This suspension is the join with the complex consisting of two isolated vertices $\{7, 8\}$, so it has two facets $F * 7$ and $F * 8$ for each facet F of \mathcal{L} , so it consists of four tetrahedra and six square pyramids, namely:

- The tetrahedra 1237, 4567, 1238, 4568, and
- The square pyramids with apices at 7 and 8 and bases at the quadrilaterals 1254, 1364 and 2365 (vertices of each quadrilateral are given on order).

Each pair of pyramids with the same base, if glued together, form a solid octahedron. Show that Barnette's sphere is obtained by a simple topological re-triangulation of each of these three octahedra into five tetrahedra.

2. If the Barnette sphere was polytopal, then it would be a regular triangulation \mathcal{T} of a certain (totally cyclic) rank 4 vector configuration \mathbf{V} . By Lemma 4.2.17, we could delete elements 7 and 8 and have the rest of the complex $\mathcal{T} \setminus \{7, 8\}$ be extendable to a regular triangulation of the deleted configuration $\mathbf{V} \setminus \{7, 8\}$. That is: there would be a rank 4 configuration $\mathbf{V} \setminus \{7, 8\}$ and a regular triangulation of it containing the tetrahedra 1245, 1346, 2356 and the triangles 123, 456. Note that $\mathbf{V} \setminus \{7, 8\}$ may or may not be acyclic.
3. Show that such a configuration and regular triangulation cannot exist. You can do show with arguments similar to those proving that Schönhardt's polyhedron is not triangulable (cf. Example 3.6.1) or using Gale transforms: observe that $\text{Gale}(\mathbf{V} \setminus \{7, 8\})$ should have rank 2.

Bibliography

- [1] P. K. Agarwal, J. Basch, L. J. Guibas, J. Hershberger, and L. Zhang. Deformable free-space tilings for kinetic collision detection. *The International Journal of Robotics Research*, 21:179–197, 2002.
- [2] O. Aichholzer. The path of a triangulation. In *Proceedings 15th Ann. ACM Symposium of Computational Geometry, Miami Beach, Florida USA*, pages 14–23, 1999.
- [3] O. Aichholzer, L.S Alboul, and F. Hurtado. On flips in polyhedral surfaces. *Internat. J. Found. Comput. Sci.*, 13(2):303–311, 2002.
- [4] O. Aichholzer, A. Aurenhammer, Hurtado F., and H. Krasser. Towards compatible triangulations. *Theoretical Computer Science*, 296(1):3 – 13, 2003.
- [5] O. Aichholzer, F. Aurenhammer, S-W. Cheng, N. Katoh, G. Rote, M. Taschwer, and Y-F. Xu. Triangulations intersect nicely. *Discrete Comput. Geom.*, 16:339–359, 1996.
- [6] O. Aichholzer, F. Aurenhammer, and R. Hainz. New results on MWT subgraphs. *Inform. Process. Lett.*, 69:215–219, 1999.
- [7] O. Aichholzer, F. Aurenhammer, H. Krasser, and P. Brass. Pseudotriangulations from surfaces and a novel type of edge flip. *SIAM J. Comput.*, 32(6):1621–1653 (electronic), 2003.
- [8] O. Aichholzer, T. Hackl, C. Huemer, F. Hurtado, H. Krasser, and B. Vogtenhuber. On the number of plane graphs. In *Proceedings of the ACM-SIAM Symp. on Discrete Algorithms, SODA’06*, 2006.
- [9] O. Aichholzer, F. Hurtado, and M. Noy. A lower bound on the number of triangulations of planar point sets. *Comput. Geom.: Theory and Applications*, 29:135–145, 2004.
- [10] O. Aichholzer and H. Krasser. The point-set order-type database: A collection of applications and results. In *Proceedings of 13th Canadian Conference on Computational Geometry, Waterloo, Ontario, Canada*, pages 13–16, 2001.
- [11] M. Aigner and G. M. Ziegler. *Proofs from the BOOK*. Springer Verlag, Berlin, 1998.
- [12] M. Ajtai, V. Chvátal, M. Newborn, and E. Szemerédi. Crossing-free subgraphs. *Annals of Discrete Math.*, 12:9–12, 1982.
- [13] E. Anagnostou and D. Corneil. Polynomial-time instances of the minimum weight triangulation problem. *Comput. Geom.*, 3:247–259, 1993.
- [14] E. E. Anclin. An upper bound for the number of planar lattice triangulations. *J. Comb. Theory, Ser. A*, 103(2):383–386, 2003.
- [15] F. Ardila and S. Billey. Flag arrangements and triangulations of products of simplices. *Adv. Math.*, 214(2):495–524, 2007.
- [16] F. Ardila and M. Develin. Tropical hyperplane arrangements and oriented matroids. *Mathematische Zeitschrift*, 262:795–816, 2009.

- [17] E. M. Arkin, M. Held, J. S. B. Mitchell, and S. Skiena. Hamilton triangulations for fast rendering. In *ESA '94: Proceedings of the Second Annual European Symposium on Algorithms*, pages 36–47, London, UK, 1994. Springer-Verlag.
- [18] B. Aronov and S. Fortune. Approximating minimum-weight triangulations in three dimensions. *Discrete Comput. Geom.*, 21:527–549, 1999.
- [19] C. Athanasiadis, J. Rambau, and F. Santos. The Generalized Baues Problem for cyclic polytopes II. *Publications De l'Institut Mathématique, Belgrade*, 66:3–15, 1999.
- [20] F. Aurenhammer. Voronoi diagrams – a survey of a fundamental geometric data structure. *ACM Comput. Surv.*, 23:345–405, 1991.
- [21] F. Aurenhammer and R. Klein. Voronoi diagrams. In J.-R. Sack and J. Urrutia, editors, *Handbook Computational Geometry*, pages 201–290. North-Holland, New York, 2000.
- [22] D. Avis and H. ElGindy. Triangulating point sets in space. *Discrete Comput. Geom.*, 2:99–111, 1987.
- [23] D. Avis and K. Fukuda. A pivoting algorithm for convex hulls and vertex enumeration of arrangements and polyhedra. *Discrete Comput. Geom.*, 8:295–313, 1992.
- [24] D. Avis and K. Fukuda. Reverse-search for enumeration. *Discrete Applied Mathematics*, 65:21–46, 1996.
- [25] M. Azaola and F. Santos. The graph of triangulations of a point configuration with $d + 4$ vertices is 3-connected. *Discrete Comput. Geom.*, 23(4):489–536, 2000.
- [26] M. Azaola and F. Santos. The number of triangulations of the cyclic polytope $C(n, n - 4)$. *Discrete Comput. Geom.*, 27(1):29–48, 2002.
- [27] E. K. Babson and L. J. Billera. The geometry of products of minors. *Discrete Comput. Geom.*, 20(2):231–249, 1998.
- [28] K. Ball. Volumes of sections of cubes and related problems. In *Geometric aspects of functional analysis (1987–88)*, volume 1376 of *Lecture Notes in Math.*, pages 251–260. Springer, Berlin, 1989.
- [29] H.-J. Bandelt and A. W. M. Dress. A canonical decomposition theory for metrics on a finite set. *Adv. Math.*, 92(1):47–105, 1992.
- [30] I. Bárány and J. M. Kantor. On the number of lattice free polytopes. *European J. Combin.*, 21(1):103–110, 2000.
- [31] M. Barile, D. Bernardi, A. Borisov, and J. M. Kantor. On empty lattice simplices in dimension 4. Preprint, arXiv.org, 2009.
- [32] D. Barnette. Diagrams and Schlegel diagrams. In *Combinatorial Structures and their Applications (Proc. Calgary Internat. Conf., Calgary, Alta)*, pages 1–4. Gordon and Breach, New York, 1970.
- [33] V. Batyrev and B. Nill. Multiples of lattice polytopes without interior lattice points. *Mosc. Math. J.*, 7(2):195–207, 349, 2007.
- [34] H. J. Baues. Geometry of loop spaces and the cobar construction. *Memoirs of the American Mathematical Society*, 25:1–171, 1980.

- [35] D. Bayer and I. Morrison. Standard bases and geometric invariant theory. I. Initial ideals and state polytopes. *J. Symbolic Comput.*, 6(2-3):209–217, 1988.
- [36] M. M. Bayer. Equidecomposable and weakly neighborly polytopes. *Israel J. Math.*, 81(3):301–320, 1993.
- [37] M. M. Bayer and B Sturmfels. Lawrence polytopes. *Canad. J. Math.*, 42(1):62–79, 1990.
- [38] M. Beck and D. Pixton. The Ehrhart polynomial of the Birkhoff polytope. *Discrete Comput. Geom.*, 30(4):623–637, 2003.
- [39] M. Beck and S. Robins. *Computing the continuous discretely: Integer-point enumeration in polyhedra*. Undergraduate Texts in Mathematics. Springer, New York, 2007.
- [40] R. Beirouti and J. Snoeyink. Implementations of the LMT heuristic for minimum weight triangulations. In *Proceedings of the 14th ACM symp. Comput. Geom.*, pages 96–105. ACM, 1998.
- [41] P. Belleville, M. Keil, M. McAllister, and J. Snoeyink. On computing edges that are in all minimum weight triangulations. In *Proceedings 12th Annual ACM symposium on computational geometry*, pages V7–V8, 1996.
- [42] A. Below, U. Brehm, J. A. De Loera, and J. Richter-Gebert. Minimal simplicial dissections and triangulations of convex 3-polytopes. *Discrete Comput. Geom.*, 21:131–142, 2000.
- [43] A. Below, J. A. De Loera, and J. Richter-Gebert. Finding minimal triangulations of convex 3-polytopes is NP-hard. In *Proceedings of the eleventh annual ACM-SIAM symposium on Discrete algorithms 2000, San Francisco, California, USA*, 2000.
- [44] A. Below, J. A. De Loera, and J. Richter-Gebert. The complexity of finding small triangulations of convex 3-polytopes. *Journal of Algorithms*, 50:134–167, 2004.
- [45] M. Bern and D. Eppstein. Mesh generation and optimal triangulations. In D. Z. Du and F. K. Hwang, editors, *Computing in Euclidean Geometry*. World Scientific Publishing Co., 1992.
- [46] D. N. Bernstein. The number of roots of a system of equations. *Funct. Anal. Appl.*, 9:1–4, 1975.
- [47] F. Bigdeli. *Triangulating General Convex d-Polytopes Based on the Notion of the Gale Transform*. PhD thesis, University of Kentucky, 1991.
- [48] L. J. Billera, P. Filliman, and B. Sturmfels. Constructions and complexity of secondary polytopes. *Adv. in Math.*, 83:155–179, 1990.
- [49] L. J. Billera, I. M. Gelfand, and B. Sturmfels. Duality and minors of secondary polyhedra. *J. of Comb. Theory Series B*, 57:258–268, 1993.
- [50] L. J. Billera, M. Kapranov, and B. Sturmfels. Cellular strings on polytopes. *Proceedings of the American Mathematical Society*, 122:549–555, 1994.
- [51] L. J. Billera and A. Sarangarajan. All 0-1 polytopes are traveling salesman polytopes. *Combinatorica*, 16(2):175–188, 1996.
- [52] L. J. Billera and A. Sarangarajan. The combinatorics of permutation polytopes. In *Formal power series and algebraic combinatorics (New Brunswick, NJ, 1994)*, volume 24 of *DIMACS Ser. Discrete Math. Theoret. Comput. Sci.*, pages 1–23. Amer. Math. Soc., Providence, RI, 1996.

- [53] L. J. Billera and B. Sturmfels. Fiber polytopes. *Ann. of Math*, 35:527–549, 1992.
- [54] A. Björner. Topological methods. In *Handbook of combinatorics, Vol. 1, 2*, pages 1819–1872. Elsevier, Amsterdam, 1995.
- [55] A. Björner, M. Las Vergnas, B. Sturmfels, N. White, and G. M. Ziegler. *Oriented Matroids*. Cambridge University Press, Cambridge, 1992.
- [56] J. Blasiak. The toric ideal of a graphic matroid is generated by quadratics. *Combinatorica*, 28(3):283–297, 2008.
- [57] A. Bliss and F. E. Su. Lower bounds for simplicial covers and triangulations of cubes. *Discrete Comput. Geom.*, 33:669 –686, 2005.
- [58] J. Bochnak, M. Coste, and M. F. Roy. *Géométrie Algébrique Réelle*, volume 12 of *Ergebnisse der Mathematik und ihrer Grenzgebiete*. Springer-Verlag, 1987.
- [59] J. Böhm. Some problems of triangulating polytopes in euclidean d -space. Technical report N-88-17, Friedrich Schiller Universität Jena, 1988.
- [60] J. Bohne. Eine kombinatorische Analyse zonotoper Raumaufteilungen. Preprint 92-041, Sonderforschungsbereich 343 “Diskrete Strukturen in der Mathematik”, 1992. Dissertation, Fachbereich Mathematik, Universität Bielefeld, 100 pp.
- [61] J. Bokowski. *Computational Oriented Matroids: equivalence classes of matrices within a natural framework*. Cambridge University Press, Cambridge, 2006.
- [62] J. Bokowski and B. Sturmfels. *Computational Synthetic Geometry*, volume 1355 of *Lecture Notes in Mathematics*. Springer, Heidelberg, 1989.
- [63] B. Bollobas. *Graph Theory*. Graduate texts in Mathematics. Springer-Verlag, 1980.
- [64] E. Bombieri and J. D. Vaaler. On Siegel’s lemma. *Invent. Math.*, 73(1):11–32, 1983.
- [65] P. Bose, L. Devroye, and W. Evans. Diamonds are not a minimum weight triangulation’s best friend. *International Journal of Computational Geometry and Applications*, 12:445–453, 2002.
- [66] G. Brightwell and P. Winkler. Counting linear extensions. *Order*, 8:225–242, 1992.
- [67] W. Bruns and J. Gubeladze. Normality and covering properties. *J. reine angew. Math.*, 510:161–178, 1999.
- [68] W. Bruns, J. Gubeladze, M. Henk, Martin A, and R. Weismantel. A counterexample to an integer analogue of Carathéodory’s theorem. *J. reine angew. Math.*, 510:179–185, 1999.
- [69] W. Bruns, J. Gubeladze, and N. V. Trung. Normal polytopes, triangulations, and Koszul algebras. *J. reine angew. Math.*, 485, 1997.
- [70] B. Büeler, A. Enge, and K. Fukuda. Exact volume computation for polytopes: a practical study. In *Polytopes – Combinatorics and Computation (Oberwolfach, 1997) 131–154, DMV Sem., 29, Birkhäuser, Basel*, ETH-Zürich, 2000.
- [71] E. R. Canfield and B. D. McKay. The asymptotic volume of the birkhoff polytope. *Online J. Anal. Comb.*, 4, 2009.

- [72] M. P. Carr and S. L. Devadoss. Coxeter complexes and graph-associahedra. *Topology Appl.*, 153(12):2155–2168, 2006.
- [73] C. Carvalho de Souza and A. Nunes. Integer programming models for minimum weight triangulations. In *Proceedings Int. Symp. on Math. Programming, Lausanne EPFL*, 1997.
- [74] C. S. Chan and D. P. Robbins. On the volume of the polytope of doubly stochastic matrices. *Experiment. Math.*, 8(3):291–300, 1999.
- [75] C. S. Chan, D. P. Robbins, and D. S. Yuen. On the volume of a certain polytope. *Experiment. Math.*, 9(1):91–99, 2000.
- [76] F. Chapoton, S. Fomin, and A. Zelevinsky. Polytopal realizations of generalized associahedra. *Canad. Math. Bull.*, 45(4):537–566, 2002.
- [77] F. Chavanon and É. Rémila. Rhombus tilings: decomposition and space structure. *Discrete Comput. Geom.*, 35(2):329–358, 2006.
- [78] B. Chazelle, H. Edelsbrunner, M. Grigni, and et al. Ray shooting in polygons using geodesic triangulations. *Algorithmica*, 12(1):54–68, 1994.
- [79] S.-W. Cheng and Y.-F. Xu. On β -skeleton as a subgraph of the minimum weight triangulation. *Theor. Comput. Sci.*, 262:459–471, 2001.
- [80] F. Y.L Chin, S. P. Y. Fung, and C. A. Wang. Approximation for minimum triangulations of simplicial convex 3-polytopes. *Disc. Comput. Geom.*, 26:499–511, 2001.
- [81] T. Christof and A. Löbel. PORTA – POlyhedron Representation Transformation Algorithm (version 1.4.1). <http://www.zib.de/Optimization/Software/Porta/>, 2009.
- [82] B. Cipra. The best of the 20th century: Editors name top 10 algorithms. *SIAM news*, 33(4):1–2, 2000.
- [83] R. Connelly and D. W. Henderson. A convex 3-complex not simplicially isomorphic to a strictly convex complex. *Math. Proc. Cambridge Philos. Soc.*, 88(2):299–306, 1980.
- [84] P. Conti and C. Traverso. Buchberger algorithm and integer programming. In *Proceedings AAECC-9 (New Orleans)*, volume 539 of *Lecture Notes in Computer Science*, pages 130–139. Springer-Verlag, 1991.
- [85] T. H. Cormen, C. E. Leiserson, R. L. Rivest, and C. Stein. *Introduction to algorithms*. MIT Press, Cambridge, MA, second edition, 2001.
- [86] R. W. Cottle. Minimal triangulation of the 4-cube. *Discrete Math.*, 40:25–29, 1982.
- [87] D. Cox, J. Little, and D. O’Shea. *Ideals, Varieties, and Algorithms*. Undergraduate Texts in Mathematics. Springer, 1992.
- [88] D. Cox, J. Little, and D. O’Shea. *Using Algebraic Geometry*. Undergraduate Texts in Mathematics. Springer-Verlag, 1999.
- [89] D. I. Dais, M. Henk, and G. M. Ziegler. All abelian quotient c.i.=singularities admit projective crepant resolutions in all dimensions. *Adv. in Math.*, 139:194–239, 1998.
- [90] G. B. Dantzig, A. J. Hoffman, and T. C. Hu. Triangulations (tilings) and certain block triangular matrices. *Mathematical Programming*, 31:1–14, 1985.

- [91] G. Das and G. Joseph. Which triangulations approximate the complete graph. In *Optimal Algorithms*, volume 401, pages 168–192. Lecture Notes in Computer Science, Springer, 1989.
- [92] E. F. D’azevedo and R. B. Simpson. On optimal interpolation triangle incidences. *SIAM Journal on Scientific and Statistical Computing*, 10:1063–1075, 1989.
- [93] M. de Berg, M. van Kreveld, M. Overmars, and O. Schwarzkopf. *Computational Geometry: Algorithms and Applications*. Springer, New York, 2000.
- [94] J. A. De Loera. *Triangulations of polytopes and computational algebra*. PhD thesis, Cornell University, 1995.
- [95] J. A. De Loera. Nonregular triangulations of products of simplices. *Discrete Comput. Geom.*, 15:253–264, 1996.
- [96] J. A. De Loera, S. Hoşten, F. Santos, and B. Sturmfels. The polytope of all triangulations of a point configuration. *Documenta Mathematica*, 1:103–119, 1996.
- [97] J. A. De Loera, E. D. Kim, S. Onn, and F. Santos. Graphs of transportation polytopes. *J. Combin. Theory Ser. A*, 116(8):1306–1325, 2009.
- [98] J. A. De Loera, F. Liu, and R. Yoshida. A generating function for all semi-magic squares and the volume of the Birkhoff polytope. *J. Algebraic Combin.*, 30(1):113–139, 2009.
- [99] J. A. De Loera, E. Peterson, and F. Su. Polytopal generalization of Sperner’s lemma. *Journal Comb. Theory Ser. A*, 100:1–26, 2002.
- [100] J. A. De Loera, F. Santos, and F. Takeuchi. Extremal properties for dissections of convex 3-polytopes. *SIAM J. Discrete Math.*, 14(2):143–161, 2001.
- [101] J. A. De Loera, B. Sturmfels, and R. R. Thomas. Gröbner bases and triangulations of the second hypersimplex. *Combinatorica*, 15:409–424, 1995.
- [102] J. A. De Loera and F. J. Wicklin. On the need of convexity in patchworking. *Adv. in Applied Math.*, 20:188–219, 1998.
- [103] B. N. Delaunay. Sur la sphère vide. *Izvestia Akademii Nauk SSSR (Bull. Acad. Sci. USSR)*, 7:793–800, 1934.
- [104] M. Develin and B. Sturmfels. Tropical convexity. *Doc. Math.*, 9:1–27 (electronic), 2004.
- [105] T. K. Dey. On counting triangulations in d dimensions. *Comput. Geom.*, 3(6):315–325, 1993.
- [106] T. K. Dey and N. R. Shah. On the number of simplicial complexes in \mathbb{R}^d . *Comput. Geom.*, 8(5):267–277, 1997.
- [107] M. T. Dickerson, J. M. Keil, and M. H. Montague. A large subgraph of the minimum weight triangulation. *Discrete Comput. Geom.*, 18:289–304, 1997.
- [108] R. L. Drysdale, S. McElfresh, and J. S. Snoeyink. On exclusion regions for optimal triangulations. *Discrete Appl. Math.*, 109:49–65, 2001.
- [109] M. E. Dyer and A. M. Frieze. On the complexity of computing the volume of a polyhedron. *SIAM J. Computing*, 17, 1988.

- [110] M. E. Dyer, A. M. Frieze, and R. Kannan. A random polynomial-time algorithm for approximating the volume of convex bodies. *J. Assoc. Comput. Mach.*, 38, 1991.
- [111] M. E. Dyer, P. Gritzmann, and A. Hufnagel. On the complexity of computing mixed volumes. *SIAM J. Computing*, 27:356–400, 1998.
- [112] P. Edelman, V. Reiner, and J. Rambau. On subdivision posets of cyclic polytopes. *European Journal of Combinatorics*, 21:85–101, 2000.
- [113] H. Edelsbrunner. *Algorithms in Combinatorial Geometry*. Springer, New York, 1987.
- [114] H. Edelsbrunner. *Geometry and topology for mesh generation*, volume 7 of *Cambridge Monographs on Applied and Computational Mathematics*. Cambridge University Press, Cambridge, 2001.
- [115] H. Edelsbrunner, F. P. Preparata, and D. B. West. Tetrahedrizing point sets in three dimensions. *Journal of Symbolic Computation*, 10:335–347, 1990.
- [116] H. Edelsbrunner and N. R. Shah. Incremental topological flipping works for regular triangulations. *Algorithmica*, 15(3):223–241, 1996.
- [117] H. Edelsbrunner and T. S. Tan. A quadratic time algorithm for the minmax length triangulation. In *Proceedings 32nd IEEE Symp. Foundations of Comp. Science*, pages 414–423. IEEE press, 1991.
- [118] H. Edelsbrunner, T. S. Tan, and R. Waupotitsch. An $O(n^2 \log n)$ time algorithm for the minmax angle triangulation. *SIAM J. Sci. Statist. Comput.*, 13(4):994–1008, 1992.
- [119] E. Ehrhart. *Polynômes arithmétiques et méthode des polyèdres en combinatoire*, volume 35 of *International Series of Numerical Mathematics*. Birkhäuser Verlag, Basel, 1977.
- [120] G. Elekes. A geometric inequality and the complexity of computing volume. *Discrete Comput. Geom.*, 1:289–292, 1986.
- [121] I. Emiris. *Sparse Elimination and Applications in Kinematics*. PhD thesis, University of California, Berkeley, 1994.
- [122] D. Eppstein. Approximating the minimum weight steiner triangulation. *Discrete Comput. Geom.*, 11:163–191, 1994.
- [123] D. K. Faddeev, N. P. Dolbilin, S. S. Ryshkov, and M. I. Shtogrin. Boris Nikolaevich Delone. on his life and creative work. *Proc. Steklov Inst. Math.*, 196:1–9, 1992.
- [124] R. T. Firla and G. M. Ziegler. Hilbert bases, unimodular triangulations, and binary covers of rational polyhedral cones. *Discrete Comput. Geom.*, 21:205–216, 1999.
- [125] S. Fomin and A. Zelevinsky. Cluster algebras. I. Foundations. *J. Amer. Math. Soc.*, 15(2):497–529 (electronic), 2002.
- [126] S. Fomin and A. Zelevinsky. Y -systems and generalized associahedra. *Ann. of Math. (2)*, 158(3):977–1018, 2003.
- [127] W. Fong. *Triangulations and Combinatorial Properties of Convex Polytopes*. PhD thesis, MIT, Cambridge, MA, 2000.
- [128] S. Fortune. A sweepline algorithm for Voronoi diagrams. *Algorithmica*, 2:153–174, 1987.

- [129] S. Fortune. Voronoi diagrams and Delaunay triangulations. In *Computing in Euclidean Geometry*. World Scientific Publishing Co., Singapore, 1995.
- [130] K. Fukuda. Homepage of cdd. http://www.ifor.math.ethz.ch/~fukuda/cdd_home/cdd.html, 2008.
- [131] K. Fukuda, A. N. Jensen, and R. R. Thomas. Computing Gröbner fans. *Math. Comp.*, 76(260):2189–2212 (electronic), 2007.
- [132] J. Galtier, F. Hurtado, M. Noy, S. Pérennes, and J. Urrutia. Simultaneous edge flipping in triangulations. *Internat. J. Comput. Geom. Appl.*, 13:113–133, 2003.
- [133] A. Garcia, M. Noy, and J. Tejel. Lower bounds on the number of crossing-free subgraphs of k_n . *Comput. Geom.*, 16:211–221, 2000.
- [134] M. R. Garey and D. S. Johnson. *Computers and Intractability: A Guide to the Theory of NP-Completeness*. Freeman, San Francisco, 1979.
- [135] E. Gawrilow and M. Joswig. polymake: a framework for analyzing convex polytopes. In Gil Kalai and Günter M. Ziegler, editors, *Polytopes — Combinatorics and Computation (Oberwolfach, 1997)*, volume 29 of *DMV Sem.*, pages 43–73. Birkhäuser, Basel, 2000.
- [136] I. M. Gelfand, M. I. Graev, and A. Postnikov. Combinatorics of hypergeometric functions associated with positive roots. In *The Arnold-Gelfand mathematical seminars*, pages 205–221. Birkhäuser Boston, Boston, MA, 1997.
- [137] I. M. Gelfand, M. M. Kapranov, and A. V. Zelevinsky. Hypergeometric functions and toric varieties. *Funct. Anal. Appl.*, 23:12–26, 1989.
- [138] I. M. Gelfand, M. M. Kapranov, and A. V. Zelevinsky. Newton polyhedra of principal a -determinants. *Soviet Math. Dokl.*, 40:278–281, 1990.
- [139] I. M. Gelfand, M. M. Kapranov, and A. V. Zelevinsky. Discriminants of polynomials in several variables and triangulations of Newton polytopes. *Leningrad Math. J.*, 2:449–505, 1991.
- [140] I. M. Gelfand, M. M. Kapranov, and A. V. Zelevinsky. *Discriminants, Resultants and Multidimensional Determinants*. Birkhäuser, Boston, 1994.
- [141] P. D. Gilbert. *New results in planar triangulations*. M.sc. thesis, Univ. of Illinois Urbana, 1979.
- [142] J. E. Goodman and R. Pollack. There are asymptotically far fewer polytopes than we thought. *Bull. Amer. Math. Soc. (N.S.)*, 14(1):127–129, 1986.
- [143] J. E. Goodman and R. Pollack. Upper bounds for configurations and polytopes in \mathbf{R}^d . *Discrete Comput. Geom.*, 1(3):219–227, 1986.
- [144] J. Gouveia, P. Parrilo, and R. Thomas. Theta bodies of polynomial ideals. *SIAM J. Optimization*, 20:2097–2118, 2010.
- [145] R. L. Graham. An efficient algorithm for determining the convex hull of a finite planar set. *Information Processing Letters*, 1:132–133, 1972.
- [146] R. L. Graham, D. E. Knuth, and O. Patashnik. *Concrete mathematics*. Addison-Wesley Publishing Company, Reading, MA, second edition, 1994.

- [147] C. Greenhill. The complexity of counting colourings and independent sets in sparse graphs and hypergraphs. *Comput. Complexity*, 9(1):52–72, 2000.
- [148] B. Grünbaum. *Convex polytopes*, volume 221 of *Graduate Texts in Mathematics*. Springer-Verlag, New York, second edition, 2003.
- [149] L. J. Guibas and J. Stolfi. Primitives for the manipulation of general subdivisions and the computation of Voronoi diagrams. *ACM Trans. Graphics*, 4:74–123, 1985.
- [150] B. Haas. Les multilucarnes: Nouveaux contre-exemples à la conjecture de Ragsdale. *C. R. Acad. Sci. Paris, Ser. I*, 320:1507–1512, 1995.
- [151] B. Haas. *Real algebraic curves and combinatorial constructions*. PhD thesis, Universität Basel, 1998.
- [152] B. Haas. A simple counterexample to Kouchnirenko’s conjecture. *Beiträge Algebra Geom.*, 43:1–8, 2002.
- [153] C. Haase, A. Paffenholz, L. C. Piechnik, and F. Santos. Existence of unimodular triangulations — positive results. In preparation, 2010.
- [154] M. Haiman. A simple and relatively efficient triangulation of the n -cube. *Discrete Comput. Geom.*, 6:287–289, 1991.
- [155] S. Hanke, T. Ottmann, and S. Schuierer. The edge-flipping distance of triangulations. *Journal of Universal Comp. Science*, 2:570–579, 1996.
- [156] L. S. Heath and S. V. Pemmaraju. New results for the minimum weight triangulation problem. *Algorithmica*, 12:533–552, 1994.
- [157] S. Herrmann. Facets of secondary polytopes. Preprint, arXiv.org, 2009. manuscript available online.
- [158] S. Herrmann. *Splits and Tight Spans of Convex Polytopes*. PhD thesis, TU Darmstadt, 2009.
- [159] S. Herrmann and M. Joswig. Splitting polytopes. *Münster Journal of Mathematics*, 1:109–142, 2008.
- [160] S. Herrmann and M. Joswig. Tight spans and coarsest subdivisions of convex polytopes. In *Proceedings of the Twenty-fifth European Workshop on Computational Geometry, Brussels*, pages 259–262, 2009.
- [161] S. Herrmann and M. Joswig. Totally splittable polytopes. *Discrete Comput. Geom.*, 44(1):149–166, 2010.
- [162] H. Hirai. A geometric study of the split decomposition. *Discrete Comput. Geom.*, 36(2):331–361, 2006.
- [163] M. Hoffmann and Y. Okamoto. The minimum weight triangulation problem with few inner points. In *Proceedings 1st International Workshop on Parameterized and Exact Computation (IWPEC 2004) September 14–17, Bergen Norway 2004*, volume 3162 of *Lect. Notes Comput. Sci.*, pages 200–212. Springer, 2004.
- [164] C. Hohlweg and C. E. M. C. Lange. Realizations of the associahedron and cyclohedron. *Discrete Comput. Geom.*, 37(4):517–543, 2007.
- [165] B. Huber, J. Rambau, and F. Santos. The Cayley trick, lifting subdivisions and the Bohne-Dress theorem on zonotopal tilings. *J. Eur. Math. Soc. (JEMS)*, 2:179–198, 2000.
- [166] B. Huber and B. Sturmfels. A polyhedral method for solving sparse polynomial systems. *Math. of Computation*, 64:1541–1555, 1995.

- [167] P. Huggins, B. Sturmfels, J. Yu, and D. S. Yuster. The hyperdeterminant and triangulations of the 4-cube. *Math. Comp.*, 77(263):1653–1679, 2008.
- [168] R. B. Hughes. Minimum-cardinality triangulations of the d -cube for $d = 5$ and $d = 6$. *Discrete Math.*, 118(1-3):75–118, 1993.
- [169] R. B. Hughes and M. R. Anderson. Simplexity of the cube. *Discrete Math.*, 158:99–150, 1996.
- [170] J. E. Humphreys. *Reflection groups and Coxeter groups*, volume 29 of *Cambridge Studies in Advanced Mathematics*. Cambridge University Press, Cambridge, 1990.
- [171] F. Hurtado and M. Noy. Counting triangulations of almost-convex polygons. *Ars Combinatoria*, 45:169–179, 1997.
- [172] F. Hurtado, M. Noy, and J. Urrutia. Flipping edges in triangulations. *Discrete Comput. Geom.*, 22:333–346, 1999.
- [173] I. Itenberg. Contre-exemples à la conjecture de Ragsdale. *C. R. Acad. Sci. Paris, Series I*, 317:277–282, 1993.
- [174] I. Itenberg. Topology of real algebraic t -surfaces. *Revista Matemática Complutense*, 10:131–152, 1997.
- [175] I. Itenberg and M. F. Roy. Multivariate Descartes’ rule. *Beiträge zur Algebra und Geometrie*, 37:337–346, 1996.
- [176] I. Itenberg and E. Shustin. Singular points and limit cycles of planar polynomial vector fields. *Duke Math. J.*, 102:1–37, 2000.
- [177] A. N. Jensen. Gfan, a software system for Gröbner fans and tropical varieties. Available at <http://www.math.tu-berlin.de/~jensen/software/gfan/gfan.html>.
- [178] B. Joe. Three dimensional triangulations from local deformations. *SIAM J. Sci. Stat. Comput.*, 10:718–741, 1989.
- [179] B. Joe. Construction of k -dimensional Delaunay triangulations using local transformations. *SIAM J. Sci. Comput.*, 14(6):1415–1436, 1993.
- [180] V. Kaibel and G. M. Ziegler. Counting lattice triangulations. In ed. C. D. Wensley, editor, *Surveys in Combinatorics 2003, Proceedings 19th British Combinatorial conference, June 29 - July 4, in Bangor/Wales*, volume 307 of *London Math. Society Lecture Notes Series*, pages 277–307. Cambridge University Press, 2003.
- [181] G. Kalai. Many triangulated spheres. *Discrete Comput. Geom.*, 3:1–14, 1988.
- [182] E. Kaltofen and G. Villard. Computing the sign or the value of the determinant of an integer matrix, a complexity survey. *Journal of Computational and Applied Mathematics*, 162(1):133–146, 2004.
- [183] J.-M. Kantor and K. S. Sarkaria. On primitive subdivisions of an elementary tetrahedron. *Pac. J. Math.*, 211(1):123–155, 2003.
- [184] M. Keil. Computing a subgraph of the minimum weight triangulation. *Comput. Geom.*, 4:289–304, 1994.
- [185] G. Kempf, F. F. Knudsen, D. Mumford, and B. Saint-Donat. *Toroidal embeddings. I*, volume 339 of *Lecture Notes in Mathematics*. Springer, Berlin, 1973.

- [186] L. G. Khachiyan. The problem of calculating the volume of a polyhedron is enumeratively hard. *Uspekhi Mat. Nauk*, 44:179–180, 1989.
- [187] V. M. Kharlamov and I. Itenberg. Toward the maximal number of components of a non-singular surface of degree 5 in \mathbb{RP}^3 . *Amer. Math. Soc. Transl.*, 173:111–118, 1996.
- [188] A. G. Khovanskii. Newton polytopes and toric varieties. *Funct. Anal. Appl.*, 10:289–298, 1977.
- [189] A. G. Khovanskii. *Fewnomials*, volume 88 of *Translations of mathematical monographs*. Amer. Math. Soc., 1991.
- [190] E. D. H. Kim. *Geometric Combinatorics of Transportation polytopes and the behavior of the simplex method*. PhD thesis, University of California, Davis, 2010.
- [191] D. G. Kirkpatrick. A note on Delaunay and optimal triangulations. *Information Processing Letter*, 10:127–128, 1980.
- [192] D. G. Kirkpatrick and J. D. Radke. A framework for computational morphology. In G. T. Toussaint, editor, *Computational Geometry*. Elsevier, Amsterdam, 1985.
- [193] G. T. Klincsek. Minimal triangulations of polygonal domains. *Annals of Discrete Mathematics*, 9:127–128, 1980.
- [194] D. E. Knuth. *Sorting and Searching*, volume 3 of *The art of computer programming*. Addison-Wesley, Reading MA, 1973.
- [195] H. Komuro. The diagonal flips of triangulations on the sphere. *Yokohama Math. J.*, 44:115–122, 1997.
- [196] J. Kratochvíl and J. Matousek. Intersection graphs of segments. *J. Comb. Theory, Ser. B*, 62:289–315, 1994.
- [197] A. G. Kushnirenko. Newton polytopes and the Bézout theorem. *Funct. Anal. Appl.*, pages 233–235, 1976.
- [198] Y. Kyoda, K. Imai, F. Takeuchi, and A. Tajima. A branch-and-cut approach for minimum weight triangulation. In *Proceedings 8th international symposium on Algorithms and Computation, ISAAC '97, December 17–19, Singapore*, volume 1350 of *Lect. Notes Comput. Sci.*, pages 384–393. Springer, 1997.
- [199] T. Lam and A. Postnikov. Alcoved polytopes. I. *Discrete Comput. Geom.*, 38(3):453–478, 2007.
- [200] T. Lambert. The Delaunay triangulation maximizes the mean inradius. In *Proceedings of the 6th Canadian Conference on Computational Geometry, Saskatoon, SK, Canada*, pages 201–206, 1994.
- [201] E. L. Lawler, J. K. Lenstra, and A. H. G. Rinnooy Kan. Generating all maximal independent sets: NP-hardness and polynomial-time algorithms. *SIAM J. Comput.*, 9(3):558–565, 1980.
- [202] C. L. Lawson. Transforming triangulations. *Discrete Math.*, 3:365–372, 1972.
- [203] C. L. Lawson. Software for c^1 -interpolation. In *Mathematical Software III*, pages 161–194. Academic Press, New York, 1977.
- [204] C. L. Lawson. Properties of n -dimensional triangulations. *Comput. Aided Geom. Design*, 3(4):231–246 (1987), 1986.
- [205] C. W. Lee. The associahedron and triangulations of the n -gon. *European J. Combin.*, pages 551–560, 1989.

- [206] C. W. Lee. Regular triangulations of convex polytopes. In P. Gritzmann and B. Sturmfels, editors, *Applied Geometry and Discrete Mathematics—The Victor Klee Festschrift*, volume 4 of *Dimacs Series in Discrete Math. and Theoretical Comp. Science*, pages 443–456. Amer. Math. Soc., 1991.
- [207] C. W. Lee. Subdivisions and triangulations of polytopes. In J. E. Goodman and J. O'Rourke, editors, *Handbook of Discrete and Computational Geometry*, pages 271–290. CRC Press, New York, 1997.
- [208] N.J. Lennes. Theorems on the simple finite polygon and polyhedron. *American Journal of Mathematics*, 33:37–62, 1911.
- [209] C. Levcopoulos and D. Krznaric. Quasi-greedy triangulations approximating the minimum weight triangulation. *J. Algorithms*, 27:303–338, 1998.
- [210] T. Y. Li and X. Wang. On multivariate Descartes’ rule—a counterexample. *Beiträge zur Algebra und Geometrie*, 39:1–5, 1998.
- [211] D. Lichtenstein. Planar formulae and their uses. *SIAM J. Comput.*, 11:329–343, 1982.
- [212] A. Lingas. The power of non-rectilinear holes. In Mogens Nielsen and Erik Meineche Schmidt, editors, *(ICALP) Automata, Languages and Programming, 9th Colloquium, Aarhus, Denmark, July 12-16, 1982, Proceedings*, volume 140 of *Lecture Notes in Computer Science*. Springer, 1982.
- [213] A. Lingas. The greedy and Delaunay triangulations are not bad in the average case. *Inf. Process. Lett.*, 22:199–208, 1986.
- [214] A. Lingas. A new heuristic for the minimum weight triangulation. *SIAM J. Algebraic and Discrete Methods*, 8:646–658, 1987.
- [215] D.E. Knuth L. J. Guibas and M. Sharir. Randomized incremental construction of Delaunay and voronoi diagrams. *Algorithmica*, 7:381–413, 1992.
- [216] E.L. Lloyd. On triangulations of a set of points in the plane. In *Proceedings 18th Annual Symposium on Foundations of Computer Science (Providence, R.I., 1977)*, pages 228–240. IEEE Comput. Soc., Long Beach, Calif., 1977.
- [217] J.-L. Loday. Realization of the Stasheff polytope. *Arch. Math. (Basel)*, 83(3):267–278, 2004.
- [218] J.-L. Loday. Parking functions and triangulation of the associahedron. In *Categories in algebra, geometry and mathematical physics*, volume 431 of *Contemp. Math.*, pages 327–340. Amer. Math. Soc., Providence, RI, 2007.
- [219] L. Lovász and M.D. Plummer. *Matching Theory*, volume 121 of *Annals of Discrete Mathematics* (29). North-Holland, 1986.
- [220] J. M. Lucas. The rotation graph of binary trees is Hamiltonian. *J. Algorithms*, 8:503–535, 1987.
- [221] M. Ludwig and M. Reitzner. Elementary moves on triangulations. *Discrete Comput. Geom.*, 35(4):527–536, 2006.
- [222] I. G. Macdonald. Polynomials associated with finite cell-complexes. *J. London Math. Soc.* (2), 4:181–192, 1971.
- [223] D. Maclagan and R.R. Thomas. Combinatorics of the toric Hilbert scheme. *Discrete Comput. Geom.*, 27(2):249–272, 2002.

- [224] G. Manacher and A. Zobrist. Neither the greedy nor the Delauney triangulation of the planar set approximates the optimal triangulation. *Information Process. Letters*, 9:31–34, 1979.
- [225] J. L. Marichal and M. J. Mossinghoff. Slices, slabs, and sections of the unit hypercube. *Online J. Anal. Comb.*, 3, 2008.
- [226] J. Matoušek and B. Gärtner. *Understanding and using linear programming*. Universitext. Springer, Berlin, 2007.
- [227] J. Matousek, M. Tancer, and Wagner U. Hardness of embedding simplicial complexes in R^d . Preprint, arXiv:0807.0336v2, 2009. Journal of the European Mathematical Society, to appear.
- [228] T. Matsui and S. Tamura. Adjacency on combinatorial polyhedra. *Discrete Applied Math.*, 56:311–321, 1995.
- [229] P. McMullen. Lattice invariant valuations on rational polytopes. *Arch. Math. (Basel)*, 31(5):509–516, 1978/79.
- [230] P. McMullen. Triangulations of simplicial polytopes. *Beiträge Algebra Geom.*, 45(1):37–46, 2004.
- [231] P. McMullen. Polyhedra and polytopes: algebra and combinatorics. In *Algebraic and geometric combinatorics*, volume 423 of *Contemp. Math.*, pages 235–267. Amer. Math. Soc., Providence, RI, 2006.
- [232] K. Meszaros. Root polytopes, triangulations, and the subdivision algebra, I. Preprint, arXiv.org, 2009. to appear in Transactions of the American Mathematical Society.
- [233] F. Meunier. Sperner labellings: a combinatorial approach. *J. Combin. Theory Ser. A*, 113(7):1462–1475, 2006.
- [234] T. Mora and L. Robbiano. The Gröbner fan of an ideal. *J. Symbolic Comput.*, 6(2-3):183–208, 1988.
- [235] W. Mulzer and G. Rote. Minimum weight triangulation is NP-hard. In *Proceedings of the 22th ACM symp. Comput. Geom.*, pages 1–10. ACM, 2006.
- [236] W. Mulzer and G. Rote. Minimum-weight triangulation is NP-hard. *J. ACM*, 55(2):1–29, 2008.
- [237] J. R. Munkres. *Algebraic Topology*. Addison Wesley, 1984.
- [238] D. Naddef. The Hirsch conjecture is true for $(0, 1)$ -polytopes. *Math. Programming*, 45(1, (Ser. B)):109–110, 1989.
- [239] S. Negami. Diagonal flips in triangulations on surfaces. *Discrete Math.*, 135:225–232, 1994.
- [240] G. L. Nemhauser and L. A. Wolsey. *Integer programming and combinatorial optimization*. Wiley-Interscience Series in Discrete Mathematics and Optimization. Wiley, New York, 1988.
- [241] H. Ohsugi. Toric ideals and an infinite family of normal $(0, 1)$ -polytopes without unimodular regular triangulations. *Discrete Comput. Geom.*, 27(4):551–565, 2002.
- [242] H. Ohsugi and T. Hibi. Normal polytopes arising from finite graphs. *Journal of Algebra.*, 207:409–426, 1998.
- [243] H. Ohsugi and T. Hibi. A normal $(0, 1)$ -polytope none of whose regular triangulations is unimodular. *Discrete Comput. Geom.*, 21:201–204, 1999.

- [244] H. Ohsugi and T. Hibi. Convex polytopes all of whose reverse lexicographic initial ideals are squarefree. *Proc. Amer. Math. Soc.*, 129(9):2541–2546 (electronic), 2001.
- [245] H. Ohsugi and T. Hibi. Unimodular triangulations and coverings of configurations arising from root systems. *J. Algebraic Combin.*, 14(3):199–219, 2001.
- [246] D. Orden and F. Santos. Asymptotically efficient triangulations of the d -cube. *Discrete Comput. Geom.*, 30(4):509–528, 2003.
- [247] D. Orden and F. Santos. The polytope of non-crossing graphs on a planar point set. *Discrete Comput. Geom.*, 33(2):275–305, 2005.
- [248] D. Orden, F. Santos, B. Servatius, and H. Servatius. Combinatorial pseudo-triangulations. *Discrete Math.*, 307:554–566, 2007.
- [249] I. Pak. Lectures on discrete and polyhedral geometry. manuscript, 2010.
- [250] S. Payne. Ehrhart series and lattice triangulations. *Discrete Comput. Geom.*, 40:365–376, 2008.
- [251] I. Peeva and M. Stillman. Toric Hilbert schemes. *Duke Math. J.*, 111(3):419–449, 2002.
- [252] J. Pfeifle. Secondary polytope models. Electronic Geometry Model Directory, available under http://www.eg-models.de/models/Polytopes/Secondary_Polytopes/, 2006.
- [253] J. Pfeifle and J. Rambau. Computing triangulations using oriented matroids. In *Algebra, Geometry, and Software Systems*. Springer-Verlag, 2003.
- [254] J. Pfeifle and G. M. Ziegler. Many triangulated 3-spheres. *Math. Ann.*, 330(4):829–837, 2004.
- [255] D. A. Plaisted and J. Hong. A heuristic triangulation algorithm. *J. Algorithms*, 8:405–437, 1987.
- [256] M. Pocchiola and G. Vegter. Pseudo-triangulations: theory and applications. In *Proceedings 12th ACM symp. Comput. Geom.*, pages 291–300. ACM press, 1996.
- [257] M. Pocchiola and G. Vegter. Topologically sweeping visibility complexes via pseudo-triangulations. *Discrete Comput. Geom.*, 16:419–453, 1996.
- [258] A. Postnikov. Permutohedra, associahedra, and beyond. *Int. Math. Res. Not. IMRN*, 2009(6):1026–1106, 2009.
- [259] D. Poulalhon and G. Schaeffer. Optimal coding and sampling of triangulations. *Algorithmica*, 46(3-4):505–527, 2006.
- [260] L. Pournin and Th. M. Liebling. Constrained paths in the flip-graph of regular triangulations. *Comput. Geom. Theory Appl.*, 37(2):134–140, 2007.
- [261] S. Provan and M. O. Ball. On the complexity of counting cuts and of computing the probability that a graph is connected. *SIAM J. Computing*, 12:777–788, 1983.
- [262] V. Ragsdale. On the arrangement of the real branches of the plane algebraic curves. *Amer. J. Math.*, 28:377–404, 1906.
- [263] J. Rambau. *Projections of Polytopes and Polyhedral Subdivisions*. Berichte aus der Mathematik. Shaker, Aachen, 1996.

- [264] J. Rambau. Triangulations of cyclic polytopes and higher Bruhat orders. *Mathematika*, 44:162–194, 1997.
- [265] J. Rambau. TOPCOM: Triangulations of point configurations and oriented matroids. In A. M. Cohen, X.-S. Gao, and N. Takayama, editors, *Mathematical Software—ICMS 2002*, pages 330–340. World Scientific, 2002.
- [266] J. Rambau. On a generalization of Schönhardt’s polyhedron. In J. E. Goodman, J. Pach, and E. Welzl, editors, *Combinatorial and Computational Geometry*, volume 52 of *MSRI Publications*, pages 510–516. Cambridge University Press, 2005.
- [267] J. Rambau and F. Santos. The Generalized Baues Problem for cyclic polytopes I. *European J. Combin.*, 21:65–83, 2000.
- [268] J. Rambau and G. M. Ziegler. Projections of polytopes and the generalized Baues conjecture. *Discrete Comput. Geom.*, 16(3):215–237, 1996.
- [269] J. G. Ratcliffe. *Foundations of hyperbolic manifolds*. Springer Verlag, Berlin, 1999.
- [270] S. Ray and R. Seidel. A simple and less slow method for counting triangulations and for related problems. In *Proceedings of the 20th European Workshop on Computational Geometry, Seville*, pages 77–80, 2004.
- [271] V. Reiner. The generalized baues problem. In *New Perspectives in Algebraic Combinatorics*, volume 38, pages 293–336. Cambridge Univ. Press, 1999.
- [272] J. Richter-Gebert. *Realization spaces of polytopes*, volume 1643 of *Lecture Notes in Mathematics*. Springer-Verlag, Berlin, 1996.
- [273] S. Rippa. Minimal roughness property of the Delaunay triangulation. *Computer Aided Geometric Design*, 7:489–497, 1990.
- [274] J. M. Rojas and X. Wang. Counting affine roots of polynomial systems via pointed Newton polytopes. *Journal of Complexity*, 12:116–133, 1996.
- [275] G. Rote, F. Santos, and I. Streinu. Expansive motions and the polytope of pointed pseudo-triangulations. In B. Aronov, S. Basu, J. Pach, and M. Sharir, editors, *Discrete and Computational Geometry – The Goodman-Pollack Festschrift*, Algorithms and Combinatorics 25, pages 699–736. Springer Verlag, Berlin, 2003.
- [276] Günter Rote, Francisco Santos, and Ileana Streinu. Pseudo-triangulations—a survey. In *Surveys on discrete and computational geometry*, volume 453 of *Contemp. Math.*, pages 343–410. Amer. Math. Soc., Providence, RI, 2008.
- [277] J. Ruppert and R. Seidel. On the difficulty of triangulating three-dimensional non-convex polyhedra. *Discrete Comput. Geom.*, 7:227–253, 1992.
- [278] F. Santos. A point configuration whose space of triangulations is disconnected. *J. Amer. Math. Soc.*, 13:611–637, 2000.
- [279] F. Santos. Triangulations with very few geometric bistellar neighbors. *Discrete Comput. Geom.*, 23:15–33, 2000.
- [280] F. Santos. On the refinements of a polyhedral subdivision. *Collect. Math.*, pages 231–256, 2001.
- [281] F. Santos. *Triangulations of oriented matroids*. American Mathematical Society, 2002.

- [282] F. Santos. The Cayley trick and triangulations of products of simplices. In A. Barvinok, M. Beck, C. Haase, B. Reznick, and V. Welker, editors, *Integer Points in Polyhedra – Geometry, Number Theory, Algebra, Optimization*, pages 151–177. American Mathematical Society, 2005.
- [283] F. Santos. Non-connected toric Hilbert schemes. *Math. Annalen*, 332:645–665, 2005.
- [284] F. Santos. Geometric bistellar flips: the setting, the context and a construction. In *International Congress of Mathematicians. Vol. III*, pages 931–962. Eur. Math. Soc., Zürich, 2006.
- [285] F. Santos. Unimodular triangulations of dilated 3-polytopes. In preparation, 2010.
- [286] F. Santos. A counter-example to the hirsch conjecture. preprint, June 2010.
- [287] F. Santos and R. Seidel. A better upper bound on the number of triangulations of a planar point set. *J. Combin. Theory Ser A*, 102:186–193, 2003.
- [288] H. Scarf. The approximation of fixed points of a continuous mapping. *SIAM J. Appl. Math.*, 15:1328–1343, 1967.
- [289] H. Scarf and T. Hansen. *Computation of economic equilibria*. Yale University press, New Haven, 1973.
- [290] E. Schönhardt. Über die Zerlegung von Dreieckspolyedern in Tetraeder. *Math. Ann.*, 98:309–312, 1928.
- [291] A. Schrijver. *Theory of Linear and Integer Programming*. Wiley-Interscience Series in Discrete Mathematics and Optimization. John Wiley and Sons, New York, 1986.
- [292] T. Seacrest and F. E. Su. Minimal triangulations of simplices.
- [293] A. Sebö. Hilbert bases, Carathéodory’s theorem and combinatorial optimization. In W. Pulleyblank R. Kannan, editor, *Proceedings of the IPCO conference University of Waterloo Press*, Waterloo, 1990.
- [294] M. I. Shamos and D. Hoey. Closest point problems. *Proceedings 16th IEEE Symp. on Foundations of computer Science*, pages 151–162, 1975.
- [295] M. Sharir and E. Welzl. Random triangulations of planar point sets. In *Proceedings 22nd ACM symp. Comput. Geom. (SoCG)*, pages 273–281. ACM, 2006.
- [296] J. Shewchuk. Delaunay refinement algorithms for triangular mesh generation. *Comput. Geom.: Theory and Applications*, 22:21–74, 2002.
- [297] E. Shustin. Critical points of real polynomials, subdivisions of newton polyhedra and topology of real algebraic hypersurfaces. *Amer. Math Soc. Transl.*, 2(173):203–223, 1996.
- [298] A. Simis, W. V. Vasconcelos, and R. H. Villarreal. The integral closure of subrings associated to graphs. *Journal of Algebra*, 199:281–289, 1998.
- [299] A. Sinclair. *Algorithms for random generation and counting: a Markov chain approach*. Birkhäuser, 1993.
- [300] D. D. Sleator, R. E. Tarjan, and W. P. Thurston. Rotation distance, triangulations and hyperbolic geometry. *J. of the AMS*, 1:647–681, 1988.
- [301] W. Smith. A lower bound for the simplexity of the n -cube via hyperbolic volumes. *Europ. J. Combinatorics*, 21:131–137, 2000.
- [302] R. P. Stanley. Combinatorial reciprocity theorems. *Advances in Math.*, 14:194–253, 1974.

- [303] R. P. Stanley. Eulerian partitions of the unit hypercube. In M. Aigner, editor, *Higher Combinatorics*, page 49. D. Reidel, 1977.
- [304] R. P. Stanley. Decompositions of rational convex polytopes. *Ann. Discrete Math.*, 6:333–342, 1980.
- [305] R. P. Stanley. Two poset polytopes. *Discrete Comput. Geom.*, 1:9–23, 1986.
- [306] R. P. Stanley. *Combinatorics and Commutative Algebra*. Birkhäuser, Boston, 2. edition, 1996.
- [307] R. P. Stanley. *Enumerative combinatorics*, volume 2. Cambridge U. Press, Cambridge, 1999.
- [308] R. P. Stanley. *Enumerative combinatorics*, volume 1. Cambridge U. Press, Cambridge, 1999.
- [309] J. D. Stasheff. Homotopy associativity of H -spaces. I, II. *Trans. Amer. Math. Soc.* 108 (1963), 275–292; *ibid.*, 108:293–312, 1963.
- [310] I. Streinu. A combinatorial approach to non-colliding robot arm motion planning. In *Proceedings 41st Ann. Annual Symposium of Foundations of Computer Science, Redondo Beach, California, USA*, pages 443–453. IEEE Computer Society press, 2000.
- [311] B. Sturmfels. Viro’s theorem for complete intersections. *Annali della Scuola Normale Superiore di Pisa, series IV*, 21:377–386, 1994.
- [312] B. Sturmfels. *Gröbner bases and Convex Polytopes*. American Mathematical Soc., Providence RI, 1995.
- [313] B. Sturmfels. *Solving systems of polynomial equations*. Published for Conference Board of the Mathematical Sciences CBMS, Washington, DC; by the American Mathematical Society, Providence RI, 2002.
- [314] B. Sturmfels. What is . . . a Gröbner basis? *Notices Amer. Math. Soc.*, 52(10):1199–1200, 2005.
- [315] B. Sturmfels and R. R. Thomas. Variations of cost functions in integer programming. *Mathematical Programming*, 77:357–387, 1997.
- [316] F. E. Su. Rental harmony: Sperner’s lemma in fair division. *Amer. Math. Monthly*, 106(10):930–942, 1999.
- [317] A. Tajima. Optimality and integer programming formulations of triangulations in general dimension. In *Proceedings 9th international symposium on Algorithms and Computation, ISAAC ’98, December 14–16, Taejon, Korea*, volume 1533 of *Lect. Notes Comput. Sci.*, pages 377–386. Springer, 1998.
- [318] A. Tajima. *Optimizing geometric triangulations using integer programming*. PhD thesis, University of Tokyo, 1999.
- [319] F. Takeuchi and H. Imai. Enumerating triangulations for products of two simplices and for arbitrary configurations of points. In *Computing and Combinatorics (Shanghai, 1997)*, volume 1276 of *Lecture Notes in Comput. Sci.*, pages 470–481. Springer, Berlin, 1997.
- [320] R. R. Thomas. A geometric Buchberger algorithm for integer programming. *Mathematics of Operations Research*, 20:864–884, 1995.
- [321] M. J. Todd. *The Computation of Fixed Points and Applications*. Springer-Verlag, Berlin, 1976.
- [322] M. J. Todd and L. Tuncel. A new triangulation for simplicial algorithms. *SIAM J. Discrete Math.*, 6:167–180, 1993.
- [323] W. T. Tutte. A census of planar triangulations. *Canad. J. Math.*, 14:21–38, 1962.

- [324] J. D. Vaaler. A geometric inequality with applications to linear forms. *Pacific J. Math.*, 83(2):543–553, 1979.
- [325] J. Verschelde, P. Verlinden, and R. Cools. Homotopies exploiting Newton polytopes for solving sparse polynomial systems. *SIAM J. Numer. Anal.*, 31:915–930, 1994.
- [326] O. Viro. Gluing of plane real algebraic curves and construction of curves of degree 6 and 7. In *Topology Proceedings*, volume 1060 of *Lecture Notes in Mathematics*, pages 187–200. Springer Verlag, 1984.
- [327] O. Viro. Real algebraic plane curves: Constructions with controlled topology. *Leningrad Math. Journal*, 1:1059–1134, 1990.
- [328] K. Wagner. Bemerkung zum Vierfarbenproblem. *Jahrerv. Deutsch. Math. Verein*, 46:26–32, 1936.
- [329] R. J. Walker. *Algebraic Curves*. Springer-Verlag, New York, 1978.
- [330] D. W. Walkup and R. J. B. Wets. Lifting projections of convex polyhedra. *Pacific Journal of Mathematics*, 28:465–475, 1969.
- [331] C. A. Wang, F. Y. Chin, and B. T. Yang. Maximum weight triangulation and graph drawing. *Information Processing Letters*, 70:17–22, 1999.
- [332] G. K. White. Lattice tetrahedra. *Canad. J. Math.*, 16:389–396, 1964.
- [333] N. L. White. A unique exchange property for bases. *Linear Algebra Appl.*, 31:81–91, 1980.
- [334] G. Wilson. Hilbert’s sixteen problem. *Topology*, 17:53–73, 1978.
- [335] B. T. Yang, Y.-F. Xu, and Z.-Y. You. A chain decomposition algorithm for the proof of a property on minimum weight triangulations. In *Proceedings 5th international symposium, ISAAC ’94, Beijing, P.R. China, August 25–27, 1994.*, volume 834 of *Lect. Notes Comput. Sci.*, pages 423–427. Springer, 1994.
- [336] J. E. Yukich. *Probability theory of classical Euclidean optimization problems*. Springer-Verlag, Berlin, 1998.
- [337] T. Zaslavsky. Facing up to arrangements: Face-count formulas for partitions of space by hyperplanes. *Mem. Am. Math. Soc.*, 154:102 p., 1975.
- [338] D. Zeilberger. Proof of a conjecture of Chan, Robbins, and Yuen. *Electron. Trans. Numer. Anal.*, 9:147–148 (electronic), 1999.
- [339] G. M. Ziegler. *Lectures on Polytopes*. Springer-Verlag, New York, 1994.
- [340] G. M. Ziegler. Lectures on 0/1-polytopes. In *Polytopes—combinatorics and computation (Oberwolfach, 1997)*, volume 29 of *DMV Sem.*, pages 1–41. Birkhäuser, Basel, 2000.
- [341] C. Zong. What is known about unit cubes. *Bull. Amer. Math. Soc. (N.S.)*, 42(2):181–211 (electronic), 2005.
- [342] C. Zong. *The cube: a window to convex and discrete geometry*, volume 168 of *Cambridge Tracts in Mathematics*. Cambridge University Press, Cambridge, 2006.

Index

Symbols

- $HST_1(n, d)$, 287
- $HST_2(n, d)$, 286
- A-triangulable, 126
- f -vector, 84
- g -vector, 489, 501
- h -vector, 87, 497
- k -split, 241
- k -split polyhedron, 242
- k -th hypersimplex of order n , 325
- n -th standard simplex, 294
- 24-cell, 353

A

- acyclic orientation, 298, 350
- adjacency graph, 84, 199
 - segment, 199
- affine
 - combination, 43
 - hull, 43
 - span, 43
 - subspaces, 43
- affine lattice, 463
- affinely independent, 44
 - basis, 44
- alcoved polytope, 32, 502, 504
- almost-triangulation, 74, 119
- arborescence, 487, 488
- associahedron, 7
 - Stasheff polytope, 33

B

- Barnette's sphere, 503
- basic feasible solution, 14, 493
- basis, 14
 - of a lattice, 463
- Baues poset, 65, 116
- binary
 - cover, 473
 - tree, 5
- Birkhoff polytope, 330
 - as compressed polytope, 333
- Buchberger's algorithm, 480

C

- carrier, 44, 52, 78
- Catalan numbers, 4, 508
- Cayley

- embedding, 295, 445, 446
- map, 454
- projection, 453
- trick, 433, 445
- Cayley trick without restrictions, 455
- cell
 - dependent, 51, 77
 - face, 51, 78
 - proper, 51, 78
 - facet, 51
 - in convex position, 51, 78
 - in general position, 51, 77
 - in special position, 51, 77
 - independent, 51, 77
 - maximal, 46
 - Minkowski —, 446
 - mixed, 448
 - of a polyhedral complex, 46
 - of a subdivision, 62, 79
 - positive span, 77
 - relative interior, 77
 - simplicial, 79
 - spanning, 51
 - Voronoi —, 97
- central
 - chamber, 262
 - fan, 490
 - subdivision, 262, 490
- cf-small, 397
- chamber, 17, 443
 - central, 262
 - complex, 246, 248, 344, 443, 493
 - equation, 406
 - fan, 246
- chirotope, 280, 377
- circuit, 72, 73, 151
 - balanced, 411
 - flip supported at, 186
 - of a toric ideal, 481
 - signature of, 151
 - type, 120
- circuit property, 154, 159
 - for triangulations, 154, 159, 160
- clause, 414
- closure property, 54, 149
- cluster algebras, 34
- cocircuit, 156
 - signature, 156
- cocircuit property, 159
 - for triangulations, 160
- coherent
- compatible subdivision, 441
- cubical flip, 437
- face flip, 435
- monotone path, 435
- triangulation, 55
- zonotopal tiling, 437
- combinatorially equivalent, 164, 278
- complex
 - associahedral, 505
 - extended, 505
- chamber —, 246, 248, 344, 493
- dual graph, 84
- order, 444
- order —, 116
- pseudo-chamber, 264
- complex torus, 25
- cone
 - inner normal —, 47
 - normal, 491
 - outer normal —, 47
 - pointed, 45, 79
 - relative interior, 45
 - secondary —, 221
 - subdivision, 14
 - triangulation, 14
- conical hull, 77
- contraction, 171
 - homogeneous, 174
- convex
 - combination, 43
 - cone, 45
 - hull, 1, 43
 - of a configuration, 50
 - polytope, 43
 - position, 108, 143
 - triangulation, 55
- coplanarity condition, 71, 223
- corank, 49, 72, 77
 - corank one, 72
- core simplex, 258
- cover
 - binary, 473
 - simplicial, 431
 - unimodular, 473
- cross-polytope, 177

- cube**
- corner-cut triangulation, 315
 - cornered simplices, 315
- cube-octahedron, 141
- cubical flip, 437
- coherent, 437
- cyclic polytope, 262, 278
- alternating oriented matroid, 282
 - canonical projection, 283
 - characteristic section, 283, 284
 - downflip, 276, 286
 - support, 286
 - downward
 - circuit, 283
 - flip, 276
 - flip support, 286
 - signature, 283
 - lower facets, 281
 - stackable triangulation, 289
- Stasheff-Tamari
- first poset, 287
 - second poset, 285
- upflip, 276, 286
- support, 286
- upper facets, 281
- upward
- circuit, 283
 - flip, 276
 - flip support, 286
 - signature, 283
- D**
- Dehn-Sommerville relations, 500
- Delaunay
- subdivision, 58
 - triangulation, 56–58, 97
 - algorithms for, 102
 - in the plane, 99
 - triangulation weighted, 55
- deletion, 86, 113, 289
- non-extendable, 344
- dependent, 44
- diagonal flip, 7, 120
- dimension, 45, 49, 50
- dissection, 318, 431
- division algorithm, 479
- dual graph, 199
- E**
- edge, 44
- light —, 105
 - locally Delaunay, 99
- equidecomposable, 410
- Euler's formula, 87
- F**
- face
- flip, 434
 - coherent, 435
 - lower, 55, 60
 - of a cone, 45
 - of a configuration, 51, 78
 - of a subdivision, 46
 - proper, 51, 78
- face property, 191, 192
- for maximal cells, 195
- facet, 44
- mixed, 23
 - of a configuration, 51, 78
 - of a simplicial complex, 493
 - width, 474
- fan
- central —, 490
 - chamber —, 246
 - complete, 46
 - normal, 16
 - normally equivalent, 47
 - outer normal —, 47
 - pointed, 46
 - polyhedral, 46
 - secondary —, 17
- feasible, 14
- fiber
- over a point, 82, 442
 - polytope, 433, 441
- finitely generated, 479
- flip, 7, 75
- direction, 285
 - adjacency oracle, 124
 - cubical —
 - coherent, 437
 - face —, 434
 - coherent, 435
 - insertion-deletion, 120
 - monotone, 137, 236, 237, 343
 - of compatible subdivisions, 441
 - parallel flip, 131
 - simultaneous flips, 131
 - successor oracle, 124
- folding condition
- strict, 223
 - strict local, 71
- Eulerian numbers, 327
- triangle, 327
- evaluation signature, 156
- exponent vector, 22
- extension, 289
- lexicographic, 204
- extremal, 51, 52
- weak, 223
- folding form, 223
- frame polytope, 427
- free Hilbert cover property, 473
- full-dimensional, 62, 79
- G**
- Gale
- affine diagram, 261
 - evenness, 280
 - gaps, 280
 - transform, 77, 160, 244
 - of the mother of all examples, 339
 - triangulation, 55
 - general position, 97, 362
 - generalized associahedron, 34
 - Generalized Baues Problem, 444
 - generically rigid, 132
 - GKZ vector, 215
 - repeated, 343
 - globally coherent string, 441
 - Gröbner
 - basis, 479
 - universal, 480, 485
 - fan, 480
- graph
- embedded in the plane, 94
 - of compatible subdivisions, 441
 - of monotone paths, 435
 - of triangulations, 7, 76
 - diameter, 239
 - disconnected, 359
 - of zonotopal tilings, 437
 - planar, 94
 - plane, 94
 - rooted, 112
- H**
- half-space, 44
- height
- function, 55
 - in a poset, 74
- homogenization
- of a configuration, 48
- hull property, 193, 194
- for adjacent maximal cells, 201
 - for maximal cells, 196, 197
- hyperdeterminant, 311
- hyperplane arrangement, 266
- hypersimplex, 311

I

- ideal, 479
- incremental, 240
- independent, 44
- initial
 - ideal, 479
 - monomial, 479
 - term, 479
- insertion, 113
- integral Carathéodory property, 473
- interior cocircuit equation, 402
- interior point property, 200, 202
- intersection
 - improper, 63, 79
 - proper, 63, 79
- intersection property, 1, 54, 149, 154
 - for maximal cells, 195

J

- join, 166
 - of subdivisions, 167

L

- l.a.o., 349
- label property, 193
 - for adjacent maximal cells, 202
 - for maximal cells, 196, 198
- Laman
 - condition, 132
 - graph, 132
- lattice
 - configuration, 464
 - linear, 463
 - polygon, 465
 - polytope, 464
 - compressed, 471, 473
 - facet-width one, 471
 - normal, 473
 - width, 471
 - triangulation, 465
- lattice-free
 - simplex, 469
 - symmetric, 469
- Lawrence
 - lifting, 265
 - polytope, 264, 454
- lexicographic
 - extension, 204
 - triangulation, 182
- lifted point configuration, 60
- lifting principle, 437
- line-stabbing, 399
- linearity space, 45, 78
- linear
 - dependence, 160

link

- evaluation, 160
- hull, 45
- lattice, 463
- in a triangulation, 488
- non-extendable, 344
- simplex, 186
- literal, 414
- LMT-graph, 106
- LMT-skeleton, 107
- locally acyclic orientation, 349
 - graph of, 349
- locally coherent string, 441

M

- map between two graphs, 359
- matrix
 - homogeneous, 49
 - totally unimodular, 481

Minkowski

- cell, 446
- projection, 451
- sum, 22, 436, 445, 447

mixed

- cell, 448
- facet, 23
- subconfiguration, 448
- subdivision, 449
- volume, 23

moment curve, 278**monomial order**, 479

- monotone
 - cellular string, 439
 - flip, 137, 236
 - sequence, 237
 - flipping, 343
 - Hirsch conjecture, 434
 - path, 434
 - coherent, 435
 - short, 434

- path polytope, 435
 - of the cube, 459
 - staircase, 302
- mother of all examples, 263, 337, 338
 - Gale transform, 339
 - lift, 340
 - perturbation, 338
 - secondary polytope, 339
- multiple face property, 191
- multiple point property, 192

N

- neighborly, 412
 - weakly —, 412

Newton polytope, 22, 480

- non-face, 478
- minimal, 481

normal

- cone, 491
- inner, 47
- outer, 47
- fan, 16, 489
- normally equivalent, 47
- outer —, 47

normal form

- 3-CNF, 415
- 3-conjunctive, 415
- conjunctive —, 414
- Gauss-Jordan, 216
- modulo an ideal, 479
- reduced column —, 379

normality, 473**O**

- octahedron, 350
- one-point suspension, 175
- order
 - complex, 116, 444
 - polytope, 11
- oriented
 - hyperplane, 156
 - matroid, 149, 164, 278, 338
 - non-realizable, 164

P

- parking function, 33
- partial triangulation, 391
- permutohedron, 298, 323, 459
- pivot, 493
- placing triangulation, 96, 179, 221
- plane graph
 - non-crossing, 94
 - rooted, 112
- point configuration, 1, 47, 488
 - convex hull, 50
 - cyclic, 278
 - dependent, 51
 - double chain, 123
 - face, 51
 - proper, 51
 - facet, 51
 - in convex position, 51
 - in general position, 51
 - in special position, 51
 - independent, 51
 - lattice —, 464
 - lifted, 55
 - relative interior, 50
 - spanning, 51

- standard cyclic, 278
 unimodular, 301
 with many triangulations, 290, 351
 zonotopal, 438
- polar, 491
 polyhedral
 complex, 45, 58
 anti-star, 46
 boundary, 46
 link, 46
 pure, 46
 star, 46
 subcomplex, 46
 subdivision, 62, 79, 149
- polyhedron, 44
 polytope, 43, 44
 dimension, 44
 edge — of a graph, 474
 face, 43
 fiber —, 441
 lattice —, 464
 monotone path —, 459
 Newton —, 480
 normally equivalent, 16, 493
 order —, 11
 relative interior, 44
 secondary —, 7, 17, 44, 215
 of the mother of all examples, 339
 unimodular, 297
- poset, 11, 65, 276
 bounded, 277
 height, 117
 refinement, 65
 refinement —, 61, 343
- positive
 circuits, 152
 hull, 45
 roots, 33, 504
 span, 45, 77
- Prim's algorithm, 101
 prism, 167, 168
 over a configuration, 168
 over a subdivision, 168
 top and bottom facets, 295
- product
 of configurations, 168
 of simplices, 294
 non-regular triangulations, 306
 simpotope, 311
 staircase triangulation, 302, 303
 of subdivisions, 168
 standard — of configurations, 168
- proper intersection property
 for adjacent maximal cells, 200
- for maximal cells, 195
 property
 circuit —, 154, 159
 for triangulations, 154, 160
 closure —, 54, 149
 cocircuit —, 159
 for triangulations, 159, 160
 face —, 191, 192
 free Hilbert cover —, 473
 hull —, 193, 194
 for adjacent maximal cells, 201
 for maximal cells, 196, 197
 integral Carathéodory —, 473
 interior point —, 200, 202
 intersection —, 1, 54, 149, 154
 for maximal cells, 195
 label —, 193
 for adjacent maximal cells, 202
 for maximal cells, 196, 198
 multiple face —, 191
 multiple point —, 192
 proper intersection —
 for adjacent maximal cells, 200
 for maximal cells, 195
 pseudo-manifold —, 155
 for maximal cells, 197, 200, 201
 union —, 1, 54, 149, 155, 159
 for maximal cells, 195–197
- pseudo-chamber, 341
 complex, 264
- pseudo-manifold property, 155
 for maximal cells, 197, 200, 201
- pseudo-triangle, 131
- pseudo-triangulation, 131
 pointed, 131
- pulling triangulation, 96, 181, 184
 pushing triangulation, 179, 184
 pyramid, 165
 apex, 165
 base, 165
 over a configuration, 165
 over a subdivision, 166
- R**
- radical of a monomial ideal, 482
 Radon partition, 73
 randomized, 240
 rank, 49, 77
 ray, 79
 ray-shooting, 399
 refinement, 65
 of subdivisions, 61, 79
 poset, 61
 long chains, 343
 pulling —, 184
- pushing —, 184
 regular, 69
 regular
 polytopes, 353
 refinement, 69
 subdivision, 59, 60
 triangulation, 55
- relative
 interior
 of a cone, 45
 of a configuration, 50, 77
 of a polytope, 44
 volume of a face, 332
- residue
 modulo an ideal, 479
 ring, 479
- reverse search enumeration, 123
 reversible edge, 349
 root system
 crystallographic, 32
 type A, 504
- S**
- Schönhardt polyhedron, 133, 170
 cupolas, 428
 skylight, 427
- secondary
 cone, 221
 fan, 17
 polytope, 7, 17, 44, 215
 diameter, 268
 of a prism, 297
 of the mother of all examples, 339
- shellable, 493
 shelling, 88, 493
 line —, 489, 494
- sign vector, 150
 signature, 150
 conformal, 150
 conformal sum, 150
 from dependence, 150
- simplex, 1, 44, 62, 79, 83
 algorithm, 14, 433
- simplicity, 318
- simplicial
 ball, 84
 cell, 79
 complex, 54
 abstract, 83
 cell, 83
 edge, 83
 facet, 493
 geometric, 46, 83
 join of two —s, 84

- link, 84
 non-face, 481
 pure, 83, 493
 size of, 84
 star, 84
 vertex, 83
 join, 166, 453
 sphere, 46, 84, 291, 500
 boundary, 46
 polytopal, 291, 397
 sparse system, 24
 stable set of a graph, 410
 standard triangulation, 7
 state polytope, 480
 subdivision, 62, 79, 149
 cell, 62, 79
 cells, 59
 central, 262, 490
 characteristic section of, 230, 284, 285
 coarser, 285
 coarsest, 66, 241
 compatible, 440
 coherent, 441
 tight, 440
 Delaunay, 97
 face, 46
 finest, 66
 induced, 441
 mixed, 449
 coherent, 452
 fine, 452
 mixed regular, 24
 path of, 126
 trivial, 64
 support, 73, 150
 of a point, 481
 of a vector, 406
 supporting hyperplane, 44, 45, 51, 78
- T**
 term order, 479
 tight
 compatible subdivision, 440
 locally coherent string, 441
 span, 242, 321, 323
 zonotopal tiling, 439
 toric
- Hilbert scheme, 360
 ideal, 480, 481
 transversal, 482
 tree, 5
 binary, 5
 minimum spanning, 101
 triangulation, 1, 54, 62, 79, 93
 coherent, 55
 convex, 55
 counting all —s, 123
 Delaunay —, 97
 edge, 94
 flip-deficient, 142, 337, 344
 full, 2, 94, 409
 Gale, 55
 greedy —, 103
 highly flip-deficient, 347, 358
 lattice —, 465
 lexicographic, 182
 locally minimal, 106
 minimum length —, 102, 105
 minimum weight —, 102
 neighborly, 136
 non-regular, 56
 number of —s, 107, 268, 291, 351, 396
 placing —, 96, 179, 221
 pulling —, 96, 181, 184
 pushing —, 179, 184
 regular, 16, 55, 96
 shallow, 412
 staircase —, 302, 303
 standard — of a unimodular triangle, 472
 t-path, 126
 topological, 111
 triangle, 94
 unimodular, 360, 464
 weight, 102
 weighted Delaunay, 55
 Tutte's formula, 112
 type (of a circuit), 73
- U**
 unimodular
 configuration, 301
 cover, 473
 lattice simplex, 464
- polytope, 297
 totally —, 473
 transformation, 464
 triangulation, 360, 464
 union property, 1, 54, 155, 159
 for maximal cells, 195–197
 universal polytope, 317, 400
 unshellable, 494
 Upper Bound Theorem, 86
- V**
 vector configuration, 48, 76, 77, 488
 acyclic, 78
 conical hull, 77
 corank, 77
 dependent, 77
 face, 78
 proper, 78
 in convex position, 78
 in general position, 77
 in special position, 77
 independent, 77
 positive span, 77
 rank, 77
 relative interior, 77
 subconfiguration, 77
 totally cyclic, 78
 unimodular, 301
 vertex, 44, 62, 79
 visibility, 96
 external, 96
 visible, 178
 Voronoi
 cell, 97
 diagram, 56, 97
- W**
 wall, 71, 188
 interior, 199
 witness —, 188
 width, 470
- Z**
 zonotopal tiling, 436, 439, 452
 coherent, 437
 tight, 436
 zonotope, 436, 452
 zone, 436